

Radiocarbon

An International Journal of Cosmogenic Isotope Research

VOLUME 46 / NUMBER 1 / 2004



Proceedings of the 18th International Radiocarbon Conference

Wellington, New Zealand
September 1–5, 2003

Part 1 of 2

Conference Editors
NANCY BEAVAN ATHFIELD
RODGER J SPARKS

Department of Geosciences
The University of Arizona
4717 East Fort Lowell Road
Tucson, Arizona 85712-1201 USA

ISSN: 0033-8222

RADIOCARBON

An International Journal of Cosmogenic Isotope Research

Editor: A J T JULL

Associate Editors: J WARREN BECK, GEORGE S BURR, AND GREGORY WL HODGINS

Managing Editor: MARK E MCCLURE

Assistant Editor: TASHA ADAMS, ROY A RAMOS

Business Manager: AGNIESZKA P BAIER

Subscriptions and Sales Manager: KRISTA LINDSAY

Published by
Department of Geosciences
The University of Arizona

Published three times a year at The University of Arizona, Tucson, AZ 85712-1201 USA.

© 2004 by the Arizona Board of Regents on behalf of the University of Arizona. All rights reserved.

Subscription rate (2004): \$200.00 (institutions), \$100.00 (individuals). Foreign postage is extra. A complete price list, including proceedings of international conferences, special publications and back issues, appears on the back pages of this issue. *Advertising rates* available upon request, or see www.radiocarbon.org/adrates.html.

Missing issues will be replaced without charge only if claim is made within three months (six months for India, New Zealand, and Australia) after the publication date. Claims for missing issues will not be honored if non-delivery results from failure by the subscriber to notify the Journal of an address change.

Authors: See our "Information for Authors" document at www.radiocarbon.org/Authors/ for guidelines on manuscript submission and format. All correspondence and manuscripts should be addressed to the Managing Editor, *RADIOCARBON*, Department of Geosciences, The University of Arizona, 4717 East Fort Lowell Road, Tucson, AZ 85712-1201 USA. Tel.: +1 520 881-0857; Fax: +1 520 881-0554; Email: editor@radiocarbon.org.

List of laboratories. Our comprehensive list of laboratories is published annually, and is also available at www.radiocarbon.org/Info/lablist.html. We ask all laboratory directors to provide their laboratory code designation, as well as current telephone and fax numbers, and email addresses. Changes in names or addresses, additions or deletions should be reported to the managing editor. Conventional and AMS laboratories are arranged in alphabetical order by country, and we include laboratories listed by code designation.

RADIOCARBON on the World Wide Web: <http://www.radiocarbon.org/>

RADIOCARBON is indexed and/or abstracted by the following sources: *Anthropological Index; Anthropological Literature; Art and Archaeology Technical Abstracts; Bibliography and Index of Geology (GeoRef); British Archaeological Bibliography; Chemical Abstracts; Chemistry Citation Index; Current Advances in Ecological and Environmental Sciences; Current Contents (ISI); FRANCIS (Institut de l'Information Scientifique et Technique – CNRS); Geographical Abstracts; Geological Abstracts; Oceanographic Literature Review; Science Citation Index; Social Sciences Citation Index.*

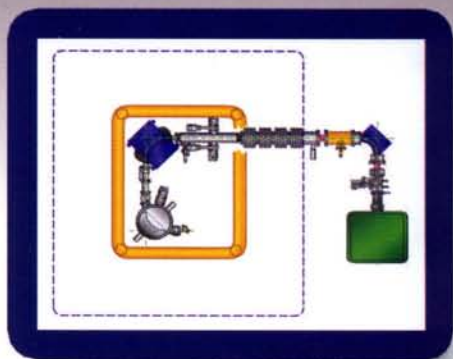
COMPACT CARBON AMS

Accelerator Mass Spectrometry Tandem and Single Stage

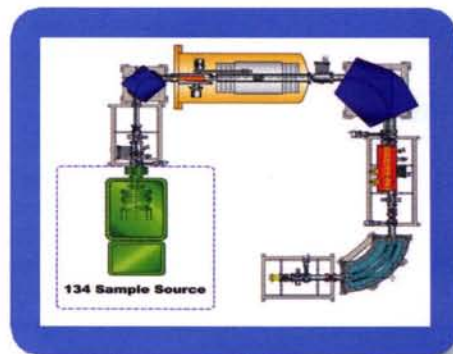
National Electrostatics Corporation offers a wide variety of compact, low voltage AMS systems for carbon radio isotope ratio measurement. All NEC systems provide high precision and low background. They can be equipped with the high throughput, multi-sample ion source or dual ion source injector for added versatility.

FEATURES INCLUDE:

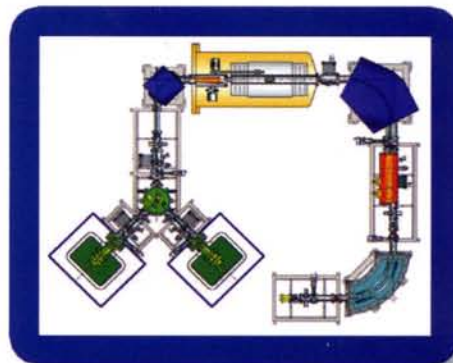
- Better than 5 per mil precision
- Better than 5×10^{-15} background
- Throughput of 400 samples/day to 2% precision for modern carbon with the 134 sample source
- Gas and solid sample source
- All metal/ceramic acceleration tubes with no organic material in the vacuum volume



Single Stage AMS



**High Through-put
Compact Carbon AMS**



**Multi Ion Source
Compact Carbon AMS**



7540 Graber Road, P.O. Box 620310
Middleton, WI USA, 53562-0310

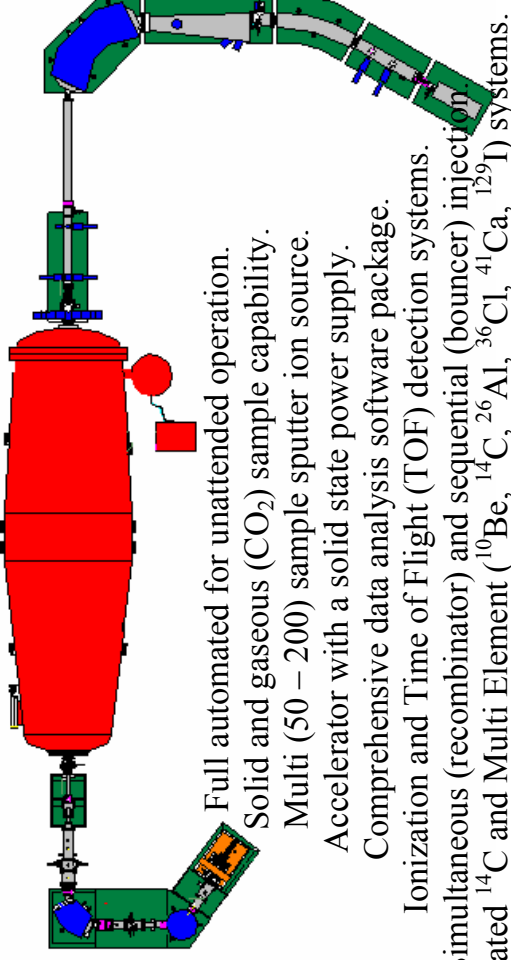
Phone: 608-831-7600 • Fax: 608-831-9591
nec@pelletron.com • www.pelletron.com

TANDETRON ACCELERATOR MASS SPECTROMETERS

Dedicated and Multi element systems

'The choice is yours....'

1.0MV, 2.0MV, 3.0MV or 5.0MV



Full automated for unattended operation.

Solid and gaseous (CO₂) sample capability.

Multi (50 – 200) sample sputter ion source.

Accelerator with a solid state power supply.

Comprehensive data analysis software package.

Ionization and Time of Flight (TOF) detection systems.

Simultaneous (recombinator) and sequential (bouncer) injection

Dedicated ¹⁴C and Multi Element (¹⁰Be, ¹⁴C, ²⁶Al, ³⁶Cl, ⁴¹Ca, ¹²⁹I) systems.



HIGH VOLTAGE ENGINEERING EUROPA B.V.

Amsterdamseweg 63, 3812 RR Amersfoort, P.O. Box 99, 3800 AB Amersfoort, The Netherlands
Phone: +31-33-4619741. Fax +31-33-4615291. Trade register Amersfoort nr. 31014544

E-mail: info@highvolteng.com – Web: www.highvolteng.com



CONTENTS

EDITORIAL BOARD	ix
------------------------------	----

SPONSORS	xi
-----------------------	----

FROM THE GUEST EDITORS	xiii
-------------------------------------	------

LIST OF PARTICIPANTS	xix
-----------------------------------	-----

ARTICLES**AMS Methods and Developments**

Initial Results with Low Energy Single Stage AMS <i>J B Schroeder, T M Hauser, G M Klody, G A Norton</i>	1
---	---

Pushing the Precision Limit of ¹⁴ C AMS <i>Peter Steier, Franz Dellinger, Walter Kutschera, Alfred Priller, Werner Rom, Eva Maria Wild</i>	5
--	---

Towards High-Precision AMS: Progress and Limitations <i>Christopher Bronk Ramsey, Thomas Higham, Philip Leach</i>	17
--	----

Using a Gas Ion Source for Radiocarbon AMS and GC-AMS <i>Christopher Bronk Ramsey, Peter Ditchfield, Martin Humm</i>	25
---	----

Ion Source Development at KCCAMS, University of California, Irvine <i>J R Southon, G M Santos</i>	33
--	----

The Keck Carbon Cycle AMS Laboratory, University Of California, Irvine: Initial Operation and a Background Surprise <i>John Southon, Guaciara Santos, Kevin Druffel-Rodriguez, Ellen Druffel, Sue Trumbore, Xiaomei Xu, Sheila Griffin, Shahla Ali, Maya Mazon</i>	41
---	----

The New ¹⁴ C Analysis Laboratory in Jena, Germany <i>A Steinhof, G Adamiec, G Gleixner, GJ van Klinken, T Wagner</i>	51
--	----

Capabilities of the New SUERC 5MV AMS Facility for ¹⁴ C Dating <i>S Xu, R Anderson, C Bryant, G T Cook, A Dougans, S Freeman, P Naysmith, C Schnabel, E M Scott</i>	59
---	----

Direct Coupling of an Elemental Analyzer and a Hybrid Ion Source for AMS Measurements <i>Thomas Uhl, Wolfgang Kretschmer, Wolfgang Luppold, Andreas Scharf</i>	65
---	----

Fast and Accurate Sequential Injection AMS with Gated Faraday Cup Current Measurement <i>M Klein, D J W Mous, A Gott dang</i>	77
--	----

¹⁰ Be Analyses with a Compact AMS Facility—Are BeF ₂ Samples the Solution? <i>L Wacker, M Grajcar, S Ivy-Ochs, PW Kubik, M Suter</i>	83
---	----

Simulation Study for the Separation of Rare Isotopes at the Seoul National University AMS Facility <i>C C Yun, C S Lee, M Youn, J C Kim</i>	89
--	----

Liquid Scintillation

Surface and Underground Ultra Low-Level Liquid Scintillation Spectrometry <i>Wolfgang Plastino, Lauri Kaihola</i>	97
--	----

Measurement of Low ^{14}C Activities in a Liquid Scintillation Counter in the Zagreb Radiocarbon Laboratory <i>Nada Horvatinčić, Jadranka Barešić, Ines Krajcar Bronić, Bogomil Obelić</i>	105
Rehabilitation of the Laboratoire De Carbone 14-Dakar (Senegal) with a Super Low-Level Liquid Scintillation Counting System <i>Maurice Ndeye, Oumar Ka, Hamady Bocoum, Alpha O Diallo</i>	117
Towards Achieving Low Background Levels in Routine Dating by Liquid Scintillation Spectrometry <i>Alan G Hogg</i>	123
Sample Processing	
Preparation of Graphite Targets from Small Marine Samples for AMS Radiocarbon Measurements <i>Laval Liong Wee Kwong, Pavel P Povinec, A J Timothy Jull</i>	133
Development of a Combustion System for Liquid or Gas Samples <i>J H Park, C S Lee</i>	141
A Pretreatment Procedure for the AMS Radiocarbon Dating of Sub-Fossil Insect Remains <i>J A Tripp, T F G Higham, R E M Hedges</i>	147
Improvements to the Pretreatment of Bone at Oxford <i>Christopher Bronk Ramsey, Thomas Higham, Angela Bowles, Robert Hedges</i>	155
Magnesium Perchlorate as an Alternative Water Trap in AMS Graphite Sample Preparation: A Report on Sample Preparation at KCCAMS at the University of California, Irvine <i>G M Santos, J R Southon, K C Druffel-Rodriguez, S Griffin, M Mazon</i>	165
Radiocarbon Dating of Iron Artifacts at the Erlangen AMS Facility <i>Andreas Scharf, Wolfgang Kretschmer, Gerhard Morgenroth, Thomas Uhl, Karin Kritzler, Katja Hunger, Ernst Pernicka</i>	175
Extraction and AMS Radiocarbon Dating of Pollen from Lake Baikal Sediments <i>Natalia Piotrowska, Andrzej Bluszcz, Dieter Demske, Wojciech Granoszewski, Georg Heumann</i>	181
^{14}C Ages of Ostracodes from Pleistocene Lake Sediments of the Western Great Basin, USA—Results of Progressive Acid Leaching <i>Irka Hajdas, Georges Bonani, Susan Herrgesell Zimmerman, Millie Mendelson, Sidney Hemming</i>	189
Preliminary Results for the Extraction and Measurement of Cosmogenic In Situ ^{14}C from Quartz <i>P Naysmith, G T Cook, W M Phillips, N A Lifton, R Anderson</i>	201
Problems Associated with the AMS Dating of Small Bone Samples: The Question of the Arrival of Polynesian Rats to New Zealand <i>T F G Higham, R E M Hedges, A J Anderson, C Bronk Ramsey, B Fankhauser</i>	207
AMS ^{14}C Dating of Iron Artifacts: Development and Application <i>Hiroki Enami, Toshio Nakamura, Hirotaka Oda, Tetsuya Yamada, Toshio Tsukamoto</i>	219
Archaeology	
^{14}C Dating Compared to Art Historical Dating of Roman and Coptic Textiles from Egypt <i>Mark Van Strydonck, Antoine De Moor, Dominique Bénazeth</i>	231
Radiocarbon Dating of Sopot Culture Sites (Late Neolithic) in Eastern Croatia <i>Bogomil Obelić, Marija Krznarić Škrivanko, Boško Marijan, Ines Krajcar Bronić</i>	245

Chronology and Possible Links Between Climatic and Cultural Change During the First Millennium BC in Southern Siberia and Central Asia <i>G I Zaitseva, B van Geel, N A Bokovenko, K V Chugunov, V A Dergachev, V G Dirksen, M A Koukova, A Nagler, G Parzinger, J van der Plicht, N D Bourova, L M Lebedeva</i>	259
Chronological Studies of the Arzhan-2 Scythian Monument in Tuva (Russia) <i>G I Zaitseva, K V Chugunov, V A Dergachev, A Nagler, G Parzinger, E M Scott, A A Sementsov, S Vasiliev, B van Geel, J van der Plicht, L M Lebedeva</i>	277
A Puzzling Body from the River Thames in London <i>Alex Bayliss, Peter Marshall, Jane Sidell</i>	285
Radiocarbon and Stable Isotope Evidence of Dietary Change from the Mesolithic to the Middle Ages in the Iron Gates: New Results from Lepenski Vir <i>C Bonsall, G T Cook, R E M Hedges, T F G Higham, C Pickard, I Radovanović</i>	293
A Review of the Evidence for Extinction Chronologies for Five Species of Upper Pleistocene Megafauna in Siberia <i>Lyobov A Orlova, Yaroslav V Kuzmin, Vyacheslav N Dementiev</i>	301
The End of the Chalcolithic Period in the South Jordan Valley: New ¹⁴ C Determinations from Teleilat Ghassul, Jordan <i>Stephen Bourke, Ugo Zoppi, John Meadows, Quan Hua, Samantha Gibbins</i>	315
Dating the Volcanic Eruption at Thera <i>Christopher Bronk Ramsey, Sturt W Manning, Mariagrazia Galimberti</i>	325
Chronology of the Beginning of Pottery Manufacture in East Asia <i>Charles T Keally, Yasuhiro Taniguchi, Yaroslav V Kuzmin, Igor Y Shewkomud</i>	345
Chronology of Prehistoric Cultural Complexes of Sakhalin Island (Russian Far East) <i>Yaroslav V Kuzmin, Alexander A Vasilevski, Sergei V Gorbunov, G S Burr, A J Timothy Jull, Lyobov A Orlova, Olga A Shubina</i>	353
Lugovskoe, Western Siberia: A Possible Extra-Arctic Mammoth Refugium at the End of the Late Glacial <i>Lyobov A Orlova, Vasily N Zenin, Anthony J Stuart, Thomas F G Higham, Pieter M Grootes, Sergei V Leshchinsky, Yaroslav V Kuzmin, Aleksander F Pavlov, Evgeny N Maschenko</i>	363
Radiocarbon Dating of <i>Kohitsugire</i> (Paper Fragments) Attributed to Japanese Calligraphists in the Heian–Kamakura Period <i>Hirota Oda, Kazuomi Ikeda, Takashi Masuda, Toshio Nakamura</i>	369
Neolithic Massacres: Local Skirmishes or General Warfare in Europe? <i>Eva Maria Wild, Peter Stadler, Annemarie Häußler, Walter Kutschera, Peter Steier, Maria Teschler-Nicola, Joachim Wahl, Helmut J Windl</i>	377
¹⁴ C Dating of the Settlement of Iceland <i>Arny E Sveinbjörnsdóttir, Jan Heinemeier, Gardar Gudmundsson</i>	387
Anomalous Radiocarbon Dates from Easter Island <i>Kevin Butler, Christine A Prior, John R Flenley</i>	395
AMS ¹⁴ C Dating Using Black Pottery and Fiber Pottery <i>Shozo Mihara, Kazuo Miyamoto, Hidefumi Ogawa, Teiji Kurosaka, Toshio Nakamura, Hiroko Koike</i>	407
Soils	
Dating of Total Soil Organic Matter Used in Kurgan Studies <i>M Molnár, K Joó, A Barczy, Zs Szántó, I Futó, L Palcsu, L Rinyu</i>	413
Calculating Sediment Compaction for Radiocarbon Dating of Intertidal Sediments <i>M I Bird, L K Fifield, S Chua, B Goh</i>	421

Preliminary ^{14}C Dates on Bulk Soil Organic Matter from the Black Creek Megafauna Fossil Site, Rocky River, Kangaroo Island, South Australia <i>Matt Forbes, Erick Bestland, Rod Wells</i>	437
^{10}Be , ^{14}C Distribution, and Soil Production Rate in a Soil Profile of a Grassland Slope at Heshan Hilly Land, Guangdong <i>CD Shen, J Beer, S Ivy-Ochs, Y Sun, W Yi, P W Kubik, M Suter, Z Li, S Peng, Y Yang</i>	445
A Novel Approach for Developing High-Resolution Sub-Fossil Peat Chronologies with ^{14}C Dating <i>T H Donders, F Wagner, K van der Borg, A F M de Jong, H Visscher</i>	455
Complexity of Soil Organic Matter: AMS ^{14}C Analysis of Soil Lipid Fractions and Individual Compounds <i>Janet Rethemeyer, Christiane Kramer, Gerd Gleixner, Guido L B Wiesenberg, Lorenz Schwark, Nils Andersen, Marie-J Nadeau, Pieter M Grootes</i>	465
Atmosphere	
Source Apportionment of Aerosols by ^{14}C Measurements In Different Carbonaceous Particle Fractions <i>S Szidat, T M Jenk, H W Gäggeler, H-A Synal, R Fisseha, U Baltensperger, M Kalberer, V Samburova, L Wacker, M Saurer, M Schwikowski, I Hajdas</i>	475
Temporal Variation of Radiocarbon Concentration in Airborne Particulate Matter in Tokyo <i>Ken Shibata, Michio Endo, Naomichi Yamamoto, Jun Yoshinaga, Yukio Yanagisawa, Osamu Endo, Sumio Goto, Minoru Yoneda, Yasuyuki Shibata, Masatoshi Morita</i>	485
Pathways for Escape of Magmatic Carbon Dioxide to Soil Air at Unzen Volcano, SW Japan <i>Hiroshi A Takahashi, Kohei Kazahaya, Hiroshi Shinohara, Toshio Nakamura</i>	491
PART II	
Groundwater	
A Direct Estimate of the Initial Concentration of ^{14}C in the Mountain Aquifer of Israel <i>Israel Carmi, Joel Kronfeld, Yoseph Yechieli, Elisabetta Boaretto, Miryam Bar-Matthews, Avner Ayalon</i>	497
Time-Dependent Factors Inherent in the Age Equation for Determining Residence Times of Groundwater Using ^{14}C : A Procedure to Compensate for the Past Variability of ^{14}C in Atmospheric Carbon Dioxide, with Application to the Wairau Deep Aquifer, Marlborough, New Zealand <i>Claude B Taylor</i>	501
Paleogroundwater in the Moutere Gravel Aquifers near Nelson, New Zealand <i>Michael K Stewart, Joseph T Thomas, Margaret Norris, Vanessa Trompeter</i>	517
Marine and Freshwater Environments	
Radiocarbon Reservoir Age Variations in the South Peruvian Upwelling During the Holocene <i>Michel Fontugne, Matthieu Carré, Ilhem Bentaleb, Michèle Julien, Danièle Lavallée</i>	531
Radiocarbon Ages and Isotope Fractionations of Beachrock Samples Collected from the Nansei Islands, Southwestern Japan <i>Kunio Omoto</i>	539
Paired ^{14}C and $^{230}\text{Th}/\text{U}$ Dating of Surface Corals from the Marquesas and Vanuatu (Sub-Equatorial Pacific) in the 3000 to 15,000 cal yr Interval <i>Martine Paterne, Linda K Ayliffe, Maurice Arnold, Guy Cabioch, Nadine Tisnérat-Laborde, Christine Hatté, Eric Douville, Edouard Bard</i>	551

Oceanic Radiocarbon and Tritium on a Transect between Australia and Bali (Eastern Indian Ocean)	
<i>Viviane Leboucher, Philippe Jean-Baptiste, Elise Fourré, Maurice Arnold, Michèle Fieux . . .</i>	567
Radiocarbon in the Water Column of the Southwestern North Pacific Ocean—24 Years After GEOSECS	
<i>Pavel P Povinec, Takafumi Aramaki, George S Burr, A J Timothy Jull, Laval Liong Wee Kwong, Orihiko Togawa</i>	583
Interannual ¹⁴ C Variations During 1977–1998 Recorded in Coral from Daya Bay, South China Sea	
<i>C D Shen, W X Yi, K F Yu, Y M Sun, Y Yang, B Zhou</i>	595
Marine Reservoir Correction for the Cocos (Keeling) Islands, Indian Ocean	
<i>Quan Hua, Colin D Woodroffe, Mike Barbetti, Scott G Smithers, Ugo Zoppi, David Fink . . .</i>	603
Holocene Variations in the Scottish Marine Radiocarbon Reservoir Effect	
<i>Philippa L Ascough, Gordon T Cook, Andrew J Dugmore, John Barber, Elaine Higney, E Marian Scott</i>	611
Radiocarbon Reservoir Ages from Freshwater Lakes, South Georgia, Sub-Antarctic: Modern Analogues from Particulate Organic Matter and Surface Sediments	
<i>Steven G Moreton, Gunhild C Rosqvist, Sarah J Davies, Michael J Bentley</i>	621
Variability of Monthly Radiocarbon During the 1760s in Corals from the Galapagos Islands	
<i>Ellen R M Druffel, Sheila Griffin, Jeomshik Hwang, Tomoko Komada, Steven R Beaupre, Kevin C Druffel-Rodriguez, Guaciara M Santos, John Southon</i>	627
Radiocarbon in Porewater of Continental Shelf Sediments (Southeast Mediterranean)	
<i>O Sivan, B Lazar, E Boaretto, Y Yecheili, B Herut</i>	633
Seasonal Radiocarbon Variation of Surface Seawater Recorded in a Coral from Kikai Island, Subtropical Northwestern Pacific	
<i>Maki Morimoto, Hiroyuki Kitagawa, Yasuyuki Shibata, Hajime Kayanne</i>	643
Temporal Changes in Radiocarbon Reservoir Age in the Dead Sea-Lake Lisan System	
<i>Mordechai Stein, Claudia Migowski, Revital Bookman, Boaz Lazar</i>	649
Marine Reservoir Correction in the South of Vietnam Estimated from an Annually-Banded Coral	
<i>Phong X Dang, Takehiro Mitsuguchi, Hiroyuki Kitagawa, Yasuyuki Shibata, Toshiyuki Kobayashi</i>	657
Past Environments	
The ‘Sterno-Etrussia’ Geomagnetic Excursion Around 2700 BP and Changes of Solar Activity, Cosmic Ray Intensity, and Climate	
<i>V A Dergachev, O M Raspopov, B van Geel, G I Zaitseva</i>	661
The Cosmic Ray Increases at 35 and 60 kyr BP	
<i>V Florinski, W I Axford, G P Zank</i>	683
Holocene Environmental Changes in Western Hungary	
<i>Zsuzsanna Szántó, Zsófia Medzihradzky</i>	691
Carbon Isotopic Composition of Tree Rings as a Tool for Biomonitoring CO ₂ Level	
<i>Stawomira Pawełczyk, Anna Pazdur</i>	701
An AMS ¹⁴ C Pollen-Dated Sediment and Pollen Sequence from the Late Holocene, Southern Coastal Hawke’s Bay, New Zealand	
<i>Pamela I Chester, Christine A Prior</i>	721
Shape Analysis of Cumulative Probability Density Function of Radiocarbon Dates Set in the Study of Climate Change in the Late Glacial and Holocene	
<i>Danuta J Michczyńska, Anna Pazdur</i>	733

Radiocarbon Chronology of the Late Pleistocene–Holocene Paleogeographic Events in the Lake Baikal Region (Siberia) <i>Sergey K Krivonogov, Hikaru Takahara, Yaroslav V Kuzmin, Lyobov A Orlova, A J Timothy Jull, Toshio Nakamura, Norio Miyoshi, Kimiyasu Kawamuro, Elena V Bezrukova</i>	745
Changes in Sediment Accumulation Rate in an Oxbow Lake Following Late 19th Century Clearing of Land for Agricultural Use: A ²¹⁰ Pb, ¹³⁷ Cs, and ¹⁴ C Study in Mississippi, USA <i>Gregg R Davidson, Meredith Carnley, Todd Lange, Stanley J Galicki, Andrew Douglas</i>	755
Late Holocene Environmental Reconstruction of St. Michiel Saline Lagoon, Curaçao (Dutch Antilles) <i>Bogumila B Klosowska, Simon R Troelstra, Jan E van Hinte, Klaas van der Borg, Arie F M de Jong</i>	765
On the Erosive Trail of a 14th and 15th Century Hurricane in Connecticut (USA) Salt Marshes <i>O van de Plassche, A J Wright, K van der Borg, A F M de Jong</i>	775
Near-Zero $\Delta^{14}\text{C}$ Values at 32 kyr cal BP Observed in the High-Resolution ¹⁴ C Record from U-Th Dated Sediment of Lake Lisan <i>K van der Borg, M Stein, A F M de Jong, N Waldmann, S L Goldstein</i>	785
Holocene Evolution of the Outer Lake of Hwajnpo Lagoon on the Eastern Coast of Korea; Environmental Changes with Holocene Sea-Level Fluctuation of the East Sea (Sea of Japan) <i>Jong-Gwon Yum, Kang-Min Yu, Keiji Takemura, Toshiro Naruse, Akihisa Kitamura, Hiroyuki Kitagawa, Jong-Chan Kim</i>	797
¹⁴ C Chronology of Mesolithic Sites from Poland and the Background of Environmental Changes <i>Anna Pazdur, Mariusz Fogtman, Adam Michczyński, Jacek Pawlyta, Mirosław Zajac</i>	809
The Modern Environment	
¹⁴ C Sources and Distribution in the Vicinity of La Hague Nuclear Reprocessing Plant: Part I—Terrestrial Environment <i>M Fontugne, D Maro, Y Baron, C Hatté, D Hebert, E Douville</i>	827
¹⁴ C Sources and Distribution in the Vicinity of La Hague Nuclear Reprocessing Plant: Part II—Marine Environment <i>D Maro, M Fontugne, C Hatté, D Hebert, M Rozet</i>	831
Testing the Use of Bomb Radiocarbon to Date the Surface Layers of Blanket Peat <i>M H Garnett, A C Stevenson</i>	841
Differentiating Bone Osteonal Turnover Rates by Density Fractionation; Validation Using the Bomb ¹⁴ C Atmospheric Pulse <i>Ji Young Shin, Tamsin O'Connell, Stuart Black, Robert Hedges</i>	853
Levels of ¹⁴ C in the Terrestrial Environment in the Vicinity of Two European Nuclear Power Plants <i>Åsa Magnusson, Kristina Stenström, Göran Skog, Diana Adliene, Gediminas Adlys, Ragnar Hellborg, Agata Olariu, Mohamad Zakaria, Christopher Rääf, Sören Mattsson</i>	863
Sources of Anthropogenic ¹⁴ C to the North Sea <i>P Gulliver, G T Cook, A B MacKenzie, P Naysmith, R Anderson</i>	869
Sellafield-Derived Anthropogenic ¹⁴ C in the Marine Intertidal Environment of the NE Irish Sea <i>G T Cook, A B MacKenzie, G K P Muir, G Mackie, P Gulliver</i>	877
Spatial and Temporal Impacts of ¹⁴ C Releases from the Sellafield Nuclear Complex on the Irish Coastline <i>Sinead M Keogh, Edward J McGee, Donal Gallagher, Peter I Mitchell</i>	885
Stepped-Combustion ¹⁴ C Dating of Bomb Carbon in Lake Sediment <i>J McGeehin, G S Burr, G Hodgins, S J Bennett, J A Robbins, N Morehead, H Markewich</i>	893

Seasonal and Secular Variations of Atmospheric $^{14}\text{CO}_2$ Over the Western Pacific Since 1994 <i>H Kitagawa, Hitoshi Mukai, Yukihiko Nojiri, Yasuyuki Shibata, Toshiyuki Kobayashi, Tomoko Nojiri</i>	901
Tree Rings	
Radiocarbon Concentration in the Atmosphere and Modern Tree Rings in the Kraków Area, Southern Poland <i>Andrzej Rakowski, Tadeusz Kuc, Toshio Nakamura, Anna Pazdur</i>	911
Wiggle-Match Dating of Tree-Ring Sequences <i>Mariagrazia Galimberti, Christopher Bronk Ramsey, Sturt W Manning</i>	917
Radiocarbon in Annual Tree Rings from Thailand During the Pre-Bomb Period, AD 1938–1954 <i>Quan Hua, Mike Barbetti, Ugo Zoppi</i>	925
Tree-Ring Records of Near-Younger Dryas Time in Central North America—Preliminary Results from the Lincoln Quarry Site, Central Illinois, USA <i>Irina P Panyushkina, Steven W Leavitt, Alex Wiedenhoeft, Sarah Noggle, Brandon Curry, Eric Grimm</i>	933
The Comparison of ^{14}C Wiggle-Matching Results for the ‘Floating’ Tree-Ring Chronology of the Ulandryk-4 Burial Ground (Altai Mountains, Siberia) <i>Yaroslav V Kuzmin, Igor Y Slusarenko, Irka Hajdas, Georges Bonani, J Andres Christen</i>	943
^{14}C Concentrations of Single-Year Tree Rings from about 22,000 Years Ago Obtained Using a Highly Accurate Measuring Method <i>Toshiyuki Gandou, Hirohisa Sakurai, Wataru Katoh, Yousuke Takahashi, Syuichi Gunji, Fuyuki Tokanai, Hiroyuki Matsuzaki</i>	949
Interpreting Radiocarbon Dates Using Evidence from Tree Rings <i>Alex Bayliss, Ian Tyers</i>	957
Variation of the Radiocarbon Content in Tree Rings During the Spoerer Minimum <i>Hiroko Miyahara, Kimiaki Masuda, Hideki Furuzawa, Hiroaki Menjo, Yasushi Muraki, Hiroyuki Kitagawa, Toshio Nakamura</i>	965
Radiocarbon Calibration	
A ^{14}C Calibration with AMS from 3500 to 3000 BC, Derived from a New High-Elevation Stone- Pine Tree-Ring Chronology <i>Franz Dellinger, Walter Kutschera, Peter Steier, Eva Maria Wild, Kurt Nicolussi, Peter Schießling</i>	969
Bayesian Periodic Signal Detection Applied to INTCAL98 Data <i>V Palonen, P Tikkanen</i>	979
Radiocarbon/Tree-Ring Calibration, Solar Activity, and Upwelling of Ocean Water <i>F B Knox, B G McFadgen</i>	987
Influence of ^{14}C Concentration Changes in the Past on Statistical Inference of Time Intervals <i>Adam Michczyński</i>	997
New ΔR Values for the Southwest Pacific Ocean <i>Fiona Petchey, Mathew Phelan, Peter White</i>	1005
ERRATUM	1015
RADIOCARBON UPDATES	1017
AUTHOR INDEX	1019
SUBJECT INDEX	1025

INTERNATIONAL ADVISORY BOARD

EDOUARD BARD	<i>France</i>
WARREN BECK	<i>USA</i>
CHRISTOPHER BRONK RAMSEY	<i>United Kingdom</i>
FRANK BRUHN	<i>New Zealand</i>
ISRAEL CARMİ	<i>Israel</i>
KEITH FIFIELD	<i>Australia</i>
DAVID FINK	<i>Australia</i>
MEBUS GEYH	<i>Germany</i>
ROBERT HEDGES	<i>United Kingdom</i>
YAROSLAV KUZMIN	<i>Russia</i>
PAVEL POVINEC	<i>Monaco</i>
ROBERT SCHNEIDER	<i>USA</i>
JOHANNES VAN DER PLICHT	<i>the Netherlands</i>

NEW ZEALAND ORGANIZING COMMITTEE

NANCY BEAVAN ATHFIELD	<i>Rafter Radiocarbon Laboratory, IGNS, New Zealand</i>
RODGER SPARKS	<i>Rafter Radiocarbon Laboratory, IGNS, New Zealand</i>
CHRISTINE PRIOR	<i>Rafter Radiocarbon Laboratory, IGNS, New Zealand</i>
BRUCE MCFADGEN	<i>Science and Research Unit, New Zealand Department of Conservation</i>
ALAN HOGG	<i>Waikato Radiocarbon Dating Laboratory, University of Waikato, New Zealand</i>
MICHELLE PARK	<i>GNS Graphics Team, IGNS, New Zealand</i>
DAWN CHAMBERS	<i>Rafter Radiocarbon Laboratory, IGNS, New Zealand</i>
LIANNE BREJNAKOWSKI	<i>Institute of Geological and Nuclear Sciences, Financial Manager</i>
JANET SIMES	<i>Absolutely Organised, Wellington, New Zealand</i>

EDITORIAL BOARD

EDOUARD BARD	<i>Aix-en-Provence, France</i>
CHRISTOPHER BRONK RAMSEY	<i>Oxford, England</i>
OWEN K DAVIS	<i>Tucson, Arizona, USA</i>
ELLEN R M DRUFFEL	<i>Irvine, California, USA</i>
PIETER GROOTES	<i>Kiel, Germany</i>
YAROSLAV KUZMIN	<i>Vladivostok, Russia</i>
STEVEN W LEAVITT	<i>Tucson, Arizona, USA</i>
TOSHIO NAKAMURA	<i>Nagoya, Japan</i>
ANN P McNICHOL	<i>Woods Hole, Massachusetts, USA</i>
PAVEL POVINEC	<i>Bratislava, Slovakia</i> <i>Monaco</i>
MICHAEL B SCHIFFER	<i>Tucson, Arizona, USA</i>
E MARIAN SCOTT	<i>Glasgow, Scotland</i>
RODGER SPARKS	<i>Lower Hutt, New Zealand</i>
JOHANNES VAN DER PLICHT	<i>Groningen, The Netherlands</i>
JOHN S VOGEL	<i>Livermore, California, USA</i>
WEIJIAN ZHOU	<i>Xi'an, China</i>

SPONSORS

The 18th International Radiocarbon Conference would not have been possible without the help of the following sponsors. The editors gratefully acknowledge the generous support of High Voltage Engineering Europa (HVEE), the National Electrostatics Corporation (NEC), and the Royal Society of New Zealand.



The editors would also like to thank the conference organizers, Absolutely Organised.



FROM THE GUEST EDITORS

Welcome to the Radiocarbon Proceedings Issue of the 18th International Radiocarbon Conference, held in Wellington, New Zealand, in September 2003. Its appearance is the last step in a process that began 4 years ago, after the 2000 Jerusalem conference.

It was a satisfying feeling on the afternoon of September 5th, 2003, as we knew that the 18th International Radiocarbon Conference had finally taken its place in that long series of conferences that stretches back 50 years. Of course, we had our concerns. The tragedy of September 11, 2001, made the world suddenly look more dangerous than most of us had ever imagined, and the prospect of travelling to distant parts of the globe lost its attraction for many people. The additional menace of the SARS virus outbreak further complicated travel to what, for many of you, was an exceedingly distant shore. Given these factors, who would come to the bottom of the Pacific to attend a conference?

Well, stone the crows, you did come. Whether through heroism, defiance, insouciance or a failure to read the newspapers is not for us to say. We missed some familiar faces, not all for the reasons given above, but there were enough old and new friends to ensure the conference was a success. Because, as with all such events, its success depended finally on the participants and what they made of it. We knew that, ultimately, we were in good hands. There was a touch of sadness when we learned that John Head, well known to many of the “old guard,” had passed away just weeks before the conference opened. Also absent was Reidar Nydal, who was prevented from coming by poor health.

What of the conference itself? It is almost with relief to note that talks were not dominated by the next “big thing” in radiocarbon. Rather, the presentations gave us a picture of a field that, although nearly 60 years old, is far from exhausted but rather is expanding into new areas, pushed by developing technology and pulled by new research priorities. AMS, after 30 years, has long since ceased being a novelty, but the continued shrinking of new AMS systems makes one wonder if someone at the next conference will announce the invention of the mass spectrometer.

What is apparent is that the promise of the AMS revolution continues to be fulfilled. Hitherto impossible measurements on hitherto impossible materials seems to be one of the roads to the future. If one were to hazard a guess as to the most promising development beginning to appear, then compound specific dating certainly appears to be the one to watch. The possibility of teasing apart the organic soup that we usually have to deal with, down to its molecular components, just has to lead to surprises in the future.

Another topic that is growing in importance and familiarity is the use of Bayesian methods in the interpretation of radiocarbon ages. The statisticians are persuading us that there is often much more information in our data than we realize, if we look at it in the right way. If they can only break the habit of beginning every paper with “Let X be a random variable with a normal distribution...”, the persuasion will be total.

For us, the highlight of the conference was at the dinner when Paul Damon asked why there was no mention of Athol Rafter in all the proceedings. How right Paul was to ask that question! It was a salutary reminder to us of how easy it is to forget the past and the contributions made by those who went before us. Certainly Rodger more than made amends with a five-minute impromptu speech on the Rafter years.

It remains to thank all those who helped make the 18th ¹⁴C Conference a success. The Rafter Radiocarbon team included Michelle Park, that powerhouse graphics wizard who corrected all the last-minute greeblies in Powerpoint presentations on site. We also acknowledge the daily support of Chris Prior, Jannine Cooper, Lisa Xie, Margaret Norris, Dawn Chambers, Kelly Sutton, Lorraine Gilligan, and Andrei Gaidamaka. Thanks to Janet Simes and her Absolutely Organised team, and the Te Papa staff who made the venue such a fantastic success. The International Advisory Panel diligently reviewed the abstracts that flooded in right on deadline; and we must thank also the reviewers who refereed the papers in this volume. Thanks to the *Radiocarbon* editorial staff, especially Tim Jull and Mark McClure, who taught us just what goes into creating every issue of the journal. And we very heartily thank our sponsors, especially HVE and NEC, whose major contributions to our budget helped us pull off the conference you all enjoyed so much.

Finally, thanks to all of you who came to Wellington in 2003. Your participation made the conference what it was; we really just tried to put on a good party for you all.

So now, relax before a roaring fire, pour a snifter of brandy, and browse this volume of the 2004 Conference Proceedings, and start thinking about the papers to be written for Oxford in 2006.

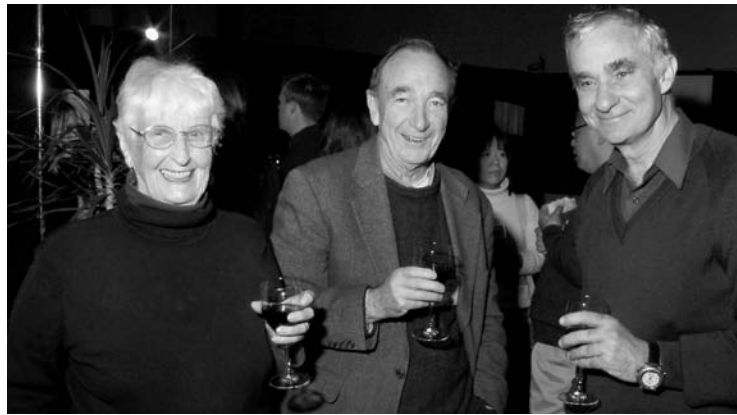
Rodger J Sparks

Nancy Beavan Athfield



Photos courtesy of Tony Athfield Photographics and Michelle Park.









CONFERENCE PARTICIPANTS¹

ASCOUGH, Philippa
SUERC
Scottish Enterprise Technology Park
Rankine Avenue
East Kilbride G75 0QF, Scotland
pasc@geo.ed.ac.uk

AXFORD, Ian
University of Alabama
Physics Department
Huntsville, Alabama 12288, USA
Ian@axford.org

BAIER, Agnieszka
University of Arizona
Department of Geosciences
4717 East Fort Lowell Road
Tucson, Arizona 85712-1201, USA
Fax +1 520-881-0554
baier@meteoritics.org

BAISDEN, W. Troy
Landcare Research
Private Bag 11052
Cnr Riddet Rd and University Loop
Palmerston North, New Zealand
Fax +64 06 355 9230
baisdent@landcare.cri.nz

BARBETTI, Mike
University of Sydney
Sydney, Australia
mikeb@emu.usyd.edu.au

BAYLISS, Alex
English Heritage
Centre for Archaeology
23 Savile Row
London, W1S 2ET, United Kingdom
Fax +44 207 973 3330
Alex.Bayliss@english-heritage.org.uk

BEAVAN ATHFIELD, Nancy
Institute of Geological and Nuclear Sciences
Rafter Radiocarbon Laboratory
PO Box 31-312, Lower Hutt, New Zealand
Fax +64 4 570 4657
n.beavan@gns.cri.nz

BECK, Warren
University of Arizona
Physics Bldg. #81, 1118 E Fourth St.
Tucson, Arizona 85721, USA
Fax +520-621-9619
wbeck@physics.arizona.edu

BECKER-HEIDMANN, Peter
University of Hamburg
Institute of Soil Science
Allende-Platz 2
Hamburg 20146, Germany
Fax +49 40 42838 2024
p.becker-heidmann@ifb.uni-hamburg.de

BEER, Juerg
EAWAG
Postfach 611
Dübendorf 8600, Switzerland
Fax +41 1 823 52 10

BENTHIEN, Albert
WHOI, Geology and Geophysics
266 Woods Hole Road
Woods Hole, Massachusetts 02543-1535, USA
Fax +1 508 457 2183
abenthi@whoi.edu

BHUSHAN, Ravi
Physical Research Laboratory
Planetary & Geosciences Division
Navrangpura Ahmedabad, Gujarat 380 009, India
Fax +91-79-6301502
bhushan@prl.ernet.in

BOARETTO, Elisabetta
Radiocarbon Dating Laboratory/ESER Dept
Weizmann Institute of Science
Rehovot 76100, Israel
Fax +972 8 9346062
Elisabetta.Boaretto@weizmann.ac.il

BOURKE, Stephen
University of Sydney
Dept. of Archaeology A14
Sydney, New South Wales 2006, Australia
Fax +61 2 9552 1412
stephen.bourke@antiquity.usyd.edu.au

BRAILSFORD, Gordon
NIWA
Private Bag 14901, Kilbirnie
Wellington, New Zealand
g.brailsford@niwa.co.nz

BRONK RAMSEY, Christopher
University of Oxford
Research Laboratory for Archaeology
6 Keble Road
Oxford OX1 3QJ, United Kingdom
Fax +44 1865 273932
christopher.ramsey@rlaha.ox.ac.uk

¹ This information was provided by the organizers of the conference.

BROWN, Tom
Lawrence Livermore National Laboratory
CAMS L-397, PO Box 808
Livermore, California 9455, USA
Fax +925 423 7884
tabrown@llnl.gov

BRUHN, Frank
Institute of Geological and Nuclear Sciences
National Isotope Centre
30 Gracefield Rd
PO Box 31312
Lower Hutt, New Zealand
Fax +64 4 570 4657
f.bruhn@gns.cri.nz

BRYANT, Charlotte
NERC Radiocarbon Lab
Scottish Enterprise Technology Park
Rankine Avenue
East Kilbride G75 0QF, Scotland
Fax +44 1355 229829
c.bryant@nercrl.gla.ac.uk

BUCK, Caitlin
University of Sheffield
Dept. of Probability and Statistics
Hicks Building, Hounsfield Road
Sheffield, South Yorkshire S3 7RH,
United Kingdom
Fax +44 114 222 3759
c.e.buck@shef.ac.uk

BURNEY, David
Fordham University
Dept. of Biological Sciences
441 E. Fordham Road
Bronx, New York 10458, USA
Fax +1 718 817 3645
burney@fordham.edu

BURR, G. S.
University of Arizona
Dept of Physics
1118 East Fourth St
Tucson, Arizona 85721, USA
Fax +1 520 621 9619
burr@u.arizona.edu

BUTLER, Kevin
Massey University
Geography, Private Bag 11122
Turitea Campus
Palmerston North 5551, New Zealand
Fax +64 6 350 5644
K.R.Butler@massey.ac.nz

CAIN, William
Loyola Marymount University
Dept of Chemistry
One LMU Drive
Los Angeles, California 90045, USA
Fax +310 338 2905
wcain@lmu.edu

CALCAGNILE, Lucio
University of Lecce
Dept. of Innovation Engineering
Via per Monteroni
Lecce 73100, Italy
Fax +39 0831 507408
lucio.calcagnile@unile.it

CARMI, Israel
Tel-Aviv University
Geophysics and Planetary Sciences
Ramat-Aviv, Tel-Aviv 6409282, Israel
Fax +973 3 6409282
carmii@internet-zahav.net

CARNLEY, Meredith
University of Mississippi
P.O. Box 3114
University, Mississippi 38677, USA
mlcarnle@olemiss.edu

CHAMBERS, Dawn
Institute of Geological and Nuclear Sciences
Rafter Radiocarbon Laboratory
30 Gracefield Road
Lower Hutt, New Zealand
Fax +64 4 570 4647
d.chambers@gns.cri.nz

CHERKINSKY, Alexander
Geochron Laboratories
711 Concord Avenue
Cambridge, Massachusetts 02138, USA
Fax +61 7 661 0148
acherkinsky@geochronlabs.com

CHESTER, Pamela I.
Massey University
Geography Department
c/o 36 Woodland Road
Wellington, New Zealand
p.chester@gns.cri.nz

COOK, Gordon
SUERC
Scottish Enterprise Technology Park
Rankine Avenue
East Kilbride G75 0QF, Scotland
Fax +44 1355 229898
g.cook@suerc.gla.ac.uk

COOPER, Jannine
Institute of Geological and Nuclear Sciences
Rafter Radiocarbon Laboratory
PO Box 31312
Wellington, New Zealand
j.cooper@gns.cri.nz

COTTEREAU, Evelyne
CNRS / CEA / IRSN / IRD / MCC
Lab de Mesure du Carbone 14
Bat 450 Porte 4^E CEA Saclay
Gif-Sur-Yvette 91191, France
Fax +33 1 69 08 15 57
cotteureau@smac14.cea.fr

CURRIE, Kim
NIWA
PO Box 56
Dunedin, New Zealand
Fax +64 3 479 5248
k.currie@niwa.co.nz

DAMON, Paul
University of Arizona
Department of Geosciences
Gould-Simpson Bldg. 77
Tucson, Arizona 85721, USA
Fax +1 520 621-2672
damon@geo.arizona.edu

DAVIDSON, Gregg
University of Mississippi
Geology & Geol. Eng.
Carrier 118
University, Mississippi 38677, USA
Fax +1 662 915 5998
davidson@olemiss.edu

DEE, Michael
28 Tavistock Rd
Lyllall Bay
Wellington, New Zealand
mikedee@fastmail.fm

DELLINGER, Franz
University of Vienna
VERA Lab
Institute for Isotope Research and Nuclear Physics
Waehringer Str 17
Vienna A-1090, Austria
Fax +43 1 4277 9517
delling@ap.univie.ac.at

DITCHBURN, Bob
Institute of Geological and Nuclear Sciences
National Isotope Centre
PO Box 31-312
Lower Hutt, New Zealand
Fax +64 4 5704 677

DONAHUE, Douglas
University of Arizona
Physics Dept.
1118 East Fourth St.
Tucson, Arizona 85721, USA
Fax +1 520 621 9619
djd@physics.arizona.edu

DONDERS, Timme
Utrecht University
Botanical Palaeoecology
Lpp Budapestlaan 4
Utrecht 3584 CD, the Netherlands
Fax +31 30 253 5096
t.h.donders@bio.uu.nl

DOUVILLE, Eric
LSCE / CEA / CNRS
Avenue de la Terrasse
Bat 12, Gif/Yvette F-91198, France
Fax +1 6982 3568
eric.douville@lsce.cnrs-gif.fr

FALCONER, Robin
Institute of Geological and Nuclear Sciences
National Isotope Centre
69 Gracefield Road
Lower Hutt, New Zealand
Fax +64 4 570 4600
r.falconer@gns.cri.nz

FALLICK, Tony
SUERC
Scottish Enterprise Technology Park
Rankine Avenue
East Kilbride G75 0QF, Scotland
Fax +44 1355 229898
T.Fallick@suerc.gla.ac.uk

FALLON, Stewart
Center for Accelerator Mass Spectrometry
Lawrence Livermore National Laboratory
7000 East Ave, L-397
Livermore, California 94550, USA
fallon4@llnl.gov

FIFIELD, Keith
Australian National University
Dept of Nuclear Physics
Research School of Physical Sciences
and Engineering
Canberra, ACT 0200, Australia
Fax +61 2 6125 0748
keith.fifield@anu.edu.au

FINK, David
ANSTO
Environment Division
PMB 1, Menai
Sydney, New South Wales 2234, Australia
Fax +61-2-9717-3257
fink@ansto.gov.au

FONTUGNE, Michel
LSCE / CEA / CNRS
Domaine du CNRS, Bat 12
Gif-Sur-Yvette 9119, France
Fax +33 1 69 82 35 68
fontugne@lsce.cnrs-gif.fr

FORBES, Matt
Flinders University
School of Chemistry, Physics and Earth Sciences
GPO Box 2100
Adelaide, South Australia 5001
mattyforbes@lycos.com

FRECHEN, Manfred
Leibniz Institute for Applied Geosciences
Geochronology and Isotope Hydrology
Stilleweg 2
Hannover 30655, Germany
Fax +49 511 643 3665
M.Frechen@gga-hannover.de

FRIEDRICH, Michael
Hohenheim University
Institute of Botany
Garbenstrasse 30
Stuttgart D-70593, Germany
Fax +49 711 4593355

GAGNON, Alan
WHOI
Ms#8 McLean Lab
Woods Hole, Massachusetts 02543, USA
Fax +1 508-457-2183
agagnon@whoi.edu

GARNETT, Mark
NERC Radiocarbon Laboratory
SUERC
Rankine Avenue
East Kilbride, Scotland G75 0QF, United Kingdom
Fax +441355229829
m.garnett@nercrcl.gla.ac.uk

GILLIGAN, Lorraine
Institute of Geological and Nuclear Sciences
Rafter Radiocarbon Laboratory
PO Box 31-312
Lower Hutt, New Zealand
Fax +64 4 570 4657

GLEIXNER, Gerd
Max-Planck-Institut Biogeochemie
Postfach 100164
Jena 07701, Germany
gerd.gleixner@bgc-jena.mpg.de

GOSLAR, Tomasz
Adam Mickiewicz University
Faculty of Physics
Poznań Radiocarbon Laboratory Ul. Rubiez 46
Poznań 61-612, Poland
Fax +48 61 8279781
goslar@radiocarbon.pl

GRAHAM, Ian
Institute of Geological and Nuclear Sciences
National Isotope Centre
PO Box 31-312
Lower Hutt, New Zealand
Fax +64 4 5704 677
i.graham@gns.cri.nz

GRIFFIN, Van
WHOI
Geology & Geophysics
Rm 254, McLean
Woods Hole, Massachusetts 02543, USA
Fax +508 457 2183
vgriffin@whoi.edu

GROOTES, Pieter
Christian-Albrechts Universität
Leibniz-Labor Max-Eyth Str. 11
Kiel 24118, Germany
Fax +49 431 880 7401
pgrootes@leibniz.uni-kiel.de

GUILDERSON, Tom
Center for Accelerator Mass Spectrometry
UC / LLNL
7000 East Avenue Ms L-397
Livermore, California 94550, USA
Fax +925 423 7884
tguilderson@llnl.gov

GULLIKSEN, Steinar
Norwegian University of Science and Technology
Radiological Dating Laboratory
Sem Saelands V.5
Trondheim N-7046, Norway
Fax +4773593383
Steinar.Gulliksen@vm.ntnu.no

GULLIVER, Pauline
NERC
Scottish Enterprise Technology Park
Rankine Avenue
East Kilbride, Glasgow G75 0QF, Scotland
Fax +44 1355 229829
p.gulliver@nercrl.gla.ac.uk

GUO, Zhiyu
Peking University
Institute of Heavy Ion Physics
Beijing 100871, China
Fax +86-10-6275 1875
zhyguo@pku.edu.cn

HAJDAS, Irka
PSIC/- ETH Honggerberg
HPK, H27 Zürich CH-8093, Switzerland
Fax +1 633 1067

HAN, Baoxi
Peking University
Institute of Heavy Ion Physics
Beijing 100871, China
Fax +86 10 62751875
bxhan@pku.edu.cn

HATTÉ, Christine
LSCE / CEA / CNRS
Domaine du CNRS, Bat 12
Gif-Sur-Yvette 91198, France
Fax +33 1 69 82 35 68
hatte@lsce.cnrs-gif.fr

HEDGES, Robert
University of Oxford Research
Laboratory for Archaeology
6 Keble Road
Oxford OX1 3QJ, United Kingdom
Fax +44 1865 273932
robert.hedges@rlaha.ox.ac.uk

HEINEMEIER, Jan
AMS Laboratory
Dept. of Physics and Astronomy
Aarhus University
Aarhus C DK-8000, Denmark
Fax +45 8612 0740
jh@phys.au.dk

HENDY, Chris
University of Waikato
Private Bag 3105
Hamilton, New Zealand
Fax +64 7 838 4312

HIGHAM, Tom
University of Oxford
6 Keble Road
Oxford OX1 3QJ, United Kingdom
Fax +44 1865 273932
thomas.igham@rlaha.ox.ac.uk

HIGNEY, Elaine
SUERC
Scottish Enterprise Technology Park
Rankine Avenue
East Kilbride G75 0QF, Scotland
Fax +44 1355 229898
e.higney@suerc.gla.ac.uk

HIROTA, Masashi
National Institute for Environmental Studies
(NIES)
16-2 Onogawa
Tsukuba Baraki 305-8506, Japan
Fax +81-29-850-2736
hirota.masashi@nies.go.jp

HJ ALIAS, Kamisah
Ministry of Science, Technology and Environment
Malaysian Institute for Nuclear Technology
Research (MINT)
Complex MINT, Bangi, Kajang
Selangor 43000, Malaysia
Fax +603 89250907
kamisah@mint.gov.my

HODGINS, Greg
University of Arizona
NSF-Arizona AMS Laboratory
Physics Department
1118 E Fourth Street
Tucson, Arizona 85721, USA
Fax +520 621 9619
ghodgins@physics.arizona.edu

HOGG, Alan
University of Waikato
Private Bag 3105
Hamilton, New Zealand
Fax +64 838 4192
alan.hogg@waikato.ac.nz

HOLDAWAY, Richard
Palaecol Research
P.O. Box 16 569
Hornby Christchurch 8004, New Zealand
Fax +64 3 349 3140
piopio@paradise.net.nz

HOWARD, Angela
University of Sheffield
Department of Probability and Statistics
The Hicks Building, Hounsfield Road
Sheffield S3 7RH, England
Fax +44 114 222 3759
a.howard@sheffield.ac.uk

HUA, Quan
ANSTO Environment Division
PMB 1 Menai, New South Wales 2234, Australia
Fax +61 2 9717 9265
qhx@ansto.gov.au

HUELS, Matthias
Christian-Albrechts Universitat Leibniz
Max-Eyth-Str. 11-13
Kiel 24118, Germany
Fax +49 431 880-7401
mhuels@leibniz.uni-kiel.de

HUGHEN, Konrad
WHOI
Marine Chemistry and Geochemistry
360 Woods Hole Rd.
Woods Hole, Massachusetts 02543, USA
Fax +1 508 457 2193
khughen@whoi.edu

IMAMURA, Mineo
National Museum of Japanese History
117 Jonai-Cho
Sakura, Chiba 285-8502, Japan
Fax +81 43 486 4299
imamura@rekihaku.ac.jp

JACOBSEN, Geraldine
ANSTO Environment Division
PMB 1 Menai, New South Wales 2234, Australia
Fax +61 2 9717 9265
gej@ansto.gov.au

JEAN-BAPTISTE, Philippe
CEA-CNRS
LSCE CEA-Saclay
Gif-Sur-Yvette 91191, France
Fax +33 169087716
pjb@lsce.saclay.cea.fr

JULL, A J Timothy
University of Arizona
Dept of Physics
1118 East Fourth St
Tucson, Arizona 85721, USA
Fax +1 520 621 9619
jull@email.arizona.edu

KEOGH, Sinead
University College Dublin
Dept of Experimental Physics
Belfield, Dublin 4, Ireland
Fax +353 1 283 7275
sineadmkeogh@eircom.net

KEY, Robert
AOS Program
Sayre Hall
Princeton University
Princeton, New Jersey 08544, USA
Fax +1 609-258-2850
key@princeton.edu

KIM, Jong-Chan
Seoul National University
School of Physics
Seoul 151-742, Korea
Fax +82 2 884 3002
jckim@phya.snu.ac.kr

KITAGAWA, Hiroyuki
Nagoya University
Graduate School of Environmental Studies
Furo-Cho, Chikusa-Ku
Nagoya, Aichi Prefecture 464-8601, Japan
Fax +81 52 789 3436
kitagawa@ihas.nagoya-u.ac.jp

KLEIN, Matthias
High Voltage Engineering Europa B.V.
P.O. Box 99
Amersfoort 3800 AB, the Netherlands
Fax +3133 4615291
mklein@highvolteng.com

KNEZOVICH, John
Center for Accelerator Mass Spectrometry
Lawrence Livermore National Laboratory
P.O. Box 808 L-397
Livermore, California 94551-0808, USA
Fax +1 925-483-7884
knezovich1@llnl.gov

KNOX, Fred
900 Ohariu Valley Road
RD, Johnsonville
Wellington 6004, New Zealand
fbmoknox@actrix.gen.nz

KORSCHINEK, Gunther
Technische Universitaet Muenchen
Fachbereich Physik E15
Garching 85748, Germany
Fax +49 89 289 14280
korschin@ph.tum.de

KRETSCHMER, Wolfgang
University of Erlangen
Physikalisches Institut
Erwin-Rommel-Str. 1
Erlangen 91058, Germany
Fax +49 9131 15249
kretschmer@physik.uni-erlangen.de

KROMER, Bernd
Heidelberg Academy of Sciences
Inf 229
Heidelberg, Germany
Fax +49 6221 546405
bernd.kromer@iup.uni-heidelberg.de

KRULL, Evelyn
CSRO Land & Water
PMB 2
Glen Osmond, South Australia 5064, Australia
Fax +64 8 8303 8550
evelyn.krull@csiro.au

KUSUMGAR, Sheela
ICHR Radiocarbon Laboratory
18 Eskimo's Enclave,
Behind TV Tower, Bodakdev
Ahmedabad, Gujarat 380 054, India
sheela@wilnetonline.net

KUTSCHERA, Walter
University of Vienna
VERA Lab
Institute for Isotope Research and Nuclear Physics
Waehringer Str 17
Vienna A-1090, Austria
Fax +43 1 4277 9517
walter.kutschera@univie.ac.at

KUZMIN, Yaroslav
Pacific Institute of Geography
Radio St. 7
Vladivostok 690041, Russia
Fax +7 4232 312159
ykuzmin@tig.dvo.ru

LANGE, Todd
University of Arizona
Physics/NSF Arizona AMS Facility
1118 E. 4th Street
PAS Bldg 81 Rm 236
Tucson, Arizona 85721, USA
Fax +1 520-621-9619
lange@physics.arizona.edu

LEAVITT, Steven W.
University of Arizona
Laboratory of Tree-Ring Research
105 W. Stadium, Bldg. 58
Tucson, Arizona 85721, USA
Fax +1 520 621 8229
sleavitt@ltr.arizona.edu

LEONARD, Alexander
University of Arizona
NSF AMS Lab
3113 North Needham Place
Tucson, Arizona 85716, USA
Fax +1 520 621 9619
alexanderleonard@hotmail.com

LIFTON, Nathaniel
University of Arizona
Geosciences Department
1040 East 4th Street, Building 77
Tucson, Arizona 85716-3521, USA
Fax +01-520-621-2672
lifton@geo.arizona.edu

LIU, Kexin
Peking University
Institute of Heavy Ion Physics
Beijing 100871, China
Fax +86 10 62751875
kxliu@pku.edu.cn

LIU, Tsung-Kwei
National Taiwan University
Geosciences
245 Choushan Road
Taipei 10617, Taiwan
Fax +886 2 236 57380
liutk@ccms.ntu.edu.tw

LOWE, Dave
NIWA
Private Bag 14901, Kilbirnie
Wellington, New Zealand
d.lowe@niwa.co.nz

LOWE, David J.
University of Waikato
Department of Earth Sciences
Private Bag 3105
Hamilton, New Zealand
Fax +64 7 856 0115
d.lowe@waikato.ac.nz

MARQUES GOUVEIA, Susy Eli
University of São Paulo
¹⁴C Laboratory
Centre for Nuclear Energy in Agriculture
Av. Centenário, 303
Piracicaba, São Paulo 13400-970, Brazil
Fax +55 19 3429 4656
susyeli@cena.usp.br

MASUDA, Kimiaki
Nagoya University
Solar-Terrestrial Environment Laboratory
Chikusa-Ku, Furo-Cho
Nagoya 464-8601, Japan
Fax +81 52 789 4313
kmasuda@stelab.nagoya-u.ac.jp

MATSUZAKI, Hiroyuki
The University of Tokyo
Research Center for Nuclear Science
and Technology
2-11-16, Yayoi, Bunkyo-Ku
Tokyo 113-0032, Japan
Fax +81-3-5841-2950
hmatsu@malt.rcnst.u-tokyo.ac.jp

MCCLURE, Mark
University of Arizona
Radiocarbon
4717 East Fort Lowell Road, Room 104
Tucson, Arizona 85712-1201, USA
Fax +520-881-0554
editor@radiocarbon.org

MCFADGEN, Bruce
Victoria University of Wellington
Stout Research Centre for NZ Studies
PO Box 600
Wellington, New Zealand
Bruce.McFadgen@vuw.ac.nz

MCGEEHIN, John
U.S. Geological Survey
12201 Sunrise Valley Drive Ms-926a
Reston, Virginia 20192, USA
Fax +1 703 648 6032
mcgeehin@usgs.gov

MCKINNON, Helen
University of Waikato
Private Bag 3105
Hamilton 2001, New Zealand
Fax +64 7 8384192
h.mckinnon@waikato.ac.nz

MCNICHOL, Ann
NOSAMS / WHOI
MS 8, McLean Laboratory
Woods Hole, Massachusetts 02543, USA
Fax +1 508 457 2183
amcnichol@whoi.edu

MEADOWS, John
University College London
Institute of Archaeology
31-34 Gordon Square
London WC1H 0PY, United Kingdom
Fax +44 20 7383 2572
j.meadows@ucl.ac.uk

MÉNOT-COMBES, Guillemette
Cerege / WHOI
Europole de L'Arbois BP50
Aix en Provence 13545, France
gmenot@who.edu

MICH CZYŃSKA, Danuta
Silesian University of Technology
Radiocarbon Laboratory
Institute of Physics
Krzywoustego 2
Gliwice 44-100, Poland
Fax +48 32 237 2254
djm@radiocarbon.gliwice.pl

MICH CZYŃSKI, Adam
Silesian University of Technology
Institute of Physics
Bolesawa Krzywoustego 2
Gliwice 44-100, Poland
Fax +48 32 237 2254
amichcz@polsl.gliwice.pl

MIHARA, Shozo
Kyushu University
Graduate School of Social and Cultural Studies
4-2-1, Ropponmatsu, Chuou-Ku
Fukuoka City, Fukuoka Prefecture
810-8560, JAPAN
Fax +81-92-726-4611
cs200027@scs.kyushu-u.ac.jp

MILLARD, Andrew
University of Durham
Department of Archaeology
South Road
Durham DH1 3LE, United Kingdom
Fax +44 191 334 1101
a.r.millard@durham.ac.uk

MIYAHARA, Hiroko
Nagoya University
Solar-Terrestrial Environment Laboratory
Furo-Cho, Chikusa-Ku
Nagoya City, Aichi 464-8601, Japan
Fax +81 52 789 4313
miyahara@stelab.nagoya-u.ac.jp

MOLLENHAUER, Gesine
WHOI
Marine Chemistry and Geochemistry
360 Woods Hole Road Ms #4
Woods Hole, Massachusetts 02543-1543, USA
Fax +1 508 457 2164
gmollenhauer@who.edu

MOLNÁR, Mihály
Hungarian Academy of Sciences
Institute of Nuclear Research
PO Box 51
Debrecen 4026, Hungary
Fax +36 52 416181
mmol@atomki.hu

MONTLUCON, Daniel
WHOI
Marine Chemistry and Geochemistry Dept. Ms# 4
Woods Hole, Massachusetts 02543-1543, USA
Fax +1 508 4572164
dmontlucon@who.edu

MORETON, Steven
NERC Radiocarbon Laboratory
Scottish Enterprise Technology Park
Rankine Avenue
East Kilbride G75 0QF, United Kingdom
Fax +44 1455 229829
s.moreton@nercrl.gla.ac.uk

MORGENSTERN, Uwe
GNS National Isotope Centre
PO Box 30368
Lower Hutt, New Zealand
Fax +64 4 570 4603
u.morgenstern@gns.cri.nz

MORIMOTO, Maki
Nagoya University
Graduate School of Environmental Studies
c/o: Hydrospheric Atmospheric Research Center
Furo-Cho, Chikusa-Ku,
Nagoya, Aichi 464-8601, Japan
Fax +81 52 789 3469
morimoto@ihas.nagoya-u.ac.jp

MURAYAMA, Masafumi
Kochi University
Center for Advanced Marine Core Research
B200 Monobe
Nankoku City, Kochi 783-8502, Japan
Fax +81 88 864 6727
murayama@cc.kochi-u.ac.jp

NADEAU, Marie-Josée
Christian-Albrechts Universität Zu Kiel
Leibniz-Labor
Max-Eyth Str. 11
Kiel 24118, Germany
Fax +49 431 880 7401
mnadeau@leibniz.uni-kiel.de

xxviii *Participants*

NADEL, Dani
University of Haifa
Zinman Institute of Archaeology
Haifa, Mt Carmel 31905, Israel
Fax +00972 4-8249876
dnadel@research.haifa.ac.il

NAEGLER, Tobias
LSCE
L'Orme des Merisiers
Gif-Sur-Yvette F-91191, France
Fax +33169087716
naegler@lsce.saclay cea.fr

NAKAMURA, Toshio
Nagoya University
Center for Chronological Research
Chikusa Ward
Nagoya City, Aichi Prefecture 464-8602, Japan
Fax +52 789 3092
nakamura@nendai.nagoya-u.ac.jp

NAYSMITH, Philip
SUERC
Scottish Enterprise Technology Park
Rankine Avenue
East Kilbride, G75 0QF, Scotland
Fax +44 1355 229898
p.naysmith@suerc.gla.ac.uk

NDEYE, Maurice
Université Cheikh Anta Diop
IFAN
BP 206 Dakar, Senegal
Fax +221 824 49 18
soukouma@hotmail.com

NICHOLLS, Geoff
Auckland University
Mathematics Department
Auckland, New Zealand
Fax +64 9 3737457
nicholls@math.auckland.ac.nz

NORRIS, Margaret
Institute of Geological and Nuclear Sciences
Rafter Radiocarbon Laboratory
30 Gracefield Rd
Lower Hutt, New Zealand
m.norris@gns.cri.nz

NORTON, Greg
National Electrostatics Corp
7540 Graber Road
PO Box 620310
Middleton, Wisconsin 53562, USA
Fax +1 608 831 9591
nec@pelletron.com

OBELIĆ, Bogomil
Rudjer Bošković Institute
Radiocarbon and Tritium Laboratory
Bijenicka 54, PO Box 180
Zagreb 10000, Croatia
Fax +385 1 4680239
Bogomil.Obelic@irb.hr

ODA, Hirotaka
Nagoya University
Center for Chronological Research
Furo-Cho, Chikusa
Nagoya, Aichi 464-8602, Japan
Fax +81 52 789 3092
oda@nendai.nagoya-u.ac.jp

OHMICHI, Juntaro
Nihon University
College of Humanities and Sciences
3-25-40 Sakurajosui
Setagaya-Ku, Tokyo 156-0045, Japan
ohmichi@chs.nihon-u.ac.jp

OKUNO, Mitsuru
Fukuoka University
Department of Earth System Science
8-19-1 Nanakuma, Jonan-Ku
Fukuoka, Fukuoka 814-0180, Japan
Fax +81 92 865 6030
okuno@fukuoka-u.ac.jp

OLSEN, Jesper
Aarhus University
Department of Physics and Astronomy
Aarhus University
Aarhus C DK-8000, Denmark
Fax +45 86 12 07 40
jespero@phys.au.dk

OMOTO, Kunio
Nihon University
Dept. Geogr., Coll. Humanities and Sciences
25-40, 3-Chome, Sakurajosui
Setagaya-Ku, Tokyo 156-8550, Japan
Fax +81 3 5317 9429
omoto@chs.nihon-u.ac.jp

ORIWALL, Angelika
CAU Kiel Leibniz-Labor
Max-Eyth Str. 11
Kiel 24118, Germany
Fax +49 431 880 7401
angelika@leibniz.uni-kiel.de

PALONEN, Vesa
Helsinki University
Accelerator Laboratory
Physics Department
P.O. Box 43
Helsingin Yliopisto 00014, Finland
Fax +358 9 191 50042
vesa.palonen@helsinki.fi

PARK, J. H.
Chung-Ang University
Department of Physics
Dongjak-Ku, Huksuk-Dong 221
Seoul 156-756, Korea
Fax +82 2 825 5892
junghun@wm.cau.ac.kr

PARK, Michelle
Institute of Geological and Nuclear Sciences
National Isotope Centre
PO Box 31-312
Lower Hutt, New Zealand
Fax +64 4 5704 677
M.Park@gns.cri.nz

PARSHOTAM, Aroon
Landcare Research
Private Bag 11 052
Palmerston North, New Zealand
Fax +64 6 355 9230
parshotama@landcareresearch.co.nz

PATERNE, Martine
LSCE / CEA / CNRS
Domaine du CNRS, Bat 12
Gif-Sur-Yvette 91198, France
Fax +33 1 69 82 35 68
paterne@lsce.cnrs-gif.fr

PAZDUR, Anna
Silesian University of Technology
Radiocarbon Laboratory
Institute of Physics
Krzywoustego 2
Gliwice 44-100, Poland
Fax +48 32 237 2254
anna.pazdur@radiocarbon.gliwice.pl

PESSEDA, Luiz Carlos Ruiz
University of São Paulo
C-14 Laboratory
Center for Nuclear Energy in Agriculture
Avenida Centenário 303
Piracicaba, São Paulo 13416-000, Brazil
pessenda@cena.usp.br

PETCHEY, Fiona
University of Waikato
Radiocarbon Dating Laboratory
Private Bag 3105
Hamilton 2001, New Zealand
Fax +64 07 838 4192
fpetchey@waikato.ac.nz

PLASTINO, Wolfango
University of Roma Tre
Department of Physics
Via Della Vasca Navale, 84
Rome I-00146, Italy
Fax +39 06 5579303
plastino@fis.uniroma3.it

POVINEC, Pavel
IAEA Marine Environment Laboratory
4 Quai Antoine 1er
Monte Carlo MC-98012, Monaco
Fax +377 9797 7273
p.povinec@iaea.org

PRIOR, Christine A.
Institute of Geological and Nuclear Sciences
Rafter Radiocarbon Laboratory
30 Gracefield Road
Lower Hutt 6315, New Zealand
Fax +64 4 570 4657
c.prior@gns.cri.nz

QUARTA, Gianluca
University of Lecce
Dept. of Innovation Engineering
Via per Monteroni
Lecce 73100, Italy
Fax +39 0831 507408
gianluca.quarta@unile.it

REIMER, Paula
Lawrence Livermore National Laboratory/CAMS
P.O. Box 808
Livermore, California 94551, USA
Fax +1 925 423 7884
pjreimer@llnl.gov

RETHEMEYER, Janet
University of Kiel Leibniz-Labor
Kiel 24118, Germany
Fax +49 431 880 7401
jrethemeyer@leibniz.uni-kiel.de

RIECK, Anke
Christian-Albrechts Universität
Zu Kiel Leibniz-Labor
Max-Eyth Str. 11
Kiel 24118, Germany
Fax +49 431 880 7401
arieck@leibniz.uni-kiel.de

ROWE, Marvin
Texas A&M University
Chemistry Dept
P.O. Box 30012
College Station, Texas 77842-3012, USA
Fax +1 979 845 4719
rowe@mail.chem.tamu.edu

SAKAMOTO, Minoru
National Museum of Japanese History
117 Jonai-Cho
Sakura, Chiba 285-8502, Japan
Fax +81 43 486 4299
sakamoto@rekihaku.ac.jp

SAKURAI, Hirohisa
Yamagata University
Dept. of Physics
1-4-12 Kojirakawa
Yamagata City, Yamagata 990-8560, Japan
Fax +81-23-628-4567
sakurai@sci.kj.yamagata-u.ac.jp

SANTOS, Guaciara dos
University of California
Earth System Science
220 Rowland Hall
Irvine, California 92697-3100, USA
Fax +1 949 824 3256
gdossant@uci.edu

SCHARF, Andreas
Universität Erlangen-Nürnberg
Abt. IV Erwin-Rommelstr. 1
Erlangen 91058 E, Germany
scharf@physik.uni-erlangen.de

SCHNEIDER, Robert
NOSAMS/WHOI
Mail Stop 8
Woods Hole, Massachusetts 02543, USA
Fax +508 457 2183
rschneider@who.edu

SCOTT, Marian
University of Glasgow
Dept of Statistics
University Gardens
Glasgow G12 8QW, United Kingdom
Fax +44 141 330 4814
marian@stats.gla.ac.uk

SEKAR, Balasubramanian
Birbal Sahni Institute of Palaeobotany
C-14 Dating
53, University Road
Lucknow, Uttar Pradesh 226 007, India
Fax +91 0522 2740485
sekar_b2001@yahoo.co.in

SERGI, Antonino
University of Rome "La Sapienza"
P. Le Aldo Moro 2
Rome 00185, Italy
Fax +39 06 4991 4208
Antonino.Sergi@Roma1.infn.it

SHANMUGANANDAN, S
Madurai Ramaraj University
Dept. of Geography
Madurai 625021, India

SHEN, Chengde
Chinese Academy of Sciences
Guangzhou Institute of Geochemistry
Wushan Guangzhou
Guangdong 510640, P. R. China
Fax +86 20 8529 0705
cdshen@gig.ac.cn

SHIBATA, Ken
The University of Tokyo
Institute of Environmental Studies
Yanagisawa Laboratory
5th Building of School of Engineering
Bunkyo-Ku, Tokyo 113-8656, Japan
Fax +81 3 5841 8583
ken.shibata@yy.t.u-tokyo.ac.jp

SKOG, Göran
Lund University
Radiocarbon Dating Laboratory
Sölvegatan 12
Lund S-223 62, Sweden
Fax +46 46 2224830
Goran.Skog@C14lab.lu.se

SLATER, Greg
WHOI
Marine Chemistry and Geochemistry
MS#4, 360 Woods Hole Road
Woods Hole, Massachusetts 02543, USA
Fax +1 508-457-2164
gslater@whoi.edu

SMITH, Andrew
ANSTO Environment
PMB 1 Menai, New South Wales 2234, Australia
Fax +61 2 9717 3257
ams@ansto.gov.au

SOUTHON, John
University of California, Irvine
Earth System Science
Dept 220 Rowland Hall
Irvine, California 92697, USA
Fax +1 949-824-3874
jsouthon@uci.edu

SPARKS, Rodger
Institute of Geological and Nuclear Sciences
Rafter Radiocarbon Laboratory
PO Box 31-312
Lower Hutt, New Zealand
r.sparks@gns.cri.nz

STEIER, Peter
University of Vienna
VERA Lab
Institute for Isotope Research and Nuclear Physics
Währinger Str 17
Vienna A-1090, Austria
Fax +43 1 4277 9517
peter.steier@univie.ac.at

STEIN, Mordechai
Geological Survey of Israel
30 Malkhe Yisrael St.
Jerusalem 95501, Israel
Fax +972 2 566 2581
motis@vms.huji.ac.il

STEWART, Michael
Institute of Geological and Nuclear Sciences
National Isotope Centre
PO Box 30368
Lower Hutt, New Zealand
m.stewart@gns.cri.nz

SUTER, Martin
ETH Physics
ETH-Hönggerberg, HPK, H31
Zürich CH-8093, Switzerland
Fax +41 1 633 1067
martin.suter@phys.ethz.ch

SUTTON, Kelly
Institute of Geological and Nuclear Sciences
Rafter Radiocarbon Lab
Lower Hutt, New Zealand

SWANSTON, Chris
Lawrence Livermore National Laboratory
Center for Accelerator Mass Spectrometry
PO Box 808, L-397
Livermore, California 94550, USA
Fax +92 5 423 7884
swanston@llnl.gov

SZÁNTÓ, Andrea Zsuzsanna
Hungarian Academy of Sciences
Institute of Nuclear Research
P O Box 51
Debrecen 4026, Hungary
Fax +36 52 416181
aszanto@atomki.hu

SZIDAT, Soenke
University of Berne
Laboratory of Radiochemistry and
Environmental Chemistry
Freiestrasse 3
Bern 3012, Switzerland
Fax +41 31 6314220
szidat@iac.unibe.ch

TAKAHASHI, Hiroshi
National Institute of Advanced Industrial Science
and Technology
Geological Survey of Japan
Central 7, 1-1-1, Higashi
Tsukuba, Ibaraki 305-8567, Japan
Fax +81 29 861 3479
h.a.takahashi@aist.go.jp

TALAMO, Sahra
Heidelberg Academy of Sciences
Inf 229
Heidelberg D-69120, Germany
Fax +49 6221 546405
sahra.talamo@iup.uni-heidelberg.de

TATE, Kevin
Landcare Research
Private Bag 11052
Palmerston North, New Zealand
Fax +6 355 9230
tatek@landcareresearch.co.nz

TAYLOR, Claude B.
Institute of Geological and Nuclear Sciences
National Isotope Centre
28 Wyndrum Avenue
Lower Hutt, New Zealand
Fax +64 4 5862124
sandbagger5@xtra.co.nz

TISNERAT-LABORDE, Nadine
LSCE / CEA / CNRS
Avenue de la Terrasse
Gif-Sur-Yvette 91198, France
Fax +33 1 69 82 35 68
tisnerat@lsce.cnrs-gif.fr

TSUCHIYA, Rie
Nagoya University
Graduate School of Environmental Studies
Furo-Cho, Chikusa-Ku
Nagoya 464-8601, Japan
s020127m@mbox.nagoya-u.ac.jp

TURNBULL, Jocelyn
University of Colorado
INSTAAR
1560 30th St, 450 UCB
Boulder, Colorado 80309-0450, USA
Fax +1 303 492 6388
jocelyn.turnbull@colorado.edu

UCHIDA, Masao
Japan Marine Science & Technology Centre
MIO 2-15 Natsushimatyou, Yokosuka, Japan

UHL, Thomas
Universität Erlangen-Nürnberg
Physikalisches Institut IV (KORA)
Erwinn-Rommel-Str. 1
Erlangen 91058, Germany
Fax +49 9131 15249
uhl@physik.uni-erlangen.de

VAN DER BORG, Klaas
Utrecht University
Faculty of Physics and Astronomy
Princetonplein 5
Utrecht 3584 CC, the Netherlands
Fax +31 30 2532532
k.vanderborg@phys.uu.nl

VAN DER PLICHT, Johannes
Groningen University
Center for Isotope Research
Nijenborgh 4
Groningen 9747 AG, the Netherlands
Fax +31 50 363 4738
plicht@phys.rug.nl

VAN STRYDONCK, Mark
Royal Institute for Cultural Heritage
Jubelpark 1
Brussels B-1000, Belgium
Fax +32 2 732 01 05
mark.vanstrydonck@kikirpa.be

WACKER, Lukas
ETH Zürich
Institute of Particle Physics
Hpk H25 ETH-Hönggerberg
Zürich 8093, Switzerland
Fax +41 1 633 1067
wacker@multisports.ch

WESTBROOK, Jessica
University of California, Berkeley
Department of Plant Biology
1 Cyclotron Rd 70a/4403
Berkeley, California 94720, USA
Fax +1 510-486-5496
jawestbrook@lbl.gov

WESTLAKE, Richard
Institute of Geological and Nuclear Sciences
P O Box 8052
The Terrace, Wellington 6015, New Zealand

WILD, Eva Maria
University of Vienna
VERA Lab
Institute for Isotope Research and Nuclear Physics
Währinger Str 17
Fax +43 1 4277 9517
eva.maria.wild@univie.ac.at

WILLIAMS, Allan
NIWA
Private Bag 14901
Wellington, New Zealand
w.allan@niwa.co.nz

WILMSHUT, Janet
Landcare Research, Ecosystems South
PO Box 69
Lincoln 8152, New Zealand
wilmshurstj@landcareresearch.co.nz

WU, Xiaohong
Peking University
Department of Conservation & Archaeological
Science
College of Archaeology & Museology
Beijing 100871, P. R. China
Fax +86 10 62757493
wuxh@pku.edu.cn

XU, Li
WHOI
Geology and Geophysics/NOSAMS
360 Woods Hole Road
Woods Hole, Massachusetts 02543, USA
Fax +1 508 457 2183
lxu@whoi.edu

XU, Sheng
SUERC
University of Glasgow
Scottish Enterprise Technology Park
East Kilbride, Glasgow G75 0QF, Scotland
Fax +44 1355 229898
s.xu@suerc.gla.ac.uk

XU, Xiaomei
University of California, Irvine
Earth System Science Department
220 Rowland Hall
Irvine, California 92697-3100, USA
Fax +949 824 3874
xxu@uci.edu

YI, Weixi
Chinese Academy of Sciences
Guangzhou Institute of Geochemistry
Wushan Guangzhou
Guangdong 510640, P. R. China
Fax +86 20 8529 0705
cdshen@gig.ac.cn

YOSHIDA, Kunio
The University of Tokyo
The University Museum
3-1 Hongo 7-Chome
Bunkyo-Ku, Tokyo 113-0033, Japan
Fax +81 3 5841 8450
gara@um.u-tokyo.ac.jp

YUM, Jong-Gwon
AMS Laboratory
National Center for Inter-University Facilities
Bldg. 139, San 56-1 Silim, Gwanak
Seoul 151-742, Korea
Fax +82 2 880 5781
paulyum@yonsei.ac.kr

YUN, Chong Cheoul
Chung-Ang University
Department of Physics
221 Huk Suk-Dong, Dong Jak-Ku
Seoul 156-756, Korea
Fax +82 2 825 4988
ccyun@ms.cau.ac.kr

ZAITSEVA, Ganna
The Institute for the History of Material Culture
Radiocarbon Laboratory
Dvortsovaya Naberezhnaya 18
St. Petersburg 191186, Russia
Fax +7 812 311 8156
ganna@mail.wplus.net

ZHOU, Weijian
Chinese Academy of Sciences
Institute of Earth Environment
No. 10 Fenghui South Rd
Hi-Tech Zone, P O Box 17
Xi'an, Shaanxi 710075, China
Fax +86 29 832 0456
weijian@loess.llqg.ac.cn

ZOPPI, Ugo
ANSTO
Environment Division
Building 53
PMB 1 Menai, New South Wales 2234, Australia
Fax +61 2 9717 3257
ugo@ansto.gov.au

INITIAL RESULTS WITH LOW ENERGY SINGLE STAGE AMS

J B Schroeder • T M Hauser • G M Klody • G A Norton

National Electrostatics Corporation, Middleton, Wisconsin, USA. Email: nec@pelletron.com.

ABSTRACT. The National Electrostatics Corporation has built and tested a prototype low energy, open-air, single stage carbon accelerator mass spectrometry (AMS) system (patent pending). The configuration tested has a standard 40-sample, multi-cathode SNICS source on a 300-kV deck. The beam is mass analyzed before acceleration to a gas stripper located at ground. The $^{14}\text{C}^+$ ions are separated from $^{13}\text{C}^+$ and $^{12}\text{C}^+$ arising from the molecular breakup by a 90° analyzing magnet immediately after the gas stripper which acts as a molecular dissociator. The $^{14}\text{C}^+$ beam passes through an electrostatic spherical analyzer before entering the particle detector. The observed $^{14}\text{C}/^{12}\text{C}$ precision is better than 5‰ with a sensitivity of better than 0.05 dpm/gmC. A first single stage AMS system has been ordered. The configuration of this system will be discussed.

INTRODUCTION

The vast majority of accelerator mass spectrometry (AMS) systems are based on dual stage (tandem), high pressure gas-insulated, high voltage, electrostatic accelerators. Briefly, in existing AMS instruments, the sample to be measured is placed in a negative ion source relatively close to ground potential. In the ion source, some of the atoms/molecules of the sample are negatively ionized, filtered, and injected into a tandem accelerator, where they are accelerated to the positively-charged high voltage terminal. There they enter a “stripper” (commonly, a long, narrow tube filled with rarified gas) where 2 or more electrons are removed (stripped) so they become positively charged. Then, they are accelerated back to ground potential and are analyzed and measured. A secondary but highly advantageous feature of the stripper is that interfering molecular ions are dissociated by collisions with the stripper gas and, hence, are prevented from introducing errors in the isotopic ratio measurements.

Until recent years, all of these systems have terminal potentials in the multimillion volt range and utilize charge states 3+ or 4+. Though the level of performance of these machines is high, they have the disadvantage of being relatively large and expensive. The group, under the direction of Martin Suter at ETH Höggerberg, has shown that a small, 0.5 MV tandem accelerator, using the 1+ charge state for carbon, provides high-precision measurements similar to the multimillion volt systems (Suter et al. 1999; Synal et al. 2000). In addition to the system built at ETH, 3 similar commercial systems are in use and a fourth system is in manufacture. During factory tests, all the systems presently in use routinely demonstrated precisions between 3‰ and 5‰ for carbon.

Experiments with these low voltage tandems indicated that complete molecular destruction can be achieved at energies as low as 250 keV. This suggested that a relatively low voltage, open-air insulated accelerator could be a practical alternative to a high pressure gas-insulated tandem. Furthermore, molecular destruction occurs after the first acceleration stage, rendering the second stage acceleration superfluous for the purposes of AMS. Indeed, this second stage has the disadvantage of allowing for charge exchange of molecular fragments, yielding ions with momentum equal to the rare isotope.

Based on these considerations, the National Electrostatics Corporation developed a new device, the Single Stage Accelerator Mass Spectrometer (SSAMS).

EXPERIMENTAL

A prototype system was built and tested over a 1-yr period. A 300-kV deck was constructed (Figure 1) with a standard 40 sample multi-cathode source of negative ions by cesium sputtering (40 MC-SNICS), followed by a 90° mass analysis magnet. The injection energy was about 40 keV.

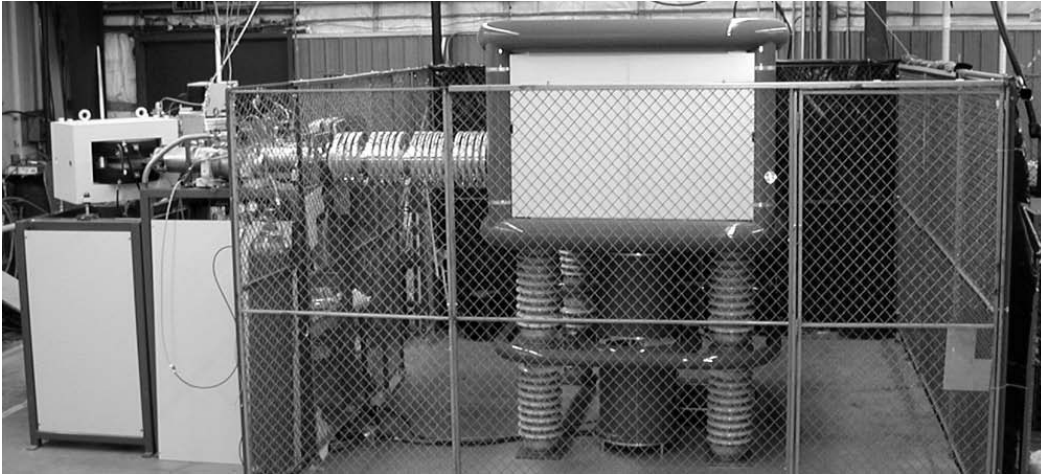


Figure 1 Prototype Single Stage AMS system with the acceleration tube exiting the 300 kV deck to the left, followed by the gas stripper and 90° energy analysis magnet.

In sequence, the gas stripper (molecular dissociator), energy analysis magnet, and electrostatic spherical analyzer are all located at ground potential, followed by the silicon surface barrier detector. This system allows for the transmission of the mass 14 beam only. The current of the mass 12 negative ion beam is measured in an offset suppressed Faraday cup immediately after the 90° analyzing magnet on the 300 kV deck. Figure 2 shows the system configuration.

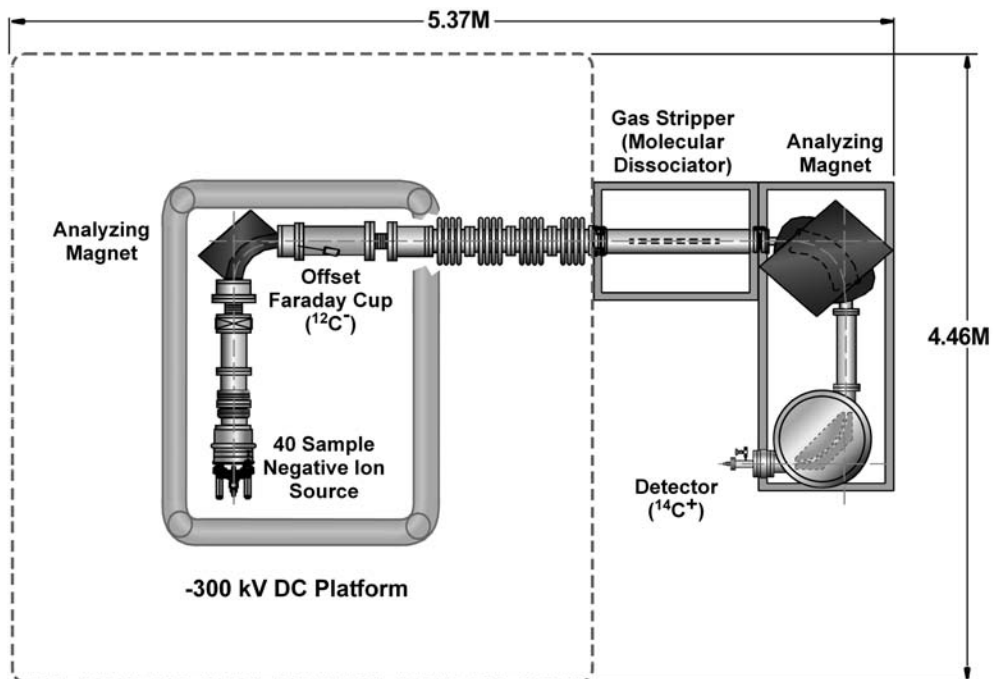


Figure 2 The prototype Single Stage AMS system has the 40 sample negative carbon source followed by a 90° permanent magnet for mass analysis. The mass 12 beam was measured before acceleration. The gas stripper, 90° analyzing magnet, 90° electrostatic spherical analyzer, and detector are located at ground potential.

The system is equipped with four 250 L/sec turbo molecular pumps. The first is located immediately after the ion source before the first 90° magnet. Two of the turbo pumps are located on the differentially-pumped gas stripper housing. It provides a stripper thickness of about 2 $\mu\text{g}/\text{cm}^2$ using either nitrogen or argon. The 4th turbo molecular pump is located on the housing of the 90° electrostatic spherical deflector. During AMS measurements, the vacuum maintained along the beamline, outside of the gas stripper, was between 10^{-6} to 10^{-7} Torr.

Experiments were conducted using graphite from Poco, ANU sucrose, OXII, beer, and Alfa Aesar for background measurements. The beam currents ranged from 80 μA to 100 μA , of which about 50% was C⁻. The deck potential was varied from 250 kV to 300 kV for a ¹⁴C⁺ beam energy at the detector of 290 keV to 340 keV.

RESULTS

Unlike all other high-precision accelerator-based AMS systems, the mass 12 and mass 13 beams were only measured at the low energy Faraday cup. Therefore, it was necessary to do an experiment to determine the actual particle transmission from the source to the detector. The system configuration would allow the transmission of the mass 13 beam through the stripper to the detector by varying the injection parameters to measure the mass 13 beam at the low energy offset cup. From this measurement, it was determined that the particle transmission was 52% at a deck bias of 300 kV, which is consistent with the expected stripping yield for carbon (Synal et al. 2000).

Background, precision, and efficiency measurements were done from a deck potential of 250 kV to 300 kV. There was no significant variation in this range. For background measurements, graphite from Alfa Aesar was used. Backgrounds from 48,000 BP (based on 724 ¹⁴C events) to 51,000 BP were seen.

Measurements of precision were done using graphite made from beer CO₂. Measurements taken over 3 cathodes positioned in 3 different quadrants of the standard 40-sample MC-SNICS cathode disk yielded a routine precision of 5‰ for 259,330 ¹⁴C events. The best precision seen was 3‰.

The increased scattering expected at these low beam energies is cause for concern related to ¹⁴C transmission through the stripper tube. The ¹⁴C events given above required a charge collection of 0.103 Coulombs on the low energy mass 12 cup. This corresponds to 69% of the typical efficiency of a 3 MV tandem AMS system. Table 1 compares the efficiencies of 3.0 MV tandem, 0.5 MV tandem, and 0.3 MV single stage AMS systems.

Table 1 Beam efficiency comparison.

AMS system	Beam energy at stripper	Sample	¹² C charge collected	¹⁴ C events	Efficiency ^a (scattering loss)
IAA ^b	2.66 MeV	ANU	0.0637 Coulombs	627,061	1.00
Poznań ^c	0.51 MeV	OXII	0.0487 Coulombs	404,403	0.95
Single stage	0.33 MeV	Beer ^d	0.1030 Coulombs ^e	259,331	0.69

^aEfficiency reduced because of scattering loss in the stripper relative to the IAA system after normalization to fraction modern.

^bInstitute of Accelerator Analysis, Japan, factory test.

^cPoznań Radiocarbon Laboratory, Poland, factory test.

^dUsed 1.08 fraction modern.

^eMeasured at low energy Faraday cup; used 0.52 particle transmission.

CONCLUSION

The prototype design was targeted at users with modest precision requirements (5%) and that goal was successfully demonstrated. However, the results of this experiment clearly indicate that a more complex design with simultaneous or sequential injection will provide the same or better background, precision, and efficiency. Accelerating only the mass 14 beam through the system does not provide the same level of confidence as sequential or simultaneous injection where mass 13 and 12 beams are measured after molecular disassociation and high-energy analysis.

The first commercial version of the system will have sequential injection and is presently in manufacture. The system is being built for the Radiocarbon Laboratory at the Geobiosphere Science Center in Lund, Sweden. In this configuration (Figure 3), the dual ion source injector is located near ground potential, with the gas stripper and the high energy analysis system with detector located on the 250 kV deck. Beam testing is scheduled to begin in Spring 2004.

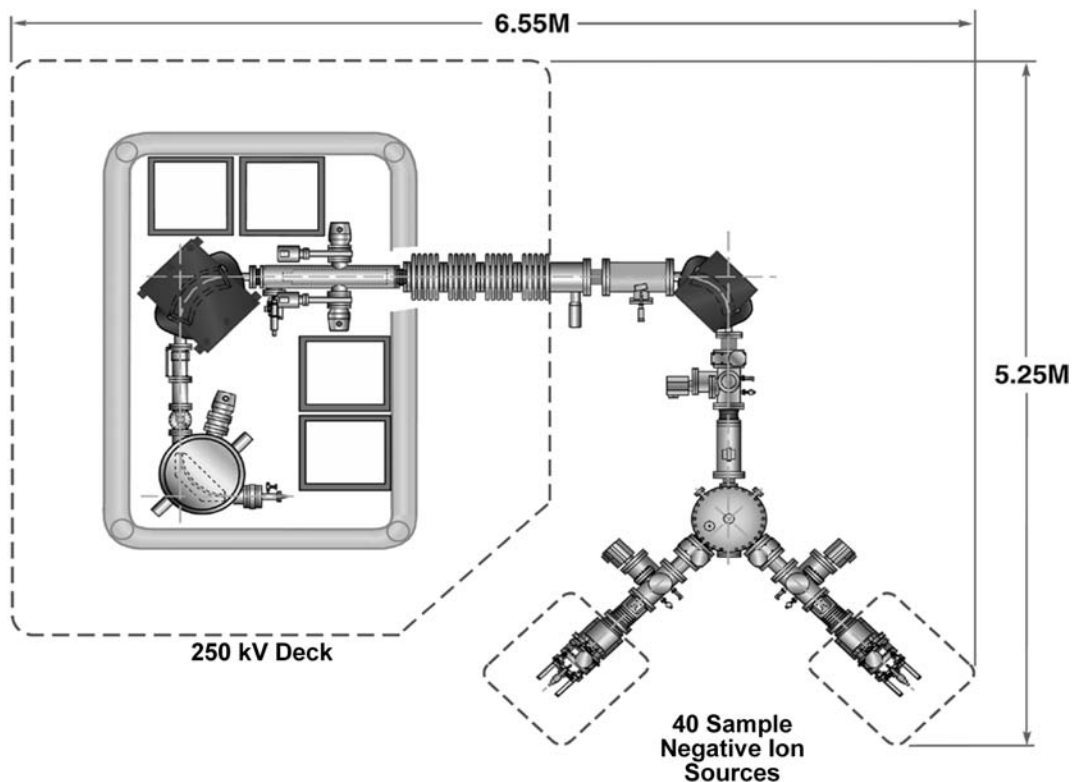


Figure 3 The first commercial Single Stage AMS system is equipped with a sequential, dual ion source injector, allowing mass 12 and 13 to be measured after the final 90° analyzing magnet on the high-voltage deck. This configuration is the reverse of the prototype with the injector system at ground potential to allow greater sample handling flexibility.

REFERENCES

- Suter M, Huber R, Jacob SAW, Synal H-A, Schroeder JB. 1999. A new small accelerator for radiocarbon dating. *15th International Conference on Application of Accelerators in Research and Industry*. 4-7 November 1998. Denton, Texas. American Institute of Physics.
- Synal H-A, Jacob S, Suter M. 2000. New concepts for radiocarbon detection systems. *Nuclear Instruments and Methods in Physics Research B* 161-163:29-36.

PUSHING THE PRECISION LIMIT OF ^{14}C AMS

Peter Steier¹ • Franz Dellinger • Walter Kutschera • Alfred Priller • Werner Rom² •
Eva Maria Wild

Vienna Environmental Research Accelerator (VERA), Institut für Isotopenforschung und Kernphysik, Universität Wien,
Währinger Strasse 17, A-1090 Wien, Austria.

ABSTRACT. High precision for radiocarbon cannot be reached without profound insight into the various sources of uncertainty which only can be obtained from systematic investigations. In this paper, we present a whole series of investigations where in some cases $^{16}\text{O}:^{17}\text{O}:^{18}\text{O}$ served as a substitute for $^{12}\text{C}:^{13}\text{C}:^{14}\text{C}$. This circumvents the disadvantages of event counting, providing more precise results in a much shorter time. As expected, not a single effect but a combination of many effects of similar importance were found to be limiting the precision.

We will discuss the influence of machine tuning and stability, isotope fractionation, beam current, space charge effects, sputter target geometry, and cratering. Refined measurement and data evaluation procedures allow one to overcome several of these limitations. Systematic measurements on FIRI-D wood show that a measurement precision of ± 20 ^{14}C yr (1σ) can be achieved for single-sputter targets.

INTRODUCTION

When accelerator mass spectrometry (AMS) for radiocarbon measurements was introduced some 25 yr ago, it was generally believed that it would not be able to reach the precision of beta counting. This was based on the notion that AMS facilities are much more complex and, thus, possess more sources of uncertainty. If counting statistics are improved by extended measurement duration, these systematic errors become significant. Thus, a precise analysis is a prerequisite for improvement.

The archaeologist usually asks for the *accuracy* of data, i.e. the maximum deviation from the “true” sample age. However, we can determine only the *precision* (i.e. the reproducibility of the result) if we would do the same measurement over and over. If only a part of the measurement is repeated (e.g. the AMS measurement but not the sample preparation), the uncertainty is underestimated. In this paper, we focus on samples containing several mg of carbon, where the sample size imposes no limit on counting statistics for AMS.

In a rough classification, uncertainty can be attributed to counting statistics, fractionation, contamination, and limited instrumental precision (e.g. of Faraday cups). Fractionation and contamination take place both in nature and in the laboratory. Carbon contamination already present when the sample arrives in the laboratory has to be carefully removed, because a suitable correction is usually not possible. Contamination in the laboratory is traced by suitable “blank” materials which undergo the same treatment as the samples. Laboratory contamination is more critical for AMS than for decay counting, since the AMS samples are significantly smaller.

In AMS, the ^{14}C content is always measured relative to ^{12}C and/or ^{13}C . These isotopes serve as an intrinsic tracer for the yield of the various processes. Therefore, knowledge of the yield is only of importance for the measurement precision if it differs for the various isotopes. Such fractionation can occur in every step where the yield is less than 100%. Many physical and chemical fractionation processes (both in nature and laboratory) show a simple dependence on the isotope mass, i.e. the

¹Corresponding author. Email: peter.steier@univie.ac.at.

²Present address: Institut für Nanostrukturierte Materialien und Photonik, Joanneum Research,
Franz-Pichler-Strasse 30, A-8160 Weiz, Austria.

fractionation of $^{14}\text{C}/^{12}\text{C}$ is twice the fractionation of $^{13}\text{C}/^{12}\text{C}$. This is called *mass dependent fractionation* by Thiemens (1999) and corresponds to “ $b = 2$ ” in Wigley and Muller (1981). In this paper, we will call it *strictly mass dependent fractionation*. The measured $^{14}\text{C}/^{12}\text{C}$ ratio can be corrected by normalizing the measured $^{13}\text{C}/^{12}\text{C}$ ratio to the nominal value of $\delta^{13}\text{C} = -25\%$ (Stuiver and Polach 1977). Precise ^{14}C dating relies on the assumption that all natural fractionation before the sample arrives in the laboratory is strictly mass dependent. Whereas AMS allows measuring $^{13}\text{C}/^{12}\text{C}$ in combination with $^{14}\text{C}/^{12}\text{C}$, decay counting requires a separate determination.

Laboratory fractionation effects are large in AMS machines. The main factors are the negative ion yield in the ion source (Nadeau et al. 1987), the stripping efficiency (Finkel and Suter 1993), and the ion-optical transmission through the whole machine. The raw $^{13}\text{C}^{3+}/^{12}\text{C}^{3+}$ and $^{14}\text{C}^{3+}/^{12}\text{C}^{3+}$ ratios measured at VERA deviate by several percent from the “true” isotopic ratios of the sample (see Table 1). This fractionation generally is not strictly mass dependent. It is handled by normalizing to a standard material which is measured together with the unknown samples.

Table 1 Unnormalized isotopic ratios for IAEA C-3 Cellulose. The nominal isotopic signature is $\delta^{13}\text{C} = -24.91 \pm 0.49\%$ and a ^{14}C content of 129.41 ± 0.06 pMC (percent Modern Carbon). For the $^{13}\text{C}^{3+}$, $^{12}\text{C}^{3+}$, and $^{14}\text{C}^{3+}$ values observed at VERA, we estimate an uncertainty of $<2\%$ from the reproducibility of the data and by comparing the reading of different Faraday cups of the same beam.

	Expected value	Observed at VERA at 2.7 MV	
		Ar stripper gas	O ₂ stripper gas
$^{12}\text{C}^{3+}$ stripping yield	Ar: $\sim 53.8\%$ ^a , O ₂ : $\sim 49.8\%$ ^a	$^{12}\text{C}^{3+}/^{12}\text{C}^- = 51.5\%$	$^{12}\text{C}^{3+}/^{12}\text{C}^- = 49.5\%$
$^{13}\text{C}/^{12}\text{C}$	1.0957×10^{-2}	$^{13}\text{C}^{3+}/^{12}\text{C}^{3+} = 1.07 \times 10^{-2}$	$^{13}\text{C}^{3+}/^{12}\text{C}^{3+} = 1.01 \times 10^{-2}$
$^{14}\text{C}/^{12}\text{C}^b$	1.529×10^{-12}	$^{14}\text{C}^{3+}/^{12}\text{C}^{3+} = 1.38 \times 10^{-12}$	$^{14}\text{C}^{3+}/^{12}\text{C}^{3+} = 1.27 \times 10^{-12}$

^aFinkel and Suter 1993.

^bin 2003.

If the contamination and the sample mass are constant, blank correction can be established by subtracting the measured $(^{14}\text{C}^{3+}/^{12}\text{C}^{3+})_{\text{blank}}$ of a nominally “dead” carbon sample from the measured $^{14}\text{C}^{3+}/^{12}\text{C}^{3+}$ of the unknown sample and the standard material:

$$(^{14}\text{C}^{3+}/^{12}\text{C}^{3+})_{\text{sample, blank corr}} = (^{14}\text{C}^{3+}/^{12}\text{C}^{3+})_{\text{sample}} - (^{14}\text{C}^{3+}/^{12}\text{C}^{3+})_{\text{blank}} \quad (1a),$$

$$(^{14}\text{C}^{3+}/^{12}\text{C}^{3+})_{\text{sample, blank corr}} = (^{14}\text{C}^{3+}/^{12}\text{C}^{3+})_{\text{standard}} - (^{14}\text{C}^{3+}/^{12}\text{C}^{3+})_{\text{blank}} \quad (1b).$$

$^{12}\text{C}^{3+}$, $^{13}\text{C}^{3+}$, and $^{14}\text{C}^{3+}$ denote the particle rates measured in the AMS analyzer. Strictly mass dependent fractionation is cancelled out by calculating

$$F_{12,13,14,\text{sample}} = (^{14}\text{C}^{3+}/^{12}\text{C}^{3+})_{\text{sample, blank corr}} \div (^{13}\text{C}^{3+}/^{12}\text{C}^{3+})_{\text{standard}}^2 \quad (2a),$$

$$F_{12,13,14,\text{standard}} = (^{14}\text{C}^{3+}/^{12}\text{C}^{3+})_{\text{standard, blank corr}} \div (^{13}\text{C}^{3+}/^{12}\text{C}^{3+})_{\text{sample}}^2 \quad (2b).$$

The following equation:

$$\text{pMC}_{\text{sample}} = \frac{F_{12,13,14,\text{sample}}}{F_{12,13,14,\text{standard}}} \times \text{pMC}_{\text{standard, nominal}} \quad (3),$$

performs the normalization to a reference standard with the nominal value $\text{pMC}_{\text{standard,nominal}}$.

These formulas are equivalent to the method described by Stuiver and Polach (1977). Relative measurements increase the precision by canceling out systematic errors. This basic principle is explicitly visible in equations (1), (2), and (3). It also reveals that most aspects of precision can be studied by investigating the reproducibility of the values $F_{12,13,14}$ obtained for samples prepared from the same material. For these investigations, no standard material is needed. The relative precision of $\text{pMC}_{\text{sample}}$ in a measurement including a standard will be the quadratic sum of the reproducibilities obtained for $F_{12,13,14,\text{sample}}$ and $F_{12,13,14,\text{standard}}$.

Fractionation only introduces uncertainty if it is not strictly mass dependent and if it is different for the standard and the unknown sample. A good correction can be expected for the fractionation in the stripping process since it is identical for all sputter targets. Slight variations in the chemical composition of the sputter targets induce fractionation differences in the ion source. However, this fractionation originates mainly in the different initial velocity of the sputtered $^{12}\text{C}^-$, $^{13}\text{C}^-$, and $^{14}\text{C}^-$ (Nadeau et al. 1987), so we expect this to be strictly mass dependent.

Finally, the use of the ^{14}C calibration curve is a normalization to independently dated samples, i.e. to the wood, coral, and varve samples incorporated in INTCAL98 (Stuiver et al. 1998). This applies both for AMS and decay counting and accounts for the varying ^{14}C content of the atmosphere in the past. We do not discuss the uncertainty introduced by the calibration process in this paper.

All measurements reported in this paper were performed at VERA. The standard operation of VERA for ^{14}C measurements was described in Priller et al. (1997) and has been basically maintained until today. Important improvements towards higher precision are described in the following.

Ion Optical Losses

Fractionation caused by ion optical beam losses will happen at every aperture where the transmission is less than 100% and where the beam profiles of ^{12}C , ^{13}C , and ^{14}C are not exactly the same. Geometrical differences of the sputter targets will lead to different beam profiles and, therefore, to different fractionation of the standard and unknown sample.

Two strategies can reduce the resulting systematic uncertainties: first, one can make the sputter target geometry as similar as possible; and second, one can try to eliminate the beam losses.

A source of variation in the sample geometry specific to our ion source (40 samples MC-SNICS; Ferry 1993) is the eccentricity of the sample wheel. As discussed in Puchegger et al. (2000), this can be partially compensated with the first beam steerers after the ion source. The reproducibility of the measured isotopic ratios was especially sensitive to the eccentricity if the whole sample wheel had a displacement bias. Therefore, a mechanism was implemented which allows to move the wheel horizontally and vertically relative to the Cs beam while the $^{12}\text{C}^-$ output of the ion source is monitored. This alignment is performed for every newly mounted wheel and every machine tuning.

Additional geometrical differences of the sputter targets are caused by sputter cratering. To reach the precision goal of less than 40 yr for all targets in the minimum total measurement time in routine ^{14}C measurements, older samples are measured longer than younger samples, resulting in deeper sputter craters. In a systematic measurement (see Figure 1), we investigated this effect up to about 5 hr of sputtering, which is about 3 times longer than the maximum sputter time in a routine measurement. Although no significant trend is visible in this experiment, deviations were observed for targets which were sputtered for extremely long periods (several hours) during machine warm-up and tun-

ing. Therefore, for high-precision measurements, we keep the sputtering times of samples and standards equal.

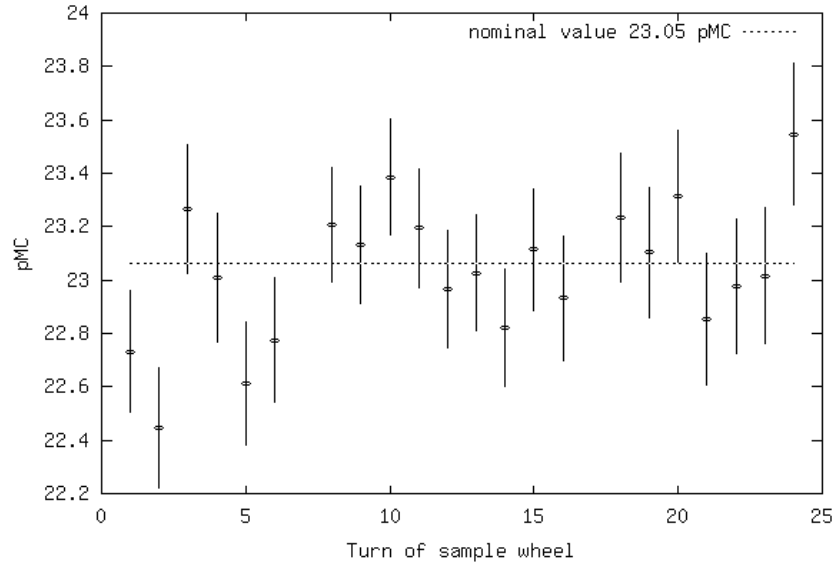


Figure 1 Cratering of sputter targets. In every turn of the sample wheel, an IAEA C-5 wood standard (23.05 pMC) was measured about twice as long as IAEA C-6 sucrose (150.61 pMC). The total sputtering time was 4.9 hr for the C-5 and 2.2 hr for C-6, respectively. The real time (including 38 other samples) was 3 days. The machine was retuned after turns 6 and 16 to eliminate the influence of machine drifts. Shown is the development of the measured pMC value of C-5 evaluated as an unknown sample, with the C-6 used as standard. The slight trend visible is most likely an artifact of retuning.

The fact that ion optical beam losses reduce measurement precision has been demonstrated by Rom et al. (1998). The main limiting aperture in VERA is the stripper canal (8 and 9 mm diameter at the entrance and exit, respectively). Figure 2 shows the progress we have achieved in accelerator transmission since the installation of VERA. It should be noted that the transmission shown is defined as $^{12}\text{C}^{3+}/^{12}\text{C}^{-}$ and includes the stripping yield to the 3+ charge state. Therefore, the values obtained with different stripper gases are shown with different symbols. From 1996 to 2002, argon was used as the stripper gas. In 2002, we switched to oxygen because this increased the stripping yield for 5+ charge states of very heavy ions by a factor of ~ 2 , whereas it lowered the $^{12}\text{C}^{3+}$ only by a factor of ~ 0.95 . The transmission for a randomly selected subset of all ^{14}C sputter targets measured so far at VERA is shown in Figure 2. Each data point corresponds to one sputter target, and one vertical set of data points corresponds to targets from the same sample wheel. The main reason for the present reliably high transmission is the use of the AUTOMAX program (Steier et al. 2000) for routine tuning. A previously limiting aperture of a small Wien filter in our analyzer (see Kutschera et al. 1997) was removed when the Wien filter was replaced by a large new electrostatic analyzer in January 2001 (Vockenhuber et al. 2003). Although ^{14}C measurements were not the primary motivation for this change, they have improved, since tuning of the analyzer is now less critical.

Although machine tuning adheres strictly to a fixed procedure, occasionally a “bad” beam tuning compromises the reproducibility of the measured isotopic ratios. This can be seen in Figure 1, where tuning took place before turn 1 and after turns 6 and 16 of the sample wheel. The scatter for the first tuning is obviously larger.

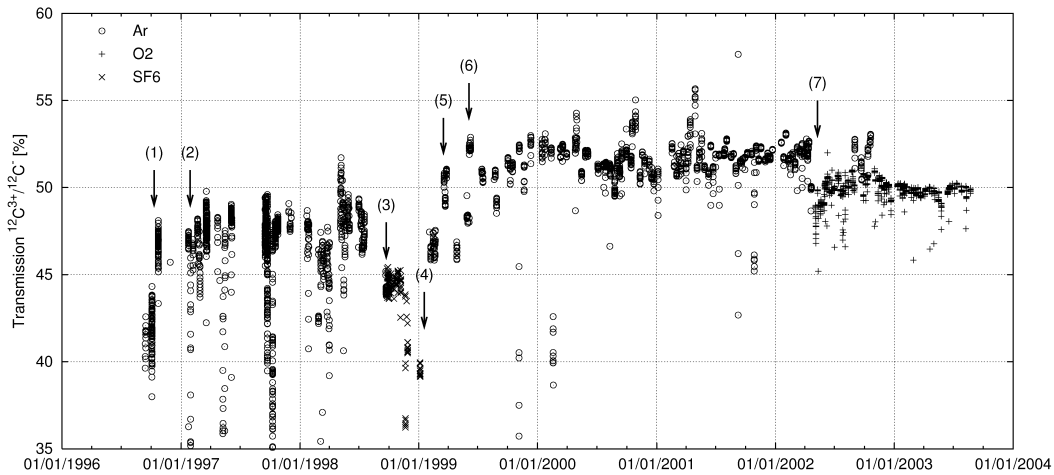


Figure 2 Progress in accelerator transmission. For the definition of the transmission, see the text. The following changes had significant influence: (1) Installation of the correcting quadrupole for the flawed injector magnet (see Priller 2000); (2) “manual” tuning procedure established; (3) sudden decrease in transmission for initially unknown reason; (4) reason found: SF_6 leak into stripper tube; (5) ion optical investigations of injector improve manual tuning procedure; (6) first use of a complete injector setup found by automatic tuning program AUTOMAX (Steier et al. 2000); (7) change from argon to oxygen as stripper gas.

Since we use a new spherical ionizer supplied by the Australian National University (ANU) (Weisser et al. 2002), we observe $^{12}\text{C}^-$ beams up to $\sim 80 \mu\text{A}$. However, in ^{14}C measurements with such currents, we encountered a significant dependency of the accelerator transmission on the beam current and a reduced measurement precision (see Figure 3). We interpret this current dependency as a space charge effect. The transmission profile became flat again when we changed our procedures to using a strong $^{12}\text{C}^-$ beam to tune the injector, instead of the previously used $^{13}\text{C}^-$ beam. Although this procedure restored the precision for routine dating, we try to stay between 40 and 50 μA for high-precision measurements.

Machine drifts can affect the precision since the standard and the sample are not measured at the same time. We perform runs of about 5-min duration on a sputter target before switching to the next one, so each of the 40 sputter targets is measured once every 3 hr. Only machine drifts which are faster will influence precision. In many measurements, we observe slow, parallel variations in the $^{13}\text{C}^{3+}/^{12}\text{C}^{3+}$ ratio of both the standard and the sample. Similar effects for the $^{14}\text{C}^{3+}/^{12}\text{C}^{3+}$ ratio are obscured by too-low counting statistics in the individual runs.

A severe problem arises if the tuned machine setup is subsequently worsened by long-term machine drifts to an extent that the ion optical transmission is compromised. In order to reach the required counting statistics for high-precision measurements, we have to run for several days. In this case, we retune the machine once every 24 hr.

$^{16}\text{O}:^{17}\text{O}:^{18}\text{O}$ as a Proxy for $^{12}\text{C}:^{13}\text{C}:^{14}\text{C}$

The use of oxygen isotopes instead of carbon isotopes to study machine fractionation has 3 main advantages. First, ^{16}O , ^{17}O , and ^{18}O are all stable isotopes, providing measurable beam currents. Thus, almost instantaneously a precision is reached which would require hours of ^{14}C event counting. Second, the ^{17}O beam can be measured and investigated at any point along the beam line with beam profile monitors and Faraday cups, whereas ^{14}C can only be detected in the final particle

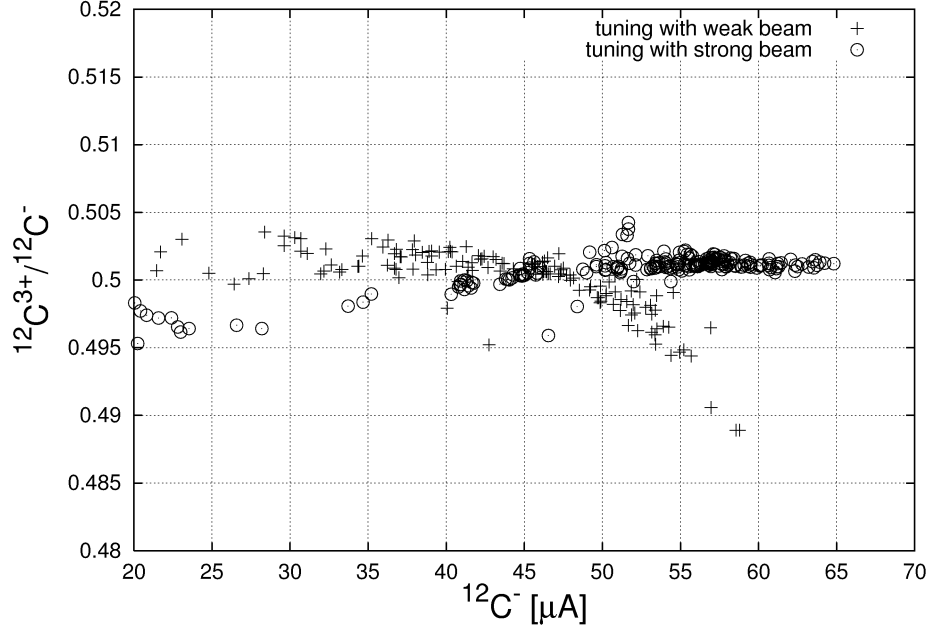


Figure 3 Accelerator transmission versus $^{12}\text{C}^-$ current for 2 different beam tunings. The transmission is measured as $^{12}\text{C}^{3+}/^{12}\text{C}^-$ and includes the stripping yield. If we tune the injector for a weak beam ($\sim 0.5 \mu\text{A } ^{13}\text{C}^-$), the transmission falls off for high beam currents (crosses). We attribute this to a space charge effect. This can be compensated by using a strong beam ($\sim 50 \mu\text{A } ^{12}\text{C}^-$) for tuning (circles). Interestingly, the setup obtained for the strong beam is also valid for sputter targets with low current yield, despite the apparent slight drop in transmission for low currents. This is caused by targets at the end of their lifetime.

detector. This helps to assess the origin of deviations in the isotopic ratios. And third, the $^{18}\text{O}/^{16}\text{O}$ ratio of all terrestrial material is $\sim 2 \times 10^{-3}$ within a few percent, whereas the $^{14}\text{C}/^{12}\text{C}$ can lie anywhere between 0 and $\sim 2 \times 10^{-12}$. For the value

$$F_{16,17,18} = (^{18}\text{O}^{3+}/^{16}\text{O}^{3+}) \div (^{17}\text{O}^{3+}/^{16}\text{O}^{3+})^2 \quad (4),$$

which is corrected for strictly mass-dependent fractionation, the variability is even smaller (Thiemens 1999). Therefore, in contrast to carbon, a small oxygen contamination will not alter the isotopic signature of the sample. Thus, oxygen allows us to study machine fractionation separately from contamination.

In a first test of this idea, we used 9 targets of commercial Al_2O_3 mixed with copper powder which were distributed evenly around the target wheel and measured with our usual ^{14}C measurement procedure, but with much shorter run times. Since VERA is a universal AMS facility, this can be easily achieved by slightly modifying magnetic fields and adjusting the offset-cup positions. With respect to the machine, the oxygen isotopes should behave very similar to carbon. The low isotopic abundance of ^{17}O (currents below 10 nA) was not a problem either for the tuning or for the measurement. Seven runs were performed on each target. It should be noted that these first experiments were too short to be sensitive to long-term machine drifts.

The observed reproducibility of the value $F_{16,17,18}$ (Equation 4) is 0.4%. This is significantly better than the reproducibility of the raw $^{17}\text{O}^{3+}/^{16}\text{O}^{3+}$ and $^{18}\text{O}^{3+}/^{16}\text{O}^{3+}$ (see Figure 4). If the same precision is achieved for carbon, it corresponds to ± 4 ^{14}C yr. This suggests that the AMS measurement is more

precise regarding the pMC value than for $\delta^{13}\text{C}$, provided there are sufficient counting statistics. This measurement also demonstrates that our Faraday cup electronics does not impose a precision limit.

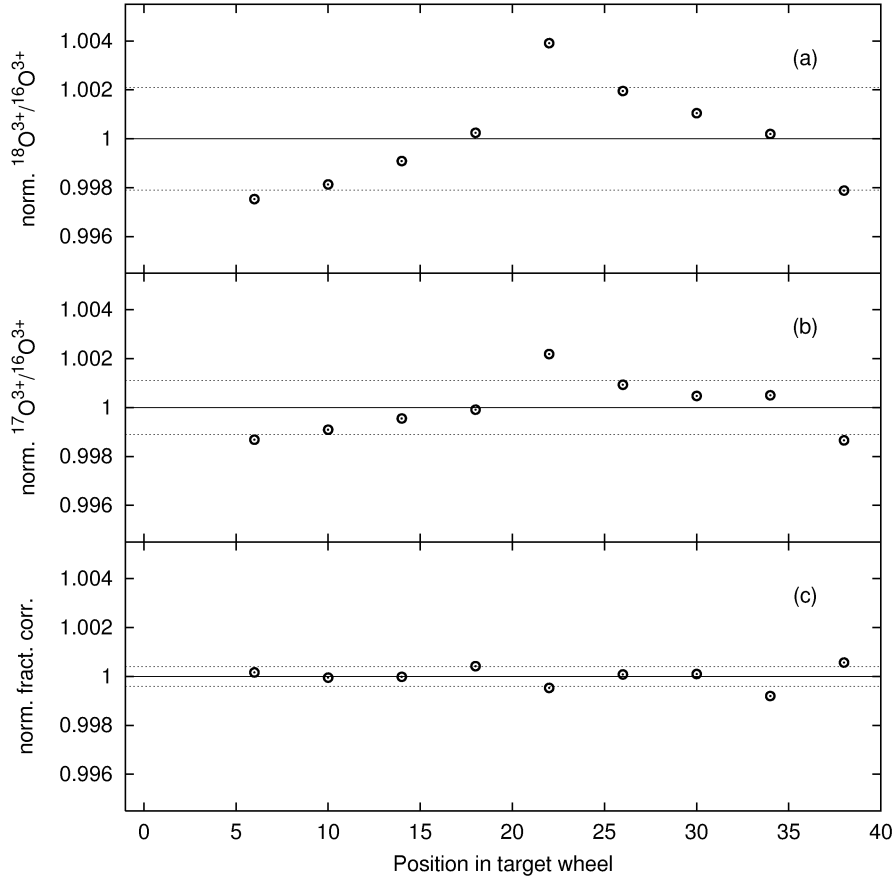


Figure 4 Measurement precision for fractionation-corrected isotopic ratios of oxygen. In the raw $^{17}\text{O}^{3+}/^{16}\text{O}^{3+}$ (a) and $^{18}\text{O}^{3+}/^{16}\text{O}^{3+}$ (b) data, systematic deviations between the targets are clearly visible, showing mainly a sinusoidal trend with their position in the wheel (eccentricity, see text). The standard deviation (indicated by the dotted lines) is 2.1‰ for $^{18}\text{O}^{3+}/^{16}\text{O}^{3+}$ and 1.1‰ for $^{17}\text{O}^{3+}/^{16}\text{O}^{3+}$. After applying the quadratic fractionation correction, the standard deviation is reduced to 0.4‰ (c).

“Turnwise” Evaluation

All new findings described above were taken into account by modifications of our automatic evaluation software “EVALGEN” (Puchegger et al. 2000). Previously (Rom et al. 1998), we first averaged the measured $^{13}\text{C}^{3+}/^{12}\text{C}^{3+}$ and $^{14}\text{C}^{3+}/^{12}\text{C}^{3+}$ ratios, and then applied blank and fractionation correction and standard normalization (Equations 1, 2, and 3). In the new scheme, the data of every turn of the sample wheel (one ~5-min run on every sputter target) is evaluated independently, and then the pMC values are averaged.

External uncertainties, which previously were calculated from the reproducibility of the raw $^{13}\text{C}^{3+}/^{12}\text{C}^{3+}$ and the $^{14}\text{C}^{3+}/^{12}\text{C}^{3+}$, are now determined from the pMC values. This new calculation scheme applies for the estimation of the scatter between the various ~5-min runs on 1 target (*inter-run scatter*, S_{IR}), the scatter between the sputter targets of the same graphite (*inter-target scatter*, S_{IT}),

and the scatter between independently prepared “graphites” from the same sample material (*inter-chemistry scatter*, S_{IC}). The S_{IC} is estimated from the scatter of the normalization factors $pMC_{\text{standard,nominal}}/F_{12,13,14,\text{standard}}$ in Equation 3 for different standards.

In the old evaluation scheme, the uncertainty was overestimated, as revealed by the investigations above. The modified scheme allows a significant reduction of the quoted error, shortening the measurement time for routine measurements.

True Wood Samples

In a final systematic investigation, we determined the maximum measurement precision possible at VERA for natural samples with a reasonable increase of effort. As material for the investigations, we chose the dendrochronologically-dated Scottish pine wood (3200–3239 BC), that is sample D of the Fourth International Radiocarbon Intercomparison (Scott et al. 2003).

From a total of 40 tree rings, we used 10 tree rings from the oldest section (3239–3230 BC) and 10 tree rings from the youngest section (3209–3200 BC). Each decade was sampled evenly by carving and homogenizing with a scalpel. Aliquots underwent separate chemical pretreatment. Additionally, standard samples from IAEA C-3 cellulose, IAEA C-5 wood, and IAEA C-6 sucrose were prepared. Samples, standards (except the sucrose), and a graphite ^{14}C blank had to undergo our standard procedure of acid-base-acid (ABA) chemical pretreatment with 1 mol/L HCl and 0.1 mol/L NaOH. Two sub-aliquots (10 mg) of each material were then oxidized separately in flame-sealed quartz tubes with 1 g CuO each, and Ag-wire to bind halogens and sulfur. The CO_2 was reduced with H_2 and Fe as catalyst at 610 °C according to the method of Vogel et al. (1984).

Since the sample material was divided in every step, a tree-like structure emerged (see Table 2). If a deviation from the nominal values is observed in the measured values, this scheme allows us to determine in which step the problem occurred.

Whereas a routine ^{14}C measurement for 1 sample wheel (40 sputter targets) reaches the required precision of <40 ^{14}C yr after about 24 hr, the duration of this systematic measurement was extended to 3 days. The machine was retuned on different sputter targets once per day. The average $^{12}\text{C}^-$ current was kept between 40 and 50 μA to avoid space charge effects, and all samples were measured equally long. Exhausted samples were skipped from further measurements once their current output dropped below ~ 25 μA .

The typical $1-\sigma$ uncertainty achieved for single targets is ± 20 ^{14}C yr (Figure 5). Our combined result for the 20 sputter targets from the earlier decade is 4493 ± 12 BP and 4524 ± 13 BP for the 8 targets of the later decade. This agrees well with the values taken from the INTCAL98 (Stuiver et al. 1998), 4492.1 ± 7.7 BP and 4531.7 ± 9.5 BP. Seven of the 28 targets deviate from the INTCAL98 value by more than 1σ , which is compatible with the statistics. Four of these targets originate from the same ABA treatment (FD/F in Table 2). The combined ^{14}C age result of these targets is 33 ± 15 yr too high, indicating a contamination in the ABA step. No single target deviates by more than 2σ .

The validity of this precision was demonstrated recently also by measurements on dendrochronologically dated wood of a new Stone Pine Chronology (Dellinger et al., these proceedings). For 58 tree-ring samples of this project, a total uncertainty of ~ 20 yr was achieved by single graphitizations, with each graphite split into 2 sputter targets. Thirty-three data points out of 58 agree within 1σ with the INTCAL98 calibration curve, while only 2 points deviate by more than 2σ .

On the other hand, the standard materials prepared for the Stone Pine measurement support the notion that the ABA step is a stage of possible contamination. For that measurement, 12 batches of

Table 2 ^{14}C ages for true wood samples. Ten tree rings from the earliest section and 10 tree rings from the latest section of the FIRI-D wood (Scott 2003) were prepared. Five aliquots of the older decade and 2 aliquots of the younger decade underwent separate chemical pretreatment. In each step of the measurement, the samples were divided, leading to a tree-like structure. The results of the individual sputter targets and also the combined results for each step are shown. For the FIRI-D samples, (d) is the measured result of each individual sputter target, (c) shows the combined results for both targets from the same graphitization, (b) the combined results for all 4 targets from the same ABA treatment, and (a) the combined result for all targets of the earlier and the later decadal section, respectively.

Sampling and homogenization with scalpel		ABA treatment		Graphitization		Sputter target		
Section	INTCAL98 ^{14}C age (BP)	Combined VERA ^{14}C age (a) (BP)	Label	Combined VERA ^{14}C age (b) (BP)	Label	Combined VERA ^{14}C age (c) (BP)	Label	Combined VERA ^{14}C age (d) (BP)
Later decade 3209–3200 BC	4531.7 \pm 9.5	4524 \pm 13	FD/1	4525 \pm 14	FD/11	4518 \pm 17	FD/11a	4522 \pm 20
			FD/11b	4514 \pm 19				
			FD/12a	4542 \pm 17				
			FD/12b	4522 \pm 21				
			FD/21a	4528 \pm 18				
			FD/21b	4498 \pm 24				
			FD/22a	4528 \pm 17				
			FD/22b	4523 \pm 23				
			FD/A1a	4466 \pm 20				
			FD/A1b	4492 \pm 19				
Earlier decade 3239–3230 BC	4492.1 \pm 7.7	4493 \pm 12	FD/A	4475 \pm 14	FD/A1	4580 \pm 19	FD/A1a	4466 \pm 20
			FD/A2a	4477 \pm 18				
			FD/A2b	4463 \pm 21				
			FD/B1a	4486 \pm 24				
			FD/B1b	4507 \pm 17				
			FD/B2a	4480 \pm 17				
			FD/B2b	4476 \pm 23				
			FD/C1a	4484 \pm 17				
			FD/C1b	4491 \pm 17				
			FD/C2a	4494 \pm 17				
FD/C2b	4490 \pm 17							
FD/E1a	4497 \pm 19							
FD/E1b	4484 \pm 17							
FD/E2a	4482 \pm 19							
FD/E2b	4493 \pm 19							
FD/F1a	4525 \pm 17							
FD/F1b	4514 \pm 20							
FD/F2a	4535 \pm 23							
FD/F2b	4526 \pm 18							

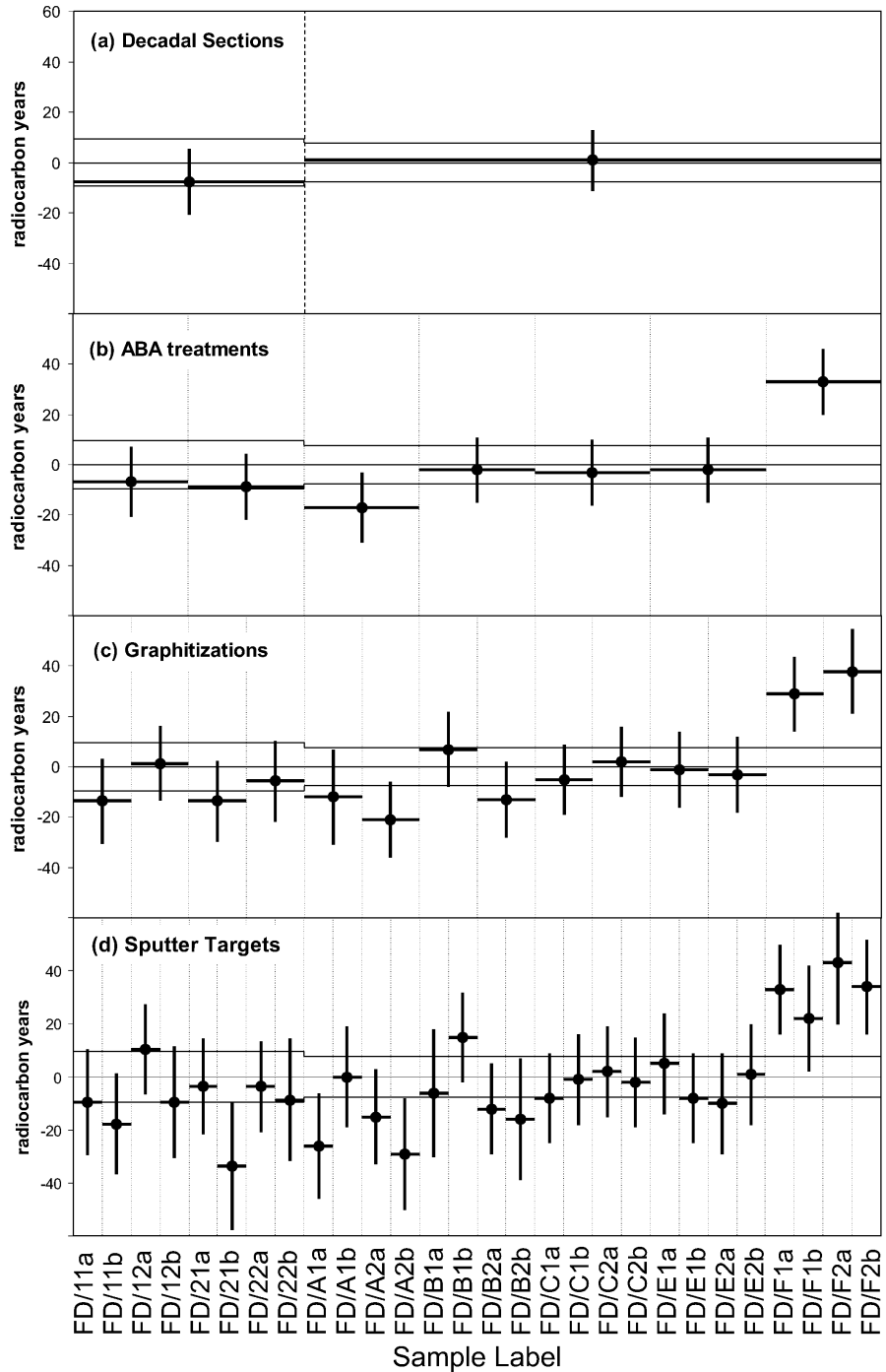


Figure 5 Deviation of FIRI-D sub-samples from the INTCAL98 master values. The values measured at VERA are shown for each individual sputter target in (d), (a), (b), and (c) are combined results. The labelling agrees with Table 2. The lines indicate the value of INTCAL98 and its uncertainty (all uncertainties are 1σ).

standard material underwent separate ABA treatment. Afterwards, the material was split into several sputter targets. For one of the 12 ABA treatments of standard material, all 4 targets were consistently measured ~ 55 ^{14}C yr too old. However, all observed deviations are too small to be significant at the precision level of routine measurements.

SUMMARY AND OUTLOOK

By systematically exploring the uncertainties in our AMS measurement and sample preparation procedures, we were able to increase our measurement precision significantly.

Systematic measurements suggest that for the AMS machine, the precision of the fractionation corrected values is better than 1%. We think that the use of oxygen as an isotopic template for carbon measurements, which was explored in this work, will be a significant advantage in further systematic measurements.

For the chemical sample preparation, a general quantification of their contribution to uncertainty cannot be given, since real samples vary significantly in their chemical composition, and the level of contamination is different. However, we recently achieved an overall precision of ± 20 ^{14}C yr (1σ) for 50 dendrochronologically-dated wood samples in the period from 3500 to 3000 BC (Dellinger et al., these proceedings). This was achieved without preparing replicates and by counting $^{14}\text{C}^{3+}$ ions for 3 to 4 hr on every sample. There is an indication that laboratory contamination during the chemical sample preparation contributes to the final uncertainty also for samples of good quality.

Investigations by Niklaus et al. (1994) on the wiggles of the tree-ring calibration curve show that an improved precision of ± 20 ^{14}C yr will also translate into smaller uncertainty intervals for the calibrated ages. However, whether this increased ^{14}C dating precision is true has to be investigated carefully. Probably systematic deviations will become significant which are caused by different sample material and quality. Additional deviations may be caused by regional offsets (Goodsite et al. 2001), seasonal variations (Dellinger et al., these proceedings; Kromer et al. 2001), or non-quadratic fractionation in nature (Wigley and Muller 1981). Up to now, such possible deviations often evaded investigation, since high measurement precision is a prerequisite for their study. Therefore, investigations on the accuracy of the ^{14}C dating method itself will most likely be the first application of increased measurement precision.

REFERENCES

- Dellinger F, Nicolussi K, Kutschera W, Schiebling P, Steier P, Wild EM. 2004. A ^{14}C calibration with AMS from 3500 to 3000 BC, derived from a new high-elevation stone-pine tree ring chronology. *Radiocarbon*, these proceedings.
- Ferry JA. 1993. Recent developments in electrostatic accelerator technology at NEC. *Nuclear Instruments and Methods in Physics Research A* 328:28–33.
- Finkel RC, Suter M. 1993. AMS in the earth sciences: technique and applications. *Advances in Analytical Geochemistry* 1:1–114.
- Goodsite ME, Rom W, Heinemeier J, Lange T, Ooi S, Appleby PG, Shotyk W, van der Knaap WO, Lohse C, Hansen TS. 2001. High-resolution AMS ^{14}C dating of post-bomb peat archives of atmospheric pollutants. *Radiocarbon* 43(2B):495–515.
- Kromer B, Manning SW, Kuniholm PI, Newton MW, Spurk M, Levin I. 2001. Regional $^{14}\text{CO}_2$ offsets in the troposphere: magnitude, mechanism, and consequences. *Science* 294:2529–32.
- Kutschera W, Collon P, Friedmann H, Golser R, Hille P, Priller A, Rom W, Steier P, Tagesen S, Wallner A, Wild E, Winkler G. 1997. VERA: a new AMS facility in Vienna. *Nuclear Instruments and Methods in Physics Research B* 123:47–50.
- Nadeau M-J, Kieser WE, Beukens RP, Litherland AE. 1987. Quantum mechanical effects on sputter source isotope fractionation. *Nuclear Instruments and Methods in Physics Research B* 29:83–6.
- Niklaus TR, Bonani G, Suter M, Wölfli W. 1994. Systematic investigation of uncertainties in radiocarbon dating due to fluctuations in the calibration curve. *Nuclear Instruments and Methods in Physics Research B* 92:194–200.

- Priller A, Golser R, Hille P, Kutschera W, Rom W, Steier P, Wallner A, Wild E. 1997. First performance tests of VERA. *Nuclear Instruments and Methods in Physics Research B* 123:193–8.
- Priller A, Brandl T, Golser R, Kutschera W, Puchegger S, Rom W, Steier P, Vockenhuber C, Wallner A, Wild E. 2000. Extension of the measuring capabilities at VERA. *Nuclear Instruments and Methods in Physics Research B* 172:100–6.
- Puchegger S, Rom W, Steier P. 2000. Automated evaluation of ^{14}C AMS measurements. *Nuclear Instruments and Methods in Physics Research B* 172:274–80.
- Rom W, Golser R, Kutschera W, Priller A, Steier P, Wild E. 1998. Systematic investigations of ^{14}C measurements at the Vienna Environmental Research Accelerator. *Radiocarbon* 40(1):255–63.
- Scott EM. 2003. Section I: The Fourth International Radiocarbon Intercomparison (FIRI). *Radiocarbon* 45(2):135–50.
- Steier P, Puchegger S, Golser R, Kutschera W, Priller A, Rom W, Wallner A, Wild E. 2000. Developments towards a fully automated AMS system. *Nuclear Instruments and Methods in Physics Research B* 161–163: 250–4.
- Stuiver M, Polach HA. 1977. Discussion: reporting of ^{14}C data. *Radiocarbon* 19(3):355–63.
- Stuiver M, Reimer PJ, Bard E, Beck JW, Burr GS, Hughen KA, Kromer B, McCormac G, van der Plicht J, Spurk M. 1998. INTCAL98 radiocarbon age calibration, 24,000–0 cal BP. *Radiocarbon* 40(3):1041–83.
- Thiemens MH. 1999. Mass-independent isotope effects in planetary atmospheres and the early solar system. *Science* 283:341–5.
- Vockenhuber Ch, Ahmad I, Golser R, Kutschera W, Liechtenstein V, Priller A, Steier P, Winkler S. 2003. Accelerator mass spectrometry of heavy long-lived radionuclides. *International Journal of Mass Spectrometry* 223–224:713–32.
- Vogel JS, Southon JR, Nelson DE, Brown T. 1984. Performance of catalytically condensed carbon for use in accelerator mass spectrometry. *Nuclear Instruments and Methods in Physics Research B* 5:289–93.
- Weisser DC, Lobanov NR, Hausladen PA, Fifield LK, Wallace HJ, Tims SG, Apushinsky EG. 2002. Novel matching lens and spherical ionizer for a cesium sputter ion source. *PRAMANA - Journal of Physics, Indian Academy of Sciences* 59:997–1006.
- Wigley TML, Muller AB. 1981. Fractionation corrections in radiocarbon dating. *Radiocarbon* 23(2):173–90.
- Wild E, Golser R, Hille P, Kutschera W, Priller A, Puchegger S, Rom W, Steier P, Vycudilik W. 1998. First ^{14}C results from archaeological and forensic studies at the Vienna Environmental Research Accelerator. *Radiocarbon* 40(1):273–81.

TOWARDS HIGH-PRECISION AMS: PROGRESS AND LIMITATIONS

Christopher Bronk Ramsey¹ • Thomas Higham • Philip Leach

Oxford Radiocarbon Accelerator Unit, University of Oxford, United Kingdom.

ABSTRACT. Precision and accuracy in accelerator mass spectrometry (AMS) dating relies on the systematic reduction of errors at all stages of the dating process, from sampling to AMS measurement. With new AMS systems providing much better precision and accuracy for the final stage of the process, we need to review the process as a whole to test the accuracy of reported results. A new High Voltage Engineering Europa (HVVE) AMS system was accepted at Oxford in September 2002. Since then, the system has been in routine use for AMS dating and here we report on our experiences during the first year. The AMS system itself is known to be capable of making measurements on single targets to a precision of better than 0.2% for the $^{14}\text{C}/^{13}\text{C}$ ratio and better than 0.1% for the $^{13}\text{C}/^{12}\text{C}$ ratio. In routine operation, we measure known-age wood to a precision of just above 0.3%, including uncertainties in background and pretreatment. At these levels, the scatter in results is no higher than reported errors, suggesting that uncertainties of ± 25 to ± 30 ^{14}C yr can be reliably reported on single target measurements. This provides a test of all parts of the process for a particular material in a particular state of preservation. More generally, sample pretreatment should remove as much contamination as feasible from the sample while adding as little laboratory contamination as possible. For more complex materials, such as bone, there is clearly more work needed to prove good reproducibility and insignificant offsets in all circumstances. Strategies for testing accuracy and precision on unknown material are discussed here, as well as the possibilities of one day reaching precisions equivalent to errors of $< \pm 20$ ^{14}C yr.

INTRODUCTION

At the last Radiocarbon Conference in Jerusalem and the last Accelerator Mass Spectrometry (AMS) Conference in Nagoya, there was some debate about the precision that can be obtained from a single AMS determination. In September 2002, the HVVE AMS system at Oxford was accepted (Bronk Ramsey et al. 2002; Gott dang et al. 2001) and showed the capability for very high-precision measurements on the AMS system itself. It was not clear at that time, however, whether the precision for routine operation on real samples would show similar improvements or be limited by other factors. We now have a year of experience of operating the new AMS and this paper draws on that experience to look at the potential for high-precision measurements by AMS.

Most very high-precision (defined here as $< 0.25\%$ or $< \pm 20$ ^{14}C yr) ^{14}C measurements have been undertaken using conventional counting methods (see, for example, Pearson 1979; McCormac 1992; Kalin et al. 1995). This is because of a number of possible factors, one of which may simply be cost. On the more scientific level, however, the 2 methods have different advantages and disadvantages.

When it comes to precision, the key theoretical disadvantages of AMS are the following:

- The difficulty of achieving isotope ratio stability over the measurement period; stability of about 0.1% is needed for high precision;
- The small sample size makes the method vulnerable to low levels of contamination either from the sample itself or more critically (since the ^{14}C isotope composition is often more radically different) from the pretreatment process;
- The danger of selecting unrepresentative portions of inhomogeneous samples.

The theoretical advantages are the following:

- The possibility of performing more rigorous sample pretreatment (even to the compound-specific level);
- The ability to select less contaminated fractions of inhomogeneous samples;

¹Corresponding author. Email: christopher.ramsey@archaeology-research.oxford.ac.uk.

- The ability to sub-sample and repeat measurements.

Each stage of the dating process (sampling, pretreatment, combustion, graphitization, and AMS measurement) play an important role in determining precision (Bryant et al. 2001). The complex subjects of taphonomy and sampling clearly depend very strongly on the specific application (e.g. Bayliss 2000; van Strydonck et al. 2000) and will not be discussed further here beyond pointing out the problems of homogeneity and the need to exclude any contamination.

Chemical pretreatment is almost certainly the key element in precision dating. It is much more difficult to check for reproducibility and accuracy at this stage than in the remaining stages where pre-prepared standards can be used. There are essentially two important questions to be asked of any pretreatment method:

1. Does the method remove contamination present in the sample (acceptable levels will depend on the relative age of the contaminants but are likely to be <1–5%)?
2. Does the method add significant levels of contamination (acceptable levels are <0.1% since ^{14}C concentration is usually radically different)?

To some extent, these work against one another in that more complex pretreatment methods are more likely to add contaminants of their own. For many materials, AMS should have the advantage that more rigorous pretreatment is possible while still retaining sufficient sample to date. However, the very small size of AMS samples makes them particularly susceptible to added contamination (for example, a sample containing 10 mg C needs to keep any added contaminants below 10 μg).

In the combustion and graphitization stages, it is important that any contaminants introduced (and there are always some) are well characterized. By this stage for AMS, the sample size is likely to be of the order of 1 mg C, so the levels of any contaminants need to be well understood at the sub-microgram level. Graphitization reproducibility is also important in that variations in the form of the graphite can give variability in beam characteristics in the AMS, which might, in turn, affect the accuracy of the AMS measurement (depending on the AMS system).

The AMS measurement itself is, of course, very important in determining precision and accuracy. However, the ability of an AMS to make precise and accurate measurements is also relatively easily tested by repeat measurements on standards of various kinds.

AMS SYSTEM AND METHODOLOGY

All of the measurements described in this paper have been performed using our routine procedures. After sampling and pretreatment (depending on type), the samples are

- Loaded into tin capsules; these capsules are pre-cleaned in cyclohexane and acetone, then a sub-sample combusted to check the blank contribution is <2 μg C;
- Combusted in a CHN analyzer furnace system; each sample combustion is preceded by the combustion of an empty tin capsule to purge the system;
- Passed through a gas chromatograph containing *Carbosieve*TM;
- Measured for stable isotope values ($\delta^{13}\text{C}$ and $\delta^{15}\text{N}$); the $\delta^{13}\text{C}$ ratio is not used in the date calculation (see below);
- Collected as CO_2 from the He stream;
- A fixed aliquot of CO_2 , equivalent to 1.5–2.0 mg C, is taken; a small proportion of samples and standards are made at half this size and then measured on the AMS in specific batches; samples smaller than this are measured as gas and are not discussed here;
- Mixed with hydrogen in a ratio 2.2:1 $\text{H}_2:\text{CO}_2$;

- Reduced to graphite on an iron catalyst at 560 °C;
- Pressed into a target (2-mm-diameter hole) for the HVEE 846 ion source.

The targets are then collected into batches for AMS measurement. A batch of up to 56 targets will typically comprise the following:

- 5–6 oxalic acid II samples;
- 2 anthracite backgrounds (graphitized in the same way as all other samples but combusted in bulk for us by the CIO Groningen laboratory);
- 2 known-age samples (tree rings and other standards);
- Other quality assurance and background samples (Mary Rose bone, Jurassic charcoal, etc.), depending on applications;
- Unknown samples making up the total.

Thus, we get several independent measurements on HOXII for each run which gives one measure of internal consistency.

The AMS used is an HVEE Tandetron with 2 recombinators (one used for the graphite measurements as outlined here on an 846 ion source, the other is used for gas or graphite measurements with a SO110 ion source).

To calculate a date, we do the following:

- Subtract the AMS/graphitization background from the measurements on anthracite;
- Calculate the $\delta^{13}\text{C}$ for each target using the $^{13}\text{C}/^{12}\text{C}$ ratio relative to the average value for the HOXII targets;
- Calculate the stable isotope corrected ^{14}C date from the $^{14}\text{C}/^{13}\text{C}$ ratio of the samples relative to the average value from the HOXII samples with the AMS derived $\delta^{13}\text{C}$ value; note that this is mathematically identical to calculating the date from the $^{14}\text{C}/^{12}\text{C}$ ratio but with a squared stable isotope correction.

The main point to note here is that we use total integrated charge ratios (less any time for cleaning up targets) and use the AMS-derived $\delta^{13}\text{C}$ rather than that from the stable isotope mass spectrometer. This corrects for any linear mass fractionation taking place in the graphitization, ion source, or AMS system. AMS labs argue whether this is necessary or not and it may depend on the AMS system itself. In our case, we have good evidence to suggest it is important. During commissioning our AMS, we measured 35 HOXII samples with a variety of graphitization and pressing methods; this gave rise to a range of $^{13}\text{C}/^{12}\text{C}$ ratios even within 1 run (Figure 1). However, if linear fractionation was corrected for as outlined above, none were more than 1.7σ from the expected value; the average precision was 0.19% (equivalent to 15 yr) with a standard deviation of 0.17% (equivalent to 14 yr). In other words, with AMS stable isotope correction, the results are within their statistical errors.

More evidence that fractionation is generally linear can be seen in Figure 2 where absolute isotope ratios are considered.

Ultimately, whatever the arguments about methodology might be, the only real test is the reproducibility and accuracy of measurements using the method, and the following sections concentrate on aspects of this.

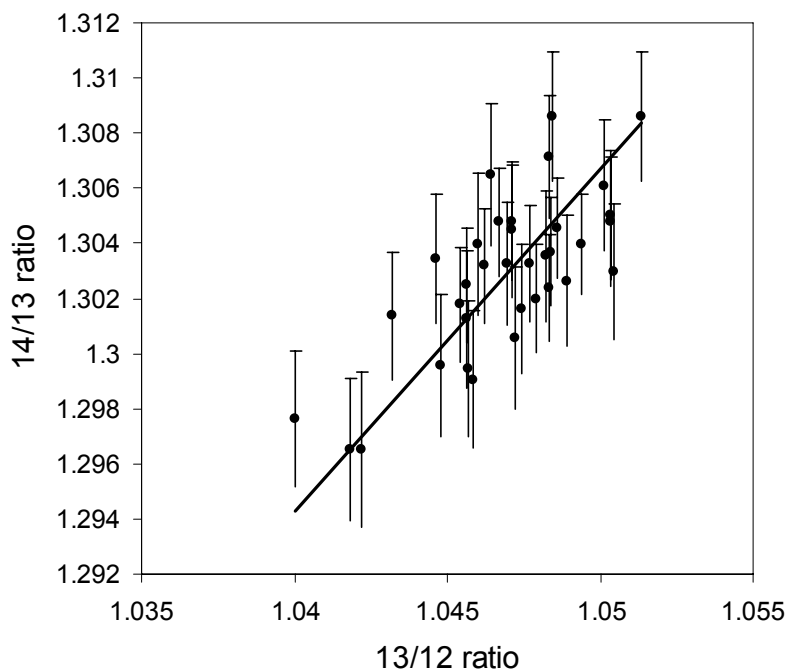


Figure 1 This figure shows a plot of $^{14}\text{C}/^{13}\text{C}$ ratio ($\times 10^{-12}$) against $^{13}\text{C}/^{12}\text{C}$ ratio ($\times 10^{-2}$) during a series of runs made throughout acceptance tests for the Oxford AMS; the stable isotope ratios have been normalized so that the average for each batch is the same as the overall average; thus, only internal run variation is displayed; the fractionation observed is linear; refer to main text for details of conclusions.

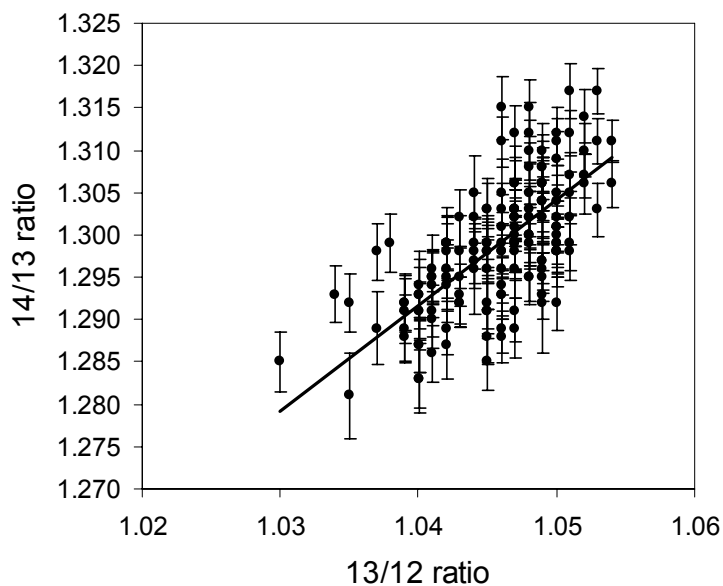


Figure 2 This plot shows the same quantities as Figure 1 but for all HOXII samples run since commissioning and, in this case, the absolute ratio has been plotted; thus, much of the variation seen here is run-run variation depending on AMS setup, stripper gas pressure, etc.; despite this, it can clearly be seen that most of the fractionation taking place is linearly mass dependent and, therefore, best corrected for by using the AMS stable isotope value.

AMS PERFORMANCE

In order to test the performance of the AMS system alone, it is really necessary to exclude some other aspects of the process. For the AMS acceptance tests, therefore, we used batches of homogenized HOXII graphite produced for HVEE by the Leibniz-Labor AMS Facility (Kiel) and pressed into targets by them. In the test of precision, 12 such targets were measured in 2 batches over 2 days. Each of them was measured to a precision of 0.2% (equivalent to 16 yr). The scatter in $^{14}\text{C}/^{13}\text{C}$ ratios was within the statistical uncertainty and the scatter in $^{13}\text{C}/^{12}\text{C}$ was 0.05% (or 0.03% if 1 outlier is removed). Thus, the intrinsic reproducibility of the system on essentially identical material seems to be better than 0.1%.

The results quoted in the previous section showed at the time that even when the graphite was of more variable consistency, the stable isotope-corrected ^{14}C concentration was still stable to well within 0.2%, implying a similar underlying instrument precision.

The machine background (no ^{14}C injected) is about 0.017% (70 ka BP). For our own graphite samples which have gone through the standard graphitization process (with about 1.5–2.0 mg C), the background is about 0.15% (52 ka BP) and in the best conditions can be as low as 0.1% (55 ka BP). For electrode graphite (no processing but unknown composition), we get a background just slightly lower than this (about 57 ka BP). This paper is really concentrated at high precision at the recent end of the ^{14}C spectrum (where precision as such is most usually an issue). Clearly, AMS backgrounds are low enough to be insignificant in this context.

Acceptance tests are, of course, not the same as routine measurements. Since the commissioning of the AMS, however, we have been quoting a precision on samples less than 2000 yr old, which averages to 27 ^{14}C yr (c.f. 38 ^{14}C yr with our old AMS) and have measured our HOXII samples to an average precision of 0.29% (equivalent to 23 ^{14}C yr, c.f. 0.43% on our old AMS). Clearly, we need to justify this in terms of accuracy and repeatability.

The first thing we can do is to look at how the HOXII values scatter around the mean value. For each HOXII target, we calculate how far away from the central value it is as a proportion of its statistical uncertainty. To correct for the loss of 1 degree of freedom, we then multiply this figure by $\sqrt{[n/(n-1)]}$, where n is the number of standards in that batch. This is to take account of the fact that the mean is defined from the values themselves. The results are shown in Table 1 and seem to be within the range expected.

Table 1 Proportion of measurements on HOXII, tree rings, and duplicate samples, lying within 1, 2, and 3 σ of expected values; in the case of the duplicate measurements and those on HOXII, the ranges have been corrected for the loss of 1 degree of freedom, since the comparisons are against an average rather than a known value.

Range offsets from true value as a factor of uncertainty (σ)	Proportion of 203 HOXII measurements lying within range	Proportion of 96 tree-ring measurements lying within range	Proportion of 66 duplicate AMS measurements on 30 samples lying within range	Proportion of 55 duplicate measurements (including pretreatment) on 27 samples lying within range
–3 to 3	100%	100%	100%	100%
–2 to 2	97.5%	95.8%	95.5%	94.6%
–1 to 1	75.9%	75.0%	69.7%	65.5%

These measurements essentially show the repeatability of the combustion, graphitization, target pressing, and AMS measurement. To see the implications of this on more normal samples, we need to include the stages of sample pretreatment and look at ratios different from those of the standard (in case of non-linearity).

Accuracy of Measurements on Wood

The most frequent other test we make on the AMS system is measurements on known-age wood, supplied to us by the Queen's University of Belfast and calibrated to the INTCAL98 calibration curve (Stuiver et al. 1998). Most of this wood has a ^{14}C concentration roughly half that of the HOXII standard, so it should provide a good measure of linearity. The wood undergoes an acid/base/acid treatment followed by chlorite bleach before the standard method described above (Hedges et al. 1989). We date decadal sections of wood similar to those used for the calibration curve. On the new AMS, we have so far measured 96 samples with an overall bias (to the older side) of 8.9 ± 3.3 yr. The proportions lying within 1, 2, and 3 σ are shown in Table 1. The implication of this is that we are not underestimating our errors.

Accuracy of Measurements on Bone

The pretreatment of bone is much more complex than any other routinely dated material (see Bronk Ramsey et al. 2004 for more details on current method and for details of known-age material). One problem here is that bone of really well-known composition is much more difficult to find because of the complexity of dietary and reservoir effects. We have chosen to work on a bone from the wreck of the Mary Rose. This ship sank in AD 1545 and the bone we are using is from pigs which were on-board the ship. From the calibration curve, we would expect the bone to have a ^{14}C date of 309 ± 4.6 BP. If we take samples in the range normally accepted within our procedures (>7 mg collagen), we have 13 measurements by our current method (some of which have a solvent extraction and some of which do not). The average uncertainty on these measurements is 23.7 ^{14}C yr and the standard deviation is 29.9 ^{14}C yr. This scatter is just low enough to pass a χ^2 test at 95% confidence. The average value is 321 ± 6.5 BP, slightly older than expected by about 10 ^{14}C yr, but calibrates to the correct age at 95% confidence.

Overall, we conclude from this that it is reasonable to quote errors lower than 30 yr on individual measurements of similar material, though clearly we would not be confident in using multiple measurements to provide an overall uncertainty of 6.5 ^{14}C yr on an unknown sample. It should also be borne in mind that in the case of bone, turnover rates and, more critically, dietary reservoir offsets can compromise accuracy of calendrical dating even if a precise and accurate measurement of the ^{14}C concentration of the bone is possible (e.g. Bonsall et al. 2004). We think that more research will be needed to improve precision much beyond current levels on bone.

Accuracy of Measurements on Charcoal

We are in the process of evaluating known-age charcoal material for routine testing. However, the pretreatment methods applied to charcoal are a subset of those applied to wood, so the tree-ring data is pertinent here. In addition, some measurements do have internal checks as in the case of wiggle-matched dating of charred wood from Miletos (Galimberti et al. 2004). In this instance, we have 7 decades of charcoal from a wiggle-matched piece of wood. The 7 measurements have an average precision of 21 yr (achieved by measuring each sample twice). The fit to the calibration curve is excellent and shows no obvious offsets, indicating that in this instance, anyway, we can measure charcoal to a precision close to 20 yr.

Testing Accuracy on Real Samples

Tests on known-age material are ideal for testing laboratory procedures. They are particularly useful for testing whether the methods themselves introduce any significant bias. However, in the case of actual samples from an archaeological or environmental context, the question of removal of sample-

specific contamination becomes more important. To some extent, all of the 3 pretreatment cases above do address this issue but of course only in one specific type of context. More generally, it is only by testing for reproducibility of duplicate measurements (including duplicate pretreatments) that we can begin to address this issue. To investigate this, we randomly select samples (about 1 in 20) for duplicate pretreatment and dating and we sometimes pretreat samples more than once for other reasons. We also perform duplicate AMS measurements on some samples.

Over a period of 1 yr (from 1 September 2002), we have 55 duplicated pretreatments on 27 individual samples. We also have 66 duplicated AMS measurements on 30 samples with 1 pretreatment. We can look at the offset in these measurements from the mean value as a proportion of the quoted uncertainty in the same way that we did for the standards in Table 1 (taking into account the fact that there are $n-1$ degrees of freedom). The results are given in Table 1 and Figure 3.

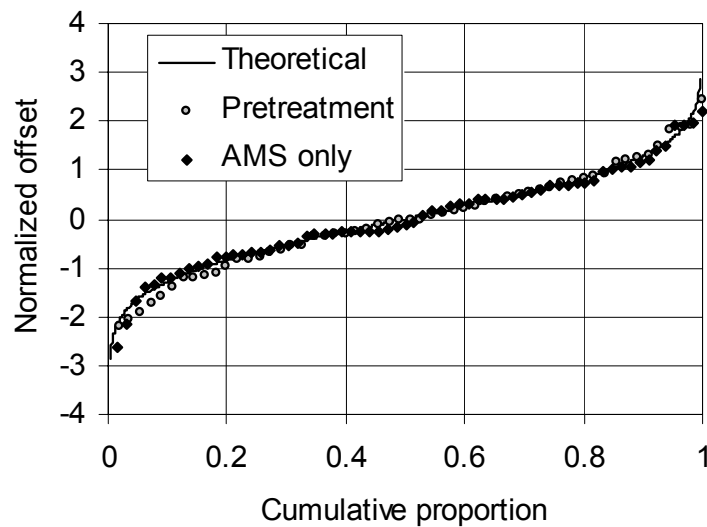


Figure 3 This figure shows the cumulative proportion of duplicate measurements lying within their quoted uncertainties. The normalized offset is the offset from the mean divided by the uncertainty and multiplied by $\sqrt{[n/(n-1)]}$, where n is the number of duplicate measurements.

In this analysis, we have included all duplicate measurements made in this period with 3 exceptions: one is a sample (P13468) which gave a very low yield (3.3 mg collagen) using our old bone pretreatment method, which was subsequently re-dated using our new method (i.e. not a true duplicate); the other two are targets (P14321 and P13951) which gave very low currents (less than one-third of the average) and for which the AMS measurement was subsequently repeated.

These data show that the reproducibility of measurements is in almost exact accord with the quoted uncertainties. As this is on normal samples rather than standards, this is a useful measure of accuracy, although it does not test for any systematic effects.

CONCLUSIONS

With the latest AMS instrumentation, it is possible to make AMS measurements to a higher precision than previously possible. At Oxford, we have been testing whether this improved AMS precision can be carried through into improved routine precision while retaining accuracy. All of the indi-

cations are that this is the case and that it is possible, for example, to quote routine precisions averaging 27 ^{14}C yr on single AMS measurements for samples from the last 2000 yr with demonstrable accuracy. Given that there is no scatter above the uncertainties quoted at this level and no measurable systematic offsets greater than about 10 yr, we would consider it valid to combine two such measurements (ideally with duplicate pretreatment) to provide an uncertainty just below 20 yr. Beyond that, we do not think we yet have sufficient evidence to draw any conclusions.

Although measurements on duplicates look encouraging, we cannot be sure that the accuracy of measurements on real samples from different contexts will always be this good, since we do not have the data to prove that contamination present in samples can always be removed sufficiently not to compromise the results at the 0.1% level. Ultimately, site-dependent issues assume importance, and we think that only by continuing to improve quoted precision and by evaluating internal consistency at specific sites will this issue really be tackled properly.

The evidence seems to suggest that AMS precision and accuracy can be improved even further. However, we recognize that it is crucial to continually monitor the accuracy and reproducibility, both using known-age material and duplicates of unknown samples to ensure that quoted errors do not become unrealistically precise. Clearly, pretreatment is the critical link in the measurement chain, both in terms of the removal of contaminants and the bias introduced by the processes themselves. The best approach would seem to be to use the most rigorous method available (to tackle contaminants in the sample) that can be demonstrated to give accurate and unbiased results on known-age material. However, it is likely that it is in pretreatment that the accuracy is ultimately limited.

REFERENCES

- Bayliss A. 2000. On the taphonomy of charcoal samples for radiocarbon dating. In: Acte du colloque "C14 and Archaeology." *Revue d'Archéométrie*. 1998. GMCPA. p 51–6.
- Bonsall C, Cook GT, Hedges REM, Higham TFG, Pickard C, Radovanovic I. 2004. Radiocarbon and stable isotope evidence of dietary change from the Mesolithic to the Middle Ages in the Iron Gates: new results from Lepenski Vir. *Radiocarbon*, these proceedings.
- Bronk Ramsey C, Hedges REM, Mous D, Gott dang A, van den Broek R. 2002. *Status of the new AMS at Oxford*. Talk given at the 9th AMS Conference, Nagoya, Japan, September 2002.
- Bronk Ramsey C, Higham TFG, Bowles A, Hedges REM. 2004. Improvements to the pretreatment of bone at Oxford. *Radiocarbon*, these proceedings.
- Bryant C, Carmi I, Cook GT, Gulliksen S, Harkness DD, Heinemeier J, McGee E, Naysmith P, Possnert G, Scott EM, van der Plicht J, van Strydonck M. 2001. Is comparability of ^{14}C dates an issue?: A status report on the Fourth International Radiocarbon Intercomparison. *Radiocarbon* 43(2A):321–4.
- Cook GT, Bonsall C, Hedges REM, McSweeney K, Boreneant V, Pettitt PB. 2001. A freshwater diet-derived ^{14}C reservoir effect at the Stone Age sites in the Iron Gates gorge. *Radiocarbon* 43(2A):453–60.
- Galimberti M, Bronk Ramsey C, Manning SW. 2004. Wiggle-match dating of tree-ring sequences. *Radiocarbon*, these proceedings.
- Gott dang A, Klein M, Mous DJW. 2001. Accelerator mass spectrometry at High Voltage Engineering Europa (HVEE). *Radiocarbon* 43(2A):149–56.
- Hedges REM, Law IA, Bronk CR, Housley RA. 1989. The Oxford accelerator mass spectrometry facility: technical developments in routine dating. *Archaeometry* 31:99–113.
- Kalin RM, McCormac FG, Damon PE, Eastoe CJ, Long A. 1995. Intercomparison of high-precision ^{14}C measurements at the University of Arizona and the Queen's University of Belfast Radiocarbon Laboratories. *Radiocarbon* 37(1):33–8.
- McCormac FG. 1992. Liquid scintillation counter characterization, optimization and benzene purity correction. *Radiocarbon* 34(1):37–45.
- Pearson GW. 1979. Precise ^{14}C measurement by LS counting. *Radiocarbon* 21(1):1–22.
- Stuiver M, Reimer PJ, Bard E, Beck JW, Burr GS, Hughen KA, Kromer B, McCormac FG, van der Plicht J, Spurk M. 1998. INTCAL98 radiocarbon age calibration, 24,000–0 cal AD. *Radiocarbon* 40(3):1041–83.
- van Strydonck M, Nelson DE, Crombé P, Bronk Ramsey C, Scott EM, van der Plicht J, Hedges REM. 2000. Rapport du groupe de travail: les limites de methode du carbone 14 appliquée a l'archéologie, What's in a ^{14}C date? In: Acte du colloque "C14 and Archaeology." *Revue d'Archéométrie*. 1998. GMCPA. p 433–48.

USING A GAS ION SOURCE FOR RADIOCARBON AMS AND GC-AMS

Christopher Bronk Ramsey¹ • Peter Ditchfield • Martin Humm

Oxford Radiocarbon Accelerator Unit, University of Oxford, United Kingdom.

ABSTRACT. This paper reports on the performance of a new method of sample injection using the High Voltage Engineering Europa (HVEE) SO-110 ion source jointly developed between HVEE and Oxford. In order to use this source, we have developed a new gas handling system which works on the direct injection of carbon dioxide mixed into a continuous flow of helium. Preliminary work has also been carried out on online gas chromatography-accelerator mass spectrometry (GC-AMS). In this application, a GC is directly coupled to the AMS system using a GC-IRMS combustion interface and Nafion™ drier. We show here results for the measurement of natural abundance in separated compounds with good peak separation and precisions of about 10%. This type of system should be ideal for source apportionment studies, biomedical, and other similar work where high precision is not required but where sample sizes are very low.

INTRODUCTION

Gas ion sources lend themselves very well to the measurement of very small samples because it removes the necessity of graphitization and the consequent handling of the very small quantities of solid material. The existing gas handling systems developed at Oxford, however, were best suited to samples $>30 \mu\text{g C}$ because of dead volumes associated with the bellows arrangement originally used (Bronk Ramsey 1994a; Bronk Ramsey and Hedges 1997). The system was also complicated because of the need for a high vacuum system and automated liquid nitrogen trap at the target potential of the ion source (typically $>24 \text{ kV}$).

With the joint project to develop a gas ion source with High Voltage Engineering Europa (HVEE) following the joint work on the design of an ion source for biomedical AMS applications (Mous et al. 1998), it was decided to try to redesign the gas inlet system to be simpler, more mechanically robust, and to operate at ground potential. This is made possible by using GC-type technology and by introducing the gas into the ion source using a helium carrier gas.

Online GC works in a similar way. It had already been demonstrated that small pulses of gas could be measured in an ion source of this kind (Bronk Ramsey and Hedges 1994c). With the SO-110 ion source, we have now demonstrated that this works in practice using an Agilent ALS 6890A GC coupled through a PDZ Europa Orchid combustion/drier system direct to the AMS.

GAS INJECTION SYSTEM

The gas injection system is shown schematically in Figure 1. The system is essentially a 2-stage concentrator and can be used either with online combustion with GC purification (as discussed in Bronk Ramsey and Humm 2000, provided here by a Carlo Erba NA1500 nitrogen/carbon analyzer) or an ampoule cracker system (Bronk Ramsey and Hedges 1994b, 1997). The dilute carbon dioxide from these systems is transferred to the AMS injection system (into the line marked “In” in Figure 1) and trapped into trap 1, while the previous sample is being injected into the AMS system from trap 2. When the analysis for the previous sample has finished, the second trap is flushed with helium and then the gas transferred from trap 1 to trap 2 (as shown in Figure 2). The second trap has a much lower internal diameter and is attached to a capillary with an overall length of about 3 m. This is sufficient to hold about $80 \mu\text{g C}$ in the form of pure CO_2 , so after the trap is warmed the smaller capillary holds a plug of fairly pure CO_2 , which is then slowly injected into the source over a period of up to 25–30 min. To control the flow into the source, a closed-split dilution (controlled

¹Corresponding author. Email: christopher.ramsey@archaeology-research.oxford.ac.uk.

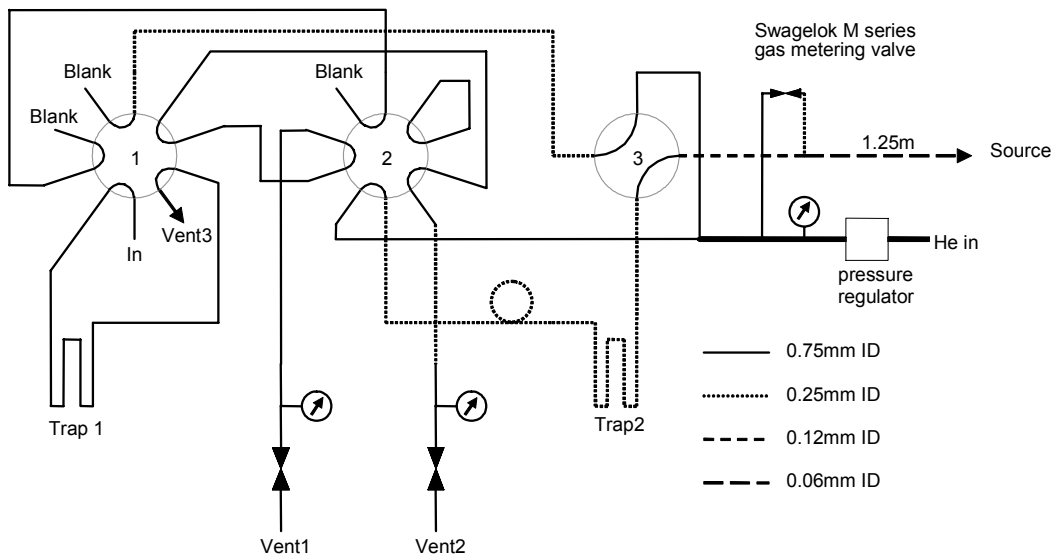


Figure 1 Schematic of the new gas handling system for the gas ion source at Oxford. The main elements of the system are 3 VICI 2-position multi-port valves (labelled 1, 2, and 3 in the diagram) and 2 automatic liquid nitrogen traps. The liquid nitrogen traps are mechanically manipulated Statebourne Bio2 long-term storage vessels which are capable of holding liquid nitrogen for about a week in this installation. See main text for description of operation. The valves in this figure are shown in the configuration for collection of CO₂ in trap 1 and injection into the AMS from trap 2.

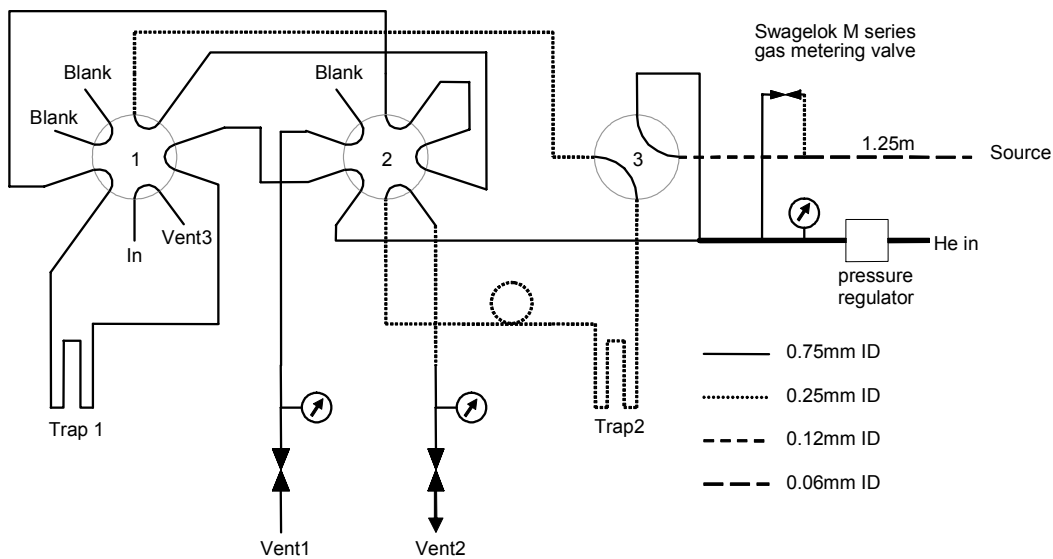


Figure 2 Gas handling system with the valves in the configuration for transfer of gas from trap 1 to trap 2. Here the mode of operation of valves 1, 2, and 3 can be seen: the central plug in the valve rotates to achieve a different selection of connections.

by the Swagelok M series gas dosing valve shown in Figure 1) is used with a He flow rate of about 0.5 mL/min. This flow of carrier gas keeps the capillary into the source flushed the whole time. For very small samples, this dilution can be switched off or reduced.

There are 3 main reasons for using a 2-stage concentrator rather than a single-stage:

- In order to obtain a fairly constant flow of CO_2 from this kind of system, the CO_2 needs to be concentrated to close to 100%; this is only possible with a low capillary diameter (0.25 mm). The output flows from online combustion systems and our ampoule rig are too high to trap CO_2 in such a fine capillary.
- The fine capillary used for injection into the AMS can only take a limited amount of CO_2 , and so a first stage concentration and expansion allows excess gas to be vented before trapping it into the AMS injection loop.
- Finally, there is an advantage, particularly when using online combustion, to perform the combustion and collection while the previous sample is being injected into the AMS. This increases the proportion of time spent making measurements by a factor of nearly 2.

Single-stage concentrators (such as that devised by Uhl et al. 2004) have the advantage of simplicity and may, therefore, be better for samples at the low end of the mass scale ($<10 \mu\text{g C}$).

The whole system operates under positive pressure and the input pressure into the source is about 2 bar. The material for the capillaries is found to be important in minimizing cross-contamination effects. Peak and other polymer-based capillaries do increase such effects, and so the system is now almost entirely stainless steel with a methyl deactivated silica capillary into the ion source. A typical application using this gas injection system (run during tests of the system on the old AMS at Oxford) is published in Staddon et al. (2003).

OPERATION OF THE GAS ION SOURCE FOR ROUTINE CO_2 DATING

In routine operation, the gas injection system is used to automatically inject a predefined sequence of samples. The whole gas system (gas injection assembly, CHN analyzer, and ampoule manifold) are controlled using NuDAM™ modules on an RS-485 network. The software used for handling the gas transfers is integrated with the HVEE AMS software via the Windows messaging system. Batches of samples can be run while the system is unattended, which is important given the relatively long collection times.

The operating parameters and characteristics of the SO-110 ion source are shown in Table 1. The maximum currents are typically several times lower than those for graphite; thus, it makes sense to use the system either when only low precision is required or when the samples are sufficiently small that there are real advantages in not having to graphitize. Overall detection efficiency is about double what we had on the original General Ionex AMS system. The typical current profile is shown in Figure 3. The duty cycle is typically about 16 min data collection and 4 min between samples, flushing the source, changing the target, and preparing the next gas. The collected data from a series of samples is shown in Figure 4. This shows a slight cross-contamination (typically 0.5%) from sample to sample. In normal operation, two or more backgrounds are run immediately after the HOXII standards in order to estimate this value for the particular run and the analysis software automatically corrects for the effect. In practice, this has very little impact on precision as the correction can be accurately corrected for.

The data analysis software, developed for analysis of the gas run data, first subtracts the average yields for all 3 isotopes that are measured prior to gas injection. The cross-contamination time constant and scale are then estimated and corrected current profiles calculated; the integrated charge for all 3 isotopes is then found. From that point on, the data can be handled in exactly the same way as for graphite sample and undergoes the same tests for reproducibility of standards and known-age

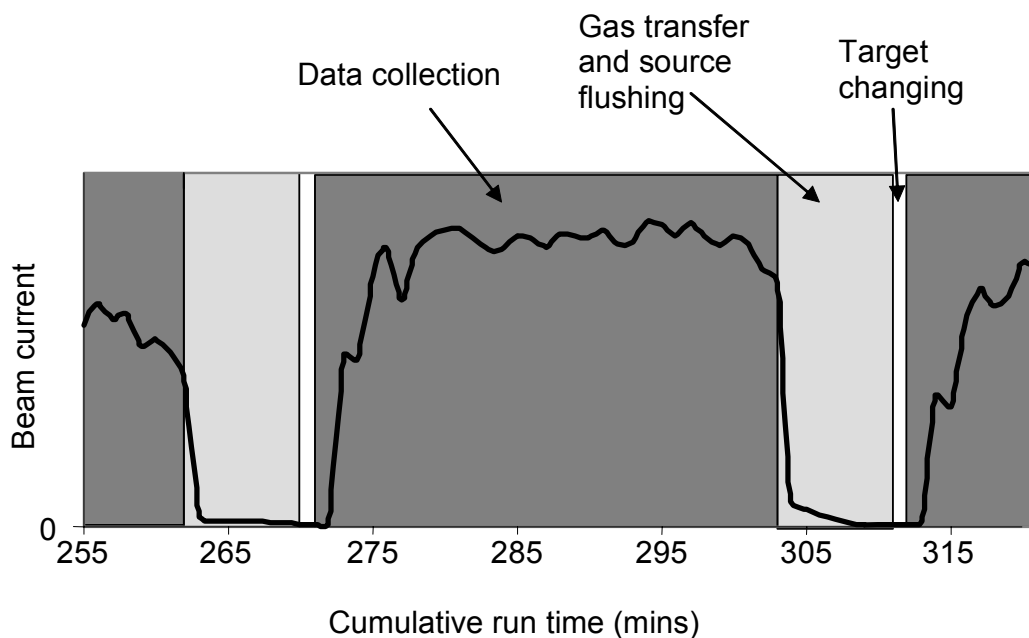


Figure 3 Current profile during a routine gas run (for typical maximum values, see Table 1 or Figure 4). While the data is being collected on one sample, the next one is being prepared. There is then a short period of about 3–4 min during which the new sample is transferred to the injection capillary and the ion source is flushed with pure Helium. A new target is then inserted into the source and the next sample injected at a fairly constant rate. The concentration and re-dilution ensures a fairly well controlled and constant gas flow, which is better suited to the source's performance than a fast pulse if the sample size is larger than a few $\mu\text{g C}$.

samples. Because the gas handling, injection, and ion source all produce some mass-dependent fractionation, the $^{13}\text{C}/^{12}\text{C}$ ratio is not as stable as it usually is for graphite samples, and between samples can vary by as much as 0.5% (within sample variation is typically higher than this). However, this does not seem to affect the accuracy of the final radiocarbon date measurements which can still be better than 0.5% (as we observe on a finer scale for graphite; see Bronk Ramsey et al. 2004).

GC-AMS

In order to use the AMS for online GC AMS, we used an Agilent ALS 6890A GC coupled through a PDZ Europa Orchid combustion/drier system. This system is designed for GC-IRMS and comprises a GC separation system, the outlet of which can be directed either to a Flame Ionization Detector (FID) or an online combustion system. The combustion system is made up of a combustion column containing platinum and oxidized copper wires followed by a Nafion™ drier. In the case of GC-AMS, because we wish to measure the CO_2 in real-time from the GC, we injected the output of the online combustion system directly into the AMS through an open split.

In our application, the flow rate is set to 2 mL/min with a 1 mL/min makeup flow into the combustion system. In order to test the system, we have made up a solution in hexane of 0.5% of 3 compounds: hexadecane (petrochemical origin), methyl palmitate (made from palm oil), and methyl oleate (made

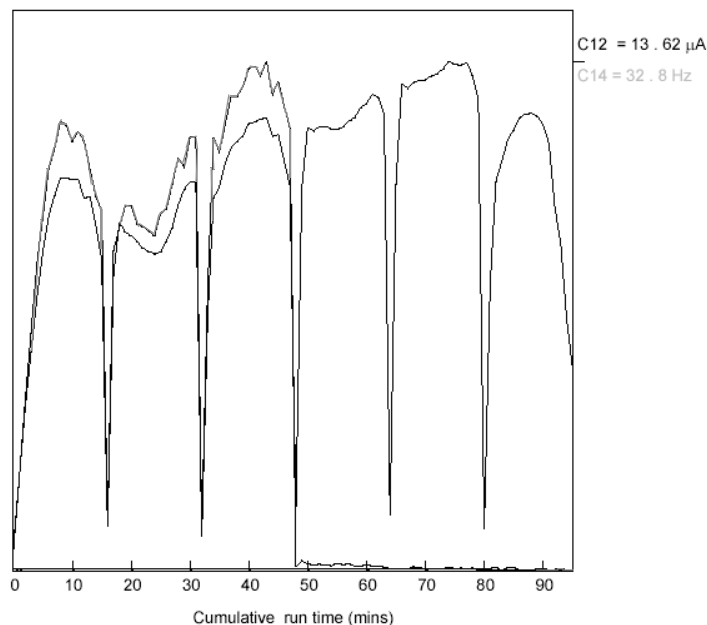


Figure 4 Data collected for a series of 3 HOXII standards followed by 3 background samples which should contain no ^{14}C . Cross-contamination is visible in the first background after the OXII—this is about 0.5% of the value of the previous sample and is corrected for by the analysis software. The currents shown are $^{12}\text{C}^{3+}$ (chopper corrected) and ^{14}C count rate.

Table 1 Operational parameters and performance of the SO-110 gas ion source. Currents given are maximal during the gas injection cycle. The source has emittance limiting apertures which are estimated to reduce the beam by 50–70% and so we can only estimate the true maximum beam from the source and its efficiency. For some applications where precision is not an issue, these apertures could probably be removed.

Parameter	Typical values
Target voltage	8.5 kV
Extraction voltage	26.7 kV
Ionizer current	15.0 A
Caesium reservoir	97 C
$^{12}\text{C}^-$ from source (before apertures)	15–20 uA (estimated)
Source efficiency	3–4% (estimated)

from olive oil). We expect the first to contain no ^{14}C and the other 2 to have modern concentrations. One μL of the solution was injected and the GC programmed to follow a temperature cycle:

- 60 s at 150 °C;
- 10 °C per min ramp to 163 °C (over 78 s);
- 60 s at 163 °C;
- 30 °C per min ramp to 300 °C (over 274 s);
- 900 s at 300 °C.

The GC column was a HP-5 (Crosslinked 5% PH ME Soloxane, 30 m × 0.32 mm × 0.25 μm film thickness, HP Part nr 19091J-413). The FID can be used to test the GC separation and identify the peaks. For GC-AMS, the flow is switched over to the combustion system/AMS after the solvent peak has come through. The injection to the source is an open split with a 500 mm × 0.075 mm (ID) methyl deactivated silica capillary (SGE prod code: 0624450) into the source, which gives rise to a flow rate of about 0.5 mL/min He. The split ratio is, therefore, about 1:5 (source:waste). For higher sensitivity, the flow rate through the GC could be lowered, but this would compromise GC performance. Figure 5 shows a GC-AMS trace with the separated compounds. All 3 isotopes of carbon are measured (the stable isotopes using CMTE 7803 digitizers, and the ^{14}C using the AMS detector) in 1-s blocks.

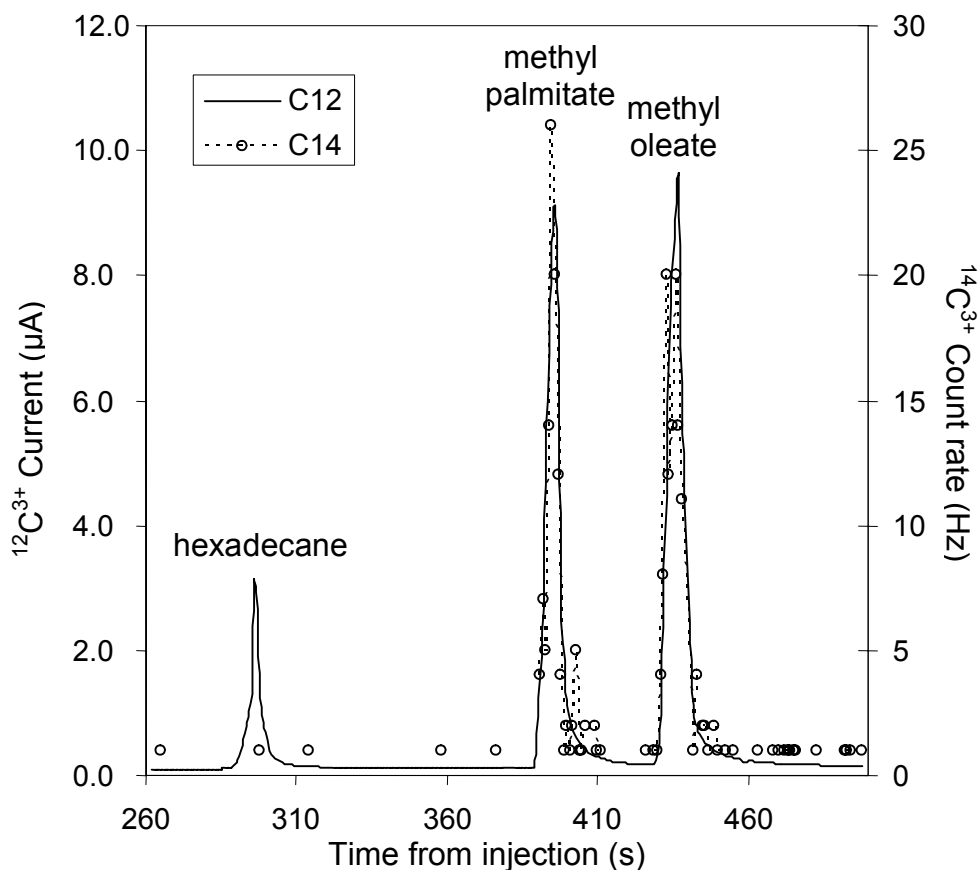


Figure 5 Example of direct GC-AMS using the SO-110 ion source. The 3 compounds injected have been easily separated and the correct isotope ratios for each compound determined (see main text for details).

The peak widths are fairly good with FWHM about 4 s on the AMS, compared to 2 s on the FID, showing that good separations can be obtained. There is some low-level tailing present (easiest to see on the ^{14}C counts on the right of Figure 5). For closely spaced peaks, some form of de-convolution would be useful. The only aspect of the trace which is not yet properly understood is the response characteristic. The hexadecane peak on the FID is broader and lower but should be similar in area—so there seems to be some non-linearity.

Using a 15-s window on the individual peaks (and normalizing to the absolute ratio for HOXII we get on routine gas runs), we obtain the following ^{14}C concentrations for the peaks:

- Hexadecane: 0.036 ± 0.036 fM;
- Methyl palmitate: 1.055 ± 0.103 fM;
- Methyl oleate: 1.076 ± 0.101 fM.

These values are, within the quoted errors, what we would expect for these samples. The stable isotope ratios are all within a range of $\pm 0.5\%$, which, likewise, is as we would expect. In this case, with just under $1 \mu\text{g C}$ per peak being injected into the source, we are getting precision on modern material of about 10%. Backgrounds would appear to be of the order of 3% or $30 \mu\text{g C}$ in the injection system, though may be non-linear.

CONCLUSIONS

The HVEE SO-110 source coupled with the gas injection system, described here, allows routine measurements on gas samples down to a few μg (Staddon et al. 2003). The whole system is completely automated and the gas injection system is substantially simpler than previous versions (Bronk Ramsey and Hedges 1994b), which should make it more reliable. The main technical advantage is that the whole sample is now flushed into the ion source instead of using a bellows system (with associated dead volumes). Mechanically, the system is simpler because there are no vacuum pumps, no bellows mechanism, and the assembly is at ground potential. Overall detection efficiency is higher by a factor of about 2 than the previous system at Oxford (in part because of the improved AMS transmission); other aspects of the performance are similar on normal-sized samples ($>30 \mu\text{g C}$).

We have shown that the ion source can also be used for online GC-AMS with very fast time response (additional FWHM about 2 s) and with precisions of about 10% for injected masses of less than $1 \mu\text{g C}$ of modern material. Absolute isotope ratios (stable isotope and ^{14}C) are in accordance with expectations. We expect this to be a valuable method for compound specific work where only low precision is required (e.g. source apportionment and biomedical work).

ACKNOWLEDGEMENTS

Funding through NERC; members of ORAU staff for building the gas handling system and helping with the GC interface; Jen Tripp, who provided invaluable advice on the GC aspects of the work; the staff of HVEE (Dirk Mous, Andreas Gottdang, Matthias Klein, and Rein van den Broek) for supporting this work and for all of the work on the new ion source for which this system has been developed; also particular thanks to Hans van Bergen (HVEE) who did so much of the installation of the new AMS system and SO-110 ion source.

REFERENCES

- Bronk Ramsey C, Hedges REM. 1994a. Carbon dioxide sputter source development at Oxford. *Nuclear Instruments and Methods in Physics Research B* 92:100–4.
- Bronk Ramsey C, Hedges REM. 1994b. Gas handling systems for radiocarbon dating by AMS. *Nuclear Instruments and Methods in Physics Research B* 92: 105–10.
- Bronk Ramsey C, Hedges REM. 1994c. Radiocarbon with gas chromatography. *Radiocarbon* 37(2):711–6.
- Bronk Ramsey C, Hedges REM. 1997. Hybrid ion sources: radiocarbon measurements from microgram to milligram. *Nuclear Instruments and Methods in Physics Research B* 123:539–45.
- Bronk Ramsey C, Humm MJ. 2000. On-line combustion of samples for AMS and ion source developments at ORAU. *Nuclear Instruments and Methods in Physical Research B* 172:242–6.
- Bronk Ramsey C, Higham TFG, Leach P. 2004. Towards high precision AMS: progress and limitations. *Radiocarbon*, these proceedings.
- Mous DJW, Fokker W, van den Broek R, Koopmans R, Bronk Ramsey C, Hedges REM. 1998. An ion source

- for the HVEE ^{14}C isotope ratio mass spectrometer for biomedical applications. *Radiocarbon* 40(1):283–8.
- Staddon PL, Bronk Ramsey C, Ostle N, Ineson P, Fitter A. 2003. Rapid turnover of hyphae of mycorrhizal fungi determined by AMS microanalysis of ^{14}C . *Science* 300:1138–40.
- Uhl T, Kretschmer W, Luppold W, Scharf A. 2004. Direct coupling of an elemental analyser and a hybrid ion source for AMS measurements. *Radiocarbon*, these proceedings.

ION SOURCE DEVELOPMENT AT KCCAMS, UNIVERSITY OF CALIFORNIA, IRVINE

J R Southon¹ • G M Santos

Earth System Science Department, University of California, Irvine, Irvine, California 92697-3100, USA.

ABSTRACT. The Keck Carbon Cycle accelerator mass spectrometry facility at the University of California, Irvine, operates a National Electronics Corporation 40-sample MC-SNICS ion source. We describe modifications that have increased beam current output, improved reliability, and made the source easier to service.

INTRODUCTION

The Keck Carbon Cycle accelerator mass spectrometry (KCCAMS) system at the University of California, Irvine, is based on a compact AMS accelerator from the National Electronics Corporation (NEC) (0.5MV 1.5SDH-1 Pelletron) with a 40 sample MC-SNICS ion source (Figure 1). The NEC source (Norton et al. 1999) operates routinely in many AMS laboratories worldwide at outputs of a few tens of μA of C^- ions. Operation above 100 μA is possible, but the source is often unstable and requires frequent cleaning. We have modified the source to increase the beam current output and to improve reliability and serviceability, and further work is planned.

SERVICEABILITY

Source Body Support

As supplied by NEC, the 40-sample version of the MC-SNICS is difficult to maintain, since no provision is made for in-situ servicing, and the entire source must be dismantled for even minor routine maintenance. Building a system for in-place servicing (Figure 2) seems mundane, but is probably the most important single change we have made. We bolted NEC's mobile high-voltage rack firmly to the floor and built into it a track system to support the source, using filing cabinet slides; longer versions of the slides are used to support the sample changer during cathode wheel changes. This allows the entire source body, or the sample changer plus isolation valve, to be rolled back for servicing, with almost all of the electrical, pneumatic, and cooling connections left in place. One person can perform a complete source cleaning in 2 hr.

Internal Changes

Maintenance is further eased if the source need only be opened at one end. The insulators supporting the Cs focus electrode (Figure 1) are unshielded, and occasionally become tracked due to buildup of sputtered material and must be replaced. As supplied, both ends of the source must be accessed in order to remove these insulators. By lock-nutting the screws which secure the downstream ends of the insulators, we can now replace the insulators with only the upstream end of the source opened.

Likewise, removing the ionizer assembly for cleaning (from the downstream end of the source) was impossible without first removing the Cs focus electrode (from the upstream end) due to interferences between these 2 assemblies and the Cs feed tube. We have cut away portions of the focus electrode according to a University of Arizona design (W Beck, personal communication), reducing it from the dished shape shown in Figure 1 to a flat plate mounted from 3 narrow legs. This was done to improve local pumping, but it also increased clearances sufficiently that the ionizer assembly can now be replaced with the Cs focus left undisturbed.

¹Corresponding author. Email: jsouthon@uci.edu.

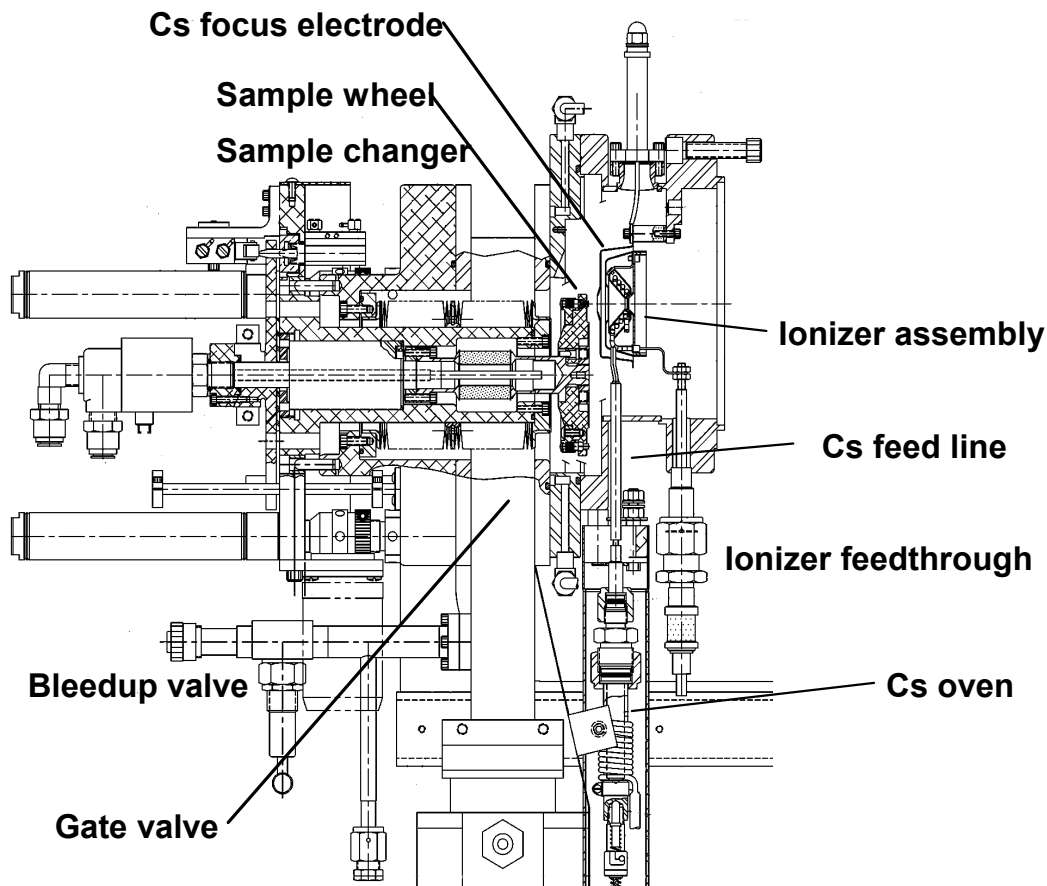


Figure 1 The NEC 40-sample ion source and sample changer. Note the tight clearances between the outer shroud of the ionizer assembly and the Cs focus electrode, and the lack of shielding of the post-type Cs focus support insulators (one of three is shown). The ionizer assembly is supported by 3 legs (not shown here) from the same internal lugs as the Cs focus electrode.

SPARKING AND INSTABILITY

After sample wheel changes, the source is often very unstable, with frequent arcing between the cathode wheel and the Cs focus electrode which can take hours to subside. The origin of the sparking remains obscure and there may be multiple causes. However, some of the instability may be due to poor contact between the aluminum sample wheel and a spring-loaded cathode voltage feedthrough. Sparking was reduced when a copper ring was temporarily bolted to the front of the wheel to make the contact. For a longer-term solution, we skimmed the front of the wheel flat on a lathe, and bolted on a stainless steel face plate (Figure 3). This has reduced (though not completely cured) the problem.

We have also found that the arcing is associated with progressive buildup over several weeks of a very hard insulating layer on the cathode side of the Cs focus. We speculate that arcing to the cathode wheel occurs due to buildup of stray charge on this layer, which is probably aluminum carbide from sputtered aluminum and graphite. We routinely swap out the focus electrode every few weeks, or when the instability becomes troublesome, and remove the deposit by grinding it with a diamond-tipped Dremel® tool.

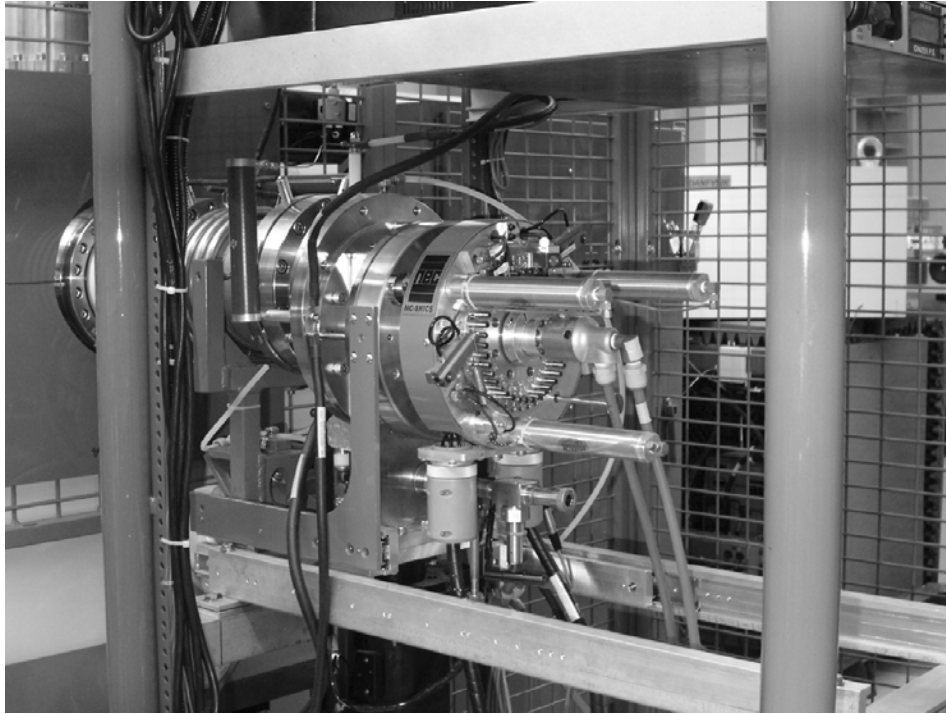


Figure 2 The track system built into the source high-voltage rack to allow the source to be serviced in situ.

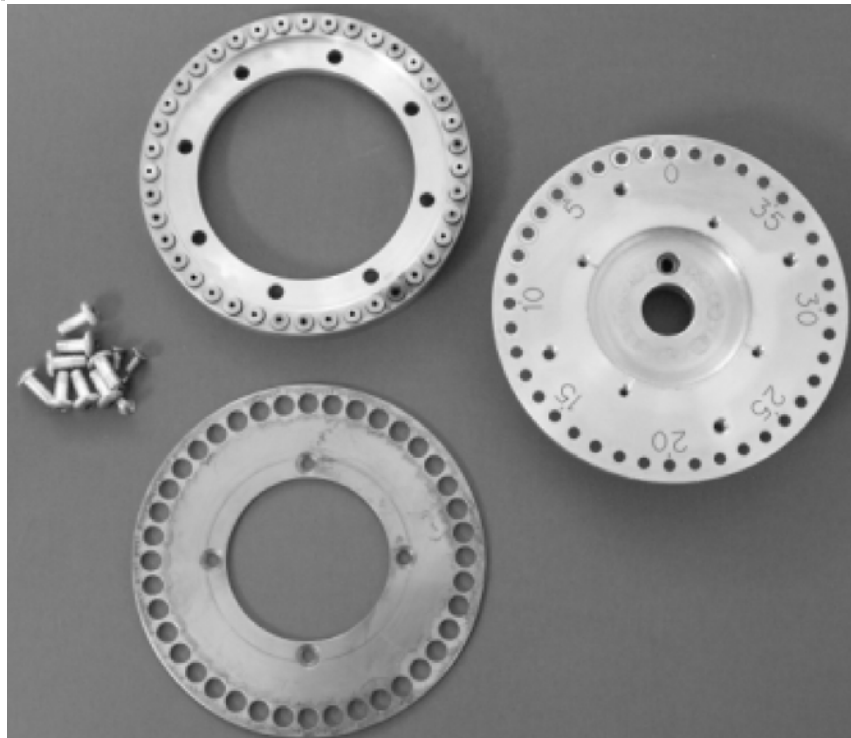


Figure 3 Modified sample wheel, sample clamp ring, and face plate.

Cs FEED

The Cs feed tube in the NEC source is actively heated but suffers from clogging problems, due in part to the small tube bore and the presence of a cold spot where the lower end of the assembly loses heat to the source body via the mounting bracket. This can lead to erratic operation at high outputs, and to frequent shorting out of insulators when the Cs oven is overheated in an effort to break through the liquid Cs plug in the line, and “burps” excess Cs into the source.

We are now running the Cs line heater at currents 40% above the original factory setting (45 A versus 33 A), following advice from other laboratories (D Knies; R Loger, personal communications). We have also added a layer of fiberboard to the existing heat shield around the Cs line and mounting bracket, and wrapped the VCR fitting at the top of the Cs oven with additional glass fiber and aluminum foil insulation. Together, these changes have raised the temperature of the cold spot where the VCR fitting attaches to the mounting bracket, and have made the Cs feed system much more controllable, though care is still required to prevent clogging. We are currently testing a new feed tube arrangement based on the double-walled, vacuum-insulated Lawrence Livermore (LLNL) design (Southon and Roberts 2000) which is completely free of this problem.

Cs OVEN

The Cs oven has been replaced to simplify and speed up Cs replenishment. The new unit (Figure 4) is based on a LLNL design (Southon and Roberts 1997), sealed with a 1.33" Conflat, and heated with an inexpensive band heater (Hotset Corporation, Battle Creek, Michigan, USA). It accepts full Cs ampoules that are opened under Ar and placed upright in the oven. It is not necessary to heat and pour out the Cs, as with the NEC design. This shorter oven is also less likely to act as a cannon when water is used to clean out residual Cs.

EXTRACTION ELECTRODE

Initially, the extractor, Cs focus, and cathode currents all tended to “run away” over time. When the source was cleaned, we saw signs of arcing (erosion) on the inside of the conical extractor snout and the end of its interior collimator assembly (Figure 5), the ionizer baseplate and the ionizer itself, the downstream side of the Cs focus electrode, and the cathode wheel. A likely explanation is that at high ionizer power levels, thermionically emitted electrons produce high space charge limited currents from sharp edges on the ionizer assembly (e.g. in the central aperture where 2 sheet-metal pressings overlap). These electrons can flow into the extraction gap and sputter positive ions from the extractor snout and collimator assembly. These positive ions then travel back upstream and strike the source. Under some conditions, this process becomes uncontrollable until the source is taken apart and cleaned.

R Loger (NEC) provided us with a new extractor electrode where the standard conical end was replaced by a large-bore tube (Figure 5), which alleviated the problem by reducing the electric field in the ionizer aperture. We have modified that design by shortening it and increasing the wall thickness to further reduce the electric field at the tip. The tubular double collimator assembly was removed to prevent arcing from the end, and was replaced by a single divergence-limiting collimator mounted at the downstream end of the electrode. Extractor currents still rise over time, but typically by 2–3 mA or less over a 12- to 24-hr run.



Figure 4 Cs oven and band heater. The new oven mates with the smaller of the 2 VCR nuts shown at the top of the NEC oven assembly in Figure 1.

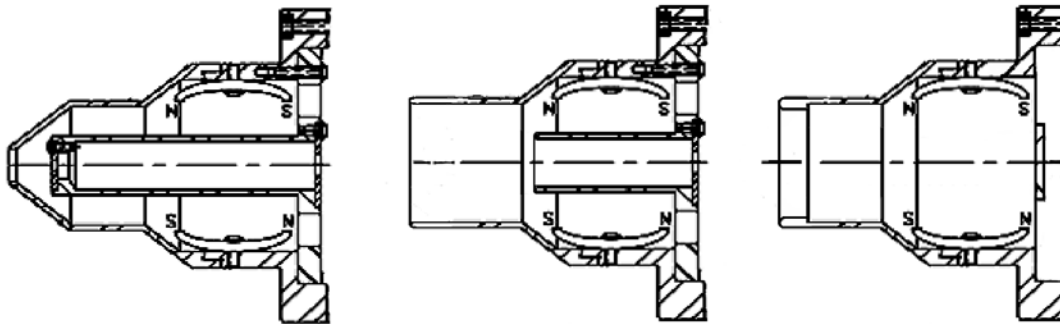


Figure 5 Extractor electrodes, with electron suppression magnets mounted above and below the beam path. Left to right: the original conical NEC design with internal 2-collimator assembly; the modified NEC straight-tube design (with shortened collimator assembly—front aperture removed); the shortened University of California, Irvine, design with a single collimator mounted on a transverse bar.

HIGH NEGATIVE ION OUTPUTS

Together, these changes have allowed us to run the source stably at higher cathode voltages and Cs oven settings to produce higher outputs. However, the key to high output currents is correct posi-

tioning of the sample wheel. As other researchers have found (M Roberts, personal communication), running with the wheel several mm back from the factory setting is necessary to obtain a suitably small (~1 mm) Cs spot at the sample for C⁻ outputs > 100 μ A.

This shift is required because as Cs currents in sputter sources increase, space charge moves the Cs beam waist (focus) back several mm further from the ionizer (Southon and Iyer 1990; Brown et al. 2000). In the NEC source, the Cs focus voltage can be varied to alter the position of the waist, but as Hausladen et al. (2002) have pointed out, when the “focus” lens is run at high voltages, it actually defocuses the Cs, pushing the waist back even further. If the lens is run at sufficiently low voltages, the waist can indeed be moved closer to the ionizer. However, since the focus voltage also determines the electric field at the ionizer surface, and hence the space charge limited Cs current, outputs are severely limited at low voltages. Moving the wheel back allows the lens to be run at high voltages, producing a correctly focused Cs beam at high intensities.

OPERATING PARAMETERS

Following these changes, typical running conditions for the source are as follows:

- Cathode voltage: 6.7 KV
- Cesium focus voltage: 3.9 KV
- Extractor voltage: 15.0 KV
- Einzel lens voltage: 1.2 KV
- Ionizer current: 24 A
- Cs heater (oven) voltage: 80 V (25 W)
- Cs oven temperature: 200 °C
- Cs line heater: 45 A
- Sample position: 3 mm back from factory setting.
- C⁻ output: 120–170 μ A
- Cs consumption: 5 g per 6 weeks

FURTHER DEVELOPMENT

We are testing a new 40-sample wheel which is a bolt-in substitute for the NEC wheel, but uses 6.3-mm-diameter \times 12.7-mm-long cylindrical sample holders held in place by spring-loaded ball inserts. These holders are large enough to be easily labeled, reducing the probability of inadvertently swapping samples. In addition, we have obtained funding from the National Science Foundation to work with NEC, Arizona, and Woods Hole on further source development. A complete new source body has been purchased from NEC and is being modified for improved cooling, provision of a vacuum-insulated Cs feed line, and changes to the Cs⁺ and negative ion geometries. We will also investigate the potential for better Cs focusing and increased negative ion output from spherical ionizers.

CONCLUSIONS

Our NEC ion source now runs with reasonable stability for periods of 2–3 weeks at 120–170 μ A of C⁻ output, with results on secondary standards indicating 2–5% precision/accuracy for ¹⁴C measurements. At these outputs, a typical wheel of 40 samples can be measured to 3–4% precision or better in well under 24 hr. Beam emittance has probably increased due to running the source harder, but the source output is still within the acceptance of the stripper canal of the 1.5 SDH-1 accelerator. Ion source sparking and instability have been reduced, so that stable operation is

reached within 1–2 hr after a sample wheel change. Although maintenance is required every few weeks to allow the source to run at high outputs, servicing it has become relatively simple and far less time consuming.

ACKNOWLEDGEMENTS

We thank Roger Loger of NEC for assistance with ion source improvements, and the W M Keck Foundation and the Dean of Physical Sciences and Vice Chancellor for Research, University of California, Irvine, for financial support

REFERENCES

- Brown TA, Roberts ML, Southon JR. 2000. Ion-source modeling and improved performance of the CAMS high-intensity Cs-sputter ion source. *Nuclear Instruments and Methods in Physics Research B* 172:344–49.
- Hausladen P, Weisser DA, Lobanov NR, Fifield LK, Wallace HJ. 2002. Simple concepts for ion source improvement. *Nuclear Instruments and Methods in Physics Research B* 190:402–4.
- Norton GA. 1992. Multi cathode SNICS ion source. In: J Benson, Rowton L, Tesmer J, Darling R, editors. Proceedings of the 25th Symposium of North Eastern Accelerator Personnel, Santa Fe, New Mexico, USA, 16–19 October 1991. World Scientific, Singapore. p 295.
- Southon JR, Iyer IS. 1990. A high-intensity multisample Cs sputter source. *Nuclear Instruments and Methods in Physics Research B* 47:299–302.
- Southon JR, Roberts ML. 2000. Ten years of sourcery at CAMS/LLNL—evolution of a Cs ion source. *Nuclear Instruments and Methods in Physics Research B* 172: 257–61.

THE KECK CARBON CYCLE AMS LABORATORY, UNIVERSITY OF CALIFORNIA, IRVINE: INITIAL OPERATION AND A BACKGROUND SURPRISE

John Southon¹ • Guaciara Santos¹ • Kevin Druffel-Rodriguez^{1,2} • Ellen Druffel¹ • Sue Trumbore¹ • Xiaomei Xu¹ • Sheila Griffin¹ • Shahla Ali^{1,3} • Maya Mazon^{1,4}

ABSTRACT. A new radiocarbon accelerator mass spectrometry (AMS) laboratory for carbon cycle studies has been established at the University of California, Irvine. The 0.5MV AMS system was installed in mid-2002 and has operated routinely since October of that year. This paper briefly describes the spectrometer and summarizes lessons learned during the first year of operation. In the process of setting up the system, we identified and largely suppressed a previously unreported ¹⁴C AMS background: charge exchange tails from ¹⁴N beams derived from nitrogen-containing molecular ions produced near the entrance of the accelerator.

THE KCCAMS FACILITY

The Keck Carbon Cycle accelerator mass spectrometry (KCCAMS) facility was established in 2001–2002 with a \$2M grant from the W M Keck Foundation and matching funds from University of California, Irvine (UC Irvine), and was set up to use carbon isotopic techniques, primarily AMS, to advance understanding of the carbon cycle and its linkages with climate. The facility consists of 3 major elements:

1. A National Electrostatics (NEC) 0.5MV 1.5SDH-1 accelerator mass spectrometry (AMS) system with a 40-sample MC-SNICS ion source;
2. A Finnegan MAT Delta Plus Isotope Ratio Mass Spectrometer equipped with Gas Bench and Elemental Analyzer (Fisons 1500NC) inputs for gas and solid organic samples, respectively;
3. A new sample preparation laboratory with two 12-head graphitizer lines to supplement existing UC Irvine sample preparation facilities.

AMS HARDWARE

The spectrometer (Figure 1) is the third NEC production model in a new generation of compact AMS systems developed in collaboration with ETH-Zurich (Synal et al. 2000). Our system has several improvements over previous versions delivered to Georgia (Roberts et al. 2003) and Poznań (Goslar et al. 2003). These include the use of large cryopumps (Cryotorr 8's) to improve vacuum and, thus, reduce backgrounds due to ions scattering from residual gas, and provision of extra beam diagnostics (beam profile monitors and adjustable slits) and additional corrective steerers (Figure 1). A larger than normal SF₆ gas handling system (NEC #952 SMB) was specified to allow the accelerator insulating gas to be transferred with minimal losses.

TIMETABLE

Funding for the facility was received in January 2001 and the AMS system was ordered in April 2001 and installed over a 3-week period in June/July 2002. After some initial delays due to ion source instability problems, the first research unknowns were measured in August 2002 and the system was accepted in October of that year; it has since run routinely. On completion of a new Earth

¹Earth System Science Department, University of California, Irvine, California 92612, USA.

²Department of Chemistry, Loyola Marymount University, Seaver Hall, Los Angeles, California, USA.

³Lamont-Doherty Earth Observatory, Columbia University, Palisades, New York, USA.

⁴Department of Biology, California State University, Fullerton, California, USA.

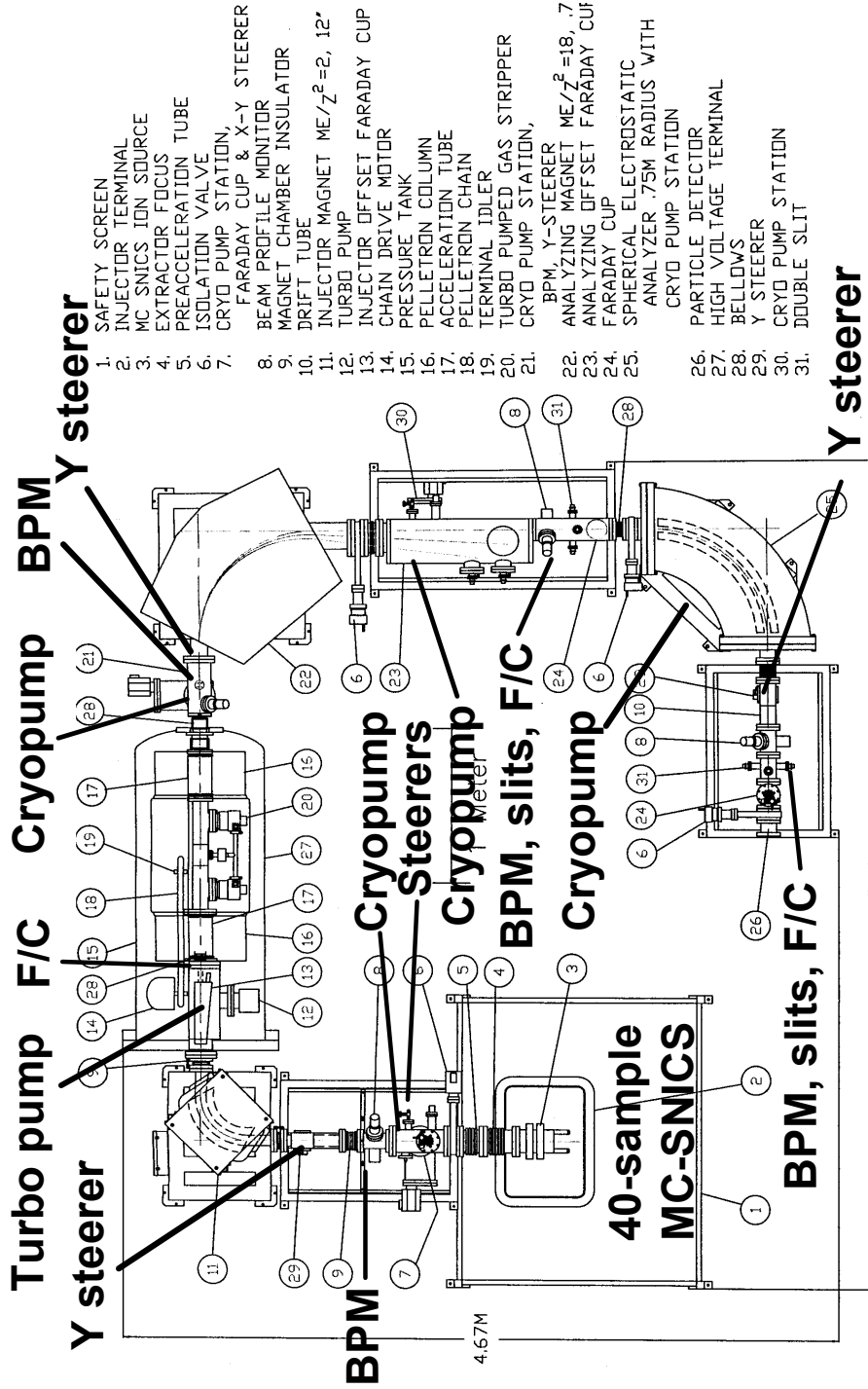


Figure 1 The 1.5 SDH-1 spectrometer. A bouncer is used to switch isotopes and a recirculating Ar gas stripper with 2 turbomolecular pumps breaks up molecules. A single 90° magnet and an Electrostatic Analyzer (ESA) comprise the High Energy (HE) beamline and ¹⁴C is detected with a single solid state detector. Positions of pumps plus beam diagnostics and steerers are shown. BPM = Beam Profile Monitor; F/C = Faraday Cup.

System Science building in July 2003, the entire facility was moved over a 4-week period, including time spent dismantling and rebuilding the sample prep lab. Four to 6 people worked on the project at any given time, including an NEC engineer who supervised reinstallation of the spectrometer. The last AMS run before the move was on June 29 and tests on July 17 showed that the spectrometer was working satisfactorily in its new home, just 19 days later. We certainly do not recommend moving an AMS system every year, but this timetable does illustrate an advantage of these small machines.

THE FIRST YEAR OF OPERATION

Our overall impression after a year of operation is that the system works well. The hardware is reliable and well interlocked, and unattended running overnight is routine. In particular, the ion source sample changer (arguably the most complex part of any AMS system) has been almost trouble-free. The small sample holders for the MC-SNICS source—too small to be labeled—are worrisome, and we are working on an alternative design (Southon and Santos, these proceedings). NEC's AccelNET control software has proven very reliable, though ease of use would be significantly improved if more features were incorporated into the present Graphical User Interface. Notable pluses of the control system are excellent implementations of a strip chart module for system monitoring and software-assignable knobs and meters for tuning. We use NEC's standard data acquisition software, but rely on the Lawrence Livermore (LLNL) Fudger code (T Ognibene, personal communication) for data analysis. However, we routinely use the strip chart feature of the NEC analysis code (abc) to scan the cycle by cycle data records to investigate anomalous results. This feature also alerted us to 2 problems which affected the $^{13}\text{C}/^{12}\text{C}$ measurements: data overwriting due to an incorrectly set jumper in a CAMAC memory module, and synchronization errors due to a wrongly selected polarity on a current integrator timing output.

Of course, significant problems have occurred. Accelerator sparks damaged cooling fans inside the tank, until we added extra shielding around the AC power inputs. Initially, the ion source showed gross instability, eventually traced to an electrical short that provided a bypass for the current heating the Cs supply line. A turbomolecular pump in the accelerator gas stripper (Leybold TMP151) developed a pressure-sensitive leak due to an aluminum KF-10 blankoff flange that had begun to split under 5 atm of SF_6 and the pump also twice suffered rotor bearing failures. Beam marks on the interior of the accelerator vacuum system indicated that the beam was oval not round and it was eventually determined that the injection magnet had been built with incorrect pole face angles due to a miscommunication between NEC and manufacturer Danfysik. We had hoped that installation of new poles would provide an increased margin for beam transmission through the stripper. However, we observed little change, though beam spots showed that the problem had indeed been corrected.

PERFORMANCE

Following a number of ion source improvements (Southon and Santos, these proceedings), the source routinely produces 120–170 μA of C^- from both Zn-reduced and hydrogen-reduced graphite. These outputs allow us to measure a typical wheel of 40 samples to 3–4% precision in well under 24 hr. Measurement precision and accuracy, based on scatter in results for multiple aliquots of a primary standard plus deviation of secondary standards from the known values are 2–5%, with some runs clearly better than others. The origin of these variations is still unknown. The $\delta^{13}\text{C}$ values measured on-line often drift by several per mil during a run, but most of these drifts normalize out and the normalized values are accurate to ~1–2%. Clearly, there is still room for improvement, but we are encouraged to have reached this level of performance after just 1 yr.

BACKGROUNDS**I. ^{14}N**

Recent results from graphitized background samples are equivalent to ^{14}C ages as high as 55 ka. Initially, however, backgrounds rarely reached 50 ka and exhibited several puzzling features. Count rates were high even with the Low Energy (injection) magnet far off-mass (Figure 2), though they did disappear when the ion source Faraday Cup was inserted. Results from Alfa Aesar synthetic graphite, commonly used as a convenient “machine” blank, were often no better than those from graphitized coal. There was no strong dependence of the background on stripper gas pressure, indicating that it was not due to incomplete destruction of molecules; and the blanks were unchanged when nitrogen was used as the stripper gas instead of argon. Experiments where selected pumps were turned off showed some dependence of blank levels on the vacuum in the HE accelerator tube, or possibly the HE analyzing magnet. Lack of sufficient pumps in suitable locations prevented us from carrying out similar experiments in the injection system.

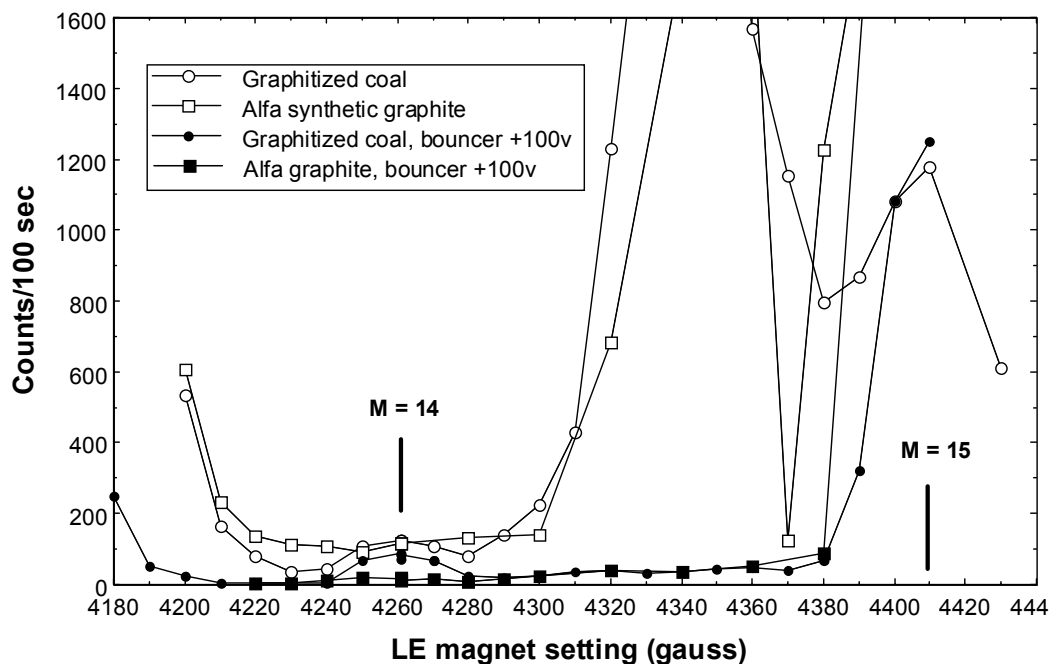


Figure 2 Detector count rate within the ^{14}C energy window versus LE magnet setting, with bouncer voltages of zero and +100 v. Count rates are far lower with a positive voltage on the bouncer.

Efforts to understand the background led us to study in detail the various trace beams emerging from the accelerator under different conditions. Scans of the HE magnet with ^{13}C injected into the accelerator revealed a surprisingly large baseline current or tail of 5–20 pA, or between 10^{-4} and 10^{-5} of the primary beam (Figure 3). This tail is due to ions which emerge from the stripper in different charge states and charge exchange to 1^+ in the HE accelerator tube. The relatively high intensity is ultimately due to the high stripper gas pressures required for destruction of molecules at 0.5 MV (Jacob et al. 2000). Figure 3 also shows a feature near the main ^{13}C peak that is probably due to secondary electrons scattered into the Faraday Cup. Small (\sim pA) peaks at magnet settings of 7340 and

7840 gauss are transmitted by the ESA at settings corresponding to E/q equal to the accelerator terminal voltage. This yields $M/q = 28$ and 32 and we believe these peaks are N_2^+ and O_2^+ from beam-induced ionization of residual air in the stripper. We also see beams of several charge states of Ar from stripper gas ionization, at intensities of nA to hundreds of pA.

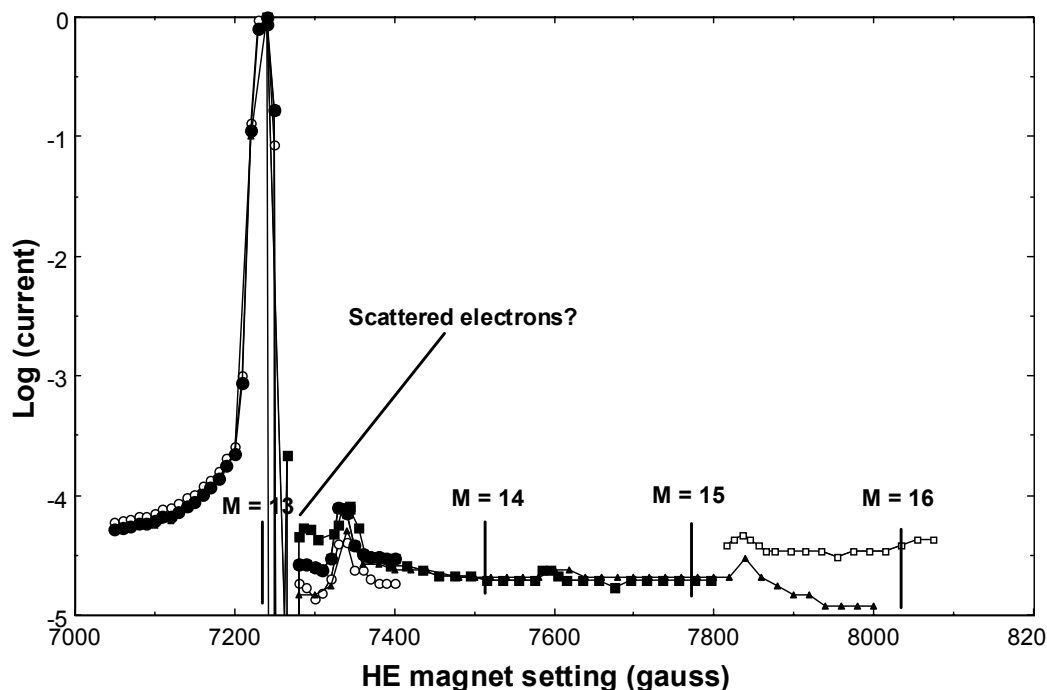


Figure 3 Current in the HE magnet Faraday Cup versus magnet setting, with ^{13}C injected (composite figure from several magnet scans). Current is plotted as a fraction of the current in the primary ^{13}C beam, on a logarithmic scale. A charge-exchange tail extends over the equivalent of several mass units, or an energy range of hundreds of keV.

Scans were also carried out with mass 14 injected and the HE magnet and ESA and the detector energy window varied together at settings appropriate for mass 14 charge state $1+$. Once again, a baseline signal—in this case a “ ^{14}C ” count rate of around 1 Hz, equivalent to 0.2 pMC (percent modern carbon) or 50 ka—was present at all HE beamline settings, though several peaks were also observed (Figure 4). Experiments where the ESA was varied showed that the ions were transmitted cleanly—i.e. the background was not due to scattering in the ESA. We were forced to accept that the background was truly mass 14 (i.e. nitrogen), made up of charge exchange tails from lower energy peaks, primarily from the intense peak at 815 keV (a 3×10^{-5} tail from a 30 KHz peak gives a count rate of ~ 1 Hz, close to that observed). Recalling that this background was present at all injector settings, we realized that we had purchased a ^{14}C AMS system that consistently produced the interfering isobar, regardless of how it was tuned.

The challenge was then to determine the origin of the ^{14}N . Eventually, we realized that the peaks at 1024, 993, and 815 keV represent energies of $(1+14/15) \times V_T$, $(1+14/16) \times V_T$, and $(1+14/26) \times V_T$, where V_T is the terminal voltage. These are the energies for nitrogen from the breakup of NH_2^- , NH_2^- , and CN^- , respectively, but for molecular ions generated after the LE magnet, NOT in the ion source. The most intense peak by far is from CN^- , a prolific and easily produced nitrogen ion (Anbar 1978). We also noted that when scanning the HE magnet with mass 14 injected, pA beams

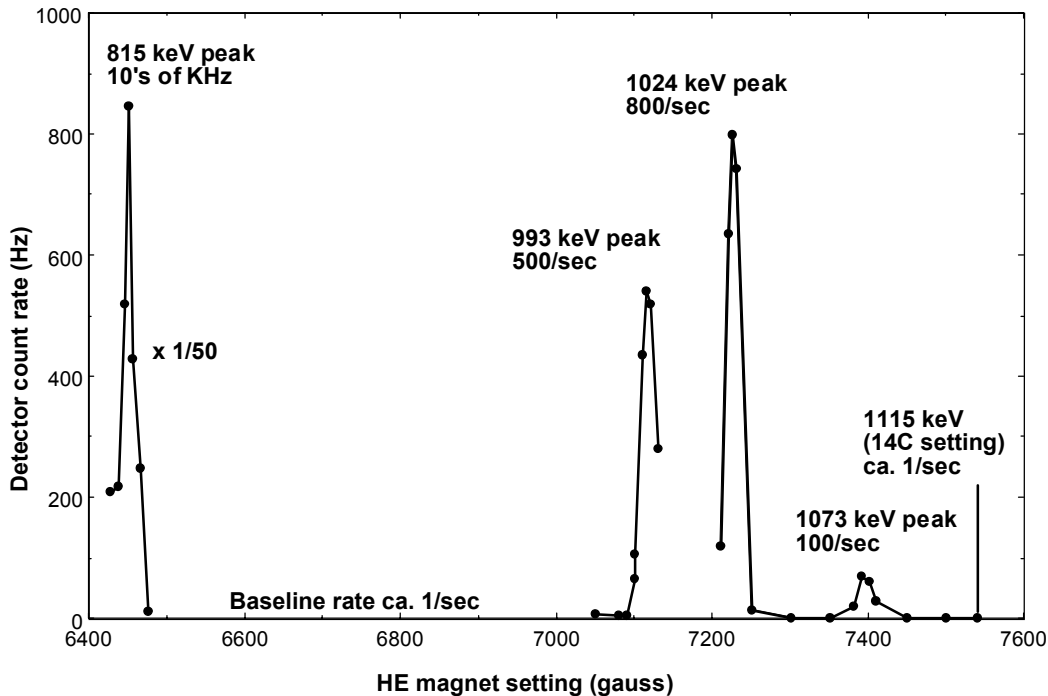


Figure 4 Detector count rate when the HE magnet and ESA are scanned together for mass 14 charge state 1+ ions of different energies. The injection energy is 55 keV and the accelerator terminal voltage is 530 kV, for a total ^{14}C energy of 1115 keV. Beam currents were reduced by a factor of ~ 50 to acquire data for the intense peak at the left of the plot. From left to right: the peaks are due to nitrogen from CN^- , NH_2^- , and NH^- generated near the base of the accelerator, and to scattering from a ^{13}C beam injected as mass-14 CH^- .

were observed at settings equivalent to ^{16}O at energies of 1060 and 1028 keV, corresponding to energies of $2 \times V_T$ and $(1+16/17) \times V_T$, or O^+ from O^- and OH^- ions, again generated at the base of the accelerator.

The basic background problem, then, is due to N-containing molecular ions generated between the LE magnet and the LE accelerator tube by some mechanism involving beams from the ion source. These low-energy ($\sim \text{eV}$) ions drift into the LE accelerator tube, and some reach the stripper and break up. Some of the resulting N ions emerge from the stripper as $2+$ and charge exchange to $1+$ in the HE tube, acquiring sufficient extra energy to mimic ^{14}C . The strong background enhancement at ~ 4340 gauss in Figure 2 must represent deflection of one of the intense beams from the source on to a region of the injector where production of the molecular ions is maximized.

Such backgrounds will typically not be a problem in larger ^{14}C AMS systems, where particle identification is used routinely; nor will they interfere in single-stage AMS systems (high-voltage decks) where only negative ions are accelerated. Small AMS systems accelerating $1+$ ions are vulnerable because they suffer from enhanced charge exchange in the HE accelerator tube due to high gas stripper pressures.

On discovering both O and N beams from the base of the accelerator, we leak-checked the area thoroughly but found nothing. Although the ultimate source of the nitrogen is probably air introduced during accelerator or ion source openings, the process is rather indirect, or use of nitrogen as the stripper gas would have had catastrophic results. It may require the buildup of nitrogen and other

atoms in close proximity on interior surfaces of the vacuum system, where they can be sputtered as molecular ions by stray beams.

We realized that since most of the critical region between the LE magnet and the LE accelerator tube is part of the bouncer, running at a small positive bouncer potential when injecting ^{14}C should trap low-energy negative ions within the bouncer structure, thereby suppressing most of the background. This proved to be the case. Running the bouncer at +50 to +100 v rather than zero reduced the count rate from Alfa graphite by up to 80% and removed the off-mass background almost completely (Figure 2), and the stray oxygen beams also disappeared. A partial re-scan of the HE magnet/ESA combination showed that the 1024-keV nitrogen peak in Figure 4 had been reduced by 90%. Backgrounds equivalent to ages of 56 ka (coal) and 54 ka (calcite) were obtained from graphitized samples, together with an age of 62 ka for Alfa graphite. Clearly, the background problem had been brought under control, if not eliminated completely.

We upgraded the injector vacuum system by adding a pumping restriction and a turbomolecular pump upstream of the LE magnet, in an attempt to reduce the background still further by reducing the periodic injections air and water from sample changer openings. However, this had little effect. Shortly, we will test the effect of adding a collimator and a negative bias ring immediately in front of the LE tube, mounted off the gap lens at the downstream end of the bouncer, to suppress the remaining 20 cm of beamline. Alternatively, since gas ΔE -E detectors with ultra-uniform silicon nitride entrance windows can resolve ^{14}C and ^{14}N even at these low energies (M Suter, personal communication), the problem could be avoided by using particle identification, though at the expense of some increase in the cost and complexity of the system.

II. Scattering

We have also begun to investigate backgrounds due to scattering, especially from ^{13}C . Figure 5 shows an oscilloscope trace of the detector amplifier output during the ^{12}C , ^{13}C , and part of the ^{14}C bounce periods. It illustrates the very high count rates that occur when ^{12}C and ^{13}C beams are brought around the HE magnet. Some of these ions scatter from residual gas and pass through the magnet image slits, and still have energies sufficiently close to the nominal value to pass the ESA and reach the detector. Even after we added a tubular extension to an existing pumping restriction at the entrance to the HE magnet and improved the vacuum to an estimated 1×10^{-7} torr at the 45° point, we observed count rates of ~ 5 KHz per μA of analyzed ^{12}C , and 50 KHz per μA of ^{13}C .

It is surprising that this mechanism can generate count rates when ^{14}C is being measured, since the only ^{13}C ions injected are mass-14 $^{13}\text{CH}^-$ or a high-energy $^{13}\text{C}^-$ sputtering tail (Litherland 1984) at 14/13 of the normal injection energy. The energy of $^{13}\text{C}^+$ from CH^- is 42 keV too low at the HE magnet (gas scattering from this ^{13}C beam in the HE magnet produces the 1073-keV peak in the HE magnet/ESA scan in Figure 4). Because of this energy mismatch, any gas-scattered ions should be rejected when the ESA is at normal ^{14}C settings. The intensity of the higher energy charge-exchange tail from this weak (~ 5 nA) beam is insufficient to provide a significant count rate via scattering. Measurements on analyzed beams after the HE magnet indicate that the sputter tail from our source (6.5 keV sputtering energy) is below 1 pA or 2×10^{-6} of the primary beam when the system is tuned for an injection energy just 1.5 keV higher than the actual source voltage setting of 55 kV. This suggests that the intensity of any beam tail injected at 14/13 of the nominal energy is very small.

Nevertheless, it does appear that scattered ^{13}C background is significant. Experiments in collaboration with LLNL colleagues showed that enriched ^{13}C samples (99% ^{13}C) gave count rates on our system equivalent to ^{14}C samples of 5 to 10 pMC. The material was known to be ^{14}C -dead from $4+$

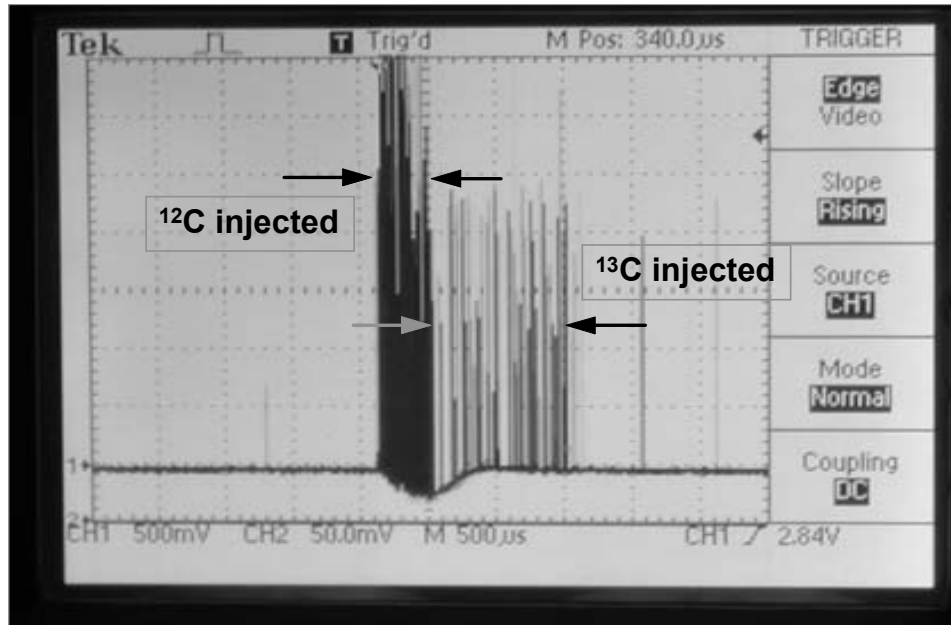


Figure 5 Detector amplifier output (oscilloscope trace). Very high scattering count rates are present when ^{12}C and ^{13}C are brought around the HE magnet—so high that pulse pileup and amplifier baseline shifts occur—though the system recovers well before ^{14}C counting begins.

AMS measurements at 6.5 MV. Count rates equivalent to 30 pMC (T Ognibene, personal communication) were observed on a small NEC AMS system at LLNL (Ognibene et al. 2000), similar to ours but with poorer vacuum in the HE magnet. Scaling the results for our system to samples of normal ^{13}C content, we can expect backgrounds in the 0.05–0.1 pMC range.

Resolving this residual ^{13}C background from ^{14}C via particle identification appears problematic at these low energies (M Suter, personal communication). In principle, the problem could be solved by adding a third dispersive element, i.e., replacing the ESA with a second 90° magnet, followed by a Wien Filter acting in the vertical. Two-magnet systems have been used since the early days of AMS, specifically to remove any scattered beam component. However, these changes would add significantly to the cost and size of the small system. Alternatively, vacuum in the HE magnet could be improved by moving it further from the accelerator to accommodate an additional pumping restriction and a second pumping stage, but this would require changes to the entire HE beamline geometry, and might result in beam losses in the magnet.

CONCLUSIONS

The Keck Carbon Cycle AMS lab is now operating routinely. In the process of setting up the system, we have identified a previously unreported ^{14}C AMS background: charge exchange tails from ^{14}N beams derived from nitrogen-containing molecular ions produced near the entrance of the accelerator. We have suppressed most of this background by appropriately biasing internal electrodes and the problem could also be solved by using E- Δ E particle identification. Scattering of ^{13}C in the HE magnet generates additional backgrounds in systems such as ours that lack a third (anti-scatter) dispersive element. Nevertheless, we have achieved blank levels in this new facility that are comparable with those of larger AMS systems, at a fraction of the cost.

ACKNOWLEDGEMENTS

We thank Jim Schroeder, Thilo Hauser, Bob Templin, Roger Loger, Mark Sundquist, and others at NEC for their assistance, Ted Ognibene and Darren Hillemonds of LLNL for help with background tests, and the W M Keck Foundation, the Vice Chancellor for Research, and the Dean of Physical Sciences, UC Irvine, for financial support.

REFERENCES

- Anbar M. 1978. The limitations of mass spectrometric radiocarbon dating using CN^- ions.
- Goslar T, Czernik J, Goslar E. Forthcoming. Low-energy ^{14}C AMS in Poznan Radiocarbon Laboratory, Poland. Proceedings of the 9th International Conference on AMS. *Nuclear Instruments and Methods in Physics Research B*.
- Gove HE, editor. *Proceedings of the 1st Conference on Radiocarbon Dating with Accelerators*. Rochester: University of Rochester. p 152–5.
- Jacob SAW, Suter M, and Synal H-A. 2000. Ion beam interaction with stripper gas—key for AMS at sub MeV. *Nuclear Instruments and Methods in Physics Research B* 172:235–41.
- Litherland AE. 1984. Accelerator mass spectrometry. *Nuclear Instruments and Methods in Physics Research B* 5:100–8.
- Ognibene TJ, Brown TA, Knezovich JP, Roberts ML, Southon JR, Vogel JS. 2000. Ion-optics calculations of the LLNL AMS system for biochemical ^{14}C measurements. *Nuclear Instruments and Methods in Physics Research B* 172:47–51.
- Roberts ML, Culp RA, Dvoracek DK, Hodgins GWL, Neary MP, Noakes JE. Forthcoming. The compact ^{14}C AMS system at the University of Georgia. Proceedings of the 9th International Conference on AMS. *Nuclear Instruments and Methods in Physics Research B*.
- Southon JR, Santos GM. 2004. Ion Source Development at KCCAMS, University of California, Irvine. *Radiocarbon*, these proceedings.
- Synal H-A, Jacob S, Suter S. 2000. The PSI/ETH small radiocarbon dating system. *Nuclear Instruments and Methods in Physics Research B* 172:1–7.

THE NEW ^{14}C ANALYSIS LABORATORY IN JENA, GERMANY

A Steinhof^{1,2} • G Adamiec³ • G Gleixner¹ • GJ van Klinken⁴ • T Wagner¹

ABSTRACT. The new accelerator mass spectrometry (AMS) Radiocarbon Analysis Laboratory in Jena is described. The laboratory developed a combustion system for solid samples and a CO_2 extraction system for air samples. Thus far, sample preparation, including graphitization, was performed in the laboratory, and the samples were measured subsequently by other AMS facilities. Currently, the laboratory owns a 3MV AMS system from HVEE (Netherlands) that has passed the acceptance tests and will be used for routine ^{14}C determinations in the near future. The AMS system is equipped with 2 ion sources, one suitable for graphite targets and the second for both graphite and CO_2 targets.

INTRODUCTION

Accelerator mass spectrometry (AMS) of radiocarbon is an important and well-established tool in many fields of science (e.g. in archaeology or biomedical applications). One of the major fields of research at the Max-Planck-Institute of Biogeochemistry is the investigation of the local and global carbon cycle of the earth system. With the ability of the AMS technique to determine the carbon isotopic composition of samples of mg size or less, AMS is also applicable to support these investigations. Therefore, the ^{14}C Analysis Laboratory was formed within the institute in 1998.

Since the year 2000, the ^{14}C Analysis Laboratory in Jena has been assisting research in the institute by providing state-of-the-art preparation of solid and gaseous samples for ^{14}C measurements. In the first years of the laboratory, the samples were pretreated, combusted, and graphitized at Jena, while the AMS measurements were performed at the Leibniz AMS Laboratory in Kiel, Germany, the Rafter Radiocarbon Laboratory in Lower Hutt, New Zealand, or the Research Laboratory for Archaeology in Oxford, Great Britain.

Below, we describe the sample preparation line, its performance, and the sample management system AMSIS (AMS Information System), which was designed and implemented for controlling the flow of samples through the processing. In September 2003, a 3MV accelerator, manufactured by High Voltage Engineering Europa (HVEE), was being installed and commissioned at the laboratory. The features of this accelerator are summarized and presented together with the first performance measurements.

SAMPLE PREPARATION

Sample Preparation Line

The majority of the samples that were prepared in the laboratory so far were soil and air samples, although other materials like wood were also prepared. The first stage of the sample preparation is chemistry. In the case of soil samples, if required, inorganic carbon was removed. For wood samples, α -cellulose was extracted.

The schematic set-up of the post-chemistry sample preparation line is shown in Figure 1. The heart of it is the UGCS (Universal Gas Collection System) which is used for solid as well as gaseous sam-

¹Max-Planck-Institut für Biogeochemie, Postfach 100164, 07701 Jena, Germany.

²Corresponding author. Email: steinhof@bgc-jena.mpg.de.

³Departamento de Física Teórica, Atómica, Molecular y Nuclear, Facultad de Ciencias, Universidad de Valladolid, 47011 Valladolid, Spain.

⁴Polykatikia Iatrou Roulia, Paralio Astros, Greece.

ples. Solid samples enter the sample preparation line through the elemental analyzer, which is a NC2500 (Carlo Erba), consisting of a combustion and a reduction oven, a chemical water trap, and a gas chromatograph (GC) column. We use the conventional set-up, i.e., in contrast to the proposal of the Groningen group, all the CO₂ passes through the GC column (Aerts-Bijma et al. 2001). A small part of the sample mass is used for the IRMS (isotope ratio mass spectrometer), model Delta Plus (ThermoQuest). The major part of the sample is extracted from the helium flow in the cryogenic CO₂ trap of the UGCS and directed into either riglets (reactors) for graphitization, special flasks for the gas source, or alternatively to ampoules for storage. Altogether there are 20 outlet ports, allowing the processing of 20 samples in 1 combustion batch. UGCS has been built in such a way that future connections to other input sources can be easily implemented, e.g., to a laser ablation system.

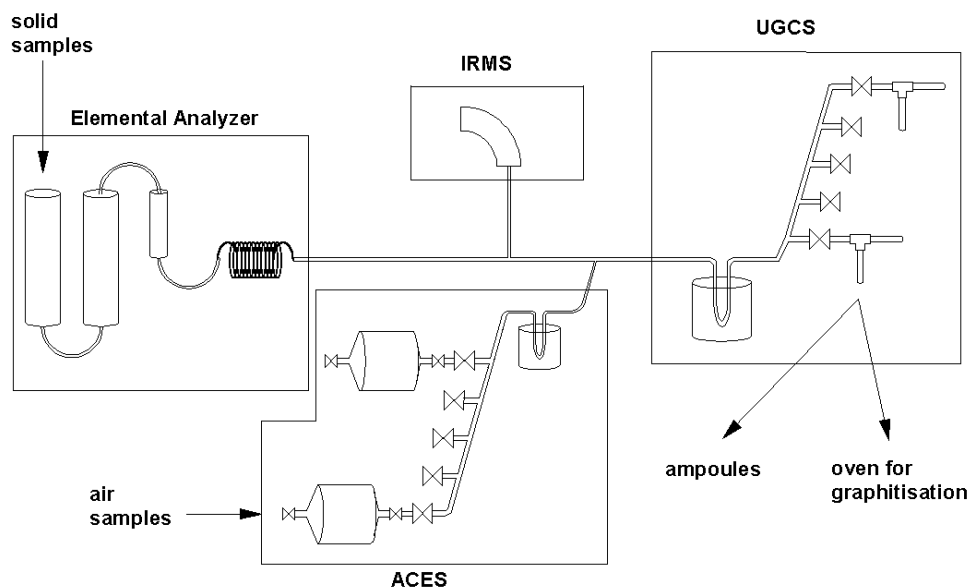


Figure 1 Schematic set-up of the post-chemistry sample preparation line showing the major parts: the elemental analyzer, the IRMS (isotope ratio mass spectrometer), the ACES (Air-CO₂-Extraction System), and the UGCS (Universal Gas Collection System). For more details, see text.

In the air samples, the bottles containing the samples are mounted to the ACES (Air-CO₂-Extraction System), which consists of a manifold for 20 bottles and a cryogenic water trap. The CO₂ is separated from the other gases (nitrogen, oxygen, and argon) in the UGCS cryogenic CO₂ trap and subsequently treated like the CO₂ from solid samples. Each individual extraction takes about 2 hr, limited by the pumping speed of UGCS, which we want to improve in the future.

The standard operation mode is semi-automated, i.e., all valves can be controlled from a switchboard, and only a small dewar with liquid nitrogen has to be positioned manually to the CO₂ trap (for the extraction of CO₂ from helium or air) and the respective sample container (for the transfer of the sample from the CO₂ trap to the sample container). For the extraction of CO₂ from air, an alternative fully-automated mode was developed: all valves in this mode are controlled through a computer interface (National Instruments) and an electronic unit built in-house. The control software is based on Measurement Studio (National Instruments) and is written in the computer language C. Instead of moving a small dewar between first the CO₂ trap and the respective sample container, a large one was designed that permanently cools all sample containers, and only the CO₂ trap is moved pneumatically in and out of the large dewar. The liquid nitrogen of this large dewar is refilled automati-

cally. With this automation, we hope that unattended overnight operation will become a standard routine in our laboratory.

Performance of the Sample Preparation Line

Presently, around 800 samples (not including standards, background, and test samples) have been prepared with the described system, mainly soil and air samples. With the soil samples, we found that it was very important to check whether the combustion oven within the elemental analyzer is really free of carbon from the previous sample. Therefore, after each soil sample we added combustion cycles without any sample and used the IRMS to measure the resulting carbon peak. The combustions without samples were repeated until the peak of the carbon was below 10^{-4} of its usual height. For soil samples with a total mass between 20 and 50 mg, up to 7 empty combustion cycles were required.

Anthracite was used initially for the combustion blank. In the first 15 batches, we reached a mean value of 0.35 pMC (45,500 BP), but starting with batch 16, we used a new piece of anthracite and the mean value increased to 0.55 pMC (41,700 BP) (Figure 2). To avoid the uncertainty due to the sample material, in the last batch (nr 22) we used the IAEA C1 marble standard (Rozanski et al. 1992) and obtained 0.216 ± 0.016 pMC (49,300 BP) as a mean value of the 3 samples. These values are not as good as the ones reached with the sealed ampoule hydrolysis technique (e.g. Nadeau et al. 2001), but are very good compared to published values of other laboratories with a comparable system (e.g. Aerts-Bijma et al. 2001). In the future, it will be checked whether the good values and the low scatter measured with the 3 C1 standard samples of the last batch can be reproduced. As soon as we have more statistics for the background, we will experiment with taking off the combusted CO_2 before the GC column, as proposed by the Groningen group (Aerts-Bijma et al. 2001).

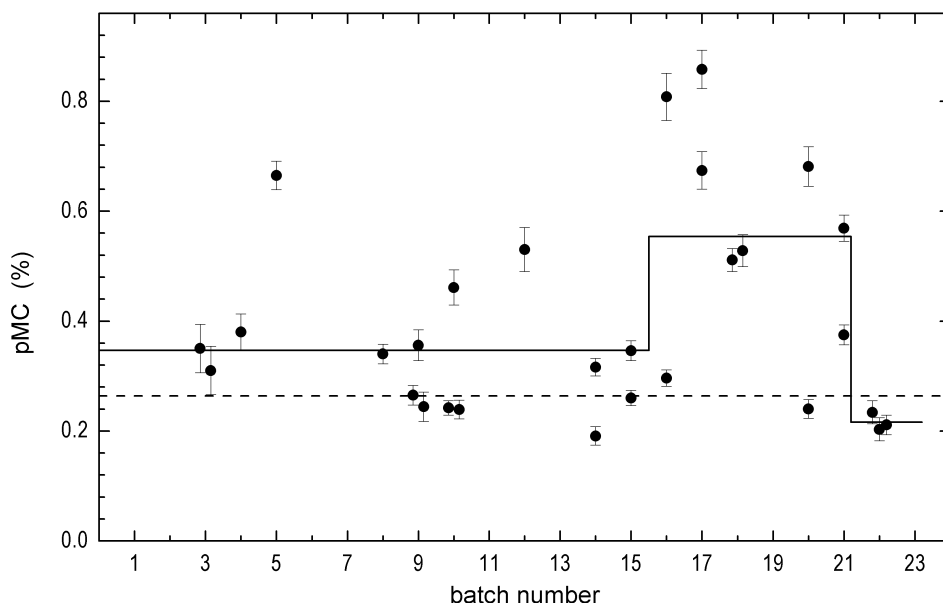


Figure 2 Background levels resulting from samples prepared in Jena, but measured at other facilities. Up to batch 15, the samples originated from a single piece of anthracite, yielding a mean value of 0.35 pMC (45,500 BP). From batch 16 to 21, another piece of anthracite was used and the mean value increased to 0.55 pMC (41,700 BP). In batch 22, the C1 marble standard of the IAEA was used and gave a mean value of 0.216 ± 0.016 pMC. These mean values are indicated by the solid line. The mean value of the graphitization background measured with bottled CO_2 gas (purity 4.8, Linde AG, Germany) is indicated in the figure by the dashed line.

To determine the graphitization background, bottled CO₂ (purity 4.8, Linde AG, Germany) was processed through the UGCS. The mean value graphitization background obtained from 12 measurements was 0.264 ± 0.084 pMC (47,700 BP). The “large” scatter is due to problems with 2 samples. But even without the 2 outliers, the mean value is 0.224 ± 0.040 pMC and, therefore, higher than one of the C1 standard samples, which indicates that our CO₂ either is not be completely free of ¹⁴C or there is a problem with contamination. Nevertheless, this mean value is satisfactory for our purpose and our system does not require modifications at the moment.

The reproducibility of processing was checked by using the measured values of the standards. The observed scatter agrees well with the expectations based on counting statistics (Figure 3). As a further test, a set of IAEA standards with different ¹⁴C concentrations was used, namely C5 (23.05 pMC) and C2 (41.14 pMC) (Rozanski et al. 1992). Up to now, we processed only 3 samples of each and found a reasonable agreement with the nominal values.

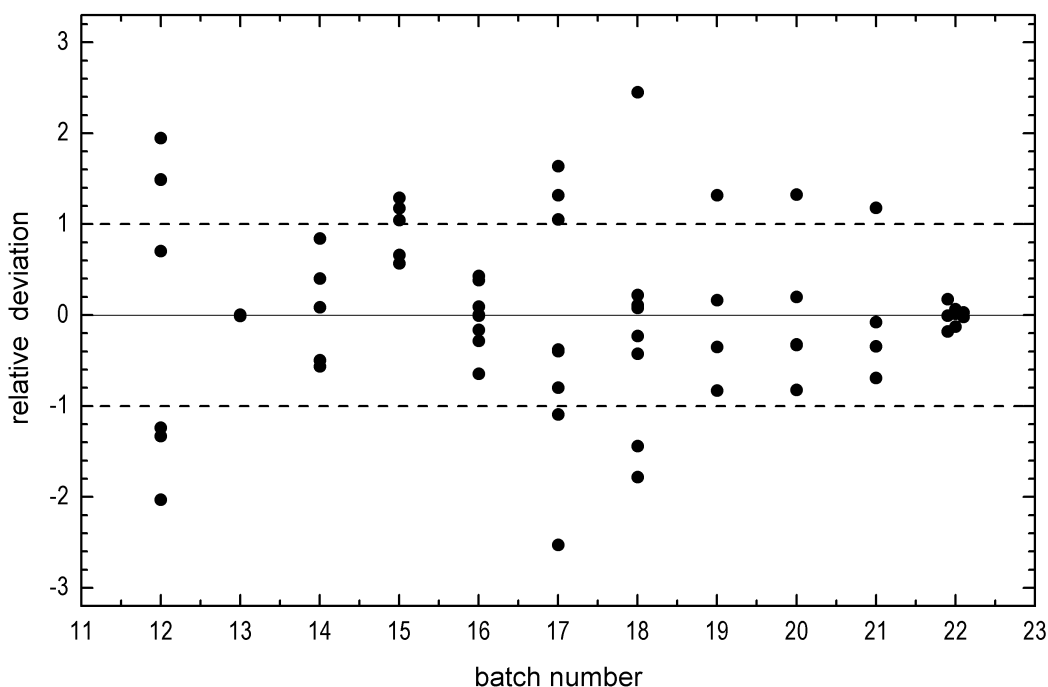


Figure 3 Precision of standards resulting from samples prepared in Jena, but measured at other facilities. Shown are the deviation of the single values from the mean value of the respective batch, divided by their statistical errors. Therefore, ± 1 corresponds to $\pm 1 \sigma$ and the percentage of 67% found within ± 1 is in good agreement with the expectation for the scatter due to statistical reasons alone.

LABORATORY MANAGEMENT SYSTEM

AMSIS (AMS Information System) is an in-house developed database system designed to allow an efficient management of the workflow in the ¹⁴C laboratory (see Figure 4). It was written in MS Visual Basic 6.0 and the data is stored in the institute database IBM DB2.

When samples are submitted to the laboratory, all sample information is stored in the database. Subsequently, AMSIS assists the laboratory staff in preparing lists of samples for the various stages of processing, i.e., chemistry, combustion, CO₂ extraction from gas samples, graphitization, and AMS measurement. It allows listing samples that are in the different stocks awaiting processing. The

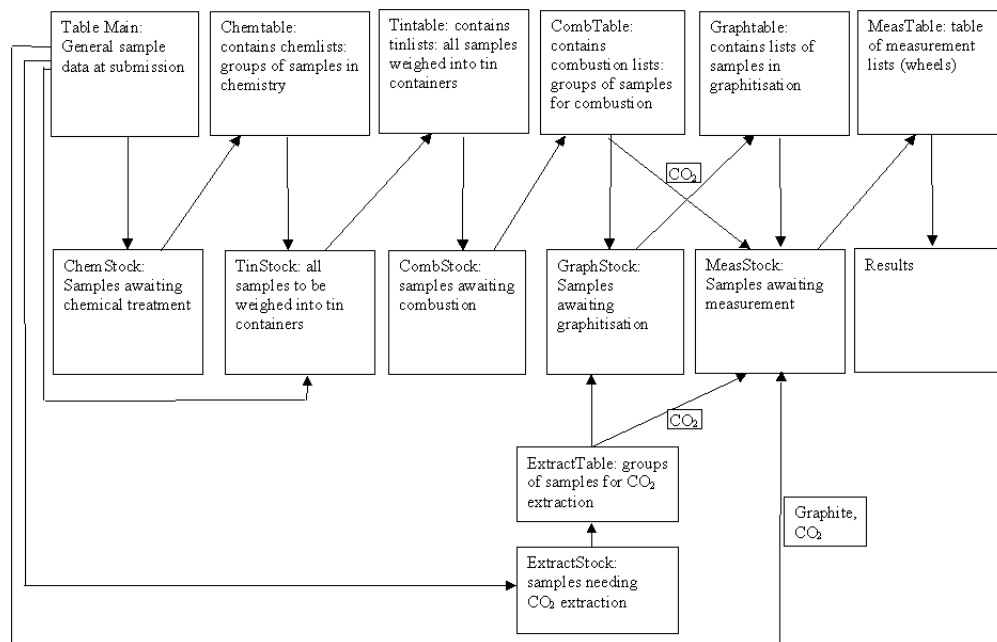


Figure 4 Logical flow chart diagram of AMSIS (AMS-Information System). The chart shows schematically the possible paths of the samples from submission to the final results. The upper rows indicates the different lists are stored. The lower rows show the different stocks from which samples can be selected for processing.

employment of AMSIS allows optimization of the process by selecting certain samples to be processed in 1 batch and determine their order. This, for example, allows minimizing the possibility of cross-contamination between samples (e.g. when a very old sample would be combusted after a very young one).

Due to the direct transfer of weight from the balances in the AMSIS database and the use of barcodes for labeling the samples, the probability of human errors is largely reduced. The barcodes are printed by AMSIS on barcode printers connected to PCs for the submission, for the test tubes in which samples are chemically processed, and for the Eppendorf vials containing the tin capsules with samples for combustion. After combustion, the CO_2 is stored in riglets that are numbered. If the sample is graphitized, the target wheel positions are stored in the database. AMSIS also allows a fast and transparent comparison according to various criteria and viewing of the “processing tree” of a given sample (the tree representing to what treatment a given sample was subjected).

AMSIS is currently being implemented in the laboratory.

AMS SYSTEM

At our laboratory, a 3MV Tandetron 4130 AMS ^{14}C system was installed by High Voltage Engineering Europa (HVEE), Netherlands, and passed all acceptance tests on 30 September 2003. The system is very similar to those operating in Groningen (Netherlands), Kiel (Germany), and Nagoya (Japan). All these systems operate at a terminal voltage of 2.5 MV and apply the so-called recombinator for simultaneous injection of the 3 carbon isotopes. Detailed information on layout, characteristics, and performance can be found elsewhere (Gott dang et al. 2001).

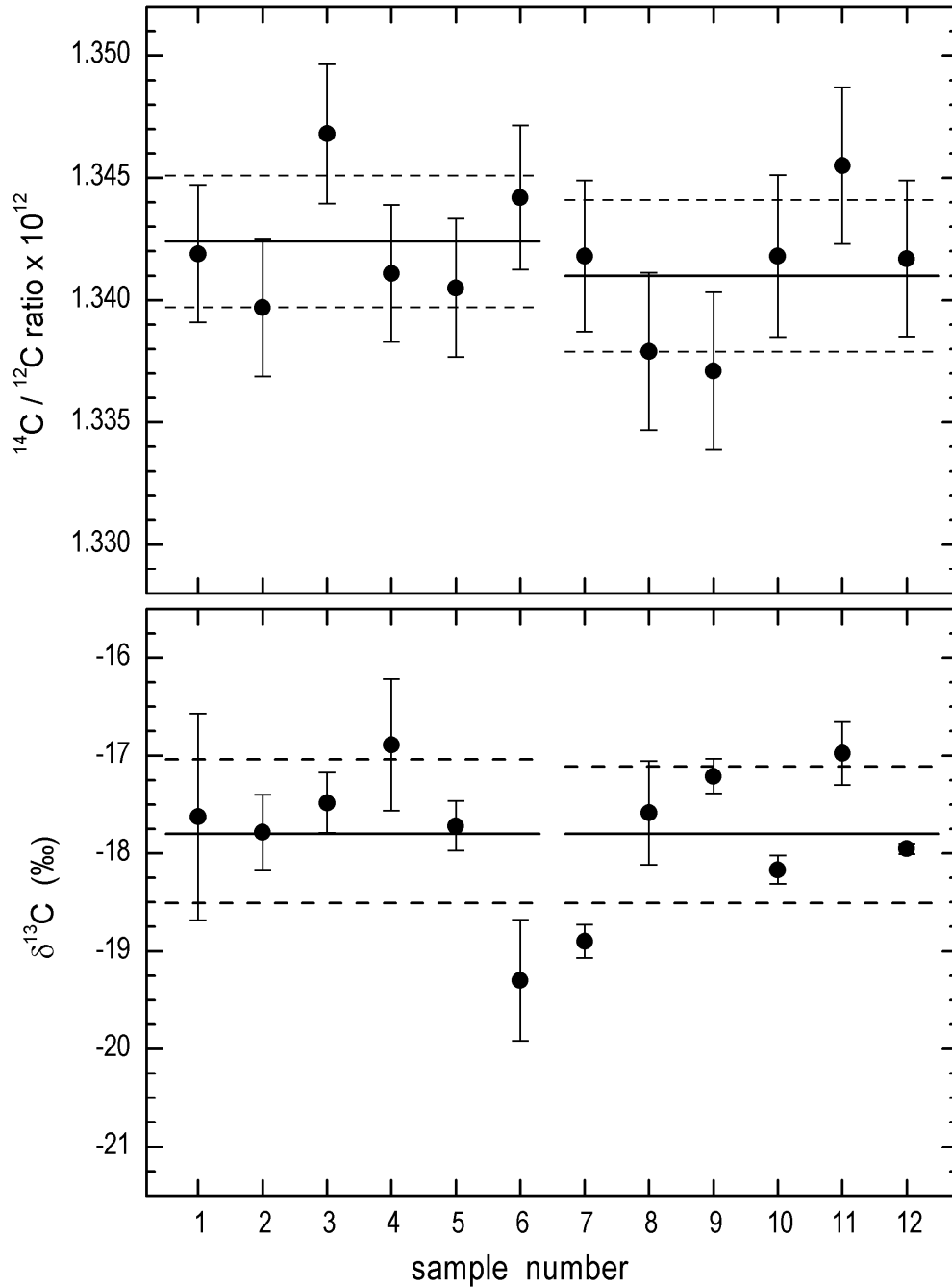


Figure 5 Results of the acceptance test of our system using Ox II targets prepared at the Leibniz AMS laboratory in Kiel, Germany. The upper diagram shows the mean $^{14}\text{C}/^{12}\text{C}$ ratios measured for each sample and the mean value for each set (i.e. each day). The error bars are calculated from counting statistics and the dashed lines show the 1- σ uncertainty for each set, determined by the scatter of the mean values of the single samples. The lower diagram shows the respective $\delta^{13}\text{C}$ values, normalized by setting the mean values of each set to -17.8‰ . The error bars are calculated from the scatter of the 4–5 runs of each samples. The solid lines show the mean values and the dashed lines their uncertainty of $\pm 0.73\text{‰}$ and $\pm 0.70\text{‰}$.

A major difference with the other AMS systems mentioned previously is the second injector with an ion source model SO-110, in addition to the standard ion source 846 B. The ion source SO-110 is a hybrid negative ion sputter source capable of handling solid graphite as well as gaseous CO_2 samples. For small samples (a considerable number of our samples), the higher efficiency of the gas source is particularly important (Bronk Ramsey et al. 1997). Detailed information on layout, characteristics, and performance can be found in Bronk Ramsey et al. (2004) and references therein. Compared with earlier HVEE AMS systems, the injectors have a higher ion optical acceptance for the isotopic carbon beams. Therefore, we can operate the system with higher ion currents of approximately $50\ \mu\text{A}$ analyzed $^{12}\text{C}^-$ under standard conditions.

The ability of the system with the ion source 846 B was demonstrated by measuring the $^{14}\text{C}/^{12}\text{C}$ and $^{13}\text{C}/^{12}\text{C}$ ratios of 2 sets of 6 standard samples (Ox II) precisely and reproducibly. Within 1 set of samples, the runs took place in a cyclical measuring sequence; in each sequence, each sample was measured for 540 s, giving approximately 50,000 ^{14}C counts. For the acceptance tests, 4–5 sequences per set were measured. Set 1 (samples 1 to 6) was measured on 15 September, and set 2 (samples 7 to 12) was measured on 18 September. The mean values of the sets reached a precision of 0.20% and 0.23%, with averaged statistical errors of 0.19% and 0.24%, respectively (see Figure 5). Furthermore, the system proved to have a low background below 54,000 BP. The used material from commercially available graphite rods has given the equal background level at other systems, too (Gott dang 2003).

The precision of the SO-110, operating with CO_2 gas, was tested analogous with 2 sets of 6 samples, measured on 29–30 September each set on 1 day, and reached a precision in $^{14}\text{C}/^{12}\text{C}$ of 0.48% and 0.44%, with averaged statistical errors of 0.44% and 0.39%, respectively. The lower precision (as compared to the 846 B ion source) is due to the lower currents. The background level was found to be at 43,000 BP.

CONCLUSION

At the ^{14}C Analysis Laboratory in Jena, a sample preparation line has been implemented successfully. This system has demonstrated all requirements needed for our applications. Because the aim of the lab is the support of the in-house scientists, the majority of the samples in the future will be soil and air samples. Our samples are expected to be small in terms of the carbon content, in particular the air samples, although they will have rather high ^{14}C concentrations. Therefore, our future development will concentrate on better precision for small samples.

ACKNOWLEDGEMENTS

We would like to thank HVEE for their cooperation during this project. We would like to especially thank Hans van Bergen for the excellent working atmosphere and the careful and precise installation of the new AMS system.

REFERENCES

- Aerts-Bijma AT, van der Plicht J, Meijer HAJ. 2001. Automatic AMS sample combustion and CO_2 collection. *Radiocarbon* 43(1):293–8.
- Bronk Ramsey C, Hedges REM. 1997. Hybrid ion sources: radiocarbon measurements from microgram to milligram. *Nuclear Instruments and Methods in Physics Research B* 123:539–45.
- Bronk Ramsey C, Ditchfield P, Humm M, Leach P. 2004. Using a gas ion source for radiocarbon AMS and GC-AMS. *Radiocarbon*, these proceedings.
- Gott dang A, Klein M, Mous DJW. 2001. Accelerator mass spectrometry at High Voltage Engineering Europe (HVEE). *Radiocarbon* 43(1):149–56.
- Nadeau M-J, Grootes PM, Voelker A, Bruhn F, Duhr A, Oriwall A. 2001. Carbonate ^{14}C background: Does it have multiple personalities? *Radiocarbon*

43(1):169–76.
Rozanski K, Stichler W, Gonfiantine R, Scott EM, Beukens RP, Kromer B, van der Plicht J. 1992. The IAEA

^{14}C intercomparison exercise 1990. *Radiocarbon*
34(3):506–19.

CAPABILITIES OF THE NEW SUERC 5MV AMS FACILITY FOR ^{14}C DATING

S Xu^{1,2} • R Anderson¹ • C Bryant³ • G T Cook¹ • A Dougans¹ • S Freeman¹ • P Naysmith¹ • C Schnabel¹ • E M Scott⁴

ABSTRACT. A new National Electrostatic Corporation (NEC) 5MV accelerator mass spectrometer became operational at the Scottish Universities Environmental Research Centre (SUERC) in July 2002. It has 2 Cs sputter negative ion sources: a 134-sample source (S1) for the routine measurement of all species, and a hybrid source (S2) with 40 spaces for radiocarbon measurements with either graphite or CO_2 samples. A number of performance tests on graphite samples have been carried out on both sources. A precision of better than 0.3% is feasible for modern samples on a routine basis. The ^{14}C background of the machine and the graphite preparation process blank are 0.04 ± 0.01 and 0.16 ± 0.05 pMC, respectively, indicating that ^{14}C dating back to ~50 kyr BP is possible. The normalized ^{14}C values for a series of reference materials agree well with the IAEA, TIRI, and FIRI consensus values. Routine measurement of ^{14}C has been underway since May 2003. Preliminary results of performance tests on the CO_2 gas ion source are also reported.

INTRODUCTION

A new NEC 5MV accelerator mass spectrometer (AMS) was installed at the Scottish Universities Environmental Research Centre in July 2002 (Freeman et al., forthcoming a, b). The SUERC spectrometer is equipped with 2 ion sources. One source (S1) accommodates up to 134 samples and is intended for the routine measurement of all species (^{10}Be , ^{14}C , ^{26}Al , ^{36}Cl , and ^{129}I), while the other 40-sample source (S2) is a hybrid ion source for radiocarbon measurements with either graphite or CO_2 samples. This paper presents the results for performance tests on graphite samples using both ion sources and also includes preliminary results for performance tests on CO_2 samples.

^{14}C Performance Tests on Solid Samples

A number of performance tests for ^{14}C have been performed for the SUERC AMS using the 2 ion sources. The tests have included the study of parameters such as precision, accuracy of normalization, background levels, as well as sample lifetime and throughput. The graphite targets were prepared by the 2 SUERC-hosted ^{14}C laboratories, NERC lab and SUERC lab, based on the method given by Slota et al. (1987). Each target is composed of 1–2 mg C mixed with 1–2 mg Fe powder. The injection energy of the extracted negative ions was 66 KeV. The measurements were performed at a terminal voltage: 4.5 MV; charge state: +4; total ion energy: 22.5 MeV; and Ar stripper gas pressure: 7–8 Torr. Each sample was scheduled for 5 measurements. For an individual measurement, the modern samples (e.g. oxalic acid and barley mash) were determined until statistical uncertainty reached 0.5% (40,000 ^{14}C counts), while the background graphite samples were counted for 9000 cycles (about 15 min). However, some samples were completed early if an assigned target value, based on the mean standard deviation of the 3 most recent measurements (0.5% for the modern samples and 10% for background samples), was reached.

For data reduction, an off-line data reduction program calculated 4 values from the measurement data: (1) mean sample isotopic ratio (a weighted average); (2) statistical uncertainty; (3) standard deviation of the mean (SDOM) uncertainty of isotopic ratios; and (4) χ^2 statistics. The program uses the χ^2 statistics to determine if the scatter of the measured isotopic ratios about the average is con-

¹Scottish Universities Environmental Research Centre, East Kilbride G75 0QF, United Kingdom.

²Corresponding author. Email: s.xu@suerc.gla.ac.uk.

³NERC Radiocarbon Laboratory, East Kilbride G75 0QF, United Kingdom.

⁴Department of Statistics, University of Glasgow, Glasgow G12 8QW, United Kingdom.

sistent with the counting statistic uncertainties of the measurements. Briefly, a sample passes the χ^2 test if its χ^2 statistics are less than or equal to the 5% χ^2 value which varies with degree of freedom, and fails the χ^2 test if its χ^2 statistics are greater than the 5% χ^2 value. For samples that pass the χ^2 test, the program sets the sample ratio equal to the weighted average of the measurement ratios and its uncertainty to the statistical uncertainty. However, for samples that fail the χ^2 test, the simple, not the weighted, average of the measurement ratios and SDOM are used for the sample ratio and its uncertainty, respectively, in subsequent calculations. Moreover, in this study, $\delta^{13}\text{C}$ values and uncertainties calculated from measured $^{13}\text{C}/^{12}\text{C}$ ratios were used for isotope fractionation correction for ^{14}C activity or age calculations.

Acceptance Tests

Three oxalic acid standards (OxII) and 3 barley mash samples were used for precision acceptance tests on source S2 (Table 1). In this batch, the $^{12}\text{C}^-$ currents were between 50 and 58 μA , with an accelerator 4+ particle transmission of 56%. The standard deviation (1σ) of the $^{13}\text{C}/^{12}\text{C}$ and $^{14}\text{C}/^{12}\text{C}$ ratios of the individual OxII sample was 0.2–0.4% and 0.2–0.3%, respectively. The latter is identical to the statistical uncertainty of 0.2–0.3%. Averaging the 3 OxII samples gives a precision of 0.15% and 0.13% for the $^{13}\text{C}/^{12}\text{C}$ and $^{14}\text{C}/^{12}\text{C}$ ratios, respectively. These results showed better than 3‰ precision on the individual and average values. In the case of the barley mash samples, precision on the $^{13}\text{C}/^{12}\text{C}$ and $^{14}\text{C}/^{12}\text{C}$ ratios of the individual samples was 0.2% and 0.4%, respectively. These 3 samples yielded better than 3‰ precision not only on the average $^{14}\text{C}/^{12}\text{C}$ ratio (0.26%) but also on the normalization value (0.27%). It should be pointed out that a repeat of the test at high currents (about 80 μA), but with reduced accelerator 4+ particle transmission (50%), gave similar results.

The same performance tests were also carried out on source S1. The negative currents extracted from S1 source were 30–35 μA , slightly lower than those from S2. The average accelerator 4+ particle transmission was 56%. Following the same experimental conditions used in S2, the S1 source gave similar precision for the $^{14}\text{C}/^{12}\text{C}$ and $^{13}\text{C}/^{12}\text{C}$ ratios as observed in S2 source. Therefore, the acceptance tests demonstrated that our new AMS system can perform high-precision measurements of $^{14}\text{C}/^{12}\text{C}$ and $^{13}\text{C}/^{12}\text{C}$ ratios.

System Background

A natural graphite sample (Alfa Aesar graphite powder 100 mesh with a purity of 99.9995%) was measured to assess machine ^{14}C background, while doublespar (TIRI F) and an interglacial wood (BK-ow) were used to assess system contamination. These materials were always placed adjacent to an OxII or modern sample to monitor any possible cross-contamination between the sample targets. The observed $^{14}\text{C}/^{12}\text{C}$ ratios of Alfa Aesar graphite were generally less than 5×10^{-16} , corresponding to 0.03 pMC (Table 1), which is equivalent to a ^{14}C age of 64 kyr. This result clearly shows that machine background and source cross-contamination are negligible.

A large volume of CO_2 was produced from doublespar and interglacial wood to minimize contamination during CO_2 production. From this volume, sub-samples of CO_2 equivalent to 1–2 mg C were graphitized. The doublespar yielded 0.16 ± 0.06 pMC, while the interglacial wood yielded 0.16 ± 0.05 pMC. This indicates that a slight contamination has occurred during the graphite target preparation process. Based on the calculation given by Donahue et al. (1990), a ^{14}C dating limit of 51 kyr was obtained.

Table 1 Precision of ^{14}C acceptance test measurement on 19 May 2003 (Source S2)^a.

Materials	^{12}C - (μA)	^{14}C counts (atoms)	$^{13}\text{C}/^{12}\text{C}$ ($\times 10^{-2}$)	$\delta^{13}\text{C}$ (‰)	$^{14}\text{C}/^{12}\text{C}^{\text{b}}$ ($\times 10^{-12}$)	^{14}C (pMC)
Oxalic acid	50	121,338	1.0641 \pm 0.0021		1.2094 \pm 0.0035	
Oxalic acid	52	121,941	1.0667 \pm 0.0045		1.2074 \pm 0.0035	
Oxalic acid	53	248,613	1.0643 \pm 0.0021		1.2063 \pm 0.0025	
<i>Mean for above 3 samples</i>			1.0650 \pm 0.0016	-17.8 \pm 1.5	1.2077 \pm 0.0016	134.07 \pm 0.27
<i>Relative deviation (%)</i>			0.15		0.13	
<i>Statistical uncertainty (%)</i>		0.14				
Barley mash (BBM-48)	50	122,202	1.0557 \pm 0.0019	-26.4 \pm 1.4	1.0426 \pm 0.0043	115.78 \pm 0.60
Barley mash (BBM-49)	55	122,557	1.0587 \pm 0.0023	-23.5 \pm 1.1	1.0474 \pm 0.0039	116.31 \pm 0.56
Barley mash (BBM-50)	58	122,717	1.0584 \pm 0.0021	-23.8 \pm 1.5	1.0426 \pm 0.0044	115.77 \pm 0.61
<i>Mean for above 3 samples</i>			1.0573 \pm 0.0014	-24.6 \pm 1.6	1.0442 \pm 0.0028	115.95 \pm 0.31
<i>Relative deviation (%)</i>			0.13		0.26	0.27
Alfa Aesar graphite	50	134	1.0781 \pm 0.0016		0.00030 \pm 0.00003	0.034 \pm 0.003

^aNo data blocks were rejected.

^bNo background was subtracted and isotope fractionation was corrected using AMS $\delta^{13}\text{C}$.

^{14}C Accuracy

A series of well-characterized samples were measured to assess the accuracy of the ^{14}C measurements. These included IAEA C6 (ANU sucrose) and barley mash (TIRI A) to assess accuracy and precision of modern samples, while IAEA C2, C5, C7, C8, Belfast cellulose (FIRI I), and 96 humin (in-house standard) provided samples with a range of ages for similar tests. The results showed that most of the individual measurements agreed with the consensus values within the 1- σ uncertainty margin. In Table 2, average measured ^{14}C values are compared with the consensus values. It is clear that the relative ^{14}C age differences between the measured and the consensus values are all in the range from -0.4 to 0.5%.

Table 2 Normalization of reference materials.

Code	Materials	Nr of samples	Measured ^{14}C		Consensus $^{14}\text{C}^{\text{a}}$		Relative difference (%)
			Activity (pMC)	Age (BP)	Activity (pMC)	Age (BP)	
IAEA C6	Sucrose	5	150.31 \pm 0.39	—	150.61 \pm 0.11	—	-0.20
TIRI A	Barley mash	25	116.35 \pm 0.52	—	116.35 \pm 0.0084	—	0.00
IAEA C7	Oxalic acid	3	49.65 \pm 0.29	—	49.54 \pm 0.13	—	0.22
IAEA C2	Travertine	3	41.13 \pm 0.27	—	41.14 \pm 0.03	—	-0.02
IAEA C5	Wood	4	23.15 \pm 0.11	—	23.05 \pm 0.02	—	0.43
IAEA C8	Oxalic acid	3	15.11 \pm 0.08	—	15.03 \pm 0.18	—	0.53
FIRI I	Belfast cellulose	16	—	4494 \pm 35	—	4485 \pm 6	0.20
96H	Humin	18	—	3365 \pm 37	—	3379 \pm 66	-0.41
TIRI F	Doublespar	41	0.16 \pm 0.06	52,000	0.180 \pm 0.006	—	—
BK-ow	Interglacial wood	23	0.16 \pm 0.05	52,000	—	—	—
Alfa Aesar	Natural graphite	22	0.04 \pm 0.01	63,000	—	—	—

^aConsensus values for IAEA C2, C5, and C6 are from Rozanski et al. (1992), IAEA C7 and C8 from Clercq et al. (1998), TIRI A and TIRI F from Gulliksen and Scott (1995), and FIRI I from Scott (2003).

In addition to the performance tests listed above, $\delta^{13}\text{C}$ values measured with the SUERC AMS were compared with those determined using dual inlet mass spectrometers (VG OPTIMA and MICRO-MASS SIRA 10). AMS $\delta^{13}\text{C}$ values were obtained from the AMS-measured $^{13}\text{C}/^{12}\text{C}$ ratio of the sample normalized to the measured $^{13}\text{C}/^{12}\text{C}$ ratio of the OxII standard materials. Figure 1 shows a comparison of $\delta^{13}\text{C}$ values from the 2 methods for a typical batch of measurements. In this batch, the

AMS $\delta^{13}\text{C}$ values for 102 of the total of 104 samples agreed with the dual inlet MS $\delta^{13}\text{C}$ values within $\pm 5\%$, which brings about a maximum of ± 40 yr difference when applying the $\delta^{13}\text{C}$ correction to the $^{14}\text{C}/^{13}\text{C}$ ratio in ^{14}C age calculation. At present, the reason for the difference is not quite clear and more precise measurements over a long term need to be done; however, we expect that the AMS $\delta^{13}\text{C}$ values can potentially be used for isotopic fractionation correction of the ^{14}C ages, as has previously only been used in very a few AMS laboratories (e.g. Bonani et al. 1987).

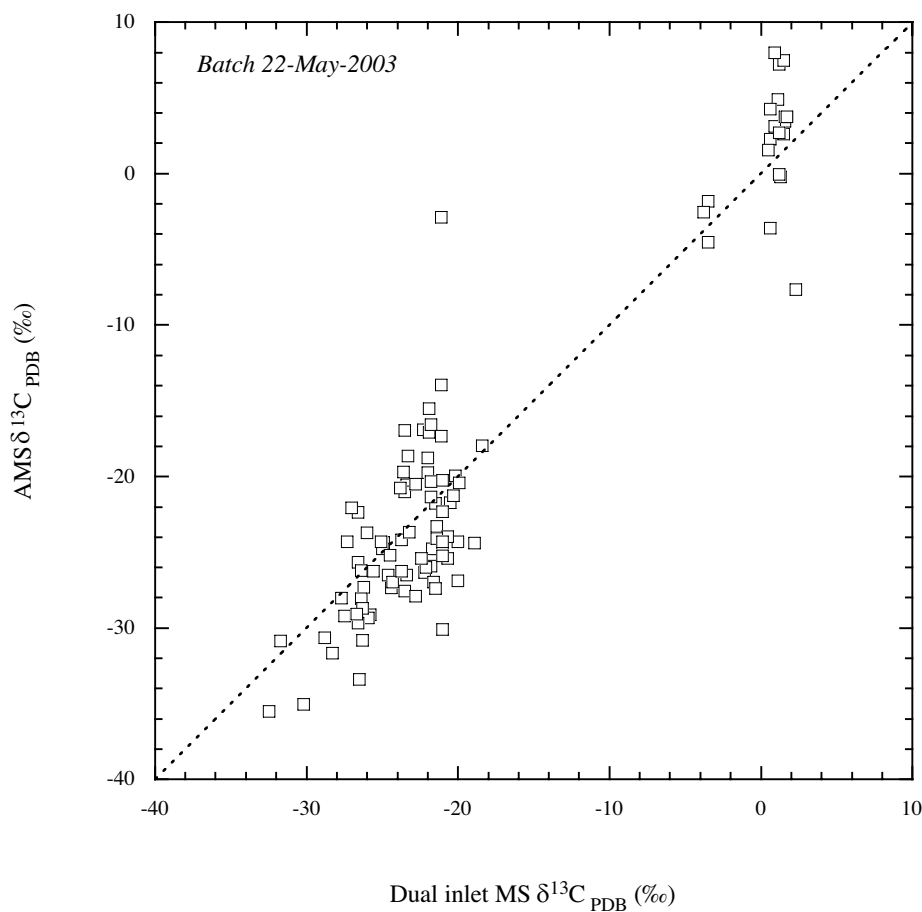


Figure 1 Comparison of $\delta^{13}\text{C}$ values measured with the SUERC AMS system and dual inlet isotope mass spectrometer (IRMS)

PRELIMINARY PERFORMANCE OF THE GAS ION SOURCE

Although the full performance tests on the gas ion source have not yet been completed, a brief description of the gas ion source with the preliminary performance results are reported as follows. The CO_2 sample is introduced into the 40-sample ion source (S2) by the gas handling system (Figure 2). This handling system uses a manifold and gas flow control system, which applies in 10 individual gas sample containers (bellows). As the bellows (116 cm^3) are much larger in volume than the manifold (9 cm^3), it can be ensured that little of the gas is wasted when the common part of the manifold is evacuated before another gas sample is introduced. The manifold is connected to the source by a 0.25 mm i.d. capillary of 1.2 m length, giving a constant gas flow for a given pressure. The pressure is measured with a pressure transducer (400 mbar) and this is used to regulate the bellows' volume.

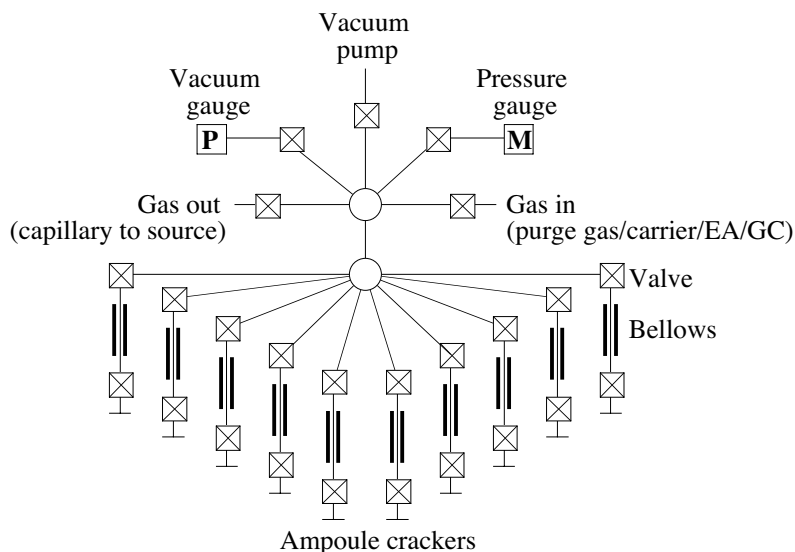


Figure 2 Diagram of the gas handling system

The sample holder used for the gas sample in the ion source is modified from that used for a solid sample by inserting a piece of titanium into the sample holder. The holders are fixed in the sample wheel where the gas tube is pressed on the back of the sample holder. The CO_2 is directly fed through the gas tube to the holder where it is passed over and adsorbed onto the titanium; sputtering by the Cs beam generates negative ions of carbon and oxygen. The targets become sufficiently contaminated with the carbon from the gas so that they must be replaced for each sample.

In operation, gas flow and current stabilization were firstly performed in order to keep the source performance the same for each sample. A typical $10 \mu\text{A}$ of C^- could be extracted. To determine the CO_2 to C^- efficiency, we used about $250 \mu\text{g}$ of carbon for a 2-hr measurement, stabilized at $6 \mu\text{A}$. This represents an overall efficiency of about 2% for negative ion production. The background beam current, however, was less than 40 nA . These values are comparable to previous reports (e.g. Middleton et al. 1989; Ramsey and Hedges 1997).

In the first measurement with the $^{12}\text{C}^-$ currents ranging from 7 to $10 \mu\text{A}$ and an average accelerator $4+$ particle transmission of 57%, the standard deviations (1σ) of the $^{14}\text{C}/^{12}\text{C}$ ratios for a single sample, 5 measurements for OxII and doublespar, and 3 for barley mash, were 0.6%, 18%, and 1.1%, respectively, which is comparable to the statistical uncertainties. On the other hand, the precision on the $^{13}\text{C}/^{12}\text{C}$ ratios for the 3 samples was 0.2–0.3%. Encouragingly, these first results imply that precision for an individual sample is comparable between graphite and the gas source.

CONCLUSION

Since May 2003, the fully-automated and high-throughput SUERC AMS system has been used routinely for ^{14}C dating. Measurements with modern samples have shown that a precision of better than 0.3% is obtainable. The levels of background for the AMS machine together with the sample preparation process are generally 0.16 pMC, indicating a ^{14}C dating limit of 51 kyr. Further performance tests on the gas ion source are in progress.

ACKNOWLEDGEMENTS

This work is supported by NERC JIF award (GR3/J0001): an AMS facility for ^{14}C and cosmogenic isotope applications. We are grateful to A Tait of SUERC and R Kitchen, G Klody, R Loger, M Sundquist of NEC for their assistance during the installation and normal operation of the SUERC AMS. We thank A Smith and R Sparks for their valuable reviews.

REFERENCES

- Bonani G, Beer J, Hofmann H, Synal HA, Suter M, Wölfli W, Pfliederer C, Kromer B, Junghans C, Münnich KO. 1987. Fractionation, precision and accuracy in ^{14}C and ^{13}C measurements. *Nuclear Instruments and Methods in Physics Research B* 29: 87–90.
- Clercq ML, van der Plicht J, Gröning M. 1998. New ^{14}C reference materials with activities of 15 and 50 pMC. *Radiocarbon* 40(1):295–7.
- Donahue DJ, Linick TW, Jull AJT. 1990. Isotope-ratio and background corrections for accelerator mass spectrometry radiocarbon measurement. *Radiocarbon* 32(2):135–42.
- Freeman S, Bishop P, Bryant C, Cook G, Fallick A, Harkness D, Metcalfe S, Scott M, Scott R, Summerfield M. Forthcoming a. A new environmental sciences AMS laboratory in Scotland. *Nuclear Instruments and Methods in Physics Research B*.
- Freeman S, Xu S, Schnabel C, Dougans A, Tait A, Kitchen R, Klody G, Loger R, Pollock T, Schroeder J, Sundquist M. Forthcoming b. Initial measurements with the SUERC 5MV spectrometer. *Nuclear Instruments and Methods in Physics Research B*.
- Gulliksen S, Scott EM. 1995. Report of the TIRI workshop, Saturday, 13 August 1994. *Radiocarbon* 37(2): 820–1.
- Middleton R, Klein J, Fink D. 1989. A CO_2 negative ion source for ^{14}C dating. *Nuclear Instruments and Methods in Physics Research B* 43:231–9.
- Ramsey CB, Hedges REM. 1997. Hybrid ion sources: radiocarbon measurements from microgram to milligram. *Nuclear Instruments and Methods in Physics Research B* 123:539–45.
- Rozanski K, Stichler W, Gonfiantini R, Scott EM, Beukens RP, Kromer B, van der Plicht J. 1992. The IAEA ^{14}C intercomparison exercise 1990. *Radiocarbon* 34(3):506–19.
- Scott EM. 2003. The Fourth International Radiocarbon Intercomparison (FIRI). *Radiocarbon* 45(2):135–291.
- Slota PJ Jr, Jull AJT, Linick TW, Toolin LJ. 1987. Preparation of small samples for ^{14}C accelerator targets by catalytic reduction of CO . *Radiocarbon* 29(2):303–6.

DIRECT COUPLING OF AN ELEMENTAL ANALYZER AND A HYBRID ION SOURCE FOR AMS MEASUREMENTS

Thomas Uhl¹ • Wolfgang Kretschmer • Wolfgang Luppold • Andreas Scharf

Physikalisches Institut, Universität Erlangen-Nürnberg, 91058 Erlangen, Germany.

ABSTRACT. The requests to measure many samples, and samples with very low carbon masses, make it necessary to develop new techniques in sample handling to accelerate sample preparation and to eliminate carbon contamination. Our 40 MC-SNICS was recently modified to a hybrid ion source. To run the hybrid ion source with a gas parameter, settings were studied and a gas handling system for the direct coupling of an elemental analyzer and a gas ion source was developed.

INTRODUCTION

The Erlangen group uses the accelerator mass spectrometry (AMS) technique for radiocarbon dating. The ratio of ^{14}C to ^{12}C is determined from graphite targets with an ion-sputter source (40 MC-SNICS). Restricting the use of solid targets is the demand for samples of carbon masses of at least 100 μg . Another disadvantage is the time-consuming and labor-intensive step of the graphitization. Motivated by projects in sectors of environmental science, where only small samples are provided (e.g. $\sim 10\ \mu\text{g}$ after a collection time of 1 yr), and life science, where many samples have to be measured, the ion source was modified by National Electrostatic Corporation (NEC) to a hybrid ion source. With this kind of ion source, it is possible to measure graphite samples as well as CO_2 samples. Due to the direct use of CO_2 , the usual graphitization and formation of solid sputter targets is not necessary. Because of the higher efficiency of gas ion sources (Bronk Ramsey and Hedges 1997) and less contamination with carbon due to the minimized preparation line, it should be possible to measure samples with carbon masses down to 1 μg . The difficulty is the handling of these small samples. In Erlangen, an elemental analyzer is used for the combustion of samples. The development of a gas handling system for a direct coupling of the elemental analyzer and the hybrid ion source for online measurements is explained in the following.

DEVELOPMENT OF A SYSTEM TO FEED GAS INTO THE HYBRID ION SOURCE

The first aim was to reach a maximum efficiency of produced carbon ions from the CO_2 samples. To determine and investigate carbon ion affecting parameters systematically, a gas-feeding system was designed. As shown in Figure 1, helium (carrier gas for CO_2) is sent to a 3-way valve which leads the gas into the ion source or into a separate vacuum system for flushing the gas-feeding system. The low flow (0.1 standard mL per minute—sccm) is pre-adjusted by the pressure of the helium and the geometry (length, inner diameter) of the glass capillary. Possible flow variations from temperature or pressure variations are regulated by a mass-flow controller. The glass capillary enables the easy tuning of He and CO_2 pressure and switching of the CO_2 valve at ground potential during operation of the ion source at high voltage. The 3-way valve at the high potential of the ion source is switched by a pneumatic actuator. CO_2 is metered (in the range of percentage) in a micro-volume Y-connector into the helium flow through a second glass capillary by the pressure difference between the CO_2 and the helium. The response time of the gas-feeding system due to switching of valves and changing of CO_2 pressure is given in the Table 1. The fast response times were reached by using short transportation ways and very low dead volume connections.

¹Corresponding author. Email: Thomas.Uhl@physik.uni-erlangen.de.

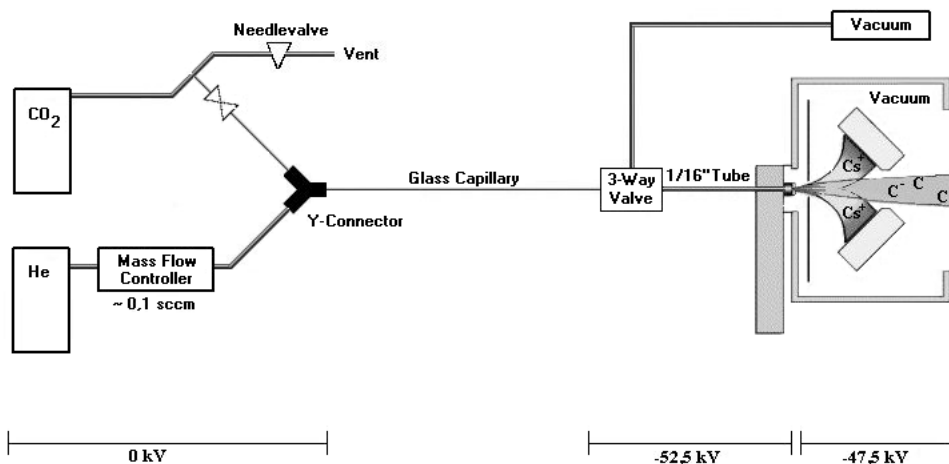


Figure 1 The gas-feeding system

Table 1 Response time of the gas-feeding system.

Operation	Time
Switching of 3-way valve	~10 s
Opening CO ₂ valve	~20 s
CO ₂ pressure changes	~20 s
Decreasing of ¹² C ⁻ current to offset current after closing CO ₂ valve	~5 min
Decreasing of ¹² C ⁻ current to offset current after reducing CO ₂ pressure beneath He pressure	~40 s

STUDY OF CATHODE SURFACES FOR GAS SAMPLES

After installation of the gas-feeding system, the geometry of the cathodes for the production of negative carbon ions was optimized. Two different cathode types are offered by NEC, one with a “flat” surface and a second with a “crater” surface (Figure 2). These cathodes differ from the cathodes for solid samples by using a titanium insert in the cathode holder. They are fixed in a cathode wheel where the gas tube is pressed on the backside of the cathode. The CO₂-He mixture is fed directly through the gas tube to the cathode where it passes the titanium insert. The titanium reduces the CO₂ to carbon and oxygen, and carbon ions are produced by cesium sputtering. The maximum obtainable ¹²C⁻ current for a pre-set cesium offer, the derived efficiency (ratio of the produced carbon ions to the CO₂ molecules introduced into the ion source), and the background current from unused cathodes are given in Table 2. The background current does not depend whether another gas target nearby was used before or not.

Table 2 Investigations of cathode surfaces.

Cathode	Maximum ¹² C ⁻ current (μA)	Maximum efficiency	Background ¹² C ⁻ current (nA)
Flat	3.5	~0.9	14
Crater	4.2	~3.4	100

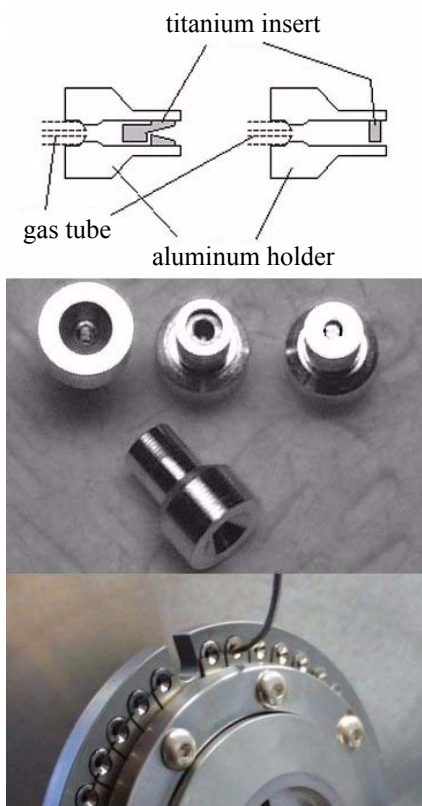


Figure 2 Comparison of 2 different styles of cathodes

Figure 3 shows a $^{12}\text{C}^-$ background-current plot of direct-sputtered gas cathodes over time. As a result of Figure 3, there must be a cleaning (sputtering) process of the titanium surface of about 2 to 3 min before using CO_2 samples.

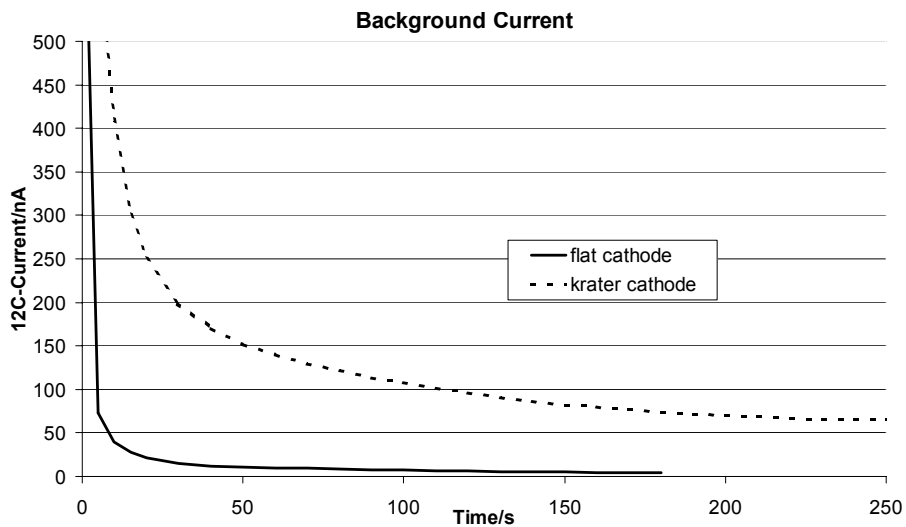


Figure 3 Background $^{12}\text{C}^-$ current over time

DETERMINATION OF OPTIMUM PARAMETER SETTINGS FOR THE GAS ION SOURCE

Due to the much higher efficiency, only the “crater” cathodes were taken for subsequent investigations. The following critical parameters for the production of the negative carbon ions have been tested: He flow, Cs oven temperature, electric power of the ionizer, and CO₂ flow (see Figure 4a–d).

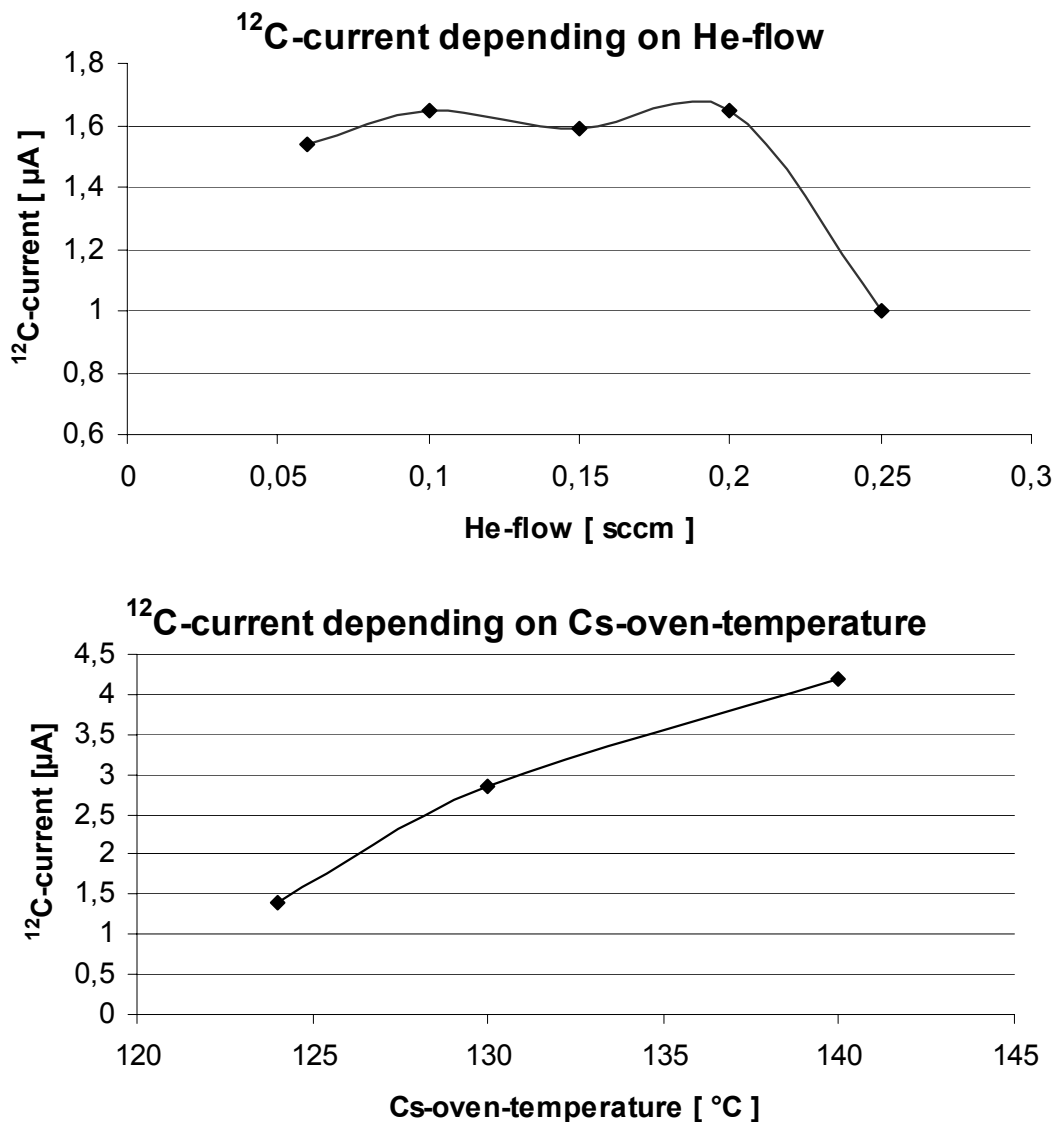


Figure 4 (a–b) Plots of ¹²C⁻ current versus He flow and Cs oven temperature, respectively.

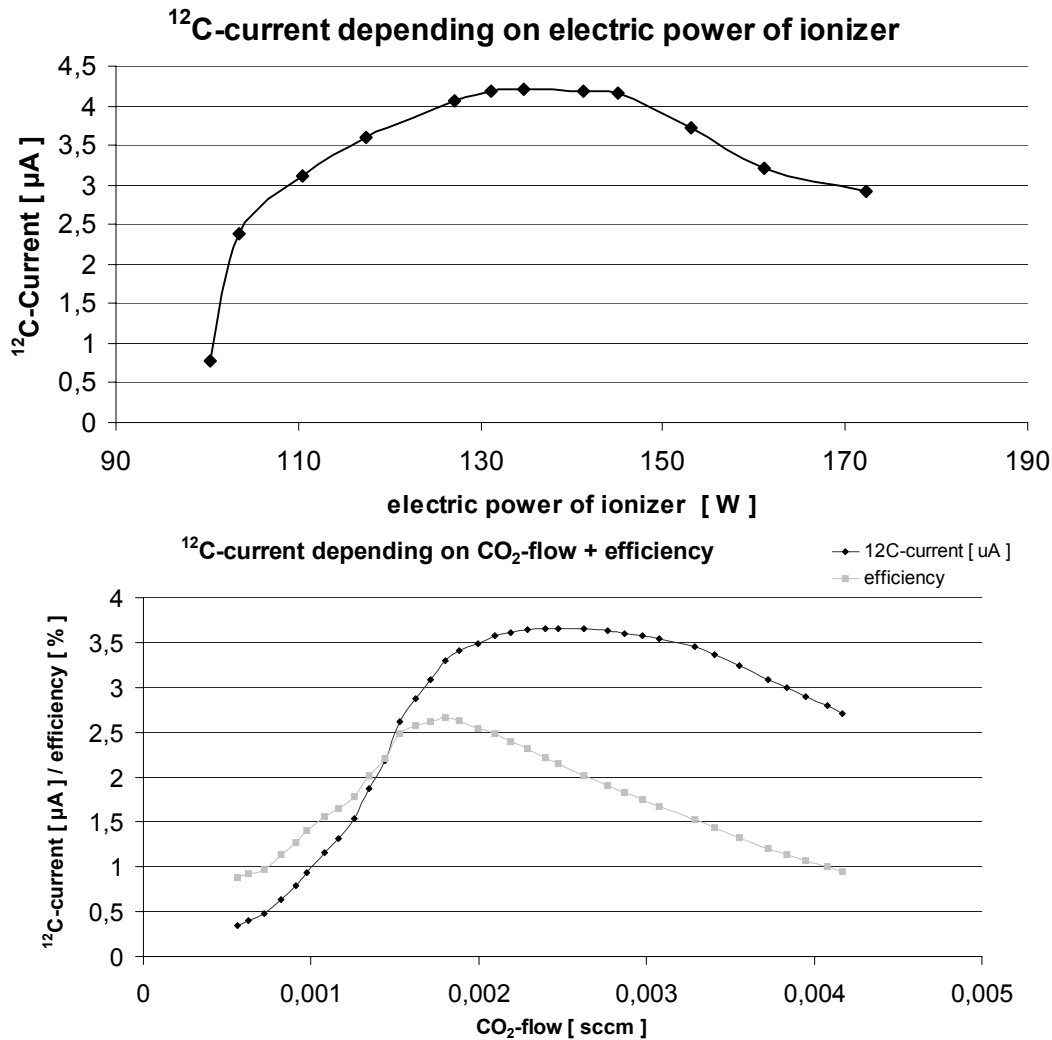
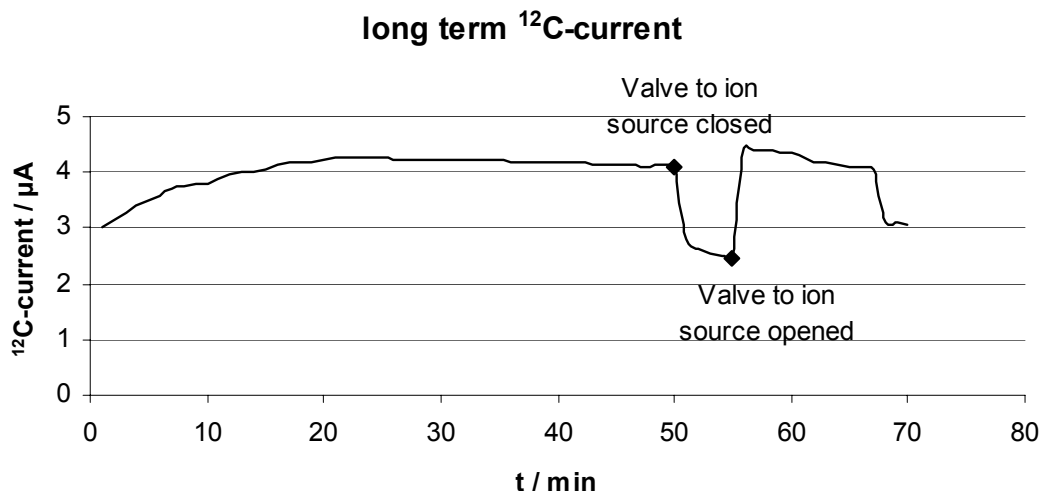


Figure 4(c-d) Plots of ¹²C⁻ current and electric power of ionizer and CO₂ flow and efficiency, respectively.

The conclusion from Figure 4a-d is:

- He flow should not exceed 0.2 sccm;
- The higher the Cs oven temperature, the higher the ¹²C⁻ current; we did not exceed the 140 °C because it is our aim to reach a maximum efficiency with a minimum use of Cs in order to reduce the contamination of the ion source with Cs;
- The optimum electric power of the ionizer is ~140 W;
- Maximum efficiency is reached at a CO₂ flow of ~0.002 sccm (0.001 sccm = 0.53 µg [carbon/min]).

Figure 5 shows a plot of the long-term sputtering of a cathode with a constant CO₂ flow. It shows a continuous increasing of the ¹²C⁻ current for 20 min, until it remains at a constant level. Closing of the 3-way valve causes a drop of the current only to 50% of maximum (so every cathode can only be used for 1 gas sample). The current rises back to the previous value after opening the valve again.

Figure 5 Long-term ^{12}C -current plot

DEVELOPMENT OF A TECHNIQUE TO HANDLE CO_2 SAMPLES: 'CRYOGENIC STORAGE AND RELEASE'

The standard method used in Erlangen for the formation of solid targets is to combust carbonaceous samples with an elemental analyzer (EA), to collect the CO_2 cryogenically, to graphitize it, and to press it into the cathode holder.

A direct coupling of the EA and the hybrid ion source skips the last 2 steps. Therefore, a method had to be developed to link the EA and the ion source that resolves 2 problems:

1. As learned from Figure 4a, the maximum helium flow is 0.2 sccm, but the EA provides a helium flow of 100 sccm.
2. CO_2 from the EA is only provided for ~ 40 s. For the optimum CO_2 flow of 0.002 sccm and a sample size of 10 μg , a constant flow should last at least 10 min.

The idea to solve these problems (similar to the method described in Bronk Ramsey et al. 2004) was to store the CO_2 that comes from the EA cryogenically and then to release it subsequently into helium with a flow rate of 0.1 sccm. Figure 6a–b demonstrates the principle of the “cryogenic storage and release” technique. In Figure 6a, the valves V1 and V2 are open so that the CO_2 coming from the EA with the high helium flow of 100 sccm is frozen in the “freezing tube” by continuously elevating a dewar vessel with liquid nitrogen. The complete freezing is done within 90 s and CO_2 is frozen over the whole inner surface of the freezing tube. Then, V1 and V2 are closed and V3 and V4 are opened (see Figure 6b). Now, a low helium flow of 0.1 sccm is flowing through the freezing tube into the ion source. By slowly lowering the dewar vessel, the CO_2 is continuously released into that helium flow and transported into the ion source. With this technique, the CO_2 content in the helium can be adjusted just by changing the lowering speed. Because of the easier handling, this interface was tested first in a direct coupling of the EA (NC 2500) and a stable mass spectrometer (see Figure 7). A typical CO_2 current plot measured with the stable mass spectrometer is shown in Figure 8. The black-filled curve is the measurement with the open-split method (Bronk Ramsey and Hedges 1994a)—typically used for GC-AMS applications—where only $\sim 10\%$ of the oxidized carbon is used for measurement. The second printout was recorded with the cryogenic storage and release technique. The black filled curve shows a steep rise followed by an exponential decrease, whereas the second printout shows an

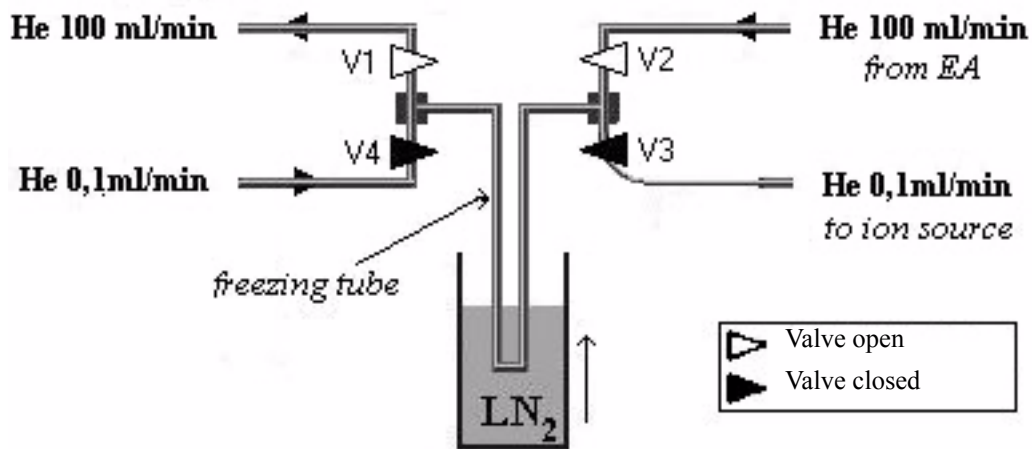


Figure 6a Cryogenic storage of CO₂

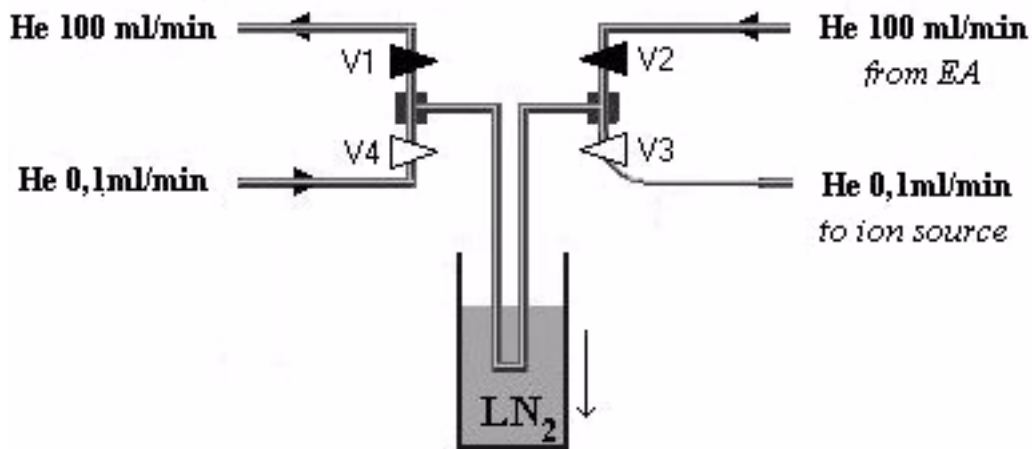


Figure 6b Continuous release of CO₂

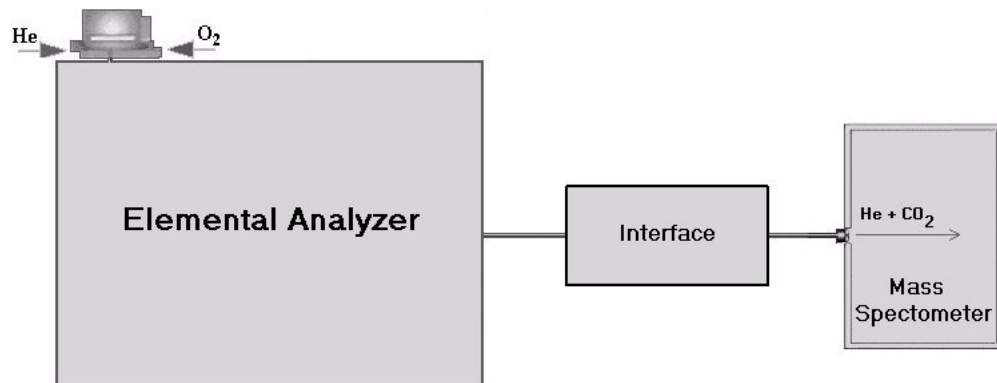


Figure 7 Set-up for testing an interface between the EA and the ion source

exponential increase followed by a steep fall. This “time inversion” is a consequence from freezing the CO₂ continuously in a forward direction in the freezing tube and subsequent releasing of the CO₂ (beginning with CO₂ that was frozen last) backwards into the mass spectrometer. Also, the second printout is lengthened by a factor of 10 (~40 s to ~400 s) and this is achieved by releasing the CO₂ slowly but continuously into the He flow that leads it into the mass spectrometer.

COUPLING OF THE ELEMENTAL ANALYZER AND THE HYBRID ION SOURCE

The last step was to perform the direct coupling of the elemental analyzer (NC 2500) and the hybrid ion source (modified 40 MC-SNICS) by the interface that is explained above. Figure 9 shows the concept and the realization. A current plot from an online measurement is given in Figure 10. The curve is the convolution of the response of the ion source and the response of the cryogenic storage and release technique. First, the current increases according to Figure 8, but when the CO₂ flow

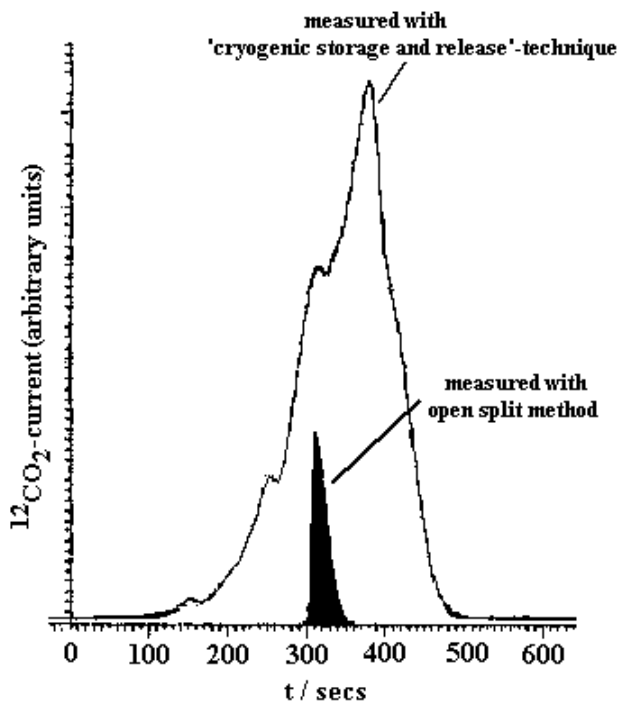


Figure 8 Increasing ¹²CO₂ current

exceeds 0.003 sccm, the current is falling as expected from the measurements in Figure 4d. When the CO₂ flow decreases, we see this behavior vice versa followed by an exponential decrease of the carbon current as expected from the curve in Figure 5. The very first online measurements of well-known reference materials are given in Figure 11 in the sequence of the measurements. The gray bars indicate the measured 1- σ range and the black bar over every gray bar marks the actual value of the reference material. The cryogenic storage and release technique proved of value as a GC-AMS online system to measure samples with carbon masses of 1–10 μ g (see the estimated combusted carbon mass of every standard, given in brackets). Note that the graphite samples have severe deviations from the actual value compared to the other standards. This could be due also to the fact that no background corrections have been made as to the measuring of modern material before every

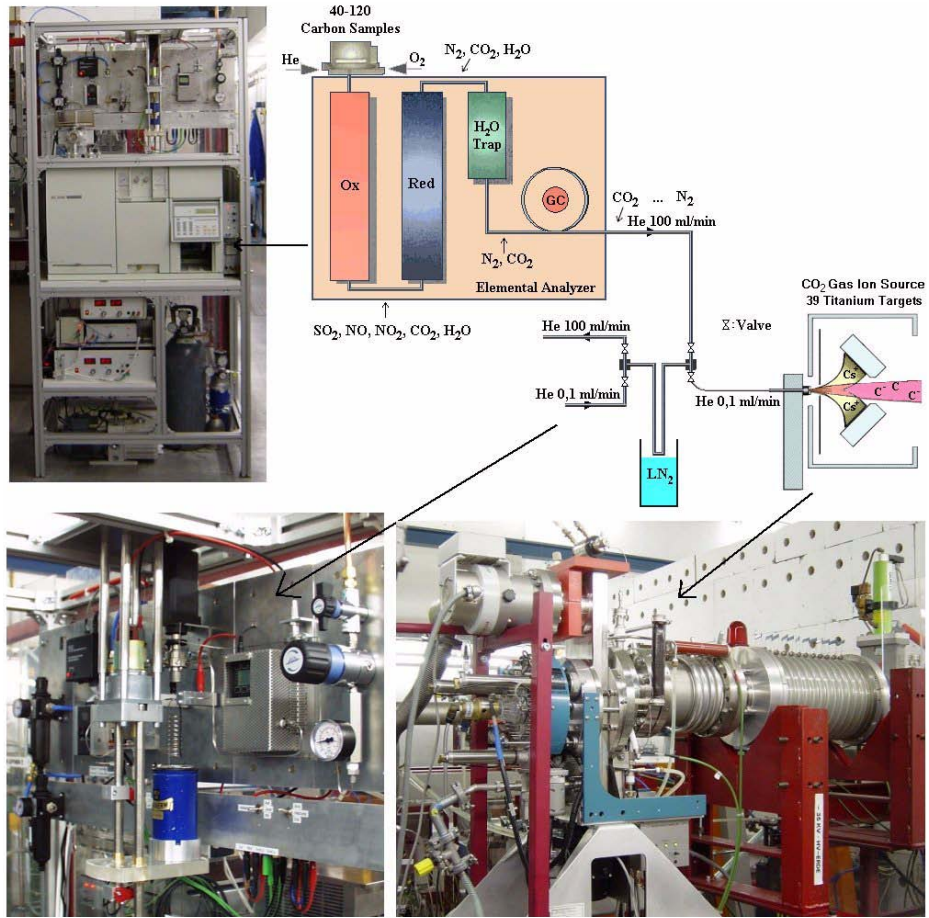


Figure 9 Coupling of EA and hybrid ion source

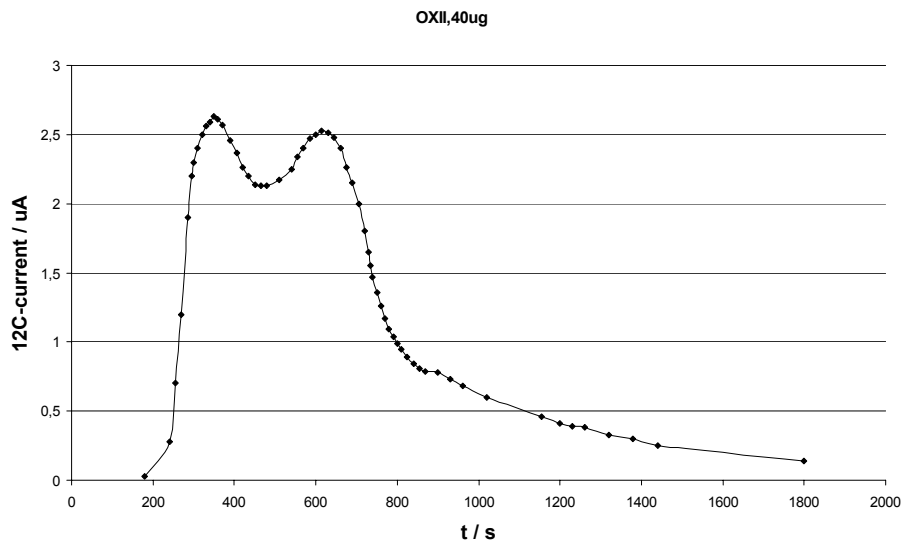


Figure 10 ¹²C⁻ current of a gas sample

graphite sample. The last indicates the level of cross-contamination. The measurement of the background curve for the carbon mass and an investigation of cross-contamination is in progress.

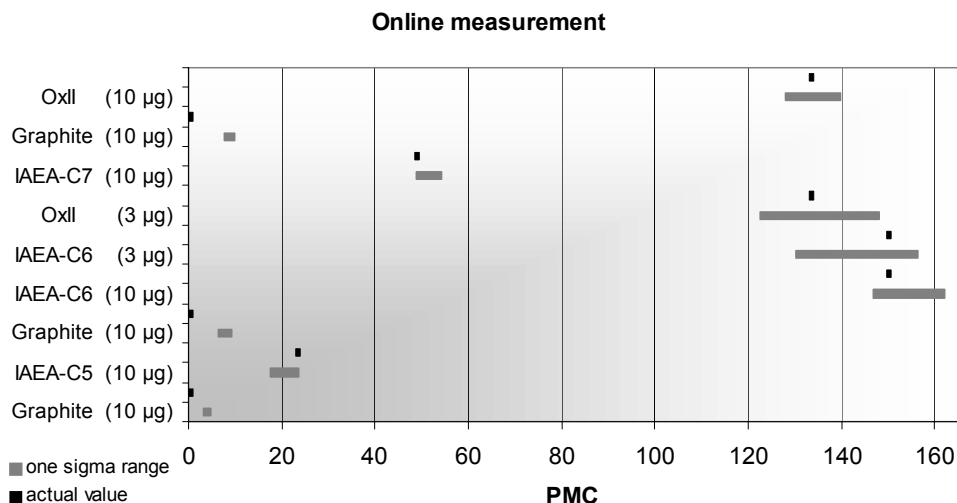


Figure 11 Results of the very first online measurements

CONCLUSION

The direct coupling of an elemental analyzer and a gas ion source for online measurements of samples with carbon masses down to 1 µg is possible with the cryogenic storage and release technique. The advantages of that system are the following:

- Easy handling;
- Omission of the step of the reduction, and so the saving of time and manpower;
- Fast cleaning of the system (within seconds) and, thus, the possibility to change rapidly to another sample;
- Direct (online) measurement and the resulting very low carbon contamination (once the sample is burnt, the CO₂ does not leave the clean system that is steadily self-checking for contamination due to the principle of the configuration);
- Very low minimum carbon mass needed, down to 1 µg (no loss of sample material due to the complete storage of the CO₂ contrary to other GC-AMS online measurement systems);
- Qualification of the technique to simplify investigations in biomedical and environmental science.

An inconvenience is the short range of the best efficiency for the production of carbon ions from CO₂. With the technique presented, it is difficult to keep a constant CO₂ flow rate. Thus, the efficiency is varying (see Figure 10). To adjust a user-defined CO₂ flow rate, the development of a technique to freeze CO₂ in a syringe (CO₂ storing in a bellow and then to dose this CO₂ into the He flow by a pressure difference—similar to the function of the gas-handling system in Figure 1 and according to Bronk Ramsey and Hedges 1994a) is in progress.

REFERENCES

- Bronk Ramsey C, Hedges REM. 1994a. Carbon dioxide sputter source development at Oxford. *Nuclear Instruments and Methods in Physics Research B* 92:100–4.
- Bronk Ramsey C, Hedges REM. 1994b. Gas handling systems for radiocarbon dating by AMS. *Nuclear Instruments and Methods in Physics Research B* 92:105–10.
- Bronk CR, Hedges REM. 1995. Radiocarbon with gas chromatography. In: Cook GT, Harkness DD, Miller BF, Scott EM, editors. Proceedings of the 15th International ^{14}C Conference. *Radiocarbon* 37(2):711–6.
- Bronk Ramsey C, Hedges REM. 1997. Hybrid ion source: radiocarbon measurements from microgram to milligram. *Nuclear Instruments and Methods in Physics Research B* 123:539–45.
- Bronk Ramsey C, Hedges REM. 2000. On-line combustion of samples for AMS and ion source developments at ORAU. *Nuclear Instruments and Methods in Physics Research B* 172:242–6.
- Bronk Ramsey C, Ditchfield P, Humm M, Leach P. 2004. Using a gas ion source for radiocarbon AMS and GC-AMS. *Radiocarbon*, these proceedings.
- Ferry JA, Loger RL, Norton GA, Raatz JE. 1996. Multiple gas feed cathode negative ion source for gas samples AMS. *Nuclear Instruments and Methods in Physics Research A* 382:316–20.
- Hughey BJ, Skipper PL, Klinkowstein RE, Shefer RE, Wishnok JS, Tannenbaum SR. 2000. Low-energy biomedical GC-AMS system for ^{14}C and ^3H detection. *Nuclear Instruments and Methods in Physics Research B* 172:40–6.
- Purser KH. 1994. A future AMS/chromatography instrument for biochemical and environmental measurements. *Nuclear Instruments and Methods in Physics Research B* 92:201–6.
- Middleton R, Klein J, Fink D. 1989. A CO_2 negative ion source for ^{14}C dating. *Nuclear Instruments and Methods in Physics Research B* 43:231–9.

FAST AND ACCURATE SEQUENTIAL INJECTION AMS WITH GATED FARADAY CUP CURRENT MEASUREMENT

M Klein • D J W Mous • A Gottdang

High Voltage Engineering Europa B.V., Amersfoort, the Netherlands. Email: info@highvolteng.com.

ABSTRACT. Sequential injection or bouncing has a number of properties which can lead to a reduction of the analysis accuracy if no appropriate measures are taken. A special injection system has been developed in order to eliminate these shortcomings. The influence of source glitches or instabilities on the measured isotopic ratio is substantially reduced by a high cycling frequency. A fast beam-blanking unit guarantees the needed accuracy of the injection periods. Background currents are avoided by synchronizing the current measurement for the stable isotopes with their injection periods. To achieve the required speed and precision of the gated measurement, new instrumentation was developed. The elimination of background contributions allows an efficiency for radiocarbon counting as high as 95% at a cycling frequency of 100 Hz.

INTRODUCTION

In accelerator mass spectrometry (AMS), the injector system has to select 2 or 3 masses of interest. Unwanted masses are rejected to reduce the measurement background and the beam-current load of the accelerator.

In a sequential injection system, the isotopes are injected one after the other. The vacuum chamber of the injector magnet is electrically isolated. A voltage applied to the chamber changes the energy of the ions that pass through the magnetic field. The voltage determines the mass of the injected ions. The cyclic change of this voltage for the injection of a sequence of isotopes is often referred to as bouncing. Data acquisition for the rare isotope is usually stopped during injection of the stable isotopes, which eliminates background originating from their injection. Sequential injection provides the flexibility to examine virtually all isotopes of the periodic system. The accuracy of the timing of the injection as well as the switching characteristics of the bouncer voltage power supply influence the achievable precision of the analysis. This is of special importance for ^{14}C dating where the highest precision is desired.

In the last 15 years, a number of AMS systems using simultaneous injection have been installed by HVE (Nadeau 1998a/b; Gottdang 1995; Aramaki 2000; Kim 2000; Nakamura 2000). Figure 1 shows a record on precision for these systems as well as for the first dedicated sequential injection ^{14}C -AMS system by HVE, which is installed in Lecce, Italy (Calcagnile 2002). The series labeled “13/12 precision” shows the standard deviation of the stable isotope ratio measurement of 6 different targets that are made from the same sample material. “14/12 precision” shows the standard deviation of the rare isotope measurements on these targets. “Statistical error ^{14}C ” is the calculated error that arises from the counting statistics. The measured 14/12 precision values scatter around the statistical errors. Apparently, there are no other contributions to the achieved precision (Gottdang 2001); this also holds for the sequential injection AMS system. The data indicates that the achieved precision was limited by counting statistics only and that principally this system allows ^{14}C analysis with higher precision. For further comparison of sequential and simultaneous injection AMS, see Nadeau (2003).

To push the performance of sequential injection AMS to its limits, HVE has optimized the bouncer set-up and its electronics, as described in the following paragraphs.

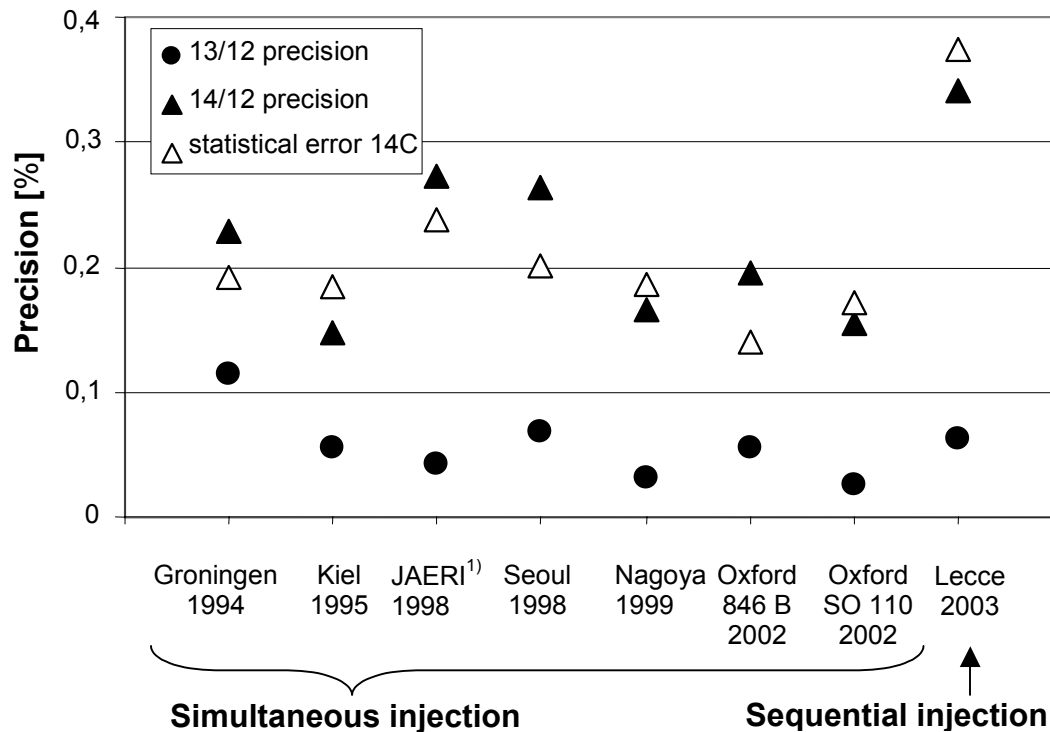


Figure 1 Precision measurements on dedicated ^{14}C AMS systems from HVE. ¹⁾ Refers to the ^{14}C section of the AMS system.

PROPERTIES OF SEQUENTIAL INJECTION DETERMINING ITS PERFORMANCE

In the following, we concentrate on 3 different properties of bouncing which can each have their own adverse contribution to the achievable precision of the analysis.

Cycling Frequency

Changes in the system conditions, like source instabilities and glitches, may affect the measurement of the various isotopes differently when they happen fast compared to the injection cycling frequency. For an accurate ratio measurement, fast cycling is required.

Isotope Switching

During switching between the isotopes, the magnet chamber voltage requires some time to settle. This settling time depends on the involved capacitances and on the characteristics of the power supply used. The voltage variation during the settling time results in an unstable beam position. This will have an influence on the system transmission and, in turn, on the achieved precision. The effect gets more pronounced with higher cycling frequencies when the settling time covers a larger part of the injection period. The settling effects can be avoided with an additional switching system for isotope injection.

Background Currents

Measurement of the stable isotopes can be influenced by background currents. Figure 2 shows typical Faraday cup currents (charge state 3+) as a function of the analyzing magnet current for the

injection of masses 12, 13, and 14 AMU. The figure shows, apart from the peaks of mass 12 and 13, that a continuum of background currents is present, which is generated by charge exchange processes in the acceleration tubes. In addition, distinct peaks originating from the injection of CH_n are visible on the traces measured during the injection of 13 and 14 AMU. It should be noted that the contribution of CH_n is not constant, but depends on the hydrogen content of the sample. The error on the measurement that is induced by background currents can be minimized by the choice of injection periods for the stable isotopes. The ^{13}C -injection period is usually about 100 times longer than the period for ^{12}C . This long time comes to the expense of the ^{14}C -injection period and reduces the measurement efficiency. Detailed analysis on the intensities of the background continuum, as well as the peaks resulting from CH_n molecules, indicated that this error can reach levels as high as 1–2%.

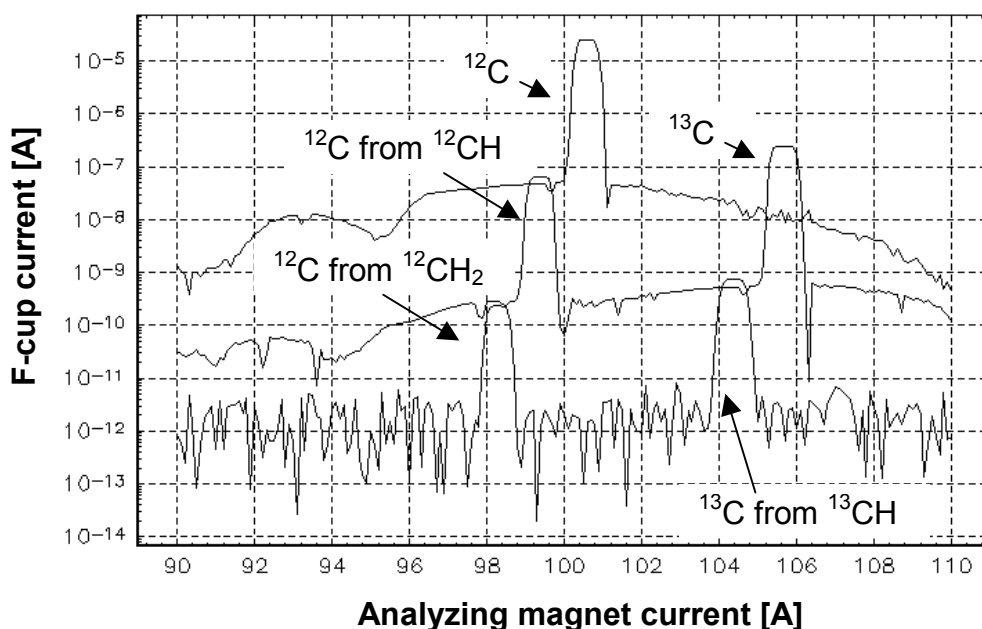


Figure 2 Analyzing magnet scans with mass 12 (upper curve), 13 (center curve), and 14 (lower curve) injected into the accelerator

CHARACTERISTICS OF THE HVE SEQUENTIAL INJECTION SYSTEM

The newly developed bouncer system is designed for high cycling frequencies to overcome the influence of ion beam instabilities. The adverse effects of the switching process are eliminated by the use of a beam-blanking unit which stops the beam unless the measurement conditions are stable and it defines the injection period with high accuracy. By synchronizing the measurement of the stable isotopes with their injection, the background currents resulting from the injection of the other isotopes are avoided. This allows the use of very short measurement times for the stable isotopes and to achieve a high time efficiency for the counting of the rare isotope.

Figure 3 gives the timing of the measurement process. The upper curve shows the magnet chamber voltage during switching of the isotopes. The voltage settling time is about 100 μs . During this time, the beam is stopped by a separate ultra-fast beam-blanking unit (second curve). This unit is a steerer acting as a fast switch, which is located between the injector magnet and the accelerator entrance.

The unit defines the injection periods with nanosecond resolution. The third curve shows the beam intensity of 1 isotope as it reaches its Faraday cup. Some delay resulting from its time of flight is present. The data acquisition time (last curve) for the stable isotopes covers the injection period (taking into account the time of flight), plus additional time for the electronic processing.

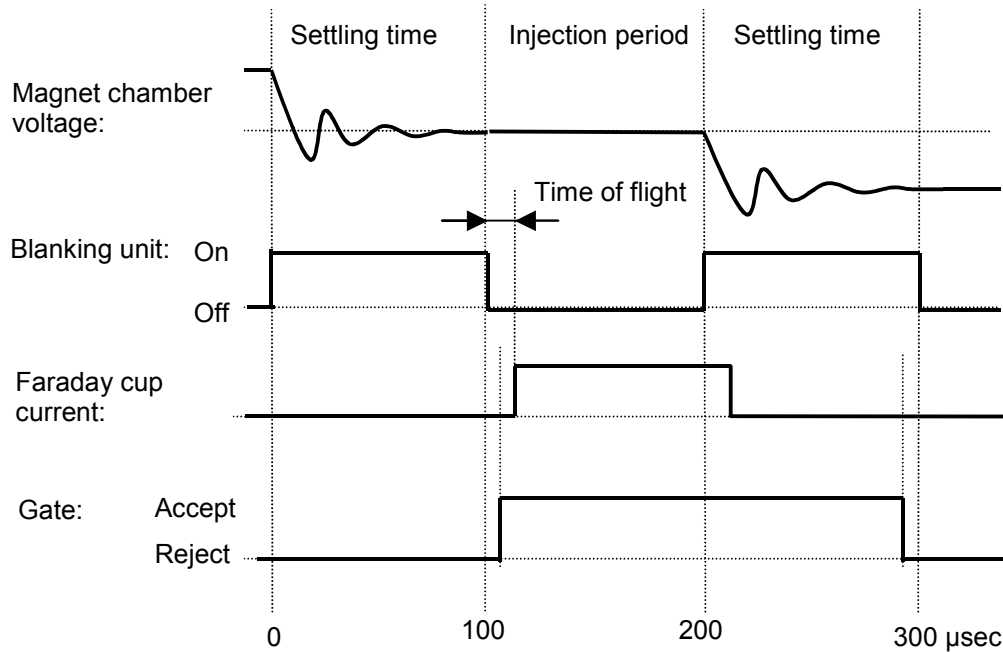


Figure 3 Timing diagram of the stable isotope measurement

For ^{14}C dating, 3 isotopes have to be switched. The settling time totals $3 \times 100 \mu\text{s}$ per injection cycle. This limits the achievable cycling frequency to about 1 kHz. However, HVE regards a 100-Hz cycling frequency sufficiently high to cope with fast source output variations. Together with typical injection times for ^{12}C and ^{13}C of 100 μs each, 9500 μs or 95% of the total injection time is used for ^{14}C counting. Thus, the sequential injection AMS system almost reaches the rare isotope counting efficiency of the simultaneous injector, in combination with the system inherent advantage of gated isotope measurement for background suppression.

The Gated Current Measurement

The stable isotopes are measured in shielded Faraday cups with secondary electron suppression. One of the cups (for ^{13}C in case of ^{14}C dating) is internally equipped with 2 slits providing information on the beam position. This slit-error signal is used in a feedback loop that adjusts the terminal voltage of the accelerator such that the beam is kept precisely in the middle of the slit system. The layout of the electronics for the gated current measurement is shown in Figure 4. The electronics unit is mounted in close vicinity of the Faraday cups for low capacitance of the interconnections and to avoid noise and hum.

The total Faraday cup current is converted into voltage. A gate, which is controlled by the bouncer electronics, passes this voltage on to a filter during the measurement intervals. The filtered, virtually

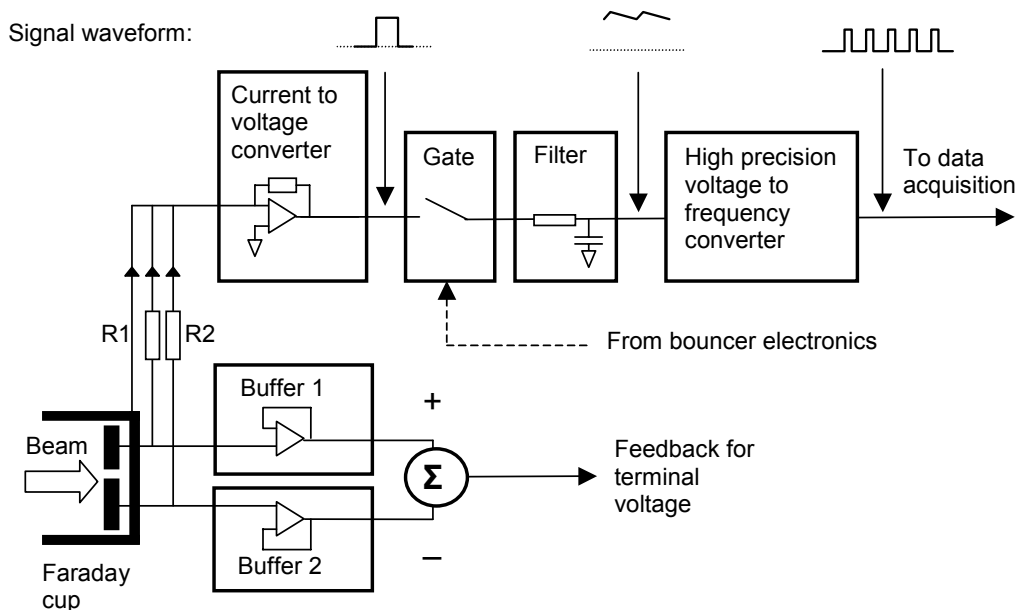


Figure 4 Layout of the electronics for gated Faraday cup current measurements

DC signal is free of background current influences. A high-precision voltage to frequency converter (VFC) converts the signal into pulses, each of them representing a well-defined amount of charge. Two buffers and 2 resistors are used to create the slit-error signal.

Tests have shown that with the high-precision amplifiers and VFCs, the overall precision is in the order of 0.01%. This low value is achieved by using VFCs that are widely applied in isotope ratio mass spectrometry (IRMS) where 10^{-5} precision is mandatory. In addition, the application of low-bias and high-speed amplifiers ensures that this accuracy is achieved with Faraday cup currents down to the low nA range and cycling frequencies up to 1 kHz.

CONCLUSION

HVE has optimized its “bouncing” set-up and electronics to enable isotope ratio measurements with a precision better than 1%. This is achieved by a high cycling frequency to suppress the influence of source output fluctuations. The adverse effects of the bouncer voltage switching on the beam are eliminated by a fast beam-blanking unit, which determines the injection periods of the different isotopes with nanosecond resolution. Gating of the Faraday cup current measurement allows the reduction of the stable isotope injection periods to 100 μ s without background current interferences. In ^{14}C dating, 95% of the analysis time is used for ^{14}C counting at a cycling frequency of 100 Hz.

REFERENCES

- Aramaki T, Mizushima T, Mizutani Y, Yamamoto T, Togawa O, Kabuto S, Kuji T, Gott dang A, Klein M, Mous DJW. 2000. The AMS facility at the Japan Atomic Energy Research Institute (JAERI). *Nuclear Instruments and Methods in Physics Research B* 172: 18–23.
- Calcagnile L, Quarta G, D’Elia M, Gott dang A, Klein M, Mous DJW. 2002. High precision radiocarbon measurements with the new sequential injector of the Lecce AMS facility. Proceedings of the AMS-9 conference. *Nuclear Instruments and Methods in Physics Research B*.
- Gott dang A, Mous DJW, van der Plicht J. 1995. The HVEE ^{14}C system at Groningen. In: Proceedings of

- the 15th International ^{14}C Conference. *Radiocarbon* 37(2):649–56
- Gott dang A, Mous DJW. 1997. The novel HVEE multi-element AMS system. *Nuclear Instruments and Methods in Physics Research B* 123:163–6.
- Gott dang A, Mous DJW. 1998. The characteristics of the HVEE multi-element AMS system. *Proceedings of the 15th International Conference on Applications of Accelerators in Research and Industry*. Denton, Texas, USA, November 1998. p 652–6.
- Gott dang A, Klein M, Mous DJW. 2001. Accelerator mass spectrometry at High Voltage Engineering Europa (HVEE). *Radiocarbon* 43(2A):149–56.
- Kim JC, Lee CH, Kim IC, Park JH, Kang J, Cheoun MK, Kim YD, Moon CB. 2000. A new AMS facility in Korea. *Nuclear Instruments and Methods in Physics Research B* 172:13–7.
- Nadeau MJ, Schleicher M, Grootes PM, Erlenkeuser H, Gott dang A, Mous DJW, Sarntheim JM, Willkomm H. 1998a. The Leibniz-Labor AMS facility at the Christian-Albrechts-University, Kiel, Germany. *Nuclear Instruments and Methods in Physics Research B* 123:22–30.
- Nadeau MJ, Grootes PM, Schleicher M, Hasselberg P, Rieck A, Bitterling M. 1998b. Sample throughput and data quality at the Leibniz-Labor AMS facility. In: Mook WG, van der Plicht J, editors. *Proceedings of the 16th International ^{14}C Conference*. *Radiocarbon* 40(1):239–45.
- Nadeau MJ, Calcagnile L, Rieck A, Quarta G, Grootes PM. 2003. *Sequential vs. Simultaneous Injection for AMS ^{14}C dating: Is there a significant difference?* Poster presented at the 18th International ^{14}C Conference.
- Nakamura T, Niu E, Oda H, Ikeda A, Minami M, Takahashi H, Adachi M, Pals L, Gott dang A, Suya N. 2000. The HVEE Tandetron AMS system at Nagoya University. *Nuclear Instruments and Methods in Physics Research B* 172:52–7.

¹⁰Be ANALYSES WITH A COMPACT AMS FACILITY—ARE BeF₂ SAMPLES THE SOLUTION?

L Wacker^{1,2} • M Grajcar¹ • S Ivy-Ochs¹ • PW Kubik³ • M Suter¹

ABSTRACT. The injection of ¹⁰BeF⁻ instead of ¹⁰BeO⁻ into a compact accelerator mass spectrometry system with a terminal voltage of 0.58 MV was investigated, because BF⁻ molecules are unstable and isobaric interference of ¹⁰B with ¹⁰Be can thus be significantly reduced. We describe the method we developed to prepare BeF₂ samples. ¹⁰Be was measured in a segmented gas ionization detector. Separation of ¹⁰Be from ¹⁰B could be achieved both for ions in the 1+ charge state with an energy of 0.8 MeV and in the 2+ charge state with an energy of 1.4 MeV. The 2+ ions are better separated, whereas the 1+ charge state has a higher transmission. ¹⁰Be/⁹Be ratios (~10⁻¹²) in a suite of rock samples were successfully determined for exposure dating in either charge state and compared with measurements made on the 6MV tandem.

INTRODUCTION

The main difficulty in ¹⁰Be accelerator mass spectrometry (AMS) is the high intensity of the isobaric ¹⁰B beam (Table 1) when samples are prepared as BeO. With a compact AMS facility operating at a terminal voltage of ≤1 MV, the energy of the ions is too low to efficiently remove ¹⁰B using the foil stack method (Grajcar et al., forthcoming) or a gas absorber before the final detector. However, if ¹⁰BeF⁻ is injected instead of ¹⁰BeO⁻, the ¹⁰B intensity is significantly reduced, allowing particle identification in a gas ionization detector (Zhao et al. 2002). This reduction is due to the lifetime of the electronic ground state of BF⁻ being much less (<1 fs) than the roughly 10 μs needed for the negative ions to reach the terminal stripper. Though excited electronic states of BF⁻ may have longer lifetimes, the total boron rate is still reduced significantly (Deuw et al. 2002).

The aim of this work was to find a method to prepare samples which would produce high BeF⁻ currents in a Cs sputter ion source, and to investigate the potential of a small AMS facility for ¹⁰Be measurements using BeF₂.

METHODS

Sample Preparation

Aqueous ¹⁰Be standard and blank solutions containing 0.1–0.5 mg of beryllium as nitrate or chloride were dried and 100 μL of a 1% silver solution (AgNO₃) was added to increase the bulk for easier sample handling. A solution of 2 mL of 40% HF was added and evaporated at 100 °C until dry to produce fluorides; this step was repeated twice. The samples were then baked at 420 °C for 90 min to reduce the silver to its metallic form. The dry BeF₂ with silver was then stored under vacuum in a desiccator because BeF₂ is very hygroscopic. The samples were mixed with 4 mg of niobium powder and then pressed into Al sample holders.

Niobium was added to improve electrical and thermal conductivity. These samples produced readily high BeF⁻ currents and had low ¹⁰B counting rates in the detector, compared with other metals, such as silver, iridium, palladium, copper, and iron, which were also tested.

¹Institute for Particle Physics, ETH Hönggerberg, CH-8093 Zürich, Switzerland.

²Corresponding author. Email: wacker@phys.ethz.ch.

³Paul Scherrer Institut (PSI), c/o Institute for Particle Physics, ETH Hönggerberg, CH-8093 Zürich, Switzerland.

In addition to blanks and standards, we prepared rock samples for measurement on both our small 0.6MV and the 6MV AMS facility for a comparison. The chemical isolation of the Be from quartz after spiking with ^9Be carrier was performed according to Ochs and Ivy-Ochs (1997). Those samples were then split into 2 fractions. One fraction was used to make BeO targets and the other for BeF_2 samples, as described above for the standards and blanks.

Measurement

The BeF_2 samples were measured using the compact PSI/ETH Tandy AMS system (Synal et al. 2000; Stocker et al., forthcoming; Grajcar et al., forthcoming; Döbeli et al. 2002). The BeF^- molecules, which were injected into the accelerator operating at the maximal terminal voltage of 0.58 MV, were dissociated in argon stripper gas. Both Be^+ and Be^{2+} ions were analyzed. ^{10}Be was measured in a gas ionization counter filled with isobutane. A 50-nm silicon nitride foil was used as a detector window (Döbeli et al. 2002), which allows the ion identification even at very low energies (Grajcar et al., forthcoming). An energy loss (ΔE) and a residual energy (E_{Res}) signal were derived from 2 anodes.

RESULTS

Targets made from commercial BeF_2 and the BeF_2 targets made according to the sample preparation procedure above, both mixed with Nb powder, gave BeF^- beam currents of up to 0.2 μA . The ^{10}B -counting rate was typically at the level of 10^{-9} to 10^{-10} relative to the ^9Be rate (Table 1), which is consistent with Zhao et al. (2002). This corresponded to counting rates of less than 1 kHz in the detector for typical beam currents, low enough to not degrade the energy resolution of the detector.

Table 1 Comparison of the 0.6 and the 6MV AMS facilities. In the present configuration of the compact facility, the ^{10}Be beam is not well focused into the detector, resulting in a much lower ^{10}Be transmission compared to ^9Be .

	BeF_2 with 0.6 MV		BeO with 6 MV
	1+	2+	3+
Extracted ions	BeF^-		BeO^-
LE current (nA)	100–200		2000–4000
$^{10}\text{B}/^9\text{Be}$ (HE side)	10^{-10} – 10^{-9}		10^{-4}
^{10}B (Hz)	100		10^8
Charge state	1+	2+	3+
Ion energy (MeV)	0.8	1.4	19
^9Be transmission	50%	12%	17%
^{10}Be transmission	25%	4%	15%

The isobars ^{10}Be and ^{10}B have different stopping powers, and so can be separated by their ΔE – E signals in the ionization chamber. Figure 1 shows a 2-dimensional spectrum for ions in charge state 2^+ ($E = 1.4$ MeV). A standard material with a $^{10}\text{Be}/^9\text{Be}$ ratio of about 10^{-10} was used. The ^{10}B peak of similar intensity is well separated. A third peak of similar height was found between the ^{10}B and the ^{10}Be peak when the stripper gas was optimized for the highest transmission of ^{10}Be . This peak can be attributed to $(^9\text{BeH})^{2+}$ molecules surviving all the way into the detector. This demonstrates the potential of this gas ionization detector for the identification of molecular ions, with AMS at low energies, where molecules in charge state 1^+ or 2^+ can survive the stripping process. By increasing the gas pressure in the stripper to about 1 $\mu\text{g}/\text{cm}^2$, the peak in the 2^+ charge state spectrum disap-

pears, e.g., most of molecules have been destroyed. At this higher pressure, the ⁹Be transmission is reduced by about 10% due to scattering processes in the stripper gas. The same gas pressure was sufficient to destroy molecules in the 1+ charge state. We did not find a significantly higher rate of 1+ molecules, though one would expect them to be formed more easily. All further measurements were made at the higher stripper pressure.

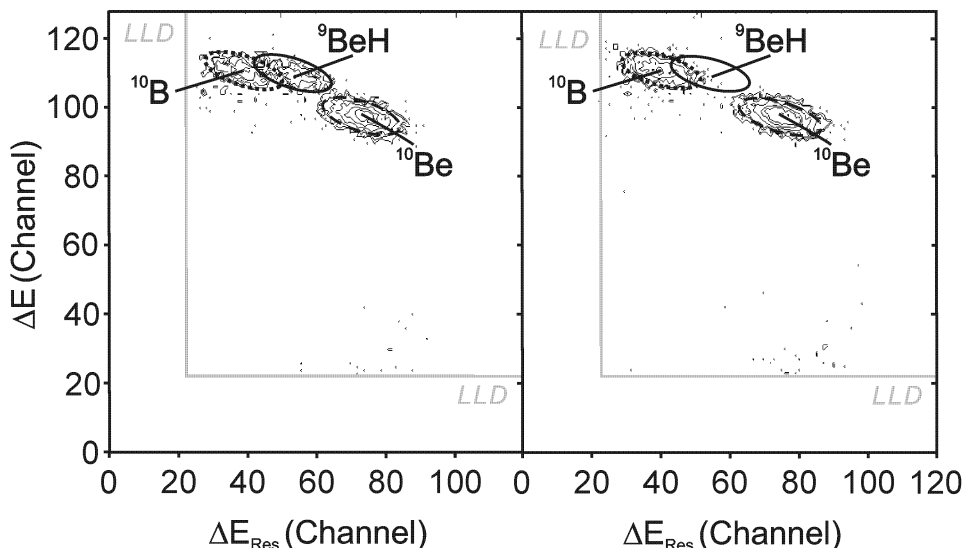


Figure 1 Left: spectrum of a ¹⁰Be standard in charge state 2+ and for a stripper gas pressure of 0.3 μg/cm² (optimum for maximal transmission of ⁹Be+). A (⁹BeH)²⁺ peak shows between ¹⁰B²⁺ and ¹⁰Be²⁺. The (⁹BeH)²⁺ can be eliminated if the gas pressure is raised to 1 μg/cm² (shown on the right).

In the upper part of Figure 2, the 2-dimensional spectrum of the same standard material is compared with one of a geological sample. In this case, the detector was optimized for the best Be-B separation. The peaks are well separated, with peak widths (FWHM) of about 50 keV. A suppression of about 5 orders of magnitude can be obtained with a peak integration of 90%. A similar peak separation has been shown in previous experiments with BeO beams (Grajcar, forthcoming). Measurements with blank samples gave values of 4×10^{-14} , i.e., higher than the result from the BeO measurements using the large tandem accelerator (Table 2) and higher than what one would expect from a tail of the boron peak. This hints at some other background source. Further experiments are needed to identify the cause for this background.

In the lower part of Figure 2, the spectra of the same samples are shown when analyzing ¹⁰Be in charge state 1+ (E = 0.8 MeV). The peak widths are about the same, but the peak separation is about a factor of 2 smaller. This allows still some ¹⁰Be-¹⁰B separation, but a reasonable background suppression can only be obtained with narrow and asymmetric software gates for ¹⁰Be as shown in Figure 2. Then, only about 60% of the real ¹⁰Be were integrated and the blank values were still at a level of 10⁻¹³. The ¹⁰B contribution to the background is now negligible. Setting the gates tighter does not improve the background.

The ⁹Be transmission given in Table 1 has been determined from current measurements on the low-energy side and after the high-energy magnet. The high transmission of about 50% for charge state 1+ reflects the high stripping yield obtained at the terminal voltage of 580 kV (corresponding to

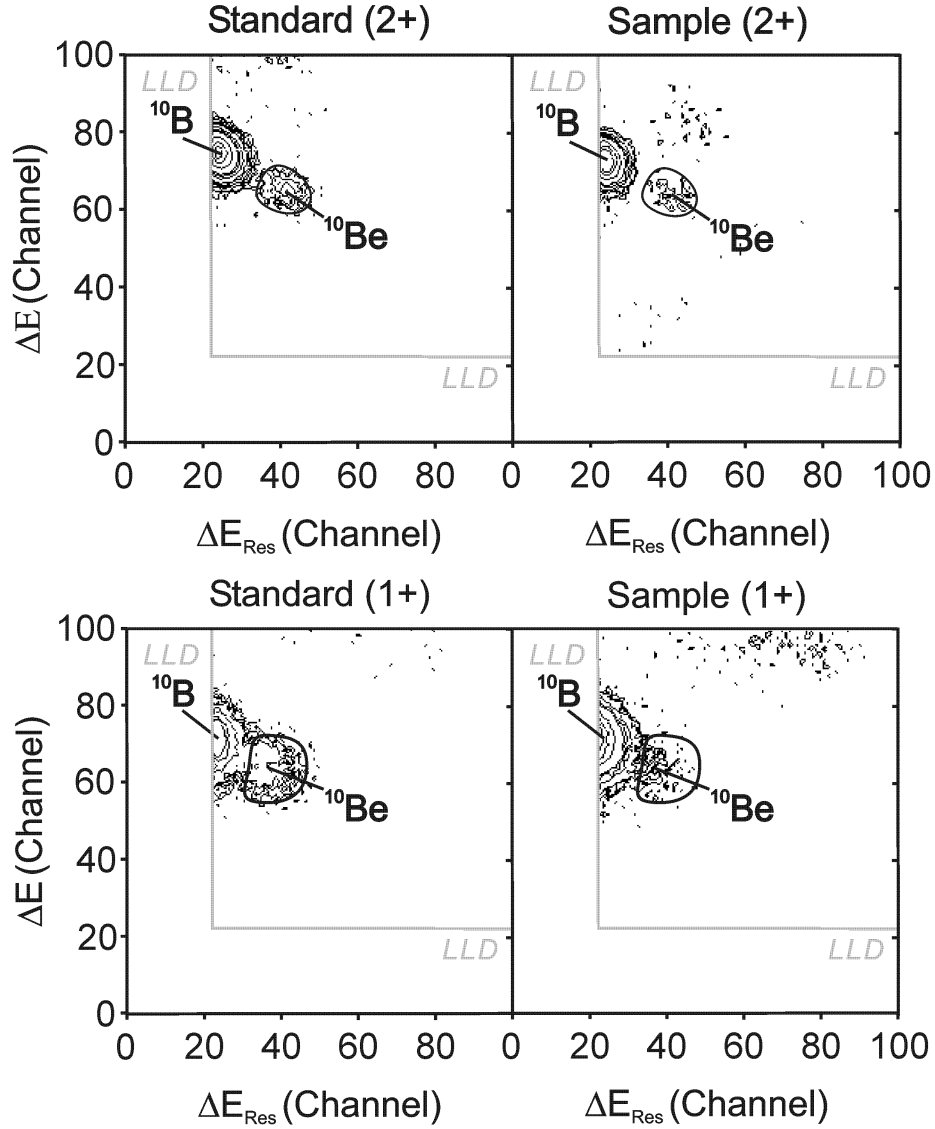


Figure 2 Two-dimensional spectra of ΔE versus ΔE_{Res} for a standard ($^{10}\text{Be}/^9\text{Be} = 10^{-10}$) and a geological sample. The 1.4-MeV $^{10}\text{Be}^{2+}$ is clearly separated from $^{10}\text{B}^{2+}$. The 0.8-MeV $^{10}\text{Be}^+$ is only partially separated from $^{10}\text{B}^+$. Events within the black contour lines were accepted as ^{10}Be events while suppressing ^{10}B by a factor of more than 10^4 . The grey lines show the low-level discriminator settings to cut off electronic noise.

205 keV for ^9Be when injecting BeF^-) and the large acceptance of the high-energy Faraday cup. For charge state 2+, the stripping yield is about a factor of 4 smaller. About a factor of 2 is lost from there to the detector for 1+ and about a factor of 3 for 2+ ions.

The normalized $^{10}\text{Be}/\text{Be}$ ratios of the rock samples are consistent with those obtained with the 6MV AMS facility, for which a description can be found in Synal et al. (1997).

Table 2 Results for geological samples measured on the 6MV Tandem and on the 0.6MV Tandy accelerator. Each rock sample was spiked with 0.5 mg ⁹Be and was split after Be separation to produce a BeO and a BeF₂ target. The BeF₂ sample was measured both in the 1+ and the 2+ charge state.

Sample	Tandy (1+), BeF ₂		Tandy (2+), BeF ₂		Tandem (3+), BeO	
	¹⁰ Be/ ⁹ Be		¹⁰ Be/ ⁹ Be		¹⁰ Be/ ⁹ Be	
	10 ⁻¹²	Error	10 ⁻¹²	Error	10 ⁻¹²	Error
S 1	5.1	12%	5.1	11%	5.06	3%
S 2	1.8	21%	not measured	not measured	1.56	4%
S 3	8	17%	7.5	26%	9.75	2%
S 4	0.5	31%	0.8	41%	0.55	4%
Blank	0.09	14%	0.04	70%	0.01	24%

DISCUSSION

BeF₂ targets of good quality can be prepared with reasonable effort using the described procedure. The hygroscopic nature of the fluorides requires the storage of the samples in a dry environment. This is inconvenient; on the other hand, BeO is more toxic. The beam currents from BeF₂ samples are still clearly lower than those obtained from BeO; however, the ¹⁰B rate is significantly reduced. Remaining ¹⁰B entering the detector is likely to be injected as (¹⁰B¹⁸O¹H)⁻, (¹⁰B₂⁹Be)⁻, or (¹⁰BF)⁻ in a meta-stable excited electronic state.

The high stripping yield of 1+ ions makes this charge state very attractive, leading to an overall transmission higher than at most existing AMS facilities. The optics system for charge state 1+ is relatively easy to improve by positioning the detector in the focal plane of the high-energy mass spectrometer and by increasing the size of the detector window, which is currently only 5 mm × 5 mm. For the charge state 2+, the situation is more complex. The high-energy accelerator tube acts as a stronger lens, leading to a convergent beam at the exit of the accelerator. To overcome this problem, a more complicated ion optics system for proper focusing would be needed.

The blank ratios are still about 1 order of magnitude higher than can be achieved at larger facilities, but a further background reduction seems to be feasible. The energy resolution of the detector can be improved, as systematic studies clearly showed that the electronic noise is presently the limiting factor for light ions. Signals from a pulser fed directly into the preamplifier showed only a 10% reduction in resolution, indicating that the noise of the preamplifier represents the main contribution. Energy straggling in the entrance window and the gas are significantly smaller. Based on preamplifier specifications, one can expect a further improvement with an appropriate design of the detector and the electronics and by the appropriate choice of the counter gas. A reduction of the peak width of 20–40% does not seem unrealistic. This should provide a reasonable ¹⁰Be-¹⁰B separation for the 1+ charge state.

CONCLUSION

We have demonstrated that BeF beams are a means of permitting ¹⁰Be AMS at low energies. For the first time, environmental samples have been measured with a compact AMS operated at 580 kV. The results are promising, but at the moment, the method is not competitive with that used at larger facilities. There is potential for improvement and it appears feasible that a facility can be developed meeting the required specifications for applications in Earth Sciences.

REFERENCES

- Döbeli M, Kottler C, Stocker M, Weinmann S, Synal H-A, Grajcar M, Suter M. Forthcoming. Gas ionization chambers with silicon nitride windows for the detection and identification of low energy ions. *Nuclear Instruments and Methods in Physics Research B*.
- Dreuw A, Sommerfeld T, Cederbaum LS. 2002. Short- and long-lived electronic states of BF^- . *Journal of Chemical Physics* 116(14):6039–44.
- Grajcar M, Döbeli M, Kubik PW, Maden C, Suter M, Synal H-A. Forthcoming. ^{10}Be measurements with terminal voltages below 1 MV. *Nuclear Instruments and Methods in Physics Research B*.
- Ochs M, Ivy-Ochs S. 1997. The chemical behavior of Be, Al, Fe, Ca and Mg during AMS target preparation from terrestrial silicates modeled with chemical speciation calculations. *Nuclear Instruments and Methods in Physics Research B* 123:235–40.
- Stocker M, Bertschinger R, Döbeli M, Grajcar M, Jakob S, Scheer J, Suter M, Synal H-A. Forthcoming. Status of the PSI/ETH Compact AMS facility. *Nuclear Instruments and Methods in Physics Research B*.
- Synal H-A, Bonani G, Döbeli M, Ender RM, Gartenmann P, Kubik PW, Schnabel Ch, Suter M. 1997. Status report of the PSI/ETH AMS Facility. *Nuclear Instruments and Methods in Physics Research B* 123:62–8.
- Synal H-A, Jacob S, Suter M. 2000. The PSI/ETH small radiocarbon dating system. *Nuclear Instruments and Methods in Physics Research B* 172:1–7.
- Zhao X-L, Litherland AE, Doup JP, Kieser WE. 2002. AMS measurements of ^{10}Be using BeF^- . Proceedings of the 9th International Accelerator Mass Spectrometry Conference, 9–13 September 2002, Nagoya, Japan. Poster presentation PTPd-5.

SIMULATION STUDY FOR THE SEPARATION OF RARE ISOTOPES AT THE SEOUL NATIONAL UNIVERSITY AMS FACILITY

C C Yun¹ • C S Lee^{1,2} • M Youn³ • J C Kim³

ABSTRACT. A simulation study for the separation of rare isotopes such as beryllium and aluminum was performed for a new beam line to be attached to the 3MV Tandatron accelerator at the accelerator mass spectrometry (AMS) facility of Seoul National University in Korea. The new beam line will also be used for other scientific applications, namely, ion implantations, Rutherford backscattering, and nuclear astrophysics experiments. It mainly consists of 30° and 100° deflection dipole magnets and drift spaces. A transfer matrix for the beam line was determined by the TRANSPORT code. Simulation of the rare isotope separation was performed by a ray tracing method using the TURTLE code. The simulation results, including the effect of the energy degrader, provide feasibility for the separation of isobars with small mass differences in ¹⁰Be-¹⁰B and ²⁶Al-²⁶Mg.

INTRODUCTION

Accelerator mass spectrometry (AMS) is a powerful technique for measuring long-lived radionuclides that occur naturally in our environment. It has been used for a wide variety of dating and tracing applications in the geological and planetary sciences, archaeology, biomedicine, etc. The AMS facility of Seoul National University (SNU-AMS) in Korea was completed in December 1998 (Kim et al. 2000). It uses a Tandatron accelerator of the Cockroft-Walton type, manufactured by High Voltage Engineering Europa in Holland, and has a dedicated radiocarbon AMS beam line, as well as 5 ports available for other experimental purposes. It uses a cesium sputtering ion source for ionizing carbon isotopes as well as other species. A recombinator system in the injection part of the SNU-AMS allows 3 carbon isotopes, ¹²C, ¹³C, and ¹⁴C, to be simultaneously measured. A detailed description of the system including detection and analysis procedures is found in Kim et al. (2001). The recent status and future plan of the SNU-AMS was presented at a symposium in October 2002 (Kim et al. 2003).

The main mission of the SNU-AMS thus far has been to count carbon isotopes. Recently, a new project to measure other radionuclides has begun with the design of a new beam line (see Figure 1). As an initial step, we decided to focus on the measurement of beryllium isotopes, ⁹Be (a stable nuclide) and ¹⁰Be (a radionuclide with a half-life of 1.5 million yr), and of aluminum isotopes, ²⁷Al (a stable nuclide) and ²⁶Al (a radionuclide with a half-life of 0.73 million yr). The ¹⁰Be and ²⁶Al radionuclides are produced in meteorites or in other extraterrestrial materials, in the atmosphere of the earth, and on the surface of the earth. They can, therefore, serve as valuable tracers, a chronological clock for prehistoric samples. In this paper, we present the simulation results, including the effect of the energy degrader through a new beam line previously reported by Yun et al. (2003).

DESIGN AND SIMULATION FOR THE NEW BEAM LINE

The new beam line was designed by the TRANSPORT code (Brown et al. 1973), which is based on a matrix approach. Transport properties of a charged particle beam can be simulated by defining a beam vector in this code. The beam vector can be written as

¹Department of Physics, Chung-Ang University, Seoul 156-756, Korea.

²Corresponding author. Email: cslee@cau.ac.kr.

³Department of Physics, Seoul National University, Seoul 151-742, Korea.

$$X(0) = \begin{pmatrix} x \\ x' \\ y \\ y' \\ \ell \\ \delta_0 \end{pmatrix} \quad (1).$$

The beam vector consists of 6 components corresponding to the horizontal (x) and vertical (y) beam extents in units of cm; the horizontal (x') and vertical (y') beam divergences or angles in units of mrad; the longitudinal beam extend (ℓ) in units of cm; and finally, the momentum spread (δ_0) in units of % for the charged particle transported through the beam line.

The transfer matrix R at a specific position can be represented by

$$X(1) = RX(0) \quad (2),$$

where $X(0)$ is the beam vector at an initial point. $X(1)$ is the beam vector at a specific position. When there are n components for the beam line, R in Equation 2 can be rewritten as a product of matrices corresponding to each component:

$$R(t) = R(n)...R(3) R(2) R(1) \quad (3),$$

where $R(i)$ ($i = 1, 2, \dots, n$) can represent a dipole magnet, a quadrupole element, the drift space, a shim angle, etc.

The new beam line (Figure 1) consists of a 30° deflection (D1) and a 100° deflection (D2) dipole magnet previously used as a gas-filled recoil mass separator and as a beam analyzer, respectively, at the SF cyclotron facility at the Center for Nuclear Study, the University of Tokyo. The basic parameters of the 2 dipole magnets are given in Table 1. The energy degrader is situated on the beam axis inside the scattering chamber located between 2 dipole magnets. A Faraday cup is also situated inside the scattering chamber but off the beam axis. The dispersion D listed in Table 1 represents separability between particles of different momenta at a magnet exit, and can be obtained from the following relation:

$$D = \frac{\rho(1 - \cos\theta)}{100} \quad (4),$$

where the dispersion D is in units of cm/% and ρ and θ are the central radius and the deflection angle of a dipole magnet, respectively. The resolving power of a beam line system can be written as (Livingood 1969):

$$R_p = \frac{P}{\Delta P} = \frac{D'}{2x_0M_x} \quad (5),$$

where x_0 and M_x are the initial beam size and the magnification, respectively. The relationship between the dispersion of the individual magnets and the overall beam line dispersion D' is a function of the beam line geometry. Therefore, the maximum resolving power should be carefully determined by taking into account the positions of the 2 dipole magnets and the drift space in the new beam line.

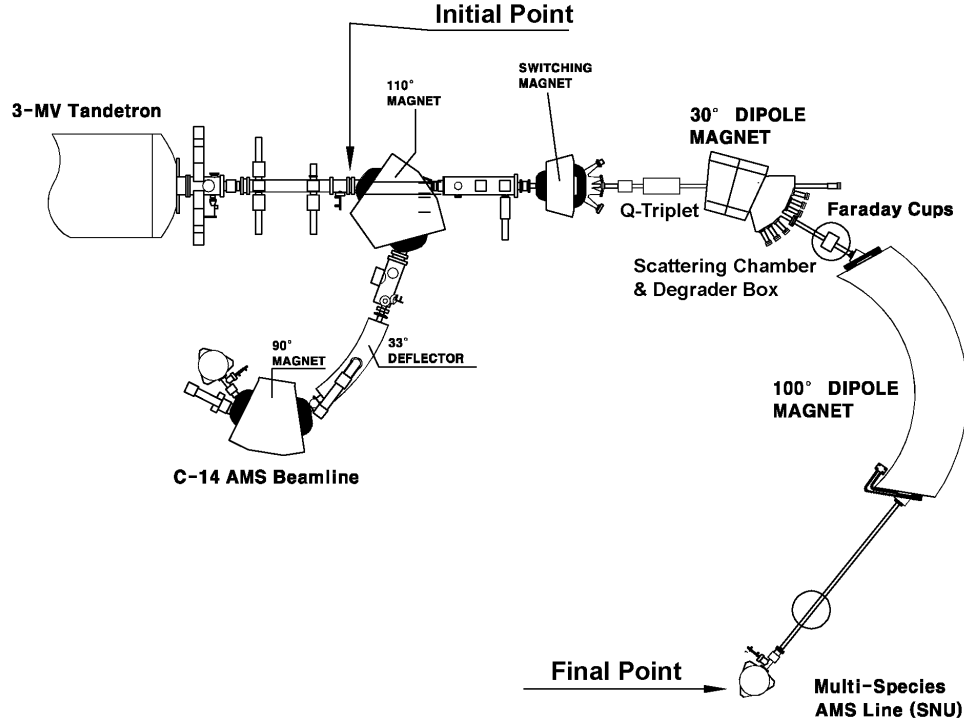


Figure 1 Schematic view of the SNU-AMS facility

Table 1 Beam-optical parameters of the D1 and D2 dipole magnets.

Parameters	D1	D2
Deflection angle (°)	30	100
Central radius (cm)	134.2	180
Pole gap (cm)	5.6	7.0
Entrance and exit angle (°)	—	30.8
Maximum field (T)	1.22	0.74
Maximum $B\rho$ (Tm)	1.6	1.33
Dispersion (cm/%)	0.18	2.11

On the other hand, the mass resolving power of the beam line system can be obtained from the following relationship:

$$R_M = \frac{1}{2} R_p \quad (6).$$

For the initial beam parameters in the subsequent calculation, we used the values supplied by the manufacturer of the SNU-AMS for the horizontal (ε_x) and the vertical (ε_y) emittance and the momentum spread (δ_0). They were $\varepsilon_x = 3.0 \pi \text{mm}\cdot\text{mrad}$ ($0.5 \text{ mm} \times 6.0 \text{ mrad}$), $\varepsilon_y = 3.0 \pi \text{mm}\cdot\text{mrad}$ ($1.2 \text{ mm} \times 2.5 \text{ mrad}$) in $3\text{-}\sigma$ emittance, and $\delta_0 = 0.01\%$, respectively. To simulate the trajectory of a charged particle through the magnetic field, we performed computation using a ray tracing method including higher order aberration, called TURTLE (Trace Unlimited Rays Through Lumped Elements) (Brown et al. 1974). The initial beam vector was created assuming the Gaussian distribution using the random number generator.

The 3- σ emittance ε_x can be obtained by

$$\varepsilon_x = \left[(3\sigma_x)^2 (3\sigma_{x'})^2 - (3\sigma_x \times 3\sigma_{x'})^2 \right]^{1/2} \quad (7),$$

where σ_x and $\sigma_{x'}$ are the standard deviations corresponding to the horizontal beam extent x and angle x' , respectively. The standard deviations are found in the general manner that

$$\sigma = \sqrt{\frac{1}{N} \sum_{i=1}^N (x_i - \bar{x})^2} \quad (8),$$

where \bar{x} is the average of x_i of each point.

The energy loss in degrading material was obtained by the Bethe-Bloch equation for higher order corrections. The energy straggling was determined using the method of Tschalär (Tschalär et al. 1968). The multiple scattering was calculated as follows (Highland 1975):

$$\sigma(\theta) = \frac{14.1 \text{ MeV} c}{\sqrt{p_i \beta_i p_f \beta_f}} Z_i \sqrt{(\Delta x / L_r)} \left[1 + \frac{1}{9} \log \frac{\Delta x}{L_r} \right] \quad (9),$$

where the angular width is given in terms of the radiation length (L_r) and the initial and final momenta (p_i and p_f) and velocities ($\beta_i c$ and $\beta_f c$). The values of the radiation length for aluminum and beryllium are 8.9 cm and 35.28 cm, respectively (Tsai 1974). The parameters used in the present simulation for beryllium-boron isotopes were assumed to have the energy of 10 MeV and the charge state of 3^+ . For aluminum-magnesium isotopes, the energy of 12.5 MeV and the charge state of 4^+ were assumed. A total of 5000 particles were considered in all the simulation.

RESULTS AND DISCUSSION

Figure 2 shows the result obtained by the TRANSPORT code for the region from the initial point to the final point (schematically shown in Figure 1). The top and bottom panels represent the beam envelope and the dispersion, respectively, for the new beam line. The upper half-plane of each panel represents the vertical beam transport while the lower half-plane represents the horizontal beam transport. The rectangles in the figure indicate a triplet quadrupole lens and dipole magnets. As shown in the bottom panel of Figure 2, the dispersion at the point of Faraday cups in Figure 1 turned out to be 0.49 cm/%, whereas the dispersion at the final point was 7.74 cm/%. From equations (5) and (6), the resolving powers at this point are $R_p \sim 2000$ and $R_M \sim 1000$, which sets the limit of separation to be $\sim 0.05\%$ in the momentum difference and $\sim 0.1\%$ in the mass difference.

Figure 3 shows the result of separation between beryllium-boron isotopes of the TURTLE code obtained by the transfer matrix from the TRANSPORT code. The 3 figures illustrate, from left to right, the x - y beam profile at the initial point, before the energy degrader, and at the final point, respectively. The values for ε_x and ε_y were 3.03 and 2.98 $\pi\text{mm}\cdot\text{mrad}$, respectively, at the initial point. The right figure illustrates the beam profile after the energy degrader at the final point. The values of ^{10}B for ε_x and ε_y were 159.14 and 63.65 $\pi\text{mm}\cdot\text{mrad}$, respectively. The values of ^{10}Be for ε_x and ε_y were 104.17 and 50.07 $\pi\text{mm}\cdot\text{mrad}$, respectively. The beam spot size of ^{10}B at final point was 7.82 cm \times 5.76 cm in the x - y beam profile. For the ^{10}Be isotope, the beam spot size at the final point was 6.16 cm \times 5.11 cm in the x - y beam profile.

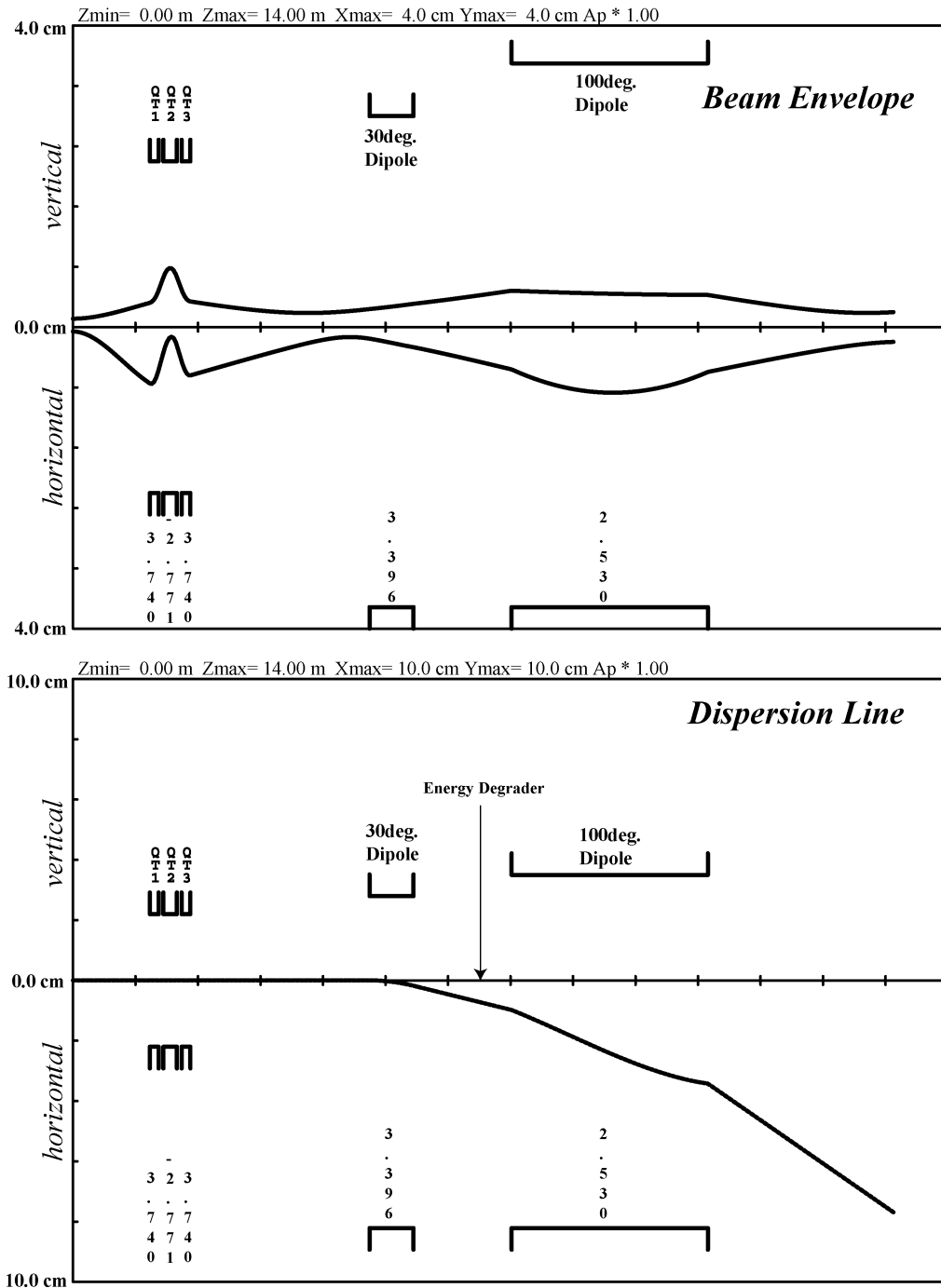


Figure 2 Beam envelope (top panel) and dispersion (bottom panel) calculated in the present work. The calculation results were plotted for the beam transport range from the initial point to the final point shown in Figure 1.

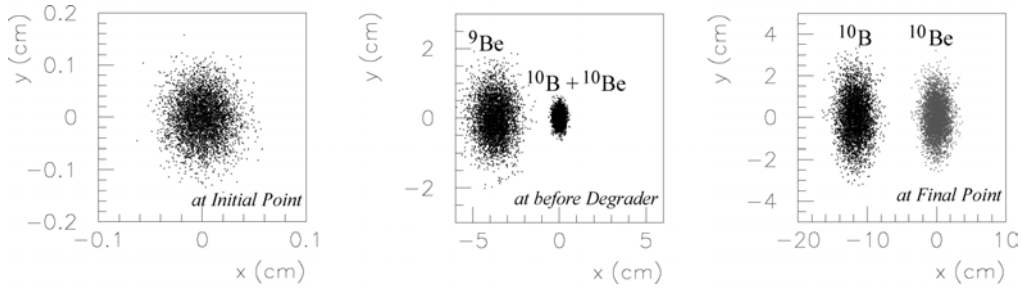


Figure 3 Result for separation of beryllium isotopes obtained by the TURTLE code. Explanations for these plots are given in the text.

As seen from the middle plot in Figure 3, ^{10}Be is clearly separated from ^9Be . However, a bundle of admixed ^{10}Be and ^{10}B is inseparable despite the large dispersion value of 7.74 cm/% at the final point. This results from the limit of separation as mentioned above: the mass difference between ^{10}B and ^{10}Be amounts was a mere 0.006%, so the momentum difference is only 0.003%. On the other hand, the isotopes passing through the energy degrader have a different energy for the different charge number (Z) because the energy loss is proportional to Z^2 of the isotopes. The energies of ^{10}B and ^{10}Be were 9.253 MeV and 9.557 MeV, respectively, after the energy degrader with a $290 \mu\text{g}/\text{cm}^2$ ($1 \mu\text{m}$) aluminum foil. This amount of 3.28% in energy difference corresponds to 1.64% in the momentum difference. This momentum difference leads to the separation of 12.7 cm between ^{10}B and ^{10}Be at the final position.

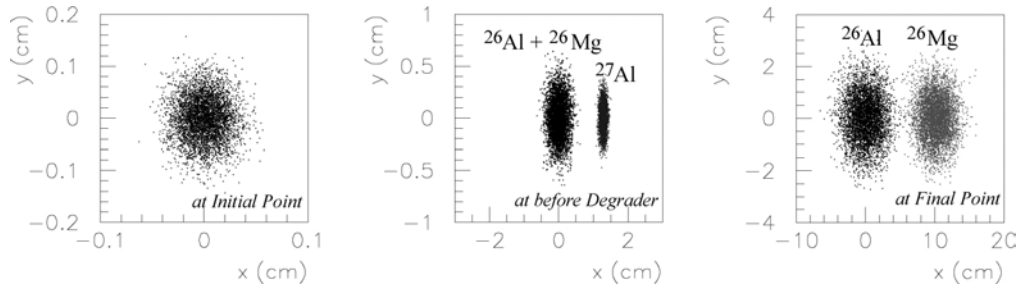


Figure 4 Result for separation of aluminum isotopes obtained by the TURTLE code. Explanations for these plots are given in the text.

Figure 4 shows the result of separation between aluminum and magnesium isotope using the TURTLE code. The figures are, from left to right, the beam profile at the initial point, before the degrader, and at the final point. The emittances of ^{26}Al after the energy degrader were $\varepsilon_x = 220.40 \pi\text{mm}\cdot\text{mrad}$ and $\varepsilon_y = 52.85 \pi\text{mm}\cdot\text{mrad}$ at the final point. The values of ^{26}Mg were $\varepsilon_x = 184.97 \pi\text{mm}\cdot\text{mrad}$ and $\varepsilon_y = 47.29 \pi\text{mm}\cdot\text{mrad}$ at the final point. The beam spot size of ^{26}Al and ^{26}Mg at the final point was $10.39 \times 5.38 \text{ cm}$ and $9.35 \times 4.98 \text{ cm}$ in the x - y beam profile, respectively. As seen in the middle figure, ^{27}Al is clearly separated from a bundle of admixed ^{26}Al and ^{26}Mg . The momentum difference between ^{26}Al and ^{26}Mg is only 0.012% for the magnetic rigidity and the mass difference is about 0.017%. The energies of ^{26}Al and ^{26}Mg were 9.475 MeV and 9.752 MeV, respectively, after the energy degrader with a $140 \mu\text{g}/\text{cm}^2$ ($0.76 \mu\text{m}$) beryllium foil. The momentum difference obtained was 1.44%, corresponding to 11.3 cm in separation between these isotopes at the final position (see right figures in Figure 4). The separation between ^{26}Al and ^{26}Mg becomes clearer with increasing degrader thickness. At the same time, growth of the beam width is inevitable.

SUMMARY

The new beam line at the SNU-AMS was designed by the TRANSPORT code for AMS counting the beryllium and aluminum nuclides. Separation of rare isotopes was simulated by the TURTLE code. For this simulation, AMS of aluminum as well as beryllium is feasible in the present design for the new beam line. In addition, the use of the energy degrader makes it possible to separate even a small mass difference in ^{10}Be - ^{10}B and ^{26}Al - ^{26}Mg isotopes. Based on the present simulation study, construction of the new beam line is underway: The 100° magnet was completely assembled and water cooling line is underway. We are also building another chamber for the 30° dipole magnet.

ACKNOWLEDGEMENTS

The authors are deeply indebted to Dr John Southon for his enlightening comments. This work was supported by Korea Research Foundation Grant (KRF-2002-070-C00031).

REFERENCES

- Brown KL, Rothacker F, Carey DC, Iseline Ch. 1973. PSI graphic transport framework by Rohrer U based on a CERN-SLAC-FERMILAB version. TRANSPORT, a computer program for designing charged particle beam transport system. *Conseil Européen pour la Recherche Nucléaire* 73-16.
- Brown KL, Iseline Ch. 1974. PSI Graphic Turtle framework by Rohrer U based on a CERN-SLAC-FERMILAB version. DECADE TURTLE. *Conseil Européen pour la Recherche Nucléaire* 74-2.
- Highland VL. 1975. Some practical remarks on multiple scattering. *Nuclear Instruments and Methods in Physics Research B* 129:497-9.
- Kim JC, Youn M, Kim IC, Park JH, Song YM, Kang J, Choi HR. 2003. Present activities and future plan at Seoul National University AMS Facility. *Journal of the Korean Physics Society* 43:S45-9.
- Kim JC, Park JH, Kim IC, Lee C, Cheoun MK, Kang J, Song YM, Jeong SC. 2001. Progress and protocol at the Seoul National University AMS Facility. *Journal of the Korean Physical Society* 39:778-82.
- Kim JC, Lee CH, Kim IC, Park JH, Kang J, Cheoun MK, Kim YD, Moon CB. 2000. A new AMS facility in Korea. *Nuclear Instruments and Methods in Physics Research B* 172:13-7.
- Livingood JJ. 1969. *The Optics of Dipole Magnet*, Chapter 2. New York: Academic Press
- Tschalär C. 1968. Straggling distributions of extremely large energy loss. *Nuclear Instruments and Methods B* 64:237-43.
- Tsai YS. 1974. Pair production and bremsstrahlung of charge leptons. *Reviews of Modern Physics* 46:815-51.
- Yun CC, Lee CS, Kim JC, Youn M. 2003. Beam line design and simulation for mass separation of beryllium isotopes at the AMS facility in Korea. *2003 IEEE International Conference on Plasma Science*. Jeju, Korea, 2-5 June 2003.

SURFACE AND UNDERGROUND ULTRA LOW-LEVEL LIQUID SCINTILLATION SPECTROMETRY

Wolfgang Plastino

Department of Physics, University of Roma Tre, via della Vasca Navale, 84, I-00146 Rome, Italy; also: INFN, Section of Roma III, via della Vasca Navale, 84, I-00146 Rome, Italy. Corresponding author. Email: plastino@fis.uniroma3.it.

Lauri Kaihola

PerkinElmer Life and Analytical Sciences, Wallac Oy, P.O.B. 10, FIN-20101 Turku, Finland.

ABSTRACT. Cosmic background and its variation have been removed in the Gran Sasso National Laboratory (National Institute of Nuclear Physics) by its 1400-m rock overburden. Stable, high-performance liquid scintillation counting conditions are obtained when any remaining variable components of the environmental background, such as radon, are eliminated. The ultra low-level liquid scintillation spectrometer Quantulus™ has an anti-Compton guard detector (guard for short) that allows monitoring of gamma radiation in the background. The guard detector efficiency in radiocarbon background reduction is 8% in the Gran Sasso National Laboratory, while 80% is observed in surface laboratories. Thus, atmospheric pressure variations in surface laboratories cause variation in cosmic radiation flux. The Quantulus anti-Compton detector is highly efficient in detecting cosmic radiation, and the sample count rate remains stable in long-term counting. Also, correlation of sample backgrounds with environmental gamma radiation in various laboratories is examined.

INTRODUCTION

Quantulus™ (PerkinElmer, Inc.) is an ultra low-level liquid scintillation spectrometer used in numerous radiocarbon laboratories for radiometric ^{14}C age determinations. Sample sizes down to a few hundred mg of carbon have been measured with various sample holder configurations (Haas 1979; Kalin and Long 1989; Hogg 1992; Kaihola et al. 1992; Buzinny and Skripkin 1995) which give lower backgrounds than larger vials.

The basic Quantulus design follows the conventional LSC configuration of 2 photomultiplier tubes (PMTs) to monitor the sample. Only coincidence events are accepted in beta counting; thus, most phototube random thermal noise is rejected. At the same time, tritium counting efficiency is maintained when compared to single phototube systems, where a threshold has to be applied to improve the signal to noise ratio. The typical single photon noise figure is 0.15 CPM and resides in the first 100 channels of the logarithmic energy scale, which are normally discarded with small ^{14}C counting efficiency loss by applying a high bias threshold. A background reduction by a factor of 50 in the full 2-MeV beta energy window is achieved by using a passive low radioactivity Boliden lead shield with a mass of 640 kg. Its shape is optimized with up to 20 cm thickness towards the zenith, from which most of the muon flux comes.

The counting chamber is inside an active anti-Compton guard detector made of OFHC copper filled with mineral oil scintillation cocktail. It is asymmetric with a larger volume on top of the sample. The guard has 2 phototubes working in conjunction which detect a fraction of the inherent tube radioactivity. The guard is a true cosmic event detector with no optical contact with the sample. Its performance does not, therefore, depend on the sample matrix, as in designs where a single phototube pair is used for both the sample and guard. Previously, the Quantulus guard used cadmium lining to remove the thermal neutron flux. This has been changed (due to health hazard reasons and non-observable background reduction) to copper lining, which together with guard copper walls, attenuates Pb X-rays generated by the small ^{210}Pb contamination in lead. The sample is lifted into the counting chamber with a massive copper piston that acts as a passive shield downwards. The

anti-Compton guard further reduces the full window background by a factor of 5. It detects cosmic muons to almost 100%, which can be verified by recording rejected sample events (spectrum 12 in ^{14}C counting mode) in high channels (channel 850 and upwards).

The low radioactivity sample phototubes are matched pairs with low thermal noise. The tube window is made of silica and its walls are built from short cylinders of graded glass to connect to Pyrex glass at the anode. Sample and guard phototubes are the radioactive components close to the sample chamber.

The multichannel analyzer collects up to 4 simultaneous spectra by Boolean logic control (Polach et al. 1984). Rejected events may be recorded and this feature is used below to estimate guard detector efficiency.

LOW-BACKGROUND LABORATORIES FOR LIQUID SCINTILLATION COUNTING

There are numerous laboratories using Quantulus, either underground or built from low-activity materials, to reduce environmental background radiation. BVFA Arsenal in Vienna (Aiginger et al. 1986) has 1.6 m of concrete, 0.6 cm of steel, and 3-cm lead linings and the positive pressure of filtered air. The reduction of gamma flux is 1:20 as in the Wallac low-level laboratory (Kaihola et al. 1986). The latter has 0.5 m of low-activity concrete and 0.5 m of normal concrete outside the first layer. The room is a Faraday cage and in overpressure of filtered air to remove radon. The University of Arizona Radiocarbon Laboratory in Tucson, Arizona, has an underground laboratory with 5 Quantuluses which have a 10-m overburden at 15 °C (Kalin and Long 1989). The instrument temperatures for ^{14}C dating are kept close to the benzene freezing point at 7 °C. The VKTA Rossendorf laboratory in Dresden is built in an old wine cellar with carefully selected construction materials and 47 m of rock (110 m water equivalent) above, which blocks 98% of the cosmic muon flux (Niese et al. 1998). The Gran Sasso National Laboratory (National Institute of Nuclear Physics) has the most overburden of rock for labs where any Quantuluses have resided so far. It has a depth of 1400 m, equivalent to 3800 m of water (Plastino et al. 2001), which reduces the cosmic flux to 1 millionth of the surface value.

BACKGROUND REDUCTION IN QUANTULUS

Phototubes contain some ^{40}K and Cerenkov radiation produced in the envelope by 1.3-MeV beta particles (89% of all decays). This radiation can also channel into the other phototube and these cross-talk events may be detected as coincidences. Similarly, there is fluorescence from glass with longer pulse length, and these events can be separated by pulse shape analysis (Kaihola 1991). Cross-talk events can be rejected by the pulse amplitude comparator (PAC), which is controlled by software to exclude events in high left/right signal amplitude disparity. This method always leads to some loss of ^{14}C signal and should be avoided for high-quench samples and for ^3H , because the number of photons from such a decay event is very low. The amplitude disparity is high in such cases and application of the PAC would cause serious efficiency loss. The PAC has been tuned to have a milder effect in the low-energy region in order not to distort the sample spectrum. Cross-talk events can also be rejected by special vial designs, where unused volume is replaced by a massive, non-transparent cap and base (copper-teflon vial by Wallac; Polach et al. 1983). This design leads to a linear dependency of sample background on its volume (Kaihola et al. 1992).

ATMOSPHERIC PRESSURE EFFECTS

Atmospheric pressure variation has an observable effect on the anti-Compton guard detector count rate (Figure 1). The cosmic muon flux is lower during a high-pressure period (Figure 2). The Comp-

ton electron spectrum of the environmental and inherent gamma background also has an additional, variable cosmic component (Figure 3).

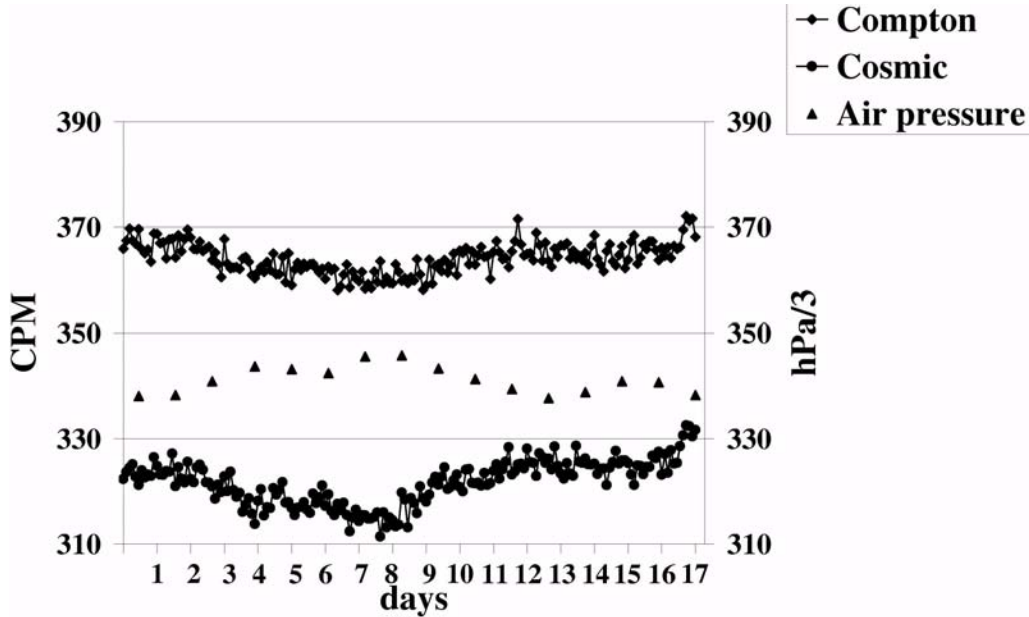


Figure 1 Guard Compton electron and muon peak count rate variation with air pressure on the surface (Wallac low-level laboratory) for 17 days. Air pressure reading (hPa) has been divided by 3 to scale down.

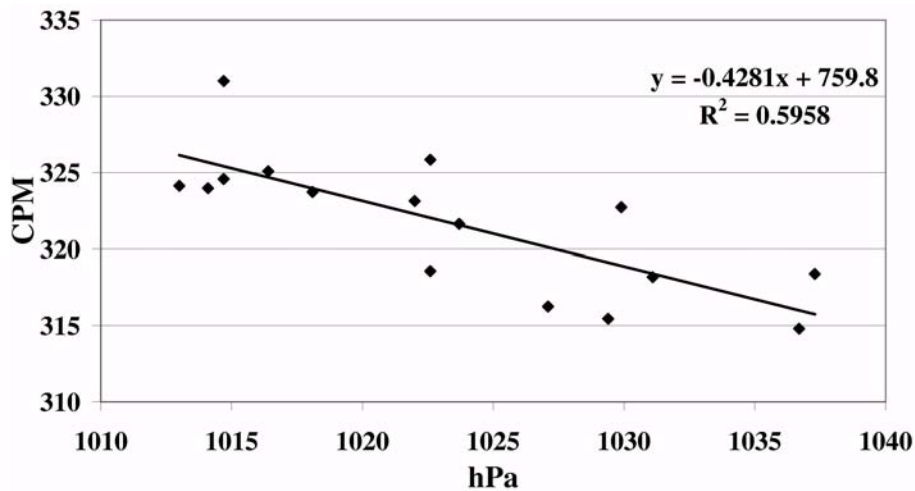


Figure 2 Guard muon count rate versus atmospheric pressure

The guard efficiency is calculated in the sample spectrum energy range, i.e., by the fraction of sample counts coincident with the guard to the total sample count rate. In the ¹⁴C counting mode, with the pulse amplitude comparator, PAC = 1 (inactive), as in the following:

$$\text{Guard efficiency} = 100 \times \text{SP12}/(\text{SP11}+\text{SP12}),$$

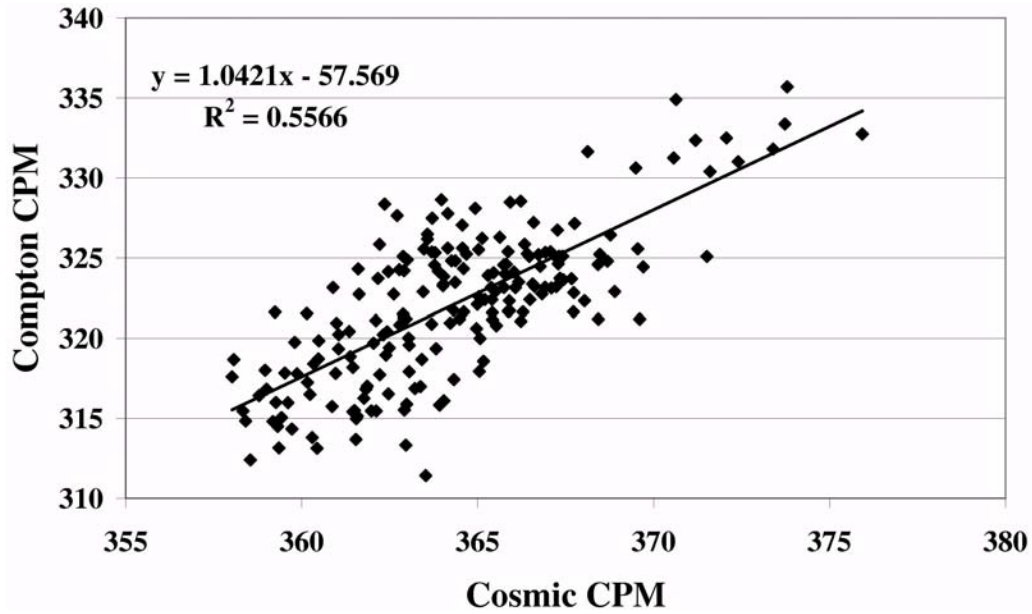


Figure 3 Compton count rate versus cosmic muon count rate under variable air pressure for 17 days

where SP12 is the guard rejected or coincidence counts and SP11 is the net accepted or anticoincidence counts. Efficiency is given as a removed fraction of background water sample events on the surface (Figure 4) and in the underground laboratory (Figure 5).

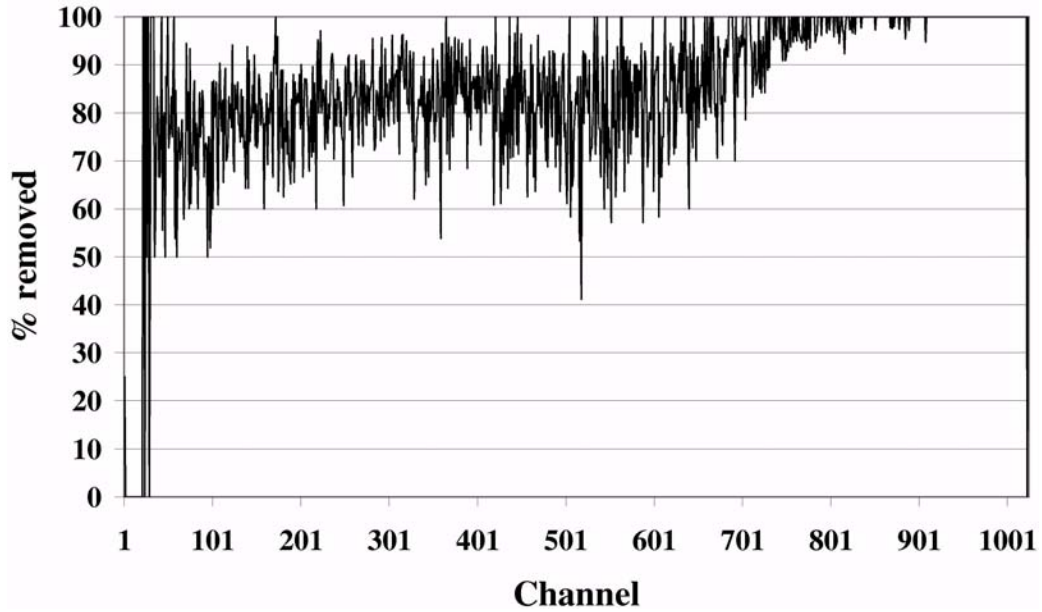


Figure 4 Guard efficiency in 6 mL water:9 mL OptiPhase HiSafe 3, measured in Wallac production hall

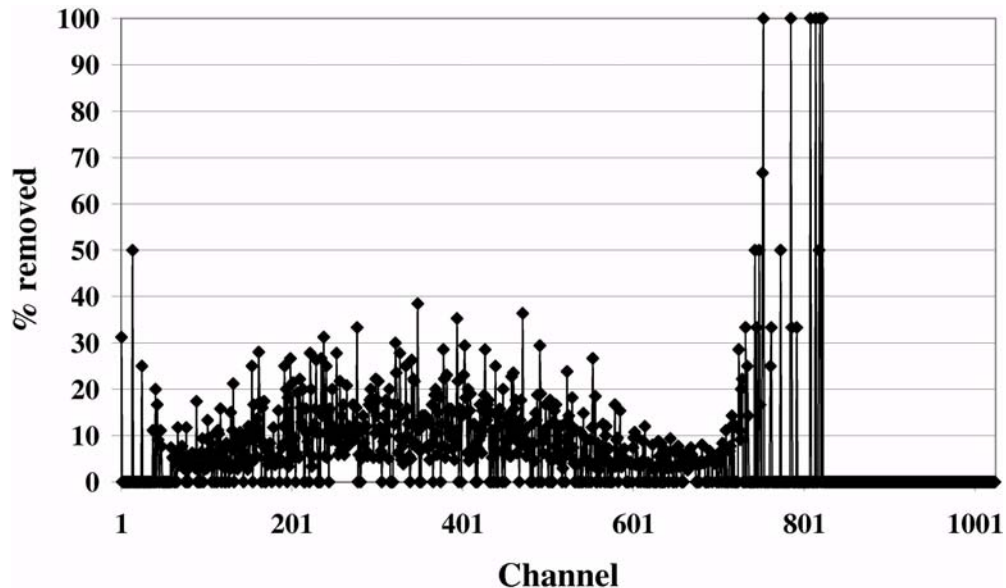


Figure 5 Guard efficiency in the Gran Sasso National Laboratory measured with a water sample, 8 mL:12 mL (water: Ultima Gold LLT)

The guard efficiency in cosmic muon channels 750–1024 is 99.0% on the surface. The full sample window (Ch 1–1024) efficiency is 86.9%, and in Ch 1–749 the efficiency is 82.3%.

In underground measurements, the efficiency is given as 100% above channels 750, if no counts were recorded. The mean guard efficiency in Compton channels 1–750 is 7.6%.

The drop of guard efficiency below 80% (PAC = 1 or inactive in ^{14}C counting mode) always means some extra activity in the vial, in the sample (which also includes cocktail) (Kaihola 1993), and/or in the counting chamber (contamination or radon). The drop is also observed in the case of the absence of cosmic radiation, when inherent sample phototube activity is a greater proportion of total background and remains undetected in the Gran Sasso lab.

BACKGROUND DEPENDENCE ON ENVIRONMENTAL GAMMA RADIATION

The sample background varies with environmental gamma background. It is possible to give an estimate of the expected ^{14}C background when the guard Compton continuum count rate is known (Figure 6).

Sample background variations between laboratories are due to different environmental gamma fluxes in each laboratory. Backgrounds are stable in each individual laboratory when the environmental conditions remain steady.

VOLUME DEPENDENCE OF SAMPLE BACKGROUND

Special vial designs eliminate cross-talk events, as in copper-teflon vials by Wallac where unused volume is replaced by a massive, non-transparent cap and base (Polach et al. 1983). This masked vial design leads to linear dependency of sample ^{14}C background on its volume. Figure 7 shows a graph (other surface labs) down to 0.3-mL masked vial size, with extrapolated 0.05-CPM empty vial

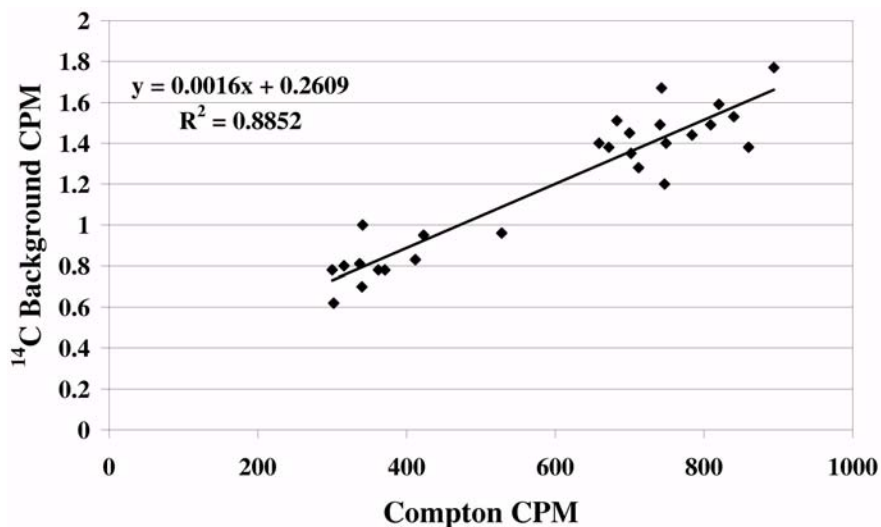


Figure 6 Background count rate in optimum ¹⁴C window versus guard Compton rate in 15-mL copper-teflon vials in 27 laboratories. Sample is benzene with 15 mg/mL butyl-PBD as scintillant.

background (Kaihola et al. 1992). When a large 9-mL teflon vial is used for variable volumes, background dependence is again linear, but additional contribution remains due to the unfilled empty volume, which is a source of air scintillations (Kaihola 1996). The surface laboratory (Bologna) has extrapolated a 0.26-CPM background at zero benzene volume in a 9-mL unmasked vial, while underground (Gran Sasso) it is 0.04 CPM (Plastino et al. 2001).

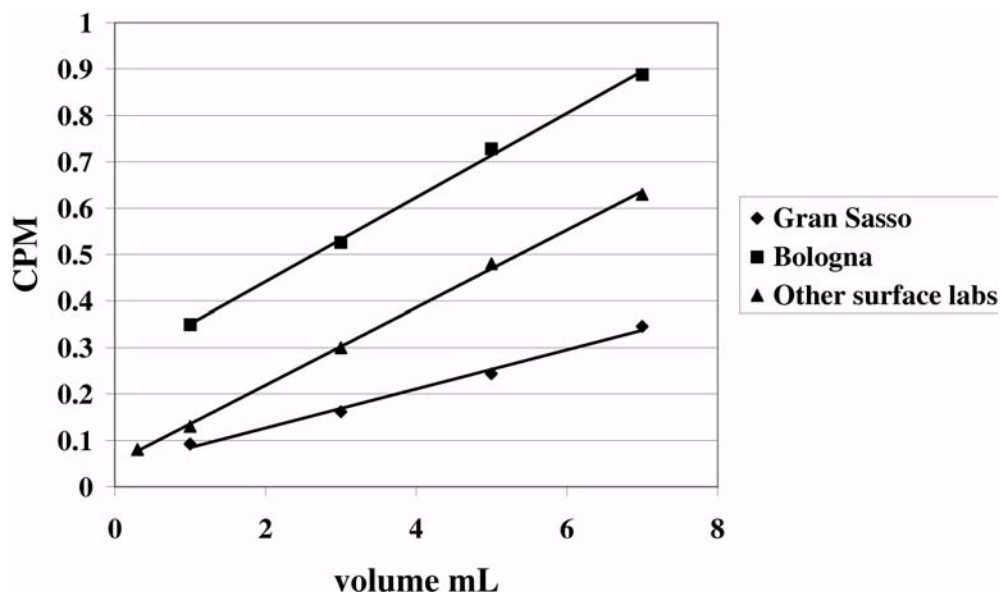


Figure 7 Background dependence on benzene volume in Gran Sasso National Laboratory, 9-mL unmasked teflon vial ($CPM = 0.0422 \times V + 0.0422$); Radiocarbon Laboratory ENEA-Bologna, 9-mL teflon vial ($CPM = 0.0908 \times V + 0.2598$); other surface laboratories, 3-, 7-, 15-, and 20-mL masked copper-teflon vials and 0.3-mL teflon vial in a black masking Delrin adapter ($CPM = 0.0844 \times V + 0.0507$).

The masked vial filled with benzene approaches the same zero volume background on the surface as an unmasked vial with equivalent benzene volumes underground in Gran Sasso. Absolute background figures in Gran Sasso are about a half of the surface figures of the ideal masked vials.

DISCUSSION

The Quantulus is well equipped with various background reduction devices. Background variation due to atmospheric pressure effects is resolved by these devices. However, the most important factor is to have a clean counting environment with no additional background variations in gamma flux. Radon concentration should be kept very low ($<10 \text{ Bq/m}^3$) and constant. Access of sunlight to the sample preparation area and counting room should be prevented; incandescent lighting is always better for such rooms than fluorescent lighting. Samples stabilize in about 4 hr to the instrument temperature and chemiluminescence decays at the same time.

Since the cosmic flux is negligible in the Gran Sasso laboratory, we can attribute the sample background to be fully derivable from the instrument's internal and external gamma radiation. The gamma flux in the laboratory is not negligible and radon is present in the water that flows into the laboratory (Plastino and Bella 2001). The laboratory is well ventilated and stable in temperature (9 °C); therefore, no cooling unit is used in the Quantulus. The instrument is placed in a steel container, which is a good Faraday cage and also shields from radon.

The guard Compton continuum, channels 50 to 850, comes from the phototubes, the environmental gamma scattering, and from secondary cosmic interactions. The latter is missing in Gran Sasso and is very small on the surface, while the environmental gamma scattering is constant. Thus, the variation of the Compton continuum reflects the environmental radioactivity of the laboratory and can be correlated with instrument performance in sample counting.

CONCLUSIONS

Atmospheric pressure variations cause both cosmic flux variations. The guard is, however, so efficient for high-energy cosmic radiation that the variation does not show as a sample signal. The guard count rate is opposite the air pressure phase.

The big difference in the guard detector efficiency between surface laboratories and underground laboratories such as Gran Sasso is related to the absence of cosmic and associated lower energy Compton radiation. The inherent radioactivity of phototubes is a larger fraction of the total background signal in Gran Sasso. The role of radon remains to be examined in an environment where its presence is eliminated.

Masked vials approach the same zero volume background on the surface as an unmasked vial in the Gran Sasso National Laboratory, where absolute backgrounds are about a half of the surface figures.

ACKNOWLEDGEMENTS

We wish to thank Prof Eugenio Coccia, Director of Gran Sasso National Laboratory, for his kind collaboration. The work was funded by EU-LNGS (INFN) (HPRI-CT-2001-00149)–LNGS (INFN)-TARI (P06/02): BACLIS (Background Characterisation for Liquid Scintillation Spectrometry at the underground laboratory of Gran Sasso).

REFERENCES

- Aiginger H, Maringer FJ, Rank D, Unfried E. 1986. A new laboratory for routine low-level measurements (BVFA Arsenal, Wien). *Nuclear Instruments and Methods in Physics Research B* 17:435–7.
- Buzinny M, Skripkin V. 1995. Newly designed 0.8-mL teflon vial for micro-volume radiocarbon dating. *Radiocarbon* 37(2):743–7.
- Haas H. 1979. Specific problems with liquid scintillation counting of small benzene volumes and background count rates estimation. In: Berger R, Suess HE, editors. *Radiocarbon Dating*. Berkeley: University of California Press. p 246–55.
- Hogg A. 1992. Assessment of 0.3-mL minivials for radiocarbon dating by liquid scintillation counting of benzene. *Radiocarbon* 34(3):389–93.
- Kaihola L, Kojola H, Kananen R. 1986. Low-level liquid scintillation counter performance in a low-level surface laboratory. *Nuclear Instruments and Methods in Physics Research B* 17:509–10.
- Kaihola L. 1991. Liquid scintillation counting performance using glass vials in the Wallac 1220 Quantulus. In: Ross H, Noakes JE, Spaulding JD, editors. *Liquid Scintillation Counting and Organic Scintillators*. Chelsea: Lewis Publishers. p 495–500.
- Kaihola L, Kojola H, Heinonen A. 1992. A minivial for small sample ^{14}C dating. *Radiocarbon* 34(3):402–5.
- Kaihola L. 1993. Glass vial background reduction in liquid scintillation counting. *The Science of the Total Environment* 130/131:297–304.
- Kaihola L. 1996. Direct detection of radon gas in air using a liquid scintillation counter. In: *Technologically Enhanced Natural Radiation by Non-Uranium Mining*. Katowice: Central Mining Institute. p 169–75.
- Kalin RM, Long A. 1989. Radiocarbon dating with the Quantulus in an underground counting laboratory: performance and background sources. *Radiocarbon* 31(3):359–67.
- Niese S, Köhler M, Gleisberg B. 1998. Low-level-counting techniques in the underground laboratory “Felsenkeller” in Dresden. *Journal of Radioanalytical and Nuclear Chemistry* 233(1–2):167–72.
- Plastino W, Bella F. 2001. Radon groundwater monitoring at underground laboratories of Gran Sasso (Italy). *Geophysical Research Letters* 28(14):2675–78.
- Plastino W, Kaihola L, Bartolomei P, Bella F. 2001. Cosmic background reduction in the radiocarbon measurement by liquid scintillation spectrometry at the underground laboratory of Gran Sasso. *Radiocarbon* 43(2A):157–61.
- Polach H, Gover J, Kojola H, Heinonen A. 1983. An ideal vial and cocktail for low-level scintillation counting: copper-shielded PTFE (Teflon) and butyl-PBD. In: McQuarrie SA, Ediss C, Wiebe LI, editors. *Advances in Scintillation Counting*. Edmonton: University of Alberta Press. p 508–25.
- Polach H, Kojola H, Nurmi J, Soini E. 1984. Multiparameter liquid scintillation spectrometry. *Nuclear Instruments and Methods in Physics Research B* 5:439–42.

MEASUREMENT OF LOW ^{14}C ACTIVITIES IN A LIQUID SCINTILLATION COUNTER IN THE ZAGREB RADIOCARBON LABORATORY

Nada Horvatinčić¹ • Jadranka Barešić • Ines Krajcar Bronić² • Bogomil Obelić

Rudjer Bošković Institute, P.O.Box 180, 10002 Zagreb, Croatia.

ABSTRACT. Two methods of chemical preparation of radiocarbon samples are implemented in the Zagreb Radiocarbon Laboratory for measurement by a new liquid scintillation counter (LSC), Quantulus 1220TM: a CO₂ absorption method (LSC-A) and a benzene synthesis method (LSC-B). For samples prepared by both methods, the optimal counting windows for measurement in LSC were determined. The total efficiency of LSC-A is 65% and that of the LSC-B is 83%, while the corresponding ^{14}C dating limits are 31,800 yr and 52,160 yr, respectively.

^{14}C activities measured by the LSC-A and LSC-B methods were compared with those measured by the gas proportional counter (GPC) method (efficiency 75%, ^{14}C dating limit 37,500 yr). The results obtained by the LSC-A method have larger errors than those measured by the GPC method, but LSC-A is quick, inexpensive, simple, and requires less carbon than the GPC method. Thus, LSC-A is suitable for ^{14}C measurements of geological, hydrological, and environmental samples. On the other hand, the results obtained by the LSC-B method give smaller errors and a larger ^{14}C dating range. Therefore, LSC-B is more suitable for ^{14}C dating of archaeological samples.

INTRODUCTION

Radiocarbon activity in archaeological, geological, environmental, and hydrological samples has been measured in the Zagreb Radiocarbon Laboratory at the Rudjer Bošković Institute since 1968 by the gas proportional counter (GPC) technique. In order to improve the capability of low-level ^{14}C measurement in our laboratory, we recently obtained a new liquid scintillation counter (LSC), Quantulus 1220TM, which is placed in the same ground-floor room with the GPC system, where we can control environmental parameters.

Sample preparation methods for the GPC technique and our participation in international intercomparison studies have been described previously (Srdoč et al. 1971; Horvatinčić et al. 1990, 1995; Krajcar Bronić et al. 1995). Briefly, after pretreatment by the acid-base-acid method, organic samples are combusted in a stream of pure oxygen. Carbonate samples are dissolved by acid (HCl or H₃PO₄). The obtained and purified CO₂ is then catalytically converted to methane, which is used as the counting gas in GPC.

Two methods of chemical preparation of samples for ^{14}C activity measurement by LSC are implemented: a CO₂ absorption method (LSC-A) and a benzene synthesis method (LSC-B). The preparation lines have been constructed following the descriptions of similar lines in previous literature (*LSC-A*: Qureshi et al. 1989; Rao and Killely 1994; Aravena et al. 1989; Nair et al. 1995; Woo et al. 1999; Momoshima et al. 1993; *LSC-B*: Noakes et al. 1965; Tamers 1975; Belluomini et al. 1978; Gupta and Polach 1985; McCormac et al. 1993; Enerson et al. 1998; Muraki et al. 1998; Pawlyta et al. 1998; Cook 2002, personal communication) with some modifications. In this paper, we describe the procedures for the absorption method and for the benzene synthesis, as well as different tests that were performed during the implementation of both methods. We have determined the optimal parameters for measurements in LSC for samples prepared by both methods, e.g. ^{14}C window, efficiency, and figure of merit. Finally, we discuss the results of ^{14}C activity measurements by both LSC-A and LSC-B methods and compare them with those obtained by the GPC method.

¹Email: Nada.Horvatincic@irb.hr.

²Corresponding author. Email: krajcar@irb.hr.

For all tests, we used CO₂ borehole gas containing no ¹⁴C ($a^{14}\text{C} = 0$ pMC), which has been used as background gas also for the GPC technique, and carbonate obtained from recent shells from the Adriatic Sea ($a^{14}\text{C} = 100$ pMC, $\delta^{13}\text{C} = 0\text{‰}$ VPBD), the activity of which has been determined previously by GPC. The ¹⁴C activity of all prepared samples was measured by LSC and the quenching effect was assessed with an index called the Standard Quench Parameter, SQP(E) (hereafter “SQP”), which represents the end-point of the external standard spectrum, i.e., the channel number beyond which 1% of the total counts are found. As an external standard, we used a built-in 37-kBq ¹⁵²Eu capsule. The LSC running and data acquisition were performed by using Wallac WinQ Windows software for controlling Wallac 1220 Quantulus™ (Version 1.2), and for data processing we used the Wallac EASY View Spectrum Analysis Program (Version 1.0).

SAMPLE PREPARATION

Method LSC-A

The vacuum line for CO₂ absorption (Figure 1) consists of the following: (1) a steel container with a CO₂ sample; (3) a U-tube with silica-gel for CO₂ purification; a manometer and (2) a needle valve for CO₂ flow regulation; (4) a 20-mL low-potassium glass vial with absorption mixture (*Carbosorb E*® + *Permafluor E*®) cooled with ice; and (5) a flow meter/bubbler. The amount of CO₂ absorbed in the absorption mixture is determined by weighing the glass vial with the mixture before and after the absorption.

In order to obtain optimal conditions for sample preparation, we performed tests by varying the CO₂ flow rate and the composition of the absorption mixture. For all prepared samples, the SQP and count rate have been determined by liquid scintillation counting.

The CO₂ flow rate in the absorption system was varied by the needle valve. Taking into account the reproducibility of the loaded CO₂, we chose a medium flow rate of about 70 mL CO₂ per min for routine sample preparation. Under such a flow rate, it takes about 15 min until the bubbles appear in the bubbler at the end of the line, indicating that the absorption mixture is almost saturated with CO₂. Some CO₂ can still be absorbed after the first bubbles have appeared; therefore, we continued the overflow of CO₂ for 10 min to assure saturation. It was established that the samples with no saturation of absorption mixture by CO₂ show stronger quenching, i.e., have lower SQP values (Figure 2) and as such are not suitable for measurement. Stronger quenching of not-completely-loaded samples was also observed by Rao and Killey (1994), while Qureshi et al. (1989) used the quenching parameter as an indirect method to estimate the amount of absorbed CO₂ instead of direct weighing. The best SQP value was obtained for about 2.15 g of the absorbed CO₂ in a mixture consisting of 10 mL *Carbosorb E* and 10 mL *Permafluor E*. In some cases, we obtained overloaded samples, i.e., the amount of absorbed CO₂ was higher than given theoretically by the manufacturer's specification (0.22 g CO₂ per 1 mL of *Carbosorb*) and the SQP of such samples decreased again (Figure 2). Nair et al. (1995) also observed stronger quenching in samples overloaded by CO₂. Therefore, the SQP of a sample for ¹⁴C activity measurement prepared by the absorption method can serve as an indicator of the amount of absorbed CO₂. For ¹⁴C activity calculation, we use only samples saturated but not overloaded with CO₂, with an SQP in the range of 710–725 (Figure 2).

To determine the best composition of the absorption mixtures, we performed test samples setting the ratio of *Carbosorb E* to *Permafluor E* to 9:11, 10:10, 11:9, 12:8, 13:7, 14:6, and 15:5. All samples were prepared by the adopted standard procedure, keeping the CO₂ flow rate constant (about 70 mL/min) with a 10 min overflow, and keeping the total volume of the absorption mixture equal to 20 mL.

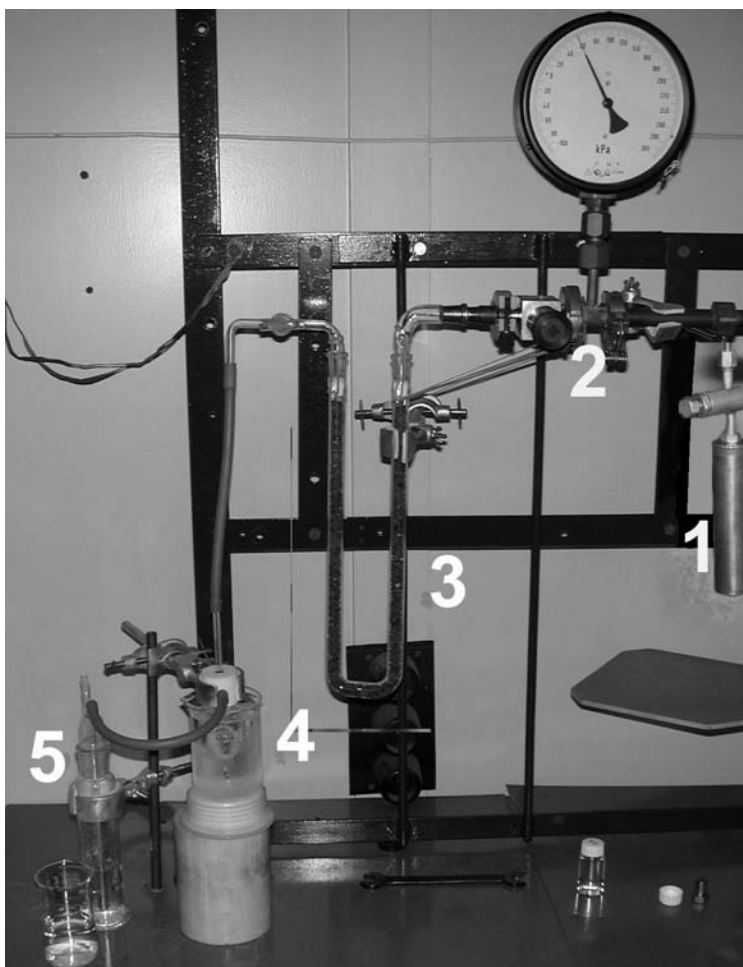


Figure 1 Preparation line for the CO_2 absorption: 1—metal container with CO_2 sample; 2—needle valve; 3—U-tube with silica-gel; 4—vial with absorption mixture (Carbosorb E + Permafluor E) immersed in mixture of ice and water; 5—bubbler.

The amount of CO_2 absorbed in the mixture increases with the amount of Carbosorb E, but the relative amount of CO_2 per mL of Carbosorb E remains constant (~ 0.21 g/mL). The SQP decreases as the quantity of Carbosorb E increases because Carbosorb E is a strong quencher (Qureshi et al. 1989; Rao and Killey 1994; Woo et al. 1999). The count rate of background samples does not depend on the amount of Carbosorb E; the count rate of the active sample shows a maximum for approximately 12 mL Carbosorb E in the absorbing mixture. The counting efficiency (Figure 3)—determined as the ratio of the measured count rate, expressed in counts per minute (cpm), to the sample activity, expressed in disintegration per minute (dpm)—shows a maximum of about 62% for the mixture containing 10 mL of Carbosorb E. A similar counting efficiency (60%) was obtained also by Qureshi et al. (1989) and Nair et al. (1995) for the component ratio 1:1 in the absorption mixture. Taking into account all these findings, we decided to use the mixture of 10 mL Carbosorb E and 10 mL Permafluor E in a routine sample preparation.

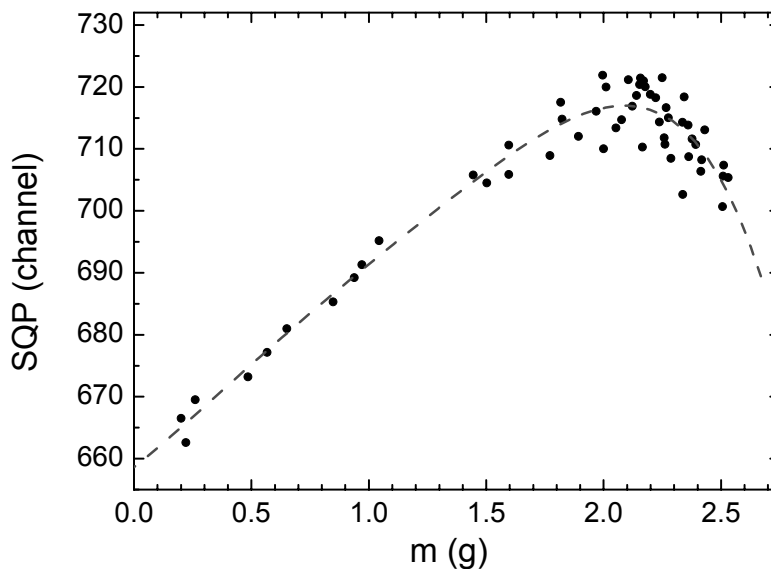


Figure 2 Standard Quench Parameter (SQP) as a function of the amount of the absorbed CO_2 in adsorption mixtures consisting of 10 mL Carbosorb E and 10 mL Permafluor E. Symbols: measurements; dotted line: polynomial fit.

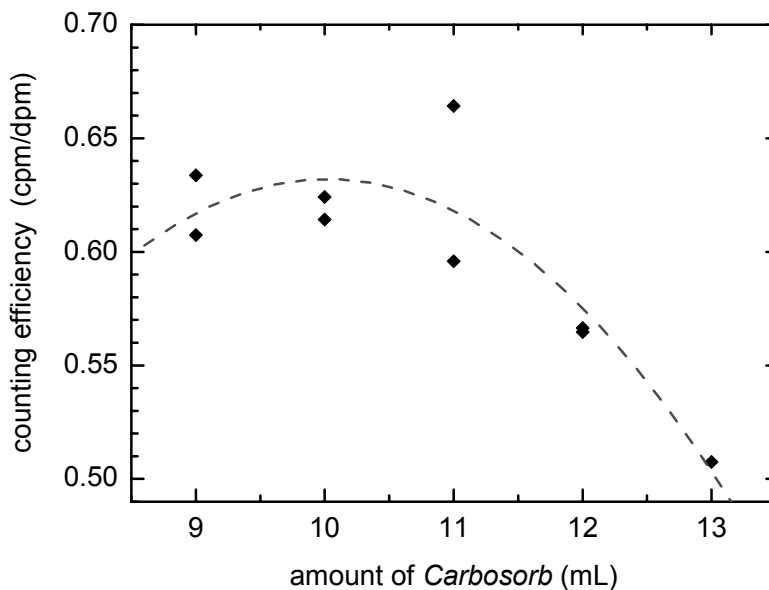


Figure 3 Counting efficiency as a function of the amount of Carbosorb in the absorbing mixture. The remaining of the total volume of 20 mL is Permafluor. Symbols: measurements; dotted line: polynomial fit.

To test the reproducibility of the procedure, we repeated the absorption of the CO_2 obtained from the same sample (replicate sample preparation). We found that the process gives reproducible results (SQP, count rate, efficiency, ^{14}C activity) if the saturation of the absorption mixture with CO_2 has been achieved.

Method LSC-B

For the LSC-B method, the vacuum line for benzene synthesis has been constructed (Figure 4). The first step involves the reaction of CO_2 with lithium at $700\text{--}900\text{ }^\circ\text{C}$ to produce lithium carbide. CO_2 stored in glass bulbs (2) is successively added into a stainless steel reactor (1) containing metallic lithium in stoichiometric quantity with an excess of 30%. The reaction is controlled by CO_2 pressure in the reactor and monitored through a glass window on the top of the reactor. After cooling and pumping of the reaction vessel, the lithium carbide is subsequently hydrolyzed to acetylene by slowly adding distilled water (15). The obtained acetylene passes through a water trap cooled to $-50\text{ }^\circ\text{C}$ (5) and is frozen in the next 2 traps (6, 7), which are cooled by liquid nitrogen under a dynamic vacuum. The purification of acetylene is realized by passing through a trap containing phosphoric acid with glass beds (8) in order to remove nitrogen compounds, and a cold trap (9) for water removing. Trimerization of acetylene to benzene is performed on the vanadium catalyst supplied from the Kyiv Laboratory (according to the procedure in Arslanov et al. 1993). Before reaction, the catalyst is activated in an oven (13) at $350\text{ }^\circ\text{C}$ for 10 hr. Acetylene from bulbs (11) slowly sublimates on the catalyst (13) while the temperature of the reaction (monitored by thermocouple 14) has been kept below $90\text{ }^\circ\text{C}$ by immersing the catalyst vessel into the mixture of water and ice. The obtained benzene is extracted into a glass finger (12) by heating the catalyst to $150\text{ }^\circ\text{C}$ and simultaneously cooling the finger with liquid nitrogen.

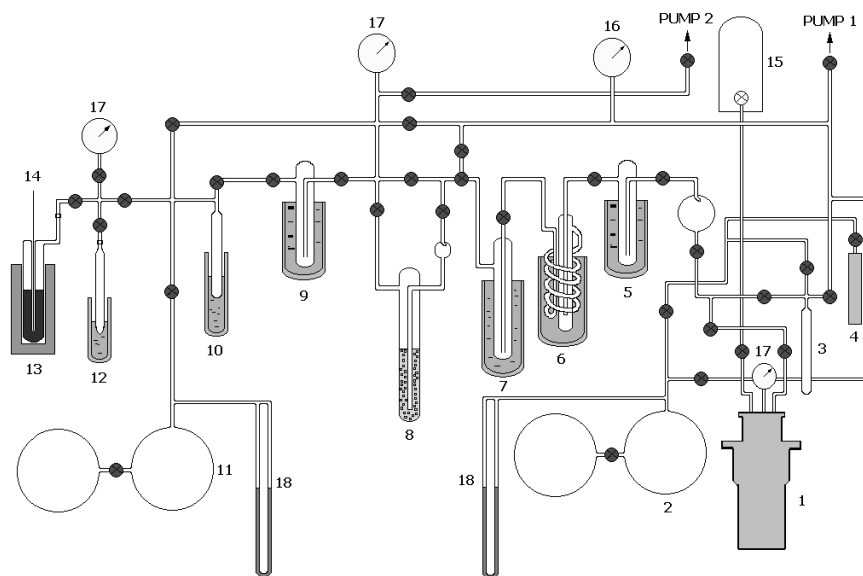


Figure 4 Benzene synthesis line: 1–reaction vessel; 2–bulbs for CO_2 storage; 3–glass finger for CO_2 ; 4–metal container for CO_2 ; 5,9–water traps cooled with mixture of ethanol and liquid nitrogen; 6,7– C_2H_2 traps cooled with liquid nitrogen; 8–trap with H_3PO_4 and glass beds; 10–glass finger for C_2H_2 cooled with liquid nitrogen; 11–bulbs for C_2H_2 storage; 12–glass finger for C_6H_6 cooled with liquid nitrogen; 13–vanadium catalyst heated by oven; 14–thermocouple; 15–reservoir with distilled water; 16–Pirani gauge; 17–Bourdon gauges; 18–Hg manometers.

Several tests for benzene synthesis were performed: duration of carbide and hydrolysis reaction, type of C_2H_2 purification, and duration and temperature of catalytic trimerization. The test results showed that the optimal time of the carbide and hydrolysis reaction is 20 min and 30–40 min, respectively. The temperature of the catalytic reaction is between $60\text{--}90\text{ }^\circ\text{C}$, with a duration of 1–2 hr, depending

on the quantity of acetylene. The acetylene yields range from 89% to 98% and benzene yields range from 77% to 90%. The purification process described above gives benzene of purity 98.9% to 99.5%, as determined by gas chromatography. The main impurity in all benzene samples is toluene.

To prepare the scintillation cocktail for LSC measurements, the recommended quantity of 15 mg of butyl-PBD per 1 g of benzene is added (Gupta and Polach 1985). The cocktail is then put into 7-mL low-potassium glass vials (pico-vials). To test the sensitivity of the cocktails on the amount of added butyl-PBD, we prepared cocktails with 7 mg and 22 mg butyl-PBD per 1 g of benzene (i.e. 50% and 150% of the recommended amount). We observed no significant changes in either count rate or SQP.

MEASUREMENTS IN LSC

We determined the optimal parameters for ^{14}C activity measurement by LSC for samples prepared by both the LSC-A and LSC-B methods. By comparing the standard deviation of the measured count rate with the number of 30-min cycles, we established the number of cycles in a run to 30 (or more), resulting in 900 (or more) min per sample measurement.

The counting efficiency (E) was determined from the ratio of measured (net) count rates (A_{meas} , expressed in cpm) and the known ^{14}C activity of the standard (A , expressed in dpm):

$$E = A_{meas} / A \quad (1).$$

Typical spectra for inactive and active standard prepared by the LSC-A and LSC-B methods are illustrated in Figure 5. The area of spectrum containing the ^{14}C spectrum, the so-called “ ^{14}C window” (between the dashed lines in Figure 5), encompasses the channels between 109 and 431 and between 127 and 580 for LSC-A and LSC-B, respectively. The counting efficiencies in these areas are 70% and 90%, respectively.

Optimization of the counting system consists of moving the boundaries of the ^{14}C window during the processing of spectra in order to decrease as much as possible the background count rate (B), and at the same time not to lose the essential part of the ^{14}C spectrum (A_{meas}). The optimal measuring window for the LSC-A technique was established to be between channels 144 and 372 (the area between the full lines in Figure 5), which encompasses 93% of the total ^{14}C spectrum and 77% the background spectrum. In such a way, we determined the total efficiency for LSC-A to be 65%. The figure of merit ($FM = A_{meas}^2/B$) has been improved from 16 to 18.4 (Table 1).

Optimization of the counting window for the LSC-B technique resulted in background reduction to 64% of that in the ^{14}C window, while 92% of the ^{14}C spectrum has remained in the window. Therefore, the total efficiency of the LSC-B technique is 82.4% and the figure of merit is considerably improved (from 2200 to 2908). Comparison of some basic parameters of the measurement of ^{14}C in the counting windows is shown in Table 1, where data for our GPC system are also shown for comparison.

Several samples prepared by the LSC-A method have been measured repeatedly during longer periods of time (4 months) to test the stability of the prepared samples. Since no significant changes in either count rate or SQP have been noticed, we concluded that measurements can be performed also some time after the sample preparation.

When the sample is measured immediately after preparation, the presence of radon may influence the count rate. However, radon can be easily detected in the upper part of the spectrum. We control the count rate in the so-called “radon window” (channels 450–700 for the LSC-A samples) for routine measurement.

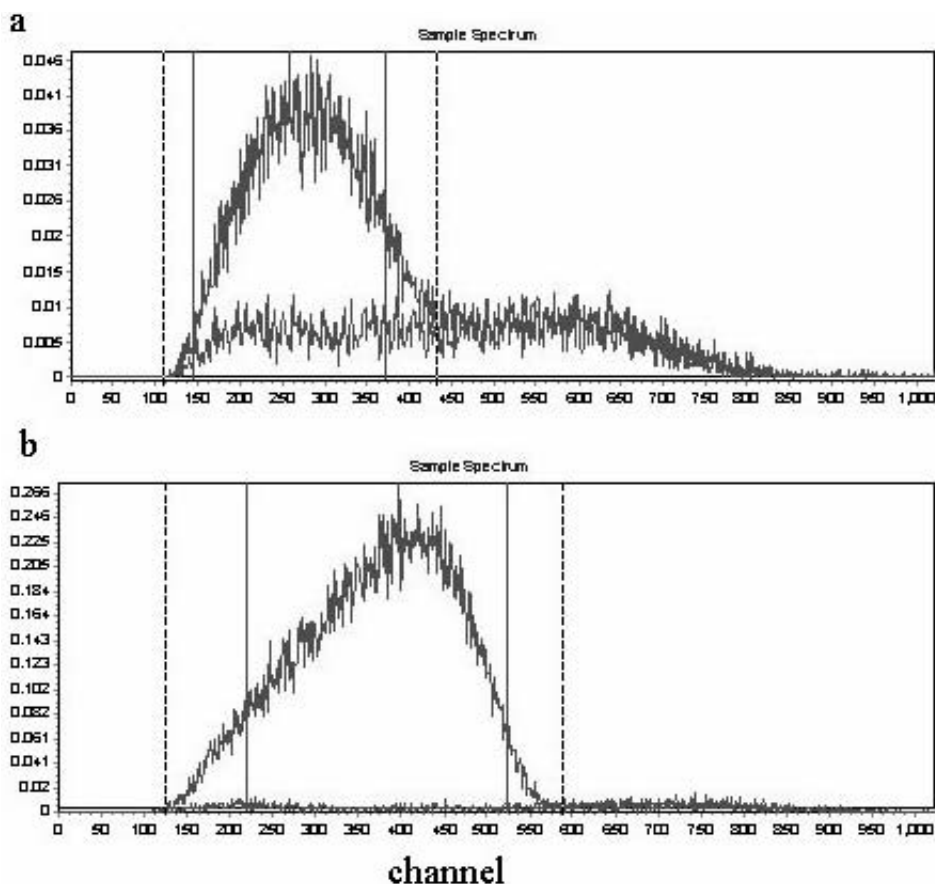


Figure 5 Characteristic ^{14}C spectra obtained in LSC. a) LSC-A preparation method (absorption of CO_2). b) LSC-B preparation method (benzene synthesis). Upper spectra: modern shells (100 pMC); bottom: background. Dashed lines: limits of the ^{14}C windows; full lines: limits of the counting windows.

Table 1 Comparison of characteristic parameters of all 3 ^{14}C measurement techniques. LSC-A: absorption of CO_2 and LSC measurement; LSC-B: benzene synthesis and LSC measurement; GPC: methane preparation and gas proportional counting. The data for LSC-A and LSC-B technique correspond to the optimized counting windows.

Value	Symbol (unit)	LSC-A	LSC-B	GPC
Amount of carbon	m (g)	0.59	4.5	2.01
Spectrum area (counting window)	(channel)	144–372	219–525	—
Real activity of standard (100 pMC)	A (dpm)	7.98	61.06	27.34
Count rate of background	B (cpm)	1.47	0.87	5.54
Net count rate of standard (100 pMC)	A_{meas} (cpm)	5.20	50.30	20.47
Efficiency	$E = A_{meas} / A$ (%)	65	82.4	75
Figure of merit	$FM = A_{meas}^2 / B$	18.4	2908	75.7
Maximum age ($t_{meas} = 1200$ min)	T_{max}^a	31,800	52,160	37,500

$$^a T_{max} = 8033 \times \ln(0.3546 \times A_{meas} \times \sqrt{t_{meas}/B})$$

We compared the benzene background count rate and the count rate of a spike sample in glass pico-vials and in special low-background teflon-copper vials (Wallac-Perkin Elmer). The use of special teflon-copper vials reduces the background count rate significantly (and the figure of merit is better, 9000, in teflon-copper vials), but the difference in the ^{14}C spectra shape and count rates of the spike sample is negligible. In both types of vials, the background count rate (5 mL of commercial petrochemical benzene, counting window 219–525 channels) was stable in the period of 6 months, and the values were 0.80 ± 0.05 cpm in pico-vials and 0.28 ± 0.03 cpm in teflon vials. Due to the limited number of teflon vials and their rather high price, we performed all test measurements in pico-vials.

The quenching correction curve was determined for the counting geometry of 5 mL of benzene in pico-vials. A small amount of acetone was added to the spike benzene and the SQP and the count rate of such samples was measured. The obtained quenching curve is shown in Figure 6, where the relative efficiency is calculated as the ratio of the count rate in the counting window of the “poisoned” samples to the count rate of the pure spike sample. Our synthesized benzene samples of purity 98.9%–99.5% resulted in SQP values above 835; therefore, the efficiency correction due to quenching was less than 1%.

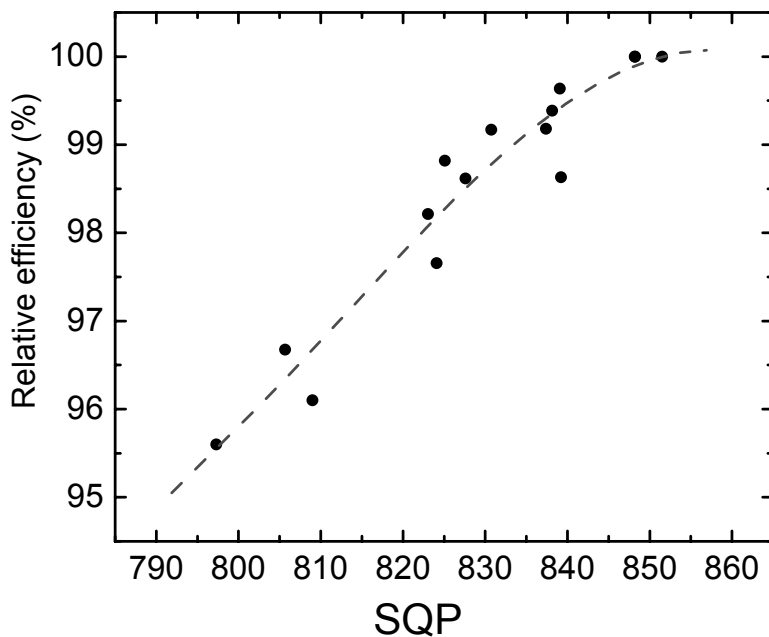


Figure 6 Quenching curve. Symbols: measured data; dashed line: polynomial fit.

RESULTS

The comparison of conventional ^{14}C ages (Stuiver and Polach 1977; Gupta and Polach 1985) of benzene samples prepared by the LSC-B method and ^{14}C ages of the same samples measured by GPC are shown in Figure 7. The LSC-B ages were corrected also for different quenching by using the quenching curve shown in Figure 6. The agreement between the LSC-B and GPC ages is good, giving the slope of the fitted line equal to 1.01 ± 0.01 . No systematic difference between the 2 sets is observed, as shown also by the intercept of the fitted line equal to 39 ± 41 yr.

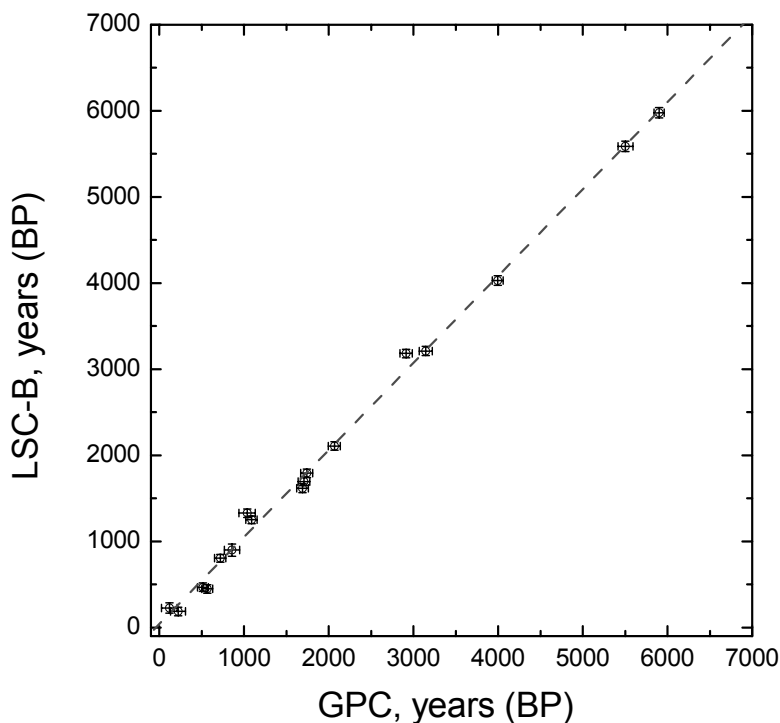


Figure 7 Comparison of conventional ^{14}C ages measured by LSC-B and GPC methods. Symbols: measured ages with corresponding $1\text{-}\sigma$ errors; line: linear fit to the measured data, slope 1.010 ± 0.015 , intercept 39 ± 41 yr, $N = 17$, $R = 0.998$.

To check the background of samples that pass different procedures of CO_2 preparation (organic and carbonate samples) in addition to the old borehole CO_2 gas that was used as a test gas in the development of the method, we synthesized benzene also from anthracite and marble. The measured count rate of all 3 kinds of background samples was the same. In Table 1, we give the mean value (0.87 ± 0.02) of all background samples in the same geometry. However, as mentioned previously, a commercially available benzene from a petrochemical source shows a slightly lower count rate (0.80 ± 0.05) under the same counting conditions.

Under the adopted counting condition, the ^{14}C dating limit (Table 1) is 52,160 yr (5-mL samples measured 1 day). The limit can be improved to 56,730 yr by using special low-background teflon-copper vials (5-mL samples measured 1 day). A larger amount of benzene (e.g., 7 mL, if the quantity of available sample allows it) would also improve the dating limit to 54,800 yr and 59,400 yr in pico and teflon vials, respectively. A longer counting time will also increase the maximal age that can be determined (57,600 yr and 62,100 yr for 7-mL samples measured 2 days in pico and teflon vials, respectively).

A comparison of ^{14}C activities (expressed in pMC) obtained by the GPC and LSC-A methods is presented in Figure 8. The agreement between the 2 sets of data is again very good (the slope of the fitted line is 1), but the uncertainties of the LSC-A results are 2–3 times larger than those of the GPC method for the same measuring time (1 day per sample). Due to the high background count rate and low efficiency (Table 1), the maximal determinable ^{14}C age is 31,800 yr. However, these characteristics are good enough for certain applications that do not require high precision and also for samples having very high ^{14}C activity.

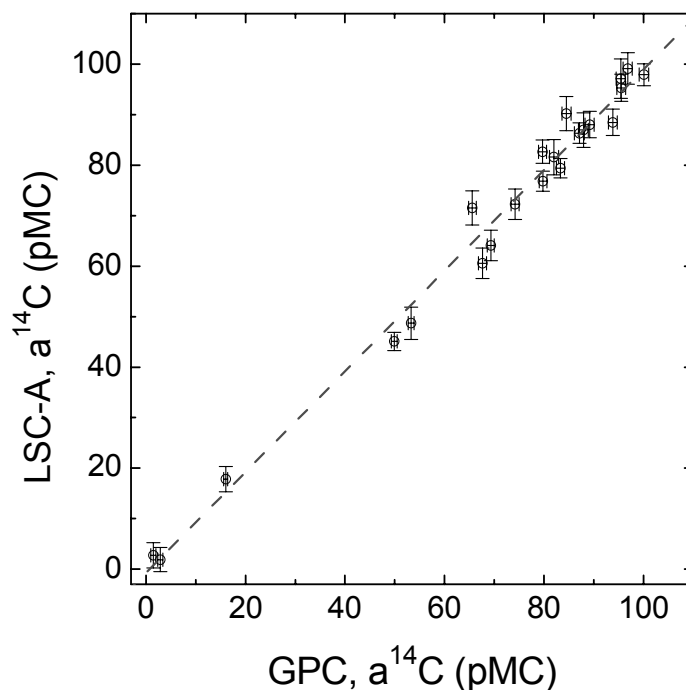


Figure 8 Comparison of ^{14}C activities measured by LSC-A and GPC methods. Symbols: measured activities with corresponding $1\text{-}\sigma$ errors; line: linear fit to the measured data, slope 0.997 ± 0.026 , intercept -0.7 ± 2.0 pMC, $N = 22$, $R = 0.993$.

As in the case of the LSC-B method, the count rate of various background materials (anthracite, marble, borehole CO_2) did not show any difference.

CONCLUSION

By introducing a liquid scintillation counter for ^{14}C activity measurement in our laboratory, we implemented also 2 new sample preparation techniques: 1) absorption of CO_2 in an absorption mixture consisting of Carbosorb E and Permaflor E (LSC-A), and 2) benzene synthesis (LSC-B). The presented methods differ in complexity, time consumed, price, and in the precision of measured results. The characteristic features of all 3 techniques—GPC, LSC-A, LSC-B—of ^{14}C measurements are compared in Table 1 and the measured activities are compared in Figures 7 and 8.

The simplest preparation method, absorption of CO_2 followed by liquid scintillation counting (LSC-A), is fast and requires only about 1 g of carbon. Its characteristics are high background, low efficiency, low ^{14}C dating limit, and large errors. However, it is accurate enough for certain applications (e.g., geological, hydrological, and environmental samples). It could be used also for quick determination of increased environmental ^{14}C contamination, e.g., in the case of a nuclear accident.

The best ^{14}C dating features are obtained by benzene synthesis and liquid scintillation counting (LSC-B): low background, high efficiency, high dating limit, and good precision. The features could be improved by using special low-background teflon-copper vials, by increasing the amount of benzene, and by prolonging the counting time. Due to these good characteristics, the LSC-B method is suitable for ^{14}C dating of archaeological samples and all other samples that require high precision or are close to the limit of the ^{14}C dating method.

The features of the GPC technique lie in between the 2 LSC techniques. The method gives accurate results, as justified by participation in the international ^{14}C intercomparison studies.

All 3 methods of ^{14}C activity measurement in our laboratory allow us to choose the preparation and counting technique which best meets the need for accuracy and precision of different kinds of samples. The 3 methods also enable a higher sample through-put.

ACKNOWLEDGEMENTS

This study was supported by the Ministry of Science of the Republic of Croatia (Project 0098014) and by the IAEA within the project CRO/2/002 of Regular Programme of Technical Co-operation (2001–2002). We appreciate the help and suggestions of IAEA expert Dr D Harkness during his stay in our laboratory. Experience gained by the co-authors in the following laboratories was useful: NERC Radiocarbon Laboratory and SURRC Radiocarbon Laboratory, East Kilbride, Scotland (UK); Queen's University of Belfast Radiocarbon Laboratory, N. Ireland (UK); RCD–Radiocarbon Dating, East Lockinge, England (UK); Geochron Laboratories, Cambridge, Massachusetts (USA); and GADAM Centre, Gliwice (Poland). We thank also Dr Z Glasovac, Rudjer Bošković Institute, for gas chromatography measurements.

REFERENCES

- Aravena R, Drimmie RR, Qureshi RM, McNeely R, Fabris S. 1989. New possibilities for ^{14}C measurements. *Radiocarbon* 31(3):387–92.
- Arslanov Kh A, Tetrychnaya TV, Chernov SB. 1993. Problems and methods of dating low-activity samples by liquid scintillation counting. *Radiocarbon* 35(3): 393–8.
- Belluomini G, Delfino A, Manfra L, Petrone V. 1978. Benzene synthesis for radiocarbon dating and study of the catalyst used for acetylene trimerisation. *International Journal of Applied Radiation and Isotopes* 29: 453–9.
- Enerson TB, Haas H, Zarrabi K, Titus RL. 1998. Comparison of vanadium oxide catalysts for synthesis of benzene: benzene purity, yields and reconditioning methods. *Radiocarbon* 40(1):167–75.
- Gupta SK, Polach HA. 1985. *Radiocarbon Dating Practices at ANU*. Canberra: Radiocarbon Laboratory Research School of Pacific Studies, ANU. p 1–175.
- Horvatinčić N, Srdoč D, Obelić B, Krajcar Bronić I. 1990. Radiocarbon dating of intercomparison samples at the Zagreb Radiocarbon Laboratory. *Radiocarbon* 32(2):295–300.
- Horvatinčić N, Obelić B, Krajcar Bronić I, Srdoč D, Bistrovic R. 1995. Sources of radon contamination in C-14 dating. *Radiocarbon* 37(2):749–57.
- Krajcar Bronić I, Horvatinčić N, Obelić B, Bistrovic R. 1995. Radiocarbon intercomparison studies at the Rudjer Bošković Institute. *Radiocarbon* 37(2):805–11.
- McCormac FG, Kalin RM, Long A. 1993. Radiocarbon dating beyond 50,000 years by liquid scintillation counting. 1993 Liquid Scintillation Spectrometry. *Radiocarbon* 32(1):125–33.
- Momoshima N, Kawamura H, Takashima Y. 1993. Determination of ^{14}C in environmental materials: combination of CO_2 absorbent and a large-volume low-background liquid-scintillation counter. *Journal of Radioanalysis and Nuclear Chemistry* 173/2:323–9.
- Muraki Y, Kocharov G, Nishiyama T, Naruse Y, Murata T, Masuda K, Arslanov Kh A. 1998. The new Nagoya Radiocarbon Laboratory. *Radiocarbon* 40(1):177–82.
- Nair AR, Sinha UK, Joseph TB, Rao SM. 1995. Radiocarbon dating up to 37,000 years using CO_2 absorption technique. *Nuclear Geophysics* 9/3:263–8.
- Noakes JE, Kim SM, Stipp JJ. 1965. Chemical and counting advances in liquid scintillation age dating. *Proceedings of the 6th International Conference on Radiocarbon and Tritium Dating*. Washington, DC: Clearinghouse for Federal Scientific and Technical Information. p 68–92.
- Qureshi RM, Aravena R, Fritz P, Drimmie R. 1989. The CO_2 absorption method as an alternative to benzene synthesis method for ^{14}C dating. *Applied Geochemistry* 4:625–33.
- Pawlyta J, Pazdur A, Rakowski AZ. 1998. Commissioning of a Quantulus 1220TM liquid scintillation beta spectrometer for measuring ^{14}C and ^3H at natural abundance levels. *Radiocarbon* 40(1):201–9.
- Rao RR, Killey RWD. 1994. Quantitative separation and determination of inorganic and organic forms of total carbon and radiocarbon in natural waters and application at a radioactive waste management site. *Radiochimica Acta* 65:63–74.
- Srdoč D, Breyer B, Sliepčević A. 1971. Rudjer Bošković Institute radiocarbon measurements I. *Radiocarbon* 13(1):135–40.
- Stuiver M, Polach HA. 1977. Discussion: reporting of

- ¹⁴C data. *Radiocarbon* 19(3):355–63.
- Tamers MA. 1975. Chemical yield optimization of the benzene synthesis for radiocarbon dating. *International Journal of Applied Radiation and Isotopes* 26: 676–82.
- Woo HJ, Chun SK, Cho SY, Kim YS, Kang DW, Kim EH. 1999. Optimization of liquid scintillation counting techniques for the determination of carbon-14 in environmental samples. *Journal of Radioanalysis and Nuclear Chemistry* 239:649–55.

REHABILITATION OF THE LABORATOIRE DE CARBONE 14-DAKAR (SENEGAL) WITH A SUPER LOW-LEVEL LIQUID SCINTILLATION COUNTING SYSTEM

Maurice Ndeye^{1,2} • Oumar Ka^{1,3} • Hamady Bocoum⁴ • Alpha O Diallo¹

ABSTRACT. Following the passing of Prof Cheikh Anta Diop in 1986, the radiocarbon laboratory (LC14) he created 20 yr earlier at the Institut Francophone d’Afrique Noire (IFAN), Dakar, Senegal, fell into a long hibernation. It took nearly 3 yr to renovate the laboratory and reinstall new equipment in order to return LC14 to full functionality and resume its activity. A new dating system has been implemented around a super low-level liquid scintillation spectrometer from Packard, the Tri-Carb 3170TR/LS, located in an underground room.

In this paper, we assess the performance of the dating setup (background level and figure of merit) using known samples from Paris 6 and international standards from the International Atomic Energy Agency (IAEA). After the calibration, the setup was used to study *bolé* seashells from the Khant area in the northern part of Senegal (West Africa). The aim is to present evidence of the correlation between the transgression of the Nouakchottan (5500 BP) and a few industries in the Khant area. The corresponding ages are difficult to assess and the dates available for this cultural site are randomly distributed, ranging from 4500 to 1500 BP, i.e., a chronological period spanning from the Neolithic to the Iron Age.

INTRODUCTION

In the early 1960s, Prof Cheikh Anta Diop, having just returned to Senegal after completing his doctoral studies in France, set up a radiocarbon laboratory at the Institut Francophone d’Afrique Noire (IFAN)⁵ (Diop 1964). The laboratory became operational in 1966 and material dating was carried out until the early 1980s using DAK as the lab code (Diop 1971). The activity of the laboratory came to a complete stop in 1986 with the passing of Prof Diop.

In 1999, the Senegalese government gave the directive to IFAN to rehabilitate the ¹⁴C laboratory. It took 3 yr to accomplish the task, from restoring buildings to acquiring new equipment, and the new laboratory became fully operational and ready to resume its dating activity in January 2003.

In this report, we present data collected during the calibration of the counting system using samples supplied by LODYC from the University Paris 6 (France) and from the International Atomic Energy Agency (IAEA). We also present the preliminary results obtained on material extracted from the Khant area in the northern part of Senegal (West Africa) in a study aimed at establishing coherent chronographic sequences for this cultural site.

EXPERIMENTAL SETUP

The best option for the new carbon dating system at LC14 was to use liquid scintillation spectrometry (Polach 1992) with benzene as the scintillation solvent. The benzene volume used each time corresponded to a weight of 2 g in a Pico glass vial (standard size 20 mL). The scintillators were a bis MSB + Butyl PBD mixture (6 mg + 6 mg). The dating setup was installed in the same underground room as the former system; however, no water overhead was used for reducing the background noise.

¹LC14, Institut Fondamental d’Afrique Noire (IFAN), Université Cheikh Anta Diop, Dakar, Sénégal.

²Email: soukouma@hotmail.com.

³Corresponding author. Email: oumar_ka@ucad.sn.

⁴Laboratoire Préhistoire-Protohistoire, IFAN, Université Cheikh Anta Diop, Dakar, Sénégal.

⁵The current name is Institut Fondamental d’Afrique Noire.

Counting was carried out using a Tri-Carb 3170TR/SL liquid scintillation analyzer from Packard, driven by the Quanta Smart software under a Windows NT operating system. The counting time used in our program was 100 min per cycle.

Assessment of the 3170TR/SL is summarized in Table 1. In the 13–85-keV energy range at an efficiency of 68% and a background noise of 0.2 cpm, the figure of merit E^2/B is 23,400. These data clearly show the high performance of the counting system. In the super low-level counting mode using a BGO (Bi₄Ge₃O₁₂) detector guard, the background is further reduced down to 0.1 cpm for a comparable efficiency. These values compare favorably with the Wallac 1220 Quantulus LSC as shown in Table 2 (see Hogg: <http://www.c14dating.com/quant.html>) and the LSC system used at the Zagreb Radiocarbon Laboratory (Horvatinčić et al., these proceedings).

Table 1 Initial assessment of the performance of the liquid scintillation counting analyzer in low-level mode through the factor of merit E^2/B . In super low-level mode, the background noise is further reduced down to 0.1 cpm.

Region (keV)	Efficiency (%)	Background (cpm)	E^2/B
13–85	68.55	0.2	23,400

Table 2 Typical counting performance of a Wallac 1220 Quantulus (<http://www.c14dating.com/quant.html>); Benzene weights used: 0.3 mL = 2.637 g; 3 mL = 2.637g; 10 mL = 10.0 g.^a

Vial volume (mL)	B (cpm)	No (cpm)	¹⁴ C efficiency (%)		tmax (yr)	tmin (yr)	
			fM	FM			
0.3	0.04	2.47	74.8	12.5	143,350	44,100	133
3.0	0.25	25.66	77.8	51.4	24,290	55,500	41
10.0	1.03	108.09	86.4	106.7	7260	61,300	20

^aB = background; No = derived net cpm for ¹⁴C reference standard, 0.95 oxalic acid; fM = factor of merit (No/ \sqrt{B}); FM = figure of merit (E^2/B); tmax = maximum determinable age (using 3000-min count time and 2- σ criterion); tmin = minimum determinable age (using 3000-min count time and 1- σ criterion).

The improvement of the new system from the one formerly used in this laboratory is around 50-fold when the background noise levels are adjusted.

CALIBRATION OF THE COUNTING SYSTEM

Since the ¹⁴C age of the samples from LODYC was already known, it was possible to determine the initial activity (A_0) from the activities measured for those samples (Table 3). The mean value of 8.56 ± 0.02 cpm (i.e. around 12.25 dpm) is in very good agreement with the expected result of 8.6. The tSIE, which is the quench indicating factor, was 650 ± 20 .

Table 3 Calibration of the LC14-Dakar carbon dating system using already-known samples from LODYC-Paris 6.

LODYC lab code	Age (BP)	Mean activity (cpm/g)	Initial activity (cpm/g)
202	3695	5.408	8.566
207	1215	7.349	8.549
205	960	7.612	8.578

Another test for the LSC system was to check the output for different samples used in the IAEA ¹⁴C intercomparison exercise (Rozanski et al. 1992). The percentage of modern carbon (pMC) obtained from C1 (carbonate) and C3 (cellulose) are shown in Table 3. A complete agreement with the reported values can be seen.

In summary, the above calibration data from the LSC system clearly show the high performance of the new system setup at LC14-Dakar, a laboratory which we would like to present under DK as the new code number.

CASE STUDY: KHANT SEASHELLS

After the qualification stage of the carbon dating system, the research program that was started relates to the study of seashells from the Khant area, northern Senegal.

Context and Excavations

The Khant depression is approximately 22 km N-NE from Saint-Louis, the main city in northern Senegal (16.5°E, 14°N), in the vast area corresponding to the delta of the Senegal River (Figure 1). The depression is approximately 14 km long, about 1.7 km wide, and is enclosed between 2 Ogolian sand-hill strings. Ravisé discovered the site in 1969 (Ravisé 1970). Her investigations allow one to surmise the complex of Khant could have begun around 5000 BP. However, on the basis of subsequent excavations and the industries evident later on, it is likely that human occupation of the area continued until the Protohistoric period and even later.

Guy Thilmans, who was involved in part of the work of Ravisé et al. (1975) and who continued prospecting the area of the delta, indeed unveiled several Neolithic sites as well as Protohistoric ones. A general chart established by this author makes it possible to realize the importance of anthropic shell accumulations in this zone.

During this work, all the surveys carried out by Ravisé could not be observed, either because of an imprecise localization or because of a location was under the backwater-flooded river bed at the time of the investigations. However, it has been possible to recognize certain excavations carried out on the clusters of the Nouakchottan terrace by piecing together the various reports established by Thilmans and the information received from the local population. They are in the same topographic position as those in which Ravisé identified Khant 2 and collected a human skeleton, which she ascribed to the Neolithic era (Ravisé et al. 1975). More recently, Mbow-Diop (1997) carried out subsequent work on the issue.

Thorough prospecting and study of existing documentation leads to identifying 3 different levels of accumulation along the transverse section of the stream in Khant (East-West section): shallow deposits, deposits on the terrace, and deposits of the Ogolian sand-hill strings.

Natural accumulation, harvests, and shell re-use are extremely old in this area. Accumulations follow the Nouakchottan transgression, with a maximum around 5500 BP. Anthropic accumulations, the subject of this study, cover a longer timespan.

The excavations carried out on the material under study should allow for a better understanding of the chronostratigraphic sequence.

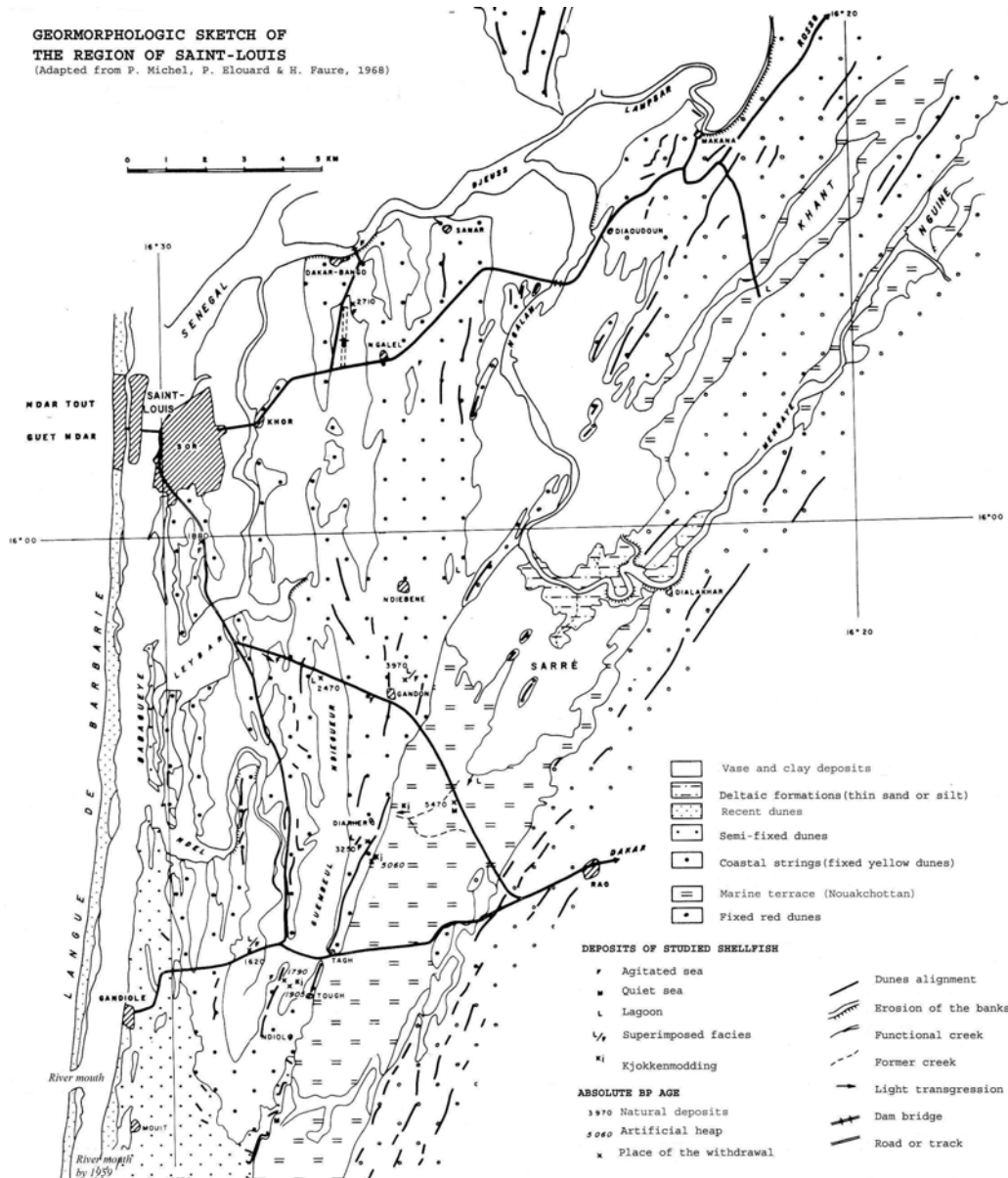


Figure 1 The Khant area in the Saint-Louis region, after Ravisé (1970). Saint-Louis is in northern Senegal, 16.5°E, 14°N.

RESULTS AND DISCUSSION

The results presented here deal with the chronological sequence of an anthropic hillock (*Bolé zone*) together with a measurement relating to a surface-collected material from a close hillock (*Xoor nook zone*). The excavated hillock has an extension of approximately 140 m in an E-W axis and 80 m in an N-S axis. The excavation was done down to a 330-cm depth. The excavated levels are composed primarily of arches and oysters which are sometimes calcined, associated osseous remains, brittle ceramics, and sediment.

Table 4 shows the chronological sequence obtained with the measurements carried out at LC14-Dakar on the *Anadara senilis* shells collected in the surveys, with a calibration according to Stuiver and Reimer (1993) revision 4.3 of the calibration program. The sequence obtained with DK-1, DK-5, and DK-7 is very coherent: 195–57, 409–294, and 498–336 cal BC (1 σ), respectively. From a preliminary analysis, it can be established that the cluster is constituted very quickly to reach 200 cm in about 2 centuries (498–294 cal BC). The progression slows down thereafter and the accumulation probably stops at about a century before our era.

Table 4 Percentage of modern carbon (pMC) measured for 2 IAEA samples compared to the mean values derived from the 1990 IAEA C14 intercomparison exercise.

Sample code	IAEA 1990 intercomparison (consensus value)	IAEA 1990 intercomparison (estimated standard error) ^a	LC14-Dakar	LC14-Dakar (estimated error)
C1	0.00 (0.02) ^b	0.02	0.04	0.01
C3	129.41	0.06	129.36	0.07

^aThis material is considered as a background sample having no measurable activity.

^bEstimated standard error calculated according to Rozanski et al. (1992).

Table 5 Measured activities, 2S%, and tSIE values for seashell samples (all samples are *Anadara* shell) extracted from the Khant area (northern Senegal, West Africa) and the corresponding dates at 1 σ . The calibration was made according to Stuiver and Reimer (1993) revision 4.3.

Lab code	Sample code	Depth (m)	Activity (cpm/g)	2S%	tSIE	¹⁴ C age BP	Cal age BP	Cal age BC
DK-1	Khant GPS	0.3	6.7052	5.35	650.21	2448 ± 34	2144–2006	195–57
DK-4	Khant	2	6.3366	6.14	651.46	2633 ± 29	2358–2243	409–294
DK-5	Khant	3.2	6.5608	5.30	649.40	2663 ± 49	2447–2285	498–336
DK-7	Xoor Nook	0	6.7052	5.35	648.27	2912 ± 29	2748–2647	799–698

The study of the survey composition makes it possible to understand relatively well the noticeable acceleration during the first 2 centuries. It is explained primarily by the prevalence of the oysters, which have a more significant volume at the beginning of accumulation. The higher levels, which are more compact, are dominated by the arches with an important sandy component, hence, a higher density.

The collected material does not deliver any metal that can be ascribed to the Iron Age. On the other hand, an adze and some bone-made objects were collected. These objects are culturally closer to those evidenced by Ravisé (1970) and this would bring them closer to a final Neolithic era.

In the case of the *Xoor nook* sample (DK-4), with a collection operated using just a superficial scouring, the age obtained is 888–698 cal BC (1 σ). This result is an incentive for further investigations to confirm that the early stage of this cluster, which culminates at 4 m, could be in the 2nd millennium BC. One would then be even nearer to the chronological sequences suggested by Ravisé (1970, 1975). However, when widening the perspective, one can note that in central Senegal, the Iron Age begins at the same time (Dème 2003). We are perhaps at a transitional period that would mark the end of the Neolithic and announces the introduction of the Iron Age in the Senegal River valley. For this reason, the extension of the investigations and the resulting additional dates of the chronological sequence should contribute to a better understanding of the Khant cultures from the Neolithic to the Iron Age.

CONCLUSIONS

The data presented here establish that the new carbon dating system setup at LC14-Dakar is a high-performance tool for the scientific community. Because of the reduced background level, the ^{14}C age may be calculated with a good precision. Thus, the carbon dating service available seems highly competitive.

Preliminary investigations have also been carried out on seashells from a cultural site in the northern part of Senegal. The results obtained are very promising and should lead to a comprehensive understanding of the chronological sequence for different entropic levels with ages spanning from the Neolithic to the Iron Age.

ACKNOWLEDGEMENTS

The authors would like to thank J-F Saliège (LODYC Paris 6, France) and J-F Tannau and M Fontugne (CEA Gif-sur-Yvette, France) for their tireless assistance during our efforts to rehabilitate the laboratory. The continuous support from the Director of IFAN is to be mentioned as well. We are also grateful to C B Gaye (AIEA, Vienna) for supplying the AIEA samples. The Khant excavation were carried out during a collaboration between H Bocoum and R Vernet, with the financial support of the French Ministry of Foreign Affairs.

REFERENCES

- Dème A. 2003. *Archeological investigations of settlement and emerging complexity in mid-Senegal valley: excavation at Walaldé* [PhD dissertation]. Houston: Rice University.
- Diop CA. 1964. Annual report 1963–1964. Institut Fondamental d’Afrique Noire (IFAN), Université de Dakar. p 20–4.
- Diop CA. 1971. Centre de datation de l’IFAN. Datation par la méthode du radiocarbone, série I et II. In: *Bulletin de l’IFAN série B, tome XXXIII, nr 3*. p 449–60.
- Hogg A. Wallac 1220 Quantulus, Liquid Scintillation Spectrometer: Performance Data. University of Waikato. (<http://www.c14dating.com/quant.html>).
- Horvatinčić N, Barešić J, Krajcar Bronić I, Obelić B. 2004. Measurement of low ^{14}C activities in a liquid scintillation counter in the Zagreb Radiocarbon Laboratory. *Radiocarbon*, these proceedings.
- Mbow-Diop MA 1997. *Les amas coquilliers du delta du Sénégal: étude ethno-archéologique* [PhD dissertation]. Paris: University Paris 1.
- Polach HA 1992. Four decades of LS counting and spectrometry. In: Taylor RE, Long A, Kra R, editors. *Radiocarbon After Four Decades. An Interdisciplinary Perspective*. New York: Springer-Verlag. p 242–61.
- Ravisé A. 1970. Industries en os de la région de Saint-Louis. *Notes africaines* 128:98–102.
- Ravisé A, Thilmans G, Marius C. 1975. Etude d’un squelette néolithique de la région de St Louis. *Bulletin IFAN* 37:687–701.
- Rozanski K, Stichler W, Gonfiantini R, Scott EM, Beukens RP, Kromer B, van der Plicht J. 1992. The IAEA C14 intercomparison exercise 1990. *Radiocarbon* 34(3):506–19.
- Stuiver M, Reimer PJ. 1993. Extended ^{14}C database and revised Calib 3.0 ^{14}C age calibration program. *Radiocarbon* 35(1):215–30.

TOWARDS ACHIEVING LOW BACKGROUND LEVELS IN ROUTINE DATING BY LIQUID SCINTILLATION SPECTROMETRY

Alan G Hogg

Waikato Radiocarbon Dating Laboratory, University of Waikato, Private Bag 3105, Hamilton, New Zealand.

Email: alan.hogg@waikato.ac.nz.

ABSTRACT. International radiocarbon intercalibration studies have revealed that radiometric laboratories using liquid scintillation (LS) spectrometry of benzene reported, on average, younger ages for near-background standards than either gas proportional counter (GPC) or accelerator mass spectrometry (AMS) laboratories. These studies suggested that the younger LS ages are probably related to the use of spectrophotometric benzene as a background standard. An analysis of successive 110-ka subfossil wood (Airedale Reef Ancient Wood: ARAW) standards shows that vacuum line memory effects occur in LS spectrometry and, consequently, must be corrected to obtain accurate ^{14}C dates. ARAW standards, measured at monthly intervals in the Waikato laboratory, are used to provide blank corrections for both research and routine dating applications. The strong correlation between the ARAW $\Delta^{14}\text{C}$ data and the sample activities that preceded the standards may provide an opportunity to obtain sample-specific blank corrections. Lithium carbide synthesis is likely to prove a source of contamination. This work suggests that reproducible background levels for routine dating of less than 0.1 pMC (55 ka ^{14}C yr) are achievable.

INTRODUCTION

International radiocarbon intercalibration studies have revealed that radiometric laboratories using liquid scintillation (LS) spectrometry of benzene reported, on average, younger ages for near-background standards than either gas proportional counter (GPC) or accelerator mass spectrometry (AMS) laboratories (e.g. the near-background FIRI Kauri standards A and B, Scott et al. 2003)—see Figure 1. These studies suggested that the younger LS ages are probably a function of laboratory standards and, in particular, relate to the use of spectrophotometric benzene to determine background count rates.

Accurate ^{14}C determinations by all 3 methods, especially of near-background samples, requires the establishment of accurate and reproducible background levels, obtained from materials containing no ^{14}C (background blanks). Anthracite, ancient wood, or ancient carbonates are commonly used as “dead” carbon sources for this purpose. Many benzene LS laboratories utilize spectrophotometric benzene derived from a petrochemical source to provide background activities for the scintillation vials. It appears that some laboratories are utilizing these values as background blanks and ignoring contamination levels in their vacuum systems.

Long and Kalin (1992) reported that the Arizona LS laboratory utilized spectrophotometric benzene as the background for routine precision, stating that with 3 mL (2.4 g) benzene counted for 2 k min, differences in ^{14}C activity between spectrophotometric benzene and anthracite are “statistically invisible” (Long and Kalin 1992: 355). However, Long and Kalin (1992) found significant differences in activity between spectrophotometric benzene and anthracite using large benzene volumes (11.5 g) and longer counting times (12 k min). Four successive anthracite blank samples were processed and a decreasing level of memory effects was observed, which Long and Kalin (1992) attributed to contamination of the lithium reaction vessel surfaces.

McCormac et al. (1993) demonstrated that spectrophotometric benzene pipetted into counting vials produced lower background count rates than those obtained from benzene synthesized from an ancient carbon source. They combusted spectrophotometric benzene and reconverted the resulting CO_2 back to benzene and compared the activities of the initial benzene with the reconverted benzene. Higher ^{14}C levels were found in the reconstituted benzene, and so McCormac et al. (1993)

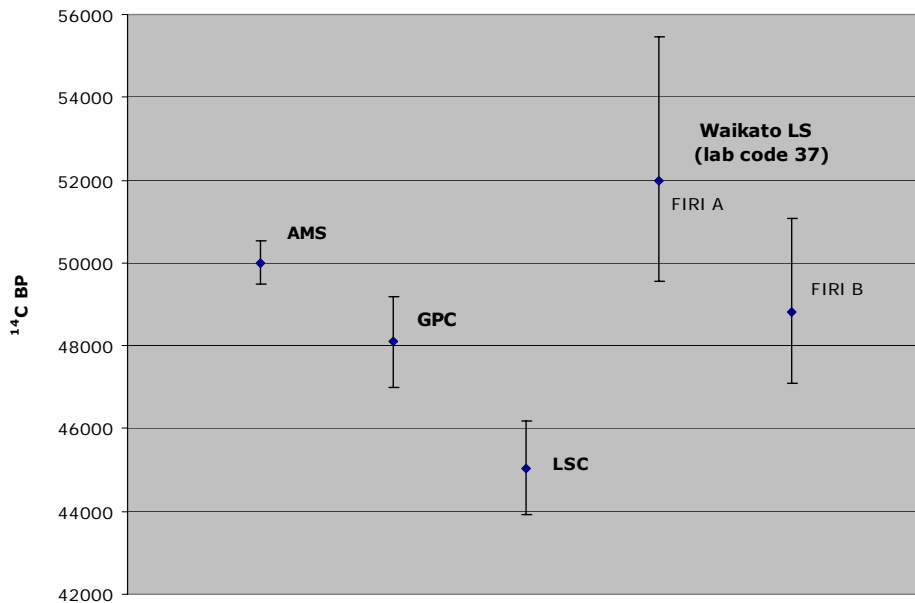


Figure 1 Mean ^{14}C ages obtained by different laboratory types for the FIRI Kauri standards A and B, showing that some LS laboratories have seriously underestimated the ages. The Waikato LS results are given for comparison.

concluded that ^{14}C was added to the reconverted benzene during combustion and synthesis. They suggested that most of the modern contamination was derived from C associated with either the lithium metal or from the reaction vessel walls.

Other possible sources of contamination during benzene synthesis include the following:

- Cross-contamination during combustion from either CuO used in furnaces or chemicals used to cleanse the CO_2 gas;
- Cross-contamination from the catalyst used in the catalytic trimerization of acetylene to benzene, where the catalyst is regenerated between samples;
- Elevation of sample activity by contamination with radon gas derived from either the ancient wood samples or from the zeolite-based vanadium-activated catalyst.

The larger numbers of LS laboratories reporting younger ages for the near-background FIRI samples indicates that some laboratories are unaware of these possible sources of contamination during benzene synthesis. Therefore, it is essential that all LS laboratories utilizing spectrophotometric benzene to establish LS vial background levels routinely analyze ^{14}C -dead background samples to provide a background correction for the contaminating ^{14}C added during benzene synthesis.

Ancient wood standards have been run at monthly intervals in the Waikato laboratory over the last 2 yr to provide accurate background levels for routine analysis. This paper is a preliminary assessment of this data undertaken to demonstrate how necessary blank determination is and the effectiveness of the LS method for dating near-background samples. It also attempts to verify the suggestion of McCormac et al. (1993) that the carbide reaction is the predominant source of contamination and highlights steps undertaken in the Waikato laboratory to achieve lower and more stable background levels, both for research samples and routine dating applications.

THE AIREDALE REEF ANCIENT WOOD (ARAW) STANDARD

Well-preserved, subfossil wood samples were collected by Dr B V Alloway from Airedale Reef, a coastal section in North Taranaki, New Zealand. The samples are from trees in growth position beneath a 4-m-thick debris avalanche deposit. Palynological and tephrochronological evidence show that the debris avalanche (and forest inundation) occurred during Marine Oxygen Isotope Stage 5c at about 110 ka (Newnham and Alloway 2001).

Wood samples were pretreated to α -cellulose (Hoper et al. 1997) to remove mobile fractions and $\Delta^{14}\text{C}$ measured by LS counting of benzene (Hogg et al. 1987) in Wallac 1220 Quantulus spectrometers (7.5-g benzene samples counted for 10k min per sample). The α -cellulose extraction procedure outlined by Hoper et al. (1997) was modified for the near-background samples by utilizing acetone (derived from a petrochemical source) as a solvent in place of ethanol (some of which may be derived from modern wood).

We also analyzed untreated wood and the Kapuni CO_2 gas standard (KCOG) for comparison. The KCOG standard is ^{14}C -dead, high-purity CO_2 , about 45 Ma in age, derived from the Kapuni Gas Field near New Plymouth, New Zealand. It is a useful standard for measuring memory effects in the lithium carbide and catalytic trimerization reactions but of course cannot be used to monitor the combustion of organic carbon. We “preconditioned” the vacuum lines before synthesizing the ARAW standard benzene samples by initial processing of 3 near-background subfossil wood samples.

We obtained statistically-identical ages on ARAW (untreated), ARAW (α -cellulose), and KCOG standards of about 60 ka BP (Figure 2).

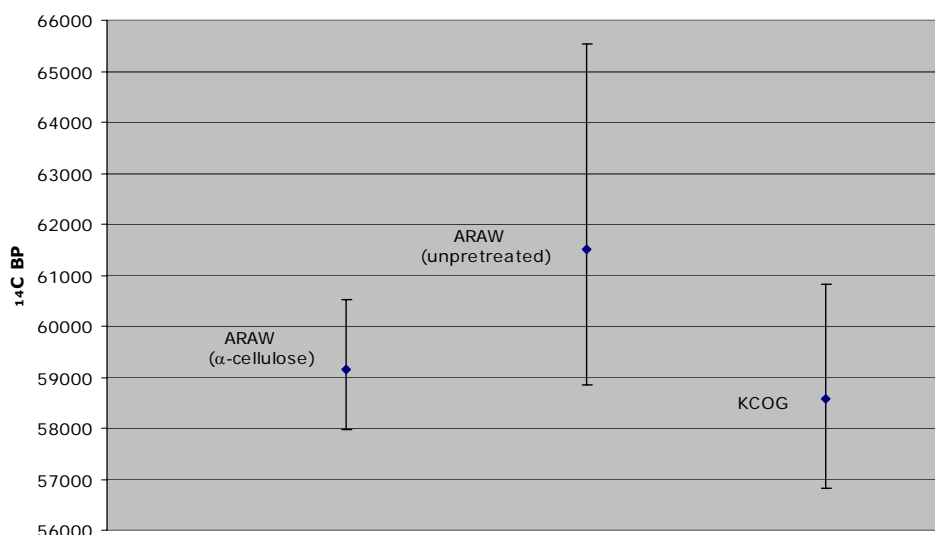


Figure 2 ^{14}C ages of the ARAW standard. The Kapuni CO_2 Gas Standard (KCOG) is given for comparison (backgrounds based upon spectrophotometric benzene—no correction for memory effects). ARAW(α -cellulose) data, mean of 5 measurements; ARAW(untreated) data, mean of 2 measurements; KCOG data, mean of 2 measurements.

METHODOLOGY EMPLOYED FOR NEAR-BACKGROUND RESEARCH SAMPLES

If known-age near-background research samples are being analyzed, we follow the procedures of Long and Kalin (1992) and McCormac et al. (1993) to reduce ^{14}C activities in the vacuum lines by

initially processing a minimum of 2 near-background standards and by processing the samples in a batch. We have found a similar pattern to that obtained by Long and Kalin (1992) and McCormac et al. (1993) with background activities diminishing with successive standards (Figure 3). Near-background research samples in the Waikato laboratory utilize 7.5 g of benzene counted for 10 k min in Wallac 1220 Quantulus spectrometers. Benzene samples are counted in Waikato 10-mL synthetic silica liquid scintillation vials (Hogg 1993). At least 2 ^{14}C -dead standards are also included in the batch to provide an accurate blank for the samples.

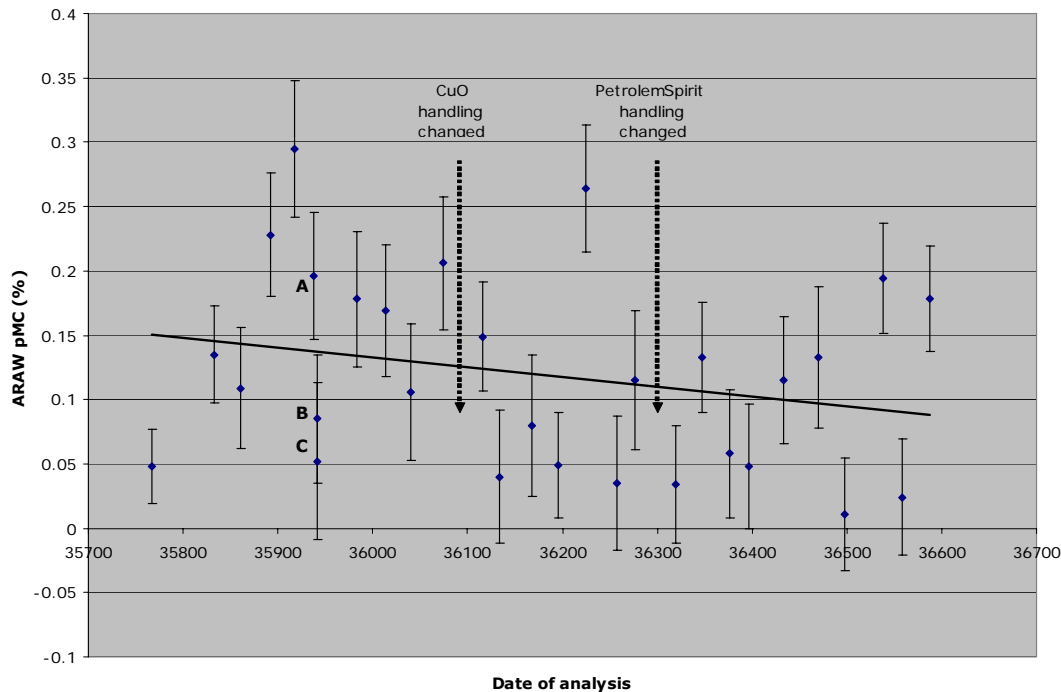


Figure 3 ^{14}C levels for routine analysis ARAW standards determined over a 24-month period at the Waikato laboratory. Backgrounds based upon spectrophotometric benzene—no blank correction. Benzene weight = 2.64 g; count time = 3 k min. Samples A, B, and C were run on successive days through the same vacuum line pathways and show decreasing activity.

METHODOLOGY EMPLOYED FOR ROUTINE DATING OF UNKNOWN-AGE SAMPLES

Low and reproducible background count rates can be readily achieved for research projects dating old material by preconditioning vacuum lines with ^{14}C -dead standards before the samples are processed, as discussed above. This procedure cannot be followed for routine dating of unknown activity samples. Routine analysis in the Waikato laboratory utilizes 2.64 g of benzene counted for 3 k min, also in Wallac 1220 Quantulus spectrometers. Benzene samples are counted in Waikato 3-mL synthetic silica liquid scintillation vials (Hogg 1993).

ARAW blank standards are analyzed at monthly intervals (Figure 3 and Table 1). The order of processing of the ARAW standards is random and no attempt is made to deliberately process any particular ARAW standard after samples known to have low activity, although they do not follow high-activity modern standards such as OXII or ANU sucrose.

Table 1 ARAW standard data accumulated in the Waikato lab over a 24-month period. The count rates (cpm) of the samples that preceded the standard, through the combustion (A), carbide reaction (B) and the catalyst trimerization (C) are also given. ARAW standard activity is given as pMC (%) ± 1 standard error (σ).

Lab nr (Wk)	pMC (%)	σ	cpm of the sample preceding the ARAW standard in:		
			A	B	C
			Combustion	Carbide reactor	Catalytic trimerization
10301	0.048	0.03	5.8	5.8	6.7
10302	0.135	0.04	19.8	5.4	15.9
10303	0.109	0.05	2.6	27.5	10.9
10858	0.228	0.05	28.5	26.1	7.2
10859	0.295	0.05	25.0	25.9	7.2
8790-4	0.196	0.05	20.8	6.7	6.7
8790-5	0.085	0.05	0.4	0.4	0.4
10860	0.052	0.06	0.4	0.4	0.4
10861	0.178	0.05	20.5	6.3	16.7
10862	0.169	0.05	1.6	15.6	8.7
10863	0.106	0.05	1.7	6.2	1.7
10864	0.206	0.05	23.2	16.9	12.6
10865	0.149	0.04	19.6	19.6	12.3
11926	0.04	0.05	21.9	13.8	3
11927	0.08	0.06	0.37	0.37	0.37
11928	0.05	0.04	0.3	0.3	3.4
12481	0.264	0.05	17.6	17.6	5.9
12482	0.035	0.05	5.5	5.5	2.7
12483	0.115	0.05	18.0	3.1	3.1
12484	0.034	0.05	13.4	4.4	10.6
12485	0.133	0.04	6.7	0.4	0.4
12486	0.058	0.05	23.1	3.7	3.7
12487	0.048	0.05	5.1	1.9	0.37
12488	0.115	0.05	21.1	9.5	0.6
13853	0.133	0.06	20.5	4.6	10.8
13854	0.011	0.04	0.5	0.5	0.5
13855	0.194	0.04	22.5	18.3	8.2
13856	0.024	0.05	6.3	2.4	0.4
13857	0.178	0.04	22.3	22.3	6.6

A line of best fit through the data of Figure 3 shows that background levels decreased over the 2-yr period. This may be due to the cumulative effect of numerous small improvements in laboratory practice, which in isolation are unlikely to significantly influence mean background levels. Two examples are given in Figure 3, the handling of CuO and petroleum spirit. The CuO, contained in combustion line furnaces, is now baked at 600 °C for 6 hr after each sample-combustion to ensure residual carbon is removed. Petroleum spirit, under which lithium metal is stored, is now changed frequently, at monthly intervals. Plotting the calendar dates on a graph (such as Figure 3) is a useful tool to evaluate the affect small changes in benzene laboratory synthesis procedures have on mean background levels.

The Waikato laboratory utilizes a mean blank correction for organic carbon samples calculated from the mean of the 10 most recent ARAW standard values. The mean ARAW activity of all measurements = 0.11 ± 0.08 pMC (54 ka BP), ranging from a high of 0.295 pMC (47 ka BP) to a low of 0.024 pMC (67 ka BP). The data for the 10 most recent measurements are significantly lower: mean = 0.095 ± 0.07 pMC (56 ka BP), with a high of 0.194 pMC (50.2 ka BP) and a low of 0.024 pMC (67 ka BP). A mean background level of less than 0.1 pMC compares favorably with AMS backgrounds, which are rarely better than 0.15 pMC (Bronk Ramsey et al., these proceedings). The low and reproducible background levels highlight the effectiveness of the LS method in the ^{14}C dating of near-background samples.

Figure 4 shows the impact of the Waikato blank correction of 0.095 pMC and demonstrates how errors increase for near-background samples if no correction is applied. In the 2003 FIRI report, 26 laboratories produced Kauri A and B ages of less than 40 ka (Scott et al. 2003). Such underestimations of age imply that a large blank correction of at least 0.4 pMC must be applied to correct them (assuming a mean Kauri age of 47,634 BP: Scott et al. 2003). The influence of the blank correction of 0.4 pMC is also shown in Figure 4. Long and Kalin's (1992) contention that differences in ^{14}C activity between spectrophotometric benzene and anthracite are "statistically invisible" implies that they can, therefore, be ignored. While the correction for memory effects may be insignificant for full-sized young samples, it can have a much larger impact upon gas-diluted, small or old samples, as is shown in Figure 4. Systematic errors are cumulative and they should, therefore, be corrected.

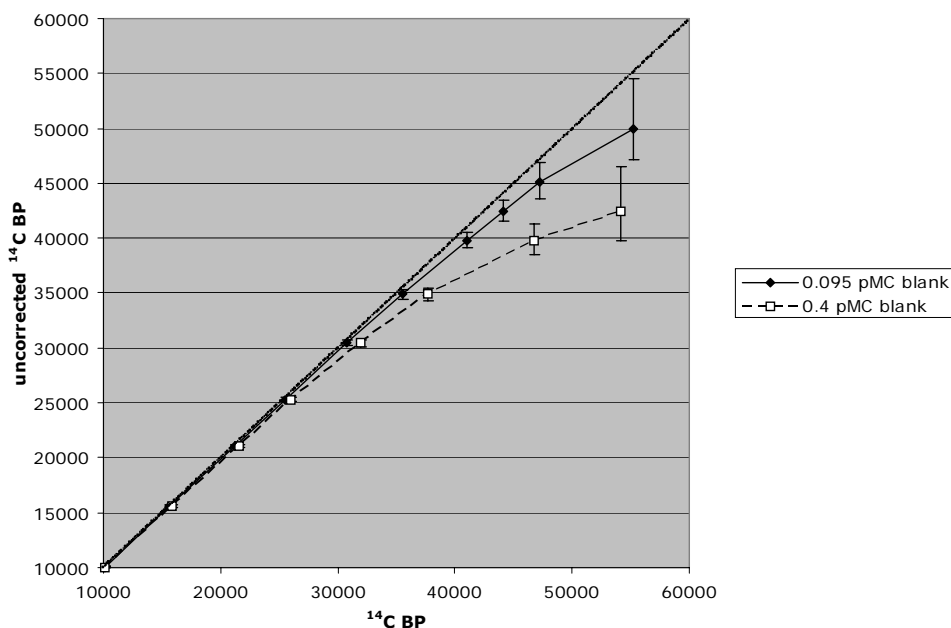


Figure 4 The influence of uncorrected ^{14}C dates on dating accuracy (blank corrections of 0.095 and 0.4 pMC shown). The dotted line represents a zero blank correction.

ANALYSIS OF ARAW STANDARD DATA

It is clear from Figure 3 that activity from 1 sample (e.g. samples A–C) can contaminate the next (memory effects). The ARAW standard activities should, therefore, show a positive correlation between previous sample activity and ARAW standard activity. The ARAW standard data may also

be able to identify which benzene synthesis reaction (i.e. combustion, lithium carbide synthesis, or catalytic trimerization) is the most likely source of contamination, and also potentially provide a means for correcting this error.

CO₂ Generation (Combustion) as a Source of Contamination

The potential for 1 sample combustion to contaminate the next is complicated by sample-size issues. Large samples may contaminate the combustion vacuum lines more than smaller samples. Unfortunately, many of the samples combusted prior to the ARAW standard combustions were undersized, obscuring any potential correlations. Therefore, all future ARAW standards will follow full-sized sample combustions to help clarify the contribution of sample combustion to memory effects.

C₂H₂ and C₆H₆ Generation-Reactions as Sources of Contamination

The Waikato benzene synthesis procedure involves gas dilution of undersized samples with dead CO₂ to ensure a constant stoichiometry between the CO₂ and lithium (also recommended by McCormac et al. 1993). The samples preceding the ARAW standards through the carbide reactors and catalyst columns are, therefore, unaffected by sample size and may provide more reliable data than the combustion data to investigate the correlation between ARAW standard levels and previous sample activity.

The ARAW standard data are given in Table 1. Also included are the count rates (in cpm) of the samples that immediately preceded the ARAW standards through the reactions involved in the synthesis of benzene:

- cpm of the sample preceding the ARAW standard in the combustion system (reaction A—oxidation of sample C to CO₂);
- cpm of the sample preceding the ARAW standard in the lithium carbide reactor (reaction B—conversion of CO₂ to C₂H₂);
- cpm of the sample preceding the ARAW standard on the catalyst column (reaction C—catalytic trimerization of C₂H₂ to C₆H₆).

Other relevant data collected, but not given in Table 1, included the number of days the benzene was stored before counting. This storage time was measured to determine if activity derived from radon gas (from either the ancient wood standard or from the catalyst column) was present. There was no significant correlation between ARAW activity and duration of benzene storage before counting, which indicates that radon does not contribute significantly to the background activity.

The ARAW standard activity was plotted against the activities of the preceding samples, for the reactions A, B, and C as outlined above (Figure 5). Correlation coefficients (R^2) were calculated from plots of the ARAW standard activity against the activities of the individual samples that preceded the standard through the various synthesis lines (Table 2). The correlation coefficient is highest for the carbide reaction (0.4712) with lower values for the combustion reaction (0.3733) and trimerization reaction (0.2265).

It is evident that there is a strong correlation between the ARAW standard activities and the sample activities that preceded them, especially for samples processed through the carbide reactor. This finding confirms those of Long and Kalin (1992) and McCormac et al. (1993). The outliers show that other memory effects are present and that they are unlikely to be derived from a primary source only (Figure 5). One explanation is that they may result from secondary effects where 2 samples have influenced a third. These results, and those of Long and Kalin (1992) and McCormac et al. (1993), suggests this is likely. There are insufficient data available at present to fully answer these questions.

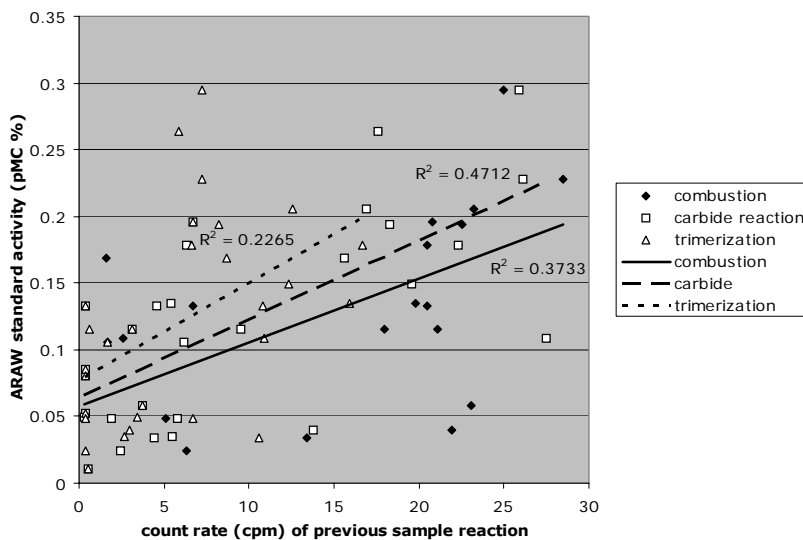


Figure 5 Dependence of ARAW activities on the count rates of the samples that preceded the combustion (A), carbide reaction (B), and the catalyst trimerization (C). The correlation coefficients (R^2) are also given.

Table 2 The correlation coefficients (R^2) for plots between ARAW standard activity and the activity of the samples preceding the ARAW standards, in reactions A (combustion), B (lithium carbide reaction), and C (catalytic trimerization). The probabilities for no correlation (calculated after Bevington 1969:124–125) are also given.

Reaction	Correlation coefficient (R^2)	Probability for no correlation
A – combustion	0.3733	0.0004
B – Li carbide synthesis	0.4712	0.0000
C – catalytic trimerization	0.2265	0.0091

FUTURE WORK

This paper highlights the importance of the routine analysis of ^{14}C -dead blanks to ensure that sources of contamination can be detected and eliminated. This process is on-going in the Waikato laboratory, with benzene synthesis procedures and their effect on the ARAW standard activities under continual review.

Future ARAW standards will be synthesized after at least 2 full-sized samples only, so that combustions and secondary effects can be seen more clearly.

The mathematical relationship between ARAW standard activity and preceding carbide sample activities could potentially be used to assign a unique background blank correction to every sample. A study is presently being conducted to test this hypothesis.

CONCLUSIONS

- ^{14}C -dead standards should be routinely analyzed so that sources of contamination can be detected and eliminated.
- LS labs which use spectrophotometric benzene measurements alone to calculate background levels are very likely to report ^{14}C ages that are too young, especially for near-background samples.

3. Research samples of near-background age can be processed in a batch through vacuum lines “pre-conditioned” by the initial processing of at least 2 low-activity samples. ^{14}C -dead standards must be included to provide an accurate blank for the samples.
4. By repeatedly analyzing at regular intervals a new ^{14}C -inert standard (ARAW), we have been able to obtain an accurate background correction for organic carbon samples routinely dated in the Waikato laboratory.
5. Analysis of the ARAW standard data shows that the activity of each sample processed through the vacuum lines is related to that of the sample preceding it. This relationship may provide a means to further improve background corrections, and hence the accuracy of ^{14}C ages, especially for near-background samples.
6. The carbide synthesis reaction is a likely source of contamination in the Waikato LS laboratory. Future research will be needed to determine if secondary contributions are also significant.
7. This work suggests that reproducible background levels for routine dating of less than 0.1 pMC (55 ka ^{14}C yr) are achievable. This is presently lower than backgrounds currently obtainable in routine AMS dating and highlights the benefits of LS spectrometry for near-background samples.

ACKNOWLEDGEMENTS

Many thanks to Helen McKinnon, Margaret Rabjohns, and Kathleen Dabell (Waikato Radiocarbon Dating Laboratory) for benzene synthesis of ARAW standards. Dr Brent Alloway (IGNS) collected the ARAW wood samples. Dr Paula Reimer (Lawrence Livermore National Laboratory) provided advice on the statistical analysis of the data. Professor John Noakes (CAIS, University of Georgia) and Dr Gordon Cook (SUERC Radiocarbon Dating Laboratory), and Professor Gerry McCormac (Queen’s University Belfast) commented on draft copies of this paper, and Associate Professor David Lowe (Earth Sciences, University of Waikato) critically reviewed it. I thank all these colleagues for their assistance.

REFERENCES

- Bevington PR. 1969. *Data Reduction and Error Analysis for the Physical Sciences*. New York: McGraw-Hill.
- Bronk Ramsey C, Higham TFG, Leach P. 2004. Towards high-precision AMS: progress and limitations. *Radiocarbon*, these proceedings.
- Hogg AG, Lowe DJ, HENDY CH. 1987. University of Waikato radiocarbon dates I. *Radiocarbon* 29(2):263–301.
- Hogg AG. 1993. Counting performance and design of 0.3-mL to 10-mL synthetic silica liquid scintillation vials for low-level ^{14}C determination. In: Noakes JE, Schönhofer F, Polach HA, editors. *International Conference on Advances in Liquid Scintillation Spectrometry 1992*. Tucson, Arizona: Radiocarbon. p 135–42.
- Hoper ST, McCormac FG, Hogg AG, Higham TFG, Head MJ. 1997. Evaluation of wood pretreatments on oak and cedar. *Radiocarbon* 40(1):45–50.
- Long A, Kalin RM. 1992. High-sensitivity radiocarbon dating in the 50,000 to 70,000 BP range without isotopic enrichment. *Radiocarbon* 34(3):351–9.
- McCormac FG, Kalin RM, Long A. 1993. Radiocarbon dating beyond 50,000 years by liquid scintillation counting. In: Noakes JE, Schönhofer F, Polach HA, editors. *International Conference on Advances in Liquid Scintillation Spectrometry 1992*. Tucson, Arizona: Radiocarbon. p 125–33.
- Newnham RM, Alloway BV. 2001. The last interglacial/glacial cycle in Taranaki, western North Island, New Zealand: a palynostratigraphic model. In: Goodman DK, Clarke RT, editors. *Proceedings of the IX International Palynological Congress, Houston (1996)*. Dallas, Texas: American Association of Stratigraphic Palynologists Foundation. p 411–22.
- Scott EM, editor. 2003. The Third International Radiocarbon Intercomparison (TIRI) and the Fourth International Radiocarbon Intercomparison (FIRI), 1990–2002. *Radiocarbon* 45(2):135–408.

PREPARATION OF GRAPHITE TARGETS FROM SMALL MARINE SAMPLES FOR AMS RADIOCARBON MEASUREMENTS

Laval Liong Wee Kwong¹ • Pavel P Povinec^{1,2} • A J Timothy Jull³

ABSTRACT. A vacuum sample processing line was set up and methods were developed for the determination of radiocarbon in small-volume seawater and biota samples. Seawater samples (500 mL per borosilicate glass bottle and poisoned with HgCl₂) were acidified with 5 mL concentrated hydrochloric acid. Pure N₂ was used as a carrier gas to strip CO₂ from the samples for 10 min in a circulation mode. After purification through several water traps, the CO₂ was isolated cryogenically. Using Na₂CO₃ standard solutions, recovery yields were calculated superior to 95 ± 5%. Freeze-dried marine biota samples were thoroughly mixed with Cu(II)O and combusted at 900 °C. The CO₂ was purified by passing through Ag wool and Cu granules at 450 °C before reduction to graphite. Finally, graphite was synthesized using Zn dust heated to 450 °C in the presence of an Fe catalyst at 550 °C. Although this method takes about 8 hr (synthesis done overnight), the advantage is that no water vapor by-product is formed to hinder the reaction. The graphite yields, measured both by gravimetric methods and by pressure readings, were 95 ± 5%. Accelerator mass spectrometry (AMS) measurements were carried out at the NSF-Arizona AMS Facility. Results for water samples from the northwest Pacific Ocean are reported which are in agreement with data reported elsewhere.

INTRODUCTION

Due to its ubiquitous nature and relatively long half-life (5730 yr), radiocarbon is a unique tracer which has been applied in a wide range of disciplines including marine sciences. ¹⁴C is a useful tool for studying the ocean carbon cycle, oceanic transport, water mass circulation, and mixing processes (e.g. Östlund and Stuiver 1980; Stuiver et al. 1983; Östlund et al. 1987; Bard et al. 1989; Östlund and Rooth 1990; Broecker et al. 1998; Lawson et al. 2000; Povinec et al. 2000; Aramaki et al. 2001; Key et al. 2002, etc.).

The 2 approaches for ¹⁴C determination are conventional radiometrics β-counting and accelerator mass spectrometry (AMS) techniques. In the first method, CO₂ is generated from the sample, purified or converted to a hydrocarbon gas, and then analyzed by a gas proportional counter (e.g. Povinec 1992; Povinec 1994; Gorczyca et al. 1998, etc.). Alternatively, carbon dioxide can be converted to benzene, which is analyzed by liquid scintillation counting (e.g. Calf 1978; Burchuladze et al. 1980, etc.). Although the 2 methods have been intensively used, they have proved to be limited when dealing with small sample sizes and low ¹⁴C levels, like, for example, in dissolved inorganic carbon (DIC) measurements in seawater for high-resolution Δ¹⁴C profiling of the water column. As ¹⁴C has a very low natural abundance and a slow decay rate, either a very long counting time is necessary or very large quantities of samples are required for good precision measurements. For example, when measuring DIC in seawater, large volumes of the order of 250–300 L are required (Bhushan et al. 1994). In polar regions, which are key areas for deep-water circulation studies, or when deep-water samples are needed for specific analyses, it is very difficult and time consuming to collect large-volume samples. A typical chemical procedure involves precipitation as Na₂CO₃ or BaCO₃, usually done on shipboard immediately after sampling. In the home laboratory, CO₂ is generated and counted in a gas proportional counter, or acetylene is produced and benzene is obtained by cyclotrimerization of acetylene before liquid scintillation counting (e.g. Calf 1978; Burchuladze et al. 1980; Bhushan et al. 1994, etc.).

¹International Atomic Energy Agency, Marine Environment Laboratory, MC 98000 Monaco.

²Corresponding author. Email address: p.povinec@iaea.org.

³NSF Arizona AMS Facility, The University of Arizona, Tucson, Arizona 85721, USA.

An alternative approach to decay counting is to measure the number of ^{14}C atoms in a sample, more precisely, the ratio of ^{14}C atoms to the stable carbon isotope atoms by AMS. With a state-of-the-art AMS technique, a sub-mg level of graphite suffices; consequently, a volume of 500 mL is enough for processing seawater samples. The major steps involved are CO_2 extraction and reduction. For seawater, the extraction is performed by first hydrolyzing the seawater and then stripping CO_2 either by bubbling with a carrier gas (e.g. Östlund et al. 1987) or by vacuum extraction (e.g. Dörr and Munnich 1980; Nydal et al. 1992; McNichol et al. 1994). For marine biota, the sample is either combusted with an oxidant at $900\text{ }^\circ\text{C}$, or, if in the form of a calcareous solid like a shell or coral, the sample can be wet-digested with phosphoric acid. The reduction to filamentous graphite is carried out using H_2 in the presence of Fe metal activated by O_2 (e.g. Vogel et al. 1984). However, an elaborate installation is required involving a heater and a water trap to eliminate the H_2O by-product which kills reduction. Zn has also been used as a reducing agent in the presence of a metal catalyst such as Fe (Jull et al. 1987). Here, the reaction usually lasts several hours. The graphite is then pressed as a target for AMS measurements.

To carry out ^{14}C assessment of small volume marine samples, a vacuum sample preparation line was constructed at the International Atomic Energy Agency's Marine Environment Laboratory (IAEA-MEL) in Monaco, and methods were developed to produce graphite targets for marine environmental studies. The adopted procedures are briefly described in the present paper.

METHODS

Seawater samples were collected in precleaned (rinsed several times with hexane and dried overnight in an oven at $100\text{ }^\circ\text{C}$), preweighed 500-mL borosilicate glass bottles and poisoned immediately with HgCl_2 (McNichol and Jones 1992). To minimize contamination, CO_2 was stripped in the bottles in which the seawater was collected. Biota samples were frozen before being lyophilized and ground into a fine homogeneous powder.

Extraction of CO_2

Seawater

In a glove box under a high-purity N_2 atmosphere, a stripping probe was inserted into the sample bottle and a glassware assembly was set up which was connected to the preparation line (Figure 1). Then a vacuum was generated up to the glassware assembly's valves. Standard water traps at $-80\text{ }^\circ\text{C}$, a slurry of ethanol and dry ice, and a liquid N_2 bath were installed before the seawater was hydrolyzed with 5 mL of concentrated HCl. High-purity carrier N_2 gas was injected into the line until a pressure of 0.1 MPa was reached. Immediately, the appropriate valves were opened to create a circulation loop, and a bellows pump (Iwaki® BA-110 SN) was switched on, forcing the carrier gas through the fritted end of the probe. The seawater sample is thus sparged along by the N_2 gas carrying CO_2 to be trapped. This stripping process was completed in 10 min. The carrier and other non-condensable gas was then purged out. While the trapped CO_2 was allowed to thaw, the liquid N_2 bath was replaced by a water bath cooled to $-80\text{ }^\circ\text{C}$. After equilibrium was reached, the CO_2 was cryogenically transferred to the calibrated volume section to which a high-precision pressure transducer was connected. The measured pressure was used to calculate the concentration of the extracted CO_2 . The calibrated volume section was also used to collect precisely known amounts of CO_2 for graphite synthesis and measurement of ^{13}C .

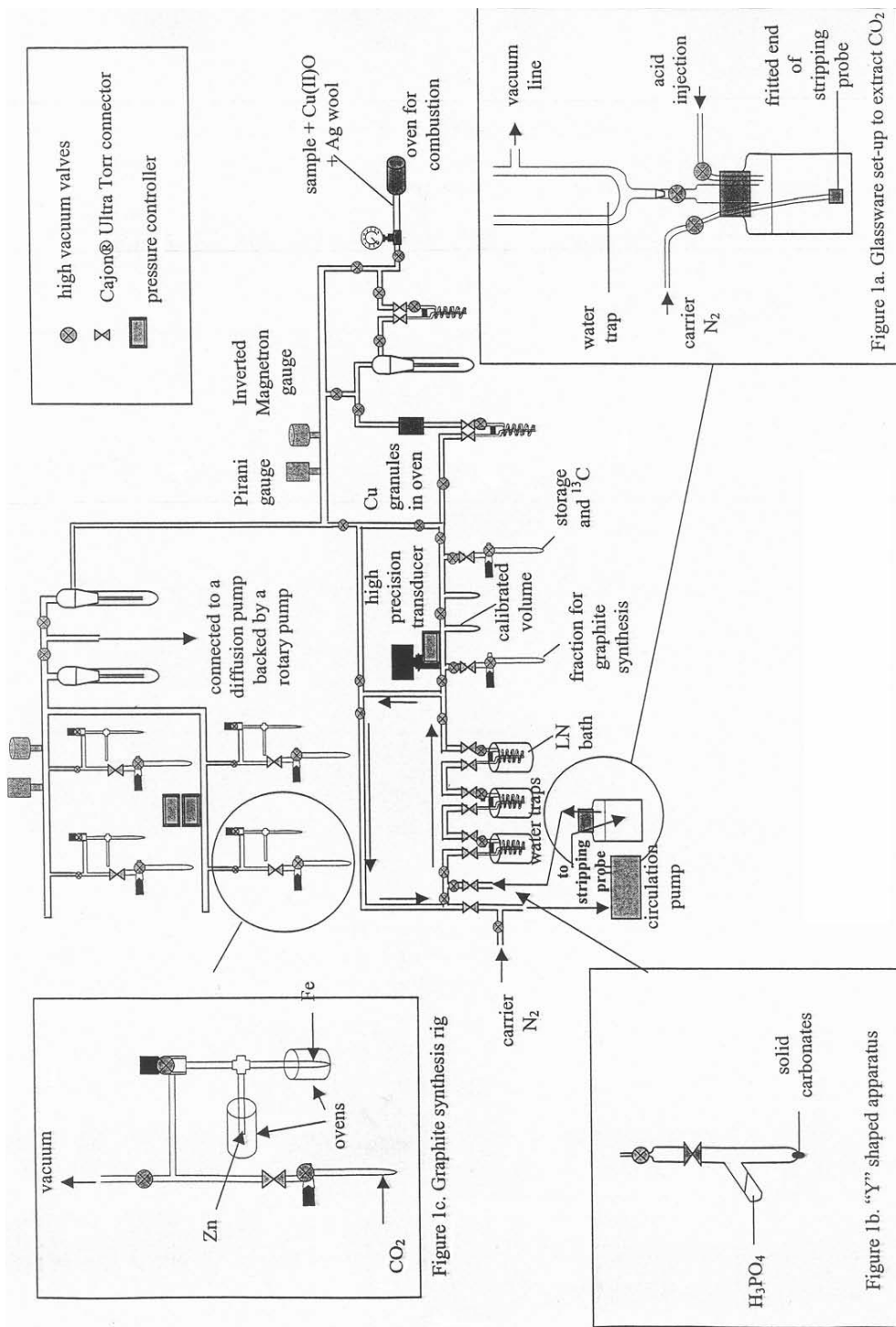


Figure 1 Processing line for preparation of samples for ^{14}C measurements

Biota

Fifty mg of freeze-dried marine biota sample was thoroughly mixed with 1000 mg of Cu(II)O and combusted under vacuum at 900 °C in a 9-mm Vycor® tube connected to the processing line. For samples of suspected higher activity, the mixture was flame-sealed in the tube before combustion in a separate oven to avoid contaminating the line. The CO₂ was purified by passing the produced gas through pure Ag wool, water traps cooled at -80 °C, and a column of packed Cu granules at 450 °C. An aliquot of the pure CO₂ of precisely known volume was reduced to graphite while a second fraction was used for δ¹³C determination.

When dealing with solid samples like shells and corals, small pieces of the material are introduced into one of the arms of the extraction glassware apparatus for solid samples depicted in Figure 1b. Five mL of H₃PO₄ was carefully introduced into the side arm before connecting the apparatus to the line and generating a vacuum. The extraction apparatus was then isolated from the processing line by means of 2 valves, enabling its disconnection from the line. No leakage was observed during this manipulation. The acid was gently tipped over the solid sample, thus liberating CO₂. For complete dissolution, gentle heating was sometimes necessary. After total digestion, the extraction apparatus was again connected to the line and the CO₂ was purified as previously described before graphite synthesis and δ¹³C measurement.

Reduction of CO₂

The reduction was carried out with Zn in the presence of dendritic Fe (200 mesh) (Slota et al. 1987). Both chemicals were carefully weighed and introduced into 6-mm-diameter Vycor tubes. They were then connected to the graphite apparatus, together with a tube filled with purified (using liquid nitrogen and dry ice traps) CO₂ extracted from a sample, as shown in Figure 1c. The air above was carefully pumped out and the CO₂ transferred cryogenically to the reactor. The Zn tube was then heated to 450 °C, which pre-reduced CO₂ to CO. After 1 hr, the Fe was heated to 550 °C and graphite was produced and deposited onto the Fe. The pressure was constantly monitored until the reaction was completed, which usually takes between 8 to 10 hr, by means of a transducer connected to a computer via a data acquisition system. The product was then weighed very carefully. The graphite yield was calculated both gravimetrically and manometrically from pressure readings.

For a 6-mm-diameter tube, 2 mg of carbon was found to be the appropriate amount for synthesis. The mass of Fe used, enabling to reach an acceptable ionic current in the AMS source, was twice the amount of carbon that needed to be reduced. For complete reduction, the pressure should drop to zero, meaning all gaseous CO₂ and CO has been reduced to solid graphite. The reactions occurring within the reactor are the following:

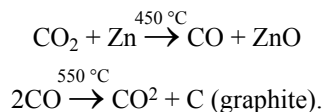


Figure 2 shows the variation of pressure with time. Curve 2 shows successful synthesis with a yield of about 98%. Curve 1 shows a synthesis with a yield of about 95%, as the curve did not return to a zero pressure state, probably because of the presence of water vapors in the system. Curves 3 and 4 are examples where no synthesis took place at all. The constant increase in pressure with time in curve 4 is an indication of a leakage in the graphite apparatus (probably due to a damaged O-ring). In reaction 5, the synthesis seemed to end prematurely at point A, which would have resulted in a poor graphite yield and probable isotopic fractionation. However, on removing the tube furnace, a

yellow deposit was noticed on the Zn surface. It was concluded that it was sulphur, obtained by the reduction of co-extracted SO_2 , which was hindering the graphite synthesis. By gently tapping the Zn tube with a spatula and re-setting the furnaces, the reaction continued to completion as depicted.

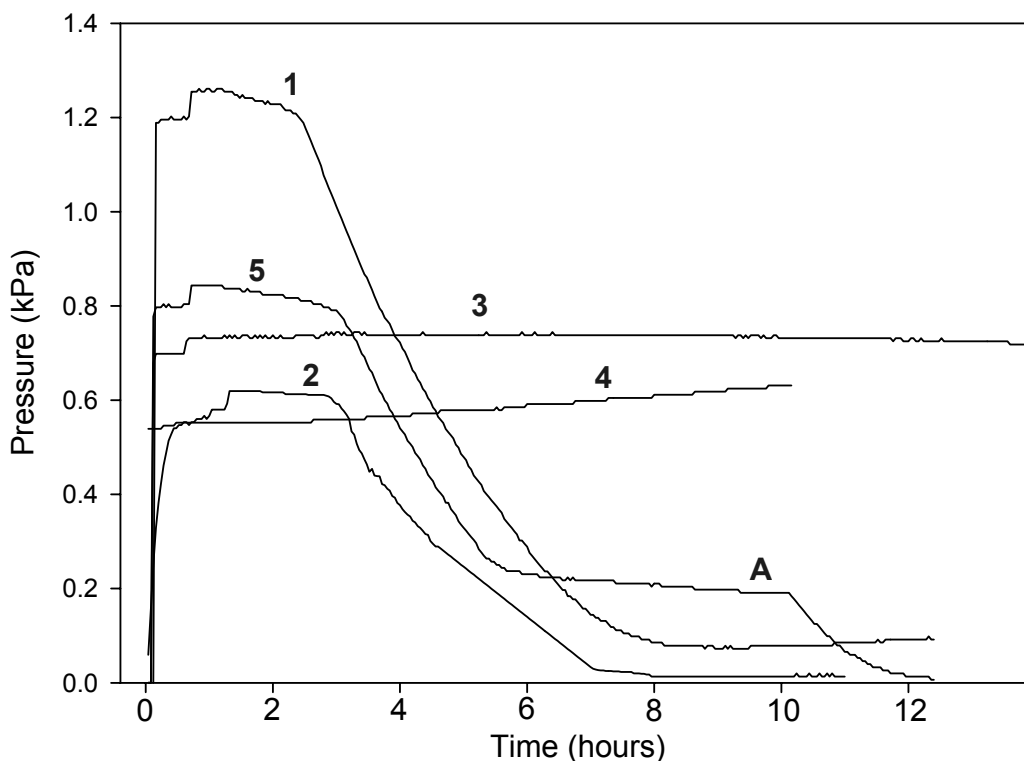


Figure 2 Variation of pressure during the graphite synthesis

RESULTS AND DISCUSSION

To verify that the CO_2 extraction procedure from water samples was quantitative, known amounts of Na_2CO_3 standards, which were dried overnight at 200°C in an oven, were dissolved in degassed Milli-Q[®] water. As soon as the dissolution was complete, the solution was processed. The mean recovery yield for 5 extractions was $95 \pm 5\%$. Similarly, to check the performance of the wet-digestion procedure, exactly known amounts of solid Na_2CO_3 were hydrolyzed with H_3PO_4 using the extraction apparatus for solid samples as described above. The mean recovery was $97 \pm 3\%$ for 5 extractions.

The combustion procedure was tested by burning 50 mg of the National Institute of Standards and Technology's (Gaithersburg, USA) oxalic-acid standard reference material (HOxII, NIST SRM 4990C) with an excess of Cu(II)O . The compounds were thoroughly mixed in a 9-mm-diameter Vycor tube and combusted at 900°C under vacuum. Aliquots of 4 mL (STP) of pure CO_2 were taken for the measurement of ^{13}C . In addition, other aliquots of CO_2 were reduced to graphite. These were then strongly heated with a torch, so that the graphite would oxidize back to CO_2 . New $\delta^{13}\text{C}$ values were again measured and they agreed with the initial ^{13}C values, proving the validity of the procedure. All stable isotope analyses were within 0.3%. The reproducibility of ^{14}C measurements on the

NIST standard reference material was better than 15%. All graphite samples discussed in this paper were analyzed by the AMS facility of the University of Arizona.

Finally, several replicate samples of seawater were collected in the Mediterranean near the port of Monaco, and processed according to the performance check tests described above. The mean concentration of CO_2 extracted was $2.64 \pm 0.18 \text{ mmol kg}^{-1}$. The $\delta^{13}\text{C}$ values ranged from -0.80 to -1.18‰ and $\Delta^{14}\text{C}$ values were in the interval of $70\text{--}80\text{‰}$. For testing purposes, seawater samples collected at Station 1 ($34^\circ 59'\text{N}$, $145^\circ 59'\text{E}$) of the IAEA 1997 Pacific Ocean expedition were also processed according to the developed procedure. The $\Delta^{14}\text{C}$ profile is shown in Figure 3 and corroborates well with results published by Aramaki et al. (2001).

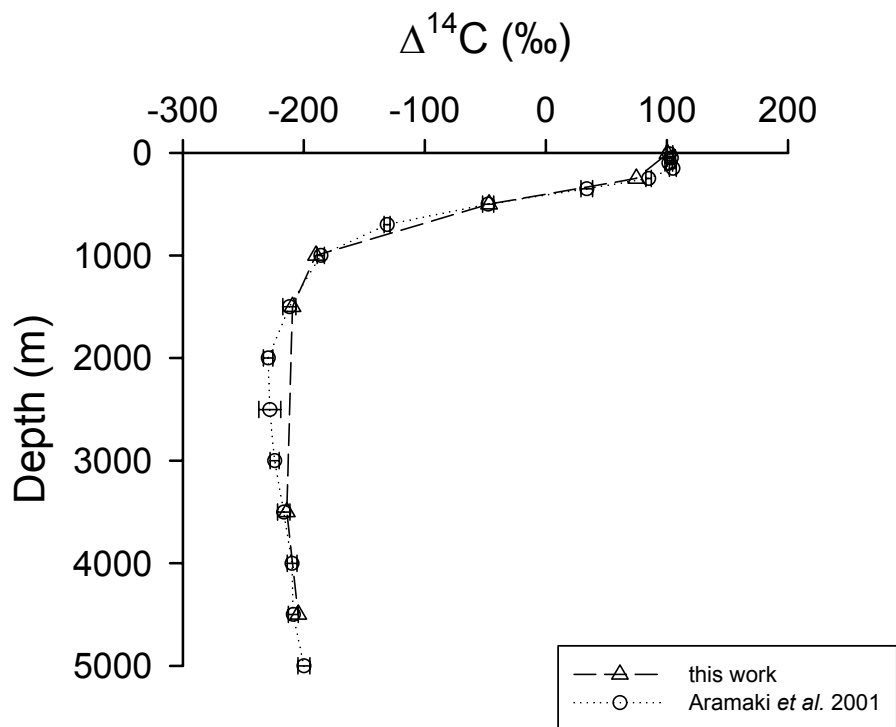


Figure 3 $\Delta^{14}\text{C}$ (‰) profile for Station 1 of the IAEA 1997 Pacific Ocean expedition (this work and Aramaki et al. 2001).

Analyses of marine biota samples (plankton, fish, and corals) have been carried out for carbon flux studies and investigations of transport and exchange processes between seawater and marine biota. The obtained results will be published in a separate paper.

CONCLUSIONS

Development of the ^{14}C line at the IAEA's Marine Environment Laboratory in Monaco and the sample processing procedures have proved to be successful, giving results comparable to published values. For routine water analyses, a rigorous internal verification procedure has been implemented and is carried out on a continuous basis. Each set of samples is processed together with Na_2CO_3 standards and another seawater sample of known concentration (a water sample collected off the port of Monaco,) which is used as an internal reference material. Measurements of ^{14}C in seawater

and marine biota such as plankton will continue to be carried out for investigations of processes in the water column, climate change and carbon flux studies, and investigations of transport and exchange processes between seawater and marine biota.

ACKNOWLEDGEMENTS

The authors are indebted to Mr T Lange of the University of Arizona's AMS Facility for the installation of the sample processing line and his advice. IAEA-MEL operates under a bilateral agreement between the International Atomic Energy Agency and the Government of the Principality of Monaco.

REFERENCES

- Aramaki T, Mizushima T, Kuji T, Povinec PP, Togawa O. 2001. Distribution of radiocarbon in the southwestern North Pacific. *Radiocarbon* 43(2B):857–67.
- Bard E, Arnold M, Toggweiler JR, Maurice P, Duplessy J-C. 1989. Bomb ^{14}C in the Indian Ocean measured by accelerator mass spectrometry: oceanographic implications. *Radiocarbon* 31(3):510–22.
- Broecker WS, Peacock SL, Walker S, Weiss R, Fahrbach E, Schroeder M, Mikolajewicz U, Heinze C, Key R, Peng TH, Rubin S. 1998. How much deep water is formed in the Southern Ocean. *Journal of Geophysical Research* 103:15,833–44.
- Burchuladze AA, Pagava SV, Povinec PP, Togonoidze GI, Usacev S. 1980. Radiocarbon variations with the 11-year solar cycle during the last century. *Nature* 287:320–2.
- Bushan R, Chakraborty S, Krishnaswami S. 1994. Physical Research Laboratory (Chemistry) radiocarbon date list 1. *Radiocarbon* 36(2):251–6.
- Calf GE. 1978. A procedure for the preparation of benzene from ^{14}C NBS oxalic acid standard. *Radiocarbon* 20(2):169–170.
- Dörr H, Munnich KO. 1980. Carbon-14 and carbon-13 in soil CO. *Radiocarbon* 22(3):909–18.
- Gorczyca Z, Jelen K, Kuc T. 1998. Gas counting system for ^{14}C dating of small samples in the Krakow Laboratory. *Radiocarbon* 40(1):129–36.
- Jull AJT, Linick TW, Toolin LJ. 1987. Preparation of small samples for ^{14}C accelerator targets by catalytic reduction of CO. *Radiocarbon* 29(2):303–6.
- Key RM, Quay PD, Schlosser P, McNichol AP, von Renden KF, Schneider RJ, Elder KL, Stuiver M, Östlund HG. 2002. WOCE Radiocarbon IV: Pacific Ocean results; P10, P13N, P14C, P18, P19 & S4P. *Radiocarbon* 44(1):239–392.
- Lawson E, Elliott G, Fallon J, Fink D, Hotchkis MAC, Hua Q, Jacobsen G, Lee P, Smith AM, Tuniz C, Zoppi U. 2000. AMS at ANTARES—the first 10 years. *Nuclear Instruments and Methods in Physics Research B* 172:95–9.
- McNichol AP, Jones GA, Hutton, DL, Gagnon AR. 1994. The rapid preparation of seawater ΣCO_2 for radiocarbon analysis at the National Ocean Sciences AMS Facility. *Radiocarbon* 36(2):237–46.
- Nydal R, Giselfoss J, Skjelvan I, Skogseth F. 1992. ^{14}C profiles in the Norwegian and Greenland Seas by conventional and AMS measurements. *Radiocarbon* 34(3):717–26.
- Östlund HG, Stuiver M. 1980. GEOSECS Pacific radiocarbon. *Radiocarbon* 22(1):25–53.
- Östlund HG, Craig H, Broecker WS, Spenser D. 1987. GEOSECS Atlantic, Pacific and Indian Ocean Expeditions. Vol. 7. Shorebased Data and Graphics. Washington, DC: *National Science Foundation*.
- Östlund HG, Rooth CGH. 1990. The North Atlantic tritium and radiocarbon transients 1972–1983. *Journal of Geophysical Research* 95(C11):20,147–65.
- Povinec PP. 1992. ^{14}C gas counting: Is there still a future? *Radiocarbon* 34(3):406–13.
- Povinec PP. 1994. Underground low-level counting. In: Proceedings of the 3rd International Conference on Low-level Measurements of Radioactivity in the Environment. Singapore: World Scientific. p 113–39.
- Povinec PP, Oregioni B, Jull AJT, Kieser WE, Zhao X-L. 2000. AMS measurements of ^{14}C and ^{129}I in seawater around radioactive waste dump sites. *Nuclear Instruments and Methods in Physics Research B* 172:672–8.
- Slota PJ, Jull AJT, Linick TW, Toolin LJ. 1987. Preparation of small samples for ^{14}C accelerator targets by catalytic reduction of CO_2 . *Radiocarbon* 29(2):303.
- Stuiver M, Quay PD, Östlund HG. 1983. Abyssal water carbon-14 distribution and the age of the world oceans. *Science* 219:849.
- Vogel JS, Southon JR, Nelson DE, Brown TA. 1984. Performance of catalytically condensed carbon for use in accelerator mass spectrometry. *Nuclear Instruments and Methods in Physics Research B* 5:289–93.

DEVELOPMENT OF A COMBUSTION SYSTEM FOR LIQUID OR GAS SAMPLES

J H Park • C S Lee¹

Department of Physics, Chung-Ang University, Seoul 156-756, South Korea.

ABSTRACT. While it is customary to use solid samples for measuring the $^{14}\text{C}/^{12}\text{C}$ ratio, it is sometimes necessary to handle liquid or gas samples. Motivated by a scientific purpose to count radiocarbon yields in deuterated acetone irradiated with energetic neutrons, we developed a new combustion system to treat liquid or gas samples. In contrast with the typical combustion system using CuO for solid samples, the new combustion system uses high-purity O_2 (99.999%) gas. As an initial investigation, we combusted deuterated acetone (acetone- d_6 , certified 100.0 atm % D) to make CO_2 under the ambient O_2 pressure. The resulting CO_2 gas then went through the reduction process to form graphite for further accelerator mass spectrometry (AMS) measurement.

INTRODUCTION

In March 2002, Taleyarkhan et al. reported an interesting result in cavitation experiments using deuterated acetone (acetone- d_6 , certified 100.0 atm % D) bombarded by 14-MeV neutrons: that tritium β -decay activity above background levels was detected and 2.5-MeV neutrons were also observed as would be expected for deuterium-deuterium (DD) fusion (Taleyarkhan et al. 2002). However, in a subsequent experiment using the same cavitation apparatus, Shapira et al. (2002) found no evidence for 2.5-MeV neutron emission correlated with sonoluminescence (SL), in which light is emitted from collapsing bubbles in a liquid subjected to an acoustic field.

Reproducibility of the claimed tritium activity will also be necessary to verify whether tritium β -decay activity was produced via DD-fusion or any other means. It is also noteworthy in the usual liquid scintillation (LS) detection that β -rays emitted from radiocarbon with the end-point energy of 156 keV might be piled on the β -ray spectrum for tritium with the end-point energy of 18 keV if the 2 β -decaying nuclides were simultaneously produced via neutron capture.

As an initial step toward investigating the possibility and verification of the claimed DD-fusion in cavitation experiments using d-acetone, we apply the accelerator mass spectrometry (AMS) technique to directly count ^{14}C atoms produced by the $^{13}\text{C}(n,\gamma)^{14}\text{C}$ reaction after d-acetone is irradiated by energetic neutrons. But a combustion system to treat liquid acetone for the AMS measurement needs to be developed by taking into account the volatility of acetone, since solids are the main type of sample in AMS measurement.

In this article, we report a new combustion system in sample treatment to convert liquid or gas to CO_2 . The new combustion system uses high-purity O_2 (99.999%) gas to combust liquid or gas samples. Since O_2 gas reacts violently with liquid or gas samples, for safety reasons, we made the pressure of both the O_2 gas and sample low and performed the combustion reaction. After the CO_2 gas was made for a further reduction procedure (Lee et al. 2000; Vogel et al. 1987) and measurement, we used the AMS facility at Seoul National University (Kim et al. 2000).

¹Corresponding author. Email: cslee@cau.ac.kr.

DEVELOPMENT OF A COMBUSTION SYSTEM FOR LIQUID OR GAS SAMPLES

Conventional Combustion Method

The combustion procedure allows one to convert the carbons of a sample to CO₂ gas. Figure 1 shows the vacuum line of the conventional combustion system to treat solid samples, which recovers the CO₂ gas after combustion (Lee et al. 2000). Chemically pretreated samples of 5–6 mg and Ag wires (each about 2 cm long and 0.2 mm thick) are inserted in a Vycor[®] tube, 5 cm in length and 6 mm in outer diameter. The Vycor tube and 1 g of CuO powder are inserted in a vacuum-sealed quartz tube. The sealed tube was placed in a muffle furnace and combusted at a temperature of 850 °C for 2 hr. The Ag wire and CuO are baked at 850 °C and 550 °C, respectively, for 2 hr before being introduced into the combustion tube in order to release any absorbed contaminants from the ambient atmosphere. After combustion, the quartz tube is inserted in flexible bellows, followed by pumping of the vacuum line, then breaking of the tube to collect CO₂. The released CO₂ gas is separated from H₂O by using dry ice/alcohol traps and cryogenically transported to the storage chamber for the further graphitization.

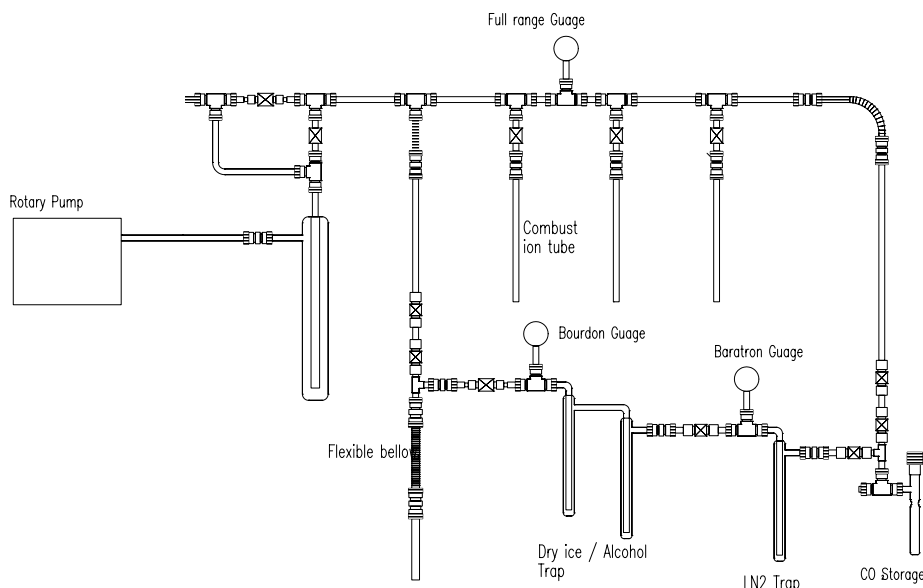


Figure 1 Schematic diagram of the conventional combustion system (Lee et al. 2000)

New Combustion System for Liquid or Gas Samples

A photograph of our combustion system for liquid or gas samples is shown in Figure 2 and its schematic diagram is given in Figure 3. Liquid samples of approximately 30–40 μL are measured using a 100-μL syringe, ensuring air is removed. The same apparatus can also be used for a gas sample by adding the gas storage chamber and a connection to the injection port. The reaction chamber consists of a quartz (or stainless steel) tube 17 cm in length and 1/2" outer diameter, and a Bourdon gauge with a range of 0–5 atm. High-purity oxygen (99.999%) is added into the system via the O₂ injection port.

We tested the combustion system using deuterated acetone (acetone-d₆, certified 100.0 atm % D). The combustion system was evacuated, then high-purity oxygen (99.999%) (600 torr) was injected



Figure 2 Photograph of the present combustion system for liquid and gas samples

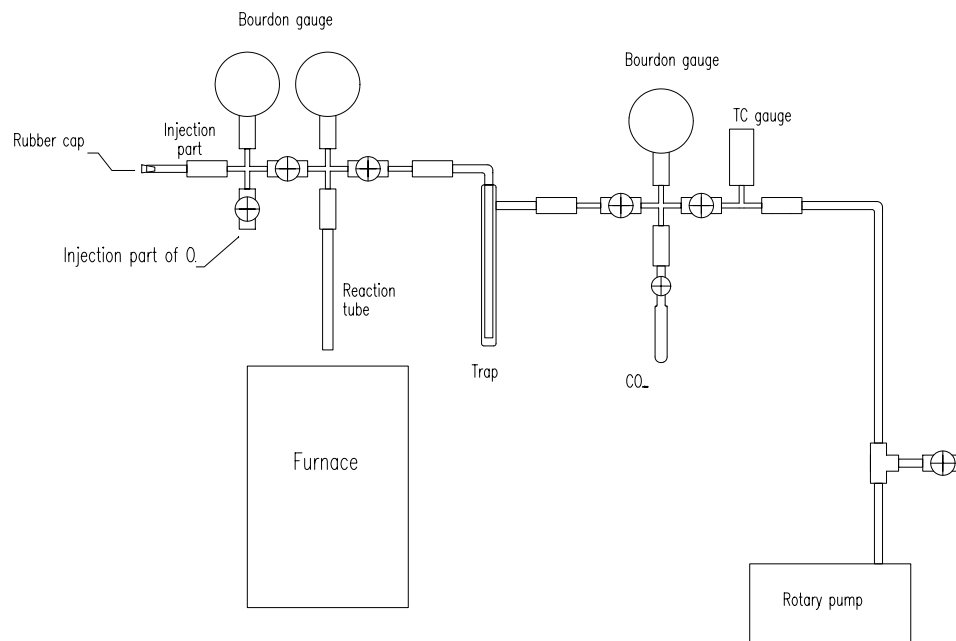


Figure 3 Schematic diagram of the present combustion line for liquid and gas samples

into the reaction chamber. The sample (10 μL) was injected via the rubber septum using a syringe. The d-acetone and oxygen were transferred to the reaction tube cryogenically, leaving 0.2 atm of O_2 in the injection area. The furnace was heated to 800 $^\circ\text{C}$ to heat the reaction tube. A flash of light occurs when the combustion reaction takes place. If the pressure inside the reaction chamber (quartz) is greater than 1.5 atm, it is possible that the reaction will break the reaction tube. Thus, we made the pressure inside the reaction chamber 1.5 atm and raised the furnace. After several seconds, a bright flash of light occurs and the reaction tube (quartz) breaks. To ensure safety, an acryl plate needs to be set in front of the reaction chamber and furnace, and the total pressure of the reaction chamber needs to be maintained around 1 atm. After 5–10 min, the furnace is lowered and the reaction chamber is allowed to cool. The reaction products are CO_2 , O_2 , H_2O , and CO . CO_2 is separated using dry ice/alcohol traps and a liquid nitrogen trap and transferred cryogenically to the storage chamber. The chamber has an approximate volume of 10 mL and the yield of carbon is then calculated from the measured pressure (typically around 0.13 atm).

RESULTS AND CONCLUSION

Three deuterated acetone samples from the same sample with a volume of 1 mL were drawn to test the various combustion methods. Using our combustion system developed for liquid or gas samples, we made CO_2 from the 3 deuterated acetone samples, followed by graphitization using a reduction system (Lee et al. 2000) housed at the AMS facility at Seoul National University (Kim et al. 2000). The $^{14}\text{C}/^{12}\text{C}$ ratios were measured at the AMS facility. Results of the measurement and the conditions of sample treatment are summarized in Tables 1 and 2.

Table 1 Conditions of sample treatment.

ID nr	Used acetone volume (μL)	Type of reaction tube	Pressure of the reaction chamber (atm)		Pressure of produced CO_2 (μmol)	Content of carbon in CO_2 (mg)
			Before reaction	After reaction		
3	15	Quartz	1.4	1.5	95	1.1
4	11	Quartz	0.8	0.7	47	0.6
5	11	Stainless steel	1.25	0.7	65	0.8

Table 2 Results of the AMS measurement.

ID nr	Sample code	Type of reaction tube	$\delta^{13}\text{C}$ (‰ , PDB)	pMC
3	SNU 03-367	Quartz	-34.1	0.6 ± 0.1
4	SNU 03-368	Quartz	-43.8	2.6 ± 0.4
5	SNU 03-369	Stainless steel	-27.4	0.8 ± 0.1

From Table 2, one can see that the $^{14}\text{C}/^{12}\text{C}$ ratio of #4 is higher than those of #3 and #5 and the $\delta^{13}\text{C}$ of #4 is also lower than those of the others. Since we used deuterated acetone samples from the same sample but found that the $^{14}\text{C}/^{12}\text{C}$ ratio and the $\delta^{13}\text{C}$ of #4 is different from the others, we conclude that #4 might be slightly contaminated. Because the content of carbon which produced the CO_2 of #4 is smaller, if #4 is contaminated, the $^{14}\text{C}/^{12}\text{C}$ ratios and $\delta^{13}\text{C}$ of #4 can change easily. However, in an effort to increase the content of carbon by raising the pressure of the reaction chamber higher than 1.5 atm, the quartz reaction tube cracked. Therefore, the pressure of the reaction chamber should be maintained at 1–1.5 atm.

The stainless steel reaction tube (for example, #5) may be more resistant to breaking, but it can introduce unwanted combustion of oxygen with the iron and carbon of stainless steel. As seen in Table 1, while the pressure of the reaction chamber for #3 and #4 after combustion is similar to that of the reaction chamber before combustion, the pressure of the reaction chamber for #5 after combustion is much lower than that of the reaction chamber before combustion. The authors believe that this phenomenon is mainly due to the combustion of oxygen with the iron of the tube. Since the resulting $^{14}\text{C}/^{12}\text{C}$ ratio of #5 (in Table 2) is low and similar to that of #3, it could indicate that #5 is not contaminated. However, the possibility of an additional combustion of oxygen with carbon contained in the stainless steel cannot be ruled out.

It is recommended that the length of the quartz reaction tube is increased to 20–25 cm in order to treat a larger quantity of the sample, which will allow a lower pressure and make the experiment safer. Furthermore, the possibility of contamination and the unwanted combustion of oxygen with the iron and carbon that are contained in stainless steel can be avoided. Regarding the deuterated acetone with energetic neutrons, we recently conducted a neutron irradiation experiment by using fast neutrons produced in the $^9\text{Be}(p,n)^9\text{B}$ induced by 20-MeV protons. Neutrons measured with the time-of-flight technique (Kim et al. 1998) were shown to be in the energy range of 6–18 MeV, with the flux intensity maximum near 14 MeV. The irradiated deuterated acetone samples were combusted using the same combustion system developed for liquid or gas samples. AMS measurement of the $^{14}\text{C}/^{12}\text{C}$ ratios for the samples is underway at the AMS facility of Seoul National University.

ACKNOWLEDGEMENTS

This work was supported by a grant (R01-2003-000-10016-0) from the Korea Science and Engineering Foundation.

REFERENCES

- Kim JC, Lee CH, Kim IC, Park JH, Kang J, Cheoun MK, Kim YD, Moon CB. 2000. A new AMS facility in Korea. *Nuclear Instruments and Methods in Physics Research B* 172:13–7.
- Kim JH, Bhang H, Ha JH, Kim JC, Kim MJ, Kim YD, Park H, Chai JS, Kim YS, Lee HY, Shin SA, Huh JY, Lee CS, Lee JH. 1998. A measurement of monoenergetic neutrons from $^9\text{Be}(p,n)^9\text{B}$. *Journal of the Korean Physical Society* 32(4):462–7.
- Lee C, Kim JC, Park JH, Kim IC, Kang J, Cheoun MK, Choi SY, Kim YD, Moon CB. 2000. Progress in sample preparation system for the Seoul National University AMS facility. *Nuclear Instruments and Methods in Physics Research B* 172:454–7.
- Shapira D, Saltmarsh M. 2002. Nuclear fusion in collapsing bubbles—Is it there? An attempt to repeat the observation of nuclear emissions from sonoluminescence. *Physical Review Letters* 89(10):104302-1–104302-4.
- Taleyarkhan RP, West CD, Cho JS, Lahey RT Jr, Nigmatulin RI, Block RC. 2002. Evidence for nuclear emissions during acoustic cavitation. *Science* 295:1868–73.
- Vogel JS, Southon JR, Nelson DE. 1987. Catalyst and binder effects in the use of filamentous graphite for AMS. In: Gove HE, Litherland AE, Elmore D, editors. Proceedings of the 4th International Symposium on Accelerator Mass Spectrometry. *Nuclear Instruments and Methods in Physics Research B* 29:50–6.

A PRETREATMENT PROCEDURE FOR THE AMS RADIOCARBON DATING OF SUB-FOSSIL INSECT REMAINS

J A Tripp • T F G Higham¹ • R E M Hedges

Oxford Radiocarbon Accelerator Unit, Research Laboratory for Archaeology and the History of Art, Oxford University, 6 Keble Road, Oxford OX1 3QJ, England.

ABSTRACT. Two pretreatment methods for accelerator mass spectrometry (AMS) dating of insect remains were explored. One method involves a simple acid wash that removes carbonate, while the other is based on the industrial purification of chitin and results in isolation of polymeric chitosan. No contamination is observed from Maillard reactions during the deacetylation reaction used to isolate the chitosan. The methods were tested on Coleoptera samples from two Roman Britain sites. Our results demonstrate that both methods produce acceptable AMS dates that correspond well to the expected age of the deposits from which they came.

INTRODUCTION

Remains of insects are often found in an archaeological context and because many of them are temperature-sensitive organisms, they have been used as temperature and climate proxies in environmental studies (Robinson 2001). Accelerator mass spectrometry (AMS) radiocarbon dating is the most common method utilized to provide the chronological framework for these studies; however, it is typically associated with organic remains from peat or swamp material that are used for dating, not the insects themselves. This is often due to difficulty in obtaining pure material for dating.

For single-compound ¹⁴C dating, the best candidate from insects is chitin or a derivative. Chitin (Figure 1) is a polymer composed of repeating *N*-acetyl-D-glucosamine units that is a major structural component of insect exoskeletons. In insects, chitin is bundled into microfibrils that are peripherally bound to proteins and arranged in a carbonate matrix to form the exoskeleton (Neville 1975). After death, the chitin-protein complex can undergo depolymerization or various condensation reactions with substances from the soil, resulting in numerous compounds, including humics, that may or may not be indigenous to or of the same age as the insects. While chitin is more resistant to diagenetic degradation when it is complexed to proteins, there is often significant chitin degradation even in cuticles that appear well-preserved (Stankiewicz et al. 1998). However, preservation of insect chitin under certain conditions in specimens as old as 25 million yr has been reported (Stankiewicz et al. 1997).

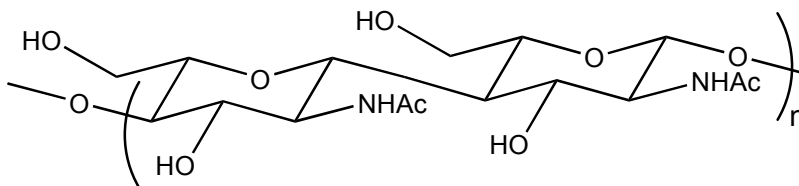


Figure 1 Structure of chitin

Certain limitations and requirements must be considered when developing a ¹⁴C pretreatment procedure. Consistent, high recovery of pure material, with some way to assess the purity, is necessary. The procedure should not be too time-intensive and should use current protocols and techniques

¹Corresponding author. Email: thomas.higham@archaeology-research.oxford.ac.uk.

where possible. In addition, isotope fractionation must be minimized. Previous work in our laboratory towards a pretreatment procedure for insects involved isolation of D-glucosamine from hydrolyzed chitin using ion-exchange chromatography, but this method identified serious problems of low recovery and incomplete purification (Hodgins et al. 2001). In addition, a significant and relatively consistent offset between AMS dates of insect remains and surrounding organic material was observed, and has also been reported by others (Elias and Toolin 1990; Elias et al. 1991; Walker et al. 2001). Possible explanations for this offset are different ecological and feeding adaptation of the insects, perhaps resulting in the uptake of differently aged ^{14}C , or insufficient purification of the isolated chitin.

In this paper, we report a study comparing two purification methods. The first is a simple acid treatment to remove carbonate (Method A), while the other involves a harsher reaction to remove the protein component and isolate only the chitin polymer (Method B). This second method is based on the industrial purification of chitin (Roberts 1992) and involves the deacetylation, with concurrent deproteinization, of insect exoskeletons, followed by isolation of chitosan (deacetylated chitin) by a dissolution-precipitation procedure. The procedures were tested on Coleoptera remains from two Roman-period sites in Britain.

EXPERIMENTAL SECTION

Materials and Methods

Commercial chitin, isolated from crab shells, was obtained from Aldrich. Water was purified using a Millipore Milli-Q system. All other solvents and reagents were purchased from Fisher Scientific. Coleoptera remains were obtained by Dr Mark Robinson of the Natural History Museum at Oxford from the sites of Priors Gate and Godmanchester in Cambridgeshire, UK. Elemental and mass spectrometric analyses were undertaken using a Europa ANCA Roboprep CHN analyzer interfaced to a Europa 20/20 MS operating in continuous-flow mode. Graphite was prepared by reduction of CO_2 over an iron catalyst in an excess H_2 atmosphere at 560°C prior to AMS ^{14}C measurement (Bronk Ramsey and Hedges 1999; Bronk Ramsey et al. 2000). Samples of insect chitin $<1.6\text{ mg C}$ in size were AMS dated as directly-injected CO_2 using the ORAU gas ion source. $\delta^{13}\text{C}$ values in this paper are reported with reference to VPDB and $\delta^{15}\text{N}$ results are reported with reference to AIR (Coplen 1994).

Deacetylation of Commercial Chitin

Chitin (1.6 g) was suspended in 50 mL of 50% NaOH and heated to 120°C for 1 hr. The reaction was filtered and the solid resuspended in purified water. Next, the 6M HCl was added to make the solution weakly acidic (about pH 3) so that the solid dissolved. The solution was again filtered to remove any residual solids, and 6 M HCl added to the filtrate to make the solution strongly acidic (pH <1). A white solid (chitosan•HCl) precipitated from the solution. This was filtered, rinsed, dried, and analyzed.

Maillard Reactions with Chitin and D-Glucosamine

One-hundred g of chitin or D-glucosamine was mixed with 100 mg of glycine (when used) and 10 mL of either water or 50% NaOH. The reactions were heated at 120°C for 1 hr. The neutral reactions were washed several times with water. Those with NaOH were filtered and acidified with HCl as described above. All samples were freeze-dried prior to analysis.

Preparation of Coleoptera Remains for ^{14}C Dating (Method A)

The insect remains (elytra, pronotum, head capsules, and legs) were picked out of suspension under a microscope, and rinsed with acetone, methylene chloride, and acetone again, and dried under vacuum for 5 hr. The insect pieces were submerged in 0.5 M HCl for 3 days. They were then filtered, rinsed, and lyophilized.

Preparation of Coleoptera Remains for ^{14}C Dating (Method B)

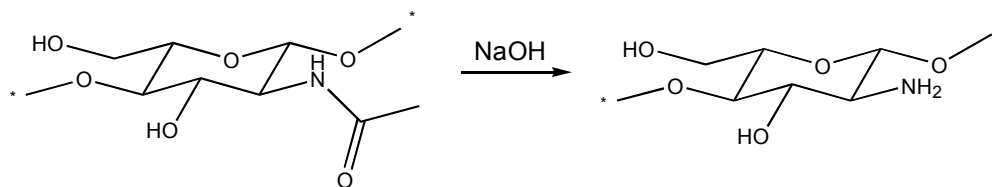
The insect remains were treated as in Method A, but following removal of the acid, they were heated in 5 mL 50% NaOH for 30 min. The resulting product was filtered and the solids resuspended in water. The resulting solution was made weakly acidic by addition of 6 M HCl, filtered to remove residual solids, and then made strongly acidic by further addition of 6 M HCl. The resulting solids were captured in pre-combusted glass-fiber filters, lyophilized, and analyzed.

Preparation of Seeds for ^{14}C Dating

Carbonized and waterlogged woody seeds were prepared using the acid-base-acid (A-B-A) method (Hedges et al. 1989) to remove carbonates, fulvics, and humics, then rinsed and dried.

RESULTS AND DISCUSSION**Deacetylation of Chitin**

In order to test the parameters for the deacetylation reaction in Method B, experiments were first performed on commercial chitin. Deacetylation (Scheme 1) results in a loss of two carbons from each residue, and thus, the C/N ratio can be used to estimate the degree of deacetylation. A completely acetylated chitin chain will have a C/N of 8, while completely deacetylated chitin (chitosan) will have a C/N of 6. Using the C/N ratio instead of the absolute values for % N and % C eliminates the effects of residual moisture in this determination (Roberts 1992). A C/N less than 6 suggests the presence of proteins, which usually have C/N between 2 and 6. Proteins present in insect samples may be either indigenous or contaminating, and thus, their removal is important.

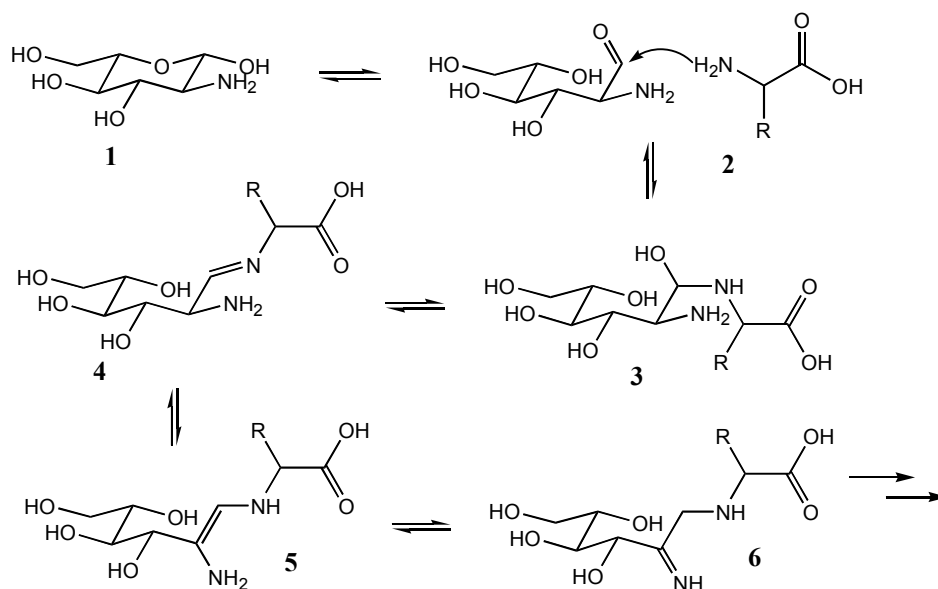


Scheme 1 Deacetylation of chitin

After deacetylation, the resulting chitosan polymer is soluble in weak acid, but will precipitate out of solution when strong acid is added due to the presence of multiple charges along the length of the polymer. It should be noted that the carbohydrate polymers are stable to even strong base, while similar conditions will result in cleavage of the amide backbone in proteins.

One necessary consideration for the deprotection reaction is the Maillard reaction, a condensation reaction that occurs between carbohydrates and amino acids that is responsible for a number of effects including the browning of cooked meat (Fayle and Gerrard 2002). The occurrence of Maillard reactions during the deprotection reaction may lead to covalent attachment of non-native and differently-aged proteins or amino acids onto the chitin. The mechanism of the initial steps of the reaction

is shown in Scheme 2 using D-glucosamine as the substrate. The first step is a nucleophilic attack of the amine group of an amino acid on the anomeric carbon of the glycoside. This step can only occur on the linear form of the glycoside (**2**), and since polymerization requires the hemiacetal form (**1**), it suggests that if the chain integrity is preserved, no Maillard reaction will be observed. The initial product condenses to a Schiff base (**4**) and rearranges to form the Amadori product (**6**), which can then undergo numerous other reactive steps to produce a variety of highly colored products.



Scheme 2 First steps of Maillard reaction mechanism

We ran a series of experiments in which D-glucosamine and chitin were reacted under conditions I–IV listed below.

- I. water
- II. 50% NaOH
- III. water + glycine
- IV. 50% NaOH + glycine.

The products of the Maillard reaction are highly colored, so this color change, as well as C/N ratios of the resulting polymeric products can be used to determine if the reactions occurred or not. Elemental analysis was not undertaken on the D-glucosamine solutions because a range of compounds was formed, thwarting our attempts to isolate specific species for analysis.

As expected, all solutions containing D-glucosamine turned dark brown upon heating. The presence of base appeared to accelerate the reaction, as solutions II and IV changed color faster and became darker brown than reactions I and III. Even solutions that did not contain glycine (I and II) darkened significantly, probably due to a related reaction involving nucleophilic attack of the amino group of one D-glucosamine on another molecule using the same mechanism as shown in Scheme 2.

In contrast, the solutions containing chitin did not change color and showed little evidence of Maillard products. Results are shown in Table 1. C/N ratios and stable isotope measurements show very little contamination of polymeric chitin from glycine which has significantly different values. This

suggests that Maillard reactions of the chitin are unlikely to occur during the deacetylation reaction even with the presence of proteins and amino acids. In addition, the chitin chain does not appear to depolymerize under the reaction conditions.

Table 1 Elemental and isotopic results from Maillard reactions with chitin.

Conditions ^a	C/N (σ) ^b	$\delta^{13}\text{C}$, ‰ (σ)	$\delta^{15}\text{N}$, ‰ (σ)
I	8.41 (0.11)	-23.01 (0.19)	-1.96 (0.17)
II	7.80 (0.30)	-22.52 (0.28)	-2.34 (0.14)
III	8.28 (0.05)	-23.04 (0.14)	-1.91 (0.31)
IV	7.23 (0.32)	-22.52 (0.42)	-2.17 (0.39)
glycine ^c	2.04 (0.01)	-37.11 (0.01)	13.33 (0.03)

^aAll reactions were heated at 120 °C for 1 hr. Conditions: I-water; II-50% NaOH; III-water + gly; IV-50% NaOH + gly.

^bn=6 for reactions I – IV, n=3 for glycine.

^cData are given for the glycine used in reactions III and IV.

¹⁴C Dating of Coleoptera

Coleoptera remains were obtained from wells at two Roman-era settlement sites in Cambridgeshire, England. The Priors Gate settlement is at the site of present-day Eaton Socon. A full analysis of the insect remains suggested that the area around the settlement was an open grassland or meadow, with trees growing in hedgerows and timber buildings (M Robinson, personal communication 2002). Pottery found in context with the Coleoptera was stylistically dated to the late 1st to 3rd century AD (Mephram and Loader 2001). The specimens were divided into 2 aliquots and treated with Methods A and B as described above.

Recovery, stable isotope, and AMS results are shown in Table 2. Clearly, Method B results in the loss of about 85% of the mass, but the increase in C/N indicates that much of the lost material may be proteinaceous. The identical $\delta^{13}\text{C}$ values indicate no carbon fractionation using the procedure. The uncalibrated AMS determinations for both procedures are indistinguishable within error and correlate well with the date of the pottery found in context with the Coleoptera. Calibrated age ranges (AD/BC) are shown in Figure 2 and these also demonstrate significant overlap.

Table 2 Elemental, isotopic, and AMS data for Coleoptera remains from Priors Gate. OxA-X-*nnnn*-*nn* numbers are given to the insect determinations because of their non-routine/experimental pre-treatment chemistry.

OxA	Method ^a	Yield, %	C/N	$\delta^{13}\text{C}$, ‰	$\delta^{15}\text{N}$, ‰	¹⁴ C age (yr BP)
OxA-X-2020-21	A	100	5.6	-25.9	9.7	1851 ± 23
OxA-X-2039-11	B	15	7.2	-25.6	4.5	1830 ± 50

^aA–acid wash, B–full isolation of polymeric chitin (see text for details).

Further AMS determinations were obtained on Coleoptera samples from the London Road excavation of the Roman settlement at Godmanchester. Godmanchester was an active Roman settlement from the late 1st century to the 4th century AD (Jones 2003), although later activity seems to have been confined to inhumation cemeteries. It was a small settlement but had certain community buildings, including a forum and temples, suggesting that it may have functioned as a seat of local government. Evidence for farming wheat and for specialization of labor within the town (including animal husbandry and pottery production) was also found.

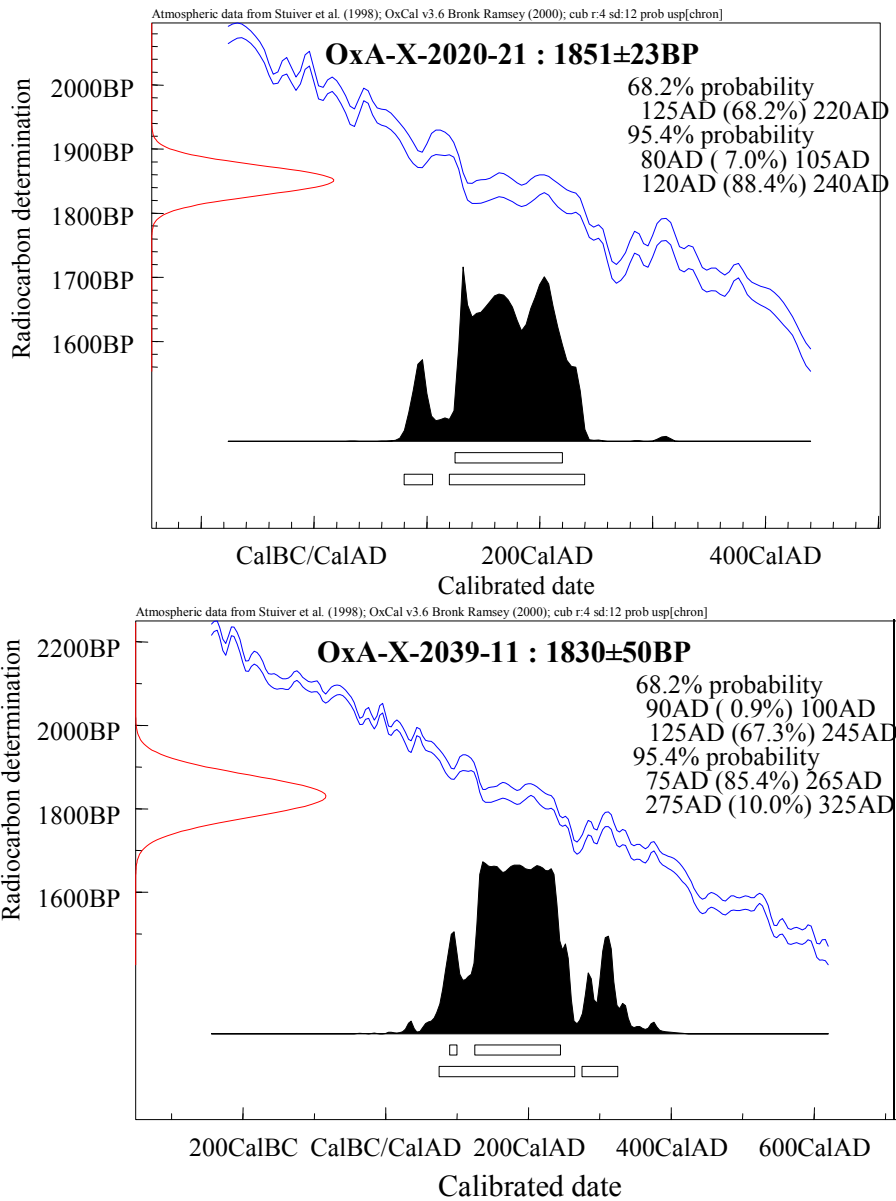


Figure 2 Calibrated AMS dates obtained from Coleoptera from Priors Gate, Eaton Socon, Cambridgeshire, treated by Methods A and B.

AMS determinations of Coleoptera (*Geotrupes* and *Aphodius*) treated with Method A were compared with carbonized (*Triticum spelta*) and waterlogged (*Malva sylvestris*, *Onopordum acanthium*, *Fallopia convolvulus*) seeds found with them. Results are shown in Table 3. The three AMS determinations are statistically indistinguishable as a group [error weighted mean = 1716 ± 19 BP ($T^2=5.55$; $\chi^2_{2;0.05}=5.99$)]. Calibrated date ranges are shown in Figure 3, and correspond to the settlement era.

Table 3 Elemental, isotope, and AMS data for Coleoptera remains and seeds from the Godmanchester site.

OxA number	Sample	C/N	$\delta^{13}\text{C}$, ‰	$\delta^{15}\text{N}$, ‰	^{14}C age (yr BP)
OxA-X-2040-22	Coleoptera	5.6	-25.9	8.4	1764 ± 29
12418	Waterlogged seeds	29.9	-26.5	7.7	1690 ± 32
12417	Carbonized seeds	18.0	-23.2	6.5	1650 ± 45

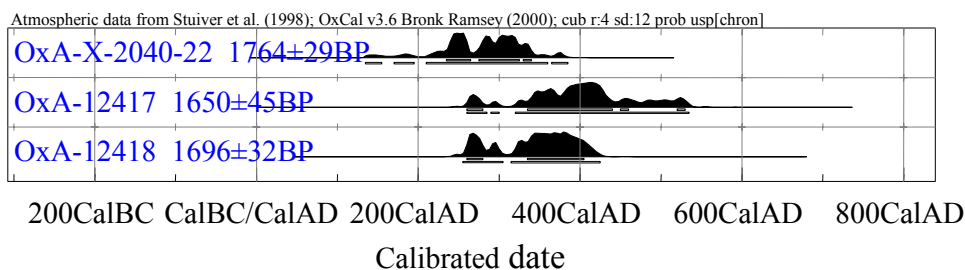


Figure 3 Calibration plots of AMS dates on beetles (OxA-X-2040-22) and carbonized (OxA-12417) and waterlogged (OxA-12418) seeds from Godmanchester, Cambridgeshire.

CONCLUSION

Our results suggest that a simple pretreatment method involving washing with organic solvents and treating the samples with acid is sufficient to yield accurate AMS dates in line with archaeological expectation. This method is simple and utilizes existing laboratory protocols. Future work will involve verification of this procedure using samples from other locations and of other ages.

Isolation of polymeric chitin is also a suitable technique, and appears to lead to ^{14}C determinations of the same age as insects purified using the simple acid wash. While this method does not result in pure isolated chitin, as seen by the C/N ratios, it is a quick and simple way of purifying insect remains for AMS dating. The substance obtained is partially deacetylated chitin with little associated protein. Experiments suggest that the chain integrity is preserved during the reactions, and no external protein contamination via a Maillard mechanism was observed. The yield of this procedure will need to be improved before it can be used routinely, but it holds promise as a purification method for the most contaminated samples.

ACKNOWLEDGEMENTS

Funding from the National Science Foundation, USA (INT-0202648) is gratefully acknowledged. We also thank Dr Mark Robinson for providing samples for dating and for helpful discussion.

REFERENCES

- Bronk Ramsey C, Hedges REM. 1999. Hybrid ion sources: radiocarbon measurements from microgram to milligram. *Nuclear Instruments and Methods in Physics Research B* 123:539–45.
- Bronk Ramsey C, Pettitt PB, Hedges REM, Hodgins GWL, Owen DC. 2000. Radiocarbon dates from the Oxford AMS system: Archaeometry Datelist 30. *Archaeometry* 42:459–79.
- Coplen TB. 1994. Reporting of stable hydrogen, carbon and oxygen isotopic abundances. *Pure and Applied Chemistry* 66:273–6.
- Elias SA, Toolin LJ. 1990. Accelerator dating of mixed assemblage of late Pleistocene insect fossils from the Lamb Spring site, Colorado. *Quaternary Research* 33: 122–6.
- Elias SA, Carrara PE, Toolin LJ, Jull AJT. 1991. Revised age of deglaciation of Lake Emma based on new radiocarbon and macrofossil analysis. *Quaternary Research* 36:307–12.
- Fayle SE, Gerrard JA. 2002. *The Maillard Reaction*.

- London: Royal Society of Chemistry. 116 p.
- Hedges REM, Law IA, Bronk CR, Housley RA. 1989. The Oxford accelerator mass spectrometry facility: technical developments in routine dating. *Archaeometry* 31:99–113.
- Hodgins GWL, Thorpe JL, Coope GR, Hedges REM. 2001. Protocol development for purification and characterization of sub-fossil insect chitin for stable isotopic analysis and radiocarbon dating. *Radiocarbon* 43(1):199–208.
- Jones A. 2003. *Settlement, Burial and Industry in Roman Godmanchester; Excavations in the Extra-Mural Area: The Parks 1998, London Road 1997-8, and Other Investigations*. BAR British Series 346. Oxford: Hadrian Books Ltd.
- Mephram L, Loader E. 2001. Finds. In: *Priors Gate, Bell Lane, Eaton Socon, St Neots, Cambridgeshire, Assessment Report on the Results of the Excavation*. The Trust for Wessex Archaeology. p 11–4.
- Neville AC. 1975. *Biology of the Arthropod Cuticle*. Berlin: Springer-Verlag. 448 p.
- Roberts GAF. 1992. *Chitin Chemistry*. Hong Kong: Macmillan Press Ltd. 368 p.
- Robinson M. 2001. Insects as palaeoenvironmental indicators. In: Brothwell D, Pollard AM, editors. *Handbook of Archaeological Sciences*. London: John Wiley & Sons. p 121–33.
- Stankiewicz BA, Briggs DEG, Evershed RP, Flannery MB, Wuttke M. 1997. Preservation of chitin in 25-million-year-old fossils. *Science* 276:1541–3.
- Stankiewicz BA, Mastalerz M, Hof CHJ, Bierstedt A, Flannery MB, Briggs DEG, Evershed RP. 1998. Biodegradation of the chitin-protein complex in crustacean cuticle. *Organic Geochemistry* 28:67–76.
- Walker MJC, Bryant C, Coope GR, Harkness DD, Lowe JJ, Scott EM. Towards a radiocarbon chronology of the Late Glacial: sample selection strategies. *Radiocarbon* 43(2B):1007–19.

IMPROVEMENTS TO THE PRETREATMENT OF BONE AT OXFORD

Christopher Bronk Ramsey¹ • Thomas Higham • Angela Bowles • Robert Hedges

Oxford Radiocarbon Accelerator Unit, University of Oxford, United Kingdom.

ABSTRACT. Bone is one of the most widely used materials for dating archaeological activity. It is also relatively difficult to pretreat effectively and new methods are an area of active research. The purpose of the chemical pretreatment of bone is to remove contaminants present from burial and to do so in a way which does not add any additional laboratory contaminant. To some extent, these two aims must be balanced since, on the whole, the more complex the procedure and the more steps included, the greater the chance for contamination. At the Oxford Radiocarbon Accelerator Unit (ORAU), the method used is a continuous-flow or manual acid/base/acid (ABA) treatment followed by gelatinization and ultrafiltration (based on Brown et al. [1988]; documented in Bronk Ramsey et al. [2000]). We find this overall method is very effective at removing more recent contamination in old bones. However, two aspects of the method have recently been improved and are reported here: the redesign of ORAU's continuous flow pretreatment and a new protocol in our pretreatment ultrafiltration stage.

INTRODUCTION

Bone is one of the most complex sample materials routinely used in radiocarbon dating. The most effective method of pretreatment for accelerator mass spectrometry (AMS) dating has been a subject of continual research over more than 20 yr since the method was first used. For many samples, a simple demineralization is effective at removing the most ubiquitous contaminants. An acid/base/acid (ABA) treatment will also remove humic contaminants which can be significant in many organic rich contexts. However, these treatments leave many organic molecules from the soil and degraded protein fragments, making the sample susceptible to contamination.

Various further stages can be applied. Gelatinization (Law and Hedges 1989) concentrates the protein components, and ultrafiltration (Brown et al. 1988) selects large molecular weight proteins which are more likely to be from the original collagen present in the bone. In 2000, ORAU adopted the ultrafiltration method after detailed consultation with existing users of the method. This method in its original form was used for bone dates in the range OxA-9361 to -11851 and OxA-12214 to -12236. Tests on deliberately contaminated material showed that the method was more effective at removing contaminants, and results on known-age material were within expected limits.

The main elements of the current method are the following:

- Coarsely ground bone powder (about 0.5–1 g) is loaded into a continuous-flow cell (Figure 1);
- An automated sequence of acid, base, acid is flowed through the cell over a period of 8 hr, rinsing with ultrapure (MilliQ™) water between each reagent (in some instances a manual version of this procedure is carried out in a test tube);
- Crude collagen is gelatinized in pH3 solution at 75 °C for 20 hr;
- The gelatin solution is filtered using a 100 µm polyethylene Eezi-filter™ and the insoluble residues discarded;
- The filtered gelatin is then pipetted into an ultrafilter (Vivaspin™ 15 30kD MWCO) and centrifuged at 2500–3000 rpm until 0.5–1 mL of the >30-kD gelatin fraction remains;
- This gelatin is freeze-dried and ready for combustion in a CHN analyzer.

¹Corresponding author. Email: christopher.ramsey@archaeology-research.oxford.ac.uk.

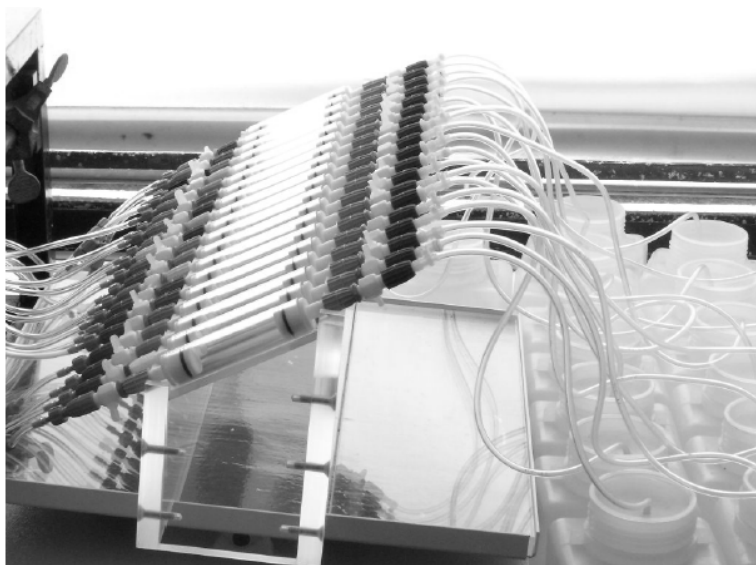


Figure 1 The continuous-flow system consists of an Ismatec IPC peristaltic pump, Omnifit™ connectors and tubing, shaking platform, glass vessels for acid/base/water, and glass flow cells. This enables semi-automated pretreatment of 20 samples of bone at once (Law and Hedges [1989] described the earlier version of what we now use).

Late in 2002, we became aware that some bone samples were giving ages which were about 100–300 yr too old in context, and this included some bone of known age. This paper describes the investigation of this problem and the means through which it was resolved.

PROBLEMS AND IMPROVEMENTS: ULTRAFILTRATION

Monitoring of the processing contamination has always been undertaken by the routine measurement of background bone samples which are believed to be beyond the range of ^{14}C . A summary of these measurements is shown in Figure 2. The data show that when we correct our bone collagen AMS measurements for known sources of contamination, there is no systematic effect with sample size, though arguably with the very oldest samples, at the lower limits of sample size, we may be underestimating our uncertainty. This is likely to be due to sample specific effects, but needs to be borne in mind in interpreting such results. There is no systematic effect with sample size, though there is slightly more variation than accounted for (about 0.1% average) and the results with yields <5 mg collagen are notably more scattered (Figure 2).

Measurements on background material do not, however, test for the presence of old contaminants in more recent samples and this was what we suspected in the case of the anomalous bone dates. We investigated possible sources of such contamination both in the original samples and in the laboratory process. Since no such systematic effect had been observed prior to the introduction of the ultrafiltration method, we suspected that the filters themselves might be responsible. The filters contain a humectant (glycerol) coated onto the regenerated cellulose filter membrane of the ultrafilters. This material is highly soluble in water and was expected to be of modern organic origin. The manufacturer's instructions are to rinse this out by centrifuging twice with ultrapure water. We had adopted the practice of centrifuging 3 times to ensure effective removal and monitoring the backgrounds as shown in Figure 2.

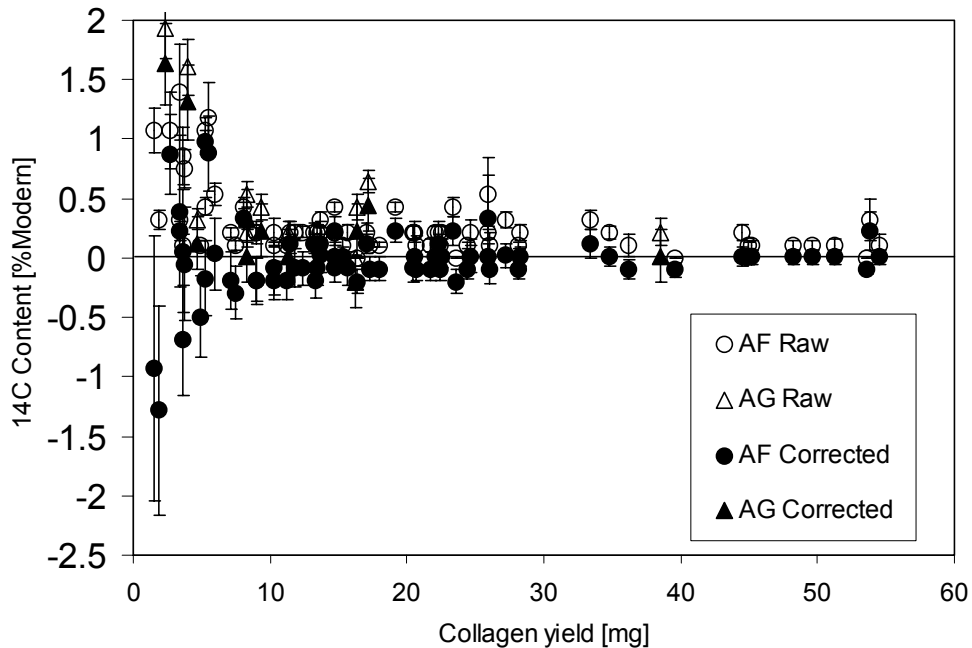


Figure 2 This figure shows a plot of ^{14}C concentration in relative percent modern as a function of collagen yield for measurements on a set of bones expected to be beyond the range of ^{14}C . Two methods have been used for these measurements: acid/base/acid and gelatinization (AG) and the same method followed by ultrafiltration (AF). Raw results are as measured on the AMS and corrected results include corrections for known sources of background. The uncertainties are plotted at 2σ and include estimates of quantified sources of background variation. Our normal cut-off for reliable measurements is 6–8 mg depending on starting weight. The scatter in pMC results for collagen yields <5 mg demonstrates the need for this acceptance threshold.

Because we suspected that the ultrafilters might be adding a fossil rather than an expected modern contaminant, we extracted and dated some glycerol from the filters and obtained a date of >35 ka BP. We devised a method for measuring the quantity of carbon remaining on the filters (most relevant in this method since the >35 kD molecular weight material remaining above the filter is pipetted off, lyophilized, and AMS dated) and in the eluent through the various phases of the ultrafilter cleaning by concentrating the glycerol onto *Chromasorb* pellets and combusting in a CHN analyzer. The results of these tests are shown in Figure 3 and were used to determine the most effective method of cleaning the ultrafilters prior to use. They show that the recommended method is clearly not sufficient, and the methods we applied to clean the filters also failed to remove all of the glycerol from the filters, despite its solubility in water. We found that 3 centrifuge rinses in ultrapure water left between approximately 20–50 $\mu\text{g C}$, which could be retained above the filter along with the retained collagen. We found that if the filters are ultrasonicated prior to centrifugation, however, there was no measurable carbon remaining after the third centrifuge (Figure 3). The quantities of carbon left above the filters using the initial cleaning method we implemented are of the right order to explain the offsets we found (see below).

By ultrasonating the filters in ultrapure water for 1 hr after the first 2 rinses, then, the glycerol is much more effectively removed. Our method for the cleaning of the filters now comprises the following:

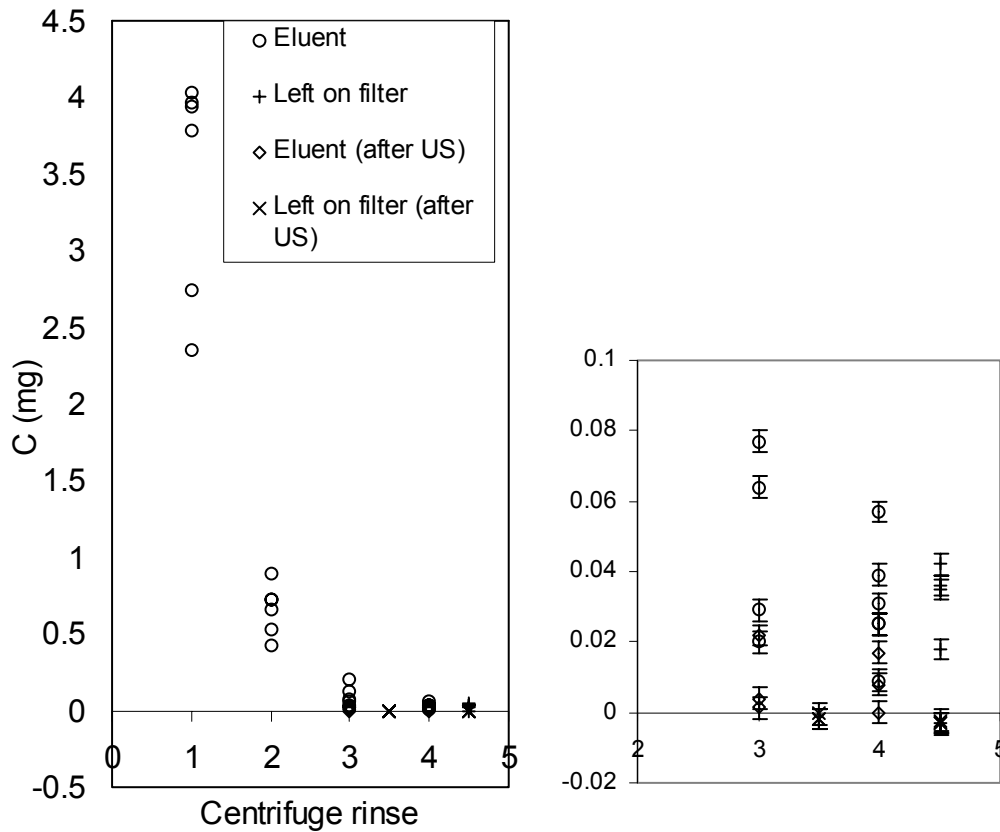


Figure 3 This figure shows the reduction in ultrafilter humectant during cleaning with centrifugation. In the cases marked “after US,” the filters have been ultrasonicated in a large volume of ultrapure water for 1 hr prior to the third centrifuge stage. In the bone pretreatment method, the eluent is discarded and the collagen above the filter is dated. The quantities remaining on the filter (that would be mixed with collagen) have been estimated by rinsing the top of the filter with ultrapure water and then concentrating this and measuring in a CHN analyzer. The figure on the right shows that 3 cleaning centrifuge rinses followed by the centrifuge of the collagen leaves about 20–50 μg C mixed with the collagen. When the filters are ultrasonicated (diamonds and crossed symbols), there is no measurable carbon remaining after the third centrifuge.

- Two centrifuge rinses in ultrapure (MilliQ™) water;
- Ultrasonication in a large volume of ultrapure water;
- One centrifuge in ultrapure water;
- A sample is taken from the top of the filter for carbon content analysis (one for each batch of filters cleaned);
- Two further centrifuges in ultrapure water.

We found that bones we redated using the new filter cleaning protocol evidenced lower C:N atomic ratios, which we correlate with the removal of a carbon-rich contaminant (Figure 4). In all cases, the original C:N ratios were well within acceptable limits (2.9–3.5 at ORAU) because the absolute proportion of contamination is very small.

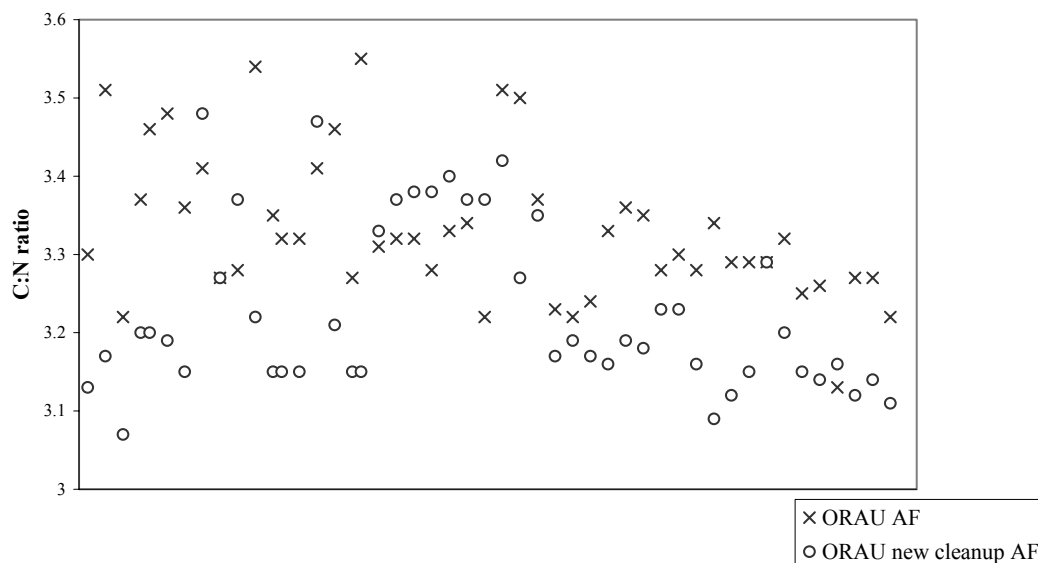


Figure 4 C:N data before and after the introduction of the new cleanup method: There is a shift in C:N ratios which occurs when original bone, dated using our ultrafiltration method, is redated using our new cleanup method for the ultrafilters. Since the humectant used in the filters has no nitrogen, the higher C:Ns in the original AF series indicate the humectant was not effectively removed.

CONTINUOUS-FLOW SYSTEM

The lower than expected yields were in some cases found to be linked to the use of the semi-automated continuous-flow system which is usually used, since the steady flow of fresh reagents is more effective at removing contaminants present in the original sample. We think that the low yields were occurring when the continuous-flow cells blocked (particularly likely in the case of fine bone powder). In these instances, the bones were subjected to the base solution for longer than intended, degrading the collagen.

We have now redesigned and constructed a new continuous-flow system. We installed an Ismatec™ IPC peristaltic pump and replaced the flowcells described in Law and Hedges (1989) with variable length (50–100 mm) preparative chromatography borosilicate glass columns fitted with Omnifit™ PTFE endpieces, caps, and viton O-rings. We use 100- μ m PTFE frits at both ends of the glass columns. We also replaced all tubing and connectors from the peristaltic pump to the glass columns and to waste, with Tygon™ tubing and Omnifit™ Peek barbed adapters (Figure 1). The glass columns sit on a shaking platform which reduces blockage and mixes reagents more effectively. This system is much less prone to blocking and eliminates leaking from the flow cells.

RESULTS

One important means of testing the reliability of a method is to monitor process blanks as described above. However, the most effective test is to make measurements on independently dated, known-age material. In the case of bone, this is not straightforward, because dietary effects and reservoir corrections account for offsets from the true age for some types of bone, particularly omnivorous species. The bones we selected are a set of pig bones recovered from the wreck of Henry VIII's flagship, the *Mary Rose*, which sank in AD 1545. Known-age bones of this sort are usually well preserved since they are usually from historic periods. *Mary Rose* bones yield routinely 130–150 mg

collagen/g, so in order to simulate low collagen yields, we have dated a series of samples using lower starting weights than usual.

The results of measurements of the Mary Rose bones are shown in Figure 5. All were measured on the new ORAU AMS, which began routine measurements in September 2002 (Bronk Ramsey et al., these proceedings). These show a very good level of agreement—certainly until the yields drop to well below 10 mg. The subset of measurements analyzed using the new filter cleaning method (denoted by AF/AF* new) shows that for collagen yields >7 mg (13 measurements), the average ^{14}C result is 321 ± 6.5 BP, with a standard deviation of 29.9 yr and an average precision of 23.7 yr [this just passes a χ^2 test ($T = 19.5$; $\chi^2_{1;0.05} = 21.0$); the combined result also passes a χ^2 test against 309 ± 4.6 BP, the INTCAL98 value for AD 1545 ($T = 2.27$; $\chi^2_{1;0.05} = 3.84$)]. None of the measurements using the original ultrafiltration cleaning method have a yield of <25 mg collagen and, notably, all of these measurements are in agreement with the expected value.

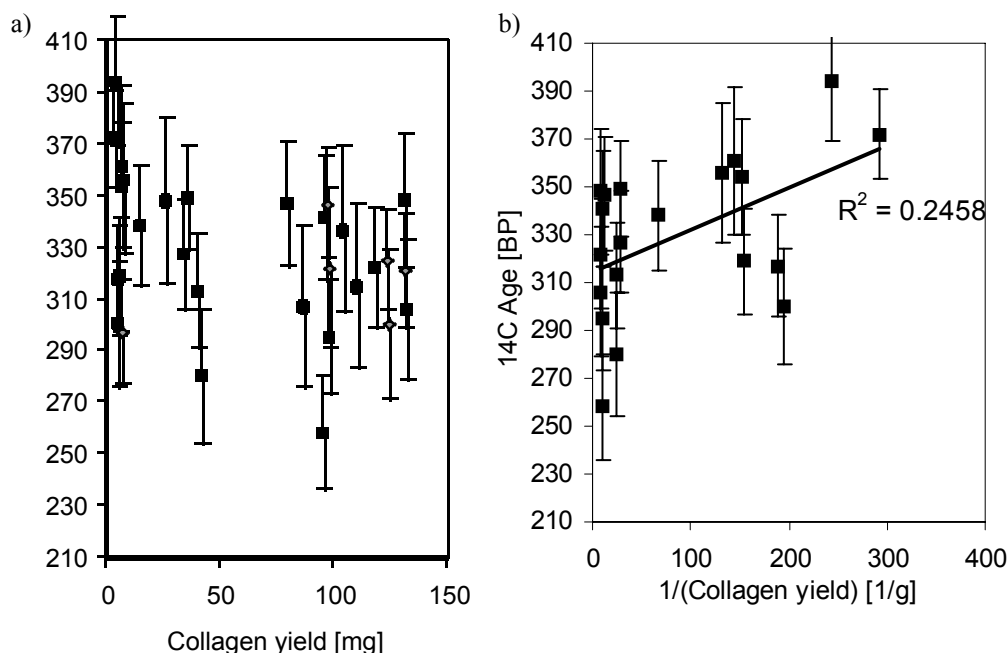


Figure 5 Results from pig bones found on the wreck of the Mary Rose (sank in AD 1545, so should be about 310 BP).
 a) All dates measured on our new AMS are shown here. AG - denotes gelatin pretreatment; AF - denotes ultrafiltration, old - with the old cleanup method and new - with the new cleanup of the ultrafilters. * - denotes solvent extraction. They are virtually indistinguishable (sigma 31, average uncertainty 27).
 b) The regression line of date versus reciprocal yield, with the intercept exactly in accord with the historical date. An increase of age with reciprocal yield suggests the possible presence of low levels of an older contaminant unrelated to bone sample size, although at a level that is not significant for the normal sample size range. The R^2 value is also low (0.2458), so we cannot be sure of the significance of the sample size effect. See main text for discussion

A linear regression of the AMS determinations versus reciprocal yield (Figure 5) for the ultrafiltration method using the new cleaning protocol indicates a small residual effect equivalent to fossil carbon contamination at the 5–10 μg level. This would produce a ^{14}C result too old by about 15–20 yr for samples with a yield of <10 mg (this encompasses a very small proportion of bone samples where the original sample is low in collagen content and poorly preserved due to post-depositional

burial conditions). It is not clear that this effect (constant amount of old carbon) is laboratory-derived, although it may well not originate from the ultrafiltration method itself. Generally speaking, the data show it to be reduced to an acceptable level for high-precision dating of bone with the normally accepted range of yields, though a bias of about 10 yr cannot be ruled out. For very low-yield bones, further research is needed before this method can be used in high-precision work.

Measurements of the Effectiveness of Ultrafiltration

Given that the ultrafiltration method involves a significant amount of technician time to ensure that the filters are effectively cleaned, one might question whether it is strictly necessary for routine, reliable dating. We have some evidence which suggests that ultrafiltration is advantageous in some instances and produces more accurate ages than less rigorous bone pretreatment methods. We redated a series of samples which were originally pretreated using the gelatinization method without ultrafiltration (ORAU code AG) and which gave anomalous ^{14}C results within their archaeological contexts. The ultrafiltered collagen samples produced AMS results in much closer agreement with other determinations. We have also tested the effect of ultrafiltration on previously determined AG pretreated samples by ultrafiltering and dating a sub-sample of collagen remaining from the original pretreatment (Table 1). The results suggest strongly that the additional ultrafiltration pretreatment does have a significant effect.

Table 1 Comparison of bone originally dated after simple gelatinization with new dates pretreated using ultrafiltration of an aliquot of the original gelatin. The changes are significant. In one case, the filtration seems to have removed a younger contaminant and in the other 3 cases has removed an older contaminant. In the case of the samples from Ecsegfalva, the results are now in better agreement with other dates from that site in related contexts and are in very good agreement with each other. Note that these results are measured using the new ultrafiltration protocol, so we are confident the differences are not because of added contaminant.

Site	Original AMS result (gelatin, AG pretreatment code)		New AMS result (ultrafiltered gelatin, AF pretreatment code)	
German Upper-Paleolithic	OxA-11964	23,990 ± 180	OxA-12057	25,050 ± 320
Ecsegfalva	OxA-9329	6950 ± 45	OxA-X-2040-09	6780 ± 45
Ecsegfalva	OxA-9327	6870 ± 50	OxA-X-2040-07	6787 ± 37
Ecsegfalva	OxA-9526	6915 ± 50	OxA-X-2040-08	6775 ± 37

More evidence is provided when we consider AMS determinations we obtained on a series of mammoth bones, performed in an inter-laboratory comparison with a conventional ^{14}C laboratory which used a modified Longin pretreatment method (Table 2). This shows that, particularly for older dates, the ultrafiltration method provides an improved removal of contaminants in the dated bones as evidenced by the older results. The implication of this is that, even for younger bones, if high levels of precision are required, ultrafiltration enables us to make a more reliable measurement on the uncontaminated collagen. To put this in context, the average offsets shown in Table 2, if due to modern contamination, would result in age offsets of about 1% (e.g. 40 ^{14}C yr at 4000 BP) for samples less than 1 half-life old. In many instances, particularly for recent, well-preserved bone, there is little doubt that the contaminants present are probably sufficiently close in age to the original material that even the simplest pretreatment methods will provide accurate ^{14}C results.

Table 2 A comparison of ultrafiltered ORAU ^{14}C determinations (original method) on mammoth bone compared with those obtained at an anonymous conventional laboratory using a more standard bone pretreatment method. The differences are in some cases greater than 1000 yr, far larger than any offsets seen from addition of humectant, and in these cases the bones give high yields and are relatively old, so the differences must arise from the removal of contaminant by the ultrafiltration.

Conventional laboratory ^{14}C age BP (using modified Longin method)	Ultrafiltered gelatin AMS ^{14}C age (ORAU)		Collagen yield (mg) (ORAU)
12,500 \pm 50	OxA-11840	13,180 \pm 60	76.1
13,200 \pm 100	OxA-11749	14,165 \pm 65	10.7
17,450 \pm 100	OxA-11842	17,740 \pm 90	170.0
28,600 \pm 600	OxA-11813	30,420 \pm 250	17.0
42,600 \pm 1000	OxA-11747	45,200 \pm 800	37.0
23,800 \pm 400	OxA-11746	23,560 \pm 140	21.8
35,600 \pm 400	OxA-11748	36,610 \pm 360	39.8

CONCLUSIONS

The data presented in this paper suggest that the ultrafiltration method as originally devised (Brown et al. 1988) and implemented at ORAU (documented in Bronk Ramsey et al. 2000) was a considerable advance in terms of removing environmental contamination and was the best method available for older bones. When isolating collagen with low mass yields and recent ages, however, significant bias to older ^{14}C ages has been shown to arise and, in these cases, the results are usually less accurate than when a simpler method is used, because environmental contamination is less of an issue with these samples.

We contacted the submitters of samples with low collagen yields when we had identified the relationship between low pretreatment yield and older than expected AMS determinations. We are in the process of repeating measurements where spare or replacement bone could be obtained and we withdrew some of the original determinations that could not be repeated. We also offered recalculated ^{14}C ages to some submitters based upon the collagen pretreatment yield and the proportion of admixed humectant carbon derived from the ultrafilters. These recalculations (given an OxA-X lab code which indicates a non-standard date calculation) will only give an indication of the scale of the effect given the variability we have subsequently seen. In a few cases, the repeated measurements even on low-yield samples were unchanged; in other cases, there were changes consistent with the effects identified through our experimental data, although the exact scale of the offsets seems to be variable and sometimes larger than expected. One such significantly affected example is shown in Figure 6. This demonstrates the age shifts between the initial series affected by ultrafiltration humectants and the redated series, which ought to have a “true age” of AD 873/4 or 1190–1205 BP. When our current re-measurement program is finished, we should be in a better position to estimate the effect on intermediate collagen yield samples, but at present it looks as if the effect could average of the order of a hundred years until collagen yields rise above about 40 mg.

The key improvements to the new protocol at Oxford are in the preparation of the ultrafilters used in the final stage of the pretreatment and in the design of the continuous-flow system used for isolating bone collagen. The method has been shown to be effective both in providing good reproducibility and accuracy on recent known-age material and in removing environmental contaminants. We have also introduced regular process tests to identify contaminants from single batches of ultrafilters prior to routine use, and implemented QA checks on known-age recent bones over a range of sizes to test for any other similar effects.

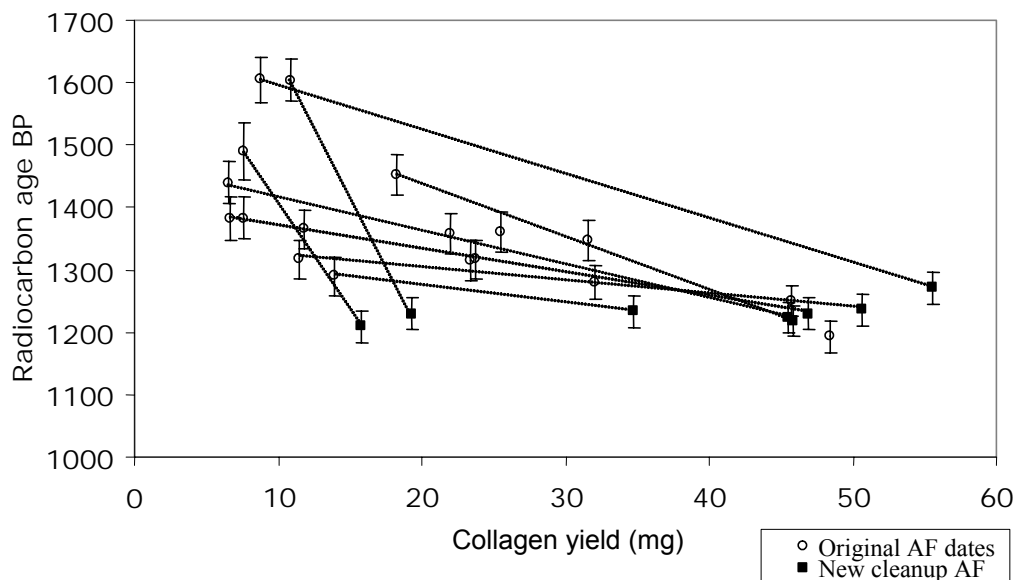


Figure 6 The Repton Viking Army site (Derbyshire, England), historically dated to AD 873/4 (1190–1205 BP). The initial humectant-affected dates are shown in open circles. The black squares are later determinations obtained with the new filter cleanup procedure. Even in this fairly severely affected batch, the higher yield dates are clearly closer to the true values.

During this research, we also conducted tests on other filter types used in ^{14}C dating and although we found that some gave no measurable additions (e.g. the Eezi-filter™ we use for removing particulate contaminants), others did have extractable carbon, although only ultrafilters had levels as high as those reported here. As ^{14}C sample requirements for AMS become smaller, this is something all ^{14}C labs will need to be aware of, and monitor.

ACKNOWLEDGEMENTS

The staff of ORAU are thanked for their involvement in all aspects of this work. We would also particularly like to thank Alex Bayliss and Peter Marshall at English Heritage for bringing this issue to our attention as well as English Heritage and NERC for funding. We are grateful to Dr A J Stuart (UCL), Professor M Biddle and B Kjolbye-Biddle (Oxford), Dr J Grunberg (Landesmuseum für Vorgeschichte, Halle), and Professor A Whittle (University of Wales, Cardiff) for permission to publish data associated with their projects. We thank Dr Margaret Rule and Mr Andrew Elkerton (Mary Rose Trust) for providing the pig bones from the Mary Rose.

REFERENCES

- Bronk Ramsey C, Higham TFG, Leach P. 2004. Towards high-precision AMS: progress and limitations. *Radiocarbon*, these proceedings.
- Bronk Ramsey C, Pettiit PB, Hedges REM, Hodgins GWL, Owen DC. 2000. Radiocarbon dates from the Oxford AMS system: Archaeometry datelist 30. *Archaeometry* 42(2):459–79.
- Brown TA, Nelson DE, Vogel JS, Southon JR. 1988. Improved collagen extraction by modified Longin method. *Radiocarbon* 30(2):171–7.
- Law IA, Hedges REM. 1989. A semi-automated bone pretreatment system and the pretreatment of older and contaminated samples. *Radiocarbon* 31(3):247–53.

MAGNESIUM PERCHLORATE AS AN ALTERNATIVE WATER TRAP IN AMS GRAPHITE SAMPLE PREPARATION: A REPORT ON SAMPLE PREPARATION AT KCCAMS AT THE UNIVERSITY OF CALIFORNIA, IRVINE

G M Santos^{1,2} • J R Southon¹ • K C Druffel-Rodriguez^{1,3} • S Griffin¹ • M Mazon^{1,4}

ABSTRACT. We present a brief discussion of sample preparation procedures at the Keck Carbon Cycle Accelerator Mass Spectrometer (KCCAMS), University of California, Irvine, and a systematic investigation of the use of $\text{Mg}(\text{ClO}_4)_2$ as an absorptive water trap, replacing the standard dry ice/ethanol cold finger in graphite sample preparation. We compare high-precision AMS measurement results from oxalic acid I and USGS coal samples using $\text{Mg}(\text{ClO}_4)_2$ under different conditions. The results obtained were also compared with those achieved using the conventional water removal technique. Final results demonstrate that the use of $\text{Mg}(\text{ClO}_4)_2$ as an alternative water trap seems very convenient and reliable, provided the $\text{Mg}(\text{ClO}_4)_2$ is replaced frequently.

THE KCCAMS PREP LABORATORY

A new sample processing laboratory was constructed and installed at the Keck Carbon Cycle Accelerator Mass Spectrometer (KCCAMS) facility in late 2002 to expand existing University of California, Irvine (UCI) radiocarbon sample handling capabilities. The KCCAMS prep laboratory has provided approximately 1500 unknown samples and quality control standards during the first 10 months of operation.

The prep laboratory is equipped for routine chemical sample cleaning and preparation of organic samples and carbonates. It also contains a sample-combustion system, 2 graphitization lines, and an accelerator target pressing station. The combustion line has 10 pump-out heads, while each graphitization line has 12 H_2/Fe reactors (Figure 1a, b), allowing us to graphitize 48 organic or carbonate samples per day. The vacuum lines are made of glass and stainless steel and are pumped by turbo-molecular pumps backed by oil-free diaphragm pumps. Water is removed during graphitization either by using magnesium perchlorate— $\text{Mg}(\text{ClO}_4)_2$ —in the graphite-reactor, or by cold fingers attached to stainless steel thermoses converted to dry ice/alcohol dewars. The progress of the reaction is monitored using pressure transducers (Figure 1b). The design was based on sample graphitization lines from CAMS/Lawrence Livermore National Laboratory (LLNL).

SAMPLE PREPARATION PROCEDURES

Submitted samples from carbonaceous raw materials are chemically and/or physically pretreated, when necessary, to remove any unwanted material before conversion to carbon dioxide by combustion or acid hydrolysis. Organic samples are pretreated initially by removal of any visually obvious contamination, followed by a standard acid-alkaline-acid treatment. Carbonate samples are leached in dilute HCl. Sample are then rinsed twice with MilliQ water and dried on a heating block at 80 °C.

Carbon dioxide is produced from pre-leached carbonates by acid hydrolysis using 85% phosphoric acid in disposable septum-sealed reactors (Vacutainer blood collection vials, 3 ml) (Figure 2a, b). Carbonates are weighed into the Vacutainers and evacuated using a 1.3-cm-long #26 hypodermic Luer-tip needle adapted to an Ultra-torr fitting in the graphitization line (Figure 2b). Once the Vacu-

¹Earth System Science, University of California, Irvine, B321 Croul Hall, Irvine, California 92697-3100, USA.

²Corresponding author. Email: gdossant@uci.edu.

³Department of Chemistry, Loyola Marymount University, Seaver Hall, Los Angeles, California, USA.

⁴Department of Biology, California State University, Fullerton, California, USA.

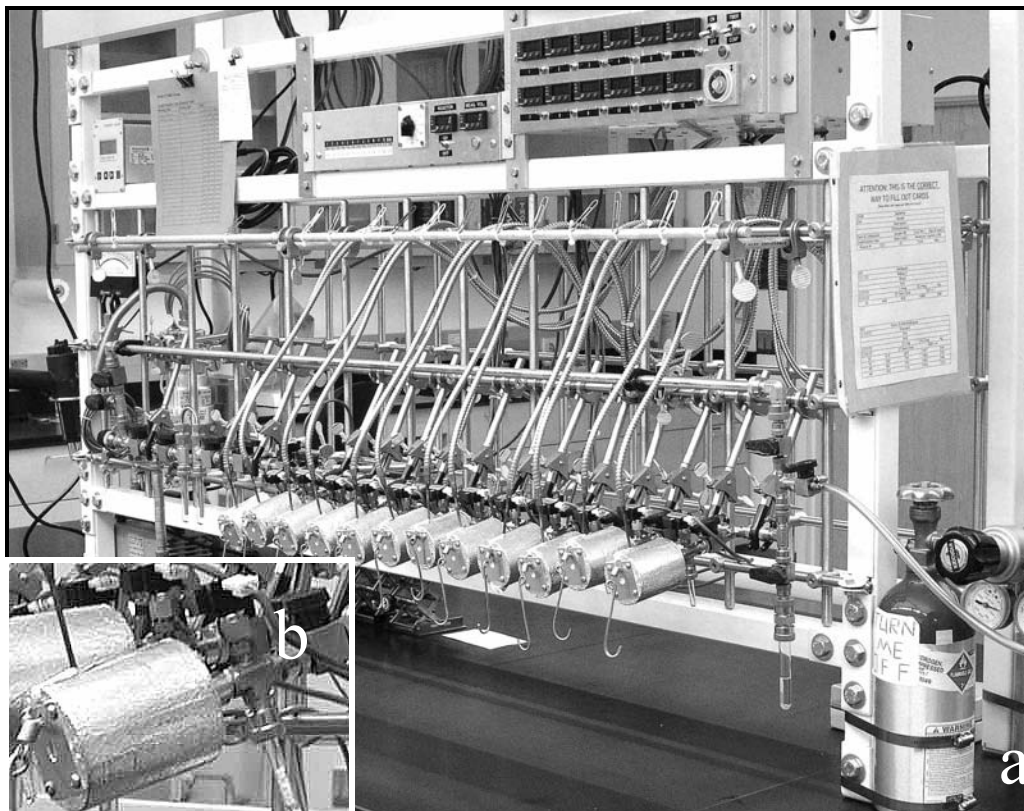


Figure 1 a) Graphitization line for target preparation showing H₂/Fe reduction reactors. Each 12-head graphitization line can produce 24 samples per day. The design is based on graphitization lines from the CAMS/LLNL laboratory. b) Reduction reactor detail showing Mg(ClO₄)₂ in the graphite-reactor.

tainers are evacuated, we detach the vial from the line and use a gas-tight Luer-lock syringe with a #26 needle to introduce 1 cc of 85% phosphoric acid (Figure 2a). The Vacutainer reactors are then placed on heating-blocks at 80 °C for at least 20 min. When the reaction ceases, they are returned to the graphitization line to extract the CO₂ via the needle fitting. To ensure complete evacuation of the needle fitting prior to CO₂ extraction, the needle is initially inserted halfway through the Vacutainer septum. The CO₂ is cryogenically purified and reduced to graphite in pyrex 6 × 50 mm culture tubes (Loyd et al. 1991), using hydrogen at 650 °C for 3–4 hr over pre-baked iron. Since the Vacutainer vials are disposable, cleaning and waste handling after sample preparation are minimized.

The carbon dioxide production of organic samples is performed by combustion at 900 °C in evacuated sealed quartz tubes in the presence of CuO and silver wire. After CO₂ extraction and purification, CO₂ is then reduced to graphite as described above.

Samples prepared on these lines have demonstrated 56 ka and 54 ka BP backgrounds for organic and carbonate materials, respectively, for samples containing 1 mg of carbon (Southon et al., these proceedings).

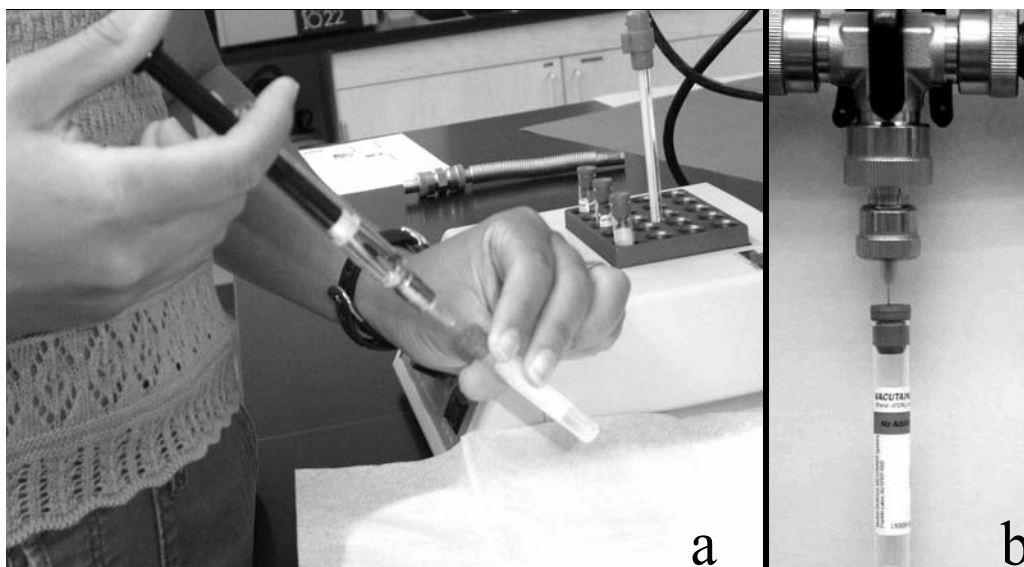


Figure 2 Acid hydrolysis procedure for carbonate sample. (a) 1cc of 85% phosphoric acid being introduced into septum-sealed reactors (Vacutainer vials). (b) Detail of Vacutainer attached to the graphitization line for evacuation. The base of a #26 hypodermic needle is placed in an Ultra-torr fitting, between the Ultra-torr ferrule and the sealing o-ring.

Use of Magnesium Perchlorate for Water Removal

Magnesium perchlorate is a well-known hygroscopic substance that has been used worldwide in the desiccant columns of stable isotope mass spectrometers. For more than 10 yr, $Mg(ClO_4)_2$ has been used to trap water during hydrogen reduction for graphite sample preparation at the UCI labs (S Zheng, personal communication).

At that time, UCI graphite was being measured at the LLNL AMS facility, where precision was initially 0.6% (J Southon, personal communication). These first investigations of the use of the substance in the graphitization process demonstrated its suitability, and 3 main advantages were immediately apparent: a) it is a very easy material to handle, allowing the user to replace it easily in the graphite-reactor in a very short period of time; b) it removes the need to prepare dry ice/ethanol slushes for each individual graphite-reactor, which can be time consuming; and c) the $Mg(ClO_4)_2$ water-trap could be re-used many times (also providing more time saving) without compromising the final measurement precision, as was demonstrated by multiple measurements of standards (S Trumbore, personal communication).

In 2002, UCI installed a compact AMS from the National Electrostatics Corporation (0.5MV 1.5SDH-1 AMS system). AMS ^{14}C precision for measurements performed with this system is currently between 0.2 to 0.5%, based on multiple measurements of oxalic acid-I (OX-I) for hydrogen reduced graphite using Fe or Co catalyst (Southon et al., these proceedings). Accuracy is being evaluated on measurement results of secondary standards, such as oxalic acid-II (OX-II) and ANU sucrose (ANU), where 4‰ fluctuations can be observed.

Since ^{14}C measurement precision has varied and some of the variation may be due to isotopic fractionation during sample preparation, we decided to perform a systematic comparison of the use of cryogenic mixtures or absorption in $Mg(ClO_4)_2$ to remove water during the graphitization reaction. Unusual variations on background samples beyond 50 ka also indicated a possible memory

or contamination effect from the $\text{Mg}(\text{ClO}_4)_2$ (or water trapped in the perchlorate), which was typically being used for 10 to 15 graphitizations before replacement based on absorptive saturation of the substance.

EXPERIMENT AND RESULTS

In the first experiment, 4 independently combusted samples of USGS coal and 4 of oxalic acid I (OX-I) were generated, each with enough material to be split into 3 aliquots. The CO_2 from each sample was purified and shared equally among 3 graphite-reactors operated under different conditions, generating the graphite-aliquots 981.1, 981.2, and 981.3, for example. We compare the effects of saturated and unsaturated $\text{Mg}(\text{ClO}_4)_2$, and pumping on the graphite-reactors for different periods of time before use (6 times previously used perchlorate and 90 min pumping time—group 1; 6 times previously used and 10 min pumping time—group 2; and wet perchlorate and 10 min pumping time—group 3). A set of 12 OX-I samples and 12 coal samples were graphitized and measured by AMS.

In the second experiment, 3 independently combusted samples of USGS coal and 3 samples of OX-I were generated, each with enough material to be split into 4 aliquots. The CO_2 from each sample was purified and shared equally among 4 graphite-reactors. In this case, we compared the use of cryogenic mixtures (group A), fresh perchlorate (group B), and previously used dry (group C) and wet (group D) perchlorate, for water removal. A set of 12 OX-I samples and 12 coal samples were graphitized and measured by AMS.

In the third experiment, we repeat the same conditions applied to the second experiment (Table 1) for the OX-I samples, but using $\text{Mg}(\text{ClO}_4)_2$ that had been previously used 8 times. We also pumped the graphite-reactor (i.e. on the perchlorate) for a longer period of time (60 min). A set of 12 OX-I samples were graphitized and measured by AMS.

Table 1 Summary of the water removal conditions in the graphitization reactor for the 3 experiments.

<p>First group 1—$\text{Mg}(\text{ClO}_4)_2$ used 6 times previously; reactor was pumped for 90 min group 2—$\text{Mg}(\text{ClO}_4)_2$ used 6 times previously; reactor was pumped for 10 min group 3—$\text{Mg}(\text{ClO}_4)_2$ used 6 times previously and exposed to MQ water vapor; reactor was pumped for 10 min</p> <p>Second group A—Dry ice and ethyl alcohol cold finger; reactor was pumped for 20 min group B—Fresh $\text{Mg}(\text{ClO}_4)_2$; reactor was pumped for 20 min group C—$\text{Mg}(\text{ClO}_4)_2$ used 2 times previously; reactor was pumped for 20 min group D—$\text{Mg}(\text{ClO}_4)_2$ used 2 times previously and exposed to MQ water vapor; reactor was pumped for 20 min</p> <p>Third group I—Dry ice and ethyl alcohol cold finger; reactor was pumped for 60 min group II—Fresh $\text{Mg}(\text{ClO}_4)_2$; reactor was pumped for 60 min group III—$\text{Mg}(\text{ClO}_4)_2$ used 8 times previously; reactor was pumped for 60 min group IV—$\text{Mg}(\text{ClO}_4)_2$ used 8 times previously and exposed to MQ water vapor; reactor was pumped for 60 min</p>

Water removal and pumping conditions from the graphite-reactors from the 3 experiments were designated as groups, and they are summarized on Table 1. AMS results from the 3 experiments are present in Tables 2, 3, and 4, respectively. All results were normalized to an independent set of OX-I samples prepared using fresh perchlorate.

DISCUSSION

From the first experiment (Table 2), we noticed that all of the $\Delta^{14}\text{C}$ data from the OX-I “unknown” samples were lower than those of the normalizing standards prepared with fresh perchlorate ($\Delta^{14}\text{C} = 33.2 \pm 2.2\text{‰}$). The difference could not be explained. It was clearly not a fractionation effect since the Fraction Modern and $\Delta^{14}\text{C}$ values in Table 2 have already been corrected for any graphitization or machine-induced isotopic fractionation (Pearson et al. 1998), using the on-line $\delta^{13}\text{C}$ values. The differences were too large to be accounted for by memory from the 6 samples (all close to Modern) run previously in each reactor.

In the second and third experiment, there were no significant differences between the AMS ^{14}C results for OX-I samples prepared using different water removal treatments and the normalizing standards prepared with fresh Mg(ClO₄)₂ (Tables 3 and 4; Figure 3). At the level of precision of these tests, 3.8 and 3.3‰, respectively, twice or 8 times previously used Mg(ClO₄)₂ appears to have no effect on $\Delta^{14}\text{C}$. However, a larger spread in the results can be noticed when Mg(ClO₄)₂ was completely wet.

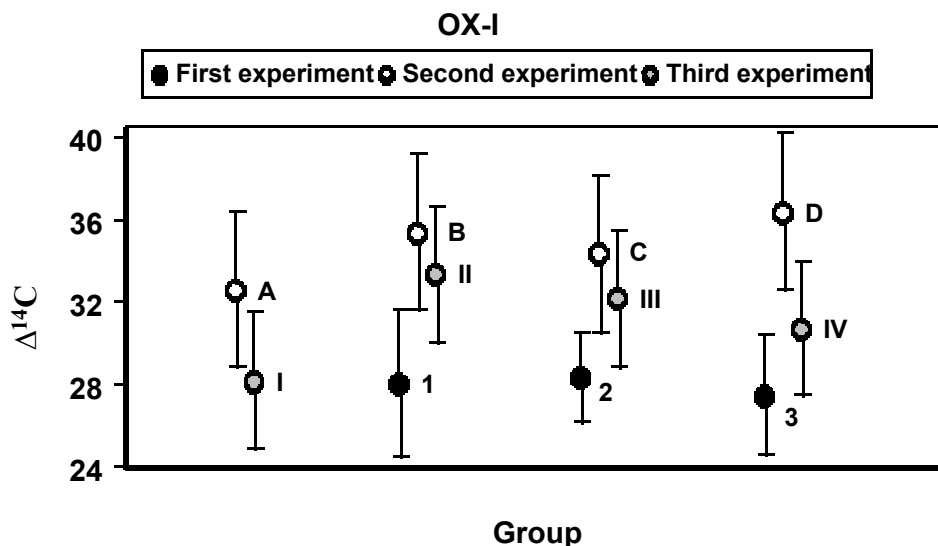


Figure 3 $\Delta^{14}\text{C}$ average and uncertainties of OX-I samples from the 3 experiments. Errors plotted represent the 1σ scatter in the results from each group, or the statistical precision, whichever is greater. Groups of samples are shifted to better show the error bars.

In Table 3, we also compare AMS $\delta^{13}\text{C}$ measurements with $\delta^{13}\text{C}$ obtained on an Elemental Analyzer (EA) coupled with an IRMS from graphite produced in the second experiment. The EA $\delta^{13}\text{C}$ results from aliquots of the graphite produced showed that there was no isotopic fractionation during graphitization (Table 3). However, machine-induced isotopic fractionation effects are clear on this second experiment.

For the background samples (USGS coals), the experiments seem more conclusive. We believe that the CO₂ samples have been contaminated by modern CO₂ trapped in water in the perchlorate (or in the perchlorate itself) since the 4 different CO₂ samples all show backgrounds improving as Mg(ClO₄)₂ wetness decreases and/or longer pumping time was applied (Figure 4). Note that none of these USGS coal samples are as good as the 54.3 ± 0.6 ka (background processed graphite) obtained with fresh perchlorate in the first experiment, for reasons which are unexplained.

Table 2 Results of OX-I and coal samples considered as unknowns. These results were normalized to an independent set of 8 OX-I samples prepared using fresh perchlorate. Measurement precision was 2.2‰ on the 8 OX-I samples and 2.2–4.0‰ on OX-II and ANU secondary standards. AMS system background on synthetic graphite was 59.2 ± 0.5 ka. The graphitization line background obtained on USGS coals prepared with fresh perchlorate was 54.3 ± 0.6 ka. Coal samples were not background corrected. AMS ^{13}C was measured on-line using offset Faraday cups after the HE analyzing magnet of the spectrometer.

OX-I samples									
UCI AMS#	Sample (lab nr)	AMS $\delta^{13}\text{C}$	Ext. err.	Fraction modern	\pm	$\Delta^{14}\text{C}$	\pm	Average	STDEV
Group 1									
3479	UCIG_981.1	-17.1	0.4	1.0312	0.0019	24.6	1.9	28.1	3.6
3480	UCIG_982.1	-15.9	0.2	1.0319	0.0020	25.3	2.0		
3481	UCIG_983.1	-16.2	0.3	1.0380	0.0024	31.4	2.4		
3482	UCIG_984.1	-16.0	0.3	1.0375	0.0019	30.9	1.9		
Group 2									
3484	UCIG_981.2	-16.7	0.2	1.0343	0.0022	27.7	2.2	28.3	1.4
3485	UCIG_982.2	-19.5	0.5	1.0367	0.0020	30.1	2.0		
3486	UCIG_983.2	-16.7	0.2	1.0353	0.0022	28.7	2.2		
3487	UCIG_984.2	-18.6	0.4	1.0335	0.0020	26.9	2.0		
Group 3									
3489	UCIG_981.3	-18.3	0.2	1.0343	0.0025	27.7	2.5	27.5	2.9
3490	UCIG_982.3	-18.3	0.3	1.0376	0.0020	30.9	2.0		
3491	UCIG_983.3	-18.2	0.3	1.0306	0.0020	24.0	2.0		
3492	UCIG_984.3	-18.4	0.3	1.0339	0.0019	27.3	1.9		
USGS coal samples									
UCI AMS#	Sample (lab nr)	AMS $\delta^{13}\text{C}$	Ext. err.	Fraction modern	\pm	Age	\pm	Average	STDEV
Group 1									
3494	UCIG_855.1	-24.0	0.3	0.0013	0.0001	53,360	410	52,010	1905
3495	UCIG_856.1	-23.2	0.3	0.0015	0.0001	52,280	310		
3496	UCIG_857.1	-22.7	0.1	0.0022	0.0001	49,240	230		
3497	UCIG_858.1	-24.4	0.3	0.0013	0.0001	53,160	460		
Group 2									
3499	UCIG_855.2	-23.0	0.3	0.0015	0.0001	52,340	290	50,893	1512
3500	UCIG_856.2	-23.3	0.3	0.0017	0.0001	51,100	330		
3501	UCIG_857.2	-23.6	0.2	0.0023	0.0001	48,770	250		
3502	UCIG_858.2	-23.8	0.3	0.0017	0.0001	51,360	250		
Group 3									
3504	UCIG_855.3	-24.2	0.3	0.0030	0.0002	46,640	410	48,273	1969
3505	UCIG_856.3	-24.1	0.3	0.0027	0.0001	47,420	310		
3506	UCIG_857.3	-24.0	0.6	0.0026	0.0002	47,910	580		
3507	UCIG_858.3	-22.7	0.2	0.0017	0.0001	51,120	500		

Table 3 Results of OX-I and coal samples considered as unknowns. These results were normalized to an independent set of 9 OX-I samples prepared using fresh perchlorate. Measurement precision was 3.8‰ on the OX-I's and 5.0‰ on OX-II secondary standards. The graphitization line background obtained on USGS coals prepared with fresh perchlorate was 52.1 ± 0.6 ka. Coal samples were not background corrected. EA/IRMS ¹³C's are measured on graphite aliquots using a Fisons NC 1500 Elemental Analyzer coupled to a Finnigan Delta Plus stable isotope ratio mass spectrometer. AMS ¹³C's are measured on-line using offset Faraday cups after the HE analyzing magnet of the spectrometer.

OX-I samples											
UCI AMS#	Sample (lab nr)	EA-IRMS $\delta^{13}\text{C}$	AMS $\delta^{13}\text{C}$	Ext. err.	Fraction modern	Age	\pm	$\Delta^{14}\text{C}$	\pm	Average	STDEV
Group A											
3777	UCIG_1136.1	-19.1	-21.7	2.4	1.0378	0.0046	31.1	4.6	32.6	2.0	
3779	UCIG_1138.1	-19.5	-19.0	2.2	1.0415	0.0033	34.8	3.3			
Group B											
3781	UCIG_1136.2	-19.9	-25.3	3.7	1.0445	0.0055	37.8	5.5	35.4	2.4	
3782	UCIG_1137.2	-19.3	-18.9	1.8	1.0397	0.0042	33.1	4.2			
3783	UCIG_1138.2	-19.8	-19.8	0.9	1.0419	0.0025	35.3	2.5			
Group C											
3785	UCIG_1136.3	-20.5	-19.7	1.1	1.0405	0.0026	33.8	2.6	34.3	0.8	
3786	UCIG_1137.3	-19.8	-19.7	0.7	1.0419	0.0024	35.2	2.4			
3787	UCIG_1138.3	-18.8	-20.8	0.7	1.0406	0.0030	34.0	3.0			
Group D											
3789	UCIG_1136.4	-19.6	-20.9	1.8	1.0409	0.0030	34.3	3.0	36.4	2.9	
3790	UCIG_1137.4	-20.1	-21.0	1.8	1.0417	0.0033	35.1	3.3			
3791	UCIG_1138.4	-19.6	-23.3	1.4	1.0464	0.0027	39.7	2.7			
USGS coal samples											
UCI AMS#	Sample (lab nr)	AMS $\delta^{13}\text{C}$	Ext. Err.	Fraction modern	Age	\pm	Average	STDEV			
Group A											
3793	UCIG_1157.1	-31.9	1.7	0.0019	0.0001	50,210	390	50,367	630		
3795	UCIG_1159.1	-26.2	1.6	0.0020	0.0001	49,830	360				
Group B											
3796	UCIG_1157.2	-28.3	1.2	0.0019	0.0001	50,270	280	50,457	180		
3797	UCIG_1158.2	-28.3	2.7	0.0019	0.0001	50,470	320				
3798	UCIG_1159.2	-25.0	1.3	0.0018	0.0001	50,630	290				
Group C											
3799	UCIG_1157.3	-27.0	2.2	0.0020	0.0001	50,020	400	49,827	729		
3800	UCIG_1158.3	-27.0	2.0	0.0019	0.0001	50,440	480				
3801	UCIG_1159.3	-26.3	1.9	0.0022	0.0001	49,020	210				
Group D											
3802	UCIG_1157.4	-25.9	3.3	0.0029	0.0001	46,840	280	46,850	1535		
3803	UCIG_1158.4	-27.0	2.3	0.0024	0.0001	48,390	300				
3804	UCIG_1159.4	-24.4	1.4	0.0035	0.0001	45,320	190				

Table 4 Results of OX-I samples considered as unknowns. These results were normalized to an independent set of 7 OX-I samples prepared using fresh perchlorate. Measurement precision was 3.3‰ on the OX-I samples and ANU secondary standards. The graphitization line background obtained on USGS coals prepared with fresh perchlorate was 49.8 ± 1.4 ka. Coal samples were not background corrected.

OX-I samples									
UCI AMS#	Sample (lab nr)	AMS $\delta^{13}\text{C}$	Ext. err.	Fraction modern	\pm	$\Delta^{14}\text{C}$	\pm	Average	STDEV
Group 1									
4329	UCIG_1483.1	-22.7	0.4	1.0338	0.0024	27.2	2.4	28.2	2.5
4330	UCIG_1484.1	-20.3	0.3	1.0329	0.0024	26.3	2.4		
4331	UCIG_1485.1	-17.9	0.4	1.0376	0.0024	31.0	2.4		
Group 2									
4332	UCIG_1483.2	-18.3	0.4	1.0438	0.0024	37.1	2.4	33.4	3.2
4333	UCIG_1484.2	-15.2	0.2	1.0382	0.0024	31.6	2.4		
4334	UCIG_1485.2	-18.2	0.4	1.0381	0.0028	31.4	2.8		
Group 3									
4337	UCIG_1483.3	-17.9	0.3	1.0385	0.0024	31.9	2.4	32.2	0.3
4338	UCIG_1484.3	-17.6	0.3	1.0389	0.0028	32.3	2.8		
4339	UCIG_1485.3	-19.2	0.4	1.0391	0.0036	32.4	3.6		
Group 4									
4340	UCIG_1483.4	-20.1	0.4	1.0380	0.0024	31.4	2.4	30.7	1.1
4341	UCIG_1484.4	-20.4	0.3	1.0379	0.0025	31.3	2.5		
4342	UCIG_1485.4	-18.6	0.4	1.0360	0.0034	29.4	3.4		

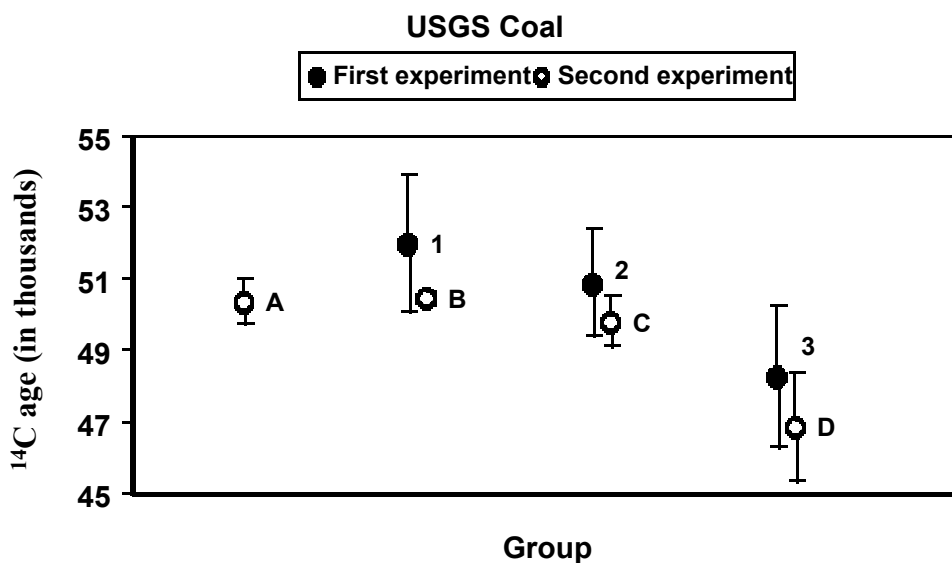


Figure 4 ^{14}C age averages for coal samples and respective errors from the 3 experiments. Errors plotted represent the 1σ scatter in the results from each group. Groups of samples are shifted to better show the error bars.

Overall, backgrounds were not as good at the time of the second experiment (e.g. compare the graphitization line backgrounds for the first and second tests cited in the table captions). Under these conditions, we saw no significant differences between results for coals graphitized using cryogenic mixtures (group A) or fresh mixtures (group B), and only minimal contamination for the twice previously used Mg(ClO₄)₂ (group C). On the other hand, a large background increase was observed for group D, as for group 3 in the first experiment, where the Mg(ClO₄)₂ was wet.

These experiments had induced us to use the Mg(ClO₄)₂ during graphitization only 3 times before replacement. Overall precision has decreased over a period of several months from a range of 0.2–0.5% to 0.2–0.3%. This improvement may not be due to changing the way we use the perchlorate, but it does demonstrate that the use of perchlorate is compatible with high precision. Backgrounds also improved and are frequently as old as 53 ka.

CONCLUSION

For ¹⁴C measurements that do not require precision better than 0.3% or backgrounds better than 53 ka, the use of Mg(ClO₄)₂ as an alternative water trap seems very convenient and reliable provided the Mg(ClO₄)₂ is replaced frequently. Variations in Δ¹⁴C are not significant when comparing dry-fresh Mg(ClO₄)₂ with standard dry ice/ethanol cold fingers.

For measurements requiring better precision (<0.2%) and/or backgrounds (>53 ka), the Mg(ClO₄)₂ should be treated with some suspicion. In such cases, cryogenic mixtures or thermoelectric cooling may be preferable solutions for removing water during the graphitization reaction. As yet, we have no direct evidence to show exactly what mechanism causes the Δ¹⁴C shifts. However, it seems that the moisture content of the Mg(ClO₄)₂ is important and we suspect that trapping of CO₂ in wet perchlorate plays a part.

ACKNOWLEDGEMENTS

We thank the W M Keck Foundation and the Dean of Physical Sciences and Vice Chancellor for Research, UCI, for financial support. Special thanks to Shuhui Zheng (pioneer in the use of Mg(ClO₄)₂ on hydrogen reduction graphite sample preparation) and Susan E Trumbore for valuable discussions. We owe special thanks to Christine Prior for her comments on the manuscript.

REFERENCES

- Loyd DH, Vogel JS, Trumbore S. 1991. Lithium contamination in AMS measurement of ¹⁴C. *Radiocarbon* 33(3):297–301.
- Pearson A, McNichol AP, Schneider RJ, von Reden KF, Zheng Y. 1998. Microscale AMS ¹⁴C measurement at NOSAMS. *Radiocarbon* 40(1):61–75.
- Southon JR, Santos GM, Druffel-Rodriguez K, Druffel E, Trumbore SE, Xu X, Griffin S, Ali S, Mazon M. The Keck Carbon Cycle AMS Laboratory, University of California, Irvine: initial operation and a background surprise. *Radiocarbon*, these proceedings.

RADIOCARBON DATING OF IRON ARTIFACTS AT THE ERLANGEN AMS FACILITY

Andreas Scharf^{1,2} • Wolfgang Kretschmer¹ • Gerhard Morgenroth¹ • Thomas Uhl¹ • Karin Kritzer¹ • Katja Hunger^{3,4} • Ernst Pernicka^{2,5}

ABSTRACT. One problem in preparing iron for radiocarbon dating is the low carbon content which makes the sample size needed too large for some sample combustion systems. Also, the metallic character of the samples complicates sample combustion or oxidation. The Erlangen accelerator mass spectrometry group uses an elemental analyzer for the sample combustion, directly followed by a reduction facility. As the carbon content and sample size for iron samples are unsuitable for combustion in an elemental analyzer, 2 alternative approaches are to (a) avoid oxidation and reduction, or (b) extract the carbon from the iron, prior to combustion. Therefore, 2 different pathways were explored. One is direct sputtering of the unprocessed iron sample in the ion source. The other is the complete chemical extraction of carbon from the iron sample and dating of the carbonaceous residue. Also, different methods for cleaning samples and removing contamination were tested. In Erlangen, a Soxhlet extraction is employed for this purpose. Also, the sampling of the iron sample by drilling or cutting can be a source of contamination. Thus, the measurement of iron drill shavings yielded ages that were far too high. The first results for iron samples of known age from 2 archaeological sites in Germany are presented and discussed.

INTRODUCTION

Radiocarbon dating of iron artifacts is, in principle, possible due to the slight carbon content of iron artifacts that originates from the iron smelting process. Up to the beginning of industrialization, smelting was usually performed with charcoal (with some exceptions, especially in East Asia; Beukens et al. 1999), which renders ¹⁴C dating possible in principle, in contrast to industrially-made steel, for which coal or lignite is used. The carbon content varies considerably due to the smelting technique. For modern steel, the carbon content can be determined exactly during processing and varies between 0.05 and 1.5%. Usually, archaeological iron artifacts have low carbon contents around 0.2%; cast iron can have a carbon content up to 5% C.

Successful attempts to date iron artifacts have been undertaken since the late 1960s (van der Merwe and Stuiver 1968; van der Merwe 1969), but it is still no routine procedure. Some of the main problems in preparing iron are the low carbon content and the metallic character of the samples, which complicates the carbon extraction and oxidation and makes the required sample size too big (about 1 g) for some sample combustion systems. In most cases, this required a separate preparation line only for iron samples, which is not applicable for many ¹⁴C laboratories (Cook 2001). The Erlangen accelerator mass spectrometry (AMS) group uses an elemental analyzer for sample combustion and a subsequent reduction facility. Iron samples that show a carbon content and a sample size as described above are not suitable for combustion in an elemental analyzer. Therefore, our approach is either to avoid oxidation and reduction of the sample, or to extract the carbon from the iron sample in order to obtain a suitable sample for combustion.

¹Physikalisches Institut Abt. IV, Erwin-Rommel-Str.1, Universität Erlangen, 91058 Erlangen, Germany.
Email: c14@physik.uni-erlangen.de.

²Corresponding author. Email: Andreas.Scharf@physik.uni-erlangen.de.

³Institut für Archäometrie, Gustav-Zeuner-Str. 5, TU Bergakademie Freiberg, 09599 Freiberg, Germany.

⁴Email: khunger79@gmx.de.

⁵Email: ernst.pernicka@am.tu-freiberg.de.

METHODS

Direct Sputtering

We tested direct sputtering of the unprepared sample material with the ion source (40 MC-SNICS) and the subsequent measurement at the Erlangen AMS facility. Ordinary sputter targets consist of a carbon-iron compound, so that direct sputtering of carbonaceous iron is also possible (Beukens et al. 1999). In this procedure, small pins that fit into the cathodes used for the 40 MC-SNICS were made by spark erosion from the sample material. After cleaning with acetone, the pins were directly pressed into a cathode and measured at the Erlangen AMS facility. The pin that fits into a cathode has a mass of about 50 mg, which corresponds to 0.5 mg C (a common sample amount for AMS targets) based on a sample containing 1% C. The carbon ion current gained from the ion source corresponds to the carbon content of the target material; thus, the ion current of directly sputtered iron samples is rather low, but sufficient for measurement (up to 40 nA of ^{13}C , regular targets provide currents between 100 and 200 nA). This requires a little more time for the measurement and probably the measurement of more than 1 pin in order to obtain good statistics. For samples with very low carbon content, the ion current may be too small for useful measurements, depending on the performance of the respective AMS facility.

Carbon Extraction Using Hydrochloric Acid

An alternative strategy for obtaining samples that are manageable for our combustion system is the chemical carbon extraction from the iron. Modifying the method described by Nakamura et al. (1995) and Cheoun et al. (2001), we dissolved the cleaned iron pieces, without treating them with CuCl_2 , in 2M hydrochloric acid at a temperature of 85 °C.

The chemical reaction taking place is the following:



The carbonaceous precipitate was separated from the FeCl_3 solution, filtered with a carbon-free glass fiber filter, repeatedly washed with deionized water, and dried at 100 °C. Subsequently, the sample was oxidized in the elemental analyzer and reduced to graphite in an analogous manner to other “standard” samples. Using 2M hydrochloric acid at 85 °C, the reaction was completed within a short time (Figure 1). If the temperature exceeds 85 °C, the chemical reaction is so intense that the carbon is distributed over the whole beaker, which makes the separation of the precipitate from the solution very difficult. The completeness of the reaction can be tested by the loss of the samples’ ferromagnetism. Most of our archaeological samples (mainly iron nails) could be used up completely; hence, it was not necessary to divide them into small fragments, which would be a possible source of contamination.

The extraction efficiency increases logarithmically with the carbon content with considerable variation and reaches up to practically 100% in the case of cast iron (Figure 2).

Removal of Contaminants

Many archaeological iron artifacts are chemically treated to inhibit corrosion. The removal of such contaminants is essential for correct dating results. We tested several cleaning methods with deionized water, methanol, acetone, tetrahydrofuran, or the application of a complete Soxhlet extraction process. The set of solvents for the Soxhlet extraction used by the Erlangen AMS group consists of tetrahydrofuran, trichloromethane, acetone, methanol, and deionized water. In principle, it is possible to apply the Soxhlet extraction to the entire artifact or to the filtered precipitate. Further research is still necessary to decide which of these methods would be more appropriate.

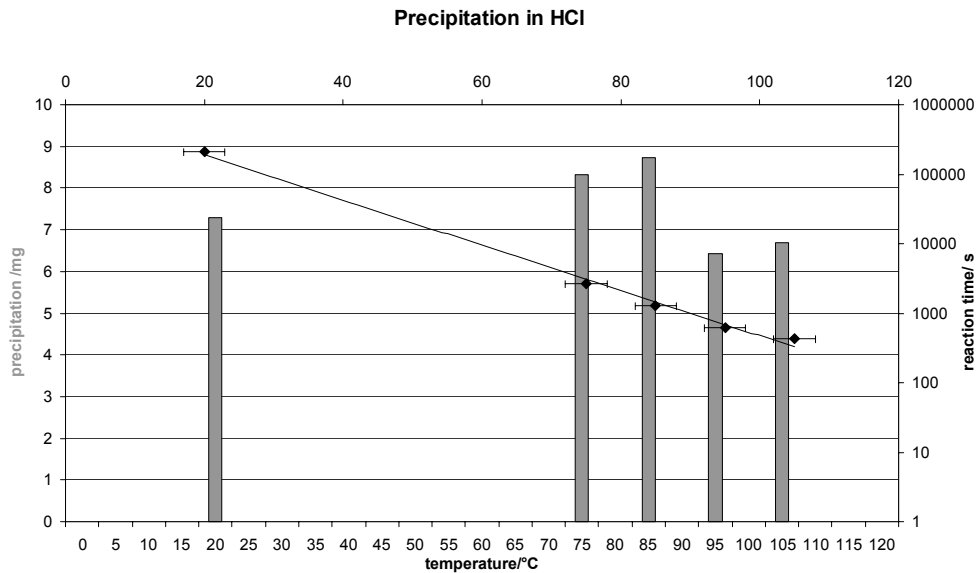


Figure 1 Amount of carbonaceous precipitate (gray bars) and reaction time for complete dissolving in 2M hydrochloric acid at different temperatures.

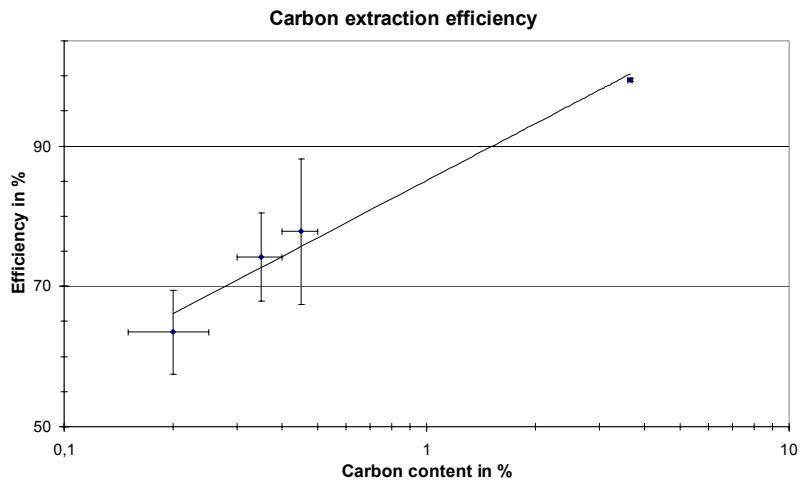


Figure 2 Efficiency of carbon extraction with 2M hydrochloric acid at 85 °C for samples with different carbon content.

SAMPLES

Samples from Sulzbach Castle

The majority of the archaeologically-dated iron samples was provided by Dr M Hensch (Hensch 2002). The artifacts were excavated at Sulzbach Castle and date from the 8th to the 16th century AD. Sulzbach is located in Upper Palatinate in northeastern Bavaria in an important medieval mining area. All in all, we received 20 samples from there, mainly including different types of nails as well as a few tool fragments (carbon content varying from 0.1% to 0.2%). The most interesting sample is

a bar of cast iron from a well-dated archaeological context of the late-11th century AD. This would make it the oldest known piece of cast iron in Central Europe. The 2 different types of sample preparation methods described above were tested with spark-eroded pieces of the cast iron bar after cleaning with deionized water, acetone, and methanol. To remove possible contaminants, 1 part of the hydrochloric acid precipitate was also treated with a Soxhlet extraction. The nails and tool fragments were dissolved in hydrochloric acid as entire pieces.

Samples from Staffelberg Mountain

The Staffelberg Mountain is located in Upper Franconia in northern Bavaria, above the valley of the Main river. Its cliffs that surround the plateau form a natural fortification which has been used by men since the 5th millennium BC. There are still remains of Celtic defense works visible on the plateau. A micrograph of a wrought-iron piece from there shows a typical La Tène welding technique; thus, it is assumed to originate from the La Tène period (about 500–15 BC). The artifact was provided by the archaeological collection of the Universität Erlangen and had been chemically treated. Therefore, it was divided into 4 pieces by spark erosion. One of them was sampled by drilling. The drill shavings and another piece were cleaned with tetrahydrofuran, acetone, and water; the two remaining ones were also cleaned with methanol. The piece from which the drill shavings were taken was cleaned by Soxhlet extraction later and also measured with the AMS facility.

RESULTS AND DISCUSSION

Samples from Sulzbach Castle

Table 1 shows the results for the cast iron bar from Sulzbach Castle. The age of the directly-sputtered iron pin was averaged over 3 individual results (Erl-4247, Erl-4248, Erl-5396), since the single results did not show any significant differences. The calibrated ages are all younger than expected; there is only a small overlap with the result from the directly-sputtered pin. But all results are compatible with an origin in the 13th century AD. The most possible contamination, besides the contamination with modern material during sample preparation, would lead to older ages, but not to younger ones. Such sources of contamination could be organic materials used for conservation, use of scrap iron, or coal or carbonate iron ores (Craddock et al. 2002) used in the smelting process. If it could have been firmly dated to the 11th century AD, then this iron bar would have been the oldest known example of cast iron in Central Europe. However, the dating results rather suggest that it was an intrusion from a younger layer. The results of the iron nails and tool fragments from Sulzbach Castle, all prepared by the hydrochloric acid extraction method, agree well with the archaeological context in all cases, with the exception of 1 sample (Table 2). The first measurement of this sample, an iron nail, yielded a result of 5448 ± 60 BP. Since part of the precipitate of this sample was not used in the first measurement, we applied Soxhlet extraction to the remaining part and measured it again. The new result was 1158 ± 104 BP, corresponding to a calibrated 2- σ range from the 7th to 12th centuries AD, whereas the archaeological layer where the nail was found originates from the 15th or 16th century, but contains also a lot of material from the 10th to 12th centuries. Accordingly, it seems that Soxhlet extraction had removed the contaminants completely.

Samples from Staffelberg Mountain

Table 3 shows the results of the artifact made of the wrought iron found on Staffelberg Mountain. Again, cleaning with tetrahydrofuran and acetone could not remove all of the organic material applied. The age of ~ 5500 BP is much too old. An additional cleaning step with methanol yielded more reasonable results, but the range of calibrated ages is still too old and would correspond to the

Table 1 Dating results for the cast iron bar from Sulzbach Castle; different types of sample pretreatment were tested.

Lab code	Target name	BP	$\delta^{13}\text{C}$ (‰)	Calibrated age ^a
Erl-4247	Cast iron pin 1	842 ± 86	-29 ± 2	AD 1023 (95.4%) AD 1290
Erl-4248	Cast iron pin 2	740 ± 78	-29 ± 2	AD 1066 (1.4%) AD 1083 AD 1124 (1.2%) AD 1136 AD 1157 (92.8%) AD 1401
Erl-5396	Cast iron pin 3	859 ± 87	-29 ± 2	AD 1020 (95.4%) AD 1286
	Cast iron pin averaged	808 ± 48	-29 ± 2	AD 1066 (2.2%) AD 1083 AD 1124 (2.1%) AD 1137 AD 1156 (91.1%) AD 1290
Erl-5532	Cast iron, extraction by hydrochloric acid	754 ± 49	-29.8	AD 1164 (0.7%) AD 1170 AD 1186 (91.5%) AD 1302 AD 1368 (3.2%) AD 1383
Erl-6002	Cast iron, extraction by hydrochloric acid and Soxhlet	717 ± 49	-29.8	AD 1218 (75.3%) AD 1323 AD 1348 (20.1%) AD 1389

^aAges were calibrated at the 95.4% confidence limit by the program Cal98 using INTCAL98 (Stuiver et al. 1998).

Table 2 Dating results for a medieval iron nail from Sulzbach Castle, before and after Soxhlet extraction.

Lab code	Target name	BP	$\delta^{13}\text{C}$ (‰)	Calibrated age ^a
Erl-5544	Iron nail, before Soxhlet extraction	5448 ± 60	-23.0	4450 BC–4050 BC (8 intervals)
Erl-5893	Iron nail, after Soxhlet extraction	1158 ± 104	-24.1	AD 660 (94.9%) AD 1036 AD 1143 (0.5%) AD 1151

^aAges were calibrated at the 95.4% confidence limit by the program Cal98 using INTCAL98 (Stuiver et al. 1998).

Table 3 Dating results for the iron artifact from Staffelberg Mountain; different types of removal of conservation material were tested.

Lab code	Target name	BP	$\delta^{13}\text{C}$ (‰)	Calibrated age ^a
Erl-5527	Staffelberg cleaned with acetone	5915 ± 69	-26.3	4945 BC (95.4%) 4600 BC
Erl-5530	Staffelberg drill shavings cleaned with acetone	15,700 ± 140	-27.5	17,399 BC (95.4%) 16,138 BC
Erl-5528	Staffelberg cleaned with acetone and methanol	2874 ± 48	-24.2	1255 BC (1.0%) 1245 BC 1213 BC (2.3%) 1200 BC 1193 BC (4.1%) 1174 BC 1170 BC (5.3%) 1140 BC 1132 BC (82.7%) 917 BC
Erl-6000	Staffelberg Soxhlet extraction	3103 ± 500	-26.8	2829 BC (0.1%) 2823 BC 2660 BC (0.1%) 2652 BC 2623 BC (0.2%) 2607 BC 2602 BC (94.9%) 148 BC 135 BC (0.2%) 116 BC

^aAges were calibrated at the 95.4% confidence limit by the program Cal98 using INTCAL98 (Stuiver et al. 1998).

Late Bronze Age, before the beginning of the Iron Age in Central Europe. The age of the drill shavings from the same artifact is very high, suggesting a massive additional contamination with old carbon, presumably originating from the drilling. This is likely because the dating of iron artifacts from another archaeological site and sampled by drilling also yielded ages that are much too high in each case. Because of the very high carbon content of steel tools and the very low carbon content of archaeological iron samples, a small amount of abrasion of the tool can affect ¹⁴C ages considerably.

These results show that the machining of the samples can be a very sensitive point in the preparation of iron samples for AMS measurements. The samples should undergo the preparation process as a whole, when possible. Drilling or cutting of the samples should be avoided. If cutting is necessary, then it should be reduced to the necessary minimum and the samples should be cleaned very carefully afterwards. Unfortunately, very little carbon could be obtained from the piece that had passed the complete Soxhlet extraction, so that the statistical errors are too large to obtain a significant result.

CONCLUSION

It could be demonstrated that both direct sputtering of iron pins and carbon extraction with hydrochloric acid can be applied for ^{14}C dating of iron artifacts. The technique of direct sputtering is more appropriate for samples with carbon contents of about 1% or above. Most archaeologically interesting iron artifacts have lower carbon contents; thus, from these, the carbon should be extracted completely. Chemical contaminants from conservation treatment could be removed to a large extent, but complete removal, even when applying the Soxhlet extraction method, is still difficult. A source of contamination that might be underestimated is the machining of the iron samples. Ideally, the artifacts should be prepared for dating as entire pieces, if possible.

REFERENCES

- Beukens RP, Pavlish LA, Wilson GC, Farquhar RM. 1999. Authenticity of a Korean iron warrior on horseback. In: Young SMM, Pollard AM, Budd P, Ixer RA, editors. *Metals in Antiquity. BAR International Series 792*:297–300. Oxford: Archaeopress.
- Cheoun MK, Kim JC, Kang J, Kim IC, Park JH, Song YM. 2001. Pretreatment of iron artifacts at SNU-AMS. *Radiocarbon* 43(2A):217–9.
- Craddock PT, Wayman ML, Jull AJT. 2002. The radiocarbon dating and authentication of iron artifacts. *Radiocarbon* 44(3):717–32.
- Cresswell RG. 1992. Radiocarbon dating of iron artifacts. *Radiocarbon* 34(3):898–905.
- Cook AC, Wadsworth J, Southon JR. 2001. AMS radiocarbon dating of ancient iron artifacts: a new carbon extraction method in use at LLNL. *Radiocarbon* 43(2A):221–7.
- Hensch M. 2002. *Burg Sulzbach in der Oberpfalz, Archäologisch-Literarische Forschungen zur Entwicklung einer Hochadelsburg des 8–14 Jahrhunderts in Hochbayern* [PhD dissertation]. Bamberg: Bamberg University. In German.
- Hunger K. 2003. *Versuche zur ^{14}C -Datierung von archäologischen Eisenartefakten mit AMS* [PhD dissertation]. Freiberg: Freiberg University of Mining and Technology. In German.
- Nakamura T. 1996. *Annual Report of AMS of Nagoya University (VII)*. Nagoya: Nagoya University, Dating and Materials Research Center. In Japanese.
- Nakamura T, Hirasawa M, Igaki K. 1995. AMS radiocarbon dating of ancient oriental iron artifacts at Nagoya University. *Radiocarbon* 37(2):629–36.
- Stuiver M, Reimer PJ, Bard E, Beck JW, Burr GS, Hughen KA, Kromer B, McCormac G, van der Plicht J, Spurk M. 1998. INTCAL98 radiocarbon age calibration, 24,000–0 cal BP. *Radiocarbon* 40(3):1041–83.
- van der Merwe NJ. 1969. *The Carbon-14 Dating of Iron*. Chicago: University of Chicago Press. 137 p.
- van der Merwe NJ, Stuiver M. 1968. Dating iron by the carbon-14 method. *Current Anthropology* 9:48–53.

EXTRACTION AND AMS RADIOCARBON DATING OF POLLEN FROM LAKE BAIKAL SEDIMENTS

Natalia Piotrowska^{1,2} • Andrzej Bluszcz¹ • Dieter Demske³ • Wojciech Granoszewski⁴ • Georg Heumann⁵

ABSTRACT. This work focuses on the preparation and dating of sporomorph (pollen and spores) concentrates of high purity. Three sediment cores recovered from Lake Baikal within the EU-Project CONTINENT were subjected to palynological analyses and accelerator mass spectrometry (AMS) radiocarbon dating. Laboratory processing of concentrates was aimed at the removal of non-sporomorph organic matter by means of chemical treatment, micro-sieving, and heavy liquid separation. The obtained concentrates were checked under the microscope and sample purity was estimated on the basis of particle counts. The results of AMS ¹⁴C dating show differences in the sedimentation rate among 3 sites of Lake Baikal.

METHODS

Lake Baikal is situated in southeast Siberia in the eastern part of the Russian Federation near the Mongolian border. It is the largest (20% of the total volume of surface freshwater), deepest (>1600 m), and probably oldest (about 25 million yr) lake on Earth.

Radiocarbon dating of Lake Baikal sediments is a difficult challenge, as previous studies have proved (Coleman 1996). The main problem is the scarcity of material suitable for dating because the sediments are very poor in organic matter and carbonates. Our work focused on the preparation and dating of high-purity sporomorph concentrates.

Three sediment cores recovered from Lake Baikal were subjected to palynological analyses and AMS ¹⁴C dating. The cores come from 3 different locations: Posolskoe Bank, Vydrino Shoulder, and Continent Ridge (see Figure 1). The cores subjected to dating were collected with the use of a Kasten corer, which gives the best assurance of complete recovery of the sediment.

The preliminary knowledge about sporomorph concentrations and sporomorph assemblages in Holocene and Late Glacial core sections, necessary for selecting appropriate subsampling levels, was gained during palynological analyses of these cores. Sample sizes ranged between 20 and 160 cm³ (see Table 1), depending on available material, pollen concentrations, and a rough calculation of pollen mass and carbon content using data available from previous studies (Erdtman 1969; Brown et al. 1989). The volume of samples taken for preparation was adjusted to obtain a minimum carbon content of about 2–4 mg per sample.

Extraction of Sporomorphs

Laboratory processing of pollen and spore concentrates was aimed at achieving a high purity of the samples. The removal of inorganic and non-sporomorph organic matter was carried out using chemical treatment, micro-sieving, and heavy liquid separation.

¹Silesian University of Technology, Institute of Physics, Department of Radioisotopes, Krzywoustego 2, PL-44-100 Gliwice, Poland.

²Corresponding author. Email: natalia.piotrowska@carbon14.pl.

³FU Berlin, Institute of Geological Sciences (Palaeontology), Malteserstr. 74-100, D-12249 Berlin, Germany.

⁴Polish Geological Institute, Carpathian Branch, Skrzatów 1, PL-31-560 Kraków, Poland.

Also: W. Szafer Institute of Botany, PAN, Lubicz 46, PL-31-512 Kraków, Poland.

⁵University Bonn, Institute of Palaeontology, Nussallee 8, D-53115 Bonn, Germany.

Table 1 Details concerning preparation of pollen concentrates and graphite targets and results of dating.

Sample code	Sample name	Depth range (cm)	Sample volume (cm ³)	Estimated purity (%)	Carbon yield (%)	Target (mg C)	Age BP (yr)	Age cal BP (yr)	$\delta^{13}\text{C}$ (‰)
Výdrino Shoulder									
1	GdA-260	0–4	60	90%	73	1.00	1950 ± 35	1820–1990	-27.2 ± 0.5
2	GdA-261	20–24	80	95%	73	1.01	2375 ± 25	2330–2710	-26.1 ± 0.4
3	GdA-263	32–35	60	95%	58	1.01	2945 ± 30	2990–3220	-26.1 ± 0.7
4	GdA-264	56–59	60	95%	62	1.01	4530 ± 40	5040–5320	-24.7 ± 0.7
5	GdA-265	77–80	60	95%	65	1.01	5455 ± 35	6170–6310	-21.5 ± 0.5
6	GdA-266	89–92	60	90%	65	1.00	6170 ± 40	6940–7230	-23.9 ± 1.1
7	GdA-267	101–104	60	85%	75	1.01	6700 ± 40	7480–7670	-20.9 ± 0.5
8	GdA-268	121–124	60	85%	79	1.01	7760 ± 40	8420–8600	-22.0 ± 0.6
9	GdA-269	138–141	60	90%	66	1.01	8620 ± 40	9520–9700	-20.1 ± 0.9
10	GdA-271	145–148	60	90%	71	1.00	8750 ± 50	9550–9950	-26.2 ± 0.7
11	GdA-272	159–163	80	90%	69	1.00	9470 ± 50	10,550–11,100	-23.0 ± 0.5
12	GdA-270	171.5–175.5	80	80%	62	1.00	10,030 ± 50	11,250–11,950	-22.3 ± 0.3
Continent Ridge									
1	GdA-247	0–4	100	70%	89	0.99	1235 ± 25	1060–1270	-25.2 ± 0.3
2	GdA-248	18–22	80	60%	75	0.99	4060 ± 30	4420–4790	-22.8 ± 0.3
3	GdA-249	24–28	80	70%	77	1.00	4955 ± 30	5600–5740	-25.0 ± 0.2
4	GdA-250	32–36	80	85%	73	1.00	5335 ± 30	5990–6270	-24.5 ± 0.2
5	GdA-251	39–43	100	70%	53	0.99	6630 ± 35	7430–7580	-26.2 ± 0.4
6	GdA-252	54–58	100	80%	69	1.01	8570 ± 40	9470–9630	-25.3 ± 0.3
7	GdA-253	60–64	80	90%	40	1.00	8690 ± 50	9540–9890	-28.7 ± 0.9
8	GdA-257	70–76	120	85%	43	1.01	10,250 ± 50	11,650–12,400	-24.2 ± 0.8
9	GdA-258	78–84	120	10%	80	0.27	11,090 ± 80	12,650–13,400	-47.0 ± 2.1
10	GdA-259	86–92	120	60%	59	0.82	11,960 ± 50	13,550–15,250	-26.5 ± 0.6
Posolskoe Bank									
1	GdA-217	29–32	30	65%	62	1.00	2425 ± 40	2340–2720	-35.2 ± 0.6
2	GdA-219	44–46	30	70%	48	1.01	3200 ± 45	3330–3560	-29.3 ± 0.7
3	GdA-231	56–57	20	85%	65	0.99	3850 ± 35	4150–4410	-25.9 ± 0.1
4	GdA-232	57–58	20	90%	64	0.99	3985 ± 40	4300–4570	-30.0 ± 0.8
5	GdA-220	66–68	30	85%	40	0.99	5520 ± 45	6200–6410	-28.8 ± 0.4
6	GdA-225	80–81	20	60%	60	0.99	9350 ± 60	10,280–10,740	-28.3 ± 0.4
7	GdA-226	81–82	20	60%	73	0.93	11,710 ± 70	13,300–13,800	-34.4 ± 0.7
8	GdA-233	84–86	40	70%	60	0.25	11,320 ± 110	13,300–13,900	-44.9 ± 0.4
9	GdA-218	89–93	60	<80%	84	0.71	12,200 ± 70	13,750–15,450	-29.6 ± 0.6
10	GdA-224	100–104	60	<30%	19	0.16	15,250 ± 210	17,410–18,370	-52.3 ± 2.6
11	GdA-223	108–112	80	<60%	65	0.93	15,040 ± 90	17,360–18,040	-27.4 ± 0.6
12	GdA-222	116–124	160	<60%	65	0.85	20,920 ± 160	23,760–25,040	-33.5 ± 0.8

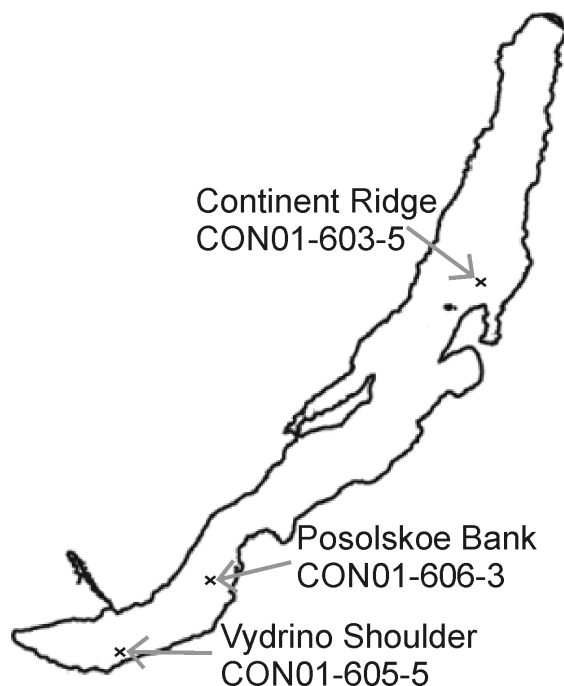


Figure 1 Map showing the location of sites: Continent Ridge (52.95460°N, 108.91370°E; water depth 130 m; collected 29 Jul 2001); Posolskoe Bank (52.08390°N, 105.86540°E; water depth 386 m; collected 3 Aug 2001); and Vydrino Shoulder (51.58350°N, 104.85180°E; water depth 665 m; collected 1 Aug 2001).

The proposed treatment steps generally follow techniques used by Brown et al. (1989), Regnéll (1992), Regnéll and Everitt (1996), and Nakagawa et al. (1998), but include a modification in specific gravity and a final acid-alkali-acid treatment combined with 10 μm micro-sieving. Heavy liquid separation combined with fine- and micro-sieving can provide pure sporomorph samples (Zhou et al. 1997; Morgenroth 2000). The steps for preparation of sporomorph concentrates are presented in Figure 2. The resulting sporomorph concentrate consists of grains of 10–90 μm in diameter, with a density of 1.13–1.66 g/cm^3 .

Sample Purity Control

The obtained concentrates were checked under the microscope and photographed (see Figure 3 for a photo example), and sample purity was estimated on the basis of particle counts. Pollen and spore spectra of the concentrates were generally similar to those obtained during standard pollen analysis. However, due to the additionally required chemical (hydrolysis, bleaching) and physical processing steps, some small and delicate pollen types (especially *Alnus fruticosa*) were partly lost. Organic matter, which could be removed from the sporomorph samples only in part, was comprised of lignin (conifer wood fragments), small globose limnic microfossils, and hyaline particles. For quantification of sample purity, the number of pollen and spores was related to the overall count of organic particles present in the concentrates. By estimation, the resulting purity was slightly adjusted according to the relative size of recorded non-sporomorph organic particles in comparison to pollen grain. Table 1 contains the estimated purity for all the samples. The best sample purity was obtained for the Vydrino core CON01-605-5 due to very high concentrations of large bisaccate pollen grains in the sediment.

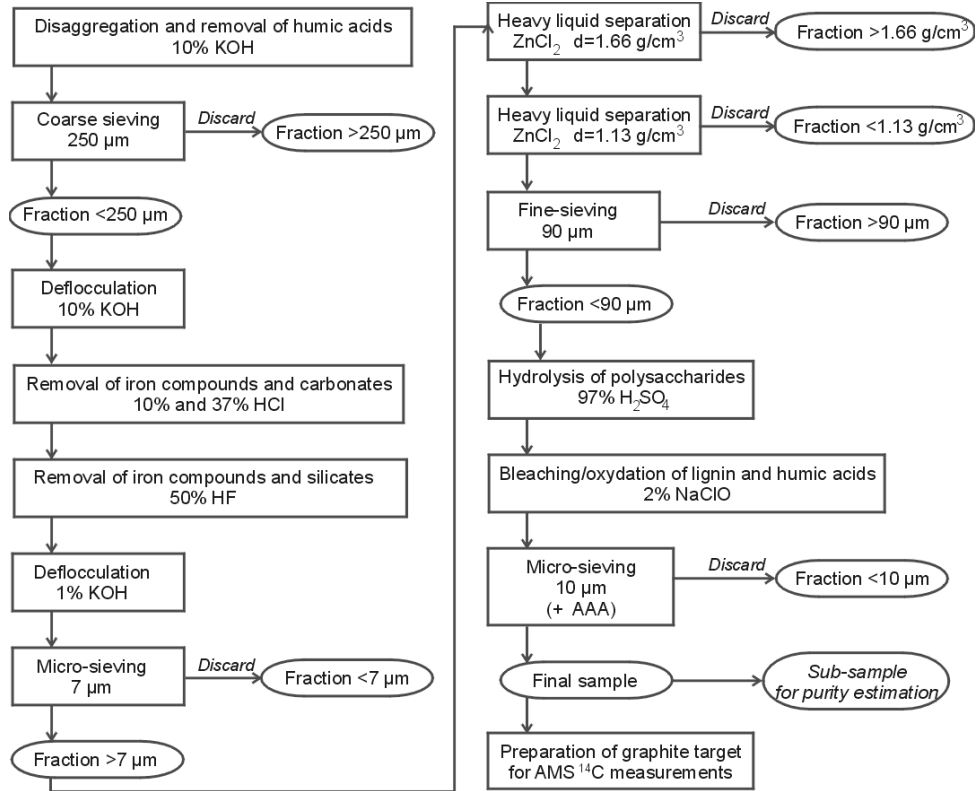


Figure 2 Flow-chart for preparation of sporomorph concentrates

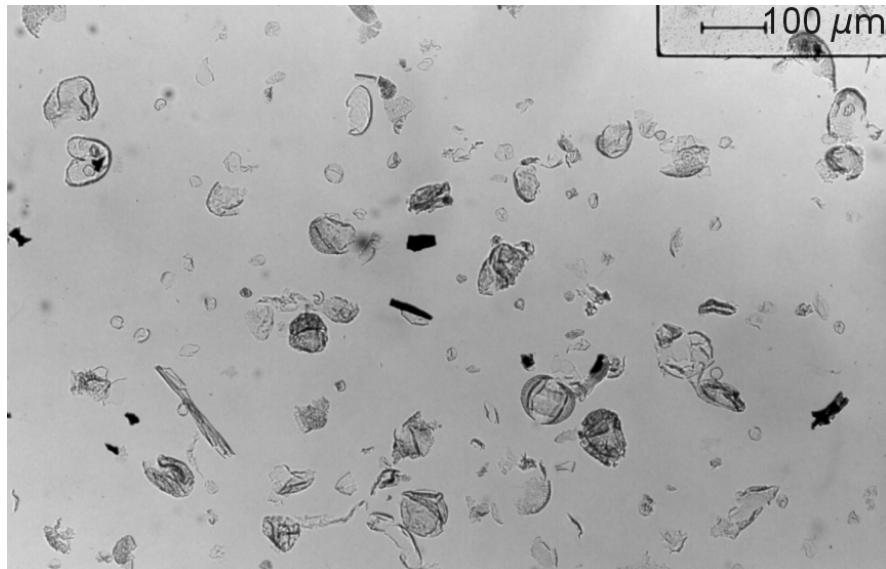


Figure 3 Photo documentation, sample LBF-AMS-8

Preparation of Graphite Targets for AMS ^{14}C Dating

The extracts were prepared for AMS measurement in the Gliwice Radiocarbon Laboratory according to the procedures described in Goslar and Czernik (2000) and Czernik and Goslar (2001). The concentration of ^{14}C in produced graphite targets was measured in the Poznań Radiocarbon Laboratory (Goslar et al., forthcoming).

RESULTS AND DISCUSSION

Details concerning sample preparation and results are given in Table 1. Most of the samples yielded CO_2 in amount corresponding to 1 or more mg of carbon, enabling the preparation of standard AMS targets. The average carbon content in pollen grains (about 64%) is in accordance with an assumed value (Erdtman 1969; Brown et al. 1989). Additionally, when the amount of CO_2 was sufficient, stable carbon isotope measurements were carried out in the Mass Spectrometry Laboratory of the Maria Curie-Skłodowska University in Lublin. The results of stable isotope measurements are within the range of values typical for terrestrial matter.

The ^{14}C ages of pollen samples were calibrated using the OxCal program (Bronk Ramsey 2001) and INTCAL98 calibration curve (Stuiver et al. 1998), except the last 3 dates from Posolskoe Bank (LBK). These dates were beyond the INTCAL98 curve and calibration was performed using the CalPal program and CalPal 2001 curve (Weninger et al. 2003; Jöris and Weninger 1998). For the construction of timescales, the ranges of calibrated ages obtained for 2 confidence intervals were taken, and the centers of the probability distribution ranges were taken as point-estimates for linear regression calculations. For 2 dates of the Posolskoe Bank (LBK-AMS-5a and b), we could have narrowed down the obtained ranges by applying the calibration of an ordered sequence of ^{14}C dates (using OxCal), taking into consideration the stratigraphic order of samples. A similar procedure could be applied to samples LBK-AMS-8 to 10, but it seems not justified at this time because the INTCAL98 calibration curve does not cover this time interval. However, we believe that the new officially accepted curve would help to solve this problem.

The results obtained for Continent Ridge and Vydrino Shoulder show a high linear correlation and were used for estimating the average sedimentation rates (Figure 4a,b). The ages of Posolskoe Bank samples are more scattered, indicating the disturbances in the sedimentation process. Two periods of sedimentation were distinguished for which the average sedimentation rates were estimated (Figure 4c). The sedimentological studies, which are still in process, will enable the recognition of possible sedimentation disturbances.

For all 3 sites, a shift in obtained sediment ages can be noticed, resulting in a non-zero age for surface sediment. Various reasons for this effect can be considered. The most likely reason is an incomplete recovery of the core (i.e. with the topmost layer missing), but the other ones also have to be considered. The surface age effect seems to be a complex problem caused by more than 1 reason. A similar effect was observed in previous studies of Lake Baikal sediments (Coleman et al. 1996; Horiuchi et al. 2000), using AMS ^{14}C dating carried out on the total organic carbon (TOC) fraction. Extraction of pollen grains was undertaken in the hope of eliminating this effect, and because macrofossils are extremely rare in Lake Baikal sediments. However, the effect of inconsistent older ages obtained on pollen extracts was observed in other studies, such as the Lake Gościąż sediments (Kilian et al. 2002), which may lead to the conclusion that this could result from specific properties of pollen grains. The surface age effect will be investigated in further studies, and the dating of more samples from the uppermost core sections and from material suspended in water is planned. We hope that this will enable the creation of reliable timescales for the sedimentation process.

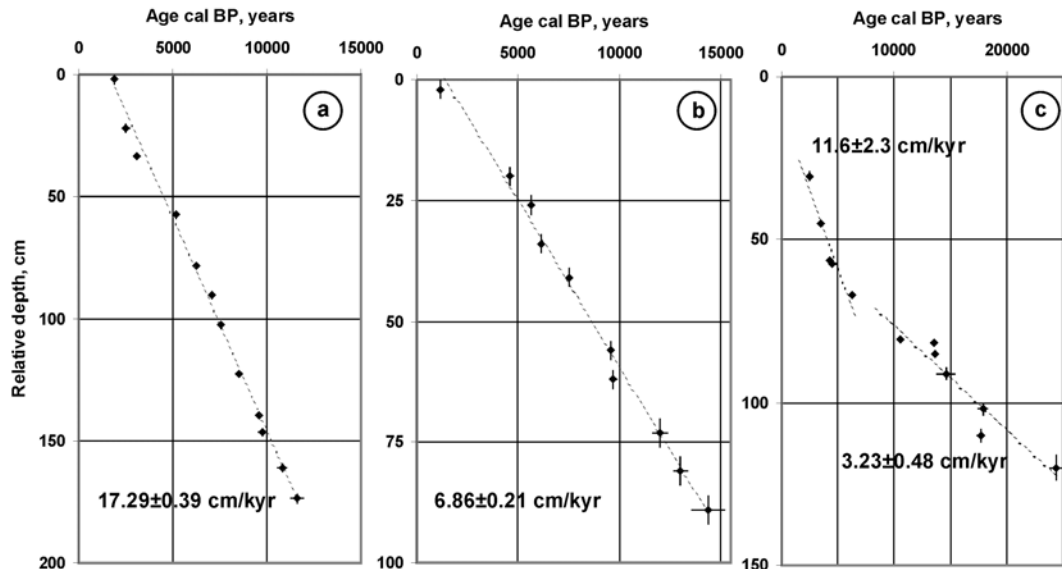


Figure 4 Calibrated age of samples versus depth for 3 investigated cores (a–Vydrino, b–Continent, c–Posolskoe). The vertical error bars represent the depth range and horizontal bars represent the range of calibrated ages. The average sedimentation rates based on linear regression are given in the graphs.

ACKNOWLEDGEMENTS

The presented work was performed as part of the European Commission project EVK2-CT-2000-00057 “CONTINENT: High-resolution continental palaeoclimate record in the Lake Baikal: A key-site for Eurasian teleconnections to the North Atlantic Ocean and monsoonal systems.”

REFERENCES

- Bronk Ramsey C. 2001. Development of the radiocarbon program OxCal. *Radiocarbon* 43(2A):355–63.
- Brown TA, Nelson DE, Mathewes RW, Vogel JS, Southon JR. 1989. Radiocarbon dating of pollen by accelerator mass spectrometry. *Quaternary Research* 32: 205–12.
- Coleman SM, Jones GA, Rubin M, King JW, Peck JA, Orem WH. 1996. AMS radiocarbon analyses from Lake Baikal, Siberia: challenges of dating sediments from a large, oligotrophic lake. *Quaternary Science Reviews* 15:669–84.
- Czernik J, Goslar T. 2001. Preparation of graphite targets in the Gliwice Radiocarbon Laboratory for AMS ^{14}C dating. *Radiocarbon* 43(2A):283–91.
- Erdtman G. 1969. *Handbook of Palynology: Morphology - Taxonomy - Ecology, An Introduction to the Study of Pollen Grains and Spores*. Copenhagen: Munksgaard. 486 p.
- Goslar T, Czernik J. 2000. Sample preparation in the Gliwice Radiocarbon Laboratory for AMS ^{14}C dating of sediments. *Geochronometria* 18:1–8.
- Goslar T, Czernik J, Goslar E. Forthcoming. Low-energy ^{14}C AMS in Poznań Radiocarbon Laboratory. *Nuclear Instruments and Methods in Physics Research B*.
- Horiuchi K, Minoura K, Hoshino K, Oda T, Nakamura T, Kawai T. 2000. Palaeoenvironmental history of Lake Baikal during the last 23000 years. *Palaeogeography, Palaeoclimatology, Palaeoecology* 157:95–108.
- Jöris O, Weninger B. 1998. Extension of the ^{14}C calibration curve to ca. 40,000 cal BC by synchronizing Greenland $^{18}\text{O}/^{16}\text{O}$ ice core records and North Atlantic foraminifera profiles: a comparison with U/Th coral data. *Radiocarbon* 40(1):495–504.
- Kilian MR, van der Plicht J, van Geel B, Goslar T. 2002. Problematic ^{14}C -AMS dates of pollen concentrates from Lake Gościąg (Poland). *Quaternary International* 88(1):21–6.
- Morgenroth G, Kerscher H, Kretschmer W, Klein M, Reichel M, Tully T, Wrzosok I. 2000. Improved sample preparation techniques at the Erlangen AMS Facility. *Nuclear Instruments and Methods B* 172:416–23.
- Nakagawa T, Brugiapaglia E, Digerfeldt G, Reille M, de Beaulieu J-L, Yasuda Y. 1998. Dense-media separation as a more efficient pollen extraction method for

- use with organic sediment/deposit samples: comparison with the conventional methods. *Boreas* 27:15–24.
- Regnéll J. 1992. Preparing pollen concentrates for AMS dating—a methodological study from a hard-water lake in southern Sweden. *Boreas* 21:373–7.
- Regnéll J, Everitt E. 1996. Preparative centrifugation—a new method for preparing pollen concentrates for radiocarbon dating by AMS. *Vegetation History and Archaeobotany* 5:201–5.
- Stuiver M, Reimer PJ, Bard E, Beck JW, Burr GS, Hughen KA, Kromer B, McCormac G, van der Plicht J, Spurk M. 1998. INTCAL98 radiocarbon age calibration, 24,000–0 cal BP. *Radiocarbon* 40(3):1041–83
- Weninger B, Jöris O, Danzeglocke U. 2003. Climate archaeology with Fortran. *Fortran Source* 19(1) Spring 2003. Lahey Computer Systems, Inc.
- Zhou WJ, Donahue D, Jull AJT. 1997. Radiocarbon AMS dating of pollen concentrated from eolian sediments: implications for monsoon climate change since the Late Quaternary. *Radiocarbon* 39(1):19–26.

¹⁴C AGES OF OSTRACODES FROM PLEISTOCENE LAKE SEDIMENTS OF THE WESTERN GREAT BASIN, USA—RESULTS OF PROGRESSIVE ACID LEACHING

Irka Hajdas¹ • Georges Bonani² • Susan Herrgesell Zimmerman³ • Millie Mendelson³ • Sidney Hemming³

ABSTRACT. Progressive dissolution experiments were performed on samples of ostracode shells from lacustrine sediments from the western Great Basin to remove contamination of the surface by secondary calcite. The observed age differences between the external and residual fractions were as great as 2000 to 6000 yr. A “plateau” in ages of the last fractions was obtained only for 1 sample; however, results of repeated experiments resulted in very good agreement of the final ages. A comparison with previously published chronologies based on bulk radiocarbon ages of ostracodes from Wilson Creek (Benson et al. 1990) shows that leaching is imperative for dating samples older than 20 ka BP. This study focuses on the problem of contamination and its removal. However, the final chronology of the Wilson Creek Formation (and other late Pleistocene lacustrine sediments) will require additional dating of other sections as well as establishment of a reservoir effect correction.

INTRODUCTION

The Great Basin (Figure 1) is a system of closed basin lakes located west of the Continental Divide, enclosed by mountains (the Sierras, the Cascades, the Wasatch Plateau) and characterized by semi-arid to arid climate. The region appears to have been very sensitive to Pleistocene climate change and the Late Glacial Maximum lake levels were uniformly high.

It was the wet/dry cycles, which are visible as ancient playa or shorelines of once deep lakes, that caught the attention of geologists. The first radiocarbon results were obtained by Libby in 1955 on samples from sediments of Searles Lake, California (Libby 1955). Research that followed established a pattern and timing of climatic oscillations in the Great Basin region and correlation with other regions such as the North Atlantic. It appears from studies by Benson et al. (1998) that rapid climatic events—perhaps equivalent to the Dansgaard/Oeschger events observed in the Greenland ice cores (GRIP and GISP2) and Heinrich events (HE) manifested by layers of ice-rafted debris in the North Atlantic (Bond et al. 1997)—might have an imprint in wet/dry cycles in the Great Basin region.

Reliable chronologies are critical for reconstructions of the past climate. Patterns of climatic changes require correlation and synchronization between regions and records. Correlations proposed by Benson et al. (1998) imply synchrony between the North Atlantic and Great Basin climatic cycles. For example, the last 2 low-stands of Lake Russell (Mono Lake) appear to correlate with HE1 (13.8 ka BP) and HE2 (21 ka BP). However, correlation of the older HE is difficult. This might be caused by chronological problems, namely contamination of the ostracodes with modern carbon and an unknown correction for reservoir effect. Kent et al. (2002) recognized the modern carbon contamination issue and they assumed that the residual carbonate measurement yielded a maximum estimate of the original ¹⁴C in the carbonate (minimum apparent age). They also recognized that the ⁴⁰Ar/³⁹Ar ash chronology is complicated and that minimum relative sanidine results yield a maximum age. Further, they considered it likely that the large magnetic excursion in the Wilson Creek Formation, known as the “Mono Lake Excursion,” was equivalent to the “Laschamp” geomagnetic

¹PSI, ETH Hönggerberg, 8093 Zürich, Switzerland. Corresponding author. Email: hajdas@phys.ethz.ch.

²Institut für Teilchenphysik, ETH Hönggerberg, 8093 Zürich, Switzerland.

³LDEO, Columbia University, New York, USA.

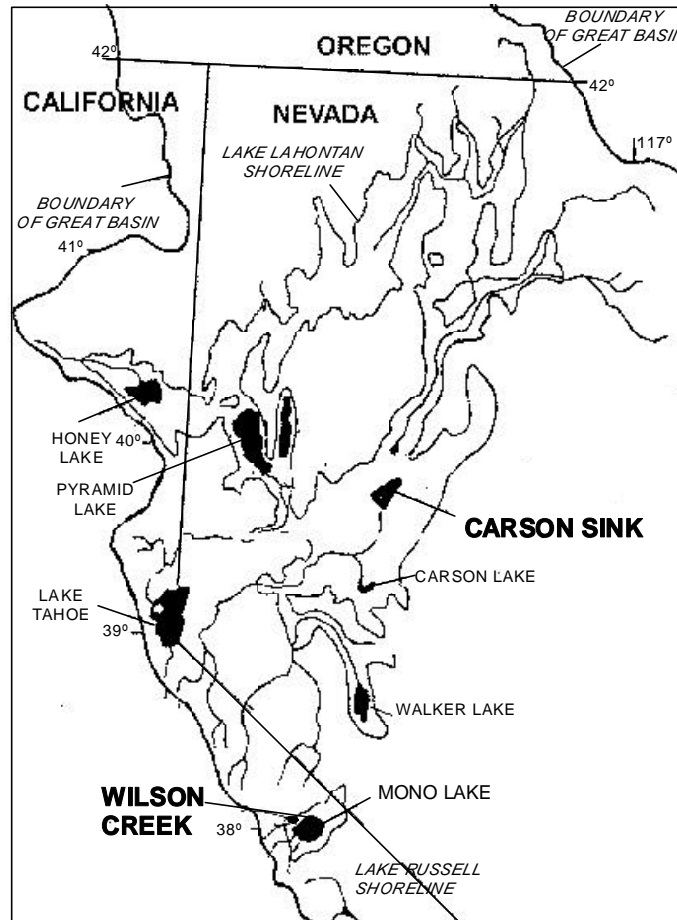


Figure 1 Map of the Great Basin adopted from Benson et al. (1990) showing location of studied sites Mono Lake and Wilson Creek Formation (California) and Carson Sink (Nevada).

excursion. Implications of such assessments are far reaching for paleoclimatic correlations, as well as correlation among paleomagnetic intensity records of the last 40 to 50 ka BP.

An alternative correlation to that of Kent et al. (2002) has already been proposed by Benson et al. (1998, 2003). Benson et al. (2003) rebutted the possibility of contamination with modern carbon and suggested an extremely large reservoir correction in order to bring the residual ^{14}C results reported by Kent et al. (2002) back into agreement with their previous assessment (Benson et al. 1998). However, such a procedure would have to be applied to both sets of data and the offset would remain unchanged. Benson et al. (2003) showed that Ash #15 of the Wilson Creek Formation has a similar composite to the ash that has been identified at Carson Sink (coincidentally, here we report ostracode data associated with that ash). A chemical match between ashes allows but does not require them correlated; thus, this issue remains unresolved.

Our study focuses on one important aspect of these issues: the ^{14}C chronology of the Wilson Creek Formation and problems connected to the possible contamination by secondary calcite deposited on the surface of ostracode shell selected from the sediments of this section.

SURFACE CONTAMINATION, DIFFUSION, AND SECONDARY CALCITE

Concerns about the possibility of contamination of carbonate samples with younger carbon pose a challenge to ^{14}C dating. One mechanism that causes contamination is young carbon dioxide diffusing through the porous surface into the core of the carbonate sample. The effects of surface contamination by modern CO_2 and diffusion into the body of the sample have been estimated and measured by Broecker and Orr (1958), who dated tufa from the Pyramid and Searles lakes. They found that, although the effect is on the order of 700 yr for a 20,000-yr-old sample, it might be avoided by leaching 80% of the surface material. In the same publication, the authors described a possibility of contamination by secondary calcite as unlikely given the arid climatic conditions in the Great Basin region. On the other hand, treatment similar to that proposed by Broecker and Orr (1958) should be sufficient for removal of younger secondary carbon. Combined ^{14}C and U/Th chronologies from Lahontan showed the effect on ages of tufa from the last high-stand of the lake, 13 ka BP (Lin et al. 1998). Burr et al. (1992) showed that 80% leaching of coral surfaces provided satisfactory ^{14}C ages.

Ostracode shells have a high surface to volume ratio; therefore, surface contamination should be taken into consideration as a potential source of error. In this study, we show results of leaching ostracodes from 2 locations in the Great Basin and the effect this procedure has on the ^{14}C chronology.

RESERVOIR EFFECT

Studies of aquatic environments require that a reservoir effect is accounted for, in addition to the problems of contamination with modern carbon. A site-specific correction is required that depends on the input of carbon-depleted water (rivers, springs), evaporation to precipitation, lake surface to volume ratios, and factors which control gas exchange (Broecker and Orr 1958; Broecker and Walton 1959). These factors can be estimated, but often they are subjected to temporal fluctuations such as lake-level variability. Moreover, due to hydrothermal inputs of ^{14}C -free CO_2 , the apparent ages of Mono Lake water might be as high as 6300 yr (Broecker et al. 1988). ^{14}C activities measured for contemporary terrestrial deposits or the ^{14}C age of water can give estimates of reservoir effect. Yet, the concern of this study is the possibility of contamination with "modern carbon," i.e., ages being too young. Our goals outlined in this study are to obtain ages of ostracodes which are free of such contamination and to build a reliable estimate of the initial ^{14}C that was incorporated into ostracode shells when formed.

^{14}C DATING OF OSTRACODES FROM CARSON SINK AND WILSON CREEK

The Sites

The section of the Wilson Creek Formation from its type locality along Wilson Creek is located at the north shore of Mono Lake, California (38°N, 118°W). The Wilson Creek Formation contains lacustrine sediments that were deposited in Lake Russell, the extended paleolake that existed during the last glacial cycle. Nineteen tephra layers found in 7-m-thick deposits of sediments can be correlated around the basin. An anomalous paleomagnetic secular variation was found at ash layer #15 and called the Mono Lake Excursion (Liddicoat 1996; Liddicoat and Coe 1979).

The Carson Sink stratigraphic section is an artificial cut exposed in the west bank of Carson River, ~20 km north east of Fallon, Nevada (39°N, 118°W). This section contains lacustrine sediments with layers composed of almost 100% ostracodes. Two white volcanic ash layers are present: the Wono ash layer and about 50 cm below the Carson Sink bed. As reported by Benson et al. (2003), the Carson Sink bed and ash layer #15 in the Wilson Creek Formation have a nearly identical chemical composition.

The Method

Sediment samples were disaggregated in deionized water and sieved. Ostracodes were hand-picked from the >250- μm fraction. Dating of fractions released in progressive leaching requires a large amount of material and, where possible, 100 mg of ostracodes were picked. However, as this is very tedious and time-consuming work, most of the samples contained 50–80 mg of ostracodes. Samples were placed in the “thumb” part of the acidification flask with 20 mL of concentrated (80%) phosphoric acid in the main tube (Figure 2). After a vacuum of 10^{-4} mb was achieved, the reaction flask was closed and the sample was mixed with the acid and left to react at 70 °C. The pressure of CO_2 released during acidification was sporadically monitored and gas was frozen in a storage tube when the amount was sufficient for 1 AMS ^{14}C sample (about 1–2 mg of C, which is based upon a 12% yield of C from of CaCO_3). As each split was collected, the remaining material was left to react and the CO_2 was collected repeatedly for dating in the same manner described above. The variation and limits on sample size weight dictated the number of fractions collected for each sample. Additionally, the number of fractions measured varied due to the sporadic measurements of the pressure, which were based on the time of the reaction. The collected CO_2 was reduced to graphite in a reaction with H_2 over cobalt at 625 °C (Vogel et al. 1984). Samples were measured at the ETH/PSI accelerator mass spectrometry (AMS) facility following the procedure described by Bonani et al. (1987). Conventional ^{14}C ages were calculated according to the protocol of Stuiver and Polach (1977).

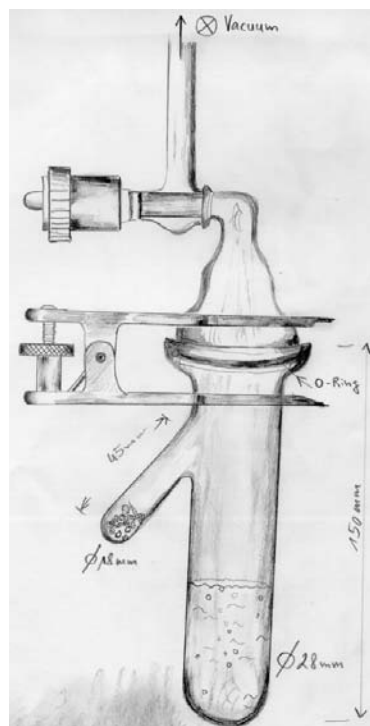


Figure 2 Attachable acidification flask used for dissolution of carbonate samples. Samples are placed in a “thumb” of the lower part using a long funnel. Acid is poured into the main chamber using an acid dispenser. The upper part with an o-ring is placed on the top and fixed with a clip. The whole chamber is attached to the vacuum and graphitization system.

RESULTS AND DISCUSSION

In the first stage of the study, several experiments were performed on ostracodes from Carson Sink. Conventional ^{14}C ages of these ostracodes are listed in Table 1. Duplicate experiments were done for 2 levels in an attempt to leach as much as possible of the ostracode shells. Each of the duplicate

experiments were performed on samples that contained at least 15 mg of ostracodes. The differences in ^{14}C ages caused by successive leaching are shown in Figure 3a and Figure 3b.

Table 1 Results of progressive leaching of ostracode shells from Carson Sink. Conventional ^{14}C ages are quoted with 1- σ error. The fraction on which age measurement was performed is based on pressure of CO_2 released during consecutive leaching steps, where '1' stands for the whole sample.

Lab nr ETH-	Sample nr	Height (cm) ^a	Fraction measured	^{14}C age (BP)	$\delta^{13}\text{C}$ (‰)	Weight (mg)
19682	CS59	-59	0-0.7	24,310 ± 190	-1.2 ± 1.2	56
			0.7-1.0	27,250 ± 220	-0.8 ± 1.2	
19682 ^b	CS59/2	-59	0-0.2	22,660 ± 160	1.6 ± 1.2	103.7
			0.2-0.31	27,180 ± 250	1.2 ± 1.2	
			0.31-1.0	27,830 ± 240	4.1 ± 1.2	
19680	CS3	-3	0-0.64	21,930 ± 160	-0.2 ± 1.2	100
			0.64-0.76	24,060 ± 180	1.1 ± 1.2	
			0.76-1.0	25,680 ± 200	-0.3 ± 1.2	
WONO	ASH	0				
19681	CS19	+19	0-0.23	24,630 ± 180	-1.6 ± 1.2	82
			0.23-0.47	27,540 ± 230	-2.0 ± 1.2	
			0.47-1.0	28,070 ± 240	-1.2 ± 1.2	
19681 ^b	CS19/2	+19	0-0.8	22,020 ± 180	1.3 ± 1.2	100.8
			0.08-0.21	26,120 ± 230	1.0 ± 1.2	
			0.28-0.32	25,000 ± 340	0.9 ± 1.2	
			0.32-1.0	28,130 ± 250	1.2 ± 1.2	

^aStratigraphic position (from bottom to top) in relation to the Wono ash layer, here at 0 cm; heights below the Wono layer are shown as negative values and heights above the layer are shown as positive values.

^bRepeat measurement on the rest material.

As well as determining the extent of exogenous carbon contamination with respect to post-leach age determinations, there were interesting results from the dating of successive leaches. The age offset between the external fraction and the residual fraction varies depending on the percentage of material in each fraction dated. For example, the largest difference is observed for sample CS19/2 (Figure 3a), where the difference between first (external) fraction and the residue is ~6000 yr. The same sample leached in the first experiment, CS19, shows a smaller difference (~3400 yr). We also observed that smaller fractions of the first leach returned the youngest ^{14}C ages in samples large enough for duplicate experiments. For example, first fractions from samples CS59 and 59/2, a 70% first leach was 24,310 ± 190 BP and a 20% first leach was only 22,660 ± 160 BP, respectively. This is shown again with CS19 and 19/2, where a 23% leach was 24,610 ± 190 BP and an 8% leach was 22,020 ± 180 BP, respectively. However, the ages for the final leaches in CS19 and CS19/2 are in very good agreement (28,099 ± 173 BP, $\chi^2 = 0.03$). Final ages obtained by leaching the samples CS59 and CS59/2 (Figure 3b) agree within the 2- σ range, despite the differences in ages of the first fractions (27,515 ± 290 BP, $\chi^2 = 3.17$). Other observed differences in ^{14}C ages between successive fractions could be associated with the size of the fraction. One fraction of CS19/2 was very small (less than 0.5 mg C, compared to all the other fractions, 1.5–2 mg of C), which might be the reason for the slightly lower age in the preceding fraction. Nevertheless, these 2 ages are in agreement in the 2- σ range.

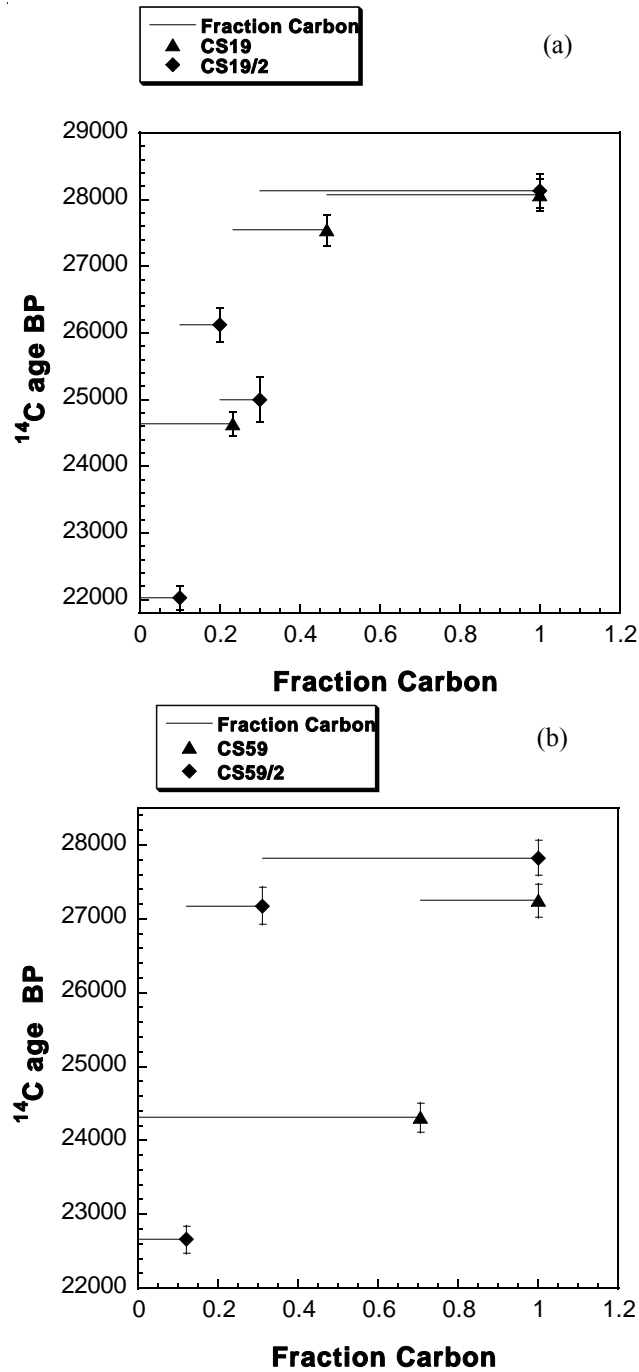


Figure 3 Results of leaching ostracodes from Carson Sink. ^{14}C ages obtained on consecutive fractions of carbon (based on pressure of CO_2 released during leaching steps) are plotted together with $1-\sigma$ error for samples (a) CS19 (ETH-19681) and (b) CS59 (ETH-19682). Triangles show the first round of measurements and diamonds show results of the second progressive leaching of ostracodes.

Results obtained on ostracodes from the Wilson Creek Formation are listed in Table 2 and plotted in Figures 4a,b. Ostracodes from 13 levels above the formation base were dated using the leaching process outlined in the Methods section. Leaching experiments were first carried out on 3 levels above the base of the section: 50 cm, 100 cm, and 160 cm. Total samples available for the 50-cm level allowed us to run 2 successive leaching experiments (WC50, WC50/2) to check on the reproducibility of results, with each leaching fraction producing sufficient carbon for analysis. The difference between the first fraction leached and the final age of the final fraction in both experiments is as high as 6000 yr. The final ages of inside fractions for WC50 and WC50/2 are within the 2- σ range (mean weighted value = 40,533 \pm 940 BP, χ^2 = 2.5). In both experiments, the first leach of 35% of the sample is \sim 35,500 BP. Moreover, the second 37% leach and the remaining 27% of residue fraction appeared to plateau in age (Figure 4a).

Table 2 Results of progressive leaching of ostracode shells from Wilson Creek. Conventional ^{14}C ages are quoted with 1- σ error. The sample number corresponds to the height given in cm. The fraction on which age measurement was performed is based on the pressure of CO_2 released during consecutive leaching steps, where '1' stands for the whole sample.

Lab nr ETH-	Sample nr	Height (cm) ^a	Fraction measured	^{14}C age (BP)	$\delta^{13}\text{C}$ (‰)	Weight (mg)
19889	WC50	50	0-0.36	35,500 \pm 530	0.7 \pm 1.2	110.0
			0.36-0.73	39,450 \pm 660	2.4 \pm 1.2	
			0.73-1.0	39,700 \pm 790 ^b	2.6 \pm 1.2	
20298	WC50/2	50	0-0.37	35,710 \pm 510	1.7 \pm 1.2	77.0
			0.37-1.0	41,590 \pm 890 ^b	2.0 \pm 1.2	
21056	WC51	51	0.41-1.0	46,100 \pm 1700 ^b	0.7 \pm 1.2	69.0
21057	WC61	61	0.43-1.0	39,200 \pm 710	1.8 \pm 1.2	46.0
21057 ^c	WC61/2	61	0-1.0	37,820 \pm 550	6.1 \pm 1.2	27.5
21059	WC81	81	0.62-1.0	39,800 \pm 730	0.4 \pm 1.2	107.0
21060	WC91	91	0.56-1.0	35,810 \pm 500	1.1 \pm 1.2	62.0
21060 ^c	WC91/2	91	0-0.47	33,680 \pm 370	3.4 \pm 1.2	46.1
			0.47-1.0	34,600 \pm 400	7.5 \pm 1.2	
20190	WC100	100	0.5-0.74	31,910 \pm 380 ^b	-0.6 \pm 1.2	55.4
	WC100	100	0.74-1.0	36,250 \pm 430 ^b	3.4 \pm 1.2	
21061	WC102	102	0.27-1.0	38,080 \pm 620	2.1 \pm 1.2	90.0
21061 ^c	WC102/2	102	0.34-1.0	39,890 \pm 690	6.4 \pm 1.2	84.4
21062	WC112	112	0.36-1.0	34,490 \pm 440	-1.0 \pm 1.2	73.0
21062 ^c	WC112/2	112	0-0.25	34,950 \pm 440	6.6 \pm 1.2	78.3
			0.25-1.0	35,660 \pm 450	6.4 \pm 1.2	
21063	WC122	122	0.43-1.0	31,270 \pm 330	0.0 \pm 1.2	77.0
21063 ^c	WC122/2	122	0-0.52	31,920 \pm 390	4.5 \pm 1.2	37.9
			0.52-1.0	32,130 \pm 320	7.3 \pm 1.2	
21064	WC132	132	0.48-1.0	32,800 \pm 380	-1.2 \pm 1.2	90.0
21064 ^c	WC132/2	132	0-1.0	32,910 \pm 350	7.5 \pm 1.2	17.7
21065	WC142	142	0.39-1.0	33,770 \pm 410	-1.0 \pm 1.2	66.0
20191	WC160	160	0.5-0.77	31,470 \pm 340	1.9 \pm 1.2	63.9
			0.77-1.0	33,610 \pm 360 ^b	3.0 \pm 1.2	
21067	WC163	163	0-0.5	31,140 \pm 330	0.2 \pm 1.2	40.3
			0.5-1.0	32,700 \pm 380	0.3 \pm 1.2	

^aHeight above the formation base.

^bAges published by Kent et al. (2002).

^cRepeat measurement on the rest material.

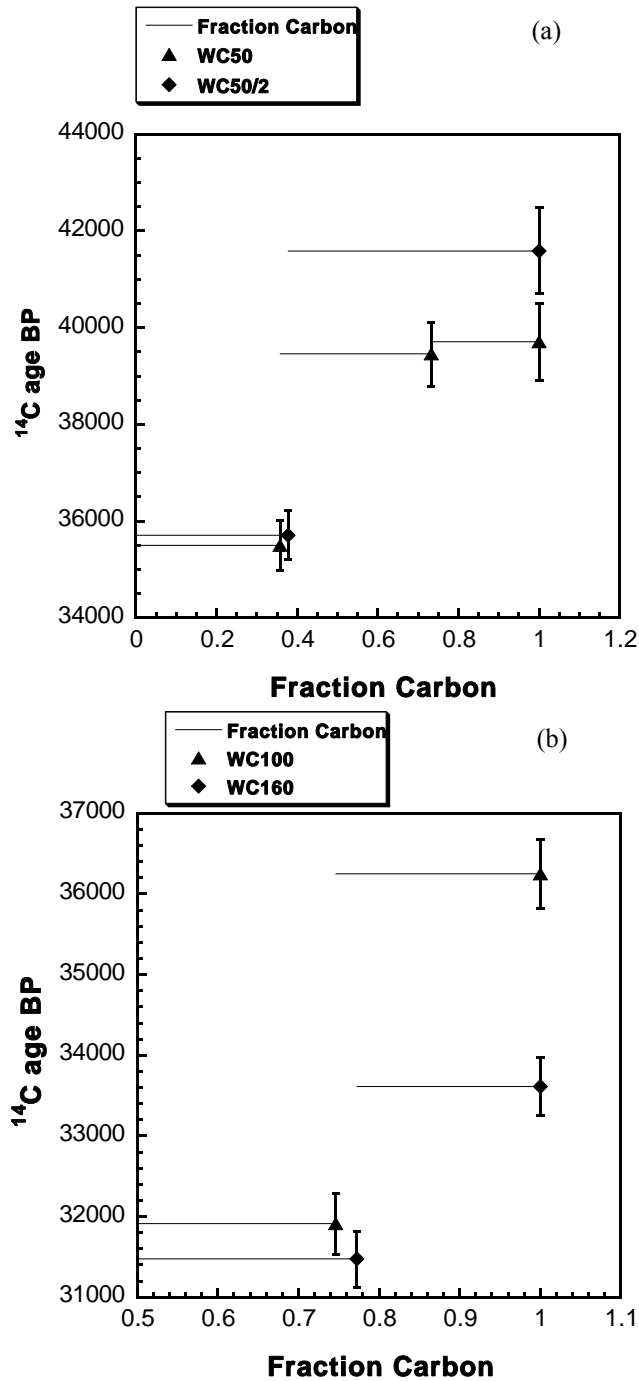


Figure 4 Results of leaching ostracodes from the Wilson Creek Formation. (a): ages obtained on fractions from 2 samples from the 50-cm level are shown as triangles (WC50, ETH-19889) and diamonds (WC50/2, ETH-20298); (b): leaching experiment was performed on 50% pre-leached samples from level 100 cm (ETH-20190) (squares) and 160 cm (ETH-20191) (diamonds).

Samples from the 100-cm and 160-cm levels had been leached (50%) prior to our “online” leaching. In these samples, the first fraction is younger than the residual fraction by ~4000 yr (Figure 4b). All of the levels listed in Table 2 were analyzed in 1999. We have recently performed our leaching experiments and analysis on some of the residual fractions of samples that contained a sufficient amount of C (Table 2, samples marked by footnote *c*). Residual fraction samples were processed and subjected to our leaching experiments (as described in the Methods section) and submitted for AMS analysis if a minimum of 1 mg carbon was collected. In general, the external fractions are younger than the residual fraction; however, the second round of measurements indicates a need for stronger than 30–50% removal of the surface as shown by the difference of ~1000 yr between ages of the both inside fractions obtained for samples WC112 and WC122 (Figure 5).

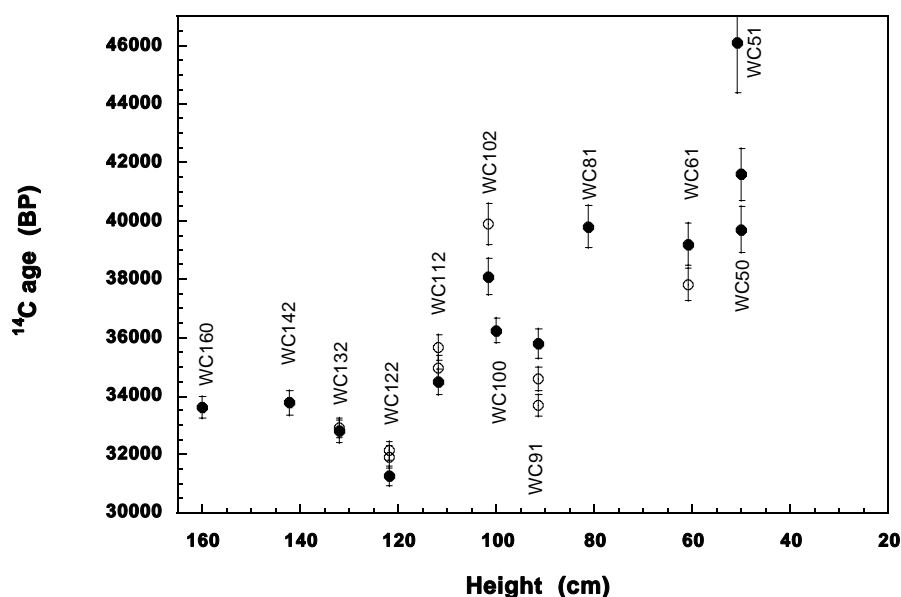


Figure 5 ^{14}C chronology of Wilson Creek. Filled circles show results from the first round of measurements. Results from repeated measurements are shown as open circles with corresponding sample number. In each of the repeated pairs, the older age corresponds to the “inside” fraction. Samples WC61 and WC132 were dated as whole shell.

Two of the samples (WC61/2 and WC132/2) were processed as a whole because they contained only 27.50 and 17.7 mg of ostracodes, respectively, which were insufficient for 2 and more fractions. The age obtained for WC61/2 was younger by ~1500 yr compared to the residual fraction measured in the first round of measurements. However, this effect is not observed for the younger sample WC132/2, which turned out to be the same age as the residual fraction of WC132.

DISCUSSION

^{14}C Chronology of the Wilson Creek Formation

We undertook the present study to address the question of the reliability of ostracode shell dating in studies such as those for the Wilson Creek Formation. A final chronology of lacustrine sediments deposited during the last 40,000 yr in the Wilson Creek Formation is urgently needed for the purpose of correlating palaeoclimatic records of the Great Basin with other regions such as the North Atlan-

tic (Benson et al. 1998). Additionally, the timing of the paleomagnetic excursion found in the Wilson Creek Formation must be resolved to allow proper correlation of paleomagnetic records (Benson et al. 2003; Kent et al. 2002).

Most of the ^{14}C ages of ostracode shells from the Wilson Creek Formation published by Kent et al. (2002) have been obtained in the younger part of the section. In that work, the ostracodes and tufa nodules were leached prior to the dating so that at least 40% of the surface was removed. In this study, we investigated the older part of the section in detail. We also applied progressive leaching and duplicated those experiments to check reproducibility where sample sizes allowed, showing that various stages of leaching do, in fact, produce different ^{14}C ages, and that the extent of the leach is an important factor for adequate removal of “modern/younger” carbon contamination. As we have shown, age differences obtained in progressive leaching of the samples underscore the need for 50 to 75% leaching of ostracode shells prior to ^{14}C dating (Figure 5).

Developing the ^{14}C chronology of this record will require determining the true reservoir correction for the section. Because the best estimates vary between 1500 and 6000 yr (Broecker et al. 1988), estimation of the reservoir correction will require additional research, such as dating terrestrial (reservoir-free) records, and correlation with the Wilson Creek Formation using tephra layers. However, the extent of the possible offsets caused by contamination with secondary calcite does not require knowledge of the reservoir effect and can be determined by comparing ages measured on whole ostracode shells with results from leached ostracode samples from the same section. In Figure 6, ^{14}C ages of leached ostracode shells (this study and Kent et al. 2002) and a chronology based on whole shells (Benson et al. 1990) are plotted for comparison. Although resolution of the dating is still not sufficient, the offset between both chronologies in the oldest parts of the section are up to

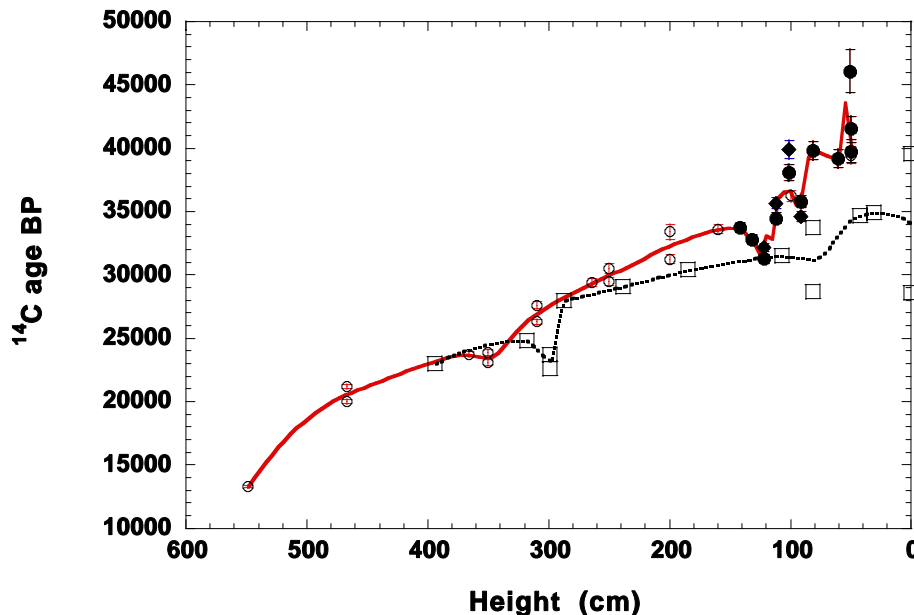


Figure 6 Comparison between chronologies based on leached ostracodes (filled circles and diamonds, this study; open circles show ages obtained by Kent et al. [2002]) and ages obtained on whole shell (open squares) by Benson et al. (1990).

6000+ yr. We also note that the younger intervals appear to agree quite well, which points to contamination becoming a significant factor for the very old samples. Benson et al. (2003) suggested that ages published by Kent et al. (2002) may have been obtained on reworked shells that were too old. Such a possibility cannot be entirely ruled out. However, there are 2 points to consider which support the Kent et al. (2002) older chronology. The first is that, as we have observed, the chronologies agree quite well in the younger part, implying that both studies used similar methods in selecting material. The second consideration is that the results of our present study show that there can be significant differences in the apparent ^{14}C ages of successive leached fractions of ostracode shells, and that another explanation for the divergence in ages between Benson et al. (1990) and Kent et al. (2002) may be due to exogenous carbon effects in untreated shells.

CONCLUSIONS

Progressive leaching of ostracode shells from Carson Sink and Wilson Creek, Mono Lake (Great Basin) resulted in older ^{14}C ages of the final fraction of progressively leached samples. Differences of up to 6000 yr between ages of the external and the residual fractions have been observed in these experiments, suggesting that the extent of leaching as a pretreatment for these samples is an important factor. Our procedure of leaching 80% of the shell improved the chronology of the record, although we concede that contamination could extend beyond this fraction and produce anomalous ages.

In samples from the oldest section of the Wilson Creek segment (+20,000 BP), the chronology based on our analysis of leached ostracodes returned ages older (by up to 6000 yr) than the previously established ^{14}C chronology of Benson et al. (1990) based on a whole shell measurements, and corroborated Kent et al. (2002) results obtained from similarly leached shell samples.

The differences between various chronologies of the region call for extensive studies that would establish a final ^{14}C chronology. This study presents a step towards such an improved chronology of the Wilson Creek Formation.

ACKNOWLEDGEMENTS

Isabel Sanchez Martinez and Saskia Laura Kaufmann are thanked for their help in sample preparation. Wolfgang Gruber drew the reaction flask. Colleagues from the AMS group are acknowledged for their help with measurements. Thanks to Jack McGeehin for his very helpful review of the first draft of the manuscript.

REFERENCES

- Benson LV, Currey DR, Dorn RI, Lajoie KR, Oviatt CG, Robinson SW, Smith GI, Stine S. 1990. Chronology of expansion and contraction of 4 Great Basin lake systems during the past 35,000 years. *Palaeogeography Palaeoclimatology Palaeoecology* 78(3–4):241–86.
- Benson LV, Lund SP, Burdett JW, Kashgarian M, Rose TP, Smoot JP, Schwartz M. 1998. Correlation of late-Pleistocene lake-level oscillations in Mono Lake, California, with North Atlantic climate events. *Quaternary Research* 49(1):1–10.
- Benson LV, Liddicoat JC, Smoot J, Sarna-Wojcicki A, Negrini RM, Lund S. 2003. Age of the Mono Lake excursion and associated tephra. *Quaternary Science Reviews* 22(2–4):135–40.
- Bonani G, Beer J, Hofmann H, Synal HA, Suter M, Wölfli W, Pfleiderer C, Junghans C, Münnich KO. 1987. Fractionation, precision and accuracy in ^{14}C and ^{13}C measurements. *Nuclear Instruments and Methods in Physics Research B* 29:87–90.
- Bond G, Showers W, Cheseby M, Lotti R, Almasi P, deMenocal P, Priore P, Cullen H, Hajdas I, Bonani G. 1997. A pervasive millennial-scale cycle in North Atlantic Holocene and glacial climates. *Science* 278(5341):1257–66.
- Broecker WS, Orr PC. 1958. Radiocarbon chronology of Lake Lahontan and Lake Bonneville. *Geological Society of America Bulletin* 69:101–10.

- ciety of America Bulletin* 69(8):1009–32.
- Broecker WS, Walton A. 1959. The geochemistry of C-14 in freshwater systems. *Geochimica et Cosmochimica Acta* 16(1–3):15–38.
- Broecker WS, Wanninkhof R, Mathieu G, Peng TH, Stine S, Robinson S, Herczeg A, Stuiver M. 1988. The radiocarbon budget for Mono Lake—an unsolved mystery. *Earth and Planetary Science Letters* 88(1–2):16–26.
- Burr GS, Edwards RL, Donahue DJ, Druffel ERM, Taylor FW. 1992. Mass spectrometric ¹⁴C and U-Th measurements in coral. *Radiocarbon* 34(3):611–8.
- Kent DV, Hemming SR, Turrin BD. 2002. Laschamp excursion at Mono Lake? *Earth and Planetary Science Letters* 197(3–4):151–64.
- Libby WF. 1955. *Radiocarbon Dating*. Chicago: University Chicago Press. 175 p.
- Liddicoat JC, Coe RS. 1979. Mono Lake Geomagnetic Excursion. *Journal of Geophysical Research* 84(NB1):261–71.
- Liddicoat JC. 1996. Mono Lake Excursion in the Lahontan Basin, Nevada. *Geophysical Journal International* 125(2):630–5.
- Lin JC, Broecker WS, Hemming SR, Hajdas I, Anderson RF, Smith GI, Kelley M, Bonani G. 1998. A reassessment of U-Th and C-14 ages for late-glacial high-frequency hydrological events at Searles Lake, California. *Quaternary Research* 49(1):11–23.
- Stuiver M, Polach HA. 1977. Discussion: reporting of ¹⁴C data. *Radiocarbon* 19(3):355–63.
- Vogel JS, Southon JR, Nelson DE, Brown TA. 1984. Performance of catalytically condensed carbon for use in accelerator mass spectrometry. *Nuclear Instruments and Methods in Physics Research B* 5:289–93.

PRELIMINARY RESULTS FOR THE EXTRACTION AND MEASUREMENT OF COSMOGENIC IN SITU ^{14}C FROM QUARTZ

P Naysmith^{1,2} • G T Cook¹ • W M Phillips³ • N A Lifton⁴ • R Anderson¹

ABSTRACT. Radiocarbon is produced within minerals at the earth's surface (in situ production) by a number of spallation reactions. Its relatively short half-life of 5730 yr provides us with a unique cosmogenic nuclide tool for the measurement of rapid erosion rates ($>10^{-3}$ cm yr⁻¹) and events occurring over the past 25 kyr. At SUERC, we have designed and built a vacuum system to extract ^{14}C from quartz which is based on a system developed at the University of Arizona. This system uses resistance heating of samples to a temperature of approximately 1100 °C in the presence of lithium metaborate (LiBO_2) to dissolve the quartz and liberate any carbon present. During extraction, the carbon is oxidized to CO_2 in an O_2 atmosphere so that it may be collected cryogenically. The CO_2 is subsequently purified and converted to graphite for accelerator mass spectrometry (AMS) measurement. One of the biggest problems in measuring in situ ^{14}C is establishing a low and reproducible system blank and efficient extraction of the in situ ^{14}C component. Here, we present initial data for ^{14}C -free CO_2 , derived from geological carbonate and added to the vacuum system to determine the system blank. Shielded quartz samples (which should be ^{14}C free) and a surface quartz sample routinely analyzed at the University of Arizona were also analyzed at SUERC, and the data compared with values derived from the University of Arizona system.

INTRODUCTION

Surface exposure dating using cosmic ray-produced nuclides, such as ^{10}Be , ^{26}Al , ^{36}Cl , ^3He , and ^{21}Ne , has revolutionized glacial and process geomorphology over the past decade by establishing accurate ages for formerly un-dateable deposits. These nuclides are produced by cosmic radiation within minerals exposed at the earth's surface. To obtain an accurate surface exposure age, the geomorphic surface must remain unburied during exposure and erode either extremely slowly or at a known rate. In theory, both burial effects and erosion rates can be resolved by measuring multiple radionuclides with differing half-lives [e.g. ^{10}Be ($t_{1/2} = 1.5 \times 10^6$ yr), ^{26}Al ($t_{1/2} = 7.05 \times 10^5$ yr), or ^{36}Cl ($t_{1/2} = 3.01 \times 10^5$ yr)]. In practice, however, the multiple-radionuclide approach does not give useful information for most samples deriving from the Last Glacial period because the long half-lives of these isotopes require burial times of >150 – 200 kyr for differential decay to be measurable. By virtue of its short half-life (5730 yr), however, in situ cosmogenic ^{14}C (in situ ^{14}C) can be used together with long-lived cosmogenic nuclides to help unravel complex exposure histories involving burial or erosion during the past 25 kyr.

In situ ^{14}C is produced within minerals at the earth's surface by spallation reactions such as $^{16}\text{O}(n,2pn)^{14}\text{C}$ and $^{17}\text{O}(n,\alpha)^{14}\text{C}$ (Gosse and Phillips 2001). Pure quartz (SiO_2) is an ideal host mineral for in situ ^{14}C analysis for the following reasons: 1) production is dominantly by spallation of oxygen; 2) its lack of cleavage makes it highly resistant to weathering and contamination by atmospheric ^{14}C ; 3) it is easily purified by etching with HF and HNO_3 ; 4) it is extremely common in the surface environment; and 5) Other cosmogenic radionuclides can also be measured in quartz.

We are developing an extraction system for in situ ^{14}C following the design of Lifton et al. (2001). This system uses lithium metaborate (LiBO_2) to dissolve the quartz sample at approximately 1100 °C in a resistance furnace. This releases any carbon within the sample into an ultra-high-purity O_2 atmosphere, where it is oxidized to CO_2 for collection and purification prior to conversion to graphite for accelerator mass spectrometry (AMS) analysis.

¹ Scottish Universities Environmental Research Centre, East Kilbride G75 0QF, Scotland.

²Corresponding author. Email: p.naysmith@suerc.gla.ac.uk.

³School of Geosciences, University of Edinburgh, Edinburgh EH8 9XP, Scotland.

⁴Geosciences Department, University of Arizona, Tucson, Arizona 85721, USA.

METHODS

Chemical Pretreatment of Quartz Samples

All pretreatments of quartz samples were carried out at the University of Edinburgh cosmogenic isotope laboratories. Before commencing the chemical pretreatment, the quartz samples were crushed and sieved to 250–500 μm , wet sieved in a 250- μm mesh sieve to remove fines, and then oven-dried at 50 °C. Eight grams of sample were added to 1 L of 2% HF and 2% HNO₃, sonically cleaned for 12–18 hr at 30 °C, and rinsed with deionized water. This process was repeated 4 times, the sample rinsed 4 times in deionized water, and then dried at 50 °C. During the pretreatment stages, the quartz samples can adsorb a small amount of atmospheric CO₂. To aid the removal of this adsorbed CO₂, the samples were sonically cleaned in a 1:1 mixture of deionized water and HNO₃ for 10 min and then placed in a vacuum oven at 50 °C overnight, immediately prior to further chemical treatment.

¹⁴C-Free CO₂ Preparation

Two liters of CO₂ were generated from “infinite age” Icelandic doublespar by acid hydrolysis. This was used as the source of ¹⁴C-free CO₂ (dead CO₂) to dilute the CO₂ extracted from quartz to give 1-mL volumes for graphitization.

Extraction of ¹⁴C from Quartz and Conversion to Graphite

All ¹⁴C extractions from quartz and CO₂ conversions to graphite were undertaken at SUERC. To start the extraction procedure, we take a 65 cm length of 41 mm o.d. quartz tubing and, using a glass-blower's hand torch, heat the tubing thoroughly in air for several minutes to burn off any surface contamination. It is important not to handle the quartz tubing as this can add contamination, so gloves and stainless steel tongs are used. An alumina boat with internal dimensions 135 mm length \times 13 mm width \times 17 mm depth is taken and cleaned using a jet of compressed nitrogen before 20 g of LiBO₂ are added. The boat is then placed in the middle of the quartz tube and the complete assembly is inserted into the Mullite tube that runs through the furnace (Figure 1). The furnace and re-circulating section are pumped for 1 hr, and then the Li BO₂ is degassed in an ultra-high-purity oxygen atmosphere at a pressure of 30–40 mbar for 2 hr at 1100 °C. The assembly is then allowed to cool overnight to 120 °C before the furnace is opened and the sleeve and boat removed. Five grams of sample quartz are then placed in the boat, which is then returned to the quartz sleeve and placed back in the furnace. The sample then undergoes a 2-stage heating process (at 500 °C and then 1100 °C). The furnace and re-circulating section are pumped for 1 hr before heating the furnace to 500 °C in a re-circulating ultra-high-purity oxygen atmosphere of 30–40 mbar for 3 hr. Any CO₂ that is produced is cryogenically trapped using liquid N₂. The volume of CO₂ collected at 500 °C is measured and stored. This CO₂ is from atmospheric contamination (Lifton et al. 2001). The next step in the process is to heat the furnace to 1100 °C for 3 hr, again in a re-circulating ultra-high-purity oxygen atmosphere at a pressure of 30–40 mbar. The CO₂ produced here is from in situ production (Lifton et al. 2001) and again it is cryogenically trapped using liquid N₂. The CO₂ is then cleaned by passing it through pentane/liquid nitrogen traps at –130 °C and then the gas is “re-combusted” with CuO and Ag at 500 °C for 2 hr. The CO₂ is measured using a highly sensitive capacitance manometer and bulked up to 1 mL using ¹⁴C-free CO₂ derived from the Icelandic doublespar. The CO₂ is then reduced to graphite using Fe and Zn as described by Slota et al. (1987) and pressed into an aluminium holder and the ¹⁴C measured by AMS.

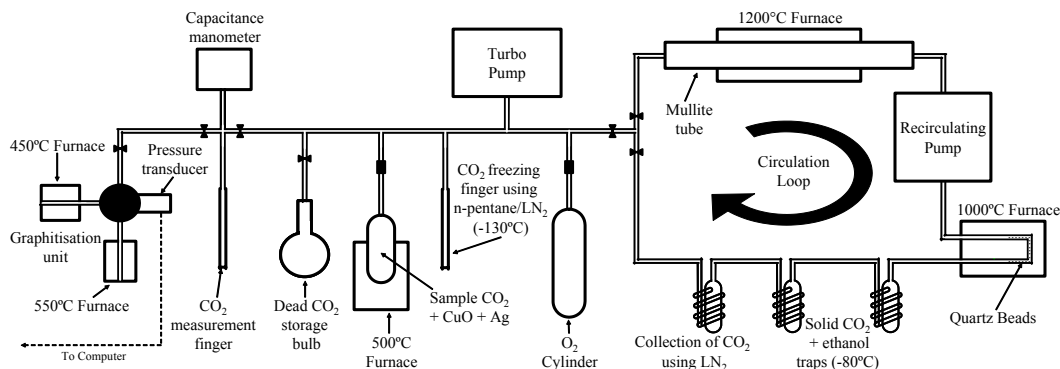


Figure 1 Vacuum system for extraction, purification, and graphitization of in situ-produced ¹⁴C

AMS Analysis

AMS analysis was initially carried out at the University of Arizona until the SUERC system was fully commissioned. Samples measured at these 2 laboratories are identified via their laboratory codes in Tables 1–4.

The volume of CO₂ for graphitization was fixed at 1 mL after tests were carried out on varying the volume of ¹⁴C-free CO₂ from 2 mL down to 0.2 mL. The measured fraction modern of the samples (*F_m*) decreased with increasing mass to a constant value between 2 mL and 0.8 mL; thus, 1 mL was chosen as the total volume for graphitization.

RESULTS

The results of the initial testing of this system are shown in Tables 1–4. Column 2 in each table indicates the number of the sample processed through the extraction line, i.e., sample 20 represents the 20th sample processed through the line. Results were calculated according to the procedures set out in Lifton (1997) and Lifton et al. (2001).

First, 1-mL aliquots of the CO₂ carrier gas that was generated from “infinite age” Icelandic doublespar were graphitized (Figure 1) and measured to check the ¹⁴C activity. The results are given in Table 1 and are used as the “graphitization” blank, which is used to correct the sample activity for contamination using the equation from Donahue et al. (1990):

$$F = F_m + f \times F_m - f$$

where *F_m* is the measured fraction modern of a sample; *f* is the measured fraction modern for a background sample (i.e. contamination); and *F* is the fraction modern corrected for contamination.

Table 1 AMS measurement of ¹⁴C activity in “dead” CO₂ dilution gas derived from Icelandic doublespar.

Laboratory code	Sample nr processed	Measured <i>F_m</i> ^a value	¹⁴ C atoms ± 1 σ (× 10 ⁵)
AA-51187	6	0.0050 ± 0.0012	1.537 ± 0.369
AA-51188	7	0.0033 ± 0.0011	0.811 ± 0.270
SUERC-14	27	0.0025 ± 0.0003	0.778 ± 0.093
SUERC-15	28	0.0024 ± 0.0003	0.692 ± 0.087

^a*f* in the equation $F = F_m + f \times F_m - f$.

The f values used were the average values from the appropriate AMS instrument. An attempt was then made to characterize the system blank for the whole process. A system blank is defined here as 1 mL of doublespar CO₂ carrier gas cycled through the entire extraction and purification procedure, including all sample heating steps in the presence of the lithium metaborate fluxing agent and ultra-high-purity O₂. The results indicated that 100% recovery of the gas was achieved on each occasion; however, when an F value was determined, it was observed that the number of ¹⁴C atoms in the system blank decreased systematically over the first 7 processings of the carrier CO₂ through the full procedure (Table 2). NB. These were not consecutive processings, but no samples with any ¹⁴C activity were processed between them. Samples 31, 33, and 34 were more stable and close to the bulk doublespar gas in activity. This suggests that the continuous running of the vacuum system with ultra-high-purity O₂ was slowly cleaning contaminant carbon from the line. It also demonstrated that great care must be taken to keep the line isolated from sources of contaminant carbon.

Table 2 Recovery yields of 1-mL aliquots of “dead” CO₂ run as system blanks and measurement of their ¹⁴C atom content.

Laboratory code	Sample nr processed	Recovery yield (%)	F value	¹⁴ C atoms $\pm 1 \sigma$ ($\times 10^5$)
AA-52891	11	103.3	0.0524 ± 0.0012	16.007 ± 0.367
AA-52892	12	101.5	0.0237 ± 0.0011	7.374 ± 0.342
SUERC-5	20	105.0	0.0354 ± 0.0020	10.970 ± 0.620
SUERC-6	21	98.0	0.0122 ± 0.0012	3.678 ± 0.362
SUERC-7	22	102.5	0.0109 ± 0.0015	3.412 ± 0.470
SUERC-16	29	100.0	0.0070 ± 0.0006	2.061 ± 0.147
SUERC-18	31	98.7	0.0009 ± 0.0004	0.268 ± 0.089
SUERC-719	33	99.8	0.0015 ± 0.0004	0.430 ± 0.115
SUERC-728	34	101.2	0.0014 ± 0.0004	0.406 ± 0.116

The results for ¹⁴C extracted from 5 g of quartz, which had >5 m of shielding by rock with a density of $\sim 2.7 \text{ g cm}^{-3}$, are given in Table 3. This material should, in principle, be free from ¹⁴C generated by cosmogenic neutron spallation reactions and can be used as a first attempt in assessing the full system contamination based on a total quartz procedural blank for the extraction procedure. As occurred for doublespar system blanks (see Table 2), initial analyses of the shielded quartz are dominated by the high system blank. However, successive measurements of repeats of full chemistry blanks (using this quartz powder) did not decrease to a stable minimum value as we observed with the doublespar procedural blanks, and it appeared to indicate that this quartz contained a measurable ¹⁴C concentration well above our lowest system blank level by a factor of 10 (apart from 1 sample where, potentially, the ¹⁴C atoms were lost from the vacuum line during processing [SUERC-9]). We also analyzed a Lake Bonneville shoreline surface quartz sample termed PP-4, which has been analyzed many times on the system designed at the University of Arizona (Lifton et al. 2001). The weighted mean of analyses carried out at the University of Arizona is $3.354 \pm 0.043 \times 10^5$ ($n = 14$) atoms per gram. The results presented here (Table 4) indicate less than half of this number of atoms have been extracted.

Table 3 Number of ^{14}C atoms extracted from 5-g shielded quartz samples.

Laboratory code	Sample nr processed	<i>F</i> value	^{14}C atoms $\pm 1 \sigma$ ($\times 10^5$) ^a
AA-52893	15	0.0215 ± 0.0011	6.514 ± 0.333
AA-52894	16	0.0371 ± 0.0011	11.311 ± 0.335
AA-52895	17	0.0217 ± 0.0015	6.657 ± 0.460
SUERC-8	25	0.0259 ± 0.0013	7.969 ± 0.400
SUERC-9	26	0.0033 ± 0.0012	0.999 ± 0.363
SUERC-729	39	0.0232 ± 0.0006	6.681 ± 0.166

^aIncludes system blank ^{14}C atoms.

Table 4 Number of ^{14}C atoms extracted per gram from aliquots of Bonneville Shoreline Surface Quartz (PP-4) sample.

Laboratory code	Sample nr processed	<i>F</i> value	^{14}C atoms per gram $\pm 1 \sigma$ ($\times 10^5$) ^a
SUERC-730	40	0.0258 ± 0.0006	1.386 ± 0.040
SUERC-731	41	0.0142 ± 0.0005	0.737 ± 0.035
SUERC-732	42	0.0278 ± 0.0006	1.509 ± 0.043

^aNet of system blank ^{14}C atoms (an average of SUERC-719 and SUERC-728 which now appears stable).

CONCLUSIONS

Significant progress has been achieved in developing a method for extraction and measurement of in situ ^{14}C , as we now appear to have a consistently low system blank and 100% CO_2 recovery. However, some issues of reproducibility, rejection of contaminant ^{14}C in the initial period of AMS measurement, and extraction efficiencies of in situ ^{14}C (perhaps as a function of temperature) persist. The shielded quartz samples appear to have some ^{14}C activity, probably due to muon production. We intend using quartz from >50 m depth for future work. At present, we do not have a definite explanation for the lack of agreement between our results and those of the University of Arizona, but we would propose the following possibilities: 1) There may be incomplete release of ^{14}C atoms from the sample. To determine whether this is happening, we plan to heat a quartz sample to 1100°C for significantly longer than the 3 hr stated in the extraction procedure and then measure the resulting gas. 2) Although our results so far suggest that a loss of ^{14}C atoms seems unlikely since recovery yields are all close to 100%, we plan to repeat this recovery test with 0.1-mL aliquots instead of 1 mL. 3) There may be release of in situ ^{14}C atoms from the 500°C combustion stage of the extraction process, resulting in a lower yield when the atoms released at 1100°C are collected and measured. However, we have noted that larger volumes of CO_2 were generated from the PP-4 sample compared to the results of Lifton et al. (2001), and at present, we can offer no explanation for this. 4) There are a number of differences in our procedures from those of Lifton et al. (2001). We intend investigating these to determine whether any have an influence on the results.

ACKNOWLEDGEMENTS

We acknowledge the financial support of the UK Natural Environment Research Council (Grant Reference: NER/B/S/2000/00698) and the expertise of the SUERC and University of Arizona AMS personnel in making the ^{14}C measurements.

REFERENCES

- Donahue DJ, Linick TW, Jull AJT. 1990. Isotope-ratio and background corrections for accelerator mass spectrometry radiocarbon measurements. *Radiocarbon* 32(2):135–42.
- Gosse JC, Phillips FM. 2001. Terrestrial in situ cosmogenic nuclides: theory and application. *Quaternary Science Reviews* 20:1475–560.
- Lifton NA. 1997. *A New Extraction Technique and Production Rate Estimate for In Situ Cosmogenic ^{14}C in Quartz* [PhD dissertation]. Tucson: University of Arizona.
- Lifton NA, Jull AJT, Quade J. 2001. A new extraction technique and production rate estimate for in situ cosmogenic ^{14}C in quartz. *Geochimica et Cosmochimica Acta* 65:1953–69.
- Lal D. 1991. Cosmic ray labeling of erosion surfaces: in situ nuclide production rates and erosion models. *Earth and Planetary Science Letters* 104:424–39.
- Slota PJ Jr, Jull AJT, Linick TW, Toolin LJ. (1987). Preparation of small samples for ^{14}C accelerator targets by catalytic reduction of CO. *Radiocarbon* 29(2):303–6.

PROBLEMS ASSOCIATED WITH THE AMS DATING OF SMALL BONE SAMPLES: THE QUESTION OF THE ARRIVAL OF POLYNESIAN RATS TO NEW ZEALAND

T F G Higham¹ • R E M Hedges¹ • A J Anderson² • C Bronk Ramsey¹ • B Fankhauser²

ABSTRACT. We have AMS dated samples of Pacific rat (*Rattus exulans*) bone “collagen” and filtered gelatin samples from the prehistoric site of Shag River Mouth, New Zealand. The age of occupation of this site has previously been determined based on 50 radiocarbon measurements. The site dates to the late Archaic phase of southern New Zealand prehistory (about 650–500 BP; 14th–15th century AD). The results of rat bones which we have dated produce a range in ages, from about 980–480 BP, a difference we attribute to a combination of effects. Pretreatment appears to be an important variable, with results showing differences in ¹⁴C age between the progressive “collagen” and filtered gelatin chemical treatment stages. Amino acid profiles suggest there is a proteinaceous but non-collagenous contaminant which is removed by the more rigorous pretreatment. Stable isotopes vary between pretreatments, supporting the removal of a contaminant, or contaminants. Variation in $\delta^{15}\text{N}$ values imply a range in uptake of dietary protein, and might suggest a potential influence from the local aquatic environment or the consumption of marine-derived protein. Rats are opportunistic, omnivorous mammals, and, therefore, obtain carbon from a variety of reservoirs and so we ought to expect that in environments where there is a variety of reservoirs, these will be exploited. Taken together, the results show that rat bone AMS ¹⁴C determinations vary in comparison with the established age of the site, but are in notably better agreement with non-collagenous data than in previously published determinations (Anderson 1996).

INTRODUCTION

Accelerator mass spectrometry (AMS) radiocarbon determinations of the Pacific rat (*Rattus exulans*) from New Zealand non-archaeological cave contexts have been used to date initial human contact, because rats are a human commensal (Holdaway 1996). The results obtained were significantly earlier than the dates of earliest human settlement established from archaeological contexts (Anderson 1991; Higham et al. 1999). AMS-dated rat bone from sites in both the North and South Islands demonstrated the presence of rats and, therefore, of human contact with New Zealand from about AD 150 (Holdaway 1996). Holdaway (1996) has emphasized that this is not equivalent to permanent settlement, since no archaeological sites have been discovered which date to this period. AMS dates obtained from archaeological rat bones, on the other hand, have produced results which range from reliable to completely erroneous (see Anderson 1996; Beavan-Athfield et al. 1999; Higham and Petchey 2000). Results from the archaeological sites of Pleasant River and Shag River Mouth, for instance, produced dates which were significantly at odds with ¹⁴C measurements obtained using reliable samples such as charcoal and shell carbonate (Anderson 1996; Smith and Anderson 1998). In contrast, AMS results of rat bones from the Pauatahunui site (Beavan-Athfield et al. 1999) were in statistical agreement with other reliable sample determinations (estuarine shell). In this paper, we present new data from the Shag River Mouth site which sheds further light on the question of the reliability of rat bone AMS ¹⁴C determinations and the reasons for variation from expected values.

Several key issues have been central to the rat bone controversy and attempts to resolve it. First, there is the question of the preservation state of rat bone. Preservation state may be assessed chemically using a suite of analytical parameters, some of which are described below (and see also van Klinken 1999). Holdaway and Beavan (1999) argued that bone from “natural” sites may be differ-

¹Oxford Radiocarbon Accelerator Unit, Research Laboratory for Archaeology and the History of Art, University of Oxford, Oxford OX1 3QJ, England.

²Department of Archaeology and Natural History, Research School of Pacific and Asian Studies, Australian National University, Canberra ACT 0200, Australia.

entally better preserved compared with bone from archaeological sites. This, they argue, is largely due to site taphonomy. Bone from coastal archaeological midden sites may be trampled, burned, and left open to the elements for periods. This results in bone which Holdaway and Beavan (1999) claim is largely unsuited for ^{14}C dating, hence the variation in the rat bone dates from archaeological sites. This contrasts with rat bones from “natural” cave contexts (as in Holdaway 1996) which are well-preserved. Second, there is the question of whether variable ^{14}C ages are the result of dietary variation amongst rats, how large this reservoir effect could conceivably be, and whether this can be corrected for using stable isotope analysis.

The Shag River Mouth Site

Shag River Mouth is an archaeological site located at the mouth of the Shag or Waihemo River near Palmerston in North Otago, New Zealand (Figure 1). Midden and putative house/hut sites (represented by hearths) cover about 2 ha of the large sand dune and spit, which extends some 600 m in a northeasterly direction from an outcrop of Tertiary rocks (McFadgen 1996). Prehistoric evidence has been identified at the edge of the nearby estuary and within the adjacent *Sarcocornia*-dominated mud flats (Anderson et al. 1996a). The faunal spectrum includes a wide range of marine and terrestrial fauna. The artifactual material recovered is typical of the late Archaic phase of New Zealand culture. The most extensive excavation undertaken at the site took place in 1988 where a 10×10 m square was opened on the highest part of the dune (SM/C:Dune) (Figure 1). The material described in this paper comes from this area (Anderson et al. 1996a).

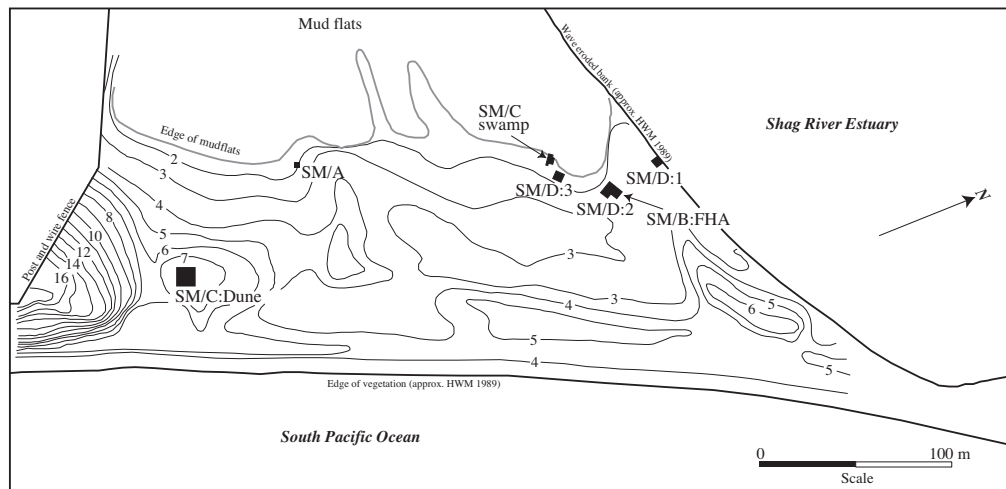


Figure 1 Excavated areas at the Shag River Mouth site, New Zealand. Rat bones dated from the site all come from the SM/C:Dune area (figure adapted after Anderson et al. 1996a). Contours are meters asl.

Fifty ^{14}C determinations have now been obtained from the site (Anderson et al. 1996b) (Figure 2). Taken together, the results of determinations on materials such as identified charcoal and marine and estuarine shell, provide support for occupation beginning in the 14th century AD. The implication of the ^{14}C results and the stratigraphic record is that prehistoric occupation may have been brief (Anderson et al. 1996b). This chronology and the presence of rat bones within cultural layers make the site ideal for testing the reliability of the material for ^{14}C , if it can be established that the bone is of reasonable preservation. Previous determinations obtained from this site by Anderson (1996) were highly variable (Figure 2) and no satisfactory explanation for them has yet been provided.

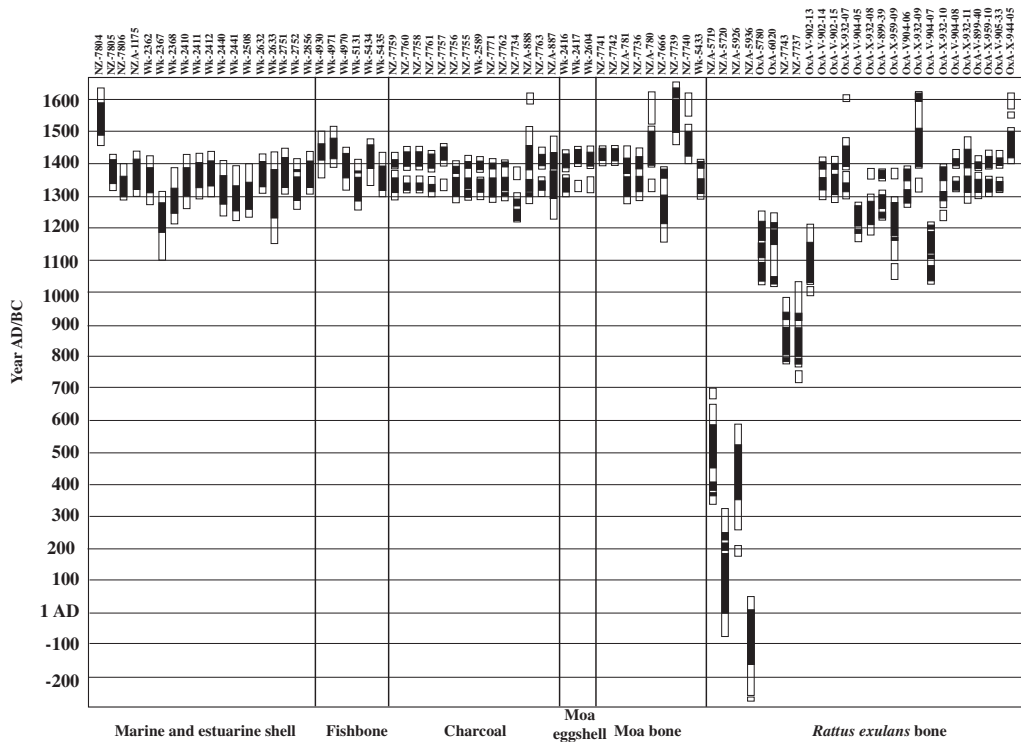


Figure 2 Calibrated age ranges of ¹⁴C determinations from the Shag River Mouth site, New Zealand. Data are taken from Anderson et al. (1996b); Higham (1993, 1994); Petchey (1998); Petchey and Higham (2000); Anderson (1996). The estuarine and marine shell, and the fish bone determinations were calibrated using the 1998 marine modelled calibration curve with a ΔR offset of -25 ± 15 yr applied (Higham and Hogg 1995). The terrestrial materials younger than about 1000 BP were calibrated using the Southern Hemisphere terrestrial curve (Hogg et al. 2003) and those older than about 1000 BP were calibrated using INTCAL98 (Stuiver et al. 1998) with a Southern Hemisphere offset of 27 ± 5 yr applied after McCormac et al. (1998).

METHOD

We aimed to investigate questions of contamination in rat bones from the site, in order to determine whether the earlier series could be influenced by old carbon contamination. Therefore, we implemented 2 pretreatment procedures on individual bones: a simple collagen extraction and the isolation of filtered gelatin. It ought to be said that neither pretreatment is our routine method, which is ultrafiltration, but the small starting weights of the rat bones meant this was not able to be implemented. The collagen fraction was dated to determine the influence of potential contaminants compared with gelatinization. We obtained 10 samples of rat bone from the SM/C:Dune site for ¹⁴C analysis (Sample reference 8 to 17; Table 1). Individual elements were used for analysis. The bones were pretreated initially at the Australian National University. They were cleaned by scraping with a scalpel to remove soil coloration, sediment detritus, and weathered surfaces, washed 3 times in MilliQ™ water and centrifuged, then dried at 35 °C for 3 days. Bones were powdered, decalcified with ~10 mL of 2% v/v HCl, and dehumified with 0.025M NaOH (Figure 3). These “collagen” samples (we use this term in quotation marks after DeNiro and Weiner [1988] and van Klinken [1999]) were submitted to the Oxford Radiocarbon Accelerator Unit (ORAU) for combustion and AMS measurement. In Table 2, they are denoted with “XB” pretreatment codes.

Table 1 Whole bone samples from Shag River Mouth, New Zealand, selected for ^{14}C dating.

Sample reference nr	Outer bag label	Inner bag label	Bone	Mass (mg)
8	SM/C A7 L2 22.11.88	BR014-01	L. mandible	110
9	SM/C AB5 L7 11.12.88	BR021-01	R. mandible	101
10	SM/C B2 L4 3.12.88	BR024-02	L. femur	111
11	SM/C D-E/1 baulk L8 10.12.88	BR054-01	L. mandible	90
12	SM/C E1 L5 8.12.88	BR057-01	R. femur	101
13	SM/C E4 L5 29.11.88	BR061-01	L. OS Innominatum	94
14	SM/C E8 L4 23.11.88	BR075-01	R. femur	140
15	SM/C F8 L6 28.11.88	BR098-03	R. tibia	75
16	SM/C G4 L4 28.11.88	BR103-01	L. tibia	150
17	SM/C I6 L8 14.12.88	BR127-01	L. femur	170

Table 2 Analytical data and AMS ^{14}C ages of rat bone from the Shag River Mouth site, New Zealand. XB samples are of “collagen”; these samples were pretreated at ANU and graphitized and AMS dated at ORAU. The samples are given OxA-V-*nnn-nn* numbers rather than OxA numbers because they were pretreated outside ORAU. The numbers denoted by *n* refer to the AMS wheel number and the position of each sample in that specific wheel. NRC (“non-routine chemistry”) denotes subsequent gelatinization of this XB fraction at ORAU. These ^{14}C determinations have been given OxA-X-*nnn-nn* numbers because of their non-routine chemistry. % carbon is the percent of carbon on combustion of gelatin or “collagen”.

OxA nr	Sample ref	Bone wgt (mg)	PCode	% wt. collagen	% wt. Nitrogen	C mg (wt dated)	% carbon	CN	$\delta^{13}\text{C}$	$\delta^{15}\text{N}$	CRA (BP) ($\pm 1 \sigma$)
V-902-13	8	71.1	XB	10.5	12.24	2.9	37.4	3.6	-13.9	17.8	985 \pm 55
V-902-14	9	82.1	XB	12.0	14.72	2.5	41.9	3.3	-20.2	11.6	640 \pm 45
X-932-07	10	71.8	NRC	12.8	16.00	0.4	39.5	2.9	-20.4	13.5	555 \pm 70
V-902-15	10		XB		14.02	4.5	42.1	3.5	-19.1	18.3	655 \pm 55
X-932-08	11	79.7	NRC	10.7	16.58	1.14	43.8	3.1	-19.0	12.6	810 \pm 50
V-904-05	11		XB		14.92	3.6	42.1	3.3	-18.4	14.5	860 \pm 40
X-959-09	12	85.6	NRC	13.2	13.57	1.4	37.1	3.2	-19.8	12.9	855 \pm 65
V-899-39	12		XB		15.47	3.6	43.5	3.3	-19.6	12.9	760 \pm 37
X-932-09	13	78.2	NRC	13.8	10.38	0.53	22.6	2.5	-18.7	12.7	510 \pm 80
V-904-06	13		XB		14.68	5.0	41.9	3.3	-16.8	19.0	715 \pm 45
X-932-10	14	109.5	NRC	13.1	17.59	2.2	45.4	3.0	-15.1	16.3	720 \pm 55
V-904-07	14		XB		14.43	3.0	42.9	3.5	-13.5	17.3	950 \pm 40
X-932-11	15	65.2	NRC	12.8	14.86	0.74	40.3	3.2	-21.3	6.7	600 \pm 80
V-904-08	15		XB		10.55	4.2	31.5	3.3	-20.8	6.8	602 \pm 40
X-959-10	16	114.2	NRC	13.4	37.86	1.03	106	3.3	-20.5	6.8	600 \pm 45
V-899-40	16		XB		15.52	6	30.8	3.2	-20.1	7.6	631 \pm 40
X-944-05	17	152.6	NRC	11.6	26.18	1.65	73.9	3.3	-20.3	10.3	480 \pm 50
V-905-33	17		XB		14.93	4.0	40.9	3.2	-20.1	10.8	598 \pm 35

Sub-samples of this “collagen” were pretreated further at ORAU. Each was gelatinized in weakly acidic water (pH3) at 75 °C for 20 hr, the supernatant was recovered using an EziFilter™ (readers should note that the EziFilters have been tested for old carbon contaminants in the light of the ultra-filtration problems outlined in Bronk Ramsey et al., these proceedings, and found to be free of extractable carbon) and lyophilized (Figure 3). In Table 2, and in the text, the gelatin samples are denoted with “NRC” pretreatment codes. Aliquots of both gelatin and “collagen” were analyzed for amino acid composition (Table 3 and Figure 4).

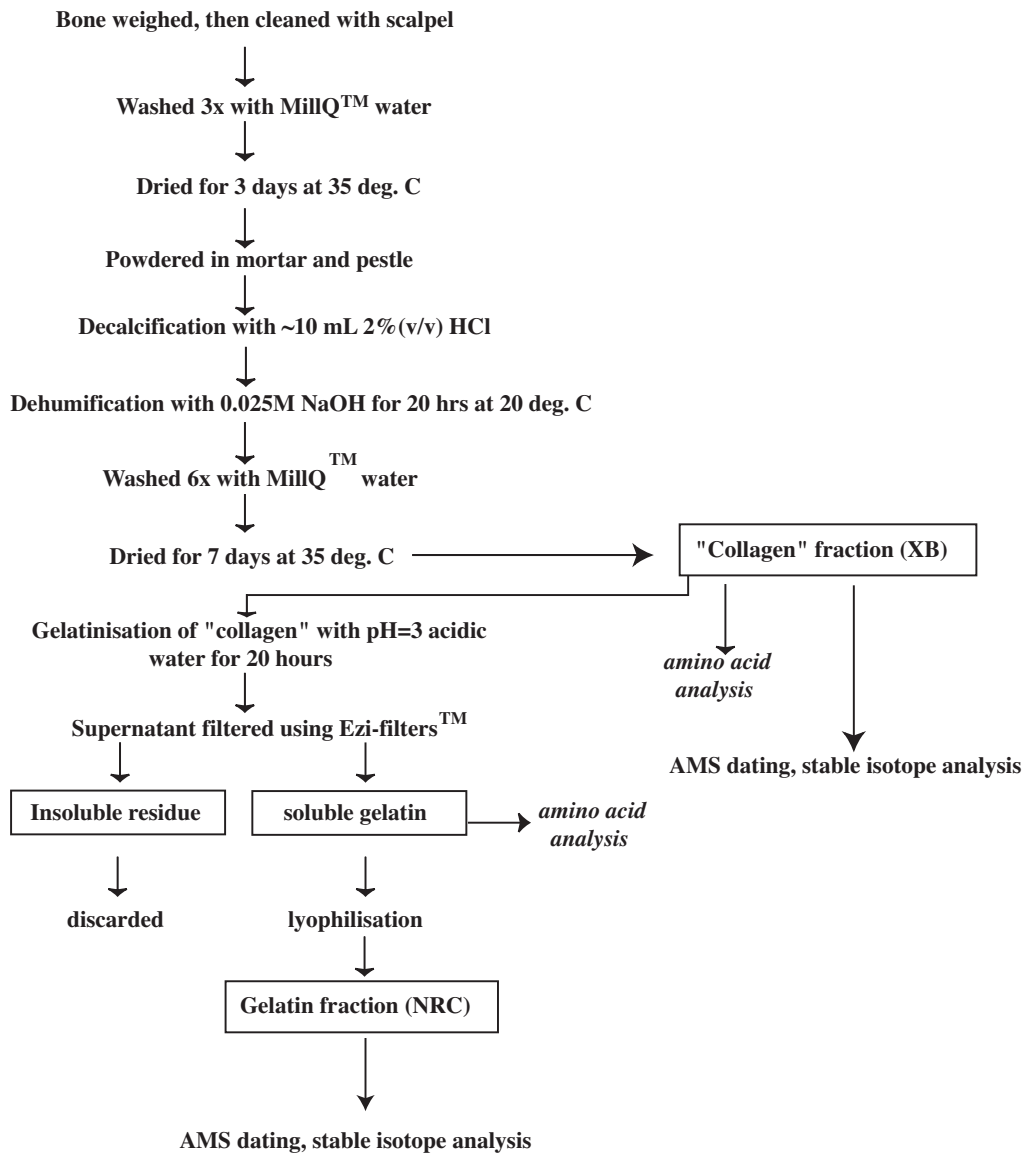


Figure 3 Pretreatment flow diagrams describing pretreatments applied to the Shag River Mouth rat bones described in this paper.

Samples of between 0.5 and 1.8 mg of bone gelatin were combusted and analyzed using a Europa Scientific ANCA-MS system consisting of a 20-20 IR mass spectrometer interfaced to a Roboprep CHN sample converter unit operating in continuous flow mode using an He carrier gas. This enables the measurement of $\delta^{15}\text{N}$ and $\delta^{13}\text{C}$, nitrogen and carbon content, and C:N ratios. $\delta^{13}\text{C}$ values in this paper are reported with reference to VPDB, and $\delta^{15}\text{N}$ results are reported with reference to AIR (Coplen 1994). Graphite was prepared by reduction of CO_2 over an iron catalyst in an excess H_2 atmosphere at 560 °C prior to AMS ^{14}C measurement (Bronk Ramsey and Hedges 1999; Bronk Ramsey et al. 2000).

Table 3 ^{14}C calibration age ranges at 68 and 95% ranges. Results were calibrated using OxCal 3.5 (Bronk Ramsey 2001) with the Southern Hemisphere calibration curve (Hogg et al. 2003; McCormac et al. 2003). No reservoir corrections have been applied in the calibration of any of the samples. See text for details.

OxA nr	PCode	^{14}C age (BP)	($\pm 1 \sigma$)	Calibrated age range AD 1 σ	Calibrated age range AD 2 σ
V-902-13	XB	985	55	1025–1155	990–11010 (3.6%) 1015–11210 (91.8%)
V-902-14	XB	640	45	1315–11360 (45.8%) 1380–11405 (22.4%)	1295–11420 (95.4%)
X-932-07	NRC	555	70	1320–11345 (10.1%) 1390–11455 (58.1%)	1295–11370 (22.6%) 1375–11505 (71.4%) 1595–11615 (1.4%)
V-902-15	XB	655	55	1300–11365 (51.8%) 1375–11400 (16.4%)	1285–11420 (95.4%)
X-932-08	NRC	810	50	1220–11285 (68.2%)	1175–11305 (91.3%) 1355–11385 (4.1%)
V-904-05	XB	860	40	1180–11195 (8.1%) 1205–11270 (60.1%)	1155–11280 (95.4%)
X-959-09	NRC	855	65	1160–11170 (2.8%) 1175–11280 (65.4%)	1040–11090 (8.3%) 1100–11300 (86.1%) 1365–11380 (1.0%)
V-899-39	XB	760	37	1230–11245 (3.8%) 1265–11305 (47.3%) 1360–11380 (17.1%)	1225–11320 (73.1%) 1350–11385 (22.3%)
X-932-09	NRC	510	80	1390–11505 (63.2%) 1595–11615 (5.0%)	1315–11355 (7.3%) 1380–11630 (88.1%)
V-904-06	XB	715	45	1285–11320 (35.2%) 1350–11385 (33.0%)	1270–11395 (95.4%)
X-932-10	NRC	720	55	1280–11320 (36.0%) 1350–11390 (32.2%)	1225–11250 (3.5%) 1265–11400 (91.9%)
V-904-07	XB	950	40	1045–11085 (26.6%) 1105–11120 (5.7%) 1130–11185 (32.9%) 1195–11210 (3.1%)	1025–11215 (95.4%)
X-932-11	NRC	600	80	1315–11360 (27.4%) 1380–11440 (40.8%)	1275–11480 (95.4%)
V-904-08	XB	602	40	1320–11345 (25.9%) 1390–11420 (42.3%)	1315–11360 (36.9%) 1380–11445 (58.5%)
X-959-10	NRC	600	45	1320–11350 (25.4%) 1385–11425 (42.8%)	1300–11365 (37.5%) 1380–11445 (57.9%)
V-899-40	XB	631	40	1315–11355 (44.0%) 1380–11405 (24.2%)	1295–11370 (59.7%) 1375–11425 (35.7%)
X-944-05	NRC	480	50	1420–11500 (68.2%)	1400–11510 (81.0%) 1545–11565 (1.4%) 1570–11625 (13.0%)
V-905-33	XB	598	35	1320–11340 (18.6%) 1390–11425 (49.6%)	1315–11355 (31.7%) 1380–11440 (63.7%)

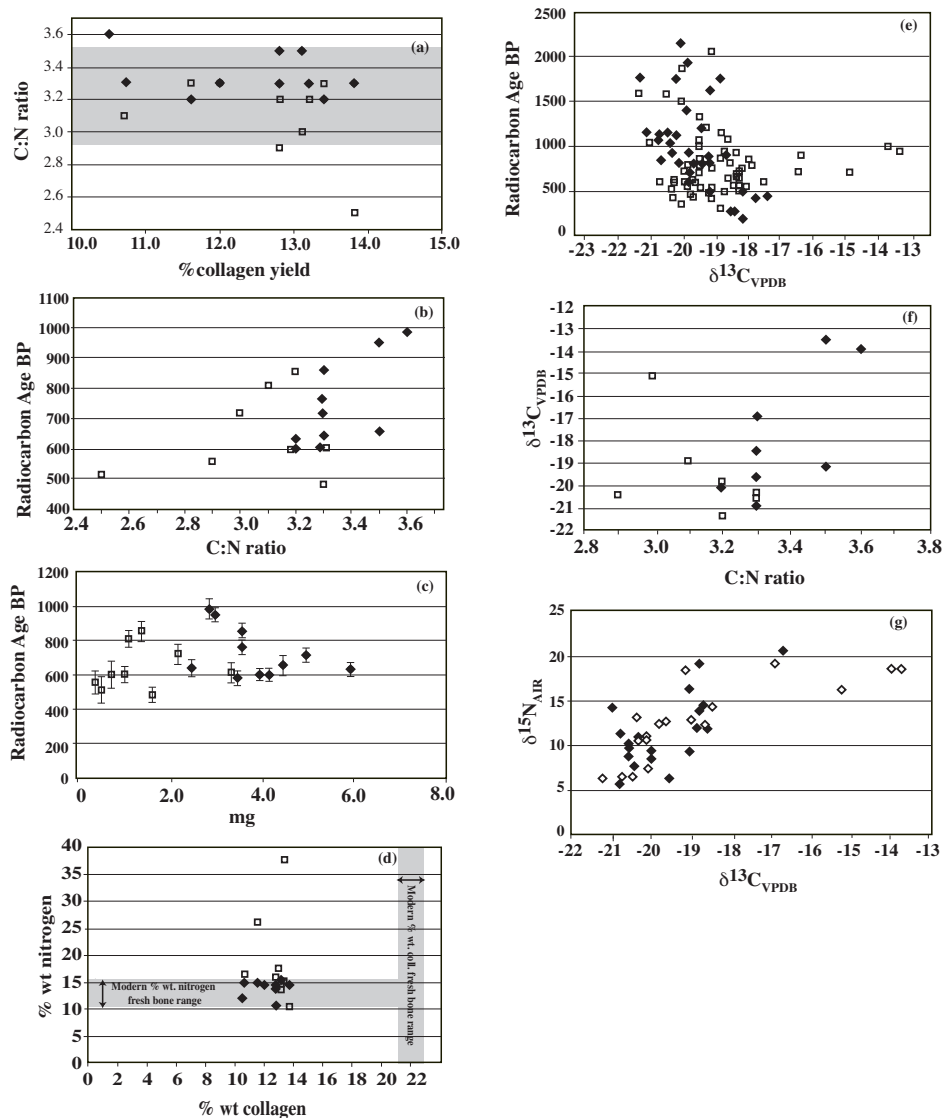


Figure 4 (a–g): for 4a–d and f; \blacklozenge : denote XB collagen samples; \square : denote NRC pretreated samples:
 a) Correlation between C:N ratio and collagen yield (%). Shaded area represents the range of acceptability at ORAU (2.9–3.5).
 b) C:N ratio plotted against conventional ^{14}C age BP.
 c) Combusted gelatin size (mg) plotted against conventional ^{14}C age BP. There is no correlation between the size of the sample dated and their ^{14}C age. Gelatin weights were uniformly lower than collagen weights, but there is no discernible effect on corresponding ^{14}C age. This confirms earlier observations by Hedges (2000) for previous rat bone gelatin determinations
 d) Relationship between % wt. nitrogen and % wt. collagen.
 e) Conventional ^{14}C age BP plotted against $\delta^{13}C$, all rat bone determinations. \blacklozenge : denote “natural” bone samples; \square : denote archaeological bone samples.
 f) C:N ratio plotted against $\delta^{13}C$ for samples described in this paper.
 g) $\delta^{15}N$ versus $\delta^{13}C$ for all archaeological rat bone samples dated (expressed in ‰). \diamond : denote samples of “collagen” and gelatin published in this study, \blacklozenge : denote samples from other archaeological contexts where there is comparable isotopic data (taken from Anderson 1996; Smith and Anderson 1998; Beavan-Athfield et al. 1999).

RESULTS

The ^{14}C ages (Tables 2 and 3) obtained range from about 480 to 980 BP. Compared with the first series of rat bones dated at the Rafter Radiocarbon Laboratory, IGNS (Anderson 1996), these are closer in age to that expected archaeologically, but they do show variance as a group. This is especially evident when the close agreement apparent from reliable samples such as charcoal and marine or estuarine shell is considered (Figure 2). We evaluate below the analytical data associated with each AMS measurement, particularly the effect of pretreatment methods upon single rat bones and the differences between “collagen” (XB) and gelatin (NRC) fractions.

The preservation state of the Shag River rat bones is important in assessing the reliability of the ^{14}C results. In instances where bone preservation is poor and the collagen yield is low, it is likely that the proportional effect of contaminants will increase if the contamination in a site is assumed to be present in a constant amount. Petchey and Higham (2000) found that bone from the Shag River site varied with location and that bone from low-lying margins adjacent to the mudflats was less well-preserved than bone from higher dune areas, such as at SM/C:Dune.

Each batch of the pretreated samples from this area that we analyzed produced “collagen” yields between 10–14% of the original bone weight (Table 2). This suggests that between 50–75% of the original collagen remains (mean = $62.9 \pm 6.8\%$), which places these samples in Hedges and van Klinken's (1992: 282, 284) “transitional preservation” category. The % weight nitrogen is within the ranges expected for unaltered or intact collagen (van Klinken 1999) (Figure 3g) with the exception of 2 samples which have much higher measured nitrogen. Percent carbon yields of combusted gelatin and “collagen” range between 30–50% as expected, with 2 exceptions.

While C:N atomic ratios are not sensitive to the uptake of small amounts of non-collagenous contamination, they will show gross exogenous contamination, particularly where the C:N ratio of the contaminating fraction is significantly different from bone collagen. C:N ratios greater than 3.6 may be taken as evidence for the presence of ~5–20% added contamination. C:N atomic ratios between 2.9–3.5 are considered acceptable at ORAU. The C:N ratios for the “collagen” series ranged between 3.2–3.6, while for the gelatin series the range was 2.9–3.3, with 1 value of 2.5. Van Klinken (1999) found that higher C:N ratios and lower % wt. collagen yields correlated closely with problematic bones. While the “collagen” samples show a slightly higher correlation between increased C:N ratios and lower % wt. collagen yields than the gelatin series, the evidence is not convincing (Figure 4a); the collagen yields are not excessively low.

The C:N ratios, the $\delta^{13}\text{C}$ and $\delta^{15}\text{N}$ values, and the ^{14}C ages together suggest the presence of a contaminant that may have affected some of the “collagen” samples. The higher C:N ratios associated with some of them (Figure 4b) tend to be associated both with the oldest ^{14}C ages and more enriched $\delta^{13}\text{C}$ values, and the gelatinization pretreatment of the same bone resulted in younger ^{14}C ages, less enriched $\delta^{13}\text{C}$ values, and reduced C:N ratios in 2 cases (for example, Sample refs 14 and 13 and perhaps also 10 [Table 2]). This suggests that simple gelatinization and filtration has removed a significant proportion of the contaminants. The high C:N ratios in the “collagen” series supports the addition of a proportion of non-proteinaceous contaminants, probably insoluble sediments, also removed by the later pretreatment. The results for bones of sample numbers 13 and 14 suggest also that contaminants in some bones are of marine origin (Table 2). In some instances, the shift in stable isotope results from XB to NRC pretreatment is as high as 6‰ in $\delta^{15}\text{N}$.

Amino acid profiles obtained from both pretreated fractions provide support for the presence of contaminants in some of the bones. They show that the XB series are largely non-collagenous in their composition. This implies the addition of a proteinaceous but non-collagenous contaminant (Figure

5, Table 4). Gelatinization and filtration pretreatment effectively removes this contamination. The amino acid profiles for the NRC sample fractions are typical of collagen. Taken together, the C:N, $\delta^{13}\text{C}$, and amino acid data suggest that there is a non-proteinaceous contaminant, as well as a proteinaceous but non-collagenous contaminant within the “collagen” sample fractions, which is significantly reduced in the gelatin fractions.

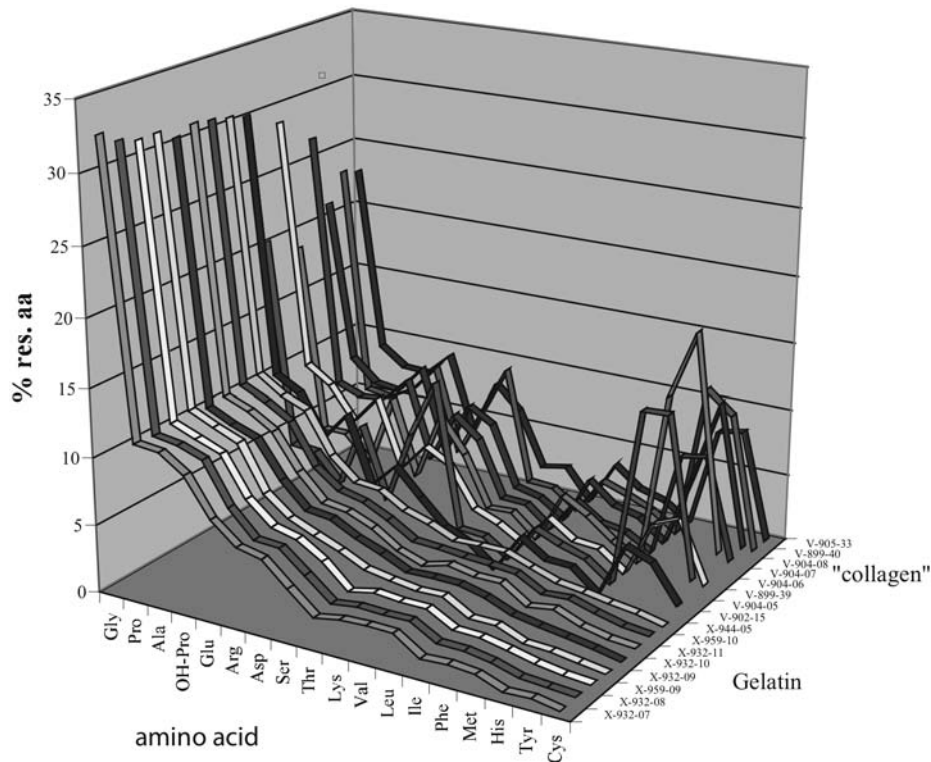


Figure 5 Amino acid profiles of rat bone gelatin (NRC) and “collagen” (XB) from Shag River Mouth; see text for details.

$\delta^{15}\text{N}$ values reflect sources for dietary protein, and since there is an enrichment in $\delta^{15}\text{N}$ from dietary protein to bone collagen of 3–4‰, important information concerning trophic level and food webs is able to be obtained from nitrogen stable isotope analyses. The $\delta^{15}\text{N}$ values for gelatin ranged from 6.7–16.3‰, indicating the uptake of a wide range of dietary protein from a range of sources and trophic levels, as one might expect in this species. Two rat bones yielded $\delta^{15}\text{N}$ values of 6–7‰ (Table 2) which are consistent with the uptake of the major proportion of dietary protein from terrestrial plant sources. These are paired with $\delta^{13}\text{C}$ values which are terrestrial (–20.5 and –21.3‰). One rat yielded a $\delta^{15}\text{N}$ value of 10.3‰, again with a terrestrial $\delta^{13}\text{C}$, which indicates dietary protein dominated by terrestrial herbivore flesh, probably land birds, which were extensively consumed by humans at the site (Anderson et al. 1996a). Two rats produced stable isotopic signatures (sample refs 8 and 14) which indicated significant marine protein uptake, again unsurprising given the high amount of marine foods consumed at the site by people (MNI estimates of Shag River faunal remains suggest marine foods comprise 15–35% of the total meat weight consumed at the site [Anderson et al. 1996a]). $\delta^{15}\text{N}$ values above 11‰ may indicate the influence of protein derived through aquatic or freshwater ecosystem foodwebs, since enrichment in $\delta^{15}\text{N}$ is not paralleled by enrichment in $\delta^{13}\text{C}$ values (Beavan-Athfield and Sparks 2001).

Table 4 Amino acid compositions (% residues) for selected Shag River Mouth rat bones. Samples were analyzed on an ABI 420A derivatiser/analyser (PE Biosystems, Warrington, UK) following hydrolysis for 24 hr in 5.7N HCl at 110 °C (Heinrikson and Meredith 1984).

GELATIN	Gly	Pro	Ala	OH-P	Glu	Arg	Asp	Ser	Thr	Lys	Val	Leu	Ile	Phe	Met	His	Tyr	Cys
X-932-07	32.5	11.3	11.2	9.9	7.2	5.6	5.2	3.6	2.0	2.4	2.4	2.4	1.1	1.2	1.1	0.3	0.5	0.1
X-932-08	31.6	11.2	11.0	10.3	7.3	5.4	5.3	3.8	2.2	2.4	2.4	2.4	1.4	1.3	1.0	0.5	0.3	0.2
X-959-09	31.2	11.5	10.7	10.1	7.2	5.6	5.1	4.0	2.2	2.6	2.5	2.5	1.4	1.4	1.0	0.6	0.3	0.1
X-932-09	31.2	11.7	10.9	10.2	6.8	5.4	4.6	3.9	3.1	2.7	2.5	2.5	1.4	1.4	0.6	0.6	0.3	0.0
X-932-10	30.5	11.3	10.4	9.7	7.1	5.3	5.1	4.1	3.4	2.5	2.6	2.6	2.1	1.4	1.0	0.7	0.4	0.0
X-932-11	31.0	11.5	10.7	9.6	7.0	5.1	4.9	4.1	2.9	2.2	2.7	2.4	2.4	1.1	1.4	0.6	0.3	0.1
X-959-10	30.8	11.6	10.7	9.6	6.6	5.3	4.9	3.9	2.8	2.7	2.5	2.4	2.3	1.2	1.4	0.8	0.3	0.1
X-944-05	30.5	11.8	10.6	9.9	6.8	5.2	5.0	3.9	3.3	2.5	2.6	2.6	1.9	1.3	1.0	0.7	0.4	0.0
COLLAGEN																		
V-902-15	30.2	11.1	10.0	7.0	9.2	4.2	6.1	4.1	2.3	1.5	0	2.9	1.7	1.6	0	4.0	3.3	0.6
V-904-05	20.3	5.0	4.8	2.7	7.7	2.3	7.8	12.1	1.4	1.2	0	2.8	2.0	1.4	0	13.3	13.4	1.7
V-899-39	28.8	10.6	9.4	7.0	9.2	4.1	6.2	5.2	2.2	1.5	0.3	2.9	1.6	1.4	0	4.2	5.0	0.5
V-904-06	18.8	4.9	4.9	3.0	8.4	2.8	7.8	5.3	1.5	1.6	0	3.8	2.7	1.2	0	12.9	18.0	2.1
V-904-07	26.7	7.9	7.2	7.4	9.2	3.4	7.3	5.7	1.6	1.5	0	2.7	1.4	1.1	0	7.8	8.2	0.8
V-904-08	21.2	9.2	7.6	7.4	9.5	3.4	7.3	6.3	1.7	1.3	0	3.6	2.0	1.5	0	5.5	11.5	1.0
V-899-40	23.2	6.1	5.8	6.8	8.9	2.6	6.2	9.9	1.4	1.4	0	2.7	2.1	1.3	0	11.5	9.9	0
V-905-33	22.7	9.0	7.7	7.5	9.3	3.6	7.8	6.0	1.9	2.3	0	3.3	1.8	1.3	0	7.6	8.0	0

The ^{14}C dates show that the contaminants we have identified in the “collagen” fractions do not appear to be of a significantly different age. The gelatin pretreated samples appear slightly younger in age than their paired “collagen” pretreated samples, but in only 2 cases is this statistically significant (sample references 13 and 14). When the calibrated ^{14}C age ranges are compared, there is overlap in all paired samples except one (sample 14).

CONCLUSIONS

The earlier set of rat bone AMS dates from Shag River Mouth disclosed significant variation in comparison with our series (Figure 2). The precise reason, or reasons for this, remain elusive, however, some possibilities are able to be set to one side. The first is contamination. The results of our analysis suggest that there is some contamination within bone from the area of the SM/C:Dune site, but this does not appear to be present in sufficiently large proportion to produce ages which approach those previously obtained (Anderson 1996). This conclusion is supported by the general agreement between the conventional ^{14}C ages of the majority of the pretreated pairs. In only one instance was the difference between pairs significant. This supports the data obtained by Higham (1993) which showed that ^{14}C determinations of humic contaminants were identical in age to those of treated and untreated charcoal from SM/C:Dune (see also Anderson et al. 1996b).

Analytical data (%C, %N, C:N atomic ratios, % wt. collagen) supported the notion that the bones were of “transitional preservation.” Each NRC-pretreated batch of bone yielded “collagen” ranging between 10–14 wt. %. This was supported by C:N ratios of 2.9–3.3, which fall within the accepted thresholds at Oxford, with 1 exception which was not reflected in a significant difference in ^{14}C age. We found that the application of 2 pretreatment methods affected the collagenous composition as shown by amino acid profiles, but this did not result in ages which were significantly different statistically.

Although the majority of AMS determinations of rat gelatin are in broad agreement with those of other materials, a small number suggest a probable reservoir depletion may exist. The stable isotope

values of OxA-X-932-10 (gelatin), for instance, show that this rat consumed protein derived from marine organisms, such as fish and shellfish, and this is consistent with an older offset. We have not applied any reservoir correction to the result because of uncertainty regarding the proportion of an offset to apply. Beavan-Athfield and Sparks (2001) applied a reservoir correction to rat bone determinations from Pleasant River Mouth, but clear anomalies resulted once the recalibrated data were obtained; one result, for instance, became much too young for the age of the site, while another remained much too old. Beavan-Athfield and Sparks (2001) argued that reservoir anomalies identified on the basis of dual (C, N) isotope analysis alone may be difficult to interpret with confidence, since foods consumed from aquatic, riverine, marine, and terrestrial environments often overlap in their isotopic range. This is particularly relevant when various protein sources from plants and animals of a variety of reservoirs are being consumed. In the case of the Shag River site, the dating of a large number of rat bones in parallel with carbon and nitrogen isotopic analysis has shown that there are small reservoir effects, but none which exceed the size of the marine reservoir effect. Three bones (sample refs 15, 16, and 17; Table 2) are likely to be unaffected by reservoir offsets since their $\delta^{15}\text{N}$ and $\delta^{13}\text{C}$ values are terrestrial in nature. Judging by the rat bone dates presented here and the age of the site as determined by other materials, no reservoir effects of the magnitude required to correct the early dated series of Anderson (1996) are apparent.

These results are in sharp contrast with previously obtained rat ^{14}C dates from the same contexts at this site (Anderson 1996). Although we have detected the presence of contaminants in the bones, and also of minor reservoir effects on the ^{14}C ages, the overall influence on the resultant dates are relatively slight. We would argue that these results, which are in broad agreement with ^{14}C dating of other materials from the site, cast doubt on the earlier published series. In the light of these results, we feel the case for rats being present in New Zealand prior to established human settlement as outlined by Holdaway (1996, 1999) remains to be proven.

ACKNOWLEDGEMENTS

We acknowledge the careful assistance of A Bowles, M Humm, P Leach, and C Tompkins (ORAU) in preparation of samples for AMS dating. T Willis, MRC Immunochemistry Unit, University of Oxford, prepared the amino acid analyses. We thank two anonymous reviewers for their constructive comments.

REFERENCES

- Anderson AJ. 1991. The chronology of colonisation in New Zealand. *Antiquity* 65:767–95.
- Anderson AJ. 1996. Was *Rattus exulans* in New Zealand 2000 years ago? AMS radiocarbon ages from Shag River Mouth. *Archaeology in Oceania* 31:178–84.
- Anderson AJ, Allingham BJ, Smith IWG, editors. 1996a. *Shag River Mouth: The Archaeology of an Early Southern Maori Village*. Canberra: Australian National University Research Papers in Archaeology and Natural History 27.
- Anderson AJ, Smith IWG, Higham TFG. 1996b. Radiocarbon chronology. In: *Shag River Mouth: The Archaeology of an Early Southern Maori Village*. In: Anderson AJ, Allingham BJ, Smith IWG, editors. 1996. *Shag River Mouth: The Archaeology of an Early Southern Maori Village*. Canberra: Australian National University Research Papers in Archaeology and Natural History 27. p 60–9.
- Beavan-Athfield NR, McFadgen BG, Sparks RJ. 1999. Reliability of bone gelatin AMS dating: *Rattus exulans* and marine shell radiocarbon dates from Pauatahanui midden sites in Wellington, New Zealand. *Radiocarbon* 41(2):119–26.
- Beavan-Athfield N, Sparks RJ. 2001. Dating of *Rattus exulans* and bird bone from Pleasant River (Otago, New Zealand): radiocarbon anomalies from diet. *Journal of the Royal Society of New Zealand* 31(4): 801–9.
- Bronk Ramsey C. 2001. Development of the radiocarbon calibration program OxCal. *Radiocarbon* 43(2A): 355–63.
- Bronk Ramsey C, Hedges REM. 1999. Hybrid ion sources: radiocarbon measurements from microgram to milligram. *Nuclear Instruments and Methods in*

- Physics Research B* 123:539–45.
- Bronk Ramsey C, Higham TFG, Bowles A, Hedges REM. 2004. Improvements to the pretreatment of bone at Oxford. *Radiocarbon*, these proceedings.
- Bronk Ramsey C, Pettitt PB, Hedges REM, Hodgins GWL, Owen DC. 2000. Radiocarbon dates from the Oxford AMS system: Archaeometry Datalist 30. *Archaeometry* 42:459–79.
- Coplen TB. 1994. Reporting of stable hydrogen, carbon and oxygen isotopic abundances. *Pure and Applied Chemistry* 66:273–6.
- DeNiro MJ, Weiner S. 1988. Chemical, enzymatic and spectroscopic characterisation of “collagen” and other organic fractions from prehistoric bones. *Geochimica et Cosmochimica Acta* 52:2197–206.
- Hedges REM. 2000. Appraisal of radiocarbon dating of kiore bones (Pacific rat *Rattus exulans*) in New Zealand. *Journal of the Royal Society of New Zealand* 30(4):385–98.
- Hedges REM, van Klinken GJ. 1992. A review of current approaches in the pretreatment of bone for radiocarbon dating by AMS. *Radiocarbon* 34(3):279–91.
- Heinrikson RL, Meredith SC. 1984. Amino-acid-analysis by reverse-phase high-performance liquid-chromatography—precolumn derivatization with phenylisothiocyanate. *Analytical Biochemistry* 136:65–74.
- Higham TFG. 1993. *Radiocarbon Dating the Prehistory of New Zealand* [PhD dissertation]. Waikato: University of Waikato.
- Higham TFG. 1994. Radiocarbon dating New Zealand prehistory with Moa eggshell: some preliminary results. *Quaternary Geochronology (Quaternary Science Reviews)* 13:163–9.
- Higham TFG, Anderson AJ, Jacomb C. 1999. Dating the first New Zealanders: the chronology of Wairau Bar. *Antiquity* 73:420–7.
- Higham TFG, Hogg AG. 1995. Radiocarbon dating of prehistoric shell from New Zealand and calculation of the ΔR value using fish otoliths. *Radiocarbon* 37(2):409–16.
- Higham TFG, Petchey FP. 2000. On the reliability of rat bone for dating in New Zealand. *Journal of the Royal Society of New Zealand* 30(4):399–409.
- Hogg AG, McCormac FG, Higham TFG, Reimer PJ, Baillie MGL, Palmer JG. 2003. High-precision radiocarbon measurements of contemporaneous tree-ring dated wood from the British Isles and New Zealand: AD 1850–950. *Radiocarbon* 44(3):633–40.
- Holdaway RN. 1996. Arrival of rats in New Zealand. *Nature* 384:225–6.
- Holdaway RN. 1999. A spatio-temporal model for the invasion of the New Zealand archipelago by the Pacific rat *Rattus exulans*. *Journal of the Royal Society of New Zealand* 29(2):91–105.
- Holdaway RN, Beavan NR. 1999. Reliable ^{14}C AMS dates on bird and Pacific rat *Rattus exulans* bone gelatin, from a CaCO_3 -rich deposit. *Journal of the Royal Society of New Zealand* 29(3):185–211.
- McCormac FG, Hogg AG, Higham TFG, Baillie MGL, Palmer JG, Xiong L, Pilcher JR, Brown D, Hoper S. 1998. Variations of radiocarbon in tree rings: Southern Hemisphere offset preliminary results. *Radiocarbon* 40(3):1153–9.
- McCormac FG, Reimer PJ, Hogg AG, Higham TFG, Baillie MGL, Palmer JG, Stuiver M. 2003. Calibration of the radiocarbon timescale for the Southern Hemisphere: AD 1850–950. *Radiocarbon* 44(3):641–51.
- McFadgen BG. 1996. Topography and geomorphology of the Shag River sand spit. In: Anderson AJ, Allingham BJ, Smith IWG, editors. *Shag River Mouth: the Archaeology of an Early Southern Maori Village*. Canberra: Australian National University Research Papers in Archaeology and Natural History 27. p 14–20.
- Petchey FJ. 1998. *Radiocarbon Analysis of a Novel Bone Sample Type: Snapper and Barracuda Bone from New Zealand Archaeological Sites* [PhD dissertation]. Waikato: University of Waikato.
- Petchey FJ, Higham TFG. 2000. Bone diagenesis and radiocarbon dating of fish bones at the Shag River Mouth site, New Zealand. *Journal of Archaeological Science* 27:135–50.
- Smith IWG, Anderson AJ. 1998. Radiocarbon dates from archaeological rat bones: the Pleasant River case. *Archaeology in Oceania* 33:88–91.
- Stafford TW Jr, Brendel K, Duhamel RC. 1988. Radiocarbon ^{13}C and ^{15}N analysis of fossil bone: removal of humates with XAD-2 resin. *Geochimica et Cosmochimica Acta* 52:2257–67.
- Stuiver M, Reimer PJ, Bard E, Beck JW, Burr GS, Hughen KA, Kromer B, McCormac FG, van der Plicht J, Spurk M. 1998. INTCAL98 radiocarbon age calibration, 24,000–0 cal AD. *Radiocarbon* 40(3):1041–83.
- van Klinken GJ. 1999. Bone collagen quality indicators for palaeodietary and radiocarbon measurements. *Journal of Archaeological Science* 26:687–95.

AMS ¹⁴C DATING OF IRON ARTIFACTS: DEVELOPMENT AND APPLICATION

Hiroki Enami¹ • Toshio Nakamura^{1,2} • Hiroataka Oda¹ • Tetsuya Yamada³ • Toshio Tsukamoto³

ABSTRACT. We have developed a prototype carbon extraction system for accelerator mass spectrometry (AMS) radiocarbon dating of archaeological iron remains by combusting them with a RF induction furnace. We have also successfully tested and used a method of carbon extraction from iron using a CuCl₂ solution. Modifications to our carbon extraction systems and methods provide us acceptable performances; carbon yield is normally around 80% and the ¹⁴C background level is as low as 42–48 ka BP in ¹⁴C apparent age. We have also conducted an iron refining experiment to examine the sources for carbon ¹⁴C age derived from iron, using established AMS ¹⁴C dating and carbon extraction systems. Our refining experiment was conducted on iron slag, which are by-products formed during iron smelting methods in the 7th century AD, and using modern charcoal as fuel. The aim of the experiment was to determine whether original carbon characteristics in the original iron materials would be preserved, or if the carbon signature would be replaced to some degree by the modern charcoal. AMS ¹⁴C measurements on the refined iron yielded ¹⁴C ages equivalent to those of the modern charcoal fuel. The result indicates that the original carbon signatures in the iron slag from 7th century production was replaced completely by modern carbon used in our experiment. The experiment confirms the assumption that ¹⁴C ages on iron products are associated with the fuel source of the iron smelting or refining process. We also report on the dating of iron slag materials excavated from the Gennaitouge iron smelting site, where ¹⁴C dates were consistent with the age of the site estimated by archaeological evidence.

INTRODUCTION

The timing of the introduction of ancient iron manufacture from China or Korea to Japan remains uncertain. Direct radiocarbon dating on archaeological iron remains is one of the most promising tools to investigate the history of iron introduction in Japan. The ages of ancient iron manufacture sites are usually determined by typological estimation, based on the shape and decoration on the surface of pottery, or ¹⁴C dating of charred wood collected from the layers in which iron-related remains were excavated. Such indirect methods, however, are not applicable for sites where pottery is absent or where charcoal deposits in relevant horizons may have been mixed with those of different horizons.

Van der Merwe and Stuiver (1968) first reported on the ¹⁴C dating of iron samples. However, their method was not practical because it required iron samples of 1 kg or more. In the 1980s, accelerator mass spectrometry (AMS) techniques were widely used to date various kinds of carbon-containing materials, and required an average of 1 mg of carbon. The ¹⁴C ages of iron artifacts were measured directly with AMS for the first time by Cresswell (1991, 1992) at the IsoTrace Laboratory, Toronto, Canada. Since then, AMS ¹⁴C dating has been applied widely for iron materials (Yoshida 1992; Igaki et al. 1994; Nakamura et al. 1995; Yokoi et al. 1998; Ono et al. 1999; Yamada et al. 1999; Yamada et al. 2001; Cheoun et al. 2001; Cook et al. 2001; Craddock et al. 2002; Cook et al. 2003a; Cook et al. 2003b; Hüls et al., forthcoming). Developments over that time on the complex apparatus developed originally by Cresswell (1991, 1992), wherein iron samples were melted and carbon was extracted under vacuum, was a simple carbon extraction method for iron based on a sealed tube combustion with CuO in quartz, which was introduced successfully by Cook et al. (2001) and further modified by Hüls et al. (forthcoming). In addition, the possibility of exact dating on carbon contained in the rusty part of iron artifacts was shown by Cook et al. (2003a, 2003b).

¹Center for Chronological Research, Nagoya University, Chikusa, Nagoya 464-8602, Japan.

²Corresponding author. Email: nakamura@nendai.nagoya-u.ac.jp.

³Center for Preservation Science, Gangoji Institute for Research of Cultural Property, 2-14-8, Moto-machi, Ikoma 630-0257, Japan.

We have applied AMS ^{14}C dating to archaeological iron materials at Nagoya University since 1994. We developed a prototype of a carbon extraction system from iron samples by combusting them with a radio-frequency (RF) induction furnace in 1994. Since 1998, we have also successfully tested and applied a method of carbon extraction by dissolving iron materials in CuCl_2 solution. We have since modified both carbon extraction systems and now the 2 methods provide us acceptable performances, as will be described below. Our test experiments had 3 stages: first, we checked ^{14}C contamination levels introduced by carbon extraction based on combustion of iron with a RF induction furnace (Nakamura et al. 1995) and iron dissolution by CuCl_2 solution (Oda et al. 1999); second, we refined ancient iron slag materials in a furnace using modern charcoal blocks to clarify the sources of carbon in the newly produced iron; third, we measured the ^{14}C ages of ancient iron slag and charcoal remains from an archaeological site, of which the period of intense occupation is clearly known. These experiments clarify whether iron artifacts can be dated directly to estimate their production ages.

SAMPLE DESCRIPTIONS

Materials used are described to estimate ^{14}C contamination introduced during carbon extraction by the RF combustion method and CuCl_2 dissolution.

Iron and Charcoal Materials Used to Estimate ^{14}C Contamination in Carbon Extraction Procedures

We used a standard iron (LECO-501-024) supplied by LECO Corporation, which is traceable to the National Institute of Standards and Technology (NIST), to test the existence of detectable ^{14}C contamination that may be introduced during carbon extraction by the RF combustion method and CuCl_2 dissolution. The LECO standard iron is granular and contains 3.35% carbon (dead carbon). Charcoal used to test the ^{14}C background level of the RF combustion system was prepared from wood fragments that were extracted from a pyroclastic flow deposit (Aso-4) formed at 85–90 ka (Shimoyama et al. 1994), and derived from Aso Volcano located in Central Kyushu, Japan.

Refining of Ancient Iron Materials with Modern Charcoal Fuel

The archaeological iron slag remains used for iron-refining experiments were collected from the Gennaitouge site, which was one of the iron smelting sites active during the second half of the 7th century AD, located in Otsu City, Shiga prefecture, Japan (Figure 1). Modern charcoal blocks used as fuel for the refining experiment were sourced from a 20- to 25-yr-old oak tree, from Zhejiang Province, People's Republic of China, in 2001.

Ancient Iron Products and Charcoal Remains from Archaeological Sites of Known Age

AMS ^{14}C ages were measured for iron slag and charcoal remains collected from the Gennaitouge site, which the iron ore probably originated. Charcoal samples were extracted from the blocks of iron slag, ensuring that the charcoal fragments tested were the remains of the fuel used in iron smelting at the site. In addition, oven remains and pottery fragments related with the iron smelting activities have been excavated (Shiga Preservation of Cultural Assets Association 2001).

EXPERIMENTS

Iron Refining Experiment

In 2001, the refining experiment was repeated twice on archaeological iron slag materials. We constructed a handmade oven, 60 cm high and 13 cm in inner diameter and made of diatomaceous earth.

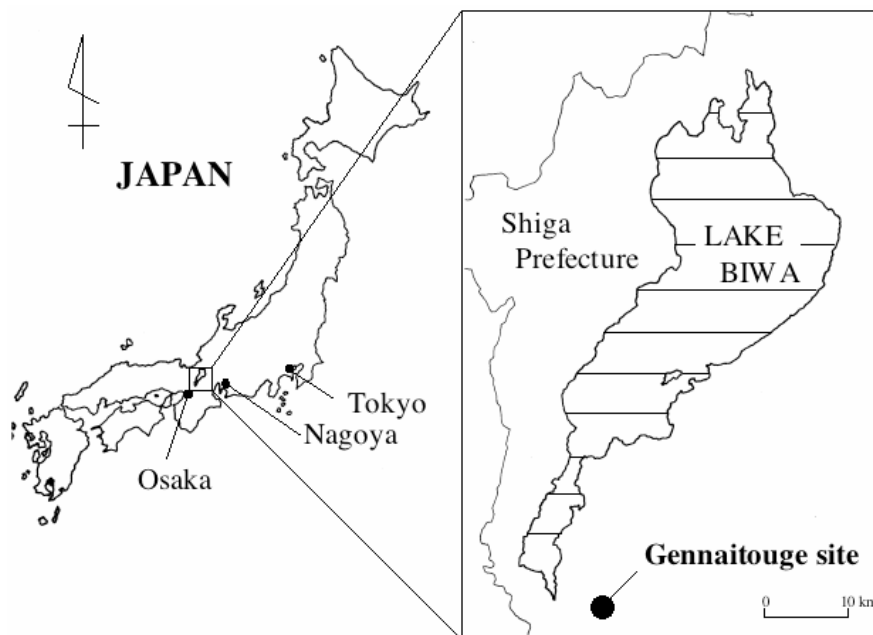


Figure 1 Location of the Gennaitouge site

The oven was first fired with charcoal. After being heated up to 1000 °C, fragmented charcoal and iron slag materials were put into the oven alternately. Air was supplied into the oven by a blower and the temperature inside the oven was maintained at 1400–1500 °C for about 5 hr. In the first run, 263.6 g of iron metal was obtained from 5.6 kg of iron slag materials and 8.9 kg of charcoal. In the second run, 222.7 g of iron metal was obtained from 3.2 kg of iron slag materials and 16.1 kg of charcoal.

Chemical Pretreatments and Graphite Preparation for AMS ^{14}C Dating

Charcoal Materials

To process charcoal samples for AMS ^{14}C dating, the charcoal was first broken into small fragments of about 1 mm³ and treated with 1.2N HCl solution at 60 °C for 2 hr to eliminate carbonate and other impurities. Next, the sample was treated with 1.2N NaOH solution at 60 °C for 2 hr to remove humic acid and other organic contaminants. A final treatment with 1.2N HCl solution was repeated under similar conditions. The samples were rinsed with distilled water and dried. Samples of about 7 mg were put in the Vycor glass tubes with about 700 mg of copper oxide wire. The glass tubes were evacuated, sealed with a torch, and then heated at 850 °C for 6 hr in an electric furnace. The resulting CO₂ gas was separated cryogenically and the amount of CO₂ collected was determined. The CO₂ gas was reduced to graphite by hydrogen under an iron catalyst (Kitagawa et al. 1993) and used for ^{14}C analysis by AMS.

Iron Materials

To prepare iron samples for AMS ^{14}C dating, we first checked the existence of metallic iron in the samples, because metallic iron preserves original carbon that was incorporated during iron production and, therefore, is suitable for ^{14}C dating. We cut the iron sample into small pieces of several

mm³ by using a metal cutting tool with a whetstone blade. The iron pieces were treated with 1.2N NaOH solution at 60 °C for 1 hr to eliminate humic acid and other organic contaminants. The samples were then treated with 1.2M HCl solution at 60 °C for 5–10 min to eliminate carbonate. Finally, the samples were rinsed with distilled water and dried.

CO₂ Extraction from Iron Samples by the RF Combustion Method

To accelerate combustion, a mixture of about 1.0 g of treated iron sample and 1.0 g of iron chips (LECO-502-231, high-purity iron chip accelerator with carbon content <8 ppm, LECO Corporation, USA) was placed in a preheated alumina crucible at 1000 °C for 10 hr. In order to remove carbonaceous contaminants from air dust, the crucible and contents were heated at 500 °C for 30 min in an electric oven. The sample was then taken from the oven and placed in a RF induction furnace (HF-10, LECO Corporation) that was connected to a glass vacuum line system used to purify the resultant CO₂. The iron sample and iron chips were heated to melting by RF induction for 4 min in a flow of ultra-high-purity oxygen (CO<0.1 ppm, CO₂<0.1 ppm, THC<0.1 ppm, Taiyo-toyo-sanso Co Ltd., Japan) at a flow rate of 200 mL/min, to ensure that all carbon in the iron sample was converted to CO₂. A schematic diagram of the glass line system used to purify CO₂ produced is shown in Figure 2. The vacuum system was evacuated in advance for 1 hr. Next, the combustion gas was passed through Pt/CuO at 450 °C to convert any remaining CO to CO₂. The CO₂ was then condensed with 3 cold traps aligned successively and cooled by liquid nitrogen, and the residual gas (mainly O₂) was pumped out slowly. The remaining CO₂ was further separated from water with an ethanol trap at –78 °C, then from any SO₂ that resisted a MnO₂ trap (Figure 2) with a normal pentane trap at –130 °C. The amount of CO₂ collected was measured volumetrically by a manometer. The CO₂ was reduced to graphite for analysis in the AMS ¹⁴C dating system.

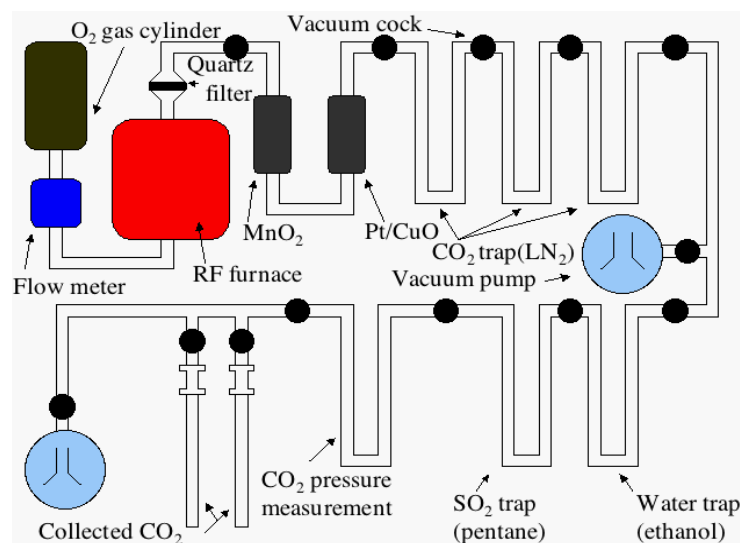


Figure 2 A schematic diagram of a RF induction furnace used to combust iron remains, and a glass line system used to purify CO₂ produced from iron remains.

The RF combustion method efficiently utilizes the O₂ and iron chips to combust iron samples completely. However, we recognized that both the O₂ and iron chips could possibly introduce modern carbon contamination to the CO₂, and a potential leak of the vacuum line system used for the iron combustion and purification of the produced CO₂ may do the same. Therefore, we tested for ¹⁴C con-

tamination by changing the amounts of iron chips (0–2000 mg) and the O₂ flow rate (100–300 mL/min), as shown in Table 1 and 2, respectively. Charcoal with dead carbon derived from the Aso-4 volcanic deposits was also treated in the RF combustion system as well as by the routine combustion procedure in a Vycor tube to compare the apparent ¹⁴C ages of graphite prepared by both procedures, as shown in Table 3.

Table 1 Yield of carbon and carbon-isotope ratios vs. amount of iron chip, for carbon extractions from standard iron using the RF combustion method. O₂ gas was supplied at a constant flow rate of 200 mL/min during the combustion period of 4 min.

Sample ^a code nr	Sample Iron chip		Carbon yield [mg C] (%) ^c	δ ¹³ C [‰]	R		Lab code [NUTA2-]
	amount [mg]	amount ^b [mg]			[(¹⁴ C/ ¹² C) _{sa} / (¹⁴ C/ ¹² C) _{st}]	¹⁴ C age [BP]	
LECO Fe 1-1	501.61	0.00	14.27 (89.4)	-25.7 ± 0.1	0.0041 ± 0.0002	44,170 ± 450	5664
LECO Fe 1-2	501.59	0.00	14.86 (88.4)	-25.8 ± 0.1	0.0033 ± 0.0002	45,780 ± 550	5666
LECO Fe 1-3	501.61	0.00	14.27 (84.9)	-25.7 ± 0.1	0.0021 ± 0.0002	49,590 ± 790	6081
LECO Fe 2-1	501.92	500.32	15.49 (92.1)	-25.0 ± 0.1	0.0035 ± 0.0002	45,510 ± 540	5667
LECO Fe 2-2	500.87	500.56	15.07 (89.8)	-25.0 ± 0.1	0.0032 ± 0.0002	46,110 ± 580	5668
LECO Fe 3-1	500.27	750.76	14.67 (87.5)	-25.2 ± 0.1	0.0031 ± 0.0002	46,380 ± 580	5669
LECO Fe 3-2	500.38	750.73	14.69 (87.6)	-25.3 ± 0.1	0.0025 ± 0.0002	48,110 ± 700	5670
LECO Fe 4-1	500.71	1000.28	16.00 (95.4)	-25.6 ± 0.1	0.0024 ± 0.0002	48,400 ± 730	5671
LECO Fe 4-2	500.67	1000.31	15.19 (90.6)	-25.6 ± 0.1	0.0031 ± 0.0002	46,420 ± 600	5672
LECO Fe 4-3	500.71	1000.28	16.00 (54.4)	-25.6 ± 0.1	0.0024 ± 0.0002	48,590 ± 730	6082
LECO Fe 5-1	500.43	1250.85	11.17 (66.6)	-25.4 ± 0.1	0.0030 ± 0.0002	46,630 ± 600	5674
LECO Fe 5-2	500.37	1250.67	11.39 (67.9)	-25.5 ± 0.1	0.0030 ± 0.0002	46,540 ± 590	5675
LECO Fe 6-1	500.71	1500.63	14.65 (87.3)	-25.6 ± 0.1	0.0036 ± 0.0002	45,240 ± 520	5676
LECO Fe 6-2	500.68	1500.21	15.01 (89.5)	-25.6 ± 0.1	0.0031 ± 0.0002	46,370 ± 590	5677
LECO Fe 7-1	500.61	1750.19	15.73 (93.8)	-25.5 ± 0.1	0.0028 ± 0.0002	47,320 ± 640	5678
LECO Fe 7-2	500.60	1750.21	15.70 (93.6)	-25.4 ± 0.1	0.0032 ± 0.0002	46,060 ± 560	5679
LECO Fe 8-1	500.82	2000.23	9.84 (58.7)	-25.9 ± 0.1	0.0042 ± 0.0002	43,960 ± 460	5680
LECO Fe 8-2	500.01	2000.71	10.34 (61.7)	-26.0 ± 0.1	0.0039 ± 0.0002	44,570 ± 490	5681
LECO Fe 8-3	500.82	2000.23	9.84 (58.7)	-25.9 ± 0.1	0.0032 ± 0.0002	46,130 ± 580	6083
		<Av.>^d	13.90 (82.9)	-25.5 ± 0.3	0.0031 ± 0.0006	46,280 ± 1430	

^aLECO standard iron (LECO-501-024): 3.35% C, 0.065% S.

^bLECO Pure iron chip accelerator (LECO-502-231): C<8 ppm, S<15 ppm.

^cCarbon collection efficiency in percent against total carbon contained in an Fe-standard material.

^dErrors quoted are 1 standard deviation.

Table 2 Yield of carbon and carbon-isotope ratios vs. amount of O₂ gas, for carbon extractions from standard iron using the RF combustion method. The flow rate of O₂ gas was changed from 100 to 300 mL/min. The combustion period was 4 min and no iron chips were added.

Sample ^a code nr	Sample amount [mg]	O ₂ [mL/min × 3 min]	Carbon yield [mg C] (%) ^b	δ ¹³ C [‰]	R		Lab code [NUTA2-]
					[(¹⁴ C/ ¹² C) _{sa} / (¹⁴ C/ ¹² C) _{st}]	¹⁴ C age [BP]	
LECO Fe 100-1	450.13	100	11.21 (74.1)	-28.9 ± 0.0002	0.0040 ± 0.0002	44,390 ± 470	5683
LECO Fe 100-2	450.12	100	12.46 (82.6)	-27.2 ± 0.0002	0.0032 ± 0.0002	46,230 ± 560	5684
LECO Fe 100-3	450.13	100	12.65 (83.9)	-27.2 ± 0.0002	0.0030 ± 0.0002	46,590 ± 580	5685
LECO Fe 200-1	450.16	200	13.67 (90.6)	-25.3 ± 0.0002	0.0034 ± 0.0002	45,680 ± 540	5686
LECO Fe 200-2	450.24	200	13.64 (90.4)	-25.4 ± 0.0002	0.0030 ± 0.0002	46,800 ± 600	5687
LECO Fe 200-3	450.11	200	13.45 (89.2)	-25.4 ± 0.0002	0.0031 ± 0.0002	46,300 ± 570	5688
LECO Fe 300-1	450.06	300	10.99 (72.9)	-25.9 ± 0.0002	0.0028 ± 0.0002	47,120 ± 610	5689
LECO Fe 300-2	450.22	300	14.49 (96.1)	-25.91 ± 0.0002	0.0028 ± 0.0002	47,200 ± 610	5691
LECO Fe 300-3	450.18	300	14.10 (93.5)	-25.2 ± 0.0003	0.0033 ± 0.0003	45,910 ± 530	6080
		<Av.>^c	12.96 (86.0)	-26.2 ± 0.0004	0.0032 ± 0.0004	46,200 ± 940	

^aLECO standard iron (LECO-501-024): 3035% C, 0.064% S.

^bCarbon collection efficiency in percent against total carbon contained in an Fe standard material.

^cErrors quoted are 1 standard deviation.

Table 3 Yield of carbon and carbon-isotope ratios for carbon extractions from charcoal (dead carbon) using the RF combustion method and a routine procedure of combustion and purification.

Sample ^a code nr	Sample amount [mg]	Iron chip amount ^b [mg]	O ₂ [mL/min × 3 min]	Carbon yield [mg C] (%) ^c	δ ¹³ C [‰]	R		Lab code [NUTA2-]
						[(¹⁴ C/ ¹² C) _{sa} / (¹⁴ C/ ¹² C) _{st}]	¹⁴ C age [BP]	
Aso4-Dry1	6.42	500.98	200	2.94 (45.8)	-25.7 ± 0.1	0.0049 ± 0.0002	42,790 ± 390	5869
Aso4-Dry2	5.79	500.96	200	5.11 (88.3)	-25.7 ± 0.1	0.0038 ± 0.0002	44,700 ± 470	5895
Aso4-Dry3	5.77	500.26	200	5.03 (87.2)	-25.8 ± 0.1	0.0044 ± 0.0002	43,520 ± 410	5896
Aso4-Dry4	5.47	500.21	200	4.61 (84.3)	-25.8 ± 0.1	0.0039 ± 0.0002	44,620 ± 460	5897
Aso4-Dry5	5.14	500.31	200	4.21 (81.9)	-25.7 ± 0.1	0.0047 ± 0.0002	43,140 ± 390	5901
Aso4-Dry6	5.85	500.04	200	4.70 (80.3)	-25.8 ± 0.1	0.0038 ± 0.0002	44,680 ± 450	5902
			<Av.> ^d	4.43 (78.0)	-25.8 ± 0.1	0.0043 ± 0.0005	43,870 ± 870	
Aso4-Line1	6.45	—	—	5.57 (86.4)	-25.7 ± 0.1	0.0028 ± 0.0002	47,190 ± 570	5903
Aso4-Line2	5.74	—	—	5.24 (91.3)	-25.5 ± 0.1	0.0030 ± 0.0002	46,570 ± 560	5904
Aso4-Line3	6.12	—	—	5.08 (83.0)	-25.9 ± 0.1	0.0033 ± 0.0002	46,000 ± 520	5905
Aso4-Line4	5.85	—	—	5.48 (93.7)	-25.6 ± 0.1	0.0023 ± 0.0002	48,920 ± 690	5906
Aso4-Line5	4.79	—	—	3.59 (74.9)	-25.7 ± 0.1	0.0023 ± 0.0002	48,870 ± 700	5910
Aso4-Line6	5.69	—	—	4.73 (83.1)	-25.9 ± 0.1	0.0023 ± 0.0002	48,720 ± 690	5911
			<Av.> ^d	4.95 (85.4)	-25.7 ± 0.1	0.0027 ± 0.0004	47,620 ± 1300	

^aAso4-Dry1-6 were prepared by the FR-combustion method. Aso4-Line1-6 were prepared with a purification line used routinely for charcoal and wood samples.

^bLECO Pure iron chip accelerator (LECO-502-231): C<8 ppm, S<15 ppm.

^cCarbon collection efficiency in percent against total weight of charcoal (Aso-4).

^dErrors quoted are 1 standard deviation.

CO₂ Extraction from Iron Samples by the Dissolution Method

¹⁴C contamination for the dissolution method was estimated with an iron standard (cast iron with carbon content of 3.35%) supplied by LECO Corporation. Both HCl and CuCl₂ solutions were used to dissolve iron samples. First, standard iron samples of about 200 mg (nr 1–3 in Table 4) were treated with 4N HCl at room temperature for about 2 weeks to be dissolved completely. The carbon residue was collected on quartz wool in a glass funnel of 6 mm outer diameter. Next, standard iron samples of about 200 mg were dissolved in CuCl₂ solutions of different concentrations (2.4–31.1 g of CuCl₂·2H₂O per 70 mL of water, nr 4–9 in Table 4) at 60 °C. A mixture of standard iron and CuCl₂·2H₂O was added with 70 mL of distilled water to dissolve the iron. Carbon in the iron was then precipitated as an aggregated colloid and metallic copper was deposited. The deposited copper was dissolved with 4N HCl at 60 °C, and the carbon residue was collected on quartz wool by filtration. We also tested the CuCl₂ solution that was filtered through a quartz wool filter before dissolving 200 mg of standard iron, to eliminate any possible carbon contaminants in the CuCl₂·2H₂O (nr 10–14 in Table 4). The separated solid carbon recovered by the quartz wool filter was combusted to produce CO₂. After purification, the CO₂ was converted to graphite and analyzed for ¹⁴C age by AMS.

¹⁴C Analysis with AMS

The graphite prepared from carbon samples (as described above) was pressed into an aluminum holder and used as a target for ¹⁴C dating with a Tandem AMS system (model 4130-AMS, HVEE, the Netherlands) at the Center for Chronological Research, Nagoya University (Nakamura et al. 2000). $R = [({}^{14}\text{C}/{}^{12}\text{C})_{\text{spl}}/({}^{14}\text{C}/{}^{12}\text{C})_{\text{std}}]$ was used to represent the carbon isotope ratio for a sample $[({}^{14}\text{C}/{}^{12}\text{C})_{\text{spl}}]$ in the ratio to the NIST oxalic acid standard $[({}^{14}\text{C}/{}^{12}\text{C})_{\text{std}}]$, after being corrected for machine ¹⁴C background and carbon isotopic fractionation, and then multiplied by a constant to normalize R=1.0 to represent the value of a sample formed in AD 1950 (Mook and van der Plicht 1999). Conventional ¹⁴C ages were also calculated from R, and calibrated to calendar yr using the INTCAL98 data sets (Stuiver et al. 1998). All errors quoted are ±1 σ.

Table 4 Yield of carbon and carbon-isotope ratios for carbon extractions from standard iron using the dissolution method. HCl solution was used for sample nr 1–3; non-filtrated CuCl_2 solution with different $\text{CuCl}_2 \cdot 2\text{H}_2\text{O}$ concentration for sample nr 4–9; and filtrated CuCl_2 solution with different $\text{CuCl}_2 \cdot 2\text{H}_2\text{O}$ concentration for sample nr 10–14. The $\text{CuCl}_2 \cdot 2\text{H}_2\text{O}$ used was from the same lot nr, except for 2 samples (nr 9 and 14).

Sample nr	Sample code nr	Filtration ^a [yes or no]	Iron amount [mg]	($\text{CuCl}_2 \cdot 2\text{H}_2\text{O}$)/Fe [g/g]	Carbon yield [mg C](%) ^b	$\delta^{13}\text{C}$ [‰]	R [($^{14}\text{C}/^{12}\text{C}$) _{sa} /($^{14}\text{C}/^{12}\text{C}$) _{st}]	^{14}C age [BP]	Lab code [NUTA2-]
1	HCl-1	—	201.18	0.0	3.00 (44.5)	-25.0 ± 0.1	0.0037 ± 0.0002	44,900 ± 480	6057
2	HCl-2	—	201.51	0.0	3.00 (44.4)	-25.1 ± 0.1	0.0040 ± 0.0002	44,280 ± 460	6058
3	HCl-3	—	201.43	0.0	2.99 (44.3)	-25.2 ± 0.1	0.0040 ± 0.0002	44,450 ± 460	6059
				<Av. ^c	(44.4)	-25.1 ± 0.1	0.0039 ± 0.0002	44,560 ± 360	
4	CuCl_2 -nf-1	no	200.67	12.0	4.83 (71.8)	-24.4 ± 0.1	0.0045 ± 0.0002	43,440 ± 420	6060
5	CuCl_2 -nf-2	no	200.97	36.0	5.99 (84.9)	-24.6 ± 0.1	0.0064 ± 0.0003	40,530 ± 320	6065
6	CuCl_2 -nf-3	no	200.43	60.0	6.27 (93.4)	-24.7 ± 0.1	0.0093 ± 0.0003	37,500 ± 250	6066
7	CuCl_2 -nf-4	no	201.68	96.0	6.12 (90.6)	-24.7 ± 0.1	0.0117 ± 0.0003	35,730 ± 220	6067
8	CuCl_2 -nf-5	no	115.36	180.0	3.49 (90.3)	-24.4 ± 0.1	0.0225 ± 0.0004	30,490 ± 150	6068
9	CuCl_2 -nf-6	no	201.63	155.0	5.56 (82.3)	-24.6 ± 0.1	0.0127 ± 0.0003	35,070 ± 210	6079
				<Av. ^c	(86.2)	-24.6 ± 0.1	0.0112 ± 0.0064	35,070 ± 7070	
10	CuCl_2 -f-1	yes	201.05	12.0	6.23 (92.5)	-24.6 ± 0.1	0.0033 ± 0.0002	45,950 ± 550	6069
11	CuCl_2 -f-2	yes	200.46	36.0	6.04 (89.9)	-24.7 ± 0.1	0.0036 ± 0.0002	45,300 ± 510	6074
12	CuCl_2 -f-3	yes	200.81	60.0	5.86 (87.1)	-24.6 ± 0.1	0.0036 ± 0.0002	45,130 ± 510	6075
13	CuCl_2 -f-4	yes	200.33	96.0	6.15 (91.6)	-24.7 ± 0.1	0.0046 ± 0.0002	43,160 ± 410	6076
14	CuCl_2 -f-5	yes	200.76	156.5	5.92 (88.0)	-24.7 ± 0.1	0.0052 ± 0.0002	42,180 ± 370	6077
				<Av. ^c	(89.8)	-24.7 ± 0.1	0.0039 ± 0.0008	44,640 ± 1580	

^aYes or no indicates with or without filtration of CuCl_2 solution during the Fe sample preparation procedure.

^bCarbon collection efficiency in percent against total carbon contained in Fe standard material.

^cErrors quoted are 1 standard deviation.

RESULTS AND DISCUSSION

Carbon Collection Efficiency from Iron

To test any possible dependence of the ^{14}C background level on iron chip amounts (Table 1) and O_2 flow rates (Table 2) in the RF combustion system, and CuCl_2 amounts for the dissolution method (Table 4), an iron standard (LECO-501-024) with carbon content of 3.35% was used. The tests resulted in a carbon collection efficiency of about 83–86% on average for both carbon-extraction methods, as shown in relevant tables. Though about 15% of carbon was lost, we detected no dependence of $\delta^{13}\text{C}$ values on the carbon collection efficiency for the separated carbon. Thus, no carbon isotopic fractionation was evident in our sample preparation procedures.

Three Types of Verifications for the RF Combustion Method

The R value was dependent on neither the amount of the iron chips nor the flow rate of O_2 gas used for carbon extraction by the RF combustion method (Tables 1, 2), i.e., an increase in contamination by modern carbon was not evident when using larger amounts of iron chips (less than 2000 mg) or O_2 gas (flow rate less than 300 mL/min). On the other hand, the average value of R for carbon which was extracted from charcoal (Aso-4) by the RF combustion method was 0.0043 ± 0.0002 , and that for carbon converted from charcoal by using an ordinary preparation line (a sealed-tube combustion with CuO in Vycor glass) was 0.0027 ± 0.0002 (Table 3). Thus, we detected a small increase in ^{14}C contamination from a leak in the glass line system used for the RF combustion procedure. However, the increase in contamination corresponds to only about a 4-yr shift towards a younger age when dating a sample of around 2000 BP. Thus, in case of dating archaeological iron products in Japan, the contamination effect was within the range of measurement error. Therefore, we conclude that the RF combustion method used at Nagoya University is applicable to ^{14}C dating of archaeological iron artifacts.

Verifications for the Dissolution Method

It was clear that CuCl_2 used in the experiment contained a small but detectable amount of modern carbon (nr 4–9 in Table 4). In fact, the R value increased from 0.0045 ± 0.0002 to 0.0225 ± 0.0002 when the maximum amount of CuCl_2 (30.7 g) was used for iron dissolution. The modern carbon contamination in CuCl_2 could, however, be considerably reduced by filtration of the CuCl_2 solution with a quartz wool filter (nr 10–14 in Table 4). In the measurement of archaeological products, the effect of residual modern carbon contamination, after the purification of the CuCl_2 solution, was estimated to be about a 3-yr shift to a younger age in dating a sample of around 2000 BP and was within the range of ^{14}C measurement error. Therefore, the dissolution method using prefiltered CuCl_2 solution is applicable to archaeological iron materials.

Iron Refining Experiment

The refining experiment suggested that the R values for 7 pieces of newly produced iron fragments selected randomly (an average value of $R [\langle R \rangle] = 1.245 \pm 0.007$, nr 32–38 in Table 5) were completely different from those for 8 pieces of original iron fragments ($\langle R \rangle = 0.838 \pm 0.002$, nr 15–22 in Table 5). They have changed from the original value to that of modern charcoal used as fuel for the refining ($\langle R \rangle = 1.193 \pm 0.004$, nr 23–28 in Table 5). The R values for refined iron samples were almost consistent with, or a bit larger than, those for the modern charcoal mixture, as shown in Figure 3. However, the former values were within the range of the R values (1.108 ± 0.003 to 1.569 ± 0.003 , nr 29–31 in Table 5) with respect to annual growth rings of wood from which the modern charcoal used for the refining was produced. The results of this experiment and of an iron

smelting experiment conducted by Yamada et al. (1999) suggested that carbon in the iron products was replaced with carbon from fuel charcoal that had been used for iron smelting or refining.

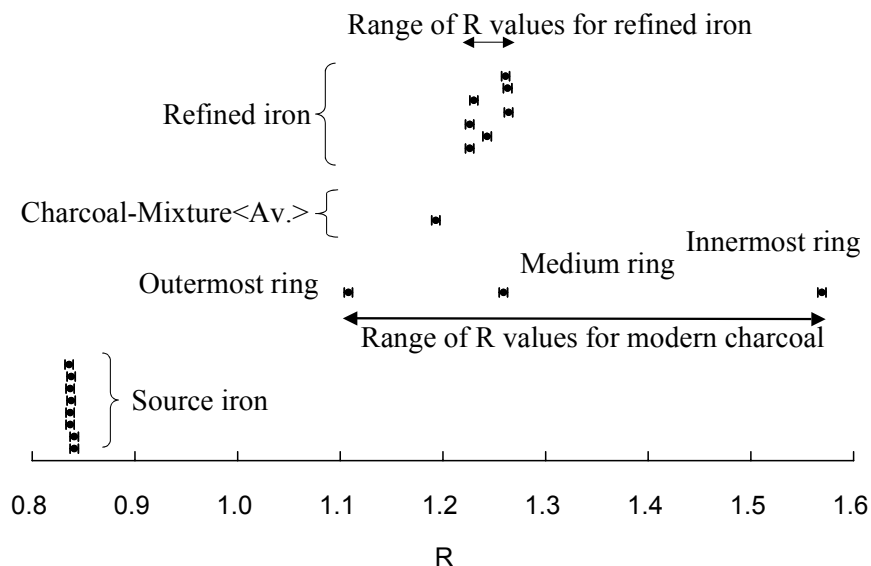


Figure 3 Comparison of R values for source iron and modern charcoal used as fuel for the refining experiment, and for produced iron. $R = (^{14}\text{C}/^{12}\text{C})_{\text{spl}} / (^{14}\text{C}/^{12}\text{C})_{\text{std}}$ to indicate the ^{14}C concentration for sample carbon, as defined in the text.

Dating of Iron Slag and Charcoal Remains from Archaeological Sites

^{14}C ages of iron slag and charcoal remains from the Gennaitouge site were dated from 1385 ± 31 BP to 1441 ± 29 BP and from 1365 ± 28 BP to 1609 ± 30 BP, respectively (Table 6). The calibrated ^{14}C ages of these samples ranged from the second half of the 6th to the 7th century AD, except for 1 charcoal sample (nr 11), and were consistent with the occupation period (around 7th century) of the site as estimated by archaeological evidence. The charcoal (nr 11) may have been derived from the inner part of a large tree, thus showing an old wood effect. Some charcoal samples were collected from the inside of iron slag blocks to certify that the charcoal fragments were the remains of charcoal blocks that were used as fuel for the iron smelting. Among such charcoal and iron slag pairs, the ^{14}C ages of charcoal samples were older by 26 to 111 yr than those of iron slag samples for 5 pairs (nr 2, 3, 4, 7, and 8 in Table 6). The charcoal ages were younger by 54 and 39 yr for 2 pairs (nr 9 and 10). In general, the ^{14}C ages for charcoal samples appeared older than those for iron slag materials, but the ^{14}C ages for the pairs (nr 4, 7, 8, 9, and 10) were quite consistent with each other. These findings suggest that we can estimate the ages of iron remains directly by dating the carbon extracted from the remains. The archaeological relevance of ^{14}C ages of iron materials from the Gennaitouge site will be discussed in a future publication.

CONCLUSION

We have estimated the ^{14}C contamination levels, i.e., the amounts of modern carbon contamination induced by the RF combustion and dissolution procedures in extracting carbon components from iron materials for AMS ^{14}C dating. The average values of R which implied the ^{14}C contamination level were 0.0043 ± 0.0002 ($43,870 \pm 870$ BP in ^{14}C age; Table 3) and 0.0039 ± 0.0008

Table 5 Change in ^{14}C concentration of carbon components from original iron to newly-produced iron by the iron-refining experiment. Yield of carbon and carbon-isotope ratios are shown for the carbon extractions using the RF combustion method from original iron (sample nr 15–22) and from produced iron (nr 32–38), as well as those using the routine charcoal preparation method from modern charcoal used as fuel (nr 23–31).

Sample nr	Sample name ^a	Sample amount [mg]	Carbon yield [mgC]	$\delta^{13}\text{C}$ [‰]	R [($^{14}\text{C}/^{12}\text{C}$) _{sa} /($^{14}\text{C}/^{12}\text{C}$) _{st}]	Lab code [NUTA2-]
15	Iron ¹ -2D	729.51	1.18	-33 ± 1	0.842 ± 0.003	3393
16	Iron ¹ -3D	384.92	1.28	-29 ± 1	0.841 ± 0.003	3394
17	Iron ¹ -4D-1	500.72	10.10	-27.7 ± 0.1	0.837 ± 0.003	3395
18	Iron ¹ -4D-2	692.73	1.54	-20.8 ± 0.1	0.837 ± 0.003	3409
19	Iron ² -1D	257.31	0.78	-25 ± 1	0.838 ± 0.003	3396
20	Iron ² -2D	581.62	1.27	-27 ± 1	0.837 ± 0.003	3397
21	Iron ² -3D	555.72	1.18	-31 ± 1	0.838 ± 0.003	3398
22	Iron ² -4D	908.30	6.47	-26.1 ± 0.1	0.836 ± 0.003	3401
			<Av.>^b	-27.5 ± 3.7	0.838 ± 0.002	
23	Charcoal-Mix-1	6.46	4.79	-26.3 ± 0.1	1.187 ± 0.005	3088
24	Charcoal-Mix-2	6.54	4.55	-25.5 ± 0.1	1.191 ± 0.005	3089
25	Charcoal-Mix-3	6.61	4.58	-26.1 ± 0.1	1.185 ± 0.005	3090
26	Charcoal-Mix-4	6.48	5.32	-26.0 ± 0.1	1.187 ± 0.005	3104
27	Charcoal-Mix-5	6.58	6.00	-26.5 ± 0.1	1.194 ± 0.004	3462
28	Charcoal-Mix-6	6.58	6.03	-26.5 ± 0.1	1.212 ± 0.004	3463
			<Av.>^b	-26.3 ± 0.2	1.193 ± 0.010	
29	Charcoal-innermost ring	7.35	6.98	-27 ± 1	1.569 ± 0.005	3658
30	Charcoal-medium ring	7.46	6.89	-25 ± 1	1.259 ± 0.004	3659
31	Charcoal-outermost ring	7.21	6.73	-24 ± 1	1.108 ± 0.004	3660
32	Refined iron ¹ -1D	1162.77	17.32	-23.0 ± 0.1	1.226 ± 0.005	3094
33	Refined iron ¹ -2D	1099.81	2.40	-20.9 ± 0.1	1.243 ± 0.005	3098
34	Refined iron ¹ -3D	697.31	7.54	-26.5 ± 0.1	1.226 ± 0.005	3097
35	Refined iron ² -1D	1115.18	7.82	-25.8 ± 0.1	1.264 ± 0.005	3095
36	Refined iron ² -2D	1099.81	13.42	-27.8 ± 0.1	1.230 ± 0.005	3096
37	Refined iron ² -3D	1366.64	21.11	-29.6 ± 0.1	1.263 ± 0.004	3410
38	Refined iron ² -4D	1059.06	23.11	-31.4 ± 0.1	1.261 ± 0.004	3411
			<Av.>^b	-26.4 ± 3.6	1.245 ± 0.018	

^aThe iron refining experiment was done 2 times (indicated superscript 1 and 2). “Charcoal-Mix” was a portion of shuffled and comminute mixture from 1 modern charred wood with about 20–25 annual rings. Charcoal-innermost ring, -medium ring, and -outermost ring indicated charcoal samples collected from innermost, medium, and outermost annual rings of 1 modern charred wood.

^bErrors cited are 1σ .

($44,640 \pm 1580$ BP; Table 4) for graphite targets prepared by the RF combustion and dissolution procedures, respectively. The contamination corresponded to only about a 3- to 4-yr shift towards a younger age in dating a sample of around 2000 BP. In dating archaeological iron artifacts, the effect of contamination was within the error range.

We described here the tests conducted using an iron standard with high carbon content (3.35%). However, we believe that we can also prepare wrought-iron samples in our RF combustion system. We can melt up to 1 g of an iron sample mixed with the same weight of an iron chip accelerator, and can date the sample if 1 mg of carbon will be recovered from it. In fact, we have collected around 1 mg of carbon for several iron slag samples and obtained consistent ^{14}C concentrations and ^{14}C ages as shown in Table 5 (nr 15, 16, 18, 19, 20, and 21) and Table 6. Of course, we consider that more systematic studies are necessary for iron samples with low carbon content (wrought-iron samples).

Table 6 AMS ^{14}C ages and calibrated calendar yr for iron slag and charcoal remains collected from the Gennaitouge archaeological site, Otsu city, Shiga prefecture, Japan.

Sample nr	Sample code nr ^a	Sample amount [mg]	Carbon yield [mg C]	$\delta^{13}\text{C}$ [‰]	^{14}C age ^b [BP]	Calibrated age range ^b [cal AD]	Lab code [NUTA2-]
1-1	Charcoal included ¹ -1	6.75	4.15	-27.4 ± 0.1	1498 ± 29	540(563,590,596)604,612(0)616	3007
2-1	Iron ¹ -2	729.51	1.18	-33 ± 1	1385 ± 31	643(657)664	3393
2-2	Charcoal included ¹ -2	6.57	4.23	-25.6 ± 0.1	1487 ± 29	542(599)619	3009
3-1	Iron ¹ -3	384.92	1.28	-29 ± 1	1387 ± 32	642(657)663	3394
3-2	Charcoal included ¹ -3	6.81	5.93	-26.4 ± 0.1	1498 ± 29	540(563,590,596)604,612(0)616	3450
4-1	Iron ¹ -4-1	500.72	10.10	-27.7 ± 0.1	1430 ± 29	604(640)654	3395
4-2	Iron ¹ -4-2	692.73	1.54	-20.8 ± 0.1	1428 ± 30	604(641)655	3409
4-3	Charcoal included ¹ -4	6.35	4.58	-26.7 ± 0.1	1465 ± 33	561(594,595 (603) 641	3091
5-1	Charcoal-free ¹ -5	6.43	4.69	-27.5 ± 0.1	1503 ± 29	539(561,595)602	3013
6-1	Charcoal-free ¹ -6	7.31	4.52	-27.0 ± 0.1	1482 ± 29	543(553,556(600)621,634(0)636	3451
7-1	Iron ² -1	257.31	0.78	-25 ± 1	1423 ± 30	613(642)656	3396
7-2	Charcoal included ² -1	6.40	4.22	-26.7 ± 0.1	1490 ± 29	541(598)618	3008
8-1	Iron ² -2	581.62	1.27	-27 ± 1	1430 ± 29	604(640)654	3397
8-2	Charcoal included ² -2	6.44	4.78	-25.6 ± 0.1	1456 ± 30	598(617)642	3012
9-1	Iron ² -3	555.72	1.18	-31 ± 1	1419 ± 30	617(643)657	3398
9-2	Charcoal included ² -3	6.55	6.50	-26.5 ± 0.1	1365 ± 28	654(661)673	3454
10-1	Iron ² -4	908.30	6.47	-26.1 ± 0.1	1441 ± 29	601(623,628,638)647	3401
10-2	Charcoal included ² -4	8.20	8.20	-26.1 ± 0.1	1402 ± 29	625(626,639(651)660	3455
11-1	Charcoal ² -free-5	5.34	2.79	-27.9 ± 0.1	1609 ± 30	416(428)440,451(0)46 485(486,504(0)506,519(0)528	3014
12-1	Charcoal-free ² e-6	10.76	6.40	-27.6 ± 0.1	1485 ± 28	543(599)620	3456

^aAll samples were excavated from the same horizon, but from 2 different locations, as indicated by superscript 1 and 2. Charcoal samples were included in iron slags, except for charcoal-free samples nr 5-1, 6-1, 11-1, and 12-1.

^bErrors quoted are 1 standard deviation.

We also conducted an iron refining experiment and confirmed that carbon in the iron products had been replaced with fuel charcoal that had been used for iron smelting or refining. Finally, we applied these methods to the measurement of ^{14}C ages of iron slag and charcoal remains from the Gennaitouge iron production site in Shiga Prefecture, Japan. The calibrated ^{14}C ages of these samples ranged from the second half of the 6th to the 7th century AD and were consistent with their archaeological ages. We conclude that the carbon extraction system from archaeological iron materials developed at Nagoya University is reliably applicable to estimate production ages of archaeological iron artifacts.

ACKNOWLEDGEMENTS

We acknowledge Mr Kazuto Omiti of Shiga Preservation of Cultural Assets Association for his kind help and useful advice in collecting and handling samples, as well as Drs Takefumi Oda, Masayo Minami, and Etsuko Niu of Nagoya University for their kind support during sample preparation and ^{14}C measurements. This study was supported partly by a ‘‘Grant-In-Aid for Scientific Research’’ from the Japanese Society for Promotion of Science (subject nr 09610421, 11610427, 13480020, and 14608004).

REFERENCES

- Cheoun MK, Kim JC, Kang J, Kim IC, Park JH, Song YM. 2001. Pretreatment of iron artifacts at SNU-AMS. *Radiocarbon* 43(2A):217–9.
- Cook AC, Wadsworth J, Southon JR. 2001. AMS radiocarbon dating of ancient iron artifacts: a new carbon extraction method in use at LLNL. *Radiocarbon* 43(2A):221–7.
- Cook AC, Wadsworth J, Southon JR, van der Merwe NJ. 2003a. AMS radiocarbon dating of rusty iron. *Journal of Archaeological Science* 30(1):95–102.
- Cook AC, Southon JR, Wadsworth J. 2003b. Using radiocarbon dating to establish the age of iron-based ar-

- tifacts. *Journal of Metallurgy* 55(5):15–22.
- Craddock PT, Wayman ML, Jull AT. 2002. The radiocarbon dating and authentication of iron artifacts *Radiocarbon* 44(3):717–32.
- Cresswell RG. 1991. The radiocarbon dating of iron artifacts using accelerator mass spectrometry. *Historical Metallurgy* 25:75–85.
- Cresswell RG. 1992. Radiocarbon dating of iron artifacts. *Radiocarbon* 34(3):898–905.
- Hüls CM, Grootes PM, Nadeau MJ, Bruhn F, Hasselberg P, Erlenkeuser H. Forthcoming. AMS radiocarbon dating of iron artefacts. *Nuclear Instruments and Methods in Physics Research B*.
- Igaki K, Nakamura T, Hirasawa M, Kato M, Sano M. 1994. Radiocarbon dating study of ancient iron artifacts with accelerator mass spectrometry. *Proceedings of the Japan Academy* 70(B):4–9.
- Kitagawa H, Masuzawa T, Nakamura T, Matsumoto E. 1993. A batch preparation method for graphite targets with low background for AMS ^{14}C measurement. *Radiocarbon* 35(2):295–300.
- Nakamura T, Hirasawa M, Igaki K. 1995. AMS Radiocarbon dating of ancient oriental iron artifacts at Nagoya University. *Radiocarbon* 37(2):629–36.
- Nakamura T, Niu E, Oda H, Ikeda A, Minami M, Takahashi AH, Adachi M, Pals L, Gott dang G, Suy a N. 2000. The HVEE Tandetron AMS system at Nagoya University. *Nuclear Instruments and Methods in Physics Research B* 172:52–7.
- Oda H, Nakamura T, Furukawa M. 1999 A wet method of carbon extraction from iron artifacts for ^{14}C age measurement with AMS. *Journal of Radioanalytical and Nuclear Chemistry* 239(3):561–4.
- Ono N, Sano M, Kuwabara M, Nakamura T, Oda H, Hirasawa M. 1999. Metallurgical and chronological studies on processing of ancient iron artifacts. *Summaries of Researches Using AMS at Nagoya University* X:77–86. In Japanese with English abstract.
- Shiga Preservation of Cultural Assets Association. 2001. *Gennaitouge Site*. 389 p. In Japanese.
- Shimoyama S, Watanabe K, Nishida T, Harada D, Tsuruta K, Komatsu J. 1994. Burnt big trees by the Aso-4 pyroclastic flow. *The Quaternary Research* 33(2):107–12. In Japanese with English abstract.
- Stuiver M, Reimer PJ, Bard E, Beck JW, Burr GS, Hughen KA, Kromer B, McCormac G, van der Plicht J, Spurk M. 1998. INTCAL98 radiocarbon age calibration, 24,000–0 cal BP. *Radiocarbon* 40(3):1041–83.
- Yamada T, Tsukamoto T, Ono N, Oda H, Nakamura T. 1999. Verifications of ^{14}C age measuring theories of iron products by an iron-manufacturing experiment and views through the experiment. *Summaries of Researches Using AMS at Nagoya University* X:87–96. In Japanese with English abstract.
- Yamada T, Tsukamoto T, Oda H, Nakamura T. 2001. Radiocarbon dating of iron manufacture remains. *Summaries of Researches Using AMS at Nagoya University* XII:103–12. In Japanese with English abstract.
- Yamada T. 2001. Report of Grant-in-Aid for Scientific Research [Grant-in-Aid for Scientific Research(C)]: 60–3. In Japanese.
- Yokoi T, Nakamura T. 1998. AMS ^{14}C dating of iron artifacts and other samples related with ancient iron production in Aichi Prefecture. *Summaries of Researches Using AMS at Nagoya University* IX:18–26. In Japanese with English abstract.
- Van der Merwe NJ, Stuiver M. 1968. Dating iron by the carbon-14 method. *Current Anthropology* 9:48–53.
- Yoshida K. 1992. Measurement of ^{14}C age by accelerator mass spectrometry. *Bulletin of the National Museum of Japanese History* 38:171–98. In Japanese with English abstract.

¹⁴C DATING COMPARED TO ART HISTORICAL DATING OF ROMAN AND COPTIC TEXTILES FROM EGYPT

Mark Van Strydonck¹ • Antoine De Moor² • Dominique Bénazeth³

ABSTRACT. A representative selection of Roman and Coptic textiles is used to compare the radiocarbon dating results with the chronology proposed by art historians. In some cases, the comparison was made on individual objects, but in other cases, groups of stylistically and/or technologically related textiles were compared. In the case of the latter, the interquartile range was calculated. The results of this comparison show that some individual samples and groups are dated older than expected, while for another group the opposite is the case. One group was matching well with the presumed period as a whole, but not on the basis of the individual pieces. The analyses showed the necessity of ¹⁴C dating to obtain a more accurate dating of Coptic textiles.

INTRODUCTION

The Coptic period (or Byzantine period) is a 400-yr span of Egyptian Christian culture, starting from the division of the Roman Empire in AD 395 to the defeat of the Byzantine Empire by the Muslim invasion in AD 641. The word “copt” itself referred to native Egyptians, as opposed to the Greek or Arab invaders and is derived from the Arab word “Qibt” (Egyptian), related to the Greek word “Aigyptos.” Although the Muslim defeat of Byzantium introduced Islam as well as Arabic as a dominant influence, Egyptian Coptic culture has persevered to the present.

Some art historians tend to rely upon a chronology for Coptic textiles based on stylistic features and are skeptical of the reliability of radiocarbon analysis, much in the same way that some Egyptologists dismiss ¹⁴C data (van der Plicht and Bruins 2001). That chronology is primarily based on a comparison of stylistic features with other media, such as paintings, sculptures, mosaics, and architectural features (De Moor et al., forthcoming). More recently, technological studies on weaving techniques (De Jonghe and Verhecken-Lammens 1993) and dye analyses have been added (Wouters 1993) as chronological tools.

It has often been said that the apparent lack of precision of ¹⁴C analysis has contributed to this skepticism, but this is not entirely true. In 1958, du Bourguet had a Coptic tunic ¹⁴C dated, resulting in a ¹⁴C date of AD 610 ± 150. This result was rejected, not on the grounds that the result was not precise enough, but because he believed, on stylistic grounds, that the result should have been younger than the 10th to 11th century AD (du Bourguet 1958).

The idea that textiles can be dated accurately and precisely on stylistic and technical grounds has less merit than for other media. Contrary to paintings and sculptures, textiles—even in historical periods—seem less influenced by technical and artistic changes. Some methods and weaving techniques stay in use for quite some time (Van Strydonck and De Jonghe 1995). Furthermore, most Roman and Coptic textiles from Egypt were not found during well-controlled archaeological excavations, but derive from unscientific excavations and grave robberies and lack all contextual dating evidence. Finally, except for some Abbasid and Fatimid textiles, the year of manufacture is never found on Coptic textiles. As a result, art historians tend to date textiles to only within a range of 1–2 centuries.

¹Royal Institute for Cultural Heritage, Jubelpark 1, B-1000 Brussels, Belgium.

²University of Ghent, Windekekouter 90, 9860 Scheldewindeke, Belgium.

³Département des antiquités égyptiennes, section Copte. Musée du Louvre, F-75058 Paris cédex 1, France.

A first attempt by our group to compare both dating methods was performed about 10 yr ago. Unfortunately, the data set was too small for the variety of textiles dated so that it was impossible to draw definite conclusions, but in some cases, an important discrepancy between both methods had already been revealed (Van Strydonck et al. 1993).

MATERIALS AND TECHNIQUES

Pretreatment

Textiles are considered to be appropriate material for dating because the ^{14}C content of the sample reflects only 1 growth season, and the difference between the age of the raw material and the time of manufacturing of the fabric is minimal. Since the textiles come from a dry and relatively isolated context with only minimal contact with the environment, most are very well preserved. From a ^{14}C point of view, it is more likely that a material will be contaminated during its handling, archiving, and conservation attempts (environmental oils and dirt, reweaving with modern fibers, glues, cleaning), from trading activities or museum storage. Thus, it is important to consider these possible contaminants when selecting and pretreating a textile.

During sampling, deteriorated and restored parts of the textiles were avoided. The chemical pretreatment depended on the nature of the textile fibers. Textiles made of plant fibers were bleached during successive washes in a hot 1M KOH solution and a NaClO_2 solution [2.7g + 3.7 mL HCl (37%) / 100 mL H_2O]. Textiles made of animal fibers were treated ultrasonically in a 0.2% Tinoventine solution. After the treatment, the samples were repeatedly washed in demineralized water.

Graphitization and Measurement

Graphite was prepared using routine analysis (Van Strydonck and van der Borg 1990–1991) and measured by accelerator mass spectrometry (AMS) at the Van de Graaff Laboratory, Utrecht (UtC) and the Leibniz Labor für Altersbestimmung und Isotopenforschung, Kiel (KIA).

Comparison

The nature of the date ranges obtained by ^{14}C is different from the ranges proposed by art historical criteria. For ^{14}C , the estimation of the true age is given by a probability distribution and this is not so for an art historical interpretation. On the other hand, the proposed art historical date range implies that there is a belief that the manufacturing dates of related fabrics are not equally distributed over the proposed range, but that there exists an introduction phase, a blooming period, and a period of decline. So as a working hypothesis, we adopted a normal distribution for the art historical estimation of the date, whereby the range is considered to be the $2\text{-}\sigma$ range and the middle of the range is the median. The difference between a single ^{14}C date and the art historical date was then calculated by OxCal. This is a different approach than in a previous study (Van Strydonck 1995).

In the case of a group of related samples, we calculated the interquartile range and the 95% probability from the summed probability of all dates.

RESULTS AND DISCUSSION

The textiles used in these study come from 2 collections: the Katoen Natie (Antwerp, Belgium) and the Louvre (département des antiquités égyptiennes, Paris, France).

First Group: Roman Textiles

Socks

Table 1 Roman sock.

Sample	Lab code	¹⁴ C age (BP)	Calibrated age (68.2%)	Calibrated age (95.4%)	Art historical date	Difference
721-01	UtC-8799	1830 ± 50	AD 90 (0.9%) AD 100 AD 120 (67.3%) AD 250	AD 70 (95.4%) AD 340	4th–6th century AD	370 (68.2%) 150 460 (95.4%) 50



Figure 1 A roman sock from Egypt (Katoen Natie DM 721-01)

These socks, “knitted” in wool with only 1 needle, are usually dated to the 4th–6th century AD. This slow technique was later replaced by the much faster true knitting. The Royal Ontario Museum in Toronto has 11 socks made with the single-needle knitting technique and stylistically dated to the 4th–5th century AD (Burnham 1972). The Victoria and Albert Museum in London has 4 similar socks dated in the same period based on archaeological grounds (Kendrick 1921). The Museo Egizio in Firenze has 1 child’s sock (inv. 12917) and a pair of larger socks (inv. 12920), both dated to the 4th–6th century AD (Del Francia Barocas 1998). There is 1 sock in the Städtischen Museum, which Simeonstift Trier dated to the Coptic period (Nauerth 1989). One similar sock is kept in the Royal Museum of Art and History in Brussels. This sock has been published 3 times and is dated to the 4th–5th century AD (Bruwier 1997; Lafontaine-Dosogne 1988; Rassart and Debergh 1988). One other sock from the Musée des Tissu de Lyon is dated to the Roman or Coptic period.

Silk Samite

Table 2 Silk Samite.

Sample	Lab code	¹⁴ C age (BP)	Calibrated age (68.2%)	Calibrated age (95.4%)	Art historical date	Difference
C269	KIA-11237	1730 ± 25	AD 250 (60.6%) AD 350 AD 360 (7.6%) AD 390	AD 240 (95.4%) AD 390	4th–6th century AD	220 (68.2%) 50 290 (95.4%) 0

The sample is a fragment from a silk weft-faced compound textile in 2 colors. A fragment from the same textile is in the Kerr collection and dated to the 4th–5th century AD (King and King 1990). One other fragment from the same textile is in the Royal Scottish Museum and dated to the 6th century AD (Bourriau 1977). Two other fragments from the same textile are in the Newark Museum (USA) and dated to the 6th to early 7th century AD (Auth 1978).



Figure 2 Silk samite from Egypt (Katoen Natie 795 / C269)

Two Roman Textiles Showing a Similar Printing Technique



Figure 3 Example of a Roman textile showing a particular printing technique (Katoen Natie 377 / DM200R)

Table 3 Two Roman textiles with similar printing techniques.

Sample	Lab code	¹⁴ C age (BP)	Calibrated age (68.2%)	Calibrated age (95.4%)	Art historical date	Difference
DM201R	UtC-9693	1700 ± 35	AD 260 (12.8%) AD 280 AD 320 (55.4%) AD 410	AD 250 (95.4%) AD 430	4th–5th cen. AD	120 (68.2%) 0 200 (95.4%) 10
DM200R	UtC-4858	1695 ± 40	AD 260 (11.9%) AD 280 AD 320 (56.3%) AD 410	AD 250 (95.4%) AD 430	5th–7th cen. AD	340 (68.2%) 60 450 (95.4%) 0

DM201R consists of a linen fragment from a shawl or a curtain. The sample was dyed with 2 shades of indigo. A similar piece is kept in the Museum of Cluny and dated on art historical grounds to the 4th–5th century AD (Lorquin 1992). DM200R is a linen fragment printed using the same technique as DM201R. The motif (not the colors nor the pattern) can be compared with that on 2 wooden panels from the monastery of Baouît (Rutschowskaya 1992). The proposed date is 6th–7th century. The motif was also found on a ceiling in Abou Girgeh dated to the 5th–6th century AD (Leclercq 1924).

Second Group: Roman and Coptic textiles

Twelve Stylistically Related Monochrome Purple (Indigo & Madder) Textiles

The results of this group of textiles are represented in Table 4 and Figure 4. Examples of this type of fabric are given in Figures 5, 6, and 7.

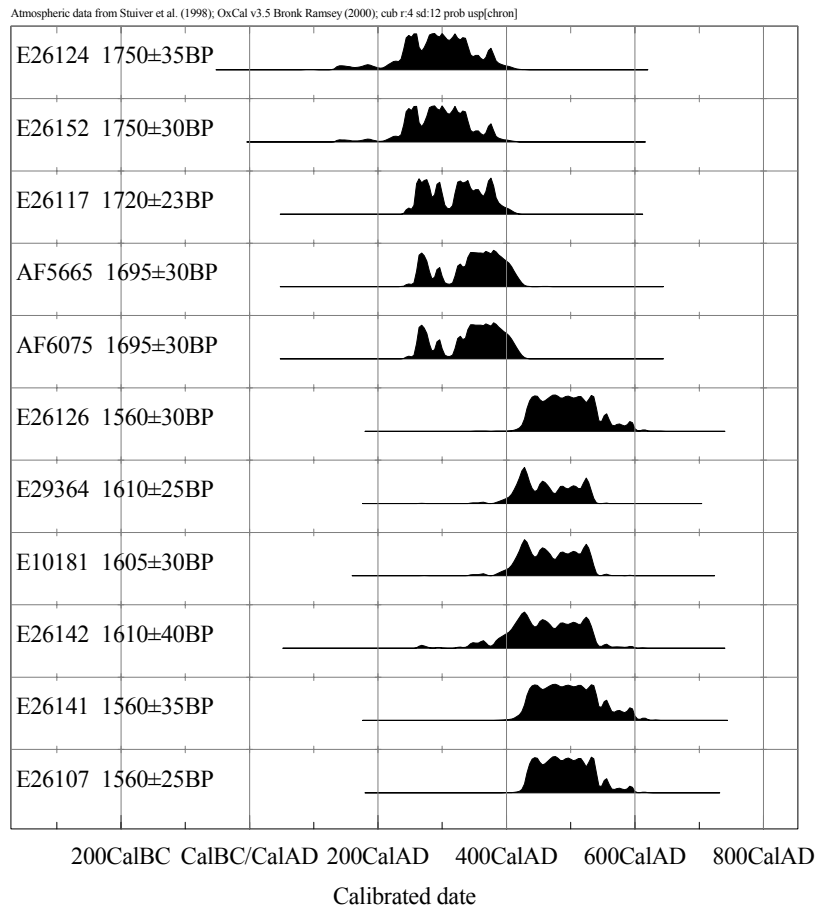


Figure 4 Results from the second group



Figure 5 Monochrome purple textile E26117 (star)

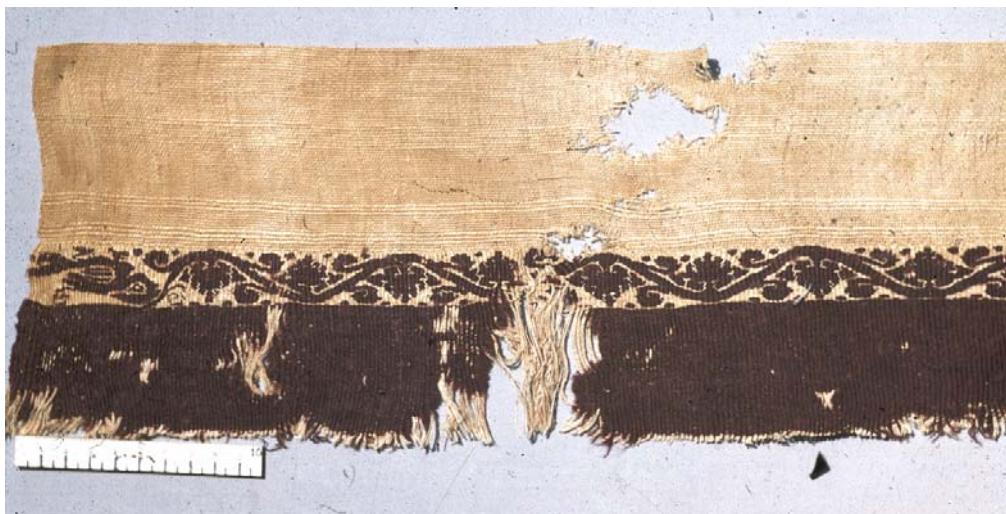


Figure 6 Monochrome purple textile E26126

This group forms a large part of the so-called “Coptic textiles” from Roman and Byzantine Egypt. It contains monochromatic tapestries, decorations for tunics or shawls woven on linen tabbies¹,

¹For technical terms such as tabby, looped weft, fringe, sprang, etc., see *Fabrics: A Vocabulary of Technical Terms, English, French, Italian, Spanish*. Centre international d’Etude des textiles anciens, 34, rue de la Charité, Lyon, France.



Figure 7 Monochrome purple textile E26142 (horseman)

Table 4 Stylistically related monochrome purple textiles.

Sample	Lab code	¹⁴ C age (BP)	Calibrated age (68.2%)	Calibrated age (95.4%)	Art historical date	Difference
E26124	KIA-14833	1750 ± 35	AD 240 (17.5%) AD 265 AD 270 (50.7%) AD 345	AD 170 (1.4%) AD 200 AD 210 (94.0%) AD 410	5th cen. AD	210 (68.2%) 90 270 (95.4%) 30
E26152	KIA-14842	1750 ± 30	AD 240 (16.9%) AD 265 AD 275 (51.3%) AD 340	AD 210 (95.4%) AD 400	3rd–4th cen. AD	80 (68.2%) 0 150 (95.4%) –10
E26117a	KIA-14839	1720 ± 35	AD 250 (28.0%) AD 300	AD 240 (95.4%) AD 400	3rd–4th cen. AD	65 (68.2%) 0
E26117b	KIA-15217	1720 ± 30 mean: 1720 ± 23	AD 320 (40.2%) AD 390			120 (95.4%) –10
AF5665	KIA-14835	1695 ± 30	AD 260 (11.8%) AD 280 AD 330 (56.4%) AD 410	AD 250 (95.4%) AD 420	3rd–4th cen. AD	60 (68.2%) –5 120 (95.4%) –10
AF6075	KIA-14837	1695 ± 30	AD 260 (11.8%) AD 280 AD 330 (56.4%) AD 410	AD 250 (95.4%) AD 420	7th cen. AD	370 (68.2%) 230 420 (95.4%) 210
E26126	KIA-14838	1560 ± 30	AD 435 (12.7%) AD 455 AD 460 (55.5%) AD 540	AD 420 (95.4%) AD 600	7th cen. AD	210 (68.2%) 105 250 (95.4%) 50
E29364	KIA-15209	1610 ± 25	AD 410 (39.8%) AD 470 AD 480 (28.4%) AD 540	AD 400 (95.4%) AD 540	—	—
E10181	KIA-14836	1605 ± 30	AD 410 (33.3%) AD 470 AD 480 (34.9%) AD 540	AD 390 (95.4%) AD 540	7th cen. AD	240 (68.2%) 120 290 (95.4%) 80
E26142	KIA-14843	1610 ± 40	AD 410 (35.9%) AD 470 AD 480 (32.3%) AD 540	AD 340 (95.4%) AD 560	6th cen. AD	150 (68.2%) 30 200 (95.4%) –10
E26141	KIA-18962	1560 ± 35	AD 430 (68.2%) AD 540	AD 420 (95.4%) AD 600	6th cen. AD	105 (68.2%) 15 140 (95.4%) –10
E26107	KIA-18963	1560 ± 25	AD 435 (12.4%) AD 455 AD 460 (48.4%) AD 520 AD 525 (7.4%) AD 540	AD 420 (95.4%) AD 570	6th cen. AD	110 (68.2%) 20 140 (95.4%) –10

which sometimes present looped wefts. The color is obtained by woolen wefts dyed with a mixture of madder and indigo, providing various shades of purple, violet, dark blue, etc. This “purple” color contrasts with the white natural linen. Tiny details are designed with a flying shuttle of undyed linen thread.

Five of these textiles (E26124, E26152, AF6075, AF5665, and E26117—accepting that E26117a and b are from the same fabric) form a distinct group within these monochrome textiles. The combination of these 5 dates gives an interquartile range from AD 270–355 and a 95% probability range from AD 220–395.

Du Bourguet (1964) dated three of them to the 3rd–4th century AD, one a century later, and another 3 centuries later.

The dating of E26117a and b (2 fragments with a very similar motif) is the same, supporting the hypothesis that they originally belonged to the same fabric. The proposed date of this star-shaped tapestry, based on its style, was quite ambiguous: it was first published as mid-4th to mid-5th century (du Bourguet 1959). The author compared this piece to a textile found in context with a coin dated AD 340 and to a Syrian mosaic dated around AD 450. Five yr later, du Bourguet (1964) dated the same textile to the 3rd–4th century. He did not explain his change of view. In the same catalog (under reference 66, B6), another textile with the same motif was placed in the 5th century.

Despite a divergence of dating based on their style, the interlaced pattern of the star E26117 and the twin stripes AF6075 (du Bourguet 1964: 121, D6) are very similar to motifs found together on a textile in the Victoria and Albert Museum, London (Kendrick 1920). A circle surrounds the star on the London piece, but the design is the same as on the one in the Louvre. A similar ¹⁴C date for both samples was, therefore, expected.

The next 6 samples also form a coherent series. The combination of these 6 gives an interquartile range of AD 435–505 and a 95% probability range of AD 390–560.

E29364 presents the same style and technique as the star-shaped decoration on E26117, the shawl roundels (medallions) E26124 and AF5665. However, they do not show the same ¹⁴C dating.

The same remark fits the vine scrolls E26152 and E26126 (see Figure 6: E26126). There are slight stylistic differences between them. E26126 has a little less elegant design and a bird is added to the vegetal scroll. Nevertheless, the presence of this bird does not mean anything in terms of dating, as it appears as well on the Victoria and Albert Museum band cited previously as a 3rd–4th century AD piece (Kendrick 1920).

The same 5th–6th century dating applies indeed to the textiles E10181, E26107, and E26141. These linen tunics are decorated with monochromatic woolen tapestries, as the whole group defined for this study. It has to be noted that the shoulder decorations with figures, sewn on E26107, do not belong to the original tunic (Cortopassi 2002). Textiles E26107 and E26141 present more sophisticated motifs: animals running through the scrolls and human beings. For this reason perhaps, art historians dated them later than the purely geometric patterns.

E26142 has linen loops around the decorated part. It also shows the sophisticated composition just mentioned above. Some red dots are added to the monochromatic purple decoration, an imperceptible change towards polychromatic tapestries. ¹⁴C dates this fabric between AD 340 and 560.

The dates show that the monochromatic group has been produced for a long time: geometrical and vegetal patterns from the 3rd–4th century AD were perpetuated in the 5th–6th century or even the 7th century if we take into account the ornamentation of tunic 862/DM42 B from Katoen Natie (KIA-17381: 1385 ± 20 BP). It is noteworthy that this set of 12 textiles can be chronologically divided in 2 very tight groups, separated by the year AD 400.

The Third Group: Coptic Textiles

Series of 12 Woolen Stylistically Related Tunics

Table 5 presents the results from this group of textiles. Figure 8 represents the probability distributions of the single dates. An example of this type of fabric is given in Figure 9.

Table 5 Woolen tunics.

Sample	Lab code	¹⁴ C age (BP)	Calibrated age (68.2%)	Calibrated age (95.4%)
DM113D	UtC-9431	1630 ± 60	AD 340 (4.2%) AD 370 AD 380 (64.0%) AD 540	AD 250 (95.4%) AD 570
DM88B	UtC-9049	1615 ± 40	AD 400 (38.4%) AD 470 AD 480 (29.8%) AD 540	AD 340 (95.4%) AD 550
DM88C	UtC-9051	1590 ± 40	AD 420 (68.2%) AD 540	AD 380 (95.4%) AD 570
DM119D	KIA-10569	1585 ± 30	AD 430 (26.0%) AD 470 AD 480 (42.2%) AD 540	AD 410 (95.4%) AD 560
DM123	UtC-2612	1540 ± 60	AD 430 (68.2%) AD 600	AD 410 (95.4%) AD 650
DM119	UtC-2619	1530 ± 70	AD 430 (68.2%) AD 610	AD 400 (95.4%) AD 660
DM88D	UtC-9050	1485 ± 40	AD 540 (67.1%) AD 620 AD 630 (1.1%) AD 640	AD 430 (95.4%) AD 660
DM88E	KIA-10570	1470 ± 35	AD 560 (68.2%) AD 640	AD 530 (95.4%) AD 660
DM119C	UtC-7253	1450 ± 50	AD 560 (17.8%) AD 590 AD 595 (50.4%) AD 655	AD 460 (1.6%) AD 500 AD 530 (93.8%) AD 680
DM119B	UtC-7240	1420 ± 60	AD 560 (68.2%) AD 670	AD 460 (1.0%) AD 490 AD 530 (92.5%) AD 720
DM88	UtC-9052	1380 ± 40	AD 620 (4.7%) AD 630 AD 635 (63.5%) AD 685	AD 740 (2.0%) AD 770 AD 590 (92.0%) AD 720
DM85	UtC-2620	1350 ± 70	AD 620 (53.3%) AD 730 AD 740 (14.9%) AD 780	AD 740 (3.4%) AD 770 AD 540 (95.4%) AD 870

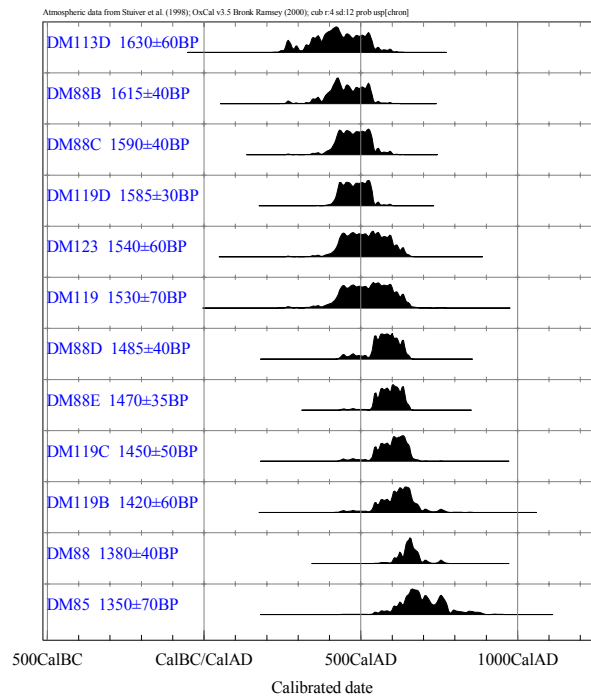


Figure 8 Probability distributions for the single dates



Figure 9 Fragment of a woolen Coptic tunic (Katoen Natie 561 / DM85)

Twelve woolen tunics of a particular type, with or without sleeves, were dated. They have clavi, vertical decorated strips next to the neck slit, frequently decorated with very stylized human figures or animals, or with geometric patterns with, for instance, octagons and interlacing (see decoration Katoen Natie 561/DM85). The clavi are nearly always running to the hem (the lower border). From a technological point of view, they form a coherent group. Most of these tunics show weft loops forming fringes at the hem. The neck slit is often carefully strengthened with weft twining and looped warp twining along the selvedge of the neck slit (Verhecken-Lammens 1994).

Some authors date these tunics as late as the 11th or 12th century (a summary of all the proposed dates can be found in De Moor et al., forthcoming). Others date them no older than the 6th–9th century AD.

The interquartile range for this set of textiles goes from AD 450–650, the 95% probability range from AD 350–740. This result shows without any doubt that these tunics do not belong to the 11th or 12th century AD as suggested by some authors. Furthermore, this data set has proven that the geometric patterns and the interlacing, very often seen in late Roman textiles from Egypt (4th century AD) did not disappear from the Coptic iconography during several centuries.

Series of 10 Woolen Caps in Sprang Technique

Table 6 and Figure 10 represent the results from the woolen caps. Figure 11 shows an example of this type of fabric.

Sprang is a plaiting technique realized by the crossing of threads. The dating of these woolen caps has been controversial. There is a general consensus that the caps date between the 4th–6th century AD, although du Bourguet (1964) dated them as late as the 9th century. A summary of all the proposed dates can be found in De Moor et al. (2002). The dates show very well that a 9th century date for this type of fabric must be excluded.

Although the dates form a very coherent series, with an interquartile range of AD 450–650 and a 95% probability range of AD 350–740, there are some technical differences between the individual

Table 6 Caps in sprang technique.

Sample	Lab code	¹⁴ C age (BP)	Calibrated age (68.2%)	Calibrated age (95.4%)
853c	KIA-15206	1615 ± 25	AD 400 (44.7%) AD 470 AD 480 (23.5%) AD 540	AD 390 (95.4%) AD 540
816f	KIA-12709	1580 ± 25	AD 430 (24.6%) AD 470 AD 480 (43.6%) AD 535	AD 420 (95.4%) AD 540
816d	KIA-12707	1545 ± 30	AD 430 (68.2%) AD 560	AD 430 (95.4%) AD 600
816e	KIA-12711	1535 ± 30	AD 430 (68.2%) AD 600	AD 430 (95.4%) AD 610
816a	KIA-12713	1525 ± 35	AD 430 (5.0%) AD 450 AD 460 (8.6%) AD 490 AD 510 (0.8%) AD 520 AD 530 (53.9%) AD 610	AD 430 (95.4%) AD 620
DM138	KIA-12710	1510 ± 25	AD 535 (68.2%) AD 600	AD 430 (95.4%) AD 640
853a	KIA-14327	1500 ± 30	AD 535 (68.2%) AD 605	AD 430 (95.4%) AD 650
816b	KIA-12712	1485 ± 25	AD 540 (68.2%) AD 615	AD 530 (95.4%) AD 640
853b	KIA-14328	1420 ± 25	AD 620 (68.2%) AD 656	AD 595 (95.4%) AD 665
816c	KIA-12708	1400 ± 25	AD 623 (6.6%) AD 628 AD 639 (61.6%) AD 662	AD 600 (95.4%) AD 675

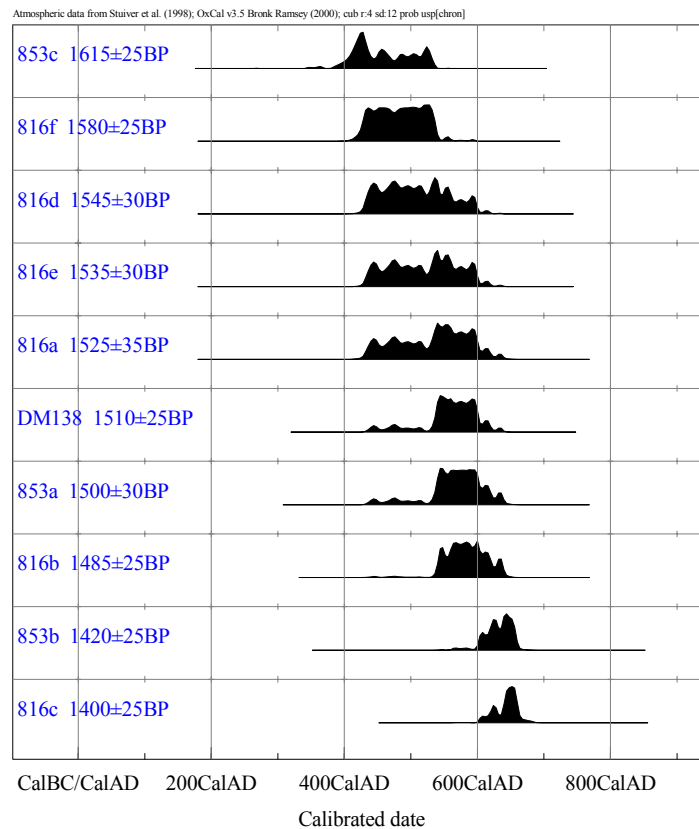


Figure 10 Probability distributions for the woolen caps

caps. In caps 816a and 816f, brocading threads were introduced. Cap 816b was made in an open sprang technique which was not very loose, and it is more related to the linen or linen and wool hair-nets. Cap 853b contains human hair from the buried person. Although caps 853b and c show the same pattern, their dates differ considerably [difference: 230–110 (68.2%), 260–80 (95.4%)].



Figure 11 A woolen cap in sprang technique (Katoen Natie 853b)

Table 7 presents the results from the woolen caps. Figure 12 shows an example of this type of textile.

Table 7 Textiles with silk embroidery of stylized floral motifs (EBERWEIN) and of a Greek cross re-crossed at the 4 ends (904 and DM1000).

Sample	Lab code	¹⁴ C age (BP)	Calibrated age (68.2%)	Calibrated age (95.4%)
EBERWEIN	UtC-7250	245 ± 30	AD 1640 (49.8%) AD 1670 AD 1780 (18.4%) AD 1800	AD 1520 (8.9%) AD 1570 AD 1620 (57.1%) AD 1680 AD 1760 (25.3%) AD 1810 AD 1930 (4.2%) AD 1950
904	KIA-20197	215 ± 20	AD 1650 (26.3%) AD 1670 AD 1780 (39.9%) AD 1800 AD 1940 (2.0%) AD 1950	AD 1640 (37.2%) AD 1680 AD 1760 (47.7%) AD 1810 AD 1930 (10.5%) AD 1950
DM1000	KIA-18957	120 ± 30	AD 1680 (19.8%) AD 1740 AD 1800 (40.8%) AD 1890 AD 1910 (7.6%) AD 1930	AD 1670 (32.6%) AD 1770 AD 1800 (62.8%) AD 1960

Textiles with Silk Embroidery, Often of a Greek Cross Re-Crossed at the 4 Ends

These linen tunics or cotton caps are often embroidered with silk floral or stylized floral motifs, sometimes with men or animals or with a large Greek cross re-crossed at the 4 ends.

Although these textiles are usually dated to the late medieval period (du Bourguet 1964), ¹⁴C analysis places them not before the mid-17th century AD.



Figure 12 A cap with a Greek cross re-crossed at the 4 ends (Katoen Natie 896 / DM1000)

CONCLUSIONS

This study has shown that for the assembled groups of textiles, the dating precision for both ¹⁴C and art historical criteria is similar and in the order of 2 centuries. We also found that, with the exception of textiles embroidered in silk, ¹⁴C analysis returned dates that were older than previous assessments based on art historical grounds. This may be due to the fact that while comparison of a textile with other media such as paintings may not provide an accurate historical example of style, ¹⁴C analysis does have the advantage of providing a calendar age range that is based on the quantitative analysis of contemporary isotopic values preserved in the material. We suggest that, rather than being viewed with some suspicion, ¹⁴C dating of textiles can indeed enhance the assessments of art historians.

REFERENCES

- Auth SH. 1978. Coptic art. *The Newark Museum Quarterly* 29(2):10–1.
- Bourriau J. 1977. Egyptian antiquities acquired in 1975 by museums in the United Kingdom. *Journal of Egyptian Archaeology* 63:171–4.
- Bruwier MC, editor. 1997. *Egyptiennes. Etoffes coptes du Nil*. Mariemont. 139 p.
- Burnham D. 1972. Coptic knitting: an ancient technique. *Textile History* 6:116–24.
- Cortopassi R. 2002. Un *amphimallon* au musée du Louvre. *Bulletin du CIETA* 79:36, Figure 1.
- De Jonghe D, Verhecken-Lammens C. 1993. Technological discussion. In: De Moor A, editor. *Coptic Textiles*. PAMZOV, buitengewone reeks 1, Zottegem, Belgium. p 31–52.
- Del Francia Barocas L. 1998. *Antinoe Cent' anni dopo*. Museo Egizio, Firenze. p 229.
- De Moor A. 1993. Dating of Coptic textiles. In: De Moor A, editor. *Coptic Textiles*. PAMZOV, buitengewone reeks 1, Zottegem, Belgium. p 23–30.
- De Moor A, Verhecken-Lammens C, Van Strydonck M. 2002. Radiocarbon dating of Coptic woolen caps in sprang technique. *CIETA-Bulletin* 79:26–32.
- De Moor A, Van Strydonck M, Verhecken-Lammens C. Forthcoming. Radiocarbon dating of a particular type of Coptic woolen tunics. *Acta of the Seventh International Congress of Coptic Studies*.
- du Bourguet P. 1958. Datations des tissus coptes et carbone 14. *Bulletin du laboratoire du musée du Louvre* juin 1958. p 53–63, tissu copte nr 45.
- du Bourguet P. 1959. La datation des tissus coptes en fonction des mosaïques méditerranéennes. Précisions nouvelles. *Ars orientalis* 3:191.
- du Bourguet P. 1964. *Musée National du Louvre. Cata-*

- Logue des Étoffes Coptes du Louvre*. Paris.
- Kendrick AF. 1921. *Catalogue of Textiles from Burying Grounds in Egypt II*. London: Victoria and Albert Museum.
- King M, King D. 1990. *European textiles in the Keir collection. 400 BC to 1800 AD* 6:17–18.
- Lafontaine-Dosogne J. 1988. *Textiles coptes des Musées Royaux d'art et d'Histoire de Bruxelles*. Bruxelles: Koninklijke Musea voor Kunst en Geschiedenis. 37 p.
- Leclercq H. 1924. *Dictionnaire d'archéologie chrétienne et de liturgie* 4(1):1246–58.
- Lorquin A. 1992. *Les tissus coptes au musée national du Moyen Age—Thermes de Cluny*, Paris, 117:282–4.
- Nauerth C. 1989. *Die koptischen textilien der Sammlung Wilhelm Rautenstrauch im Städtischen Museum Trier*: 190.
- Rassart-Debergh M. 1988. Art tardifs et chrétiens d'Égypte 52:36–7.
- Rutschowskaya M-H. 1992. *Musée du Louvre, département des antiquités égyptiennes. La peinture copte*, Paris: Réunion des Musées nationaux (RMN).
- van der Plicht J, Bruins HJ. 2001. Radiocarbon dating in Near-Eastern contexts: confusion and quality control. *Radiocarbon* 43(3):1155–66.
- Van Strydonck M, van den Borg K. 1990–91. The construction of a preparation line for AMS-targets at the Royal Institute for Cultural Heritage Brussels. *Bulletin Koninklijk Instituut voor het Kunstpatrimonium* 23:228–34.
- Van Strydonck M, van der Borg K, De Jong A. 1993. The dating of Coptic textiles by radiocarbon analysis. In: De Moor A, editor. *Coptic textiles*. PAMZOV, buitengewone reeks 1, Zottegem, Belgium. p 65–71.
- Van Strydonck M. 1995. Koptisch textiel uit Vlaamse privé-verzamelingen: bevestigen de kunsthistorische en de ¹⁴C dateringen elkaar? *VVOHT bulletin* 1995: 17–20.
- Van Strydonck M, De Jonghe D. 1995. Radiocarbon dating of Liseré linen: a comparison. *N.S.T.* 13 (2–3–4), 461–6.
- Verhecken-Lammens C. 1994. Two Coptic wool tunics in the collection of the Abegg-Stiftung: a detailed analysis of the weave technique used. *Riggisberger Berichte* 2:73–103.
- Wouters J. 1993. Dye analysis of Coptic textiles. In: De Moor A, editor. *Coptic textiles*, PAMZOV, buitengewone reeks 1, Zottegem, Belgium. p 53–64.

RADIOCARBON DATING OF SOPOT CULTURE SITES (LATE NEOLITHIC) IN EASTERN CROATIA

Bogomil Obelić^{1,2} • Marija Krznarić Škrivanko³ • Boško Marijan⁴ • Ines Krajcar Bronić¹

ABSTRACT. The results of radiocarbon dating of several Late Neolithic archaeological sites in Slavonia, eastern Croatia, are presented. According to the archaeological findings, the sites belong to the Sopot culture. Stages I-B, II-A, II-B, and III were identified at the eponym site Sopot near Vinkovci, stages I-B and II at the site Dubovo-Košno near Županja, while findings for other investigated sites (Herrmann's Vineyard near Osijek, Mandek's Vineyard from Otok, Privlaka near Vinkovci, and Slavča near Nova Gradiška) were placed to phases II and III. ¹⁴C results place the I-B stage to the period 5480–5070 cal BC, stage II-A to 5030–4770 cal BC, stage II-B to 4800–4250 cal BC, and phase III to 4340–3790 cal BC. These dates were compared to those obtained for other Late Neolithic cultures in the Pannonian Valley. The results confirmed the Protolengyel character of Sopot culture.

INTRODUCTION

Sopot culture was set apart for the first time by Milošević (1949) as an autonomous appearance in the Late Neolithic of SE Europe and named the *Slavonian-Syrmian* or *Babska-Lengyel* culture. As a consequence of later investigations, the name *Sopot-Lengyel* was proposed (Dimitrijević 1968). The first part of the name was used after the eponym to designate the area of Sopot near Vinkovci, and the second part in order to stress the important role of this culture to the Lengyel culture complex in the Pannonian Valley. Subsequent excavations performed in Transdanubia showed the Protolengyel character of this culture. Therefore, only the first part of the name (Sopot) has been used since 1971, which is also in concordance with the fact that the culture is, in its essence, closer to Vinča than to Lengyel.

In this paper, we attempt to justify these assumptions by radiocarbon dating of several Sopot culture sites in eastern Croatia and by comparison with the dating of neighboring Lengyel and Vinča culture sites. Our contribution is the relative chronology of almost contemporary cultures, the genesis of the Sopot and related cultures and their chronological and cultural links.

At the Third ¹⁴C and Archaeology Symposium in Lyon, Obelić et al. (1999) presented the results of ¹⁴C dating of about 500 archaeological samples of charcoal, wood, grains, and human and animal bones from Slovenia, Croatia, Bosnia and Herzegovina, Serbia and Montenegro, Macedonia, and Hungary in the form of a period of existence of an archaeological site. The ¹⁴C chronology of the oldest important Neolithic culture in this region, Starčevo, was systematically presented by Krajcar Bronić et al. (2003) at the Fourth ¹⁴C and Archaeology Symposium in Oxford on the basis of 2 settlements. This paper, dealing with the younger Neolithic in eastern Croatia, is based mainly on excavations performed at the eponym site Sopot near the town Vinkovci (Iskra-Janošić and Krznarić Škrivanko 1997; Krznarić Škrivanko 1998a, 1998b, 1999, 2000, 2002, 2003) and the site Dubovo-Košno near the town Županja (Marijan 2001). It represents a further step in the systematization of ¹⁴C dating of prehistoric cultures in SE Europe performed at the Rudjer Bošković Institute in Zagreb. The results of the ¹⁴C measurements were published in the Rudjer Bošković Institute data list XV (Obelić et al. 2002a).

¹Rudjer Bošković Institute, P.O. Box 180, 10002 Zagreb, Croatia.

²Corresponding author. Email: Bogomil.Obelic@irb.hr.

³Vinkovci Municipal Museum, 32100 Vinkovci, Croatia.

⁴Županja Municipal Museum "Stjepan Gruber", 32270 Županja, Croatia.

CHARACTERISTICS OF THE SOPOT CULTURE

The region Slavonia in eastern Croatia was one of the main arteries of cultural and ethnic trends during all prehistoric periods. There are more than 100 registered sites belonging to the Neolithic, mostly to the Sopot culture (Minichreiter 1996–97). On the area covered by the Vinkovci Municipal Museum (1022 km²), 17 hill-forts and 6 open settlements were localized, and on the basis of casual findings, 11 more sites are supposed to exist. The favorable natural conditions enabled the high population density of the region during a continuous period of 8000 yr.

The Sopot culture is assumed to be caused by the movement of the Vinča population from present-day Serbia towards the northwest by the pressing of the ethnically superior, but culturally inferior, Starčevo culture elements into the Slavonian area. The result was the partial transformation of Starčevo ceramography, expressed in the successive introduction of biconic fine ceramic and in the decline of painted pottery. The Sopot culture is not a derivation of the Vinča culture because it is closer to Starčevo. Its ceramic production is, in essence, a very simple and static production category. Although a member of the Balkan-Anatolian cultural complex and, thus, close to the Vinča culture, it differs greatly from Vinča decorative splendor, except for a very polished surface on this simple pottery. A characteristic feature of this culture is the dark monochrome ceramic and carving and tally ornament, which was found also at the very end of the Starčevo culture under the influence of the Vinča culture. Other forms of the Sopot culture are cannelling, pressing, and ribbon decoration by incision and pricking, which is imported from the Vinča (Dimitrijević 1979). The novel feature of the Vinča is the reductive heating of ceramics (black polished), a characteristic of Balkan-Anatolian culture complex.

Archaeologists divide the Sopot culture into 3 phases (I, II, III). Dimitrijević (1968) subdivided the oldest phase into 2 stages (I-A, I-B), while newer investigations performed at the eponym site Sopot (Krznarić Škrivanko 2002) distinguish also the older (II-A) and the younger (II-B) stages of phase II. The youngest phase is denoted by III.

The central area of the Sopot culture is situated between the rivers Danube, Drava, and Sava from the Croatian-Serbian border at the east. The western border was subjected to changes during the expansion of the culture, and in its final stage, reached almost the region of today's Zagreb. By the end of the I-B stage, there was an expansion of the Sopot population towards the south, across the Sava River to northern Bosnia, as well as to the north into the Transdanubian zone in Hungary, where this Sopot manifestation was named the Sopot-Bicske culture (Dimitrijević 1979). By the beginning of phase III, an expansion towards the east, across the Danube, into the territory of the Vinča group in western Vojvodina was noticed (Brukner 1974). The main sites are presented in Figure 1.

The Sopot population was mostly agricultural. Cattle breeding, fishing, and hunting were intensive. Analyses of osteological material found at the Dubovo-Košno site confirm the existence of cow, horse, deer, boar, swine, sheep, goat, dog, and various kinds of birds. The cows and pigs are of primitive breed, i.e., changes in bones caused by domestication were not found (Jurišić, private communication). Handicraft was concentrated to pottery and production of tools and arms from stone and bones. Since a large amount of polished chisels and wedges were found at some sites, we can consider carpentry as an important activity.

The only graves of the Sopot culture in any of the investigated sites were found at Herrmann's Vineyard in Osijek, and a partial burial was found at the site Ervenica (Krznarić Škrivanko 1997), which provided minimal examples upon which to comment on the burial ritual and the spiritual life of Sopot inhabitants. It can be supposed that burial within the settlement was not usual.



Figure 1 Main sites of Sopot culture denoted by •. Numbers correspond to the sites from which samples were taken for ¹⁴C analysis: 1–Sopot near Vinkovci, 2–Dubovo-Košno near Županja, 3–Mandek's Vineyard in Otok, 4–Privlaka, 5–Herrmann's Vineyard in Osijek, 6–Slavča near Nova Gradiška.

Investigations performed up to now indicate that the Sopot population built 2 types of houses (Krznarić Škrivanko 2002): those belonging to the II-A stage have walls constructed from horizontal beams coated with a mixture of clay and grain-husks, and those belonging to phase III were built from vertically bolted posts connected by interwoven brushwood and coated by clay and grain-husks. The strutted double roof was covered by straw.

SITE DESCRIPTION

The earliest site of the Sopot culture found in the region that covers the Vinkovci Municipal Museum was Ervenica in Vinkovci, where 7 half-buried objects were found (Krznarić Škrivanko 1997). In one of the earth-huts, a partially buried child skull was found. This ritual burial, considered as stage I-B, can be connected with the initial period of the life at the settlement. Unfortunately, no ¹⁴C measurement from this site was possible.

Tell Sopot

After some investigations done in 1939 and 1940 by M Klein and 1957 by Dimitrijević (1968), systematic excavations started in 1996 at the eponym settlement Sopot near Vinkovci in eastern Slavonia (Figure 2). An elliptical tell, fortified with a palisade and a moat filled with water, is situated on the right bank of the Bosut River. Four probes of different sizes were opened, three of them within the hill-fort itself (Figure 3), and the fourth at the neighboring SW elevation.

In probe 1, several house basements from phases Sopot II to Sopot III were found. All of them were burned, except the deepest one which belongs to the oldest phase of Sopot culture. Two charcoal samples (Z-2752 and Z-2753) from this probe, taken from the basements of burned houses belonging to phase II, were submitted for ¹⁴C analysis.

Further excavations were concentrated around probe 3 (Figure 3). This probe encompassed 250 m² and was situated at the edge of the fortification close to the moat with a palisade cemented by mud. The moat was functioning during the early stage II of Sopot culture and was later filled due to the widening of the settlement.

Two house basements (SU 11 and SU 13), belonging to the latest phase III of the Sopot culture, were discovered in probe 3. The house basement, denoted as stratigraphic unit 11 (SU 11), was found on the moat. Dimensions of the house are 4 × 6 m and the orientation is NW-SE. The basement was 16 cm deep and along it there are holes for vertical poles. An oven connected with the basement had an ash and soot infill, and numerous broken dishes were found, as well as clay weights for fishing nets or looms. The distribution of these household items seems to indicate that the inhabitants abandoned their settlement very quickly, and may be the point at which this settlement was abandoned. Three charcoal samples were taken for ¹⁴C analysis (Z-2754, Z-2826, Z-2827).

Two rectangular house basements from stage II-B (SU 17 and SU 20) were discovered in probe 3 between 1–1.5 m depth, along a vertical line at the same position of the houses belonging to stage III (SU 11 and SU 13). They have the same orientation (NW-SE) and are made of yellow, beaten clay. Although burned, they were partially preserved in their original form. Around the houses, post holes and bigger pieces of burned clay-daub from wall construction with traces of red coloring were found. Two charcoal samples from SU 20 were dated (Z-2909, Z-2911), as well as one from SU 53 (Z-3143, nivelation of the house SU 20).

Further excavations uncovered a 7 × 4-m house (SU 23). Its orientation was different from that of the houses excavated at probe 3 (NE-SW). The remains of the house indicate that it was destroyed by fire. *In situ* finds include a large quantity of crudely fashioned household vessels and fine polished bowls and bowls with legs and numerous objects made of bone and stone. A quantity of clay weights was discovered in the SW part of the house. On the basis of a rounded pot with a low ring-like neck decorated in a typically Vinča fashion, the house was dated back to the older II-A Sopot stage. Under the house, a trench (6 m wide) was uncovered which surrounded the settlement on 3 sides (the Bosut River runs along the NW side). Below the house, there was a grayish-black layer (SU 24) with ashes and soot containing less ceramic and bone remains than the upper layers. The deepest and the oldest horizon had a lower density of houses than in the younger II-B and III stages. Charcoal samples were taken from stage II-A for ¹⁴C analyses (Z-3139, Z-3140, Z-3141).

Site Dubovo-Košno

During the construction of the Zagreb-Belgrade highway section near Županja in east Slavonia, rescue excavations along the route were performed in 2000 (Figures 4 and 5). A Neolithic settlement was uncovered at the Dubovo-Košno location, where an area of 8575 m² has been excavated. The shape of the settlement is typical for Neolithic period and belongs to the type of plain, non-fortified settlements. It consists of numerous objects, both above and below the ground. It appears that most of the sites served as workshops, while some were used as stores, wells, or waste pits, but seldom as housing objects. Conventional techniques of construction, mostly a combination of wood and mud-daub, were used.



Figure 4 Position of site Dubovo-Košno



Figure 5 Dubovo-Košno site from the air. The highway route is visible.

A significant quantity of ceramic, clipped and polished stone artifacts, clay plaster, half-charred wood, animal bones, and seeds was found. A range of pottery from coarse to transitional and fine ceramic can be recognized, with pots, dishes, and beakers on solid feet. Stone and bone tools were also found, as well as a dozen weights perhaps used in trade activities. No object for exclusively cer-

emonial or religious purposes was found. Generally, it can be concluded that it was a temporary (seasonal) settlement. Typological characteristics of the finds indicate that it was a Sopot culture settlement, a transition from stage I-B to phase II. Five samples of charred wood were taken for ¹⁴C analyses (Z-2969, Z-2973, Z-2998, Z-3045, Z-3046).

Other Sites

One of the first excavations on Sopot culture sites was done by Celestin in 1897 (Celestin 1896/97) on a tell which was then Herrmann's Vineyard near Osijek. Although without stratigraphic data, the finds show at least 2 building horizons with characteristics of phases II and III of Sopot culture. Finds of interest were animal figures, numerous stone and bone artifacts, and several pendants from *Spondylus*. During the construction of a collector for municipal sewerage in Osijek, the excavations were continued (Šimić 1998, 1999, 2000). A sample of charcoal found near the fireplace (Z-2830) and a sample of human bone (Z-2831) were dated from this site.

The hill-fort at Mandek's Vineyard near the village of Otok, close to Vinkovci, is the ellipsoidal tellsite, bounded by a trench of 4 m relative height. Dimitrijević directed the excavation from 1957 and 1970 (Dimitrijević 1979). Finds belonging to all 3 phases of the Sopot culture were recovered. Samples of charcoal (Z-2762) and grain (Z-2761, Z-2913) were collected in 1970 and recently submitted for ¹⁴C analysis (Obelić et al. 2002a). Grain (*Triticum aestivum* L.) was identified as *Thell sp. vulgare* by J McKey, Institute of Genetics, Uppsala, Sweden (Horvatinčić et al. 1999).

Excavations on the site Privlaka (Gradina) near Vinkovci were led by Pandžić-Majnarić in 1979. According to typological analyses, this settlement existed during phases II and III. Two samples were taken for ¹⁴C analyses, Z-727 and Z-728 (Srdoč et al. 1981).

Recently, the excavation started at the Slavča site near Nova Gradiška in western Slavonia. Three samples (Z-3234, Z-3290, Z-3291) were analyzed for ¹⁴C. No additional information by the archaeologists is yet available and our ¹⁴C dates will help in developing a chronology for the site.

¹⁴C DATING

¹⁴C dating of charcoal and bones was performed in the Rudjer Bošković Institute Radiocarbon Laboratory. The samples were dated according to the standard laboratory procedures (Srdoč et al. 1971, 1979; Krajcar Bronić et al. 1995). Charcoal samples are first mechanically cleaned. The chemical treatment includes boiling in 4% HCl, neutralization, boiling in 2% NaOH, and additional boiling in a low-acid solution of HCl (A-B-A procedure). For bone measurements, we extracted collagen following the method introduced by Longin (1970). The dried samples are then combusted in a stream of purified oxygen. The obtained CO₂ is hydrogenated to CH₄ over a Ru catalyst at 470 °C and then purified from the residual gas impurities. Measurement of ¹⁴C activity is performed in the gas proportional counter after methane was stored for about 2 weeks to allow radon to decay. Each sample is routinely measured twice and the mean value is calculated. The age is calculated following the recommendations given by Stuiver and Polach (1977) and the fractionation correction for δ¹³C is applied. The conventional ¹⁴C age is calibrated using the Oxford University program OxCal (Bronk Ramsey 2001, 2003).

The quality system used in the laboratory since its beginning has been recently improved and the ISO 17025 standard has been implemented (Obelić et al. 2002b). Participation in several ¹⁴C inter-comparison studies (Horvatinčić et al. 1990; Krajcar Bronić et al. 1995; *Radiocarbon* 2001) and proficiency tests are part of the quality assurance program.

DATING RESULTS

The results of ^{14}C dating of 25 samples from various Sopot culture sites are shown in Table 1. Both the conventional ^{14}C age and the calibrated age ranges within a 1- σ confidence interval are given. Probabilities of the calibrated age ranges are also given and the probabilities <5% are omitted. The graphical representation of calibrated results, sorted according to currently understood phases, is presented in Table 2.

Table 1 Overview of samples and ^{14}C results.

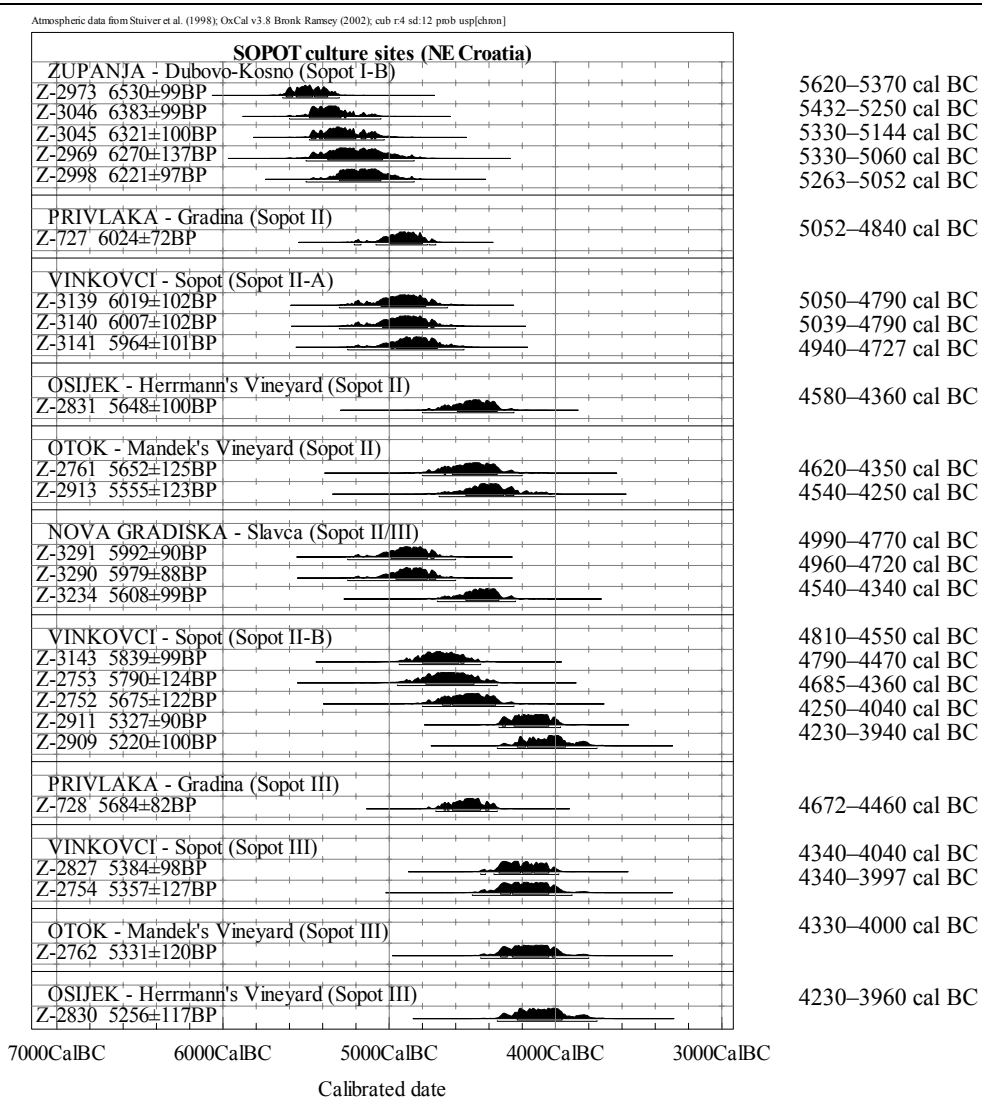
Sample code	Sample description	Conventional ^{14}C age (BP) ^a	Calibrated ranges ($\pm 1 \sigma$) and probabilities (%) ^b	Ref ^c
Županja—Dubovo-Košno				
Z-2969	Charcoal No.152 from pit SU 160, square H-38	6270 \pm 140	cal 5320–4990 BC (68.2%)	[1]
Z-2973	Charcoal No.214 from earth hut SU148, square F-38, western part	6530 \pm 100	cal 5620–5580 BC (8.1%) cal 5560–5460 BC (38.4%) cal 5450–5370 BC (21.7%)	[1]
Z-2998	Charcoal from earth hut SU 1144, square R-38/39	6220 \pm 100	cal 5300–5050 BC (68.2%)	[1]
Z-3045	Charcoal, SU 1804, square Z-43d, PU 339	6320 \pm 100	cal 5390–5200 BC (51.2%) cal 5170–5140 BC (5.1%)	[1]
Z-3046	Charcoal SU 308, square H-49d, PU 228	6380 \pm 100	cal 5480–5290 BC (67.0%)	[1]
Vinkovci—Sopot				
Z-2752	Charcoal from basement of house, probe 1, square E-6, depth 1.05–1.25 m	5675 \pm 120	cal 4680–4630 BC (5.8%) cal 4620–4360 BC (62.4%)	[1]
Z-2753	Charcoal from basement of house, probe 1, square C/D-4, depth 1.05–1.25 m	5790 \pm 125	cal 4780–4490 BC (68.2%)	[1]
Z-2754	Charcoal from house SU 11, probe 3, square G-9	5360 \pm 130	cal 4320–4270 BC (14.4%) cal 4260–4040 BC (53.8%)	[1]
Z-2827	Charcoal from house SU 11, probe 3, square I-6, depth 2.11 m	5380 \pm 100	cal 4340–4210 BC (36.8%) cal 4200–4140 BC (13.5%) cal 4130–4040 BC (17.9%)	[1]
Z-2909	Charcoal from house SU 20, probe 3, square I-6, depth 2.11 m	5220 \pm 100	cal 4230–4180 BC (8.9%) cal 4170–3940 BC (59.3%)	[1]
Z-2911	Charcoal from house SU 20, probe 3, square J-6, depth 3.54–3.67 m	5330 \pm 90	cal 4250–4040 BC (66.1%)	[1]
Z-3139	Charcoal from house SU 23, probe 3, square A-8, depth 3.89–3.99 m	6020 \pm 100	cal 5050–4780 BC (68.2%)	[3]
Z-3140	Charcoal from house SU 23, probe 3, square C-6, depth 3.61 m	6010 \pm 100	cal 5040–4770 BC (66.35%)	[3]
Z-3141	Charcoal from SU 6 of the house SU 23, probe 3, square D-11, depth 2.74 m	5960 \pm 100	cal 4960–4710 BC (67.2%)	[3]
Z-3143	Charcoal from SU 53 (nivation of house SU 20), probe 3, square G/H-7, depth 3.58–3.99 m	5840 \pm 100	cal 4800–4580 BC (64.2%)	[3]
Otok—Mandek's Vineyard				
Z-2761	Grain from ceramic pot, square 10/ij, depth 0.70–0.80 m	5650 \pm 120	cal 4620–4350 BC (67.2%)	[1]
Z-2762	Charcoal, square 10/ij, depth 0.77 m	5330 \pm 120	cal 4330–4290 BC (7.1%) cal 4260–4040 BC (57.6%)	[1]
Z-2913	Grain, same as Z-2761	5555 \pm 120	cal 4540–4310 BC (59.1%) cal 4300–4250 BC (9.1%)	[1]
Osijek—Hermann's Vineyard				
Z-2830	Charcoal from fireplace, depth 1.8–2.0 m	5260 \pm 120	cal 4230–4180 BC (7.7%) cal 4170–3930 BC (53.2%) cal 3860–3810 BC (7.3%)	[1]
Z-2831	Human bone, depth 1.9 m	5650 \pm 100	cal 4590–4350 BC (68.2%)	[1]
Privlaka—Gradina				
Z-727	Charcoal from a partially burned beam in house floor, hill-fort Gradina	6030 \pm 100	cal 5000–4800 BC (68.2%)	[2]
Z-728	Wheat grains in soil 1.7 m below floor of the burned house, hill-fort Gradina	5700 \pm 80	cal 4620–4450 BC (60.1%)	[2]

Table 1 Overview of samples and ¹⁴C results. (Continued)

Sample code	Sample description	Conventional ¹⁴ C age (BP) ^a	Calibrated ranges (±1 σ) and probabilities (%) ^b	Ref ^c
Nova Gradiška—Slavča				
Z-3234	Charcoal from SU 37, probe 2, square B-1,2	5610 ± 100	cal 4540–4340 BC (68.2%)	[3]
Z-3290	Charcoal from SU 37, probe 1, square BC-3	5980 ± 90	cal 4960–4770 BC (61.2%) cal 4760–4720 BC (8.2%)	[3]
Z-3291	Charcoal from SU 110, probe 1, square C-4	5990 ± 90	cal 4990–4770 BC (68.2%)	[3]

^a Conventional ¹⁴C age has been calculated with 1-σ error. Rounding of results according to suggestions of *Radiocarbon*.
^b Calibration range is given in historical ages together with the probability (in %) according to dendrochronological curves (Stuiver et al. 1998; Bronk Ramsey 2001, 2003). Only intervals for probabilities greater than 5% are presented.
^c [1] Obelić et al. 2002a; [2] Srdoč et al. 1981; [3] this paper.

Table 2 Graphical presentation of ¹⁴C results.



Results of all samples from the site Županja–Dubovo–Košno confirm the supposition that this site belongs to stage I-B of Sopot culture and existed for about 600 yr.

One sample from Privlaka runs into phase II and the other into phase III. Therefore, it can be supposed that the settlement existed during both phases and spanned about 600 yr.

Three samples (Z-3139, Z-3140, Z-3141) from probe 3 at tell Sopot near Vinkovci which belong to the stratigraphic unit 23 fit well into stage II-A. Samples Z-2752, Z-2753, Z-3143 agree with the supposed stage II-B, which chronologically follows and partly overlaps the previous stage II-A. However, 2 samples (Z-2909, Z-2911) from house SU 20 are younger than expected and they probably do not belong to stage II-B.

A sample of charcoal from the Herrmann's Vineyard site in Osijek found near the fireplace (Z-2830) belongs to phase III and the sample of human bone (Z-2831), found 1.9 m below the cultural layer, coincides with phase II of Sopot culture.

Dating of samples from Otok, the Mandek's Vineyard site, confirmed the supposition that samples of grain (Z-2761, Z-2913) belonged to phase II of Sopot culture and the charcoal sample (Z-2762) to phase III.

¹⁴C results of the 2 samples from the Slavča site near Nova Gradiška show the early stages of phase II, while the third one is younger and confirms the transition from phase II to phase III.

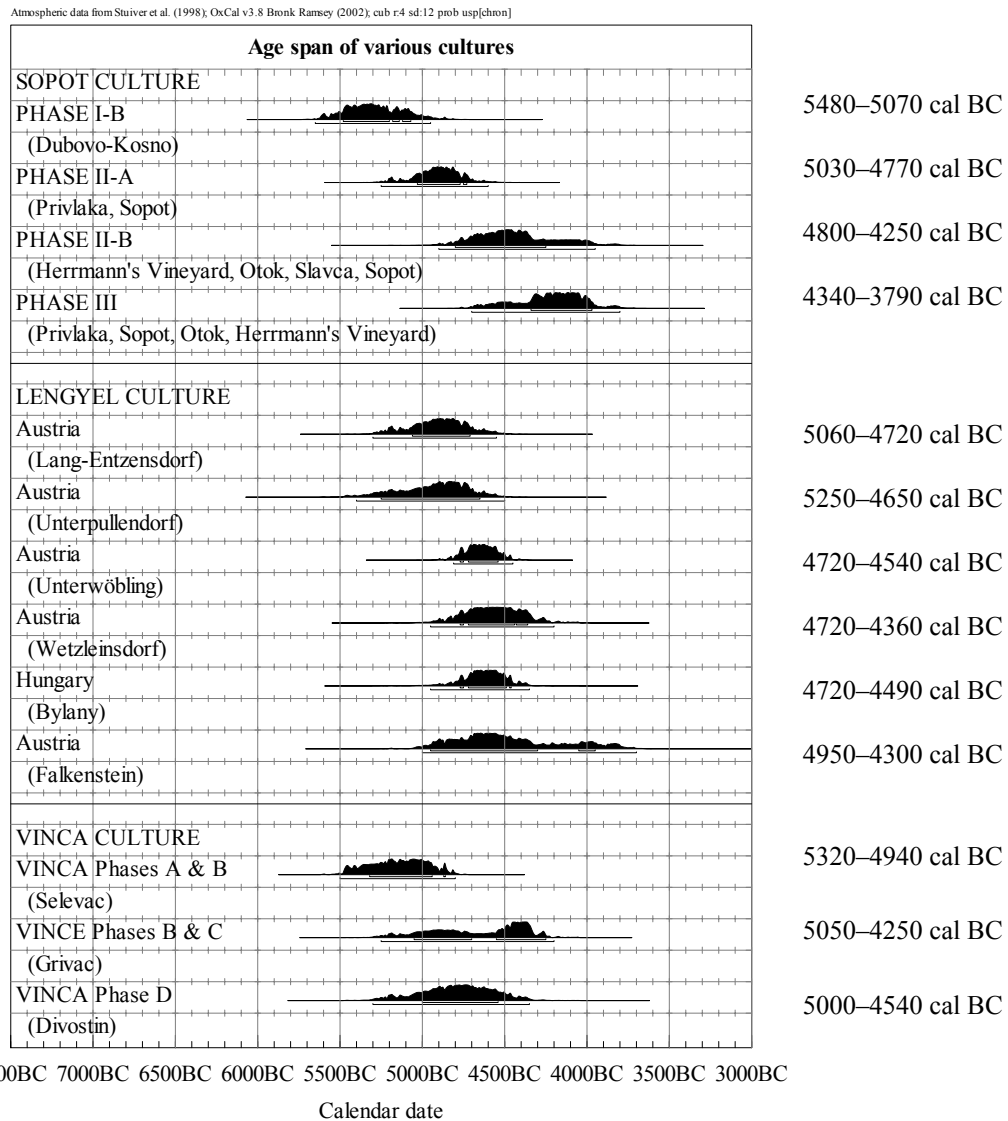
DISCUSSION

Table 3 represents the summary of calibrated age ranges from Sopot culture sites in Slavonia, divided into phases and stages. The results of ¹⁴C measurements are compared with those obtained for the Lengyel (Raetzl-Fabian 1986; Breunig 1987; Midgley 1992; Baldia 2003; Furholt et al. 2003) and Vinča cultures (Srdoč et al. 1975, 1977, 1987). The chronological distribution for a given site or phase was obtained by summation of probability distributions of individual measurements, resulting in the cumulative curve of probability of existence (Bronk Ramsey 2001, 2003). The results are summarized and compared with the ¹⁴C dates of other Late Neolithic cultures from the Pannonian Valley in Figure 6.

According to Table 3 and Figure 6, stage I-B of the Sopot culture spans from 5480 to 5070 cal BC and precedes by about 160 yr the appearance of the Vinča culture in Serbia, as well as the appearance of the Lengyel culture by about 200 yr. This fact confirms the Protolengyel character of the Sopot culture. Lenneis and Stadler (1995) in their discussion on Middle-European Linearbankeramik quote results of ¹⁴C dating of 88 samples from the Vinča culture that gave the age span from 5300 to 4500 cal BC. The same span is obtained on the basis of samples from the Vinča culture sites Selevac, Grivac, and Divostin dated in our laboratory (Srdoč et al. 1975, 1977, 1987). Sopot phase I is earlier also than the Middle Neolithic cultures of the Great Hungarian Plain: Vinča-Tordoš (5390–4960 cal BC) and Alföld linear pottery (5330–5000 cal BC) (Figure 6). Stage II-A coincides with the formation phase of the Tisza culture (5120–4710 cal BC) and II-B with the Prototiszapolgár culture in the Great Hungarian Plain (4570–4270 cal BC) (Hertelendi et al. 1995).

Unfortunately, no ¹⁴C dating of the earliest (I-A) stage of the Sopot culture has been obtained. Its beginnings should coincide with the dawn of the earliest Neolithic culture which preceded Sopot, namely, the Starčevo culture (phase Linear A). Two sites of this culture in Slavonia (Zadubravlje-Dužine and Slavonski Brod-Galovo) are dated between 6600 and 5000 BC (Krajcar Bronić et al. 2003). Stage I-B of Sopot appeared in 5480 BC during the existence of the Starčevo culture. It means that both cultures coexisted for several hundred years in a relatively small area (approximately 50 km apart).

Table 3 Comparison of age span of Sopot culture with Late Neolithic cultures in the neighborhood.



In our introduction, we stated that Sopot culture is supposed to appear as the result of the movement of the Vinča culture towards the north. Here we present dates of stage I-B of the Sopot culture (5480–5070 cal BC) that are older than about 100 samples (Lenneis and Stadler 1995; Srdoč et al. 1975, 1977, 1987) of the Vinča culture (5300–4500 cal BC). This chronology would, thus, not justify the assumption. Therefore, a question remains: If the Sopot culture is the consequence of forcing the Starčevo culture elements towards the west by the second wave of the Vinča population (Dimitrijević 1979: 262), why are there no dates of the Vinča which precede the earliest Sopot ¹⁴C results?

The Sopot culture was succeeded by the Copper (Eneolithic) Lasinja culture, which in its essence represents still a proper offspring of the Late Neolithic. No one copper object was found at the Las-

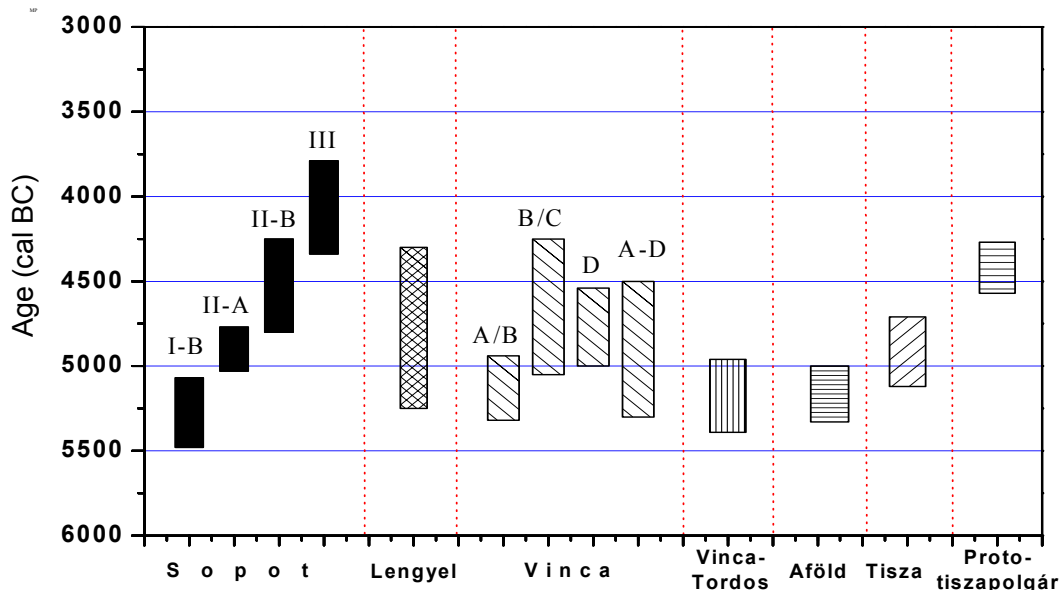


Figure 6 Comparative ^{14}C chronology of Late Neolithic cultures in Pannonian valley. **Sopot**: present results; **Lengyel**: Baldia 2003; Furhold et al. 1995; **Vinča A/B, B/C and D**: Srdoč et al. 1975, 1977, 1987; Vinča A–D: Lenneis and Stadler 1995; **Vinča-Tordos, Aföld, Tisza, Prototiszapolgár**: Hertelendi et al. 1995

inja sites in Croatia until now. The earliest dates for the Lasinja culture are from the site Koprivnički bregi in NW Croatia, giving 3500 BC (Obelić et al. 1999). The proper representatives of the Early Eneolithic are the bearers of the Baden culture (Težak-Gregl 1998). The beginning of Baden culture in eastern Croatia was dated to 3800 BC (Obelić et al. 1999).

Further ^{14}C dates from early Sopot culture sites are certainly required to further define the role of the Vinča culture in the development of the Sopot. From our own excavations and analysis, a possible revision of established archaeological assumptions for the region is foreseen in light of new dates and archaeological investigation of Sopot culture sites.

REFERENCES

- Baldia M. 2003. The Comparative Archaeology WEB. URL: <http://www.comp-archaeology.org>. Accessed 15 January 2004.
- Breunig P. 1987. ^{14}C Chronologie des vorderasiatischen, südost- und mitteleuropäischen Neolithikums [^{14}C chronology of the Preasiatic, South-East and Middle-European Neolithic]. *Fundamenta (Köln)*: Reihe A, Band 13.
- Bronk Ramsey C. 2001. Development of the radiocarbon program OxCal. *Radiocarbon* 43(2A):355–63.
- Bronk Ramsey C. 2003. *OxCal Program v.3.9—The Manual*. University of Oxford, Radiocarbon Accelerator Unit. URL: <http://www.rlaha.ox.ac.uk/oxcal/oxcal.htm>. Accessed 15 January 2004.
- Brukner B. 1974. Sopotsko-Lendelska grupa [The Sopot-Lengyel group]. In: *Praistorija Vojvodine*, Novi Sad: 95–103.
- Celestin V. 1896/97. Neolitska naseobina kod Osijeka [A Neolithic Settlement near Osijek]. *Vjesnik Hrvatskog arheološkog društva*, Zagreb.
- Dimitrijević S. 1968. Sopotsko-Lendelska kultura [The Sopot-Lengyel culture]. *Monographiae Archaeologicae (Zagreb)* 1:1–123.
- Dimitrijević S. 1979. Sjeverna zona [Northern zone]. In: Benac A, editor. *Praistorija jugoslavenskih zemalja: Neolit*. Sarajevo: Academy of Sciences and Arts of Bosnia and Herzegovina. p 229–362.
- Furholt M, Müller J, Raetzl-Fabian D, Rinne C, Wotzka HP. 2003. RADON: Radiocarbon dates online (in German). URL: <http://www.jungsteinsite.de/radon/radon.htm>. Accessed 15 January 2004.
- Hertelendi E, Kalicz N, Raczky P, Horváth F, Veres M, Svingor E, Futó I, Bartosiewicz L. 1995. Re-evaluation of the Neolithic in Eastern Hungary based on calibrated radiocarbon dates. *Radiocarbon* 37(2):239–44.

- Horvatinčić N, Obelić B, Krajcar Bronić I, Srdoč D, Čalić R. 1999. Rudjer Bošković Institute radiocarbon measurements XIV. *Radiocarbon* 41(2):199–214.
- Horvatinčić N, Srdoč D, Obelić B, Krajcar Bronić I. 1990. Radiocarbon dating of intercomparison samples at the Zagreb Radiocarbon Laboratory. *Radiocarbon* 32(3):295–300.
- Iskra-Janošić I, Krznarić Škrivanko M. 1997. Sustavno istraživanje neolitičkog naselja Sopot pokraj Vinkovaca [Systematic explorations of Sopot Neolithic settlement near Vinkovci]. *Obavijesti Hrvatskog arheološkog društva (Zagreb) year XXIX, nr 1*:20–4.
- Krajcar Bronić I, Horvatinčić N, Obelić B, Bistović R. 1995. Radiocarbon intercomparison studies at the Rudjer Bošković Institute. *Radiocarbon* 37(2):805–11.
- Krajcar Bronić I, Minichreiter K, Obelić B, Horvatinčić N. Forthcoming. The oldest early Neolithic (Starčevo culture) settlements in Croatia: Zadubravlje-Dužine and Slavonski Brod-Galovo. 4th International Symposium “¹⁴C and Archaeology”, Oxford, England, UK, 9–14 April 2002.
- Krznarić Škrivanko M. 1997. Prapovijesno naselje na Ervenici u Vinkovcima [The prehistoric settlement of Ervenica in Vinkovci]. *Opuscula Archaeologica (Zagreb)* 21:205–15.
- Krznarić Škrivanko M. 1998a. Druga etapa sustavnog arheološkog iskopavanja gradine Sopot [Second stage of systematic archaeological excavations on gradina Sopot]. *Obavijesti Hrvatskog arheološkog društva (Zagreb) year XXX, nr 1*:30–4.
- Krznarić Škrivanko M. 1998b. Treća sezona iskopavanja na gradini Sopot [Third stage of excavations on gradina Sopot]. *Obavijesti Hrvatskog arheološkog društva (Zagreb) year XXX, nr 3*:71–4.
- Krznarić Škrivanko M. 1999. Mlade kameno doba [Neolithic in Vinkovci]. In: Catalogue *Vinkovci u svijetu arheologije*. p 11–21.
- Krznarić Škrivanko M. 2000. Četvrta sezona sustavnog istraživanja gradine Sopot [Fourth season of systematic investigations of gradina Sopot]. *Obavijesti Hrvatskog arheološkog društva (Zagreb) year XXXII, nr 2*:49–52.
- Krznarić Škrivanko M. 2002. Peta i šesta sezona sustavnog istraživanja gradine Sopot [Fifth and sixth season of systematic investigations of gradina Sopot]. *Obavijesti Hrvatskog arheološkog društva (Zagreb) year XXXIV, nr 2*:36–45.
- Krznarić Škrivanko M. 2003. Sedma sezona sustavnog istraživanja gradine Sopot (godina 2002.) [Systematic Excavations at the Sopot hill-fort, seventh campaign—2002]. *Obavijesti Hrvatskog arheološkog društva (Zagreb) year XXXV, nr 1*:37–46.
- Lenneis E, Stadler P. 1995. Zur Absolutchronologie der Linearbandkeramik aufgrund von ¹⁴C-daten [Absolute chronology of Linear-band Ceramic according to ¹⁴C dates]. *Archäologie Österreichs* 6/2:4–13.
- Longin R. 1970. New method of collagen extraction for radiocarbon dating. *Nature* 230:231–42.
- Marijan B. 2001. Zaštitna istraživanja arheoloških lokaliteta uz južni trak autoceste Zagreb-Lipovac, dionica Velika Kopanica—Županja, poddionica Babina Greda—Županja [Archaeological rescue excavations at the site along the southern carriageway of the motorway Zagreb-Lipovac, section Velika Kopanica—Županja, subsection Babina Greda—Županja]. *Obavijesti Hrvatskog arheološkog društva (Zagreb) year XXXIII, nr 2*:35–45.
- Midgley MS. 1992. *TRB Culture: The First Farmers of the North European Plain*. Edinburgh: Edinburgh University Press. 550 p.
- Milojčić V. 1949. Chronologie der Jüngerer Steinzeit Mittel- und Südosteuropas [Chronology of the Neolithic in Middle and Southern Europe]. Berlin: Deutsches Archaeologisches Institut. 136 p.
- Minichreiter K. 1996–1997. Zoomorfna idoloplastika obredno-ukopnog prostora starčevačkog lokaliteta na Galovu u Slavonskom Brodu [Zoomorphic idols of the Starčevo ceremonial and burial area site at Galovo, Slavonski Brod]. *Prilozi Instituta za arheologiju u Zagrebu* 13–14:7–22.
- Obelić B, Horvatinčić N, Durman A. 1999. Radiocarbon chronology of archaeological sites in southeastern Europe. *Mémoires de la Société Préhistorique Française (Supplément 1999 de la Revue d'Archéométrie)* Tome 26:233–8.
- Obelić B, Horvatinčić N, Krajcar Bronić I. 2002a. Rudjer Bošković Institute radiocarbon measurements XV. *Radiocarbon* 44(3):601–30.
- Obelić B, Horvatinčić N, Krajcar Bronić I. 2002b. Improving of quality control and quality assurance in Radiocarbon and Tritium Laboratory; participation in the IAEA model project. Regional IRPA Congress on Radiation Protection in Central Europe—“Radiation Protection and Health”, Dubrovnik, 20.05.2001–25.05.2001., Proceedings: 10-09.
- Radiocarbon. 2001. Report on the FIRI Workshop, Edinburgh March 2001. University of Arizona, Tucson. URL: <http://www.radiocarbon.org_Announcements/FIRI-results.html>. Accessed 2004 January 15.
- Raetzl-Fabian D. 1986. Phasenkartierung des mitteleuropäischen Neolithikums [Phase mapping of Middle-European Neolithic]. *Chronologie und Chorologie. B.A.R. International Series*: 316.
- Šimić J. 1998. Istraživanje neolitičkog nalazišta Osijek-Filipovica/Hermanov vinograd [Investigations of the Neolithic site Osijek-Filipovica/Herrmann's Vineyard]. *Glasnik slavonskih muzeja (Županja)* 2(57): 69–72.
- Šimić J. 1999. Osijek-Filipovica (Hermanov vinograd), zaštitno iskopavanje neolitičkog naselja [Osijek-Filipovica (Herrmann's Vineyard), rescue excavations of a Neolithic settlement]. *Obavijesti Hrvatskog arheološkog društva (Zagreb) year XXXI, nr 1*:30–3.

- Šimić J. 2000. Istraživanje neolitičkog lokaliteta Hermanov vinograd u Osijeku [Investigations of the Neolithic site Herrmann's Vineyard in Osijek]. *Histria antiqua (Pula)* 6:223–30.
- Srdoč D, Breyer B, Sliepčević A. 1971. Rudjer Bošković Institute radiocarbon measurements I. *Radiocarbon* 13(1):135–40.
- Srdoč D, Obelić B, Horvatinčić N, Sliepčević A. 1979. Measurement of the ^{14}C activity of the ANU sucrose secondary standard by means of the proportional counter technique. *Radiocarbon* 21(3):321–8.
- Srdoč D, Obelić B, Sliepčević A, Krajcar Bronić I, Horvatinčić N. 1987. Rudjer Bošković Institute radiocarbon measurements X. *Radiocarbon* 29(1):135–47.
- Srdoč D, Sliepčević A, Obelić B, Horvatinčić N. 1977. Rudjer Bošković Institute radiocarbon measurements IV. *Radiocarbon* 19(3):465–75.
- Srdoč D, Sliepčević A, Obelić B, Horvatinčić N. 1981. Rudjer Bošković Institute radiocarbon measurements VI. *Radiocarbon* 23(3):410–21.
- Srdoč D, Sliepčević A, Planinić J. 1975. Rudjer Bošković Institute radiocarbon measurement III. *Radiocarbon* 17(1):149–55.
- Stuiver M, Polach HA. 1977. Discussion: reporting of ^{14}C data. *Radiocarbon* 19(3):355–63.
- Stuiver M, Reimer PJ, Bard E, Beck JW, Burr GS, Hughen KA, Kromer B, McCormac G, van der Plicht J, Spurk M. 1998. INTCAL98 radiocarbon age calibration, 24,000–0 cal BP. *Radiocarbon* 40(3):1041–83.
- Težak-Gregl T. 1998. Neolitik i eneolitik [Neolithic and Eneolithic]. In: Dimitrijević S, Težak-Gregl T, Majnarić-Pandžić N, editors. *Prapovijest*. Zagreb: Naprijed. p 59–151.

CHRONOLOGY AND POSSIBLE LINKS BETWEEN CLIMATIC AND CULTURAL CHANGE DURING THE FIRST MILLENNIUM BC IN SOUTHERN SIBERIA AND CENTRAL ASIA

G I Zaitseva^{1,2} • B van Geel³ • N A Bokovenko¹ • K V Chugunov⁴ • V A Dergachev⁵ • V G Dirksen⁶ • M A Koulikova¹ • A Nagler⁷ • G Parzinger⁶ • J van der Plicht⁸ • N D Bourova² • L M Lebedeva¹

ABSTRACT. We reconstructed climate change during the second half of the Holocene for the Minusinsk (southern Siberia) and the Uyuk (Central Asia) valleys in the Eurasian steppe zone. Sediment cores from 2 lakes and a soil profile from the Arzhan-2 burial mound were investigated. We combined pollen and geochemical analyses and radiocarbon dating with the archaeological record. A sharp increase of human population density occurred at the transition from the Bronze Age to Iron Age (about 2700 cal BP). The most representative Scythian culture started in the Uyuk and the Minusinsk valleys after increased humidity and occupation capacity of the steppe zone during the 9th century BC.

INTRODUCTION

Long-term and short-term climatic variations during the Holocene have been recorded in high-resolution studies of tree rings, ice cores, and peat deposits (cf. Dergachev et al. 2001; van Geel et al. 1996). Studies of cosmogenic isotopes, such as the radiocarbon content in tree rings and the ¹⁰Be concentration in ice cores, show that cyclic climate variations with a duration of about 200 and 2300 yr are caused by changes in solar activity (Vasiliev et al. 2002). At around 2700 cal BP (9th century BC), a sharp climatic shift was observed in different parts of Europe. This change had a global character and was associated with an abrupt decline of solar activity (van Geel et al. 1996, 1998; Speranza et al. 2002; Gracheva 2002). Some recently published studies evaluate possible evidence for climate change in the 1st millennium BC in Central Asia. Peck et al. (2002) studied the Holocene sediments of Lake Telmen in Mongolia and, based on the high-level terraces of the lake, concluded that an effective moisture balance greater than the present-day occurred between 2710 and 1260 cal BP. Grunert et al. (2000) studied geomorphic changes in landforms and lake-level changes in the Uvs Nuur basin and adjacent areas in western Mongolia. The lakes Uvs Nuur and Bayan Nuur are situated just south of the Russian-Mongolian border and 100 to 200 km southwest of the Uyuk valley in Tuva. The reconstructed lake-level fluctuations indicate a decline in precipitation since about 5000 cal BP. A sudden rise of lake levels, glacial advances, and solifluction started between 3000 and 2000 cal BP, indicating enhanced rainfall and lower temperatures. Pollen analysis for a peat

¹Institute for the History of Material Culture, Russian Academy of Sciences, St. Petersburg, Russia, Dvortsovaya nab. 18, 191186, St. Petersburg, Russia.

²Corresponding author. Email: ganna@mail.wplus.net.

³Institute for Biodiversity and Ecosystem Dynamics, Faculty of Science, University of Amsterdam, Kruislaan 318, 1098 SM Amsterdam, the Netherlands. Email: vangeel@science.uva.nl.

⁴State Hermitage Museum, Dvortsovaya nab. 36, 191186 St. Petersburg, Russia. Email: oaves@hermitage.ru.

⁵A.F. Ioffe Physical-Technical Institute, Russian Academy of Sciences, Politechnicheskaya str. 26, 19402 St. Petersburg, Russia. Email: v.dergachev@pop.ioffe.rssi.ru.

⁶Institute of Volcanic Geology and Geochemistry, Russian Academy of Sciences, Piipa blvd. 9, 683006 Petropavlovsk-Kamchatsky, Russia. Email: dirksen@VD3155.spb.edu.

⁷Deutsches Archäologisches Institut, Eurasien-Abteilung, Podbielskiallee 69-71, 14195 Berlin, Germany. Email: eurasien@dainst.de.

⁸Centre for Isotope Research, University of Groningen, Nijenborgh 4, 9747 AG Groningen, the Netherlands. Email: plicht@phys.rug.nl.

deposit showed wetter climatic conditions since about 2500 cal BP (Lehmkuhl et al. 1998), and that the vegetation around Bayan Nuur displayed a transition from steppe to a temporary forest phase.

The main focus in the present study has been on the Minusinsk and Uyuk valleys (Figure 1). These isolated mountain depressions in southern Siberia and Central Asia form part of the Eurasian steppe belt. These valleys are located in the central part of Eurasia, where the Altai-Sayan mountain ridges form a barrier for moist air masses from the Atlantic Ocean. Low and irregular precipitation, strongly depending on the topography, is the main factor controlling environmental changes and, possibly, the occupation history of the territory by ancient populations.

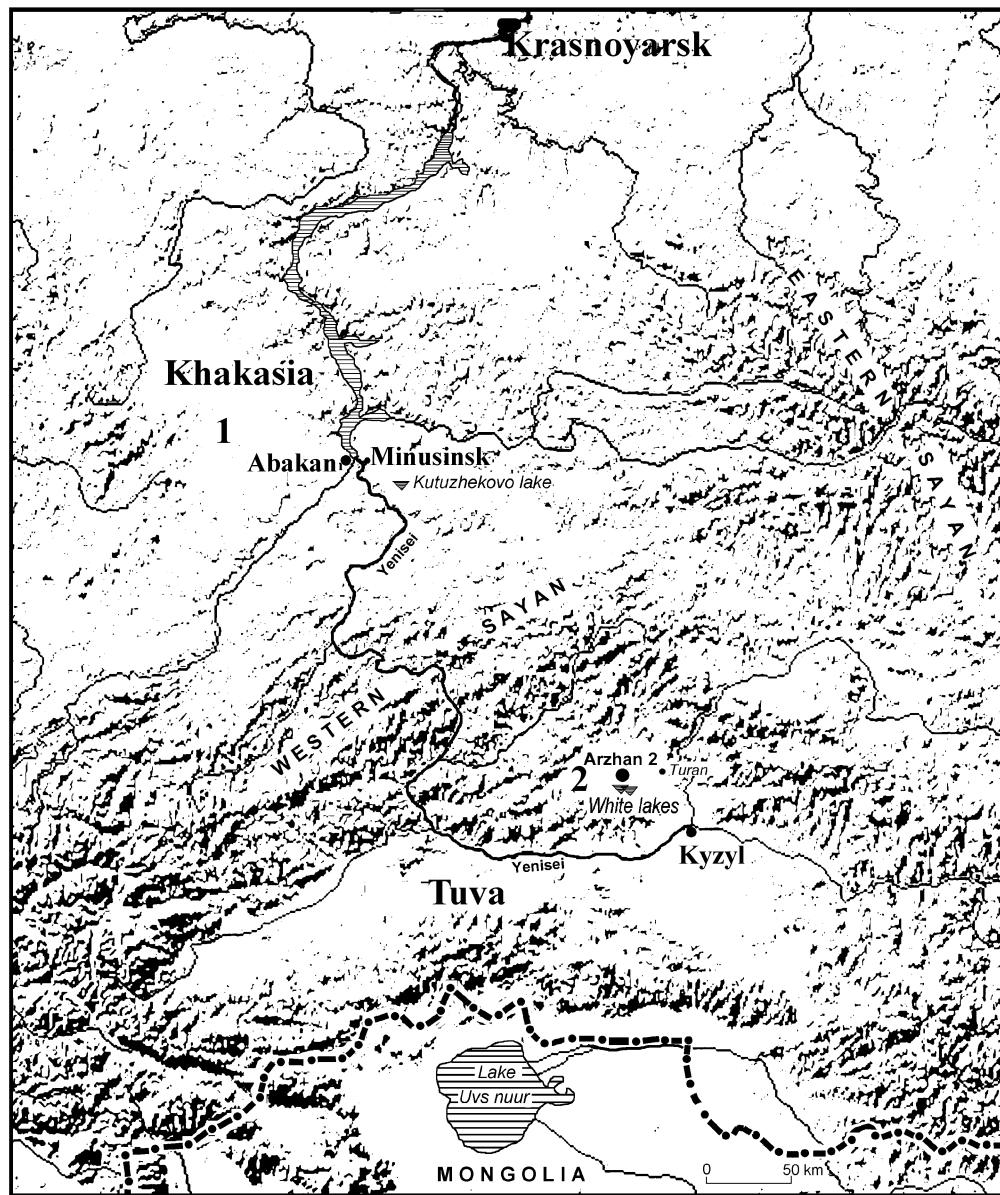


Figure 1 Map of the investigated region indicating the Minusinsk (1) and Uyuk valleys (2)

The Minusinsk valley is located in the southern part of the Krasnoyarsk district and the Republic of Khakasia. The bottom of the valley, surrounded by the high mountain chains of the Sayans, is located at a height of 300–350 m. Sand dunes and some freshwater lakes are present in the central part of the valley; they probably originate from the ancient Yenisey River valley. The modern climate is continental with a mean annual temperature of about 0 °C. The mean annual precipitation ranges from 250 mm in the western part of the valley (Khakasia) to 1500 mm in the eastern part, where the Western and Eastern Sayan Mountain ridges meet (Galvina 1954). A major part of the valleys was originally covered with bunchgrass steppe vegetation. Today, this area is mainly used for agriculture and settlements. Some patches of dense pine forests occur on the sand dunes. A piedmont of mountain ridges lies within the forest-steppe zone, while mountain taiga (coniferous and mixed forests) rises to a height of 1300–1800 m.

The Uyuk valley is the section of the Turan-Uyuk mountain depression located in the northern part of the Tuva Republic. In the west and east, this valley is surrounded by the Sayan Mountain chains; in the south, it is bordered by the Uyuk Mountain ridge. The bottom of the valley is located at 650–850 m. The present climate is extremely continental with a mean annual temperature below 0 °C. The mean annual precipitation is about 300 mm and most of the rainfall occurs during the summer (Efimtsev 1957). The main vegetation types of the valley are steppe and saline meadows, while the mountain slopes are covered by forest.

These regions have long been investigated by archaeologists, and links between cultural and environmental changes may exist.

The St. Petersburg Radiocarbon Laboratory Database produced about 300 ¹⁴C measurements for 80 sites located in Khakasia, and 140 ¹⁴C measurements for 25 sites located in Tuva. Not all known sites have been ¹⁴C dated, but a representative picture is obtained. The frequency of Holocene ¹⁴C dates for the archaeological sites in the territory of the Eurasian steppe between 42° and 55°N are shown in Figure 2 (curve 1), and for southern Siberia (Khakasia) combined with those from Central Asia (Tuva) (curve 2).

During the period between 8000 and 4000 BC, Mesolithic and Neolithic cultures were present all over the Eurasian territory, with the exception of southern Siberia and the Central Asian part of Russia (southern part of Krasnoyarsk district, Khakasia and Tuva). Occupation of these regions began during the Bronze Age and became more intense during the Iron Age. Figure 2 shows that both regions were essentially uninhabited during the Mesolithic-Neolithic periods up to 4500–4000 BP. Figure 2 also shows a sharp increase of archaeological sites after 3000 BP. The increase in settlements may be connected with the changed environmental conditions that influenced the economy of the ancient populations. Thus, we conducted our investigations to better understand the character of climatic changes and their possible influence on the development of archaeological cultures.

METHODS

We used pollen analysis and geochemical methods for the study of the lake deposits, supplemented by archaeological information and ¹⁴C data. Most archaeological sites in the study area were ¹⁴C dated (see Figure 2 for their distribution).

The lakes investigated were Kutuzhekovo (KTH; 53°36'N, 91°56'E) Lake in the Minusinsk valley, and the 2 White Lakes (WL-1; 52°05'11"N; 93°42'18"E and WL-2; 52°03'59"N; 93°43'40"E) in the Uyuk valley. During 2001 and 2002, we collected lacustrine sediment cores along the borders of these lakes using a Dakhnovsky sampler (Faergi and Iversen 1989) for sand deposits and a Russian

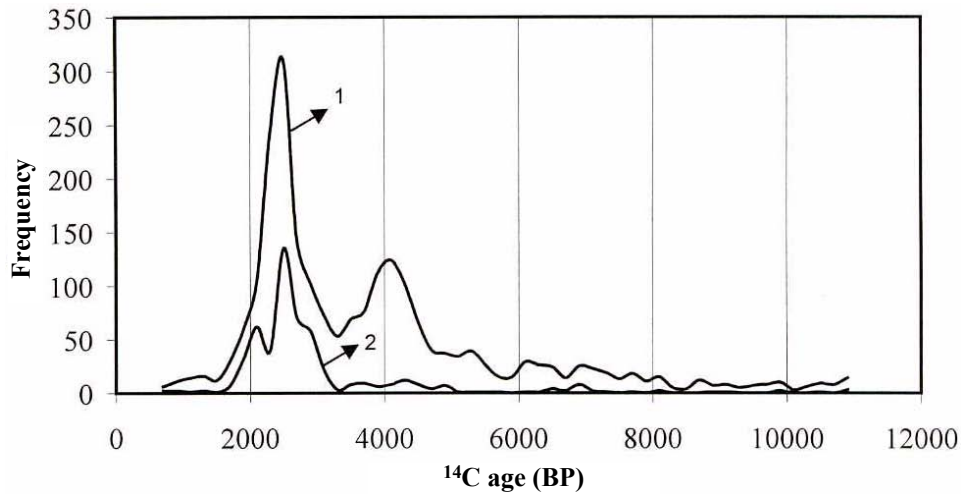


Figure 2 Distribution of ^{14}C dates of monuments located in the Eurasian steppe belt: 1) all of the Eurasian steppe; 2) southern Siberia (Khakasia) and Central Asia (Tuva).

sampler for the soft gyttja deposits. Subsamples from the longest cores were used for pollen and geochemical analyses.

The pollen samples were prepared at the University of Amsterdam using standard procedures (Faegri and Iversen 1989). An average of 507, 384, and 448 pollen grains were counted in samples from the WL-2 and KTH cores and from the Arzhan-2 site, respectively. Pollen percentages were calculated based on the total pollen sum, excluding spores and aquatic taxa. The WL-2 samples yielded scarce pollen and were omitted from the calculation. The percentages of other microfossils were also calculated based on the total pollen sum. The results are shown as percentage diagrams of the selected taxa. The pollen concentrations of the major components are also given in the diagrams, with the exception of the diagram for Arzhan-2, where the absolute pollen concentration was not calculated.

The samples for the geochemical analysis were collected together with the samples for pollen analysis. The aeolian-soil deposits were sampled from the open cross-section buried under the Arzhan-2 monument. The samples for geochemical analysis were taken from each layer of the stratigraphical successions.

Standard analytical techniques were used to measure the chemical composition of the samples (Soltanpour et al. 1996). We determined the elements Na, Ca, Mg, Al, Fe, Mn, P, Ti, Zn, Cu, Ni, Cr, Ba, Sr, S, and N, as well as the CO_2 and C_{org} yield.

The correlation between the elements allows us to determine the mineral complexes of the samples. Sedimentological parameters were applied as paleoclimatic markers. The decay of vegetation during colder periods increases the CO_2 concentration in the deposits. Such processes destroy the carbonate minerals (Eusterhaues et al. 2002). Precipitation with evaporation also results in the destruction of carbonate minerals. Dry environments favor carbonate precipitation (Hassan 1985). The Ba/Sr ratio is used as a marker of relative temperature, following Chen et al. (1999) and Goldberg et al. (2000). We used the Chemical Index Alteration (CIA) to estimate the relative temperature. This indicator determines the weathering grade during increasing temperature and humidity (Bor-ming et al. 2001). An increasing CIA index in soil profiles is an indication of warmer climate.

The ^{14}C dates were produced by 2 laboratories: ^{14}C laboratory of the Institute for the History of Material Culture (Zaitseva et al. 1999) and the Centre for Isotope Research, University of Groningen (van der Plicht et al. 1995; van der Plicht and Wijma 2000). The Institute for Material Culture (Le) employs the liquid scintillation technique and the Groningen laboratory (GrA) uses accelerator mass spectrometry (AMS). The counting form for measuring the ^{14}C concentration is benzene for the traditional methods, and graphite for AMS methods.

Chemical pretreatments to isolate the organic fractions from the lake soil deposits are similar for both dating techniques and consist of standardized washes with acid-alkali solutions (Arslanov 1986; Chichagov 1985). First, to eliminate exogenous carbonate, the soil samples were heated in 3% HCl solution for 30 min and then washed to neutral. The residue is then treated with cold 2% NaOH solution for 20 hr. The alkali solution and residue are filtered, and from the alkali solution, the humic acids are precipitated by HCl, then isolated by centrifugation. This humic acid fraction obtained is here named “cold humic.” The residue filtered from the acid/alkali wash is boiled in 2% NaOH solution for 4 hr, and after cooling, the humic acids are precipitated by HCl and separated by centrifugation. After washing to neutral and drying, this fraction of humic acids is here named “hot humic.” Meanwhile, the charcoal was chemically pretreated with a standard acid-alkali-acid solution (2% HCl and 2% NaOH).

The chemically treated humic acids and charcoal were then prepared for either liquid scintillation (Zaitseva et al. 1999) or AMS analysis (van der Plicht et al. 1995; van der Plicht and Wijma 2000) according to each laboratory’s standardized procedures for ^{14}C dating.

Our choice of ^{14}C analysis type for certain samples was limited by the recovered sample size. Sample size limits on the amount of charcoal for liquid scintillation are between 0.8 g and 1 g. For the humic samples, if the separate fractions of the humic acids (cold and hot) were not sufficient for dating, we chose to combine both fractions, and the ^{14}C date was produced from the total humic acids fraction (“Total humic acids,” Tables 1, 2, 3).

RESULTS

The Minusinsk Valley

Organic layers from the sediment core collected from Kutuzhekovo Lake were ^{14}C dated in St. Petersburg (Le, conventional) and Groningen (GrA, AMS). We note that these deposits contain a low amount of organic material, particularly in the deepest part. The results are shown in Table 1.

The Kutuzhekovo (KTH) pollen record is constructed from 53 samples, including a surface sample from the lacustrine mud, and shown in Figure 3. Three main zones are distinguished in the pollen diagram:

- **Zone KTH-I** (235–165 cm; 4310 ± 120 BP [Le-6233], upper half of the zone) is characterized by domination of shrub pollen and by the highest values of xerophytic taxa. In the middle of the zone, the *Betula sect. Nanae/Fruticosae* pollen reach their maximum value (up to 48%) and a sudden rise of pine pollen frequency occurs, while *Artemisia* and *Chenopodiaceae* show their peaks at the lower and upper parts of the zone. These xerophytic components taken together prevail over *Cyperaceae* and *Poaceae* and indicate dry conditions during this time interval, when steppe and desert-steppe persisted in the valley. All these features are indications of an arid period interrupted by a minor amelioration just before 4300 BP. The upper dry interval was obviously less arid than the lower one because of the higher *Artemisia/Chenopodiaceae* ratio (van Campo and Gasse 1993). The extremely low values of tree pollen (<10%) found at the

Table 1 Results of ^{14}C dating of deposits from Kutuzhekovo Lake.

Nr	Lab nr	Depth (cm)	Material	^{14}C age (BP)	Calibrated dates, cal BC/AD	
					1 σ	2 σ
KTH 1	Le-6234a	106–120	Hot humic acids	1530 \pm 90	430–610 cal AD	330–670 cal AD
KTH 2	Le-6234b	106–120	Total humic acids	1600 \pm 150	320–610 cal AD	50–700 cal AD
KTH 3	Le-6231	146–158	Total humic acids	2470 \pm 70	770–510 cal BC	790–400 cal BC
KTH 4	Le-6232	158–176 (upper layer)	Total humic acids	2630 \pm 180	1000–520 cal BC	1300–350 cal BC
KTH 5	GrA-20687	158–176 (lower layer)	Total humic acids	2985 \pm 45	1320–1130 cal BC	1390–1060 cal BC
KTH 6	Le-6233	176–195	Total humic acids	4310 \pm 120	3300–2650 cal BC	3350–2600 cal BC
KTH 1	Le-6234a	106–120	Hot humic acids	1530 \pm 90	430–610 cal AD	330–670 cal AD

base of the core also indicate the maximum aridity of the record, with strongly reduced mountain forest.

- **Zone KTH-II** (165–117 cm; 2985 \pm 45 BP [GrA-20687], beginning of the zone). This zone is characterized by abrupt starting pollen concentrations. The most significant features are the sharp rise of *Cyperaceae*, from 10% at the beginning of the interval up to 32% at the top, and a decrease of xerophytic taxa. This reflects a rapid vegetation shift due to an increase in moist conditions at about 3000 BP. The shrub birch percentages decrease quite rapidly to 5–10%, and tree birch (*Betula sect. Albae*) appears. A gradual increase of *Pinus sylvestris*, which grows predominantly in the lower part of mountain forest and is adapted to grow on sand dunes in the valley, suggests a progressive forest shift down-slope as a response to increased moisture conditions. The KTH-II zone corresponds to a period with maximum humidity.
- **Zone KTH-III** (117–30 cm; 1600 \pm 150 BP [Le-6234b] and 1530 \pm 90 BP [Le-6234a], lower part of the zone). An increase in the frequency of highland pine species *Pinus sibirica* at the beginning of the zone indicates a warmer climate compared to the KTH-II interval. The values of xerophytic taxa are rather stable, while *Poaceae* shows a sharp rise from 13% to 33% and reaches the highest values of the whole record. The change of domination from sedges to grasses reflects a drop in water level and a change in trophic conditions, stimulating the expansion of *Phragmites* vegetation around the lake. However, it is difficult to prove an exclusively local origin for grasses, because some *Poaceae* pollen grains could also originate from the surrounding steppe, rich in *Stipa*, *Festuca*, and *Koeleria*. In both cases, we can also deduce that the sudden change of *Cyperaceae* by *Poaceae* corresponds to the end of a period with maximum humidity.

The climatic changes as derived from the pollen data support our observations from our geochemical data.

For Kutuzhekovo Lake, the geochemical results are summarized as follows: 1) a detrital (alumosilicate) element group, consisting of K, Na, Al, Ti, Ba, Fe; (2) a carbonate group, consisting of Ca, Sr, CO_2 ; (3) an organic group, consisting of N, C_{org} , S. The analysis shows anti-correlation between alumosilicate elements and elements found in the organic material. The increase of detrital sediments in the lake deposits compared with organic material can take place in cool climatic conditions, or as the result of soil erosion. The amount of aluminum is the detrital (alumosilicate) index. The increase

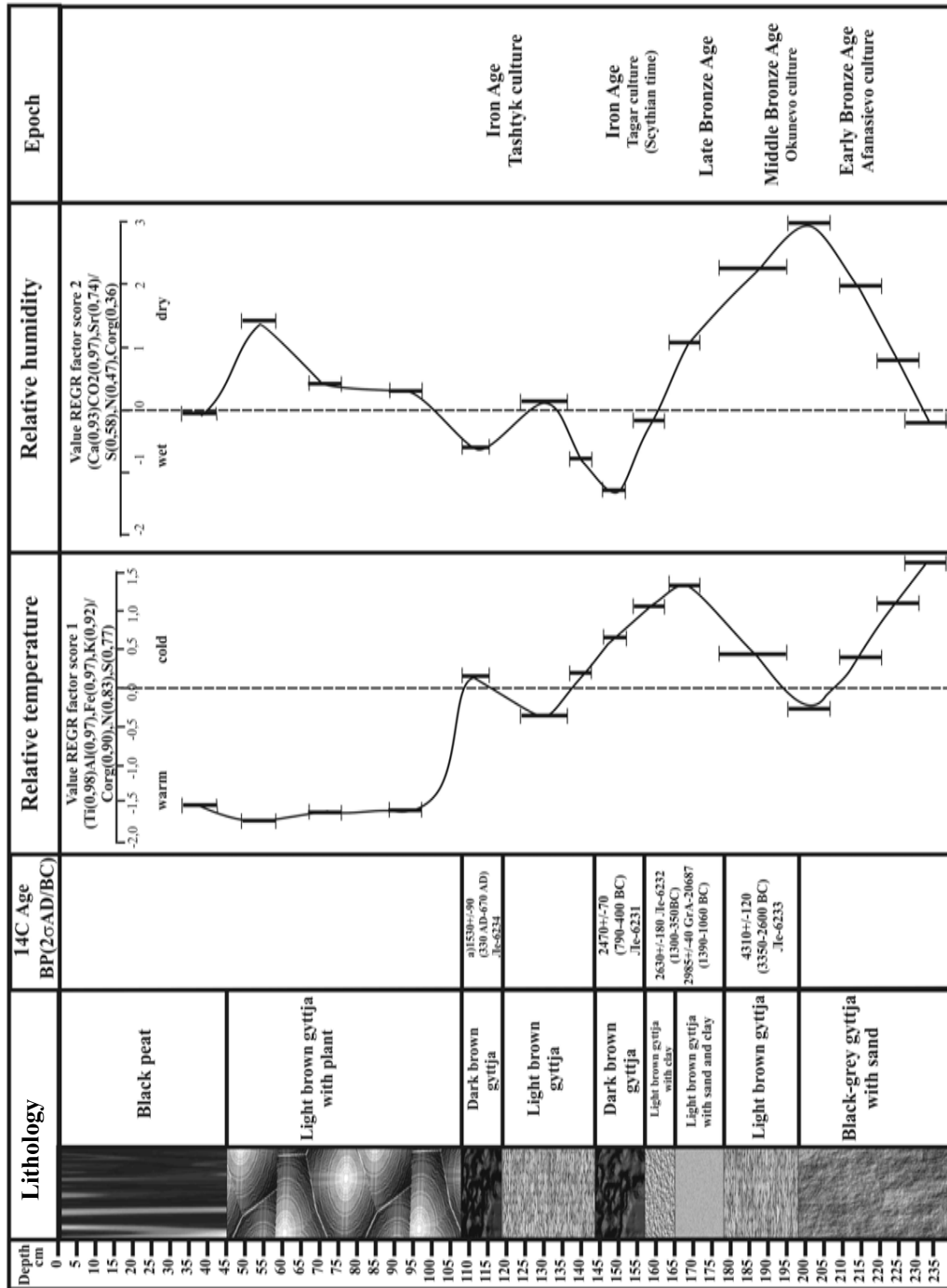


Figure 4 Lithology and geochemistry for Kutuzhekovo Lake.

of clay-feldspar concentration in the lake deposits depends on the terrestrial sediment supply during the cold period (Eusterhaues et al. 2002). The analysis shows that temperature fluctuations can be determined this way, as well as relative humidity.

Figure 4 shows temperature and humidity changes, as derived from the geochemical data. A cool phase occurred during the 11th–8th centuries BC. An increase in humidity reached a maximum during the early Iron Age, when there was also a warming trend. In summary, the pollen record and the geochemical data both show a pronounced shift to humid climatic conditions at the start of the early Iron Age.

The Uyuk Valley

Results of the ^{14}C dating of the organic materials from the White Lake deposits are shown in Table 2.

Table 2 Results of ^{14}C dating of deposits from White Lake.

Nr	Lab nr	Material	Depth (cm)	^{14}C age (BP)	Calibrated dates, cal BC/AD	
					1 σ	2 σ
WL1 1	Le-6195	Hot humic acids	20–40	2090 \pm 100	360 cal BC–20 cal AD	390 cal BC– 80 cal AD
WL2 2	Le-6499	Total humic acids	21–26	3930 \pm 90	2580–2290 cal BC	2900–2100 cal BC
WL2 3	Le-6501	Total humic acids	36–41	5840 \pm 50	4790–4670 cal BC	4850–4580 cal BC
WL2 4	Le-6502	Hot humic acids	41–44	4670 \pm 400	3900–2900 cal BC	—
WL2 5	Le-6503	Hot humic acids	44–49	6530 \pm 400	5800–5000 cal BC	—
WL2 6 ^a	Le-6623	Total humic acids	22–35	2460 \pm 120	770–480 cal BC	850–200 cal BC
WL2 7 ^a	Le-6624	Total humic acids	35–50	4360 \pm 150	3650–3100 cal BC	3700–2900 cal BC

^aSamples collected in 2002.

For WL-2, only ^{14}C dates for the deposits between 20 and 50 cm depth could be obtained. The lower layers did not contain sufficient organic material for dating. One ^{14}C date could be produced for WL-1 for the layer of 20–40 cm (2090 \pm 100 BP; Le-6195). During the 2001 season, we collected a small number of samples using both a Dakhnovsky and a Russian corer. The deposits had a low organic content, resulting in larger measurement errors in the liquid scintillation analysis. In 2002, we opened another trench at White Lake to collect additional samples with sufficient material for dating. The layer at 22–35 cm, corresponding to the Scythian period, was dated 2460 \pm 120 BP (Le-6623). A deeper layer, corresponding to the Middle Bronze Age, was dated 4360 \pm 50 BP (Le-6624).

Of the 33 samples in the White Lake-2 (WL-2) core, only 19 samples contained enough pollen for percentage calculations. The total length of this core was 130 cm, but most samples from the lowest 25 cm did not contain pollen. The pollen and microfossil diagram is shown in Figure 5. The following zones are distinguished in the diagram:

- **Zone WL-I** (105–60 cm). From the base of the core, *Artemisia* pollen are dominating and reach the highest value of the whole record (around 70%), while *Chenopodiaceae*, *Poaceae*, and *Ephedra* are present permanently as minor components. Tree-pollen percentages are very low

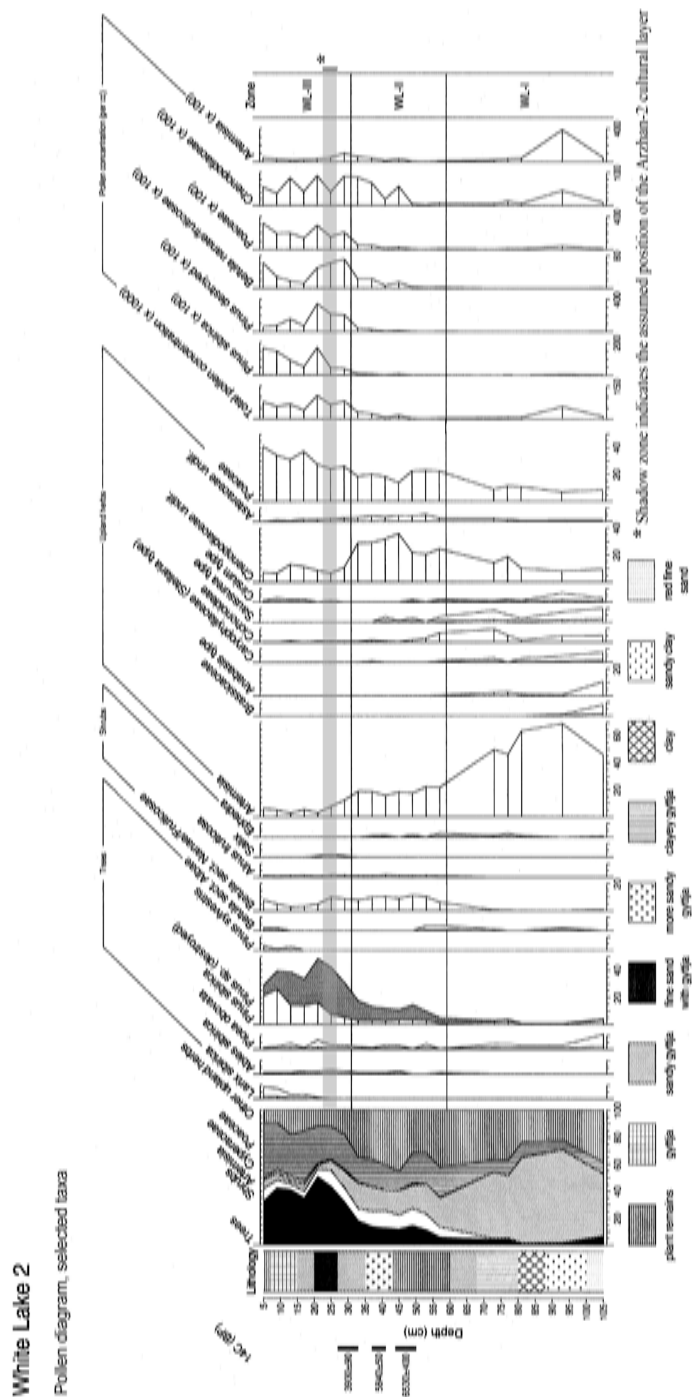


Figure 5 Pollen diagram for White Lake (Tuva)

and constant. The pollen concentrations are extremely low, except for the only sample at the basal part of zone. All these features suggest low local and regional pollen production, a persistence of stony steppe within the valley, and scarce forest or even tree-less conditions in the mountains during a relatively dry and cold climate.

- **Zone WL-II** (60–32 cm; 6530 ± 400 BP [Le-6503] in the middle of zone, 5840 ± 50 BP [Le-6501], upper part of the zone). The *Chenopodiaceae* frequency increases to 37%, and dominates over *Artemisia* and *Poaceae* at the second half of zone, indicating that desert and semi-desert conditions persisted in the depression, and/or that halophytic vegetation was present in the lake area. This suggests lower moisture, i.e., there is more evaporation than precipitation. Low pollen concentrations, a sign of low biomass production during this period, also indicate arid conditions. A gradual increase of pine pollen, taken together with the appearance of shrub birch pollen, suggests the establishment of forest and shrub belts in the mountains. These phenomena are all indications of dry and warm climate conditions during this period.
- **Zone WL-III** (32–5 cm; 3930 ± 90 BP [Le-6499], beginning of the zone). The most remarkable feature of this zone is a sudden rise of tree-pollen values to 54%, together with a sharp increase of the total pollen concentration. Xerophytic taxa, *Artemisia* and *Chenopodiaceae*, decline to 3% and 7%, respectively; *Ephedra* disappears completely, while *Poaceae* pollen gradually increase towards the top of core, reaching their highest value of 41%. *Cyperaceae* become more frequent, indicating its settlement in the local wetlands. Both grasses and sedges start to colonize the lake shores and replace halophytic wetland plant communities. This reflects a significant vegetation shift from semi-desert to herbaceous steppe in the valley, and a relatively rapid spreading of mountain forest; this also indicates the onset of more humid conditions. The highest concentration of shrub birch pollen suggests a relatively cold climate at the transition between dry and wet periods.

Three groups of elements are found in the deposits of WL-2: (1) a detrital (alumosilicate) element group, consisting of K, Al, Ti, Ba, Fe; (2) Sr, Ca, S, CO₂, N, C_{org}; and (3) an organic group consisting of carbonates, sulfates, and organic complexes. Since all CO₂ is bound to Ca in carbonate, the calcium excess combined with strontium constitutes sulfate complexes. Sodium shows minor correlation with all elements; Na probably combines into halogen minerals. Our analysis also shows that there is no correlation between alumosilicate elements and elements included in organic material, indicating relative temperature variations. Increasing salinity (Na) of the lake reflects a dry environment, indicating humidity changes.

The results of the climatic reconstructions based on geochemistry are shown in Figure 6. The following major fluctuations are observed:

1. The period when the lower layers (135–95 cm) were deposited was characterized by a cool, dry climate, and (based on the data of the granulometric analysis) the depth of the lake basin was rather low.
2. During the next period (95–58 cm), the climate was even cooler, but the lake level was relatively high. The higher concentration of N and Mn indicates oxidation processes in the lake.
3. During the following period (57–30 cm), one can observe a temperature rise and relatively dry conditions (shallow lake).
4. Maximal dry conditions occurred around 3900 BP (33–30 cm).
5. During the youngest period (30–15 cm), beginning around 3000–2500 BP, more wet conditions and higher temperatures prevailed. Local organic production was high, leading to terrestrialization of the lake at the sampling site.

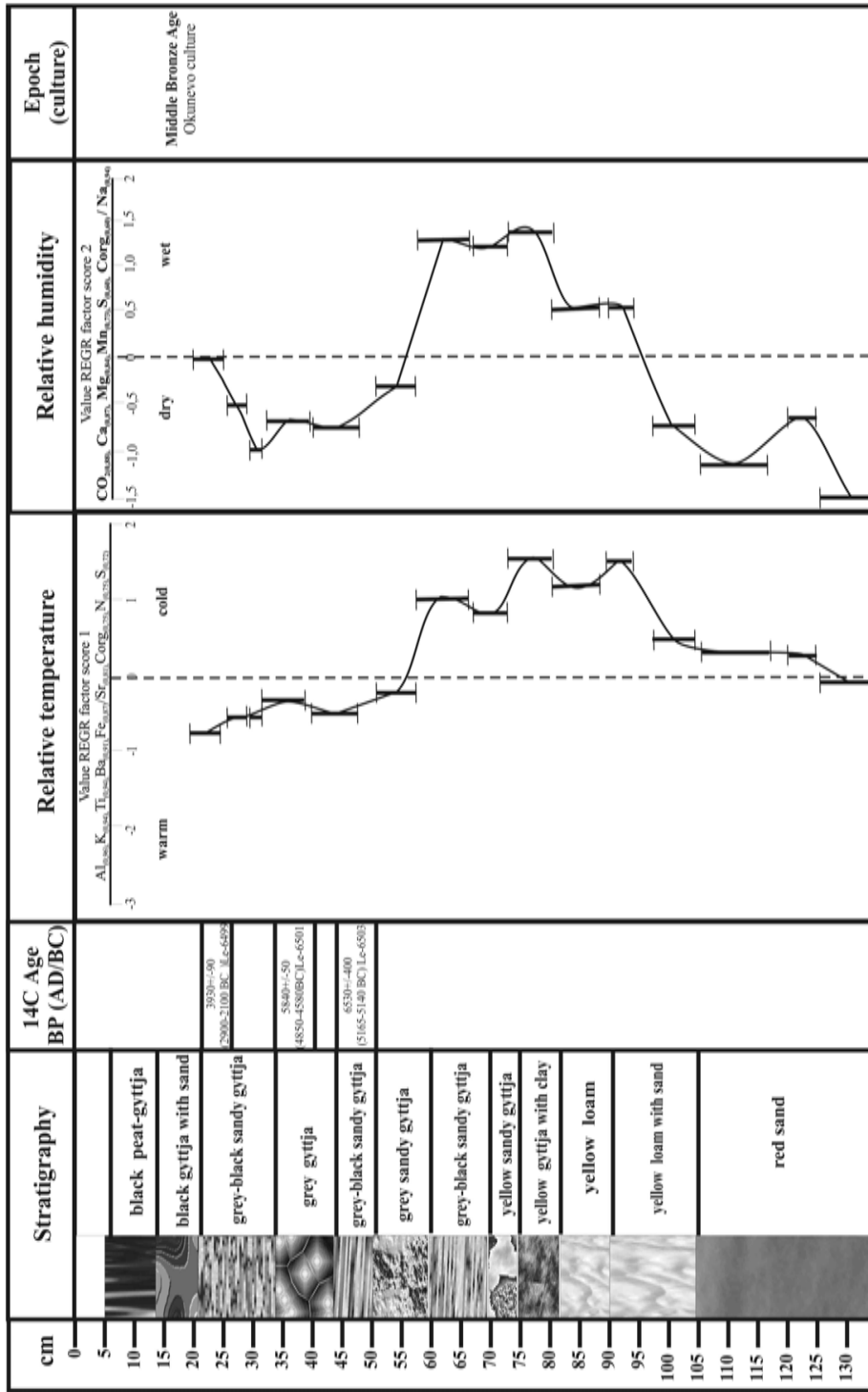


Figure 6 Lithology and geochemistry for White Lake (Tuva).

The famous Arzhan-2 Scythian monument (52°03'N; 93°35'E) is located about 1 km from the White Lakes. This monument was discovered in 2001 (Chugunov et al., forthcoming). The first chronological study is presented in these proceedings (Zaitseva et al., these proceedings). This monument is dated to the 7th century BC. The ^{14}C dates of the deposits from the Arzhan-2 monument are in Table 3.

Table 3 The ^{14}C results for the deposits from Arzhan-2 monument.

Nr	Lab nr	Material	Location	^{14}C age (BP)	Calibrated dates, cal BC	
					1 σ	2 σ
1	Le-6219	charcoal	Outside the royal grave 5	3000 ± 20	1300–1130	1370–1120
2	GrA-18938	Total humic acids from soil	Inside the royal grave 5	2530 ± 70	800–520	810–410

Unfortunately, during the monument construction, the soil layers were disturbed. Based on archaeological evidence, it was suggested that this location was occupied by people of the Okunevo culture before the burial mound was built. A ^{14}C date of charcoal from a pit fill (3000 ± 20 BP, Le-6219) supports this hypothesis. Several profiles were sampled during the excavation of the barrow; a pollen diagram was produced (Figure 7) and samples were analyzed geochemically (Figure 8).

The pollen diagram is composed of 4 sets of samples representing stratigraphical levels:

1. A buried cultural level (1 sample) belonging to the Okunevo culture dated to 3000 ± 20 BP (Le-6219);
2. The bottom of buried soil below the Arzhan-2 monument;
3. The surface of buried soil directly connected with the Arzhan-2 barrow construction, dated to 2530 ± 70 BP (GrA-18938);
4. The modern surface.

The low temporal resolution of the WL-2 sediment core did not allow us to make a direct correlation between the WL-2 pollen record (Figure 5) and pollen data from the Arzhan-2 monument (Figure 7). To determine a possible stratigraphical position of the main cultural layer of Arzhan-2 within the WL-2 pollen record, we used the changes in tree-pollen curves. These long-distance transported taxa have a regional significance, while the values of non-arboreal taxa are more variable and dependent on the local environments. According to the Arzhan-2 pollen data, the total tree-pollen sum from the surface of the buried soil is higher than that from the Okunevo cultural level and lower than that from the modern surface. Based on these data, we suppose that the Scythian cultural layer corresponds stratigraphically to the lower part of the WL-III zone in the WL-2 pollen diagram.

Based on these paleoenvironmental data, it is possible to connect the development of archaeological culture with the climatic changes. It is clear that the Arzhan-2 monument was erected during a period of relatively wet and warm climatic conditions.

DISCUSSION

Cultural Developments in the Minusinsk Valley

We compared our detailed paleoclimatic data with the occupation records of ancient cultures to determine possible relationships. After more than 200 yr of archaeological research in the Minusinsk basin, much is known about the sequence of cultures (Vadeckaya 1986; Vasiliev 2001).

The steppe areas in Khakasia were occupied only since the end of the Neolithic period, (Lisytsin 1988). The first Bronze Age cultures found in this territory, the Afanasievo, dated to 4th–3rd millennium BC, and the Okunevo, dated to the end of the 3rd millennium BC (Görsdorf et al. 1998, 2001), have no local origin. They could have come from the Black Sea region, from the southern Caspian territory, or from Central Asia. The Middle Bronze Age of the northern part of the Minusinsk valley is characterized by the Andronovo culture, dated to the 18th–14th century BC (Görsdorf et al. 1998).

The archaeological data do not reveal why the Andronovo population did not move to the southern part of the Minusinsk valley; it is possible that environmental conditions were a limiting factor. At the end of the 2nd millennium BC, the climate in the Minusinsk valley was relatively dry and cool. The best represented Late Bronze Age culture in the Minusinsk valley is the Karasuk culture, dated to the 14th–10th century BC (Görsdorf et al. 1998, 2001; Bokovenko 1995; Bokovenko and Legrand 2000). Thousands of burial mounds and settlements of this culture were discovered in the steppe zone of the Yenisei River valley. Artifacts of this culture were found in a large region, ranging from central Kazakhstan to Mongolia and China (Novgorodova 1970; Chlenova 1972). The archaeological materials show that in this period horse-riding became important and that the transition to a nomadic stock-breeding economy took place.

The Karasuk culture developed into the early Iron Age Tagar culture (1st millennium BC; Vadeckaya 1986), which is contemporary and closely related to Scythian cultural groups in other parts of the Eurasian steppe belt. The change from the latest phase of the Late Bronze Age to the beginning of the Iron Age, when the Tagar culture began to develop, does not show a break in the cultural development. The earlier stage of the Scythian epoch (the Tagar culture) is dated to the 8th–9th century BC (Sementsov et al. 1997; Alekseev et al. 2001). We note that the evidence for climate change at the Subboreal-Subatlantic transition is also dated to the 9th century BC (van Geel et al. 1996, 1998). In the Kutuzhekovo lake deposits, the dates of 2985 ± 40 BP (GrA-20687) and 2630 ± 180 BP (Le-6232) mark the transition to wetter climatic conditions. However, in the region to the north of the Sayan Mountains, there is no evidence pointing to causal relationships between climate change and cultural developments.

Cultural Development in the Uyuk Valley

There are considerable differences in cultural development for the regions of the Minusinsk and Uyuk valleys, even though they are relatively close to each other. In Tuva, only a few Neolithic sites were found in the Sayan Canyon of the Yenisey River (Toora-Dash and Ust'-Khemchik III). The multi-layered Toora-Dash site is well stratified, showing the cultural development from the late Neolithic up to the Bronze and Iron Ages (Semenov 1992, 2003). According to archaeological data, some occupation of the Tuvanian steppe started during the second half of the 2nd millennium BC, when the pastoral stock-breeding population appeared (the Okunevo culture). This culture existed to the time of the Scythian cultures, which began to occupy this territory during the 1st millennium BC.

The almost complete lack of Bronze Age archaeological records is remarkable. The situation changed completely after the 9th century BC, when the Scythian culture emerged in Tuva, much earlier than in the western parts of the Eurasian steppe zone. The great Arzhan-1 barrow, excavated by the famous Russian archaeologist M Gryaznov, yielded very early Scythian material dated to the late 9th–early 8th century BC (Gryaznov 1980; Gryaznov 1984). This early date is confirmed by the ^{14}C dates as well as by archaeological arguments, because certain types of horse bridles from the central grave can be connected with the pre-Scythian phase in the Black Sea region.

Climate Changes

The reconstruction of the climate change can be compared with the cultural development in both the Minusinsk and the Uyk valleys. Despite some similarities, there are major differences in the occupation of both territories. Practically no Mesolithic and Neolithic cultures (10,000–5000 BP) are known in both areas. This is difficult to explain here, because only 2 cores of lake deposits were studied which mainly represent the Late Holocene. Some early nomads appeared in both territories during the Bronze Age. In the Minusinsk valley, early Bronze Age occupation (Aphanasievo culture) was quite intense. However, in the Uyk valley (Tuva), only a few traces of the Middle Bronze Age Okunevo culture were recorded. The most intensive occupation of both territories occurred in the beginning of the 1st millennium BC, when the more impressive Scythian time cultures started to exist (Tagar culture in the Minusinsk valley and Aldy-Bel culture in the Uyk valley). The comparison between archaeological material available and the paleoenvironmental data yields important information about the influence of climate change.

The relatively thick deposits from Kutuzhekovo Lake (Minusinsk valley) have a better time-resolution than the record from White Lake. Unfortunately, in both cases, the lower parts of the core did not contain enough organic matter for ^{14}C dating. But it is evident that in both cases more humid conditions started during the Middle Bronze Age and culminated during the early Iron Age (shown by increased local and regional biomass production). The major change occurred between 2700 and 2500 BP (Figures 3, 5: zone boundaries KTH-I/II and WL-II/III). The pollen, sedimentological, and geochemical records all show that the climate suddenly became more humid than during the preceding period. Humidity is a major factor influencing the plant biomass production of the steppe. This may well be the reason that in first instance the steppe of the Minusinsk valley was more densely occupied by nomadic tribes than the Uyk valley. In the Uyk valley, the conditions for biomass production were less good, taking into account the more continental climate and lower precipitation, than in the Minusinsk valley. According to our data, the forests have never covered the Uyk valley during the Holocene, while today forest-steppe areas occur in the Minusinsk valley.

Only in the early part of the 1st millennium BC did the climatic conditions in the Uyk valley improve sufficiently so that the occupation capacity was high enough for a dense human population. The Arzhan-1 barrow located in this region was constructed during the 9th century BC, while the Arzhan-2 monument dated to the 7th century BC. We suppose that a climatic factor played a major role in the settlement history of Tuva (van Geel et al., forthcoming). Prehistoric communities living in marginal areas (in terms of climatic conditions and related with food production) may react in a very sensitive way to environmental changes, because such changes can have an enormous impact on their way of life and even survival.

CONCLUSION

The main occupation of the Minusinsk valley (Krasnoyarsk district) and the Uyk valley (Tuva) started during the Bronze Age, when the humidity of the steppe areas was increasing. Based on the available record, we conclude that the Minusinsk valley was at first more attractive than the southern, too-dry Uyk valley. Increased humidity and related biomass production and carrying capacity were the main factors influencing the start of the early Iron Age occupation of the Uyk valley in Tuva.

ACKNOWLEDGEMENTS

This research was supported by the Russian Humanitarian Foundation (03-01-00099a) and the Dutch-Russian Scientific Cooperation Program of the Netherlands Organisation for Scientific Research (NWO grant 047.009.005).

REFERENCES

- Alekseev AY, Bokovenko NA, Boltrik Y, Chugunov KA, Cook G, Dergachev VA, Kovalyukh N, Possnert G, van der Plicht J, Scott EM, Sementsov A, Skripkin V, Vasiliev S, Zaitseva G. 2001. A chronology of the Scythian antiquities of Eurasia based on new archaeological and ^{14}C data. *Radiocarbon* 43(2B):1085–107.
- Arslanov KhA. 1987. *Radiocarbon: Geochemistry and Geochronology* [translated from Russian]. Leningrad: University Press. 296 p.
- Bokovenko NA. 1995. The Tagar culture in the Minusinsk basin. In: Davis-Kimball J, Bashilov VA, Yablonskiy LT, editors. *Nomads of the Eurasian Steppes in the Early Iron Age*. Berkeley, California: Zinat Press. p 296–314.
- Bokovenko NA, Legrand S. 2000. Das karasukzeitliche Gräberfeld Anchil Chon in Chakassien. *Eurasia Antiqua* 6:209–48.
- Bor-ming J, Sylvain G, Jiamao H. 2001. Geochemistry of the Xining Jixian sections, loess plateau of China: eolian dust provenance and paleosol evolution during the last 140 ka. *Chemical Geology* 178:71–94.
- Chen J, Zhisheng A, Head J. 1999. Variation of Rb/Sr ratio in the loess-paleosol sequences of central China during the last 130,000 years and their implications for monsoon paleoclimatology. *Quaternary Research* 51: 215–9.
- Chichagova OA. 1985. *Radiocarbon Dating of Numinic Acids from Solid*. Gerasimov IP, editor. Moscow: Nauka Press. 272 p. In Russian.
- Chlenova NL. 1972. The chronology of the monuments belong to the Karasuk epoch [translated from Russian]. Moscow: Nauka press. *The Materials and Investigations on Archaeology of the Institute of Archaeology* (182):248.
- Chugunov KV, Dergachev VA, Nagler A, Parzinger G, Possnert G, Sementsov AA, Scott EM, van Geel B, van der Plicht J, Vasiliev SS, Zaitseva GI. Forthcoming. First data on the chronological study of the unique Tsar burial mound Arzhan-2 in Central Asia (Tuva Republic). *4th International Symposium on ^{14}C and Archaeology*. Oxford, 2002.
- Dergachev VA, Vasiliev SS, Sementsov AA, Zaitseva GI, Chugunov KA, Slusarenko IJ. 2001. Dendrochronology and radiocarbon dating methods in archaeological studies of Scythian sites. *Radiocarbon* 43(2A):417–24.
- Efimtsev EA. 1957. Environments of Tuva In: Klimenko P, editor. *Climate Review* [translated from Russian]. Moscow: Nauka Press. p 46–65.
- Eusterhaues K, Lechterbreck J, Schneider J, Wolf-Brozio U. 2002. Late- and post-glacial evolution of Lake Steisslingen (I). Sedimentary history, palynological record and inorganic geochemical indicators. *Palaeogeography, Palaeoclimatology, Palaeoecology* 187: 341–71.
- Faegri K, Iversen J. 1989. *Textbook of Pollen Analysis*. Fourth Edition. New York: John Wiley & Sons. 328 p.
- Gavlina GB. 1954. The climate of Khakassia. *Natural Environment and Agriculture of the Khakassia Republic* [translated from Russian]. Moscow: Nauka Press. p 14–42.
- Goldberg L, Fedorin MA, Grachev MA, Bobrov VA. 2000. Periodic signals of orbital forcing during Brunhes in geochemical records of Baikal Lake deposits. In: *The Problems of Climatic and Environmental Reconstructions of Holocene and Pleistocene* [translated from Russian] 2:121–31.
- Görsdorf J, Parzinger H, Nagler A, Leontev N. 1998. Neue ^{14}C -Datierungen für die Sibirische Steppe und ihre Konsequenzen für die regionale Bronzezeitchronologie. *Eurasia Antiqua* 4:73–80.
- Görsdorf J, Parzinger H, Nagler A. 2001. New radiocarbon dates of the north Asian steppe zone and its consequences for the chronology. *Radiocarbon* 43(2B): 1115–20.
- Gracheva R. 2002. Abrupt environmental change and depopulation of Upper Volga lowland, central Russia, around 2600 BP. Abstracts “*Environmental Catastrophes and Recoveries in the Holocene*” Conference. Brunel University, UK. (<http://atlas-conferences.com/cgi-bin/abstract/caiq-71>).
- Grunert J, Lehmkuhl F, Walther M. 2000. Paleoclimatic evolution of the Uvs Nuur basin and adjacent areas (western Mongolia). *Quaternary International* 65/66: 171–92.
- Gryaznov MP. 1980. *Arzhan—The Tsar barrow of the Early Scythian Time* [translated from Russian]. Leningrad: Nauka Press. 62 p.
- Gryaznov MP. 1984. Der Großkurgan von Arzhan in Tuva, Südsibirien. *Materialien zur Allgemeinen und Vergleichenden Archäologie* 23. München: Verlag C.H. Beck.
- Haasan FA. 1985. Fluvala system and geoarchaeology in arid lands: with examples from North Africa, Near East, and the American Southwest. In: Stein JK, Farrant WR, editors. *Archaeological Sediments in Context*. Peopling of the Americans Edited Volume Series: Volume 1. Orono, Maine: Center for Study of Early Man Institute for Quaternary Studies, University of Maine. p 53–68.
- Lehmkuhl F, Schlütz F, Beckert C, Klinge M. 1998. Zur Jungpleistozänen und Holozänen Klimageschichte des Turgen-Charichira, Mongolischer Altai. *Jenaer Geographische Manuskripte* 19:43–4.
- Lisitsyn NF. 1988. To the question about the Neolithic in Khakassia [translated from Russian]. *Short Reports of the Institute of Archaeology (KSIA)* 193:15–20.
- Novgorodova EA. 1970. *Central Asia and the Karasuk Problem*. Moscow: Nauka Press. 192 p. In Russian.
- Peck JA, Khosbayer P, Fowell SJ, Pearce RB, Ariunbileg S, Hansen BCS, Soninkhishig N. 2002. Mid to Late Holocene climate change in north central Mongolia as

- recorded in the sediments of Lake Telmen. *Palaeogeography, Palaeoclimatology, Palaeoecology* 183: 135–53.
- Semenov VA. 1992. *The Neolithic and the Bronze Age in Tuva*. Saint Petersburg: IHMC Press. 152 p. In Russian.
- Semenov VA. 2003. The Neolithization of the Minusinsk valley and Tuva (The Upper Yenisey Neolithic culture) [translated from Russian]. In: Timofeev V, Zaitseva G, editors. *The Chronology and the Interaction of the Neolithization of Eurasia*. Saint Petersburg: IHMC press. p 212–6.
- Sementsov AA, Zaitseva GI, Gorsdorf J, Bokovenko NA, Parzinger G, Nagler A, Chugunov KV, Lebedeva LM. 1997. The chronological questions of the Scythian nomads for the southern Siberia and Central Asia regions [translated from Russian]. *Radiocarbon and Archaeology* 2:86–94.
- Soltanpour PN, Johnson GW, Workman SM, Benton JS, Miller RJO. 1996. Inductively coupled plasma emission spectrometry and inductively coupled plasma-mass spectrometry. In: *Methods of Soil Analysis*. Madison, Wisconsin, USA: Soil Science Society of America, Inc.; American Society of Agronomy, Inc. p 91–135.
- Speranza A, van Geel B, van der Plicht J. 2002. Evidence for solar forcing of climate change at ca. 850 cal BC from a Czech peat sequence. *Global and Planetary Change* 35:51–65.
- Vadeckaya EB. 1986. *The Archaeological Sites in the Steppe Zone of the Middle Yenisey River Basin* [translated from Russian]. Leningrad: Nauka Press. 179 p.
- van Campo E, Gasse F. 1993. Pollen- and diatom-inferred climatic and hydrological changes in Sumxi Co basin (western Tibet) since 13,000 yr BP. *Quaternary Research* 39:300–13.
- van der Plicht J, Aerts A, Wijma S, Zondervan A. 1995. First results from the Groningen AMS facility. *Radiocarbon* 37(2):657–61.
- van der Plicht J, Wijma S, Aerts AT, Pertuisot MH, Meijer HAJ. 2000. The Groningen AMS Facility: status report. *Nuclear Instruments and Methods in Physics Research B* 172:58–65.
- van Geel B, Buurman J, Waterbolk HT. 1996. Archeological and paleoecological indications for an abrupt climate change in the Netherlands and evidence for climatological teleconnections around 2650 BP. *Journal of Quaternary Science* 11:451–60.
- van Geel B, van der Plicht J, Kilian MR, Klaver ER, Kouwenberg JHM, Renssen H, Reynaud-Farrera I, Waterbolk HT. 1998. The sharp rise of $\Delta^{14}\text{C}$ ca. 800 cal BC: possible causes, related climatic teleconnections and the impact on human environments. *Radiocarbon* 40(1):535–50.
- van Geel B, Zaitseva GI, Bokovenko AN, Chugunov KV, Dergachev KV, Dirksen VG, Koulikova MA, Nagler A, Parzinger G, van der Plicht J, Bourova ND, Lebedeva LM. Forthcoming. Chronology and possible links between climatic and cultural change during the first millenium BC in southern Siberia and Central Asia. *Journal of Archaeological Sciences*.
- Vasiliev SA. 2001. The later complexes of the multilayer site Uy-II and the problem of the development of the Stone Age cultures in the Upper Yenisey River Basin during the Holocene. St. Petersburg: *Archaeological News* 8:62–76. In Russian.
- Vasiliev SS, Dergachev VA. 2002. The ~2400-year cycle in atmospheric radiocarbon concentration: bispectrum of ^{14}C data over the last 8000 years. *Annales Geophysicae* 20:115–20.
- Zaitseva GI, Chugunov KV, Dergachev VA, Nagler G, Parzinger G, Scott EM, Sementsov AA, Vasiliev S, van Geel B, van der Plicht J, Lebedeva LM. 2004. Chronological studies of the Arzhan-2 Scythian monument in Tuva. *Radiocarbon*, these proceedings.
- Zaitseva GI, Timofeev VI, Sementsov AA. 1999. C14 dating in the Institute for the History of Material Culture of Russian Academy of Sciences: history, status of work, results and prospects. *Russian Archaeology* 3:5–22. In Russian.

CHRONOLOGICAL STUDIES OF THE ARZHAN-2 SCYTHIAN MONUMENT IN TUVA (RUSSIA)

G I Zaitseva¹ • K V Chugunov² • V A Dergachev³ • A Nagler⁴ • G Parzinger⁴ • E M Scott⁵ • A A Sementsov¹ • S Vasiliev³ • B van Geel⁶ • J van der Plicht⁷ • L M Lebedeva¹

ABSTRACT. The first radiocarbon dates from the unique early Scythian monument Arzhan-2, discovered in 2001, are presented. The monument contained a royal burial (grave nr 5). Unfortunately, precise dating is hampered by the Hallstatt plateau in the calibration curve. However, using both accelerator mass spectrometry measurements from buried materials and conventional dates for floating tree rings from the burial chamber, we were able to date the construction of the monument to the 7th century BC. This is consistent with archaeological expectations. Other graves located inside the barrow were also dated. Grave nr 11, located on the edge of the barrow, is younger, showing that the monument was a place of burial ritual for many years for this ancient population.

INTRODUCTION

In 1970, the famous Arzhan-1 barrow was discovered in Tuva, Russia (Gryaznov 1980). This barrow is considered the earliest pre-Scythian or early Scythian monument in Eurasia, and it became the key monument for the study of all Eurasian Scythian cultures.

During 2001, a Russian-German research project discovered the Arzhan-2 monument in the Uyuk hollow, about 7 km from the Arzhan-1 barrow (Chugunov et al. 2001a–c; 2003). Arzhan-2 is unique because it has not been robbed or otherwise disturbed and appears untouched since its construction. The abundance and variety of well-preserved archaeological material in this monument has no equal among Eurasian Scythian monuments. Consequently, Arzhan-2 plays an important role in understanding the history of the Eurasian Scythian nomads. Concerning Scythian cultures, major questions concerning their origin, development, spread, and ways of life still need to be answered (Alekseev et al. 2001).

The Arzhan-2 barrow contains many graves. In 2001, grave nr 5 was discovered. Two skeletons dressed in richly decorated clothes, buried along with gold artifacts made in the typical Scythian animal style, show that this grave must have belonged to the upper levels of the nomadic nobility. Grave nr 5 is now known as the “royal grave” of Arzhan-2. The continuation of the excavation during the following season yielded further discoveries, and now we know that this monument contains more than 20 different graves. There are graves for women, children, and warriors, and a common horse grave with 14 skeletons. In addition, there were several graves made at later times. The chronology of the different graves and the period of construction and use of the monument itself needs to be established, using both archaeological and radiocarbon dating techniques.

¹The Institute for the History of Material Culture, Russian Academy of Sciences, St. Petersburg, Russia.

Corresponding author. Email: ganna@mail.wplus.net

²The State Hermitage Museum, St. Petersburg, Russia.

³A.F.Ioffe Physical-Technical Institute, Russian Academy of Sciences, St. Petersburg, Russia.

⁴German Archaeological Institute, Berlin, Germany.

⁵Glasgow University, Glasgow, United Kingdom.

⁶Institute for Biodiversity and Ecosystem Dynamics, University of Amsterdam, the Netherlands.

⁷Centre for Isotope Research, Groningen University, the Netherlands.

RESULTS**Wooden Logs: Conventional Dating**

Arzhan-2 is located in the Uyuk hollow of the Tuva Republic (52°05'N and 93°42'E). It contains organic material suitable for both accelerator mass spectrometry (AMS) and conventional ^{14}C dating. First, we investigated the chronology of the royal grave, nr 5. The chamber of this grave consists of a wooden floor and 2 walls (external and internal) made from horizontally stacked logs. In 2001, before the reconstruction of the chamber, one of these logs (D3) containing 133 rings from the covering was used for both ^{14}C dating and dendrochronological measurements. The results are shown in Table 1.

Table 1 ^{14}C dates of tree-ring samples for log D3.

Nr	Lab code	Tree rings (counted from the center)	^{14}C age	Corrected ^{14}C age (BP)
1	Le-6260	0–20	2635 ± 60	not used
2	Le-6261	21–30	2444 ± 50	2515 ± 50
3	Le-6262	31–40	2421 ± 24	2492 ± 24
4	Le-6263	41–50	2359 ± 18	2430 ± 18
5	Le-6264	51–60	2390 ± 18	2461 ± 18
6	Le-6265	61–70	2400 ± 18	2471 ± 18
7	Le-6266	71–80	2391 ± 18	2462 ± 18
8	Le-6267	81–90	2420 ± 18	2491 ± 18
9	Le-6268	91–100	2327 ± 18	2398 ± 18
10	Le-6269	101–127	2437 ± 21	2508 ± 21

The first chronology for the Arzhan-2 monument was obtained using wiggle-matching of these dates, showing that the construction dates to the calendar interval (2σ) 670–625 cal BC (Chugunov et al. 2003). After the reconstruction of the chamber, logs from the walls could be used as well. We selected log C3 from the internal wall; log C3 contained 150 rings. The results for this log are shown in Table 2.

Table 2 ^{14}C dates of tree-ring samples for log C3.

Nr	Lab code	Tree rings	^{14}C age	Corrected ^{14}C age (BP)
1	Le-6561	1–10	2435 ± 20	2518 ± 20
2	Le-6562	11–30	2408 ± 20	2505 ± 20
3	Le-6563	31–50	2409 ± 18	2475 ± 18
4	Le-6564	51–70	2354 ± 16	2462 ± 16
5	Le-6565	71–90	2419 ± 16	2485 ± 16
6	Le-6566	91–100	2391 ± 16	2506 ± 16
7	Le-6567	101–110	2458 ± 20	2503 ± 20
8	Le-6568	111–120	2377 ± 16	2488 ± 16
9	Le-6569	121–130	2374 ± 16	2473 ± 16
10	Le-6570	131–140	2408 ± 20	2471 ± 20
11	Le-6571	141–150	2401 ± 15	2495 ± 15

By comparing the dating results for the 2 logs (Tables 1 and 2), one can see that the ^{14}C ages cover practically the same interval. However, the ^{14}C dates fall on the large so-called Hallstatt plateau

(about 800–400 BC) of the calibration curve. This makes it difficult to calibrate the ^{14}C dates to the calendar ages for this monument. The plateau follows a period with increased atmospheric $\Delta^{14}\text{C}$ caused by solar activity changes (van Geel et al. 1998).

Logs D3 and C3 were subdivided into sections of 10–20 tree rings and were ^{14}C dated at the Institute for the History of Material Culture, St Petersburg (lab code Le) using liquid scintillation spectrometry (Zaitseva et al. 1999). $\delta^{13}\text{C}$ values were not measured; instead, a correction factor, taking into account systematic errors resulting from instrumental errors and isotopic fractionation effects, was determined. We used a method of low-frequency filtration to exclude the high-frequency noise (Der-gachev et al. 2001). ^{14}C dates determined this way for logs C3 and D3 are shown in column 5 (Tables 1 and 2). These corrected ^{14}C ages were used for the assessment of the concordance of the dates with the calibration curve using a statistical approach. The ^{14}C dates are matched to the calibration curve by minimizing the statistical parameter χ^2_{n-1} , where n is the number of the samples from the log. The results are shown in Figures 1 and 2.

As one can see from Figures 1 and 2, the felling dates for these logs show that the construction of grave nr 5 can be dated to the middle or end of the 7th century BC.

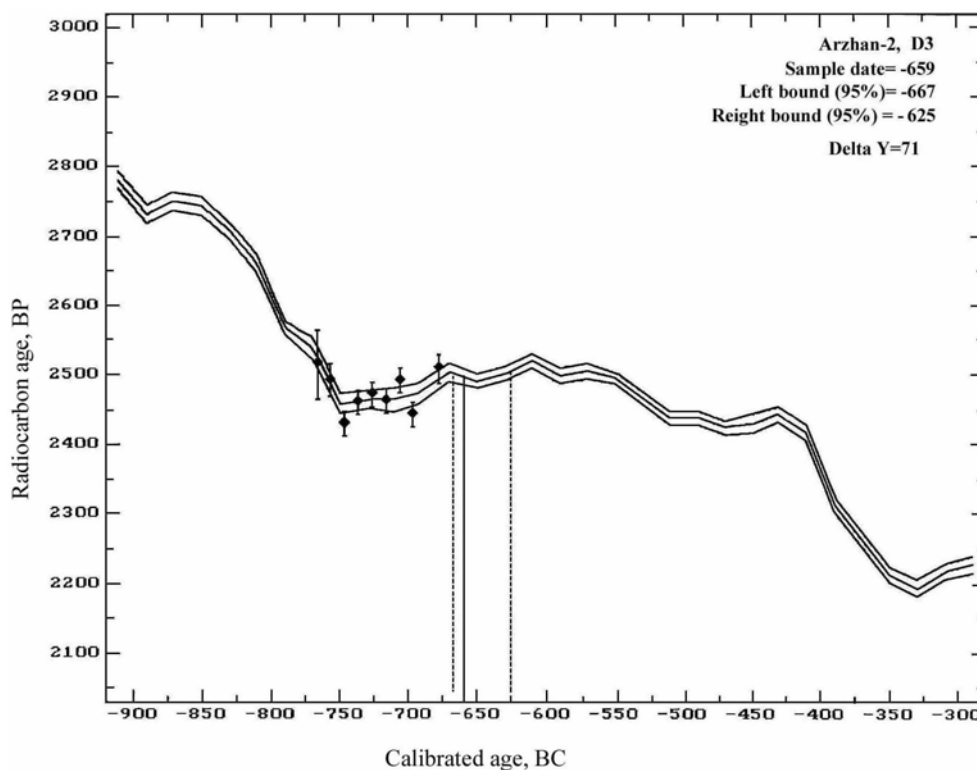


Figure 1 The position of the corrected ^{14}C ages for log C3 from the inside wall of grave nr 5. The date of the felling of this log is 622 cal BC (solid line). The left limit of the 95% confidence interval is 642 cal BC; the right limit is 602 cal BC (vertical lines).

The most probable felling date for these logs is 659 BC, with 2- σ confidence limits of 671–609 BC. We tried to estimate the reliability of this date mathematically; this approach is presented in Figures 3 and 4.

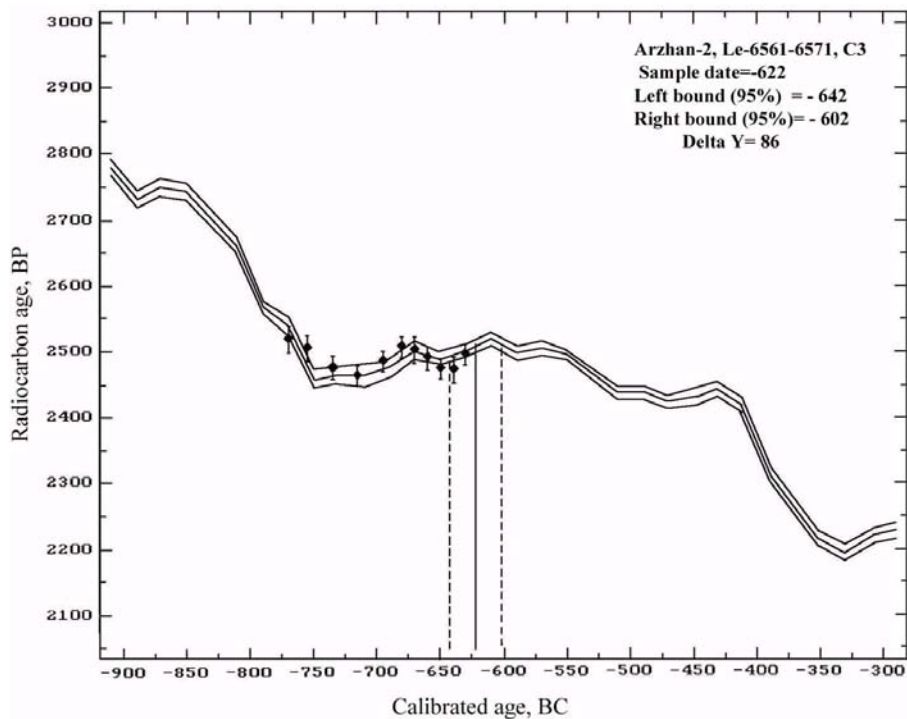


Figure 2 The position of the corrected ¹⁴C age for log D3 from the covering of grave nr 5. The date of the felling of this log is 660 cal BC (solid line). The left limit of the 95% confidence interval is 670 cal BC; the right limit is 610 cal BC (vertical lines).

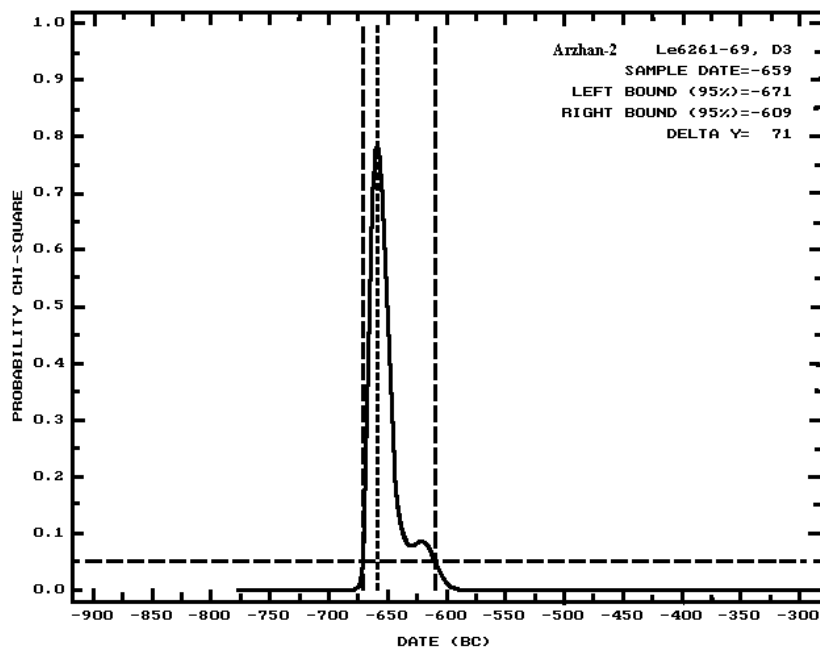


Figure 3 The reliability of the ¹⁴C dates for log C3. The dotted vertical line is the position of the most probable date. The dashed lines are the right and left confidence limits; the dashed horizontal line corresponds to a probability of 0.05. The most probable date for the felling of this log is 622 BC. The right and left confidence limits are 642 and 602 BC.

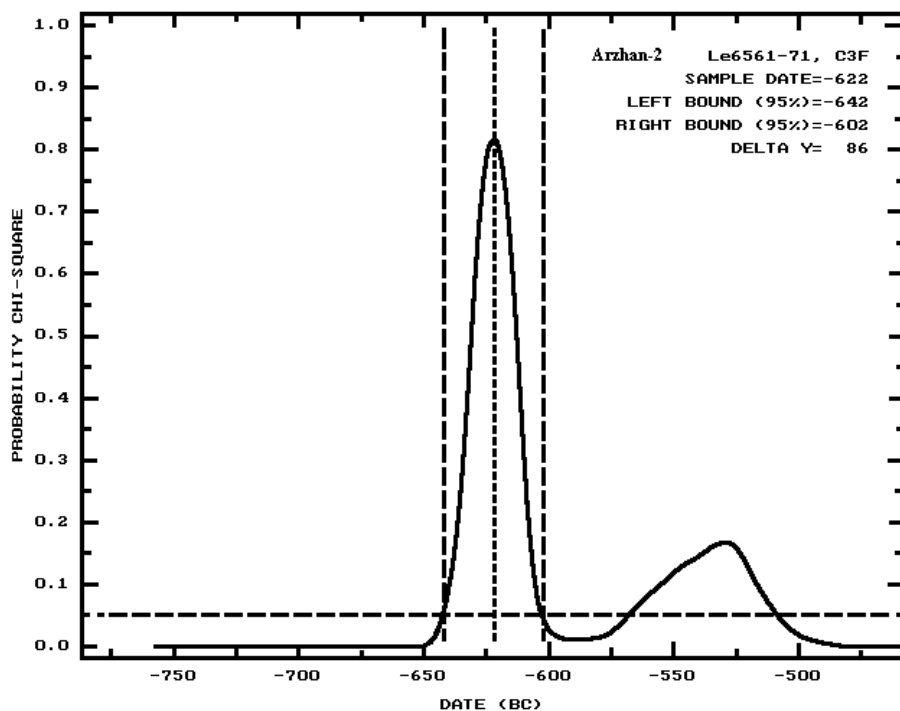


Figure 4 The reliability of the ^{14}C dates for log D3. The most probable date of the felling of this log is 659 BC. The right and left confidence limits are 671 and 609 BC.

AMS Results

In grave nr 5, many different organic materials were found and were AMS dated. Among them are the remains of clothing (textile, leather, felt), various seeds, bone, and wooden objects. The results of these AMS-dated finds are shown in Table 3.

Table 3 AMS ^{14}C dates for the Arzhan-2 barrow, grave nr 5.

Nr	Lab code	^{14}C age BP	Dated material
1	GrA-18910	2520 \pm 40	Grain
2	GrA-18920	2540 \pm 45	Textile
3	GrA-18931	2465 \pm 40	Grain
4	GrA-18932	2565 \pm 40	Leather
5	GrA-18935	2470 \pm 40	Wood
6	GrA-18938	2535 \pm 45	Soil
7	GrA-18939	2455 \pm 45	Textile, alkali fraction
8	GrA-18948	2485 \pm 40	Grain
9	GrA-18949	2565 \pm 40	Grain
10	GrA-18962	2520 \pm 45	Leather
11	Ua-18487	2475 \pm 50	Wood from branch
12	Ua-18488	2350 \pm 50	Small grains
13	Ua-18489	2495 \pm 50	Leather
14	AA-46872	2533 \pm 39	Wood from artifact
15	AA-46873	2503 \pm 39	Bark from bow
16	AA-46874	2494 \pm 40	Seeds
17	AA-46875	2496 \pm 43	Wood from artifact

All these ^{14}C dates lie close to 2500 BP. The weighted mean ^{14}C age calculated by the OxCal program (Bronk Ramsey 1994, 1998) is 2501 ± 10 BP. Calibration for this combined age is shown in Figure 5.

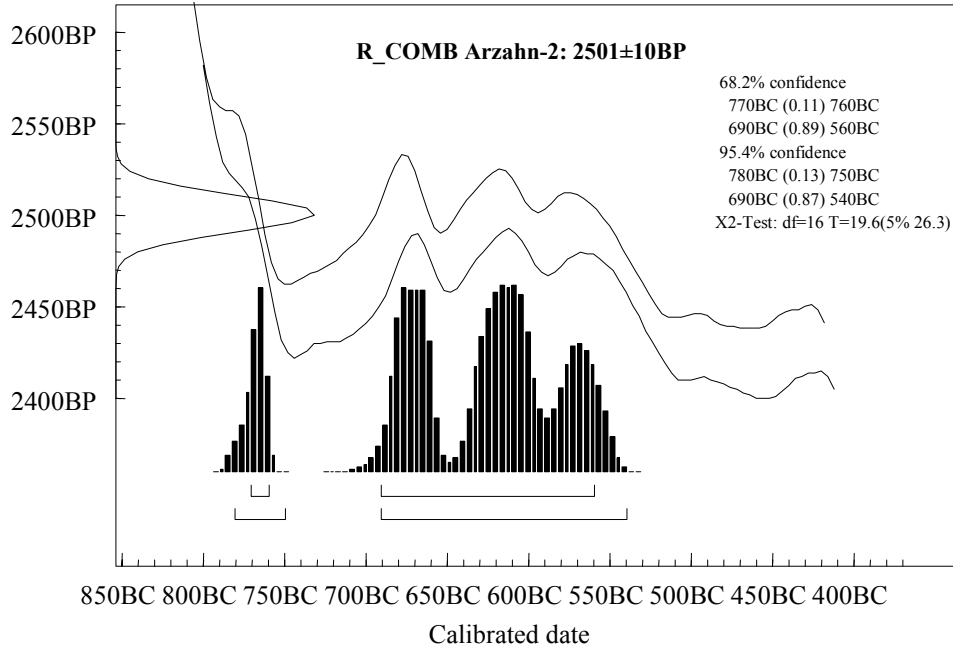


Figure 5 The combined ^{14}C date from the 17 ^{14}C ages produced by AMS from different organic materials in grave nr 5 and their calibration.

The combined ^{14}C date, albeit very precise, corresponds to a rather wide calendar interval: 780–540 cal BC (2σ) and 770–560 cal BC (1σ). Nevertheless, the AMS dates agree with the wiggle matching result from the wood (grave construction), indicating that grave nr 5 was constructed during the beginning-middle of the 7th century BC. This corresponds well with the archaeological perspective that Arzhan-2 dates from the 6th to the 7th centuries BC.

In 2002, additional graves were discovered in this monument; at present, more than 20 graves have been identified. Many of them are important but contain fewer gold artifacts. Graves nr 13a and 13b are stone burial mounds for females, separated by a stone wall. In the first chamber, 1 woman was buried and 2 women were buried in the other chamber. The clothing of the women is well preserved and of a very complicated design. It consists of several textile layers with different weaves, felt, fur, and other materials. The color of the different cloth layers can be seen. ^{14}C dates were produced from the different organic components of the clothes by both AMS (Groningen, GrA) and conventional dating (St Petersburg, Le). The very unusual collective burial of horses (grave nr 16) was found inside the monument and contains 14 horse skeletons. Some artifacts made with similar ornamentation to those in the royal grave nr 5 were found in this grave. The horses' equipment and even the grass in their mouths was preserved. A variety of organic remains were used for ^{14}C dating. Not far from the royal grave nr 5, a warrior burial (grave nr 20) with bronze artifacts and weapons was found. In stone-lined grave nr 26, male individuals were buried. Between the stone slabs covering the grave, charcoal was found, which was used for ^{14}C dating. All these graves are located inside the barrow of Arzhan-2. In addition, there are graves inserted on the edge of the barrow. Grave nr 11 is such an inserted grave, made from stone slabs. Charcoal found between the slabs was used for ^{14}C dating. ^{14}C results from the different graves belonging to Arzhan-2 are shown in Table 4.

Table 4 ^{14}C dates of the different graves belonging to Arzhan-2.

Nr	Lab code	^{14}C age (BP)	Grave nr	Dated material	cal BC interval (1 σ)	cal BC interval (2 σ)
1	GrA-21532	2240 \pm 45	13a	Leather	390–240	400–200
2	GrA-21533	2555 \pm 45	13a	Fur	810–550	820–520
3	GrA-21341	3010 \pm 70	13b	Felt	1400–1160	1430–1040
4	GrA-21534	2330 \pm 45	13b	Leather	510–370	550–200
5	Le-6338	2530 \pm 70	13b	Fur	810–530	810–410
6	Le-6339	2410 \pm 70	16	Wood	760–400	770–390
7	Le-6639	2320 \pm 60	16	Bone, skeleton 17	520–250	800–200
8	GrA-21526	2100 \pm 60	16	Grass, skeleton 4	200–40	360 BC–AD 20
9	GrA-21527	2500 \pm 50	20	Destroyed leather near knife, skeleton 1	790–530	800–410
10	Le-6337	2385 \pm 45	26	Charcoal	730–390	770–380
11	Le-6335	2290 \pm 25	11	Charcoal	397–376	410–250

The ^{14}C for different materials from the same grave are scattered, which is difficult to explain. It appears that the monument had been used during an extended period of time. The results will be discussed in more detail in the next section.

DISCUSSION

Chronological research is essential for historical reconstructions. Key monuments form the basis of chronological correlations. Such a key monument is Arzhan-1, which is the earliest Scythian monument in Eurasia and dates to the 10th–9th century BC (Marsadolov et al. 1994; Zaitseva et al. 1998; Alekseev 2003). The latest period of the Scythian time cultures is represented by the key monuments of Pazyryk in the Altai, dating to the 3rd–4th century BC (Alekseev et al. 2001, 2003). It is noteworthy that there are only a few Scythian monuments which can be dated to the 7th–6th century BC.

The significance of Arzhan-2, discussed in this paper, is difficult to overestimate. Monuments in which all materials are preserved, reflecting practically all aspects of the way of life of the ancient population, are unique. In Arzhan-2, all the graves located inside the monument have not been disturbed, so that the objects found in this monument shed light on past life, ancient clothing, ritual traditions, and the relationship between nobility and other levels of the population. Therefore, the chronology of this unique monument is very important for all Eurasian Scythian history.

Most material from the royal grave nr 5 in Arzhan-2 corresponds to the early Scythian tradition, but sometimes it is rather difficult to find an analogy with materials and techniques from other known Scythian monuments. From an archaeological perspective, the Arzhan-2 monument can be dated to the 6th–7th century BC. In spite of the ^{14}C dates produced from the logs of the different elements of the burial chamber, considerable difficulties remain in determining the calendar date of this burial due to the large plateau on the calibration curve. Various organic materials from this grave have also been dated by AMS. The average AMS ^{14}C date and the date for the wiggle-matched wood indicate that the construction of grave nr 5 took place during the 7th century BC, which corresponds well with archaeological evidence.

The other graves inside the Arzhan-2 barrow play an important role too, because they provide material from other levels of the ancient population. The clothes in the women's graves (nr 13a and 13b) have a very complex design with many layers of different textiles, fur, and felt. The ^{14}C dates from the textile and fur show that these graves are contemporaneous with the royal grave nr 5. Organic materials

from warrior grave nr 20, where a weapon assemblage was found, date from the same time. For the collective horse burial (grave nr 16), unfortunately, we are not yet able to present a definite date.

One of the inserted graves (nr 11) contained charcoal. The ^{14}C date measured indicates that this grave was constructed later than the main barrow construction. Therefore, we conclude that the monument has been a ritual site for the ancient nomads, used for more than 100 yr.

Only 2 yr have passed since the discovery of this already famous Arzhan-2 monument. We present here the first results, and will continue its chronological study in the near future. We expect that, as the complete series of ^{14}C and dendrochronological dates from other logs of the chamber construction are measured by different ^{14}C laboratories, and as ^{14}C dates are measured for other graves in this monument, we will be able to determine the age of this unique monument with more precision.

CONCLUSION

The first ^{14}C dates measured for a number of graves from the Arzhan-2 monument show that the time of construction dates back to the 7th century BC. A later date for an inserted grave indicates that this monument has been used as a place of ritual for the nomads over a long period of time, without the destruction of the main barrow.

ACKNOWLEDGEMENTS

This study was supported by Russian Humanitarian Foundation nr 03-01-00099a and NWO, grant nr 047.009.005.

REFERENCES

- Alekseev A Yu. 2003. *Chronography of the European Scythia (VII–IV Centuries BC)*. St. Petersburg: State Hermitage Press. 416 p. In Russian.
- Alekseev A Yu, Bokovenko NA, Boltrik Yu, Chugunov KV, Cook GT, Dergachev VA, Kovaliukh N, Possnert G, van der Plicht J, Scott EM, Sementsov A, Skripkin V, Vasiliev S, Zaitseva G. 2001. The chronology of the Scythian antiquities of Eurasia (on new archaeological and ^{14}C data). *Radiocarbon* 43(2B):1085–107.
- Chugunov K, Nagler A, Parzinger H. 2001a. The Golden Grave from Arzhan. *Minerva* V13(1):39–42.
- Chugunov K, Nagler A, Parzinger H. 2001b. Der First von Arzhan. Ausgrabungen im Skythischen Ferstengrabhegel Arzhan-2 in der Südsibirischen Republik Tuva. *Antike Welt* 32(6):607–14.
- Chugunov K, Parzinger H, Nagler A. 2001c. The elite burial mound of the nomads of the early Scythian time in Tuva. The preliminary results of the field research of the Russian–Germany expedition in 2001. *Archaeology, Ethnology and Anthropology of Eurasia* 2:115–24. In Russian and English.
- Chugunov KV, Dergachev VA, Nagler A, Parzinger H, Possnert G, Sementsov AA, Scott EM, van Geel B, van der Plicht J, Vasiliev SS, Zaitseva GI. Forthcoming. First chronological data for the unique Tsar burial mound Arzhan-2 in Tuva, Central Asia. *Proceedings of the Conference ^{14}C and Archaeology*, Oxford, April 2002.
- Dergachev VA, Vasiliev SS, Sementsov AA, Zaitseva GI, Chugunov KA, Sljusarenko I Ju. 2001. Dendrochronology and radiocarbon dating methods in archaeological studies of the Scythian sites. *Radiocarbon* 43(2A):417–25.
- Grjaznov MP. 1980. *Arzhan*. Leningrad: Nauka. 62 p. In Russian.
- Marsadolov LS, Zaitseva GI, Lebedeva LM. 1994. The correlation of the dendrochronological and radiocarbon determinations for the great barrows of the Sayan–Altai. *Elite Barrows of the Eurasian Steppe in the Scythian–Sarumathian Epoch*. St. Petersburg: IHMC & SHM press. p 141–56. In Russian.
- Bronk Ramsey C. 1994. Analysis of chronological information and radiocarbon calibration: the program OxCal. *Archaeological Computing Newsletter* 41:11–6.
- Bronk Ramsey C. 1998. Probability and dating. *Radiocarbon* 40(1):461–74.
- Van Geel B, van der Plicht J, Kilian MR, Klaver ER, Kouwenberg JHM, Renssen H, Reynaud-Farrera I, Waterbolk HT. 1998. The sharp rise of $\Delta^{14}\text{C}$ ca. 800 cal BC: possible causes, related climatic teleconnections and the impact of human environments. *Radiocarbon* 40(1):535–50.
- Zaitseva GI, Vasiliev SS, Marsadolov LS, van der Plicht J, Sementsov AA, Dergachev VA, Lebedeva LM. 1998. A tree-ring and ^{14}C chronology of the key Sayan–Altai monuments. *Radiocarbon* 40(1):571–80.
- Zaitseva GI, Timofeev VI, Sementsov AA. 1999. Radiocarbon dating in the Institute of the History of Material Culture: history, work status, results and perspectives. *Journal of Russian Archaeology* (3):3–21. In Russian.

A PUZZLING BODY FROM THE RIVER THAMES IN LONDON

Alex Bayliss^{1,2} • Peter Marshall^{1,3} • Jane Sidell⁴

ABSTRACT. Radiocarbon measurements on a partially articulated female human skeleton, recovered from the foreshore of the river Thames in London, raised interesting questions of interpretation when the body did not produce the anticipated Neolithic date. A relatively recent ¹⁴C age and a strong marine component to the individual's diet, identified by stable isotope measurements, means that the date of death is difficult to estimate accurately, although the body probably does not constitute a forensic case.

INTRODUCTION

In February 2002, a partial, articulated, female human skeleton was recovered from the eroding foreshore of the river Thames downstream of Tower Bridge close to Chamber's Wharf (Figure 1; NGR, TQ 53430 17975; 53°56'24"N, 00°11'20"W). The body was apparently associated with twigs, 6 fragments of Peterborough Ware pottery, and characteristic Neolithic flintwork (Figure 2). Radiocarbon dating was undertaken to confirm the suspected Neolithic date of this burial, and to determine whether she is the earliest Londoner so far discovered.



Figure 1 Excavating the skeleton on the foreshore

¹English Heritage, 23 Savile Row, London, W1S 2ET, United Kingdom.

²Corresponding author. Email: alex.bayliss@english-heritage.org.uk.

³Email: peter.marshall@english-heritage.org.uk.

⁴Institute of Archaeology, University College London, 31-34 Gordon Square, London, WC1H 0PY, United Kingdom.
Email: j.sidell@ucl.ac.uk.



Figure 2 The Chamber's Wharf skeleton

METHODS AND RESULTS

Replicate bone samples from the left scapula of the skeleton were dated by the Oxford Radiocarbon Accelerator Unit, using methods described by Bronk Ramsey et al. (2000), Brown et al. (1988), and Bronk Ramsey and Hedges (1997). It is not thought that these results were affected by the older contaminant subsequently discovered in this filtration protocol (Bronk Ramsey et al., these proceedings). Two ^{14}C measurements were obtained (OxA-11141-2; 421 ± 31 BP and 415 ± 35 BP) which are statistically consistent according to the χ^2 test described by Ward and Wilson (1978; $T'=0.0$; $n=1$; $T'(5\%)=3.8$), and so a weighted mean was taken before calibration (418 ± 23 BP).

Using the probability method of calibration and INTCAL98, this calibrates to cal AD 1430–1495 (94% probability; Figure 3a) (Stuiver et al. 1998a; Stuiver and Reimer 1993; Bronk Ramsey 1995 [OxCal v3.5]). There is, however, a considerable complication when considering these results.

The skeleton also produced statistically consistent $\delta^{13}\text{C}$ values of $-17.0 \pm 0.3\text{‰}$ and $-16.7 \pm 0.3\text{‰}$ [$T'=0.5$; $T'(5\%)=3.8$; $n=1$; $-16.9 \pm 0.3\text{‰}$], and consistent $\delta^{15}\text{N}$ values of $+12.4 \pm 0.5\text{‰}$ and $+12.6 \pm 0.5\text{‰}$ [$T'=0.1$; $T'(5\%)=3.8$; $n=1$; $+12.5 \pm 0.4\text{‰}$]. These results indicate that there is a strong marine component in the ultimate source of carbon in the dated individual (Figure 4).

Methods of estimating this proportion accurately are not well understood (Bayliss et al. 2004), but using the methodology published by Arneborg et al. (1999) in which a simple linear extrapolation is made between a 100% terrestrial diet ($\delta^{13}\text{C}$ value of -21.0‰) and a 100% marine diet ($\delta^{13}\text{C}$ value of -12.5‰), it can be estimated that 49% of this individual's protein intake was of marine origin. This information can be used in the interpretation of the ^{14}C results by mixing the atmospheric calibration curve with the marine calibration curve in the proportion suggested by the estimate of marine protein. This has been done using OxCal v3.5 and the methodology outlined in Bronk Ramsey (2001: 356) in which the 2 curves are mixed in user-defined proportions (in this case, 51% terrestrial, 49% marine) on the basis of ^{14}C concentration (<http://www.rlaha.ox.ac.uk/oxcal/>).

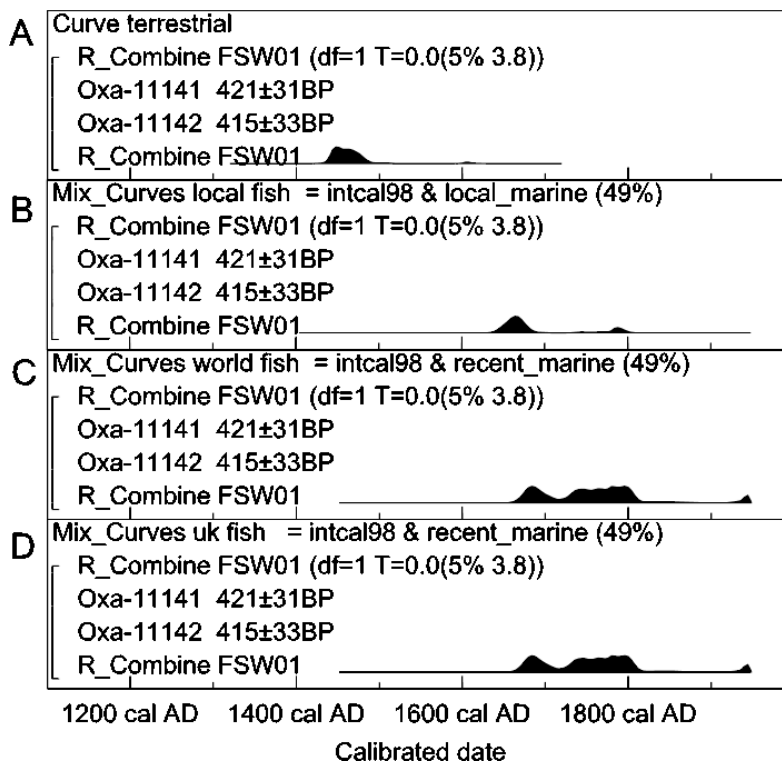


Figure 3 Probability distribution of the calibrated date for the Thames skeleton (a) using the terrestrial curve of Stuiver et al. (1998a); (b) using the marine curve of Stuiver et al. (1998b) and a ΔR value of -5 ± 40 BP; (c) using a ΔR value of 112 ± 37 BP; and (d) using a ΔR value of 112 ± 47 BP.

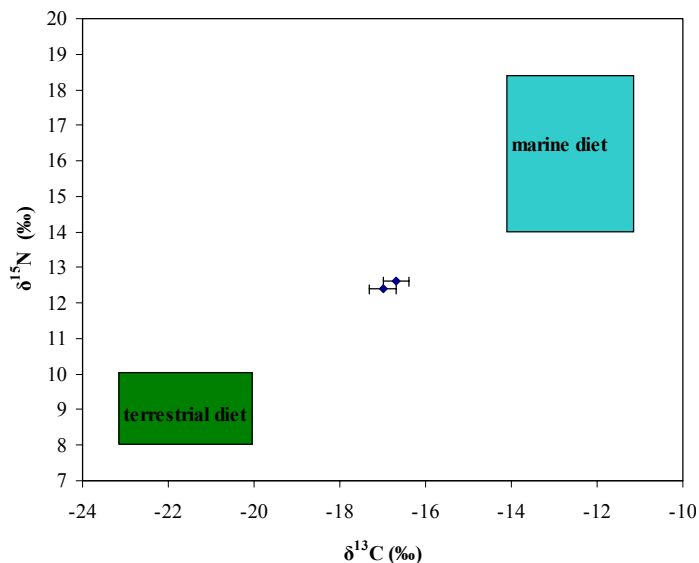


Figure 4 Graph of $\delta^{13}\text{C}$ and $\delta^{15}\text{N}$ values of bone collagen from Chamber's Wharf, related to the values expected for archaeological populations consuming pure C3 and marine diets (after Mays 1998).

Using a ΔR value of -5 ± 40 BP for the coastal waters off England (Stuiver and Braziunas 1993) and the marine calibration curve of Stuiver et al. (1998b), this provides calibrated date ranges for the burial of cal AD 1635–1695 (77% probability) or cal AD 1740–1750 (1%) or cal AD 1760–1805 (17% probability) (Figure 3b). Using the same methodology, but introducing an error on the estimate of marine protein in the individual's diet ($\pm 10\%$), produces the calibrated date shown in Figure 5b (cal AD 1520–1820 at 95% probability). The choice of an error of $\pm 10\%$ is simply illustrative as there are so many unknowns inherent within dietary reconstructions from stable isotope values.

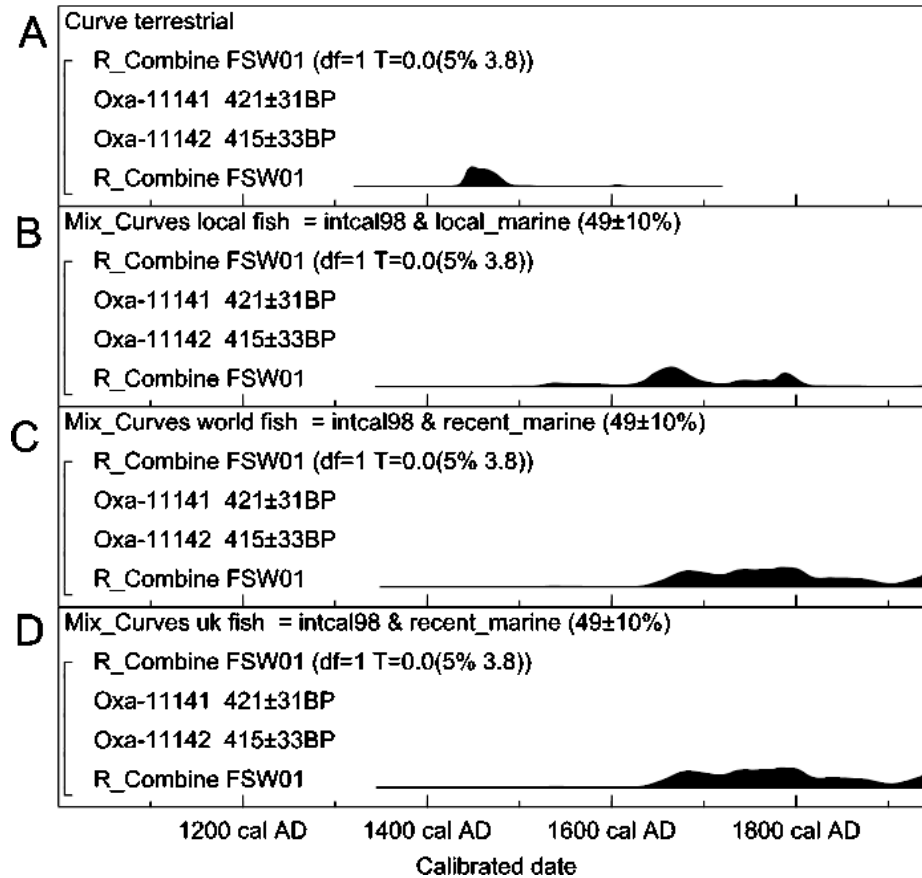


Figure 5 Probability distribution of the calibrated date for the Thames skeleton, with an estimated proportion of marine protein of $49 \pm 10\%$: (a) using the terrestrial curve of Stuiver et al. (1998a); (b) using the marine curve of Stuiver et al. (1998b) and a ΔR value of -5 ± 40 BP; (c) using a ΔR value of 112 ± 37 BP; and (d) using a ΔR value of 112 ± 47 BP.

It is unclear whether the use of an entirely local marine offset is reasonable for a skeleton of this age. Seafaring in northwestern Europe appears to have originated in the Early Bronze Age (Wright et al. 2001), although most fish seem to have been caught locally until the rise of the stockfish market in the medieval period (Heinrich 1986). Cod was certainly being caught and salted by English seamen off Greenland in the early 15th century (Carus-Wilson 1954: Chapter 11). Between the 16th and 18th centuries, the English were largely excluded from the Icelandic fishing grounds by the Danish authorities, and so were forced to develop new fisheries off the North Atlantic coast of America

(Innis 1940). In contrast, salt herring in late medieval England was largely supplied by traders from the Hanseatic League and derived from the Baltic (Lewis and Runyan 1985: 128–30). By the 17th century, however, the focus of this trade had moved and was controlled by the Dutch from fisheries in the eastern North Sea (Unger 1980). Consequently, from the later medieval period, not only does the scale of the marine component in an individual’s diet have to be considered, but also the proportion of marine resources consumed from different sources¹.

The unexpected ¹⁴C age produced by the Chamber’s Wharf skeleton meant that the possibility that it is of recent date has to be considered. We have done this by attempting to assess the reservoir age of fish consumed by modern populations. Figure 6 shows the percentage (by weight) of the world marine fish catch in each region of the oceans in 1999 (MAFF 2000), and the approximate marine reservoir correction applicable in each region (after Stuiver and Braziunas 1993). From these statistics, using a simple average of the ΔR values of the world fish catch proportional to the weight of fish caught in each region, it can be estimated that the fish consumed in the world in 1999 had an average ΔR value of 112 ± 37 BP. Using this value, the ¹⁴C age of the Thames skeleton calibrates to cal AD 1660–1820 (92% probability) or cal AD 1930–1945 (3% probability) (Figure 3c) or cal AD 1640–1955* (95% probability) (Figure 5c).

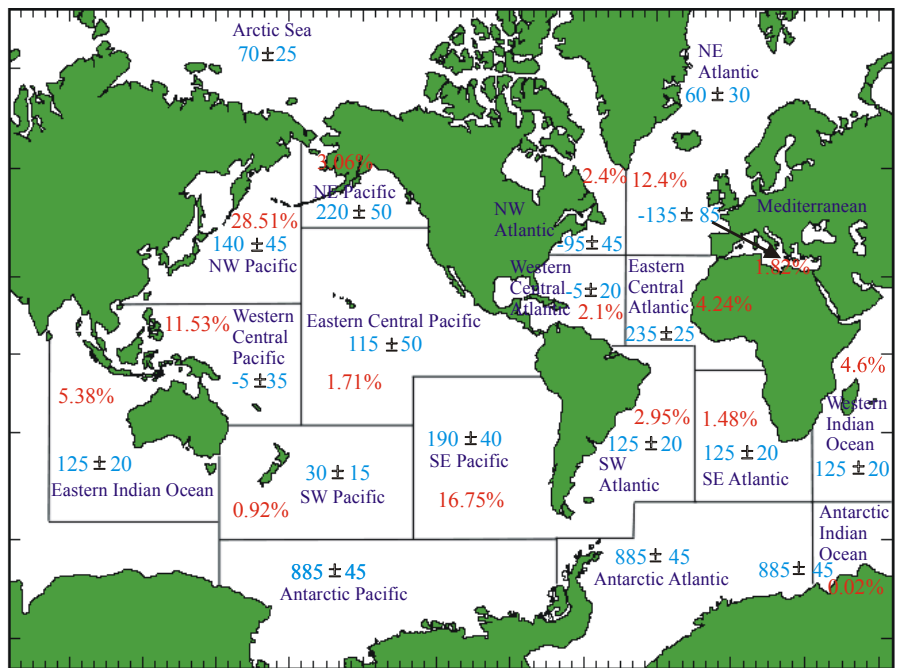


Figure 6 The percentage (by weight) of the world marine fish catch in each region of the oceans in 1999 (MAFF 2000), and the approximate marine reservoir correction applicable in each region (after Stuiver and Braziunas 1993).

¹With the exception of the Salmonids, most marine species which have been widely exploited in England have migration patterns on a regional scale (Taggart 1997; Huse et al. 2002; McKeown 1984). This means that the fish can be expected to have a reservoir age in equilibrium with the region of the sea in which they were caught.

A slightly more sophisticated approach has also been attempted, based on statistics for fish consumed in the UK in 1999. Approximately 20% was landed in the UK, with the remaining 80% imported from the regions shown in Table 1 (MAFF 2000). From these statistics, it can be estimated that the fish consumed in the UK in 1999 had an average ΔR value of 112 ± 47 BP (calculated in the same way as above), and so the skeleton again calibrates to cal AD 1660–1820 (92% probability) or cal AD 1930–1945 (3% probability) (Figure 3d) or cal AD 1640–1955* (95% probability) (Figure 5d).

Table 1 Origin of fish consumed in the UK in 1999 (MAFF 2000).

Landings by country/trade area	Percentage by weight	Assumed ΔR value
UK	20%	60 ± 30 BP
European Union	22%	58 ± 35 BP
European Free Trade Area	27%	60 ± 30 BP
Faroe Islands	7%	60 ± 30 BP
Russia	9%	220 ± 50 BP
USA	2%	220 ± 50 BP
Other	13%	112 ± 37 BP

CONCLUSION

This analysis has shown conclusively that the Chamber's Wharf skeleton is not Neolithic. It has also shown that the body is not sufficiently recent to warrant police investigation. Uncertainty reigns at every stage in attempting to correct these ^{14}C measurements for a marine component in the individual's diet. In these circumstances, any estimate for the absolute date of the skeleton is hazardous, although she certainly died in the 15th century or later, and perhaps is most likely to have died between ~1650 and ~1800.

REFERENCES

- Arneborg J, Heinemeier J, Lynnerup N, Nielsen HL, Rud N, Sveinbjörnsdóttir ÁE. 1999. Change of diet of the Greenland Vikings determined from stable carbon isotope analysis and ^{14}C dating of their bones. *Radiocarbon* 41(1):157–68.
- Bayliss A, Shepherd-Popescu E, Beavan-Athfield N, Bronk Ramsey C, Cook GT, Locker A. 2004. The potential significance of dietary offsets for the interpretation of radiocarbon dates: an archaeologically significant example from medieval Norwich. *Journal of Archaeological Science* 31:563–75.
- Brown TA, Nelson DE, Vogel JS, Southon JR. 1988. Improved collagen extraction by modified Longin method. *Radiocarbon* 30(1):171–7.
- Bronk Ramsey C. 1995. Radiocarbon calibration and analysis of stratigraphy: the OxCal Program. *Radiocarbon* 37(2):425–30.
- Bronk Ramsey C. 2001. Development of the radiocarbon calibration program. *Radiocarbon* 43(2A):355–64.
- Bronk Ramsey C, Hedges REM. 1997. A gas ion source for radiocarbon dating. *Nuclear Instruments and Methods in Physics Research B* 29:45–9.
- Bronk Ramsey C, Higham TFG, Hedges REM. 2004. Improvements to the pretreatment of bone at Oxford. *Radiocarbon*, these proceedings.
- Bronk Ramsey C, Pettitt PB, Hedges REM, Hodgins GWL, Owen DC. 2000. Radiocarbon dates from the Oxford AMS system: Archaeometry datelist 30. *Archaeometry* 42:459–79.
- Carus-Wilson EM. 1954. *Medieval Merchant Venturers*. London: Methuen.
- Heinrich D. 1986. Fishing and consumption of cod (*Gadus morhua* L.) in the Middle Ages. In: Brinkhuizen DC, Clason AT, editors. Fish and Archaeology. *British Archaeological Reports, International Series* 294:42–52.
- Huse G, Railsback S, Fernö A. 2002. Modelling changes in migration patterns of herring: collective behaviour and numerical domination. *Journal of Fish Biology* 60:571–82.
- Innis HA. 1940. *The Cod Fisheries: The History of an International Economy*. Toronto: University of Toronto Press. 522 p.
- Lewis AR, Runyan TJ. 1985. *European Naval and Maritime History, 300–1500*. Bloomington: Indiana University Press. 192 p.
- Mays S. 1998. *The Archaeology of Human Bones*. London: Routledge. 256 p.

- Ministry of Agriculture, Fisheries, and Food. 2000. *United Kingdom Sea Fisheries Statistics*. London: HMSO.
- McKeown BA. 1984. *Fish Migration*. London: Croom Helm Ltd. 224 p.
- Stuiver M, Braziunas TF. 1993. ^{14}C ages of marine samples to 10,000 BC. *Radiocarbon* 35(1):137–89.
- Stuiver M, Reimer PJ. 1993. Extended ^{14}C database and revised Calib 3.0 ^{14}C age calibration program. *Radiocarbon* 35(1):215–30.
- Stuiver M, Reimer PJ, Bard E, Beck JW, Burr GS, Hughen KA, Kromer B, McCormac G, van der Plicht J, Spurk M. 1998a. INTCAL98 radiocarbon age calibration, 24,000–0 cal BP. *Radiocarbon* 40(3):1041–83.
- Stuiver M, Reimer PJ, Braziunas TF. 1998b. High-precision radiocarbon age calibration for terrestrial and marine samples. *Radiocarbon* 40(3):1127–51.
- Taggart CT. 1997. Bank-scale migration patterns in northern cod. *Northwest Atlantic Fisheries Organization (NAFO) Scientific Council Studies* 29:51–60.
- Unger R. 1980. Dutch herring, technology, and international trade in the seventeenth-century. *Journal Economic History* 40:253–79.
- Ward GK, Wilson SR. 1978. Procedures for comparing and combining radiocarbon age determinations: a critique. *Archaeometry* 20:19–31.
- Wright EV, Hedges REM, Bayliss A, van de Noort R. 2001. New AMS radiocarbon dates for the North Ferriby boats—a contribution to dating prehistoric seafaring in northwestern Europe. *Antiquity* 75:726–34.

RADIOCARBON AND STABLE ISOTOPE EVIDENCE OF DIETARY CHANGE FROM THE MESOLITHIC TO THE MIDDLE AGES IN THE IRON GATES: NEW RESULTS FROM LEPENSKI VIR

C Bonsall^{1,2} • G T Cook³ • R E M Hedges⁴ • T F G Higham⁴ • C Pickard¹ • I Radovanović⁵

ABSTRACT. A previous radiocarbon dating and stable isotope study of directly associated ungulate and human bone samples from Late Mesolithic burials at Schela Cladovei in Romania established that there is a freshwater reservoir effect of approximately 500 yr in the Iron Gates reach of the Danube River valley in southeast Europe. Using the $\delta^{15}\text{N}$ values as an indicator of the percentage of freshwater protein in the human diet, the ^{14}C data for 24 skeletons from the site of Lepenski Vir were corrected for this reservoir effect. The results of the paired ^{14}C and stable isotope measurements provide evidence of substantial dietary change over the period from about 9000 BP to about 300 BP. The data from the Early Mesolithic to the Chalcolithic are consistent with a 2-component dietary system, where the linear plot of isotopic values reflects mixing between the 2 end-members to differing degrees. Typically, the individuals of Mesolithic age have much heavier $\delta^{15}\text{N}$ signals and slightly heavier $\delta^{13}\text{C}$, while individuals of Early Neolithic and Chalcolithic age have lighter $\delta^{15}\text{N}$ and $\delta^{13}\text{C}$ values. Contrary to our earlier suggestion, there is no evidence of a substantial population that had a transitional diet midway between those that were characteristic of the Mesolithic and Neolithic. However, several individuals with “Final Mesolithic” ^{14}C ages show $\delta^{15}\text{N}$ and $\delta^{13}\text{C}$ values that are similar to the Neolithic dietary pattern. Provisionally, these are interpreted either as incomers who originated in early farming communities outside the Iron Gates region or as indigenous individuals representing the earliest Neolithic of the Iron Gates. The results from Roman and Medieval age burials show a deviation from the linear function, suggesting the presence of a new major dietary component containing isotopically heavier carbon. This is interpreted as a consequence of the introduction of millet into the human food chain.

INTRODUCTION

The Iron Gates section of the Danube River valley has an exceptional record of human occupation extending back to the Late Glacial period, about 12,600 BP. It is known especially for a large series of open-air settlements with evidence of Mesolithic and/or Early Neolithic occupation. The most famous of these is the site of Lepenski Vir, which is the focus of this paper (Figure 1). There has long been a debate over the dating of this site. The excavations at Lepenski Vir were conducted between 1965 and 1970 by Dragoslav Srejović, who identified a stratigraphic sequence of 5 occupation phases: Proto-Lepenski Vir (Early Mesolithic), Lepenski Vir I and II (Late Mesolithic), and Lepenski Vir IIIa and IIIb (Early Neolithic) (Srejović 1969, 1972). The results of radiocarbon dating have been inconsistent with this interpretation. A series of charcoal samples from contexts associated with LV I–II buildings gave ^{14}C ages between about 6560 and about 7360 BP (Quitta 1972), which are similar to those for Early Neolithic (Starčevo–Körös–Criş) sites in the surrounding regions (Gimbutas 1991; Radovanović 1996; Whittle et al. 2002). Subsequent accelerator mass spectrometry (AMS) dating of human remains assigned to the later phase, LV III, produced ages between about 6910 and 7770 BP (Bonsall et al. 1997), which are earlier than expected on the basis of the stratigraphic interpretation.

A series of human bone ages from another Iron Gates site, Vlasac, about 2 km downriver from Lepenski Vir, were also offset from previously measured charcoal ages. The similar trends in these

¹School of Arts, Culture and Environment, University of Edinburgh EH1 1LT, United Kingdom.

²Corresponding author. Email: C.Bonsall@ed.ac.uk.

³Scottish Universities Environmental Research Centre, East Kilbride G75 0QF, United Kingdom.

Email: g.cook@suerc.gla.ac.uk.

⁴Radiocarbon Accelerator Unit, Research Laboratory for Archaeology and the History of Art, Oxford OX1 3QJ, United Kingdom.

⁵Department of Anthropology, University of Kansas, 616 Fraser, Lawrence, Kansas 66045, USA.

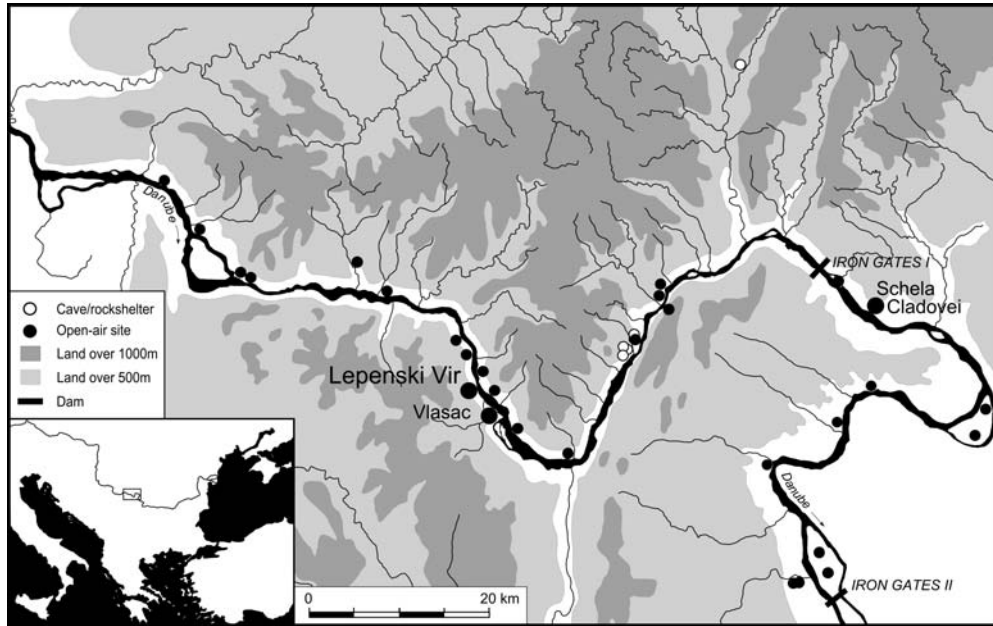


Figure 1 Mesolithic and Early Neolithic sites in the Iron Gates section of the Danube Valley

2 sites raised the possibility that some type of reservoir effect was in operation, making the human bone ages appear too old.

A third Iron Gates site, Schela Cladovei, provided a means of investigating this question. The ^{14}C ages of Late Mesolithic human bones were compared with directly associated ungulate bones, in the form of arrowheads embedded in, or otherwise directly associated with, the human skeletons (Cook et al. 2001, 2002). An age offset was observed between the 2 sample types in which the human bone ages were always several hundred years older than the associated ungulate bone projectile points, implying that the human population was deriving at least part of its diet from a carbon reservoir that was depleted in ^{14}C relative to the contemporaneous atmosphere. Stable isotope analyses ($\delta^{13}\text{C}$ and $\delta^{15}\text{N}$) of both sets of samples indicated that the $\delta^{13}\text{C}$ values for the human bones were always slightly heavier than those of the ungulates, while the $\delta^{15}\text{N}$ values were enriched significantly. These data were compared with published values (e.g. Ambrose 1991; Lanting and van der Plicht 1998; Little and Little 1997) and it was concluded that the human diet must have contained a significant proportion of freshwater fish and, therefore, the River Danube was the source of the reservoir effect. Since virtually all of the nitrogen that humans assimilate is derived from protein (Conn and Stumpf 1972), it was assumed that the $\delta^{15}\text{N}$ values recorded in the human bone collagen would be the result of a linear mixing of terrestrial and riverine resources. It was postulated that provided one had end-member values for these resources, it should be possible to estimate both the contribution of each resource to the diet and the reservoir age that should be subtracted from any human bone ^{14}C age prior to calibration on the calendar timescale. To achieve this, the following data were used:

1. Human bone samples from 3 individuals, all of which had $\delta^{15}\text{N}$ values of approximately +15‰;
2. An average offset for these individuals from the ungulate bone ages of 425 ± 55 yr;
3. An assumed $\delta^{15}\text{N}$ value for the terrestrial diet end-member of +8‰ (based on literature values: Mays 1998; Ogrinc 1999);

4. An aquatic resources end-member for $\delta^{15}\text{N}$ of +17‰, based on the heaviest value for an individual from the Iron Gates (Bonsall et al. 1997).

From this, we determined that +15‰ corresponded to a diet with approximately 79% of aquatic protein, for which the average reservoir age was 425 ± 55 yr. Thus, a reservoir age of 540 ± 70 yr would be applicable to someone subsisting wholly on riverine resources. This reservoir correction was then applied to the available human bone ages from Lepenski Vir and Vlasac.

Reservoir correction of the previously reported human bone ages from Lepenski Vir (Bonsall et al. 1997) brought the results broadly into the same range as the charcoal ages (Cook et al. 2001), but still in conflict with the stratigraphic dating unless phases LV I–IIIb occupy a very short time-span. In a separate study of the stable isotope data from Lepenski Vir, Bonsall et al. (2000) demonstrated that there was a linear correlation between $\delta^{13}\text{C}$ and $\delta^{15}\text{N}$ in human bone collagen. The data also implied that there were 3 compositional patterns to the human diet during the time-range represented by the burials—one dominated by aquatic resources, one dominated by terrestrial resources, and a third that was intermediate in character. Furthermore, once the reservoir age appropriate to the diet of individual humans had been subtracted from the age of the human bone samples, the data implied that the diet dominated by aquatic resources was from the Late Mesolithic; the diet dominated by terrestrial resources was from the Early Neolithic; and the intermediate diet was from the Mesolithic/Neolithic transition. However, this conclusion was based on a limited number of ^{14}C age measurements. This paper reports on a much more extensive suite of AMS ^{14}C and associated $\delta^{13}\text{C}$ and $\delta^{15}\text{N}$ analyses of human bone collagen from Lepenski Vir.

METHODS

Bone samples were prepared for AMS ^{14}C dating at the Oxford Radiocarbon Accelerator Unit (ORAU) using routine collagen extraction procedures (Bronk Ramsey et al. 2000; Law and Hedges 1989). An additional ultrafiltration pretreatment step was used to further purify the bone gelatin and retain only the >30-kD molecular weight fraction for ^{14}C assay (Brown et al. 1988; Bronk Ramsey et al. 2000). The <30-kD fraction may include degraded collagen fragments, salts, and contaminants that may be of a different ^{14}C age to the gelatin. We used the ratio of carbon to nitrogen (C:N ratio) to determine the chemical integrity of the extracted gelatin. All ratios were within the 2.9–3.6 range of acceptability for bone collagen used at ORAU. Yields of ultrafiltered gelatin that are below 10 mg g^{-1} are not dated routinely because they indicate poor levels of collagen preservation. All of the ultrafiltered samples from Lepenski Vir were above this threshold.

The >30-kD fraction was lyophilized and analyzed using a Europa Scientific ANCA-MS system consisting of a 20–20 IR mass spectrometer interfaced to a Roboprep CHN sample converter unit operating in continuous flow mode. CO_2 from the combustion was trapped cryogenically and graphite was prepared by reduction of CO_2 over iron within an excess H_2 atmosphere. Graphite targets were then measured by AMS (Bronk Ramsey and Hedges 1997). Small samples of CO_2 (<1.6 mg C) were dated directly using the ORAU gas ion source (Bronk Ramsey and Hedges 1997). $\delta^{13}\text{C}$ values in this paper are reported in per mil (‰) with reference to VPDB and $\delta^{15}\text{N}$ results are reported with reference to AIR (Coplen 1994).

RESULTS AND DISCUSSION

The data presented here comprise 5 previously published (Bonsall et al. 1997) and 19 new sets of analyses. Table 1 summarizes the reservoir corrected ^{14}C data for the 24 AMS ^{14}C measurements and the number of samples, following this reservoir correction, which can be assigned to the various archaeological periods. Figure 2 summarizes the $\delta^{13}\text{C}$ and $\delta^{15}\text{N}$ results for all 24 human bone samples.

Table 1 Phasing of 24 AMS ^{14}C -dated skeletons from Lepenski Vir. Reservoir corrected ^{14}C ages were calculated using Method 1 of Cook et al. (2002).

Reservoir corrected ^{14}C age range	Notional archaeological period	Nr of samples
9020 ± 80 – 8784 ± 72 BP	Early Mesolithic	2
about 8500–7400 BP	Late Mesolithic	0
7374 ± 80 – 7133 ± 75 BP	Final Mesolithic	12
7036 ± 95 – 6718 ± 93 BP	Early Neolithic (Starčevo)	5
5269 ± 54 BP	Chalcolithic (Salcuța)	1
1724 ± 44 – 339 ± 38 BP	Roman and Medieval	4

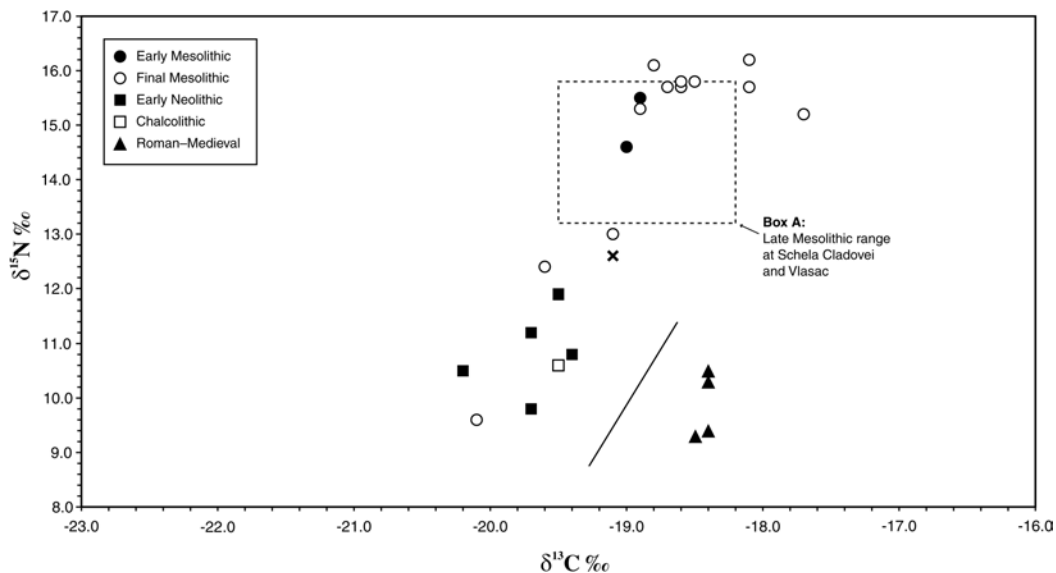


Figure 2 $\delta^{13}\text{C}$ versus $\delta^{15}\text{N}$ for 24 AMS ^{14}C -dated human skeletons from Lepenski Vir. The cross (x) represents an undated burial of Starčevo type.

From Table 1, it can be observed that there are no skeletons from Lepenski Vir that are dated to the period 8500–7400 BP (“Late Mesolithic”), but this time range is represented at 2 other sites. At Vlasac, 4 skeletons have been dated between 8400–7600 BP, while at Schela Cladovei, 6 skeletons have been dated between 8100–7700 BP (Bonsall et al. 1997; Cook et al. 2001, 2002). In contrast, the period 7400–7100 BP (“Final Mesolithic”) is only represented at Lepenski Vir and not currently at any other site in the Iron Gates region. This appears to have been a period of general site abandonment in the Iron Gates, possibly linked to increased flooding along the Danube which coincided with the “8200 cal BP global cooling event” (Bonsall et al. 2002).

It is interesting to consider the “isotopic profiles” of humans belonging to the different time ranges that are set out in Table 1.

Late Mesolithic (8500–7400 BP)

This period is considered first because the stable isotope profile of Late Mesolithic populations in the Iron Gates is well known from our earlier research. Ten skeletons from Schela Cladovei and Vlasac have been dated to the time range 8500–7400 BP (Bonsall et al. 1997, 2000). The $\delta^{13}\text{C}$ and $\delta^{15}\text{N}$

values of these 10 skeletons fall within the range circumscribed by Box A in Figure 2, $\delta^{13}\text{C}$: -19.5 to -18.2‰ and $\delta^{15}\text{N}$: $+13.2$ to $+15.8\text{‰}$. These values have been interpreted as indicative of diets rich in protein derived from aquatic sources, primarily larger Danube fish such as carp, catfish, and sturgeon (Bonsall et al. 1997).

Early Mesolithic (>8500 BP)

Two skeletons from Lepenski Vir (and one from Vlasac) are dated to the period before 8500 BP (Figure 2, filled circles). Here, the $\delta^{13}\text{C}$ and $\delta^{15}\text{N}$ values all fall within the range of Late Mesolithic skeletons from Vlasac and Schela Cladovei (Figure 2, Box A). This suggests that the range defined by Box A is typical for Iron Gates Mesolithic populations older than 7400 BP. Using the $\delta^{15}\text{N}$ -based calculation method described in Cook et al. (2001), this is consistent with diets in which >58% of the protein was derived from aquatic resources.

Early Neolithic (7100–6700 BP)

Five skeletons from Lepenski Vir are dated to this time range (Figure 2, filled squares) and have $\delta^{13}\text{C}$ values in the range -20.2 to -19.4‰ and $\delta^{15}\text{N}$ values of $+9.8$ to $+11.9\text{‰}$. These values indicate a diet that is very different from that of the Mesolithic populations. It is dominated by terrestrial resources and has a much smaller contribution (20–43%) from aquatic resources. However, this may underestimate the range of Early Neolithic diets. An undated Starčevo-type burial has more elevated $\delta^{13}\text{C}$ and $\delta^{15}\text{N}$ values (Figure 2, cross). Thus, we would expect the true $\delta^{15}\text{N}$ range to be at least $+9.8$ to $+12.6\text{‰}$, reflecting diets in which 49–80% of the protein was derived from terrestrial resources. This is consistent with the presence of bones of livestock in Iron Gates sites after about 7100 BP, together with other evidence of a Neolithic farming economy (pottery, bread ovens). Comparison with similar age (Starčevo–Körös–Criş) sites on the Great Hungarian Plain (Whittle et al. 2002), where the majority of dated skeletons have $\delta^{15}\text{N}$ values in the range $+8.3$ to $+9.5\text{‰}$, confirms that fishing continued to play a significant role in the Iron Gates economy during this period. This is supported by archaeozoological evidence (Clason 1980; Bartosiewicz et al. 1995).

Final Mesolithic (7400–7100 BP)

The majority (12) of dated skeletons from Lepenski Vir fall into this time range and show a very broad range of $\delta^{13}\text{C}$ and $\delta^{15}\text{N}$ values (Figure 2, open circles), much broader than one would expect in a single population with access to the same resources. Nine of the skeletons have very high $\delta^{15}\text{N}$ values ($+15.2$ to $+16.2\text{‰}$) and relatively heavy $\delta^{13}\text{C}$ values (-17.7 to -18.8‰). Although the range of $\delta^{15}\text{N}$ and $\delta^{13}\text{C}$ values overlaps that of the earlier Mesolithic populations (Figure 2, Box A), on average, both the $\delta^{13}\text{C}$ and $\delta^{15}\text{N}$ values are heavier. This may reflect either: (1) a higher percentage of aquatic food in the diet, or (2) a change in composition of the aquatic food intake, such as an increase in the average size of fish consumed or concentration on certain species. Possible causes of this change include the following:

- Social—e.g., higher status individuals with preferential access to large fish or certain species.
- Environmental—e.g., effect of increased flooding on fish populations.
- Technological—change in fishing methods resulting in catches of different species or larger specimens.
- A combination of these.

Three skeletons have much lighter $\delta^{13}\text{C}$ and $\delta^{15}\text{N}$ values. The $\delta^{15}\text{N}$ values are also lighter than those from any Mesolithic skeletons from either Schela Cladovei or Vlasac. In 2 cases, the $\delta^{15}\text{N}$ values are intermediate between aquatic and terrestrial diets and similar to the upper end of our “expected”

Early Neolithic range, while the third has a $\delta^{15}\text{N}$ value which is lighter than any of the dated Early Neolithic skeletons from Lepenski Vir and similar to values recorded from Starčevo sites on the Hungarian Plain (Whittle et al. 2002), suggesting a diet based on terrestrial food sources. There are several possible explanations for these results:

- The individuals with light or intermediate $\delta^{15}\text{N}$ values were incomers (e.g. on marriage) whose bone collagen had not undergone complete turnover. The age-at-death profiles of the individuals concerned (Roksandić 1999) are consistent with this interpretation. The individual with the light $\delta^{15}\text{N}$ value is relatively young (20–40 yr), while the individuals with intermediate $\delta^{15}\text{N}$ values are older (>40 yr) and would have had longer to adjust. If so, the question is whether these individuals transferred from a hunter-gatherer (Mesolithic) community(-ies) or a farming community(-ies). The only evidence for the existence of hunter-gatherer communities in the northern Balkans with an economy based on terrestrial food sources derives from an age of 8085 ± 55 BP (OxA-8504) for a burial from the Starčevo culture site of Topole-Bač in northern Serbia (Whittle et al. 2002). A $\delta^{13}\text{C}$ value of -19.9‰ and a $\delta^{15}\text{N}$ value of $+8.6\text{‰}$ for this individual indicate a terrestrially-based diet, but the dating is inconsistent with the archaeological evidence. This is one of two crouched inhumations (implying an Early Neolithic age) that were situated back to back (further implying that the burials were more or less contemporaneous). The 2 skeletons have similar $\delta^{13}\text{C}$ and $\delta^{15}\text{N}$ values; however, the second has a ^{14}C age of 7170 ± 50 BP (OxA-8693), which is consistent with the archaeological context. Thus, the ^{14}C age of the first skeleton requires verification. If individuals with light/intermediate $\delta^{15}\text{N}$ values in the Final Mesolithic group are “incomers”, they are more likely to be derived from Early Neolithic farming communities. There is no unequivocal evidence that farming was practiced anywhere in the Middle or Lower Danube Basin (outside the Iron Gates) during the period 7400–7100 BP. However, by about 7300 BP, Neolithic communities were present in the Morava valley, about 120 km southwest of Lepenski Vir (Whittle et al. 2002).
- The ^{14}C ages lie at the lower extremes of the $2\text{-}\sigma$ ranges, and these skeletons belong to the later part of the time-range (about 7250–7100 BP), when agriculture began to make a significant contribution to diet. That is, the burials are those of indigenous people who represent the earliest Neolithic of the Iron Gates. The implication of this hypothesis is that the transition to farming occurred as early as, or earlier than, elsewhere in the Danube Basin. This is in conflict with the view espoused by some authors (e.g. Radovanović and Voytek 1997) that the transition in the Iron Gates was significantly delayed compared to neighboring regions such as the Great Hungarian Plain, where the earliest ^{14}C ages for short-lived terrestrial material from Early Neolithic (Starčevo-Kőrös) contexts are about 7100 BP (Whittle et al. 2002). If the 3 individuals with light/intermediate $\delta^{15}\text{N}$ values do belong to the earliest Neolithic, it is interesting that the burial rite in each case follows the Mesolithic tradition of extended supine inhumation, rather than the crouched or tightly flexed inhumation rite of the Early Neolithic (Starčevo culture).
- A third hypothesis—a variant on hypothesis 2, above—is that the lifetimes of the individuals with light/intermediate $\delta^{15}\text{N}$ values overlapped with a short-lived phase(s) when terrestrial food resources became (temporarily) more important in the Iron Gates economy. It is possible that in the relatively “difficult” environment of the Danube gorges, there were one or more “false starts” to agriculture, lasting years to decades. Under these circumstances, the people might be forced to revert to the traditional Mesolithic subsistence pattern, based on aquatic resources, before a farming economy was successfully established about 7100 BP.

It is not possible to decide between the above hypotheses on present evidence; however, analysis of Sr-, Pb-, and O-isotopes in teeth might indicate whether the individuals with light/intermediate $\delta^{15}\text{N}$ values originated outside the Iron Gates (e.g. Budd et al. 2001; Price et al. 2001). An implication

common to all the hypotheses is that the Lepenski Vir population had knowledge of agriculture, regardless of whether they practiced it prior to 7100 BP.

Chalcolithic (Eneolithic)

One skeleton from Lepenski Vir (Figure 2, open square) was assigned to the Chalcolithic (Salcuța culture) on archaeological grounds (Zoffmann 1983). This dating is confirmed by the reservoir corrected ¹⁴C age of 5269 ± 54 BP. It is interesting that the δ¹³C and δ¹⁵N values fall within the range of the Early Neolithic skeletons, suggesting a similar diet, i.e., one dominated by terrestrial resources with low to moderate levels of aquatic protein.

Roman and Medieval Periods

One individual is dated to the Roman period and 3 to the Medieval period (Figure 2, filled triangles). Like the Early Neolithic and Chalcolithic skeletons, these individuals have light δ¹⁵N values (+9.3 to +10.5‰), but they are unusually enriched in ¹³C (δ¹³C: -18.5 to -18.4‰). The most likely explanation is the incorporation of C₄ plant material into the food chain (Bonsall et al. 2000). There is evidence that millet started to be grown in this part of southeast Europe during the Iron Age (Murray and Schoeninger 1988) and its addition into the human diet, either directly or indirectly in the form of forage fed to livestock, would result in enrichment in δ¹³C without enriching the δ¹⁵N values.

CONCLUSIONS

The results of paired ¹⁴C and stable isotope measurements on 24 skeletons from Lepenski Vir provide evidence of substantial dietary change over the period from about 9000 BP to about 300 BP. The data from the Early Mesolithic to the Chalcolithic are consistent with a 2-component dietary system, where the linear plot of isotopic values reflects mixing between the 2 end-members to differing degrees. Typically, the individuals of Mesolithic age have much heavier δ¹⁵N signals and slightly heavier δ¹³C, while individuals of Early Neolithic and Chalcolithic age have lighter δ¹⁵N and δ¹³C values. Contrary to Bonsall et al. (2000), there is no evidence of a substantial population that had a transitional diet midway between those that were characteristic of the Mesolithic and Neolithic. However, several individuals with “Final Mesolithic” ¹⁴C ages show δ¹⁵N and δ¹³C values that are similar to the Neolithic dietary pattern. Provisionally, these are interpreted either as incomers who originated in early farming communities outside the Iron Gates region or as indigenous individuals representing the earliest Neolithic of the Iron Gates region. The results from Roman and Medieval age burials show a deviation from the linear function, suggesting the presence of a new major dietary component containing isotopically heavier carbon. This is interpreted as a consequence of the introduction of millet into the human food chain.

REFERENCES

- Ambrose SH. 1991. Effects of diet, climate and physiology on nitrogen isotope abundances in terrestrial foodwebs. *Journal of Archaeological Science* 18:293–317.
- Bartosiewicz L, Bonsall C, Boroneanț V, Stallibrass S. 1995. Schela Cladovei: a preliminary review of the prehistoric fauna. *Mesolithic Miscellany* 16(2):2–19.
- Bonsall C, Lennon R, McSweeney K, Stewart C, Harkness D, Boroneanț V, Payton R, Bartosiewicz L, Chapman JC. 1997. Mesolithic and Early Neolithic in the Iron Gates: a palaeodietary perspective. *Journal of European Archaeology* 5(1):50–92.
- Bonsall C, Cook G, Lennon R, Harkness D, Scott M, Bartosiewicz L, McSweeney K. 2000. Stable isotopes, radiocarbon and the Mesolithic-Neolithic transition in the Iron Gates. *Documenta Praehistorica* 27:119–132.
- Bonsall C, Macklin MG, Payton RW, Boroneanț A. 2002. Climate, floods and river gods: environmental change and the Meso-Neolithic transition in southeast Europe. *Before Farming: The Archaeology of Old World Hunter-Gatherers* 3–4(2):1–15.
- Bronk Ramsey C, Hedges REM. 1997. Hybrid ion sources: radiocarbon measurements from microgram

- to milligram. *Nuclear Instruments and Methods in Physics Research B* 123:539–45.
- Bronk Ramsey C, Pettitt PB, Hedges REM, Hodgins GWL, Owen DC. 2000. Radiocarbon dates from the Oxford AMS system: Archaeometry Datelist 30. *Archaeometry* 42(2):459–79.
- Brown TA, Nelson DE, Vogel JS, Southon JR. 1988. Improved collagen extraction by modified Longin method. *Radiocarbon* 30(1):171–7.
- Budd P, Montgomery J, Evans J, Chenery C. 2001. Combined Pb-, Sr- and O-isotope analysis of human dental tissue for the reconstruction of archaeological residential mobility. In: Holland JG, Tanner SD, editors. *Plasma Source Mass Spectrometry: The New Millennium*. Cambridge: Royal Society of Chemistry Special Publication. p 311–26.
- Clason AT. 1980. Padina and Starčevo: game, fish and cattle. *Palaeohistoria* XXII:142–73.
- Cook GT, Bonsall C, Hedges REM, McSweeney K, Boroneanț V, Pettitt PB. 2001. A freshwater diet-derived ¹⁴C reservoir effect at the Stone Age sites in the Iron Gates gorge. In: Carmi I, Boaretto E, editors. Proceedings of the 17th International Radiocarbon Conference, Judean Hills, Israel, 18–23 June 2000. *Radiocarbon* 43(2A):453–60.
- Cook GT, Bonsall C, Hedges REM, McSweeney K, Boroneanț V, Bartosiewicz L, Pettitt PB. 2002. Problems of dating human bones from the Iron Gates. *Antiquity* 76:77–85.
- Coplen TB. 1994. Reporting of stable hydrogen, carbon and oxygen isotopic abundances. *Pure and Applied Chemistry* 66:273–6.
- Gimbutas M. 1991. *The Civilization of the Goddess: The World of Old Europe*. San Francisco: Harper.
- Hedges REM, Law IA, Bronk CR, Housley RA. 1989. The Oxford accelerator mass spectrometry facility: technical developments in routine dating. *Archaeometry* 31:99–113.
- Lanting JN, van der Plicht J. 1998. Reservoir effects and apparent ¹⁴C ages. *Journal of Irish Archaeology* IX: 151–65.
- Law IA, Hedges REM. 1989. A semi-automated bone pretreatment system and the pretreatment of older and contaminated samples. *Radiocarbon* 31(2):247–53.
- Little JDC, Little EA. 1997. Analysing prehistoric diets by linear programming. *Journal of Archaeological Science* 24:741–7.
- Mays S. 1998. *The Archaeology of Human Bones*. London: Routledge.
- Murray M, Schoeninger M. 1988. Diet, status and complex social structure in Iron Age Central Europe: some contributions of bone chemistry. In: Gibson DB, Geselowitz MN, editors. *Tribe and Polity in Late Prehistoric Europe: Demography, Production and Exchange in the Evolution of Complex Social Systems*. New York: Plenum. p 155–76.
- Ogrinc N. 1999. Stable isotope evidence of the diet of the Neolithic population in Slovenia—a case study: Ajdovska jama. *Documenta Praehistorica* 26:193–200.
- Price T, Bentley R, Luning J, Detlef G, Wahl J. 2001. Prehistoric human migration in the Linearbandkeramik of central Europe. *Antiquity* 75:593–603.
- Quitta H. 1972. The dating of radiocarbon samples. In: Srejović D. *Europe's First Monumental Sculpture. New Discoveries at Lepenski Vir*. London: Thames and Hudson. p 205–10.
- Radovanović I. 1996. Mesolithic/Neolithic contacts: a case of the Iron Gates region. *Poročilo o raziskovanju paleolitika, neolitika in eneolitika v Sloveniji* 23:39–48.
- Radovanović I, Voytek B. 1997. Hunters, fishers and farmers: sedentism, subsistence and social complexity in the Djerdap Mesolithic. *Analecta Praehistorica Leidensia* 29:19–31.
- Roksandić M. 1999. *Transition from Mesolithic to Neolithic in the Iron Gates Gorge: Physical Anthropology Perspective* [PhD dissertation]. Burnaby, Canada: Simon Fraser University.
- Srejović D. 1969. The roots of the Lepenski Vir culture. *Archaeologia Jugoslavica* 10:13–21.
- Srejović D. 1972. *Europe's First Monumental Sculpture. New Discoveries at Lepenski Vir*. London: Thames and Hudson.
- Whittle A, Bartosiewicz L, Borić D, Pettitt P, Richards M. 2002. In the beginning: new radiocarbon dates for the Early Neolithic in northern Serbia and southeast Hungary. *Antaeus* 25:64–117.
- Zoffmann Z. 1983. Prehistorical skeletal remains from Lepenski Vir (Iron Gate, Yugoslavia). *Homo* 34:129–48.

A REVIEW OF THE EVIDENCE FOR EXTINCTION CHRONOLOGIES FOR FIVE SPECIES OF UPPER PLEISTOCENE MEGAFaUNA IN SIBERIA

Lyobov A Orlova¹ • Yaroslav V Kuzmin² • Vyacheslav N Dementiev^{1,3}

ABSTRACT. A review of the radiocarbon chronology of some late Upper Pleistocene mammals from Siberia is presented. Previously published data has been supplemented by new ¹⁴C dates for 5 species (woolly mammoth, woolly rhinoceros, bison, horse, and muskox) to reconstruct chronological extinction patterns. The final extinction of woolly rhinoceros and bison in Siberia can be dated to approximately 11,000–9700 BP, but some megafaunal species (woolly mammoth, horse, and muskox) survived into the Late Holocene, about 3700–2200 BP.

INTRODUCTION

Determining the extinction patterns of Upper Pleistocene megafauna using radiocarbon dating was first conducted in Siberia in the early 1960s (Heintz and Garutt 1964, 1965; Heintz 1966). Since that time, the number of ¹⁴C dates obtained directly from megafaunal species has significantly increased and now constitutes several hundred values. The majority of dates were obtained for such species as woolly mammoth (*Mammuthus primigenius* Blum.), woolly rhinoceros (*Coelodonta antiquitatis* Blum.), Pleistocene bison (*Bison priscus* Boj.), Pleistocene-type horse (*Equus caballus* L.), and muskox (*Ovibos moschatus* Zimm.). These data provide a basis for establishing the timing of the megafauna's final extinction in Siberia and the Russian Far East, and in the adjacent territories of Kazakhstan and Northeastern China. The aim of this paper is to present an extended data set which enhances our understanding of extinction patterns for the species and compare the data set to previous summaries (cf. Stuart 1991; Sulerzhitsky 1997; Vasil'chuk et al. 1997).

MATERIAL AND METHODS

We have compiled data from published sources (mainly from Sulerzhitsky 1997; Sulerzhitsky and Romanenko 1999; Vasil'chuk et al. 1997; Orlova et al. 2000; Stuart et al. 2002; MacPhee et al. 2002; Schirmermeister et al. 2002; Kuzmin et al. 2003), with new ¹⁴C dates produced at the Institute of Geology, Siberian Branch of the Russian Academy of Sciences, Novosibirsk (Lab code SOAN). The number of ¹⁴C dates known for extinct megafaunal species in Siberia is skewed towards woolly mammoth, with about 530 ¹⁴C values from 230 localities. Of these, we have concentrated on only the "youngest" dates, less than about 12,000 BP, because they are directly related to the issue of extinction (Table 1; Figure 1). Other species have far fewer ¹⁴C determinations; for example, there are 59 dates on bison from 51 localities, 55 dates on horse from 33 localities, 41 dates on woolly rhinoceros from 35 localities, and 29 dates on muskox from 19 localities (Tables 2–5; Figures 2–3).

The dating of megafaunal remains was conducted mainly using bone collagen as the source of carbon. Dates produced in Russian laboratories, located in Moscow, Novosibirsk, and St Petersburg, comprise 85% of the total ¹⁴C values discussed in this paper. The main technique of collagen extraction for bone dating in Russian laboratories since the late 1960s is the dissolution of the mineral part of the bone in weak hydrochloric acid (HCl) (Arslanov and Svezhentsev 1993; Sulerzhitsky 1997;

¹Institute of Geology, Siberian Branch of the Russian Academy of Sciences, Koptuyg Ave. 3, Novosibirsk 630090, Russia. Email: orlova@uiggm.nsc.ru.

²Pacific Institute of Geography, Far Eastern Branch of the Russian Academy of Sciences, Radio St. 7, Vladivostok 690041, Russia. Email: ykuzmin@tig.dvo.ru.

³Email: dementev@uiggm.nsc.ru.

see detailed description in Vasil'ev et al. 2002:505–7). Slow dissolution of the mineral part of whole pieces of bone in diluted HCl makes it possible to extract non-contaminated collagen and to see the degree of preservation of the initial fiber-like internal collagen structure after demineralization. The reliability of the slow dissolution technique for collagen extraction is also supported by good agreement of results of parallel dating on the same pieces of bone conducted in Russian, US, and European laboratories (Vartanyan et al. 1995; Vasil'chuk et al. 2000; Kuzmin et al. 2001; MacPhee et al. 2002).

The date of final extinction was estimated using the latest ^{14}C date available for a particular species, an approach employed in similar studies (cf. Stuart et al. 2002; MacPhee et al. 2002; Guthrie 2003). The extent of the species' habitats (i.e. the natural home or environment of an organism) were assumed by the geographic distribution of their fossil remains (cf. Kuzmin et al. 2003:223–5) and are listed in Tables 1–5 by latitude and longitude, given as decimal values (e.g. 70.50 N means 70°30' northern latitude), as per the US Defense Mapping Agency Operational Navigation Charts (scale of 1:1,000,000). GIS ArcView 3.2 software was used for map generation.

RESULTS AND DISCUSSION

Woolly Mammoth

As previously noted, we selected 56 of the latest ^{14}C dates from 26 localities covering the Late Glacial and the Holocene, about 12,000–3700 BP (Table 1; Figure 1). As for earlier times, about 50,000–12,000 BP, it is clear that the woolly mammoth habitat extended through all of Northern Asia-Siberia, the Russian Far East, northeastern China, and northern Kazakhstan (cf. Sulerzhitsky 1997; Kuzmin et al. 2003). The distribution pattern appears to have changed significantly, by about 12,000–10,000 BP (Figure 1). The mammoth habitat was substantially reduced in size and located mainly in arctic Siberia, including the lower part of the Indigirka River basin, the Taymyr, Yamal, and Gydan peninsulas, the Severnaya Zemlya archipelago, and Wrangel Island. The Taymyr Peninsula mammoths have the youngest ^{14}C dates in continental Siberia of about 9800–9700 BP. New ^{14}C dates obtained in 2000–2002 also reveal several mammoth sites in the temperate belt of Siberia dated to approximately 11,980–10,210 BP, including the central and southern West Siberian Plain (Volchya Griva, Sosva River, and Lugovskoe) and the Upper Yenisei River basin (Konzhul) (Table 1; Figure 1). In our opinion, these localities represent the “patchy” nature of the mammoth habitat in Siberia after about 12,000 BP, with few isolated “pockets” outside of the High Arctic. Finally, in the Middle Holocene, about 7700–3700 BP, smaller mammoths (a subspecies, *M. primigenius vrangeliensis*; Averyanov et al. 1995) existed only on Wrangel Island.

These data suggest that the final extinction of woolly mammoth in Siberia and elsewhere in the Northern Hemisphere occurred at about 9700 BP in the continental part (Taymyr Peninsula), and at about 3700 BP in the insular part (Wrangel Island). Our extended data set presented here indicates mammoth survival in temperate Siberia after shrinking and fragmentation of its habitat at about 12,500–12,000 BP. Based on this, it is possible to assume that even after approximately 12,000 BP some mammoth populations survived outside of arctic regions in a few places in continental Eurasia (Western Siberia, north Russian Plain in Eastern Europe) until the beginning of the Holocene (Stuart et al. 2002; Lõugas et al. 2002).

Woolly Rhinoceros

The distribution of woolly rhinoceros ^{14}C dates indicates its habitat covered Northeastern Siberia and the southern parts of Western and Eastern Siberia (Figure 2) in the late Upper Pleistocene, from

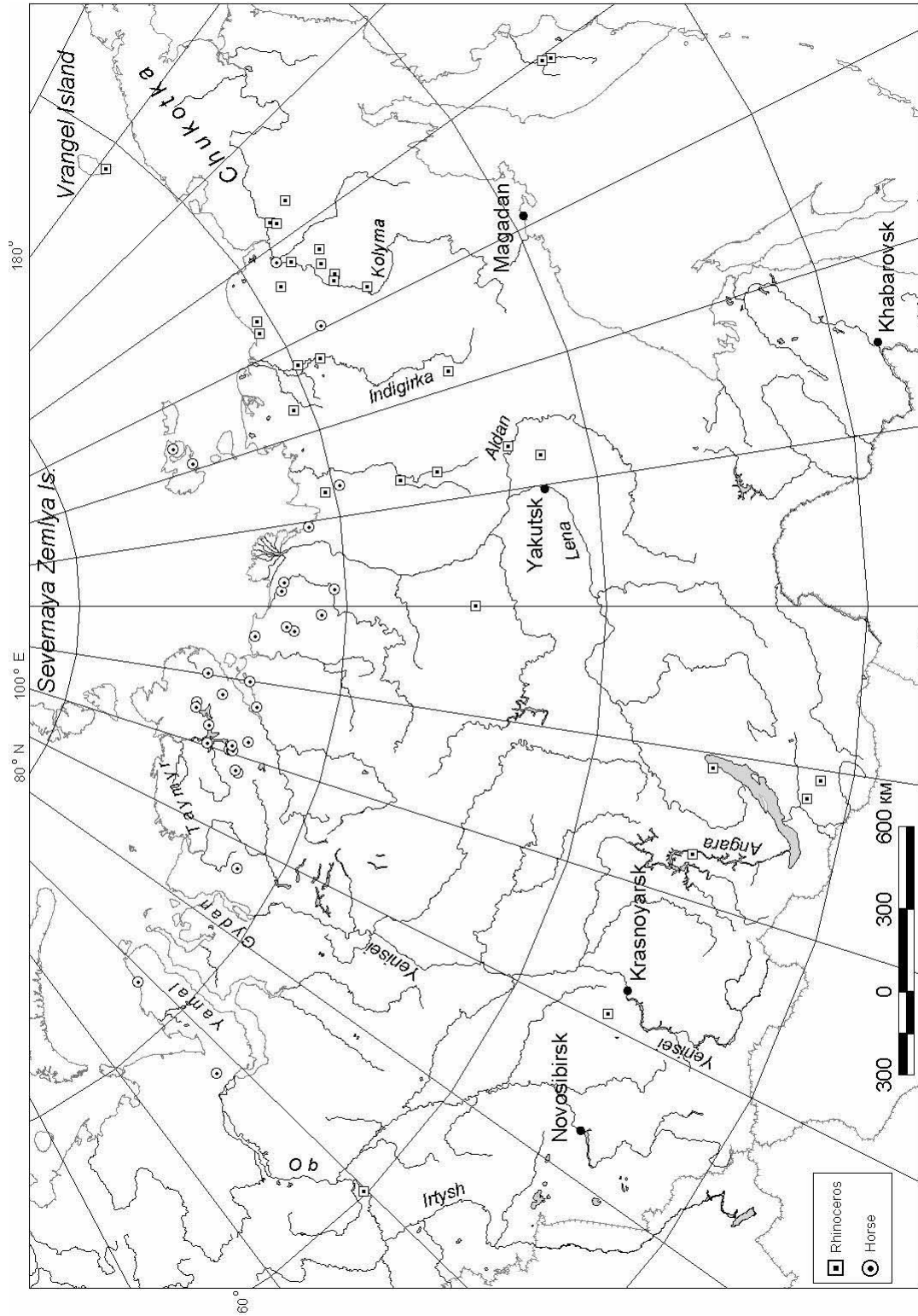


Figure 2 Location of ¹⁴C-dated woolly rhinoceros and horse remains in Siberia

about 49,000 BP, as well as the Russian Far East (without direct ^{14}C dates). In the northern parts of Western and Eastern Siberia (Putorana Plateau, and the Taymyr, Gydan, and Yamal peninsulas), no remains of woolly rhinoceros have been recovered, perhaps indicating that these areas were not part of its natural habitat as was earlier assumed by R-D Kahlke (1998). The latest ^{14}C dates for the species are from the Bolshoi Khomus-Yuriakh River, Yakutia (about 15,130 BP); Yukagir Plateau, Northeastern Siberia (about 14,260 BP); Zlatoustovka, Ashkadar River, southern Trans-Urals (about 12,330 BP); and Lugovskoe, central Western Siberia (about 10,770 BP) (Table 2). It is worthwhile highlighting that the ^{14}C dates from temperate Siberia (Zlatoustovka and Lugovskoe) are significantly younger than those from arctic regions.

With the new ^{14}C date from the Lugovskoe locality, the final extinction of woolly rhinoceros could be as late as the end of the Late Glacial (about 10,800 BP), rather than as suggested at approximately 14,000–12,000 BP by Vereshchagin and Baryshnikov (1984:497–9). Further study is thus necessary on this ^{14}C chronology in Siberia to confirm/reject the 10,800 BP age for its final extinction, especially in the areas with the youngest dates such as Western Siberia and the Trans-Urals.

Bison

The bison habitat in the late Upper Pleistocene extended throughout all of the Siberian and the Russian Far Eastern territory (Figure 3). In most of Siberia, bison were extinct by approximately 15,000–11,600 BP (Table 3). Bison persisted only in a few places into the Holocene. The latest bison ^{14}C date, about 8860 BP, comes from the Popigai River basin, northern Eastern Siberia, next to the Taymyr Peninsula (MacPhee et al. 2002). At the Sushikha locality, southern West Siberian Plain, the tentative age of bison occupation, about 9320 BP, requires further study due to only a single ^{14}C value obtained so far from this locality and the fragmentary nature of the fossils. Similar aged bison remains are known from the Ust-Belaya site (layers 3–4) at the Angara River headwaters, southern Eastern Siberia, with an associated ^{14}C bone date of 8960 ± 60 BP (GIN-96) (Kuzmin and Orlova 1998:18; MacPhee et al. 2002:1033). Nevertheless, no details are available about the association of ^{14}C -dated bone and the bison remains, and this value should, therefore, be treated with caution. The existence of *Bison priscus* in southern Siberia in the Early Holocene is still in doubt and requires additional study.

Horse

Although there are many Upper Pleistocene findings of horse fossils in Siberia (cf. Vangengeim 1977; Vereshchagin and Baryshnikov 1984; Markova et al. 1995), ^{14}C -dated localities are known mostly from the northern parts of Western, Eastern, and Northeastern Siberia (Figure 2). Most of the youngest dates correspond to the Late Glacial and the Pleistocene-Holocene boundary, about 15,300–9010 BP (Table 4). However, in the Holocene, small populations of horse existed on the Laptev Sea coast and the Taymyr Peninsula. At the Bykovsky Peninsula locality, on the Laptev Sea coast near the modern town of Tiksi, a ^{14}C date of 4610 ± 40 BP was obtained; and on the Bolshoi Lyakhovsky Island (Novosibirsk archipelago), the value of 2200 ± 50 BP was generated (Kuznetsova et al. 2001). On the Taymyr Peninsula, ^{14}C dates of 3250 ± 60 BP (Agapa River basin) and 2150 ± 200 BP (Bolshaya Balakhnya River basin) have been previously reported (MacPhee et al. 2002). These dates support that horse existed in arctic Siberia into the Late Holocene.

The data shows an extinction pattern which illustrates a disappearance of horse in Siberia at about 11,700–9000 BP, but an apparent reappearance in arctic Siberia at about 4600 BP, and finally becoming extinct throughout the region at about 2200 BP. The cause of the hiatus in the existence of horse in this region between approximately 9000 and 4600 BP is not clear (MacPhee et al. 2002: 1034–40).

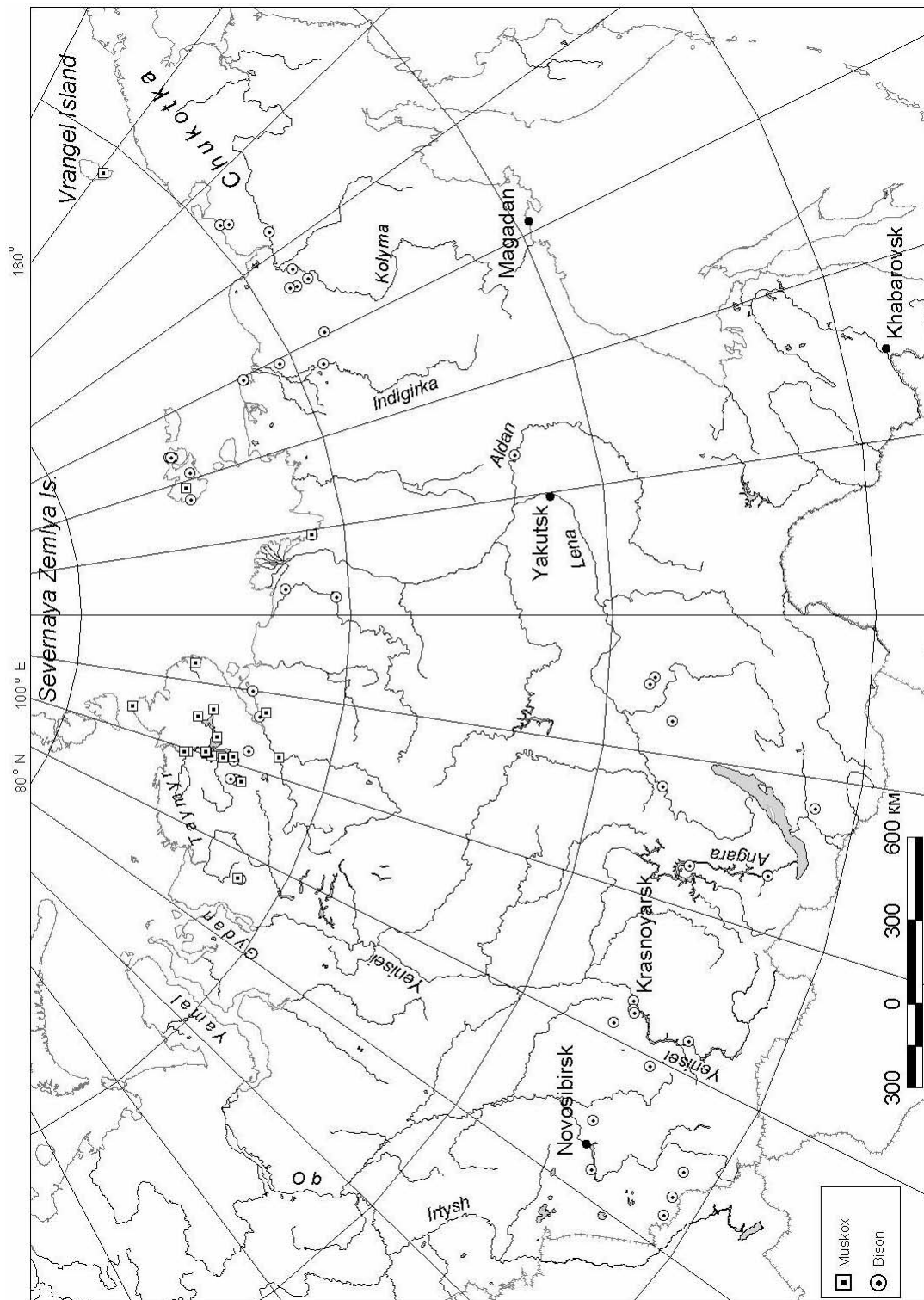


Figure 3 Location of ¹⁴C-dated bison and muskox remains in Siberia

Muskox

Fossils of muskox are rare in Siberia and are concentrated mainly in what are today arctic regions, from where ^{14}C -dated remains are found (Figure 3). The highest concentration of dates is on the Taymyr Peninsula (MacPhee et al. 2002). The majority of the latest ^{14}C dates run on muskox belong to the Late Glacial, about 12,150–10,750 BP (Table 5). However, in the Late Holocene, muskox reappeared on the Laptev Sea coast and the Taymyr Peninsula at about 3200–2900 BP, and continued to exist until about 2700 BP (Sulerzhitsky and Romanenko 1999; Kuznetsova et al. 2001). This pattern is similar to the Holocene dynamics of horse in the same region, with a significant hiatus on the Taymyr Peninsula from approximately 12,150 BP to 2900 BP (MacPhee et al. 2002:1030–3).

CONCLUSION

From the data presented, we conclude that the major extinction of the Pleistocene fauna representatives in continental Siberia can be dated to approximately 11,000–9700 BP. In the insular territories, (for example, Wrangel Island), a few species such as woolly mammoth survived until the Late Holocene, about 3700 BP. Some species, such as horse and muskox, reappeared in continental arctic Siberia in the Holocene. Thus, the dynamics of the megafaunal species was quite complex and “mosaic-like” in their geographic and chronological patterns, with hiatuses in the ^{14}C age distribution for some species, possibly reflecting the re-colonization after a long absence.

Our data also allows us to assume that the central and southern parts of the West Siberian Plain contained several apparent refuge areas for Pleistocene species, including mammoth (until about 10,200 BP), woolly rhinoceros (until about 10,800 BP), and possibly bison (until about 9000 BP). The existence of isolated megafaunal populations beyond the Arctic after about 12,000 BP is at odds with current Pleistocene extinction models, but will provide an interesting challenge for future research.

ACKNOWLEDGEMENTS

We are grateful to colleagues who helped us to collect original data which were used in this study, including Drs Leopold D Sulerzhitsky, Tatiana V Kuznetsova, Ross D E MacPhee, Aleksei N Tikhonov, Nikolai D Ovodov, Evgeny M Ineshin, Vasily N Zenin, Sergei K Vasiliev, and Fedor A Romanenko. We are also grateful to Dr Susan G Keates for grammar polishing and useful suggestions. We are grateful to anonymous reviewer for helpful suggestions and remarks. This study was supported by grants from Russian RFFI (00-06-80410, 03-06-80289 and 03-05-64434).

REFERENCES

- Arslanov KA, Svezhentsev YS. 1993. An improved method for radiocarbon dating fossil bones. *Radiocarbon* 35(3):387–91.
- Averianov AO, Vartanyan SL, Garutt VE. 1993. Melky mamont, *Mammuthus primigenius vrangeliensis* (Garutt, Averianov et Vartanyan, 1993) s ostrova Vrangelya (Severo-Vostochnaya Sibir) [The small size mammoth, *Mammuthus primigenius vrangeliensis* (Garutt, Averianov et Vartanyan, 1993), from the Wrangel Island (Northeastern Siberia)]. In: Baryshnikov GF, editor. *Issledovaniya po pleistotsenovym i sovremennym mlekopitayushchim*. St. Petersburg: Zoologichesky Institut RAN. p 184–99.
- Garutt NV, Boeskorov GG. 2001. Sherstistye nosorogi: k istorii roda [Woolly rhinoceros: to the history of genus]. In: Rozanov AY, editor. *Mamont i ego okruzhenie: 200 let izucheniya*. Moscow: GEOS. p 157–67.
- Guthrie RD. 2003. Rapid body size decline in Alaskan Pleistocene horses before extinction. *Nature* 426(6963):169–71.
- Heintz AE. 1966. New radiocarbon (^{14}C) age determinations from the permafrost in Siberia. *Norsk Geologisk Tidsskrift* 46(2):215–7.
- Heintz AE, Garutt VE. 1964. Opredelenie absolutnogo vozrasta iskopaemykh ostatkov mamonta i sherstistogo nosoroga iz vechnoi merzloty Sibiri pri pomoshchi radioaktivnogo ugleroda ^{14}C [The age determination of the fossil remains of mammoth and woolly

- rhinoceros from the permafrost of Siberia with the help of radioactive carbon ^{14}C]. *Doklady Akademii Nauk SSSR* 154(6):1367–70.
- Heintz AE, Garutt VE. 1965. Determination of the fossil remains of mammoth and woolly rhinoceros from the permafrost in Siberia with the help of radiocarbon (^{14}C). *Norsk Geologisk Tidsskrift* 45(2):74–9.
- Kahlke R-D. 1998. *The History of the Origin, Distribution and Dispersal of the Late Pleistocene Mammuthus-coelodonta Faunal Complex in Eurasia (Large Mammals)*. Hot Springs, South Dakota: Fenske Company. 219 p.
- Kuzmin YV, Baryshnikov GF, Jull AJT, O'Malley JM, Orlova LA, van der Plicht J. 2001. Radiocarbon chronology of the Pleistocene fauna from Geographic Society Cave, Primorye (Russian Far East). *Current Research in the Pleistocene* 18:106–8.
- Kuzmin YV, Orlova LA. 1998. Radiocarbon chronology of the Siberian Paleolithic. *Journal of World Prehistory* 12(1):1–53.
- Kuzmin YV, Orlova LA, Zolnikov ID. 2003. The dynamics of mammoth (*Mammuthus primigenius* Blum.) population in Northern Asia: radiocarbon evidence. In: Reumer JWF, de Vos J, Mol D, editors. *Advances in Mammoth Research*. DEINSEA (Annual of the Natural History Museum Rotterdam) 9:221–37.
- Kuznetsova TV, Sulerzhitsky LD, Siegert C. 2001. New data on the “mammoth” fauna of the Laptev shelf land (East Siberian Arctic). In: Cavaretta G, Giola P, Mussi M, Palombo MR, editors. *The World of Elephants*. Rome: Consiglio Nazionale delle Ricerche. p 289–92.
- Latypova EK, Yakheemovich BL. 1993. Geochronology of the Pleistocene and Holocene in the Fore-Urals. *Radiocarbon* 35(3):441–8.
- Lõugas L, Ukkonen P, Jungner H. 2002. Dating the extinction of European mammoths: new evidence from Estonia. *Quaternary Science Reviews* 21(6):1347–54.
- MacPhee RDE, Tikhonov AN, Mol D, de Marliave C, van der Plicht J, Greenwood AD, Fleming C, Agenbroad L. 2002. Radiocarbon chronologies and extinction dynamics of the Late Quaternary mammalian megafauna of the Taymyr Peninsula, Russian Federation. *Journal of Archaeological Science* 29(10):1017–42.
- Markova AK, Smirnov NG, Kozharinov AV, Kazantseva NE, Simakova AN, Kitaev LM. 1995. Late Pleistocene distribution and diversity of mammals in Northern Eurasia (PALEOFAUNA Database). *Paleontologia i Evolucio* 28-29:5–143.
- Orlova LA, Kuzmin YV, Zolnikov ID. 2000. Time-space systematics for mammoth (*Mammuthus primigenius* Blum.) and prehistoric humans in Siberia (on the basis of radiocarbon dating). *Archaeology, Ethnology, and Anthropology of Eurasia* 1(3):31–41.
- Schirrrmeister L, Siegert C, Kuznetsova T, Kuzmina S, Andreev A, Kienast F, Meyer H, Bobrov A. 2002. Paleoenvironmental and paleoclimatic records from permafrost deposits in the arctic region of Northern Siberia. *Quaternary International* 89:97–118.
- Stuart AJ. 1991. Mammalian extinctions in the Late Pleistocene of Northern Eurasia and North America. *Biological Reviews of the Cambridge Philosophical Society* 66(4):453–562.
- Stuart AJ, Sulerzhitsky LD, Orlova LA, Kuzmin YV, Lister AM. 2002. The latest woolly mammoths (*Mammuthus primigenius* Blumenbach) in Europe and Asia: a review of the current evidence. *Quaternary Science Reviews* 21(7):1559–69.
- Sulerzhitsky LD. 1997. Cherty radiouglerodnoi khronologii mamontov Sibiri i severa Vostochnoi Evropy (kak substrata dlya rasseleniya cheloveka) [The features of radiocarbon chronology of mammoths in Siberia and northern Eastern Europe (as substratum for human dispersal)]. In: Velichko AA, Soffer O, editors. *Chelovek zaselyaet planetu Zemlya*. Moscow: Institut Geografii RAN. p 184–202.
- Sulerzhitsky LD, Romanenko FA. 1999. The “twilight” of the mammoth fauna in the Asiatic Arctic. *Ambio* 28(3):251–5.
- Vangengeim EA. 1977. *Paleontologicheskoe obosnovanie stratigrafii antropogena Severnoi Azii (po mlekopitayushchim)* [Paleontological justification of the Anthropogene stratigraphy of the Northern Asia (according to mammals)]. Moscow: Nauka Publishers. 172 p.
- Vartanyan SL, Arslanov KA, Tertychnaya TV, Chernov SV. 1995. Radiocarbon evidence for mammoths on Wrangel Island, Arctic Ocean until 2,000 BC. *Radiocarbon* 37(1):1–6.
- Vasil'chuk Y, Punning J-M, Vasil'chuk A. 1997. Radiocarbon ages of mammoths in Northern Eurasia: implications for population development and Late Quaternary environment. *Radiocarbon* 39(1):1–18.
- Vasil'chuk YK, Vasil'chuk AC, Long A, Jull AJT, Donahue DJ. 2000. AMS dating mammoth bones: comparison with conventional dating. *Radiocarbon* 42(2):281–4.
- Vasil'ev SA, Kuzmin YV, Orlova LA, Dementiev VN. 2002. Radiocarbon-based chronology of the Paleolithic in Siberia and its relevance to the peopling of the New World. *Radiocarbon* 44(2):503–30.
- Vereshchagin NK, Baryshnikov GF. 1984. Quaternary mammalian extinctions in Northern Eurasia. In: Martin PS, Klein, RG, editors. *Quaternary extinctions: a prehistoric revolution*. Tucson, Arizona: University of Arizona Press. p 483–516.

Table 1 ^{14}C dates for Late Glacial and Holocene (about 12,000–3700 BP) woolly mammoth in Siberia (after Sulerzhitsky 1997; Sulerzhitsky and Romanenko 1999; Vasil'chuk et al. 1997; MacPhee et al. 2002; Kuzmin et al. 2003) (*, **, *** = dates were run on the same sample).

Nr	Site name, location	Latitude, N	Longitude, E	^{14}C date, BP	Sigma ($\pm \sigma$)	Lab code and nr
1	Wrangel Island	71.00	179.00	3685	60	Ua-13366
2	Wrangel Island	71.00	179.00	3730	40	LU-2741
3	Wrangel Island	71.00	179.00	3920	30	GIN-6980
4	Wrangel Island	71.00	179.00	4010	50	LU-2798
5	Wrangel Island	71.00	179.00	4040	30	LU-2808
6	Wrangel Island	71.00	179.00	4370	70	GIN-8249
7	Wrangel Island	71.00	179.00	4400	40	LU-2756
8	Wrangel Island	71.00	179.00	4410	50	LU-2768
9	Wrangel Island	71.00	179.00	4740	40	LU-2556
10	Wrangel Island	71.00	179.00	4900	40	LU-2740
11	Wrangel Island	71.00	179.00	5110	40	LU-2794
12	Wrangel Island	71.00	179.00	5200	30	LU-2745
13	Wrangel Island	71.00	179.00	5250	40	LU-2744
14	Wrangel Island	71.00	179.00	5310	90	LU-2742
15	Wrangel Island	71.00	179.00	5480	50	LU-2535
16	Wrangel Island*	71.00	179.00	6260	50	LU-2799
17	Wrangel Island*	71.00	179.00	6360	60	AA-11529
18	Wrangel Island	71.00	179.00	6610	50	LU-2558
19	Wrangel Island**	71.00	179.00	6750	30	GIN-6990
20	Wrangel Island**	71.00	179.00	6760	50	LU-2736
21	Wrangel Island	71.00	179.00	6890	50	LU-2810
22	Wrangel Island	71.00	179.00	7040	60	LU-2746
23	Wrangel Island***	71.00	179.00	7250	60	LU-2809
24	Wrangel Island***	71.00	179.00	7295	95	AA-11530
25	Wrangel Island	71.00	179.00	7360	50	LU-2559
26	Wrangel Island	71.00	179.00	7710	40	GIN-6995
27	Nizhnaya Taymyra River	75.25	99.73	9670	60	GIN-1828
28	Pronchishev Coast	76.75	110.50	9780	40	GIN-8256
29	Nizhnaya Taymyra River	75.25	99.73	9860	50	GIN-1495
30	Bikada River	74.92	106.58	9920	60	GrA-17350
31	Yuribey River (Gydan Peninsula)	68.92	71.00	10,000	70	LU-1153
32	Nyengatiatari	74.83	106.17	10,070	60	GIN-10508
33	Engelgardt Lake	75.10	110.30	10,100	100	GIN-1489
34	Kupchiktakh Lake	73.58	101.13	10,200	40	GIN-11138a
35	Lugovskoe	61.05	68.57	10,210	135	SOAN-4752
36	Goltsovaya River	76.80	104.58	10,270	40	Beta-148640
37	Nyunkarakutari River	75.35	105.50	10,270	120	GIN-10507
38	Nizhnaya Taymyra River	75.25	99.73	10,300	100	GIN-1828k
39	Mutnaya Seyakha River	70.15	69.00	10,350	50	GIN-6386
40	Berelekh	70.55	149.05	10,370	70	SOAN-327
41	Sabettayakha River	71.15	71.33	10,420	130	AA-27378
42	Yuribei River (Yamal Peninsula)	68.92	69.70	10,460	120	AA-27378
43	Nganasanskaya River	74.40	99.41	10,680	70	GIN-3768

Table 1 ^{14}C dates for Late Glacial and Holocene (about 12,000–3700 BP) woolly mammoth in Siberia (after Sulerzhitsky 1997; Sulerzhitsky and Romanenko 1999; Vasil'chuk et al. 1997; MacPhee et al. 2002; Kuzmin et al. 2003) (*, **, *** = dates were run on the same sample). (*Continued*)

Nr	Site name, location	Latitude, N	Longitude, E	^{14}C date, BP	Sigma ($\pm \sigma$)	Lab code and nr
44	Krasnaya River	74.57	98.50	10,790	100	GIN-10552
45	Lugovskoe	61.05	68.57	10,820	170	SOAN-4943
46	Sosva River	59.16	62.08	11,080	160	SOAN-4842
47	Volchya Griva	54.50	80.20	11,090	120	SOAN-4921
48	Taymyr Lake	74.05	93.10	11,140	180	GIN-3067
49	Lugovskoe	61.05	68.57	11,310	380	SOAN-4755
50	Mamont River	75.15	96.00	11,450	250	T-297
51	Oktyabrskoi Revolutsii Island	78.82	97.67	11,500	60	LU-610
52	Lugovskoe	61.05	68.57	11,840	95	SOAN-4753
53	Arilakh Lake	74.42	107.58	11,940	40	Beta-148663
54	Konzhul	55.33	92.47	11,980	155	SOAN-4953
55	Berelekh	70.55	149.05	12,000	130	LU-149
56	Wrangel Island	71.00	179.00	12,010	110	LU-2823

Table 2 ^{14}C dates for woolly rhinoceros in Siberia (after Heintz and Garutt 1965; Latypova and Yakheemovich 1993; Kuzmin and Orlova 1998; Sulerzhitsky and Romanenko 1999; Garutt and Boeskorov 2001).

Nr	Site name, location	Latitude, N	Longitude, E	^{14}C date, BP	Sigma ($\pm \sigma$)	Lab code and nr
1	Lugovskoe	61.05	68.57	10,770	250	SOAN-4757
2	Zlatoustovka	52.97	55.32	12,330	120	BashGI-107
3	Yukagir Plateau	67.00	157.17	14,260	150	GIN-6007
4	Bolshoi Khomus-Yuriakh River	71.16	153.45	15,130	50	GIN-6023
5	Bolshoi Khomus-Yuriakh River	71.16	153.45	15,130	90	GIN-6024
6	Indigirka River	69.87	147.58	15,850	80	GIN-6020
7	Churapcha	62.00	132.50	19,500	120	GIN-9594
8	Zhuya River	58.15	115.51	19,610	670	SOAN-4732
9	Ikhine	63.17	133.75	20,080	150	SOAN-3185
10	Khroma River	70.70	143.00	20,400	200	GIN-6021
11	Kamchatka Peninsula	55.50	159.50	20,800	200	GIN-3400
12	Rel River	55.38	109.00	25,880	350	SOAN-829
13	Ikhine 2	63.17	133.75	26,030	200	IM-239
14	Kozlovka	56.35	90.77	26,620	240	SOAN-3158
15	Kolyma River	68.20	157.67	26,900	400	GIN-6005
16	Maly Anui River	68.00	162.17	27,300	300	GIN-6018
17	Maly Anui River	68.00	162.17	27,300	300	GIN-3209
18	Wrangel Island	71.00	179.00	29,800	340	GIN-8259a
19	Wrangel Island	71.00	179.00	>30,000	—	GIN
20	Lugovskoe	61.05	68.57	30,090	800	SOAN-4756
21	Bolshoi Khomus-Yuriakh River	71.16	153.45	>30,400	—	GIN-6023a

Table 2 ¹⁴C dates for woolly rhinoceros in Siberia (after Heintz and Garutt 1965; Latypova and Yakheemovich 1993; Kuzmin and Orlova 1998; Sulerzhitsky and Romanenko 1999; Garutt and Boeskorov 2001). (Continued)

Nr	Site name, location	Latitude, N	Longitude, E	¹⁴ C date, BP	Sigma (± σ)	Lab code and nr
22	Varvarina Gora	51.62	108.12	30,600	500	SOAN-850
23	Bolshoi Khomus- Yuriakh River	71.16	153.45	30,900	200	GIN-6022
24	Emige	70.40	133.00	31,500	300	GIN-6013
25	Ozernaya Balya	55.45	103.05	31,860	780	SOAN-4251
26	Achchagy-Allaikha	69.00	147.30	>32,000	—	GIN-6017
27	Khalbui River	67.50	132.67	>33,000	—	T-172
28	Irelyakh-Sien River	66.17	151.67	33,100	400	GIN-6010
29	Varvarina Gora	51.62	108.12	>34,050	—	AA-8875
30	Tolbaga	51.25	109.33	34,860	2100	SOAN-1522
31	Bolshaya Chukochya River	69.03	156.00	37,100	1100	GIN-6009
32	Elga River	64.58	141.50	>38,000	—	T-173
33	Dzhelon-Siene	67.27	155.87	39,900	500	GIN-6011
34	Yana River headwaters	66.02	132.75	40,000	500	GIN-6012
35	Bourdakh	67.02	154.30	41,600	800	GIN-6006
36	Khetechan	67.80	161.67	>42,300	—	GIN-6014
37	Baltagai	67.17	153.75	>42,300	—	GIN-6015
38	Tyung River	65.08	120.00	>43,000	—	GIN-5926
39	Bolshaya Chukochya River	69.03	156.00	43,700	1000	GIN-6008
40	Kamchatka Peninsula	55.83	159.67	46,700	1200	GIN-3424
41	Bolshoi Anui River	66.98	163.00	>49,000	—	GIN-6014

Table 3 ¹⁴C dates for bison in Siberia (after Kuzmin and Orlova 1998; Sulerzhitsky and Romanenko 1999; Schirmermeister et al. 2002; MacPhee et al. 2002).

Nr	Site name, location	Latitude, N	Longitude, E	¹⁴ C date, BP	Sigma (± σ)	Lab code and nr
1	Popigai River	72.83	107.42	8860	40	Beta-148623
2	Sushikha	54.37	81.70	9320	95	SOAN-4568
3	Krasnoyarsk	56.10	92.90	11,610	110	SOAN-1683
4	Keremensit River	70.50	149.50	12,800	60	GIN-4038
5	Listvenka, layer 10	55.95	92.40	13,200	110	SOAN-5083
6	Birusa, layer 3a	55.87	92.20	14,480	400	LE-3777
7	Malta, layers 9.1–9.2	52.83	103.55	14,720	190	GIN-8476
8	Kolyma River	68.30	157.70	14,800	250	GIN-3208a
9	Kozhevnikov Bay	73.50	110.00	16,390	120	GIN-5727
10	Shlenka	53.55	92.00	17,660	700	GIN-2862a
11	Ust-Mashinka 3	51.05	82.00	17,910	265	SOAN-4570
12	Ikhine	63.12	133.62	19,695	100	SOAN-3186
13	Tesa River	57.50	112.50	20,040	765	SOAN-4419
14	Malta, layer 8	52.83	103.53	21,600	170	GIN-8475
15	Kudelin	55.33	84.50	23,050	255	SOAN-3633

Table 3 ^{14}C dates for bison in Siberia (after Kuzmin and Orlova 1998; Sulerzhitsky and Romanenko 1999; Schirmermeister et al. 2002; MacPhee et al. 2002). (*Continued*)

Nr	Site name, location	Latitude, N	Longitude, E	^{14}C date, BP	Sigma ($\pm \sigma$)	Lab code and nr
16	Yuzhny	55.83	102.83	23,400	455	SOAN-3155
17	Western Chukotka	69.50	166.00	23,590	1560	GIN-8251
18	Tobol River	56.00	66.00	24,600	300	SOAN-3849
19	Balyshevo 3	57.48	107.77	25,100	940	LE-3950
20	Faddeevsky Island	75.70	144.20	26,100	300	GIN-4329
21	Vacha River	58.24	115.31	27,140	330	SOAN-4734
22	Logata River	73.20	98.15	27,600	400	GIN-3814
23	Mylakchyn	69.00	147.50	29,500	100	SOAN-1007
24	Ust-Karakol	51.38	84.68	28,700	850	SOAN-2614
25	Belkovsky Island	75.50	135.83	30,500	400	GIN-8222
26	Bykovsky Peninsula	71.28	129.42	>31,300	—	GIN
27	Logata River	73.30	98.20	31,800	500	GIN-3825
28	Agapa River	71.60	87.10	31,900	500	GIN-3241
29	Vacha River	58.24	115.31	32,170	250	SOAN-4733
30	Faddeevsky Island	75.60	144.05	32,200	600	GIN-8228
31	Logovo Gieny Cave	51.25	83.05	32,700	2800	SOAN-110
32	Bykovsky Peninsula	71.28	129.42	32,800	400	GIN
33	Bolshoi Kuduskit	58.33	115.50	>33,000	—	GIN-8877
34	Vacha River	58.50	115.00	>33,000	—	GIN-9069
35	Faddeevsky Island	75.65	144.05	33,100	320	GIN-8231
36	Logata River	73.50	98.00	33,750	1200	GIN-3824
37	Lopatka Peninsula	72.00	149.67	33,800	1200	GIN-8235
38	Duvanny Yar	68.45	150.45	34,700	400	GIN-8235
39	Maly Anui River	68.20	162.17	>35,300	—	GIN-7308
40	Varvarina Gora, layer 3	51.63	108.17	>35,300	—	AA-8993
41	Bederbo-Tarida	73.16	102.20	35,800	800	GIN-3100/1
42	Olenek River	70.55	122.10	36,800	500	GIN-6097
43	Kolyma River	68.00	156.00	37,100	500	GIN-3207
44	Kolyma River	68.50	156.00	38,400	800	GIN-5711
45	Western Chukotka	69.20	165.50	>39,000	—	GIN-8239
46	Bolshaya Balakhnya River	73.60	100.50	39,200	800	GIN-2764a
47	Bykovsky Peninsula	71.28	129.42	39,200	900	GIN
48	Sabler Cape (Lake Taymyr)	74.53	100.50	39,760	870	Beta-148624
49	Proskuryakov Grotto	54.45	89.47	40,595	875	SOAN-1518
50	Proskuryakov Grotto	54.45	89.47	40,690	1150	SOAN-1517
51	Proskuryakov Grotto	54.45	89.47	40,770	1075	SOAN-1519
52	Malta	52.83	103.53	41,100	1500	GIN-7707
53	Olenek River	70.55	122.10	41,300	800	GIN-6098
54	Olenek River	72.45	123.20	41,700	1500	GIN-6428
55	Kolyma River	68.75	156.20	42,800	700	GIN-5710
56	Kotelny Island	75.20	141.00	43,400	2200	GIN-8253
57	Birusa River	55.55	97.90	>45,000	—	SOAN-3157
58	Duvanny Yar	68.45	150.45	45,400	1200	GIN-3860
59	Talalakh Lake	73.07	106.83	45,320	1740	Beta-148625

Table 4 ¹⁴C dates for horse in Siberia (after Sulerzhitsky and Romanenko 1999; Kuznetsova et al. 2001; Schirrmeister et al. 2002; MacPhee et al. 2002).

Nr	Site name, location	Latitude, N	Longitude, E	¹⁴ C date, BP	Sigma (± σ)	Lab code and nr
1	Bolshaya Balakhnya River	73.65	100.48	2150	200	GIN-2744
2	Bolshoi Lyakhovsky Island	73.63	143.10	2200	50	GIN
3	Agapa River	71.62	87.00	3250	60	GIN-3243
4	Bykovsky Peninsula	71.28	129.42	4160	40	GIN
5	Nyunkarakutari River	75.30	105.75	9010	140	GIN-10509
6	Olenek River	72.50	122.00	11,660	450	GIN-6427
7	Logata River	73.10	98.00	14,100	160	GIN-3823a
8	Olenek River	70.50	122.00	14,560	250	GIN-6096
9	Omolon River mouth	68.67	158.50	15,300	60	GIN-5371
10	Bykovsky Peninsula	71.28	129.42	16,380	120	GIN
11	Bolshaya Balakhnya River	73.53	100.49	17,000	150	GIN-11133
12	Taymyr Lake	74.66	103.00	17,950	60	Beta-148659
13	Arilakh Lake	74.43	107.58	18,090	80	GrA-17351
14	Bolshaya Balakhnya River	73.55	100.45	18,300	200	GIN-3140b
15	Kotelny Island	75.00	141.00	19,100	120	GIN-8252
16	Duvanny Yar	68.45	150.45	19,480	100	GIN-3868
17	Sabler Cape (Taymyr Lake)	74.53	100.50	20,700	500	GIN-3241a
18	Bederbo-Tarida River	73.06	102.16	21,500	200	GIN-2744
19	Bykovsky Peninsula	71.28	129.42	23,850	700	GIN
20	Bolshaya Balakhnya River	73.54	100.50	23,900	400	GIN-11132
21	Olenek River	70.50	122.00	24,000	400	GIN-6426
22	Sabler Cape	74.53	100.50	24,690	110	Beta-148660
23	Engelgardt Lake	75.10	110.30	25,200	200	GIN-1817a
24	Sabler Cape	74.53	100.50	26,400	300	GIN-2142b
25	Shchuchya River	67.40	67.90	27,360	170	GIN-6448a
26	Bykovsky Peninsula	71.28	129.42	27,500	400	GIN
27	Sabler Cape	74.53	100.50	27,900	300	GIN-3841b
28	Anabar-Olenek watershed	72.00	117.00	28,180	270	GIN-8219
29	Kozhevnikov Bay	73.50	110.00	28,300	400	GIN-5732
30	Bykovsky Peninsula	71.28	129.42	28,400	300	GIN
31	Bykovsky Peninsula	71.28	129.42	29,000	450	GIN
32	Bykovsky Peninsula	71.28	129.42	29,000	900	GIN
33	Faddeevsky Island	75.50	144.00	29,100	400	GIN-4330
34	Sabler Cape	74.53	100.50	29,700	700	GIN-3141a
35	Pavel-Saiyngi-Yuriakh River	41.00	119.00	29,800	1200	GIN-5047
36	Kupchiktakh Lake	73.61	101.15	>30,000	—	GIN
37	Bykovsky Peninsula	71.28	129.42	31,100	400	GIN
38	Bykovsky Peninsula	71.28	129.42	>31,300	—	GIN
39	Sabler Cape	74.53	100.50	32,000	1000	GIN-3141c
40	Bykovsky Peninsula	71.28	129.42	32,000	1000	GIN
41	Bykovsky Peninsula	71.28	129.42	33,000	400	GIN
42	Bykovsky Peninsula	71.28	129.42	34,000	400	GIN
43	Bykovsky Peninsula	71.28	129.42	34,800	700	GIN
44	Bykovsky Peninsula	71.28	129.42	>34,600	—	GIN
45	Bykovsky Peninsula	71.28	129.42	35,800	500	GIN
46	Bykovsky Peninsula	71.28	129.42	>35,800	—	GIN
47	Anabar-Olenek watershed	72.30	117.50	36,300	640	GIN-8221

Table 4 ^{14}C dates for horse in Siberia (after Sulerzhitsky and Romanenko 1999; Kuznetsova et al. 2001; Schirrmeister et al. 2002; MacPhee et al. 2002). (*Continued*)

Nr	Site name, location	Latitude, N	Longitude, E	^{14}C date, BP	Sigma ($\pm \sigma$)	Lab code and nr
48	Bolshaya Balakhnya River	75.30	105.00	36,300	900	GIN-3119
49	Bykovsky Peninsula	71.28	129.42	35,900	600	GIN
50	Talalakh Lake	73.07	106.83	36,770	610	Beta-148622
51	Olenek River	72.40	123.00	38,100	800	GIN-6430
52	Kular Ridge	69.83	133.50	38,700	1000	GIN-4965
53	Anabar-Olenek watershed	73.50	116.00	39,600	500	GIN-3519
54	Western Yamal Peninsula	72.00	68.67	>40,000	—	GIN-8544
55	Logata River	73.20	98.15	40,200	1200	GIN-3823

Table 5 ^{14}C dates for muskox in Siberia (after Sulerzhitsky and Romanenko 1999; Kuznetsova et al. 2001; Schirrmeister et al. 2002; MacPhee et al. 2002).

Nr	Site name, location	Latitude, N	Longitude, E	^{14}C date, BP	Sigma ($\pm \sigma$)	Lab code and nr
1	Logata River	73.12	98.03	2700	70	GIN-3803
2	Pronchishchev Bay	75.73	112.83	2900	60	GIN-10529
3	Cheluskin Cape	77.72	104.25	2920	50	GIN-2945
4	Bykovsky Peninsula	71.28	129.42	3180	100	GIN
5	Bykovsky Peninsula	71.28	129.42	3200	80	GIN
6	Kotelny Island	75.50	139.00	10,750	90	LU-1666
7	Bolshaya Balakhnya River	74.00	100.40	12,150	40	GIN-3131
8	Wrangel Island	71.08	179.50	15,250	60	GIN-8248
9	Sabler Cape (Lake Taymyr)	74.53	100.50	15,800	50	Beta-148653
10	Agapa River	71.70	87.00	16,080	100	GIN-3239
11	Nizhniya Taymyra River	75.30	99.70	17,800	300	GIN-1815
12	Sabler Cape	74.53	100.50	17,800	160	GIN-3140c
13	South of Sabler Cape	74.50	100.40	18,370	70	Beta-148628
14	Sabler Cape	74.53	100.50	19,310	80	Beta-148627
15	Bolshaya Balakhnya River	75.30	105.00	19,710	70	Beta-148654
16	Taymyr Lake	74.42	100.17	20,770	180	GrA-17500
17	Yalutarida River	74.42	102.83	21,190	90	Beta-148629
18	Khatanga	71.97	102.42	21,330	70	Beta-148658
19	Popigai River ^a	72.83	107.42	21,500	100	Beta-148655
20	Popigai River ^a	72.83	107.42	22,530	220	GrA-17605
21	Taymyr Lake	74.42	100.17	22,370	80	Beta-156194
22	Taymyr Lake	74.42	100.17	22,610	100	Beta-148652
23	Nizhniya Taymyra River	75.45	99.50	24,660	110	Beta-148657
24	Bykovsky Peninsula	71.28	129.42	>27,000	—	GIN
25	Bolshaya Balakhnya River	73.60	100.50	27,440	150	Beta-148656
26	Bolshaya Balakhnya River	73.60	100.50	32,540	150	GrA-17349
27	Bikada River	74.80	106.50	36,700	700	UtC-10156
28	Bolshaya Balakhnya River	73.60	100.50	>39,000	—	GIN-11130
29	Sabler Cape	74.53	100.50	42,680	1240	Beta-148626

^aDates were run on same sample

THE END OF THE CHALCOLITHIC PERIOD IN THE SOUTH JORDAN VALLEY: NEW ¹⁴C DETERMINATIONS FROM TELEILAT GHASSUL, JORDAN

Stephen Bourke^{1,2} • Ugo Zoppi³ • John Meadows⁴ • Quan Hua³ • Samantha Gibbins¹

ABSTRACT. This article reports on 12 new accelerator mass spectrometry (AMS) dates from the latest phases of the Chalcolithic period occupation (late 5th millennium cal BC) at Teleilat Ghassul, type site for the south Levantine Ghassulian Chalcolithic culture. The new AMS dates from Teleilat Ghassul favor an amendment to a previous suggestion (Bourke et al. 2001), that all significant occupation at the site had ceased by 4000/3900 cal BC. This end-date should now be amended to 3900/3800 cal BC. Follow-up statistical modelling sourced to published ¹⁴C data drawn from a wide selection of south Levantine Chalcolithic period sites (Bourke 2001; Burton and Levy 2001) raises the possibility that Chalcolithic period occupation had ceased at virtually all major centers by 3800/3700 cal BC. This, in turn, suggests that the new data bearing on the end-date for occupation at Teleilat Ghassul may reflect a more widespread horizon of abandonment in the southern Levant.

INTRODUCTION

Traditionally, the transition from the Chalcolithic period to the Early Bronze Age (EBA) in the southern Levant has been placed around the middle of the 4th millennium BC (Weinstein 1984; Joffe and Dessel 1995). However, recent radiocarbon determinations from Chalcolithic period Teleilat Ghassul suggested an end-date for occupation at that site around the end of the 5th millennium cal BC (Bourke et al. 2001:1221). The new dates from Ghassul were consistent with unexpectedly early 4th millennium cal BC dates for the earliest phases of the EBA at Afridar (Braun 2000; Braun 2001:1290), Tell Shuna North (Bronk Ramsey et al. 2002:82–84), and Chalcolithic Aqaba (Görsdorf 2002).

These new dates suggested a transition between the Chalcolithic and the EBA between 300 and 500 yr earlier than traditionally assumed, sharply truncating the length of the Chalcolithic period and (more problematically) greatly increasing the length of the already relatively sparsely occupied EBA I period (Braun 2001:1282). Were this new scenario to have wide application in south Levantine archaeology, whole periods (such as Joffe and Dessel's "Terminal Chalcolithic") would have to be subsumed into earlier Chalcolithic horizons (Burton and Levy 2001:1223–1224) and the early phases of the succeeding Early Bronze Age (e.g. EBA IA–B) greatly lengthened and significantly reworked (Braun 2001).

It was, therefore, a matter of some importance to examine in more detail the suggestion that the final horizon of occupation at Teleilat Ghassul did indeed come to an end around 4000/3900 cal BC. To further investigate this issue, another 12 short-life botanical samples, drawn from relevant contexts, were processed at the ANSTO Accelerator Mass Spectrometry (AMS) Centre in 2001/2002. Most samples derive from the latest Chalcolithic strata in 4 widely separated areas of the site, allowing us to determine for the first time a reliable end-date for occupation across the entire 20 hectare ruinfield.

¹Department of Archaeology, University of Sydney, Sydney, Australia.

²Corresponding author. Email: stephen.bourke@arts.usyd.edu.au.

³ANSTO, PMB1, Menai, New South Wales 2234, Australia.

⁴Institute of Archaeology, University College London, London, United Kingdom.

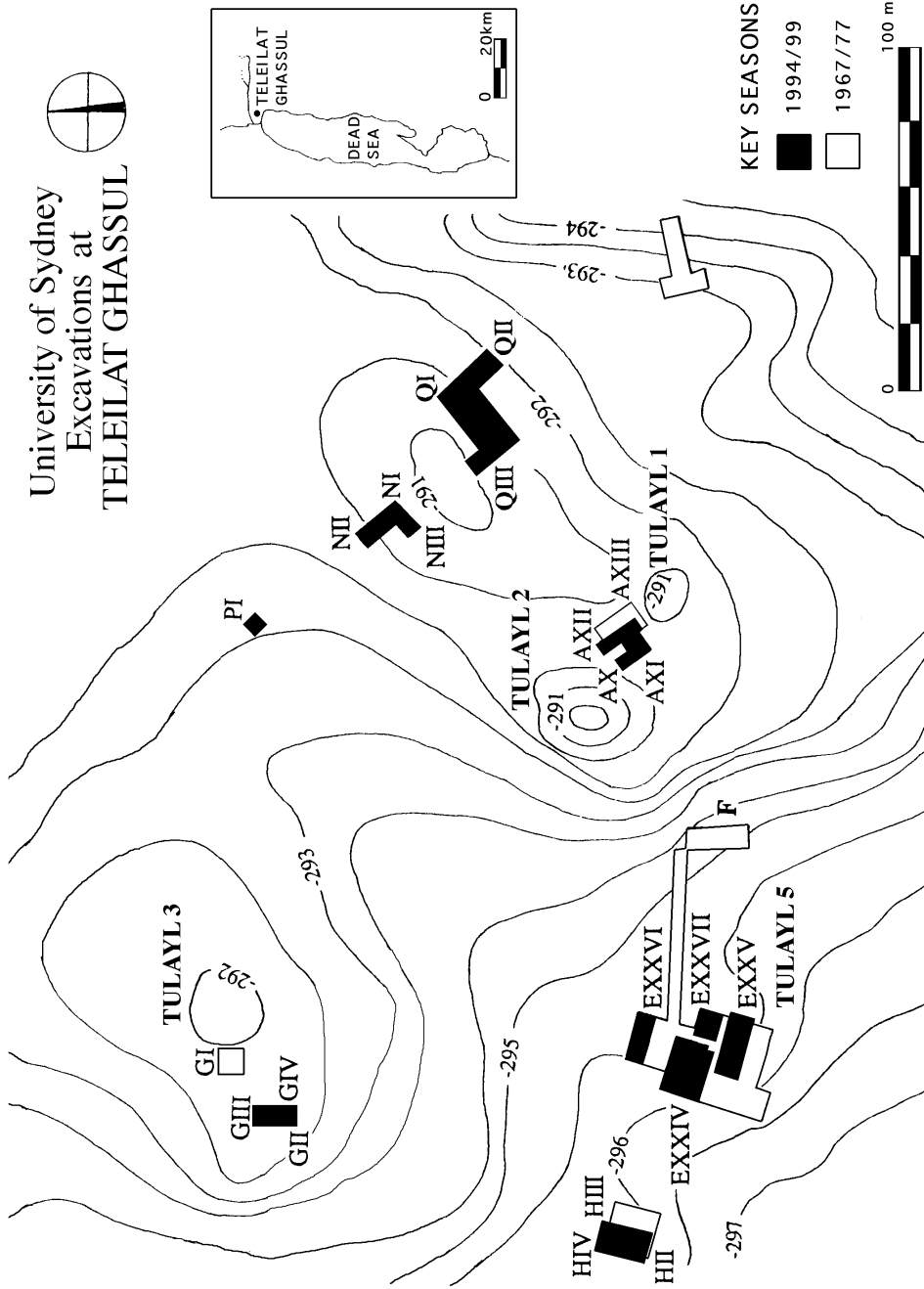


Figure 1 Plan of the University of Sydney excavation areas at Teleilat Ghassul

PREVIOUS LATE CHALCOLITHIC PERIOD ¹⁴C DATES FROM TELEILAT GHASSUL

Before the current assays, 7 ¹⁴C dates were known from the latest archaeological horizons at Teleilat Ghassul (Table 1). One derives directly from J Basil Hennessy's University of Sydney excavations in the 1970s (Hennessy 1982); three were taken from standing sections in the 1980s (Neef 1990); and three come from most recent work at the site (Bourke et al. 2001). While the Hennessy (SUA) and Bourke (OZD) assays come with reliable context details, the Groningen (GrN) materials (of necessity) have less specific context details, although they very probably derive from Hennessy Phase A horizons.

Table 1 Previous work: latest Chalcolithic ¹⁴C dates from Teleilat Ghassul.

Ref	Lab	Date BP	2 σ cal BC	Material	Context phase/area	
1	Hennessy 1982	SUA-511	5655 ± 120	4765–4250	Wood	Phase A/E
2	Bourke 2001	OZD030	5550 ± 165	4725–4040	Grain	Phase A/Q
3	Bourke 2001	OZD033	5455 ± 60	4399–4219	Grain	Phase A/G
4	Bourke 2001	OZD034	5340 ± 70	4262–4035	Grain	Phase A/G
5	Neef 1990	GrN-15194	5330 ± 25	4254–4040	Wood	Phase A/A
6	Neef 1990	GrN-15195	5270 ± 100	4334–3937	Wood	Phase A/E
7	Neef 1990	GrN-15196	5110 ± 90	4051–3697	Dung	Phase A/A

The first of these dates (SUA-511) is a pooled mean from 3 separate assays (SUA 511a–c), all taken from 1 large wooden beam (Bourke et al. 2001:1218). The beam formed part of the collapsed roof of Sanctuary A, the larger building in the Area E sanctuary complex (Hennessy 1982:56; Bourke 2001:130–133). The destruction horizon was interpreted by Hennessy as marking the end of substantial occupation in Area E (Hennessy 1989: 234–235). The next 3 dates (OZD030 and OZD033–034) derive from Late Chalcolithic horizons in northern Area G and eastern Area Q, although the large standard deviation in OZD030 (due to small sample size) renders it of little use to our deliberations.

The final 3 dates (GrN-15194 to 15196) were taken from Hennessy's standing sections in Areas A and E by Reindeer Neef a decade after excavations had ceased. However, Neef provided Hennessy with clear photographs of the areas from which his samples were taken (Neef 1988), which theoretically allow a reasonably reliable context to be allocated to each of the samples. GrN-15194, identified as olive wood by Neef, was taken from baulk material equivalent to excavated Phase A deposits in Hennessy trench A II (Hennessy 1969:3–4). GrN-15196, composed of threshing and dung material according to Neef, comes from a closely related context. Neef accounted for the variance in date between GrN-15194 and GrN-15196 as due to the different materials sampled. GrN-15195, identified as olive wood by Neef, comes from the southern end of Hennessy trench E XXIII (Hennessy, personal communication) and is probably best associated with late occupational horizons in the area.

The 7 ¹⁴C determinations previously assayed derive from latest occupational horizons in 3 widely separated areas of the site (Areas A, E, and G). While some doubt must still adhere to Neef's GrN contexts, they are likely to sample latest Chalcolithic (Phase A) occupational horizons. However, they do not sample Hennessy's hypothetical Phase A+ horizons as Blackham (2002:80–81) has recently suggested, since these horizons were not present in either Areas A or E (Hennessy, personal communication).

TECHNICAL DATA: PREPARATION AND PROCESSING

All samples presented in this study were ¹⁴C dated at the AMS facility at ANSTO (Fink et al., forthcoming). To remove contamination, the standard AAA method (Mook and Streurman 1983) was

employed. Pretreated samples were then converted to CO₂ by combustion at 900 °C for 5 hr in a sealed tube in the presence of precleaned CuO and Ag wires. Graphite targets were prepared by reducing CO₂, using zinc (400 °C) and iron (600 °C) catalysts in the presence of a small amount of hydrogen. Finally, the graphite was loaded into an aluminium sample holder ready for the AMS measurement. The technical details of these methods are described in Hua et al. (2001).

The ¹⁴C/¹³C isotopic ratio was measured relative to the internationally accepted HOxI standard material (Stuiver 1983). Corrections were then applied for the spectrometer background, for the contamination incorporated during the preparation of the graphite target, and for the isotopic fractionation. Using the corrected radioisotopic ratio, the conventional ¹⁴C age was calculated and finally calibrated using the CALIB software (Stuiver and Reimer 1993) and the tree-ring dataset of Stuiver et al. (1998).

Table 2 Twelve new AMS dates from Late Chalcolithic Teleilat Ghassul.

ANSTO code	Material	Graphite mass (mg C)	δ ¹³ C (PDB)	¹⁴ C age [BP]	2 σ calibrated age [BC]	Relative probability
OZF418	Cereal grain	2.25	-24.5	5750 ± 40	4698–4496 cal BC	98.5%
OZF419	Cereal grain	0.66	-21.9	5490 ± 40	4369–4248 cal BC	88.2%
OZF420	Cereal grain	2.29	-23.2	5395 ± 40	4337–4219 cal BC	71.5%
OZF421	Cereal grain	2.02	-25.0	5870 ± 40	4808–4667 cal BC	91.8%
OZF422	Cereal grain	2.04	-22.2	5505 ± 40	4403–4320 cal BC	64.2%
					4293–4252 cal BC	20.2%
					4450–4416 cal BC	15.6%
OZF423	Cereal grain	2.37	-24.2	5370 ± 40	4202–4048 cal BC	53.7%
					4329–4216 cal BC	46.3%
OZG248	Olive stone	1.09	-26.2	5510 ± 40	4405–4321 cal BC	66.9%
					4450–4415 cal BC	17.7%
					4290–4253 cal BC	15.3%
OZG249	Olive stone	1.33	-26.4	5475 ± 40	4369–4237 cal BC	91.9%
OZG250	Olive stone	1.58	-23.9	5445 ± 40	4355–4227 cal BC	98.4%
OZG251	Olive stone	1.46	-23.3	5110 ± 45	3982–3792 cal BC	100.0%
OZG252	Olive stone	1.98	-23.5	5335 ± 60	4260–4037 cal BC	85.4%

THE NEW DETERMINATIONS AND THE SEQUENCE AT GHASSUL

Each of the 12 new samples consisted of short-lived plant remains, either carbonized cereal grains or olive stones (Table 2). The olive stones are “single entity samples” (Ashmore 1999), but the cereal grain samples consisted of between 3 and 5 individual grains. Samples are drawn from discrete concentrations of ashy material wherever possible and brick debris layers are generally avoided. This strategy aims at reducing the likelihood of sampling residual materials. Ongoing archaeobotanical work at Ghassul (Bourke et al. 2000:79–84; Meadows, forthcoming) demonstrates the persistence of spatial and temporal patterns in the incidence of plant remains, even in secondary contexts. This suggests that even if some of the dated grains were residual, they were probably derived from nearby contexts and are very nearly contemporaneous with the contexts in which they were found. The coherence of the sequence of ¹⁴C results from Area G (see below) reinforces our belief that few, if any, of the dated grains were significantly older or younger than their contexts.

The 12 new determinations include 6 samples from the latest archaeological horizon (Phase A) across the site. They are drawn from 4 widely separated areas (two each from Areas E and Q, and one each from Areas H and N). Three samples come from slightly earlier (Phase B–C) horizons (two

from Area E and 1 from Area G). The final 3 samples derive from significantly earlier horizons (one each from Areas A, H, and N).

All six of the latest (Phase A) ¹⁴C results are broadly comparable, and reinforce earlier suggestions that significant occupation across the site came to an end by 4000/3900 cal BC. One of the 2 samples (OZG251) from the easternmost area of excavations (Area Q) might suggest a slight modification to this view. The sample (OZG251) comes from a pit (F.18) cut into the latest (Phase A) occupational horizon, making it one of the very latest deposits in Area Q. While it is possible that OZG251 could simply be an outlier in an otherwise relatively homogenous Phase A grouping, it is probably best to regard it (along with sample OZF423, which derives from the earliest Phase A living/work surface in Area Q) as delimiting the maximum span of the Phase A occupational horizon in Area Q. Given the similar reading from Neef's (less reliably contexted) sample of short-lived material (GrN-15196) from Area A, it suggests that the final end-date for occupation at the site should be amended from its previously suggested 4000/3900 cal BC to a slightly later 3900/3800 cal BC date.

The 3 earlier (Phase B–C) assays are stratigraphically coherent in relation to Phase A determinations. That being said, given the broadly similar stratigraphy and material assemblages of OZF418 and OZG249, the quite early date of the former comes as something of a surprise. This suggests that although carefully selected short-life material was employed, it may nonetheless have been residual in the Phase B courtyard assemblage (Bourke et al. 2000:47). The Phase B–C determination from Area G (OZG250) is stratigraphically and radiometrically earlier than 1 later assay (OZD034) and stratigraphically and radiometrically later than 3 earlier (OZD031–033) determinations (Bourke et al. 2001:1220). This would suggest that the Area G radiometric sequence is internally coherent and provides for the first time a reliable chronology for the full occupational history of Tulayl 3, extensively excavated by Pontifical Biblical Institute (PBI) archaeologists in the 1930s (Lee 1973:168–176).

The 3 earlier phased determinations from Areas A, H, and N are broadly in line with stratigraphic positioning, although the earliest date provokes some comment when detailed material cultural affiliations are examined. In Area H, OZF421 records a surprisingly early date for basal levels in this westernmost area of excavations, given the previous cultural attribution to Early Chalcolithic (Phase F–G) horizons (Bourke et al. 2000:56). It may well be that the small cultural assemblage from the base of the H II sondage has been mis-attributed, if the assemblage is Late Neolithic (Hennessy H–I) as the ¹⁴C determination would suggest. If so, it would seem that Late Neolithic occupation was far more extensive across the site than previously assumed (Bourke 1997:405). Alternatively, if the material assemblage is Early Chalcolithic as previously stated, then OZF421 may have sampled material residual from the mixed wash deposits that lay at the base of the sondage (Bourke et al. 2000:55–56).

The close agreement between current Phase D determinations (OZF422 and OZG248) and previously reported assays OZD028–029 (Bourke et al. 2001:1220) would suggest that Areas A and N have relatively similar stratigraphic histories and that the radiometric date (about 4400 cal BC) for the earliest phase (Phase D) of the Late Chalcolithic period in both areas is secure.

BAYESIAN MODELLING AND GHASSULIAN CHRONOLOGY

Calibration of the individual ¹⁴C results suggests that Phase A dates to at most a century or two either side of 4000 cal BC and that Ghassul was abandoned by 3800 cal BC, if not earlier. The use of Bayesian techniques of chronological modelling (Buck et al. 1996) provides a means of visualizing the calendar ages of the ¹⁴C samples and of estimating the date of events that cannot be dated

Table 3 Archaeological contexts and phasing.

Site context	ANSTO code	BP age	Calibrated age	Site phasing
EXXV 2.13	OZF417	5450 ± 40	4332–4257 BC	Hennessy Phase A
EXXV 4.9	OZF418	5750 ± 40	4666–4544 BC	Hennessy Phase B–C
EXXIV 12.12	OZF419	5490 ± 40	4360–4268 BC	Hennessy Phase A
HIII 2.10	OZF420	5400 ± 40	4309–4158 BC	Hennessy Phase A
HII 3.31	OZF421	5870 ± 40	4780–4698 BC	Hennessy Phase F–G
NI 15.11	OZF422	5500 ± 40	4420–4279 BC	Hennessy Phase D
QI 17.18	OZF423	5370 ± 40	4296–4094 BC	Hennessy Phase A
AXIII 1.5	OZG248	5520 ± 40	4429–4336 BC	Hennessy Phase D
EXXVII 2.40	OZG249	5490 ± 50	4378–4268 BC	Hennessy Phase B–C
GIV 30.43	OZG250	5440 ± 40	4327–4247 BC	Hennessy Phase B–C
QIII 7.3	OZG251	5100 ± 50	3946–3818 BC	Hennessy Phase A
NIII 3.1	OZG252	5320 ± 60	4233–4059 BC	Hennessy Phase A

directly by the ^{14}C method. It must be emphasized that such estimates depend heavily on the known or assumed relative ages of the ^{14}C samples and will change under different sets of assumptions.

The simplest model is the bounded phase, which is based on the assumption that the dated samples are drawn evenly from a continuous phase of activity (Bronk Ramsey 2000). Probability distributions for the dates of the beginning and end of this phase can be calculated using the program OxCal (Bronk Ramsey 1995, 1998). If the results of all short-lived samples are placed in a bounded phase (i.e. excluding SUA-511 and GrN-15194), the end-date falls in the range 4040–3690 cal BC (95% probability). There is a 49% probability that the end-date falls before 3900 cal BC, a 73% probability that it falls before 3850 cal BC, and an 88% probability that it falls before 3800 cal BC.

A more sophisticated version of the model assumes not only that the samples are representative of a continuous phase of activity, but that samples in earlier strata are actually older than samples in later strata. One result, OZF-418, is clearly inconsistent with this proposition¹ and evidently represents residual material from an earlier stratum. This is not surprising given the relatively low incidence of plant remains in Area E (Meadows, forthcoming). However, if this result is regarded as a *terminus post quem* for phases B–C, the model shows that the remaining results can accurately date their contexts (Figure 2).

Under this model, the end-date is estimated to fall in the range 4040–3710 cal BC (95% probability). There is a 46% probability that the Chalcolithic at Ghassul ends before 3900 cal BC, a 69% probability that it ends before 3850 cal BC, and an 86% probability that it ends before 3800 cal BC. The probability that the Chalcolithic ends before 3950 cal BC, however, is only 14%. Therefore, our current estimate for the date of abandonment is between 3950 and 3800 cal BC. Although this is slightly later than the 4000–3900 cal BC previously proposed (Bourke et al. 2001:1221), it remains significantly earlier than the traditional date (approximately 3500 cal BC) of the Chalcolithic–EBA transition (Joffe and Dessel 1995:514). New ^{14}C data from Tell Shuna North (Bronk Ramsey et al. 2002:82–84) are broadly consistent with the Ghassul results.

The model structure, which is defined by the OxCal keywords and brackets at the left of Figure 2, assumes that the Phase H–I samples are older than Phase E–G samples, which in turn, are older than

¹ This is indicated by an unsatisfactory overall index of agreement ($A = 34.7\%$), well below the threshold level of 60%, and a negligible individual index of agreement (0.6%) for the result OZF-418.

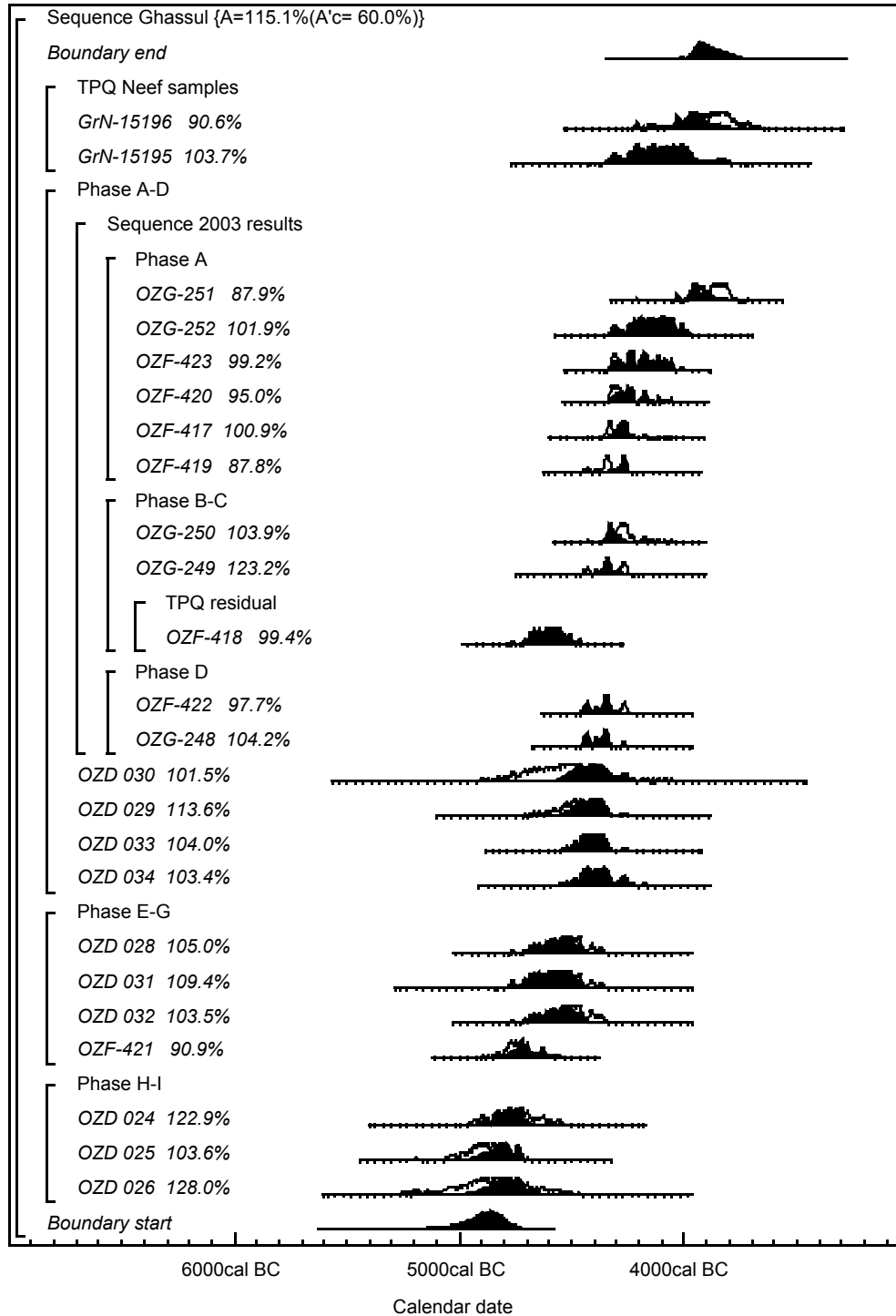


Figure 2 Modeled ¹⁴C results for short-lived samples from Teleilat Ghassul

all Phase A–D samples. OZD-029, OZD-030, OZD-033, and OZD-034 are not assigned to a sub-phase within the Phase A–D group, but the 2002 results are placed in a sequence which assumes that the Phase A samples are more recent than the Phase B–C samples, which in turn, are more recent than the Phase D samples. Three results are treated as *termini post quem*: OZF-418, which the model assumes is older than the Phase A samples, and GrN-15195 and GrN-15196, which are assumed to pre-date the abandonment of the site. The distributions in outline show the calibration of the ^{14}C results by the probability method (Stuiver and Reimer 1993). The solid distributions are “posterior density estimates” of the actual age of each sample given its calibrated ^{14}C result and its age relative to the other dated samples. The distributions *Boundary start* and *Boundary end* are the estimated dates of the beginning and end of occupation at Ghassul given the ^{14}C results and the structure of the model.

DISCUSSION

The new dates from Teleilat Ghassul suggest that occupation at that site ended by 3800 cal BC at the latest, fully 300 yr earlier than the generally accepted end-point for the south Levantine Chalcolithic as a whole (Stager 1992; Joffe and Dessel 1995). Recent radiometric data bearing on the earliest phase of the succeeding Early Bronze Age at Afridar (Braun 2000, 2001) and Tell Shuna North (Bronk Ramsey et al. 2002:82–84) is nonetheless consistent with such a revision. While Braun’s observations on the very real archaeological difficulties involved in the acceptance of such a revision are valid (Braun 2001:1281–1283), studies of the succeeding EB II–III period at Jericho (Bruins and van der Plicht 2001:1327) also report a 300-yr discrepancy between traditional and recent radiometric chronologies. Commentary on recent EB IV period dates from Tell Abu en-Niaj in the Jordan Valley (Bronk Ramsey et al. 2002:82) report a similar 300-yr difference between radiometric and traditional chronologies. Taken together, the recent radiometric data from Late Chalcolithic Ghassul, EB I Afridar and Tell Shuna North, EB II–III Jericho and EB IV Tell Abu en-Niaj are all consistent in suggesting the need for a significant upwards revision in the chronology of the Chalcolithic/EB I transitional period in the southern Levant.

CONCLUSION

The 12 new dates from Teleilat Ghassul have provided much needed data relating to the origins, site history, and eventual demise of the largest site occupied during the south Levantine Chalcolithic. A consideration of the latest dates suggests occupation ended around 3900/3800 cal BC. This is consistent with new assays bearing on the inception date and internal periodization of the succeeding Early Bronze Age.

ACKNOWLEDGEMENTS

The 12 new AMS dates were processed under AINSE Grants 01/196 and 02/199. The authors would like to thank AINSE for these grants and all members of the AMS dating facility at ANSTO (Lucas Heights, Sydney) for their assistance in the preparation of the new dates. As well, we thank Emeritus Professor J Basil Hennessy (Department of Archaeology, University of Sydney) for much fruitful discussion on the early Sydney University excavations at Teleilat Ghassul.

REFERENCES

- Ashmore P. 1999. Radiocarbon dating: avoiding errors by avoiding mixed samples. *Antiquity* 73:124–30.
- Blackham M. 2002. *Modeling Time and Transition in Prehistory: The Jordan Valley Chalcolithic (5500–3500 BC)*. Oxford: British Archaeological Reports.
- Bourke S. 1997. The ‘pre-Ghassulian’ sequence at Teleilat Ghassul. In: Gebel H-G, Kafafi Z, Rollefson G, editors. *The Prehistory of Jordan II: Perspectives from 1997*. Berlin: Ex Oriente. p 395–417.
- Bourke S. 2001. The Chalcolithic period. In: MacDonald B, Adams R, Bienkowski P, editors. *The Archaeology of Jordan*. Sheffield: Sheffield Academic Press. p 107–62.
- Bourke S, Lovell J, Sparks R, Seaton P, Mairs L, Meadows J. 2000. Preliminary report on a second and third season of renewed excavations at Teleilat Ghassul by the University of Sydney, 1995/1997. *Annual of the Department of Antiquities Jordan* 44:37–89.
- Bourke S, Lawson E, Lovell J, Hua Q, Zoppi U, Barbetti M. 2001. The chronology of the Ghassulian Chalcolithic period in the southern Levant: new ¹⁴C determinations from Teleilat Ghassul, Jordan. *Radiocarbon* 43(3):1217–22.
- Braun E. 2000. Area G at Afridar, Palmahim Quarry 3 and the earliest pottery of Early Bronze Age I: part of the “missing link.” In: Philip G, Baird D, editors. *Ceramics and Change in the Early Bronze Age of the Southern Levant*. Sheffield: Sheffield Academic Press. p 113–28.
- Braun E. 2001. Proto, Early Dynastic Egypt and Early Bronze I–II of the southern Levant: some uneasy ¹⁴C correlations. *Radiocarbon* 43(3):1279–96.
- Bronk Ramsey C. 1995. Radiocarbon calibration and analysis of stratigraphy: the OxCal program. *Radiocarbon* 37(2):425–30.
- Bronk Ramsey C. 1998. Probability and dating. *Radiocarbon* 40:461–74.
- Bronk Ramsey C. 2000. Comment on ‘The use of Bayesian statistics for ¹⁴C dates of chronologically ordered samples: a critical analysis.’ *Radiocarbon* 42(2):199–202.
- Bronk Ramsey C, Higham T, Owen D, Pike A, Hedges R. 2002. Radiocarbon dates from the Oxford AMS system: datelist 31. *Archaeometry* 44(3):1–149.
- Bruins H, van der Plicht J. 2001. Radiocarbon challenges archaeo-historical time frameworks in the Near East: the Early Bronze Age of Jericho in relation to Egypt. *Radiocarbon* 43(3):1321–32.
- Buck C, Cavanagh W, Litton C. 1996. *Bayesian Approach to Interpreting Archaeological Data*. Chichester: Wiley.
- Burton M, Levy T. 2001. The Chalcolithic radiocarbon record and its use in southern Levantine archaeology. *Radiocarbon* 43(3):1223–46.
- Fink D, Hotchkis M, Hua Q, Jacobsen G, Smith A, Zoppi U, Child D, Mifsud C, van der Gaast H, Williams A, Williams M. Forthcoming. The ANTARES AMS facility at ANSTO. *Nuclear Instruments and Methods in Physics Research B*.
- Görsdorf J. 2002. New ¹⁴C datings of prehistoric settlements in the south of Jordan. *Orient Archäologie* 5: 333–9.
- Görsdorf J, Dreyer G, Hartung U. 1998. New ¹⁴C dating of the archaic Royal Necropolis Umm al-Qaab at Abydos. *Radiocarbon* 40(2):641–7.
- Hennessy J. 1969. Preliminary report on a first season of excavations at Teleilat Ghassul. *Levant* 1:1–24.
- Hennessy J. 1982. Teleilat Ghassul and its place in the archaeology of Jordan. *Studies in the History and Archaeology of Jordan* 1:55–8.
- Hennessy J. 1989. Ghassul, Teleilat. In: Homes-Fredericq D, Hennessy J, editors. *Archaeology of Jordan. Vol. II.1 Field Reports. Surveys and Sites A-K*. Leuven: Peeters. p 230–41.
- Hua Q, Jacobsen G, Zoppi U, Lawson E, Williams A, Smith A, McGann M. 2001. Progress in radiocarbon target preparation at the ANTARES AMS Centre. *Radiocarbon* 43(2A):275–82.
- Joffe A, Dessel J-P. 1995. Redefining chronology and terminology for the Chalcolithic of the southern Levant. *Current Anthropology* 36:507–18.
- Lee J. 1973. *Chalcolithic Ghassul: New Aspects and Master Typology*. [Unpublished PhD dissertation]. Jerusalem: Hebrew University Jerusalem.
- Lovell J. 2001. *The Late Neolithic and Chalcolithic Periods in the Southern Levant*. Oxford: British Archaeological Reports.
- Meadows J. Forthcoming. *Early Farmers and Their Environment: Archaeobotanical Studies of Neolithic and Chalcolithic Sites in Jordan*. [PhD dissertation]. Melbourne: La Trobe University.
- Neef R. 1988. Letter to J.B Hennessy, 28/4/88. *Teleilat Ghassul Archive*. Sydney: University of Sydney.
- Neef R. 1990. Introduction, development and environmental implications of olive culture. In: Bottema S, Enjes-Nieborg G, Van Zeist W, editors. *Man’s Role in the Shaping of the Eastern Mediterranean Landscape*. Rotterdam. p 295–306.
- Stager L. 1992. The Periodisation of Palestine from the Neolithic through Early Bronze times. In: Ehrlich R, editor. *Chronologies in Old World Archaeology*. 3rd edition. Chicago: University of Chicago Press. p 22–60.
- Stuiver M. 1983. Business meeting: international agreements and the use of the new oxalic acid standard. *Radiocarbon* 25(2):793–5.
- Stuiver M, Reimer P. 1993. Extended ¹⁴C database and revised CALIB 3.0 radiocarbon calibration program. *Radiocarbon* 35(1):215–30.
- Stuiver M, Reimer P, Bard E, Beck J, Burr G, Hughen K, Kromer B, McCormac G, van der Plicht J, Spurk M. 1998. INTCAL98 radiocarbon age calibration, 24,000–0 cal BP. *Radiocarbon* 40(3):1041–83
- Weinstein J. 1984. Radiocarbon dating in the southern Levant. *Radiocarbon* 26(2):297–366.

DATING THE VOLCANIC ERUPTION AT THERA

Christopher Bronk Ramsey^{1,2} • Sturt W Manning³ • Mariagrazia Galimberti¹

ABSTRACT. The eruption of the volcano at Thera (Santorini) in the Aegean Sea undoubtedly had a profound influence on the civilizations of the surrounding region. The date of the eruption has been a subject of much controversy because it must be linked into the established and intricate archaeological phasings of both the prehistoric Aegean and the wider east Mediterranean. Radiocarbon dating of material from the volcanic destruction layer itself can provide some evidence for the date of the eruption, but because of the shape of the calibration curve for the relevant period, the value of such dates relies on there being no biases in the data sets. However, by dating the material from phases earlier and later than the eruption, some of the problems of the calibration data set can be circumvented and the chronology for the region can be resolved with more certainty.

In this paper, we draw together the evidence we have accumulated so far, including new data on the destruction layer itself and for the preceding cultural horizon at Thera, and from associated layers at Miletos in western Turkey. Using Bayesian models to synthesize the data and to identify outliers, we conclude from the most reliable ¹⁴C evidence (and using the INTCAL98 calibration data set) that the eruption of Thera occurred between 1663 and 1599 BC.

INTRODUCTION

The question of the date of the eruption of Thera (or Santorini) is of great importance because it defines the relationship between different cultural developments in the east Mediterranean in the middle of the 2nd millennium BC (Manning 1999). Dating of the eruption has been determined by “traditional” archaeological techniques through the study of trade links, particularly to Egypt (see Bietak 2003 for a summary of this evidence; previously, Warren and Hankey 1989), linking it into the Egyptian historical chronology, which is thought to be secure for this time period because of the extensive documentary evidence (e.g. Kitchen 2000).

Radiocarbon dating since the mid-1970s has suggested a date for the eruption some 100–150 yr earlier than the traditional archaeological (“conventional”) chronology (e.g. Michael 1976; Betancourt 1987; Manning 1988; Friedrich et al. 1990; Housley et al. 1990; Manning and Bronk Ramsey 2003). In the 1980s, it was suggested that tree-ring and ice-core evidence also suggested similarly “early” dates in the mid- to later-17th century BC (LaMarche and Hirschboeck 1984; Hammer et al. 1987; Baillie and Munro 1988).

But recent work has seriously questioned the case from ice-core evidence for a Thera eruption about 1645 BC (argued for by Hammer et al. 2003); there was a major volcanic eruption, just not it seems of Thera, given critical review of the currently available geochemical characterization data (Pearce et al. 2004a,b; Keenan 2003). Similarly, the case for a dendrochronologically-derived date has only ever been based on a hypothetical and suggestive proxy linkage. There is as yet no positive evidence for a causal association.

Thus, attention turns ever more centrally and critically to the ¹⁴C evidence since at present this alone offers direct and independent science-based dating evidence for the great and archaeologically pivotal Thera eruption in the mid-2nd millennium BC. In this paper, we report on further ¹⁴C measurements which we have recently made on material from Thera and from a related Aegean site. These add important new elements to the ¹⁴C picture.

¹Oxford Radiocarbon Accelerator Unit, University of Oxford, United Kingdom.

²Corresponding author. Email: christopher.ramsey@archaeology-research.oxford.ac.uk.

³Department of Fine Art, University of Toronto, Canada/Department of Archaeology, University of Reading, United Kingdom.

STRATEGY

One of the main problems with the dating of material from the eruption at Thera is the form of the calibration curve in the period from about 1675 cal BC to 1525 cal BC. In this period, there is an approximate plateau in the curve, which means that the ^{14}C dates do not differ by more than about 50 yr (see Figure 1). Thus, with the usual levels of precision obtainable, it is difficult to distinguish between the 2 main contending dates for the eruption: a mid- to later-17th century BC date (proposed variously from ^{14}C , ice-core, and tree-ring evidence: LaMarche and Hirschboeck 1984; Baillie 1995; Zielinski et al. 1994; Manning 1999; Manning et al. 2001; Hammer et al. 2003), or one about 100–150 yr later (the “conventional” position based on interpretation of archaeological linkages between the Aegean and Egypt: e.g. Warren 1984, 1998; Warren and Hankey 1989; Bietak 2003). However, the calibration curve in periods preceding and postdating this plateau does show considerable variation and, therefore, allows more precise calendar dating.

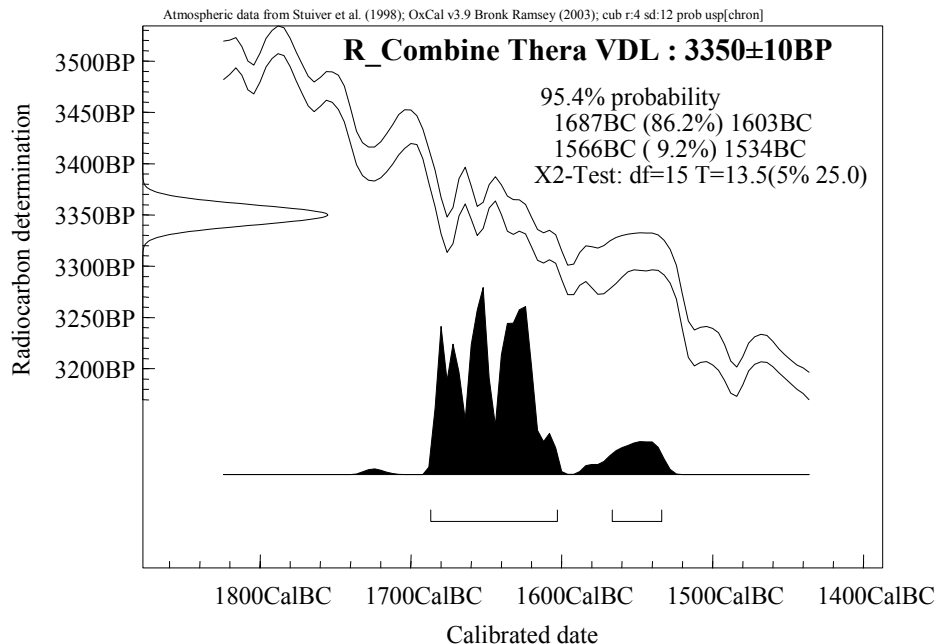


Figure 1 This shows the combined result from the 16 measurements, using standard pretreatment methods, run at ORAU on charred seeds from the final volcanic destruction layer at Akrotiri. This evidence, on its own, suggests that a 17th century cal BC date for the eruption is more likely by a factor of 10 than a date in the mid-16th century cal BC. However, on its own, the result is not conclusive.

The aim of this dating program (see Manning et al. 2002 and Manning and Bronk Ramsey 2003 for previous reports) has, therefore, been to date material from throughout the Late Minoan I period (from the end of the Middle Bronze Age) and to the close of the Late Minoan II period. If the chronology is shifted in the way that has been suggested by, or argued from, the ice-core evidence, tree-ring evidence, and past ^{14}C analyses from Thera, then these periods should show compatible offsets. Where possible at other sites, we have used wiggle-match dating (see Galimberti et al., these proceedings) to achieve the highest precision currently possible. In the analysis, we have also included normally pretreated data from measurements previously obtained at Oxford on material from Thera (Housley et al. 1990).

In addition to these measurements, we have also conducted multiple high-precision accelerator mass spectrometry (AMS) measurements on short-lived material from the volcanic destruction level at Akrotiri (Thera) to see if this can help to resolve the date of the eruption itself.

In terms of sample selection, we have concentrated on short-lived material, identified to species, which is sealed in secure contexts (architectural features, storage jars, etc.) and labeled “secure” in this paper. In previous publications, these have been the samples on which our conclusions have been based. However, such material is not easy to find in many sites and periods. We have, therefore, also dated a range of bone and charcoal samples from well-defined stratigraphic contexts. Because the bones are not articulated and the charcoal is from wood of unknown age, we can only use this material as a *terminus post quem* for the phases, and, since there is always the possibility of intrusion from higher levels, even this cannot be done with complete certainty. These samples will be labeled “phased” here. In this paper, we will present all of the results from “secure” and “phased” samples.

THE ¹⁴C MEASUREMENTS

The ¹⁴C dates considered in this paper are all listed in Appendix I. The results cover the whole range from the Middle Bronze Age to Late Minoan II:

- From Kommos, Akrotiri, and Trianda, we have long-lived wood charcoal samples which are from early Late Minoan IA (LM IA) levels. These either derive from this period or an earlier one. One Trianda sample has 30 visible rings and 3 decades have been measured in duplicate in order to try to wiggle-match the sequence. From Miletos, we also have bone samples from Middle Bronze Age (MBA) phases.
- From Miletos, we have wiggle-matched 7 decades (each measured twice) from a 72-yr-long tree-ring sequence from an oak timber that had been quartered and stripped of bark before being fashioned into an ornate chair. This chair burned in a fire dated by the excavator, Wolf-Dietrich Niemeier, to late in the LMIA period, and as excavated was covered in Thera ash (Niemeier, personal communication, September 2003). The last ring of the sample, present around the entirety of the preserved circumference, appears to indicate the presence of the wane edge, i.e., the last ring before the tree was cut down (Peter Ian Kuniholm and Maryanne Newton, personal communications, December 2002, February 2004; they note that this is their best interpretation of what is visible on the basis of their experience, but also that it cannot be regarded as certain given the absence of the morphological features that in oak wood might indicate sapwood—color change, filled tyloses in the earlywood vessels). Though this chair is from late in the LM IA level, it could, in principle, have been manufactured earlier. This wiggle-matched dendrochronological sequence is, thus, best considered in our Bayesian-modelled scenarios (below) as being bounded on the most recent end by the Volcanic Destruction Level (VDL) at Thera.
- From the VDL at Thera itself, there is short-lived material in the form of charred seeds. The original series of these seeds (submitted by A Sarpaki, OxA-1548 to -1556) were from pithoi in the West House. The new series also comprises seeds from storage jars from the 2000–2001 excavations at Akrotiri (M10/23A N012 from pithos A15, M2/76 N003 from vase A12, M31/43 N047 from pithos A105, and M7/68A N004 from basket M05). We also have material from the LMIA levels of other sites which should be contemporary (or earlier if residual). Such material includes samples from Tsoungiza, near Nemea, in mainland Greece, which is from what is interpreted as its LHI phases.
- From the LMIB destruction levels of Chania and Myrtos-Pyrgos in Crete, we have more seeds (i.e. short-lived material, originally submitted by Hallager and Cadogan [see Housley et al.

1999] and re-dated for this project). These should date the period towards the end of LMIB and should be roughly contemporary. More charcoal from Kommos should also relate to this period, as should LHI/II charcoal from Tsoungiza.

- For LMII, we have dates on charred seeds from the destruction layers at Knossos (originally submitted by M Popham and re-dated for this project).

OVERVIEW OF ¹⁴C EVIDENCE FROM THIS PROJECT

As the principal purpose of this paper is to examine the dating of the eruption of the volcano at Thera, we will first look at the results on samples from the volcanic destruction layer itself. All 16 measurements on the short-lived material (cereals and pulses) pass a χ^2 test (Figure 1). They suggest a 17th century cal BC date for the eruption with a lower probability (by a factor of about 10) for a date in the mid-16th century cal BC.

Later in the paper, we will consider a wider statistical analysis of these results, but first we will examine the calibrated results for each of the other periods.

- The secure context long-lived samples from early LMIA (which may very well date to during the Middle Bronze Age) are apart from one (OxA-11252) earlier than 1700 cal BC. OxA-11252 could be anything between about 1520 cal BC and 1750 cal BC. These samples suggest that the early part of LMIA might lie from about 1700 cal BC, but it could be later given the nature of the material. The material taken from contemporary phases gives a more mixed picture, on average being a little later. Two samples are particularly late (OxA-10618 from Kommos and OxA-10623 from Trianda, marked “?” in Figure 2).
- For the later LMIA (Figure 3), the individual calibrations are not very specific, except in the case of the wiggle-matched sample from Miletos, which could, in principle, be residual. However, note that the sample 65/N001/I2 combined date must be later than about 1683 cal BC and M4N003 must be earlier than 1625 cal BC (both samples from Akrotiri). The short-lived material from the VDL itself (as discussed above) is most likely to be from the mid-later 17th century cal BC. Again the samples from contemporary phases give a very mixed picture. Early dates can be explained as being residual within context, but the 3 LHI dates from Tsoungiza seem later as does one of the bone samples from Miletos (OxA-11952—this sample and the almost similarly late looking OxA-11953 have, subsequent to the initial writing of this text for submission, now been recognized as later, probably Mycenaean, intrusive material from a pit cut into the LMIA stratum [Wolf-Dietrich Niemeier, personal communication, December 2003]; they may, therefore, be discounted).
- For the LMIB destruction layers (Figure 4), the dates cluster around about 1500 cal BC, but with considerable scatter because of the calibration. Given that these dates are meant to be very similar in age, the only date consistent with all of the measurements is about 1520 cal BC, where there is a steep fall in the INTCAL98 calibration curve (Figure 1), which explains the range in values obtained for the 2 sites. But we might also note that 1 sample from Chania (of peas: OxA-2517, 10322) is perhaps significantly older than the other samples from this site (and the set of data from the Chania LMIB destruction horizon fails a 95% χ^2 test with this sample included—it passes without them) and without this sample the need to include the older 16th century BC calibration curve segment is reduced; we might also note that the steep slope in the INTCAL98 calibration curve relies on the effect of a Belfast bi-decadal datum centered at 1510 BC—significantly different from the surrounding Seattle data—without this datum, the “slope” in the calibration curve moves more to about 1500–1490 BC (cf. analysis of Housley et al. 1999 main text based on the Seattle 1993 data set). Thus, an initial date range of possibly

about 1520–1490 BC might be considered. The sample from LMIB levels at Kommos is compatible with the Chania and Myrtos-Pyrgos ages. The samples from LHI/II at Tsoungiza are much earlier.

- The LMII samples from Knossos (Figure 5) show a similar pattern with all of the calibrated dates scattering about 1420 cal BC.

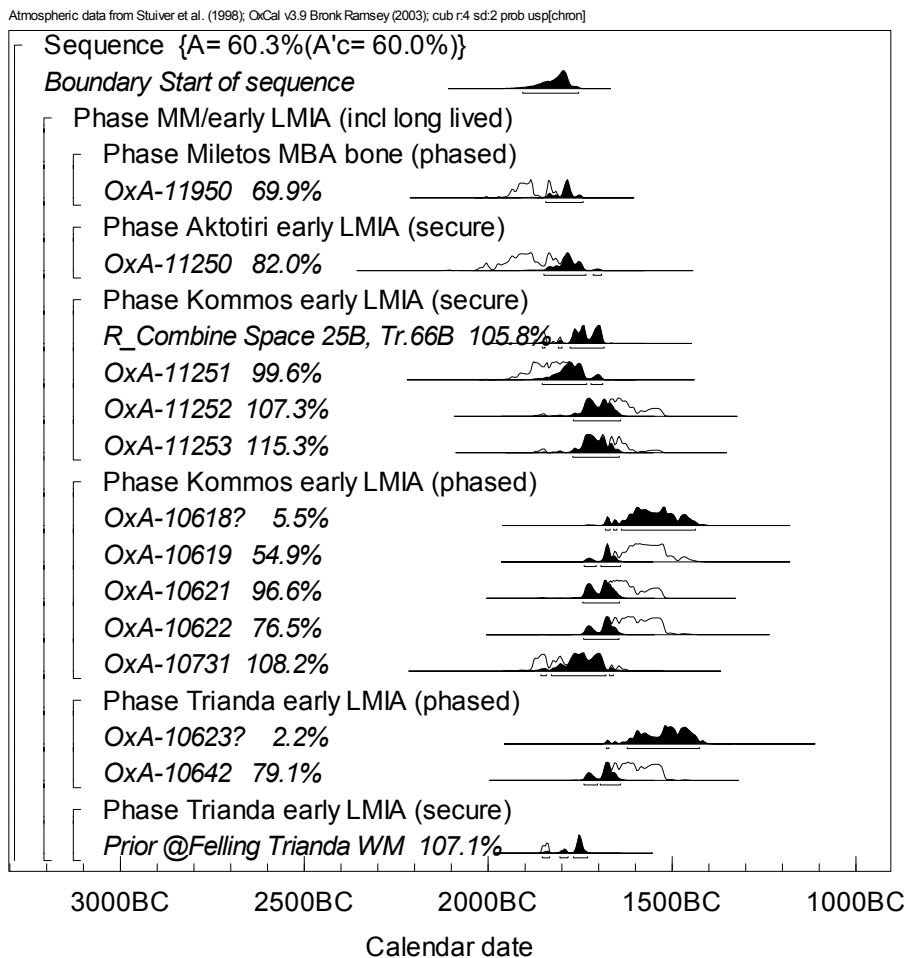


Figure 2 This figure shows the results of the calibrations (in outline) of the samples dated from the MM and early LMIA levels. The solid black distributions are the result of applying Model 3 to the data using a Bayesian analysis. The ¹⁴C dates marked with a “?” have been excluded from the analysis in this model and the distributions for those samples are for a simple calibration. The figures in percentages are the agreement indices for the samples. Where the sample is excluded from the model (those marked “?”), the figure gives the probability that the sample is in the context specified in the model.

What is immediately clear is that the dates from stratigraphic phases give more mixed results than those from the secure contexts with short-lived material. This is not very surprising.

Because we can always account for early dates through likely instances of residuality, it is useful to look in more detail at the 6 later dates mentioned above. Three of these samples are from LHI levels at Tsoungiza. Two of the samples (OxA-11312 and -11313) come from contexts also dated using

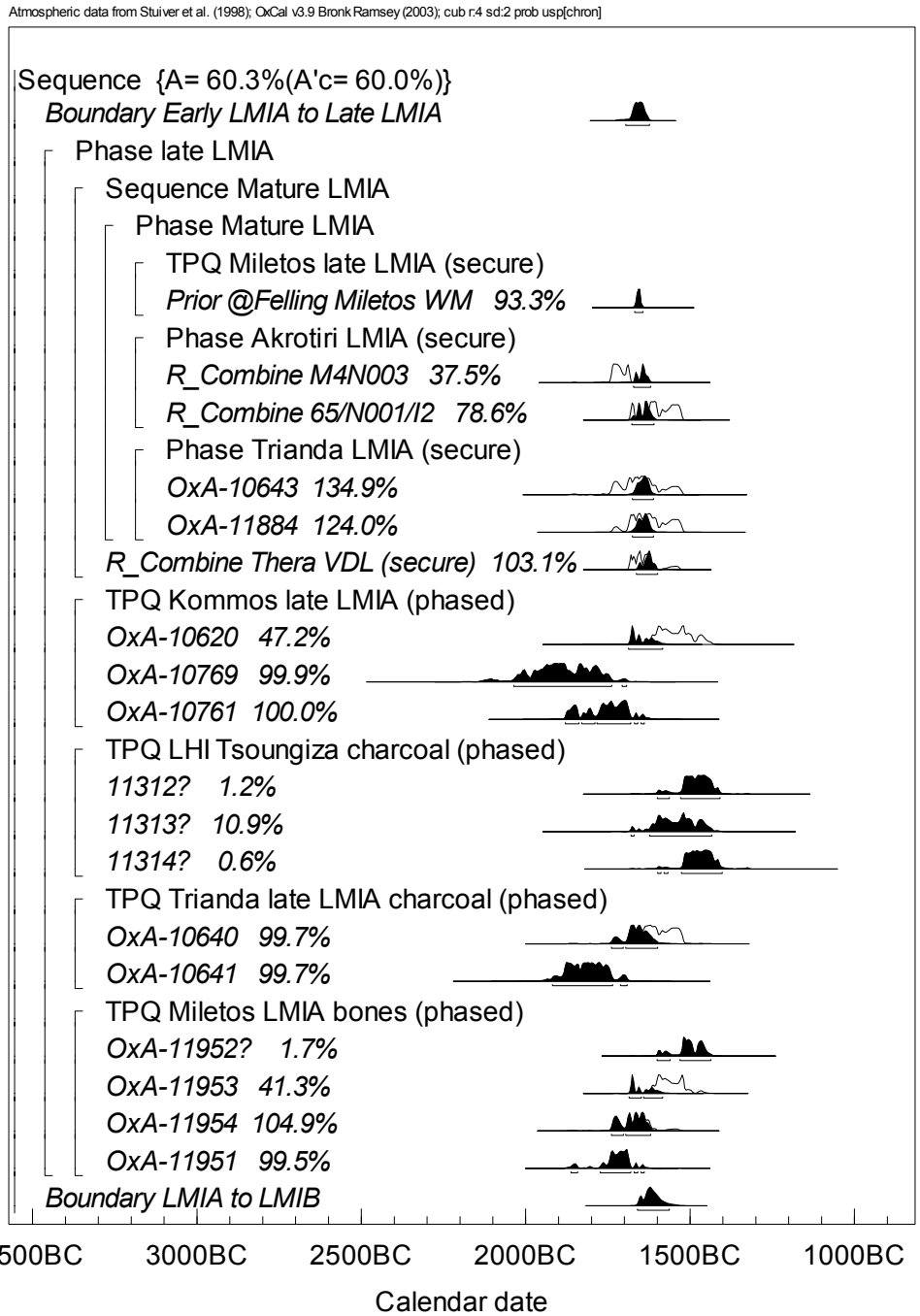


Figure 3 This shows the results from the late LMIA phase; see Figure 2 caption for details.

Atmospheric data from Stuiver et al. (1998); OxCal v3.9 Bronk Ramsey (2003); cub r:4 sd:2 prob usp[chron]

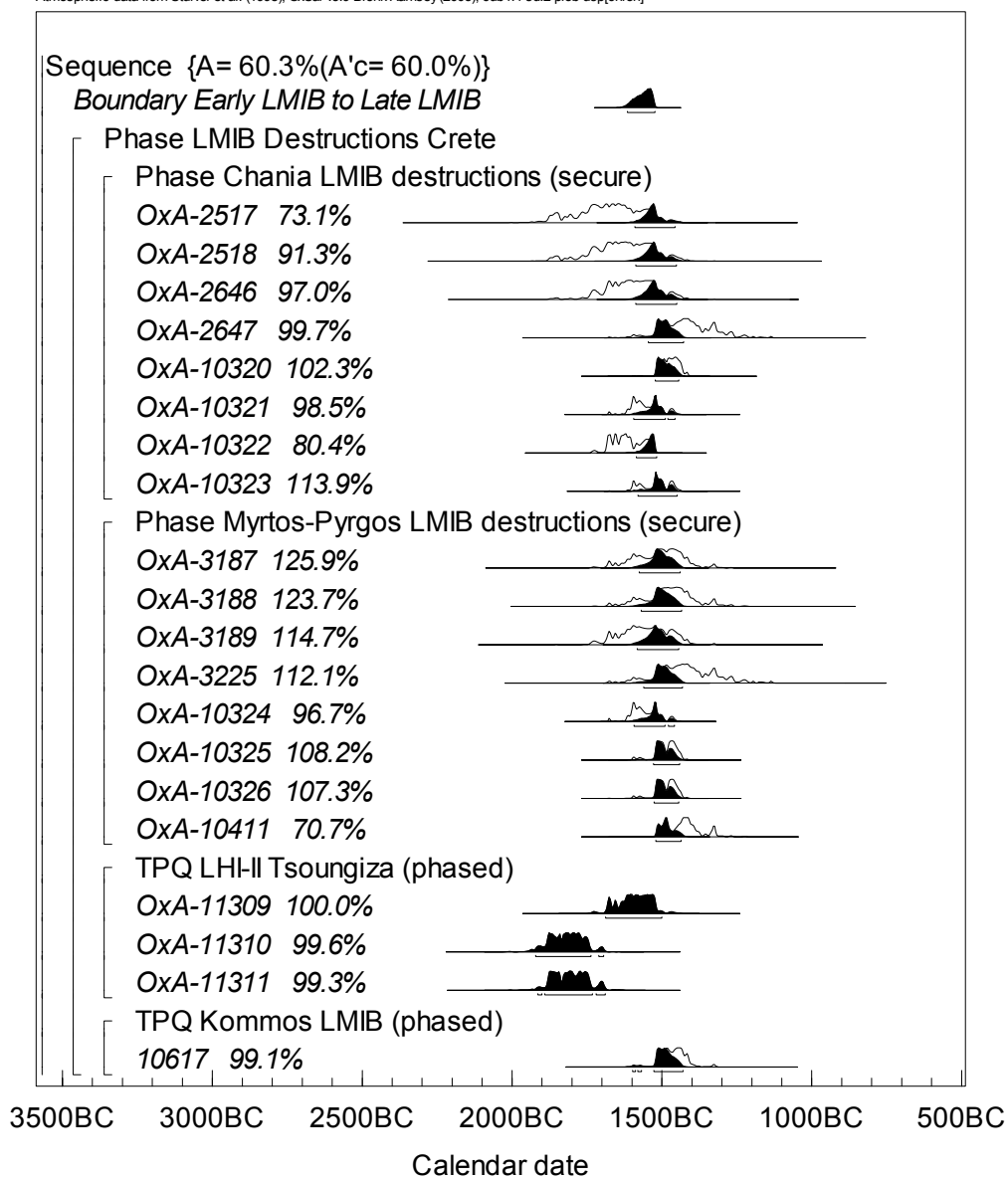


Figure 4 This shows the results from the LMIB phase; see Figure 2 caption for details.

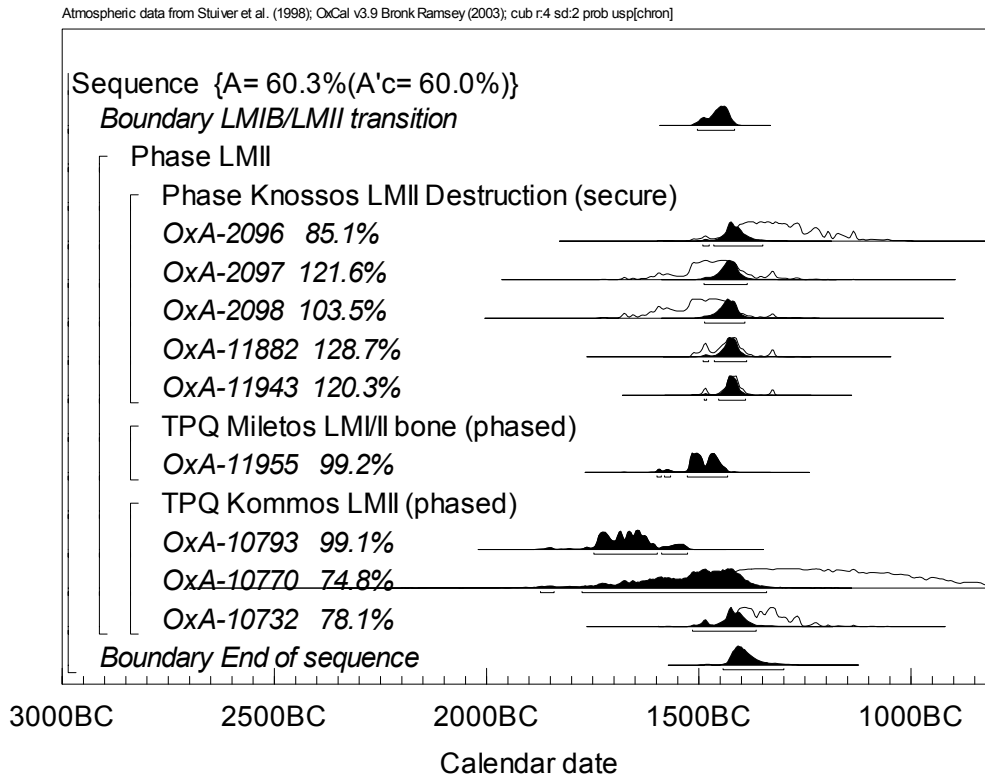


Figure 5 This shows the results from the late LMII phase; see Figure 2 caption for details.

other charcoal fragments by the Arizona ^{14}C lab to 3322 ± 54 BP (AA-10816) and 3317 ± 55 BP (AA-10818)—earlier dates which suggest that the material from these contexts is mixed in age. A third sample (a grape seed, *vitis vinifera*) from this site, 3308 ± 39 BP (OxA-11309), matches well with another sample on charcoal fragments from the same context, 3313 ± 5 BP (AA-10820). Of the other 3 samples that seem later than the majority, two are un-identified charcoal fragment samples (one from Kommos and one from Trianda) and one is a bone sample from Miletos. In the case of the Trianda sample, subsequent analysis of the archaeological record suggests that the context may be disturbed (Toula Marketou, personal communication, 2002).

From this information, several points emerge. Firstly, the dates from the LMIB period point strongly to the period of the destruction of the sites/palaces in Crete being around 1520 cal BC (INTCAL98), where there is a strong shift in the ^{14}C calibration curve (see Section 6 and Table 2 for discussion of calibration data sets). This is about 50–100 yr earlier than the conventional archaeological chronology would suggest (e.g. a date of about 1425 BC is given in Warren and Hankey 1989:169; Warren 1999:902 suggests a date of “around 1430 B.C.”). If we accept such a shift, then 6 samples (none of them in the “secure” context category) from the preceding LMIA period seem to be too late for their context as they lie on the young side of this same rapid ^{14}C concentration shift and, therefore, date to later than 1520 cal BC (INTCAL98). All of the dated “secure” samples from LMIA are consistent with a volcanic eruption date in the mid- to later-17th century cal BC, and with a much lower probability in the mid-16th century cal BC.

BAYESIAN ANALYSIS USING OXCAL

In order to be more numerically specific, we have constructed a Bayesian model for the analysis of these dates using OxCal (Bronk Ramsey 1995, 2001). This takes all of the material together and uses it to constrain a basic model for the chronology of the region. In this model, we have taken the following transitions:

- early LMIA to late LMIA,
- late LMIA to early LMIB,
- early LMIB to late LMIB,
- late LMIB to LMII,

as the major transitions in the chronology. We have then fitted all of the dates within this framework, assuming, for example, that the volcanic destruction at Thera occurs in the late LMIA period. Where material is long lived, we have defined it merely as a *terminus post quem* (TPQ), which will constrain the model to be later than these dates. We have also treated any material which is taken from stratigraphic phases, as opposed to secure contexts, as being a TPQ for the end of the relevant phase. If anything, this should make the chronology later rather than earlier; it allows for residual material but not for intrusion from higher levels.

In order to test for intrusion and outliers, we used the OxCal agreement index (Bronk Ramsey 1995, 2001). This is a calculation of the overlap of the simple calibrated distribution with the distribution after Bayesian modelling. If the overlap falls below 60%, it is equivalent to a combination of normal distributions failing a χ^2 test at 95% level. In this case, we have over 100 ¹⁴C dates, so we would expect some samples (5%) to fail this test but not by much. An extension of this method tests the model as a whole to see if the overall agreement is acceptable or not. In this case, we decided to include all relevant dates in the analysis and then remove the most extreme outliers in a sequential fashion. The characteristics of the 6 models considered are shown in Table 1. We have used INTCAL98 in this exercise.

Table 1 Models 1 and 2 are not acceptable in terms of internal consistency. By removing 6 (all from non-secure contexts) out of the 102 samples dated, the agreement becomes acceptable and the model converges on conclusions that are fairly robust. The best agreement (Model 6) is with only the secure context samples included.

	Excluded samples	Reason	Overall agreement	
Model 1	None	—	26%	Very poor
Model 2	Tsougiza charcoals OxA-11312, 11313, 11314	Very low agreement and AA comparisons	43%	Poor
Model 3	+ OxA-10618 (Kommos), 10623 (Trianda), 11952 (Miletos)	Low agreement and contexts not secure	60%	Marginal
Model 4	+ OxA-10619 (Kommos), 10620 (Kommos), 11953 (Miletos)	Low agreement and contexts not secure	81%	OK
Model 5	+ M4N003 (Akrotiri) combination	Low agreement despite secure context	96%	OK
Model 6	All non-secure contexts (M4N003 included)	M4N003 agreement now OK	100%	OK

Model 1 includes all measurements; Model 2 excludes the 3 most extreme outliers, which are the 3 measurements from LHI (as discussed above). Model 3 excludes the next most extreme outliers (also as discussed above), which are from non-secure contexts. The full details of Model 3 are given in Appendix II and the results of the analysis are given in the Figures 2–5. This is the first model

where the overall agreement is acceptable (just over 60%). In Model 4, we have then examined the effect of removing the remaining 3 samples from non-secure contexts where the agreement index is lower than 60% (even though these may simply be statistical outliers). Model 5 removes 1 “secure” sample (M4N003) which has been dated 5 times because its agreement index is still just below the 60% threshold.

Given that almost all of the anomalous measurements come from the “phased” rather than “secure” contexts, it seems better simply to consider the “secure” material on its own and exclude all “phased” elements from the model. If we do this, all of the agreement indices are above the 60% threshold (including M4N003) and this is what we have considered in Model 6.

The results of all of the analyses are summarized in Table 2. It shows the dates for the main archaeological transitions as estimated from the Bayesian models under the different assumptions outlined above. Models 1 and 2 are not acceptable because they are internally inconsistent—the anomalous dates discussed in the previous section are, in ^{14}C terms, clearly too late to fall before the early/late LMIB transition which must pre-date 1520 BC. All of the models give a very consistent picture of the chronology of the middle of the LMIB phase. All models, except 1 and 2, constrain the date of the eruption at Thera to be in the 17th century BC. The 6 dates that are inconsistent with this date are fragments (five of charcoal, one of bone) from “phased” contexts. Given the very large number of dates measured in this project (over 100), this inconsistency is not too surprising.

Table 2 This shows the date ranges for key transitions inferred from the different models. Note that the date for early LMIB to late LMIB is fairly sensitive to the model and is always earlier than 1520 BC. Models 1 and 2 are the only ones consistent with a 16th century BC date for the Thera eruption, but suffer from very low levels of internal consistency (as measured by the agreement index—see Table 1). However, given that the start of the LMIB destruction events must be earlier than 1520 BC (see this table), Models 1 and 2 would have to require a very short end to LMIA and a very short LMIB phase. Between each of Models 3 and 6, only the date of the early to late LMIA transition is significantly affected by the assumptions made. The “conventional” dates are taken from Warren (1999). All data marked * are based on the INTCAL98 calibration curve (Stuiver et al. 1998). The last model, marked †, has been calculated on the basis of the University of Washington decadal calibration data set (UWTEN98: Stuiver, Reimer, and Braziunas 1998).

	LMIA early/ LMIA Late		VDL	LMIA/LMIB		LMIB early/ LMIB late		LMIB/LMII		
	From	To		From	To	From	To	From	To	
Model 1*	1677	1625	1632	1600	1593	1533	1575	1520	1510	1423
	1586	1546	1587	1536						
Model 2*	1678	1624	1638	1598	1624	1532	1591	1520	1508	1420
	1579	1549	1587	1537						
Model 3*	1696	1623	1663	1599	1660	1563	1615	1523	1504	1416
Model 4*	1709	1628	1662	1611	1661	1595	1620	1524	1503	1416
Model 5*	1698	1613	1661	1601	1661	1577	1618	1523	1504	1416
Model 6*	1747	1643	1662	1608	1661	1581	1621	1522	1507	1416
Model 6†	1743	1639	1663	1605	1662	1577	1621	1516	1501	1421
Conventional			~1520/1500		~1500				~1430	

POSSIBLE FLAWS IN THE ANALYSIS

There are various possible flaws in the ^{14}C dating program presented here. They center on 4 main issues:

- *Certainty of association:* We have considered this in some detail previously in this paper. If we rank the samples in terms of their certainty of association with the archaeological phases into the 2 categories “secure” and “phased,” all of the outliers are in the second category and one of these is now known to lie in a disturbed context. The most secure context samples (the charred seeds from storage vessels at Akrotiri) all give a perfectly consistent set of results and imply a date for the eruption in the 17th century BC.
- *Regional offsets in ^{14}C concentration:* This is an area that has been much discussed and studied (e.g. Kromer et al. 2001; Manning et al. 2001; Manning and Bronk Ramsey 2003). There is little to add here, except to point out that the wiggle-matched sample from Miletos (Galimberti et al., these proceedings) confirms that material from the eastern Mediterranean does match well with the general Northern Hemisphere calibration curve in this particular period. Even if one discounts the material from Thera itself on the grounds that it may have been cultivated near some volcanic vent (and this is very unlikely for all samples from different crop types), such an explanation will not hold for the LMIB material from Crete, nor the LMIA data from Rhodes.
- *Laboratory offset in measurements:* All of these measurements have been measured in conjunction with known-age material from tree-rings. These average <10 ^{14}C yr offset from the INTCAL98 values (see Bronk Ramsey et al., these proceedings, for the latest measurements on this). The results on the short-lived material from Thera have also been measured over a very long timeframe, with the first measurements being made in the 1980s and then the more recent dates on 2 different accelerators. The fact that all of the dates are in good agreement at least shows strong internal consistency. They are also in good agreement with the Copenhagen dates on fully charred short-lived material from the destruction level (Friedrich et al. 1990).
- *Calibration curve:* We have employed what is, at the time of writing, the standard internationally recommended ^{14}C calibration curve (INTCAL98: Stuiver et al. 1998). This curve is, of course, far from definitive (and a new revised and more robustly-based INTCAL04 calibration will appear soon). We have noted, for example, the issue of the reality of the steep slope in the curve ~ 1520 BC, and how this relies largely on 1 Belfast datum that is perhaps an outlier from the general trend at this time. Ignoring this datum would place the relevant slope more about 1505–1485 BC. Thus, statements in this text referring to the 1520 BC slope and age divide would have to be modified, and might be lowered to about 1490 BC (compare Housley et al. 1999 which used only the Seattle data set in its main text). However, overall, such issues of relatively minor differences between the underlying calibration data sets have little significant impact on the analysis of the entire sequence of data. See, for example, the 2 rows of Table 2 for Model 6 (Model 6* and Model 6†), where the results of using INTCAL98 may be compared with the outcome of calibration employing just the Seattle data on German oak (UWTEN98: Stuiver et al. 1998); the differences are very small and insignificant.

The Bayesian analysis performed has explored a number of possible interpretations of the data set presented, and provides some measure of the sensitivity of the analysis to different assumptions. All of the models that which acceptable levels of internal consistency (i.e. Models 3–6 inclusive) provided very similar conclusions about the chronology of this period, despite the different underlying assumptions.

CONCLUSIONS

The first conclusion we draw from the data presented here is a recurrent theme in publications on ^{14}C dating: that where high-precision work is to be undertaken, high-quality samples of short-lived material and with very secure contexts are critical. In this case, we do have quite a few measurements which do not fit this category, and in the end, they do not add much to the analysis. We have 102 ^{14}C measurements to consider here and, of these, six are inconsistent with the others; all come from phases of sites but do not have the same certainty of context as the samples from secure architectural contexts, storage jars, etc.

By looking at the calibrated ^{14}C dates, it is clear that the chronology, particularly of the late LMIB period, must be earlier than the conventional archaeological chronology. We can also see from the secure short-lived material from Akrotiri and other related sites that the eruption of Thera is much more likely (by a factor of about 10) to be in the mid-later 17th century cal BC than a 100 yr (or more) later.

If we combine this information in a Bayesian model and take only those models that are internally consistent, we can see that 4 different analyses (Models 3–6) all give dates for the eruption of Thera in the range of about 1663–1599 BC. This is consistent with suggestions from the mid-1970s onwards of a mid- to late-17th century BC date for the Thera eruption. We emphasize that this dating is direct on the context of interest; it is not a proxy (as current tree-ring evidence) nor subject to debate over the provenance of the tephra-derived glass shards/acidity spike in Greenland ice cores (e.g. Zielinski and Germani 1998a, 1998b; Manning 1998, 1999: 288–307; Hammer et al. 2003; Keenan 2003; Pearce et al. 2004a, b). Following our conclusions above, we think that Model 6, which discards all evidence from fragmentary charcoal and bone found in stratified contexts, is likely to give us the most accurate results. Figure 6 shows the resultant distribution for the volcanic destruction layer material from Akrotiri.

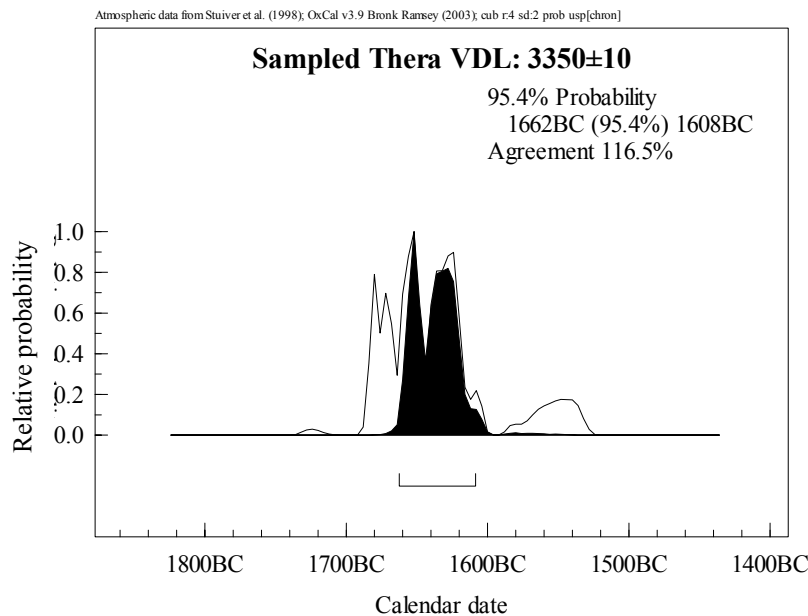


Figure 6 This shows in outline the ^{14}C calibration for the samples from the volcanic destruction layer at Thera (cf. Figure 1, but now after Bayesian analysis using Model 6*, in which only the samples from “secure” contexts are used).

We conclude that if the ^{14}C evidence is considered in isolation, one would deduce that the eruption of Thera took place sometime between 1663 and 1599 BC with 95% confidence. However, there is other archaeological evidence and specific interpretations of this, which clearly need to be taken into account (see Bietak 2003). Ultimately, one's conclusions will depend on how much weight is given to the alternative evidence and especially its interpretation. If, for example, after considering the archaeological evidence, it is concluded that a mid-16th century BC date for the eruption of Thera is 10 times as likely as a 17th century BC date, then this will lead to a different final conclusion. Others, meanwhile, have argued that the archaeological evidence is potentially consonant with a 17th century BC date for Thera (Kemp and Merrillees 1980; Betancourt 1987, 1998; Manning 1988, 1999).

Perhaps most interesting of all is that new evidence is now beginning to suggest that the historical-numerical chronology of Egypt in this period may not be as secure as had been supposed (see Kutschera et al., submitted). Such evidence might open the way for the reconciliation of archaeological linkages with Egypt to the ^{14}C evidence.

ACKNOWLEDGEMENTS

We thank NERC for funding (both for the specific grant held by Manning and Bronk Ramsey and for the funding of the Oxford laboratory's infrastructure) and all of the members of ORAU staff who worked on the dating. For samples, assistance, and collaboration, we gratefully thank Gerald Cadogan, Christos Doumas, Erik Hallager, Peter Ian Kuniholm, Toula Marketou, Maryanne Newton, Wolf-Dietrich Niemeier, Charlotte Pearson, Mervyn Popham, Jeremy Rutter, Joseph and Maria Shaw, Yannis Tzedakis, and James Wright. We also acknowledge the important groundwork done for this project by Rupert Housley and colleagues in the 1980s, and the support given to this area of research by Manfred Bietak with the SCIEM2000 project, and the useful on-going collaborations with Walter Kutschera and the VERA group in Vienna.

REFERENCES

- Baillie MGL. 1995. *A Slice Through Time: Dendrochronology and Precision Dating*. London: B.T. Batsford Ltd. 176 p.
- Baillie MGL, Munro MAR. 1988. Irish tree rings, Santorini and volcanic dust veils. *Nature* 332:344–6.
- Betancourt PP. 1987. Dating the Aegean Late Bronze Age with radiocarbon. *Archaeometry* 29:45–9.
- Betancourt PP. 1998. The chronology of the Aegean Late Bronze Age: unanswered questions. In: Balmuth MS, Tykot RH, editors. *Sardinian and Aegean Chronology: Towards the Resolution of Relative and Absolute Dating in the Mediterranean*. Studies in Sardinian Archaeology V. Oxford: Oxbow Books. p 291–6.
- Bietak M. 2003. Science versus archaeology: problems and consequences of High Aegean chronology. In: Bietak M, editor. *The Synchronisation of Civilisations in the Eastern Mediterranean in the Second Millennium BC II*. Proceedings of the SCIEM 2000—Euroconference, Haindorf, 2001, Vienna. p 23–33.
- Bronk Ramsey C. 1995. Radiocarbon calibration and analysis of stratigraphy: the OxCal program. *Radiocarbon* 37(2):425–30.
- Bronk Ramsey C. 2001. Development of the radiocarbon program OxCal. *Radiocarbon* 43(2A):355–63.
- Bronk Ramsey C, Higham TFG, Leach P. 2004. Towards high-precision AMS: progress and limitations. *Radiocarbon*, these proceedings.
- Friedrich WL, Wagner P, Tauber H. 1990. Radiocarbon dated plant remains from the Akrotiri excavations on Santorini, Greece. In: Harder DA, Renfrew AC, editors. *Thera and the Aegean World III. Volume Three: Chronology*. London: Thera Foundation. p 188–96.
- Galimberti M, Bronk Ramsey C, Manning SW. 2004. Wiggle-match dating of tree ring sequences. *Radiocarbon*, these proceedings.
- Hammer CU, Clausen HB, Friedrich WL, Tauber H. 1987. The Minoan eruption of Santorini in Greece dated to 1645 BC? *Nature* 328:517–9.
- Hammer CU, Kurat G, Hoppe P, Grum W, Clausen HB. 2003. Thera eruption date 1645 BC confirmed by new ice core data? In: Bietak M, editor. *The Synchronisation of Civilisations in the Eastern Mediterranean in the Second Millennium BC II*. Proceedings of the SCIEM 2000—Euroconference, Haindorf, 2001, Vienna. p 87–94.
- Housley RA, Hedges REM, Law IA, Bronk CR. 1990.

- Radiocarbon dating by AMS of the destruction of Akrotiri. In: Harder DA, Renfrew AC, editors. *Thera and the Aegean World III. Volume Three: Chronology*. London: Thera Foundation. p 207–215.
- Housley RA, Manning SW, Cadogan G, Jones RE, Hedges REM. 1999. Radiocarbon, calibration, and the chronology of the Late Minoan IB phase. *Journal of Archaeological Science* 26:159–71.
- Keenan DJ. 2003. Volcanic ash retrieved from the GRIP ice core is not from Thera. *Geochemistry, Geophysics, Geosystems* 4:1097.
- Kemp BJ, Merrillees RS. 1980. *Minoan Pottery in Second Millennium Egypt*. Mainz am Rhein: P. von Zabern. 340 p.
- Kitchen KA. 2000. Regnal and genealogical data of Ancient Egypt (Absolute Chronology I). The historical chronology of Ancient Egypt, a current assessment. In: Bietak M, editor. *The Synchronisation of Civilisations in the Eastern Mediterranean in the Second Millennium B.C.* Vienna: Austrian Academy. p 39–52.
- Kromer B, Manning SW, Kuniholm PI, Newton MW, Spurk M, Levin I. 2001. Regional ¹⁴C₂ offsets in the troposphere: magnitude, mechanism, and consequences. *Science* 294:2529–32.
- Kutschera W, Bietak M, Stadler P, Thranheiser U, Wild EM. Submitted. Sequencing ¹⁴C data from Tel el-Daba in Egypt, and the puzzle of the Thera Volcano Eruption. *Radiocarbon*.
- LaMarche VC Jr, Hirschboeck KK. 1984. Frost rings in trees as records of major volcanic eruptions. *Nature* 307:121–6.
- Manning SW. 1988. The Bronze Age eruption of Thera: absolute dating, Aegean chronology and Mediterranean cultural interrelations. *Journal of Mediterranean Archaeology* 1:17–82.
- Manning SW. 1998. Correction. New GISP2 ice-core evidence supports 17th century BC date for the Santorini (Minoan) eruption: response to Zielinski and Germani (1998). *Journal of Archaeological Science* 25:1039–42.
- Manning SW. 1999. *A Test of Time: The Volcano of Thera and the Chronology and History of the Aegean and East Mediterranean in the Mid-Second Millennium BC*. Oxford: Oxbow Books. p 494 + xxxiii.
- Manning SW, Bronk Ramsey C, Doumas C, Marketou T, Cadogan G, Pearson CL. 2002. New evidence for an early date for the Aegean Late Bronze Age and Thera eruption. *Antiquity* 76:733–44.
- Manning SW, Bronk Ramsey C. 2003. A Late Minoan I-II absolute chronology for the Aegean—combining archaeology with radiocarbon. In: Bietak M, editor. *The Synchronisation of Civilisations in the Eastern Mediterranean in the Second Millennium B.C.* Vienna: Austrian Academy. p 111–33.
- Manning SW, Kromer B, Kuniholm PI, Newton MW. 2001. Anatolian tree-rings and a new chronology for the east Mediterranean Bronze-Iron Ages. *Science* 294:2532–5.
- Michael HN. 1976. Radiocarbon dates from Akrotiri on Thera. *Temple University Aegean Symposium* 1:7–9.
- Pearce NJG, Westgate JA, Preece SJ, Eastwood WJ, Perkins WT, Hart JS. Forthcoming. Reinterpretation of Greenland ice-core data recognises the presence of the late Holocene Aniakchak tephra (Alaska), not the Minoan tephra (Santorini), at 1645 BC. In: Bietak M, editor. *The Synchronisation of Civilisations in the Eastern Mediterranean in the Second Millennium B.C.* Vienna: Austrian Academy.
- Pearce N, Westgate J, Preece S, Eastwood W, Perkins W. 2004. Identification of Aniakchak (Alaska) tephra in Greenland ice core challenges the 1645 BC date for Minoan eruption of Santorini. *Geochemistry, Geophysics, Geosystems* 5(3):Q03005 doi:10.1029/2003GC000672.
- Stuiver M, Reimer PJ, Bard E, Beck JW, Burr GS, Hughen KA, Kromer B, McCormac G, van der Plicht J, Spurk M. 1998. INTCAL98 radiocarbon age calibration, 24,000–0 cal BP. *Radiocarbon* 40(3):1041–83.
- Stuiver M, Reimer PJ, Braziunas TF. 1998. High-precision radiocarbon age calibration for terrestrial and marine samples. *Radiocarbon* 40(3):1127–51.
- Warren P. 1984. Absolute dating of the Bronze Age eruption of Thera (Santorini). *Nature* 308:492–3.
- Warren PM. 1998. Aegean Late Bronze 1-2 absolute chronology—some new contributions. In: Balmuth MS and Tykot RH, editors. *Sardinian and Aegean Chronology: Towards the Resolution of Relative and Absolute Dating in the Mediterranean*. Studies in Sardinian Archaeology V. Oxford: Oxbow Books. p 323–31.
- Warren PM. 1999. LMIA: Knossos, Thera, Gournia. In: Betancourt PP, Karageorghis V, Laffineur R, Niemeier WD, editors. *Meletemata: Studies in Aegean Archaeology Presented to Malcolm H. Wiener As He Enters His 65th year*. Liège and Austin: Université de Liège & University of Texas at Austin. p 893–903.
- Warren P, Hankey V. 1989. *Aegean Bronze Age chronology*. Bristol: Bristol Classical Press. 246 p.
- Zielinski GA, Germani MS. 1998a. New ice-core evidence challenges the 1620s BC age for the Santorini (Minoan) eruption. *Journal of Archaeological Science* 25:279–89.
- Zielinski GA, Germani MS. 1998b. Reply to: Correction. *Journal of Archaeological Science* 25:1043–5.
- Zielinski GA, Mayewski PA, Meeker LD, Whitlow S, Twickler MS, Morrison M, Meese DA, Gow AJ, Alley RB. 1994. Record of volcanism since 7000 BC from the GISP2 Greenland ice core and implications for the volcano-climate system. *Science* 264:948–52.

Appendix I List of all samples and dates (108) used in this study. The six samples shown in grey are not considered further because they are either too early to be relevant, or TPQ for late periods and, therefore, would have no impact on the chronology considered here.

Site	Submitter's reference	Material	Species	OxA	BP	\pm	$\delta^{13}\text{C}$	Period	Context
Akrotiri, Thera	M31/67 N069	charred seed		11819	3768	32	-25.5	<LM	secure
Akrotiri, Thera	M31/67 N069	charred seed		12173	3788	29	-25.2	<LM	secure
Akrotiri, Thera	M31/67 N069	charred seed		12174	3745	29	-25.5	<LM	secure
Miletos, Turkey	AT 98.196	bone		11950	3549	24	-19.8	MM	phased
Kommos, Crete	TP-KE-32	charcoal		10621	3359	39	-25.5	MMIII	phased
Kommos, Crete	TP-KE-32	charcoal		10622	3330	45	-25.3	MMIII	phased
Miletos, Turkey	AT 99.915	bone		11951	3423	23	-19.5	LMIA ^a	phased
Miletos, Turkey	AT 99.729	bone		11952	3243	22	-20.1	Intrusive into LMIA	phased
Miletos, Turkey	AT 99.779	bone		11953	3279	26	-20.0	LMIA ^a	phased
Miletos, Turkey	AT 99.811	bone		11954	3377	24	-19.4	LMIA	phased
Trianda, Rhodes	Trianda 4	charcoal		10640	3338	40	-25.4	LMIA	phased
Akrotiri, Thera	M54/2/VI/60/δε>247	charcoal	<i>Olea europaea</i>	11250	3550	45	-23.4	LMIA(early)	secure
Kommos, Crete	Space 25B Tr.66B	charcoal	<i>Chamaecyparis sp.</i>	3429	3350	70	-27.8	LMIA(early)	secure
Kommos, Crete	Space 25B Tr.66B	charcoal	<i>Chamaecyparis sp.</i>	11883	3485	33	-25.3	LMIA(early)	secure
Kommos, Crete	Space 25B Tr.66B	charcoal	<i>Olea europaea</i>	11944	3435	25	-24.4	LMIA(early)	secure
Kommos, Crete	TP-KE-30	charcoal		10618	3270	45	-22.6	LMIA(early)	phased
Kommos, Crete	TP-KE-30	charcoal		10619	3295	45	-22.8	LMIA(early)	phased
Kommos, Crete	K85A/62D/9:92	charcoal	<i>Quercus sp.</i>	11251	3505	40	-23.6	LMIA(early)	secure
Kommos, Crete	K85A/66B/4:22+23	charred twig		11252	3375	45	-23.6	LMIA(early)	secure
Kommos, Crete	K85A/62D/8:83	charcoal	<i>Quercus sp.</i>	11253	3397	38	-23.2	LMIA(early)	secure
Kommos, Crete	38/TP-KC-22	charcoal		10731	3450	45	-24.1	LMIA(early)	secure
Trianda, Rhodes	Trianda 1	charcoal		10623	3245	45	-23.5	LMIA(early)	phased
Trianda, Rhodes	Trianda 9	charcoal	<i>?Olea sp.</i>	10642	3333	39	-25.2	LMIA(early)	phased
Trianda, Rhodes	34/AE1024/A	charcoal	<i>Quercus sp.</i>	10728	3455	45	-25.3	LMIA(early)	secure
Trianda, Rhodes	34/AE1024?B	charcoal	<i>Quercus sp.</i>	10729	3410	45	-25.9	LMIA(early)	secure
Trianda, Rhodes	36/AE1024/C	charcoal	<i>Quercus sp.</i>	10730	3490	45	-25.5	LMIA(early)	secure
Trianda, Rhodes	34/AE1024/A	charcoal	<i>Quercus sp.</i>	11945	3473	24	-24.9	LMIA(early)	secure
Trianda, Rhodes	34/AE1024/C	charcoal	<i>Quercus sp.</i>	11946	3474	24	-26.1	LMIA(early)	secure
Trianda, Rhodes	36/AE1024/C	charcoal	<i>Quercus sp.</i>	11948	3526	25	-25.2	LMIA(early)	secure

^aTwo bone samples from Miletos were received and dated on the basis of being from Late Minoan IA contexts. Subsequent to this work, the excavator of the site, Wolf-Dietrich Niemeier (personal communication, December 2003), has informed us that these 2 samples derive from what is now recognized as a later (probably Mycenaean) pit cut into the LMIA stratum. These 2 dates may therefore be dismissed as relevant to LMIA. The analysis (see text) had already identified these 2 data as outliers.

Appendix I List of all samples and dates (108) used in this study. The six samples shown in grey are not considered further because they are either too early to be relevant, or TPQ for late periods and, therefore, would have no impact on the chronology considered here. (Continued)

Site	Submitter's reference	Material	Species	OxA	BP	\pm	$\delta^{13}\text{C}$	Period	Context
Akrotiri, Thera	F/65/N001/12	charcoal	<i>Tamarix sp.</i>	10312	3293	27	-24.0	LMIA(late)	secure
Akrotiri, Thera	G/65/N001/12	charcoal	<i>Tamarix sp.</i>	10313	3353	27	-24.1	LMIA(late)	secure
Akrotiri, Thera	H/65/N001/12	charcoal	<i>Tamarix sp.</i>	10314	3330	27	-24.5	LMIA(late)	secure
Akrotiri, Thera	A/M4N003	charcoal	<i>Olea europaea</i>	10315	3446	39	-24.0	LMIA(late)	secure
Akrotiri, Thera	B/M4N003	charcoal	<i>Olea europaea</i>	10316	3342	38	-24.4	LMIA(late)	secure
Akrotiri, Thera	C/M4N003	charcoal	<i>Olea europaea</i>	10317	3440	35	-24.1	LMIA(late)	secure
Akrotiri, Thera	D/M4N003	charcoal	<i>Olea europaea</i>	10318	3355	40	-24.2	LMIA(late)	secure
Akrotiri, Thera	E/M4N003	charcoal	<i>Olea europaea</i>	10319	3424	38	-24.4	LMIA(late)	secure
Kommos, Crete	TP-KE-31	charcoal		10620	3269	38	-22.4	LMIA(late)	phased
Kommos, Crete	40/TP-KC-20	charcoal		10761	3440	38	-24.3	LMIA(late)	phased
Kommos, Crete	39/TP-KC-21	charcoal		10769	3555	60	-24.8	LMIA(late)	phased
Miletos, Turkey	1:C-TU-MIL-1/RY1000-1010	charcoal	<i>Quercus sp.</i>	12301	3439	30	-25.4	LMIA(late)	secure
Miletos, Turkey	1:C-TU-MIL-1/RY1000-1010	charcoal	<i>Quercus sp.</i>	12302	3386	31	-26.0	LMIA(late)	secure
Miletos, Turkey	2:C-TU-MIL-1/RY1010-1020	charcoal	<i>Quercus sp.</i>	12303	3467	31	-25.5	LMIA(late)	secure
Miletos, Turkey	3:C-TU-MIL-1/RY1020-1030	charcoal	<i>Quercus sp.</i>	12304	3404	31	-25.5	LMIA(late)	secure
Miletos, Turkey	3:C-TU-MIL-1/RY1020-1030	charcoal	<i>Quercus sp.</i>	12305	3459	31	-25.7	LMIA(late)	secure
Miletos, Turkey	4:C-TU-MIL-1/RY1030-1040	charcoal	<i>Quercus sp.</i>	12306	3416	31	-25.7	LMIA(late)	secure
Miletos, Turkey	4:C-TU-MIL-1/RY1030-1040	charcoal	<i>Quercus sp.</i>	12307	3425	31	-25.6	LMIA(late)	secure
Miletos, Turkey	5:C-TU-MIL-1/RY1040-1050	charcoal	<i>Quercus sp.</i>	12308	3361	31	-26.0	LMIA(late)	secure
Miletos, Turkey	5:C-TU-MIL-1/RY1040-1050	charcoal	<i>Quercus sp.</i>	12309	3397	31	-26.0	LMIA(late)	secure
Miletos, Turkey	6:C-TU-MIL-1/RY1050-1060	charcoal	<i>Quercus sp.</i>	12310	3345	32	-26.3	LMIA(late)	secure
Miletos, Turkey	6:C-TU-MIL-1/RY1050-1060	charcoal	<i>Quercus sp.</i>	12311	3397	32	-26.3	LMIA(late)	secure
Miletos, Turkey	7:C-TU-MIL-1/RY1060-1070	charcoal	<i>Quercus sp.</i>	12312	3388	30	-26.3	LMIA(late)	secure
Miletos, Turkey	7:C-TU-MIL-1/RY1060-1070	charcoal	<i>Quercus sp.</i>	12313	3352	31	-26.1	LMIA(late)	secure
Miletos, Turkey	2:C-TU-MIL-1/RY1010-1020	charcoal	<i>Quercus sp.</i>	12407	3385	34	-25.8	LMIA(late)	secure
Trianda, Rhodes	Trianda 8	charcoal		10641	3498	39	-24.4	LMIA(late)	phased
Trianda, Rhodes	Trianda 13	charred twig	<i>Quercus sp.</i>	10643	3367	39	-26.3	LMIA(late)	secure
Trianda, Rhodes	Trianda 13	charred twig	<i>Quercus sp.</i>	11884	3344	32	-26.0	LMIA(late)	secure
Tsougiza, Nemea	Tsougiza 4	charcoal		11312	3215	38	-24.2	LHI(late) (LMIA(late)) LHI (late)	phased

Appendix I List of all samples and dates (108) used in this study. The six samples shown in grey are not considered further because they are either too early to be relevant, or TPQ for late periods and, therefore, would have no impact on the chronology considered here. (Continued)

Site	Submitter's reference	Material	Species	OxA	BP	\pm	$\delta^{13}\text{C}$	Period	Context
Tsougiza, Nemea	Tsougiza 5	charcoal		11313	3261	39	-24.1	(LMIA(late)) LHI (late)	phased
Tsougiza, Nemea	Tsougiza 6	charcoal	<i>Allium sp.</i>	11314	3202	38	-22.7	LMIA(late)	phased
Akrotiri, Thera	M2/76 N003	charred seed	? <i>Lens. sp.</i>	11817	3348	31	-22.9	LMIA(V)	secure
Akrotiri, Thera	M7/68A N004	charred seed	<i>Hordeum sp.</i>	11818	3367	33	-25.8	LMIA(V)	secure
Akrotiri, Thera	M10/23A N012	charred seed	<i>Hordeum sp.</i>	11820	3400	31	-25.2	LMIA(V)	secure
Akrotiri, Thera	M31/43 N047	charred seed	<i>Hordeum sp.</i>	11869	3336	34	-22.8	LMIA(V)	secure
Akrotiri, Thera	M2/76 N003	charred seed	? <i>Lens. sp.</i>	12170	3336	28	-22.9	LMIA(V)	secure
Akrotiri, Thera	M7/68A N004	charred seed	<i>Hordeum sp.</i>	12171	3372	28	-25.7	LMIA(V)	secure
Akrotiri, Thera	M31/43 N047	charred seed	<i>Hordeum sp.</i>	12172	3321	32	-23.1	LMIA(V)	secure
Akrotiri, Thera	M10/23A N012	charred seed	<i>Hordeum sp.</i>	12175	3318	28	-24.7	LMIA(V)	secure
Akrotiri, Thera	1	charred seed	<i>Lathyrus sp.</i>	1548	3335	60	-26	LMIA(V)	secure
Akrotiri, Thera	1	charred seed	<i>Lathyrus sp.</i>	1549	3460	80	-26	LMIA(V)	secure
Akrotiri, Thera	2	charred seed	<i>Lathyrus sp.</i>	1550	3395	65	-26	LMIA(V)	secure
Akrotiri, Thera	4	charred seed	<i>Lathyrus sp.</i>	1552	3390	65	-26	LMIA(V)	secure
Akrotiri, Thera	8	charred seed	<i>Lathyrus sp.</i>	1553	3340	65	-26	LMIA(V)	secure
Akrotiri, Thera	8	charred seed	<i>Lathyrus sp.</i>	1554	3280	65	-26	LMIA(V)	secure
Akrotiri, Thera	9	charred seed	<i>Lathyrus sp.</i>	1555	3245	65	-26	LMIA(V)	secure
Akrotiri, Thera	11	charred seed	<i>Hordeum sp.</i>	1556	3415	70	-26	LMIA(V)	secure
Tsougiza, Nemea	Tsougiza 2	charred seed	<i>Vitis vinifera</i>	11309	3308	39	-23.4	LHI-II (LMIA/ LMIB)	phased
Tsougiza, Nemea	Tsougiza 3	charcoal	? <i>Quercus sp.</i>	11310	3503	38	-24.5	LHI-II (LMIA/ LMIB)	phased
Tsougiza, Nemea	Tsougiza 3	charcoal	? <i>Quercus sp.</i>	11311	3487	38	-22.7	LHI-II (LMIA/ LMIB)	phased

Appendix I List of all samples and dates (108) used in this study. The six samples shown in grey are not considered further because they are either too early to be relevant, or TPQ for late periods and, therefore, would have no impact on the chronology considered here. (Continued)

Site	Submitter's reference	Material	Species	OxA	BP	\pm	$\delta^{13}\text{C}$	Period	Context
Chania, Crete	15/TR10, Rm E	charred seed	<i>Pisum sativum</i>	2517	3380	80	-25.6	LMIB	secure
Chania, Crete	13/TR17, 1984, Rm C	charred seed	<i>Vicia faba</i>	2518	3340	80	-24.9	LMIB	secure
Chania, Crete	14/TR17, 1984 Rm C	charred seed	<i>Hordeum sp.</i>	2646	3315	70	-23.9	LMIB	secure
Chania, Crete	16/TR24, 1989, L6, BA1	charred seed		2647	3150	70	-25.1	LMIB	secure
Chania, Crete	13/TR17, 1984, Tm C	charred seed	<i>Vicia faba</i>	10321	3208	26	-22.8	LMIB	secure
Chania, Crete	14/TR17, 1984, Rm C	charred seed	<i>Hordeum sp.</i>	10321	3268	27	-22.1	LMIB	secure
Chania, Crete	15/TR10, Rm E	charred seed	<i>Pisum sativum</i>	10322	3338	26	-23.9	LMIB	secure
Chania, Crete	16/TR24, 1989, L6, BA1	charred seed		10323	3253	25	-23.3	LMIB	secure
Kommos, Crete	TP-KE-29	charcoal		10617	3190	40	-24.2	LMIB	phased
Myrtos-Pyrgos, Crete	17/K5,2,1	charred seed	<i>Hordeum sp.</i>	3187	3230	70	-22.2	LMIB	secure
Myrtos-Pyrgos, Crete	18/K5,2,4	charred seed	<i>Hordeum sp.</i>	3188	3200	70	-26.5	LMIB	secure
Myrtos-Pyrgos, Crete	19/K5/K6,2,1	charred seed	<i>Vicia ervilia</i>	3189	3270	70	-26.0	LMIB	secure
Myrtos-Pyrgos, Crete	20/K5/L6,2,2	charred seed	<i>Vicia ervilia</i>	3225	3160	80	-23.6	LMIB	secure
Myrtos-Pyrgos, Crete	17/K5,2,1	charred seed	<i>Hordeum sp.</i>	10324	3270	26	-22.4	LMIB	secure
Myrtos-Pyrgos, Crete	19/K5/K6,2,1	charred seed	<i>Vicia ervilia</i>	10325	3228	26	-23.4	LMIB	secure
Myrtos-Pyrgos, Crete	20/K5/L6,2,2	charred seed	<i>Vicia ervilia</i>	10326	3227	25	-22.4	LMIB	secure
Myrtos-Pyrgos, Crete	18/K5,2,4	charred seed	<i>Hordeum sp.</i>	10411	3150	40	-26.5	LMIB	secure
Miletos, Turkey	AT 99.787	bone		11955	3233	23	-17.8	LMIB/II	phased
Knossos, Crete	LMII	charred seed	<i>Hordeum sp.</i>	2096	3070	70	-23.3	LMII	secure
Knossos, Crete	LMII	charred seed	<i>Hordeum sp.</i>	2097	3190	65	-23.6	LMII	secure
Knossos, Crete	LMII	charred seed	<i>Hordeum sp.</i>	2098	3220	65	-22.9	LMII	secure
Knossos, Crete	LMII	charred seed	<i>Hordeum sp.</i>	11882	3156	33	-22.7	LMII	secure
Knossos, Crete	LMII	charred seed	<i>Hordeum sp.</i>	11943	3148	23	-23.0	LMII	secure
Kommos, Crete	TP-KE-28	charcoal		10793	3382	37	-23.7	LMII	phased
Kommos, Crete	43/TP-KC-17	charcoal		10732	3095	45	-22.2	LMII	phased
Kommos, Crete	42/TP-KC-18	charcoal		10762	7440	50	-23.4	LMII	phased
Kommos, Crete	41/TP-KC-19	charcoal		10770	3040	190	-26.9	LMII	phased
Kommos, Crete	45/TP-KC-27	charcoal		10734	3185	45	-24.1	LMIIIA1	phased
Kommos, Crete	44/TP-KC-26	charcoal		10733	2930	45	-24.2	LMIIIA2	phased

Appendix II Bayesian OxCal Model 3 used in this analysis.

```

Plot
{
  D_Sequence "Trianda WM"
  {
    First;
    R_Date "OxA-10730" 3490 45;
    R_Date "OxA-11948" 3526 25; Gap 10;
    R_Date "OxA-10729" 3410 45;
    R_Date "OxA-11946" 3474 24; Gap 10;
    R_Date "OxA-10728" 3455 45;
    R_Date "OxA-11945" 3473 24; Gap 5;
    Event "Felling Trianda WM";
  }
  Page;
  D_Sequence "Miletos WM"
  {
    First;
    R_Date "OxA-12301-2" 3413 22; Gap 10;
    R_Date "OxA-12303_407" 3430 23; Gap 10;
    R_Date "OxA-12304-5" 3432 22; Gap 10;
    R_Date "OxA-12306-7" 3420 22; Gap 10;
    R_Date "OxA-12308-9" 3379 22; Gap 10;
    R_Date "OxA-12310-11" 3371 23; Gap 10;
    R_Date "OxA-12312-3" 3371 22; Gap 5;
    Event "Felling Miletos WM";
  }
  Page;
  Sequence
  {
    Boundary "Start of sequence";
    Phase "MM/early LMIA (incl long lived)"
    {
      Phase "Miletos MBA bone (phased)"
      {
        R_Date "OxA-11950" 3549 24;
      }
    }
  }
  Phase "Aktotiri early LMIA (secure)"
  {
    R_Date "OxA-11250" 3550 45;
  }
  Phase "Kommos early LMIA (secure)"
  {
    R_Combine "Space 25B, Tr.66B"
    {
      R_Date "OxA-3429" 3350 70;
      R_Date "OxA-11883" 3485 33;
      R_Date "OxA-11944" 3435 25;
    }
    R_Date "OxA-11251" 3505 40;
    R_Date "OxA-11252" 3375 45;
    R_Date "OxA-11253" 3397 38;
  }
  Phase "Kommos early LMIA (phased)"
  {
    R_Date "OxA-10618" 3270 45?
    R_Date "OxA-10619" 3295 45;
    R_Date "OxA-10621" 3359 39;
    R_Date "OxA-10622" 3330 45;
    R_Date "OxA-10731" 3450 45;
  }
  Phase "Trianda early LMIA (phased)"
  {
    R_Date "OxA-10623" 3245 45?
    R_Date "OxA-10642" 3333 39;
  }
  Phase "Trianda early LMIA (secure)"
  {
    Prior "@Felling Trianda WM";
  }
}
Page;
Boundary "Early LMIA to Late LMIA";
Phase "late LMIA"
{
  Sequence "Mature LMIA"
  {
    Phase "Mature LMIA"
    {
      TPQ "Miletos late LMIA (secure)"
      {
        Prior "@Felling Miletos WM";
      }
      Phase "Aktotiri LMIA (secure)"
      {
        R_Combine "M4N003"
        {
          R_Date "OxA-10315" 3446 39;
          R_Date "OxA-10316" 3342 38;
          R_Date "OxA-10317" 3440 35;
          R_Date "OxA-10318" 3355 40;
          R_Date "OxA-10319" 3424 38;
        }
        R_Combine "65/N001/I2"
        {
          R_Date "OxA-10314" 3330 27;
          R_Date "OxA-10313" 3353 27;
          R_Date "OxA-10312" 3293 27;
        }
      }
      Phase "Trianda LMIA (secure)"
      {
        R_Date "OxA-10643" 3367 39;
        R_Date "OxA-11884" 3344 32;
      }
    }
  }
}

```

Appendix II Bayesian OxCal Model 3 used in this analysis (*Continued*).

```

R_Combine "Thera VDL (secure)"
{
  R_Date "OxA-11954" 3377 24;
  R_Date "OxA-11951" 3423 23;
};
};
R_Date "OxA-11817" 3348 31;
R_Date "OxA-11818" 3367 33;
R_Date "OxA-11820" 3400 31;
R_Date "OxA-11869" 3336 34;
R_Date "OxA-12170" 3336 28;
R_Date "OxA-12171" 3372 28;
R_Date "OxA-12175" 3318 28;
R_Date "OxA-12172" 3321 32;
R_Date "OxA-1552" 3390 65;
R_Date "OxA-1555" 3245 65;
R_Date "OxA-1548" 3335 60;
R_Date "OxA-1549" 3460 80;
R_Date "OxA-1550" 3395 65;
R_Date "OxA-1553" 3340 65;
R_Date "OxA-1554" 3280 65;
R_Date "OxA-1556" 3415 70;
};
};
TPQ "Kommos late LMIA (phased)"
{
  R_Date "OxA-10620" 3269 38;
  R_Date "OxA-10769" 3555 60;
  R_Date "OxA-10761" 3440 38;
};
TPQ "LHI Tsoungiza charcoal (phased)"
{
  R_Date "11312" 3215 38?
  R_Date "11313" 3261 39?
  R_Date "11314" 3202 38?
};
TPQ "Trianda late LMIA charcoal (phased)"
{
  R_Date "OxA-10640" 3338 40;
  R_Date "OxA-10641" 3498 39;
};
TPQ "Miletos LMIA bones (phased)"
{
  R_Date "OxA-11952" 3243 22?
  R_Date "OxA-11953" 3279 26;
};
};
};
R_Date "OxA-11954" 3377 24;
R_Date "OxA-11951" 3423 23;
};
};
Boundary "LMIA to LMIB";
Page:
Boundary "Early LMIB to Late LMIB";
Phase "LMIB Destructions Crete"
{
  Phase "Chania LMIB destructions (secure)"
  {
    R_Date "OxA-2517" 3380 80;
    R_Date "OxA-2518" 3340 80;
    R_Date "OxA-2646" 3315 70;
    R_Date "OxA-2647" 3150 70;
    R_Date "OxA-10320" 3208 26;
    R_Date "OxA-10321" 3268 27;
    R_Date "OxA-10322" 3338 26;
    R_Date "OxA-10323" 3253 25;
  };
};
Phase "Myrtos-Pyrgos LMIB destructions (secure)"
{
  R_Date "OxA-3187" 3230 70;
  R_Date "OxA-3188" 3200 70;
  R_Date "OxA-3189" 3270 70;
  R_Date "OxA-3225" 3160 80;
  R_Date "OxA-10324" 3270 26;
  R_Date "OxA-10325" 3228 26;
  R_Date "OxA-10326" 3227 25;
  R_Date "OxA-10411" 3150 40;
};
TPQ "LHI-II Tsoungiza (phased)"
{
  R_Date "OxA-11309" 3308 39;
  R_Date "OxA-11310" 3503 38;
  R_Date "OxA-11311" 3487 38;
};
TPQ "Kommos LMIB (phased)"
{
};
};
};
R_Date "10617" 3190 40;
};
};
Page:
Boundary "LMIB/LMII transition";
Phase "LMII"
{
  Phase "Knossos LMII Destruction (secure)"
  {
    R_Date "OxA-2096" 3070 70;
    R_Date "OxA-2097" 3190 65;
    R_Date "OxA-2098" 3220 65;
    R_Date "OxA-11882" 3156 33;
    R_Date "OxA-11943" 3148 23;
  };
  TPQ "Miletos LMI/II bone (phased)"
  {
    R_Date "OxA-11955" 3233 23;
  };
};
TPQ "Komos LMII (phased)"
{
  R_Date "OxA-10793" 3382 37;
  R_Date "OxA-10770" 3040 190;
  R_Date "OxA-10732" 3095 45;
};
};
Boundary "End of sequence";
};
};

```

CHRONOLOGY OF THE BEGINNING OF POTTERY MANUFACTURE IN EAST ASIA

Charles T Keally¹ • Yasuhiro Taniguchi² • Yaroslav V Kuzmin³ • Igor Y Shewkomud⁴

ABSTRACT. This paper presents an updated radiocarbon chronology of the earliest pottery sites in the Old World. Ceramic production originated in the Late Glacial period in several regions of East Asia—the Japanese Islands, the Russian Far East, and southern China—at approximately the same time, about 13,700–13,300 BP (about 17,200–14,900 cal BP).

INTRODUCTION

The emergence of pottery had a significant impact on prehistoric people's lifestyle and subsistence, increasing the usable food resources and leading to a sedentary life. By the mid-1960s, the Japanese already had dates of 12,700–12,200 BP for the beginning of pottery manufacture there, despite the limited number of radiocarbon dates available at that time (Watanabe 1966). Since then, the number of dates associated with the earliest pottery in Japan and neighboring East Asia, including the Russian Far East and China, has increased dramatically, but this information is not well known to Anglophone scholars because the original sources are written mostly in Japanese, Russian, and Chinese. Some of the ¹⁴C dates associated with the earliest pottery from East Asia have been summarized before (Morlan 1967; Kuzmin and Keally 2001), and here we present the most complete corpus of data available as of mid-2003.

MATERIALS AND METHODS

¹⁴C dates for Japanese and Russian sites (Figure 1) were collected from published reports and the authors' own research materials (Keally and Muto 1982; Kuzmin 1998, 2001, 2002; Kuzmin and Keally 2001; Kuzmin and Orlova 2000; Nakamura et al. 2001; Taniguchi 2002); these were critically evaluated. For Japan, the 97 most reliable age measurements from 30 sites clarify the ¹⁴C ages of the 4 oldest phases of pottery development there (Keally et al. 2003). For the present study, we included only the 28 earliest pottery-associated dates, those belonging to Phases 1 and 2 (Table 1). For the Russian Far East, the ¹⁴C dates of the Osipovka and Gromatukha cultural complexes in the Amur River basin were included (Table 1). To evaluate the reliability of the age of the earliest Russian pottery, both ¹⁴C dating of pottery temper (sedge grass, *Carex* sp.) and thermoluminescent (TL) dating of potsherds were performed. For the Chinese sites (Figure 1), the most recent summaries were used (Zhang 1999, 2002; Zhao and Wu 2000; Wu and Zhao 2003). Data from the Xianrendong, Miaoyan, Yuchanyan, and Diaotonghuan sites were incorporated and critically evaluated. These sites are all located south of the Yangtze River. Due to uncertainty about the direct association of ¹⁴C values and earliest pottery in southern China (see below), only the most reliable ¹⁴C pottery-associated dates are given (Table 1), and problematic dates are discussed separately. For consistency, original Chinese dates were re-calculated for the Libby ¹⁴C half-life value, 5568 yr, whenever necessary.

¹Sophia University, 4 Yonban-cho, Chiyoda-ku, Tokyo 102-0081, Japan. Email: c-keally@t-net.ne.jp.

²Kokugakuin University, 4-10-28 Higashi, Shibuya-ku, Tokyo 150-8440, Japan. Email: stoneage@h7.dion.ne.jp.

³Pacific Institute of Geography, Far Eastern Branch of the Russian Academy of Sciences, Radio St. 7, Vladivostok 690041, Russia. Corresponding author. Email: ykuzmin@tig.dvo.ru.

⁴Grodekov's State Museum, Turgenev St. 86, Khabarovsk 680000, Russia. Email: amur_neo@yahoo.com.

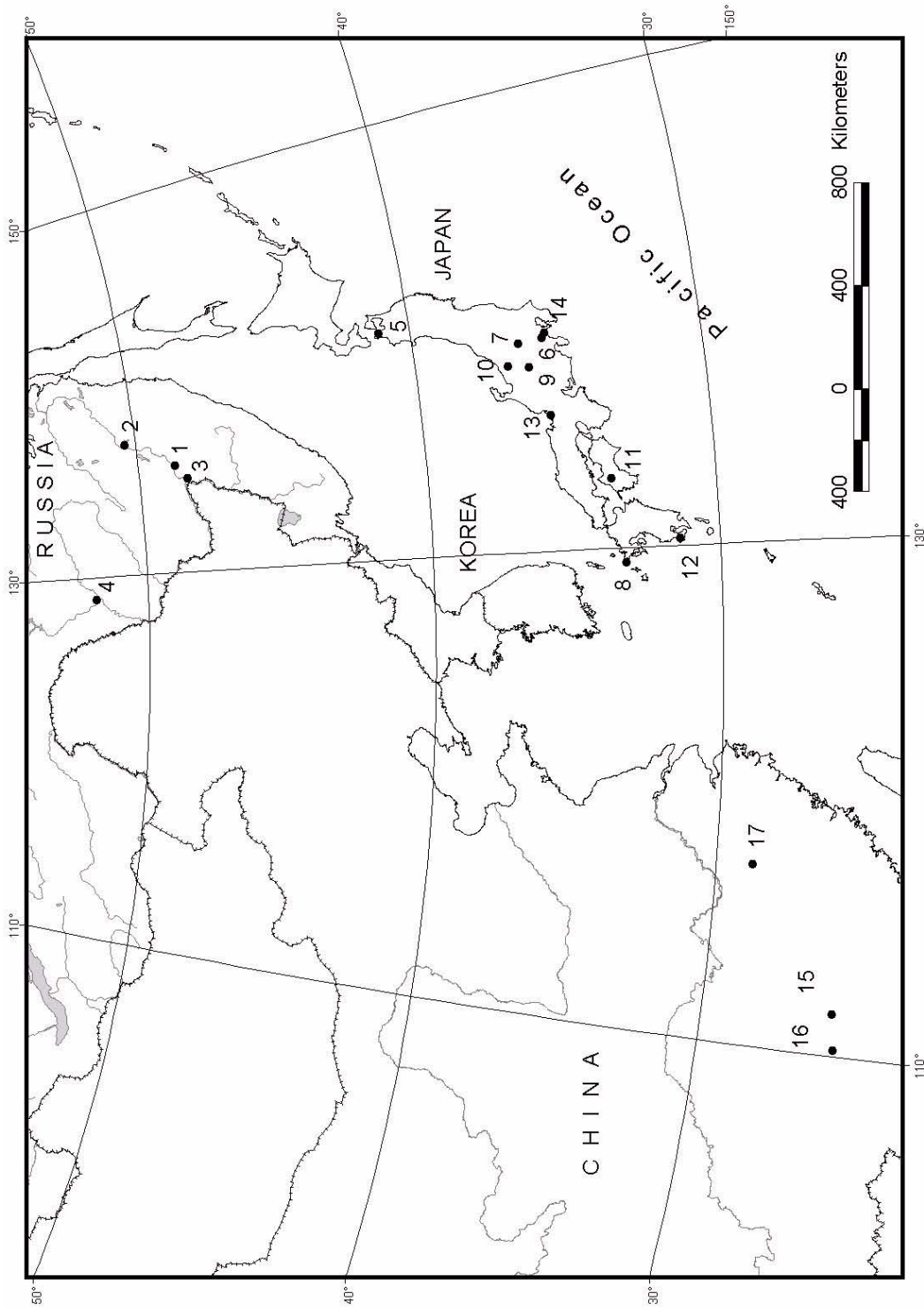


Figure 1 Location of the earliest sites with pottery in East Asia: 1–Gasya; 2–Khummi; 3–Goncharka 1; 4–Gromatukha; 5–Odai Yamamoto 1; 6–Kitahara; 7–Tokumaru Nakata; 8–Fukui Cave; 9–Nakajima B; 10–Seiko Sansou B; 11–Kamikuroiwa; 12–Sikazegashira; 13–Toriama; 14–Keio SFC; 15–Miaoyan; 16–Miaoyan; 17–Xianrendong.

Table 1 ^{14}C dates associated with the earliest pottery in East Asia (after Kuzmin and Jull 1997; Jull et al. 2001; Taniguchi 2002).

Nr	Site	Phase	Lab code & nr	Material dated	^{14}C age, BP ($\pm 1 \sigma$)	cal BP ($\pm 2 \sigma$) ^a
JAPAN						
1	Odai Yamamoto 1	1	NUTA-6510	adhesion	13,780 \pm 170	17,160–15,950
2	Odai Yamamoto 1	1	Beta-125550	charred wood	13,480 \pm 70	16,680–15,730
3	Odai Yamamoto 1	1	NUTA-6515	adhesion	13,210 \pm 160	16,470–14,750
4	Odai Yamamoto 1	1	NUTA-6507	adhesion	13,030 \pm 170	16,270–14,470
5	Odai Yamamoto 1	1	NUTA-6509	adhesion	12,720 \pm 160	15,880–14,240
6	Odai Yamamoto 1	1	NUTA-6506	adhesion	12,680 \pm 140	15,800–14,220
7	Kitahara	1	Beta-105398	charred wood	13,060 \pm 80	16,190–14,640
8	Kitahara	1	Beta-105401	charred wood	13,060 \pm 100	16,210–14,620
9	Kitahara	1	Beta-105400	charred wood	13,050 \pm 80	16,180–14,620
10	Kitahara	1	Beta-105403	charred wood	13,050 \pm 80	16,180–14,620
11	Kitahara	1	Beta-105402	charred wood	13,020 \pm 80	16,140–14,590
12	Tokumaru Nakata	2	PAL-381	wood	13,700 \pm 560	17,830–14,420
13	Tokumaru Nakata	2	PAL-383	wood	12,770 \pm 225	16,050–14,170
14	Tokumaru Nakata	2	PAL-384	wood	12,420 \pm 205	15,600–13,850
15	Tokumaru Nakata	2	PAL-380	wood	12,410 \pm 225	15,620–13,840
16	Tokumaru Nakata	2	PAL-379	wood	11,810 \pm 240	15,290–13,180
17	Tokumaru Nakata	2	PAL-382	wood	11,550 \pm 235	15,060–13,020
18	Fukui Cave, layer 3	2	Gak-950	charred wood	12,700 \pm 500	16,530–13,550
19	Nakajima B	2	I-13767	charred wood	12,460 \pm 310	15,850–13,820
20	Seiko Sanso B	2	Beta-133847	adhesion	12,340 \pm 50	15,480–14,110
21	Seiko Sanso B	2	Beta-133849	adhesion	12,160 \pm 40	15,390–13,840
22	Seiko Sanso B	2	Beta-133848	adhesion	12,000 \pm 40	15,310–13,660
23	Kamikuroiwa, layer 9	2	I-944	charred wood	12,165 \pm 600	16,130–12,980
24	Sikazegashira	2	Beta-118963	adhesion	11,860 \pm 50	15,230–13,620
25	Sikazegashira	2	Beta-118964	adhesion	11,780 \pm 50	15,170–13,470
26	Torihama	2	KSU-1028	wood	11,830 \pm 55	15,210–13,550
27	Torihama	2	KSU-1029	wood	11,800 \pm 55	15,190–13,480
28	Keio SFC	2	Gak-15904	charred wood	11,350 \pm 160	13,810–13,000
RUSSIAN FAR EAST						
29	Gasya	—	LE-1781	charcoal	12,960 \pm 120	16,110–14,480
30	Gasya	—	GEO-1413	charcoal	11,340 \pm 60	13,780–13,030
31	Gasya	—	AA-13393	charcoal	10,875 \pm 90	13,140–12,640
32	Khummi	—	AA-13392	charcoal	13,260 \pm 100	16,450–14,900
33	Khummi	—	SOAN-3583	charcoal	12,425 \pm 850	16,990–12,690
34	Khummi	—	AA-13391	charcoal	10,345 \pm 110	12,830–11,690
35	Goncharka 1	—	LLNL-102169	charcoal	12,500 \pm 60	15,550–14,160
36	Goncharka 1	—	AA-25437	charcoal	12,055 \pm 75	15,350–13,670
37	Goncharka 1	—	LLNL-102168	charcoal	10,590 \pm 60	12,940–12,190
38	Goncharka 1	—	AA-25438	charcoal	10,280 \pm 70	12,750–11,700
39	Goncharka 1	—	AA-25439	charcoal	10,280 \pm 70	12,750–11,700
40	Goncharka 1	—	Gak-18981	charcoal	9890 \pm 230	12,330–10,600
41	Gromatukha	—	AA-36079	charcoal	12,340 \pm 60	15,480–14,110
42	Gromatukha	—	AA-36447	charcoal	9895 \pm 50	11,550–11,200
SOUTHERN CHINA						
43	Yuachanyan, layer 3E	—	BA95058	charcoal	13,680 \pm 270	17,210–15,660
44	Miaoyan, layer 4M	—	BA92034	charcoal	13,320 \pm 270	16,780–14,720
45	Xianrendong, zone 3B1	—	UCR-3561	charcoal	12,430 \pm 80	15,530–14,130

^aCALIB rev. 4.3 software (Stuiver et al. 1998; <http://depts.washington.edu/qil/calib/>) was used for date calibration.

RESULTS AND DISCUSSION

Approximate dates of the earliest phases of Japanese Jomon culture have been known for a long time (Watanabe 1966; Keally and Muto 1982). These sources give the Phase 1 dates as about 13,000 BP, and for Phase 2, about 12,500–12,000 BP. The large number of additional ^{14}C dates collected during the past 20 yr, especially the AMS dates, have greatly improved the earliest pottery chronology in Japan (Taniguchi 2002). The most reliable measurements indicate the ages of the 2 earliest phases of pottery in Japan to be about 13,500–12,700 BP for Phase 1, and about 12,700–11,400 BP for Phase 2. The calibrated ^{14}C ages for the beginnings and endings of these phases are listed below:

- Phase 1, beginning at about 16,750–15,700 cal BP (approximately 14,800–13,750 cal BC);
- Phase 1/2 boundary, about 15,750–14,350 cal BP (approximately 13,800–12,400 cal BC);
- Phase 2, ending at about 13,500–13,150 cal BP (Keally et al. 2003).

In the Amur River basin in the Russian Far East, ^{14}C dates on charcoal indicate that the Osipovka culture comprises such sites as Gasya, Khummi, and Goncharka 1, and existed about 13,300–10,000 BP (approximately 16,100–11,700 cal BP or 14,150–9750 cal BC) (Table 1). The pottery temper ^{14}C dates for the Gasya and Khummi sites are about 12,000–9000 BP (O'Malley et al. 1999), which are generally close to the charcoal dates. The TL dates of the Gasya site pottery are $13,460 \pm 1460$, $10,430 \pm 1160$, and 8580 ± 1490 yr ago (Kuzmin et al. 2001). They are very close to the calibrated dates of the charcoal ^{14}C dates they correspond to in Table 1. The charcoal ^{14}C dates of the Gromatukha site are of about 12,340–9900 BP (approximately 15,500–11,200 cal BP or 13,550–9250 cal BC) (Table 1). The pottery temper ^{14}C dates are in the range from about 13,300 to about 7300 BP (O'Malley et al. 1999; Jull et al. 2001).

There are several age determinations for the earliest pottery-bearing sites in southern China (Zhao and Wu 2000; Wu and Zhao 2003). Some of them—such as Bailiandong and Dushizai, dated to about 21,000–14,000 BP (An 1989; Wu and Zhao 2003: 17)—were considered as problematic and later were not associated with the Neolithic. The best studied sites associated with the earliest pottery in China are Yuchanyan, Miaoyan, and Xianrendong.

^{14}C dates from the Yuchanyan site are $13,680 \pm 270$ BP (BA95058) for charcoal from a layer with pottery and rice grains, and $14,390 \pm 230$ BP (BA95057b) and $11,970 \pm 120$ BP (BA95057a) for pottery organics (Zhao and Wu 2000). ^{14}C ages of $15,220 \pm 260$ BP (BA94137b) and $15,120 \pm 500$ BP (BA94137a) were obtained for organic matter in the pottery from layer 5 of the Miaoyan site. Earlier, a ^{14}C age of $13,320 \pm 270$ BP (BA92034-1) was obtained for charcoal from layer 4M of this site (Yuan et al. 1995; Wu and Zhao 2003). The underlying layer 5 was without pottery and dated to about 17,600 BP (Wu and Zhao 2003); this is consistent with the age of pottery-containing layers and potsherd organics. Organics in pottery for the Yuchanyan and Miaoyan sites might represent the time of clay formation, but not pottery manufacture, because pottery from both sites is not organic-tempered (Zhao 2002). Thus, dates range from about 15,200 BP to about 14,400 BP for these sites are less reliable, rather than charcoal dates, about 13,700–13,300 BP (Table 1). For the Diaotonghuan site, the newly released bone ^{14}C date from layer D is $15,090 \pm 210$ BP (BA00014) (Wu and Zhao 2003). No details about the degree of association of the dated sample and the pottery were provided, so this age determination must be considered a provisional one.

For the Xianrendong site, charcoal associated with pottery from zone 3B1 was dated to $12,430 \pm 80$ BP (UCR-3561) (MacNeish and Taylor 1995). There are also earlier ^{14}C dates reported for the Xianrendong site— $14,185 \pm 290$ BP (BA93181) for zone 3B1, and $15,180 \pm 90$ BP (UCR-3300) for zone 3 (MacNeish and Taylor 1995)—but these should be excluded from consideration

because there is a possibility that the cultural materials are mixed. For example, ^{14}C dates of $17,420 \pm 130$ BP (AA-15008) (MacNeish and Taylor 1995:83–84) and $16,440 \pm 190$ BP (BA00009) (Wu and Zhao 2003) were obtained from a stratigraphically higher layer in zone 3C1B, showing clearly that there is disturbance of the layers in the Xianrendong site. A new bone date from zone 3C1a is $15,210 \pm 190$ BP (BA00006) (Wu and Zhao 2003). Thus, the youngest ^{14}C age measurement from zone 3B1, about 12,430 BP (UCR-3561), is probably the most reliable age estimate for the earliest pottery-bearing component from this site. Lu (1999:95) estimates the age of the earliest pottery layers in the Xianrendong site as about 13,000 BP.

The origins of pottery technology in East Asia remains one of the main questions yet to be answered. Our present interpretation of the dates and materials available is that a) the oldest pottery in Japan, the Russian Far East, and southern China represents 3 independent origins, and b) none of these regions was influenced from any other outside source. We base this interpretation on 2 factors: 1) the oldest pottery in all 3 regions is typological very different, and 2) the dates are very similar, while the regions are quite distant.

The oldest pottery in Japan (Phase 1) is mostly plain ware; a few vessels with impressed or incised marks are also known, and some vessels have fiber tempering. The forms are not clear; however, some vessels had flat bases. Linear-relief and bean-relief wares mark phase 2 of Incipient Jomon. Vessel shapes are somewhat varied and both pointed bases and flat bases occur. In the Amur River basin, the Osipovka complex pottery from the Gasya and Khummi sites has flat bottoms, thick walls (up to 1.7 cm), and a clay matrix tempered with grass. The design is represented by vertical grooves on the external surface (Derevianko and Medvedev 1993). At the Goncharka site, there is no plant-fiber tempering in the potsherds, and the design is more elaborate compared with Gasya and Khummi, with cord and comb impressions and vertical zigzags. The Gromatukha pottery is flat-based with grooves on both sides and plant-fiber temper (Okladnikov and Derevianko 1977). In southern China, the earliest pottery from the Xianrendong site has round bottoms and stripe-marked designs and it is tempered with coarse quartzite grains. Other early pottery types from the Xianrendong site have cord-marked designs and woven patterns; plain pottery also was discovered there (Zhang 2002). The Yuchanyan site pottery also has round bottoms and cord-marked designs and it is tempered with quartzite grains. The Miaoyan site pottery does not have a definite design, but it is tempered with coarse quartzite grains (Zhang 2002).

CONCLUSION

In Japan, the earliest pottery can be dated to about 13,500 BP (about 16,750–15,700 cal BP). The beginning of pottery manufacture in the Amur River basin can be now dated to about 13,300 BP (about 16,500–14,900 cal BP). The most reliable ^{14}C age determinations for the earliest pottery complexes in southern China are in the range from approximately 13,700 to about 13,300 BP (about 17,200–14,700 cal BP). The oldest pottery in East Asia and in the whole Old World is now reliably dated to about 13,700–13,300 BP (about 17,200–14,700 cal BP) in 3 regions: 1) Japan, 2) lower and middle parts of the Amur River basin in the Russian Far East, and 3) southern China (Figure 2). Due to very different pottery types in these regions, it is probable that pottery-making originated in several places within East Asia independently, rather than being the result of migration or technological exchange.

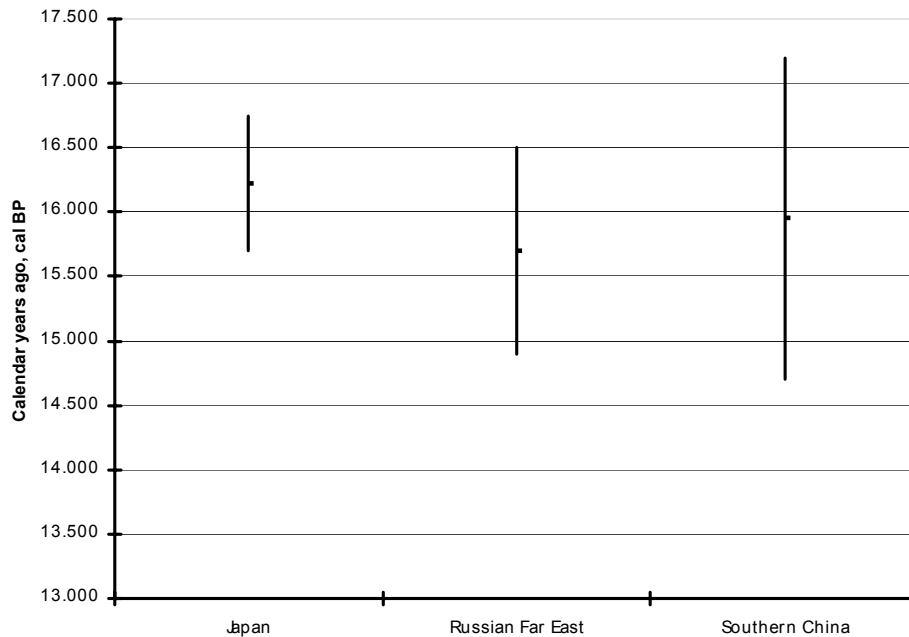


Figure 2 The calibrated ages for the beginning of pottery manufacture in East Asia

ACKNOWLEDGEMENTS

We are grateful to several colleagues who provided assistance in collection and evaluation of the data included into this review. Among them are Profs A P Derevianko, V E Medvedev, and M Budja; Drs Zhang C, Wu X, and Z S Lapshina, and Mr N N Zaitsev. We are also grateful to Dr B Obelić for useful comments. This research was supported by grants from several foundations, including RFFI, # 96-06-80688, 99-06-80348, and 02-06-07015; ISF (1995); IREX (1995); U.S. NSF, # EAR95-08413 and EAR97-30699; the Japan Foundation (1996); the Fulbright Program, # 21230 (1997); the BK21 Fund (2000), the Korea Foundation (2002), and Ministry of Education, Culture, Sports, Science and Technology of Japan (Mombu-Kagakusho) (2003).

REFERENCES

- An Z. 1989. Application of ^{14}C dating to the Early Neolithic in South China. *Di Si Yanjiu* 6(2):123–33.
- Derevianko AP, Medvedev VE. 1993. *Issledovaniya poseleniya Gasya (predvaritelnye rezultaty, 1980 god)* [The study of the Gasya site (preliminary results of the 1980 excavations)]. Novosibirsk: Institut Arkheologii i Etnografii SO RAN. 110 p.
- Jull AJT, Burr GS, Derevianko AP, Kuzmin YV, Shevkunov IY. 2001. Radiouglerodnaya khronologiya perekhoda ot paleolita k neolitu v Priamurie (Dalny Vostok Rossii) [The radiocarbon chronology of the Paleolithic-Neolithic transition in the Amur River basin, Russian Far East]. In: Derevianko AP, Medvedev GI, editors. *Sovremennye problemy evraziiskogo paleolitovedeniya*. Novosibirsk: Izdatelstvo Instituta Arkheologii i Etnografii SO RAN. p 140–2.
- Keally CT, Muto Y. 1982. Jomon jidai no nendai [Dating of the Jomon period]. In: Kato S, Kobayashi T, Fujimoto T, editors. *Jomon Bunka no Kenkyu*. Vol. 1. Tokyo: Yuzankaku. p 246–75.
- Keally CT, Taniguchi Y, Kuzmin YV. 2003. Understanding the beginnings of pottery technology in Japan and neighbouring East Asia. *The Review of Archaeology* 24(2):3–14.
- Kuzmin YV, editor. 1998. *Radiouglerodnaya khronologiya drevnikh kultur kamennogo veka Severo-Vostochnoi Azii* [Radiocarbon chronology of the Stone Age of Northeast Asia]. Vladivostok: Tikhookeansky Institut Geografii DVO RAN. 126 p.
- Kuzmin YV. 2001. Radiocarbon chronology of Paleolithic and Neolithic cultural complexes from the Russian Far East. *Journal of East Asian Archaeology*

- 3(3-4):227-54.
- Kuzmin YV. 2002. The earliest centers of pottery origin in the Russian Far East and Siberia: review of chronology of the oldest Neolithic cultures. *Documenta Praehistorica* 29:37-46.
- Kuzmin YV, Hall S, Tite MS, Bailey R, O'Malley JM, Medvedev VE. 2001. Radiocarbon and thermoluminescence dating of the pottery from the early Neolithic site of Gasya (Russian Far East): initial results. *Quaternary Science Reviews* 20:945-8.
- Kuzmin YV, Jull AJT. 1997. AMS radiocarbon dating of the Paleolithic-Neolithic transition in the Russian Far East. *Current Research in the Pleistocene* 14:46-8.
- Kuzmin YV, Keally CT. 2001. Radiocarbon chronology of the earliest Neolithic sites in East Asia. *Radiocarbon* 43(2B):1121-8.
- Kuzmin YV, Orlova LA. 2000. The Neolithization of Siberia and the Russian Far East: radiocarbon evidence. *Antiquity* 74(284):356-65.
- Lu TL-D. 1999. *The Transition from Foraging to Farming and the Origin of Agriculture in China (BAR International Series 774)*. Oxford: John and Erica Hedges Ltd. 233 p.
- MacNeish RS, Taylor RE. 1995. Chronometrics. In: MacNeish RS, Libby JG, editors. *Origins of Rice Agriculture: the Preliminary Report of the Sino-American Jiangxi (PRC) Project SAJOR (Publications in Anthropology No. 13, El Paso Centennial Museum)*. El Paso, Texas: The University of Texas at El Paso. p 77-86.
- Morlan RE. 1967. Chronometric dating in Japan. *Arctic Anthropology* 4(2):180-211.
- Nakamura T, Taniguchi Y, Tsuji S, Oda H. 2001. Radiocarbon dating of charred residues on the earliest pottery. *Radiocarbon* 43(2B):1129-38.
- Okladnikov AP, Derevianko AP. 1977. *Gromatukhinskaya Kultura* [The Gromatukha Culture]. Novosibirsk: Nauka Publishers. 286 p.
- O'Malley JM, Kuzmin YV, Burr GS, Donahue DJ, Jull AJT. 1999. Direct radiocarbon AMS dating of the earliest pottery from the Russian Far East and Transbaikalia. *Mémoires de la Société Préhistorique Française* 26:19-24.
- Stuiver M, Reimer PJ, Bard E, Beck JW, Burr GS, Hughen KA, Kromer B, McCormac G, van der Plicht J, Spurk M. 1998. INTCAL98 radiocarbon age calibration, 24,000-0 cal BP. *Radiocarbon* 40(3):1041-83.
- Taniguchi Y. 2002. Nihon oyobi Kyokuto ni okeru doki shutsugen no nendai [Dating of the oldest pottery culture in Japan and the Far East]. *Kokugakuin Daigaku Kokogaku Shiryokan Kiyo* 18:45-67.
- Watanabe N. 1966. Radiocarbon dates of the Jomon and Yayoi periods in Japan. *Daiyonki Kenkyu* 5(3-4):157-68.
- Wu X, Zhao C. 2003. Chronology of the transition from Palaeolithic to Neolithic in China. *The Review of Archaeology* 24(2):15-20.
- Yuan S, Zhou G, Guo Z, Zhang Z, Gao S, Li K, Wang J, Liu K, Li B, Lu X. 1995. ¹⁴C AMS dating the transition from the Paleolithic to the Neolithic in South China. *Radiocarbon* 37(2):245-9.
- Zhang C. 1999. The Mesolithic and the Neolithic in China. *Documenta Praehistorica* 26:1-13.
- Zhang C. 2002. The discovery of early pottery in China. *Documenta Praehistorica* 29:29-35.
- Zhao C, Wu X. 2000. The dating of Chinese early pottery and a discussion of some related problems. *Documenta Praehistorica* 27:233-9.

CHRONOLOGY OF PREHISTORIC CULTURAL COMPLEXES OF SAKHALIN ISLAND (RUSSIAN FAR EAST)

Yaroslav V Kuzmin^{1,2} • Alexander A Vasilevski³ • Sergei V Gorbunov⁴ • G S Burr⁵ • A J Timothy Jull^{5,6} • Lyobov A Orlova⁷ • Olga A Shubina⁸

ABSTRACT. A chronological framework for the prehistoric cultural complexes of Sakhalin Island is presented based on 160 radiocarbon dates from 74 sites. The earliest ¹⁴C-dated site, Ogonki 5, corresponds to the Upper Paleolithic, about 19,500–17,800 BP. According to the ¹⁴C data, since about 8800 BP, there is a continuous sequence of Neolithic, Early Iron Age, and Medieval complexes. The Neolithic existed during approximately 8800–2800 BP. Transitional Neolithic-Early Iron Age complexes are dated to about 2800–2300 BP. The Early Iron Age may be dated to about 2500–1300 BP. The Middle Ages period is dated to approximately 1300–300 BP (VII–XVII centuries AD).

INTRODUCTION

Sakhalin Island in the Russian Far East, known as the “landbridge” which connects the northern part of the Japanese archipelago with mainland Asia, is important for the study of prehistoric human migrations in Northeast Asia. The first radiocarbon dates of the archaeological sites on Sakhalin Island were obtained in the 1970s (Vasilievsky and Golubev 1976), but during the following decades, the chronology of the prehistoric cultural complexes on Sakhalin (cf. Shubin and Shubina 1987; Vasilevski 1995) was studied inadequately compared to the neighboring mainland Russian Far East (cf. Kuzmin 2001; Kuzmin et al. 1994, 1998a). During the last few years, dozens of new ¹⁴C dates were obtained from Paleolithic, Neolithic, and Early Iron Age complexes on Sakhalin. Here, we present the first systematic study of the ¹⁴C chronology of Sakhalin Island prehistory, and the main aim is to give original data and its interpretation to scholars who study the archaeology and paleoecology of Northeast Asia.

MATERIALS AND METHODS

The prehistory of Sakhalin may be sub-divided into several periods, namely Paleolithic, Neolithic, Early Iron Age, and the Middle Ages (Golubev and Lavrov 1988; Vasilevski 1992, 1995, 2000). The definition of the Neolithic in the Russian Far East is mostly based on the presence of pottery in the artifact assemblage (Kuzmin and Orlova 2000; Kuzmin 2003). The term “Early Iron Age” in Sakhalin is close to that of “Paleometal” in the mainland Russian Far East (Aleksandrov et al. 1982), and this definition is used for the complexes which existed after the Neolithic but are lacking metal production. There are several cultural complexes associated with the transition from the Neolithic to the Early Iron Age. Due to the small scale of excavations at some sites, they can not be affiliated with a particular culture and are indicated as an “unidentified culture” (Table 1, see pages 359–362).

¹Pacific Institute of Geography, Russian Academy of Sciences, Radio St. 7, Vladivostok 690041, Russia.

²Corresponding author. Email: ykuzmin@tig.dvo.ru.

³Department of History, Sakhalin State University, Lenin St. 290, Yuzhno-Sakhalinsk 693008, Russia.
Email: vasilevski@sakhgu.ru.

⁴Tymovsky Museum, Kharitonov St. 14, Tymovsky, Sakhalin District 694400, Russia.

⁵NSF-Arizona AMS Facility, University of Arizona, Tucson, AZ 85721-0081, USA. Email: burr@u.arizona.edu.

⁶Email: jull@u.arizona.edu.

⁷Institute of Geology, Russian Academy of Sciences, Koptyug Ave. 3, Novosibirsk 630090, Russia.

Email: orlova@uiggm.nsc.ru.

⁸Sakhalin State Museum, Kommunistichesky Ave. 29, Yuzhno-Sakhalinsk 693010, Russia. Email: isam@ostrov.sakhalin.ru.

The chronology of the prehistoric complexes of Sakhalin is now based on about 160 ^{14}C dates (Table 1) from 74 sites (Figure 1). Dates were produced mostly in 3 laboratories located in Novosibirsk, Tucson, and Magadan (86% of the total amount). The main material dated was wood charcoal (89%) and burnt food attached to the pottery (10%). Calibration of ^{14}C dates was done with the help of the CALIB rev. 4.3 software (Stuiver et al. 1998).

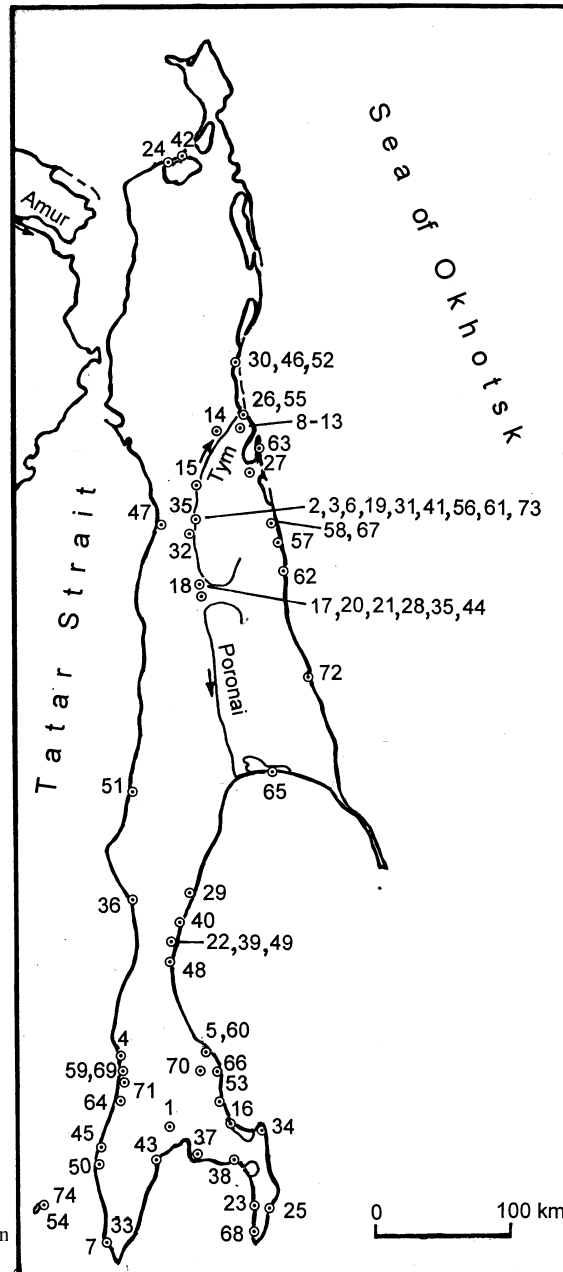


Figure 1 The location of ^{14}C -dated sites on Sakhalin Island (numbers correspond to those in Table 1).

RESULTS AND DISCUSSION

There is a single ^{14}C -dated Paleolithic site on Sakhalin, Ogonki 5 (Vasilevski 2003) (Table 1, nr 1). The series of dates shows that it existed at approximately 19,500–17,800 BP, during the Last Glacial Maximum (Kuzmin et al. 1998b). After about 17,900 BP, there is a hiatus in the prehistoric chronology of Sakhalin until about 8800 BP (Figure 2). Recently produced ^{14}C dates for the Ostantsevaya cave ($11,140 \pm 100$ BP, SOAN-5178; and 8040 ± 85 BP, SOAN-5176) allow placement of the Final Paleolithic of Sakhalin after about 11,100 BP. However, the time of the Paleolithic-Neolithic transition on Sakhalin is still uncertain, compared with the mainland Russian Far East where it occurred at approximately 13,300–10,300 in the Amur River basin and at about 10,800–9300 BP in Primorye (Jull et al. 2001; Kuzmin 2003).

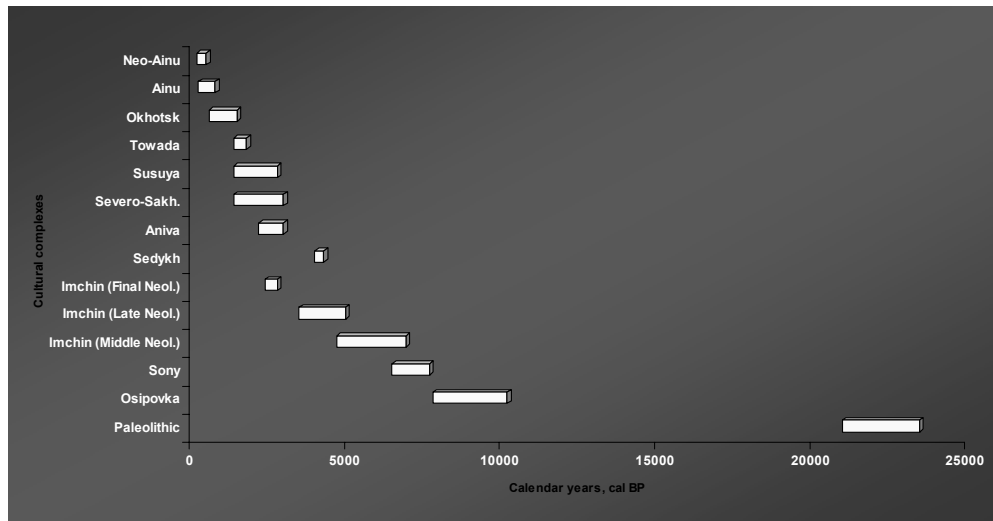


Figure 2 Calibrated ages of the main archaeological complexes of Sakhalin Island

The Neolithic of Sakhalin may be sub-divided into Early, Middle, and Late stages (Table 1). The Early Neolithic or the Paleolithic-Neolithic transitional site of Sokol has no ^{14}C dates; it was dated by the obsidian hydration method to about 11,800 yr ago, but no pottery was found at this site. The first pottery-containing assemblage is associated with the Early Neolithic at the Puzi 2 site and is dated to about 8800 BP. The Early Neolithic sites dated to approximately 8800–7000 BP may be roughly associated with the Osipovka culture, which could have survived at the Sakhalin after it disappeared in the lower stream of the Amur River at about 10,000 BP (Kuzmin 2001, 2002, 2003). The Middle Neolithic is associated with the Yuzhno-Sakhalinsk culture, earlier identified by Japanese scholars as Sony, and it existed at about 6700–5800 BP. The Imchin culture, originally determined as a single complex (Vasilievsky and Golubev 1976), now may be sub-divided into 3 components belonging to the Middle and Late Neolithic and to the Neolithic-Early Iron Age transition (Table 1). The earliest Imchin component is dated to about 5900–4300 BP and the middle component to about 4100–3300 BP. The latest Imchin culture sites correspond to approximately 2600–2500 BP (~970–260 cal BC) (Vasilevski 1995). A single ^{14}C date, about 3800 BP, is associated with the Sedykh culture of the Late Neolithic.

The Neolithic-Early Iron Age transition on Sakhalin continued for a long time, during about 2600 to 1700 BP. At that time, the Aniva culture (as part of the early Epi-Jomon sphere) existed in southern

Sakhalin at approximately 2800–2300 BP (~1000–200 cal BC). The Susuya culture, located in southern and central Sakhalin, is dated to about 2500–1600 BP (~800 cal BC–800 cal AD). Two ¹⁴C dates, 2750 ± 150 BP (MAG-693) from the Kuznetsovo 1 site and 2700 ± 200 BP (MAG-692) from the Svobodnoe 1 site, are earlier than the rest of the values for the Susuya culture (Table 1). It is possible that a hearth at Kuznetsovo 1 dated to about 2750 BP might correspond to the Late Jomon or the earliest Epi-Jomon component. At Svobodnoe 1, a small test pit was excavated, and it is not clear if, besides the Susuya component, earlier cultural component might exist at this site. The Severo-Sakhalinsk (Nhabil) culture, located in northern and central Sakhalin, may be provisionally dated to about 2900–1100 BP (~1400 cal BC–1150 cal AD).

The Towada culture is associated with the Early Iron Age period; 2 ¹⁴C dates place it at about 1600 BP (~200–700 cal AD). Taking into account the few late dates of the Susuya culture (~1600–1500 BP), we can determine the existence of the Towada culture during the V–VII centuries AD. The most important Early Iron Age complex on Sakhalin is the Okhotsk culture, widely distributed also in Hokkaido and the southern Kurile Islands (Vasilievsky and Golubev 1976; Vasilevski 1990; Amano and Vasilevski 2002). According to the most recent ¹⁴C dates and archaeological information, the Okhotsk culture existed in southern and central Sakhalin at about 1400–800 BP (~500–1300 cal AD) (Table 1). There are some earlier ¹⁴C dates which may be associated with the Okhotsk culture (Nevelsk 1, Venskoe 2, Ivanovka, and Sedykh 1 sites, ~2100–1800 BP), and additional study is necessary to establish the exact timing of this cultural complex. The Middle Ages period on Sakhalin is associated with the Ainu (or Neiji) and Neo-Ainu cultures, at about 800–200 BP (~1300–1800 cal AD).

Using the chronological outline for ancient cultural complexes of the Sakhalin Island, it is possible to firmly date the important events in the prehistoric economy. The exchange of high-quality raw material for stone tool manufacture, namely obsidian, between Sakhalin Island (where it does not occur) and the neighboring sources on Hokkaido Island, began as early as the Upper Paleolithic, about 19,500 BP (Kuzmin et al. 2002). Obsidian exchange was practiced for most of the prehistory of Sakhalin, until about 1500 BP. The distance of exchange in the Upper Paleolithic was about 300 km, and since the Early Neolithic (~10,000–8000 BP), it increased to up to 1000 km.

The earliest evidence of maritime adaptation on Sakhalin, such as seal hunting, corresponds to the Early Neolithic (~6000 BP). Shellfish exploitation was most intensive during the Neolithic–Early Iron Age transition and the Early Iron Age (mainly the Susuya and Okhotsk cultures) in southern and central Sakhalin, at about 2700–800 BP.

CONCLUSION

Recent ¹⁴C dating of the prehistoric cultural complexes of Sakhalin Island allows us to establish the main chronological framework (Figures 2 and 3). The Upper Paleolithic was ¹⁴C dated to about 19,500–17,800 BP (~21,500–19,000 cal BC or ~23,500–21,000 cal BP) (Figure 2). At about 8800 BP (~8200–7600 cal BC or ~10,100–9600 cal BP), pottery appeared on Sakhalin for the first time and marked the beginning of the Early Neolithic (Figure 3). The Middle Neolithic (Sony and middle stage of the Imchin complex) is dated to approximately 6700–4300 BP (~5700–2700 cal BC or ~7700–4700 cal BP). The Imchin culture can now be sub-divided into 2 main complexes: the early complex is dated to about 5900–4300 BP (~4950–2700 cal BC or ~7900–6300 cal BP) and the late one to about 4100–3300 BP (~3000–1500 cal BC or ~5000–3500 cal BP). Several Middle and Late Neolithic sites without clear cultural complex affiliation were dated to about 5500–2900 BP. The Neolithic–Early Iron Age transitional Epi-Jomon complex represented by the Aniva culture was

dated to about 2800–2300 BP (~1000–200 cal BC or ~3000–2200 cal BP). The Early Iron Age complexes are dated to about 1600–600 BP (~200 cal BC–1400 cal AD or ~1800–600 cal BP). The Ainu and Neo-Ainu complexes, attributed to the Middle Ages, are dated to about 800–200 BP (~1200–1800 cal AD or ~800–150 cal BP). Intensive contacts between the Sakhalin and Hokkaido islands began very early, at least at about 19,500 BP. Marine food resource exploitation in southern Sakhalin was practiced in the Middle and Late Holocene at about 6000–1500 BP.

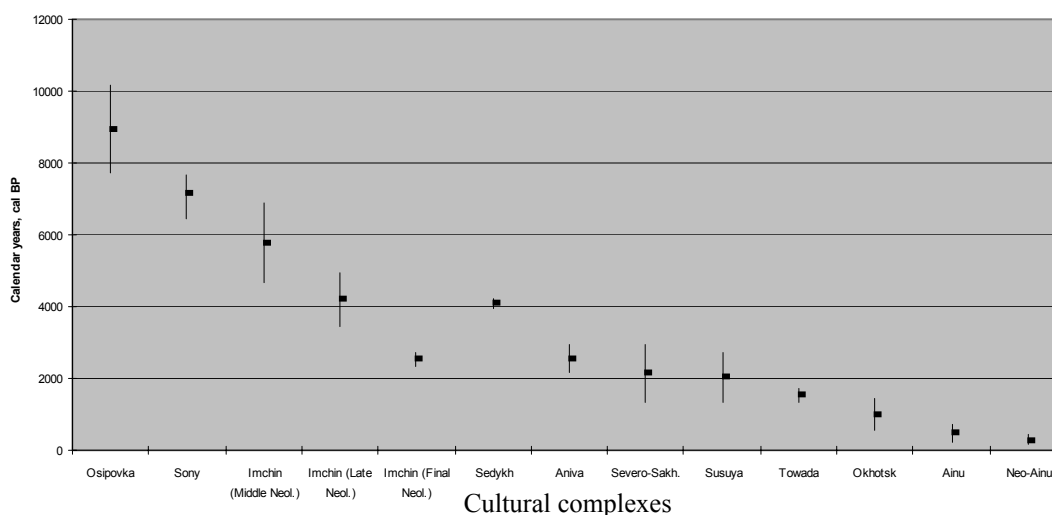


Figure 3 Calibrated ages of the Neolithic, Early Iron Age, and Middle Ages archaeological complexes of Sakhalin Island (ambiguous dates and values with a large standard deviation were not used).

ACKNOWLEDGEMENTS

We are grateful to colleagues who conducted the ^{14}C dating of the Sakhalin archaeological sites prior to our studies, Drs A V Lozhkin, G I Zaitseva, T Nomura, V I Razov, and Y A Mikishin; Mr V G Volkov and Mr A V Orishchenko. We are also grateful to Dr S G Keates for grammar polishing and to Dr B Obelić for useful comments of the earlier version of this paper. This study was supported partly by grants from US NSF (EAR97-30699, EAR01-15488) and Russian RFFI (96-06-80688, 02-06-80282).

REFERENCES

- Aleksandrov AV, Arutyunov SA, Brodiansky DL. 1982. *Paleometall severo-zapadnoi chasti Tikhogo okeana* [Paleometal of the Northwestern Part of the Pacific Ocean]. Vladivostok: Izdatelstvo Dalnevostochnogo Universiteta. 103 p.
- Amano T, Vasilevski AA, editors. 2002. *The Okhotsk Culture Formation, Metamorphosis and Ending*. Proceedings of the 5th Open Symposium of the Hokkaido University Museum. Sapporo: Hokkaido University Museum. 174 p.
- Golubev VA, Lavrov EL. 1988. *Sakhalin v epokhu kamnya* [Sakhalin in the Stone Age]. Novosibirsk: Nauka Publishers. 240 p.
- Jull AJT, Burr GS, Derevianko AP, Kuzmin YV, Shevkovud IY. 2001. Radiouglerodnaya khronologiya perekhoda ot paleolita k neolitu v Priamurie (Dalny Vostok Rossii) [The radiocarbon chronology of the Paleolithic-Neolithic transition in the Amur River basin, Russian Far East]. In: Derevianko AP, Medvedev GI, editors. *Sovremennye problemy evraziiskogo paleolitovedeniya*. Novosibirsk: Izdatelstvo Instituta Arkheologii i Etnografii SO RAN. p 140–2.
- Kuzmin YV. 2001. Radiocarbon chronology of Paleolithic and Neolithic cultural complexes from the Russian Far East. *Journal of East Asian Archaeology* 3(3–4):227–54.
- Kuzmin YV. 2002. The earliest centers of pottery origin in the Russian Far East and Siberia: review of chronol-

- ogy of the oldest Neolithic cultures. *Documenta Praehistorica* 29:37–46.
- Kuzmin YV. 2003. The Paleolithic-Neolithic transition and the origin of pottery production in the Russian Far East: a geoarchaeological approach. *Archaeology, Ethnology and Anthropology of Eurasia* 4(3):16–26.
- Kuzmin YV, Glascock MD, Sato H. 2002. Sources of archaeological obsidian on Sakhalin Island (Russian Far East). *Journal of Archaeological Science* 29(7):741–50.
- Kuzmin YV, Jull AJT, Orlova LA, Sulerzhitsky LD. 1998a. Radiocarbon chronology of the Stone Age cultures, Russian Far East. *Radiocarbon* 40(1):675–86.
- Kuzmin YV, Orlova LA. 2000. The Neolithization of Siberia and the Russian Far East: radiocarbon evidence. *Antiquity* 74(284):356–65.
- Kuzmin YV, Orlova LA, Sulerzhitsky LD, Jull AJT. 1994. Radiocarbon dating of the Stone and Bronze Age sites in Primorye (Russian Far East). *Radiocarbon* 36(3):359–66.
- Kuzmin YV, Vasilevski AA, O'Malley JM, Jull AJT. 1998b. The age and environment of the Paleolithic occupation of Sakhalin Island, the Russian Far East. *Current Research in the Pleistocene* 15:124–6.
- Shubin VO, Shubina OA. 1987. Novye radiouglerodnye datirovki arkheologicheskikh pamyatnikov Sakhalinskoi oblasti [The new radiocarbon dates of the archaeological sites in the Sakhalin Province]. In: Larichev VE, editor. *Drevnosti Sibiri i Dalnego Vostoka*. Novosibirsk: Nauka Publishers. p 95–103.
- Stuiver M, Reimer PJ, Bard E, Beck JW, Burr GS, Hughen KA, Kromer B, McCormac G, van der Plicht J, Spurk M. 1998. INTCAL98 radiocarbon age calibration, 24,000–0 cal BP. *Radiocarbon* 40(3):1041–83.
- Vasilevski AA. 1990. *Formirovanie okhotskoi kultury na Sakhaline (1-e tys. do n. e.)* (The formation of the Okhotsk culture at the Sakhalin [1st millennium BC]). [PhD dissertation synopsis]. Kemerovo: Kemerovskiy Gosudarstvennyy Universitet. 14 p.
- Vasilevski AA. 1992. Neolithic cultures of the Sakhalin Island. *Hokkaido Kokogaku* 28:115–36.
- Vasilevski AA. 1995. Kalibrovka radiouglerodnykh datirovok i khronologiya arkheologicheskikh kultur Sakhalina [Calibration of radiocarbon dates and chronology of archaeological cultures at the Sakhalin]. *Kraevedchesky bulletin* 2:93–110.
- Vasilevski AA. 2000. K ponyatiyu “Neolit” i ego periodizatsii na ostrove Sakhalin [About the term “Neolithic” and its periodization at the Sakhalin Island]. In: Vostretsov YE, Klyuev NA, editors. *Vpered...v proshloe*. Vladivostok: Dalnauka Publishers. p 150–60.
- Vasilevski AA. 2003. Periodization and classification of the Upper Paleolithic of Sakhalin and Hokkaido in the light of the research conducted at the Ogonki-5 site. *Archaeology, Ethnology and Anthropology of Eurasia* 4(3):51–69.
- Vasilievsky RS, Golubev VA. 1976. *Drevnie poseleniya na Sakhaline (Susuiszkaya stoyanka)* [The Ancient Settlements on the Sakhalin (Susuya site)]. Novosibirsk: Nauka Publishers. 271 p.

Table 1 ¹⁴C dates for the prehistoric sites on Sakhalin Island.

Site nr ^a	Site name	Coordinates ° ' N / ° ' E	¹⁴ C date, BP (±1 σ)	Calibrated age ^b	Lab code and nr	Material dated ^c	Cultural affiliation ^d
UPPER PALEOLITHIC							
1	Ogonki 5	46 46 / 142 28	19,440 ± 140	21,520–20,710 BC	Beta-115987	C	
			19,380 ± 190	21,470–20,620 BC	Beta-115986	C	
			19,320 ± 145	21,380–20,570 BC	AA-20864	C	
			18,920 ± 150	20,900–20,120 BC	AA-25434	C	
			17,880 ± 120	19,670–18,960 BC	AA-23137	C	
NEOLITHIC							
Early and Middle Neolithic							
2	Puzi 2	51 09 / 142 39	8780 ± 135	8200–7600 BC	SOAN-3819	C	Os
			7790 ± 65	6980–6460 BC	AA-36388	C	Os
			7610 ± 60	6590–6270 BC	AA-36389	C	Os
			7535 ± 135	6470–6230 BC	SOAN-4064	C	Os
			7520 ± 70	6460–6230 BC	AA-36387	C	Os
3	Ado-Tymovo 4	51 08 / 142 40	7035 ± 40	5990–5810 BC	AA-36391	C	Os
4	Sadovniki 2	47 10 / 142 04	6740 ± 150	5740–5510 BC	MAG-694	C	YS (S)
			6100 ± 300	5370–4620 BC	MAG-691	C	YS (S)
5	Starodubskoye 3	47 25 / 142 49	6465 ± 85	5610–5300 BC	TIG-269	C	YS (S)
6	Ado-Tymovo 5	51 09 / 142 40	6190 ± 40	5300–5000 BC	AA-36437	C	UEN
7	Kuznetsovo 3	46 04 / 141 56	5960 ± 140	5000–4690 BC	LE-4044	C	YS (S)
			5770 ± 140	4780–4460 BC	LE-4043	C	YS (S)
8	Imchin 2	51 42 / 143 01	5890 ± 90	4950–4540 BC	SOAN-1145	C	MNI
			5650 ± 250	4780–4250 BC	MAG-680	C	MNI
			4750 ± 300	3910–3100 BC	MAG-674	C	MNI
			4550 ± 100	3500–3100 BC	MAG-683	C	MNI
			4250 ± 30	2910–2710 BC	SOAN-1040	C	MNI
Late Neolithic							
8	Imchin 2	51 42 / 143 01	4100 ± 200	2900–2350 BC	MAG-688	C	LNI
			4060 ± 50	2860–2470 BC	SOAN-1041	C	LNI
			3700 ± 250	2470–1740 BC	MAG-673	C	LNI
			3500 ± 100	1940–1690 BC	MAG-689	C	LNI
			3400 ± 80	1890–1520 BC	MAG-671	C	LNI
9	Imchin 10	51 42 / 143 01	4200 ± 200	3020–2490 BC	MAG-686	C	LNI
10	Imchin 11	51 42 / 143 01	4200 ± 200	3020–2490 BC	MAG-688	C	LNI
11	Imchin 4	51 42 / 143 01	4040 ± 85	2880–2310 BC	SOAN-1148	C	LNI
			3730 ± 70	2400–1920 BC	SOAN-1149	C	LNI
			3490 ± 75	2030–1620 BC	SOAN-1147	C	LNI
			3950 ± 100	2580–2290 BC	MAG-690	C	LNI
			3500 ± 100	1940–1690 BC	MAG-687	C	LNI
12	Imchin 7	51 42 / 143 01	3750 ± 150	2460–1940 BC	MAG-685	C	LNI
13	Imchin 12	51 42 / 143 01	3430 ± 70	1920–1530 BC	MAG-745	C	LNI
			3340 ± 20	1690–1530 BC	MAG-744	C	LNI
14	Tym-Zona	51 43 / 143 00	5470 ± 45	4430–4250 BC	AA-37188	BF	UN
15	Chkharnya	51 23 / 142 44	5440 ± 40	4350–4170 BC	AA-37079	C	UN
5	Starodubskoye 3	47 24 / 142 49	4500 ± 140	3490–2920 BC	SOAN-3580	C	UN
16	Sedykh, layer 2	46 51 / 143 09	4220 ± 55	2920–2600 BC	AA-23133	BF	UN
			3760 ± 50	2330–1980 BC	AA-23134	BF	S
17	Kirpichny 3	50 42 / 142 40	4140 ± 75	2900–2470 BC	SOAN-4066	C	UN
3	Ado-Tymovo 4		4110 ± 125	2880–2470 BC	SOAN-3821	C	UN
			3575 ± 50	2110–1750 BC	AA-36390	C	UN

Table 1 ^{14}C dates for the prehistoric sites on Sakhalin Island. (*Continued*)

Site nr ^a	Site name	Coordinates ° ' N / ° ' E	^{14}C date, BP ($\pm 1 \sigma$)	Calibrated age ^b	Lab code and nr	Material dated ^c	Cultural affiliation ^d
18	Yasnoye	50 38 / 142 41	4065 \pm 40	2860–2470 BC	AA-37463	C	UN
19	Puzi 4	51 10 / 142 39	3870 \pm 45	2470–2200 BC	SOAN-3717	C	UN
16	Sedykh 1	46 51 / 143 09	3760 \pm 40	2290–2040 BC	AA-37190	BF	UN
20	Beloje 1	50 44 / 142 39	3460 \pm 35	1880–1690 BC	AA-37078	C	UN
			3250 \pm 35	1620–1430 BC	AA-37125	C	UN
			2570 \pm 35	810–560 BC	AA-37226	C	UN (?)
			2200 \pm 35	380–170 BC	AA-37077	C	UN (?)
21	Kirpichny 12	50 41 / 142 40	3435 \pm 35	1880–1640 BC	AA-37127	C	UN
22	Pugachevo 7	48 11 / 142 34	3150 \pm 175	1620–1130 BC	SOAN-3564	C	UN
23	Yuzhnaya 2	46 18 / 143 24	3015 \pm 40	1390–1130 BC	AA-37824	BF	UN
			3005 \pm 125	1410–1020 BC	TIG-249	C	UN
24	Ush 4	53 32 / 142 18	2920 \pm 65	1370–920 BC	SOAN-3563	C	UN
TRANSITION FROM THE NEOLITHIC TO THE EARLY IRON AGE							
8	Imchin 2		2570 \pm 110	830–520 BC	MAG-672	C	FI
			2460 \pm 100	790–400 BC	MAG-670	C	FI
23	Yuzhnaya 2		2550 \pm 160	830–410 BC	LE-4038	C	An
			2450 \pm 100	790–400 BC	LE-4041	C	An
			2360 \pm 110	760–260 BC	LE-4040	C	An
			2320 \pm 160	760–180 BC	LE-4039	C	An
6	Ado-Tymovo 5		1905 \pm 100	20 BC–AD 240	SOAN-3723	C	SS (N)
25	Predreflyanka	46 33 / 143 33	2800 \pm 45	1050–830 BC	AA-23131	BF	An
			2740 \pm 45	990–800 BC	AA-25440	BF	An
26	Nyivo 9	51 51 / 143 11	2695 \pm 50	970–800 BC	SOAN-3248	C	SS (N)
27	Nhabyl 1	51 28 / 143 17	2495 \pm 40	790–410 BC	SOAN-3817	C	SS (N)
28	Beloje 3	50 43 / 142 40	2470 \pm 40	790–410 BC	AA-37125	C	UC
5	Starodubskoe 3		2265 \pm 50	400–180 BC	AA-20865	C	UC
29	Porechye 1	48 34 / 142 46	2365 \pm 35	520–390 BC	AA-37076	C	Su
			2315 \pm 35	410–260 BC	AA-37225	C	Su
			2180 \pm 35	380–120 BC	AA-37124	C	Su
31	Ado-Tymovo 16	50 10 / 142 41	2875 \pm 30	1210–940 BC	SOAN-3719	C	UC
32	Noksi 2	51 00 / 142 40	2870 \pm 90	1370–830 BC	NU-431	C	SS (N)
33	Kuznetsovo 1	46 04 / 141 56	2750 \pm 150	1110–800 BC	MAG-693	C	Su (?)
			2385 \pm 270	810–120 BC	DVGU-91	C	Su
34	Svobodnoye 1	46 48 / 143 26	2700 \pm 200	1110–560 BC	MAG-692	C	Su (?)
35	Ado-Tymovo 20	51 08 / 142 39	2610 \pm 165	920–460 BC	SOAN-3823	C	SS (N)
			2495 \pm 30	790–410 BC	SOAN-3822	C	SS (N)
			2200 \pm 35	380–170 BC	AA-36438	C	SS (N)
36	Ust-Ainskoye	48 27 / 142 04	2540 \pm 45	800–460 BC	AA-36621	BF	Su
37	Susuya	46 45 / 142 44	2520 \pm 35	800–450 BC	SOAN-782	C	Su
			2040 \pm 65	200 BC–AD 80	SOAN-783	C	Su
			1850 \pm 150	AD 1–380	SOAN-1025	C	Su
38	Ozersk 1	46 36 / 143 13	2360 \pm 35	520–390 BC	AA-37363	BF	Su
			2070 \pm 100	200 BC–AD 50	MAG-677	C	Su
			1920 \pm 55	40 BC–AD 240	SOAN-1019	C	Su
			1910 \pm 65	40 BC–AD 240	SOAN-1018	C	Su
			1750 \pm 100	AD 130–410	MAG-676	C	Su
39	Pugachevo 9	48 10 / 142 35	1600 \pm 100	AD 340–600	MAG-678	C	Su
			1590 \pm 200	AD 240–560	MAG-669	C	Su
			2315 \pm 55	480–210 BC	SOAN-3264	C	Su

Table 1 ^{14}C dates for the prehistoric sites on Sakhalin Island. (Continued)

Site nr ^a	Site name	Coordinates ° ' N / ° ' E	^{14}C date, BP ($\pm 1 \sigma$)	Calibrated age ^b	Lab code and nr	Material dated ^c	Cultural affiliation ^d
40	Tagyu	48 19 / 142 40	2265 \pm 35	400–200 BC	AA-37227	C	Su
30	Venskoye 2	51 57 / 143 06	1855 \pm 30	AD 80–240	AA-36620	BF	Okh (?)
41	Ado-Tymovo 1	51 09 / 142 40	2220 \pm 35	390–170 BC	AA-36440	C	SS (N)
			2105 \pm 100	350 BC–AD 1	SOAN-4280	C	SS (N)
			1905 \pm 100	20 BC–AD 240	SOAN-3723	C	SS (N)
42	Ush 2	53 35 / 142 27	2170 \pm 60	390–50 BC	SOAN-3562	C	SS (N)
43	Taranai	46 37 / 142 26	2155 \pm 65	390–1 BC	SOAN-1023	C	Su
			2050 \pm 30	170 BC–AD 20	SOAN-1021	C	Su
			1970 \pm 45	50 BC–AD 130	SOAN-1022	C	Su
44	Blagodatny 1	51 10 / 142 39	2110 \pm 40	350–1 BC	SOAN-3718	C	SS (N)
			2030 \pm 30	110 BC–AD 50	SOAN-3637	C	SS (N)
			1715 \pm 30	AD 240–420	AA-36395	C	SS (N)
			1700 \pm 35	AD 240–420	AA-36394	C	SS (N)
45	Nevelsk 1	46 40 / 141 52	2080 \pm 35	200 BC–AD 1	AA-37180	BF	Okh (?)
46	Tabush	52 02 / 143 08	2075 \pm 80	360 BC–AD 80	SOAN-3361	C	UC
47	Vtoraya Polovinka	50 57 / 142 11	2040 \pm 60	200 BC–AD 80	SOAN-3818	C	UC
48	Buruny 1	48 06 / 142 33	1990 \pm 25	40 BC–AD 70	SOAN-3250	C	Su
49	Pugachevo 38	48 11 / 142 36	1890 \pm 55	20 BC–AD 240	SOAN-3565	C	Su
50	Ivanovka	46 44 / 141 53	1850 \pm 90	40 BC–AD 400	TIG-270	W	Okh (?)
51	Shakhtersk	49 11 / 142 03	1780 \pm 60	AD 80–410	SOAN-1024	C	Su
6	Sedykh 1	46 52 / 143 09	1775 \pm 40	AD 130–380	AA-37466	BF	Okh (?)
52	Bauri 2	51 58 / 143 08	1720 \pm 85	AD 90–540	SOAN-3415	C	SS (N)
			1080 \pm 60	AD 780–1150	SOAN-3414	C	SS (N)
53	Mys Krugly	47 00 / 143 04	1700 \pm 100	AD 240–430	MAG-675	C	Su
EARLY IRON AGE AND THE MIDDLE AGES							
54	Kitakotan 1	46 16 / 141 14	1640 \pm 80	AD 240–600	NU-430	C	T
33	Kuznetsovo 1		1640 \pm 370	40 BC–AD 770	DVGU-90	C	T
55	Nyivo 2	51 51 / 143 12	1620 \pm 40	AD 340–540	SOAN-3269	C	SS (N)
56	Ado-Tymovo 28	51 07 / 142 40	1610 \pm 30	AD 390–540	AA-36349	C	UC
			1220 \pm 45	AD 690–960	SOAN-4065	C	UC
57	Delil-de-la-Kroiye	50 48 / 143 40	1600 \pm 45	AD 360–600	SOAN-3279	C	Su
			1440 \pm 35	AD 540–660	AA-37128	C	Okh
			1430 \pm 40	AD 540–670	AA-37229	C	Okh
			1235 \pm 60	AD 660–960	SOAN-3376	C	Okh
58	Kiri 2	51 03 / 143 31	1550 \pm 50	AD 410–640	AA-37465	C	UC
59	Antonovo 2	47 07 / 142 04	1550 \pm 35	AD 420–600	SOAN-3820	C	Okh
60	Starodubskoye 2	47 25 / 142 48	1540 \pm 30	AD 430–620	SOAN-1143	C	Su
61	Puzi Grotto	51 11 / 142 41	1540 \pm 50	AD 420–640	SOAN-3814	C	UC
62	Vengeri 1	50 31 / 143 43	1515 \pm 35	AD 430–640	AA-37080	C	UC
63	Stary Nabyl 1	51 29 / 143 18	1450 \pm 45	AD 540–660	SOAN-3815	C	SS (N)
38	Ozersk 1		1400 \pm 100	AD 560–690	MAG-679	C	Okh
			1140 \pm 45	AD 780–1000	SOAN-1020	C	Okh
			1035 \pm 35	AD 900–1030	SOAN-1140	C	Okh
			760 \pm 25	AD 1220–1290	SOAN-1141	C	Okh
64	Kholmok 4	47 02 / 142 03	1350 \pm 45	AD 620–770	AA-36738	BF	Okh
50	Ivanovka 1		1280 \pm 100	AD 660–890	NU-492	W	Okh
65	Promyslovoye 2	49 19 / 143 29	1210 \pm 35	AD 690–940	SOAN-3403	C	Okh
66	Peschanoye 1	47 15 / 143 01	1040 \pm 105	AD 890–1150	DVGU-149	C	Okh
67	Ygvo 2	51 17 / 143 30	1015 \pm 35	AD 980–1150	AA-37228	C	UC

Table 1 ^{14}C dates for the prehistoric sites on Sakhalin Island. (*Continued*)

Site nr ^a	Site name	Coordinates ° ' N / ° ' E	^{14}C date, BP ($\pm 1 \sigma$)	Calibrated age ^b	Lab code and nr	Material dated ^c	Cultural affiliation ^d
68	Mramornaya 1	46 09 / 143 25	1010 \pm 40	AD 980–1160	UPI-805	C	Okh
			1000 \pm 100	AD 900–1160	LE-4042	C	Okh
39	Pugachevo 9		970 \pm 80	AD 900–1240	NU-597	C	Okh
			630 \pm 20	AD 1300–1400	SOAN-3249	C	Okh
69	Antonovo-Chasi	47 08 / 142 04	940 \pm 30	AD 1020–1190	SOAN-3636	C	Okh
34	Kuznetsovo 1		905 \pm 75	AD 990–1280	DVGU-92	C	Okh
70	Takoe 2	47 18 / 142 47	805 \pm 80	AD 1030–1380	SOAN-1144	C	Okh (A?)
71	Simakovo 1	47 05 / 142 03	515 \pm 30	AD 1330–1440	SOAN-3716	C	Okh (A?)
72	Bogataya 1	49 59 / 143 59	805 \pm 30	AD 1190–1280	AA-36618	BF	FA
38	Ozersk 1		770 \pm 60	AD 1160–1380	AA-37230	BF	FA
			300 \pm 100	AD 1470–1800	MAG-668	C	A
34	Svobodnoye 1		610 \pm 30	AD 1300–1410	AA-36619	BF	A
73	Ado-Tymovo 6	51 08 / 142 40	550 \pm 25	AD 1330–1430	SOAN-3725	C	UC
			180 \pm 30	AD 1660–1950	AA-36392	C	UC
5	Starodubskoye 3		380 \pm 85	AD 1410–1790	TIG-250	C	NA
74	Kitakotan 2	46 15 / 141 14	200 \pm 70	AD 1520–1950	NU-493	C	NA

^aSite numbers correspond to those in Figure 1.

^bFor ^{14}C dates with $\pm 1 \sigma$ less than 100 yr, the $\pm 2 \sigma$ calibration range is given; for ^{14}C dates with $\pm 1 \sigma$ more than 100 yr, the $\pm 1 \sigma$ calibration range is applied.

^cC: charcoal; BF: burnt food attached to the pottery; W: wood.

^dOs–Osipovka culture; YS (S)–Yuzhno-Sakhalinsk (Sony) culture; UEN–unidentified Early Neolithic; MNI–Middle Neolithic Imchin culture; LNI–Late Neolithic Imchin culture; S–Sedykh culture; UN–unidentified Neolithic culture; FI–Final Imchin culture; An–Aniva (Early Epi-Jomon) culture; SS (N)–Severo-Sakhalinsk (Nhabil) culture; UC–unidentified culture; Su–Susuya culture; Okh–Okhotsk culture; T–Towada culture; A–Ainu (Neiji) culture; NA–Neo-Ainu culture.

LUGOVSKOE, WESTERN SIBERIA: A POSSIBLE EXTRA-ARCTIC MAMMOTH REFUGIUM AT THE END OF THE LATE GLACIAL

Lyobov A Orlova¹ • Vasily N Zenin² • Anthony J Stuart³ • Thomas F G Higham⁴ • Pieter M Grootes⁵ • Sergei V Leshchinsky⁶ • Yaroslav V Kuzmin⁷ • Aleksander F Pavlov⁸ • Evgeny N Maschenko⁹

ABSTRACT. Eleven woolly mammoth bone samples from Lugovskoe (central West Siberian Plain, Russia) were radiocarbon dated in 3 laboratories: Institute of Geology, Novosibirsk; Oxford University, Oxford; and Christian Albrechts University, Kiel. Each laboratory used its own protocol for collagen extraction. Parallel dating was carried out on 3 samples in Novosibirsk and Oxford. Two results are in good agreement. However, there is a major discrepancy between 2 dates obtained for the third sample. The dates obtained so far on the Lugovskoe mammoths range from about 18,250 BP to about 10,210 BP. The Lugovskoe results thus far confirm the possibility of woolly mammoth survival south of Arctic Siberia in the Late Glacial after about 12,000 BP, which has important implications for interpreting the process of mammoth extinction. The site has also produced the first reliable traces of human occupation from central Western Siberia at the Late Glacial, including unique direct evidence of mammoth hunting.

INTRODUCTION

Establishing a chronology of Pleistocene megafaunal extinctions is very important for understanding their cause(s), and placing the events in the wider context of Quaternary paleoenvironment history (Martin and Klein 1984; Stuart 1991; MacPhee 1999). A large radiocarbon data set is available for the woolly mammoth (*Mammuthus primigenius* Blum; hereafter, “mammoth”) (Stuart 1991; Sulerzhitsky 1997; Vasil’chuk et al. 1997; Kuzmin et al. 2003). Previous research suggests that mammoths retreated at about 12,000 BP from most of its former extensive distribution in Northern Eurasia, but survived in the far north of mainland Siberia for another 2 millennia (cf. Sulerzhitsky 1997; Sher 1997). This model of spatial-temporal pattern of mammoth dynamics at the end of the Pleistocene can be called the “retreat to the north after ca. 12,500–12,000 BP” (cf. Sher 1997).

Recent research, however, indicates that mammoths were present until about 10,000 BP in the Baltic States and North Russian Plain, outside of the Arctic regions (Stuart et al. 2002: 1567; Lõugas et al. 2002). These European occurrences probably represent recolonization from the refugium in Northern Siberia during the renewed cold of the Younger Dryas phase (Stuart, forthcoming). The possibility that mammoths also survived in Siberia outside the Arctic region after 12,000 BP is very important in interpreting the process of mammoth extinction. Lugovskoe, in the central West Siberian Plain, is a key locality for the study of mammoth’s late survival because it was dated to the critical period of about 12,000–10,300 BP. ¹⁴C dates on woolly mammoth remains were carried out in 2000–2002. Here, we present the ¹⁴C results obtained so far and their preliminary interpretation.

¹Institute of Geology, Siberian Branch of the Russian Academy of Sciences, Koptyug Ave. 3, Novosibirsk 630090, Russia. Corresponding author. Email: orlova@uiggm.nsc.ru.

²Institute of Archaeology and Ethnography, Siberian Branch of the Russian Academy of Sciences, Lavrentiev Ave. 17, Novosibirsk 630090, Russia.

³Department of Biology, University College London, Gower St., London WC1E 6BT, United Kingdom.

⁴Oxford Radiocarbon Accelerator Unit, University of Oxford, 6 Keble Rd., Oxford OX1 3QJ, United Kingdom.

⁵Leibniz-Labor, Christian Albrechts University, Max-Eyth-Str. 11, 24118 Kiel, Germany.

⁶Tomsk State University, Lenin Ave 36, Tomsk 634050; Russia.

⁷Pacific Institute of Geography, Far Eastern Branch of the Russian Academy of Sciences, Radio St. 7, Vladivostok 690041, Russia.

⁸Museum of Nature and Humans, Mira St. 11, Khanty-Mansiysk 628011; Russia.

⁹Paleontological Institute, Russian Academy of Sciences, Profsoyuznaya St. 123, Moscow 117647, Russia.

MATERIAL AND METHODS

The Pleistocene fossil mammal locality of Lugovskoe is in the modern forest zone of the central Western Siberian Plain (60°57'N; 68°32'E) about 25 km west of Khanty-Mansiysk City and the confluence of the Ob and Irtysh Rivers (Figure 1). Paleontological research has been conducted here since 1994 (Mashchenko et al. 2003). The bone bed occurs at a depth of 0.5–1.5 m below the modern surface within the muddy clay deposits of a small stream that flows into the Ob River. Although it is impossible to conduct proper excavations because the deposits are saturated with stream water, about 4500 fossil mammal bones were recovered in 1998–2002, of which 98% belong to mammoth. Remains of at least 27 individual mammoths were collected from the muddy clay, and several skeletal elements were found in anatomical association (Pavlov et al. 2002). Lugovskoe represents one of the richest so-called “mammoth cemeteries” in Siberia.

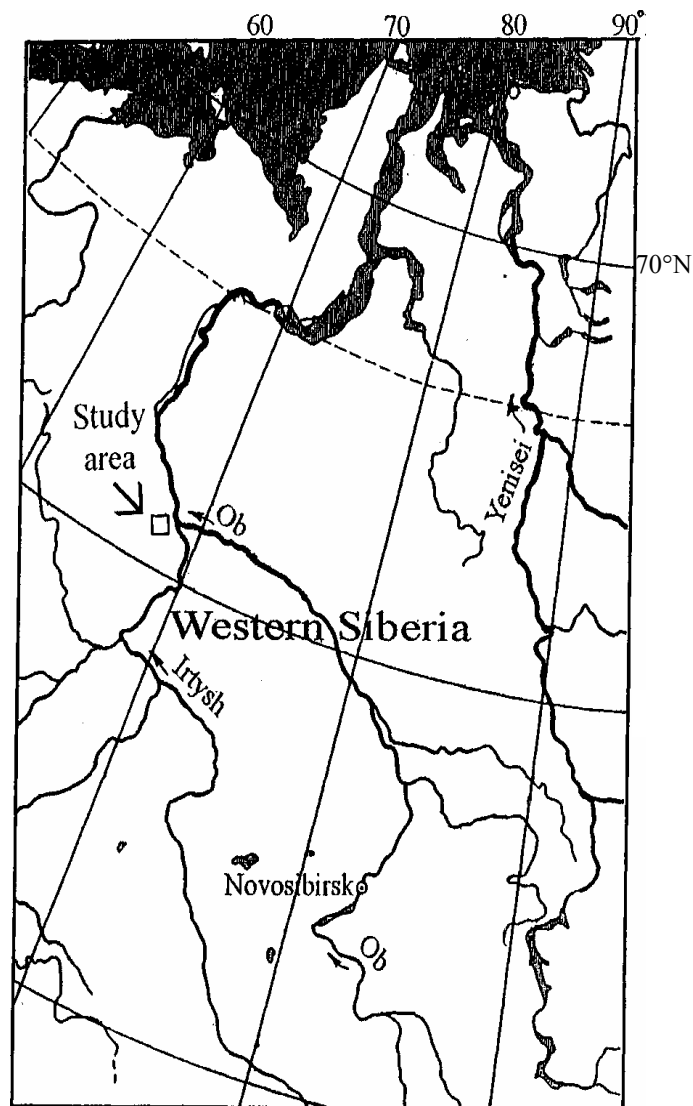


Figure 1 The position of the Lugovskoe locality in Western Siberia

^{14}C dating of the mammoth bones was undertaken in 3 laboratories: the Institute of Geology, Novosibirsk (Russia); Oxford University, Oxford (UK); and Christian Albrechts University, Kiel (Germany). Collagen extracted from mammoth bones was dated by the liquid scintillation counting (LSC) (Novosibirsk) and accelerator mass spectrometry (AMS) (Oxford and Kiel) techniques. In each laboratory, the collagen extraction protocol is different.

In Novosibirsk, pieces of bone 10–20 cm long were mechanically cleaned of any surface contamination and were demineralized with a 5% HCl solution (at 7–8 L of solution for 1 kg of bone) at 2–3 °C. Since the process may take 1–2 weeks, the sample is refrigerated. The extracted gelatin-like collagen was thoroughly washed with distilled water. The collagen was then treated with an 0.1-N solution of sodium base (NaOH) for several hours in order to remove the humic acids. The remaining collagen was again washed with distilled water, dried, and carbonized by heating in an 800 °C oxygen-free environment. To remove the phosphorous compounds, the carbonized collagen was treated with a mixture of nitric acid (HNO_3) and HCl (“aqua regia”). Finally, the purified collagen was washed with distilled water, dried, and used for benzene preparation and LSC measurements.

At the Oxford Radiocarbon Accelerator Unit (ORAU), bones were cleaned by scraping with a scalpel to remove soil coloration, sediment detritus, and weathered surfaces. Bone was then chemically pretreated using the ORAU continuous-flow semi-automated method (Bronk Ramsey et al., these proceedings), with an acid-base-acid sequence to isolate crude collagen, then gelatinization with weakly acidic water (pH=3) for 20 hr in an incubator at 75 °C. Ultrafilters were used to isolate the >30-kD fraction of the bone hydrolyzate. This fraction was then lyophilized. Samples were combusted using a Europa Scientific ANCA-MS system consisting of a 20-20 IR mass spectrometer interfaced to a Roboprep CHN sample converter unit operating in continuous flow mode. Graphite was prepared by reduction of CO_2 over an iron catalyst in an excess H_2 atmosphere at 560 °C prior to AMS ^{14}C measurement (Bronk Ramsey and Hedges 1999; Bronk Ramsey et al. 2000).

At the Leibnitz Laboratory for Radiometric Dating and Isotope Research (Kiel), bone sample was checked and mechanically cleaned under the microscope. The collagen content was calculated from the concentration of nitrate, determined by colorimetry as nitrate in about 2 mg of bone material. The sample was first treated with acetone, rinsed with demineralized water, and subsequently demineralized in 1% HCl. This was followed by 1% NaOH at room temperature for 1 hr to remove humic acids, then washed and subsequently acidified with 1% HCl. After filtering, the purified collagen was gelatinized overnight in 1.6 mL of H_2O at 90 °C and pH=3. The gelatin solution was dried in quartz tubes, to which CuO and silver wool was added and combusted to CO_2 at 900 °C. The CO_2 gas was reduced with H_2 over about 2 mg of Fe powder as catalyst, and the resulting carbon/iron mixture was pressed into a pellet for AMS analysis.

RESULTS AND DISCUSSION

Measurements of stable carbon and nitrogen isotopes ($\delta^{13}\text{C}$ and $\delta^{15}\text{N}$) were made at the Oxford Laboratory for 3 samples, OxA-12029, 12030, and 12031. $\delta^{13}\text{C}$ values are within –20.7 to –21.3‰ (Table 1), and $\delta^{15}\text{N}$ values are within +4.7 to +5.9‰. The collagen yield from 3 samples dated at Oxford is 1.9–4.8%, which indicates poor preservation and low survival of collagen >30 kD MW. The collagen yield for 1 sample dated at Kiel (KIA-19643) was 23%, about the content of a fresh bone, indicating excellent preservation. The minimum threshold for yield acceptance at Oxford is 10 mg/g^{-1} (1% weight collagen). Differences between the collagen yields by laboratory are liable to be a function of pretreatment method. The Oxford ultrafiltration method often produces lower yields

in comparison with simpler bone hydrolyzate filtration methods, a fact we attribute to the removal of degraded collagen, salts, and low molecular weight particulates. The C/N ratios for the Oxford samples ranged between 3.3–3.4, and values between 2.9–3.5 are considered acceptable (DeNiro 1985).

Table 1 ^{14}C dates for woolly mammoth from Lugovskoe^a.

Lab code	Sample	^{14}C age (BP)	$\delta^{13}\text{C}$ (‰)	$\delta^{15}\text{N}$ (‰)	C/N ratio
SOAN-3838	Tibia	18,250 ± 1100	—	—	—
SOAN-5065	Scapula fragment	15,420 ± 215	—	—	—
SOAN-4940	Thoracic vertebra ^b	13,720 ± 160	—	—	—
OxA-12030	Thoracic vertebra ^b	13,455 ± 60	-21.1	+4.7	3.4
SOAN-4942	Pelvic bone ^c	13,490 ± 155	—	—	—
OxA-12029	Pelvic bone ^c	13,450 ± 50	-20.7	+5.9	3.4
KIA-19643	Thoracic vertebra ^d	13,465 ± 50	-21.4	—	—
OxA-12031	Molar fragments ^e	13,205 ± 60	-21.3	+4.9	3.3
SOAN-4943	Molar fragments ^e	10,820 ± 170	—	—	—
SOAN-5063	Femur	12,970 ± 160	—	—	—
SOAN-4754	Cervical vertebrae	12,830 ± 350	—	—	—
SOAN-4753	Femur	11,840 ± 95	—	—	—
SOAN-4755	Ulna	11,310 ± 380	—	—	—
SOAN-4752	Femur	10,210 ± 135	—	—	—

^a $\delta^{13}\text{C}$ values are reported with reference to VPDB, and $\delta^{15}\text{N}$ results are reported with reference to AIR (Coplen 1994).

^bDates were run on the same sample.

^cDates were run on the same sample.

^dContains hole made by notched point.

^eUncertain if dates were run on the same specimen (see text).

Three samples of mammoth material from Lugovskoe were submitted for parallel dating to the Novosibirsk and Oxford laboratories, both to corroborate the results and to compare the effect of different collagen extraction methods. Two out of 3 samples (SOAN-4940, 4942; and OxA-12029, 12030) are in good agreement (see Table 1), but there is a serious discrepancy between SOAN-4943 and OxA-12031. When submitted, the samples were believed to be fragments of the same tooth. The samples, represented by lamellas of mammoth tooth, were collected from mud deposits. Several lamellas were used for liquid scintillation dating at Novosibirsk. The difference in the results raises the possibility that they may have come from different individuals. Alternatively, the samples may have come from the same tooth, in which case there is a significant disagreement between the 2 laboratories. Additional mammoth samples from Lugovskoe of the putative post-12,000 BP age are being submitted to resolve this important question.

Results of ^{14}C dating of the Lugovskoe mammoths (Table 1) show that bones accumulated at the site over a long period of time, from about 18,250 BP to about 10,200 BP. The 3 youngest ^{14}C values for the Lugovskoe mammoths (11,840 ± 95 BP [SOAN-4753]; 11,310 ± 380 [SOAN-4755]; and 10,210 ± 135 BP [SOAN-4752]; Table 1), are of particular importance. During the last few years, a number of mammoth dates post-12,000 BP have been reported from southern and central Siberia: Volchya Griva (about 11,090 BP), Sosva River (about 11,080 BP), and Konzul (about 11,980 BP) (Orlova et al. 2004); and from the North European Plain: Puurmani (about 10,100–10,200 BP) and Cherepovets (about 9800 BP) (Lõugas et al. 2002; Stuart et al. 2002). The contribution of the Lugovskoe date series is that it might be one of the areas with very late mammoths which survived

until the end of the Pleistocene, about 10,200 BP. In addition, a very late ^{14}C date for woolly rhinoceros from the Lugovskoe, $10,770 \pm 250$ BP (SOAN-4757) (Orlova et al., these proceedings) makes it one of the most important localities in terms of research on late survival of the Upper Pleistocene megafauna in Northern Asia.

One of the mammoth vertebrae has direct evidence of mammoth hunting by prehistoric humans, the single example known from Siberia so far. The mammoth thoracic vertebra, which is attributed to an adult female mammoth of about 23–25 yr old, has a cone-shaped hole resulting from the penetration of a notched point, and there are fragments of quartzite flakes lodged in the hole (Pavlov et al. 2002; Zenin et al. 2003). The vertebra has been ^{14}C dated to about 13,470 BP (Table 1).

CONCLUSION

The available evidence from Lugovskoe, and from several other localities in Siberia and Europe, confirm survival of woolly mammoth south of the Arctic region after about 12,000 BP, which has important implications for our understanding of the process of mammoth extinction. The Lugovskoe ^{14}C date series indicate that the nature of the mammoth habitat in Siberia after about 12,000 BP was quite “patchy,” with few isolated populations outside of the High Arctic. This is distinct from the model of “retreat to the north after approximately 12,000 BP,” which is now challenged by the new post-12,000 BP mammoth ^{14}C dates from Siberia and North Russian Plain, including the Lugovskoe. In order to test this hypothesis of extra-Arctic survival, more ^{14}C dating, including parallel dating by Russian, West European, and North American laboratories, is being undertaken. This compliments ongoing research on the chronology and paleoenvironment of mammoths and other extinct megafauna, especially in temperate Western Siberia where there may have been several megafaunal refugia after about 12,000 BP.

ACKNOWLEDGEMENTS

This work was supported by grants from the Russian RFFI (00-06-80410, 02-04-48458, 03-06-80289, 03-05-64434, and 03-05-65252); Institute of Archaeology and Ethnography, Siberian Branch of the Russian Academy of Sciences (“Initial Human Colonization and Settling of Eurasia: Formation and Evolution of Paleolithic Cultures, Correlation of Mechanisms of Cultural Adaptation with Climate Fluctuations”); Presidium of the Russian Academy of Sciences (Fundamental Studies Program “Ethnocultural Interaction in Eurasia”); Governor of the Khanty-Mansiysk Autonomous District; and the UK NERC (GR3/12599). We are grateful to an anonymous reviewer for useful comments.

REFERENCES

- Bronk Ramsey C, Hedges REM. 1999. Hybrid ion sources: radiocarbon measurements from microgram to milligram. *Nuclear Instruments and Methods in Physics Research B* 123:539–45.
- Bronk Ramsey C, Higham TFG, Bowles A, Hedges REM. 2004. Improvements to the pretreatment of bone at Oxford. *Radiocarbon*, these proceedings.
- Bronk Ramsey C, Pettitt PB, Hedges REM, Hodgins GWL, Owen DC. 2000. Radiocarbon dates from the Oxford AMS system: Archaeometry Datelist 30. *Archaeometry* 42:459–79.
- Coplen TB. 1994. Reporting of stable hydrogen, carbon and oxygen isotopic abundances. *Pure and Applied Chemistry* 66:273–6.
- DeNiro MJ. 1985. Postmortem preservation and alteration of *in vivo* bone collagen isotope ratios in relation to paleodietary reconstruction. *Nature* 317(6043): 806–9.
- Kuzmin YV, Orlova LA, Zolnikov ID. 2003. Dynamics of mammoth (*Mammuthus primigenius* Blum.) population in Northern Asia: radiocarbon evidence. In: Reumer JWF, de Vos J, Mol D, editors. *Advances in Mammoth Research*. DEINSEA (Annual of the Natural History Museum Rotterdam) 9:221–37.
- Lõugas L, Ukkonen P, Jungner H. 2002. Dating the extinction of European mammoths: new evidence from

- Estonia. *Quaternary Science Reviews* 21(6):1347–54.
- MacPhee RDE, editor. 1999. *Extinctions in Near Time: Causes, Contexts, and Consequences*. New York: Plenum Press. 384 p.
- Martin PS, Klein RG, editors. 1984. *Quaternary Extinctions: A Prehistoric Revolution*. Tucson, Arizona: University of Arizona Press. 892 p.
- Maschenko EN, Pavlov AF, Zenin VN, Leshchinskiy SV, Orlova LA. 2003. The Lugovskoe site: relations between the mammoth assemblage and Late Palaeolithic humas. In: *3rd International Mammoth Conference Program and Abstracts. Occasional Papers in Earth Sciences 5*. Whitehorse: Dawson City Museum. p 77–80.
- Orlova LA, Kuzmin YV, Dementiev VN. 2004. A review of the evidence for extinction chronologies for five species of Upper Pleistocene megafauna in Siberia. *Radiocarbon*, these proceedings.
- Pavlov AF, Mashchenko EN, Zenin VN, Leshchinsky SV, Orlova LA. 2002. Predvaritelnye rezultaty mezhdistsiplinarnykh issledovaniy mestonakhozhdeniya Lugovskoe (Khanty-Mansiysky avtonomnyy okrug) [The preliminary results of the multidisciplinary studies of the Lugovskoe locality (Khanty-Mansiysk Autonomous District)]. In: Derevianko AP, Molodin VI, editors. *Problemy Arkheologii, Etnografii, Antropologii Sibiri i Sopredelnykh Territoriy*. Novosibirsk: Izdatelstvo Instituta Arkheologii i Etnografii SO RAN. p 165–72.
- Sher AV. 1997. Late-Quaternary extinction of large mammals in northern Eurasia: a new look at the Siberian contribution. In: Huntley B, Cramer W, Morgan AV, Prentice HC, Allen JRM, editors. *Past and Future Rapid Environmental Changes: The Spatial and Evolutionary Responses of Terrestrial Biota*. Berlin-Heidelberg-New York: Springer-Verlag. p 319–39.
- Stuart AJ. 1991. Mammalian extinctions in the Late Pleistocene of Northern Eurasia and North America. *Biological Reviews of the Cambridge Philosophical Society* 66(4):453–562.
- Stuart AJ. Forthcoming. The extinction of woolly mammoth (*Mammuthus primigenius*) and straight-tusked elephant (*Palaeoloxodon antiquus*) in Europe. *Quaternary International*.
- Stuart AJ, Sulerzhitsky LD, Orlova LA, Kuzmin YV, Lister AM. 2002. The latest woolly mammoths (*Mammuthus primigenius* Blumenbach) in Europe and Asia: a review of the current evidence. *Quaternary Science Reviews* 21(7):1559–69.
- Sulerzhitsky LD. 1997. Cherty radiouglerodnoi khronologii mamontov Sibiri i severa Vostochnoi Evropy (kak substrata dlya rasseleniya cheloveka) [The features of radiocarbon chronology of mammoths in Siberia and northern Eastern Europe (as substratum for human dispersal)]. In: Velichko AA, Soffer O, editors. *Chelovek Zaselyaet Planetu Zemlya*. Moscow: Institut Geografii RAN. p 184–202.
- Vasil'chuk Y, Punning J-M, Vasil'chuk A. 1997. Radiocarbon ages of mammoths in Northern Eurasia: implications for population development and Late Quaternary environment. *Radiocarbon* 39(1):1–18.
- Zenin VN, Maschenko EN, Leshchinskiy SV, Pavlov AF, Grootes PM, Nadeau M-J. 2003. The first direct evidence of mammoth hunting in Asia (Lugovskoe site, Western Siberia). In: *3rd International Mammoth Conference Program and Abstracts. Occasional Papers in Earth Sciences 5*. Whitehorse: Dawson City Museum. p 152–5.

RADIOCARBON DATING OF *KOHITSUGIRE* (PAPER FRAGMENTS) ATTRIBUTED TO JAPANESE CALLIGRAPHISTS IN THE HEIAN–KAMAKURA PERIOD

Hiroataka Oda^{1,2} • Kazuomi Ikeda³ • Takashi Masuda⁴ • Toshio Nakamura¹

ABSTRACT. A *kohitsugire* is a paper fragment from an old manuscript written mainly in the Heian and Kamakura periods. Although they contain significant information for historical, literary, and paleographical study, because of their antique handwriting and description of historical incidents, there are many copies and counterfeits written several centuries later. In this study, radiocarbon ages of *kohitsugire* were measured by accelerator mass spectrometry (AMS). On the *kohitsugire* attributed to the famous calligraphists in the Kamakura period (Fujiwara no Sadaie and Prince Munetaka), ¹⁴C dating indicated that they were not genuine and should be excluded from the materials for study of the calligraphists. Calibrated ¹⁴C ages of the *kohitsugire* attributed to Fujiwara no Yukinari indicated the middle Heian period. This calligraphy was written on *Tobikumogami* paper, which has a billowing cloud pattern decorated with indigo-blue-dyed fiber. Although it was commonly accepted that the *Tobikumogami* is peculiar to the middle 11th to early 12th century, the results from ¹⁴C dating also suggested that the origin of the *Tobikumogami* would date back to the last of the 10th or the early 11th century, when Fujiwara no Yukinari flourished as a calligraphist. Calibrated ¹⁴C ages of the *kohitsugire* attributed to Nijo Tameuji and Reizei Tamesuke showed that they are fragments of old manuscripts describing lost tales and were written in the 13th–14th century. Consequently, ¹⁴C dating clarified the existence of ancient tales which had been unknown and indicated their worth as a material for the study of classical Japanese literature.

INTRODUCTION

In Japanese history, the Heian period usually indicates a span from AD 794, when Emperor Kanmu relocated the capital in Heiankyo (present-day Kyoto Prefecture), to AD 1192, when the Kamakura Shogunate was established as the first military government by Minamoto no Yoritomo. The Kamakura period corresponds to the duration of the Kamakura Shogunate (1192–1333).

The literary history of the Heian and Kamakura periods is surveyed below. The composition of Chinese poetry was considered as an obligatory accomplishment for nobles; accordingly, the major genre of literature were anthologies of Chinese poetry during the first 100 yr of the Heian period. The development of the Japanese *kana* syllabary in the early 10th century, however, brought about a burst of native literature because it was now possible to write calligraphy without depending on Chinese characters. Nobles occasionally held the competitions of *waka* (Japanese poetry) and poetry anthologies of *waka* were compiled. The *kana* syllabary also caused the creation of a prose literature, including the *monogatari* (tale), the *nikki* (diary), and the *zuihitsu* (essay). The most famous of these literatures is perhaps *Genji monogatari* (The Tale of Genji), which recounts the life of a nobleman named Hikarugenji in the Heian period court. During the last Heian and the Kamakura periods, this field produced various literary forms: the *gunkimono* (war tale), the *rekisi monogatari* (historical narrative), the *kiko* (itinerary), and the *setsuwa shu* (anthology of short narratives, legends, and historical incidents). *Heike monogatari* (The Tale of the Heike), which is well known and recited to a biwa accompaniment, followed the establishment of the Kamakura shogunate; the tale centers on the rise and fall of the Taira warrior and gives a description of the Taira-Minamoto War.

Classical literature also provides significant information for historians because of the description of historical incidents, and for the study of paleography because of the antique calligraphy. The study

¹Center for Chronological Research, Nagoya University, Chikusa, Nagoya 464-8602, Japan.

²Corresponding author. Email: oda@nendai.nagoya-u.ac.jp.

³Chuo University, Higashinakano, Hachioji, Tokyo 192-0351, Japan.

⁴Aichi Bunkyo University, Komaki, Aichi 485-0802, Japan.

of classical literature, history, and paleography generally requires the source book or the old manuscripts to be copied with few mistakes or alterations. However, complete manuscripts written during the Heian and Kamakura period are quite rare. One of the main reasons can be ascribed to the Onin War (1467–1477), which was the nationwide war triggered by a conflict over the successor of shogun. The greater part of Kyoto was burned down and a large quantity of ancient documents and treasures kept in temples, shrines, and nobles' mansions were reduced to ashes in the war. In addition, the development of the tea ceremony indirectly accelerated the decrease of the old manuscripts. Because the tea ceremony was popular among military lords and wealthy merchants in the 16th century, in order to appreciate their elegant and antique calligraphy in the teahouses, the old manuscripts had been cut page by page and mounted on hanging scrolls for decoration.

Although the old manuscripts are rarely discovered as complete books, the kohitsugire paper fragments hold potentially significant information for historical study. There are, however, many copies and counterfeits written several centuries later among the kohitsugire fragments attributed to the famous calligraphists. While the written age or the author of the ancient manuscript can be generally presumed by the paleographical views, it is generally difficult to ascertain whether kohitsugire with only a few calligraphic lines are genuine or not.

We have been working on radiocarbon dating focused on ancient Japanese documents and sutras of known age (Oda et al. 2000, 2003). These previous studies indicated that calibrated ^{14}C ages of Japanese paper are in good agreement with assumed corresponding historical ages of the documents or sutras. In this paper, we further examine the suitability of this material for historical study, and have measured the ^{14}C ages of the kohitsugire fragments traditionally attributed to the famous Japanese calligraphists in the Heian-Kamakura period.

SAMPLES

In this study, ^{14}C ages of 9 kohitsugire samples were measured. They include 3 samples (nr I–III, Table 1) of which the written ages were determined by evidence based on historical, paleographical, and bibliographical views. Sample nr I is a fragment of the *Chusonji konshi kinginkosho issaikyo* sutra. This sutra was written on indigo-blue-dyed paper with gold and silver Indian inks in alternate lines. It is assumed to have been written in the early 12th century (1117–1125) at the request of Fujiwara no Kiyohira (1056–1128) for the completion ritual of the Golden Hall of the Chusonji temple (1126) in Hiraizumi (present-day Iwate Prefecture). Sample nr II is an ancient letter with the compliments of the New Year. It was attached to the back of a sheet of the *Inmyo mondo sho* sutra. Several letters from the same sender were pasted together and the sutra was written on the back side of the recycled paper. Such sutras were commonly written as condolences for death of the original sender. The sutra was written in 1315; accordingly, the date when the letter was originally sent should be a few years or decades before. Sample nr III is a paper fragment of the last page of an ancient book. Since this part corresponds to a colophon, it has a writer's signature, "Nakanoin Nobutane", a signature stamp, and an account that the book was written in 1501 at the request of a person by the name of Kijumaru. Based on the handwriting and the ancient records on Nakanoin Nobutane, it is fairly certain that the kohitsugire is a genuine calligraphy of Nakanoin Nobutane.

Table 1 The kohitsugire samples of known age.

Nr	Sample name	Written age (AD)
I	Chusonji konshi kinginkosho issaikyo sutra	1117–1125
II	A letter on the back on Inmyo mondosho sutra	1315
III	The last page of a book by Nakanoin Nobutane	1501

The written ages of the other 6 samples (nr 1–6, Table 2) have no reliable evidence from paleographical studies and leave room for further examination, especially by ¹⁴C dating. The estimated paleographical ages are listed in Table 2. Some kohitsugire fragments had small labels attached (called *kiwamefuda*) upon which are the calligraphists' names. The calligraphists noted on the *kiwamefuda* are also indicated in Table 2. Most of them, however, have no evidence based on paleographical studies.

Table 2 The kohitsugire samples of unknown age.

Nr	Sample name	Calligraphist on the <i>Kiwamefuda</i>	Estimated paleographical age
1	<i>Itsumei honcho kaku gire</i>	Fujiwara no Yukinari (971–1027)	971–1027 or middle 11th–early 12th century
2	<i>Ise monogatari</i>	Fujiwara no Sadaie (1162–1241)	14th century
3	<i>Kokin wakasyu</i> anthology	Fujiwara no Sadaie (1162–1241)	—
4	The anthology of Fujiwara no Sanekata's poetry	Prince Munetaka (1242–1274)	The latter half of the 11th century
5	A lost tale by Nijo Tameuji	Nijo Tameuji (1222–1286)	—
6	A lost tale by Reizei Tamesuke	Reizei Tamesuke (1260–1328)	—

METHODS

The kohitsugire fragment is commonly mounted on another paper sheet. In addition, some of them have double or triple sheets. Paper samples (20–130 mg) were cut from the margins of the calligraphies and were soaked with distilled water to peel the surface fragments from the mounts. All the sample fragments were first washed with distilled water in an ultrasonic cleaner and then treated with 1.2N HCl and 1.2N NaOH solutions on a hot plate (each step was repeated 5 times for 2–3 hr at 60–70 °C). Next, alpha-cellulose was prepared from samples nr II, III, 1, 3–5: they were bleached 4 times with 0.07M NaClO₂ solution under acidic conditions adjusted with HCl (70–80 °C, 1 hr), treated with 17.5% NaOH solution for 30 min at room temperature, and finally rinsed with 1.2N HCl and distilled water. The surface sheets of 3 kohitsugire (nr I, 2, 6) are small fragments; therefore, they were treated again with 1.2N HCl (3 times, 3–4 hr, 60–70 °C) and rinsed with distilled water instead of alpha-cellulose extraction in a lower yield. After drying in a vacuum desiccator, each sample was sealed in a Vycor glass tube with CuO and converted to CO₂ at 850 °C for 2 hr. The CO₂ gas was purified on an evacuated glass line with successive traps cooled with chilled ethyl alcohol, solid n-pentane, and liquid nitrogen. The purified CO₂ gas was reduced with hydrogen to graphite in the presence of an iron catalyst at 650 °C for 6 hr.

The AMS measurements were run on a Tandemtron accelerator mass spectrometer manufactured by HVEE (High Voltage Engineering Europa) at the Center for Chronological Research, Nagoya University, Japan. NBS oxalic acid (SRM-4990) was used as the standard material. Isotopic fractionation was corrected with ¹³C/¹²C ratios measured on the Tandemtron spectrometer during the analysis. Each sample was measured 3 or 6 times.

RESULTS

Tables 3 and 4 show the averaged ¹⁴C ages of the samples with 1 σ and 2 σ errors. The ¹⁴C ages were calibrated to calendar yr using data from INTCAL98 (Stuiver et al. 1998). In the columns of calibrated ¹⁴C age, the values inside parentheses are the calibrated yr of the mean ¹⁴C age and the values outside indicate the error ranges.

Table 3 Results of ^{14}C dating on the kohitsugire samples of known age.

Sample nr	Lab nr (NUTA2-)	^{14}C age (BP)	Calibrated ^{14}C age (cal AD)
I	5209, 5231	935 ± 14 (1 σ)	1036(1041)1065, 1084(1094,1117)1123, 1137(1141)1144, 1147(1153)1157
		935 ± 28 (2 σ)	1028(1041,1094,1117,1141,1153)1160
II	383	656 ± 22 (1 σ)	1295(1300)1304, 1367(1374,1376)1384
		656 ± 45 (2 σ)	1288(1300)1326, 1348(1374,1376)1391
III	385	348 ± 18 (1 σ)	1487(1516)1523, 1567(1598,1617)1627
		348 ± 37 (2 σ)	1477(1516)1531, 1543(1598,1617)1635

Table 4 Results of ^{14}C dating on the kohitsugire samples of unknown age.

Sample nr	Lab nr (NUTA2-)	^{14}C age (BP)	Calibrated ^{14}C age (cal AD)
1	2042	1104 ± 20 (1 σ)	897(903,916)922, 943(964,972,975)982
2	5212, 5233	1104 ± 41 (2 σ)	891(903,916,964,972,975)995
		685 ± 14 (1 σ)	1289(1295)1298
		685 ± 28 (2 σ)	1284(1295)1301, 1371()1379
3	380	240 ± 23 (1 σ)	1647(1656)1663
		240 ± 46 (2 σ)	1640(1656)1670, 1780()1797
4	379	202 ± 20 (1 σ)	1661(1667)1673, 1777(1782,1795)1800, 1942()1946
		202 ± 41 (2 σ)	1654(1667)1679, 1740()1753, 1756(1782,1795)1804, 1935()1947
5	382	766 ± 23 (1 σ)	1258(1275)1280
		766 ± 45 (2 σ)	1221(1275)1286
6	5214, 5234	670 ± 14 (1 σ)	1294(1297)1300, 1372()1378
		670 ± 28 (2 σ)	1288(1297)1304, 1367()1384

DISCUSSION

Kohitsugire Samples of Known Age

As shown in Table 3, the calibrated ^{14}C ages of samples nr I–III include the presumed paleographical ages. Similar corroboration of historical ages with ^{14}C dates were also found in the previous studies on the ^{14}C dating of ancient Japanese paper samples of known age (Oda et al. 2000, 2003). The results from these known-age samples indicate that the Japanese handmade paper these documents are written on is a suitable material for ^{14}C dating. There are several reasons for this. Japanese

paper sheets were made mainly from branches of the following shrubs: Kozo (*Broussonetia kazinoki* × *Broussonetia papyrifera*), Ganpi (*Diplomorpha sikokiana*), and Mitsumata (*Edgeworthia chrysantha*). Fresh branches less than a few years old were also selected for paper manufacture since old branches yield paper of poor quality. Long preservation of Japanese handmade paper reduces the absorbency of the Indian ink and thin ink used to write on the old paper. Therefore, it is fairly certain that a new paper sheet was used for kohitsugire writing in which particular attention is paid to the deep-black tone of ink. In addition, if an old paper sheet was used for calligraphy, it can be paleographically distinguished because of its watery shade of ink.

We have also considered the tints given to the paper sheets themselves. Although the blue-dyed sample (nr 1) was not completely bleached with acid-alkali-acid treatment and required further chemical treatment as described in the “Methods” section, the paper was tinted during production with indigo, which is a yearly plant and, thus, not a factor of contamination for our dating.

Itsumei Honcho Kaku Gire

Itsumei honcho kaku gire (nr 1) is a tale traditionally attributed to Fujiwara no Yukinari (familiarily called Kouzei, 971–1027), who is one of the most famous calligraphists in the middle Heian period. The handwriting of this kohitsugire is identical with that of *Hakushishikan* written by Kouzei in 1018; consequently, it was regarded as his genuine calligraphy. However, there remained a question. This calligraphy was written on the paper decorated with indigo-blue-dyed fiber, as if clouds are billowing in the sky. Such paper is called *Tobikumogami*. In the historical study on Japanese paper production, it is suggested by the extant *Tobikumogami* with known age that the *Tobikumogami* paper is peculiar to the middle 11th to early 12th century (Yotsutsuji 2001). There was, thus, a question as to the difference between the timing of Kouzei’s writings and the beginning of *Tobikumogami* paper production.

Our results show that the calibrated ¹⁴C age of *Itsumei honcho kaku gire* indicates that it was written in the 10th century (891–995 cal AD, 2 σ). It is suggested that all the extant *Tobikumogami* of known age postdate *Itsumei honcho kaku gire*. The cloud patterns in the *Tobikumogami* paper gradually varied: the old examples in the middle 11th century have relatively large clouds; the size became smaller in the late 11th century; and it changed into mere external decoration in the early 12th century (Yotsutsuji 2001). *Itsumei honcho kaku gire* has large and excellent cloud patterns. It is, therefore, fairly certain that *Itsumei honcho kaku gire* is the oldest example among the extant *Tobikumogami*. Although it had been commonly accepted that *Tobikumogami* paper was produced during quite a short period (middle 11th–early 12th century), we propose, from our ¹⁴C analysis and paleographical views, that the origin ascends back to the late 10th or early 11th century, when Kouzei flourished as a calligraphist. As to ascertaining whether the calligraphist was indeed Kouzei, we cannot make an unequivocal statement; there remains a possibility of other calligraphists in the middle Heian period, especially Prince Kaneakira (914–987) whose calligraphy is similar to that of Kouzei. However, based on the result of ¹⁴C dating and the paleographical comparison with the handwriting of *Hakushishikan* (his genuine calligraphy), it seems reasonable that *Itsumei honcho kaku gire* was written by Kouzei.

Kohitsugire Traditionally Attributed to the Famous Calligraphists

Among the kohitsugire fragments, there are many copies and counterfeits written several centuries later by the following historical circumstances. The kohitsugire fragments of the ancient calligraphists in the Heian-Kamakura period had been used as models of calligraphy because of their antique, rare, and elegant handwriting. Moreover, the development of the tea ceremony in the 16th

century increased the value of the kohitsugire as hanging scrolls. In the Edo period (17th–middle 19th century), collectors of kohitsugire appeared and compiled the albums of kohitsugire (called *kohitsutekagami*). These albums were treasured among upper-class samurai and court nobles. The *kohitsutekagami* has a definite order of calligraphists; therefore, many copies or counterfeits were required for incomplete *kohitsutekagami* albums. As a result, genuine calligraphies from *kohitsutekagami* authors are, in fact, quite rare.

Fujiwara no Sadaie (1162–1241) is the greatest calligraphist of the Kamakura period; he is familiarly called Teika. The kohitsugire fragments of samples nr 2 and 3 are traditionally attributed to him. Sample nr 2 is a part of a scroll composed of 9 kohitsugire sheets. The subject of the scroll is a combination of a part of a waka poem recorded in the *Shin kokin wakashu* (the 8th imperial anthology, the original was compiled in 1205; Teika was an editor of the anthology); sentences with classical Chinese from *Kinpisho* written during 1219–1222 (including some words of the public posts in the Korean government from the 10th century downward: Koryo [918–1392] and Yi [1392–1910] dynasties); and the text of *Ise monogatari* (“The Tale of Ise”, the original of which was written in the first half of the 10th century). If this kohitsugire are genuinely by Teika, it should be an essential reference not only for the study of calligraphy but for classic literature, especially because of the waka poem from *Shin kokin wakashu* and the description of the ancient tale, *Ise monogatari*. The waka and the text of the *monogatari*, however, appear to be written later in the margin of Chinese sentences of *Kinpisho* and the unidentified document. The calibrated ^{14}C age of sample nr 2 indicates the late 13th or late 14th century (1284–1301, 1371–1379 cal AD, 2σ), and it is reasonable to suppose that the kohitsugire is not a genuine calligraphy of Teika.

Sample nr 3 is also attributed to Teika. This fragment is part of a selection of amorous poems from the *Kokin Wakashu* (the first imperial anthology; the original was compiled in 905). The thin handwriting, an individual style of Teika’s writing in his youth, suggests that the anthology was written in about 1200. In addition, another kohitsugire fragment of amorous poems written in the identical handwriting of sample nr 3 had been already authenticated as genuine calligraphy of Teika. However, these 2 fragments of amorous poems have a few kana characters which seem to be different from those of other genuine kohitsugire of Teika. Our ^{14}C results for sample nr 3 indicated that this kohitsugire was written in the middle 17th or the late 18th century and, thus, not attributable to Teika.

Sample nr 4 is part of the anthology of Fujiwara no Sanekata’s poetry. The original of the Sanekata anthology was edited in the 10th century (the middle Heian period). According to the Kiwamefuda label, it was written in the middle Kamakura period by Prince Munetaka (1242–1274). The Kiwamefuda label usually has no valid evidence based on paleographical studies. Actually, this kohitsugire is written in a second Koyagire style which is peculiar to the latter half of the 11th century. However, the handwriting appears to be less adept; therefore, the written age was not determined by the paleographical information. The calibrated ^{14}C age of the kohitsugire indicated a production period from the middle 17th century downward and that the paper sheet was manufactured in the Edo period; thus, the handwriting with this second Koyagire style was a counterfeit. Kohitsugire fragments nr 3 and 4 written in the Edo period would be for a hanging scroll or a *kohitsutekagami* album. They are not genuine calligraphies of Fujiwara no Teika and Prince Munetaka.

The Lost Monogatari

Some ancient tales created in the Heian and Kamakura period are still known in the present day: *Genji monogatari*, *Taketori monogatari*, and *Ise monogatari* are famous examples. However, many other tales were lost by the subdivision of the old manuscripts. Among kohitsugire, there are some fragments with parts of a certain tale which do not match any extant ancient tales and seem to be the

kohitsugire of heretofore unknown tales. If the date of production or the author of such Kohitsugire fragments were uncovered, it would be a significant material clue for reconstruction of the lost tale.

We chose 2 kohitsugire fragments of lost tales for AMS analysis. Because of their tone of ink, it is fairly certain that they were not written on long-preserved paper sheets. Kohitsugire nr 5 is attributed to Nijo Tameuji (1222–1286), and our analysis indicated that this fragment was written in the middle Kamakura (1221–1286 cal AD, 2 σ). This result corresponds to the period when Tameuji flourished as a calligraphist. Fragment nr 6 comes from a lost tale attributed to Reizei Tamesuke (1260–1328). The results on this kohitsugire (1288–1304, 1367–1384 cal AD, 2 σ) also includes the time when Tamesuke flourished. Although the error range reached to the late 14th century, it is obvious that the kohitsugire was not a counterfeit made from the 16th century downward. Our analysis indicated that these 2 kohitsugire are not forgeries for hanging scrolls or kohitsutegagami albums. It also supports their worth for the study of classical literature as fragments from old manuscripts of lost tales. The collection of other kohitsugire fragments with identical handwriting and dating by paleographical views or ¹⁴C method will, thus, assist the reconstruction of lost tales written in the Kamakura period.

CONCLUSION

¹⁴C ages of kohitsugire fragments were measured by the AMS method. The results on the kohitsugire of known age supported that Japanese paper is suitable sample for ¹⁴C dating because of the small discrepancy between the calibrated ¹⁴C age and the historical age. The ¹⁴C dating on samples of unknown age provided new information for the written age, the author, the history of paper manufacture, and also the estimation of the worth as a material for the study on classical literature, history, and paleography.

ACKNOWLEDGEMENTS

This research was supported in part by a Grant-in Aid for Young Scientists (B) (nr 14780091) from the Japan Society for the Promotion of Science.

REFERENCES

- Oda H, Yoshizawa Y, Nakamura T, Fujita K. 2000. AMS radiocarbon dating of ancient Japanese sutras. *Nuclear Instruments and Methods in Physics Research B* 172:736–40.
- Oda H, Masuda T, Niu E, Nakamura T. 2003. AMS radiocarbon dating of ancient Japanese documents of known age. *Journal of Radioanalytical and Nuclear Chemistry* 255(2):375–9.
- Stuiver M, Reimer PJ, Bard E, Beck JW, Burr GS, Hughen KA, Kromer B, McCormac FG, van der Plicht J, Spurk M. 1998. INTCAL 98 radiocarbon age calibration, 24,000–0 cal BP. *Radiocarbon* 40(3):1041–83.
- Yotsutsuji H. 2001. *Glossary. Decorative Papers*. Aichi, Japan: The Tokugawa Museum. p 220–9. In Japanese, with English abstract.

NEOLITHIC MASSACRES: LOCAL SKIRMISHES OR GENERAL WARFARE IN EUROPE?

Eva Maria Wild¹ • Peter Stadler² • Annemarie Häußner³ • Walter Kutschera¹ • Peter Steier¹ • Maria Teschler-Nicola⁴ • Joachim Wahl⁵ • Helmut J Windl⁶

ABSTRACT. The Neolithic site of Schletz in Lower Austria comprises a fortified settlement from the end of the *Linearbandkeramik* (LBK) culture. Large numbers of human bones were found at the base of the fortification ditches, and many of the excavated bones and skulls showed evidence of trauma which most likely originates from violence. This remarkable deposit of human remains has been considered evidence for an abrupt end to the Early Neolithic settlement at Schletz. In order to investigate this interpretation, radiocarbon accelerator mass spectrometry (AMS) measurements of human bone samples from this site were performed at VERA. The χ^2 test of the results from specimens with clearly identified lesions suggests that these may be contemporaneous. Further, it may be concluded that all individuals with evidence of trauma from Schletz were probably the victims of a single event: a massacre at the end of the LBK.

Similar evidence is found at Early Neolithic sites at Talheim and Herxheim in the western part of Germany. Analysis of the ¹⁴C ages of bones from both sites suggests that the Talheim event may have been coeval with the massacre of Schletz, whereas an event at Herxheim might have happened some time earlier. For Herxheim, the massacre theory is still under discussion, and a change in the burial rite is also considered as an alternative interpretation.

INTRODUCTION

The *Linearbandkeramik* (LBK) is a European culture which developed in the central part of Europe in Early Neolithic times. This culture was spread over a large area of Europe, from the northwestern regions of Germany to the southeastern parts of Europe around the Black Sea. In contrast to all succeeding cultures, the LBK rarely showed local characteristics in ceramic styles. People of the LBK lived in the period after the fundamental transition in human lifestyle from hunter-gathering to farming. Generally, the LBK time is considered to have been a peaceful period (Petrasch 1999). At the end of the LBK, though, living conditions must have become more violent, seen by the occurrence of settlements with fortifications.

THE EARLY NEOLITHIC SITE AT SCHLETZ IN LOWER AUSTRIA

One of the fortified settlements from the end of the LBK period is the archaeological site at Schletz in eastern Austria. Schletz is located about 50 km north of Vienna in Lower Austria (Figure 1a). A map of the settlement, derived from aerial survey and geophysical investigations, is given in Figure 1b. The 2 oval fortification ditches of the settlement are indicated. Systematic excavations at the site started in 1983 and are still on-going (Windl 1996, 2001).

¹Vienna Environmental Research Accelerator (VERA), Institut für Isotopenforschung und Kernphysik, Universität Wien, Währinger Strasse 17, A-1090 Wien, Austria. Corresponding author. Email: eva.maria.wild@univie.ac.at.

²Prähistorische Abteilung, Naturhistorisches Museum, Burgring 7, A-1014 Wien, Austria.

³Landesamt f. Denkmalpflege, Amt Speyer, Kleine Pfaffengasse 10, D-67345 Wiesbaden, Germany.

⁴Anthropologische Abteilung, Naturhistorisches Museum, Burgring 7, A-1014 Wien, Austria.

⁵Landesdenkmalamt Baden-Württemberg, Osteologie, Stromeyersdorfstraße 3, D-78467 Konstanz, Germany.

⁶Museum für Urgeschichte des Landes Niederösterreich, A-2151 Asparn/Zaya, Austria.

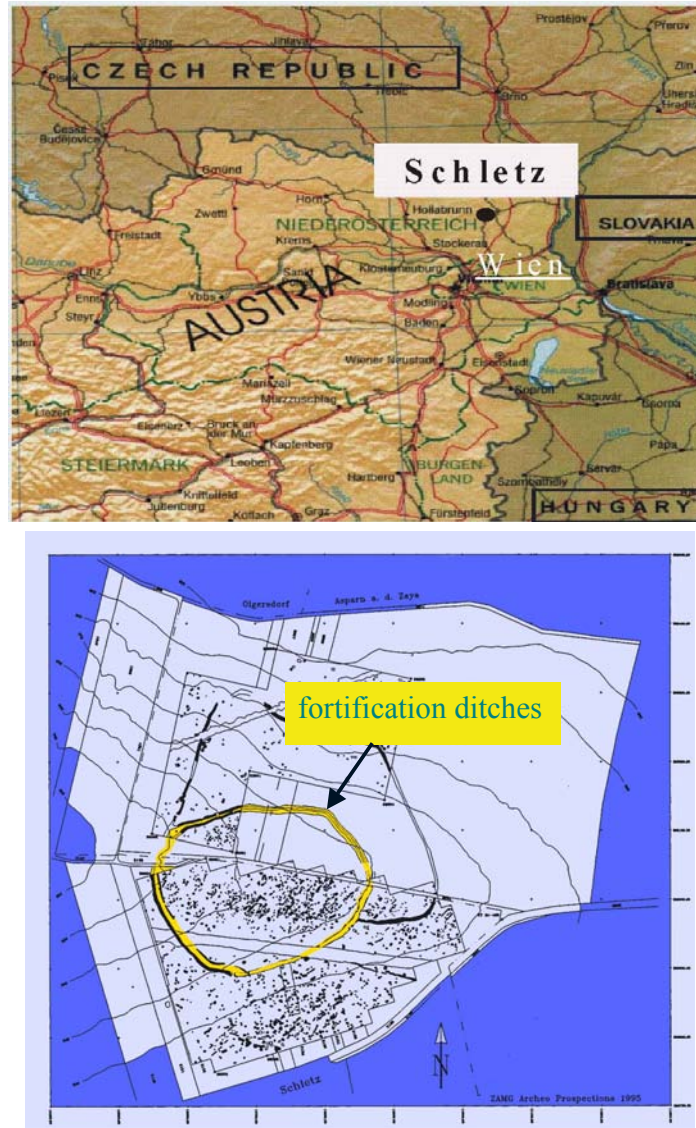


Figure 1 (a) Map of the northeastern part of Austria showing the location of Schletz, north of Vienna; (b) Map of the Early Neolithic site of Schletz derived from aerial survey and geophysical prospection (Windl 1996).

Anthropologic Investigations of Human Remains from Schletz

In the course of the excavations at Schletz, large numbers of human remains were found at the base of the outer ditch. It is estimated from the number of cranial and postcranial remains that approximately 200 individuals were deposited in the ditches. Up to now, about 100 individuals have been excavated. The skeletons were found mainly in strange positions, and often several skeletons were grouped together (see Figure 2). The bodies were deposited prone and many skeletons were incomplete with extremities missing.



Figure 2 Photograph from the Early Neolithic excavation area at Schletz showing human remains as found in the fortification ditches.

A subsample of 67 individuals has been investigated by osteologists. This investigation showed that all the skulls were lethally fractured (Figure 3), and many of the postcranial remains exhibit unusual features too. A large number of the bones showed carnivore gnawing marks. The age and the sex distribution of the individuals was also determined, and it is evident that the occurrence of females among the young adult population is significantly reduced. From these results, it has been suggested that the traumatic lesions originate from inter-human aggressive acts. It was also suggested that the carnivore bite marks, which are definitely post-mortem alterations of the bones, indicate that the individuals were left unburied for some time. The reduced abundance of females amongst the young adults was interpreted as an indication of the abduction of women of child-bearing age. It was further deduced that these humans were probably the victims of a massacre which led to the abrupt end of the LBK settlement at Schletz (Teschler-Nicola et al. 1999).

Other European Early Neolithic Sites with Evidence of Massacre

A similar situation as in Schletz is also found at 2 Neolithic sites from the LBK period in Germany: at Herxheim in Rheinland-Pfalz and in Talheim near Heilbronn in Baden-Württemberg. These 2 sites are located approximately 750 km to the northwest and 660 km to the west from Schletz, respectively.

Talheim

The remains of 34 human individuals were excavated from a mass grave found at Talheim in 1983/84. This mass grave was located outside the (assumed) settlement area, which was detected by a surveying project more than 50 yr ago. In contrast to Schletz, no fortifications have yet been found. The position of the skeletons indicated that these human remains were not buried according to usual LBK burial rites. Many bodies were lying face down, others in a very unusual twisted posture, and

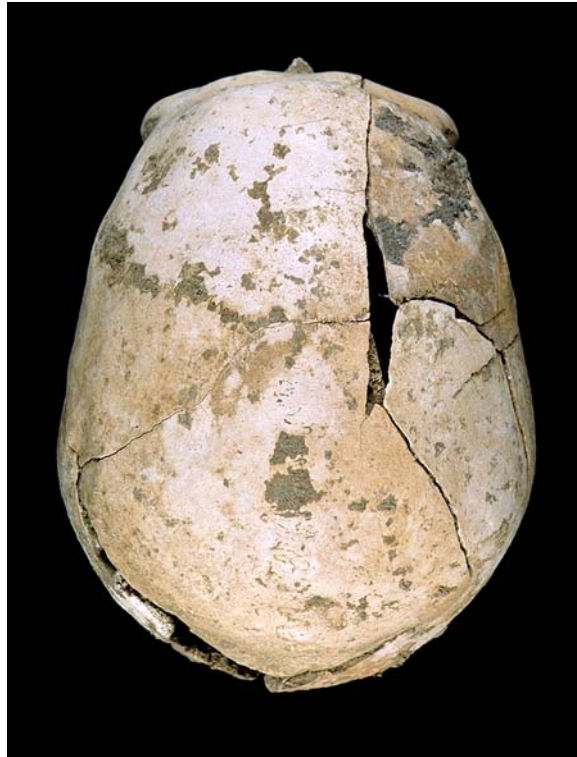


Figure 3 Human skull excavated at Schletz with a typical bending fracture

several skeletons were mixed together. In contrast to the Schletz remains described above, animal gnawing marks were not found. The whole assemblage was interpreted as a mass grave, with bodies quickly thrown into a pit and covered. Anthropological investigation of the bones showed that several skulls were lethally fractured. This again suggests that the humans found in the mass grave were the victims of a massacre. A possible deficit of infants in the age group of below 4 yr was suggested from the age and sex profile of the burial assemblage. It was calculated from the number of women of child-bearing age that no more than 4 additional children should have been present in the grave. Three reasons were considered for the possibility of missing infants: the new-born children may have died of natural causes before the massacre and been buried according to usual custom; the average time between pregnancies could have been almost doubled by nutrition deficiencies and/or physical, plus psychological stress of the women; and third, that these children have been kidnapped by the attackers (Wahl and König 1987).

Herxheim

In the Herxheim area, archaeological finds are known since 1900. Up to now, more than 75 sites have been detected. Early excavations showed that they date from the Hallstatt and the La Tène periods and also from the Neolithic. In a big excavation campaign in 1996–1999, a large LBK settlement was excavated. The settlement was equipped with an outer and an inner fortification ditch—similar to Schletz—where a huge amount of human remains was found. It has been estimated from the excavated bones that more than 500 individuals are buried/deposited in the excavation area, most of them in the ditches (Häußer 1998). Many skeletons were incomplete and were not lying in a correct

anatomical position. Several bones were fragmented and deposited together with animal bones, pottery, and other waste material from the settlement. The most extraordinary findings at Herxheim are calottes from human skulls which at some places appeared to be grouped together. Also, cut marks have been detected on some skulls and bones. For the Herxheim site, a massacre is not the only reason put forward for the atypical burial of the human remains. It is also suggested that these remains may be the result of a change in burial rites at the end of the LBK (Orschiedt 2003; Häußler 1998).

¹⁴C DATING AND DATA EVALUATION

In order to test the hypothesis that people were killed at the same time, 15 human bone samples from Schletz were ¹⁴C dated at the Vienna Environmental Research Accelerator (VERA).

The dated bones originated from the fortification ditches as well as from regular graves within the settlement. Our standard procedures for the preparation of bone samples and the ¹⁴C measurement protocol which we use for archaeological samples were also applied for the Schletz samples (Wild et al. 1998, 2001).

The age determinations are listed in Table 1, together with information on whether the sample originates from a massacred individual or an individual buried in a grave. Two bone samples from Schletz excavated from the ditches were dated some years ago at ETH Zurich. The ¹⁴C ages of 6145 ± 55 BP (ETH 14373) and 6025 ± 55 BP (ETH 14374) were determined by accelerator mass spectrometry (AMS). From the entire data set (VERA plus ETH data), the unrounded results from samples with clearly identified trauma were combined. The sample from the ditch with the anthropological assessment “massacre not proved” was not included. A χ^2 test of the selected data was performed to check whether the distribution of the results is in agreement with the hypothesis that all samples are of the same age (e.g. Geyh and Schleicher 1990). After the removal of 1 outlier (VERA-2020/VERA-2738, see Table 1), a χ^2 value of 15.4 at 10 degrees of freedom (df) was calculated. The age determination of sample VERA-2020 was repeated (VERA-2738) and the age is in agreement with the result of the first measurement. The outlying of this sample is unexplained. Usually, for the rejection of the “Null hypothesis” (in the present case: all dated samples are coeval), a 5% significance level is used. For a data set with 10 df, a χ^2 value of 18.3 corresponds to the 5% significance level. As the χ^2 value determined for the measured data set is smaller than this, the Null hypothesis (H_0 in statistical textbooks) can be accepted, i.e., no significant differences between the sample ages have been detected. The Schletz data suggest that the samples may originate from the same time. This result seems to support the massacre theory. In addition, no regular grave was dated (see Table 1) to be younger than the time of the massacre. Thus, the massacre could have been the cause of the end of the Neolithic settlement at Schletz.

Human bones from the 2 German sites were also dated at VERA: 4 samples from Herxheim and 7 samples from Talheim (Table 2). The respective data sets were combined and again χ^2 tests were performed. Two samples from Talheim were ¹⁴C dated in the 1980s by GPC (gas proportional counting) at Heidelberg. Sample HD 8606-8827, gave a ¹⁴C age of 5960 ± 80 BP, and for sample HD 8607-8828, a ¹⁴C age of 6045 ± 80 BP was determined. Although consistent with the AMS ¹⁴C ages determined at VERA, these results were not included in the present study because of the relatively large uncertainty on these ages. Adding these data to the AMS data set does not have a significant effect on the result of the weighted mean or on the result of the χ^2 test.

According to the χ^2 value of 1.5 (required value for the rejection of H_0 at a 5% significance level and 3 df: 7.8) determined for the Herxheim data, no deviation from the contemporaneity of the investigated samples is detected. One outlier (VERA-2021, see Table 2) had to be rejected from the Tal-

Table 1 ^{14}C data (rounded off according to Stuiver and Polach 1977) of all bone samples from Schletz measured at VERA and ETH Zurich.

^{14}C lab nr	Sample material	Find inventory nr, provenance, and anthropological assessment	Individual nr	$\delta^{13}\text{C}^{\text{a}}$ [‰]	^{14}C age ^a [BP]	Calibrated time range ^b 2 σ confidence interval
VERA-2007	human bone	4470 4224 ^e , ditch, probably massacred	1993/12	-21.7 ± 0.4	6175 ± 35	5260 BC (95.4%) 4990 BC
VERA-2008	human bone	4518, ditch, massacred	1993/5	-23.9 ± 0.5	6145 ± 35	5260 BC (25.0%) 5160 BC 5150 BC (70.4%) 4940 BC
VERA-2009	human bone	4518, ditch, massacred	1993/4	-21.5 ± 0.6	6055 ± 35	5050 BC (93.1%) 4840 BC 4820 BC (2.3%) 4800 BC
VERA-2010	human bone	4520 ^d , ditch, massacred	1993/2	-20.5 ± 0.5	6130 ± 35	5230 BC (18.4%) 5160 BC 5150 BC (75.7%) 4940 BC 4870 BC (1.2%) 4860 BC
VERA-2011	human bone	4520 ^d , ditch, massacred	1993/17	-21.1 ± 0.5	6100 ± 35	5210 BC (7.0%) 5170 BC 5140 BC (1.8%) 5120 BC 5080 BC (81.2%) 4900 BC 4880 BC (5.4%) 4850 BC
VERA-2012	human bone	5076, ditch, massacred	1996/3	-22.4 ± 0.6	6075 ± 35	5200 BC (1.2%) 5180 BC 5070 BC (81.1%) 4900 BC 4890 BC (13.1%) 4840 BC
VERA-2737	human bone	5839 6072 6076 ^c , ditch, massacred	1997/4	-19.3 ± 0.4	6175 ± 30	5260 BC (93.7%) 5030 BC 5020 BC (1.7%) 5000 BC
VERA-2014	human bone	685/S11, ditch, massacred	Ind. 41	-21.1 ± 0.5	6125 ± 35	5230 BC (16.4%) 5160 BC 5150 BC (77.2%) 4930 BC 4880 BC (1.8%) 4850 BC
VERA-2015	human bone	302/S6-7, ditch, massacred	Ind. 61	-20.9 ± 0.4	6160 ± 35	5260 BC (95.4%) 4960 BC
VERA-2016	human bone	374/S7, regular grave	Ind. 24	-18.9 ± 0.5	6210 ± 40	5300 BC (95.4%) 5050 BC
VERA-2017	human bone	264/S4-6, ditch, massacre not proved	Ind. 62	-21.8 ± 0.4	6200 ± 35	5300 BC (95.4%) 5040 BC
VERA-2019	human bone	unclear provenance	88/5?	-21.8 ± 0.6	6175 ± 40	5280 BC (95.4%) 4990 BC
VERA-2020	human bone	4455, ditch, massacred	1993/11	-22.4 ± 0.5	6235 ± 40	5310 BC (95.4%) 5060 BC
VERA-2738	human bone	4455, ditch, massacred, VERA-2020 repeated	1993/11	-20.5 ± 0.5	6205 ± 30	5290 BC (95.4%) 5050 BC
VERA-2198	human bone	666, regular grave	—	-18.6 ± 1.6	6210 ± 35	5300 BC (95.4%) 5050 BC
VERA-2441	human bone	692, regular grave	—	-18.7 ± 0.4	6165 ± 35	5260 BC (95.4%) 4990 BC
ETH 14373	human bone	4223, ditch, massacred	n.a. ^e	-19.3 ± 1.1	6025 ± 55	5060 BC (95.4%) 4770 BC
ETH 14374	human bone	4521, ditch, massacred	n.a.	-20.6 ± 1.2	6145 ± 55	5280 BC (93.7%) 4910 BC 4880 BC (1.7%) 4850 BC

^a 1 σ uncertainty.

^b The ^{14}C age calibration was performed with the INTCAL98 calibration curve (Stuiver et al. 1998).

^c One individual can be represented by more find inventory numbers.

^d A single find inventory number may include more than one individual.

^e n.a. = not available.

heim data. We concluded that this sample was probably contaminated by a consolidant. The χ^2 test of the reduced data set (7.5 compared to a value of 11.1 at 5 df for the rejection of the H_0 at the 5% significance level) also indicates that these samples may be of the same age.

In the calculation of the weighted mean, the fact that several samples were measured in 1 measurement run was taken into account. In routine ^{14}C measurement at VERA, about 30 sputter targets of “unknowns” are mounted in a target wheel together with a set of ^{14}C standards and 1 blank sample (“dead” carbon) which were produced at the same time. The $^{14}\text{C}/^{12}\text{C}$ ratio determined for each of the measured unknowns present in 1 wheel is corrected with the same blank value and normalized to the same set of standards. Therefore, in the evaluation of the standard deviation of the weighted mean value of all ^{14}C ages, correlated uncertainties had to be taken into account. (For details of the routine evaluation procedures, see Steier et al., these proceedings.) The results of the combination of the data and the calibration of the thus derived ^{14}C ages are displayed in Figure 4. The respective χ^2 value of each data set is also indicated in the plot.

Table 2 ¹⁴C data (rounded off according to Stuiver and Pollach 1977) of the Early Neolithic bone samples from Talheim and Herxheim measured at VERA and at the Academy of Science at Heidelberg.

¹⁴ C lab nr	Find inventory nr sample material, location	δ ¹³ C ^a [‰]	¹⁴ C age ^a [BP]	Calibrated time range ^b 2 σ confidence interval
VERA-2021	SK16, human bone, Talheim	-22.9 ± 0.5	5930 ± 35	4910 BC (7.5%) 4870 BC 4860 BC (87.9%) 4710 BC
VERA-2022	83/1, human bone, Talheim	-21.9 ± 0.5	6130 ± 35	5230 BC (18.4%) 5160 BC 5150 BC (75.7%) 4940 BC 4870 BC (1.2%) 4860 BC
VERA-2023	83/10, human bone, Talheim	-22.0 ± 0.4	6085 ± 30	5200 BC (1.7%) 5180 BC 5070 BC (85.1%) 4900 BC 4890 BC (8.6%) 4850 BC
VERA-2025	SK22, human bone, Talheim	-21.5± 0.5	6015 ± 35	5000 BC (95.4%) 4780 BC
VERA-2026	83/13, human bone, Talheim	-21.4 ± 0.3	6095 ± 35	5210 BC (5.6%) 5170 BC 5140 BC (1.2%) 5120 BC 5080 BC (82.3%) 4900 BC 4890 BC (6.3%) 4850 BC
VERA-2046	SK21?, human bone, Talheim	-22.7 ± 1.1	6115 ± 35	5210 BC (11.8%) 5170BC 5150 BC (5.6%) 5110 BC 5100 BC (75.0%) 4910 BC 4880 BC (2.9%) 4850 BC
VERA-2047	83/19, human bone, Talheim	-21.6 ± 0.9	6140 ± 40	5260 BC (22.9%) 5160 BC 5150 BC (72.5%) 4940 BC
HD 8606-8827	SK4, human bone, Talheim	-21.18 ^c	5960 ± 80	5060 BC (94.3%) 4670 BC 4640 BC (1.1%) 4610 BC
HD 8607-8828	SK14, human bone, Talheim	-20.59 ^c	6045 ± 80	5250 BC (95.4%) 4700 BC
VERA-1826	E96/102 281-14-6 human bone, Herxheim	-19.1 ± 1.3	6145 ± 35	5260 BC (25.0%) 5160 BC 5150 BC (70.4%) 4940 BC
VERA-1827	E96/102 281-117-4 human bone, Herxheim	-20.1 ± 1.2	6165 ± 40	5260 BC (95.4%) 4960 BC
VERA-1828	E96/102 282-7-6 human bone, Herxheim	-20.7 ± 1.3	6190 ± 30	5260 BC (95.4%) 5040 BC
VERA-1830	E96/102 296-16 human bone, Herxheim	-22.5 ± 1.3	6195 ± 35	5290 BC (95.4%) 5040 BC

^a 1 σ uncertainty.

^b The ¹⁴C age calibration was performed with the INTCAL98 calibration curve (Stuiver et al. 1998).

^c 1 σ standard deviation smaller than 0.03‰.

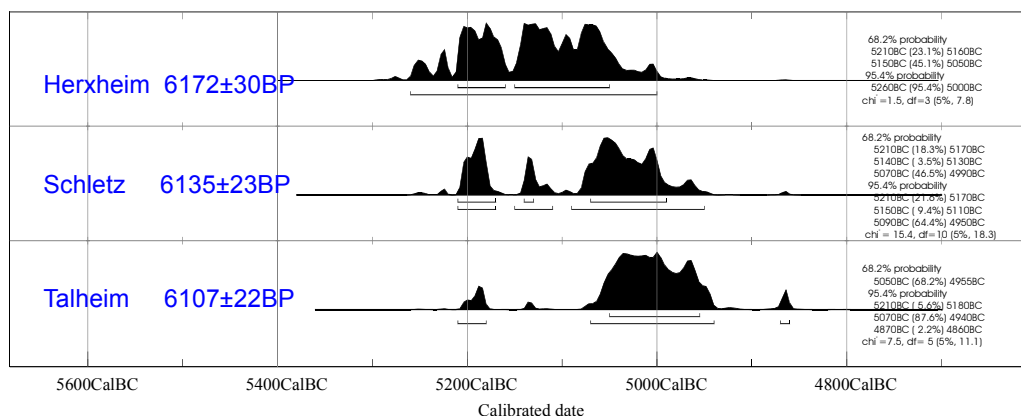


Figure 4 Calibration of the mean ¹⁴C age values from the 3 sites investigated in this study. The results of the χ^2 are also listed.

DISCUSSION

Although it is known that bone collagen of humans shows a variable turnover time which depends on the biological age of the individual (Wild et al. 1998), it is not expected to detect such an effect in archaeological bone samples with the precision presently achieved in AMS ^{14}C determinations. It must also be noted that variations in the ^{14}C age must be very small due to the relatively short lifetime of people from this time period; for instance, the mean lifespan of the Neolithic Talheim population was estimated to be about 24 yr (Wahl and König 1987). Thus, it was assumed that the χ^2 test of data from human bone samples should not fail if all the individuals died at the same time, because such samples would be of the same ^{14}C age. This could be shown for the data of each of the LBK sites investigated in this study. The χ^2 tests show no indication that these data sets include samples of different age. Therefore, according to our results, the massacre theory seems plausible for all 3 sites. But once again, it should be noted that the complex Herxheim site is not directly comparable to the others and a different interpretation is under discussion (see above).

From the calibrated date ranges shown in Figure 4, it can be deduced that the events at Talheim and at Schletz may have been contemporary. According to the calibration results, the event at Herxheim may have taken place earlier than the 2 other sites, although the possibility that the Herxheim event is coeval with the others cannot be fully excluded.

These results induce further questions about the reasons for increased violence at the end of the LBK period. Obvious aggression is documented by the appearance of fortification ditches at settlements from this time. Three reasons are discussed as possible causes for inter-human attacks and massacres: a) these events were the consequence of the breakdown of local economic systems, leading to local skirmishes between neighbors in isolated regions in Europe; b) these events were triggered by a more general disturbance (e.g. climate) affecting a larger area of Europe; and c) the massacres were caused by a wave of migration that overran Central Europe and may also have been triggered by climatic changes (see Teschler-Nicola et al. 1999).

CONCLUSION

The ^{14}C data of the Early Neolithic site at Schletz described above support the massacre theory derived from the osteological investigation of the human remains. No younger Neolithic material was found at this site, which suggests that this massacre was the end of the Neolithic settlement period. For the 2 German sites, the ^{14}C data indicate that the human remains may be coeval, and a massacre theory seems to be possible for these sites, although for the Herxheim site another explanation for the atypical burial of the Neolithic human remains is under discussion.

ACKNOWLEDGEMENTS

The investigation of the Schletz samples was performed in the course of the research project P12253-PHY "Absolute Chronology for Early Civilizations in Austria and Central Europe using ^{14}C Dating with Accelerator Mass Spectrometry" funded by the Austrian Science Fund. We wish to thank Harald Humberger and Martin Janner for their help in sample preparation.

REFERENCES

- Geyh M, Schlicher H. 1990. *Absolute Age Determination. Physical and Chemical Dating Methods and Their Application*. Berlin-Heidelberg, New York: Springer-Verlag.
- Häußer A, editor. 1998. *Krieg oder Frieden? Herxheim vor 7000 Jahren*. Exhibition catalog printed in Odenwald, Bellheim, Germany.
- Orschiedt J. 2003. Ein überlebtes, mehrfaches Schädeltrauma aus dem frühen Neolithikum. In: *Abstracts of the Workshop: Frühe Spuren der Gewalt-Schädelverletzungen und Wundversorgung an prähistorischen Menschenresten aus interdisziplinärer Sicht*,

- 28.11.2003–30.11.2003. Rostock-Warnemünde. p 9–10.
- Petrasch J. 1999. Mord und Krieg in der Bandkeramik. *Archäologisches Korrespondenzblatt* 29:505–16.
- Steier P, Dellinger F, Kutschera W, Rom W, Wild EM. 2003. Pushing the precision of ^{14}C measurements with AMS. *Radiocarbon*, these proceedings.
- Stuiver M, Polach HA. 1977. Discussion: reporting of ^{14}C data. *Radiocarbon* 19(3):355–63.
- Stuiver M, Reimer PJ, Bard E, Beck JW, Burr GS, Hughen KA, Kromer B, McCormac G, van der Plicht J, Spurk M. 1998. INTCAL98 radiocarbon age calibration, 24,000–0 cal BP. *Radiocarbon* 40(3):1041–83.
- Teschler-Nicola M, Gerold F, Bujatti-Narbeshuber M, Prohaska T, Latkoczy Ch, Stingeder G, Watkins M. 1999. Evidence of genocide 7000 BP—Neolithic paradigm and geoclimatic reality. *Collegium Antropologicum* 23:437–50.
- Wahl J, König HG. 1987. Anthropologisch-Traumatologische Untersuchung der menschlichen Skelettreste aus dem Bandkeramischen Massengrab bei Talheim, Kreis Heilbronn. *Fundberichte Baden-Württemberg* 12:65–193.
- Wild EM, Stadler P, Bondá MR, Draxler S, Friesinger H, Kutschera W, Priller A, Rom W, Ruttkey E, Steier P. 2001. New chronological frame for the Young Neolithic Baden culture in Central Europe (4th millennium BC). Proceedings of the 17th International Radiocarbon Conference. *Radiocarbon* 43(2B):1057–64.
- Wild E, Golser R, Hille P, Kutschera W, Priller A, Puchegger S, Rom W, Steier P, Vycudilik W. 1998. First ^{14}C results from archaeological and forensic studies at the Vienna Environmental Research Accelerator. *Radiocarbon* 40(1):273–81.
- Windl H, editor. 1996. *Rätsel um Gewalt und Tod vor 7000 Jahren. Katalog des NÖ Landesmuseums*. Asparn a.d. Zaya, Austria.
- Windl H. 2001. Erdwerke der Linearbandkeramik in Asparn an der Zaya/Schletz, Niederösterreich. *Preistoria Alpina* 37:137–44.

¹⁴C DATING OF THE SETTLEMENT OF ICELAND

Arny E Sveinbjörnsdóttir¹ • Jan Heinemeier² • Gardar Gudmundsson³

ABSTRACT. The dating of the settlement of Iceland has been debated for many years. According to written sources (sagas) from the early 12th century, the first Norwegian settlers arrived in Iceland in AD 874. However, some ¹⁴C dates from the earliest archaeological sites in Iceland, invariably from samples of birch and other indigenous wood species, have yielded surprisingly old ages, older by 100–150 yr than the historical date, suggesting that the settlement took place in the 7th or 8th century. In this paper, we report 16 new ¹⁴C dates of pairs of barley grain and wood samples from an excavation in Reykjavík in 2001. The new results show that the wood samples tend to be older than the grain samples by up to about 100 yr. We argue that the barley grains give the true date (AD 890), whereas the wood dates are too old. The grain dates are in close agreement with the settlement year quoted in the written sources. In particular, our new data eliminate the need of any of the ad hoc theories introduced up to now to explain the suspiciously high ¹⁴C ages of wood samples from the settlement of Iceland, namely, 1) the island effect, 2) the volcanic or geothermal effect, or 3) that settlement actually took place significantly before the time recorded in the sagas.

INTRODUCTION

Written Sources

The time of the settlement of Iceland has been the subject of intense debate for many years, fueled by the fact that radiocarbon dates of early human occupation often give an older age than the historical tradition, which places the first settlement in the late 9th century. The traditional settlement time is based on written sources (sagas) from the early 12th century according to which the first Norwegian settlers are said to have arrived in Iceland in AD 874 (Íslendingabók Ara fróða).

The Settlement Tephra Layer

The changes in land use following the beginning of permanent settlement show up in soil profiles as a change in soil type and pollen composition (Einarsson 1962; Hallsdóttir 1987, 1996). This stratigraphic transition is located close to a volcanic ash (tephra) layer (denoted the “Settlement” layer), which has been found in soil profiles over a large part of Iceland. Larsen (1996) reported that the tephra layer was formed in a volcanic eruption from Vatnaöldur, southeast Iceland, in the last part of the 9th century based on a relative age determination. The tephra layer was first noted in the 1940s, during an excavation in Thjórsárdalur, south Iceland, where it was found just below the oldest remains of settlement (Thórarinnsson 1944). Pollen analyses have shown that changes in land use following the start of permanent settlement in some places occurred just before the volcanic eruption in Vatnaöldur, but in other places occurred just after the eruption (Hallsdóttir 1996).

Dating of the Settlement Layer

Three attempts have been made to ¹⁴C date organic remains adjacent to the Settlement tephra layer in Iceland (see Figure 1a,b). Thórarinnsson (1977) reported 2 ¹⁴C dates with a mean calibrated value of AD 845 ± 45. Theodórsson (1993) pointed out that due to the plateau on the calibration curve between AD 770 and 880, Thórarinnsson’s results should not be reported as a mean value since their age range spans the plateau time interval. Haraldsson (1981) reported the calibrated age AD 860 ± 75

¹Science Institute, University of Iceland, IS107 Reykjavík, Iceland. Corresponding author. Email: arny@raunvis.hi.is.

²AMS Dating Centre, Department of Physics and Astronomy, University of Aarhus, DK-8000 Aarhus, Denmark.

³Institute of Archaeology, Bárugata 3, 101 Reykjavík, Iceland.

based on 1 bog sample. Hallsdóttir (1987) collected 5 samples of organic remains, one from the tephra layer, two 1-cm slices above the layer, and 2 slices below the layer, and reported a mean calibrated age of AD 845. Wiggle-matching of Hallsdóttir’s results gives AD 835 ± 20 (Theodórsson 1993). In addition, the Settlement tephra layer has been recognized in Irish bogs and ¹⁴C dated to AD 860 ± 20 (calibrated age, Hall et al. 1993). Although all the attempts to ¹⁴C date the Settlement tephra layer are mutually compatible, the age of the layer cannot be determined very accurately due to the plateau in the calibration curve. The ¹⁴C dates agree, however, with the precise result AD 871 ± 2 obtained by absolute dating of the tephra layer in the GRIP ice core in Greenland (Grönvold et al. 1995). The results of both methods agree with the historical date of the settlement.

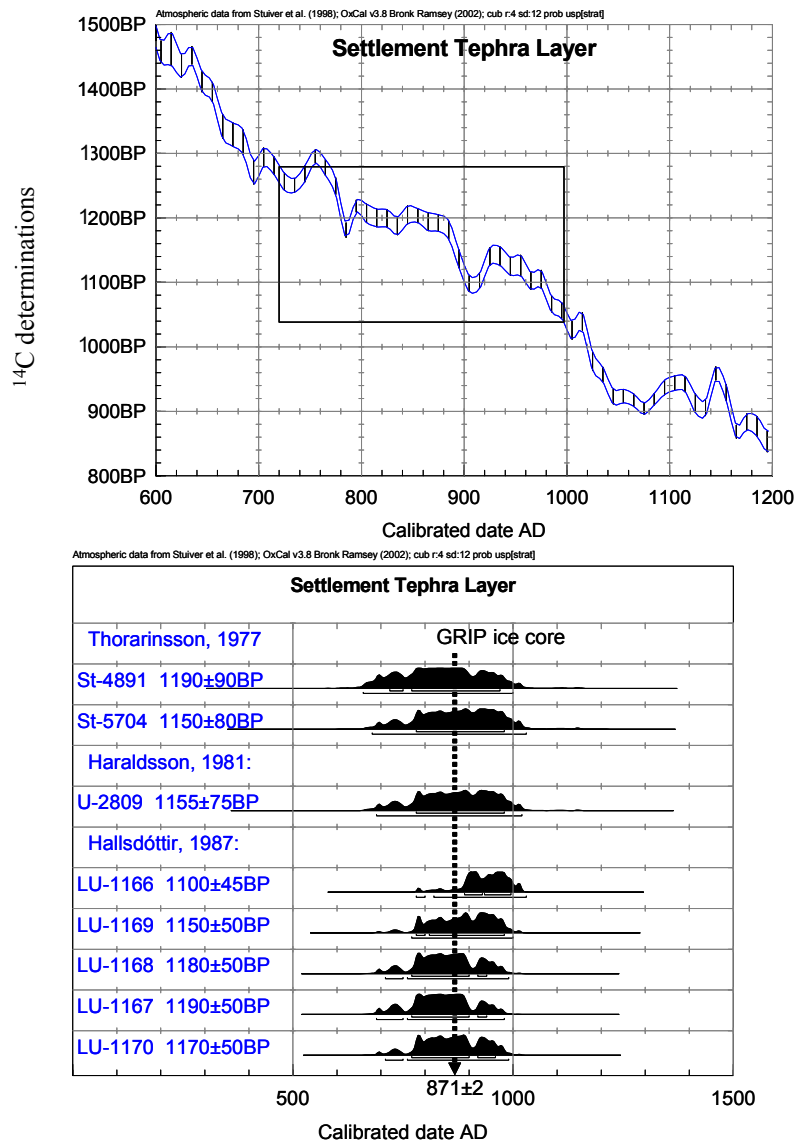


Figure 1 a) The calibration curve with the region of interest for the settlement time period indicated. The age plateau makes it difficult to achieve accurate ¹⁴C-based age determination of samples from the settlement period. b) Attempts to date the Settlement ash layer are mutually compatible, as shown by the probability distributions as calculated by the OxCal v3.8 calibration program (Bronk Ramsey 2001).

Previous ¹⁴C Dates of Archaeological Sites from the Settlement Period

Although we now know precisely the age of the Settlement tephra layer, the age of the settlement is still debatable, since the chronological association between the tephra layer and the earliest strata of human occupation is not always clear and the ¹⁴C dates of archaeological remains often indicate earlier settlement (Nordahl 1988; Hermanns-Audardóttir 1989). Vilhjálmsson (1991) has compiled ¹⁴C dates from archaeological sites in Iceland and criticized ¹⁴C dating laboratories, archaeologists, and geologists for misinterpreting ¹⁴C dates. In the following, we examine the previous results from Reykjavík and Vestmannaeyjar for comparison with our new ¹⁴C dates from Reykjavík reported below.

Reykjavík Site

In the 1970s, archaeological excavations were undertaken in Reykjavík at sites from the settlement period. About 30 ¹⁴C dates were obtained (Nordahl 1988). Of the 35 results shown in Figure 2, 13 dates have their 68.2% (1 σ) probability interval older than the Settlement tephra layer, the difference being as much as 100 yr for the 6 oldest samples. Based on these, one would have to accept a *terminus ante quem* (TAQ) for the first settlement of about AD 780 (indicated by the dotted line), assuming negligible lifespan and deposition time before the wood was charred. The same TAQ would result using the 2- σ interval (based on the 2 oldest samples). All of the samples in Figure 2 are from birch, *Betula pubescens*, *B. tortuosa*, and/or *B. nana*, apart from 1 European larch-sample, *Larix decidua* (U-2082), and 1 grain sample (U-2674). In the case of wood samples, the measured ¹⁴C age depends on the biological age of the dated tree rings and the time interval between death and subsequent use of the wood. The highest biological age for Icelandic birch is about 100 yr. The maximum age of the European larch is about 200 yr. These trees grow in Central Europe and the wood has probably been shipped to Iceland as building material (Grimsson and Einarsson 1970). In light of this, wood samples can be expected to give greater ¹⁴C ages than that of the archaeological event. Grain, on the other hand, is probably from the latest harvest and, therefore, most likely to give a reliable date of the human activity. The 2- σ calibrated age range of the grain sample (U-2674) is AD 860–1160 (Figure 2 *continued*, last sample).

Vestmannaeyjar Site

Figure 3 shows the ¹⁴C results of samples from an excavation in Herjólfsdalur in Vestmannaeyjar (the Westman Islands) off the southwest coast of Iceland (Hermanns-Audardóttir 1989). Six out of 10 results give older calibrated ¹⁴C ages (1 σ) than the Settlement tephra layer by 100 yr or more for three of them. With the assumptions discussed for the Reykjavík site the TAQ for the settlement of Vestmannaeyjar would be AD 690 or, omitting the oldest sample, AD 780 (shown by the dotted line on Figure 3). All measurements were done on wood samples, mostly Icelandic birch (*Betula*) and 1 larch (*Larix*) sample (U-4403). Two samples were not species-determined (U-2529 and U-2533). On the basis of these measurements, Hermanns-Audardóttir (1989) concluded that the settlement of Iceland had taken place in the 8th century, or even as early as the 7th century.

Abnormal ¹⁴C Condition in Iceland?

Most of the igneous rocks in Iceland are basaltic (about 90%), the rest is of rhyolitic and intermediate composition. About 90% of Iceland above sea level consists of volcanic rocks, only about 10% being consolidated sediments, which are mainly interbedded tuffaceous layers of short transport, and tillite. Icelandic bedrock contains no calcareous rocks and, therefore, hardwater effect is absent. Volcanic and geothermal activity is widespread. According to Saemundsson (1979), 24 volcanic

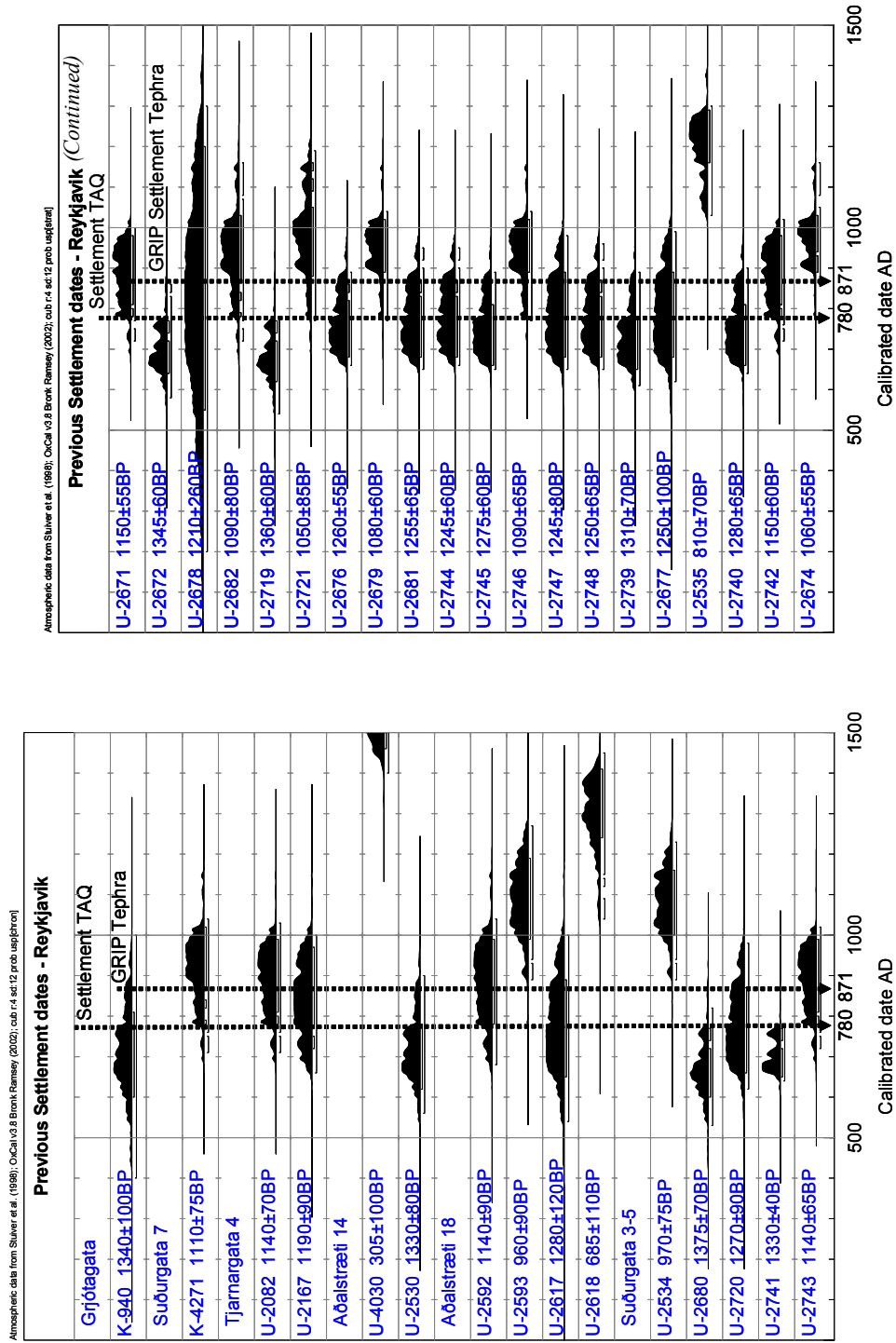


Figure 2. Probability distribution (OxCal v3.8) of calibrated ages of samples from the center of Reykjavik previously ¹⁴C dated (Nordahl 1988; Grímsson and Einarsson 1970). The dotted lines indicate *terminus ante quem* (TAQ) for the settlement, derived from the 1-σ intervals, and the Settlement tephra date AD 871 (Grönvold et al. 1995).

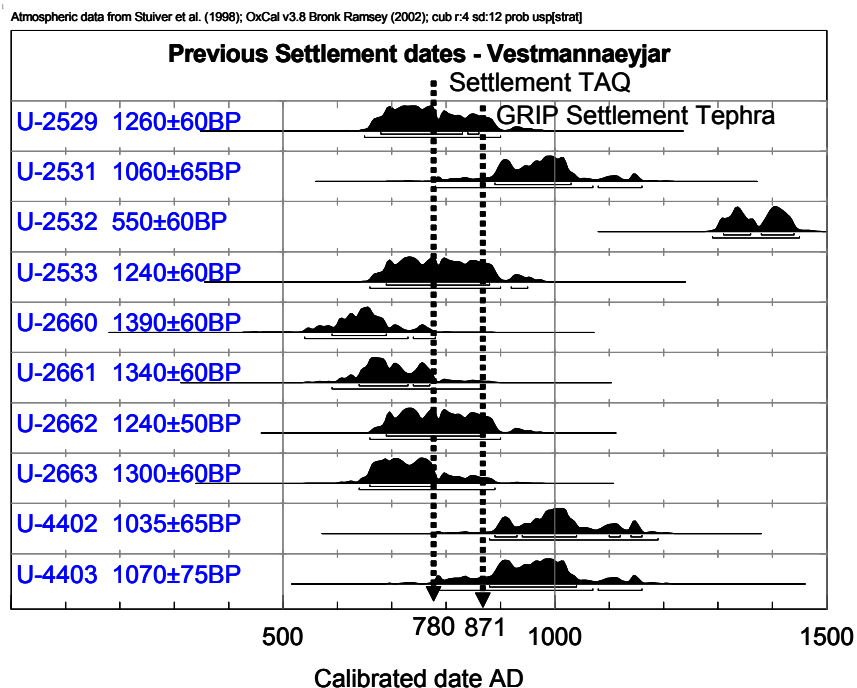


Figure 3 Probability distribution (OxCal v3.8) of calibrated ages of samples from Vestmannaeyjar previously ¹⁴C dated (Hermanns-Audardóttir 1989). The dotted lines indicate *terminus ante quem* (TAQ) for the settlement, derived from the 1-σ intervals (see text), and the Settlement tephra date AD 871 (Grönvold et al. 1995).

systems have been active in postglacial time, producing about 400–500 km³ of lava, and geothermal areas are frequently associated with these volcanic complexes. Despite the volcanic activity, ¹⁴C dates of mollusks and plant remains have produced consistent results, with wood samples from the settlement period as an exception. In only 1 case, anomalously high ¹⁴C ages (older by 8000 yr) have been reported that can be explained by volcanic activity (Sveinbjörnsdóttir et al. 1992), namely aquatic moss samples that have grown in geothermal water. Apart from this, volcanic activity has not been known to have caused any major errors in ¹⁴C results of geological samples. Shore et al. (1995) explicitly studied modern moss samples in the vicinity of the Katla volcano, Iceland (3 samples) and compared them to modern moss (2 samples) in Scotland and found no difference in the ¹⁴C/¹²C ratio. After extensive data collection, Olsson (1983) proposed a general ¹⁴C depletion in atmospheric CO₂ in Iceland, which she explained by the so-called “island effect,” which would make ¹⁴C ages in Iceland appear slightly too high due to isotopic exchange between the atmosphere and the sea surface.

RESULTS AND DISCUSSION

In the present work, we have measured ¹⁴C dates on samples from an excavation (site AST-01) in the center of the city of Reykjavík. The operation was part of a larger excavation program carried out in the early 1970s (Nordahl 1988). The excavations in 2001 revealed a complete Viking Age longhouse and also cultural layers from later times. The longhouse was erected shortly after the deposition of the Settlement tephra. A sampling program carried out throughout the excavation was designed to address some of the questions regarding the Icelandic ¹⁴C dating problems. Eight pairs

of barley seeds and wood samples (Icelandic birch) from the same, oldest stratigraphic context of the site were ^{14}C dated by accelerator mass spectrometry (AMS).

After standard chemical pretreatment of the samples with 1M HCl and 1M NaOH, the carbon was combusted to CO_2 , which was partly converted to graphite for AMS ^{14}C dating with the EN tandem accelerator at the University of Aarhus and partly used for $\delta^{13}\text{C}$ measurements by conventional mass spectrometry at the Science Institute, University of Iceland. The accuracy of the $\delta^{13}\text{C}$ measurements is better than 0.1‰. The AMS results are given in Table 1 with the 1- σ precision indicated. That the accuracy is of the order of the precision is demonstrated by our results in the Fourth International Radiocarbon Intercomparison (FIRI, Scott 2003a), where our weighted average deviation from consensus values on 18 measurements was only 0.8 ± 12 ^{14}C yr (Scott 2003b, participant laboratory #88).

Table 1 ^{14}C dates and $\delta^{13}\text{C}$ values for grain (*Hordeum Sativum*) and charcoal (*Betula*) samples paired according to context from an excavation in the center of Reykjavík (site AST-01). Calendar age single interval corresponding to 68.2% probability (1 σ), calculated by the OxCal v3.8 calibration program (Bronk Ramsey 2001).

Lab nr AAR-	Object ID nr	Sample type	Conventional ^{14}C age (yr BP)	Calendar age (cal AD)	$\delta^{13}\text{C}$ (‰ VPDB)	Context location
7610	AST01-AMS-1	grain	1102 \pm 35	895–985	–21.44	Context 646: Fill of temp. hearth
7618	AST01-AMS-18	charcoal	1082 \pm 37	890–1020	–25.71	Context 792: Upper fill of longfire
7611	AST01-AMS-2	grain	1092 \pm 39	895–1000	–25.63	Context 795: Lower upper fill of longfire
7618	AST01-AMS-19	charcoal	1282 \pm 35	685–775	–24.83	Context 802: Upper lower fill of longfire
7612	AST01-AMS-3	grain	1150 \pm 36	780–980	–23.94	Context 831: Bottom fill of longfire
7620	AST01-AMS-20	charcoal	1184 \pm 35	780–890	–25.29	Context 858: Floor deposit N of longfire
7613	AST01-AMS-4	grain	1087 \pm 35	895–1000	–25	Context 864: Upper floor deposit, W of longfire
7621	AST01-AMS-21	charcoal	1210 \pm 33	770–890	–26.35	Context 873: Lower floor deposit W of longfire
7614	AST01-AMS-5	grain	1218 \pm 40	720–890	–25.9	
7622	AST01-AMS-22	charcoal	1262 \pm 35	685–780	–26.35	
7615	AST01-AMS-6	grain	1153 \pm 36	780–970	–25.21	
7623	AST01-AMS-23	charcoal	1226 \pm 33	720–880	–27.98	
7616	AST01-AMS-7	grain	1129 \pm 35	890–980	–24.32	
7624	AST01-AMS-24	charcoal	1192 \pm 36	780–890	–25.88	
7617	AST01-AMS-8	grain	1152 \pm 36	780–980	–23.42	
7625	AST01-AMS-25	charcoal	1236 \pm 35	690–870	–27.31	

The ^{14}C dates of the 8 grain/wood sample pairs are given in Table 1 and the calibrated probability distribution shown in Figure 4. The results show that the wood samples (Icelandic birch) tend to be older than grain samples. With the same assumptions for these wood samples as for the previous sample series discussed above, one would reach the same conclusion, namely, that the settlement in Reykjavík has occurred no later than around AD 780 (dotted line in Figure 4). However, the grain samples date the settlement in Reykjavík to no later than around AD 890.

We argue that wood samples often give too-high ages and are not suited to date the settlement. Grain, on the other hand, is probably from the last harvest and, therefore, most suitable to give the true age of the human occupation. Similarly, Olafsson (1995) found that a birch sample from a fireplace in west Iceland from the settlement time period was 150 yr older than an associated cow bone. The fireplace is located in a cave within a lava flow (Hallmundarhraun) that sits on the Settlement tephra layer. Therefore, any human activity must be younger than the tephra layer. However, the age of the fireplace sample is older than the tephra layer and, therefore, cannot reflect the true date of the event.

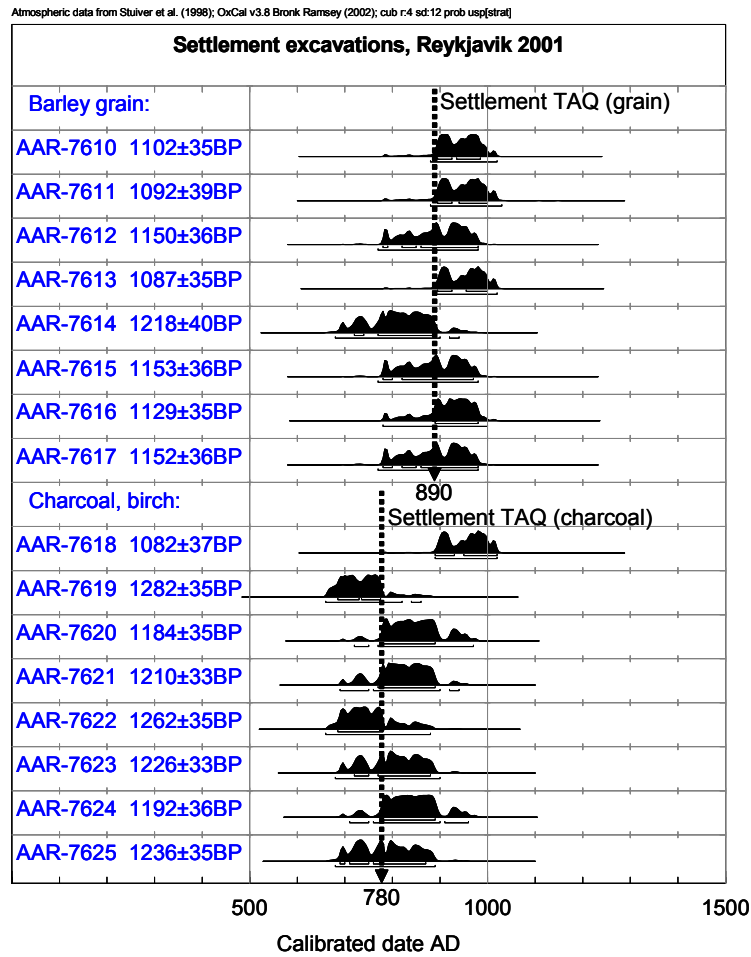


Figure 4 Probability distribution (OxCal v3.8) of calibrated ages of the series of ¹⁴C dates on paired wood/grain samples from an excavation (site AST-01) in the center of the city of Reykjavík. The wood samples are shown in the same sequence as their grain counterparts. The dotted lines indicate the *terminus ante quem* (TAQ) AD 780 and AD 890, respectively, for the settlement, derived from 1-σ intervals of the wood samples and the grain samples. The grain samples have a shorter lifespan and a safer association with the settlement.

As pointed out by Ólafsson (1998), the wood collected by the first settlers in Iceland to build their fire had very likely been dead, possibly for more than a century. This makes “Settlement” wood unsuited for ¹⁴C dating as it can be much older than the archaeological context. Work in progress indicates that the supply of old firewood was gradually exhausted, thus reducing the age offset of charcoal samples from the following centuries.

The interpretation of our new ¹⁴C results on paired grain and wood samples eliminates the necessity of any of the ad hoc theories introduced up to now to explain the surprisingly early ¹⁴C dates of the settlement of Iceland, namely, 1) island effect, 2) volcanic and/or geothermal effect, 3) early settlement. We argue that the ¹⁴C dating results of wood samples in the settlement time period simply do not give the true date of human occupation.

REFERENCES

- Bronk Ramsey C. 2001. Development of the radiocarbon program OxCal. *Radiocarbon* 43(2A):355–63
- Einarsson Th. 1962. Vitnisburður frjógreiningar um gróður, vedurfur og landnám á Íslandi. *Saga* 3:442–69.
- Grímsson Th, Einarsson Th. 1970. Fornminjar í Reykjavík og aldursgreiningar. *Árbók Fornleifafélagsins*, 1969. p 80–97.
- Grönvold K, Óskarsson N, Johnsen SJ, Clausen C, Hammer CU, Bond G, Bard E. 1995. Ash layer from Iceland in the Greenlandic GRIP ice core correlated with oceanic and land sediments. *Earth and Planetary Science Letters* 135:149–55.
- Hall VA, Pilcher JR, McCormac FG. 1993. Tephra dated lowland landscape history of the north of Ireland, AD 750–1150. *New Phytologist* 125:193–202.
- Halldóttir M. 1987. *Pollen Analytical Studies of Human Influence on Vegetation in Relation to the Landnám Tephra Layer in Southwest Iceland* [PhD dissertation]. Lund: Lund University.
- Hallsdóttir M. 1996. Frjógreining. Frjókorn sem heimild um landnám. In: Grímsdóttir GÁ, editor. *Um Landnám Á Íslandi*. Reykjavík: Societas scientiarum Islandica. p 123–34.
- Haraldsson H. 1981. The Markarfljót sandur area, southern Iceland: sedimentological, petrographical and stratigraphical studies. *Striae* 15:1–65.
- Hermanns-Audardóttir M. 1989. Islands tidiga bosättning. *Studia Archaeologica Universitatis Umensis* 1, Umeå. 184 p.
- Larsen G. 1996. Gjósulagatímatal og gjóskulög frá tíma norræns landnáms á Íslandi. In: Grímsdóttir GÁ, editor. *Um Landnám Á Íslandi*. Reykjavík: Societas scientiarum Islandica. p 81–106.
- Nordahl E. 1988. Reykjavík from the archaeological point of view. Aun 12, *Societas Archaeologica Upsalensis*, Uppsala. 150 p.
- Olsson IU. 1983. Radiocarbon dating in the arctic region. *Radiocarbon* 25(3):393–4.
- Ólafsson G. 1998. Fylgsmid í Vidgelmi. *Árbók Hins íslenska Fornleifafélags*. p 125–42.
- Saemundsson K. 1979. Outline of geology of Iceland. *Jökull* 29:7–28.
- Scott EM, editor. 2003a. Section 1: The Fourth International Radiocarbon Intercomparison (FIRI). *Radiocarbon* 45(2):135–50.
- Scott EM, editor. 2003b. Section 7: Characterization of the reference materials by consensus values. *Radiocarbon* 45(2):249–75.
- Shore JS, Cook GT, Dugmore AJ. 1995. The ¹⁴C content of modern vegetation samples from the flanks of the Katla volcano, southern Iceland. *Radiocarbon* 37(3): 525–9.
- Sveinbjörnsdóttir ÁE, Heinemeier J, Rud N, Johnsen SJ. 1992. ¹⁴C anomalies observed for plants growing in Icelandic geothermal waters. In: Long A, Kra RS, editors. Proceedings of the 14th International ¹⁴C Conference. *Radiocarbon* 34(3):696–703.
- Theodórsson P. 1993. Geislakolsgreining gjóskulaga og aldur landnámslagsins. *Náttúrufræðingurinn* 63:275–83.
- Thórarinsson S. 1944. Tefrokronologiska studier på Island. Thjórsárdalur och dess förödelse. *Geografiska annaler* 26:1-217.
- Thórarinsson S. 1977. Jarðvísindi og Landnáma. In: *Sjöttú ritgerdir, helgadar Jakobi Benediktssyni*. Reykjavík: The Árni Magnússon Institute. p 665–76.
- Vilhjálmsson VÖ. 1991. Radiocarbon dating and Icelandic archaeology. *Laborativ Arkeologi* 5:101–14.

ANOMALOUS RADIOCARBON DATES FROM EASTER ISLAND

Kevin Butler^{1,2} • Christine A Prior³ • John R Flenley¹

ABSTRACT. The largest volcanic crater on Easter Island in the South Pacific contains a lake 1 km in diameter with large floating mats of vegetation, mainly *Scirpus californicus*. A core taken through a mat near the center produced anomalous dates, with older dates above younger ones. The possibility that the mat had become inverted was considered, but palynological evidence refutes this idea because it shows a progressive upward decline of forest pollen, which is well known from other swamp cores on the island. A new series of radiocarbon dates made directly on pollen concentrates was obtained. These dates also produced inconsistencies, particularly when pollen concentrate ages were compared with ¹⁴C ages on plant fragments from the same depth. This series of ¹⁴C ages seems to indicate that both old and young organic components in the sediment are deposited contiguously and that the depositional history of these cores is more complex than previously known. Previous age determinations on bulk sediments from Easter Island, which also show anomalous dates, may be too simplistic. This paper provides a warning to other researchers dating sediments from Easter Island. We suggest that sample selection and dating procedures be carefully considered for these sediments.

INTRODUCTION

Easter Island has been the subject of much research and speculation in recent years. Palynological evidence clearly shows that Easter Island, for at least the past 35,000 yr, was extensively forested, mostly by a now-extinct palm. Travellers to the island in recent times, however, are greeted by a landscape of grasslands where the much admired statues, or *Moai*, far outnumber the few scrubby trees present. Deforestation occurred mostly between AD 700 and AD 1680, which is within the accepted time of human occupation. Most debate and controversy occurs concerning the causal factors leading to the disappearance of the forest and rapid decline of the society. Flenley et al. (1991), Bahn and Flenley (1992), and Flenley and Bahn (2003) argue that the collapse of the Easter Island economy and the severe decline in its population were caused primarily by exhaustion of the island's resources, principally its timber resource. McCall (1993) has speculated that these major changes resulted from a severe drought induced by the Little Ice Age. Hunter-Anderson (1998) has totally dismissed the "human impact scenario," claiming the decline of forest was the sole result of climate change. If the disagreement between the "human impact" and "climate change" hypotheses is to be resolved, then a high-resolution chronology of vegetational change on Easter Island must be obtained.

Easter Island is volcanic in origin, roughly triangular in shape, and covers an area of 117 km² (Figure 1). The landscape is dominated by the 3 volcanic peaks which give the island its triangular shape. The coastline is mostly rugged with few sandy beaches. The nearest inhabited landmass is Pitcairn Island, some 2092 km to the west, and the nearest continental landmass is South America, 3599 km to the east. This makes Easter Island one of the most isolated places to live on this planet. The isolation is probably partly responsible for the extremely depauperate flora, with less than 50 vascular species known from the island.

Sediment from the 3 swamps/lakes on Easter Island has been the subject of palynological analysis. Flenley et al. (1991) describe the vegetational history from cores taken in Rano Raraku and Rano Aroi, and at the edge of the Rano Kao caldera. Dating of sediments from these 3 sites was performed by the Scottish Universities Research and Reactor Centre (SURRC). The age-depth graphs pro-

¹School of People, Environment and Planning, Massey University, Palmerston North, New Zealand.

²Corresponding author. Email: K.R.Butler@massey.ac.nz.

³Rafter Radiocarbon Laboratory, Institute of Geological & Nuclear Sciences, Lower Hutt, New Zealand.

duced show a relatively good fit with the dates, but a number of anomalous dates do occur. From the Rano Raraku sediments, 10 bulk samples were submitted for dating. Of these, three seem too old and one appears too young. The possibility of contamination by inwashed soil carbon was suggested for some of these anomalies. Eleven bulk sediment samples were submitted from Rano Aroi, of which one in the top meter was much too old. The upper ~1 m of these sediments has been severely disturbed during the building of a small dam in the 1920s. Flenley et al. (1991) considered that some of the older dates from Rano Aroi appear younger than expected and suggest the possibility of young roots from above contaminating the older sediments. Five bulk sediment samples were submitted from Rano Kao (borehole 1). One date appeared much too young. In this case, young roots from above were offered as a possible explanation. Flenley et al. (1991) also report observing an inversion of a smaller, modern floating mat on Rano Kao during field work.

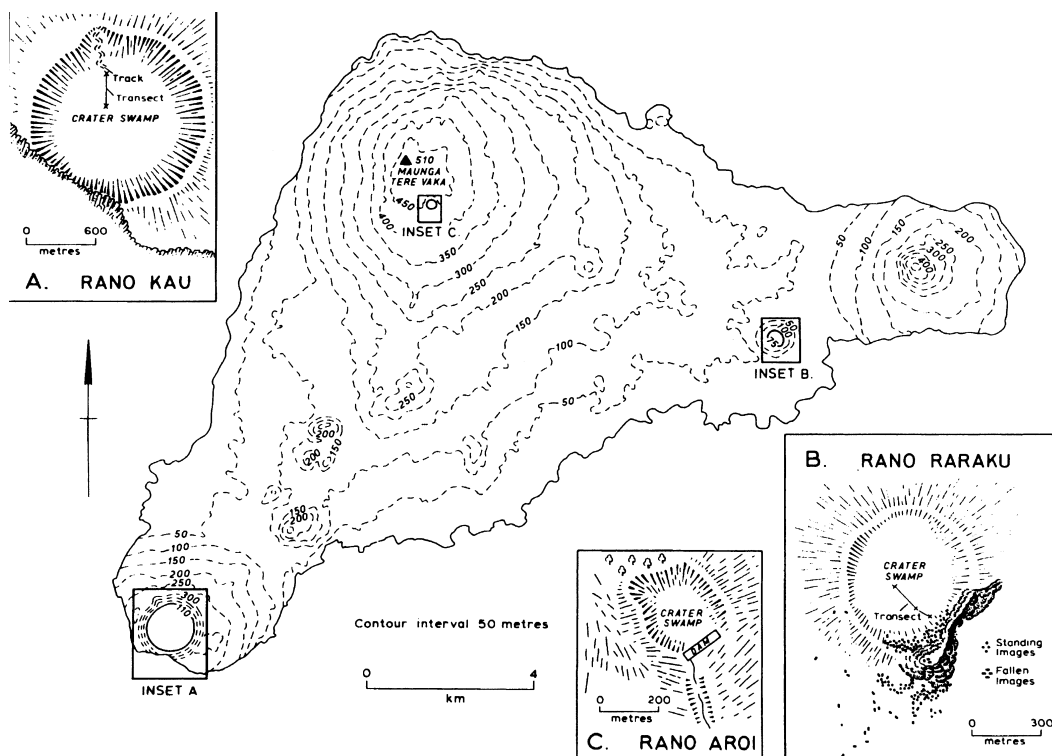


Figure 1 Map of Easter Island. Inserts show the 3 coring sites. Rano Kao (Kau) borehole 2 (near the center of the crater), which is the focus of this paper, is shown in insert A.

METHODS

Site Description and Coring

This paper describes a second sediment core recovered from nearer the center of Rano Kao in 1984. Preliminary work on this core (borehole KAO 2) was reported in Flenley (1996) and Butler and Flenley (2001). Rano Kao is a collapsed crater (caldera) almost circular in shape, located in the southwest part of the island. The inner walls slope down at an angle of about 30° to a circular floating swamp about 1 km in diameter. The swamp surface consists of several floating mats of various sizes and thicknesses, which occupy large areas, although open water does exist between the float-

ing mats. The dominant species on the floating mats is the totora reed, *Scirpus californicus*. An interesting feature of this vegetation is the apparently dead patches found in the center of some of the larger floating mats.

Borehole 2 (KAO 2) was extracted using a Russian D-section corer (Jowsey 1966), approximately 300 m in from the eastern edge. The core consists of 2 separate parts, 3 m of floating mat and 10 m of lake sediment, the 2 parts being separated by 8 m of water. Unfortunately, coring could not proceed past this point due to insufficient extension rods being available for the corer. The stratigraphy of the core is fairly uncomplicated. The 3-m floating mat consists of very soft, coarse organic detritus with rhizomes of *Scirpus californicus* in the uppermost meter. The lake sediment consists entirely of coarse organic detritus, although the lowest 15 cm was darker and more consolidated than that above. The 2 parts of this core were sampled for palynological analysis at 10-cm intervals. The vegetation patterns of the resulting pollen diagrams reinforced the findings of the previous pollen diagrams from Rano Raraku and Rano Aroi. In general, a 3-zonal pattern of vegetation exists. The lower zone is dominated by trees and shrubs with Palmae being predominant. Ferns are variable in abundance and Poaceae are virtually absent. The middle zone shows a steady, but sometimes saw-toothed, decline in trees and shrubs. Ferns are abundant and Poaceae become prominent. Charcoal particles appear in significant quantities. In the upper zone, trees and shrubs decline and disappear. Ferns and Poaceae dominate completely and charcoal is abundant. A summary diagram of the Rano Kao 2 pollen profiles is provided in Figures 2 and 3. For the full pollen diagrams, see Butler and Flenley (2001).

Dating

Initial dates from the KAO 2 cores were accelerator mass spectrometry (AMS) dates on bulk sediment obtained from Nagoya University and reported in Flenley (1996). In an attempt to establish a preliminary chronology, 5 sediment samples were measured. With the exception of NUTA-3516, these initial dates seem to fit expectations once compared with the data from Flenley et al. (1991), considering the few pollen samples analyzed at that time (samples were taken at 50-cm intervals). Once the pollen analysis (sampling at 10-cm intervals) was completed some years later, it was decided to obtain additional ^{14}C analyses. A new method of AMS dating of pollen concentrates had been developed at the Rafter Radiocarbon Laboratory and this was considered an ideal opportunity to compare ages from pollen concentrates with the original bulk sediment ages.

Sediment from several depths in KAO 2 were treated for pollen separation and concentration by the method described in detail in Prior and Chester (2001) and Vandergoes and Prior (2003). After chemical pretreatment with HCl, HF, HNO_3 , and ammonia solution, the samples were sieved and then subjected to a density separation with sodium polytungstate (SPT). The samples were centrifuged with SPT solutions of decreasing specific gravity, with the precipitates of each centrifugation saved as separate fractions. Individual fractions were examined under the microscope and those containing the highest pollen concentrations were selected for combustion and dating. These pollen fractions are identified in Table 1 by the specific gravity at which they precipitated. At 2 depths, 16.75–16.85 m and 18.25–18.35 m, 2 additional fractions were dated for comparison: large plant fragments (~1 mm) sieved from the sediment and a different density fraction containing fine plant debris but no pollen.

In an experiment to determine whether Rano Kao showed evidence of a reservoir effect, we also dated several fractions from the top 7.5 cm of the floating mat. The original material removed in taking this core consisted of mostly basal stems and roots of *Scirpus californicus* and a smaller component consisting of plant fragments, mineral, and charcoal. Dating of this material was expected to

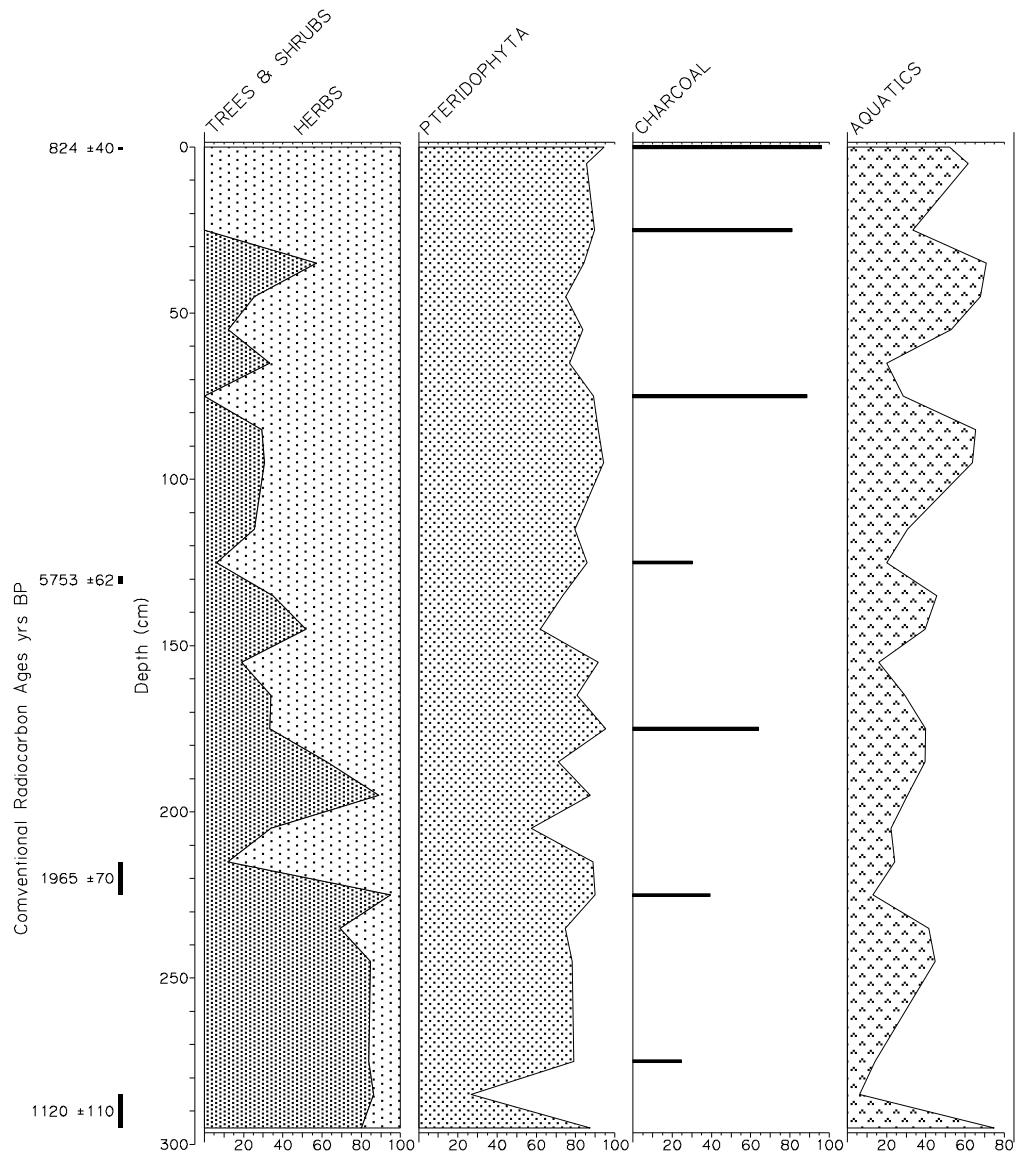


Figure 2 Summary pollen profile for the Rano Kao floating mat. The ages given are for bulk sediment dates when these were the only ages available, else ages are those obtained from AMS dating the specific gravity separation containing pollen and spores.

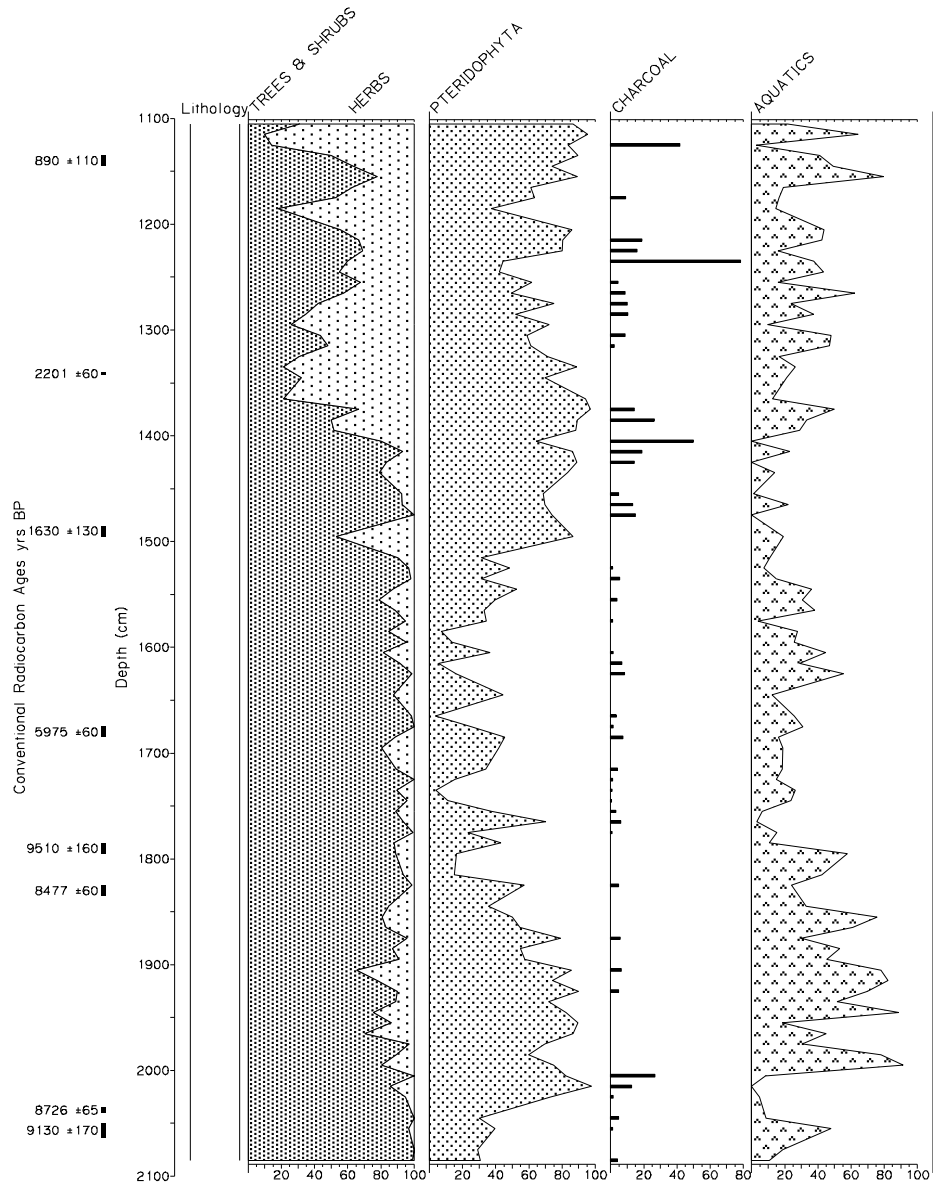


Figure 3 Summary pollen profile for the Rano Kao lake sediment. The ages given are for bulk sediment dates when these were the only ages available, else ages are those obtained from AMS dating the specific gravity separation containing pollen and spores.

Table 1 ^{14}C dates for Rano Kao 2.

Core depth (m)	Fraction dated	Lab code nr	CRA ^a (BP)	$\delta^{13}\text{C}$ (‰)	Calibrated age ^b (2 σ interval)	Calibrated age, BP (2 σ interval)
0-0.075	bulk sediment	NZA-18033	312 \pm 40	-25.0	AD 1471-1659	479-291
0-0.075	plant fragments > 100 micron	NZA-17986	191 \pm 40	-24.3	AD 1646-1945	304-5
0-0.075	plant frag, pollen & spores, 1.20 sg ^c	NZA-18034	824 \pm 40	-26.1	AD 1159-1280	791-670
1.29-1.315	plant frag, pollen & spores	NZA-15461	5753 \pm 62	-25.0	4770-4454 BC	6719-6403
2.15-2.25	plant frag, pollen & spores	NZA-15462	1965 \pm 70	-26.3	157 BC-224 AD	2106-1726
2.85-2.95	bulk sediment	NUTA-3515	1120 \pm 110	n/a ^d	AD 671-1161	1279-789
	water					
11.35-11.45	bulk sediment	NUTA-3011	890 \pm 110	n/a	AD 904-1295	1046-655
13.40-13.425	plant frag, pollen & spores	NZA-15463	2201 \pm 60	-26.3	392-64 BC	2341-2013
14.85-14.95	bulk sediment	NUTA-3013	1630 \pm 130	n/a	AD 94-662	1856-1288
16.75-16.85	coarse plant remains > 1mm	NZA-11603	4009 \pm 60	-25.9	2844-2348 BC	4793-4297
16.75-16.85	fine plant frag, 1.25 sg	NZA-11639	5716 \pm 60	-27.2	4712-4401 BC	6661-6350
16.75-16.85	plant frag, pollen & spores, 1.30 sg	NZA-11638	5975 \pm 60	-27.2	5001-4717 BC	6950-6666
17.85-17.95	bulk sediment	NUTA-3516	9510 \pm 160	n/a	9262-8324 BC	11,211-10273
18.25-18.35	coarse plant remains > 850 μm	NZA-11604	8418 \pm 60	-26.8	7582-7332 BC	9531-9281
18.25-18.35	plant frag, 1.30 sg	NZA-11640	8498 \pm 60	-27.2	7599-7479 BC	9548-9428
18.25-18.35	plant frag, pollen & spores, 1.35 sg	NZA-11641	8477 \pm 60	-27.2	7595-7377 BC	9544-9326
20.35-20.40	pollen & spores	NZA-15464	8726 \pm 65	-27.2	8157-7592 BC	10,106-9541
20.50-20.63	bulk sediment	NUTA-3012	9130 \pm 170	n/a	8750-7831 BC	10,699-9780 BP

^aCRA = Conventional Radiocarbon Age, as defined in Stuiver and Polach (1977).

^bCalibrations made with WINSICAL (Institute of Geological and Nuclear Sciences), based on INTCAL98 (Stuiver et al. 1998).

^csg = specific gravity.

^dn/a = not available.

return ages no older than 150 yr. The upper 7.5 cm was split longitudinally into 2 equal parts. One half remained intact and was dated as a “bulk sediment” sample, receiving a standard acid/alkali/acid pretreatment. This “bulk” sample contained all the constituent parts of the original material. The other half was treated to separate a pollen concentrate as described above. Two fractions from this procedure were chosen for dating: large plant fragments >100 microns and the plant fragments, pollen, and spores that precipitated at a specific gravity of 1.20.

Results for all of the ^{14}C age analyses are presented in Table 1. Nagoya University ages are identified by the NUTA laboratory code and Rafter Radiocarbon Laboratory ages are identified by the NZA lab code.

RESULTS

The depths in KAO 2 chosen for dating by the pollen concentrate procedure were selected to elucidate some age inversions which appeared in the suite of ages from Nagoya. The base of the floating mat at 2.85–2.95 m produced an age of 1120 ± 110 (NUTA-3515), while the sediment at 11.35–11.45 m produced an age of only 890 ± 110 (NUTA-3011). Also, either the date of 9510 ± 160 BP (NUTA-3516) at 17.90 m is much too old, or the basal date of 9130 ± 170 BP (NUTA-3012) at 20.5 m is much too young. Tentative initial acceptance of the basal date was based on the opinion that the basal 15 cm of darker consolidated sediment could represent the end of the Pleistocene (Flenley 1996). On the other hand, once pollen analysis was complete, sustained peaks of Poaceae and Asteraceae (Tubuliflorae) for approximately 1.5 m below the depth, dated at 9510 ± 160 BP, suggests that the depth of 18.0 m to 18.5 m could represent the Pleistocene-Holocene boundary. Both Poaceae and Asteraceae (Tubuliflorae) have a preference for cooler/drier conditions. Peaks of cool/dry preference taxa are also present in the other pollen diagrams from Easter Island, some of which date well into the Pleistocene with basal ages of 34,000 BP. It was thought that if the date at 20.5 m was too young, then this was probably due to incorporation of younger carbon. AMS dating of pollen concentrates was considered an ideal solution to the quandary, as this method gave us the opportunity to remove inwashed and aerially-derived contaminants.

The ^{14}C age estimates from the 3 fractions at the 18.3 m depth are statistically identical. In contrast, the ages from the 3 fractions at the 16.8 m depth vary considerably. The coarse plant fragments sieved from 16.8 m are about 1800 yr younger than the density fractions. Of the 2 density fractions, the 1.3 specific gravity (sg) fraction (visually identified as containing palynomorphs) was older than the 1.25-sg fraction which contained fine plant fragments. Although the difference is not as great as with the large plant fragments, when the ages of the 2 fractions are calibrated, they do not intersect at the $2\text{-}\sigma$ confidence interval. Initially, there seemed no obvious explanation for why the large plant remains should be so much younger than the pollen in one depth but not the other.

The date from 18.30 m of 8477 ± 60 BP (NZA-11641) was not that much younger than the NUTA-3516 date of 9510 ± 160 BP obtained previously, which seems to give reasonable confidence in the age of this depth. Some 2 m of sediment separates these 2 depths (18.3 m and 17.9 m) from the basal (20.5 m) age of 9130 ± 170 BP (NUTA-3012), yet very little difference in age is seen. This led us to question whether the basal date at 20.5 m of 9130 ± 170 BP (NUTA-3012) was too young (see Table 1). The pollen evidence showing peaks of cool preference taxa below the 18.0 m to 18.5 m depth would suggest this basal date was too young.

Four additional ages using AMS on extracted pollen were obtained from the 1.29–1.315, 2.15–2.25, 13.40–13.425, and 20.35–20.40 m depths. It was hoped that these would clarify the basal date of the lake sediment and establish a chronology for the floating mat. The pollen concentrate density fraction

was the only fraction dated for these 4 samples. The basal age of the lake sediment was given some confirmation when a date from 20.40 m of 8726 ± 65 BP (NZA-15464) was returned. Previously, only 1 bulk sediment date had been obtained from the base (2.90 m) of the floating mat, 1120 ± 110 BP (NUTA-3515). The 2 pollen samples submitted from the floating mat returned ages which seemed the inverse of what we expected. The sample from 2.20 m produced an age of 1965 ± 70 BP (NZA-15462) and the sample from 1.30 m an age of 5753 ± 60 BP (NZA-15461). The middle of the mat appeared to be older than the bottom, giving the appearance that the mat had flipped over. Despite the field team witnessing the inversion of 1 mat, this explanation was considered unlikely based on the pollen evidence. Had the mat been subject to inversion/s, the pollen evidence would not give the characteristic profile of large numbers of tree pollen at the base continuing up the profile to 2.2 m where tree pollen shows a saw-toothed decline and ultimately disappears 35 cm from the top (see Figures 2 and 3).

DISCUSSION

With such a pattern of seemingly contradictory dates, we considered possible sources of contamination. In-wash of old carbon from the inner walls of the crater is unlikely to be a major contaminant, as the core site was 300 m out from the eastern edge of the crater lake. Airborne contamination of mineral and/or organic dust or charcoal from old trees or peat was a possibility. Since most of the samples dated were pollen extracts, it was easy to analyze microscopically both the constituent parts being dated and the residues from separations. Mineral particles are removed from the sample during preparation with the particles smaller than 10 μm being removed during sieving and the larger mineral particles being removed during density separation. When present in a sample, charcoal particles were removed at specific gravities of 1.6 to 1.4. The pollen fraction dated was at specific gravity 1.2 and only contained pollen, spores, and small pieces of plant material. These sediments are not rich in palynomorphs; pollen and spores made up $<20\%$ of the sample which was dominated by small, light plant fragments. The idea of humic acids moving freely through the profile was also considered, but this is unlikely as a source of contamination as these would have been removed by alkali washes during pretreatment. We then considered the possibility that the source of contamination might be depleted CO_2 emitted from the caldera and entering the plant during photosynthesis (Pasquier-Cardin et al. 1999).

To test this hypothesis, we had originally planned to ^{14}C date a sample of the living reed currently growing in Rano Kao, and perhaps a water sample. Unfortunately, that was not possible at the time of this study, so we decided to test the age of the material at the surface of the floating mat. We dated 3 fractions from the top 7.5 cm with the expectation that sample material from this depth should be somewhere between 0 and 150 yr. The ^{14}C age measured for the bulk sample was 312 ± 40 BP (NZA-18033). The 1.2-sg fraction which contained pollen, spores, and small plant fragments produced an age of 824 ± 40 BP. These 2 dates are significantly older than expected, especially the treated sample containing the smaller plant remains. Even the fraction of sieved plant fragments >100 microns returned an age greater than would have been expected for plants presumably growing after 1965 and enriched with bomb carbon (Table 1).

The variability in ages among different fractions separated from the same sediment depth suggests the situation may be even more complex. The inconsistency in age between the 2 fractions separated from the 0–7.5-cm level of the floating mat (191 ± 40 BP for the plant fragments sieved out at 100 microns and 824 ± 40 BP for the fine material collected at 1.2 sg) suggests that at least 2 components of very different ^{14}C ages combine to make up the bulk of the material collecting in the floating mat. The “bulk sediment” age can be explained as a mixture of the 2 components. It would

require only about 20% input of a component aged 824 yr to shift the apparent ^{14}C age of a 191-yr component into the 300-yr range.

The variation in ages among different fractions obtained for the top 7.5 cm is also seen in the deeper lake sediments at 16.8 m. Coarse plant remains >1 mm sieved from the sediment at the beginning of the pollen separation procedure yielded a CRA that is significantly younger than the fine fractions separated at specific gravities of 1.3 and 1.25. Even the 2 specific gravity fractions produced CRAs that differ by more than 2σ (Figure 4 and Table 1). This pattern is not repeated though at 18.30 m, where the large plant remains and 2 fractions from 1.35 and 1.30 specific gravities yield statistically identical ages.

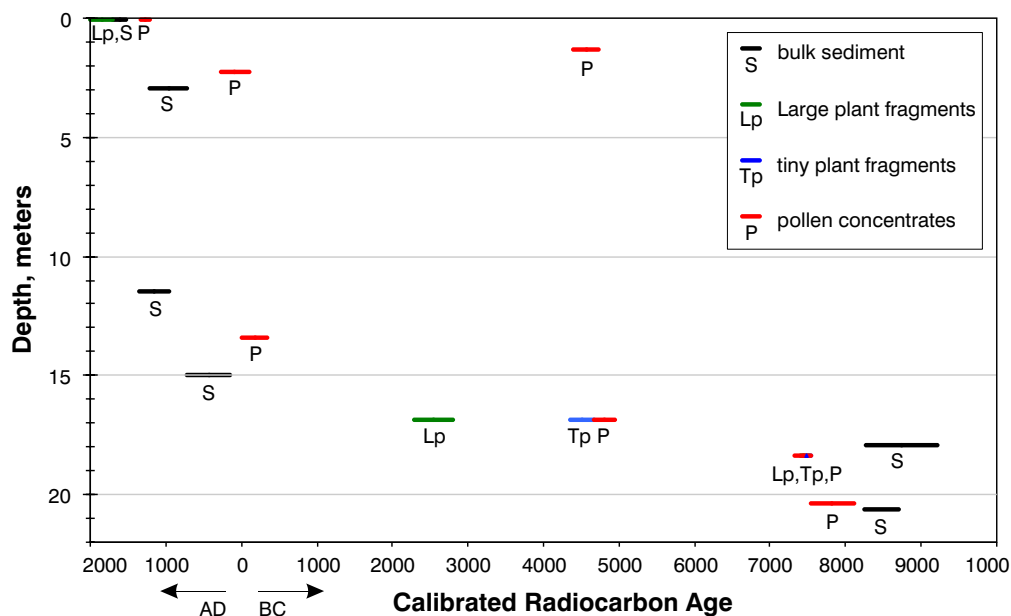


Figure 4 Calibrated ^{14}C ages versus depth diagram for all dated fractions of the Rano Kao 2 core. Length of bar represents 2σ confidence interval.

What remains to be explained is the origin of the “old” component. Some possibilities include the following:

- *Fine charcoal particles derived from the burning of aged trees outside the crater:* There is much evidence for this burning (e.g. Mieth and Bork 2003). The older small plant fragments dated with the pollen do not appear to contain any charcoal. Microscopic analysis of the dated samples has shown no charcoal present, although charcoal may be a factor in the “bulk sediment” ages.
- *Depleted CO_2 emitted as gas from the caldera floor and incorporated by photosynthesis:* Depleted volcanic CO_2 alone does not seem to provide an explanation for these anomalously old ages, but there are some indications that it could be a factor. This will be tested by ^{14}C dating live-collected plants and determining their apparent age. It is possible that depleted CO_2 is being emitted in varying quantities over time. The 2 fractions (small plant fragments and >100- μm plant fragments) differ in age considerably, and this would require a different source for each to produce such an anomaly. If variably-depleted CO_2 contributes to ^{14}C age variability, it may be necessary to date live-collected plants from both the middle of the crater and from the edge to

ascertain whether emissions are spatially variable within the crater, as well as water sourced from different locations within the lake.

- *Periodic droughts leading to lowering of the lake level and erosion of the marginal sediments:* There is, however, currently no evidence for such droughts. Although there are occasional droughts on the island, they are not severe or long lived. Droughts due to ENSO are unlikely, as the island is on the fulcrum between the ENSO extremes of the East and West Pacific (Genz and Hunt 2003; MacIntyre 2001). Inside the caldera, it is quite sheltered from wind, but it is possible that during drought years older small plant fragments are blown from the edge out into the center areas and then incorporated into the floating mats. Placing modified pollen traps onto the floating mats, and/or onto the open water between the floating mats, to catch any small plant fragments may be worthwhile. Biological identification of the small plant fragments would greatly assist in identifying possible source areas.

Additional coring of Rano Kao and Rano Raraku, plus the collection of water and of living material from these sites, is planned for later in 2004. Our research design for sampling will incorporate testing of each of these possibilities.

CONCLUSION

The floating mats seem to be quite complex and their reliability as chronological indicators or archives of vegetational change may be in question. Pollen evidence would seem to rule out the inversion of the floating mats. The possibility that these mats have been inverted, or “flipped over,” on more than one occasion in the past cannot, however, be ruled out. Whilst there is evidence of variable age with both young and old components in 1 sample, the lake sediment ages produce a more regular pattern of increasing age with depth. Further analysis and interpretation is needed in order to correlate the Rano Kao lake sediment with that in Rano Raraku. Some anomalies are also apparent with the SURRC “bulk sediment” dates of the Rano Raraku lake sediments (Flenley et al. 1991). Component-specific AMS dating of different fractions from the Rano Raraku sediments may also produce variable ages of both younger and older components.

Future research will include the ^{14}C dating of live-collected samples of the plants living within the craters of Rano Kao and Rano Raraku to determine whether depleted CO_2 in the lake water contributes to anomalously old ages and, if so, to what degree. Additionally, small plant fragments will be identified to help determine their source of origin. In the meantime, we regard bulk sediment ^{14}C ages in this region with some degree of caution.

REFERENCES

- Bahn P, Flenley JR. 1992. *Easter Island, Earth Island*. London: Thames & Hudson. 240 p.
- Butler K, Flenley JR. 2001. Further pollen evidence from Easter Island. In: Stevenson CM, Lee G, Morin FJ, editors. *Pacific 2000: Proceedings of the Fifth International Conference on Easter Island and the Pacific*. p 79–86.
- Flenley JR. 1996. Further evidence of vegetational change on Easter Island. *South Pacific Study* 16(2): 135–41.
- Flenley JR and Bahn P. 2003. *The Enigmas of Easter Island*. Oxford: Oxford University Press. 256 p.
- Flenley JR, King ASM, Teller JT, Prentice ME, Jackson J, Chew C. 1991. The Late Quaternary vegetational and climatic history of Easter Island. *Journal of Quaternary Science* 6(2):85–115.
- Genz J, Hunt TL. 2003. El Niño/Southern Oscillation and Rapa Nui prehistory. *Rapa Nui Journal* 17(1):7–14.
- Hunter-Anderson RL. 1998. Human vs climatic impacts at Rapa Nui. In: Stevenson CM, Lee G, Morin FJ, editors. *Easter Island in Pacific Context: South Seas Symposium. Proceedings of the Fourth International Conference on Easter Island and East Polynesia*. Easter Island Foundation, Bearsville & Cloud Mountain Press: California. p 85–99.
- Jowsey PC. 1966. An improved peat sampler. *New Phytologist* 65:245–8.
- McCall G. 1993. Little Ice Age: some speculations for

- Rapa Nui. *Rapa Nui Journal* 7(4):65–70.
- MacIntyre F. 2001. ENSO, climate variability, and the Rapanui, Part II. Oceanography and Rapa Nui. *Rapa Nui Journal* 15:83–94.
- Mieth A, Bork H-R. 2003. Diminution and degradation of environmental resources by prehistoric land use on Poike Peninsula, Easter Island (Rapa Nui). *Rapa Nui Journal* 17(1):34–41.
- Pasquier-Cardin A, Allard P, Ferreira T, Hatté C, Coutinho R, Fontugne M, Jaudon M. 1999. Magma-derived CO_2 emissions recorded in ^{14}C and ^{13}C content of plants growing in Furnas caldera, Azores. *Journal of Volcanology and Geothermal Research* 92: 195–207.
- Prior CA, Chester PI. 2001. Precision radiocarbon dating of a Late Holocene vegetation history. In: Jones M, Sheppard P, editors. *Australasian Connections and New Directions: Proceedings of the 7th Australasian Archaeometry Conference* Auckland: University of Auckland, Research in Anthropology and Linguistics series, volume 5. p 285–94.
- Stuiver M, Polach HA. 1977. Discussion: reporting of ^{14}C data. *Radiocarbon* 19(3):355–63.
- Stuiver M, Reimer PJ, Bard E, Beck JW, Burr GS, Hughen KA, Kromer B, McCormac FG, van der Plicht J, Spurk M. 1998. INTCAL98 radiocarbon age calibration, 24,000–0 cal BP. *Radiocarbon* 40(3):1041–83.
- Vandergoes MJ, Prior CA. 2003. AMS dating of pollen concentrates—a methodological study of late Quaternary sediments from South Westland, New Zealand. *Radiocarbon* 45(3):479–91.

AMS ¹⁴C DATING USING BLACK POTTERY AND FIBER POTTERY

Shozo Mihara^{1,2} • Kazuo Miyamoto³ • Hidefumi Ogawa⁴ • Teiji Kurosaka⁵ • Toshio Nakamura⁶ • Hiroko Koike¹

ABSTRACT. A technique of accelerator mass spectrometry (AMS) has made it possible to directly measure radiocarbon ages of pottery by isolating organic materials sealed in the pottery when the pottery was formed. We analyzed the carbon contents and ¹⁴C ages for “black pottery” from the Philippines and “fiber pottery” from Japan using the relevant carbonaceous materials extracted from the pottery samples, i.e., adhered chaff or grass fibers that were incorporated in the pottery matrix, respectively. The carbon yield of the pottery sample varied largely depending on the pottery types, the preservation conditions, as well as the chemical pretreatment methods to purify carbonaceous materials for ¹⁴C dating. We will discuss criteria for sample selection of well-preserved pottery, and a modified method, instead of the standard alkali treatment, to obtain sufficient material for precise ¹⁴C dating.

INTRODUCTION

Radiocarbon ages for pottery have previously been measured on charcoal blocks and shell fragments existing in association with the pottery in the sedimentary layers (Kuzmin et al. 1997) or on carbonized materials such as soot and charred food residues on pottery surfaces (Nakamura and Iwahana 1990; Nakamura et al. 1990; Kolic 1995; Nakamura et al. 2001; Oda and Yamamoto 2001). However, there are 2 possibilities in ¹⁴C age offsets for these sample types. First, soot extracted from exterior surfaces of the pottery may have been deposited during pottery firing using wood of unknown age, which could possibly introduce a ¹⁴C reservoir effect. Secondly, carbonized materials on interior surfaces are usually from foods, and unless the types of foods that were processed in these vessels are known, they could introduce an offset such as a “marine reservoir effect” from cooking marine foods. In this study, instead of using soot or charred food residues, we have targeted short-lived organic materials, either sealed in the matrix of pots (grass) or deposited on the pot surface when they were fired (chaff). These types of organic temper are considered to be reliable materials for ¹⁴C dating (Hedges et al. 1992).

We examined “black pottery” from the Philippines and “fiber pottery” from Japan, and extracted the respective carbon contents, using these to determine ¹⁴C ages. Black pottery (Figure 1) is distributed from China to Southeast Asia, and is still produced today at San Nicolas, Northern Luzon, the Philippines. Raw pottery is fired in a pit in the ground using wood for fuel. After the pottery turns red, it is covered with a large amount of chaff (husks of rice or millet) which chars on the pottery surface to produce a black, carbon-adsorbed coloring. Pottery fragments containing the carbon that was transferred from chaff were selected for ¹⁴C dating.

Black pottery samples came from excavations at the Lal-lo shell midden sites located in the lower basin of the Cagayan River, Northeast Luzon. In this area, the shell midden layer on the river terrace yielded black pottery assigned to the Iron Age in the Philippines, and the silt layers under the shell midden layer yielded the red pottery belonging to the Pre-Iron Age (Ogawa 2000).

¹Graduate School of Social and Cultural Studies, Kyushu University, 4-2-1, Ropponmatsu, Chuo-ku, Fukuoka, Japan.

²Corresponding author. Email: cs200027@scs.kyushu-u.ac.jp.

³Faculty of Humanities, Kyushu University, 6-19-1, Hakozaki, Higashi-ku, Fukuoka, Japan.

⁴Dept. of Philippine Studies, Tokyo University of Foreign Studies, 3-11-1, Asahi-machi, Fuchu, Tokyo, Japan.

⁵Saitama Cultural Deposits Research Corporation, 4-4-1, Funakidai, Ohzato, Saitama, Japan.

⁶Dating and Materials Research Center, Nagoya University, Furo-cho, Chikusa-ku, Nagoya, 464-8602 Japan.

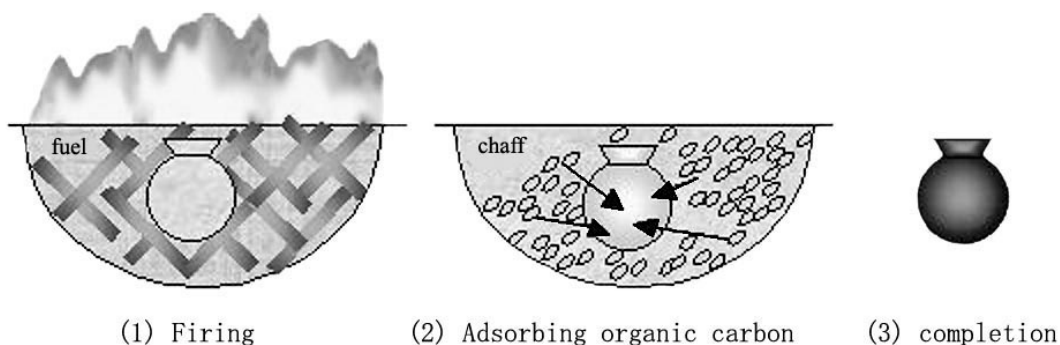


Figure 1 Fired pottery (1) in China and Philippines adsorbs carbon from organic materials such as chaff (2) and is stained black (3). This method was evident in San Nicolas in the Philippines where the black pots are now made.

The fiber pottery samples were collected from the Myouonji cave site, Saitama prefecture, Japan. Fiber pottery (Figure 2) is a class of Jomon pottery that contains charred fibers within the pot matrix. The fiber pottery was produced during the Earliest and Early Jomon periods, and was distributed mainly in central Japan. To make fiber pottery, grasses such as *Gramineae*, which are rich in silica, were mixed into the clay in order to strengthen the pottery matrix. After firing, charred grass fibers remain in the pottery, and it is possible to isolate these residues for AMS dating (Kuzmin et al. 2001). Fiber pottery has previously been analyzed by Yoshida et al. (forthcoming) and is known to give reasonable ages for selected carbonaceous materials after an acid-alkali-acid (AAA) treatment.

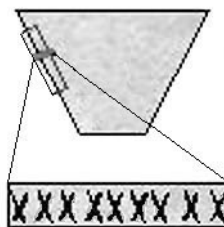


Figure 2 Fiber pottery contains charred fibers within the pot matrix.

MATERIALS AND METHODS

The pottery samples used here are the following: a) modern black pottery shards that were obtained at San Nicolas for a check on our carbon extraction methods and a reliability test of dating this type of sample; b) Philippine Black Pottery I, which was excavated from a cultural layer between the Red Pottery II and Black Pottery II; and c) Japanese Jomon pottery in 4 styles: 1) Todo-Kasou, 2) an unidentified type of pottery decorated with incised lines, 3) Sekiyama, and 4) Kurohama.

Surface dirt was removed from all pottery samples with a dental disk. Powder samples were then taken from the cleaned pottery sherds and were chemically treated by AAA to remove acid and alkali soluble materials, such as humic acids and fulvic acids which may have been incorporated from burial soil. The AAA treatment consisted of successive cleaning by 0.1N HCl at 80 °C, 0.1N NaOH at 80 °C, and again by 0.1N HCl at 80 °C. The residues were rinsed to neutral and dried.

After being chemically treated, the charred materials were analyzed for carbon content and $\delta^{13}\text{C}$ using an automated nitrogen and carbon analysis mass spectrometer (ANCA-MS, Europa Scientific Ltd). Analyses were done on 2 sets of 10-mg fractions from each pottery sample, and the average was calculated.

For AMS analysis, samples of the pretreated charred material containing about 2 mg of carbon were combusted at 850 °C for 4 hr in evacuated and sealed Vycor tubes together with CuO and Ag. The CO₂ was then purified cryogenically (using normal-pentane slush at -130 °C and ethanol slush at -90 °C) on a vacuum line. The purified CO₂ samples were then reduced to graphite (Kitagawa et al. 1993). The graphite samples were measured against a standard (NBS-II) using the Tandemron AMS (Model-4130 AMS, HVEE) at Nagoya University (Nakamura et al. 2000). We corrected for carbon isotopic fractionation using the $\delta^{13}\text{C}$ values provided by the AMS.

RESULTS

Significant differences were observed in carbon content among all samples (0.21% to 0.77%; Table 1). The carbon contents of the Philippine Black pottery samples were 0.51% in the modern sample, and from 0.23% to 0.45% in the archaeological samples. In fiber pottery of the Japanese Jomon period, carbon contents were 0.39% and 0.21% for 2 badly preserved samples, and from 0.33% to 0.77% for the better preserved samples (Table 1). Pottery matrix including charred carbon was lower for the badly preserved samples and yielded a lower carbon content. It is not easy to explain the large variation of extracted carbon, which may be due to chemical pretreatment procedures. The concentration of NaOH in the standard AAA procedure may cause a varying loss of organic carbon. In addition, the large variation in extracted carbon yields may also depend upon the preservation condition of the material and the amount of material used for treatment.

The ^{14}C ages obtained for the different types of pottery appear to confirm the reliability of chaff residues as a target material for dating. Chronologically, both black pottery and red pottery appears to have changed from a decorated type (I) to a non-decorated type (II). The calibrated calendar age of the Black Pottery II phase is already known to be from 1800 cal BP to 1000 cal BP, and that of the Red Pottery II phase is older than 3000 cal BP (Mihara et al. 2002). Samples in this study are of the decorated type (I) and belong to the cultural layer between the Red Pottery II and Black Pottery II.

^{14}C ages for the 2 Black Pottery I samples are 2170 ± 30 BP and 2290 ± 30 BP (2310–2095 cal BP and 2350–2180 cal BP; Figure 3). For the Japanese fiber pottery samples, the Todo-Kasou style pottery was dated to 8660 ± 45 BP (9770–9535 cal BP). The unidentified pottery type was dated to 7855 ± 45 BP (8780–8540 cal BP), the Sekiyama type to 7220 ± 40 BP (8110–7940 cal BP), and the Kurohama type to 7540 ± 45 BP and 6540 ± 45 BP (8405–8205 and 7560–7330 cal BP) (Figure 4).

DISCUSSION

This is the first report applying AMS to directly dating the Black Pottery I phase; no other ^{14}C ages have been published for this phase. The possibility of using AMS to date these black pottery samples should enable researchers to establish a more detailed chronology.

Two ^{14}C ages for Black Pottery I samples, a decorated type, are consistent with the archaeological interpretation that Black pottery I belongs to the cultural phase between Red Pottery II and Black Pottery II.

The variation in carbon recovery for both black pottery and fiber pottery samples suggests that there is a possibility for improvements in carbon yield, and in particular, the alkali treatment method, perhaps in the concentrations of NaOH solution. The alkali treatment at lower concentrations than 0.1N, possibly 0.05N, may preserve more residual organic carbon in the sample, and a higher carbon recovery would also provide greater amounts of material for ^{14}C dating.

Table 1 Carbon contents and ^{14}C ages for pottery samples.

Sample nr	Sample	Site	Type	Preservation state	Carbon content (%)	$\delta^{13}\text{C}$ (‰)	Size of graphite	Conventional ^{14}C age (BP)	Calibrated ^{14}C age (cal BP)	(%) ^a	Lab # (NUTA2-)
01PO18	black pottery	San Nicoras, Philippines	—	hard	0.51	—	—	modern	1990s	—	—
01PO13	black pottery	Bangag I, Philippine	Black Pottery I	hard	0.31	—	1.77 mg	2170 \pm 30	2310–2220 2185–2095	45 46	5367
01PO14	black pottery	Bangag I, Philippines	Black Pottery I	hard	0.23	—	1.30 mg	2290 \pm 30	2350–2300 2245–2180	60 37	5368
01PO21	fiber pottery	Myouonji Cave, Japan	Tado kasou	fragile	0.39	-26.2	0.95 mg	8660 \pm 45	9770–9535	100	5983
01PO25	fiber pottery	Myouonji Cave, Japan	unidentified ^b	hard	0.33	-24.7	1.03 mg	7855 \pm 45	8900–8830 8780–8540	6 89	5991
01PO27	fiber pottery	Myouonji Cave, Japan	Sekiyama	hard	0.36	-23.9	1.37 mg	7220 \pm 40	8110–8075 8065–7940	19 76	5992
01PO28	fiber pottery	Myouonji Cave, Japan	Kurohama	fragile	0.21	-23.2	1.02 mg	7540 \pm 40	8405–8290 8260–8205	81 19	5984
01PO29	fiber pottery	Myouonji Cave, Japan	Kurohama	hard	0.77	-24.3	1.11 mg	6540 \pm 40	7560–7535 7510–7415 7395–7370 7350–7330	11 77 7 5	5985

^aPercentage of main peak in the probability distribution of calibrated age.^bAn unidentified pottery type decorated with incised lines.

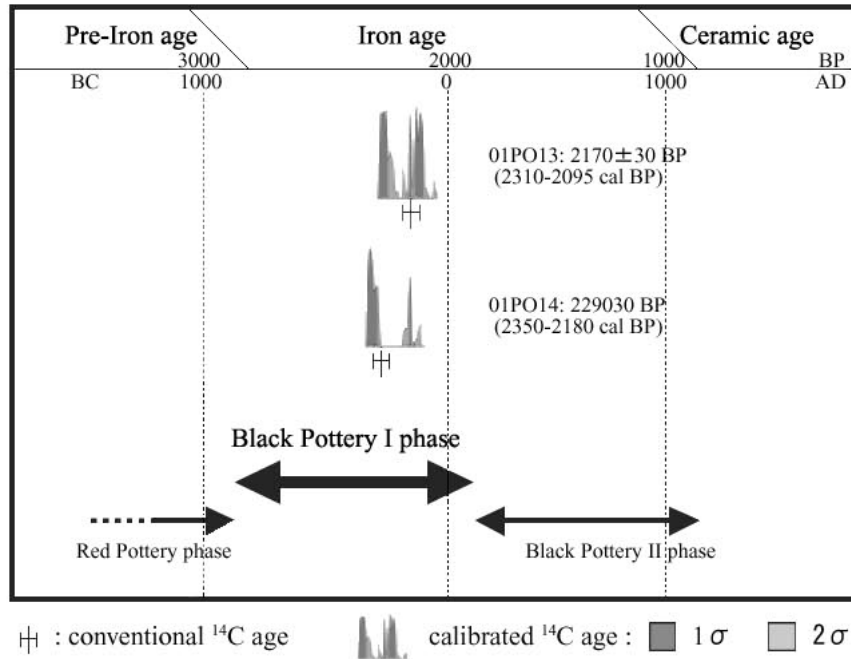


Figure 3 ¹⁴C ages for the Black Pottery I from Lal-lo shell midden sites, the Philippines. The ages of the Red Pottery II phase and Black Pottery II phase were analyzed from bone and charcoal samples (Mihara et al. 2002).

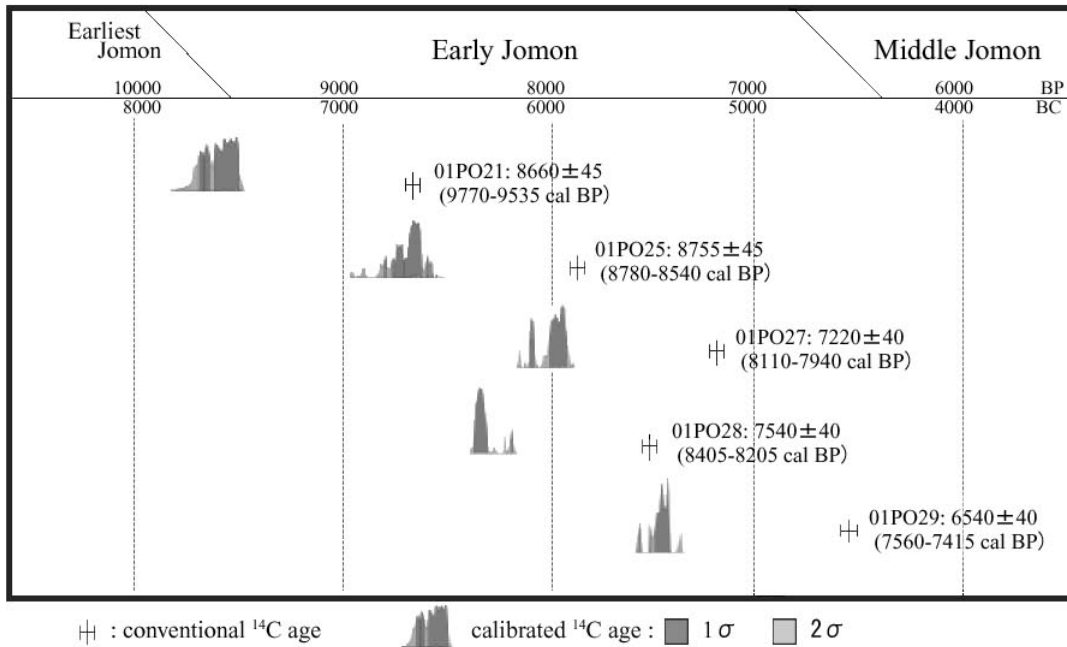


Figure 4 ¹⁴C ages for fiber pottery in Myouonji Cave site, Japan, during the Jomon period

^{14}C ages for the Japanese fiber pottery samples fluctuated largely. One of the fiber pottery samples (01PO28) belonging to the Kurohama style was older than the sample from the Sekiyama style which appeared before the Kurohama type. The anomalous date was for the Kurohama sample which was badly preserved and showed the lowest carbon content at 0.21%. The source of an older carbon contaminant which might have caused the ^{14}C age offset has not been identified.

We are now applying this method for analyzing black pottery from China, which is thought to be the origin for black pottery in Southeast Asia. We will also extend our research using this method to other black pottery samples and fiber pottery samples.

ACKNOWLEDGEMENTS

We would like to thank Prof K Yoshida of Tokyo University, Dr M Sakamoto of the National Museum of Japanese History, and Dr M Okuno of Fukuoka University for their useful comments and suggestions, and Dr B Chisholm of University of British Columbia for careful reading of the manuscript.

REFERENCES

- Hedges REM, Chen T, Housley RA. 1992. Results and methods in the radiocarbon dating of pottery. *Radiocarbon* 34(3):906–15.
- Kitagawa H, Masuzawa T, Nakamura T, Matsumoto E. 1993. A batch preparation method for graphite targets with low background for AMS ^{14}C measurements. *Radiocarbon* 35(2):295–300.
- Kolic ED. 1995. Direct radiocarbon dating of pottery: selective heat treatment to retrieve smoke-derived carbon. *Radiocarbon* 37(2):275–84.
- Kuzmin YV, Jull AJT, Lapshida ZS, Mendvedev VE. 1997. Radiocarbon AMS dating of the ancient sites with earliest pottery from the Russian Far East. *Nuclear Instruments and Methods in Physics Research, Section B: Beam Interaction with Materials and Atoms* 123:496–7.
- Mihara S, Okuno M, Ogawa H, Tanaka K, Nakamura T, Koike H. 2002. AMS ^{14}C dating and dietary analysis for Lal-lo shell midden sites, Philippines. *Summaries of Researches Using AMS at Nagoya University* (XIII):82–104. In Japanese with English abstract.
- Nakamura T, Iwahana H. 1990. Comparison of ^{14}C ages by accelerator mass spectrometry between solid-carbon and humic acid ingredients from charcoal remains collected at Moroka Site, Gifu prefecture. *Archaeology and Natural Science* 22:59–76. In Japanese with English abstract.
- Nakamura T, Nakai N, Ishihara T, Iwahana H. 1990. Radiocarbon ages by accelerator mass spectrometry of charred carbonaceous residues on buried Jomon potteries from Morinoshita Site, Gifu prefecture. *Quaternary Research* 28(5):389–97. In Japanese with English abstract.
- Nakamura T, Niu E, Oda H, Ikeda A, Minami M, Takahashi H, Adachi M, Palis L, Gottdang A, Suya N. 2000. The HVEE Tandem AMS system at Nagoya University. *Nuclear Instruments and Methods in Physics Research B* 172:52–7.
- Nakamura T, Taniguchi Y, Tsuji S, Oda H. 2001. Radiocarbon dating of charred residues on the earliest pottery in Japan. *Radiocarbon* 43(2B):1129–38.
- Oda T, Yamamoto N. 2001. AMS radiocarbon ages and the calibration ages of Jomon Pottery: from early to final stages of the Jomon Period in Ishikawa prefecture, Japan. *Archaeology and Natural Science* 42:1–13. In Japanese with English abstract.
- Ogawa H, editor. 2000. *Excavation of the Lal-lo Shell Middens—Report for the Grant-in-Aid for the International Scientific Research (Field Research)*. Monbusho: The Ministry of Education, Science Sports and Culture. 269 p.
- Yoshida K, Ohmichi J, Kinose M, Iijima H, Oono A, Abe N, Miyazaki Y, Matsuzaki H. Forthcoming. The application of ^{14}C dating to potsherds of the Jomon period. *Nuclear Instruments and Methods in Physics Research B*.

DATING OF TOTAL SOIL ORGANIC MATTER USED IN KURGAN STUDIES

M Molnár^{1,2} • K Joó³ • A Barczy³ • Zs Szántó¹ • I Futó¹ • L Palcsu¹ • L Rinyu¹

ABSTRACT. We investigated Csípő-halom, one of the kurgans that served as a burial place in the Hortobágy area of the Hungarian Great Plain. For pedological description and other studies of the protected mound and its surroundings, only a few monitoring drillings were permitted to get soil samples. On the basis of morphological and visual studies, the structure and layers of the mound were reconstructed. The Laboratory of Environmental Studies of the Institute of Nuclear Research at the Hungarian Academy of Sciences (INR/HAS) performed radiocarbon measurements of soil samples, applying a bulk combustion pretreatment method. The measured ¹⁴C ages of soil samples from reference points, such as the top layer of the mound, the center of mound body, the base layer of the mound, the near surroundings, and the distant surroundings, are in good agreement with the preliminary archaeological concept for this field and give substantial information about the rate of soil generation processes in this area.

INTRODUCTION

“You are our cathedrals,” wrote the Hungarian poet Gyula Illyés about our burial mounds. In fact, these land elevations are one of the oldest and the most valuable pieces of the human heritage of Hungary and the Great Plain. They are the witnesses of past ages, demonstrating the culture of our ancestors, their burial habits, and their relationship to nature.

The isolated burial mounds, called “kurgans,” belong to the landscape of the Great Hungarian Plain. Many of them were actually a settlement, a settlement border, or a guarding hillock. Since 1996, all of the artificially formed mounds in the Hungarian landscape are protected by law, considered as “kunhalom” (cumanian hillock), no matter their origin, purpose, or their time of derivation. According to these laws, every tomb-mound (kurgan), living-mound (tell-telep), defensive and protective mound, and the delineation of county, district, and settlement borders are counted among the wide concept of “kunhalom” (Tóth 1999).

Kurgans were built in the Stone and Iron Ages (4000–1000 BC) until the Hungarian conquest. The ground was piled simultaneously so that the corpse was held in a half-sitting position, with its head shorn (Kovács 1977; Kalicz 1970). These tumuli are more than archaeological findings; they are also special landscape features that have botanical importance, and provide records for the soil sciences (Alexandrovskiy et al. 2001).

Mounds in Hungary were generally built from the surrounding soil. Their outlines are oval. In general, after building up the mound, the construction provided a surface on which the new soil formation could begin. Under the mound, the several thousand-year-old soil surface has been buried so it has preserved the soil forms that existed in the time of the mound’s construction, while the distant surroundings of the mound preserved marks of soil formation since then (Alexandrovskiy 1996). Thus, securing the soil surface around the mound gives important information about the recent soil formation, and it can widen our knowledge about soil development (Gennadiev and Ivanov 1989).

In our research, we applied radiocarbon dating, a powerful tool in soil and archaeological studies. When lacking enough alternative material for the applied dating technique (proportional counting),

¹Institute of Nuclear Research of the Hungarian Academy of Sciences (INR/HAS), Laboratory of Environmental Studies, H-4026 Debrecen, Bem tér 18/c., Hungary.

²Corresponding author. Email: mmol@atomki.hu.

³Szent István University, Department of Landscape Ecology H-2103 Gödöllő Páter Károly u 1., Hungary.



Figure 1 Map of Hungary within Europe. Since 1996, laws protect all of the artificially formed mounds in Hungary.

the dating of total soil organic matter was carried out (Magyari et al. 2001; Pessenda et al. 2001). This paper presents the results and availability of ^{14}C dating of total soil organic matter in the case of the studied kurgan.

MATERIALS AND METHODS

Csípő-halom is one of the kurgans that served as burial place. It is located in the Hortobágy area of the Hungarian Great Plain (Figure 2). The height of the kurgan is 5.0 m (elevation 95.15 m) (Figure 3). This territory had developed on loess-like sediment. It was possibly slightly disturbed (ploughing, afforestation, or buildings, etc.) and soil formation was undisturbed (prevented from floods, low human influence, protection).

After the general description of the area, the pedological study of the body of the mound was carried out. The instrument used for sampling was a Styl-style double-armed auger. The diameter of the auger was 5 cm; the helical drill was 100 cm long, and the attachable extensions were 100 cm each. The maximum depth of the boring was 10 m (Figure 4).

The principle of the sampling was based on the Birks and Birks (1980) type of palaeoecological network. The first series of drillings was performed on the body of the mound in the higher third of the slope. The purpose was to study the material of the mound and the buried soil. The second series of drillings, located at the foot of the mound, examined the destroyed and regenerated area, and the third one, performed farther from the mound, examined those areas which had not been disturbed by the building. We carried out the boring with 5 replications at each site. We studied differences between the samples regarding color, structure, humidity, and solidity on the site. The content of lime was tested in every 10 cm with 10% HCl, disregarding the dividing lines between the horizons

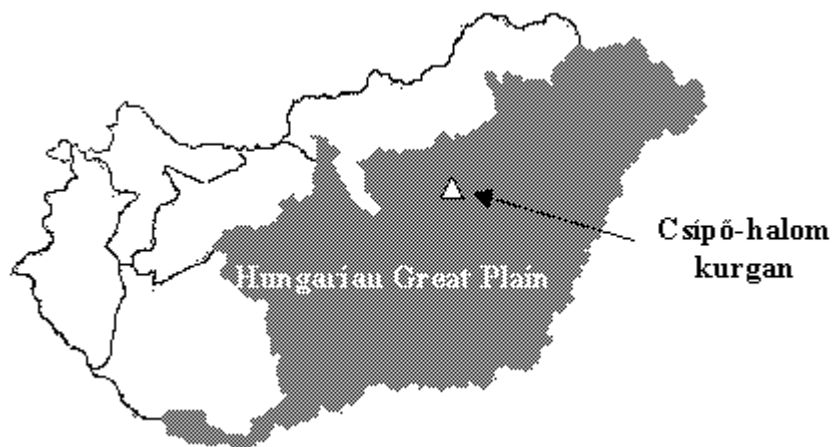


Figure 2 The Csíró-halom kurgan is located in the Hungarian Great Plain



Figure 3 The height of the kurgan is 5.0 m

or layers. We also noted the location of various concretions and morphological features, like roots, tunnels of animals, iron and silica separations, bones, etc. According to these, we could separate the layers and horizons from each other on the scene; accordingly, we classified and prepared the samples for laboratory studies.

Dating of soil samples was performed by the Laboratory of Environmental Studies of the Institute of Nuclear Research at the Hungarian Academy of Sciences. When lacking enough alternative material from soil core samples for ^{14}C dating (with proportional counters), the total organic matter of the soil samples was dated. After removing inorganic carbonate fraction (0.1N HCl) and the obviously recent macroscopic biomass fragments, 200–300 g of air-dried soil sample was taken for wet chemical oxidation, using H_2SO_4 and H_2O_2 as oxidants, at 200 °C temperature for 8 hr reaction time in a special combustion system. The produced CO_2 gas from the carrier N_2 gas flow was collected in traps with $\text{Ba}(\text{OH})_2$ solutions (Figure 5). A trap with H_2SO_4 , located before the CO_2 traps, was applied to retain SO_2 .

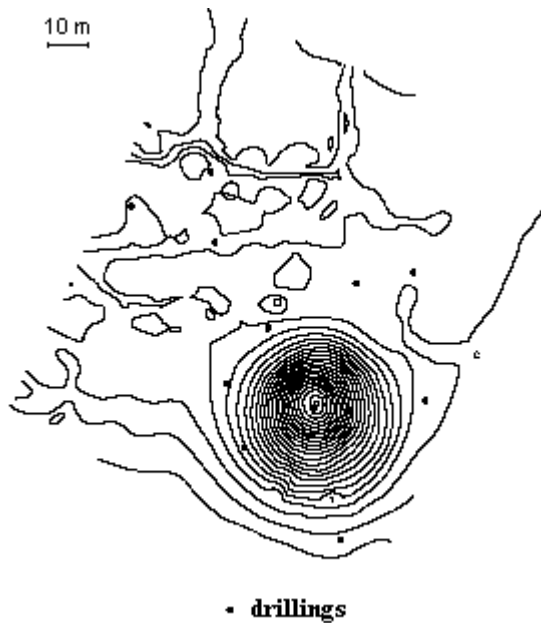


Figure 4 The location of drillings on the mound

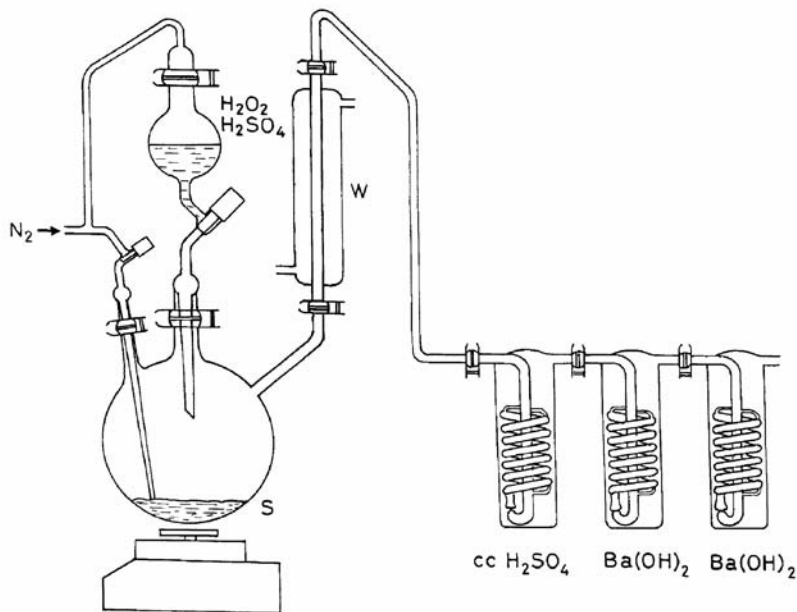


Figure 5 Combustion system applied for chemical oxidizing of soil organic matter

The carbonate precipitate from the traps was digested by 75% H_3PO_4 , and the produced CO_2 gas, after purification in a chromatographic system, was used for ^{14}C dating (Csongor et al. 1982). This special bulk combustion pretreatment method provides enough gas amount (at least 0.04 mol) for the gas proportional counters (Hertelendi et al. 1989).

RESULTS AND DISCUSSION

The depths of the drillings that were carried out on the higher third of the slope were 580 cm, 480 cm, 405 cm, respectively. We bored down to 165 cm deep around the mound (supposedly the building zone) and in the distant surroundings in the same way.

Figure 6 presents the schematic drawing of recorded main layers in the mound and the surrounding area. The structure and layers of the mound were reconstructed on the basis of their morphological and visual studies. The measured ^{14}C dates are presented in Table 1.

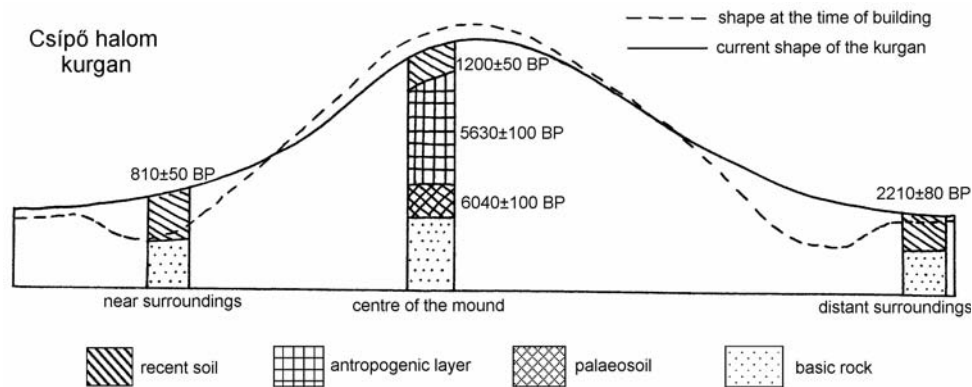


Figure 6 Schematic drawing of recorded main layers in the mound and the surroundings area

Table 1 ^{14}C dates for the Csípő-halom kurgan. Calibrated ages are given as 1- σ age range (Stuiver et al. 1998).

Laboratory code	Sample	^{14}C age (BP $\pm 1 \sigma$)	Calibrated age (1 σ)
Deb-9071	Top soil of the mound	1200 \pm 50	780–880 cal AD
Deb-9086	Anthropogenic core of the mound	5630 \pm 100	4550–4360 cal BC
Deb-9087	Buried paleosoil	6040 \pm 100	5040–4800 cal BC
Deb-9073	Soil of near surroundings of the kurgan	810 \pm 50	1200–1260 cal AD
Deb-9070	Soil of distant surroundings of the kurgan	2210 \pm 80	360–200 cal BC

In each case, a 20- to 30-cm-deep A-horizon was identifiable on the top of the mound. Under this zone, 50- to 70-cm-deep layers showed lime dynamics, which is a characteristic in the B-horizon of chernozem soils. We could also identify the fur of lime in 3 samples. The ^{14}C age of this recent layer was 1200 \pm 50 BP, which is younger than the lower layers of the body of the mound, and younger than the undisturbed surroundings; this shows that this is a recent layer which formed on the top of the mound.

Under the recent layer of the mound, we could not find the usual basic rock, since the body of the mound consists of the piled, uniformly dark brown, humic soil. The structure of this layer is strikingly different from the upper one, and shows conchoidal fracture when it was dried. The ^{14}C age of the piled body was 5630 \pm 100 BP.

Under this layer, after more or less transition, there is another unified layer (A-paleo-soil) in which we could find hydromorphic marks with clayey texture, solid structure, and bones. Under the A-paleo-soil layer, there was a slightly better structured, dark brown horizon (B-paleo-soil) with higher lime content which changed into loess in a 30- to 50-cm transition. The ^{14}C measurement of the soil sample of this buried palaeosoil was 6040 ± 100 BP, similar to the upper piled body.

The order of the layers was the same in every sample, only their thickness varied. With the exception of the upper A-horizon, we could not identify the genetical horizons unambiguously. This is particularly important because presently we can only estimate the location of the anthropogenic layer and the buried soil.

In the drillings adjacent to the mound, we found a 20- to 30-cm-deep dusty-crumbly structured A-horizon that changed into the loess basic material with increasing proportions of lime. In the loess, we found lime concretions. The ^{14}C age of the sample from this zone was 810 ± 50 BP, which confirmed that this was a very young soil that formed on the eroded zone since the building of the kurgan.

The morphological survey of the areas that had not been affected by the building of the mound gave more unambiguous results. On the higher areas, we could identify chernozem soils. Their A-horizon was followed by a clearly identifiable, gradual B-horizon, which contained tunnels of animals. The basic rock is loess in which the marks of the moving groundwater can be identified (blots of iron, spots of rust). On the lower areas, there are solonetz-type alkanian soils; in the basic rock of this level, we observed a stronger effect of water (gley spots). The ^{14}C age of the sample from this distant surroundings was 2210 ± 80 BP. This measured age showed that the sample from this region is older than the soil of the building zone or the upper recent soil of the mound.

CONCLUSIONS

As a result of the morphological surveys, we conclude that the layers and horizons can be clearly divided by the outside studies of the sample, and can be used for further identification. The structure of the mound can be ascertained: the mound is covered with new soil formation (1200 BP). Under the mound, the body consists of an anthropogenic core (5630 BP), and the buried soil (6040 BP) has remained protected. The coincidence of the ages of the anthropogenic core and the buried soil are in good agreement with the archaeological concept that the kurgan was built in one step, not step by step over a long period of time. The age of the soil in nearby surroundings (810 BP) also confirmed the preliminary concept that this area was eroded almost to the basic rock for the building of the kurgan, and the new soil formation began after the birth of the mound. The ^{14}C age of the soil of distant surroundings (2210 BP) was older than the soil samples from the top of the kurgan and the near surroundings, which confirmed that this distant region was possibly undisturbed.

Although these bulk ages obtained after a special pretreatment of the total soil organic matter have to be considered only as maximum ages, the presented ^{14}C dates are in good agreement with the anthropological concept about the conditions and chronology of the building of the investigated Csípő-halom kurgan.

REFERENCES

- Alexandrovskiy AL. 1996. Natural environment as seen in soil. *Eurasian Soil Science* 29(3):277–87.
- Alexandrovskiy AL, van der Plicht J, Belinskiy AB, Khokhlova OS. 2001. Chronology of soil evolution and climatic changes in the dry steppe zone of the Northern Caucasus, Russia, during the 3rd millennium BC. *Radiocarbon* 38(2):629–35.
- Birks HJ, Birks HH. 1980. *Quaternary Palaeoecology*. London: E. Arnold Press. 297 p.
- Csongor É, Szabó I, Hertelendi E. 1982. Preparation of

- counting gas of proportional counters for radiocarbon dating. *Radiochemical and Radioanalytical Letters* 55:303.
- Gennadiev AN, Ivanov IV. 1989. Generation of soil and palaeopedology: problems, conceptions, and methodology. *Pocsvovedenije* 10(1):34–43. In Russian.
- Hertelendi E, Csongor É, Záborszky L, Molnár J, Dajkó G, Györfi M, Nagy S. 1989. A counter system for high-precision ^{14}C dating. *Radiocarbon* 31(1):399–406.
- Kalicz N. 1970. *Claygods. The Memories of Age of Neolithic and Brass in Hungary*. Budapest: Corvina Kiadó. p 48–58. In Hungarian.
- Kovács T. 1977. *Bronze Age in Hungary*. Budapest: Corvina Kiadó. p 51–6. In Hungarian.
- Magyari E, Sümegi P, Braun M, Jakab G, Molnár M. 2001. Retarded wetland succession: anthropogenic and climatic signals in a Holocene peat bog profile from northeast Hungary. *Journal of Ecology* 89:1019–32.
- Pessenda LC, Gouveia SE, Aravena R. 2001. Radiocarbon dating of total soil organic matter and humin fraction and its comparison with ^{14}C ages of fossil charcoal. *Radiocarbon* 38(2):595–601.
- Stuiver M, Reimer PJ, Bard E, Beck JW, Burr GS, Hughen KA, Kromer B, McCormac G, van der Plicht J, Spurk M. 1998. INTCAL98 radiocarbon age calibration, 24,000–0 cal BP. *Radiocarbon* 40(3):1041–83.
- Tóth A. 1999. *Cumanian Mounds*. Kísújszállás: Alföldkutatásért Alapítvány Kiadványa. 77 p. In Hungarian.

CALCULATING SEDIMENT COMPACTION FOR RADIOCARBON DATING OF INTERTIDAL SEDIMENTS

M I Bird^{1,2} • L K Fifield³ • S Chua¹ • B Goh¹

ABSTRACT. This study estimates the maximum and minimum degrees of autocompaction for radiocarbon-dated Holocene mangrove sediments in Singapore, in order to correct apparent sediment accretion rates for the effects of sediment compression due to autocompaction. Relationships developed for a suite of modern (surface) sediment samples between bulk density, particle-size distribution, and organic matter content were used to estimate the initial (uncompacted) bulk density of buried and variably compressed Holocene sediments, based on the grain-size distribution and organic matter content of the sediment. The difference between measured (compacted) and initial (uncompacted) bulk density of each buried sediment interval can be interpreted as the amount of length shortening experienced by each interval since burial. This allows the elevation of samples selected for ¹⁴C dating to be corrected for the effects of autocompaction of the underlying sediment sequence, so that accurate estimates of vertical sediment accretion rates can be calculated.

The 3 Holocene mangrove sequences analyzed and dated for this study ranged in age from 2000 to 8500 cal BP. The effects of autocompaction are significant, even in comparatively thin sequences, with subsidence of up to 56 cm calculated for carbon-dated samples presently 2 m above incompressible basement. The vertical sediment accretion rates for these mangrove sequences ranged from 0.99 to 6.84 mm/yr and carbon sequestration rates ranged from 0.9 to 1.7 t/ha/yr, all within the range observed for comparable Holocene and modern mangrove sediments elsewhere.

INTRODUCTION

Autocompaction refers to the tendency of newly deposited sediments to increase in bulk density over time through compaction, as new sediments are deposited above them. This leads to the gradual subsidence of Holocene sedimentary sequences “insidiously, continuously and irreversibly lowering the level of the (ground) surface, especially where the sequence beneath is rich in silts and peat...” (Allen 2000).

This compaction and subsidence, in turn, creates space for the continued vertical accretion of new sediment in marginal marine and estuarine environments. Radiocarbon dating of organic and carbonate material from such sediments has been widely used to determine relative sea-level histories through the Holocene (e.g. Pirazzoli 1996) as well as for the calculation of vertical sediment accumulation rates (e.g. Ellison and Stoddart 1991; Ellison 1993) and carbon sequestration rates (e.g. Fujimoto 2000).

While autocompaction does not effect the calculation of mass accumulation rates of mineral or organic matter, it does potentially introduce large errors into the calculation of rates of sea-level rise and vertical sediment accretion rates (Allen 2000; Stanley and Hait 2000). This is because a sample selected for dating from a particular elevation in a sedimentary sequence will have been lowered since deposition by autocompaction of the sediment pile beneath it. The degree to which a sample has been lowered will be a time-dependent function of the thickness and type of sediments beneath it and the thickness and type of sediment subsequently accumulated above it. Sands tend to have a comparatively high initial bulk density and are relatively incompressible, whereas fine-grained sed-

¹National Institute of Education, Nanyang Technological University, 1 Nanyang Walk, Singapore, 637616.

²Present address: School of Geography and Geosciences, University of St. Andrews, St. Andrews, Fife, KY16 9AL, Scotland, United Kingdom. Corresponding author. Email: Michael.bird@st-andrews.ac.uk.

³Department of Nuclear Physics, Research School of Physical Sciences and Engineering, Australian National University, Canberra, A.C.T. 0200, Australia.

iments (silts and clays) and peaty material have low initial bulk density, but may be compacted by 40–80% when buried a few tens of meters (Allen 2000).

The rate of autocompaction is likely to be rapid in the initial stages (Cahoon and Lynch 1997), slowing asymptotically to zero as it approaches a maximum value determined again by the characteristics and thickness of sediment pile above (Allen 2000). While, in principle, the effects of autocompaction can be modeled (Allen 2000), in many cases the timing of the imposition of the sediment load above a sample collected for ^{14}C dating will not be known in detail.

Since the time dependence of autocompaction is often unknowable, this study instead calculates the maximum amount of compaction that could have occurred to a given interval of sediment within a sedimentary sequence. This is obtained by comparison of the measured (compacted) dry bulk density of the sample and a calculated initial (uncompacted) dry bulk density of the sample, determined on the basis of the particle size distribution and organic matter content of the compacted sample. The study examines mangrove sediments in Singapore but, in principle, can be applied to any intertidal sediments.

EXPERIMENTAL TECHNIQUES

Conceptual Framework

The major determinants of the bulk density of a sediment sample are its particle size distribution, particularly the proportion of fine mineral material, and the proportion of organic material. In this study, fine minerals (silt and clay) are operationally defined as material $<63\ \mu\text{m}$ in size. Organic matter content is defined as (i) the total organic carbon content of the sample, and (ii) the mass loss on ignition of material $>63\ \mu\text{m}$ in size. The loss on ignition measurements were made on the $>63\text{-}\mu\text{m}$ fraction as this reduces complications that might arise from the dewatering of clays and amorphous phases; also, it is possible that large fragments of organic detritus exert a greater control on the compressibility of a sediment sample than fine organic matter.

It is assumed that when initially deposited, a sediment sample will have a wet bulk density largely determined by the above parameters. In the intertidal zone, where the sediment surface is exposed and partly drained with each tidal cycle, sediments can undergo initial settling into a coherent mass of sediment with a definable sediment surface. In detail, bulk density may be influenced by elevation in the intertidal zone and, thus, the amount of time over which the sediment pile can drain in a single tidal cycle, but this complication is not addressed in this study.

Carbon in mangrove sediments will continue to be mineralized by microbial processes after burial, but carbon is also added into the sub-surface sediments as dead root biomass. Alongi et al. (2001) found that mineralization efficiencies for mangrove sediments in Thailand ranged from 27 to 40% in the mixed layer (16–38 cm). The same study also found that carbon densities through the mixed layer could both increase and decrease with depth, depending on location and season, suggesting that there is no reason to expect that sediment buried below the mixed layer will have a systematically lower carbon content than sediment at the surface. Once sediment is buried below the mixed layer, mineralization may proceed, but the rates of mineralization can be considered small for the purposes of this study (Alongi et al. 2000).

It is therefore assumed that once buried, a given volume of sediment will retain its particle size distribution and organic matter content. Thus, the amount of compaction of a sediment interval can be estimated from the difference between the bulk density of the compacted sediment and the bulk density of a modern (uncompacted) sediment sample with the same grain size and organic matter char-

acteristics. The estimate of initial bulk density for a compacted sample is derived from empirical relationships between dry bulk density, particle size distribution, and organic matter content developed for a suite of modern intertidal sediment samples of widely divergent characteristics from mangrove regions in Singapore (as described below).

This comparison can be repeated for successive intervals up a sedimentary sequence, and the cumulative amount of compaction can be calculated from the base of a sedimentary sequence to the elevation from which a sample was taken for ¹⁴C dating. Since some, or all, of this compaction could have occurred before the sample was deposited, however, this amount of compaction does not necessarily reflect the amount of lowering that the sample has experienced since deposition. Because the time dependence of the rate of autocompaction is in general not known, only the 2 end-member values for the cumulative lowering of a sample from its original depositional elevation are well defined.

The first end-member assumes that autocompaction occurs rapidly after deposition of the sediment. In this case, the amount of lowering of a sample selected for ¹⁴C dating at any point in the sedimentary sequence is zero, because the sedimentary pile beneath was already fully compacted before the sample selected for dating was deposited. The second end-member assumes that compaction of the sequence underlying a sample collected for dating occurs only after deposition of the sample. This yields the maximum amount of lowering that a sample could possibly have experienced. Neither of these end-members is realistic, but the “true” amount of lowering experienced by a sample must lie between these 2 values and can be reported as the average of the two, plus or minus half the difference between the two.

Samples and Analysis

Modern Samples

A set of 45 modern reference sediment samples (0–5 cm) and 12 sub-recent sediments (15–20 cm) were collected from mangrove environments distributed around the coast of Singapore, with sample locations selected in order to obtain as wide a range of particle size distributions and carbon contents as possible. In each case, a PVC tube 3.8 cm in diameter was pushed into the sediment surface to a depth of 5 cm from the sediment surface (0–5 cm) or from a pit dug to 15 cm depth (15–20 cm). Then, each sediment was quantitatively extracted, yielding a volume of 175 cm³ of wet sediment. This sediment was transferred to a plastic bag and sealed for transport to the laboratory where the wet weight of sediment was determined. While sampling does compact the sediment in the tube, the weight of sediment collected is representative of the uncompacted material in the volume sampled, and, hence, compaction during sampling does not affect the bulk density calculations.

Approximately 20–30 g of wet sediment was weighed and then dried for 2 days at 60 °C to determine water content and dry bulk density of each sample (grams of dry sediment per cubic cm of original volume). A separate aliquot of 30 g of wet sediment was weighed and then wet sieved at 63 μm to separate the most compressible silt and clay fraction of the sediment. The >63-μm fraction was dried and weighed, and the proportion of <63-μm material calculated by difference after correcting for water content. The dried >63-μm fraction was then sieved at 2000 μm and 500 μm and these fractions weighed to obtain more detailed information on particle size distribution. All >63-μm material was then recombined into a single sample for the determination of loss on ignition in the >63-μm fraction (LOI_{>63μm}). This was calculated from the weight loss accompanying the heating of 1–2 g of well-mixed >63-μm material in a furnace at 450 °C for 4 hr.

Total organic carbon and total inorganic carbon were determined on dried and crushed aliquots of bulk sediment (~150 mg) using a Shimadzu total carbon analyzer. Total carbon (TC) was determined by combustion at 900 °C, total inorganic carbon (TIC) by acidification, and total organic carbon (TOC) from the difference between the TC and TIC determinations.

Relationships between calculated dry bulk density (DBD), fraction of <63- μm ($F_{<63\mu\text{m}}$) material and either TOC or $\text{LOI}_{>63\mu\text{m}}$ for all modern samples were explored using Tablecurve-3D surface fitting software.

Compacted Samples

Three sedimentary sequences buried to different depths were used to test the “decompaction” methodology (Figure 1). The first was a ~2.5-m sequence of mangrove peat underlying modern mangroves at Lim Chu Kang in northwest Singapore (LCK-4; 1.446737°N, 103.709312°E; determined by differential GPS to ± 0.5 m). The core was obtained using a 50-mm-diameter modified Livingstone piston corer. The base of the sequence (–2.0 m rsl: relative to mean sea-level) represents a pre-Holocene-transgression weathered profile developed on highly compacted but not lithified Pleistocene “Old Alluvium.” The profile grades upwards from peaty muds and sands to essentially pure peat +0.5 m above modern mean sea level. The sediments were extracted in 1-m increments, with each section extruded on site and wrapped in plastic to prevent water loss. In the laboratory, each section of the core was cut into 10-cm segments and weighed. Thereafter, sample preparation and analysis protocols followed those described above for the modern sediments.

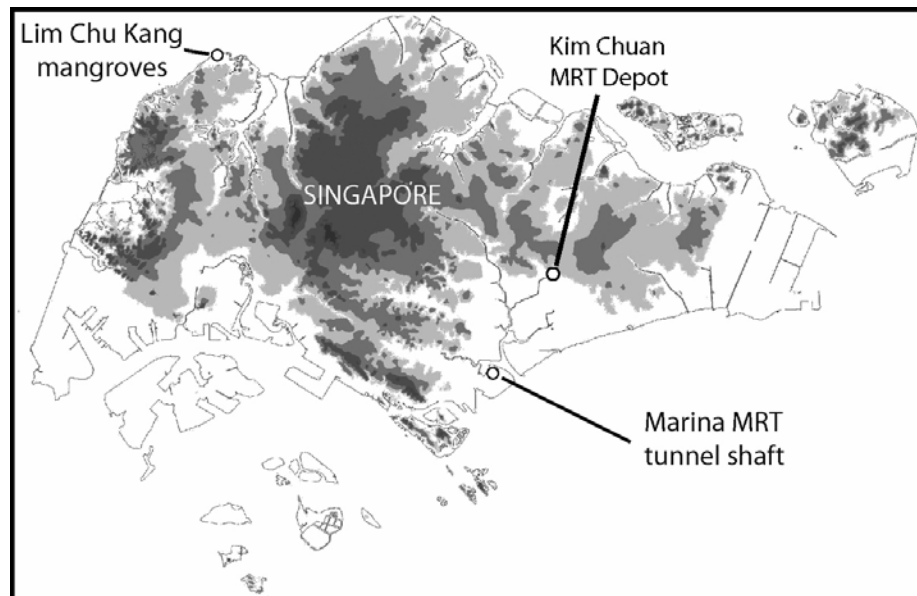


Figure 1 Locations of the Holocene mangrove sequences analyzed in this study. The outline of modern Singapore is shown as a line. The extent of Singapore above tidal influence during the mid-Holocene sea-level highstand is shown as a shaded area. Higher land is shown with darker shading.

The second sequence was exposed in a deep excavation in the downtown area for the future underground Marina Mass Rail Transit line (MAR-5; 1.290896°N; 103.861090°E). A 1.5-m sequence from –7.82 to –6.32 m rsl was sampled from a vertical face by pushing a sample tube horizontally

into the exposure at 10-cm intervals. The base of the sequence (−7.82 to −7.42 m) represents a pre-Holocene-transgression soil developed on the sedimentary “Old Alluvium,” overlain from −7.42 to −7.0 m by a sandy mangrove peat, overlain in turn by ~4 m of shallow marine clays. This location was originally beneath the sea, but reclamation in the 1970s added another ~5 m of sand to the top of the sedimentary pile, raising the sediment surface about 4 m above mean sea level. All samples collected from this sequence were treated in the manner described for the modern sediment samples.

The third sequence was sampled from the excavation that will become the Kim Chuan underground train servicing facility for the Circle Line Mass Rapid Transit train line (KCD-6; 1.340096°N 103.886743°E) The samples were collected from an excavation face exposed from +1.0 to +3.0 m rsl. The lowermost 30 cm of the section represents highly compacted “Old Alluvium” transgressed between +1.3 and +1.6 m rsl by Holocene interbeds of clay and sandy clay. A sequence of mangrove mud was deposited from +1.6 m, grading gradually into a mangrove peat at +2.6 m. The top of the natural sequence was at +3.0 m, but this was overlain by 1–2 m of fill material (probably dumped in the 1950s) that was not sampled. All samples were collected as described for MAR-5, and were subsequently treated in the manner described for the modern sediment samples.

For all sedimentary sequences, woody material was selected from the basal Holocene layers and from the upper parts of the sequences for ^{14}C dating. Samples were given an acid-base-acid pretreatment before analysis by accelerator mass spectrometry at the Research School of Physical Sciences and Engineering, Australian National University (ANU-A prefix) or by conventional scintillation counting at the Research School of Earth Sciences, Australian National University (ANU-prefix).

RESULTS

Modern Samples

The modern samples covered a wide spectrum of compositions from peaty sands and muds to inorganic sands. DBD for the samples ranged from 0.12 g/cm³ to 1.62 g/cm³, water content from 19.4% to 83.3%, $F_{<63\mu\text{m}}$ from 0.44% to 85.5%, TOC from 0.41% to 34.7%, and $\text{LOI}_{>63\mu\text{m}}$ from 0.56% to 85.6%. In general, coarse-grained sediments were characterized by high DBD and low water content, TOC, $F_{<63\mu\text{m}}$ and $\text{LOI}_{>63\mu\text{m}}$, while fine-grained sediments were characterized by low DBD and high water content, $F_{<63\mu\text{m}}$ and $\text{LOI}_{>63\mu\text{m}}$, and variable TOC. There are good relationships between DBD and water content, TOC, and $\text{LOI}_{>63\mu\text{m}}$, but poor correlation between DBD and $F_{<63\mu\text{m}}$, suggesting that organic content is a more significant determinant of DBD than particle size distribution (Figure 2). Samples from 15–20 cm tend to plot above the line defined by the 0–5-cm samples, suggesting that these samples have been compacted to a variable degree.

Compacted Samples

Core LCK-4 (Figure 3) is generally composed of muddy to sandy peats with less than 10% of >2000- μm material and 20–50% of <63- μm material, except for a sandier unit from −0.4 to −0.1 m rsl. Water content and DBD tend to decrease up the core, while TOC increases up the core from ~2 to 10%. $\text{LOI}_{>63\mu\text{m}}$ remained approximately constant at around 10% up to +0.1 m rsl, increasing in the uppermost part of the core to 40–50%. This core spanned a range of sediment types, and, hence, some uncertainty is introduced by the compacting effect of the coring process. The degree of compaction along the length of the core may not be uniform and may vary depending on the compressibility of the sediments encountered. This effect is probably small, and is accounted for in the decompaction procedure.

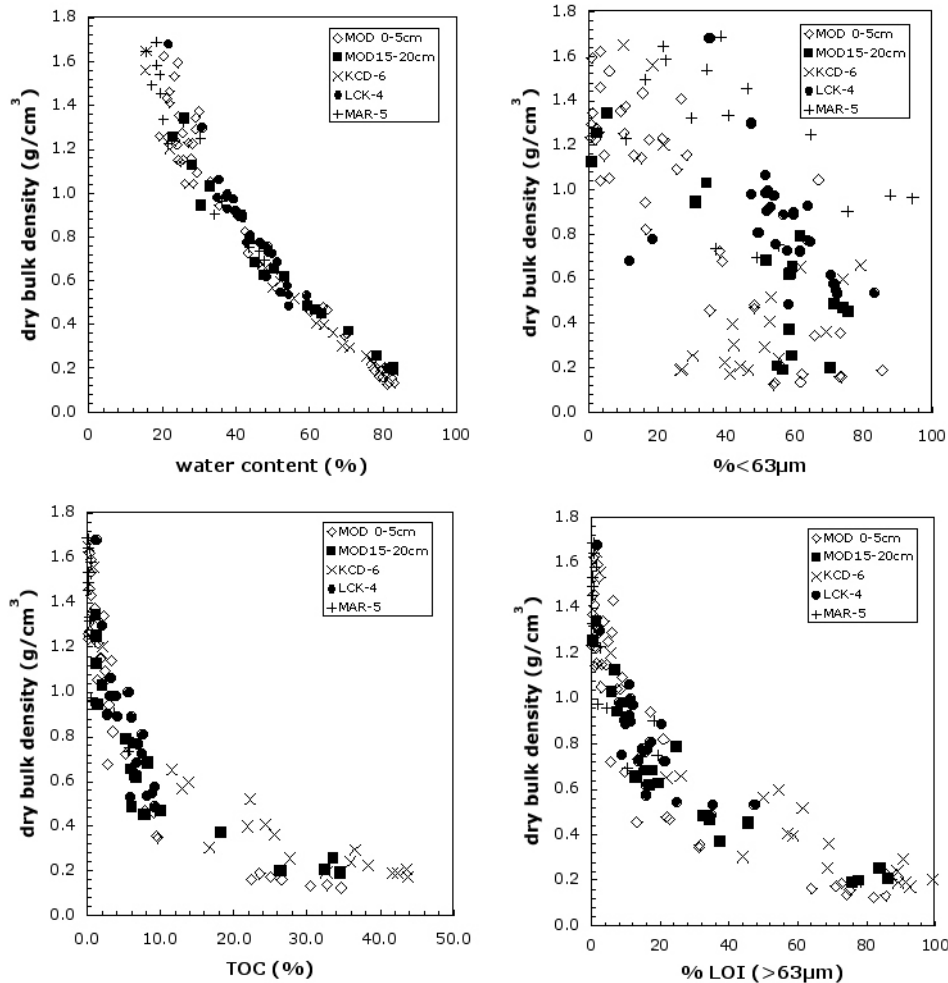


Figure 2 Relationships between DBD, $F_{<63\mu\text{m}}$, TOC, and $\text{LOI}_{>63\mu\text{m}}$ for all samples analyzed in this study

The composition of the Holocene sequence of mangrove peat and shelly marine clay in core MAR-5 is markedly different from the underlying soil profile (Figure 4). The grain size distribution of the underlying soil was dominated by fractions $>63\ \mu\text{m}$, with $F_{<63\mu\text{m}}$ being $<50\%$ in all cases. In the underlying soil, DBD was uniformly very high ($>1.5\ \text{g/cm}^3$), water contents were $<20\%$, and organic matter was present only in very small amounts. In contrast, the mangrove peat was generally composed of sediments containing $>50\%$ $F_{<63\mu\text{m}}$ material with DBD ranging from 0.6 to $1.0\ \text{g/cm}^3$ and high organic matter content (10–20% $\text{LOI}_{>63\mu\text{m}}$ and 2–8% TOC). The shelly marine clay overlying the peat was dominated by $F_{<63\mu\text{m}}$, increasing rapidly towards the top of the section to values in excess of 90%. DBD ranged from ~ 1.0 to $1.5\ \text{g/cm}^3$ and both TOC and $\text{LOI}_{>63\mu\text{m}}$ comprised $<1\%$ of the material.

As with MAR-5, the soil underlying the Holocene sequence in KCD-6 is characterized by high DBD and, in this case, is dominated by sand-sized material with low TOC (Figure 5). The overlying interbedded sandy muds contain comparatively little organic carbon and high $F_{<63\mu\text{m}}$ ($>50\%$), with DBD values of $\sim 0.6\ \text{g/cm}^3$. Above this unit, TOC and $\text{LOI}_{>63\mu\text{m}}$ increase to about +2.0 m and then remain

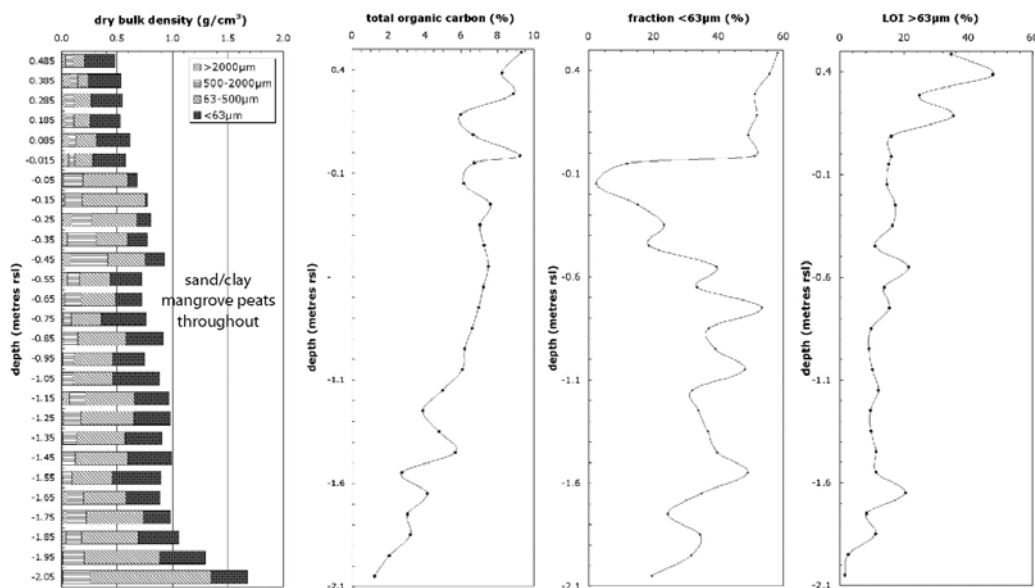


Figure 3 Contributions of different size fractions to the observed bulk density of LCK-4. Also shown are variations in $F_{<63\mu\text{m}}$, TOC, and $\text{LOI}_{>63\mu\text{m}}$ through the sequence.

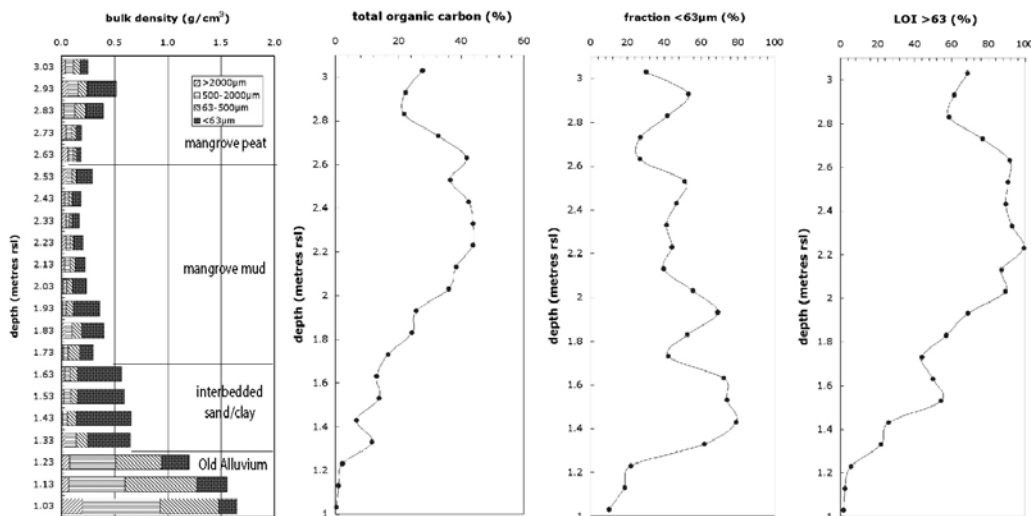


Figure 4 Contributions of different size fractions to the observed bulk density of MAR-5. Also shown are variations in $F_{<63\mu\text{m}}$, TOC, and $\text{LOI}_{>63\mu\text{m}}$ through the sequence.

approximately constant at 30–40% and 80–90%, respectively, decreasing slightly in the uppermost 30 cm of the section. DBD values are $<0.4 \text{ g/cm}^3$ throughout this interval except in the upper 30 cm, reflecting the very organic-rich nature of the sediments.

The ^{14}C dates obtained from all 3 sediment sequences are shown in Table 1, and range from 1880 to 7650 BP, indicating that these sequences were deposited through the Holocene, following sea-level rise after the Last Glacial Maximum (Hesp et al. 1998).

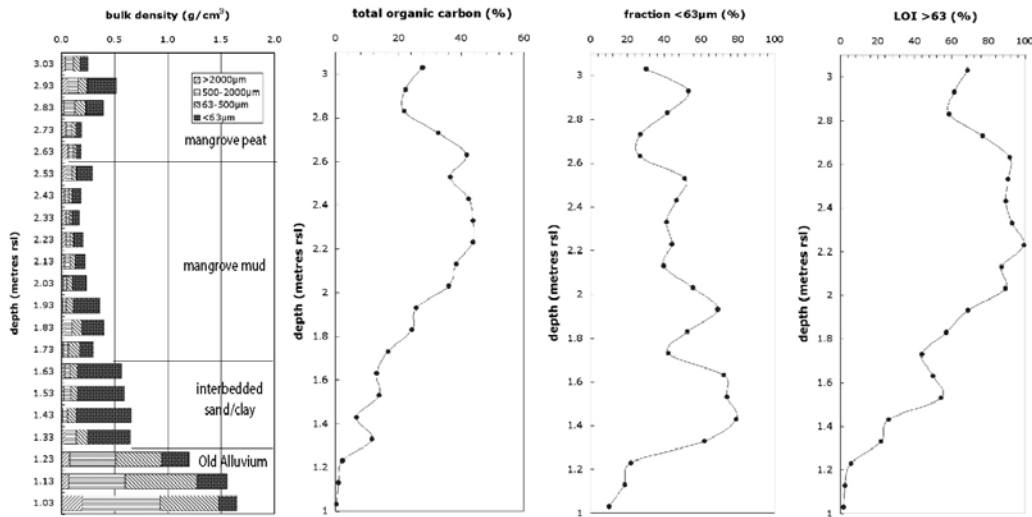


Figure 5 Contributions of different size fractions to the observed bulk density of LCK-6. Also shown are variations in $F_{<63\mu\text{m}}$, TOC, and $\text{LOI}_{>63\mu\text{m}}$ through the sequence.

Table 1 ^{14}C dates for sedimentary sequences analyzed in this study. All samples were woody material and have been corrected for fractionation using an assumed $\delta^{13}\text{C}$ value of -25% . Calibration from ^{14}C yr (yr BP) to calendar yr (cal BP) was achieved using the Calib 4.4 dataset (Stuiver et al. 1998). Only the calibrated date with the highest probability is shown.

	m (rsl)	yr BP	cal BP
KCD-6			
ANU-11808	+2.63	4470 ± 120	5300–4970
ANU-11807	+1.63	5270 ± 170	6210–5890
ANU-11806	+1.33	6300 ± 80	7315–7160
LCK-4			
ANUA-22221	-0.01	2400 ± 190	2740–2310
ANUA-25705	-0.35	1880 ± 190	2000–1570
ANUA-22223	-2.04	7090 ± 190	8040–7715
MAR-5			
ANU-11841	-6.97	7530 ± 80	8390–8315
ANU-11840	-7.42	7650 ± 100	8540–8360

DISCUSSION

Figure 6 shows the relationship between DBD, $F_{<63\mu\text{m}}$, and TOC for modern sediments (0–5 cm), while Figure 7 shows the relationship between DBD, $F_{<63\mu\text{m}}$, and $\text{LOI}_{>63\mu\text{m}}$ for modern sediment. These figures show that the DBD of the modern intertidal sediments can be predicted by a knowledge of $F_{<63\mu\text{m}}$ and either TOC or $\text{LOI}_{>63\mu\text{m}}$ using the following equations:

$$\ln(\text{DBD}) = 0.316 + \{[(0.0032 \times (F_{<63\mu\text{m}})) \times \ln(F_{<63\mu\text{m}})] + \{[(0.0665 \times (\text{TOC}))^{0.5} \times \ln(\text{TOC})]\} r^2=0.94 \quad (1)$$

$$\ln(\text{DBD}) = 0.399 + [0.0145 \times (F_{<63\mu\text{m}})] + [0.0142 \times (\text{LOI}_{>63\mu\text{m}})] r^2=0.91 \quad (2)$$

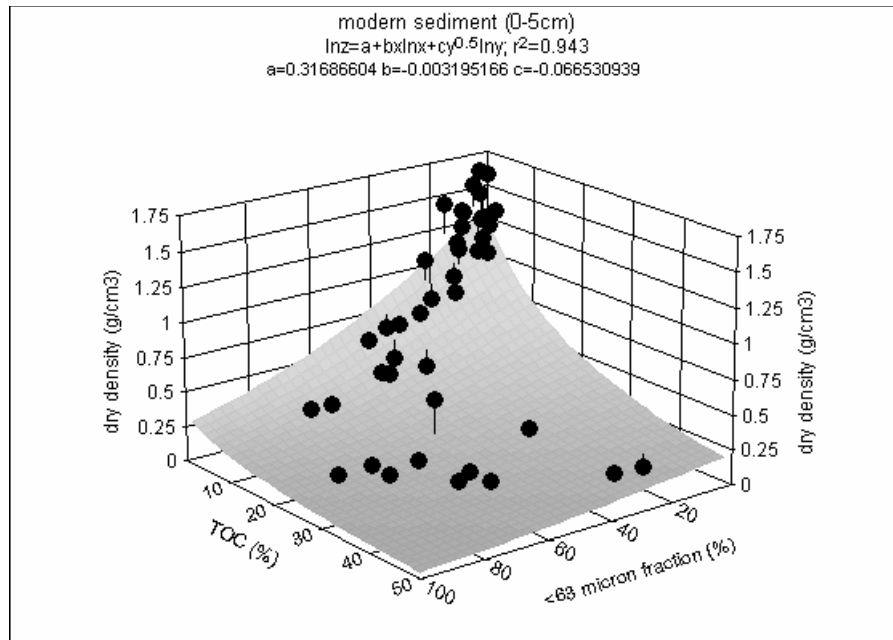


Figure 6 Relationship between DBD, $F_{<63\mu\text{m}}$, and TOC for modern (0–5 cm) mangrove sediments in Singapore

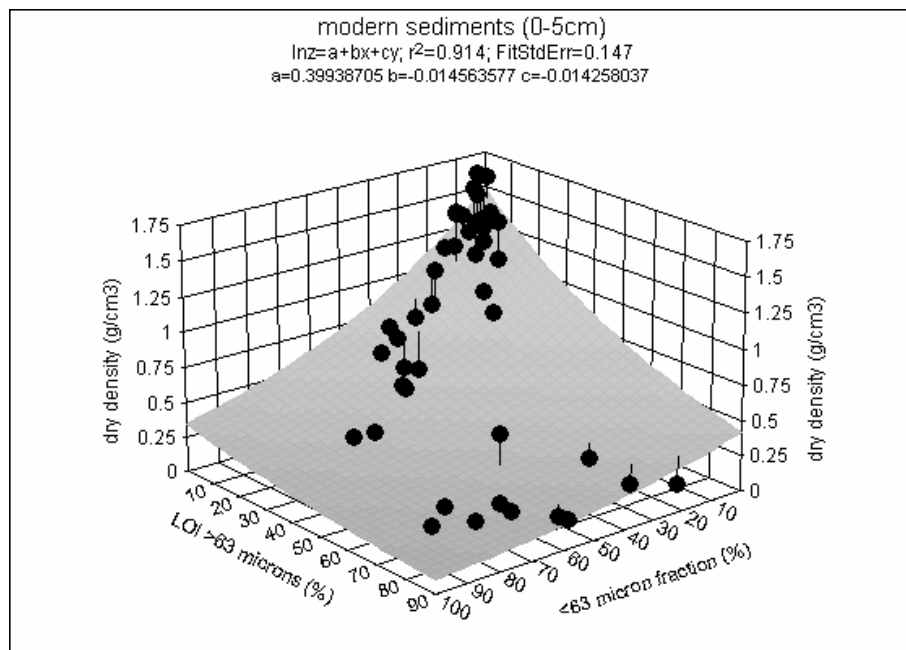


Figure 7 Relationship between DBD, $F_{<63\mu\text{m}}$, and $\text{LOI}_{>63\mu\text{m}}$ for modern (0–5 cm) mangrove sediments in Singapore

The fit of both these equations is good, suggesting that the initial “uncompacted” dry bulk density (DBD_i) of any sediment interval in a sedimentary sequence can be calculated from a knowledge of the other parameters, all of which can be measured directly. The 2 equations above provide 2 quasi-independent estimates of DBD_i , and, therefore, the average value is used in subsequent calculations.

From comparison of average calculated DBD_i with the measured dry bulk density of the sample (DBD_f), the initial vertical length (L_i) of uncompact sediment of DBD_i required to yield a 1-cm vertical interval of compacted sediment of DBD_f can be calculated via the following equation:

$$L_i = 1 + [(DBD_f - DBD_i)/DBD_f] \quad (3)$$

Application of this relation to 10-cm intervals along the sedimentary sequence allows determination of the cumulative compaction below any point in the sequence, and, hence, of the *maximum* amount of lowering that could have been experienced by a sample in the sequence due to compaction of the sediments below it. Due to uncertainties in the sampling and analysis, this equation can yield values less than 1 (apparent expansion). Since expansion under an imposed sediment load is unlikely and an estimate of maximum compaction is required, negative values for the apparent change in length are set to zero.

The percent compaction of each 10-cm interval in the 3 sampled sedimentary sequences is shown in Figures 8, 9, and 10. Also shown are the calibrated ^{14}C ages for each core and the calculated maximum amount of lowering that could have been experienced by each ^{14}C -dated sample. TOC and DBD measurements for these cores allow the calculation of carbon sequestration rates, while the “decompaction” of the cores allows the calculation of maximum rates of sediment accumulation.

Table 2 shows that the average amount of maximum compaction experienced by the sedimentary sequences analyzed in this study ranges from 17 to 55%. While the “true” rate of sediment accretion can only be said to lie between the observed and “decompact” values, the results do suggest that autocompaction is likely to have a significant impact on sediment accretion rate calculations, even over comparatively narrow intervals, in sediments buried to even shallow depths.

Table 2 Accretion rates calculated assuming rapid compaction (uncorrected accretion rate) and slow compaction (decompact accretion rate) as described in the text. The probable accretion rate can be reported as the average of these 2 values \pm half the difference between them. Also shown is the average maximum compaction for the intervals over which the accretion rates were calculated, and the depths over which these were calculated are given in Figures 8–10. The carbon sequestration rate was calculated from TOC and DBD_f values.

Core/sediment type	Uncorrected accretion rate (mm/yr)	Decompacted accretion rate (mm/yr)	Maximum compaction (%)	TOC accumulation (t/ha/yr)
LCK-4, mangrove mud/peat	(0.31)	(0.38)	18	(0.16)
MAR-5, mangrove peat	4.73	6.84	31	1.7
KCD-6, mangrove mud	0.99	1.19	17	0.91
KCD-6, interbedded sand/clay	0.25	0.56	55	0.23

The uppermost sample ^{14}C dated in the mangrove unit in MAR-5 may have been lowered by up to 28 cm by compaction of the underlying 40 cm of mangrove peat (Figure 8). These sediments exhibit the most rapid accretion rate (4.73–6.84 mm/yr). Nevertheless, this rate is less than half the rate of sea-level rise between 8350 and 8450 cal BP (Hesp et al. 1998); hence, it is not surprising that the mangrove sequence was rapidly transgressed and buried by marine clay. The calculated maximum compactions for each interval are comparatively high (5–56%; Figure 8), consistent with the comparatively thick sequence (9 m) of marine clay and landfill material that overlie the sediments. Given that the mangrove peat is narrow and was deposited over a short time interval, it is likely that the “true” amount of compaction approaches the calculated maximum amount of compaction in this

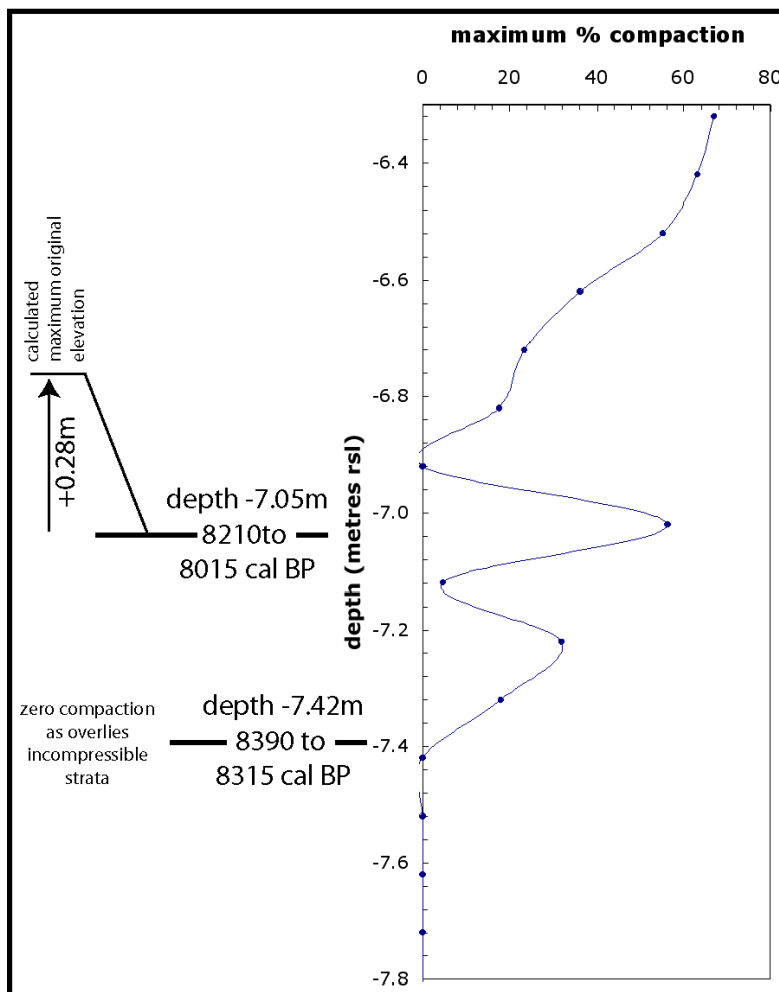


Figure 8 Percent compaction calculated for each 10-cm interval of MAR-5. Also shown is the effect of “decompacting” the sediments on the elevation of samples selected for ^{14}C dating. The lowermost sample is immediately above incompressible basement, and, hence, cannot be lowered by compaction. The approach used in this study yields an estimate of maximum compaction. Since the true amount of compaction is not known, the average of the values for “no compaction” and “maximum compaction” should be used for calculation of accretion rate, with the error given by half the difference between the 2 estimates.

case. Compaction of the interval of marine clay above the mangrove unit has also been significant, increasing from 0 to 67% as $F_{<63\mu\text{m}}$ increases from 11% to 94% of the total sediment. Carbon sequestration rates over the period during which the mangrove sequence was deposited averaged 1.7 t/ha/yr.

Accretion rates for 2 intervals can be calculated for KCD-6. The lowest transgressive unit, an interbedded unit of sand and clay, accumulated in the uppermost intertidal zone beyond the landward fringe of the mangroves at a comparatively low rate of 0.25–0.56 mm/yr. This sequence exhibits the highest amount of compaction, with the carbon-dated sample at the top of the unit having been lowered by up to 36 cm by compaction of the underlying 30 cm of sediment (Figure 9). Carbon sequestration during this interval between ~6000 and ~7200 cal BP was low (0.23 t/ha/yr), consistent with its depositional context.

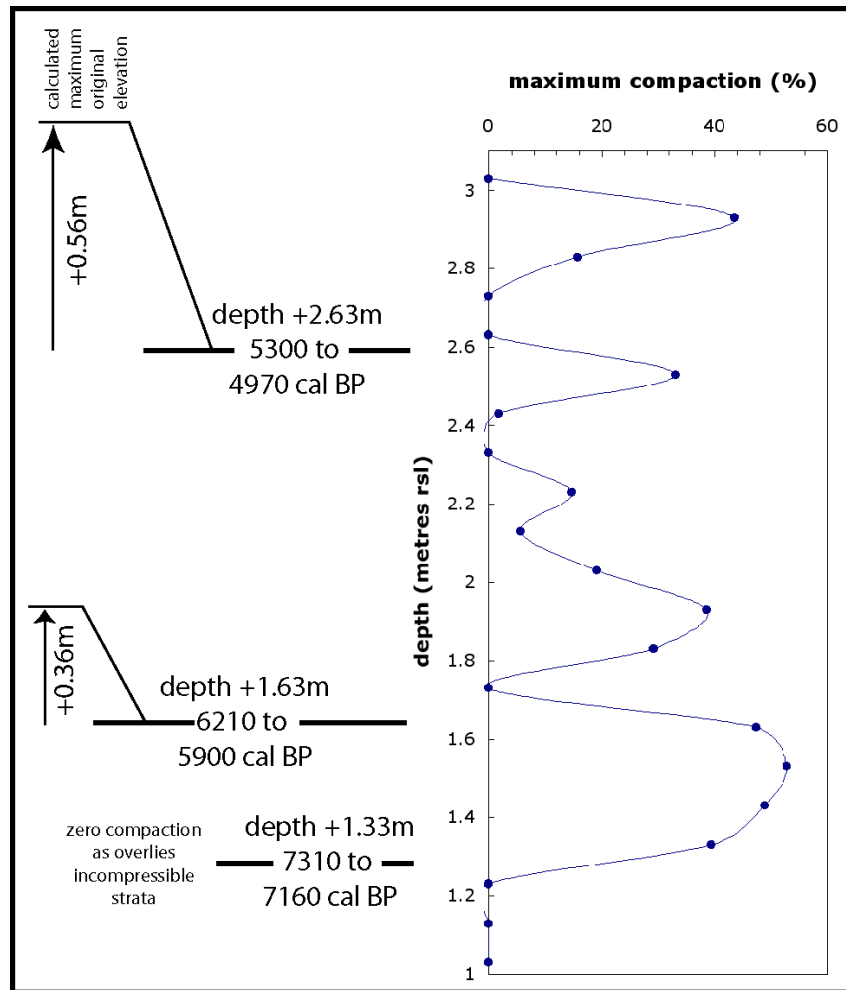


Figure 9 Percent compaction calculated for each 10-cm interval of KCD-6. Also shown is the effect of “decompacting” the sediments on the elevation of samples selected for ^{14}C dating. The lower-most sample is immediately above incompressible basement, and, hence, cannot be lowered by compaction (errors same as for Figure 8).

The elevation of the dated sample from the top of the mangrove mud unit in KCD-6 has been lowered by up to 56 cm through compaction of the underlying 1.3 m of sediment. Allowing for this compaction, the sequence of organic-rich mangrove muds accreted at rates of 0.99–1.19 mm/yr between ~5000 and ~6000 cal BP. The sea level during this period peaked at a mid-Holocene highstand of ~+2 to +3m and then began to decline slowly (Hesp et al. 1998), so the mangrove sediments were readily able to maintain their position by vertical accretion. During this period, the mangroves sequestered 0.91 t/ha/yr of carbon.

The uppermost dated sample in core LCK-4 has been lowered by up to 43 cm through compaction of the underlying 2 m of sediment (Figure 10), but the ^{14}C dates present several problems in interpretation. It is clear that the mangrove sediments began accumulating ~7850 cal BP, but the upper 2 dates in the sequence are reversed, and assuming either leads to very low sediment accretion rates

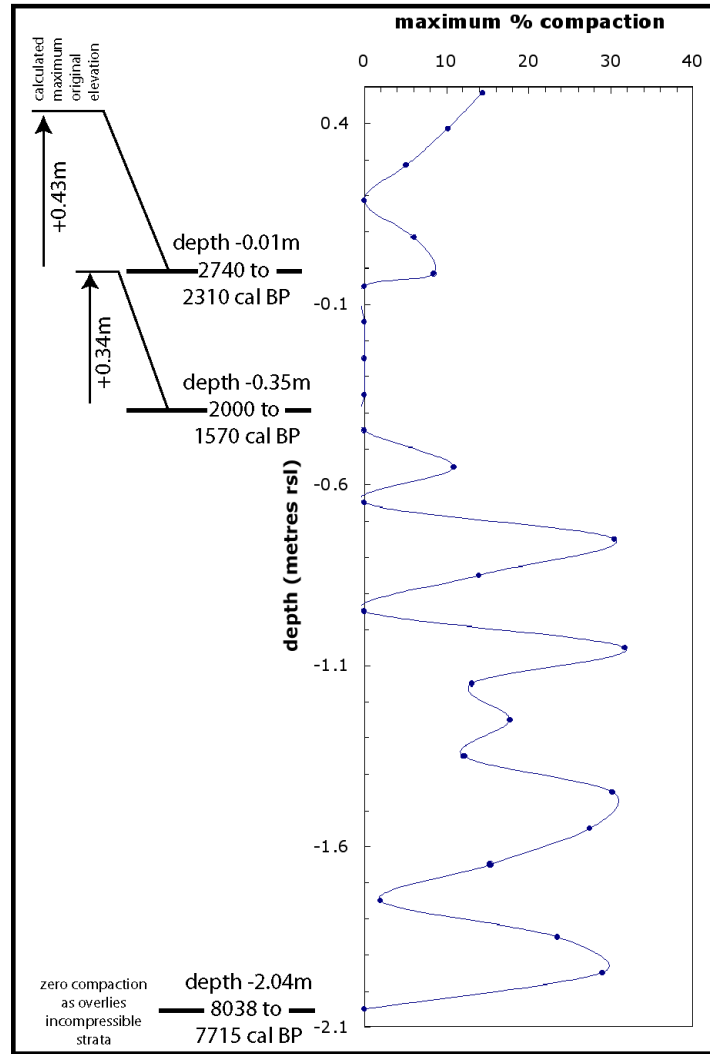


Figure 10 Percent compaction calculated for each 10-cm interval of LCK-4. Also shown is the effect of “decompacting” the sediments on the elevation of samples selected for ¹⁴C dating. The lowermost sample is immediately above incompressible basement, and, hence, cannot be lowered by compaction (errors same as for Figure 8).

(0.31–0.38 mm/yr) and very low carbon sequestration rates (0.17 t/ha/yr) for such an organic-rich mangrove peat. Three km west of LCK-4 at Sungei Buloh, a similar mangrove peat accreted at a rate of ~2.3 mm/yr between ~7250 and 7900 cal BP (Chua 2002). The peat at Sungei Buloh is truncated at the modern low tide mark by marine erosion and forms part of a wide shore platform. The same low-tide platform composed of truncated early Holocene mangrove sediments occurs immediately in front of the LCK-4 location. Thus, it seems likely that the increase in coarse sandy material above -0.45 m in the core marks an erosional surface, cut as the sea retreated from its mid-Holocene highstand (Hesp et al. 1998). A new series of mangrove sediments prograded over the erosional surface around ~2000 cal BP. Therefore, no sediment accretion rates or carbon sequestration rates can be calculated for this core. It is clear from the bulk density data that the lower portions of the sequence

have been compacted by up to 30%, while sediments currently above mean sea level have been compacted very little (<15%), consistent with burial depth being important in determining the degree of compaction.

Comparison between the mangrove sediments of MAR-5 and KCD-6 provides a consistent picture of accretion and carbon sequestration. The mangrove sediments in MAR-5 accumulated at a time when the sea level was rising rapidly and were subsequently buried under 9 m of sediment, while KCD-6 accumulated when sea-level change was slow and the sequence was not deeply buried. Hence, it is not surprising that the accretion rates, carbon sequestration rates, and degree of compaction calculated for the mangrove sediments of MAR-5 are all considerably higher than for KCD-6 (Table 2).

The accretion rates calculated for mangrove units in MAR-5 and KCD-6 (total range=0.99 to 6.84 mm/yr) compare favorably with values calculated for other mangrove areas. Ellison (1998) has compiled a summary of short-term sediment accumulation rates in 9 modern mangrove sediments and found a total range from 0.6–10.0 mm/yr. In contrast, long-term sediment accretion rates based on carbon dating of Holocene mangrove sequences have yielded a smaller range of values between 0.7 and 1.8 mm/yr (Woodroffe 1981; Ellison 1989; Ellison and Stoddart 1991; Ellison 1993), but none of these authors considered the effects of autocompaction in their studies, and, hence, the published Holocene rates may be biased towards lower values.

Likewise, the carbon sequestration rates calculated for the mangrove units of MAR-5 and KCD-6 (1.70 and 0.91 t/ha/yr, respectively) compare favorably with the rates calculated on centennial to millennial timescales for mangroves in the Asia-Pacific region which range between 0.14 and 2.98 t/ha/yr (Fujimoto 2000).

CONCLUSIONS

This study has demonstrated that there are predictable empirical relationships between the dry bulk density of a modern surface sample and its organic matter content and particle size distribution. Thus, for a sample buried in a sedimentary sequence, the measured dry bulk density of the sample can be compared with an estimate of the initial bulk density derived from the physical characteristics of the sample (grain size distribution and organic carbon content) in order to obtain an estimate of the maximum amount of autocompaction experienced by the sample. Using this approach, it has been demonstrated that significant autocompaction can occur even when a sediment interval has been subjected to a load equivalent to <2 m of overlying sediments. Inorganic sands appear less susceptible to autocompaction than organic-rich and/or fine-grained sediment.

The average maximum compactions for 3 mangrove sediment sequences ranged from 17–55%, indicating that significant subsidence of samples selected for ¹⁴C dating from within compressible intertidal sedimentary sequences can occur even when the thickness of compressible sediment beneath the sample is <1 m. The approach is likely to be most useful when the total thickness of the sediment pile is comparatively small (generally less than a few meters, depending on sediment characteristics), and in this study yielded rates of sediment accretion and carbon sequestration within the range observed for mangroves sediments elsewhere.

The advantage of the approach used in this study is that it is based on readily quantifiable physical characteristics of the sediment, but its drawback is that it provides only a maximum estimate of autocompaction. Combining this approach, however, with a time-dependent modeling approach, such as

employed by Allen (2000), should yield better estimates of the magnitude of autocompaction than either approach used in isolation.

ACKNOWLEDGEMENTS

This work was supported by a grant RP19/01 from the Academic Research Fund of the National Institute of Education, Nanyang Technological University. The authors would like to acknowledge N Shirlaw, N Osbourne, and H Rosser of the Land Transport Authority of Singapore, and J Lai of the National Parks Board for facilitating access to the sites sampled for this study. L Vellen assisted with AMS target preparation.

REFERENCES

- Allen JRL. 2000. Holocene coastal lowlands: autocompaction and the uncertain ground. In: Pye K, Allen JRL, editors. Coastal and estuarine environments: sedimentology, geomorphology and geoarchaeology. *Geological Society Special Publication* 175:239–52.
- Alongi D, Tirendi F, Dixon P, Trott LA, Brunskill GJ. 1999. Mineralization of organic matter in intertidal sediments of a tropical semi-enclosed delta. *Estuarine Coastal and Shelf Science* 48:451–67.
- Alongi D, Tirendi F, Clough BF. 2000. Below-ground decomposition of organic matter in forests of the mangroves, *Rhizophora stylosa* and *Avicennia marina*, along the arid coast of Western Australia. *Aquatic Botany* 68:97–122.
- Alongi D, Wattayakorn G, Pfitzner J, Tirendi F, Zagorskis I, Brunskill GJ, Davidson A, Clough BF. 2001. Organic carbon accumulation and metabolic pathways in sediments of mangrove forests in southern Thailand. *Marine Geology* 179:85–103.
- Blasco F, Saenger P, Janodet E. 1996. Mangroves as indicators of coastal change. *Catena* 27:167–78.
- Chua CW. 2003. *Environmental History of the Sungei Buloh-Kranji Mangrove coast*. [BA honors thesis]. Singapore: Nanyang Technological University.
- Ellison JC. 1989. Pollen analysis of mangrove sediments as a sea-level indicator. *Palaeogeography, Palaeoclimatology and Palaeoecology* 74:327–41.
- Ellison JC. 1993. Mangrove retreat with rising sea-level, Bermuda. *Estuarine, Coastal and Shelf Science* 37:75–87.
- Ellison JC. 1998. Impacts of sediment burial on mangroves. *Marine Pollution Bulletin* 37:420–6.
- Ellison JC, Stoddart DR. 1991. Mangrove ecosystem collapse with predicted sea-level rise: Holocene analogues and implications. *Journal of Coastal Research* 7:151–65.
- Fujimoto K. 2000. Below-ground carbon sequestration of mangrove forests in the Asia-Pacific region. *International Workshop Asia-Pacific Cooperation on Research for Conservation of Mangroves*. 26–30 March 2000, Okinawa, Japan.
- Hesp PA, Chang CH, Hilton M, Ming CL, Turner IM. 1998. A first tentative Holocene sea-level curve for Singapore. *Journal of Coastal Research* 14:308–14.
- Pirazzoli PA. 1996. *Sea-Level Changes. The Last 20,000 Years*. Chichester: John Wiley.
- Stanley DJ, Hait AK. 2000. Deltas, radiocarbon dating, and measurements of sediment storage and subsidence. *Geology* 28:295–8.
- Stuiver M, Reimer PJ, Braziunas TF. 1998. High-precision radiocarbon age calibration for terrestrial and marine samples. *Radiocarbon* 40(3):1127–51. (Data available at <http://www.calib.org/>).
- Woodroffe CD. 1981. Mangrove swamp stratigraphy and Holocene transgression, Grand Cayman Island, West Indies. *Marine Geology* 41:271–94.

PRELIMINARY ^{14}C DATES ON BULK SOIL ORGANIC MATTER FROM THE BLACK CREEK MEGAFUNA Fossil SITE, ROCKY RIVER, KANGAROO ISLAND, SOUTH AUSTRALIA

Matt Forbes^{1,2} • Erick Bestland¹ • Rod Wells³

ABSTRACT. Radiocarbon age determinations and stratigraphy suggest that the deposits in Black Creek Swamp on Kangaroo Island record 3 phases of deposition and associated soil development which spanned at least the last 20,000 yr. Four new ^{14}C age determinations on bulk soil organic matter and their stratigraphic context are presented in this paper. Three of these age determinations (FP6: $15,687 \pm 110$ BP [WK11487]; FP7: $16,326 \pm 385$ BP [WK11488]; and FP8: $17,618 \pm 447$ BP [WK11489]), are from the organic-rich fossil layer located 45–75 cm below the current floodplain surface. The fourth, a much younger date, FP5: 5589 ± 259 BP (WK11486), was obtained from the base of the overlying modern soil. The dates for the fossil layer increase systematically with depth and correlate well with 5 previous ^{14}C dates (Hope et al., unpublished), ranging between $15,040 \pm 120$ BP and $19,000 \pm 310$ BP. This suggests that the data set represents a possible minimum age of the bulk organic matter, and considering the high organic matter contents of approximately 8%, has implications for the age of the megafauna buried in this layer. The overlying modern soil, with its much younger date, contains lower levels of organic matter (3–7%) and gastropods not seen in the fossil layer. This suggests a substantial change in environmental conditions probably due to an alteration in the floodplain drainage conditions. This chronological and sedimentological discontinuity indicates that 2 distinct depositional regimes existed and were separated by up to 10,000 ^{14}C yr. A calcareous, sandy silt deposit underlying the fossil layer is a calcarenite deposit with low total organic content and is considered the base of the section; it suggests a third separate depositional episode. As such, the Black Creek Swamp in the southwest corner of Kangaroo Island formed intermittently over at least the last 20,000 yr during 3 distinct depositional phases, one of which was the formation of the fossil-laden, organic-rich floodplain surface, which has a possible minimum age of approximately 15,000 to 19,000 BP.

INTRODUCTION

The Black Creek Swamp, located in the Rocky River catchment in the southwest region of Kangaroo Island South Australia (Figure 1), has had intermittent geological (Tindale et al. 1935; Hope et al., unpublished; Tyler et al. 1979), paleontological (Tindale et al. 1935; Hope et al., unpublished), archaeological (Tyler et al. 1979), and paleoenvironmental (Gröcke 1996, 1998) research over the last 90 yr. The Black Creek Swamp is nestled between the calcareous dune ridges of the west and south coasts and the laterite plateau that comprises the northern two-thirds of Kangaroo Island (Figure 1). It is a unique deposit because it contains a significant, dense, and well-preserved megafauna fossil deposit (including *Diprotodon*, *Zygamaturus*, and *Sthenurus*). Chaplin (1972) has showed that highly alkaline conditions, similar to those in the Black Creek Swamp, contribute to the high level of bone preservation.

A description of the stratigraphy of Black Creek Swamp by Tindale et al. (1935) included 4 sedimentary horizons (from top to bottom: A, B, C, and D): a brown earth (A, 0–10 cm) and a reddish-colored swamp earth (B, 10–30 cm), followed by the fossil-bearing black swamp earth (C, 30–60 cm). Underlying these deposits and representing the base of the swamp was a greyish calcareous sand (layer D), consisting of worn marine shells, foraminifera, freshwater shell fragments (*America pyramidatus*, *Sphaerium sp.*), and salt-lake-frequenting *Coxiella sp.* The varied suite of shells in this basal layer indicated a sediment accumulation well below water, most likely under estuarine conditions (Tindale et al. 1935). Importantly, 2 key erosional boundaries were

¹School of Chemistry, Physics and Earth Sciences, Flinders University, GPO Box 2100 Adelaide, South Australia 5001, Australia.

²Corresponding author. Email: mattforbes@lycos.com.

³School of Biological Sciences, Flinders University, GPO Box 2100 Adelaide, South Australia 5001, Australia.

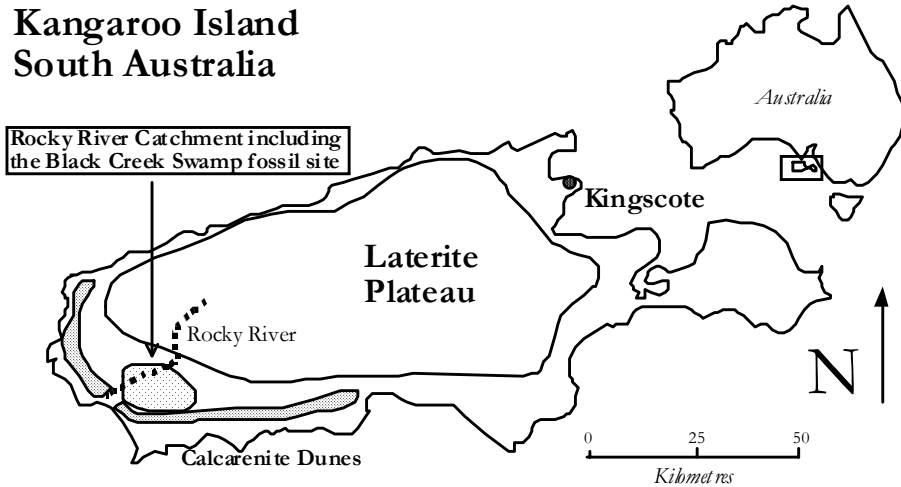


Figure 1 Location map of the Black Creek Swamp in the Flinders Chase National Park, Kangaroo Island, South Australia.

identified in the stratigraphic section. A marked change in coloration was seen between layers B and C. Also noted was the existence of boulders and cobbles of hardened calcrete crust at the top of layer D, consolidated during a period of sub-aerial denudation and kunkarization. Tindale et al. (1935) tentatively suggested a Pleistocene age for the deposit based on a geomorphological comparison of the Rocky River site with the Pleistocene coastal limestone hills located on the island.

Research by Hope et al. (unpublished) recognized layers A, B, and C; however, they divided the calcareous layer D into 2 separate horizons consisting of a grey silt sand overlying a light grey calcareous marl which graded into decomposed calcarenite. Five dates, which span $15,040 \pm 120$ BP and $19,000 \pm 310$ BP, were obtained for layer C (the fossil horizon), both from the excavation pit itself and a sediment core taken nearby for pollen analysis. An age of 1960 ± 120 BP (ANU 2170) for the overlying layer B, obtained by Hope et al. (unpublished), further supported an early Holocene depositional hiatus in the stratigraphic section, as suggested by Tindale et al. (1935). Another radiocarbon date of 4260 ± 90 BP was obtained for the organic material extracted from the calcarenite layer (layer D), which is stratigraphically the oldest of the units. This anomalous ^{14}C age was primarily attributed to carbon contamination from humates in groundwater.

Recent age determinations of the site using other methods, such as Optical Stimulated Luminescence (OSL), are proving to be problematic due to the high uranium content of the deposit. This amounts to 10 parts per million (ppm) for groundwater sampled from the site (Gill 1996), as well as 37.9 ppm (FP6) and 21.7 ppm (FP8) obtained from recent X-ray fluorescence analysis for bulk soil samples taken from the fossil pit (this study). An attempt to obtain ^{14}C dates from collagen extracted from the fossil material has also proved to be difficult due to the minimal amounts of dateable material preserved in the excavated bones. Hence, the ^{14}C dating of bulk soil organic matter (SOM) is a first step in determining the approximate age of the site. More detailed age determinations currently being undertaken are aimed at placing the geomorphological, paleoenvironmental, and paleontological interpretations to be put into a chronological context and will allow for a comparison to other late Pleistocene megafauna sites and paleoenvironmental databases.

METHODS

A stratigraphic profile was constructed from a section located in the southwestern corner of the 4 × 4-m 2003 fossil excavation pit (FP). A 120-cm vertical trench was excavated in order to obtain fresh samples. These were described in cm scale using standard geological techniques to estimate grain size, texture, mineralogy, and color, following methods described by Retallack (1988), while color codes follow Munsell (1994). Inspection of numerous samples in each horizon was undertaken in order to determine the representative features. Twelve samples (FP1 to FP12) were taken for geochemical analysis at 10-cm intervals.

Four of these samples (FP5, FP6, FP7, and FP8) were hand-sieved to remove root material, bone and shell fragments, with the portion ≤1 mm in diameter being retained and milled to a fine powder. These samples were forwarded to the Radiocarbon Laboratory at the University of Waikato in Hamilton, New Zealand for dating. Physical pretreatment at the Waikato laboratory involved removal of any visible contaminants (roots and stones). This was followed by a chemical pretreatment involving an initial acid wash using 10% concentrated HCl (to remove carbonates), followed by a DI rinse. Samples were then washed in hot 0.5% NaOH solution (to remove humic acids), then again washed in 10% concentrated HCl, rinsed and dried. From this, the base soluble fraction was selected for ¹⁴C age determination (Alan Hogg, personal communication, 2003).

¹⁴C age determinations in this paper (Table 1) follow Godwin (1962), Stuiver and Polach (1977), and Gillespie (1986). They are based on the Libby half-life of ¹⁴C (5568 yr), the assumption of constancy of ¹⁴C atmospheric concentrations during the past, and the use of oxalic acid (direct or indirect) as the modern ¹⁴C standard. Isotopic fractionation normalization of all sample activities to the base of δ¹³C = -25‰ (relative to the ¹³C/¹²C ratio of PDB) is assumed. Finally, BP ages are presented with the year 1950 automatically designated as the base year (i.e. present is AD 1950). Dates are given ±1 standard deviation (±1 σ) due to counting statistics multiplied by an experimentally determined laboratory error multiplier of 1.217 (Alan Hogg, personal communication, 2003).

Table 1 δ¹⁴C‰, δ¹³C‰, Δ¹⁴C‰, and % modern carbon (pMC) for the 4 ¹⁴C dates WK11486 (FP5), WK11487 (FP6), WK11488 (FP7), and WK11489 (FP8) provided by the University of Waikato, Radiocarbon Dating Laboratory, Hamilton, New Zealand. Note: WK numbers are catalog numbers provided by the University of Waikato Radiocarbon Dating Laboratory.

Sample	Depth	δ ¹⁴ C‰	δ ¹³ C‰	Δ ¹⁴ C‰	pMC	Result
FP 5	40 cm	-504.6 ± -12.9	-28.3 ± -0.2	-501.3 ± -15.8	49.9 ± -1.6	5589 ± -259 BP
FP 6	50 cm	-858.6 ± -0.2	-26.8 ± -0.2	-858.1 ± -1.9	14.2 ± -0.2	15,687 ± -110 BP
FP 7	60 cm	-870.8 ± -5.0	-32.0 ± -0.2	-869.0 ± -6.1	13.1 ± -0.6	16,326 ± -385 BP
FP 8	70 cm	-889.7 ± -4.9	-30.7 ± -0.2	-888.4 ± -6.0	11.2 ± -0.6	17,618 ± -447 BP

RESULTS

The 4 main units initially identified by Tindale et al. (1935) and expanded on by Hope et al. (unpublished) are further described (Figure 2). The modern soil horizon grades from a 10YR brown to a 10YR 4/2 dark greyish brown through approximately the top 40 cm of the profile. It is moderately calcareous with a PH_w of 8.57 and contains a substantial modern root system, charcoal fragments, and sub-rounded quartz grains of sand and silt. A visual non-quantitative inspection of mega-scopic charcoal content indicates that it increases down-profile to 40 cm. Total organic carbon (TOC) content varies between 7% at the top, decreasing down to 3% at the base of the horizon. These values were derived from the non-calcareous residual portion of the sample retained after 1M hydrochloric

acid treatment at 85 °C for 45 min. Of particular note is the presence of the gastropod species *Hydrococcus brazieri* in the top 40 cm of the profile (layers A, B) of the profile (John Cann, personal communication, 2003). This small species has a wide temperature and salinity tolerance and prefers marginal salt lakes, back dune swamps, estuaries, and tidal flats (Ludbrook and Gowlett-Holmes 1989).

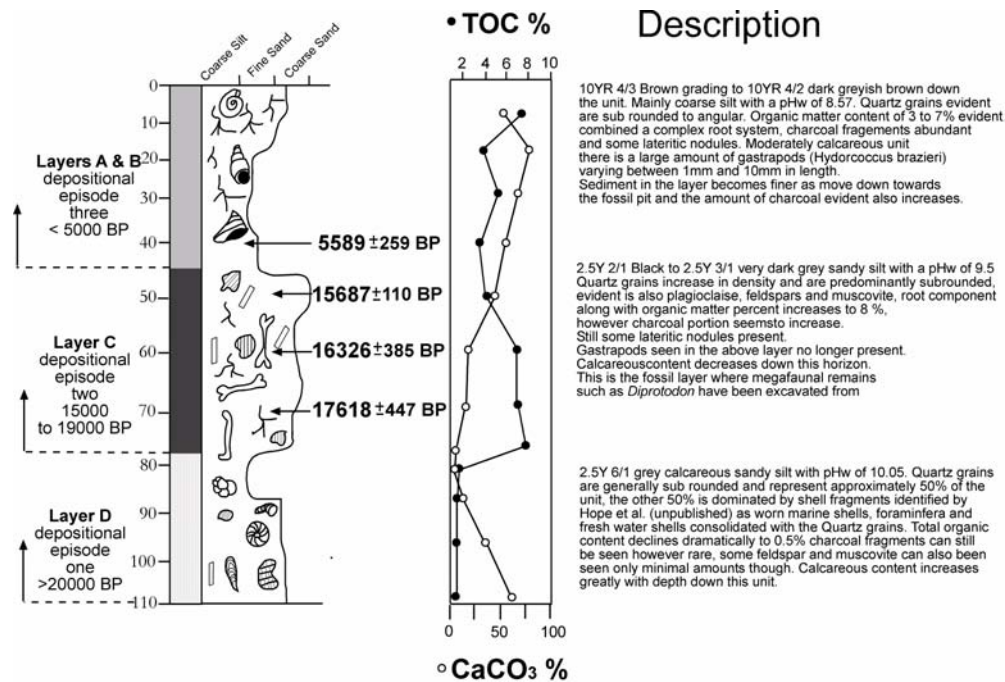


Figure 2 Stratigraphical reconstruction of the Black Creek Swamp fossil excavation pit. Included are pH_w values, ^{14}C dates, and TOC data provided with $\delta^{13}\text{C}$ values from the Rafter Isotope Lab, Lower Hutt, New Zealand.

A distinct yet gradational boundary between this unit and the underlying 2.5Y 2/1 black to 2.5Y 3/1 very dark grey, silty organic-rich fossil layer is evident between 30 and 40 cm. Below this boundary, there is a total lack of megascopic gastropods, suggesting a different depositional regime. The fossil layer, which extends down to 70–75 cm, has a pH_w of 9.5 and a TOC of between 6 and 8% for the HCl-treated residual portion of the samples. The percentage of quartz grains in this unit is greater than in the overlying modern soil and there are minor occurrences of feldspars and muscovite. The quantity of modern root material decreases significantly down-profile, while macroscopic charcoal content increases and the calcareous content decreases. A distinct boundary is evident between the dark fossil horizon (layer C) and the underlying 2.5Y 6/1 grey calcareous silt and sand (layer D) identified by Tindale et al. (1935). It is recognized by the existence of boulders and cobbles of hardened calcrete crust, clearly visible in the fossil pit stratigraphy. Quartz grains are sub-rounded and represent approximately 40% of the horizon decreasing in abundance with depth and corresponding with an increase in the percentage of shell fragments. The latter include worn and rounded marine shell fragments, freshwater shells, and foraminifera of likely calcarenite aeolian origin. Both the calcareous component and the pH_w (10.05) of the unit corresponding to increasing shell fragment content. Macroscopic charcoal is almost non-existent in this unit and TOC on the residual sample decreases to 0.5%. There is also a small percentage (1–2%) of feldspars and muscovite. The distinct variations between this layer and the overlying organic-rich soil (layer C) infer the existence of 2 separate depositional modes: the first being aeolian deposition of calcarenite grains and the second being a floodplain, organic-rich soil.

Table 1 presents the $\delta^{14}\text{C}\text{‰}$, $\delta^{13}\text{C}\text{‰}$, $\Delta^{14}\text{C}\text{‰}$, and pMC for the 4 dates obtained from the Waikato Laboratory in New Zealand. Three of the dates (FP6, FP7, and FP8) were taken at 10-cm intervals from the 2.5Y 2/1 black peat-like horizon at depths from the top datum of 50, 60, and 70 cm, respectively (Figure 2). The fourth date was obtained at the base of the overlying 10YR 4/2 dark greyish brown silt at a depth of 40 cm (sample FP5).

DISCUSSION

¹⁴C dating of organic matter soils, sediment, and their individual components is not a routine procedure. This is due largely to difficulties in determining the origin of the carbon in these materials (Gillespie 1986). Although treated to remove sources of modern carbon (plant rootlets, humic acids, and carbonates), some level of contamination of the ¹⁴C sample will occur. This becomes a problem for samples older than 20,000 yr, due to the small amounts of original ¹⁴C carbon that remain (Roberts et al. 1994; Fauve 1986; Gillespie 1986). However, for samples younger than 20,000 yr in age, it is still necessary to have an independent check of the dates obtained.

Radiocarbon (¹⁴C) dating has been used in conjunction with other dating methods, such as uranium-thorium (U/Th), thermoluminescence (TL), electron spin resonance (ESR), and more recently, optical stimulated luminescence (OSL). ¹⁴C dates have been compared to these methods at many archaeological sites in Australia with varying degrees of success (Turney et al. 2001; Gillespie 2002; Bowler et al. 2003; Stone and Cupper 2003). Cave sediments in Western Australia's Devil's Lair produced strong correlation between ¹⁴C dates of charcoal, and OSL and ESR ages for sediments (Turney et al. 2001). This was consistent for ages up to approximately 30 ka BP; however, older dates obtained produced differences of up to 10,000 yr between the various techniques. At Lake Mungo in western New South Wales, site of Australia's oldest human remains, both comparative and non-comparative results are informative (Bowler et al. 2003). Good correlation existed between ¹⁴C dates of charcoal and TL dates of sediment spanning the Lake Mungo geomagnetic excursion (Barbetti and McElhinny 1972; Huxtable and Aitken 1977; Bell 1994). However, ¹⁴C estimates for the Mungo I cremation site are approximately 15 to 20 ka younger than those provided by OSL dating (Bowler et al. 2003). Another archaeological site at Kow Swamp was dated, giving ¹⁴C ages of 15–9 ka BP obtained from charcoal, shells, and bone apatite, and OSL dates of 22 and 19 Ka from the surrounding sediment (Stone and Cupper 2003). At both Lake Mungo and Kow Swamp, differences in ages were attributed primarily to contamination by younger carbon that had moved downward through the profile.

Investigations into the soil organic matter (SOM) grain size fractions have been undertaken to better appreciate the contribution of carbon fractions to ¹⁴C age determinations (Gillespie et al. 1992; Trumbore 1993; Bol et al. 1996; Leavitt et al. 1996; Paul et al. 1997). Acid hydrolysis, humus fractionation, density separation, and size separation are all examples of methods that have been employed to isolate and date certain components of SOM. In general, the residual or recalcitrant components retained after separation provided older ages than those obtained for bulk SOM. Lipid fractions (Bol et al. 1996), fine silt and coarse clay fractions (Anderson and Paul 1984), denser particle fractions (Trumbore et al. 1989), and fine-grained charcoal (Gillespie et al. 1992) are examples of SOM components that contain carbon older than the bulk SOM from which they were extracted. The method employed to extract this older carbon fraction from SOM varies with environment of deposition. Hence, it is important to identify the carbon components that exist in the SOM before an extraction processes is chosen. ¹³C nuclear magnetic resonance (NMR) spectra of bulk and treated SOM is one such method that can achieve this.

^{13}C NMR spectroscopy is a technique that can be used to characterize SOM (Baldock and Skjemstad 2000; Mathers et al. 2000; Quideau et al. 2000; Krull and Skjemstad 2002). This technique produces spectra that roughly divide SOM samples into chemical shift regions in which the chemistry of the C atoms within each region is similar. Examples of such shift regions are alkyl, o-alkyl, aromatic, methoxyl, and carbonyl C atoms. Hence, the application of ^{13}C NMR to the dated bulk SOM from the Black Creek Swamp will help to identify the SOM components present. This will allow for a better appreciation of in situ and contaminant carbon constituents in the sediment. As such, the extraction and dating of these in situ fractions will provide an age comparison to the most likely minimum ages provided by the bulk SOM dating process. This type of work is now in progress for the Black Creek Swamp SOM samples. Preliminary results indicate a substantial aromatic and lignin component, as well as an absence of any significant carbohydrate component (Jan Skjemstad and Evelyn Krull, personal communications, 2003). This suggests that the carbon of the organic-rich layer has not been contaminated extensively by more modern SOM, and that the ^{14}C age determinations are a reasonably accurate age estimation of the SOM accumulation in the fossil layer soil zone.

CONCLUSION

The ^{14}C dates presented in this paper give an approximate age of the bulk SOM contained within the organic-rich layer of the Black Creek Swamp excavation site at Rocky River, Kangaroo Island. The dates for FP6: $15,687 \pm 110$ BP (WK11487); FP7: $16,326 \pm 385$ BP (WK11488); and FP8: $17,618 \pm 447$ BP (WK11489) correlate with the time frame of 15,000 to 19,000 BP obtained by Hope et al. (unpublished). These dates also combined with a fourth, FP5: 5589 ± 259 BP (WK11486, base of Layer B), have been useful in placing the site's stratigraphy into a better chronological context. It seems clear that the Black Creek Swamp experienced 3 separate depositional periods that spanned at least the last 20,000 yr. The 3 dates (FP6, FP7, and FP8) obtained for the overlying organic-rich horizon (layer C) suggest a possible minimum age of between 15,000 and 18,000 BP for this unit. Thus, it can be assumed that the underlying calcareous, sandy silt layer D was most likely deposited prior to 20,000 BP. The ^{14}C age for the base of layer B constrains the horizons above it to a possible mid-Holocene age of 5000 BP. It also suggests that the erosional boundary between layers A and B and the fossil layer below spans a minimum of approximately 10,000 ^{14}C yr.

It should be made clear, however, that these ^{14}C dates are of bulk SOM only, and do not imply a similar age for the fossils excavated from this site. The ^{14}C ages given are purely from the TOC, which is most likely residual carbon retained since the time of deposition. It is also likely that the ages also reflect some component of younger carbon that has been translocated by surface or groundwater processes. Hence, these preliminary dates are likely to represent a possible minimum age of the bulk SOM. In situ and contaminant carbon components contained in the SOM will be quantified using ^{13}C nuclear magnetic resonance (NMR). In turn, the extraction of these older carbon constituents identified for ^{14}C age determinations will allow the on-going palaeoenvironmental reconstruction to be put into the clearest chronological context yet.

ACKNOWLEDGEMENTS

The Department of Environment and Heritage Research Grant is acknowledged for funding this project. Dr Alan Hogg and staff at the Radiocarbon Dating Laboratory at the University of Waikato, Hamilton, New Zealand, are acknowledged for providing the 4 ^{14}C dates and associated sample preparation methodology. Discussion with Drs Jan Skjemstad and Evelyn Krull at CSIRO, Land and Water, Adelaide, helped clarify preliminary NMR results. We also acknowledge Dr John Cann at the University of South Australia for invertebrate slide preparation and identification of gastropod species.

REFERENCES

- Anderson DW, Paul EA. 1984. Organo-mineral complexes and their study by radiocarbon dating. *Soil Science Society of America Journal* 48:298–301.
- Baldock JA, Skjemstad JO. 2000. Role of the soil matrix and minerals in protecting natural organic materials against biological attack. *Organic Geochemistry* 31: 697–710.
- Barbetti M, McElhinny M. 1972. Evidence of a geomagnetic excursion 30,000 yr BP. *Nature* 239:327–30.
- Bell WT. 1991. Thermoluminescence dating of Lake Mungo geomagnetic polarity excursion. *Nature* 265: 40–1.
- Bol R, Huang Y, Meridith JA, Eglinton G, Harkness DD, Ineson P. 1996. The ¹⁴C age and residence time of organic matter and its lipid constituents in a stagnohumic gley soil. *European Journal of Soil Science* 47: 215–22.
- Bowler JM, Johnston H, Olley JM, Prescott JR, Roberts RG, Shawcross W, Spooner NA. 2003. New ages for human occupation and climate changes at Lake Mungo, Australia. *Nature* 421:837–40.
- Chaplin RE. 1971. *The Study of Animal Bones from Archaeological Sites*. London: Seminar Press Ltd. 171 p.
- Faure G. 1986. *Principles of Isotopic Geology, 2nd Edition*. New York: John Wiley & Sons. 589 p.
- Gill RL. 1996. *The Application of Uranium-Series Disequilibrium Dating to Utilise Fossil Bones as Palaeo-Environmental Indicators in the Naracoorte Caves, South Australia* [Honors thesis]. Flinders: University of South Australia.
- Gillespie R. 1986. *Radiocarbon User's Handbook*. Oxford University Committee for Archaeology. Oxford: Oxbow Books. 36 p.
- Gillespie R, Prosser IP, Dlugokencky E, Sparks R, Wallace G, Chappell JMA. 1992. AMS dating of alluvial sediments on the southern tablelands of New South Wales, Australia. *Radiocarbon* 34(1):29–36
- Gillespie RL. 2002. Dating the first Australians. *Radiocarbon* 44(2):455–72.
- Godwin H. 1962. Radiocarbon dating. *Nature* 195(4845): 943–5.
- Gröcke DR, Bocherens H. 1996. Isotopic investigation of an Australian island environment. *Comptes Rendus de l'Académie des Sciences, Series II* (322):713–9.
- Gröcke DR. 1998. Carbon-isotope analyses of fossil plants as a chemostratigraphic and palaeoenvironmental tool. *Lethaia* 31:1–13.
- Hope JH, Clark RL, Hope GS. Unpublished. A preliminary analysis of palaeoenvironmental of the Rocky River bone bed, Kangaroo Island, South Australia. *Royal Society of South Australia*.
- Huxtable J, Aitken MJ. 1977. Thermoluminescent dating of Lake Mungo geomagnetic polarity excursion. *Nature* 265:40–1.
- Krull ES, Skjemstad JO. 2002. $\delta^{13}\text{C}$ and $\delta^{15}\text{N}$ profiles in ¹⁴C-dated oxisol and vertisols as a function of soil chemistry and mineralogy. *Geoderma* 1890:10–29.
- Leavitt SW, Follett RF, Paul EA. 1996. Estimation of slow- and fast-cycling soil organic carbon pools from 6N HCl hydrolysis. *Radiocarbon* 38(2):231–9.
- Ludbrook NH, Gowlett-Holmes KL. 1989. Introduction to the Mollusca. In: Shepherd SA, Thomas IM, editors. *Marine Invertebrates of Southern Australia. Part II*. Adelaide: South Australian Government Printing Division.
- Mathers NJ, Mao XA, Xu ZH, Saffigna PG, Berners-Price SJ, Perera MCS. 2000. Recent advances in the application of ¹³C and ¹⁵N NMR spectroscopy to soil organic matter studies. *Australian Journal of Soil Research* 38:769–87.
- Paul EA, Follett RF, Leavitt SW, Halvorson A, Peterson GA, Lyon DJ. 1997. Radiocarbon dating for determination of soil organic matter pool sizes and dynamics. *Soil Science Society of America Journal* 61:1058–67.
- Quideau SA, Anderson MA, Graham RC, Chadwick OA, Trumbore SE. 2000. Soil organic matter processes: characterisation by ¹³C NMR and ¹⁴C measurements. *Forest Ecology and Management* 138:19–27.
- Retallack GJ. 1988. Field recognition of palaeosols. In: Reinhardt J, Sigleo WR. Palaeosols and Weathering Through Geologic Time: Principles and Applications. *Geological Society of America Special Paper* 216:1–20.
- Roberts RG, Jones R, Smith MA. 1994. Beyond the radiocarbon barrier in Australian prehistory. *Antiquity* 68:611–6.
- Stone T, Cupper ML. 2003. Last Glacial Maximum ages for robust humans at Kow Swamp, Southern Australia. *Journal of Human Evolution* 45(2):99–111.
- Stuiver M, Polach HA. 1977. Discussion: reporting of ¹⁴C data. *Radiocarbon* 19(3):355–63.
- Tindale NB, Fenner FJ, Hall FJ. 1935. Mammal bone beds of probable Pleistocene age, Rocky River, Kangaroo Island. *Transactions Royal Society of South Australia* 59:103–6.
- Trumbore SE. 1993. Comparison of carbon dynamics in tropical and temperate soils using radiocarbon measurements. *Global Biogeochemical Cycles* 7:275–90.
- Turney CSM, Bird MI, Fifield LK, Roberts RG, Smith M, Dortch CE, Grün R, Lawson E, Ayliffe LK, Miller GH, Dortch J, Cresswell RG. 2001. Early human occupation at Devil's Lair, southwestern Australia 50,000 years ago. *Quaternary Research* 55:3–13.
- Tyler MJ, Twidale CR, King JK. 1989. *Natural History of Kangaroo Island*. Adelaide: Royal Society of South Australia.

¹⁰BE, ¹⁴C DISTRIBUTION, AND SOIL PRODUCTION RATE IN A SOIL PROFILE OF A GRASSLAND SLOPE AT HESHAN HILLY LAND, GUANGDONG

CD Shen^{1,2} • J Beer³ • S Ivy-Ochs⁴ • Y Sun¹ • W Yi¹ • P W Kubik⁵ • M Suter⁴ • Z Li⁶ • S Peng⁵ • Y Yang¹

ABSTRACT. Concentrations of organic carbon, carbon isotopes (¹³C and ¹⁴C), atmospheric ¹⁰Be in soil, and in situ ¹⁰Be in bedrock and weathering rock were determined in a study of a profile of a grassland slope at the Heshan Hilly Land Interdisciplinary Experimental Station, Chinese Academy of Sciences, in Guangdong Province, China. A good linear relationship between depth and the ¹⁴C apparent age of the organic carbon demonstrates that the rock weathering process and the accumulation process of organic matter in the slope are relatively stable. Both ¹⁴C and ¹⁰Be results show that about 34% of soil in the grassland slope has been eroded during the past 3800 yr. The ¹⁰Be results for interstitial soil from weathered rocks show that the 90-cm-thick weathering rock layer above the bedrock has evolved over a period of 1.36 Myr. The concentrations of in situ ¹⁰Be in the weathered rock and bedrock are 10.7×10^4 atoms/g and 8.31×10^4 atoms/g, respectively. The weathering rate of the bedrock, equivalent to the soil production rate, was estimated at 8.8×10^{-4} cm/yr, and the exposure ages of the weathered rock and the bedrock were 72 kyr and 230 kyr, respectively.

INTRODUCTION

Soil contains abundant paleoclimatic information and is also an important source or sink for major greenhouse gases such as carbon dioxide, methane, and nitrogen oxides. With respect to global change, interaction between the pedosphere and other spheres of the crust has attracted more and more attention from researchers. The key to understanding soil development lies in the rate of pedogenesis and the rate of soil erosion, which requires precise dating. Only after the timescale for the development of soil is established can the paleoclimatic and paleoenvironmental information revealed by the geochemical evolution of nuclides and elements in the soil be interpreted.

Since soil is developed from the accumulation of erosional products or sedimentary deposition above the bedrock, the age of soil can be determined from the ages of the erosional surface and the sediments. The ¹⁴C method has already been used in soil dating and in quantitative discussion of soil development processes (Goh et al. 1975; Trumbore 1993). ¹⁰Be is a product of spallation nuclear reactions between cosmic ray particles and atmospheric gases (O, N), and has a half-life ($T_{1/2}$) of 1.5 Myr. Within a short time after its production, ¹⁰Be becomes attached to aerosols and is deposited on the earth's surface via precipitation or dust fallout. ¹⁰Be can be produced also through spallation reactions between cosmic ray particles and rocks on the earth's surface. The former is called "atmospheric ¹⁰Be" and the latter is called "in situ ¹⁰Be." In soils, Be exists mainly as oxide, or in the alkaline environment as complex anions such as $\text{Be}(\text{OH})\text{CO}_3^{3-}$ or $\text{Be}(\text{CO}_3)_2^{2-}$. Organic matter can also complex Be, which in part explains why Be concentration in soils is relatively high (Pavich et al. 1984). The geochemical properties and the distribution of ¹⁰Be in soil have been extensively investigated in relation to the emerging field of soil dynamics and dating. Recently, researchers have applied either an open-system model (Monaghan et al. 1983; Pavich et al. 1984, 1986; McKean et al. 1993) or a closed-system model (Lal 1991; Barg et al. 1997; Heimsath et al. 1997) to estimate the

¹Guangzhou Institute of Geochemistry, Chinese Academy of Sciences, Guangzhou 510640, China.

²Corresponding author. Email: cdshen@gig.ac.cn.

³Swiss Federal Institute of Environmental Science and Technology, EAWAG, CH-8600 Dübendorf, Switzerland.

⁴Particle Physics, ETH-Hönggerberg, CH-8093 Zürich, Switzerland.

⁵Paul Scherrer Institute, c/o ETH-Hönggerberg, CH-8093 Zürich, Switzerland.

⁶South China Institute of Botany, Chinese Academy of Sciences, Guangzhou 510640, China.

age of soil formation using ^{10}Be . In the closed-system model, it is assumed that ^{10}Be has been locked up in authigenic minerals since soil formation, so that ^{10}Be decay can be used to determine the formation age of the authigenic minerals.

This research focuses on a soil profile of a grassland slope in Guangdong Province, China. Both atmospheric ^{10}Be in soil and in situ ^{10}Be in bedrock and weathering rock were determined, as well as organic carbon in soil and its ^{14}C and ^{13}C composition.

SAMPLING SITES AND SOIL SAMPLES

The sampling sites are located in a grassland slope in the catchment area at the Heshan Hilly Land Interdisciplinary Experimental Station, Chinese Academy of Sciences (HHLIES-CAS) ($22^{\circ}41'\text{N}$, $112^{\circ}54'\text{E}$) at an elevation of about 92 m asl and slope of 18.5° . The geomorphic feature of the hilly land is convex and the underlying bedrocks are sandy shale. The land is covered by vast stretches of lawn mixed with sparsely populated shrubs. In the summer of 1999, the authors excavated 3 soil profiles along 1 side of the watershed: Profile I is located in the upper part of the slope; Profile II in the middle of the slope, about 20 m away from Profile I; and Profile III in the lower part of the slope, about 50 m further away from Profile I.

This paper deals only with investigations on Profile I. Figure 1 shows that Profile I is comprised of 3 parts: a soil layer (60 cm), a weathering layer (90 cm), and bedrock. The soil layer is itself comprised of 4 layers, while the weathering layer consists mainly of rock fragments of different sizes, with weathering clays filling the interstices. With increasing depth, this layer contains less clay and a greater amount of weathered rock fragments, the fragments becoming larger in volume. For ^{10}Be and $\delta^{13}\text{C}$ determination, the sampling interval is 2 cm above 20 cm depth, 5 cm for 20–60 cm depth, and 20 cm or 30 cm for 60–150 cm depth. One sample of the bedrock was taken. For ^{14}C determination, the sampling interval is, on average, 4 cm above 20 cm depth and 10 cm or 20 cm for 20–60 cm depth (Figure 1).

EXPERIMENT AND RESULTS

^{14}C Determination

After air-drying and picking out visible roots and fragmentary stone, all soil samples were passed through a 1-mm sieve to remove rootlets and coarse sand. All samples were treated with 0.1N HCl to remove carbonates and then rinsed with distilled water repeatedly until they became neutral. Soil samples were dried prior to analysis of ^{14}C , ^{13}C , and organic carbon. The samples for ^{14}C measurements were further ground and put into a quartz tube, where they were combusted in an oxygen stream at 800°C to produce CO_2 . The CO_2 was purified repeatedly using dry ice-acetone and liquid-nitrogen traps and then converted into Li_2C_2 in a Li-reactor under vacuum at 900°C . Li_2C_2 was hydrolyzed into C_2H_2 , which was then synthesized into C_6H_6 under catalysis. ^{14}C measurements were carried out using a 1220 Quantulus ultra low-level liquid scintillation spectrometer with a scintillation cocktail teflon vial.

^{13}C Determination

The ^{13}C content for soil samples is usually expressed as $\delta^{13}\text{C}$:

$$\delta^{13}\text{C} = \left[\left(\frac{^{13}\text{C}/^{12}\text{C}}{^{13}\text{C}/^{12}\text{C}} \right)_{\text{sample}} / \left(\frac{^{13}\text{C}/^{12}\text{C}}{^{13}\text{C}/^{12}\text{C}} \right)_{\text{standard}} - 1 \right] \times 1000,$$

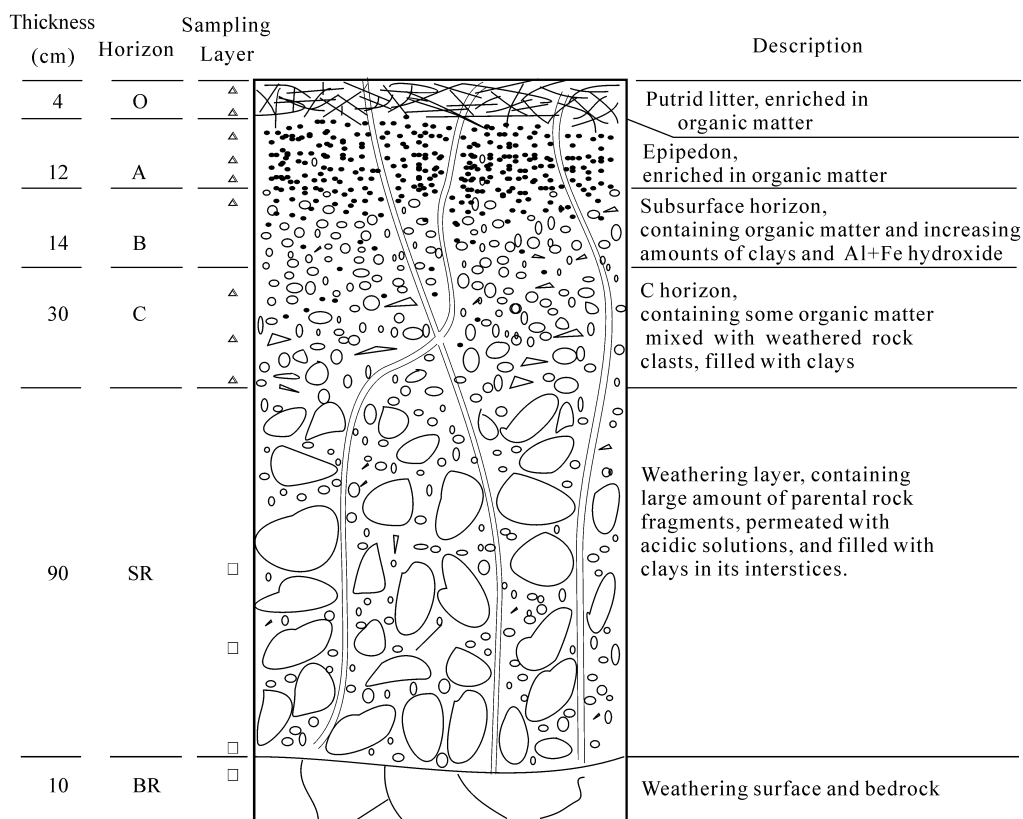


Figure 1 Sketch of Profile I of a grassland slope at Heshan Hilly Land, Guangdong. △ = the sampling layer for ^{14}C ; □ = the sampling layer for in situ ^{10}Be .

where $(^{13}\text{C}/^{12}\text{C})_{\text{sample}}$ is the isotope ratio for organic carbon in soil samples and $(^{13}\text{C}/^{12}\text{C})_{\text{standard}}$ is the carbon isotope ratio for the PDB standard. All ^{13}C measurements were completed using the Finigen Model-251 mass spectrometric system in the Xi'an State Key Laboratory of Loess and Quaternary Geology. The modern mass spectrometry has a $\delta^{13}\text{C}$ measurement precision of $\pm 0.02\text{‰}$ and a sample preparation error of generally less than $\pm 0.2\text{‰}$. Therefore, when the difference in the $\delta^{13}\text{C}$ value for soil samples is less than $\pm 1\text{‰}$, special attention should be paid to the interpretation of the $\delta^{13}\text{C}$ data. In this work, the $\delta^{13}\text{C}$ value ranges from -27.6‰ to -15.7‰ , while the average $\delta^{13}\text{C}$ values for the various horizons are -27.4‰ for Layer O, -23.3‰ for Layer A, -18.5‰ for Layer B, and -16.7‰ for Layer C.

Organic Carbon Determination

Soil samples were first oxidized into CO_2 in a vacuum system, then CO_2 volume and pressure were measured and converted into organic carbon concentration. All results are listed in Table 1 and illustrated in Figure 2. The organic carbon concentrations for the various soil horizons are as follows: 4.29% for Layer O; 1.22–0.58% for Layer A; 0.35–0.37% for Layer B, which tends to be stable; 0.21–0.16% for Layer C, which still remains stable despite the concentration being rather low.

Table 1 The concentrations of ^{10}Be , ^{14}C , ^{13}C , and organic carbon in Profile I of a grassland slope at Heshan Hilly Land, Guangdong.

Lab code	Field code	Horizon	Depth (cm)	Organic carbon (%)	$\Delta^{14}\text{C}$ (‰)	^{14}C apparent age (BP)	$\delta^{13}\text{C}$ (‰)	Atmospheric ^{10}Be (10^8 atoms/g)	In situ ^{10}Be (10^4 atoms/g)
GC-001037	HSC1-0	Litter	0	—	126	modern	-28.4	—	—
GC-001038	HSC1-1	O	2	4.29	100	modern	-27.2	0.048	—
GC-001039	HSC1-2	O	4	1.30	—	—	-25.8	0.051	—
GC-001040	HSC1-3	A	6	1.22	—	—	-23.2	0.071	—
GC-001041	HSC1-4	A	8	1.19	62	modern	-25.8	0.084	—
GC-001042	HSC1-5	A	10	0.94	—	—	-24.6	0.102	—
GC-001043	HSC1-6	A	12	0.65	—	811 ± 70	-23.9	0.112	—
GC-001044	HSC1-7	A	14	0.58	—	—	-21.8	0.094	—
GC-001045	HSC1-8	A	16	0.36	—	1032 ± 75	-20.6	0.166	—
GC-001046	HSC1-9	B	18	0.43	—	—	-17.9	0.141	—
GC-001047	HSC1-10	B	20	0.35	—	1770 ± 75	-21.1	0.13	—
	HSC1-11	B	25	0.35	—	—	-16.3	0.164	—
GC-001048	HSC1-12	B	30	0.37	—	—	-18.8	0.152	—
	HSC1-13	C	35	—	—	—	—	0.162	—
GC-001049	HSC1-14	C	40	0.21	—	2210 ± 90	-16.3	—	—
	HSC1-15	C	45	—	—	—	—	0.161	—
GC-001050	HSC1-16	C	50	0.17	—	3080 ± 105	-15.7	0.16	—
	HSC1-17	C	55	—	—	—	—	0.159	—
GC-001051	HSC1-18	C	60	0.16	—	3840 ± 110	-18.2	0.244	—
	HSC1-19	SR	80	—	—	—	—	0.119	—
	HSC1-20	SR	100	—	—	—	—	0.125	10.7
	HSC1-21	SR	120	—	—	—	—	0.073	6.4
	HSC1-22	SR	150	—	—	—	—	0.097	8.3
	HSC1-23	BR	160	—	—	—	—	—	8.13

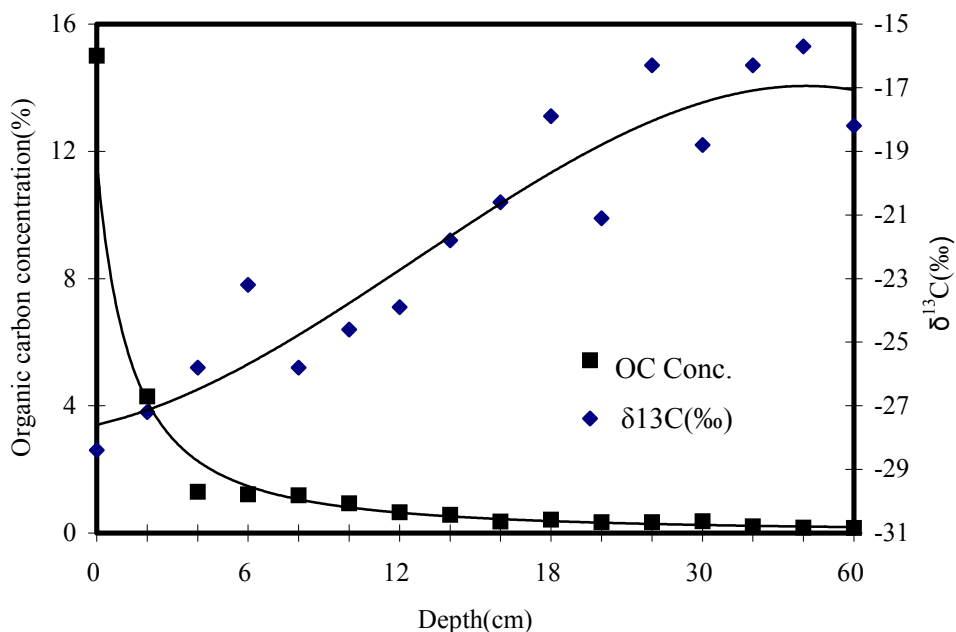


Figure 2 Relationships of organic carbon concentration versus depth and stable carbon isotope versus depth for Profile I.

¹⁰Be Determination

Atmospheric ¹⁰Be

After removal of roots and large detrital stones, the soil was desiccated under natural ventilation conditions for 24 hr and screened with a 710- μ m sieve. The screened soil samples were ground in an agate mortar to form a homogeneous mixture. One gram of sample was weighed and placed in a 100-mL plastic beaker, to which a 1-mL ⁹Be carrier solution (containing 0.254 mg of ⁹Be) was added. Organic matter was removed with H₂O₂, then 6M HCl was added for leaching (Shen et al. 1992). The leaching solution was placed in a teflon beaker and evaporated to dryness on an electric hot plate. The residue was dissolved in 1M HCl and then transferred to an ion exchange column (DOWEX-50W \times 8, 100- to 200-mesh size) which was washed 10 times with 10 mL 1M HCl. The ¹⁰Be-bearing residue was preserved in the effluent, then heated to reduce the volume to 20 mL, NH₄OH solution was added, and Be(OH)₂ was separated out. In a 900 °C quartz oven coated with gold, Be(OH)₂ was oxidized to BeO, which was then mixed homogeneously with copper powder and pressed into ¹⁰Be targets,—just as for accelerator mass spectrometry (AMS) measurements—using a 5T target-preparation machine. All ¹⁰Be measurements were carried out in the ETH/PSI AMS system in Switzerland. The blank ¹⁰Be/⁹Be ratio is 10⁻¹⁴, which is about 2 orders of magnitude lower for the soil sample. At least 2 measurements were made for each sample and the measurement precision (1 σ) was 3–5% (Suter et al. 1984).

In situ ¹⁰Be

About 30 g of quartz grains were carefully separated from the rock samples and placed in a 500-mL plastic bottle, to which was added 300 mL of 5% HF solution. The plastic bottle was placed and fixed on a vibrator and vibrated at a rate of 200 times per min for 24 hr. The supernatant liquid was discarded and the remaining quartz grains rinsed with deionized water 5 times. Then, 300 mL of 5% HF solution was added and the quartz grains were vibrated and rinsed for the second time. The well-rinsed quartz grains were dried and 20 g weighed for analysis. A 5-ml 40% HF solution and 1-ml ⁹Be carrier (containing 1.0 mg of ⁹Be) were added to a teflon bottle containing 20 g of quartz; the bottle was placed on a hot plate, and the solution evaporated at 80 °C. Even though the quartz grains were completely altered, residues of other minerals might remain. After adding 2 mL of 1M HCl into the dried sample, the component containing in situ ¹⁰Be was completely dissolved, and the residues and the solution were thus separated centrifugally. The separated solution was loaded on to the DOWEX-50W \times 8 (100- to 200-mesh) cation exchange resin column and washed 10 times with 10 mL of 1M HCl. A 100-mL effluent was collected in a teflon bottle. The effluent was evaporated to 10 mL on a hot plate and its pH value was adjusted to 8–9 with NH₄OH to precipitate Be(OH)₂. It was then oxidized at 900 °C to obtain BeO, which was mixed with an appropriate amount of copper powder and pressed into ¹⁰Be targets for AMS measurement at the ETH/PSI AMS system in Switzerland. S555 was used as ¹⁰Be standards in the in situ ¹⁰Be determinations with the blank ¹⁰Be/⁹Be ratio of 10⁻¹⁴. At least 3 measurements were made for each sample and standard sample and the measurement precision (1 σ) was 5% (Kubik et al. 1998; Ivy-Ochs et al. 1995). The measurement results are listed in Table 1.

DISCUSSION

¹⁴C Apparent Age

The 0–4-cm section of Profile I is comprised mainly of litter and humic substances with ¹⁴C radioactivity consistently greater than the standard value for modern carbon, demonstrating that it has

already been affected by atmospheric nuclear tests. Comparisons with the radioactivity of atmospheric ^{14}C show that the organic carbon originated from plants accumulated in the past 10 yr. As illustrated in Table 1, the penetration depth of bomb ^{14}C is 8–10 cm. Layer B (16–30 cm) has a pedogenesis duration estimated to be at least 700 yr based on the ^{14}C results. Layer C (30–60 cm) has an apparent age for the organic carbon at its base of 3840 ± 110 BP. Figure 3 illustrates the relationship between the ^{14}C apparent age for Profile I and its burial depth. One can see that there is a good linear relationship between the depth and the ^{14}C age for organic matter, which reveals that the weathering of rocks in the slope and the accumulation of organic matter are both stable.

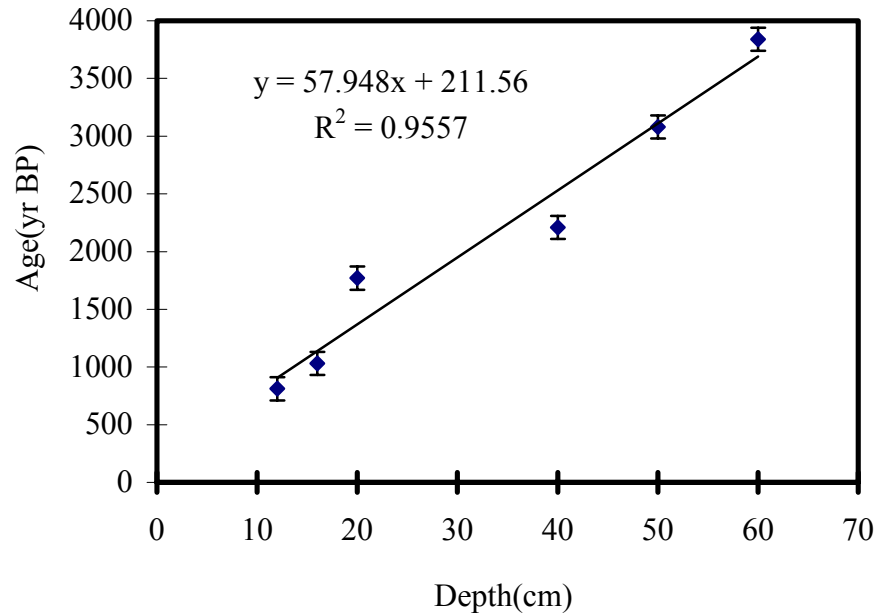


Figure 3 Relationship between ^{14}C apparent age and depth of Profile I

Organic Carbon Content and $\delta^{13}\text{C}$ Distribution

Figure 2 gives evolution curves for the organic carbon content in the soil of Profile I versus depth and also the $\delta^{13}\text{C}$ value versus depth. The 2 curves exhibit similar shaped but opposite trends: a rapid change for the section from the surface to 4 cm in depth, a slow change for the section from 4–10 cm in depth, and slight variation for the section from 10–60 cm in depth. It can thus be inferred that the organic carbon in the soil contains 2 completely different components: one of which has rapidly decomposed with increase in depth, while the other has decomposed extremely slowly. Under the action of microorganisms, the plant residues in the soil are broken down into amino compounds, hydroxybenzenes, saccharides, lignins, etc., and further into humic substances. Organic carbon mainly originates from humic substances, so the distribution characteristics of organic carbon can reflect the accumulation of humic substances in the soil. In general, the soil layer above 10 cm depth is characterized by a relatively loose structure with good air permeability, and the root distribution is well developed with intense biological activity. Therefore, the residual plant material decomposes rapidly, and the dissolved humic substances can be easily removed due to the gley moisture in the surface soil. However, below the 10 cm depth, the physical and chemical properties of the soil and the biogeochemical reactions in the soil are all relatively stable and, consequently, the organic carbon component tends to be stable.

Based on photosynthetic pathways, natural plants can be divided into 3 types: C₃, C₄, and CAM. The $\delta^{13}\text{C}$ value for C₃ plants is in the range of -34‰ to -23‰ ; the $\delta^{13}\text{C}$ value for C₄ plants ranges from -22‰ to -6‰ ; and the $\delta^{13}\text{C}$ value for CAM plants is from -20‰ to -10‰ (Deines 1980). The difference between the mean $\delta^{13}\text{C}$ values for C₃ and C₄ plants at the same location is about 14‰. Isotope fractionation in organic matter commonly occurs during decomposition and humification processes and the $\delta^{13}\text{C}$ value slightly increases, generally by 1–4‰. Organic carbon in soil originates from vegetation and the variation of its $\delta^{13}\text{C}$ value reflects the $\delta^{13}\text{C}$ variation of the vegetation. The $\delta^{13}\text{C}$ values for soil in Profile I ranges from -27.6‰ to -15.7‰ . Average $\delta^{13}\text{C}$ values for the various soil horizons are -27.4‰ for Layer O, -23.3‰ for Layer A, -18.5‰ for Layer B, and -16.7‰ for Layer C. Based on the $\delta^{13}\text{C}$ and ¹⁴C apparent ages, the grass and the sparse shrubbery, which cover the slope at the site today, should belong to the C₃ type of vegetation. However, most of the vegetation of this same grassland slope would have belonged to the C₄ type 3000 yr ago.

Atmospheric ¹⁰Be and Soil Erosion

Variation curves of ¹⁰Be concentration versus depth in Profile I are shown in Figure 4, from which it can be seen that the ¹⁰Be concentration distribution has the following characteristics: an exponential increase from 2–30 cm, stability from 30–60 cm, an abrupt 50% increase at 60 cm, and an exponential decrease from 60–150 cm. The total amount of ¹⁰Be for the profile can be used to evaluate the retentivity of ¹⁰Be in the soils. The ¹⁴C apparent age at the boundary of the soil layer is 3840 BP. The age of the weathering pedogenic substances occurring on the rocks is close to or even older than this ¹⁴C apparent age. The average global production rate of ¹⁰Be is approximately 1.8×10^{-2} atoms $\text{cm}^{-2}\text{s}^{-1}$ (Beer et al. 1994; Masarik and Beer 1999). On this basis, the gross amount of ¹⁰Be accumulated in Profile I should be at least 21.8×10^8 atoms/cm². However, ¹⁰Be measurements show that the gross amount of ¹⁰Be accumulated in the 60-cm-thick soil layer is only 14.4×10^8 atoms/cm², the shortfall suggesting a major lateral migration of ¹⁰Be. ¹⁰Be preservation is closely related to the chemical and mineralogical compositions of the soil grains and the parent materials, and it is generally considered that ¹⁰Be can be well retained in soils enriched in clay minerals (Barg et al. 1997). For any given soil profile, ¹⁰Be is usually displaced downward together with the migration of organic substances and fine-grained particles. In case of a slope, ¹⁰Be can be displaced both physically and chemically. Moreover, it can be displaced transversely toward the valley of the slope due to runoff. In neutral conditions, the distribution coefficient K_d of ¹⁰Be between the solid phase (the particle phase) and the liquid phase is as high as 10^5 to 10^6 (Baumgartner et al. 1997). Thus, ¹⁰Be is firmly adsorbed on the surfaces of soil particles, and it is probable that the significant lateral migration of ¹⁰Be results from soil and ¹⁰Be being carried away by underground water, or by the slope wash, in a systematic manner. If so, then the migration of ¹⁰Be reflects the status of erosion of this region. This work suggests that about 34% of the pedogenic substances in the area studied have been eroded in the past 3800 yr.

The exponential decrease with depth of the ¹⁰Be that is preserved in the interstitial soil of the weathering rocks in the 60–150-cm section suggests that the retention of ¹⁰Be is good in this section of soil. It can be seen from Table 1 that the highest ¹⁰Be concentration is 0.244×10^8 atoms/g, and the average ¹⁰Be concentration is 0.16×10^8 atoms/g at the boundary between the soil and weathering rocks. The ¹⁰Be concentration in the upper part of the bedrock is 0.085×10^8 atoms/g. Based on these data, it can be estimated that the 90-cm-thick weathering rock layer above the bedrock has evolved for a period of 1.36 Myr. In this calculation, the average ¹⁰Be concentration at the boundary between the soil and the weathering rocks was taken as the initial concentration of the atmospheric ¹⁰Be in the 90-cm-thick weathering rock layer. The actual initial concentration of the atmospheric ¹⁰Be is difficult to estimate accurately since it is constrained by several factors, such as the precipitation

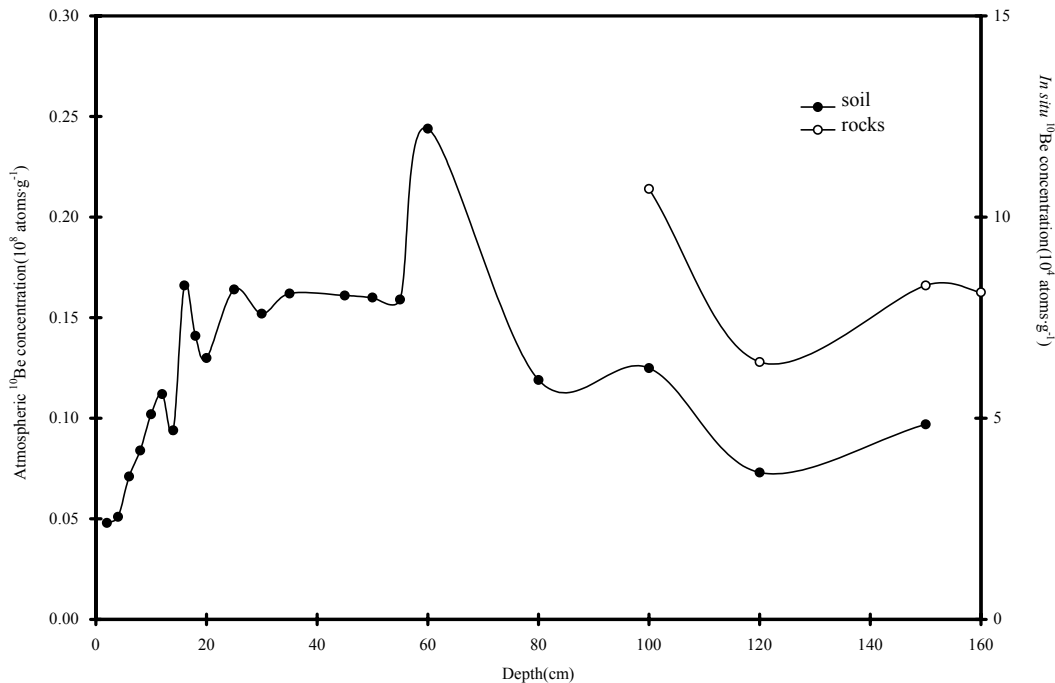


Figure 4 Relationship between ¹⁰Be concentration and depth for Profile I. The left ordinate axis and the right ordinate axis represent atmospheric ¹⁰Be concentrations in the soil and in situ ¹⁰Be concentrations in the rocks, respectively.

flux of ¹⁰Be, change of soil erosion rate, ¹⁰Be accumulation rate and preservation, etc. Although 1.36 Myr is only a rough estimation, it indicates that the production of soil in this area is rather slow (Heimsath et al. 2000).

In Situ ¹⁰Be and Soil Production Rate

The Heshan area (HHLIES-CAS) in Guangdong has a tropical, humid climate which causes intense weathering action. The bedrock in the lower part of the profile is sandy shale, which is overlain by a 90-cm-thick layer of weathering rocks. This layer is comprised mainly of weathered rock fragments of a variety of sizes mixed with interstitial soil. For this work, 3 weathered rock samples were taken at depths of 100 cm, 120 cm, and 150 cm, respectively, together with 1 bedrock sample at 150–160 cm. Quartz was separated from all rock samples and the in situ ¹⁰Be concentrations in the quartz were measured by AMS (Table 1 and Figure 4). Concentrations of in situ ¹⁰Be vary in the range of $(10.7\text{--}6.4) \times 10^4$ atoms/g, which is 2 to 3 orders of magnitude lower than that of the atmospheric ¹⁰Be in the same horizon.

Soil in the Heshan Hilly Land comprises mainly accumulated weathering products of the bedrock. In tropical, humid climate zones, dust fallout is negligible. The weathering rate of rock for a stable geomorphic unit is equivalent to the soil production rate (Heimsath et al. 1997). Based on the concentration of the in situ ¹⁰Be in rocks, the weathering rate of rocks can be calculated and the relationship between the soil production rate and depth can be derived. Assuming that the soil body is stable with a thickness of h , the soil density is constant, and the bedrock-soil transformation rate is constant, then the ¹⁰Be concentration C (atoms/g) of the bedrock at the boundary is the following (Lal 1991):

$$C = P(h, \theta) [\lambda + (\rho_r \epsilon / \lambda)]^{-1}.$$

Here, $P(h, \theta)$ is the production rate (atoms $\text{g}^{-1}\text{yr}^{-1}$) of ^{10}Be at a depth of h and a gradient of θ ; Λ = average attenuation length = 165 g/cm^2 ; λ = ^{10}Be decay constant = $\ln 2/T_{1/2} = 4.33 \times 10^{-7}\text{yr}^{-1}$; ρ_r = rock bulk density; ϵ = rate of weathering, which is equivalent to the soil production rate, $\epsilon = (\Lambda/\rho_r)[P(h, \theta)/C - \lambda]$.

In order to calculate the rate of weathering ϵ , the following values can be used based on this work: $h = 60 \text{ cm}$, $\rho_r = 2.6 \text{ g/cm}^3$, $\theta = 18.5^\circ$. The production rate P of ^{10}Be at the boundary of weathered rock is $1.49 \text{ atoms g}^{-1}\text{yr}^{-1}$ (Stone 2000). In Table 1, the measured in situ ^{10}Be concentration on the upper part of the weathering rock is $10.7 \times 10^4 \text{ atoms/g}$, so the weathering rate ϵ is estimated to be $8.8 \times 10^{-4} \text{ cm/yr}$, which is equivalent to the soil production rate. The cosmic ray exposure time of the upper part of the weathered rock is about 72 kyr. In Table 1, the in situ ^{10}Be concentration in the bedrock is $8.31 \times 10^4 \text{ atoms/g}$. After correcting for shielding effects, the production rate P of ^{10}Be in the bedrock is $0.36 \text{ atoms g}^{-1}\text{yr}^{-1}$, yielding a cosmic ray exposure time of about 230 kyr.

As the global ^{10}Be production rate is not known with certainty and its estimates vary by a factor of 2 (Beer et al. 1994; Brown et al. 1989; Kubik et al. 1998; Lal 1991; Monaghan et al. 1985; Pavich et al. 1986; Stone 2000), it is necessary to further reduce the inherent uncertainty regarding the ^{10}Be production rate and improve to reliability of estimating the soil production rate and exposure age.

CONCLUSIONS

A linear relationship between the depth of sample and the ^{14}C apparent age of organic carbon demonstrates that the rock weathering process and the accumulation of organic matter in the slope are relatively stable. The apparent age of the organic carbon at the bottom of Horizon C is $3.8 \pm 0.1 \text{ kyr}$.

The ^{13}C value of the grassland slope soil ranges from -27.6‰ to -15.7‰ . The grass and the sparsely populated shrubs, which extensively cover the slope in the modern hilly land, all belong to C_3 type vegetation, but most of the vegetation of the grassland slope could have belonged to type C_4 3000 yr ago.

Both ^{14}C and ^{10}Be data indicate that about 34% of the soil substances in the grassland slope have been eroded during the past 3800 yr.

The concentration of in situ ^{10}Be in the weathering rock and the bedrock are $10.7 \times 10^4 \text{ atoms/g}$ and $8.31 \times 10^4 \text{ atoms/g}$, respectively, indicating a weathering rate equivalent to the soil production rate of $8.8 \times 10^{-4} \text{ cm/yr}$, and exposure ages of the weathering rock and the bedrock are 72 and 230 kyr, respectively.

ACKNOWLEDGEMENTS

This work was performed at the Zürich AMS facility, jointly operated by the Swiss Federal Institute of Technology, Zürich, and the Paul Scherrer Institut, Villigen, Switzerland. We thank the Zürich AMS group for their contributions during ^{10}Be measurements. This work was supported by grants from NSFC (40231015, 49872093), Chinese NKBRFSF (G1999043401), CAS Knowledge Innovation Project (KZCX2-SW-118, KZCX2-108), and also from the Swiss NSF, ETH Zürich, and the Paul Scherrer Institute.

The authors are indebted to Dr Yongliang Yang for his help in the preparation of this manuscript and to two reviewers for their constructive comments and suggestions.

REFERENCES

- Barg E, Lal D, Pavich MJ, Caffee MW, Southon JR. 1997. Beryllium geochemistry in soils: evaluation of $^{10}\text{Be}/^9\text{Be}$ ratios in authigenic minerals as a basis for age models. *Chemical Geology* 140:237–58.
- Baumgartner S, Beer J, Wagner G, Kubik P, Suter M, Raisbeck GM, Yiou F. 1997. ^{10}Be and dust. *Nuclear Instruments and Methods in Physics Research B* 123: 296–301.
- Beer J, Joos F, Lukaschik C, Mendel W, Rodriguez J, Siegenthaler U, Stettin R. 1994. ^{10}Be as an indicator of solar variability and climate. In: Nesme-Ribes E, editor. *The Solar Engine and Its Influence on Terrestrial Atmosphere and Climate, NATO ASI-Series* 25:221–33.
- Brown L, Stensland GJ, Klein J, Middleton R. 1989. Atmospheric deposition of ^7Be and ^{10}Be . *Geochimica et Cosmochimica Acta* 53:135–42.
- Deines P. 1980. The isotopic composition of reduced organic carbon. In: Fritz P, Fontes J-Ch, editors. *Handbook of Environment Isotope Geochemistry I: The Terrestrial Environment*. Amsterdam: Elsevier. p 329–406.
- Goh KM, Tonkin PJ, Rafter TA. 1975. Implications of improved radiocarbon dates of Timaru peats on Quaternary loess stratigraphy. *New Zealand Journal of Geology and Geophysics* 21:463–7.
- Heimsath AM, Dietrich WE, Nishizumi K, Finkel RC. 1997. The soil production function and landscape equilibrium. *Nature* 388:358–61.
- Heimsath AM, Chappell J, Dietrich WE, Nishizumi K, Finkel RC. 2000. Soil production on a retreating escarpment in southeastern Australia. *Geology* 28(9): 787–90.
- Ivy-Ochs S, Schluchter C, Kubik P W, Dietrich-Hannen B, Beer J. 1995. Minimum ^{10}Be exposure ages of early Pleistocene for the Table Mountain plateau and the Sirius Group at Mount Fleming, Dry Valleys, Antarctic. *Geology* 23:1007–10.
- Kubik PW, Ivy-Ochs S, Masarik J, Frank M, Schluchter C. 1998. ^{10}Be and ^{26}Al production rates deduced from an instantaneous event within the dendro-calibration curve, the landslide of Kofels, Oetz Valley, Austria. *Earth and Planetary Science Letters* 161:231–41.
- Lal D. 1991. Cosmic ray labeling of erosion surface: in situ nuclide production rates and erosion models. *Earth and Planetary Science Letters* 104:424–39.
- Masarik J, Beer J. 1999. Simulation of particle fluxes and cosmogenic nuclide production in the earth's atmosphere. *Journal of Geophysical Research*. 104(D10): 12,099–111.
- McKean JA, Dietrich WE, Finkel RC, Southon JR, Caffee MW. 1993. Quantification of soil production and down slope creep rates from cosmogenic ^{10}Be accumulations on a hillslope creep profile. *Geology* 21: 343–6.
- Monaghan MC, Krishnaswami S, Thomas JH. 1983. ^{10}Be concentrations and the long-term fate of particle-reactive nuclides in fire soil profiles from California. *Earth and Planetary Science Letters* 65:51–60.
- Monaghan MC, Krishnaswami S, Turekian KK. 1985. The global-average production rate of ^{10}Be . *Earth and Planetary Science Letters* 76:279–87.
- Pavich MJ, Brown L, Klein J, Middleton R. 1984. ^{10}Be accumulation in a soil chronosequence. *Earth and Planetary Science Letters* 68:198–204.
- Pavich MJ, Brown L, Harden J, Klein J, Middleton R. 1986. ^{10}Be distribution in soils from Merced terraces, California. *Geochimica et Cosmochimica Acta* 50: 1727–35.
- Shen CD, Beer J, Liu TS, Oeschger H, Bonani G, Suter M, Wolfli W. 1992. ^{10}Be in Chinese loess. *Earth and Planetary Science Letters* 109:169–77.
- Stone JO. 2000. Air pressure and cosmogenic isotope production. *Journal of Geophysical Research*. 105(B10):23,753–9.
- Suter M, Balzer R, Bonani G, Hofmann H, Morenzoni E, Nèssi M, Wolfli W, Andree M, Beer J, Oeschger H. 1984. Precision measurements of ^{14}C in AMS—some results and prospects. *Nuclear Instruments and Methods in Physics Research* 233(B5):117–22.
- Trumbore SE. 1993. Comparison of carbon dynamics in tropical and temperate soils using radiocarbon measurements. *Global Biogeochemical Cycles* 7:275–90.

A NOVEL APPROACH FOR DEVELOPING HIGH-RESOLUTION SUB-FOSSIL PEAT CHRONOLOGIES WITH ^{14}C DATING

T H Donders^{1,2} • F Wagner¹ • K van der Borg³ • A F M de Jong³ • H Visscher¹

ABSTRACT. Sub-fossil sections from a Florida wetland were accelerator mass spectrometry (AMS) dated and the sedimentological conditions were determined. ^{14}C data were calibrated using a combined wiggle-match and ^{14}C bomb-pulse approach. Repeatable results were obtained providing accurate peat chronologies for the last 130 calendar yr. Assessment of the different errors involved led to age models with 3–5 yr precision. This allows direct calibration of paleoenvironmental proxies with meteorological data. The time frame in which ^{14}C dating is commonly applied can possibly be extended to include the 20th century.

INTRODUCTION

Modern paleoclimatology focuses on the development and validation of biological proxies, which are indicative for climate parameters rapidly changing under ongoing greenhouse gas forcing. The ability to understand the dynamics of major weather determining systems such as the El Niño Southern Oscillation (ENSO) is a basic requirement to predict the consequences of human interference with the global system. Although increasing amounts of instrumental precipitation and temperature records are available, the relatively short timespan covered in these records generally does not encompass the total range of natural variability.

On this background, the development of proxies able to detect high-frequency changes on near-annual to sub-decadal scale is needed. To test the applicability of any potential proxy, it is essential to first assess the natural range of variability within a single site and compare changes to meteorological data.

Among the available proxies for paleoclimatological reconstructions, pollen and plant macro-remain analysis have been demonstrated to be highly indicative for fast changes in their growth environments (Birks and Birks 2003). Peat-accumulating systems provide well-preserved organic-rich sediments and are, thus, a suitable source for paleobotanical investigations.

Validation and application of these proxies, for studies involving climatological changes occurring on multi-annual to sub-decadal scale, requires meticulous calibration of paleo-records with modern meteorological data series. The proxy quality thereby strongly depends on an extremely accurate age assessment of young sediment cores. Contrary to lake sediments, peat is generally not (annually) laminated. Consequently, radiometric dating is required to obtain a reliable core chronology.

Commonly used ^{137}Cs and ^{210}Pb dating methods depend on analysis of particles that potentially migrate in the sediment due to changing water levels, and the results are not always satisfactory (Jensen et al. 2002) or in mutual agreement (Cohen et al. 1999). Errors in determination of water content and dry bulk densities and the estimation of initial concentrations provide further uncertainties in ^{210}Pb dating (Appleby 2001). In this study, we assess the applicability of radiocarbon dating in creating high-precision peat chronologies for the 20th century and into the time frame where ^{14}C dating is commonly applied. Furthermore, we consider the different errors involved and provide some recommendations for future application.

¹Botanical Palaeoecology, Laboratory of Paleobotany and Palynology, Utrecht University, Budapestlaan 4, 3584 CD Utrecht, the Netherlands.

²Corresponding author. Email: t.h.donders@bio.uu.nl.

³R.J. Van de Graaff Laboratorium, Utrecht University, Princetonplein 5, 3584 CC Utrecht, the Netherlands.

SITE DESCRIPTION

Extensive peat-accumulating wetlands exist in southern Florida (USA). This area is highly suitable for high-resolution studies on climate variability because of the distinct linkage of precipitation and temperature to the ENSO system (Cronin et al. 2002). High-quality ecological and meteorological data for the region are abundant. The site studied is located in a relatively undisturbed wetland ecosystem, part of the Fakahatchee Strand Preserve State Park (25°95'N, 81°49'W, hereafter FSPSP, see Figure 1).

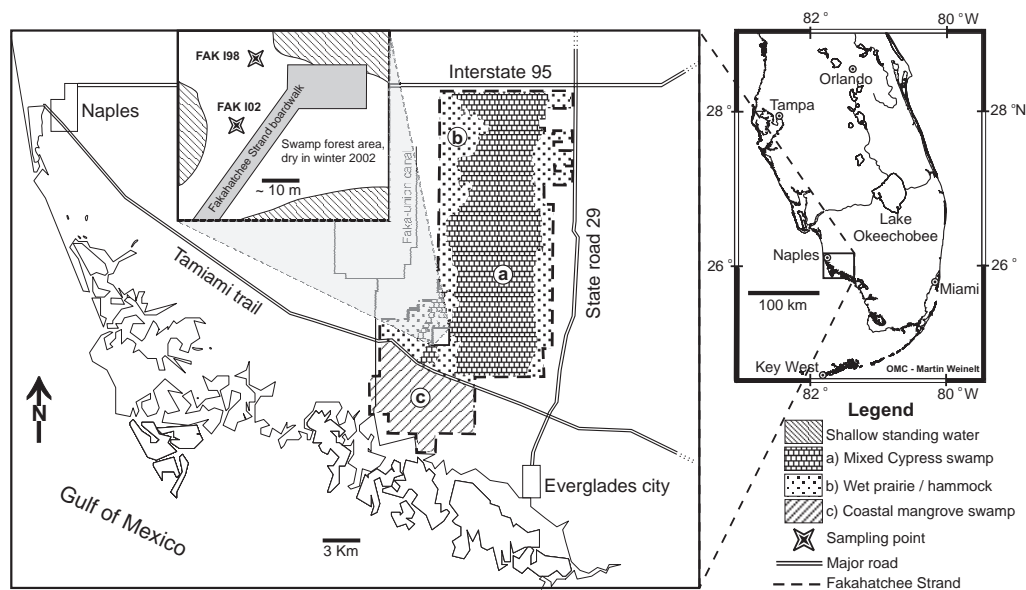


Figure 1 Location and environmental setting of the Fakahatchee Strand Preserve State Park (FSPSP) in south-central Florida

Although widespread in Florida, human impacts by lumbering and drainage activities have not directly affected the area studied; old-growth forest is still dominant (Burns 1984). Swamp conditions persist within the wide and shallow 40-km-long karst structure or “strand” where a peat layer seals off the underlying limestone. This organic-rich layer retains water which extends the local hydroperiod. These continuous moist conditions create anoxia that inhibits organic degradation and bioturbation. The strong seasonality, however, creates large fluctuations in water level throughout the year, which allows small inorganic particles to migrate within the sediment column. The wetland forest ecosystem and general low topography of the terrain (Watts and Hansen 1994) act together as a water capacitor, resulting in a wide sheet flow that deposits no clastic material and creates stable high sedimentation rates. These factors combined make the FSPSP highly suitable for collecting organic-rich undisturbed sediments for both ^{14}C dating and subsequent paleoecological reconstructions.

MATERIAL AND METHODS

Coring and Sampling Procedures

Two peat cores were taken in the FSPSP for palynological/paleobotanical studies. The first peat core was taken in 1998 (FAK I98) from the end of a 300-m FSPSP boardwalk that penetrates into an undisturbed mixed cypress forest. The 43-cm-long core was frozen and cut into 1-cm slices for further analysis. A second core (FAK I02) was collected in 2002 at approximately 50 m from FAK I98

in a slightly deeper and wetter section of the swamp. This 83-cm core was cut in 0.5-cm slices for more detailed analysis. Both cores were taken with a manual 21-cm-diameter peat corer designed for minimal sediment disturbance (Clymo 1988). The obtained peat sequences consist of dark, organic-rich, non-laminated peat with abundant leaf and plant fragments. Tops were not consolidated and contained the best-preserved plant remains. The peat slices were sub-sampled for AMS ^{14}C dating, plant macrofossil-analysis, pollen analysis, and loss-on-ignition (LOI, FAK I02 only).

For AMS ^{14}C dating, leaf samples from 9 slices of core FAK I98 and 10 slices of core FAK I02 were picked out and determined to highest possible taxonomic level (see Table 1 for details). Material from tall canopy trees (*Quercus* and *Taxodium*) was used exclusively to eliminate reservoir effects from any old carbon outgassing and subsequent uptake by low-growing vegetation. The remains were cleaned from any rootlet material that might contaminate the samples, dried for 12 hr at 60 °C, and stored in dry and cool conditions.

Table 1 Samples and results of AMS ^{14}C dating.

Depth ^a (cm)	UtC # ^b	Material	Dry weight (mg)	$\delta^{13}\text{C}$ (‰)	^{14}C age $\pm 1 \sigma$ (yr BP)	Calibrated ages (cal AD $\pm 1 \sigma$)	Total error ^c (yr)
Core FAK I98							
4	11709	leaf (<i>Quercus</i> / <i>Acer</i>)	2.17	-30.7	-1018 \pm 34	1993 \pm 3 ^d	5
6	11710	leaf (<i>Quercus</i> / <i>Acer</i>)	1.31	-32.6	-877 \pm 27	1995 \pm 3 ^d	5
9	11711	leaf (<i>Quercus</i> / <i>Acer</i>)	2.08	-29.8	-1476 \pm 27	1985.5 \pm 2.5 ^d	4.5
12	11712	leaf (<i>Quercus</i> / <i>Acer</i>)	0.59	-29.7	-1522 \pm 31	1985 \pm 2 ^d	4
15	11713	leaf (<i>Quercus</i> / <i>Acer</i>)	0.45	-29.9	-1671 \pm 32	1983 \pm 2 ^d	4
20	11714	leaf (<i>Quercus</i> / <i>Acer</i>)	0.2	-28.1	-1507 \pm 70	1960.5 \pm 1.5 ^d	3.5
23	11715	seed (cf. <i>Quercus</i>)	2.29	-26.7	-353 \pm 29	1955 \pm 1 ^e	3
26	11716	leaflets (<i>Taxodium d.</i>)	1.01	-28.9	-100 \pm 70	1954 \pm 1 ^e	3
39	11717	leaflets (<i>Taxodium d.</i>)	1.35	-28.1	170 \pm 29	1937 \pm 17 ^e	19
Core FAK I02^f							
6	12080	leaflets / buds	14	-28.9	-756 \pm 34	1998.5 \pm 3.5 ^d	5.5
15	12081	leaflets / buds	9	-29.1	-840 \pm 40	1995.5 \pm 2.5 ^d	4.5
20	12082	leaflets / buds	9.9	-29.2	-825 \pm 33	1996 \pm 2 ^d	4
30	12083	leaflets / buds	7.4	-29.5	-1851 \pm 49	1981.5 \pm 1.5 ^d	3.5
40	12084	leaflets / buds	12.4	-27.9	-976 \pm 34	1957.5 \pm 1 ^e	3
50.5	12085	leaflets / buds	8.6	-28.7	146 \pm 45	1937 \pm 18 ^g	18
60	12114	leaflets / buds	9	-25.0	124 \pm 33	1919 \pm 15 ^g	15
70	12086	leaflets / buds	8.7	-28.0	-131 \pm 32	1954.5 \pm 0.5 ^{e,h}	2.5
75	12087	leaflets / buds	10.8	-27.9	66 \pm 47	1890 \pm 15 ^g	15
80.5	12088	leaflets / buds	8.9	-28.3	121 \pm 32	1881 \pm 10 ^g	10

^aDepths measured from core top; value is for underside of sample; sample thickness is 1.0 cm (FAK I98) and 0.5 cm (FAK I02).

^bLaboratory code: R.J. Van de Graaff laboratorium, Utrecht University.

^cTotal error consists of ^{14}C calibration error plus a 2-yr error factor covering sample thickness and transport/coring inaccuracies in samples calibrated with the bomb pulse.

^dCalibrated with bomb peak; data from Levin et al. (1994).

^eCalibrated with Cain and Suess (1974).

^fAll material for Core FAK I02 is *Taxodium distichum*.

^gWiggle-match with UWSY98, Stuiver et al. (1998).

^hSample identified as outlier; not used in construction of age-depth model.

¹⁴C Analysis

Plant remains were visually inspected using a binocular microscope, and attached allochthonous organic material was removed. The samples were pretreated according to an acid-alkali-acid procedure (Mook and Streurman 1983) to remove contaminating humic acids. The prepared material was combusted and the carbon dioxide formed was subsequently converted into graphite. The graphite targets were analyzed by the AMS facility of Utrecht University (van der Borg et al. 1997). The $\delta^{13}\text{C}$ values were obtained from analysis by the gas mass spectrometer at the Earth Sciences Department of Utrecht University, the Netherlands.

Pollen and Loss-on-Ignition (LOI)

Pollen from a weighed volumetric sediment sample was counted under the light microscope. A known amount of marker grains (*Lycopodium clavatum*) was added to the sample before standard palynological processing (Faegri and Iversen 1989) to allow for calculation of pollen concentration (grains/cm³) per sample. At a constant pollen influx on a decadal timescale (Middeldorp 1982; Hicks 2001), stability of sedimentation rates can be assessed.

Sediment samples for loss-on-ignition (LOI) were dried for 12 hr at 100 °C, and combusted at 550 °C and 1000 °C. Percent weight loss after each step is a measure of organic and carbonate fractions, respectively. Results of Dean (1974) show that organic material begins combustion at 200 °C and is completely ignited when temperature reaches 550 °C.

RESULTS

Results of the AMS ¹⁴C analysis are given in Table 1, represented as ¹⁴C ages. The obtained $\delta^{13}\text{C}$ values are between -32.6 and -25.0‰, in agreement with the characteristic range of $\delta^{13}\text{C}$ values in leaves and wood of canopy trees (Lockheart et al. 1998; Loader et al. 2003).

Results of the LOI and pollen counts are presented in Figure 2. As Australian pine (*Casuarina equisetifolia*) was introduced to Florida only after AD 1900 (Alexander and Crook 1974), the deepest occurrence of *C. equisetifolia* pollen in FAK I02 at 52.5 cm depth provides a maximum age of 100 calendar yr for the upper part of the core.

LOI at 550 °C (Figure 2) reveals a down-core decrease of the organic fraction, pointing to gradual decomposition of organic material. No sudden large influxes of clastic material were observed. Pollen concentrations show significant annual variability but no long-term trend; an apparent small decrease within the top 20 cm is in line with the expected low compaction at this level.

Calibration and Age Models

Twentieth century nuclear bomb testing created a distinct high-amplitude profile of elevated atmospheric ¹⁴C levels, which can be used to calibrate recent samples into calendar yr. For better comparability with our ¹⁴C ages, the ¹⁴C data were converted into ¹⁴C ages. This conversion creates a post-AD 1950 calibration curve with negative ¹⁴C ages (Figure 3a, atmospheric and tree-ring ¹⁴C data from Northern Hemisphere rural areas, adapted from Cain and Suess 1976; Levin et al. 1994; Stuiver et al. 1998).

In case of multiple curve intercepts, stratigraphic information (order and depth of samples) was used to either assign data to the up- or down-slope of the bomb pulse (Figure 3a). Assuming stratigraphic order represents a true chronology in FAK I98 and I02, all ages below -100 BP could be accurately calibrated (Table 1). ¹⁴C data calibrated in this manner have very small 1- σ errors (1–2 yr) as a result

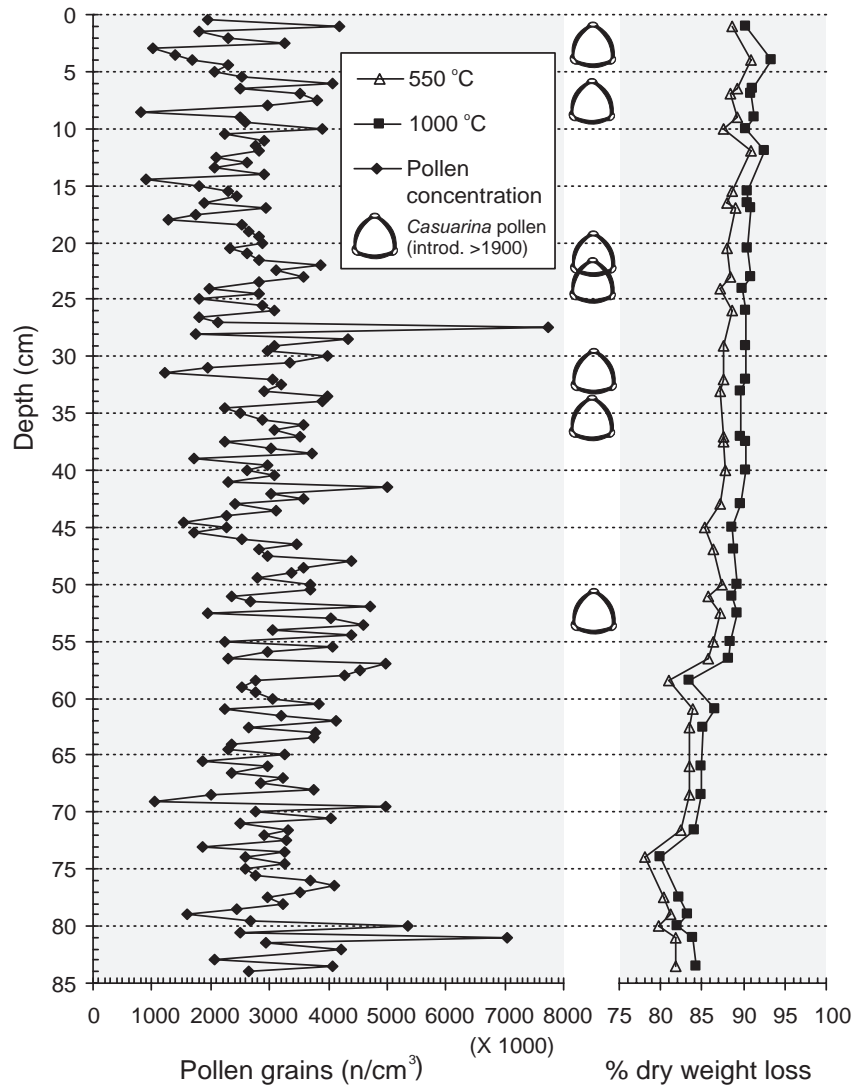


Figure 2 Loss-on-ignition (LOI) and pollen concentrations of core FAK I02. Occurrences of *Casuarina equisetifolia* pollen indicate post-AD 1900 sediment deposition.

of the well-determined ¹⁴C bomb pulse. Especially evident is the fourfold better precision of the ¹⁴C dates calibrated post-AD 1950 in comparison with the single pre-AD 1950 date in core FAK I98 (Figure 3b).

A smooth transition could be obtained between the pre- and post-AD 1950 sections of core FAK I02 (Figure 4a) by wiggle-matching the pre-bomb ¹⁴C dates. The core was well compacted below 25 cm (taking pollen concentration and LOI data into account, Figure 2); thus, a linear accumulation rate could be expected below this level. Four ¹⁴C data were calibrated by wiggle-matching with the high-resolution UWSY98 curve (Stuiver et al. 1998). The best fit was obtained visually by varying the slope between and position of the ¹⁴C dates relative to the calibration data. The accumulation rate thus found is a continuation of values encountered in the upper half of core FAK I02 (0.53 cm/yr,

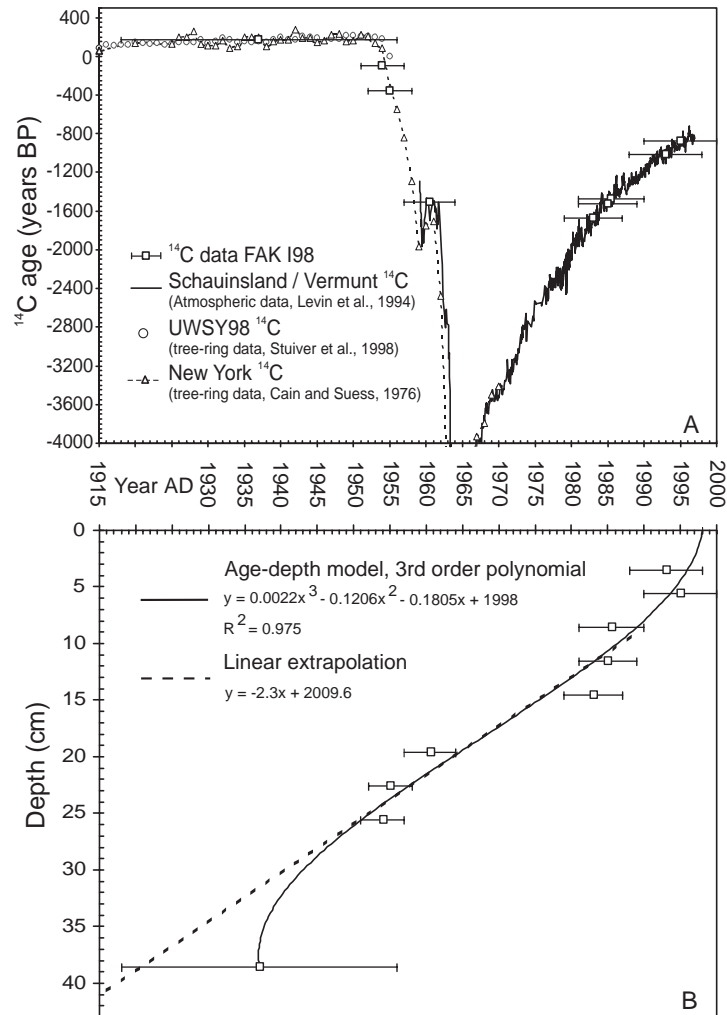


Figure 3 Modern ^{14}C bomb-peak anomaly used for calibrating recent samples of core FAK I98. (a) Calibrated samples are used to construct an age-depth model (b). x = depth in cm, y = age in yr AD (axes inverted for comparison between Figures a and b). Errors shown contain an additional 2-yr factor for coring/sampling inaccuracies.

Figure 4b), in agreement with the stable sedimentation conditions below the top 25 cm and generally undisturbed setting of the site. Since no intercept is determined with wiggle-matching, error ranges were obtained by calculating the minimum value at which the ^{14}C measurement would fall outside the UWSY98 curve when shifted along the calendar axis.

Age models for both cores were obtained by fitting polynomial curves through the calibrated ^{14}C data, while fixing the core top at the year of collection (Figures 3b and 4b). In FAK I02, 1 data point was excluded from the age model since it most likely represents an outlier. The resulting age determination range is 90 calendar yr for FAK I98 and 130 calendar yr for FAK I02 (see discussion).

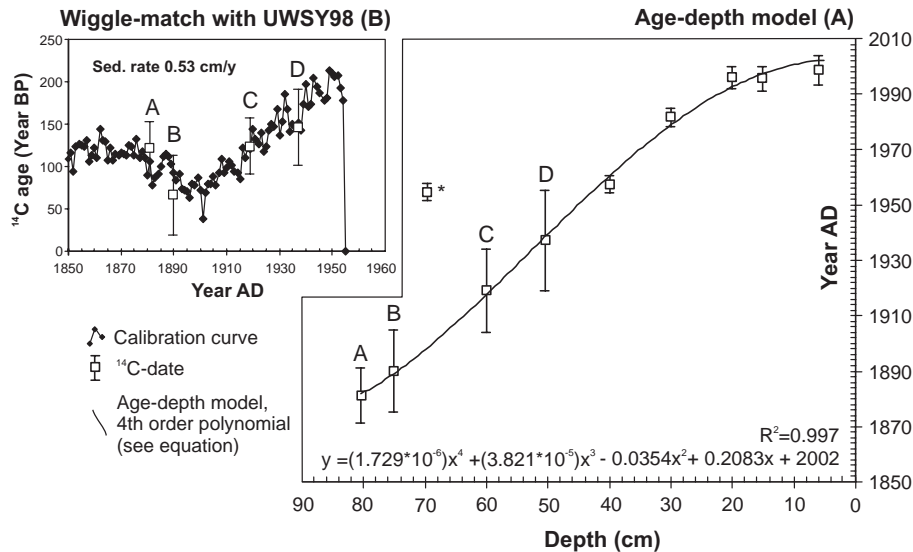


Figure 4 Age-depth model of core FAK I02 (a) containing data calibrated with bomb-peak and wiggle-matching approaches (Figure b, samples indicated A–D), x = depth in cm, y = age in yr AD. Errors shown contain an additional 2-yr factor for coring/sampling inaccuracies when calibrated with the bomb-peak. The sample marked with an asterisk (*) was considered an outlier and was not used for constructing the age-depth model (see discussion).

DISCUSSION

Error Factors

Since ¹⁴C data calibrated with the bomb pulse anomaly have very small 1-σ errors (1–2 yr), the accuracy of coring and sampling contributes significantly to the total error of the date. To account for these effects in the cores studied, a 2-yr error factor was added to the 1-σ interval of ¹⁴C data calibrated by this method (Table 1). Possible artifacts of coring procedure, transport, sampling precision, and resolution are accounted for in this additional factor. The improvement by higher sampling resolution and precision of FAK I02 compared to FAK I98 (with 0.5-cm and 1-cm sampling intervals, respectively) is apparent from a better fit of the age-depth model in FAK I02.

Since in core FAK I98 only 1 data point is present in the pre-AD 1950 period, the lower limit of the age-depth curve cannot be accurately determined. Hence, an unrealistic age-reversal is present that cannot be explained from the ¹⁴C and LOI data of the nearby core FAK I02. A linear extrapolation of the polynomial function was, therefore, used below 27 cm. Based on the local sedimentation regime, this is considered the most realistic age model available for core FAK I98.

The outlier identified in FAK I02 is possibly due to down-sliding of individual leaves during coring. However, it most likely presents an isolated case since the outside of the core was removed during sample preparation.

The compaction difference between the unconsolidated top and lower sediment section is very apparent in the age models of both cores (Figures 3b and 4a). This change is less obvious from the pollen concentrations in the FAK I02 core top (Figure 2). The pollen sub-sampling method used (small volumetric punch core) most likely caused some additional compaction, not fully reflecting the loose non-decomposed nature of the youngest sediment. The lower pollen concentration in the

top is apparent, however, and therefore, in agreement with the core descriptions and the depth-models obtained.

Pre-bomb samples from areas with more than average fossil fuel combustion (i.e. cities, industries) can show a locally enhanced Suess effect (Cain and Suess 1976). For the early 20th century, these local effects could create additional uncertainty that cannot be resolved with high precision unless a calibration data set from the same area is present or industrial areas are avoided.

Use of Method

Although southern Florida is known to be highly sensitive to changes in the ENSO system, systematic paleoecological and paleoclimatological investigations on very high temporal resolution was hampered until now by the insufficient accuracy of age assessments for the peat deposits by conventional dating methods as ^{137}Cs and ^{210}Pb (Cohen et al. 1999). By following the approach presented here, the homogenous organic-rich peat accumulations from this key area can be dated with far greater accuracy. The combined wiggle-match and bomb-pulse calibration of ^{14}C data of the peat deposits from South Florida has resulted in extremely accurate age models, especially for core FAK I02. Despite uncertainties about the different error factors mentioned above, the precision is still very high with maximum errors of 5 yr for the post-AD 1950 period. The quality of the age assessments improves both the validation procedure for new proxies and their applicability.

Paleoecological proxies are commonly calibrated by comparison with surface samples as modern analogues. However, this modern analogue approach often suffers from error factors that arise from geographically widespread data sets. The high dating precision obtained here provides the opportunity for direct comparison of proxy data with measured historical meteorological records, thus enabling secure proxy validation and calibration in a restricted geographical area.

The high accumulation rates in both cores studied, with approximately 0.5 cm/yr in the main part of the sections, allows the build-up of proxy records for the time beyond the range of instrumental measurements, with a temporal resolution high enough to detect changes occurring on multi-annual to sub-decadal scale.

In addition, we have obtained a smooth transition between samples calibrated by the bomb pulse and the UWSY98 data set. Therefore, the time frame where ^{14}C dating is commonly applied can be extended to include the 20th century.

The dating strategy outlined above thus meets the requirements for sound proxy validation and application, which is of prime importance in actualizing research fields dealing with dynamic climate systems that vary on multi-annual to centennial timescales, such as ENSO.

ACKNOWLEDGEMENTS

The authors wish to thank staff members of the Fakahatchee Strand Preserve State Park for their field assistance and overall support, in particular, Mike Owen and Ken Alvarez of the Florida Park Service. Ton van Druten, Wolfram Kürschner, Dan Zwart, and Claire Schreurs are thanked for their fieldwork assistance. We greatly acknowledge the comments of the reviewer on the manuscript. This study was supported by the Council of Earth and Life Sciences, Netherlands Organization for Scientific Research. This is publication number 2004.05.02 of the Netherlands School of Sedimentary Geology (NSG).

REFERENCES

- Alexander TJ, Crook AG. 1974. Recent vegetational changes in southern Florida. In: Gleason PJ, editor. *Environments of South Florida: Present and Past*. Miami: The Miami Geological Society. p 61–72.
- Appleby PG. 2001. Chronostratigraphic techniques in recent sediments. In: Last WM, Smol JP, editors. *Basin Analysis, Coring and Chronological Techniques*. Dordrecht, the Netherlands: Kluwer Academic. p 171–203.
- Birks HH, Birks HJB. 2003. Reconstructing Holocene climates from pollen and plant macrofossils. In: Mackay AW, Battarbee RW, Birks HJB, Oldfield F, editors. *Global Change in the Holocene*. London: Arnold publishers. p 342–57.
- Burns LA. 1984. Productivity and water relations in the Fakahatchee Strand of South Florida. In: Ewel KC, Odum HT, editors. *Cypress Swamps*. Gainesville: University Press of Florida. p 318–33.
- Cain WF, Suess HE. 1976. Carbon 14 in tree rings. *Journal of Geophysical Research* 81:3688–94.
- Clymo RS. 1988. A high-resolution sampler of surface peat. *Functional Ecology* 2(3):425–31.
- Cohen AD, Gage CP, Moore WS. 1999. Combining organic petrography and palynology to assess anthropogenic impacts on peatlands Part 1. An example from the northern Everglades of Florida. *International Journal of Coal Geology* 39:3–45.
- Cronin TM, Dwyer GS, Schwede SB, Vann CD, Dowsett H. 2002. Climate variability from the Florida Bay sedimentary record: possible teleconnections to ENSO, PNA and CNP. *Climate Research* 19:23–45.
- Dean WE. 1974. Determination of carbonate and organic matter in calcareous sediments and sedimentary rocks by loss on ignition: comparison with other methods. *Journal of Sedimentary Petrology* 44(1):242–8.
- Faegri K, Iversen J. 1989. *Textbook of Pollen Analysis*. New York: Wiley and Sons. 340 p.
- Hicks S. 2001. The use of annual arboreal pollen deposition values for delimiting tree-lines in the landscape and exploring models of pollen dispersal. *Review of Palaeobotany and Palynology* 117:1–29.
- Jensen C, Kunzendorf H, Vorren K-D. 2002. Pollen deposition rates in peat and lake sediments from the *Pinus sylvestris* L. forest-line ecotone of northern Norway. *Review of Palaeobotany and Palynology* 121:113–32.
- Levin I, Kromer B, Schoch-Fischer H, Bruns M, Munnich M, Berdau D, Vogel JC, Munnich KO. 1994. Delta ¹⁴CO₂ records from two sites in Central Europe. In: Boden TA, Kaiser DP, Sepanski RJ, Stoss FW, editors. *Trends 93-A* compendium of data on global change p 203–22 and online updates (Online Trends). Oak Ridge: Carbon Dioxide Information Analysis Centre. Oak Ridge National Laboratory.
- Loader NJ, Robertson I, McCarroll D. 2003. Comparison of stable carbon isotope ratios in the whole wood, cellulose and lignin of oak tree rings. *Palaeogeography, Palaeoclimatology, Palaeoecology* 196:395–407.
- Lockheart MJ, Poole I, van Bergen PF, Evershed RP. 1998. Leaf carbon isotope compositions and stomatal characters: important considerations for palaeoclimate reconstructions. *Organic Geochemistry* 29(4):1003–8.
- Middeldorp AA. 1982. Pollen concentration as a basis for indirect dating and quantifying net organic and fungal production in a peat bog ecosystem. *Review of Palaeobotany and Palynology* 37(3–4):225–82.
- Mook WG, Streurman HJ. 1983. Physical and chemical aspects of radiocarbon dating. In: Mook WG, Waterbolk HT, editors. *Proceedings of the First International Symposium on ¹⁴C and Archaeology*. *PACT* 8:31–55.
- Stuiver M, Reimer PJ, Braziunas TF. 1998. High-precision radiocarbon age calibration for terrestrial and marine samples. *Radiocarbon* 40(3):1127–51.
- van der Borg K, Alderliesten C, de Jong AFM, Van den Brink A, de Haas AP, Kersemaekers HJH, Raaymakers JEMJ. 1997. Precision and mass fractionation in ¹⁴C analysis with AMS. *Nuclear Instruments and Methods in Physics Research B* 123(1–4):97–101.
- Watts WA, Hansen BCS. 1994. Pre-Holocene and Holocene pollen records of vegetation history from the Florida peninsula and their climatic implications. *Palaeogeography, Palaeoclimatology, Palaeoecology* 109:163–76.

COMPLEXITY OF SOIL ORGANIC MATTER: AMS ^{14}C ANALYSIS OF SOIL LIPID FRACTIONS AND INDIVIDUAL COMPOUNDS

Janet Rethemeyer^{1,2} • Christiane Kramer³ • Gerd Gleixner³ • Guido L B Wiesenberg⁴ • Lorenz Schwark⁴ • Nils Andersen¹ • Marie-J Nadeau¹ • Pieter M Grootes¹

ABSTRACT. Radiocarbon measurements of different lipid fractions and individual compounds, isolated from soil samples collected on 2 different agricultural long-term study sites, located in the rural area of Rothalmünster (Germany) and in the city of Halle/Saale (Germany), were analyzed to obtain information about sources and the stability of soil organic matter (SOM). Different lipid compound classes were isolated by automated solvent extraction and subsequent medium-pressure liquid chromatography. Generally, ^{14}C contents of lipid compound classes from topsoil samples of maize plots at Rothalmünster are close to the modern atmospheric ^{14}C content. Lower ^{14}C values of aliphatic and aromatic hydrocarbons isolated from neutral lipids suggest a contribution of old carbon to these fractions. In contrast, ^{14}C values of bulk soil (52 pMC) as well as isolated lipid classes from Halle are highly depleted. This can be attributed to a significant contribution of fossil carbon at this site. Extremely low ^{14}C contents of aromatic (7 pMC) and aliphatic hydrocarbons (19 pMC) reflect the admixture of fossil hydrocarbons at the Halle site. Individual phospholipid fatty acids (PLFA), which are used as a proxy for viable microbial biomass, were isolated by preparative capillary gas chromatography (PCGC) from topsoils at Rothalmünster and Halle. PLFA ^{14}C values are close to atmospheric ^{14}C values and, thus, indicate a clear microbial preference for relatively young SOM. At Rothalmünster, the ^{14}C concentration of short-chain unsaturated PLFAs is not significantly different from that of the atmosphere, while the saturated PLFAs show a contribution of sub-recent SOM extending over the last decades. At Halle, up to 14% fossil carbon is incorporated in PLFAs *n*-C17:0 and *cy*-C18:0, which suggests the use of fossil carbon by soil microorganisms. Moreover, it can be concluded that the ^{14}C age of soil carbon is not indicative of its stability.

INTRODUCTION

Soil organic matter (SOM) is an important factor in the global carbon cycle. As SOM is composed of a complex mixture of organic components in various stages of decomposition and transformation, the objective of diverse studies is to differentiate between different organic matter pools or components to be able to follow carbon transformation and sequestration in the soil system.

Radiocarbon measurements have been helpful to classify bulk SOM separated into physically- or chemically-defined organic matter pools (O'Brien 1986; Balesdent 1987; Trumbore et al. 1990; Trumbore 1993; Trumbore and Zheng 1996). ^{14}C concentrations of SOM pools represent the mean residence time and, thus, the stability of the organic matter (Scharpenseel and Becker-Heidmann 1992; Trumbore 1996). However, most physical and chemical SOM fractions still consist of a complex mixture of organic molecules with different origin and decomposability. Additionally, SOM properties may be influenced by the contribution of anthropogenic pollutants, such as fossil fuel-derived carbon, which complicates the interpretation of the ^{14}C data (Rumpel et al. 2003; Rethemeyer et al., forthcoming). Our results on SOM samples from Halle showed this fossil contamination persisted to varying degrees in the usual physical and chemical fractions, including a lipid and phospholipid fraction (Rethemeyer et al., forthcoming). More specific separation methods are thus needed.

Lipids, representing 4–8% of SOM, are assumed to be of high importance for SOM stabilization. In soils, they mainly derive from plants and microorganisms, but they also can be of anthropogenic ori-

¹Leibniz-Laboratory for Radiometric Dating and Isotope Research, University of Kiel, Germany.

²Corresponding author. Email: jrethemeyer@leibniz.uni-kiel.de.

³Max Planck Institute for Biogeochemistry, Jena, Germany.

⁴Geological Institute, University of Cologne, Germany.

gin (Gregorich et al. 1996; Lichtfouse et al. 1997). Soil lipids are a relatively stable organic carbon fraction that contain several biomarker compounds which can be related to the input of plant constituents to the soil and to their transformations (Lichtfouse et al. 1994, 1997; Bol et al. 1996; van Bergen et al. 1997).

Compound-specific accelerator mass spectrometry (AMS) ^{14}C analysis is a modern technique which can help to exclude contaminating carbon sources, and to obtain information on the origin and biodegradability of organic matter in soils and sediments (Eglinton et al. 1996, 1997; Uchida et al. 2000). Different biomarker compounds, which can be attributed to specific sources, have been used to study pathways of organic carbon in soils and sediments (Hedges 1991; Lichtfouse et al. 1997; Eglinton et al. 1997). In this study, we combined organic geochemical isolation methods with AMS ^{14}C measurements to identify sources of SOM and, moreover, to find fractions that are not influenced by anthropogenically-derived, fossil carbon contamination and, thus, can be used to study C dynamics in soils. Different chemically-defined lipid compound classes (Willsch et al. 1997; Wiesenberg et al., forthcoming a), separated by medium-pressure liquid chromatography, as well as individual phospholipid fatty acids isolated by preparative capillary gas chromatography, were analyzed. PLFAs are integral components of the cell membrane. They are degraded within days or weeks after cell death (White et al. 1979) and, thus, can be used as indicators of viable microbial biomass in soils (Frostegård and Bååth 1996; Zelles 1999; Petsch et al. 2001). The investigations were done on soil samples from 2 agricultural long-term field trials located in a rural and in an industrialized region of Germany.

MATERIALS AND METHODS

Study Sites and Soil Sampling

Samples from 2 study sites in Germany with agricultural long-term field experiments were used for the investigations. The study site at Rotthalmünster is located in a rural area in the south of Germany. The mean annual temperature in this region is 8.2 °C and the mean annual precipitation is 890 mm. The soil is a Haplic Luvisol (FAO 1990) derived from loess (10% sand, 73% silt, 17% clay). Samples were taken from a plot with continuously cropped maize since 1979. The field trials of the University of Halle are located in a heavily industrialized region in the middle eastern part of Germany. The mean annual temperature is 9.2 °C and the mean annual precipitation is 465 mm. The soil type is a Haplic Phaeozem (FAO 1990) derived from sandy loess consisting of about 70% sand, 20% silt, and 10% clay (Merbach et al. 1999). Soil samples from plots with continuous rye since 1878 and continuous maize since 1961 were used for this study.

Samples of the field trials in Rotthalmünster were collected in 2002, and from the experiments in Halle in 2000. Soil samples of the ploughed surface soil (0–30 cm) were taken with a spade from different locations of each plot and mixed to obtain a representative sample. Mixed subsoil samples, taken from 8–10 locations per plot, were collected by corer.

Extraction and Separation of Lipid Compound Classes

The extraction of total lipids from bulk soil samples was done via accelerated solvent extraction (Dionex ASE 200) at the University of Cologne. Each sample of 150 g of dried soil was distributed into 5 extraction vessels. They were extracted twice for 20 min at 50 bar and at a temperature of (1) 75 °C, and (2) 140 °C, using a mixture of dichloromethane and methanol (DCM:MeOH: 93:7 by volume). The 5 extracts and both isolation steps were combined resulting in the total lipid extract (Ex) (Wiesenberg et al., forthcoming a).

Total lipids were separated by medium-pressure liquid chromatography (H-MPLC) into 6 fractions of different polarity (Willsch et al. 1997): neutral lipids (N), medium polar compounds (F), high molecular lipids (W), acid fraction (H), basic fraction (Q), and high polar fraction (V). The neutral fraction (N) was further separated by a second MPLC described by Radke et al. (1980), resulting in 3 additional fractions: aliphatic- (A) and aromatic hydrocarbons (B), and low polar heterocompounds (C). The extracts were evaporated to dryness using rotary evaporation.

Purity of the individual compound classes was checked by gas chromatography-mass spectrometry analysis (Wiesenberg et al., forthcoming a). A small proportion of the total extract (Ex) (<15%) remained insoluble in DCM or could not be recovered from the MPLC columns.

Isolation of Phospholipid Fatty Acids

Fresh soil samples were shaken for 3 hr with chloroform, methanol, and a phosphate buffer (2.5:5:2.5 by volume). The resulting total lipid extract was then separated into 3 fractions by chromatography using silica gel columns conditioned with chloroform. Neutral-, glyco-, and phospholipids were eluted with chloroform, acetone, and methanol (White et al. 1979; Zelles et al. 1993). The phospholipid fraction was derivatized to fatty acid methyl ester by mild alkaline methanolysis as described by White et al. (1979). Individual saturated- and monounsaturated-PLFA methyl esters were isolated at the Max Planck Institute for Biogeochemistry (Jena, Germany) by PCGC (HP 6890 GC, Gerstel preparative trapping device). To obtain sufficient quantities (about 100 µg carbon) for AMS ^{14}C measurements, only the most abundant PLFAs (*i/a*-C15:0, *n*-C16:0, *cy*-C16:0, *n*-C18:0, *cy*-C18:0, *n*-C16:1, *n*-C17:1, and *n*-C18:1) were isolated.

The isolation procedure and sample preparation for AMS were checked repeatedly using fatty acid methyl ester standards in the sample size range of the isolated PLFAs. The standards had ^{14}C contents of about 70 pMC (*n*-C28:0) and about 110 pMC (*n*-C12:0, *n*-C18:0), allowing the detection of both modern and fossil contamination (C Kramer, personal communication). No significant contamination by background was detected. Since 1 carbon atom is added during derivatization, ^{14}C results have to be corrected by isotopic mass balance calculation:

$$^{14}\text{C}_{\text{free}} = (C_n + 1) / C_n \cdot ^{14}\text{C}_{\text{ester}} - 1/C_n \cdot ^{14}\text{C}_{\text{Methanol}} \quad (1),$$

where $^{14}\text{C}_{\text{free}}$ is the ^{14}C concentration of the PLFA without the contribution of the methyl group, $^{14}\text{C}_{\text{ester}}$ is the measured ^{14}C concentration of its methyl ester ($^{14}\text{C}_{\text{Methanol}} = 0.1$ pMC), and C_n represents the number of carbon atoms of the PLFA prior to derivatization. PLFA methyl ester, subsequently abbreviated as PLFA, are designated according to A:B, with *A* indicating the number of carbon atoms and *B* the number of double bonds. The prefixes indicate the following: *n*—unbranched chain; *i*—iso-; *a*—anteiso-branching; and *cy*—cyclopropyl. We calculated mean values of individual PLFAs from 2 cropping variants of each site (Rotthalmünster: maize, wheat; and Halle: maize, rye) if they did not show statistically significant differences (1- σ level).

Sample Treatment for AMS

The dried lipid compound classes were dissolved again using dichloromethane and methanol, depending on the polarity of the fraction. Lipid classes and PLFAs were pipetted in solution into pre-combusted (4 hr, 900 °C) quartz combustion tubes. The solvent was removed by evaporation overnight and, in case of incomplete removal, under a gentle N_2 stream. Samples with carbon contents of >500 µg were combusted with 450 mg CuO and 150 mg silver wool. For combustion of small samples containing <500 µg of carbon, reduced portions of 75 mg CuO and 30 mg silver were added. The tubes were evacuated to a pressure of about 10^{-4} mbar while immersed in dry ice/ethanol

to avoid possible loss of highly volatile compounds, and subsequently flame-sealed. Samples were combusted at 900 °C for 4 hr. The resulting CO₂ was collected in a cold trap with liquid nitrogen, and subsequently reduced to graphite with a 10% excess of hydrogen at 600 °C over an iron catalyst (Nadeau et al. 1997, 1998). The AMS measurements were made at the Leibniz Laboratory in Kiel, Germany. ¹⁴C data are reported as percent modern carbon (pMC) with 1-σ measurement uncertainty. The measurement precision lies in the range of 0.3 pMC for modern, standard-sized (about 1 mg C) samples (Nadeau et al. 1998). The precision achievable for small samples is worse, as the relative importance of the blank correction increases and its uncertainty (about 1/3 of the blank value) makes an ever larger contribution to the overall measurement uncertainty of small samples. Figure 1 shows the 1-σ uncertainties for our PLFA samples with carbon weights of 40 to 340 μg C (between 3.9 to 0.6 pMC).

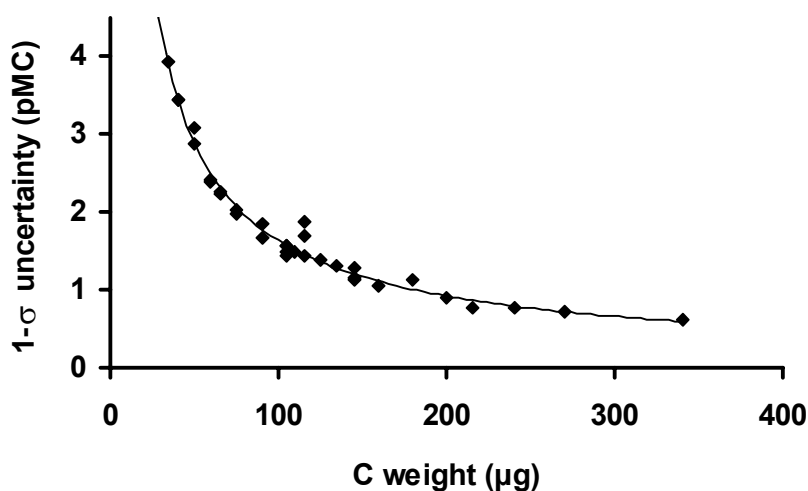


Figure 1 Uncertainty (1 σ) for PLFAs as a function of sample carbon weight. All PFLA single measurements are displayed.

RESULTS AND DISCUSSION

Lipid Compound Classes

¹⁴C concentrations of the different lipid compound classes from surface soil samples of the field trials at Rotthalmünster and Halle are compared in Figure 2. ¹⁴C values of compound classes at Rotthalmünster are close to the modern atmospheric ¹⁴C level (Figure 2a). The total lipid extract (Ex) is 3.3 ± 0.7% depleted in ¹⁴C compared to the bulk soil (S) (106.5 pMC). ¹⁴C contents of the isolated compound classes range from 98.7 ± 0.3 pMC for the neutral lipids (N), with closely similar values for the acid (H) and basic fraction (Q), to 105 pMC for the high molecular fraction (W). Aliphatic (A) and aromatic hydrocarbons (B), isolated from the neutral lipids (N), have a low ¹⁴C content of 44 ± 0.3 pMC (A) and 25 ± 1.7 pMC (B), which may be caused by a contribution of fossil carbon to these fractions. These ¹⁴C-depleted fractions represent only a small proportion (about 0.5% [B] to 6.0% [A]) of the total extract. Main constituents (about 85%) of neutral lipids are low polar heterocompounds (C) with a relatively high ¹⁴C content of 103.4 ± 0.3 pMC. Since N was subdivided into fractions A, B, and C, the weighted mean ¹⁴C concentration of the 3 fractions should be equal to the ¹⁴C content of N. Actually, the resulting ¹⁴C value, calculated by mass balance of fractions A, B, and C, suggests a small loss of about 4.4% modern carbon compared to the higher

^{14}C content of the directly measured fraction N. This may result from volatilization of substances during solvent evaporation and/or incomplete recovery in the preparation of fractions A, B, and C.

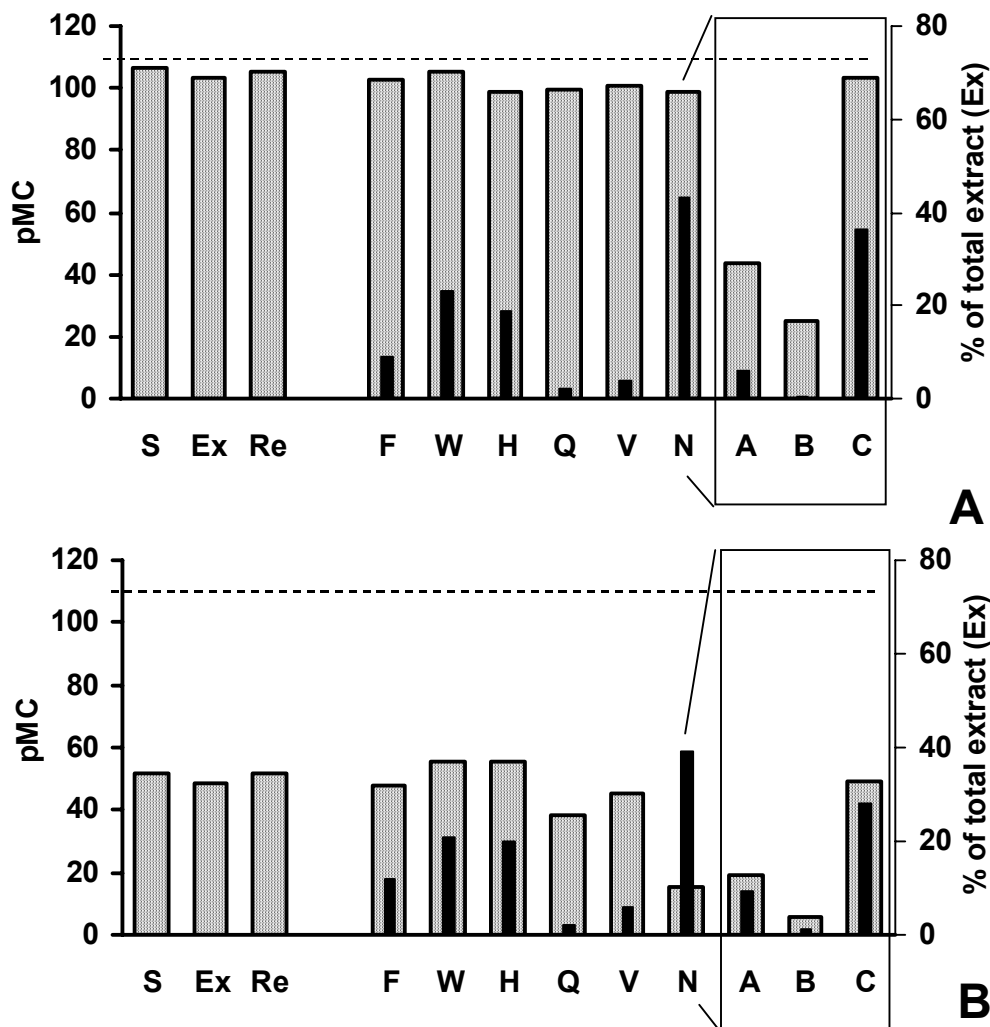


Figure 2 ^{14}C values of lipid compound classes from topsoil samples (0–30 cm) of (a) the rural site at Rotthalmünster (maize plots) and (b) the urban site at Halle (continuous rye). The black bars refer to the right y-axis. The dashed line represents the ^{14}C content of the atmosphere in 2000. Lipid compound classes are designated according to the following: F-medium polar compounds; W-high molecular lipids; H-acid fraction; Q-basic fraction; V-high polar fraction; and N-neutral fraction. Other abbreviations display: S-bulk soil; Ex-total lipid extract; and Re-residue after extraction.

In contrast to the rural, uncontaminated Rotthalmünster site, lipid compound classes from surface soil samples of the rye plots at Halle show highly depleted ^{14}C values (Figure 2b). Low ^{14}C concentrations were measured in aromatic (B: 5.7 ± 0.3 pMC) and aliphatic hydrocarbons (A: 19 ± 0.2 pMC) isolated from the neutral lipids, which can be attributed to a high contribution of old, ^{14}C -free carbon. Wiesenberg et al. (forthcoming b), using molecular markers combined with $\delta^{13}\text{C}$ analysis, showed that lignite, derived from nearby open-pit mining, and coke particles, from steam trains running close to the experimental site until the 1980s, are major sources of fossil carbon at

Halle. Fossil carbon compounds contribute preferentially to the aromatic and aliphatic hydrocarbon fraction. Additionally, significantly higher proportions of aromatic (1.2%) and aliphatic hydrocarbons (9.4%) were found in the total extract from Halle in comparison to that from Rotthalmünster. ^{14}C concentrations of about 55 ± 0.2 pMC, measured in the acid (H) and the high molecular fraction (W), reflect a lower contamination of these more functionalized fractions which, however, still include about 50% fossil carbon.

The ^{14}C data of lipid compound classes from the rural Rotthalmünster and the urban Halle site revealed that the isolated fractions are composed of a mixture of substances originating from natural sources as well as from anthropogenic sources with quite different ^{14}C contents. Furthermore, these fractions have shown to be highly susceptible to contaminations such as fossil fuel-derived carbon. To exclude contaminations as observed in Halle, it is essential to isolate and analyze compounds on the molecular level.

Phospholipid Fatty Acids

PLFAs were obtained from the maize and wheat plots at Rotthalmünster and from maize and rye at Halle. As the sample quantities were extremely small (40 to 340 μg of carbon), the standard deviations were relatively large, and no statistically significant differences were visible between maize and wheat at Rotthalmünster and maize and rye at Halle. The weighted averages of the ^{14}C content of individual phospholipid fatty acids at Rotthalmünster and Halle are given with their (reduced) uncertainty for each site in Figure 3, displayed in relation to the atmospheric ^{14}C level of about 109 pMC in 2000 (Schauinsland, Germany; B Kromer, personal communication).

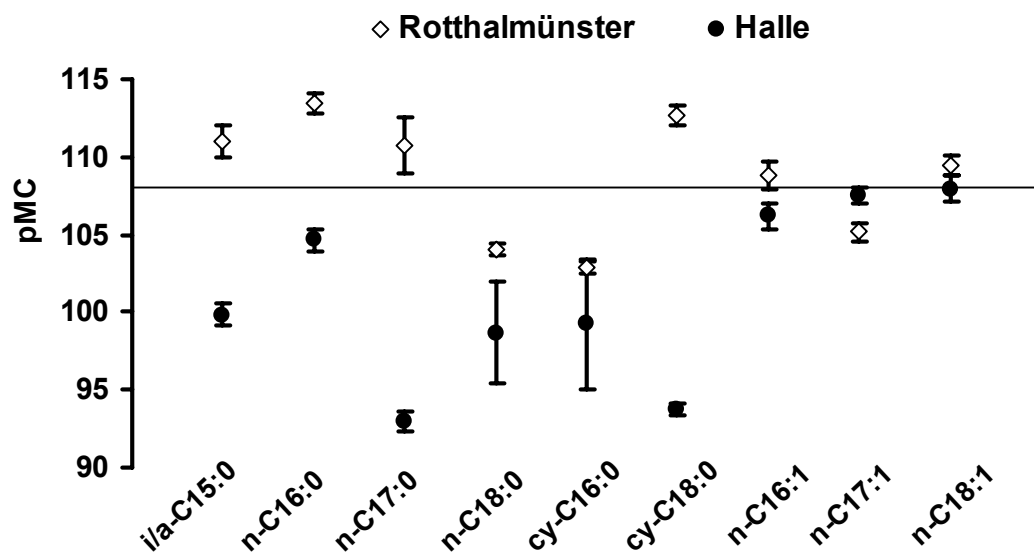


Figure 3 Comparison of calculated ^{14}C concentrations of individual PLFAs from surface soil samples (0–30 cm) collected at Rotthalmünster (average of maize, wheat values) and Halle (average of maize, rye). The error bars show the calculated uncertainties for these averages and for single values of *n*-C17:0 from Rotthalmünster (wheat) and *cy*-C16:0 and *n*-C18:0 from Halle (maize). The x-axis displays the atmospheric ^{14}C content in 2000.

In contrast to the extremely low ^{14}C content of the bulk soil (52 pMC) at Halle, the ^{14}C values of its PLFAs are surprisingly high, ranging from about 93 pMC to 108 pMC. The relatively low ^{14}C contents of monounsaturated PLFAs, particularly *n*-C17:0 (93.0 ± 0.6 pMC) and *cy*-C18:0

(93.8 ± 0.4 pMC), still suggest an assimilation of fossil, most probably lignite-derived carbon by soil microorganisms. Assuming that the input materials are fresh crop residues with atmospheric ^{14}C levels, the proportion of fossil carbon can be estimated by a mass balance calculation to amount to about 14% in *n*-C17:0 and *cy*-C18:0, and about 9% in *n*-C18:0, *cy*-C16:0, and *i/a*-C15:0 fatty acids from Halle soil. The saturated PLFAs *i/a*-C15:0, *n*-C16:0, *n*-C17:0, and *cy*-C18:0 yield statistically significant ($2\text{-}\sigma$ criterion) differences in ^{14}C values in Halle and Rotthalmünster. At Rotthalmünster, their ^{14}C levels, with the exception of *n*-C17:0, are significantly above that of the present atmosphere, reflecting the contribution of organic material from the last 40 yr containing bomb ^{14}C . Relatively low ^{14}C values of these PLFAs at Halle reflect the incorporation of fossil, supposedly refractory carbon. The pMC values of the *n*-C18:0 and *cy*-C16:0 PLFAs at Halle and Rotthalmünster are not statistically different, but are both significantly below atmospheric ^{14}C levels. This suggests the contribution of pre-bomb SOM to these compounds as fossil carbon contamination is low or absent at Rotthalmünster. At both sites, the monounsaturated PLFAs show no significant difference from each other, nor from the atmospheric ^{14}C level at their time of growth. These PLFAs are apparently synthesized exclusively from fresh organic material. Thus, ^{14}C data of the different PLFAs show an interesting range of substrate use from fresh SOM (monounsaturated PLFAs) via a preference for material from the last decades to pre-bomb SOM.

CONCLUSIONS

^{14}C measurements of lipid biomarkers, such as different compound classes, obtained by medium-pressure liquid chromatography and individual phospholipid-derived fatty acids, and isolated by preparative gas chromatography, have proven valuable to identify sources of organic carbon.

^{14}C concentrations of lipid compound classes reflect their heterogeneous composition, consisting of a mixture of material ranging from plant-derived substances with modern ^{14}C concentrations, to old, ^{14}C -free compounds. At the field trial in Halle, particularly, the neutral fraction, which contains aromatic and aliphatic hydrocarbons and low polar heterocompounds, was found to be strongly influenced by fossil carbon (Wiesenberg et al., forthcoming b). The highest proportions of most probably fossil fuel-derived carbon were detected in the aromatic and aliphatic hydrocarbon fraction, resulting in extremely low ^{14}C contents of about 6 pMC (aromatic) and 19 pMC (aliphatic fraction). In contrast, these fractions are less abundant and, moreover, contain higher portions of younger, vegetation-derived substances at Rotthalmünster. Lipid classes that are supposed to consist of recent plant constituents, such as the carboxylic acid fraction and the high molecular fraction containing long-chain wax esters, yield higher values of about 55 pMC at Halle.

^{14}C data of individual PLFAs, which are not supposed to be influenced by anthropogenic contaminations, suggest a preference of soil microorganisms for the uptake of modern organic carbon. Depleted ^{14}C contents of saturated PLFA at Halle indicate an incorporation of up to 14% fossil carbon. This ability of soil microorganisms to use old and supposedly refractory material as carbon sources (Petsch et al. 2001; Rumpel et al. 2003) complicates the use of ^{14}C as a tracer for soil carbon turnover if fossil carbon is present. It also questions the concept of a pool of refractory organic compounds, used in soil carbon models, that are biologically inert (Falloon et al. 1998).

ACKNOWLEDGEMENTS

This study was financially supported by grants of the Deutsche Forschungsgemeinschaft within the Priority Program 1090 "Soils as sources and sink for CO_2 —mechanisms and regulation of organic matter stabilization in soils." We thank the Leibniz staff for the AMS ^{14}C measurements and Ann McNichol for her constructive review.

REFERENCES

- Balesdent J. 1987. The turnover of soil organic fractions estimated by radiocarbon dating. *The Science of the Total Environment* 62:405–8.
- Bol R, Huang Y, Merdith JA, Eglinton TI, Harkness DD, Ineson P. 1996. The ^{14}C age and residence time of organic matter and its lipid constituents in a stagnohumic gley soil. *European Journal of Soil Science* 47: 215–22.
- Eglinton TI, Aluwihare LI, Bauer JE, Druffel ERM, McNichol AP. 1996. Gas chromatographic isolation of individual compounds from complex matrices for radiocarbon dating. *Analytical Chemistry* 68:904–12.
- Eglinton TI, Benitez-Nelson BC, Pearson A, McNichol AP, Bauer JE, Druffel ERM. 1997. Variability in radiocarbon ages of individual organic compounds from marine sediments. *Science* 277:796–9.
- Falloon P, Smith P, Coleman K, Marshall S. 1998. Estimating the size of inert organic matter pool for use in the Rothamsted Carbon Model. *Soil Biology and Biochemistry* 30:1207–11.
- FAO-ISRIC. 1990. *Guidelines for Soil Description*, 3rd edition. Rome: Food and Agricultural Organization.
- Frostegård Å, Bååth E. 1996. The use of phospholipid fatty acid analysis to estimate bacterial and fungal biomass in soil. *Biology and Fertility of Soils* 22:59–65.
- Gregorich EG, Monreal CM, Schnitzer M, Schulten HR. 1996. Transformation of plant residues into soil organic matter: chemical characterization of plant tissues, isolated soil fractions, and whole soil. *Soil Science* 161:680–93.
- Hedges JJ. 1991. Lignin, cutin, amino acid and carbohydrate analysis of marine particulate organic matter. In: Hurd DC, Spencer DW, editors. *Marine Particles: Analysis and Characterization. Geophysical Monograph* 63. Washington, DC: American Geophysical Union. p 129–37.
- Lichtfouse E, Elbisser B, Balesdent J, Mariotti A, Bardoux G. 1994. Isotope and molecular evidence for direct input of maize leaf wax n-alkanes into crop soil. *Organic Geochemistry* 22:349–51.
- Lichtfouse E, Bardoux G, Mariotti A, Balesdent J, Balleentine DC, Mackod SA. 1997. Molecular, ^{13}C , and ^{14}C evidence for the allochthonous and ancient origin of C16–C18 n-alkanes in modern soils. *Geochimica et Cosmochimica Acta* 61:1891–8.
- Merbach W, Schmidt L, Wittmayer L, editors. 1999. *Die Dauerdüngungsversuche in Halle (Saale)*. Stuttgart/Leipzig: Teubner. 150 p.
- Nadeau MJ, Schleicher M, Grootes PM, Erlenkeuser H, Gott dang A, Mous DJW, Sarnthein JM, Willkomm H. 1997. The Leibniz-Labor AMS facility at the Christian-Albrechts-University, Kiel, Germany. *Nuclear Instruments and Methods in Physics Research B* 123: 22–30.
- Nadeau MJ, Grootes PM, Schleicher M, Hasselberg P, Rieck A, Bitterling M. 1998. Sample throughput and data quality at the Leibniz-Labor AMS facility. *Radiocarbon* 40(1):239–45.
- O'Brien BJ. 1986. The use of natural and anthropogenic ^{14}C to investigate the dynamics of soil organic carbon. *Radiocarbon* 28(2A):358–62.
- Petsch ST, Eglinton TI, Edwards KJ. 2001. ^{14}C -dead living biomass: evidence for microbial assimilation of ancient organic carbon during shale weathering. *Science* 292:1127–31.
- Radke M, Willsch H, Welte DH. 1980. Preparative hydrocarbon group type determination by automated medium pressure liquid chromatography. *Analytical Chemistry* 52:406–11.
- Rethemeyer J, Bruhn F, Kramer C, Gleixner G, Andersen N, Nadeau MJ, Grootes PM. Forthcoming. Age heterogeneity of soil organic matter. *Nuclear Instruments and Methods in Physics Research B*.
- Rumpel C, Balesdent J, Grootes PM, Weber E, Kögel-Knabner I. 2003. Quantification of lignite- and vegetation-derived soil carbon using ^{14}C activity measurements in a forested chronosequence. *Geoderma* 112: 155–66.
- Scharpenseel HW, Becker-Heidmann P. 1992. Twenty-five years of radiocarbon dating soils: paradigm of erring and learning. *Radiocarbon* 34(3):541–9.
- Stuiver M, Polach HA. 1977. Discussion: reporting of ^{14}C data. *Radiocarbon* 22(1):1–24.
- Trumbore SE, Bonani G, Wölfli W. 1990. The rates of carbon cycling in several soils from AMS ^{14}C measurements of fractionated soil organic matter. In: Bouwman AF, editor. *Soils and the Greenhouse Effect*. New York: John Wiley & Sons. p 407–14.
- Trumbore SE. 1993. Comparison of carbon dynamics in tropical and temperate soils using radiocarbon measurement. *Global Biogeochemical Cycles* 7(2):275–90.
- Trumbore SE. 1996. Applications of accelerator mass spectrometry to soil science. In: Boutton TW, Yamasaki S, editors. *Mass Spectrometry of Soils*. New York: Marcel Dekker. p 311–40.
- Trumbore SE, Zheng S. 1996. Comparison of fractionation methods for soil organic matter ^{14}C analysis. *Radiocarbon* 38(2):219–29.
- Uchida M, Shibata Y, Kawamura K, Yoneda M, Mukai H, Tanaka A, Uehiro T, Morita M. 2000. Isolation of individual fatty acids in sediments using preparative capillary gas chromatography (PCGC) for radiocarbon analysis at NIES-TERRA. *Nuclear Instruments and Methods in Physics Research B* 172:583–8.
- van Bergen PF, Bull ID, Poulton PR, Evershed RP. 1997. Organic geochemical studies of soil from the Rothamsted Classical Experiments—I. Total lipid extracts, solvent insoluble residues and humic acids from Broadbalk Wilderness. *Organic Geochemistry* 26: 117–35.
- Wiesenberg GLB, Schwark L, Schmidt MWI. Forthcom-

- ing (a). Improved automated extraction and separation procedure for soil lipid analyses. *European Journal of Soil Science*.
- Wiesenberg GLB, Schwarzbauer J, Schmidt MWI, Schwark L. Forthcoming (b). Sources and turnover of soil organic matter derived from *n*-alkane/*n*-carboxylic acid compositions and C-isotope signature. *Organic Geochemistry*.
- Willsch H, Clegg H, Horsfield B, Radke M, Wilkes H. 1997. Liquid chromatographic separation of sediment, rock, and coal extracts and crude oil into compound classes. *Analytical Chemistry* 69:4203–9.
- White DC, David WM, Nickels JS, King JD, Bobbie RJ. 1979. Determination of the sedimentary microbial biomass by extractable lipid phosphate. *Oecologia* 40: 51–62.
- Zelles L, Bai QY. 1993. Fractionation of fatty acid derived from soil lipids by solid phase extraction and their quantitative analysis by GC-MS. *Soil Biology and Biochemistry* 25:495–507.
- Zelles L. 1999. Fatty acid patterns of phospholipids and lipopolysaccharides in the characterization of microbial communities in soil: a review. *Biology and Fertility of Soils* 29:111–29.

SOURCE APPORTIONMENT OF AEROSOLS BY ^{14}C MEASUREMENTS IN DIFFERENT CARBONACEOUS PARTICLE FRACTIONS

S Szidat¹ • T M Jenk^{1,2} • H W Gäggeler^{1,2,3} • H-A Synal⁴ • R Fisseha² • U Baltensperger² • M Kalberer⁵ • V Samburova⁵ • L Wacker⁶ • M Saurer² • M Schwikowski² • I Hajdas⁴

ABSTRACT. Radiocarbon enables a distinction between contemporary and fossil carbon, which can be used for the apportionment of biogenic and anthropogenic sources in environmental studies. In order to apply this approach to carbonaceous atmospheric aerosols, it is necessary to adapt pretreatment procedures to the requirements of ^{14}C measurements. In this work, we followed an approach in which total carbon (TC) is subdivided into fractions of different chemical and physical properties. ^{14}C data of ambient aerosols from Zürich (Switzerland) are presented for the 2 sub-fractions of TC, organic carbon (OC) and elemental carbon (EC). Furthermore, OC is separated into water-insoluble OC (WINSOC) and water-soluble OC (WSOC). Results demonstrate the importance to differentiate between these fractions for ^{14}C -deduced source apportionment, as the contributions can range between both extremes, nearly exclusively biogenic and anthropogenic.

INTRODUCTION

Atmospheric carbonaceous particles include a huge variety of organic substances, which can sum up to half of the mass of the fine urban aerosol (Jacobson et al. 2000; Turpin et al. 2000). For their source apportionment, 2 different strategies are often employed, which can be classified as the “bottom” and “top” approach. The bottom approach pursues a complete identification of every single organic compound (Zheng et al. 1997; Kubátová et al. 2002). The top approach considers the carbonaceous particles as a whole with a given total carbon (TC) content, followed by a more specific division into the sub-groups organic carbon (OC) and elemental carbon (EC) with different physical and chemical properties (Krivácsy et al. 2001; Kleefeld et al. 2002). Moreover, OC can be separated into water-insoluble OC (WINSOC) and water-soluble OC (WSOC). Some classes of organic compounds that are found in these sub-groups are n-alkanes, aromatic compounds (e.g. PAHs), and long-chained carboxylic acids for WINSOC; polyols, polyethers, mono-, di-, and poly-carboxylic acids for WSOC; and a complex mixture of graphitic and high molecular weight refractory organic species for EC (Rogge et al. 1993; Jacobson et al. 2000; Turpin et al. 2000; Decesari et al. 2001). Whereas the bottom approach involves very extensive analytical procedures and allows only an identification of typically less than 10% of the organic mass at present (Rogge et al. 1993; Kubátová et al. 2002), the top approach leads to method-dependent sum parameters (Schmid et al. 2001; Currie et al. 2002).

Concerning the process of formation in the atmosphere, carbonaceous particles are often classified into primary organic aerosol, which is directly emitted as particles, and secondary organic aerosol (SOA), which is generated from gaseous precursors by atmospheric oxidation (Pun et al. 2000). During this process, less volatile compounds are formed, which then partition to the aerosol phase. This exposure to atmospheric oxidants introduces oxygenated groups to organic aerosol compounds, which enhances water solubility of SOA. Therefore, WSOC mainly consists of secondary aerosol.

¹Department of Chemistry and Biochemistry, University of Bern, Freiestrasse 3, CH-3012 Bern, Switzerland.

²Paul Scherrer Institut (PSI), CH-5232 Villigen, Switzerland.

³Corresponding author. Email: heinz.gaeggeler@iac.unibe.ch.

⁴Paul Scherrer Institut (PSI), c/o Institute for Particle Physics, ETH Hönggerberg, CH-8093 Zürich, Switzerland.

⁵Laboratory of Organic Chemistry, ETH Hönggerberg, CH-8093 Zürich, Switzerland.

⁶Institute for Particle Physics, ETH Hönggerberg, CH-8093 Zürich, Switzerland.

Radiocarbon measurements of carbonaceous particles bear the potential to distinguish between fossil carbon and contemporary carbon and, consequently, between anthropogenic and biogenic emission sources of aerosols (Currie et al. 1989; Klinedinst and Currie 1999; Currie 2000; Lemire et al. 2002). Whereas first studies were restricted to the analysis of TC (see Currie 2000 for a review), recent work also focused on ^{14}C analysis in specific fractions of the carbonaceous aerosol. On the one hand, preparative chromatography made it possible to perform compound specific studies of different PAHs (Currie et al. 1997; Currie et al. 2002; Reddy et al. 2002) and fatty acids (Matsumoto et al. 2001) according to the bottom approach. However, a large amount of aerosol had to be collected for these studies to achieve enough material for ^{14}C determination, resulting in a poor time resolution. On the other hand, ^{14}C measurements in EC (Slater et al. 2002; Currie et al. 2002; Reddy et al. 2002) and OC (Szidat et al. 2004a) followed the top approach.

Furthermore, the determination of ^{13}C has a potential to trace the extent of atmospheric photochemical processing. Rudolph et al. (2003) observed for the gas phase that isoprene is enriched in ^{13}C with increasing average lifetime, which suggests for the particulate phase that SOA is depleted in ^{13}C compared to the gaseous precursors.

In a previous work, we presented a separation scheme for the determination of ^{14}C in TC, OC, and EC and demonstrated its potential as an environmental tracer by investigation of Standard Reference Material (SRM) 1649a, Urban Dust (Szidat et al. 2004a). For this study, this separation scheme is extended to water-insoluble OC (WINSOC) and applied to ambient aerosol samples collected in Zürich, Switzerland.

METHODS

Sampling of Aerosols

Between 16 August and 8 September 2002, 4 aerosol samples were collected on pre-baked quartz fiber filters ($D = 150$ mm, QF 20, Schleicher and Schuell) with a high-volume sampler (Digital DA80) and a PM_{10} inlet at the Swiss National Air Pollution Monitoring Network (NABEL) station in the city center of Zürich, Switzerland ($47^{\circ}22'42''\text{N}$, $8^{\circ}31'52''\text{E}$, 410 m asl). After collection, samples were wrapped in aluminum foil, packed into air-tight plastic bags, and stored at -20 °C. For the ^{14}C analysis of EC and WINSOC, a long sampling duration (3–5 days) was necessary to get the carbon mass of approximately 20 μg required (Szidat et al. 2004a). The NABEL station Zürich represents an “urban background site”, as primary emissions from traffic or industries have only a small impact (EMPA 2000). Meteorological parameters and concentrations of PM_{10} (half-hourly values using a betameter) as well as ozone were routinely determined at this station by the Swiss Federal Laboratories for Materials Testing and Research, Dübendorf.

Separation of Carbon Fractions for ^{14}C AMS Measurements

Seven sub-samples of 16 mm each of the air filters were used to perform the analysis of the different carbon fractions (1 for TC, OC, and WINSOC, 2 for total and water-insoluble EC). With the device *THEODORE* (Two-step heating system for the EC/OC determination of radiocarbon in the environment) (Szidat et al. 2004a), different carbonaceous particle fractions were separated within 10 min in a stream of oxygen under the following conditions and as illustrated in Figure 1.

TC was combusted at 650 °C; a previous acidification was not necessary because carbonates can be neglected in mid-latitude aerosols (Chow and Watson 2002). OC was separated from other carbon fractions at 340 °C. For WINSOC analysis, a water-extracted filter was obtained by soaking in

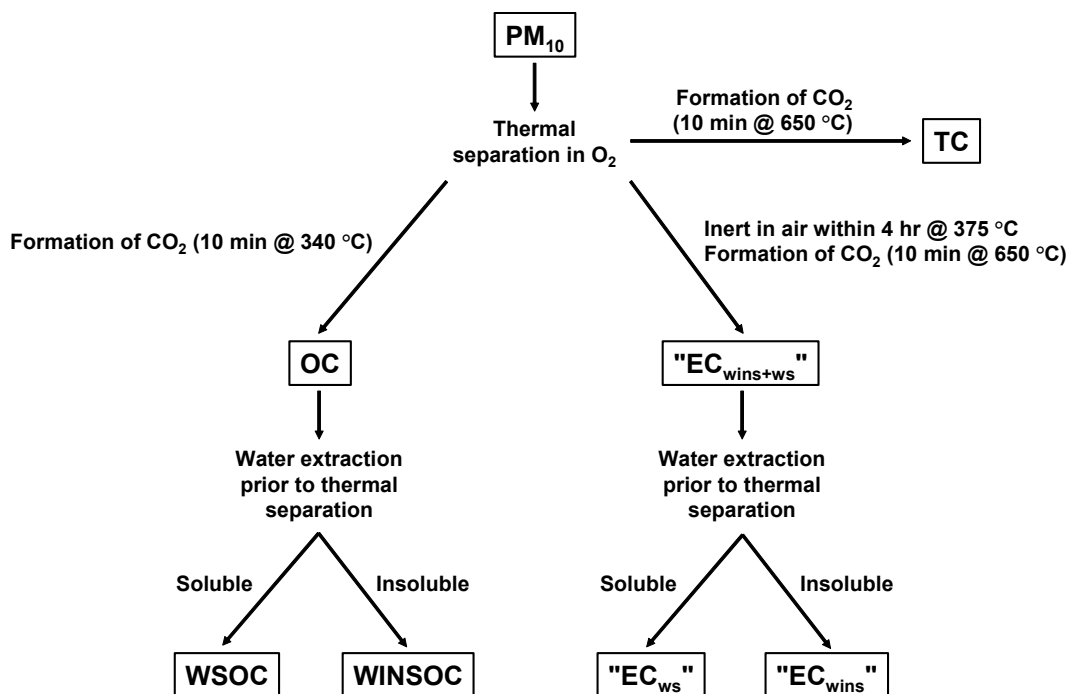


Figure 1 Separation scheme of the different carbon fractions

10 mL of high-purity water overnight (Gelencsér et al. 2000). Filters were dried and OC separation was conducted as described above. Determination of WSOC was performed by subtraction ($\text{WSOC} = \text{OC} - \text{WINSOC}$). For the analysis of EC, 2 methods were used: For the determination of EC according to Szidat et al. (2004a), OC was eliminated for 4 hr at 375 °C in a muffle furnace and EC was then combusted at 650 °C. This EC fraction represented a sum of 2 fractions and is named $\text{EC}_{\text{wins}+\text{ws}}$. In order to remove high-molecular polyacidic species, which rapidly form EC by pyrolysis on heating, a water extraction pretreatment as described above was carried out prior to the elimination of OC at 375 °C. The remaining fraction represented water-insoluble EC (i.e. EC_{wins}). The water-soluble fraction (EC_{ws}) was determined by subtraction ($\text{EC}_{\text{ws}} = \text{EC}_{\text{wins}+\text{ws}} - \text{EC}_{\text{wins}}$).

In order to achieve a highly efficient separation and isolation of OC and EC, an average total recovery of 60–80% was accepted. The residual OC included large polymeric polar molecules such as humic-like substances, which may hinder the separation of OC and EC and, therefore, were disregarded. These losses during the thermal treatment are tolerable for isotopic ratio measurements assuming identical $^{14}\text{C}/^{12}\text{C}$ ratios of the measured and the neglected fraction, which was shown to be valid for SRM 1649a, Urban Dust (Szidat et al. 2004a).

Sample Analyses

TC concentrations were determined by manometrical measurements of the produced carbon dioxide using the system *THEODORE* (Szidat et al. 2004a). $\text{EC}_{\text{wins}+\text{ws}}$ and EC_{wins} concentrations were measured with nearly quantitative yields using a longer combustion time of 42 min (Lavanchy et al. 1999). OC was calculated as the difference of TC and EC_{wins} , which was regarded as the best proxy for EC as described below.

Concentrations of water-soluble inorganic ionic species were analyzed in the water extract with standard ion chromatography (IC). Filter debris and suspended insoluble particles were removed using a 0.45- μm PTFE syringe filter. Uncertainties of IC analyses were less than 10%.

^{14}C measurements were performed at the PSI/ETH compact AMS system, which is based on a 500-kV pelletron accelerator (Synal et al. 2000). For details of measurement parameters and data evaluation of sub-mg samples, see Szidat et al. (2004a). Using both the isotopic ratio and the carbon concentration, data were corrected for an overall blank, which was dominated by the filter blank but also included the blank of storage and chemical pretreatment of the samples. In this paper, ^{14}C results are presented as the fraction of contemporary carbon (f_{C}), which equals the biogenic contribution according to a simple ^{14}C model (Currie et al. 1989; Klinedinst and Currie 1999; Currie 2000; Lemire et al. 2002; Reddy et al. 2002; Szidat et al. 2004a). The correction factor for the residual nuclear bomb excess for mid-Europe was extrapolated as 1.077 ± 0.002 for August/September 2002 using atmospheric $^{14}\text{CO}_2$ data from the Schauinsland and Jungfraujoch stations (Levin and Kromer 1997 and 2002; Levin, personal communication).

$\delta^{13}\text{C}$ measurements of the different carbon fractions were performed with the AMS target material using an isotope ratio mass spectrometer (IRMS) with an on-line elemental analyzer injection (Saurer et al. 1997; Szidat et al. 2004a).

RESULTS AND DISCUSSION

Aerosol Composition

Details of aerosol sampling, meteorological parameters, and concentrations of different chemical species are given in Table 1 and Figure 2. PM_{10} concentrations and temperature as well as ozone maxima show rather constant values due to the time resolution of 3–5 days. The lengths of the dry period before sampling (t_{dry}) differed significantly and the samples were classified accordingly. For samples II and IV, sampling started 15.5 hr and 5 hr after a rainfall, respectively; thus, these samples represent aerosol of relatively short average lifetime. On the other hand, t_{dry} amounted to several days for samples I and III, indicating aerosol of longer average lifetime. The different lifetimes had an influence on concentrations of all chemical species and carbon fractions. Rainfall leads to wet deposition of airborne particles. Thus, the fraction of fresh primary particles is increased immediately after a precipitation event. During dry days, aged aerosols accumulate and mix continuously with new primary and secondary particles. As a consequence, aerosol with a longer average lifetime shows higher concentrations of all parameters. This also includes the secondary inorganic compounds SO_4^{2-} , NO_3^- , and NH_4^+ . Sea salt and mineral dust only contributed <6% to SO_4^{2-} according to the method of Schwikowski et al. (1999), indicating that observed concentrations originated nearly exclusively from oxidation of SO_2 , which is predominantly emitted anthropogenically in a present urban environment. K^+ concentrations were low for all samples and in the range of typical values for Swiss urban and rural locations in summer (Hüglin et al., forthcoming). Sea salt contributed to less than 5%, assuming constant Na^+/K^+ ratios (Keene et al. 1986), but the fraction of K^+ originating from mineral dust is quite uncertain. Following the concept of Andreae (1983), who used crustal average $\text{K}^+/\text{Ca}^{2+}$ ratios for the correction, a contribution to K^+ from mineral dust between 36% and >100% resulted. Because of this large uncertainty, an estimation of the fraction of EC derived from biomass burning using K^+/EC ratios was not possible, but ^{14}C analyses of EC as discussed below indicate that this fraction was 6% at most.

Table 1 Meteorological conditions, aerosol sampling parameters, and concentrations of carbonaceous particle fractions as well as some inorganic ions for the campaign in Zürich in summer 2002. Concentrations of carbonaceous particle fractions are presented with combined standard uncertainties (ISO 1995).

Sample	I	II	III	IV
Sampling period	16 Aug, 19:00– 21 Aug, 19:00	21 Aug, 20:00– 26 Aug, 20:00	30 Aug, 09:00– 02 Sep, 09:00	03 Sep, 20:00– 08 Sep, 20:00
Air volume (m^3)	3600	3600	2160	3600
PM_{10} ($\mu\text{g m}^{-3}$)	26.3	25.8	25.4	23.3
T_{max} ($^{\circ}\text{C}$) ^a	26.9	23.9	23.2	22.5
Ozone _{max} (ppbv) ^a	57	46	44	46
h_p (mm) ^b	3.3	0.0	45.6	1.0
t_{dry} (d) ^b	4.3	0.6	(3.0) 9.2 ^c	0.2
TC ($\mu\text{g m}^{-3}$)	7.2 ± 0.3	3.6 ± 0.1	6.2 ± 0.2	2.5 ± 0.1
OC ($\mu\text{g m}^{-3}$)	5.7 ± 0.3	2.9 ± 0.2	5.0 ± 0.3	2.1 ± 0.1
WINSOC ($\mu\text{g m}^{-3}$)	2.0 ± 0.4	1.1 ± 0.2	2.0 ± 0.4	0.8 ± 0.2
WSOC ($\mu\text{g m}^{-3}$)	3.1 ± 0.4	1.5 ± 0.2	2.5 ± 0.4	1.0 ± 0.2
EC _{wins+ws} ($\mu\text{g m}^{-3}$)	2.1 ± 0.1	1.0 ± 0.1	1.7 ± 0.1	0.6 ± 0.1
EC _{wins} ($\mu\text{g m}^{-3}$)	1.5 ± 0.2	0.7 ± 0.1	1.2 ± 0.2	0.4 ± 0.1
EC _{ws} ($\mu\text{g m}^{-3}$)	0.6 ± 0.2	0.3 ± 0.1	0.5 ± 0.2	0.2 ± 0.1
EC/TC	0.20 ± 0.03	0.19 ± 0.03	0.19 ± 0.03	0.18 ± 0.03
SO_4^{2-} ($\mu\text{g m}^{-3}$)	3.5	2.1	4.8	1.6
NO_3^- ($\mu\text{g m}^{-3}$)	0.5	1.0	2.0	0.5
NH_4^+ ($\mu\text{g m}^{-3}$)	1.1	1.0	2.3	0.7
K^+ ($\mu\text{g m}^{-3}$)	0.16	0.07	0.13	0.02

^a= As means of daily maxima for the period of aerosol sampling.

^b= Precipitation depth (h_p) during sampling, dry period before beginning of sampling (t_{dry}).

^c= 3.0 days before sampling, only a minor event with a precipitation depth of 0.1 mm occurred.

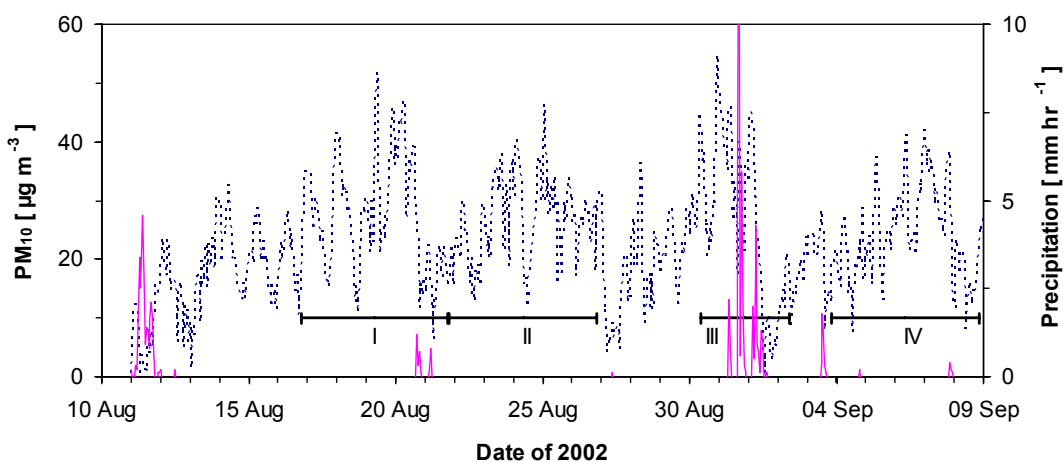


Figure 2 Hourly data of PM_{10} concentrations (dashed lines) and precipitation intensities (solid lines) during collection of aerosol samples I–IV.

Isotopic Signals of Carbonaceous Particle Fractions

Table 2 gives isotopic results for the different carbon fractions. Whereas $f_C(\text{TC})$ was rather constant at a level of 0.60–0.67, $f_C(\text{OC})$ indicated a significantly higher biogenic contribution for aerosol with a longer average lifetime (samples I and III). On the average, 82% of OC originated from biogenic sources in these samples compared to 69% in aerosol with shorter average lifetime. Equivalent results were observed for the sub-fractions of OC, WINSOC and WSOC. Similar to TC, f_C values were quite constant for all EC fractions at 0.30, 0.06, and 0.84 for $EC_{\text{wins+ws}}$, EC_{wins} , and EC_{ws} , respectively. $\delta^{13}\text{C}$ of all fractions ranged from -25.7‰ to -28.6‰ . Mean values showed slightly more negative $\delta^{13}\text{C}$ for WINSOC ($-27.9 \pm 0.6\text{‰}$) than for OC ($-27.0 \pm 0.2\text{‰}$) and TC ($-26.3 \pm 0.3\text{‰}$). However, this effect is not significant due to the high uncertainties; thus, a possible response of $\delta^{13}\text{C}$ to the influence of atmospheric processes (Rudolph et al. 2003) could not be detected.

Table 2 Carbon isotope results of different carbon fractions for the campaign in Zürich in summer 2002 with combined standard uncertainties (ISO 1995). “n.d.” means “not determined.”

Sample	I	II	III	IV
Sampling period	16 Aug, 19:00– 21 Aug, 19:00	21 Aug, 20:00– 26 Aug, 20:00	30 Aug, 09:00– 02 Sep, 09:00	03 Sep, 20:00– 08 Sep, 20:00
$f_C(\text{TC})$	0.67 ± 0.02	0.60 ± 0.02	0.62 ± 0.03	n.d.
$f_C(\text{OC})$	0.80 ± 0.02	0.67 ± 0.06	0.84 ± 0.03	0.71 ± 0.03
$f_C(\text{WINSOC})$	0.63 ± 0.02	0.55 ± 0.04	0.68 ± 0.03	0.58 ± 0.04
$f_C(\text{WSOC})$	0.91 ± 0.14	0.76 ± 0.16	0.96 ± 0.17	0.82 ± 0.15
$f_C(\text{EC}_{\text{wins+ws}})$	0.30 ± 0.02	0.30 ± 0.02	0.30 ± 0.02	0.31 ± 0.02
$f_C(\text{EC}_{\text{wins}})$	0.062 ± 0.020	0.064 ± 0.015	n.d.	n.d.
$f_C(\text{EC}_{\text{ws}})$	0.84 ± 0.30	0.83 ± 0.29	n.d.	n.d.
$\delta^{13}\text{C}(\text{TC})$ [‰]	-25.7 ± 0.4	-26.5 ± 0.6	-26.6 ± 0.6	n.d.
$\delta^{13}\text{C}(\text{OC})$ [‰]	-26.9 ± 0.9	-27.4 ± 1.2	-26.5 ± 0.4	-27.0 ± 2.6
$\delta^{13}\text{C}(\text{WINSOC})$ [‰]	-26.2 ± 0.5	-28.4 ± 0.5	-28.5 ± 0.8	-28.6 ± 1.0
$\delta^{13}\text{C}(\text{EC}_{\text{wins+ws}})$ [‰]	n.d.	-26.9 ± 0.9	-25.7 ± 0.5	n.d.
$\delta^{13}\text{C}(\text{EC}_{\text{wins}})$ [‰]	-27.3 ± 0.7	-26.1 ± 0.9	n.d.	n.d.

As stated above, the fraction of secondary aerosol increases with increasing aerosol lifetime. $f_C(\text{OC})$ also increased with increasing t_{dry} , indicating that SOA is to a significant fraction biogenic. This effect is even more pronounced for WSOC, and the highest f_C value was observed for $f_C(\text{WSOC})$ of sample III, which was preceded by the longest dry period. Thus, WSOC might be viewed as a proxy for SOA, which has a high content of water-soluble compounds (Kalberer et al. 2004), and the biogenic contribution of $96 \pm 17\%$ to WSOC of sample III indicates that SOA was mainly of biogenic origin.

Origin of Different EC Fractions

In Tables 1 and 2, two different methods for the separation of EC are considered. EC_{wins} resulted from the thermal EC separation with water extraction prior to combustion and $EC_{\text{wins+ws}}$ without this extraction (Figure 1). EC_{ws} (the difference between both) amounted to 30% of $EC_{\text{wins+ws}}$ on average. This value is surprisingly high because EC is supposed to be completely insoluble in water.

Measurements of the urban model aerosol SRM 1649a (see Table 3) apportioned EC as about 95% anthropogenic (Currie et al. 2002; Reddy et al. 2002; Szidat et al. 2004a). This value was confirmed to be the best estimate for EC sources at present by snow samples from Summit, Greenland (Slater

et al. 2002). $f_{\text{C}}(EC_{\text{wins}})$ was close to this value, whereas $f_{\text{C}}(EC_{\text{wins+ws}})$ was much higher and $f_{\text{C}}(EC_{\text{ws}})$ corresponds to results of $f_{\text{C}}(\text{WSOC})$. This implies that actually EC_{wins} represents EC correctly due to the f_{C} value and the water insolubility so that $f_{\text{C}}(EC_{\text{wins}})$ was set as $f_{\text{C}}(\text{EC})$ in Figures 3a and b as well as in Table 3. Furthermore, EC_{ws} seems to belong to the WSOC fraction as indicated by $f_{\text{C}}(EC_{\text{ws}})$ and to be artificially transformed into EC during analysis by pyrolysis. Obviously, this fraction is enriched with polymeric polar OC (e.g. polyacidic, humic-like substances), which is soluble in water and often interferes with OC/EC separations (Lavanchy et al. 1999; Kalberer et al. 2004). This suggests that $EC_{\text{wins+ws}}$ accounts for a mixture of EC and polymeric polar OC.

Table 3 Comparison of ^{14}C measurements in different carbonaceous particle fractions with results from Standard Reference Material SRM 1649a, Urban Dust (NIST 2001; Currie et al. 2002), and 2 American studies of ambient urban aerosols. Results are given as mean values with the whole range of values in parentheses, except for SRM 1649a (weighted mean of 3–5 repeated measurements with standard uncertainties of the mean). “n.d.” means “not determined.”

Source/site	NABEL Zürich	NABEL Zürich	SRM 1649a	Aldine	Welby (summer)	Welby (winter)
Date	Aug/Sep 2002	Aug 2002	1976/1977	Aug 2000	Aug 1996	Dec 96/Jan 97
Location	Zürich	Zürich	Washington, DC	Houston, Texas	Denver, Colorado	Denver, Colorado
$f_{\text{C}}(\text{TC})$	0.63 (0.60–0.67)	n.d.	0.39 ± 0.01	0.48 (0.25–0.68)	0.42 (0.09–0.68)	0.26 (0.13–0.69)
$f_{\text{C}}(\text{OC})$	0.75 (0.67–0.84)	0.69 (0.51–0.80)	0.52 ± 0.03	0.49 (0.14–0.74) ^a	n.d.	n.d.
$f_{\text{C}}(\text{EC})$	~0.06	n.d.	0.05 ± 0.01	n.d.	n.d.	n.d.
Particle size	PM ₁₀	PM ₁₀	100 μm (sieved)	PM _{2.5}	PM _{2.5}	PM _{2.5}
Sampling time [d]	3–5	0.5–1.5	~365	0.25–1	0.25	0.25
Individual samples	4	13	1	9	24	18
Reference	This work	Szidat et al. 2004b	Szidat et al. 2004a	Lemire et al. 2002	Klinedinst and Currie 1999	Klinedinst and Currie 1999

^aEstimated values based on determinations of $f_{\text{C}}(\text{TC})$ and OC/TC ; for details, see Lemire et al. (2002).

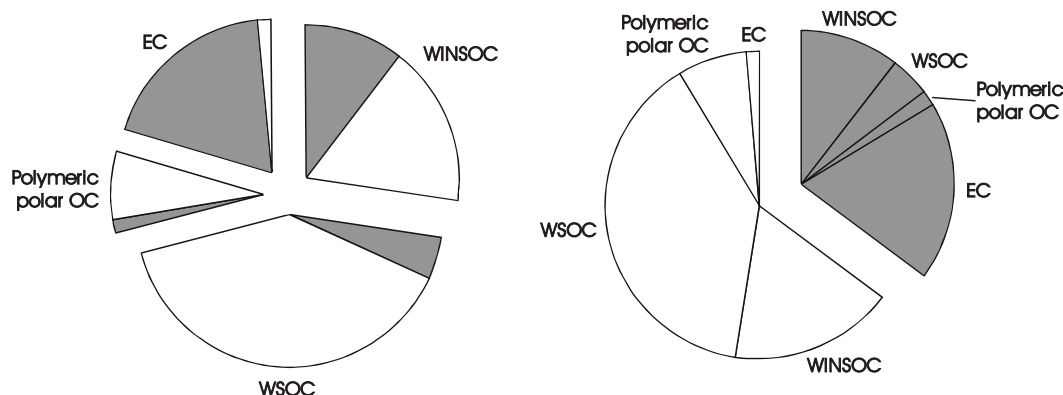


Figure 3a Biogenic (white) and anthropogenic (gray) contributions to different carbonaceous particle fractions of sample I representing aerosol of longer average lifetime, arranged by carbon fractions (left) and biogenic/anthropogenic contributions (right). Note that the fraction EC_{ws} is renamed “polymeric polar OC” (see “Sources of Different EC Fractions”).

Source Apportionment Information

Figures 3a and b illustrate the source apportionment information for samples I and II. Results underline that measurements of $f_{\text{C}}(\text{TC})$ alone cannot provide a reliable identification of emission sources

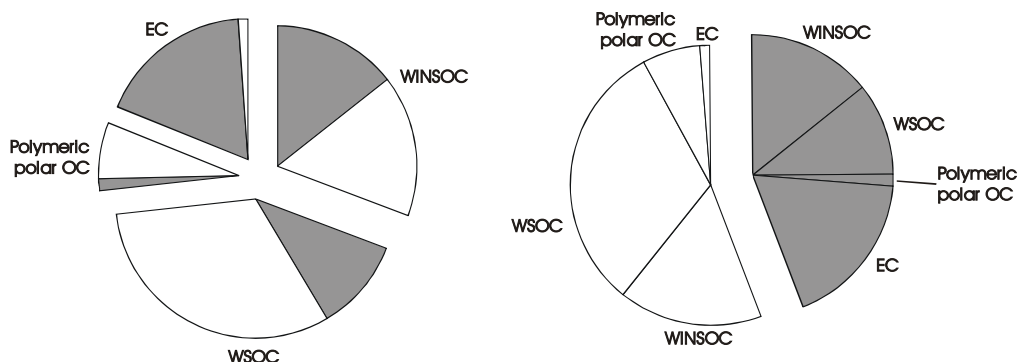


Figure 3b Same as Figure 3a but for sample II representing aerosol of shorter average lifetime

of carbonaceous aerosol, and that at least a separation of OC and EC is required, as these fractions may differ in physical and chemical properties as well as their origin. Moreover, the distinction between WSOC and WINSOC exposed a significantly higher anthropogenic contribution for the water-insoluble fraction.

Comparison of Results

$f_C(\text{TC})$, $f_C(\text{OC})$, and $f_C(\text{EC})$ values are compared with data from other studies in Table 3. Within a parallel campaign (Szidat et al. 2004b), we measured samples for $f_C(\text{OC})$ at the same site separated for day and night conditions with a higher time resolution. Both studies yielded similar $f_C(\text{OC})$ values. Some samples of the parallel campaign, which were collected immediately after a precipitation event and represented aerosol of very short average lifetime, showed slightly lower $f_C(\text{OC})$ values, which was caused by a higher fraction of fresh primary particles. A lower average of $f_C(\text{TC})$ was observed for cities in the US compared to Zürich. Some samples within the studies at Houston and Denver reached biogenic contributions of nearly 70%, similar to this work. In contrast to that, high anthropogenic emissions of up to 91% were also determined, which indicates completely different sources for those samples compared to Zürich. Moreover, $f_C(\text{OC})$ values are lower for SRM 1649a and Houston than for Zürich. However, as SRM 1649a represents an annual average and $f_C(\text{OC})$ values for Houston only give an estimate, a reliable comparison of ^{14}C results for OC is not possible. Finally, EC was nearly exclusively influenced by anthropogenic emissions in this work and in SRM 1649a as discussed above.

CONCLUSIONS

^{14}C measurements of different carbon fractions of airborne particulate matter according to the top approach enable an insight into emission sources of carbonaceous aerosols. Results from an urban background site in Zürich demonstrate that OC was derived from biogenic emissions to 75% of the average, whereas EC originated to 94% from anthropogenic sources. Furthermore, WSOC was determined as up to 96% biogenic, which suggests that SOA may be formed nearly exclusively from biogenic precursor gases even in an urban environment.

ACKNOWLEDGEMENTS

This work is supported by the Swiss National Science Foundation (project 2169-061393.00). We thank R Gehrig and C Hüglin (EMPA), as well as R Weber (BUWAL) for providing NABEL data. The assistance of K Henderson (PSI) with the EC determinations and of S Brütsch (PSI) with the IC

measurements is also acknowledged. We are grateful to the Paul Scherrer Institut (PSI) and the Swiss Federal Institute of Technology (ETH), who jointly operate the Zürich AMS facilities.

REFERENCES

- Andreae MO. 1983. Soot carbon and excess fine potassium: long-range transport of combustion-derived aerosols. *Science* 220:1148–51.
- Chow JC, Watson JG. 2002. $\text{PM}_{2.5}$ carbonate concentrations at regionally representative Interagency Monitoring of Protected Visual Environment sites. *Journal of Geophysical Research* 107:8344, doi: 10.1029/2001JD000574.
- Currie LA, Stafford TW, Sheffield AE, Klouda GA, Wise SA, Fletcher RA, Donahue DJ, Jull AJT, Linick TW. 1989. Microchemical and molecular dating. *Radiocarbon* 31(3):448–63.
- Currie LA, Eglinton TI, Benner Jr BA, Pearson A. 1997. Radiocarbon “dating” of individual chemical compounds in atmospheric aerosol: first results comparing direct isotopic and multivariate statistical apportionment of specific polycyclic aromatic hydrocarbons. *Nuclear Instruments and Methods in Physics Research B* 123:475–86.
- Currie LA. 2000. Evolution and multidisciplinary frontiers of ^{14}C aerosol science. *Radiocarbon* 42(1):115–26.
- Currie LA, Benner Jr BA, Kessler JD, Klinedinst DB, Klouda GA, Marolf JV, Slater JF, Wise SA, Cachier H, Cary R, Chow JC, Watson J, Druffel ERM, Masiello CA, Eglinton TI, Pearson A, Reddy CM, Gustafsson Ö, Quinn JG, Hartmann PC, Hedges JI, Prentice KM, Kirchstetter TW, Novakov T, Puxbaum H, Schmid H. 2002. A critical evaluation of interlaboratory data on total, elemental, and isotopic carbon in the carbonaceous particle reference material, NIST SRM 1694a. *Journal of Research of the National Institute of Standards and Technology* 107:279–98.
- Decesari S, Facchini MC, Matta E, Lettini F, Mircea M, Fuzzi S, Tagliavini E, Putaud J-P. 2001. Chemical features and seasonal variation of fine aerosol water-soluble organic compounds in the Po Valley, Italy. *Atmospheric Environment* 35:3691–9.
- EMPA. 2000. Technischer Bericht zum Nationalen Beobachtungsnetz für Luftfremdstoffe (NABEL). *Swiss Federal Laboratories for Materials Testing and Research (EMPA)*. Dübendorf, Switzerland.
- Gelencsér A, Hoffer A, Molnár A, Krivácsy Z, Kiss G, Mészáros E. 2000. Thermal behaviour of carbonaceous aerosol from a continental background site. *Atmospheric Environment* 34:823–31.
- ISO. 1995. Guide to the expression of uncertainty in measurement. *International Organization for Standardization*. Geneva, corrected and reprinted.
- Jacobson MC, Hansson H-C, Noone KJ, Charlson RJ. 2000. Organic atmospheric aerosols: review and state of the science. *Reviews of Geophysics* 38:267–94.
- Kalberer M, Paulsen D, Sax M, Steinbacher M, Dommen J, Fisseha R, Weingartner E, Frankevich V, Zenobi R, Baltensperger U. 2004. First identification of polymers as major components of atmospheric organic aerosols. *Science* 303:1659–62.
- Keene WC, Pszenny AAP, Galloway JN, Hawley ME. 1986. Sea-salt corrections and interpretation of constituent ratios in marine precipitation. *Journal of Geophysical Research* 91:6647–58.
- Kleefeld S, Hoffer A, Krivácsy Z, Jennings SG. 2002. Importance of organic and black carbon in atmospheric aerosols at Mace Head, on the west coast of Ireland ($53^{\circ}19'N$, $9^{\circ}54'W$). *Atmospheric Environment* 36:4479–90.
- Klinedinst DB, Currie LA. 1999. Direct quantification of $\text{PM}_{2.5}$ fossil and biomass carbon within the Northern Front Range Air Quality Study's domain. *Environmental Science and Technology* 33:4146–54.
- Krivácsy Z, Sávári Z, Temesi D, Baltensperger U, Nyeki S, Weingartner E, Kleefeld S, Jennings SG. 2001. Role of organic and black carbon in the chemical composition of atmospheric aerosol at European background sites. *Atmospheric Environment* 35:6231–44.
- Kubátová A, Vermeylen R, Claeys M, Cafmeyer J, Maenhaut W. 2002. Organic compounds in urban aerosols from Gent, Belgium: characterization, sources, and seasonal differences. *Journal of Geophysical Research* 107:8343, doi: 10.1029/2001JD000556.
- Lavanchy VMH, Gaggeler HW, Nyeki S, Baltensperger U. 1999. Elemental carbon (EC) and black carbon (BC) measurements with a thermal method and an aethalometer at the high-alpine research station Jungfraujoch. *Atmospheric Environment* 33:2759–69.
- Lemire KR, Allen DT, Klouda GA, Lewis CW. 2002. Fine particulate matter source attribution for southeast Texas using $^{14}\text{C}/^{13}\text{C}$ ratios. *Journal of Geophysical Research* 107:4613, doi: 10.1029/2002JD002339.
- Levin I, Kromer B. 1997. Twenty years of atmospheric $^{14}\text{CO}_2$ observations at Schauinsland station, Germany. *Radiocarbon* 39(2):205–18.
- Levin I, Kromer B. 2002. Long-term measurements of $^{14}\text{CO}_2$ at Jungfraujoch: observing fossil fuel CO_2 over Europe. In: Workshop on “Atmospheric research at the Jungfraujoch and in the Alps,” Davos, Switzerland, 20 September 2002 (available at: http://acp.web.psi.ch/acp_public/ProceedingDavos02.pdf). p 19–20.
- Matsumoto K, Kawamura K, Uchida M, Shibata Y, Yoneda M. 2001. Compound specific radiocarbon and $\delta^{13}\text{C}$ measurements of fatty acids in a continental aerosol sample. *Geophysical Research Letters* 28:

- 4587–90.
- NIST. 2001. Certificate of analysis for Standard Reference Material 1649a, Urban Dust. *National Institute of Standards and Technology*. Gaithersburg, Maryland, revised.
- Pun BK, Seigneur C, Grosjean D, Saxena P. 2000. Gas-phase formation of water-soluble organic compounds in the atmosphere: a retrosynthetic analysis. *Journal of Atmospheric Chemistry* 35:199–223.
- Reddy CM, Pearson A, Xu L, McNichol AP, Benner Jr. BA, Wise SA, Klouda GA, Currie LA, Eglinton TI. 2002. Radiocarbon as a tool to apportion the sources of polycyclic aromatic hydrocarbons and black carbon in environmental samples. *Environmental Science and Technology* 36:1774–82.
- Rogge WF, Mazurek MA, Hildemann LM, Cass GR, Simoneit BRT. 1993. Quantification of urban organic aerosol at a molecular level: identification, abundance and seasonal variation. *Atmospheric Environment* 27A:1309–30.
- Rudolph J, Anderson RS, Czapiewski KV, Czuba E, Ernst D, Gillespie T, Huang L, Rigby C, Thompson AE. 2003. The stable carbon isotope ratio of biogenic emissions of isoprene and the potential use of stable isotope ratio measurements to study photochemical processing of isoprene in the atmosphere. *Journal of Atmospheric Chemistry* 44:39–55.
- Saurer M, Borella S, Schweingruber F, Siegwolf R. 1997. Stable carbon isotopes in tree rings of beech: climatic versus site-related influences. *Trees* 11:291–7.
- Schmid H, Laskus L, Abraham HJ, Baltensperger U, Lavanchy V, Bizjak M, Burba P, Cachier H, Crow D, Chow J, Gnauk T, Even A, ten Brink HM, Giesen K-P, Hitznerberger R, Hueglin C, Maenhaut W, Pio C, Carvalho A, Putaud J-P, Toom-Sauntry D, Puxbaum H. 2001. Results of the “Carbon Conference” international aerosol carbon round robin test stage I. *Atmospheric Environment* 35:2111–21.
- Schwikowski M, Döscher A, Gäggeler HW, Schotterer U. 1999. Anthropogenic versus natural sources of atmospheric sulphate from an Alpine ice core. *Tellus* 51B:938–51.
- Slater JF, Currie LA, Dibb JE, Benner Jr BA. 2002. Distinguishing the relative contribution of fossil fuel and biomass combustion aerosols deposited at Summit, Greenland through isotopic and molecular characterization of insoluble carbon. *Atmospheric Environment* 36:4463–77.
- Synal H-A, Jacob S, Suter M. 2000. The PSI/ETH small radiocarbon dating system. *Nuclear Instruments and Methods in Physics Research B* 172:1–7.
- Szidat S, Jenk TM, Gäggeler HW, Synal H-A, Hajdas I, Bonani G, Saurer M. 2004a. THEODORE, a two-step heating system for the EC/OC determination of radiocarbon (^{14}C) in the environment. *Nuclear Instruments and Methods in Physics Research B*, in press.
- Szidat S, Jenk TM, Gäggeler HW, Synal H-A, Fisseha R, Baltensperger U, Kalberer M, Samburova V, Reimann S, Hajdas I. 2004b. Radiocarbon (^{14}C) deduced biogenic and anthropogenic contributions to organic carbon (OC) of urban aerosols from Zürich, Switzerland. *Atmospheric Environment*, in press.
- Turpin BJ, Saxena P, Andrews E. 2000. Measuring and simulating particulate organics in the atmosphere: problems and prospects. *Atmospheric Environment* 34:2983–3013.
- Zheng M, Wan TSM, Fang M, Wang F. 1997. Characterization of the non-volatile organic compounds in the aerosols of Hong Kong—identification, abundance and origin. *Atmospheric Environment* 31:227–37.

TEMPORAL VARIATION OF RADIOCARBON CONCENTRATION IN AIRBORNE PARTICULATE MATTER IN TOKYO

Ken Shibata¹ • Michio Endo¹ • Naomichi Yamamoto¹ • Jun Yoshinaga^{1,2} • Yukio Yanagisawa¹ • Osamu Endo³ • Sumio Goto⁴ • Minoru Yoneda⁴ • Yasuyuki Shibata⁴ • Masatoshi Morita⁴

ABSTRACT. The temporal radiocarbon variation (in terms of percent Modern Carbon: pMC) of size-fractionated airborne particulate matter (APM) collected in Tokyo between April 2002 and February 2003 was analyzed in order to get an insight into the sources of carbonaceous particles. Results indicated significant biogenic origins (approximately 40 pMC on average). In general, the seasonal and particle size variations in pMC were relatively small, with 2 exceptions: elevated pMC in coarse particles in April and October 2002, and relatively low pMC in the finest particle size fraction collected in August 2002. The former finding could be tentatively attributed to the abundance of coarse particles of biological origins, such as pollen; the latter might be due to an increased fraction of anthropogenic secondary particles.

INTRODUCTION

Health and meteorological effects caused by airborne particulate matter (APM) have been extensively investigated (Dockery et al. 1993; Charlson et al. 1992). The major emission sources of the APM in Tokyo are thought to include diesel exhaust, gas-to-particle conversion, road dust, iron and steel industries, fuel oil combustion, natural (soil, marine, biogenic emissions, and so on), and refuse incineration origins (Yoshizumi 1991). A chemical mass balance method in conjunction with the use of atmospheric tracers, such as metals and ions, has been one of the major approaches for the source apportionment of the APM (Gordon 1988). Radiocarbon has been introduced as a promising measure to determine the mixing ratio of fossil and biomass components (Currie 2000). Since ¹⁴C completely decays to radioactive decay during the fossilization period, fossil fuels do not contain ¹⁴C. Therefore, the amount of ¹⁴C expressed in a unit of percent modern carbon (pMC) (Stuiver and Polach 1977) can approximate the biogenic contribution of target materials, although the ambient ¹⁴C excess from atmospheric bomb tests of the 1950s (Currie et al. 1989) needs to be corrected for more accurate source dissection. Since ¹⁴C for the APM source apportionment was first introduced by Clayton et al. (1955), various studies have been performed to characterize APM using ¹⁴C as a tracer to offer quantitative distinctions between fossil and biomass origins (Currie et al. 1989; Hildemann et al. 1994; Currie et al. 1997; Klinedinst et al. 1999; Weissenböck et al. 2000; Lemire et al. 2002; Reddy et al. 2002). These studies indicated biogenic sources contributed significantly to the total and fine particles in the USA. In our previous study (M Endo, J Yoshinaga, N Yamamoto, Y Yanagisawa, O Endo, S Goto, M Yoneda, Y Shibata, M Moriata, unpublished data), the pMC value of the APM collected in Tokyo was found to be approximately 30. In this paper, seasonal variations in ¹⁴C concentrations in the size-fractionated APM are further reported to provide a detailed insight into the sources of carbonaceous particles.

¹Institute of Environmental Studies, The University of Tokyo, Hongo 7-3-1, Bunkyo-ku, Tokyo 113-0033, Japan.

²Corresponding author. Email: junyosh@k.u-tokyo.ac.jp.

³National Institute of Public Health, 4-6-1 Shirokanedai, Minato-ku, Tokyo, 108-8638, Japan.

⁴National Institute for Environmental Studies, 16-2 Onogawa, Tsukuba-shi, 305-8506, Japan.

MATERIALS AND METHODS

Sample Collection

A high-volume Andersen sampler with 5 cascaded stages (<1.3, 1.3–2.2, 2.2–3.8, 3.8–7.9, and >7.9 μm of aerodynamic diameter) (Model AH-600, Sibata Scientific Technology Ltd., Tokyo, Japan) was used for the size-fractionated APM collection. Quartz filters (2500QAST, Pallflex; about 30 cm in diameter) to be loaded in the Andersen sampler were pre-combusted at 850 $^{\circ}\text{C}$ to remove carbon contamination before sampling. The APM samples were collected bimonthly from April 2002 to February 2003 for the duration of 7 days on the rooftop (approximately 20 m from the ground level) of the National Institute of Public Health (NIPH) in Minato-ku, located in the center of the metropolitan Tokyo. The sampler was operated at a nominal flow rate of 566 L/min (total air volume 5705 m^3). The sampled filters were kept in a freezer until the ^{14}C analysis.

^{14}C Measurement

The APM collected on a quartz filter (minimum 1 mg carbon) was combusted in a specially designed large-volume quartz tube with 5.0 g copper oxide, 2.5 g copper, and 0.1 g silver foil. After combustion at 850 $^{\circ}\text{C}$ for 2 hr, the resultant gas was cryogenically purified to obtain CO_2 , which was subsequently heated to 650 $^{\circ}\text{C}$ for 8 hr with an iron catalyst and hydrogen in a graphite reaction tube (Kitagawa et al. 1993). The produced graphite was packed into targets for accelerator mass spectrometry (AMS) measurement. The AMS analysis was undertaken at the National Institute for Environmental Studies Tandem Accelerator for Environmental Research and Radiocarbon Analysis (NIES-TERRA) Facility (Tanaka et al. 2000). For ^{14}C measurements, a certified reference material from the National Institute of Standards and Technology (NIST SRM 4990c, Hox II, USA) was used as a standard (certified pMC value of 134.07). Precision of pMC analysis at the NIES-TERRA was evaluated by repeated analyses of the Hox II and the result was 134.21 ± 0.21 ($n=10$) (M Endo, J Yoshinaga, N Yamamoto, Y Yanagisawa, O Endo, S Goto, M Yoneda, Y Shibata, M Moriata, unpublished data). The absolute concentrations of biomass and fossil carbons, in addition to their ratios, were calculated with information of the CO_2 pressure generated during the purification process, since it corresponds with absolute carbon content in the APM sample. The surface of the filter for coarse particle fraction (>7.9 μm) was observed with a scanning electron microscope (SEM), and the numbers of pollen in $325 \times 225\text{-}\mu\text{m}$ area units were counted.

RESULTS AND DISCUSSION

The annual means and standard deviations of ^{14}C concentrations in the size-fractionated APM were 36.4 ± 5.3 , 43.1 ± 4.9 , 44.5 ± 7.1 , 49.0 ± 11.0 , and 44.8 ± 8.8 pMC for the following particles, respectively, <1.3, 1.3–2.2, 2.2–3.8, 3.8–7.9, and >7.9 μm . There is an increasing tendency in pMC in accordance with an increase of the particle size (Figure 1). The overall mass-weighted mean pMC in an entire particle size range through the year was 40.2. A study conducted in Los Angeles (USA) showed that contemporary carbon constituted 20–43% of the fine particulate matter (Hildemann et al. 1994). Therefore, the present results clearly demonstrated that a certain amount of modern (biomass) carbon also contributed to the APM in metropolitan Tokyo as was observed in Los Angeles. It should be noted, however, that our study used the unit of pMC for the purpose of characterizing seasonal and size-fractional trends instead of using the fraction of contemporary carbon for which the ambient ^{14}C excess needed to be corrected. The potential sources of the biomass carbon include the emissions from the refuse incineration and secondary particle formation from atmospheric oxidation of volatile organic compounds (VOCs) emitted from vegetation. The observed pMC values were higher than that of the reference APM (33.7 pMC), the composite of total

suspended particles collected by an electrostatic precipitator over 2 yr between 1997 and 2000 at the same sampling site (M Endo, J Yoshinaga, N Yamamoto, Y Yanagisawa, O Endo, S Goto, M Yoneda, Y Shibata, M Moriata, unpublished). The pMC values observed in each particle size fraction distributed in narrow range around 40 pMC through the year with 2 exceptions. First, pMC elevation was observed in coarse particles collected in April and October 2002. Second, relatively low pMC was found in the finest fraction collected in August 2002. To characterize the reasons for these 2 exceptions, the absolute concentrations of biomass and fossil carbon, derived by multiplication of pMC and carbon concentrations in μm^3 for each size fraction, are calculated (Figure 2). Carbon concentrations were calculated with information of the CO_2 pressure generated during purification process as was previously mentioned. As indicated in the figure, the elevated pMC in the coarse fraction ($>7.9 \mu\text{m}$) in April and October 2003 may result from an excess of biomass carbon with the constant fossil levels compared to other months. This elevation could be attributed to the coarse particles of biological origin, such as pollens observed by the SEM (Figure 3), and identified as those of the Japanese cedar and oak species. We also observed a seasonal trend in the frequency distribution of pollens in the $>7.9\text{-}\mu\text{m}$ fraction (Figure 4). Whereas the fossil carbon concentrations were quite constant through all samples, with the exception of December 2002, the results from our SEM observations semi-quantitatively indicated that pollens might increase pMC values in the coarse fraction in April and October 2002.

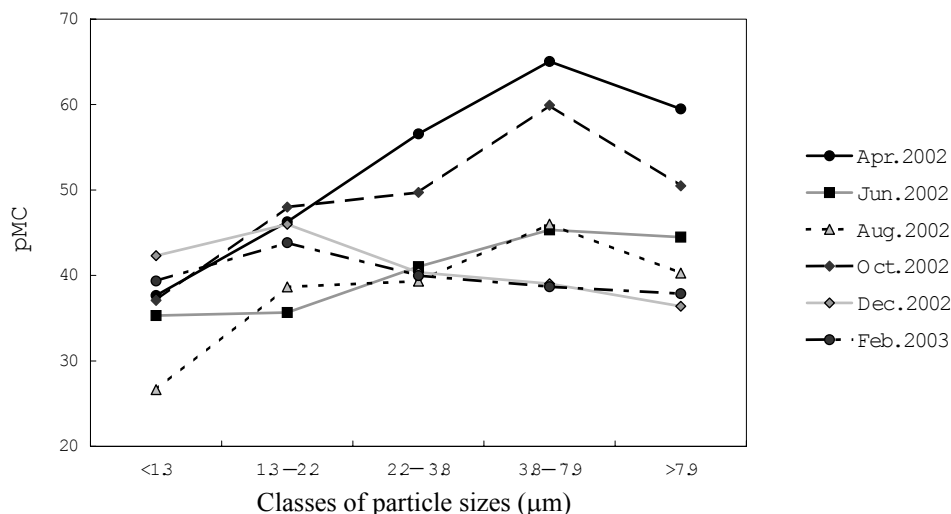


Figure 1 Temporal variations of ^{14}C concentrations

A relatively low pMC value was observed in the finest particle fraction in August (Figure 1) due to the larger amount of fossil carbon (Figure 2). There were no clear tendencies of increased production of electricity or traffic density in this month. This might be attributed to the increased volatilization of VOCs from anthropogenic sources (e.g. asphalt surface) due to the hot weather in Tokyo in this season, which could result in the increased formation of fine secondary particles by atmospheric condensation. Further investigation is necessary to clarify the cause of this variation.

The pMC of the elemental carbon in the APM is currently under investigation to identify the combustion sources from either fossil or biomass origins using elemental carbon as an indicator of the combustion sources. We conclude from the results of the present study that the analysis of temporal

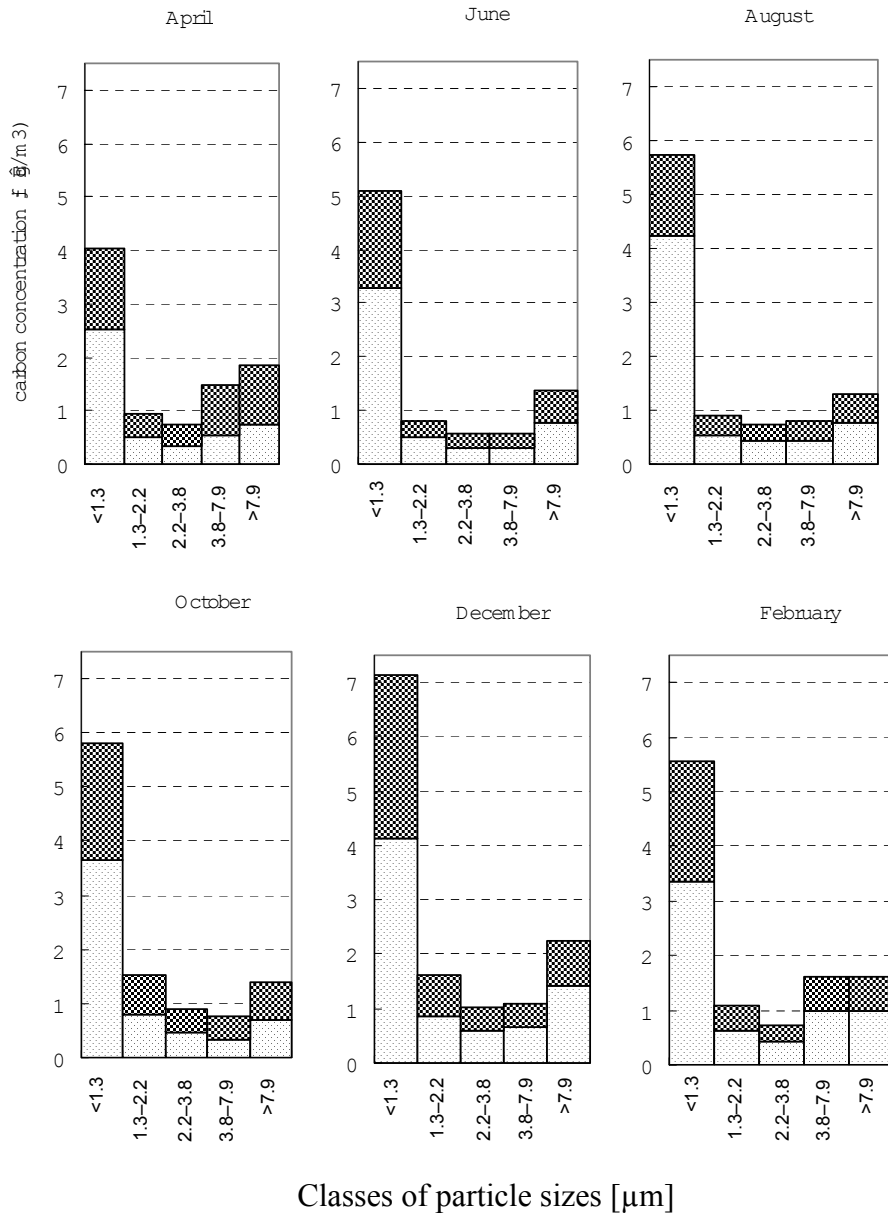


Figure 2 Temporal variations of the concentrations of biomass (dark) and fossil carbons (light)

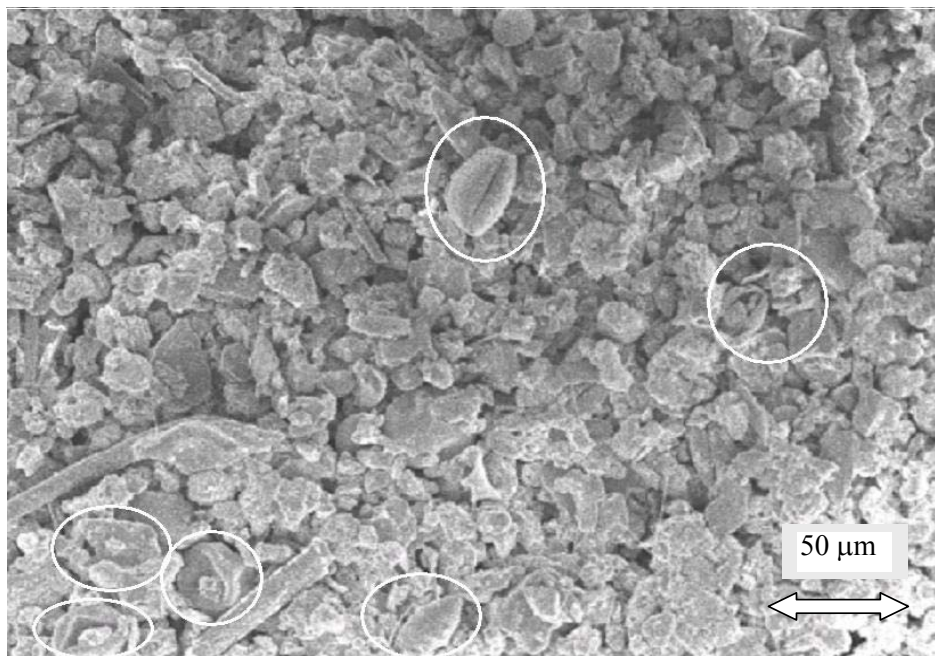


Figure 3 APM (>7.9 μm) collected in April 2002 (325 × 225 μm)

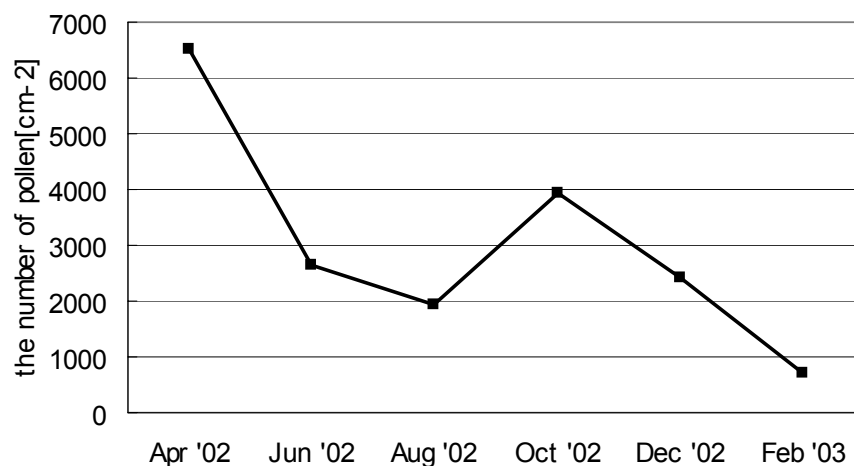


Figure 4 Number of pollen grains on the filter (>7.9 μm)

and across size-fraction variations can be an effective approach to generate hypotheses regarding source(s) of carbonaceous particles in the APM.

ACKNOWLEDGEMENTS

The authors gratefully acknowledge Mr R Suzuki, Mr T Kobayashi, and Ms M Nakamura of the NIES for their technical assistance. The authors sincerely appreciate the work of Dr Sahashi, Toho University, for identifying the species of pollens in the APM.

REFERENCES

- Charlson RJ, Schwartz SE, Hales JM, Cess RD, Coakley JA, Hansen JE, Hofmann DJ. 1992. Climate forcing by anthropogenic aerosols. *Science* 255:423–30.
- Clayton G, Arnold J, Patty F. 1955. Determination of sources of particulate atmospheric carbon. *Science* 122:751–53.
- Currie LA, Stafford TW, Sheffield AE, Klouda GA, Wise SA, Fletcher RA, Donahue DJ, Jull AJT, Linick TW. 1989. Microchemical and molecular dating. *Radiocarbon* 31(3):448–63.
- Currie LA, Eglinton TI, Benner BA, Pearson A. 1997. Radiocarbon “dating” of individual chemical compounds in atmospheric aerosol: first results comparing direct isotopic and multivariate statistical apportionment of specific polycyclic aromatic hydrocarbons. *Nuclear Instruments and Methods in Physics Research B* 123:475–86.
- Currie LA. 2000. Evolution and multidisciplinary frontiers of ^{14}C aerosol science. *Radiocarbon* 42(1):115–26.
- Dockery DW, Pope CA, Xu XP, Spengler JD, Ware JH, Fay ME, Ferris BG, Speizer FE. 1993. An association between air pollution and mortality in six U.S. cities. *New England Journal of Medicine* 329:1753–9.
- Gordon GE. 1988. Receptor models. *Environmental Science and Technology* 22:1132–42.
- Hildemann LM, Klinedinst DB, Klouda GA, Currie LA, Cass GR. 1994. Sources of urban contemporary carbon aerosol. *Environmental Science and Technology* 28:1565–76.
- Kitagawa H, Masuzawa T, Nakamura T, Matsumoto E. 1993. A batch preparation method for graphite targets with low-background for AMS C-14 measurements. *Radiocarbon* 35(2):295–300.
- Klinedinst DB, Currie LA. 1999. Direct quantification of PM_{2.5} fossil and biomass carbon within the Northern Front Range Air Quality Study’s domain. *Environmental Science and Technology* 33:4146–54.
- Lemire KR, Allen DT, Klouda GA, Lewis CW. 2002. Fine particulate matter source attribution for southeast Texas using $^{14}\text{C}/^{13}\text{C}$ ratios. *Journal of Geophysical Research* 107:4613. doi: 10.1029/2002JD002339.
- Reddy CM, Pearson A, Xu L, McNichol AP, Benner Jr. BA, Wise SA, Klouda GA, Currie LA, Eglinton TI. 2002. Radiocarbon as a tool to apportion the sources of polycyclic aromatic hydrocarbons and black carbon in environmental samples. *Environmental Science and Technology* 36:1774–82.
- Stuiver M, Polach HA. 1977. Discussion: reporting of ^{14}C data. *Radiocarbon* 19(3):355–63.
- Tanaka A, Yoneda M, Uchida M, Uehiro T, Shibata Y, Morita M. 2000. Recent advances in ^{14}C measurement at NIES-TERRA. *Nuclear Instruments and Methods in Physics Research B* 172:107–11.
- Weissenböck RH, Currie LA, Gröllert C, Kutschera W, Marolf J, Priller A, Puxbaum H, Rom W, Steier P. 2000. Accelerator mass spectrometry analysis of non-soluble carbon in aerosol particles from high alpine snow (Mt. Sonnblick, Austria). *Radiocarbon* 40(1): 285–94.
- Yoshizumi K. 1991. Source apportionment of aerosols in the Tokyo metropolitan area by chemical element balances. *Energy and Buildings* 15–6: 711–7.

PATHWAYS FOR ESCAPE OF MAGMATIC CARBON DIOXIDE TO SOIL AIR AT UNZEN VOLCANO, SW JAPAN

Hiroshi A Takahashi^{1,2} • Kohei Kazahaya¹ • Hiroshi Shinohara¹ • Toshio Nakamura³

ABSTRACT. Estimation of the magmatic contribution to soil air at Unzen Volcano, SW Japan, was carried out using carbon isotopes, both ¹⁴C and ¹³C, and a mixing model of isotopic mass balance in order to assess the spatial variation of magmatic influence from the volcano. The advantage of using soil air samples is that a wide range of gas sampling sites can be selected. Magmatic CO₂ contributed mostly in the eastern region from Unzen Volcano. The high magmatic contribution to soil air appeared along the Akamatsudani fault zone located southeast of the volcano. Our observations across the fault also showed remarkable peaks of CO₂ concentration and δ¹³C values, suggesting that magmatic fluid comes up along the fracture zone as for the normal fault system of the graben.

INTRODUCTION

Unzen Volcano is on the western part of Beppu-Shimabara Graben (20 km NS wide and 200 km EW long) in Kyushu Island, SW Japan, and is located at the center of a smaller-scale graben (Unzen Graben) in Shimabara Peninsula. During the latest activity (1990–1995), a lava dome eruption occurred and made the new highest peak (1486 m in elevation). Ohsawa et al. (2002) discussed a magmatic carbon contribution using δ¹³C of dissolved inorganic carbon (DIC) in groundwater and estimated a flux of magmatic CO₂ to be 9.1 t/day to the shallow groundwater system in Shimabara Peninsula. However, their study area was limited to the eastern coastal zone of the peninsula, since it was difficult to find a well or springs where samples outside the coastal zone could be taken. We used soil air samples (air occupying pore space among soil grains) instead of groundwater samples in the present study. Hernández (2001) reported on an advective CO₂ degassing from a volcanic body using a soil air survey. Use of soil air allows us to measure CO₂ concentration and flux easily in the field, and to select a large number of observation points.

In this study, we focused on estimating the spatial variation of magmatic CO₂ around Unzen Volcano using soil air samples for comparison with results from a hydrological survey. We also made supplementary observations across the fault to determine the possible path of magmatic carbon to the ground surface.

STUDY SITE AND METHOD

Observation and sampling of soil air at a soil depth of 30 cm were carried out in January 2002 at 51 observation points around Unzen Volcano (Figure 1). In order to discuss the path of magmatic CO₂ to the ground surface, an observation traverse across the fault was also established. The strike of our traverse was in a North-South direction, since the strike of the Akamatsudani fault, located southeast of the volcano, was West-East. Soil gas was sampled using pre-evacuated bottles (150 mL) or aluminumized plastic bags (3 L), and the CO₂ was purified cryogenically on a vacuum line within a few days after sampling. At each observation point, CO₂ concentration in the soil air and CO₂ flux from the soil surface were measured by a portable gas detector (GasTec) and a portable CO₂ flux meter (West System), respectively. The CO₂ flux meter was used in association with a dynamic closed-chamber method with NDIR (LI-800, Licor). The δ¹³C values of 33 samples were measured by IR-

¹Geological Survey of Japan, AIST, 1-1-1 Higashi, Tsukuba, 305-8567, Japan.

²Corresponding author. Email: h.a.takahashi@aist.go.jp.

³Center for Chronological Research, Nagoya University, Chikusa-ku, Nagoya, 464-8602, Japan.

MS with a dual inlet system (Delta Plus, Thermoquest) at the Geological Survey of Japan. The $\delta^{14}\text{C}$ values of 21 samples were measured by accelerator mass spectrometry (AMS) (model 4130-AMS, HVVE) at the Center for Chronological Research, Nagoya University.

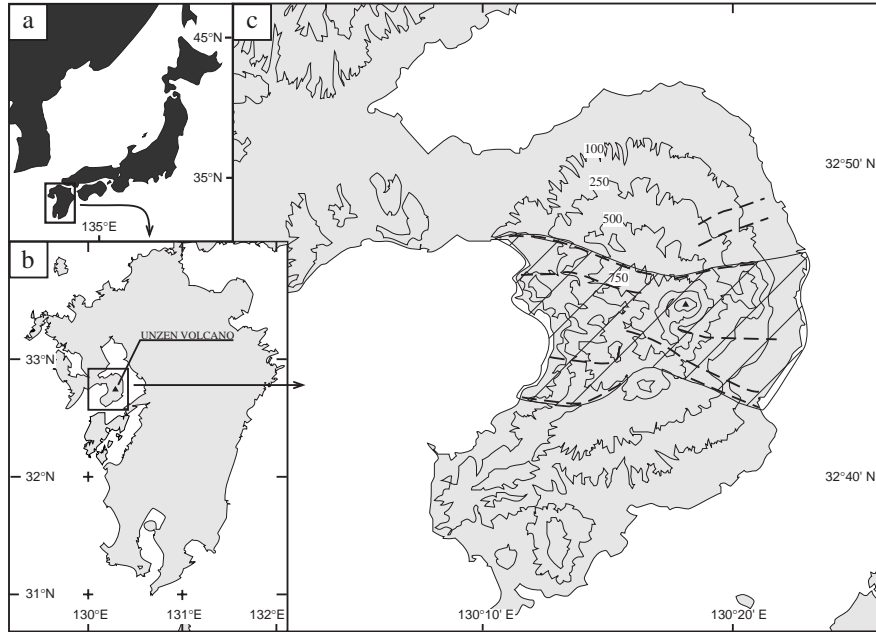


Figure 1 Locality of Unzen Volcano, Kyushu Island, SW Japan. The area of Unzen Graben and the faults are indicated by the striped pattern and dotted lines, respectively (1c, after Hoshizumi et al. 2002).

A mixing model of isotopic mass balance was used to distinguish the magmatic (m), soil organic matter (s), and atmospheric (a) components in order to estimate the magmatic CO_2 contribution to soil air CO_2 . The respective contributions can be computed by the following equations,

$$\delta^{14}\text{C}_i = \delta^{14}\text{C}_m \cdot F_m + \delta^{14}\text{C}_s \cdot F_s + \delta^{14}\text{C}_a \cdot F_a \quad (1),$$

$$\delta^{13}\text{C}_i = \delta^{13}\text{C}_m \cdot F_m + \delta^{13}\text{C}_s \cdot F_s + \delta^{13}\text{C}_a \cdot F_a \quad (2),$$

$$F_m + F_s + F_a = 1 \quad (3),$$

where F is the contribution of respective components, and $0 \leq F \leq 1$. The subscript i indicates a measured sample. The $\delta^{14}\text{C}$ value of the magmatic CO_2 is defined as -1000‰ theoretically, since magmatic carbon was supplied from subducted slab or mantle. The $\delta^{13}\text{C}$ value of magmatic CO_2 is -5.3‰ (Takahashi et al., forthcoming), with an error of $\pm 3\text{‰}$ at 1σ , which is slightly larger than the $\delta^{13}\text{C}$ range of the upper-mantle carbon (Sano and Marty 1995). We assumed the average and error (1σ) values of carbon isotopic ratios of atmosphere and soil organic matter in the study area because their exact values were not measured. The $\delta^{14}\text{C}$ and $\delta^{13}\text{C}$ values of atmospheric CO_2 were computed from the observation data of atmospheric CO_2 and their secular trends (Levin and Kromer 1997). Levin and Kromer (1997) reported an exponential trend of $\Delta^{14}\text{C} = 417 \cdot \exp(-t/16.0)$; $t =$ years after 1974 and a linear decreasing trend of $0.017\text{‰} \cdot \text{yr}^{-1}$ in $\delta^{13}\text{C}$. These fitting trends show us the secular decrements of annual mean values from 1996 to 2002. Then, we combined the comparable values from January 1996 (Levin and Kromer 1997) and the secular decrements. The $\delta^{14}\text{C}$ and $\delta^{13}\text{C}$ values

of atmospheric CO₂ obtained in the present study were 106‰ and -8.9‰, respectively. We estimated the error ranges widely to be ±7.5‰ and ±1‰, respectively, since these values were measured in Germany, not in Japan. Comparable values for soil organic matter were 66 ± 7.5‰ and -27 ± 5‰, respectively, since the Δ¹⁴C of vegetation seems to establish equilibrium with the atmosphere, and the δ¹³C value is used as the approximate mean value of C3 plant, ranging from -32‰ to -22‰ (Smith and Epstein 1971; Wickman 1952). ¹⁴C-dead carbon is not expected from the magmatic contribution because limestone is not present in the Unzen area. Although we have assumed large error ranges in some components, our estimations using Equations 1–3 have a small standard deviation, i.e., better than ±0.02 at 1 σ.

RESULTS AND DISCUSSION

The spatial results of CO₂ concentration, δ¹⁴C, δ¹³C, and flux are shown in Figure 2. The CO₂ concentrations inside Unzen Graben were relatively higher than those outside the graben. The carbon isotopic compositions suggest that the magmatic CO₂ contribution is greater at some of the sample sites inside the graben, shown by relatively lower δ¹⁴C and higher δ¹³C values, than at other sample sites outside the graben. The CO₂ flux, however, was higher along the coastal area than inside the graben. The higher CO₂ flux in the coastal area is probably caused by the difference in soil organic matter content between the 2 regions. The outer rim of the graben is a mountain area (Figure 1c) which was mainly covered with pyroclastic deposits (Hoshizumi et al. 2002). Greater amounts of organic matter are formed along the coastal area as compared to inside the graben (mountain area), indicating that there is a greater biological contribution of CO₂ flux along the coastal area. Carbon isotopic values also indicate a greater contribution of biogenic CO₂ in the coastal region.

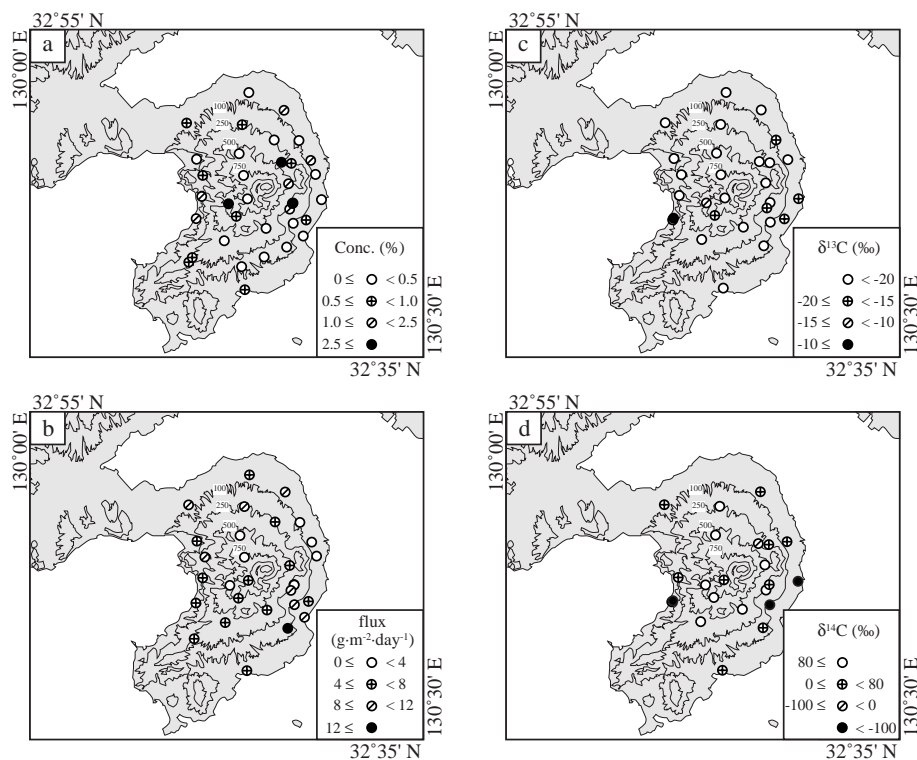


Figure 2 Spatial variations of (a) CO₂ concentration, (b) flux, (c) δ¹³C, and (d) δ¹⁴C in Shimabara Peninsula.

The spatial variation of the magmatic CO₂ contribution to soil air (Figure 3a) was estimated using Equations 1–3. Using the magmatic contribution and the observed results, magmatic CO₂ concentration in soil air and flux from soil surface can be computed (Figure 3b, c). The highest values of magmatic CO₂ contribution, concentration, and flux were 30%, 0.2%, and 1.7 g CO₂·m⁻²·day⁻¹, respectively. The magmatic CO₂ is not degassing uniformly across the soil surface, suggesting that degassing from a volcanic body, measured as the soil CO₂ flux, occurred through a specific path to the ground surface. The observed points show that the high magmatic CO₂ flux are located near the fault zones (Figures 1c, 3c). We measured the remarkable peaks of CO₂ concentration and δ¹³C in traverse observations across the Akamatsudani fault (Figure 4). The field observation did not allow us to identify whether they were located on the fault or not, since there is no outcrop around this traverse point to confirm the exact location of the fault. However, these peaks suggest that magmatic fluid comes up along the fracture zone, just as in a fault system. It is noteworthy that the spatial variability of CO₂ shows a high magmatic CO₂ contribution, flux, and concentration along the Akamatsudani fault zone located southeast of the volcano.

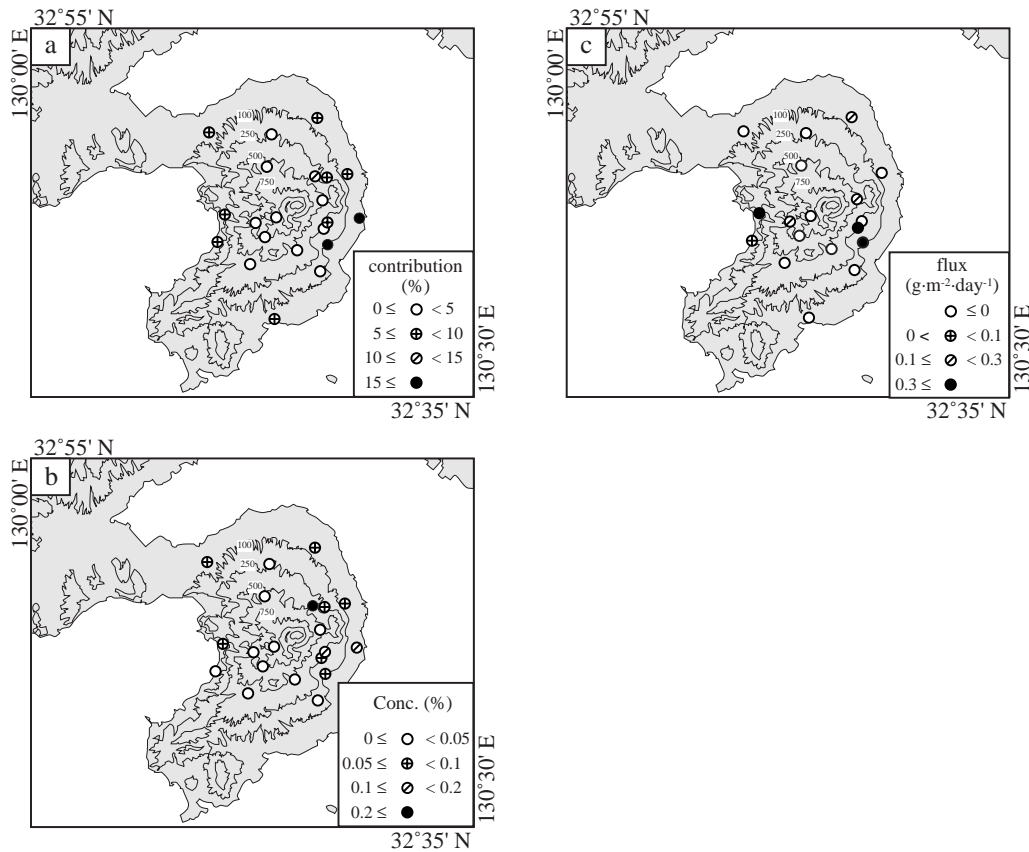


Figure 3 Spatial variations of magmatic CO₂ (a) contribution, (b) concentration, and (c) flux in Shimabara Peninsula.

Even inside the graben, the eastern region showed the relatively high contribution of magmatic CO₂. This agrees well with the groundwater survey (Ohwasa et al. 2002) which suggested that the magmatic fluid in soil air and groundwater might be supplied by the same or a similar system to that of Unzen Graben. Moreover, the approach using soil gas can be used as a tool to substitute for a

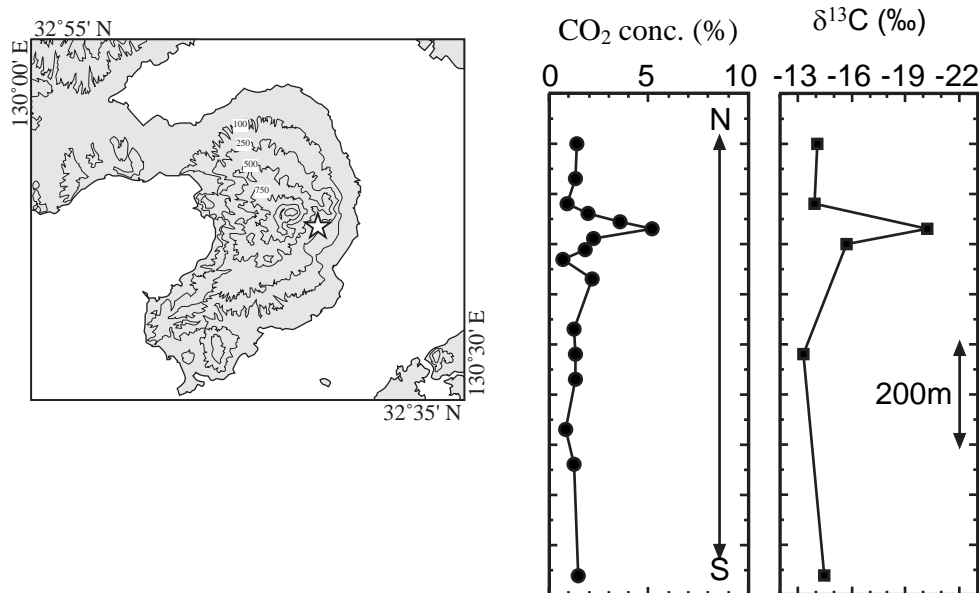


Figure 4 Results of CO₂ concentration and $\delta^{13}\text{C}$ along the traverse across the Akamatsudani fault located south-east of Unzen Volcano. The star indicates the observation locality.

groundwater survey to identify magmatic influence. However, we consider that the magmatic contribution may be underestimated because the incorporation of ^{14}C enrichment from nuclear testing is not considered in the present study.

CONCLUSION

The spatial variations of magmatic CO₂ contribution, concentration, and flux were obtained using CO₂ concentration, flux, and carbon isotopic compositions in soil air around Unzen Volcano, SW Japan. The magmatic influence was large inside the Unzen Graben, especially in the eastern region. The spatial variations from soil gas survey were identical to those from the groundwater survey. On the other hand, the traverse across the fault zone suggested that the fracture zone of the fault system played a key role in providing a path for a magmatic fluid from a deep environment to the ground surface. Our study shows that the soil gas survey can provide a convenient tool for the identification of magmatic influences.

ACKNOWLEDGEMENTS

The authors wish to thank Dr Etsuko Niu of Nagoya University for the operation of the AMS system. During the sample preparation, Dr Eiichi Konohira, Ms Rie Tsuchuya, Ms Tomoko Ohta, and Ms Akiko Ikeda of Nagoya University provided kind assistance.

REFERENCES

- Hernández PA, Notsu K, Salazar M, Mori T, Natale G, Okada H, Virgili G, Shimoike Y, Sato M, Pérez NM. 2001. Carbon dioxide degassing by advective flow from Usu Volcano, Japan. *Science* 292:83–6.
- Hoshizumi H, Uto K, Matsumoto T, Shu S, Kurihara A, Sumii T. 2002. History of Unzen Volcano. *Gekkan Chikyū* 282:828–34. In Japanese.
- Levin, I, Kromer B. 1997. Twenty years of high precision atmospheric ^{14}C observations at Schauinsland station, Germany. *Radiocarbon* 39(2):205–18.
- Ohsawa S, Kazahaya K, Yasuhara M, Kono T, Kitaoka K, Yusa Y, Yamaguchi K. 2002. Escape of volcanic gas

- into shallow groundwater system at Unzen Volcano (Japan): evidence from chemical and stable carbon isotope compositions of dissolved inorganic carbon. *Limnology* 3:169–73.
- Sano Y, Marty B. 1995. Origin of carbon in fumarolic gas from island arcs. *Chemical Geology* 119:265–74.
- Smith BN, Epstein S. 1971. Two categories of $^{13}\text{C}/^{12}\text{C}$ ratios for higher plants. *Plant Physiology* 47:380–4.
- Takahashi HA, Kazahaya K, Shinohara H, Nakamura T. Forthcoming. Application of radiocarbon to detect a deep source CO_2 in soil air. *Nuclear Instruments and Methods in Physics Research B*.
- Wickman FE. 1952. Variations in the relative abundance of the carbon isotopes in plants. *Geochimica et Cosmochimica Acta* 2:243–54.



Australian Government

Ansto

ANTARES AMS

Established at the Australian Nuclear Science and Technology Organisation (ANSTO) in 1991, we offer AMS services and collaborative arrangements to Australian and international researchers in a wide range of applications.

Capabilities

- Designed for Multi-isotope analysis with high precision and high throughput.
- ^{10}Be , ^{14}C , ^{26}Al , ^{129}I and ^{236}U are routinely analysed.
- A suite of chemistry laboratories for sample processing and target preparation for a wide range of sample types.
- Stable isotope analysis ($\delta^{13}\text{C}$ and $\delta^{15}\text{N}$).

Current Applications

- Radiocarbon dating
- Geological exposure dating
- Nuclear safeguards

We specialise in

- Small radiocarbon sample size
- Atmospheric carbon dioxide analysis
- High sensitivity actinide analysis

To find out more contact

ANTARES AMS Facility
Australian Nuclear Science and Technology Organisation
PMB 1, Menai NSW 2234, AUSTRALIA
antares.ams@ansto.gov.au
www.ansto.gov.au/ansto/environment1/ams

^{129}I

^{26}Al

^{10}Be

^{14}C

^{236}U

ADVERTISE IN *RADIOCARBON*

REACH YOUR TARGET AUDIENCE EFFECTIVELY & AFFORDABLY

Prices good through March 1, 2004

Display Ads

<i>Inside page</i>	<i>Inside back cover</i>	<i>Back cover^a</i>
\$350/issue	\$500/issue	\$600/issue
\$900/volume	\$1250/volume	\$1500/volume

^aReserved through 2003.

Color Ads and Folded Inserts^a

<i>Color ad (inside page)</i>	<i>Folded inserts</i>
\$1600/issue	\$300/issue
\$4500/volume	\$700/volume

^aThe prices above are for prepared inserts and ads provided by the customer. Call for estimates on typesetting, design, duplicating and folding services.

Radiocarbon reaches libraries, labs, individuals, and institutions in North America, South America, Europe, the Middle East, Asia, Africa, and Australasia. We can help you reach your target market, wherever it is.

We publish three issues per volume year. Advertise in two consecutive issues and get the third at a significant discount (must reserve all three ads at once for discount to apply).

We accept full-page and multipage advertisements in black and white or full-color. You may send camera-ready copy, film negatives, or digital files. Or, for a small fee, we will create an ad from your supplied text and graphics.

*For more information, please contact Managing Editor
Mark McClure at editor@radiocarbon.org.*



RADIOCARBON

\$5 Back Issues Clearance Sale

YEAR	VOL.	Write in the number of copies desired for each issue					
		NR 1	NR 2	NR 2A	NR 2B	NR 3	NR 4
1980	22						
1981	23						
1982	24						
1983	25						
1984	26						
1985	27						
1986	28						
1987	29						
1988	30						
1989	31						
1990	32						
1991	33						
1992	34						

Calculate Payment

___ copies × \$5 ea. = \$ _____

Subtotal: \$ _____

Shipping via surface mail:
(Contact us for other shipping methods)

Add \$2 ea. book for US
Add \$3 ea. book outside US

___ copies × \$ ___ ea. = \$ _____

Shipping total: \$ _____

Total due: \$ _____

Payment & Shipping Address

- MasterCard Visa
 Check enclosed Please bill me

Name: _____

Address: _____

Fax: _____ E-mail: _____

For Credit-Card Orders

Card number: _____ Expiration date: _____

Signature: _____ Phone: _____

For online Contents see: <http://www.radiocarbon.org/Pubs/contents.html>

Prices good while supplies last. Mail or fax this form to:

RADIOCARBON, 4717 East Fort Lowell Road, Room 104, Tucson, Arizona 85712-1201 USA
 Phone: +1 520 881-0857; Fax: +1 520 881-0554; orders@radiocarbon.org



RADIOCARBON

An International Journal of
Cosmogenic Isotope Research

The University of Arizona
Department of Geosciences
4717 E. Fort Lowell Rd, Rm. 104
Tucson, AZ 85712-1201 USA

E-mail: orders@radiocarbon.org
<http://www.radiocarbon.org/>

2004 PRICE LIST

Proceedings of the 17th International Radiocarbon Conference (Vol 43, Nrs 2A, 2B and 3, 2001)	\$60.00*
Proceedings of the 16th International Radiocarbon Conference (Vol 40, Nrs 1 and 2, 1998)	50.00
INTCAL98 (1998 Calibration issue; Vol 40, Nr 3, 1998)	40.00
Calibration 1993 (Vol 35, Nr 1, 1993)	40.00
Proceedings of the 15th International Radiocarbon Conference (Vol 37, Nr 2, 1995)	50.00
Liquid Scintillation Spectrometry 1994 (ISBN: 0-9638314-3-7; 1996)	20.00
Liquid Scintillation Spectrometry 1992 (ISBN: 0-9638314-0-2; 1993)	10.00
Liquid Scintillation Spectrometry 2001 (ISBN: 0-9638314-4-5; 2002)	60.00
<i>Special offer—LSC 92 , LSC 94, LSC 01 package—save \$5.00</i>	85.00
Tree Rings, Environment and Humanity (ISBN 0-9638314-2-9; 1996) (Proceedings of the International Tree-Ring Conference, Tucson, Arizona, 1994)	20.00
SUBSCRIPTION RATES VOLUME 46, Nrs 1–3, 2004 (subscriptions include free online access)	
Institution (Includes domestic shipping)	190.00
Institution (Includes foreign shipping)	205.00
Individual (Includes domestic shipping)	90.00
Individual (Includes foreign shipping)	105.00
Lifetime Subscription—Institutional	2500.00
Lifetime Subscription—Individual	1100.00
BACK ISSUES (except conference proceedings and special issues)	Single issue 40.00
VOLUMES 1–9 each volume	40.00
VOLUMES 10–21 each volume	65.00
VOLUMES 22–44 each volume	100.00
Radiocarbon Conference Proceedings	50.00
SPECIAL FULL-SET OFFER—Volumes 1–44 (1959–2002)	1300.00
Big savings. Includes bound copies of 35 out-of-print issues. Take \$50.00 off for each additional set.	

2004 POSTAGE AND HANDLING CHART

	U.S.	Foreign
Subscription	--	\$15.00
Single back issue	\$4.00	\$9.00
Book or Proceedings	\$5.00	\$14.00
Full set	\$200.00	varies

Surface mail rates are listed here. Please contact us for airmail or express delivery rates.

Orders must be prepaid. We accept payments by Visa and MasterCard, or by check or money order payable in US\$ to *Radiocarbon*. Bank funds transfers are also accepted. Please contact us for instructions.

Federal tax ID 86-6004791

*Postage will be added; see above chart. Subscription rates and book prices are subject to change.

RAFTER

RADIOCARBON LABORATORY

The test of time

Accelerator Mass Spectrometry Radiocarbon Dating

Rafter provides:

- ◆ **Prompt reporting times**
 - ◇ *never more than 8 weeks*
- ◆ **Competitive prices**
 - ◇ *NZ\$ 820 per sample*
- ◆ **Stable isotope corrections**
 - ◇ *$\delta^{13}\text{C}$ measurement at no extra charge*
- ◆ **Additional services**
 - ◇ *3 week express turnarounds*
 - ◇ *enhanced precision measurements*
 - ◇ *radiometric ^{14}C dating for large samples*
 - ◇ *bone C:N analysis:- %C, %N, $\delta^{13}\text{C}$, $\delta^{15}\text{N}$*
 - ◇ *direct dating of pollen*
 - ◇ *X-ray diffraction for shells*
 - ◇ *calibration assistance*
 - ◇ *consultancy services*

At the Rafter Radiocarbon Laboratory we have been successfully meeting the test of time for more than 50 years.

The Rafter Radiocarbon Laboratory has an international reputation for accurately dating a wide range of organic materials, sediments, textiles, bone, ivory, paper, wood, parchment, charcoal, shell, foraminifera and peat.

At Rafter we understand what our clients expect: accurate dating, at competitive rates and superior turn around times and service.

For more information, visit our website

www.RafterRadiocarbon.co.nz

or contact us at:

Rafter Radiocarbon Laboratory
Institute of Geological & Nuclear Sciences
30 Gracefield Road, Lower Hutt, New Zealand

☎: +64-4-570 4647

Fax: +64-4-570 4657

Email: r.sparks@gns.cri.nz



Institute of
**GEOLOGICAL
& NUCLEAR
SCIENCES**
limited